frontiers

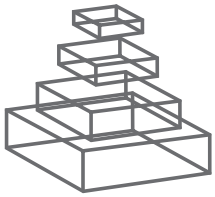
RESEARCH TOPICS

BRAIN CONNECTIVITY ANALYSIS: INVESTIGATING BRAIN DISORDERS

Hosted by
Barry Horwitz and Silvina G. Horovitz



frontiers in
SYSTEMS NEUROSCIENCE



frontiers

FRONTIERS COPYRIGHT STATEMENT

© Copyright 2007-2012
Frontiers Media SA.
All rights reserved.

All content included on this site, such as text, graphics, logos, button icons, images, video/audio clips, downloads, data compilations and software, is the property of or is licensed to Frontiers Media SA ("Frontiers") or its licensees and/or subcontractors. The copyright in the text of individual articles is the property of their respective authors, subject to a license granted to Frontiers.

The compilation of articles constituting this e-book, as well as all content on this site is the exclusive property of Frontiers. Images and graphics not forming part of user-contributed materials may not be downloaded or copied without permission.

Articles and other user-contributed materials may be downloaded and reproduced subject to any copyright or other notices. No financial payment or reward may be given for any such reproduction except to the author(s) of the article concerned.

As author or other contributor you grant permission to others to reproduce your articles, including any graphics and third-party materials supplied by you, in accordance with the Conditions for Website Use and subject to any copyright notices which you include in connection with your articles and materials.

All copyright, and all rights therein, are protected by national and international copyright laws.

The above represents a summary only. For the full conditions see the Conditions for Authors and the Conditions for Website Use.

Cover image provided by Ibbl sarl, Lausanne CH

ISSN 1664-8714
ISBN 978-2-88919-020-1
DOI 10.3389/978-2-88919-020-1

ABOUT FRONTIERS

Frontiers is more than just an open-access publisher of scholarly articles: it is a pioneering approach to the world of academia, radically improving the way scholarly research is managed. The grand vision of Frontiers is a world where all people have an equal opportunity to seek, share and generate knowledge. Frontiers provides immediate and permanent online open access to all its publications, but this alone is not enough to realize our grand goals.

FRONTIERS JOURNAL SERIES

The Frontiers Journal Series is a multi-tier and interdisciplinary set of open-access, online journals, promising a paradigm shift from the current review, selection and dissemination processes in academic publishing.
All Frontiers journals are driven by researchers for researchers; therefore, they constitute a service to the scholarly community. At the same time, the Frontiers Journal Series operates on a revolutionary invention, the tiered publishing system, initially addressing specific communities of scholars, and gradually climbing up to broader public understanding, thus serving the interests of the lay society, too.

DEDICATION TO QUALITY

Each Frontiers article is a landmark of the highest quality, thanks to genuinely collaborative interactions between authors and review editors, who include some of the world's best academicians. Research must be certified by peers before entering a stream of knowledge that may eventually reach the public - and shape society; therefore, Frontiers only applies the most rigorous and unbiased reviews.
Frontiers revolutionizes research publishing by freely delivering the most outstanding research, evaluated with no bias from both the academic and social point of view.
By applying the most advanced information technologies, Frontiers is catapulting scholarly publishing into a new generation.

WHAT ARE FRONTIERS RESEARCH TOPICS?

Frontiers Research Topics are very popular trademarks of the Frontiers Journals Series: they are collections of at least ten articles, all centered on a particular subject. With their unique mix of varied contributions from Original Research to Review Articles, Frontiers Research Topics unify the most influential researchers, the latest key findings and historical advances in a hot research area!
Find out more on how to host your own Frontiers Research Topic or contribute to one as an author by contacting the Frontiers Editorial Office: researchtopics@frontiersin.org

BRAIN CONNECTIVITY ANALYSIS: INVESTIGATING BRAIN DISORDERS

Hosted By
Barry Horwitz, National Institutes of Health, USA
Silvina G. Horovitz, National Institutes of Health, USA

In the last few years, advances in human structural and functional neuroimaging (fMRI, PET, EEG/MEG) have resulted in an explosion of studies investigating the anatomical and functional connectivity between different regions of the brain. More and more studies have employed resting and task-related connectivity analyses to assess functional interactions, and diffusion-weighted tractography to study white matter organization. Many of these studies have addressed normal human function, but recently, a number of investigators have turned their attention to examining brain disorders.

The study of brain disorders is a complex endeavor; not only does it require understanding the normal brain, and the regions involved in a particular function, but also it needs a deeper understanding of brain networks and their dynamics. This special issue will provide the scientific community with an overview of how to apply connectivity methods to study brain disease, and with perspectives on what are the strength and limitations of each modality.

For this Research Topic, we solicit both reviews and original research articles on the use of brain connectivity analysis, with non-human or human models, to explore neurological, psychiatric, developmental and neurodegenerative disorders from a system perspective. Connectivity studies that have focused on one or more of the following will be of particular interest:

(1) detection of abnormal functional/structural connectivity;
(2) neural plasticity, assessed by changes in connectivity, in patients with brain disorders;
(3) assessment of therapy using connectivity measures;
(4) relation of connectivity changes to behavioral changes.

Table of Contents

The Review Articles

06 ***Introduction to Research Topic – Brain Connectivity Analysis: Investigating Brain Disorders. Part 1: The Review Articles***
Barry Horwitz and Silvina G. Horovitz

08 ***Connectivity Analysis is Essential to Understand Neurological Disorders***
James B. Rowe

21 ***Identifying abnormal connectivity in patients using Dynamic Causal Modelling of fMRI responses***
Mohamed L Seghier, Peter Zeidman, Nicholas H Neufeld, Alex P Leff and Cathy Price

35 ***Transcranial Magnetic Stimulation and Connectivity Mapping: Tools for Studying the Neural Bases of Brain Disorders***
M. Hampson and R. E. Hoffman

43 ***Studying Network Mechanisms Using Intracranial Stimulation in Epileptic Patients***
Olivier David, Julien Bastin, Stéphan Chabardès, Lorella Minotti and Philippe Kahane

53 ***From Intracerebral EEG Signals to Brain Connectivity: Identification of Epileptogenic Networks in Partial Epilepsy***
Fabrice Wendling, Patrick Chauvel, Arnaud Biraben and Fabrice Bartolomei

66 ***Concepts of Connectivity and Human Epileptic Activity***
Louis Lemieux, Jean Daunizeau and Matthew C. Walker

79 ***Disrupted Modularity and Local Connectivity of Brain Functional Networks in Childhood-Onset Schizophrenia***
Aaron F. Alexander-Bloch, Nitin Gogtay, David Meunier, Rasmus Birn, Liv Clasen, Francois Lalonde, Rhoshel Lenroot, Jay Giedd and Edward T. Bullmore

95 ***Inter-Regional Brain Communication and Its Disturbance in Autism***
Sarah E. Schipul, Timothy A. Keller and Marcel Adam Just

106 ***Brain Connectivity in Pathological and Pharmacological Coma***
Quentin Noirhomme, Andrea Soddu, Rémy Lehembre, Audrey Vanhaudenhuyse, Pierre Boveroux, Mélanie Boly and Steven Laureys

112 ***Functional Connectivity in Relation to Motor Performance and Recovery After Stroke***
Kelly P. Westlake and Srikantan S. Nagarajan

124 ***Relevance of Structural Brain Connectivity to Learning and Recovery from Stroke***
Heidi Johansen-Berg, Jan Scholz and Charlotte J. Stagg

Original Research Articles

133 Introduction to Research Topic – Brain Connectivity Analysis: Investigating Brain Disorders. Part 2: Original Research Articles

Silvina G. Horovitz and Barry Horwitz

135 A Linear Structural Equation Model for Covert Verb Generation Based on Independent Component Analysis of fMRI Data from Children and Adolescents

Prasanna Karunanayaka, Vincent J. Schmithorst, Jennifer Vannest, Jerzy P. Szaflarski, Elena Plante and Scott K. Holland

150 A Baseline for the Multivariate Comparison of Resting-State Networks

Elena A. Allen, Erik B. Erhardt, Eswar Damaraju, William Gruner, Judith M. Segall, Rogers F. Silva, Martin Havlicek, Srinivas Rachakonda, Jill Fries, Ravi Kalyanam, Andrew M. Michael, Arvind Caprihan, Jessica A. Turner, Tom Eichele, Steven Adelsheim, Angela D. Bryan, Juan Bustillo, Vincent P. Clark, Sarah W. Feldstein Ewing, Francesca Filbey, Corey C. Ford, Kent Hutchison, Rex E. Jung, Kent A. Kiehl, Piyadasa Kodituwakku, Yuko M. Komesu, Andrew R. Mayer, Godfrey D. Pearlson, John P. Phillips, Joseph R. Sadek, Michael Stevens, Ursina Teuscher, Robert J. Thoma and Vince D. Calhoun

173 Neural substrates of reliability-weighted visual-tactile multisensory integration

Michael S Beauchamp, Siavash Pasalar and Tony Ro

184 The Neural Architecture of the Language Comprehension Network: Converging Evidence from Lesion and Connectivity Analyses

And U. Turken and Nina F. Dronkers

204 Greater Pre-Stimulus Effective Connectivity from the Left Inferior Frontal Area to other Areas is Associated with Better Phonological Decoding in Dyslexic Readers

Richard E. Frye, Meng-Hung Wu, Jacqueline Liederman and Janet McGraw Fisher

217 Influences of Neural Pathway Integrity on Children's Response to Reading Instruction

Nicole Davis, Qiuyun Fan, Donald L. Compton, Doug Fuchs, Lynn S. Fuchs, Laurie E. Cutting, John C. Gore and Adam W. Anderson

228 Prefrontal Compensatory Engagement in TBI is due to Altered Functional Engagement Of Existing Networks and not Functional Reorganization

Gary R. Turner, Anthony R. McIntosh and Brian Levine

240 Effects of Visual Experience on the Human MT+ Functional Connectivity Networks: An fMRI Study of Motion Perception in Sighted and Congenitally Blind Individuals

Lorenzo Sani, Emiliano Ricciardi, Claudio Gentili, Nicola Vanello, James V. Haxby and Pietro Pietrini

249 Diffusion Tensor Imaging Detects Early Cerebral Cortex Abnormalities in Neuronal Architecture Induced by Bilateral Neonatal Enucleation: An Experimental Model in the Ferret

Andrew S. Bock, Jaime F. Olavarria, Lindsey A. Leigland, Erin N. Taber, Sune N. Jespersen and Christopher D. Kroenke

260 Reduced Interhemispheric Functional Connectivity in the Motor Cortex during Rest in Limb-Onset Amyotrophic Lateral Sclerosis

Laura M. Jelsone-Swain, Brett W. Fling, Rachael D. Seidler, Rebecca Hovatter, Kirsten Gruis and Robert C. Welsh

268 Altered Resting State Cortico-Striatal Connectivity in Mild to Moderate Stage Parkinson's Disease

Youngbin Kwak, Scott Peltier, Nicolaas I. Bohnen, Martijn L. T. M. Müller, Praveen Dayalu and Rachael D. Seidler

293 Whole Brain Resting-State Analysis Reveals Decreased Functional Connectivity in Major Depression

Ilya M. Veer, Christian F. Beckmann, Marie-José van Tol, Luca Ferrarini, Julien Milles, Dick J. Veltman, André Aleman, Mark A. van Buchem, Nic J. van der Wee and Serge A.R.B. Rombouts

303 Is Social Phobia a "Mis-Communication" Disorder? Brain Functional Connectivity during Face Perception Differs between Patients with Social Phobia and Healthy Control Subjects

Sabrina Danti, Emiliano Ricciardi, Claudio Gentili, Maria Ida Gobbini, Pietro Pietrini and Mario Guazzelli

frontiers in
SYSTEMS NEUROSCIENCE

EDITORIAL
published: 13 February 2012
doi: 10.3389/fnsys.2012.00003

Introduction to research topic – Brain connectivity analysis: investigating brain disorders. Part 1: the review articles

***Barry Horwitz*[1]* and *Silvina G. Horovitz*[2]**

[1] *Brain Imaging and Modeling Section, National Institute on Deafness and Other Communication Disorders, National Institutes of Health, Bethesda, MD, USA*
[2] *Human Motor Control Section, National Institute of Neurological Disorders and Stroke, National Institutes of Health, Bethesda, MD, USA*
**Correspondence: horwitzb@nidcd.nih.gov*

In the past few years, advances in human structural and functional neuroimaging, especially with respect to magnetic resonance imaging, have resulted in an explosion of studies exploring the anatomical and functional connectivities between different regions of the brain. More and more studies have employed resting and task-related connectivity analyses to assess functional interactions, and other studies have used diffusion-weighted tractography to examine the organization and integrity of white matter tracts. Many of these studies have addressed normal human function, but recently, a number of investigators have turned their attention to examining brain disorders. We are on the verge of being able to better understand the pathophysiology of neurological and psychiatric disorders and the effect of treatments on brain function. The study of brain disorders is a complex endeavor: not only does it require understanding the normal brain, and the regions involved in a particular function, but also it needs a deeper understanding of brain networks and their dynamics. Moreover, in many cases, disorders are progressive, and thus imaging could potentially become a source of biomarkers for early detection and assessment of the course of a disease (Horwitz and Rowe, 2011), and for evaluating potential treatments. The articles that appear in this special topics ebook represent the current status of the applications that employ brain connectivity analysis to investigate brain disorders.

Although certain types of connectivity analyses have become very popular recently [e.g., resting state fMRI functional connectivity – see the special topics issue of Frontiers in Systems Neuroscience edited by Uddin and Menon (2010)], we have chosen to cover articles that represent the broadest possible set of connectivity methods, employing the widest possible spectrum of imaging techniques, and applied to the full range of neurological, psychiatric, and developmental disorders. In this way, we hope that readers acquire an understanding of how these relatively new connectivity analysis methods enable investigators to address brain disorders from a network perspective. Even pathology localized to one area of the brain can lead to dysfunctional network behavior, since no brain region is an island onto itself. The insights offered by the network paradigm have, therefore, important ramifications for using neuroimaging to help detect and diagnose brain disorders, interpret the symptoms of many disorders, and assess potential treatments.

Two types of articles comprise this special topics ebook – review articles and papers that include primarily the results of original research. Here, we provide a brief overview of the review articles. See the Horovitz and Horwitz editorial (Introduction to research topic – Brain connectivity analysis: investigating brain disorders. Part 2: original research articles) for a corresponding overview of the research papers.

The review articles can be roughly divided into (1) those that focus on a connectivity method, and use one or more disorders to illustrate the method, and (2) those whose emphasis is placed on a particular disorder, and discuss a number of relevant functional and structural connectivity studies investigating the disorder. In the first category of reviews, Rowe (2010) provides an overview of fMRI-based functional and effective connectivity, with a focus on its applications to neurological disorders. One of the most widely used effective connectivity techniques is dynamic causal modeling (DCM; Friston et al., 2003), and Seghier et al. (2010) present an extensive review of its application to all brain disorders. This article also includes a useful introduction to Bayesian model selection (Penny et al., 2004), a key component of DCM. Another "functional" connectivity method that has been applied to investigate brain disorders is transcranial magnetic stimulation (TMS), and the article by Hampson and Hoffman (2010) contains a nice overview of the method, along with a review of its applications to psychiatric and neurological disorders. In TMS, an externally applied changing magnetic field is used to induce electrical stimulation in a cortical brain area which propagates through long-range connections to other brain regions. David et al. (2010) discuss a similar method, direct electrical stimulation (DES), applied using intracranial electrodes in some epileptic patients during presurgical evaluation prior to epileptogenic tissue resection. DES is applied directly to cortical tissue and tracts with extremely well-defined spatial definition, and in this sense, it provides human data that are unattainable by any other method. Epilepsy also provides the basis for two other reviews. Wendling et al. (2010) discuss a variety of functional connectivity techniques that have been applied to electrophysiological data obtained from scalp and intracerebral EEG recordings, whereas the review by Lemieux et al. (2011) offers a broad overview of both EEG-based and fMRI-based functional and effective connectivity analyses. Finally, Alexander-Bloch et al. (2010) provide a useful overview of the basic concepts and mathematics of graph theory as applied to fMRI resting data. As an example of graph theory as applied to resting state fMRI, they present results of a study comparing childhood-onset schizophrenia with normal controls, showing disrupted modularity and local connectivity in the patients.

The second category of review articles focuses on disorders. Schipul et al. (2011) provide a detailed review of autism. In many ways autism represents the classic example of a disorder where analyses of imaging data at the single brain region level yielded very little insight, but network analyses have proven quite fruitful in furthering our understanding of the condition. A second brain disorder that is reviewed here is coma (and related disorders of consciousness). Noirhomme et al. (2010)

show that such studies can shed important light on what mediates conscious awareness. Two articles address stroke, in particular focusing on using brain connectivity analyses to assess functional recovery. Westlake and Nagarajan (2011) provide an overview of functional connectivity in relation to motor performance. Their review emphasizes PET, fMRI, and EEG/MEG studies. In the other review, Johansen-Berg et al. (2010) examine white matter connectivity results, obtained using diffusion tensor imaging (DTI). Their paper includes information on how this technique can be used to test for dynamic changes in structural connectivity with learning or with recovery from the effects of a stroke.

ACKNOWLEDGMENTS

This work was supported by the Intramural Research Programs of NIDCD (BH) and NINDS (SGH).

REFERENCES

Alexander-Bloch, A. F., Gogtay, N., Meunier, D., Birn, R., Clasen, L., Lalonde, F., Lenroot, R., Giedd, J., and Bullmore, E. T. (2010). Disrupted modularity and local connectivity of brain functional networks in childhood-onset schizophrenia. *Front. Syst. Neurosci.* 4:147. doi: 10.3389/fnsys.2010.00147

David, O., Bastin, J., Chabardes, S., Minotti, L., and Kahane, P. (2010). Studying network mechanisms using intracranial stimulation in epileptic patients. *Front. Syst. Neurosci.* 4:148. doi: 10.3389/fnsys.2010.00148

Friston, K. J., Harrison, L., and Penny, W. (2003). Dynamic causal modelling. *Neuroimage* 19, 1273–1302.

Hampson, M., and Hoffman, R. E. (2010). Transcranial magnetic stimulation and connectivity mapping: tools for studying the neural bases of brain disorders. *Front. Syst. Neurosci.* 4:40. doi: 10.3389/fnsys.2010.00040

Horwitz, B., and Rowe, J. B. (2011). Functional biomarkers for neurodegenerative disorders based on the network paradigm. *Prog. Neurobiol.* 95, 505–509.

Johansen-Berg, H., Scholz, J., and Stagg, C. J. (2010). Relevance of structural brain connectivity to learning and recovery from stroke. *Front. Syst. Neurosci.* 4:146. doi: 10.3389/fnsys.2010.00146

Lemieux, L., Daunizeau, J., and Walker, M. C. (2011). Concepts of connectivity and human epileptic activity. *Front. Syst. Neurosci.* 5:12. doi: 10.3389/fnsys.2011.00012

Noirhomme, Q., Soddu, A., Lehembre, R., Vanhaudenhuyse, A., Boveroux, P., Boly, M., and Laureys, S. (2010). Brain connectivity in pathological and pharmacological coma. *Front. Syst. Neurosci.* 4:160. doi: 10.3389/fnsys.2010.00160

Penny, W. D., Stephan, K. E., Mechelli, A., and Friston, K. J. (2004). Comparing dynamic causal models. *Neuroimage* 22, 1157–1172.

Rowe, J. B. (2010). Connectivity analysis is essential to understand neurological disorders. *Front. Syst. Neurosci.* 4:144. doi: 10.3389/fnsys.2010.00144

Schipul, S. E., Keller, T. A., and Just, M. A. (2011). Inter-regional brain communication and its disturbance in autism. *Front. Syst. Neurosci.* 5:10. doi: 10.3389/fnsys.2011.00010

Seghier, M. L., Zeidman, P., Neufeld, N. H., Leff, A. P., and Price, C. J. (2010). Identifying abnormal connectivity in patients using dynamic causal modeling of FMRI responses. *Front. Syst. Neurosci.* 4:142. doi: 10.3389/fnsys.2010.00142

Uddin, L. Q., and Menon, V. (2010). Introduction to special topic – resting-state brain activity: implications for systems neuroscience. *Front. Syst. Neurosci.* 4:37. doi: 10.3389/fnsys.2010.00037

Wendling, F., Chauvel, P., Biraben, A., and Bartolomei, F. (2010). From intracerebral EEG signals to brain connectivity: identification of epileptogenic networks in partial epilepsy. *Front. Syst. Neurosci.* 4:154. doi: 10.3389/fnsys.2010.00154

Westlake, K. P., and Nagarajan, S. S. (2011). Functional connectivity in relation to motor performance and recovery after stroke. *Front. Syst. Neurosci.* 5:8. doi: 10.3389/fnsys.2011.00008

Received: 25 January 2012; accepted: 27 January 2012; published online: 13 February 2012.
Citation: Horwitz B and Horovitz SG (2012) Introduction to research topic – Brain connectivity analysis: investigating brain disorders. Part 1: the review articles. Front. Syst. Neurosci. ***6****:3. doi: 10.3389/fnsys.2012.00003*
Copyright © 2012 Horwitz and Horovitz. This is an open-access article distributed under the terms of the Creative Commons Attribution Non Commercial License, which permits non-commercial use, distribution, and reproduction in other forums, provided the original authors and source are credited.

frontiers in
SYSTEMS NEUROSCIENCE

REVIEW ARTICLE
published: 17 September 2010
doi: 10.3389/fnsys.2010.00144

Connectivity analysis is essential to understand neurological disorders

James B. Rowe*[1,2,3]

[1] Department of Clinical Neurosciences, University of Cambridge, Cambridge, UK
[2] Cognition and Brain Sciences Unit, Medical Research Council, Cambridge, UK
[3] Behavioural and Clinical Neurosciences Institute, University of Cambridge, Cambridge, UK

Edited by:
Barry Horwitz, National Institutes of Health, USA

Reviewed by:
Barry Horwitz, National Institutes of Health, USA
Arun Bokde, Trinity College Dublin, Ireland

Correspondence:
James B. Rowe, Cognition and Brain Sciences Unit, Medical Research Council, 15 Chaucer Road, Cambridge CB2 7EF, UK.
e-mail: james.rowe@mrc-cbu.cam.ac.uk

Neurological and neuropsychiatric disorders are major causes of morbidity worldwide. A systems level analysis including functional and structural neuroimaging is particularly useful when the pathology leads to disorders of higher order cognitive functions in human patients. However, an analysis that is restricted to regional effects is impoverished and insensitive, compared to the analysis of distributed brain networks. We discuss the issues to consider when choosing an appropriate connectivity method, and compare the results from several different methods that are relevant to fMRI and PET data. These include psychophysiological interactions in general linear models, structural equation modeling, dynamic causal modeling, and independent components analysis. The advantages of connectivity analysis are illustrated with a range of structural and neurodegenerative brain disorders. We illustrate the sensitivity of these methods to the presence or severity of disease and/or treatment, even where analyses of voxel-wise activations are insensitive. However, functional and structural connectivity methods should be seen as complementary to, not a substitute for, other imaging and behavioral approaches. The functional relevance of changes in connectivity, to motor or cognitive performance, are considered alongside the complex relationship between structural and functional changes and neuropathology. Finally some of the problems associated with connectivity analysis are discussed. We suggest that the analysis of brain connectivity is an essential complement to the analysis of regionally specific dysfunction, in order to understand neurological and neuropsychiatric disease, and to evaluate the mechanisms of effective therapies.

Keywords: effective connectivity, functional connectivity, structural equation modeling, dynamic causal modeling, psychophysiological interactions, MRI

INTRODUCTION

Neurological and neuropsychiatric disorders are major causes of morbidity and mortality worldwide. They include developmental and degenerative processes, as well as focal brain injury from stroke or trauma, and are subject to many genetic and environmental influences. The heterogeneity and complexity of individual clinical syndromes reflect interactions among patterns of neuropathology, individual differences in premorbid function and the distributed functional anatomy of normal cognitive and motor processes. This presents a double challenge for clinical translational cognitive neuroscience – to define simultaneously the processes or systems underlying neuropsychiatric syndromes, and to understand their functional anatomical abnormalities.

For many years, a neuropsychological approach was the only way to dissociate functional components of behavioral syndromes, and often localize clinical phenomena to specific brain regions. With the advent of structural brain imaging, combined with behavioral analysis and larger case series, this approach remains informative (Mort et al., 2003; Sapir et al., 2007; Verdon et al., 2010). However, methods that identify localized or functionally segregated disease effects are fundamentally limited, for several reasons.

First and foremost is that cognitive processes depend fundamentally on interactions among multiple brain regions, rather than on isolated processes within regions. Even seemingly basic early sensory cortical functions are not simply determined by inputs from the periphery, but are modulated by back-projections within networks of primary, secondary, and association cortices. Neurological disorders that are manifest by dysfunction of distributed cognitive processes may arise from changes in the interactions (connectivity) within the cortical and subcortical networks, as well as isolated abnormalities within any one "node" of the network. This principle was established in early modern neurology by Lichtheim's anticipation and identification of conduction aphasia, and it remains highly relevant today.

Second, many neuropathologies are themselves distributed widely (Braak and Braak, 1997; Braak et al., 2006). The reasons for selective vulnerability of a subset of brain networks to disease are rarely clear cut, but a consequence of distributed pathology is that there may be severely impaired function of the network without consistent and sufficiently severe localized abnormalities to detect group-based localized deficits. This applies not only to neurodegenerative disorders such as Parkinson's disease (PD) but also multifocal cerebral insults such as subcortical ischemia or demyelination.

Third, a localized lesion may not cause relevant functional abnormalities in only its own location and immediate connections. There can also be remote consequences within the neural network in which the lesion is embedded. In complex networks,

with reciprocal connections or large scale circuit loops, the local and remote changes in connectivity can be difficult to predict, in clinical (Sharma et al., 2009) and simulated data (Kim and Horwitz, 2009).

Several methods to study connectivity are commonly used at present (see **Table 1**). We begin by considering the choice of methods. Subsequent sections will emphasize the commonalities of methods, and the importance of using these methods in order to fully understand disorders of the nervous system, as well as effective treatments. The challenges of these complex network interactions apply not only to disease, but also the neural basis of healthy individual differences. Although this review focuses on neurological disorders, the principles are also relevant to individual differences in the healthy population.

WHICH METHOD OF CONNECTIVITY SHOULD ONE CHOOSE?

There are many available methods to study large scale neural networks from functional neuroimaging data (**Table 1**). I will illustrate several of them in this review including psychophysiological interactions (PPIs), structural equation modeling (SEM), dynamic causal modeling (DCM), independent components analysis (ICA), and partial least squares (PLS), with an emphasis on fMRI data in neurological conditions.

A distinction is often drawn between functional connectivity and effective connectivity. Functional connectivity refers to covariance over time among spatially distributed brain regions which may arise because they are part of a common network. However, it may also be observed in the absence of causal influences among the regions if there are common inputs from other areas; multifocal effects of drugs; or common sources of noise. In contrast, effective connectivity refers explicitly to the causal influences of one region over another (see Limitations, Counter Intuitive Results and Naive Expectations). It often also implies that these influences are related to the study paradigm or an intervention such as transcranial magnetic stimulation. Some methods are clearly designed to study effective connectivity, based on temporal precedence (e.g., GCM) or dynamic causal models (e.g., DCM). Other methods (e.g., PPIs)

Table 1 | Glossary and outline of methods discussed.

DCM	Dynamic causal modeling	A deterministic approach within a generative model that characterizes neural activity in terms of driving inputs to a distributed neural network, intrinsic connections, and linear or non-linear modulations of connectivity arising from tasks or neural activity (Friston et al., 2003). Critical features of DCM as implemented by SPM software are the simultaneous estimation of a forward model of neurovascular coupling and the interactions among network regions at the level of neuronal activity. These are estimated to optimize a free energy estimate of the log-evidence of a model in a Bayesian framework. DCM is currently applicable to single subject and group studies of fMRI and M/EEG data, with extensions able to incorporate multiple state representations at each region and stochastic or spontaneous activations. See www.fil.ion.ucl.ac.uk/spm
GCM	Granger causality modeling and Granger causality mapping	These methods examine connectivity in terms of "Granger causality" (Roebroeck et al., 2005, 2009a), emphasizing the role of temporal precedence in the inference of causality. They are closely related to multivariate autoregressive modeling, which like SEM has its roots in econometrics, and can be applied to test anatomically defined neural network models (Granger causality modeling), or explore the interactions between a source region all other regions (Granger causality mapping). An invaluable discussion of issues related to GCM for fMRI data is contained in the exchange between Friston and Roebroeck (see Friston, 2009; Roebroeck et al., 2009a,b). See www.brainvoyager.com
ICA	Independent component analysis	Model-free fMRI analysis which may in some packages also estimate the number of interesting noise and signal sources in the data (McKeown et al., 1998; Beckmann et al., 2005). This approach does not assume anatomical connectivity or directionality of influences within the networks, but component networks can be mapped to task events or contexts. See www.fmrib.ox.ac.uk/fsl/melodic or afni.nimh.nih.gov/sscc/gangc/ica
PLS	Partial least squares	Related to principal components analysis, PLS identifies functionally connected brain networks and can identify subject- or experimental-variables associated with them (McIntosh et al., 1996; McIntosh and Lobaugh, 2004) as well as identifying psychophysiological interactions. See www.rotman-baycrest.on.ca/
PPI	Psycho–physiological interactions	A general conceptual framework in which physiological interactions between regions are modulated by psychological or physiological contexts. It can be used to test hypotheses of effective connectivity (Friston et al., 1997), or explore functional connectivity. However, the term PPI is also used to refer to a specific implementation within general linear models (PPI-GLMs). These PPI-GLMs use moderator variables that express the interactions between regional activations and contexts (and higher order interactions with between-subjects factors like age or disease risk factors) (Buchel and Friston, 1997; Rowe et al., 2006; Passamonti et al., 2009). See www.fil.ion.ucl.ac.uk/spm
RSN	Resting state networks	ICA of fMRI data acquired at rest identifies a small number (~10) of consistent spatially distributed covarying brain networks. One of these is also commonly identified by the brain state when not engaged in typical experimental tasks, known as the default mode network (DMN)
SEM	Structural equation modeling	Introduced into neuroimaging from econometrics and social sciences for the analysis of brain effective connectivity analysis (McIntosh and Gonzalez-Lima, 1994; McIntosh et al., 1994), to determine task-dependent (McIntosh et al., 1994; Buchel and Friston, 1997; Honey et al., 2002) or group-dependent (Grafton et al., 1994; Horwitz et al., 1995; Rowe et al., 2002b) changes in a hypothesized causal structure formalized in a path model. Commonly implemented for fMRI data by LISREL or SPM toolbox software.

can be used either to test causal models (effective connectivity) or to explore changes in task related covariance (functional connectivity). If functional connectivity is sufficient to generate or test hypotheses, then validated options include partial least squares (PLS) (McIntosh et al., 2004; McIntosh and Lobaugh, 2004), principal components analysis (PCA), or independent components analysis (ICA) (McKeown et al., 1998).

It is therefore necessary for each study to be clear about the hypotheses being tested and the biophysical interpretation of connectivity parameters (Buchel and Friston, 2000; Penny et al., 2004b; Ramnani et al., 2004; Lee et al., 2006; Friston, 2009; Roebroeck et al., 2009a,b; Cole et al., 2010). With this in mind, I will show these different methods can each contribute to our understanding of the complex network interactions in the brain; their relevance to neurological disease; and discuss how to choose an appropriate method.

Few studies directly compare multiple methods on the same data, despite the lack of consensus for many years (Horwitz, 2003). There are many reasons why two methods might differ in the inferred changes in connectivity, including a different biophysical interpretation of connectivity parameters and differential sensitivity to artifacts. Nonetheless, direct comparisons are interesting. Passamonti et al. (2008) directly compared psychophysiological interactions in general linear models (PPI-GLM) and dynamic causal modeling (DCM). They examined the connectivity between amygdala and medial frontal cortex, in relation to individual personality differences. The conclusions of these two methods were congruent. In the context of Parkinson's disease (PD), Palmer et al. (2009) compared SEM and multivariate autoregressive modeling. Both methods revealed similar dopamine-dependent group differences in connectivity, despite significant differences in methods and their interpretation. Using simulated data, Witt and Meyerand (2009) compared SEM, autoregression analysis, Granger causality modeling (GCM), and DCM and again found that each method was able to detect the underlying system dynamics (although GCM was adversely sensitive to differences in imaging and modeling parameters). Thus, methods do appear to yield consistent, although not identical results. However, different methods permit different inferences, and they are not all appropriate for every circumstance.

How then should one choose the right method to study the effects of disease or treatments? This depends on a number of practical considerations. First, what types of inference are relevant? For example, are inferences of directional and causal influences required? If so, then dynamic causal modeling (DCM) (Friston et al., 2003; Penny et al., 2004a; Sonty et al., 2007; Stephan et al., 2008; Rowe et al., 2010), SEM (McIntosh and Gonzalez-Lima, 1994; Buchel and Friston, 1997; Rowe et al., 2002b; Sharma et al., 2009) or Granger causality modeling (GCM) (Roebroeck et al., 2005) should be considered. Note that GCM of fMRI data is the youngest of these methods, and important theoretical considerations have been discussed recently (Friston, 2009; Roebroeck et al., 2009a,b). Alternatively, is it sufficient to establish differences in spatiotemporal covariance? If so, functional connectivity methods such as simple correlations analysis, partial least squares (PLS) (McIntosh et al., 2004; McIntosh and Lobaugh, 2004), principal components analysis or independent components analysis (McKeown et al., 1998) may be preferable to infer the presence or connectivity of spatiotemporally covarying networks. If one is able to predefine the specific experimental manipulations or disease factors that determine the changes in connectivity, these factors may be incorporated as hypothesized modulatory influences, e.g., in DCM, SEM or PPI-GLMs. Alternatively, data driven approaches such as PLS or *post hoc* interrogation of independent components analysis may be used to identify relevant factors that define a network's function.

Second, the appropriate methods may be restricted by the clinical conditions, by disease-related confounding factors such as medication, or by the cognitive systems of interest. Some tasks are not well suited to temporally precise network models, e.g., tasks with long epochs without discrete events are not easily modeled accurately in DCM. Such tasks include imagination of movements without precise timing of imagined "events"; observation of video clips with imprecise timing of critical perceptions; or long working memory delays. Another problem arises from the use of a canonical hemodynamic response function to estimate interactions between task, context and disease, e.g., SEM or PPI-GLMs. These might be confounded by a disease or medication that fundamentally alters the hemodynamic response function (Iannetti and Wise, 2007). In contrast, other methods such as DCM, which estimate a subject-, session-, and region-specific forward model of the neurovascular BOLD response, can accommodate disease or drug dependent differences in hemodynamic response function. In addition, general linear models of psychophysiological interactions are less suited to rapid event-related designs, which might be required to study the psychological or behavioral phenomenon of relevance to the disease such as the response to unexpected events.

A third factor is the information already available from the literature. Can one justify a set of cognitive and anatomical models, within which to evaluate the effects of disease on network connectivity? If so, then models embodying anatomically defined regions of interest and the causal relations among them can be tested, e.g., DCM or SEM. In addition, DCM, can be used to compare the effects of disease or treatment within multiple plausible models, and identify the most likely causal network model for a given cognitive process even in heterogeneous groups with between-subject differences in network dynamics (Penny et al., 2004a; Stephan et al., 2009a). Alternatively, an exploratory approach may be required, using PPIs, GCM, or ICA of whole brain data. These methods can be applied without restricting the analysis of disease effects on connectivity to a predefined anatomical network and without defining unidirectional or bidirectional interactions among regions.

A related question is whether it is justified to restrict analysis to connectivity changes induced by experimental manipulations? Deterministic models, such as those embodied by DCM, are powerful tools to define linear or non-linear networks related to experimental tasks, and their interactions with psychological contexts, diseases or pharmacology. However, current versions of DCM do not support stochastic or spontaneous processes within defined networks. The latter call for SEM which includes spontaneous activity ("innovations") arising within the network, rather than external or driving inputs to the network. However, a variational Bayes approach to DCM can approximate non-linear and stochastic dynamic models (Stephan et al., 2008; Daunizeau et al., 2009), encompassing endogenous sources of changing connectivity. Alternatively, connectivity may be inferred from model independent

functional connectivity methods such as independent components analysis (ICA) of "spontaneous" resting state fluctuations (see Distributed (dis-)Connectivity for Distributed Neuropathology). In brief, different methods are currently required to examine connectivity changes resulting from spontaneous processes compared to changes resulting from to experimental manipulations.

Whilst there are important theoretical considerations behind the right choice of method, each of the methods has been helpful in understanding the effects of disease. These methods may broadly agree, where commonalities are sufficient to enable direct comparisons. Often, the connectivity analysis is presented alongside an analysis of regionally specific effects (e.g., mass univariate voxel-wise analysis underlying traditional statistical parametric mapping) and the two approaches should be seen as complementary. In the next sections we focus on specific advantages or insights gained from connectivity analyses.

CONNECTIVITY ANALYSES DEMONSTRATE INCREASED SENSITIVITY TO DISEASE

Many studies of neurological disease have reported significant effects in terms of network integration when none was found in terms of activation of individual nodes of the network. This phenomenon has been observed with many different connectivity methods, from some of the earliest applications in aging (Horwitz et al., 1986), Parkinson's disease (Grafton et al., 1994) and neurodevelopmental disorders (Horwitz et al., 1988) to more recent fMRI studies (below).

Rowe et al. (2007) combined fMRI and focal brain lesions in adults, to test the predictions of a model of prefrontal cortical function that had been developed from neuroimaging of healthy subjects (Sakai and Passingham, 2003, 2006). It was proposed that prefrontal cortex was essential to support task-set activations within task-specific non-prefrontal cortical regions in anticipation of future cognitive tasks. However, prefrontal lesions that included sites of activation in normal subjects did not diminish activation in surviving regions of the dorsal and ventral streams associated with anticipated future spatial and letter tasks. Could it really be that activation of prefrontal cortex in healthy volunteers was redundant? The authors then examined the correlations among surviving task-related brain regions during long delay intervals (**Figure 1**). Unlike DCM or SEM, no assumptions were required about the presence or direction of causal influences among these regions, nor the sources of perturbation of network activity. It was clear that the functional connectivity was impaired among surviving regions following prefrontal cortical lesions, even though the mean level of activation of each region during the task was not altered in patients. This illustrates that even a simple correlations method was sufficient to test the hypothesis regarding necessity of a region, and to identify group differences that were not apparent from the analysis of regional activations.

Many neurological disorders affect movement and action – how actions are chosen, learned, imagined, and executed. These "motor" processes depend on an extended motor system of cortical and subcortical regions, including motor and premotor cortex, prefrontal and parietal association cortex, striatum, thalamus, and cerebellum. The anatomical connections among these regions of the motor network have been extensively described in non-human primates (Kotter, 2004; Stephan et al., 2001), sufficient to build simple but plausible anatomical models related to action which can be supplemented by human anatomical connectivity estimates using diffusion weighted imaging (Johansen-Berg and Rushworth, 2009; Stephan et al., 2009b).

The function of this extended motor system is clearly relevant to understanding the common movement disorder Parkinson's disease (PD) and its treatment. Many studies have used mass univariate analyses of regional activation (e.g., Statistical Parametric Mapping of the fMRI response arising from focal neural activity) to compare movement related activations in PD "on" or "off" medication, against healthy adults (Hughes et al., 2010). These studies have identified abnormalities in the supplementary or pre-supplementary motor area (SMA) and lateral premotor cortex (PMC). However, the network function could not be inferred from differences in localized activations alone.

Whereas Rowe et al. (2007) examined a few specified connections, the correlations or covariances among multiple brain regions can be examined without prior specification of network nodes or structure. Orthogonal spatiotemporal patterns of activation may be identified by partial least squares (PLS) or principal components analysis (PCA) and related back to task demands or disease states (McIntosh et al., 2004; McIntosh and Lobaugh, 2004). This enables exploration but also hypothesis testing for complex networks. For example, PLS analysis of PET data has shown that to learn motor sequences as effectively as controls, patients with PD over-express the same fronto-parietal network that is associated with the task in healthy adults (Mentis et al., 2003). One cannot infer the structure of direct or indirect causal connections within this covarying network, or the temporal dynamics of the network from PET data. Nonetheless, the PLS was sufficient to test major hypotheses regarding efficiency versus additional recruitment of brain networks in PD. Relatively few studies of neurological disorders have so far used PLS/PCA for fMRI data. However, they may be more sensitive to group effects than mass-univariate methods (McIntosh and Lobaugh, 2004) and the lack of assumptions about the anatomy or architecture of affected networks is a potential advantage.

One of the earliest examples of network analysis of neuroimaging data was SEM of cortico-subcortical interactions in PD, using positron emission tomography (PET) before and after treatment by pallidotomy (Grafton et al., 1994). Grafton et al. (1994) used published anatomical and electrophysiological data (e.g., Alexander et al., 1990) to build an anatomical model, and then used SEM to identify differences in movement-related connectivity between groups, before and after therapeutic pallidotomy. Their path analysis again revealed significant differences in connectivity even when categorical differences in activity within regions was not observed between groups.

Grafton et al. (1994) also showed that treatment by pallidotomy attenuated thalamocortical connectivity, "downstream" from the lesion. This illustrates another recurrent finding, that connectivity changes may be remote from the lesion in complex networks. Indeed, in circuits with recurrent projections, the effects of a lesion may be seen in altered connectivity apparently "upstream" of the lesion. For Grafton et al. (1994), this occurred in SMA projections to the putamen, but it also occurs in SEM simulations of focal lesions in complex networks (Kim and Horwitz, 2009).

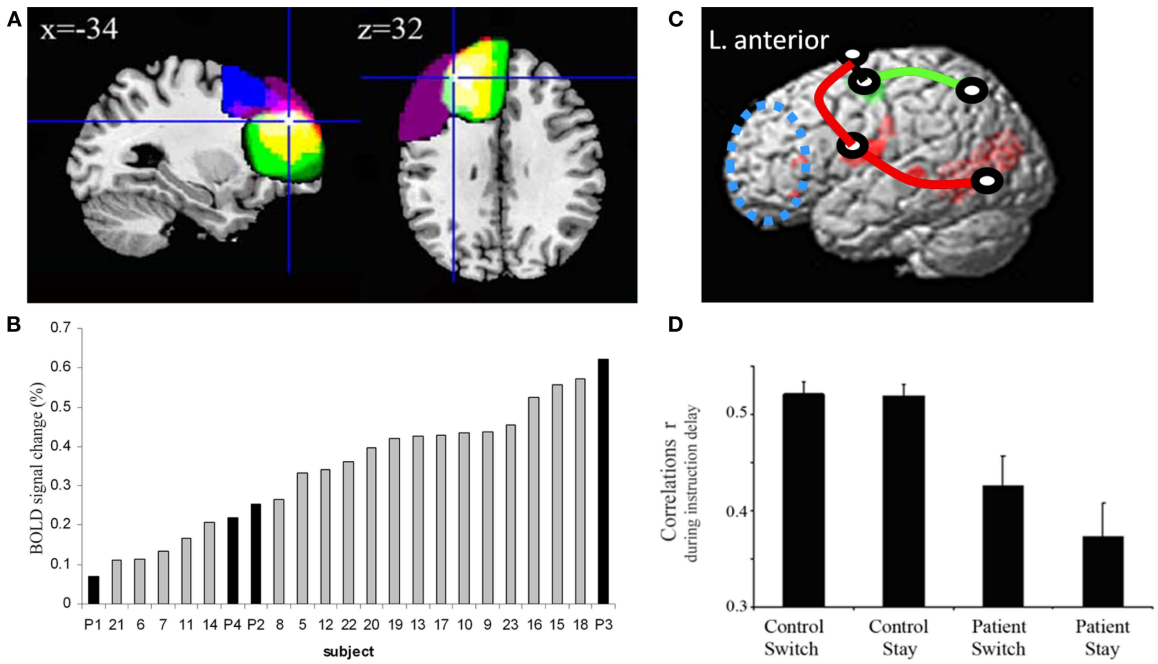


FIGURE 1 | During sustained task set, for future verbal or spatial working memory tasks, the lesions of left prefrontal cortex (A) made no significant difference to behavior or activations in surviving non-prefrontal cortex. For example, the estimates percent BOLD signal change in left inferior frontal gyrus **(B)** were not lower in four patients (black bars) compared with health controls (gray bars). However, the correlations among five surviving regions **(C)** associated with verbal set (red) or spatial set (green) were reduced in patients **(D)**, especially when the same task set was repeated in subsequent trials (stay trials) (Rowe et al., 2007).

Rowe et al. (2002a,b) used SEM of fMRI to study simple finger movement and attention to action in Parkinson's disease. The SEM again used an anatomical model derived from human and animal data in the literature. The model also embodied psychophysiological interactions (Friston et al., 1997) in terms of modulatory influences of attention on inter-regional connectivity. Voxel-wise analysis revealed no significant group activation differences in prefrontal cortex or lateral premotor cortex. SMA activation was greater in patients than controls for simple movements, but less in patients for attention to action, consistent with previous fMRI studies (Catalan et al., 1999; Sabatini et al., 2000). SEM indicated that attention to action specifically enhanced connectivity from prefrontal cortex to SMA and premotor cortex (PMC) in healthy adults. However, the SEM also revealed that the modulatory effect of attention to action on connectivity disappeared in patients with PD. This was interpreted as a functional disconnection of the SMA (Dick et al., 1986). In other words, the SEM approach showed that the SMA was not inherently over- or under-active in Parkinson's disease, but instead it was no longer subject to appropriate modulation by prefrontal afferents.

One feature of the model used by Rowe et al. (2002a,b) was that the changes in connectivity might have arisen within either direct cortico-cortical connections or at some unspecified point in the cortico-striato-thalamo-cortical loops. For some readers, the ability to identify cortico-cortical connectivity at a systems level, without specifying intermediate paths, is an advantage. However, for others, the inadequacy of the models leaves unanswered important questions about the mechanisms of effect of PD on movement related networks.

Structural equation modeling has several other limitations (Buchel and Friston, 1997; Penny et al., 2004b; Kim et al., 2007). These include the inability to compare non-nested alternative network models (where one network is not a component of the other); the assumption of stationary of neural responses; severe restrictions on the complexity of models; and in some implementations an inflexible canonical hemodynamic response function. These disadvantages can be circumvented by DCM while retaining the hypothesis led investigation of the effects of PD on intrinsic network connectivity and context-dependent modulatory influences of connectivity (note that DCM still requires the same data, i.e., nodes, in all models, even if they are not nested).

Rowe et al. (2010) therefore revisited the effects of PD on an extended cortical motor network in the frontal lobe using DCM. Participants made simple hand movements that were either self-selected or externally specified (rather than attended to as in the earlier study). Again, voxel-wise analysis revealed no significant action-related or choice-related activation differences between PD and control subjects in the SMA or PMC. The DCM employed a Bayesian framework to identify subject-specific and region-specific neurovascular forward models; the effects of choice on connectivity; and estimated the model-evidence of each member of a large set of candidate models. DCM model selection procedures re-identified the same optimal model in young and old healthy controls, and were reliable across repetitions several weeks apart. In accordance with the earlier SEM study, there was contextual modulation of connectivity from the lateral prefrontal cortex to the pre-SMA (**Figure 2**). Given the commonalities between attention

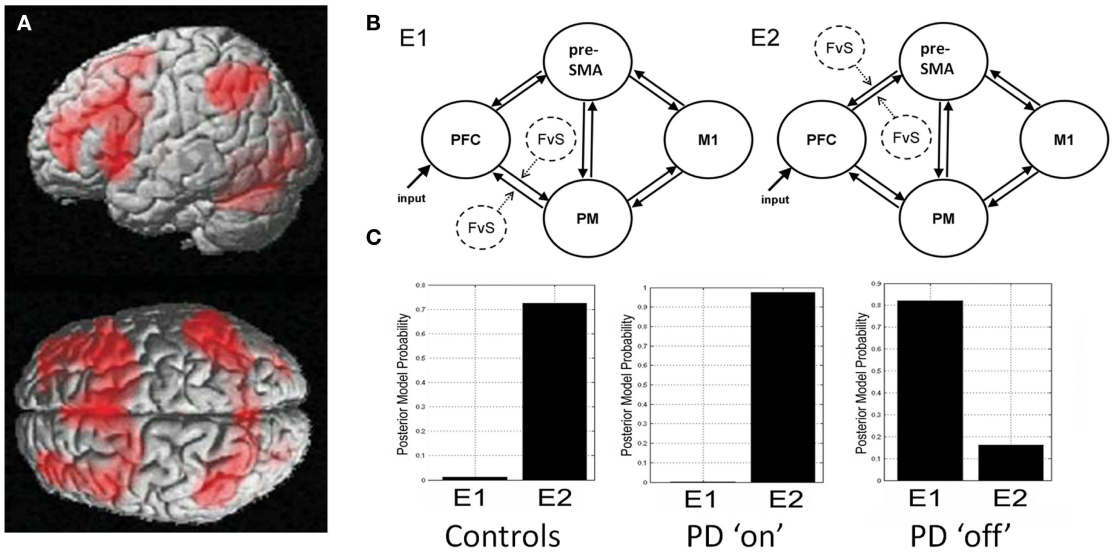


FIGURE 2 | (A) During manual action selection, there is activation of prefrontal cortex (PFC), pre-supplementary motor area (pre-SMA), lateral premotor cortex (PMC) and primary motor cortex (M1). These activations did not differ between patients with Parkinson's disease (PD) and control subjects, by voxel-wise group comparisons. **(B)** Dynamic causal modeling (DCM) was used to model the interactions among these regions. Forty-eight models were compared in all, differing in terms of anatomical connections, feed-forward versus feedback, and the connections which are subject to modulation by selection of action (FvS). The two leading models are shown in detail here (E1 and E2). **(C)** In healthy subjects, and patients on their dopaminergic medication, model E2 was more likely (by the posterior model probability, based on the free energy estimate of the log of model-evidence, adjusted for model complexity) in which the selection of action (FvS) was associated with greater connectivity of PFC to pre-SMA. When withdrawn from medication, to a relative "off" state, the connectivity pattern in PD patients changed to a state in which the selection of action was associated with greater connectivity between PFC and the PMC, model E1. This confirmed the hypothesis of a functional disconnection of the pre-SMA, and an enhanced role of the lateral PMC in action selection in PD. From Rowe et al. (2010).

to action and attentional selection of action, it is notable that the two very different connectivity methods – SEM and DCM – led to similar conclusions.

Despite the lack of significant differences in local activations between PD and controls, the DCM revealed clear differences in group connectivity. Not only was DCM more sensitive than classical voxel-wise analysis to the effects of PD, it was also sensitive to the connectivity changes associated with effective dopaminergic therapy (Rowe et al., 2010; cf Grafton et al., 1994). For patients in an "off" state after drug withdrawal, PD abolished the contextual modulation of prefrontal connectivity to the pre-SMA (self-selected versus specified actions), replaced by contextual modulation of connectivity from prefrontal cortex to lateral PMC. When patients were "on" after dopaminergic medication, the normal pattern of connectivity was restored.

Rowe et al. (2010) also showed that DCM was reproducible in health, at least in terms of the model selection procedures. However, there were significant posterior covariances among parameter estimates. These meant that individual parameters were not uniquely identifiable. The lack of unique identification means that estimated parameter values may correlate poorly across sessions even for the same tasks in the same subjects across sessions, making them unsuitable for use as dependent variables in statistical comparisons of groups. This is despite the excellent reliability of model selection procedures. For other tasks and models, DCM connectivity parameter estimates may be identifiable and therefore more reliable (Schuyler et al., 2009). In practice, we suggest that the major hypotheses regarding the effects of PD on motor network connectivity could be formulated in terms of model selection, as this was both reliable and sensitive.

The superior sensitivity of DCM to neurodegenerative disease, compared to analysis of regional activation, has also been observed for primary progressive aphasia (PPA), a subtype of frontotemporal dementia (Sonty et al., 2007). PPA is a structurally and cognitively restricted syndrome, with left perisylvian and temporal lobe atrophy and progressive language impairments, clearly suited to an hypothesis-led anatomically constrained approach like DCM. For a semantic task during fMRI, there were clear task-specific activations in the left inferior frontal gyrus (Broca's area) and posterior superior temporal gyrus (Wernicke's area) regions in both groups. Neither region's activity differed significantly between groups. However, despite the lack of differential activation within these regions, connectivity between Wernicke's and Broca's area was reduced in patients. The functional relevance of this connectivity difference is considered in the next section.

The previous studies of PD and PPA might have revealed changes in connectivity because either area or the connections between them are directly affected by the pathology. This direct effect of pathology in a network is not always the case. For example, Sharma et al. (2009) studied the imagination of movement following subcortical stroke. This was primarily motivated by the need to study the motor system in patients with weakness of actual movements. With the exception of primary motor cortex, healthy subjects trained to imagine hand movements demonstrated activation throughout the motor network, to a very similar degree as actual movements of

the same rate. However, without actual movements, it is difficult to specify the times of imagined movements. This led Sharma et al. (2009) to use SEM of fMRI data, rather than DCM, adopting the assumptions of stationarity rather than dynamic networks and sacrificing model selection procedures in favor of an anatomical model based on the literature.

Following significant partial recovery from stroke, the regional activations in patients were not different from healthy control subjects (Sharma et al., 2009). However effective connectivity within the motor system remained abnormal, both for actual and imagined movements (**Figure 3**). An earlier study of stroke patients performing manual actions data had also shown functionally relevant changes in cortical connectivity using DCM rather than SEM (Grefkes et al., 2008). Importantly for Sharma et al. (2009) the cortical motor network model did not include the subcortical lesions. Connectivity differences were concentrated on the interactions between prefrontal cortex, the premotor cortex and SMA, reminiscent of the abnormalities of frontal motor networks seen in PD. Thus, this study of stroke reiterates two findings: that connectivity analyses can be more sensitive to disease than analyses of regional activations, and that connectivity effects may be distant from a focal pathology.

DISTRIBUTED (DIS-)CONNECTIVITY FOR DISTRIBUTED NEUROPATHOLOGY

Neurodegenerative diseases often have characteristic anatomical distributions reflecting selective vulnerability of neurons (Braak and Braak, 1997; Braak et al., 2006). Even within frontotemporal dementia there are distinct behavioral and language clinical phenotypes characterized by different anatomical distributions

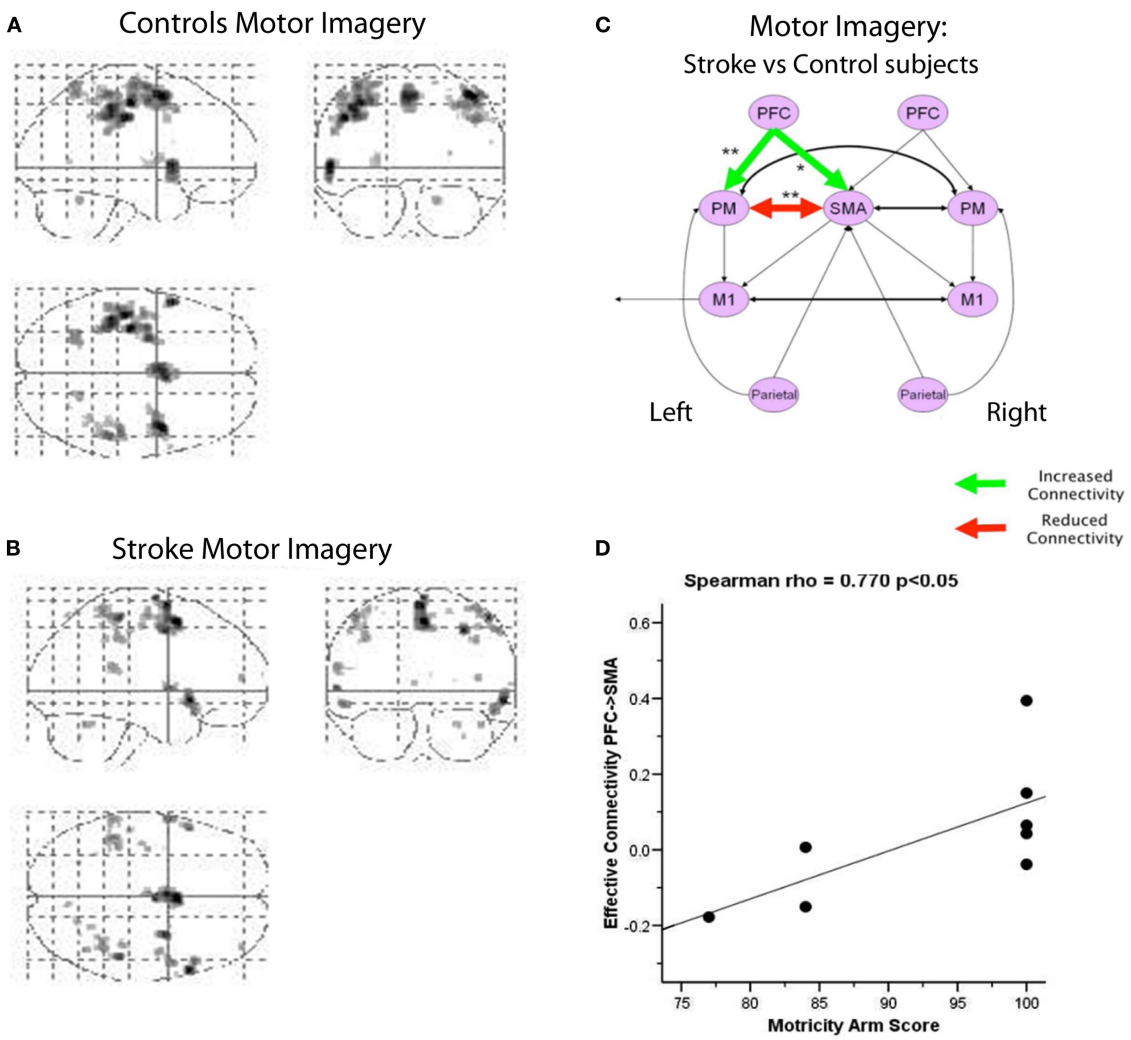


FIGURE 3 | During the imagination of movement, healthy subjects (A) and patients with subcortical strokes **(B)** show similar patterns of voxel-wise activation during fMRI, with no significant group differences in regional activations. However, Structural equation modeling of fMRI data revealed persisting abnormities of connectivity between groups **(C)** even after substantial clinical recovery. Patients showed increased connectivity from left prefrontal cortex to the SMA and premotor cortex. Moreover, the connectivity path coefficient from right PFC to the SMA correlated with the function of the recovered arm **(D)**. From Sharma et al. (2009).

of disease burden (Pereira et al., 2009; Rohrer et al., 2010). How do these relate to distributed functional systems in the normal brain?

Progress in understanding the relationship between pathology, structural, and functional networks has been made in recent years by the integration of multiple imaging modalities. This stems from the recognition of a small set of functionally connected (co-activated) networks, conserved across spontaneous fluctuations in primate networks (Vincent et al., 2007); humans with impaired consciousness (Boly et al., 2008; Greicius et al., 2008); and during rest in awake humans (Beckmann et al., 2005; Damoiseaux et al., 2006; Fox and Raichle, 2007; Smith et al., 2009). One of these "resting state networks" (RSNs) is a "default mode" that is prominent during the interval between focused cognitive tasks in humans (Fox and Raichle, 2007; Buckner et al., 2008). The robustness of RSNs has attracted considerable interest to understand or predict the effects of distributed neuropathologies.

Resting state networks are particularly useful for studying severely impaired clinical populations. The advantage lies not only the avoidance of some practical difficulties such as training and differential performance on cognitive tasks; long scanning sessions; and dependence on prior specification of anatomical model connectivity. RSNs also enable the comparison across multiple clinical conditions on multiple brain networks.

In two seminal papers, Seeley et al. (2009; Zhou et al., 2010) analyzed RSNs in several heterogeneous neurodegenerative diseases, including Alzheimer's and frontotemporal dementia. The disorders varied in their pathology and the distribution of disease burden across cortical and subcortical regions. There were corresponding disease-specific changes in RSNs that were robust enough to enable classification of disease (Zhou et al., 2010). The abnormal RSNs were in accordance with functional deficits typical of each disorder with evidence that the RSNs are selectively vulnerable to neuropathology, measured by focal atrophy (Greicius, 2008; Supekar et al., 2008; Seeley et al., 2009).

The correspondence of structural and functional connectivities does not imply that the progression of neuropathology through the networks depends on the same structural interconnections. This might be the case, especially for diseases with prior-like behavior of aggregating proteins, including PD and Alzhiemer's disease (Soto and Estrada, 2008; Angot and Brundin, 2009; Morales et al., 2010). However, it may also result from developmentally or environmentally determined predispositions to neuropathology in functionally related neurons, even when distributed widely across the RSN and in the absence of direct connection. In addition, artifactual sources of functional connectivity must also be considered, such as aliased cardiorespiratory signals or gross head movements (Birn et al., 2006) which may differ systematically between patient groups. Fortunately, where these sources of noise are measured, ICA can be used to identify and account for their otherwise misleading contributions to disease-specific RSNs (Beckmann et al., 2005).

Interestingly, disease-specific changes in RSN functional connectivity can occur in the absence of known direct structural connectivity (Damoiseaux and Greicius, 2009; Honey et al., 2009). The presence of indirect structural connections is one possible explanation. However, recall that the task-based changes in effective connectivity in the previous section (Rowe et al., 2007; Sharma et al., 2009) occurred in parts of a network that were not directly affected by the lesion (tumor resection and stroke respectively). It is also possible that neurochemical depletion rather than focal atrophy or white matter disease may cause differences in connectivity (Rowe et al., 2002b, 2008b,c; Palmer et al., 2009; Wu et al., 2009).

CONNECTIVITY CHANGES CAN BE FUNCTIONALLY RELEVANT

In this section, we consider the functional relevance of changes in effective and functional connectivity. We have already seen that in primary progressive aphasia, DCM measures of connectivity were abnormal even when regional activations were not. Sonty et al. (2007) went on to show that the abnormality of DCM connectivity correlated with cognitive tests of disease severity. Specifically, in patients but not controls, the connectivity between Wernicke's and Broca's areas correlated with performance on a semantic task but not a lexical task. Thus, the change in connectivity reflected the functionally relevant cognitive defects that characterize the PPA syndrome.

It is interesting to compare the task-specific abnormal frontotemporal connectivity in PPA (Sonty et al., 2007) with the abnormal RSN in other forms of frontotemporal dementia (Seeley et al., 2009). The former provides a direct connectivity-based mechanism of the cognitive clinicopathological correlations within PPA. In contrast, the latter study helps one begin to understand the basis of selective vulnerability of distributed neural networks to different pathological processes between neurodegenerative syndromes. This difference reinforces the suggestion (Section Which Method of Connectivity Should One Choose?) that the method to study connectivity should be chosen according to the hypothesis to be tested and type of inferences that are sought.

There is further evidence of the functional relevance of differences in connectivity. Following subcortical stroke, prefrontal interactions with premotor cortex and SMA were abnormal even though none of the regions was directly affected by the stroke or differentially activated during the task (Sharma et al., 2009). Moreover, the degree of connectivity (SEM path coefficients) in the frontal lobe motor network correlated with functional indices of recovery (**Figure 3**). For example the SEM path coefficient for prefrontal cortex to SMA during motor imagery correlated with the motricity index of arm function.

In the studies of PD outlined above, the analyses of effective connectivity have been shown to be sensitive to conventional effective therapies. Both pallidotomy and L-DOPA medication lead to significant differences in effective connectivity using SEM and DCM respectively (Grafton et al., 1994; Rowe et al., 2010). Interestingly, not all PD related changes in connectivity are normalized by l-DOPA (Palmer et al., 2009), consistent with noradrenergic and serotonergic contributions to cognitive dysfunction in PD (Marsh et al., 2009; Rodriguez-Oroz et al., 2009).

Even the RSN abnormalities may be directly related to functional ability, over and above their indexing of network dysfunction. For example, although RSNs are recorded at "rest," the properties of these networks are functionally relevant to performance on specific cognitive tasks (Kelly et al., 2008; Hayden et al., 2009). Despite the evidence presented so far of the sensitivity, reproducibility, and functional relevance of connectivity measures, there are serious problems and caveats to be considered. We turn to these in the next section.

LIMITATIONS, COUNTER INTUITIVE RESULTS, AND NAIVE EXPECTATIONS

The analysis of effective connectivity and the terminology used in neuroimaging are inspired by neurophysiology, neuropsychology, and a computational analysis of neuronal interactions (Gerstein and Perkel, 1969; Aertsen et al., 1989; Friston, 2007). There are attempts to explicitly bridge between cellular and whole brain methods (Chawla et al., 1999; Riera et al., 2006), and the conceptual framework from cellular models has proven useful in imaging analysis. However, it should be borne in mind that there is much that we do not know about the translation between neuronal activity and the PET and BOLD signals (Logothetis and Pfeuffer, 2004; Goense and Logothetis, 2008). Pre- and post synaptic functions of neurotransmission as well as spike rates are relevant to the generation of a vascular response, via complex and incompletely characterized coupling mechanisms. The BOLD signal underlying most of the results discussed here is therefore only an indirect measure of neuronal function, and this may be an important caveat for neuroimaging applications to specific diseases or treatments. More generally, it means that the connectivity measures in, say, DCM, PPIs, or SEM, cannot therefore be interpreted in terms of single excitatory or inhibitory synapses.

This limitation partly reflects the fact that current structural models in DCM or SEM are specified at a systems level, rather than the mono- or poly-synaptic connections of direct, indirect, or parallel connections between regions. In addition, current fMRI provides a single state representation for each node (voxel or region) in which the functions of all types of neuron and all types of synapse in a voxel are collapsed to a single value at any given timepoint. A richer descriptive framework with multi-state representations per region is beginning to emerge, at least for M/EEG data (Chen et al., 2008, 2009; Marreiros et al., 2008). Meanwhile, the uncertainty over the physical basis of connectivity in, say, PPI-GLMs, may explain some results that otherwise appear contradictory (Passamonti et al., 2009).

Confounding factors and correlations among model parameters must also be considered (Deneux and Faugeras, 2006; Rowe et al., 2010). For example, Rowe et al. (2010) found that DCM model comparison was very reliable, but posterior covariances among parameters meant that individual model parameters were no longer uniquely identifiable, and were therefore not reliable. This would inflate the false negative rate of group or drug comparisons. In addition, correlations among parameters can lead to the counter-intuitive result that the arithmetic mean of parameters for a group may differ markedly (even in terms of sign) from the precision weighted Bayesian "averaging" of parameters across the group. If using DCM, a consistent, principled and prior specification of the analysis protocol must therefore be developed to reduce bias (Stephan et al., 2010). Alternative approaches to causal dynamic models (related conceptually to DCM and GCM) have also been developed (Smith et al., 2010a) with a view to reliable parameter estimation, but it is too soon to comment on their application to clinical populations.

Connectivity approaches like DCM have further highlighted the problems of simplistic interpretations or inconsistent applications of "top-down" and "bottom-up" processes in terms of feed-back and feed-forward connections (Mechelli et al., 2003; Penny et al., 2004a; Garrido et al., 2007). For example, "top-down" cognitive control may manifest as changes in feed-forward connections (Rowe et al., 2008a). This was identified using DCM, as modality specific changes in connectivity from prestriate to parietal and temporal cortex during a task in which cognitive set varied between visual and spatial domains (**Figure 4**). Fortunately, evidence-based model selection procedures in DCM can be used to determine whether the functional anatomical network has significant feed-forward and feed-back connections, even where these do not map directly to cognitive psychological constructs such as "top-down" and "bottom-up" control (Mechelli et al., 2003; Rowe et al., 2008a).

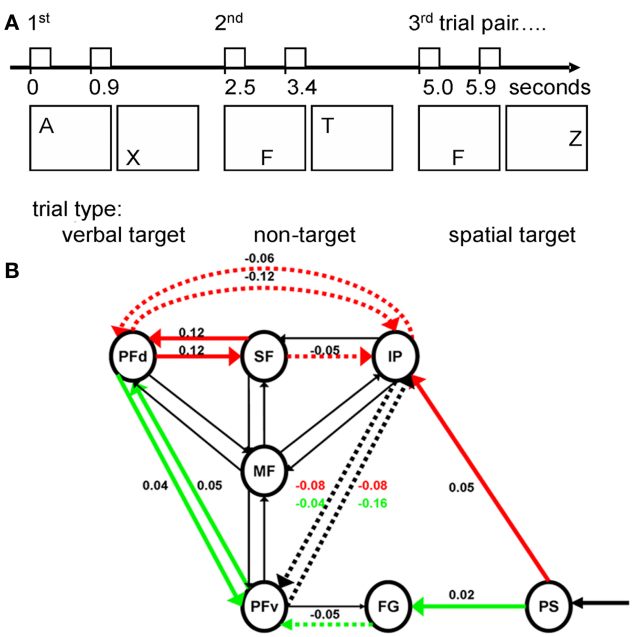


FIGURE 4 | (A) During a two-modality continuous performance task, subjects monitored a letter stream for successive verbal targets (A then X) or successive spatial targets (3 then 6 o'clock positions). Three correct targets within a modality were rewarded. Reward expectations lead to a graduated bias toward verbal or spatial cognitive sets, according to the recent history of spatial versus verbal targets. **(B)** The effects of this "top-down" modulation from cognitive set were studied using dynamic causal modeling of fMRI data. The figure shows modulatory (bilinear) effects representing psycho–physiological interactions in the most likely causal model (selected by Bayesian model comparison). This model included the medial frontal (MF) cortex, the dorsal (PFd) and ventral (PFv) lateral prefrontal cortex, the superior frontal sulcus (SF), the intraparietal cortex (IP), the fusiform gyrus (FG), and the prestriate cortex (PS), with intrinsic connections indicated by the presence of arrows (of any color). Values are time constants (Hz) for the modulatory influences of task bias for which the group posterior mean was positive (solid lines) or negative (dashed lines) for verbal bias (thick green), spatial bias (thick red), or both (thick black). These modulatory effects have strong evidence that they are non-zero, confirmed by *post hoc t*-tests. The "top-down" modulation of task set resulting from higher reward expectations was associated not only with changing connectivity of the lateral prefrontal cortical regions, but also the feed-forward connections from pre-striate cortex. Moreover, the feed-forward connections were enhanced to parietal cortex with spatial task set bias, and to temporal cortex with verbal task set bias. This illustrates that domain specific "top-down" control is not restricted to changes in feedback connections from higher cortical areas, but is also manifest by changes in feed-forward connectivity. From Rowe et al. (2008a).

Like mass-univariate modeling of regional activations, connectivity methods are also prone to technical, statistical, and inferential problems arising from clinical group differences in confounds, sources of variance, and performance. Important confounding factors to consider are motion artifacts (which are often greater in clinical populations), cardiorespiratory signals (altered by anxiety or medications such as beta-blockers), age, and systematic differences in the hemodynamic response function (Iannetti and Wise, 2007). A patient population will often have additional sources of variance due to the heterogeneity of disease phenotype, duration, severity and response to treatments, or differences in artifacts as above. Group level inferences of connectivity should attempt to accommodate or adjust for these inequalities of variance, whether at the first level adjustment of the data to include in time-series analysis (Glover et al., 2000) or second level random effects models (Stephan et al., 2009a). Otherwise, outlying subjects or mixed generative models within a group may compromise group comparisons.

The problem of differential sources of variance between groups can have other counterintuitive consequences. Using simulated fMRI data, Kim and Horwitz (2009) compared SEM network connectivity in controls with patients following a focal network lesion. Surprisingly, goodness of fit (GFI) estimates were better for the patients, yet patients showed significantly larger error variances throughout the network. The better GFI values had resulted from better modeling of error variance on each node rather than the values of inter-regional connectivity. High GFI values for models of patient data might therefore arise when regional activations are affected mostly by their noise inputs. Understanding, minimizing, and controlling for group differences in variance is therefore essential.

We have presented several cases in which connectivity analysis revealed effects of disease or treatment when the analysis of regional activations did not. This may reflect a true higher sensitivity to the neurophysiological effects of disease or treatment, although one cannot rule out a publication bias and investigator bias toward connectivity analysis when traditional approaches "fail." Multivariate methods like PLS or PCA may have intrinsically higher power than univariate analyses. This is supported by simulated and clinical data (McIntosh et al., 2004; Asllani et al., 2008; Habeck et al., 2008), but methods differ widely (Smith et al., 2010b) and increased sensitivity to network changes is generally at the expense of information about the organization of interactions within that network. For the analysis of effective connectivity, within theoretically motivated and anatomically constrained networks, it does not seem that methods like DCM have inherently higher power to detect underlying effects. For example, in a fMRI study of face emotion processing in two populations (Goulden et al., 2010) the number needed to achieve reasonable power (>0.7) to detect large effects (0.8) in DCM parameters was approximately 20 subjects. This estimate is similar to the number indicated for typical mass-univariate analysis of voxel-wise activations (Desmond and Glover, 2002; Murphy and Garavan, 2004; Mumford and Nichols, 2008).

Performance difference between groups must also be considered. If patients do not perform a task, then there is an inherent ambiguity to differences in neuroimaging data (Price and Friston, 1999; Price et al., 2006). This ambiguity is often not resolved in clinical studies, although the use of parametric modulations of task or performance indices can be used to try to circumvent the difficulty in interpreting categorical differences. Connectivity studies have the added problem of interpreting connectivity differences if there are differences in regional activations. In the extreme case, if a disease reduces a region to noise only, or removes a region altogether, then changes in its connectivity are not meaningful. However, as we have seen, diseases can cause significant changes in connectivity among surviving regions with normal activation (Rowe et al., 2007, 2008b; Sonty et al., 2007; Sharma et al., 2009).

CONCLUDING REMARKS

We have shown that the analysis of brain connectivity has much to contribute to understanding the consequences and mechanisms of neurological disease, and complements other neuroimaging methods. It is sensitive to disease and therapies, and relates to functional loss or recovery, following a wide variety of focal and distributed pathologies.

Colleagues have sometimes asked "I have this experiment that hasn't really worked so should I do connectivity analysis?" or "A reviewer has asked me to do a connectivity analysis, but isn't clear why. What should I do?" There are clearly cases in which the standard analysis of regional activations has yielded minimal results, despite functionally relevant difference in connectivity. The investment of time and resources in undertaking the connectivity analysis is certainly worthwhile. However, if a planned study of regional activations has failed in its main aims, it is best to begin by revisiting the hypotheses that led to the experiment and considering potential causes and confounds underlying negative results. Many of the same problems will undermine a connectivity analysis as well.

Despite the yield from the analysis of connectivity, these methods should be motivated by specific hypotheses. Moreover, it is often better to plan a new experiment with the intention of connectivity analysis in mind. This may require modifications to the range of stimulus conditions, or the reformulation of specific hypotheses, e.g., in terms of model selection rather than non-zero path parameters. Bear in mind that an experimental design may not be suitable for some connectivity methods, even if optimal for other forms of analysis (Henson, 2007). As for other neuroimaging studies, it is important to specify in advance the protocols for construction of models, optimization, and inference, in order to reduce biases in inference and estimation of the presence or size of connectivity effects (Kraft, 2008; Kriegeskorte et al., 2009; Vul et al., 2009).

Through this article, we hope to encourage researchers to engage in formal analyses of brain connectivity. These methods are practicable, insightful, and exciting. Each of the methods I have discussed here is supported by readily available freeware or commercial software (see **Table 1**), with discussion forums and on-line support to supplement published methods. Although the methods are evolving rapidly, we have no doubt that they will continue to make an essential contribution to our understanding of neurological and neuropsychiatric disease.

ACKNOWLEDGMENTS

James B. Rowe is supported by the Wellcome Trust (088324) and the Medical Research Council (Cognition and Brain Sciences Unit).

REFERENCES

Aertsen, A. M., Gerstein, G. L., Habib, M. K., and Palm, G. (1989). Dynamics of neuronal firing correlation: modulation of "effective connectivity." *J. Neurophysiol.* 61, 900–917.

Alexander, G. E., Crutcher, M. D., and DeLong, M. R. (1990). Basal ganglia-thalamocortical circuits: parallel substrates for motor, oculomotor, "prefrontal" and "limbic" functions. *Prog. Brain Res.* 85, 119–146.

Angot, E., and Brundin, P. (2009). Dissecting the potential molecular mechanisms underlying alpha-synuclein cell-to-cell transfer in Parkinson's disease. *Parkinsonism Relat. Disord.* 15(Suppl. 3), S143–S147.

Asllani, I., Habeck, C., Scarmeas, N., Borogovac, A., Brown, T. R., and Stern, Y. (2008). Multivariate and univariate analysis of continuous arterial spin labeling perfusion MRI in Alzheimer's disease. *J. Cereb. Blood Flow Metab.* 28, 725–736.

Beckmann, C. F., DeLuca, M., Devlin, J. T., and Smith, S. M. (2005). Investigations into resting-state connectivity using independent component analysis. *Philos. Trans. R. Soc. Lond. B Biol. Sci.* 360, 1001–1013.

Birn, R. M., Diamond, J. B., Smith, M. A., and Bandettini, P. A. (2006). Separating respiratory-variation-related fluctuations from neuronal-activity-related fluctuations in fMRI. *Neuroimage* 31, 1536–1548.

Boly, M., Phillips, C., Tshibanda, L., Vanhaudenhuyse, A., Schabus, M., Dang-Vu, T. T., Moonen, G., Hustinx, R., Maquet, P., and Laureys, S. (2008). Intrinsic brain activity in altered states of consciousness: how conscious is the default mode of brain function? *Ann. N. Y. Acad. Sci.* 1129, 119–129.

Braak, H., Bohl, J. R., Muller, C. M., Rub, U., de Vos, R. A., and Del Tredici, K. (2006). Stanley Fahn Lecture 2005: the staging procedure for the inclusion body pathology associated with sporadic Parkinson's disease reconsidered. *Mov. Disord.* 21, 2042–2051.

Braak, H., and Braak, E. (1997). Diagnostic criteria for neuropathologic assessment of Alzheimer's disease. *Neurobiol. Aging* 18, S85–S88.

Buchel, C., and Friston, K. (2000). Assessing interactions among neuronal systems using functional neuroimaging. *Neural. Netw.* 13, 871–882.

Buchel, C., and Friston, K. J. (1997). Modulation of connectivity in visual pathways by attention: cortical interactions evaluated with structural equation modelling and fMRI. *Cereb. Cortex* 7, 768–778.

Buckner, R. L., Andrews-Hanna, J. R., and Schacter, D. L. (2008). The brain's default network: anatomy, function, and relevance to disease. *Ann. N. Y. Acad. Sci.* 1124, 1–38.

Catalan, M. J., Ishii, K., Honda, M., Samii, A., and Hallett, M. (1999). A PET study of sequential finger movements of varying length in patients with Parkinson's disease. *Brain* 122, 483–495.

Chawla, D., Lumer, E. D., and Friston, K. J. (1999). The relationship between synchronization among neuronal populations and their mean activity levels. *Neural. Comput.* 11, 1389–1411.

Chen, C. C., Henson, R. N., Stephan, K. E., Kilner, J. M., and Friston, K. J. (2009). Forward and backward connections in the brain: a DCM study of functional asymmetries. *Neuroimage* 45, 453–462.

Chen, C. C., Kiebel, S. J., and Friston, K. J. (2008). Dynamic causal modelling of induced responses. *Neuroimage* 41, 1293–1312.

Cole, D. M., Smith, S. M., and Beckmann, C. F. (2010). Advances and pitfalls in the analysis and interpretation of resting-state FMRI data. *Front. Syst. Neurosci.* 4:8. doi: 10.3389/fnsys.2010.00008.

Damoiseaux, J. S., and Greicius, M. D. (2009). Greater than the sum of its parts: a review of studies combining structural connectivity and resting-state functional connectivity. *Brain Struct. Funct.* 213, 525–533.

Damoiseaux, J. S., Rombouts, S. A., Barkhof, F., Scheltens, P., Stam, C. J., Smith, S. M., and Beckmann, C. F. (2006). Consistent resting-state networks across healthy subjects. *Proc. Natl. Acad. Sci. U.S.A.* 103, 13848–13853.

Daunizeau, J., Friston, K. J., and Kiebel, S. J. (2009). Variational Bayesian identification and prediction of stochastic nonlinear dynamic causal models. *Physica D* 238, 2089–2118.

Deneux, T., and Faugeras, O. (2006). Using nonlinear models in fMRI data analysis: model selection and activation detection. *Neuroimage* 32, 1669–1689.

Desmond, J. E., and Glover, G. H. (2002). Estimating sample size in functional MRI (fMRI) neuroimaging studies: statistical power analyses. *J. Neurosci. Methods* 118, 115–128.

Dick, J. P., Benecke, R., Rothwell, J. C., Day, B. L., and Marsden, C. D. (1986). Simple and complex movements in a patient with infarction of the right supplementary motor area. *Mov. Disord.* 1, 255–266.

Fox, M. D., and Raichle, M. E. (2007). Spontaneous fluctuations in brain activity observed with functional magnetic resonance imaging. *Nat. Rev. Neurosci.* 8, 700–711.

Friston, K. (2007). "Functional integration," in *Statistical Parametric Mapping*, eds K. Friston, J. Ashburner, S. Kiebel, T. Nichols and W. Penny (London: Elsevier), 471–491.

Friston, K. (2009). Dynamic causal modeling and Granger causality comments on: the identification of interacting networks in the brain using fMRI: model selection, causality and deconvolution. *Neuroimage*. doi: 10.1016/j.neuroimage.2009.1009.1031

Friston, K. J., Buechel, C., Fink, G. R., Morris, J., Rolls, E., and Dolan, R. J. (1997). Psychophysiological and modulatory interactions in neuroimaging. *Neuroimage* 6, 218–229.

Friston, K. J., Harrison, L., and Penny, W. (2003). Dynamic causal modelling. *Neuroimage* 19, 1273–1302.

Garrido, M. I., Kilner, J. M., Kiebel, S. J., and Friston, K. J. (2007). Evoked brain responses are generated by feedback loops. *Proc. Natl. Acad. Sci. U.S.A.* 104, 20961–20966.

Gerstein, G. L., and Perkel, D. H. (1969). Simultaneously recorded trains of action potentials: analysis and functional interpretation. *Science* 164, 828–830.

Glover, G. H., Li, T. Q., and Ress, D. (2000). Image-based method for retrospective correction of physiological motion effects in fMRI: RETROICOR. *Magn. Reson. Med.* 44, 162–167.

Goense, J. B., and Logothetis, N. K. (2008). Neurophysiology of the BOLD fMRI signal in awake monkeys. *Curr. Biol.* 18, 631–640.

Goulden, N., McKie, S., Suckling, J., Williams, S. R., Anderson, I. M., Deakin, J. F., and Elliott, R. (2010). A comparison of permutation and parametric testing for between group effective connectivity differences using DCM. *Neuroimage* 50, 509–515.

Grafton, S., Sutton, J., Couldwell, W., Lew, M., and Waters, C. (1994). Network analysis of motor system connectivity in Parkinson's disease: modualtion of thalamocortical interactions after pallidotomy. *Hum. Brain Mapp.* 2, 45–55.

Grefkes, C., Nowak, D. A., Eickhoff, S. B., Dafotakis, M., Kust, J., Karbe, H., and Fink, G. R. (2008). Cortical connectivity after subcortical stroke assessed with functional magnetic resonance imaging. *Ann. Neurol.* 63, 236–246.

Greicius, M. (2008). Resting-state functional connectivity in neuropsychiatric disorders. *Curr. Opin. Neurol.* 21, 424–430.

Greicius, M. D., Kiviniemi, V., Tervonen, O., Vainionpaa, V., Alahuhta, S., Reiss, A. L., and Menon, V. (2008). Persistent default-mode network connectivity during light sedation. *Hum. Brain Mapp.* 29, 839–847.

Habeck, C., Foster, N. L., Perneczky, R., Kurz, A., Alexopoulos, P., Koeppe, R. A., Drzezga, A., and Stern, Y. (2008). Multivariate and univariate neuroimaging biomarkers of Alzheimer's disease. *Neuroimage* 40, 1503–1515.

Hayden, B. Y., Smith, D. V., and Platt, M. L. (2009). Electrophysiological correlates of default-mode processing in macaque posterior cingulate cortex. *Proc. Natl. Acad. Sci. U.S.A.* 106, 5948–5953.

Henson, R. (2007). "Efficient experimental design for fMRI," in *Statistical Parametric Mapping*, eds K. Friston, J. Ashburner, S. Kiebel, T. Nichols and W. Penny (London: Elsevier), 193–210.

Honey, G. D., Fu, C. H., Kim, J., Brammer, M. J., Croudace, T. J., Suckling, J., Pich, E. M., Williams, S. C., and Bullmore, E. T. (2002). Effects of verbal working memory load on corticocortical connectivity modeled by path analysis of functional magnetic resonance imaging data. *Neuroimage* 17, 573–582.

Honey, C. J., Sporns, O., Cammoun, L., Gigandet, X., Thiran, J. P., Meuli, R., and Hagmann, P. (2009). Predicting human resting-state functional connectivity from structural connectivity. *Proc. Natl. Acad. Sci. U.S.A.* 106, 2035–2040.

Horwitz, B. (2003). The elusive concept of brain connectivity. *Neuroimage* 19, 466–470.

Horwitz, B., Duara, R., and Rapoport, S. I. (1986). Age differences in intercorrelations between regional cerebral metabolic rates for glucose. *Ann. Neurol.* 19, 60–67.

Horwitz, B., McIntosh, A. R., Haxby, J. V., Furey, M., Salerno, J. A., Schapiro, M. B., Rapoport, S. I., and Grady, C. L. (1995). Network analysis of PET-mapped visual pathways in Alzheimer type dementia. *Neuroreport* 6, 2287–2292.

Horwitz, B., Rumsey, J. M., Grady, C. L., and Rapoport, S. I. (1988). The cerebral metabolic landscape in autism. Intercorrelations of regional glucose utilization. *Arch. Neurol.* 45, 749–755.

Hughes, L. E., Barker, R. A., Owen, A. M., and Rowe, J. B. (2010). Parkinson's disease and healthy aging: Independent and interacting effects on action selection. *Hum. Brain Mapp.* doi: 10.1002/hbm.20979.

Iannetti, G. D., and Wise, R. G. (2007). BOLD functional MRI in disease and pharmacological studies: room for improvement? *Magn. Reson. Imaging* 25, 978–988.

Johansen-Berg, H., and Rushworth, M. F. (2009). Using diffusion imaging to study human connectional anatomy. *Annu. Rev. Neurosci.* 32, 75–94.

Kelly, A. M., Uddin, L. Q., Biswal, B. B., Castellanos, F. X., and Milham,

M. P. (2008). Competition between functional brain networks mediates behavioral variability. *Neuroimage* 39, 527–537.

Kim, J., and Horwitz, B. (2009). How well does structural equation modeling reveal abnormal brain anatomical connections? An fMRI simulation study. *Neuroimage* 45, 1190–1198.

Kim, J., Zhu, W., Chang, L., Bentler, P. M., and Ernst, T. (2007). Unified structural equation modeling approach for the analysis of multisubject, multivariate functional MRI data. *Hum. Brain Mapp.* 28, 85–93.

Kotter, R. (2004). Online retrieval, processing, and visualization of primate connectivity data from the CoCoMac database. *Neuroinformatics* 2, 127–144.

Kraft, P. (2008). Curses – winner's and otherwise – in genetic epidemiology. *Epidemiology* 19, 649–651; discussion 657–648.

Kriegeskorte, N., Simmons, W. K., Bellgowan, P. S., and Baker, C. I. (2009). Circular analysis in systems neuroscience: the dangers of double dipping. *Nat. Neurosci.* 12, 535–540.

Lee, L., Friston, K., and Horwitz, B. (2006). Large-scale neural models and dynamic causal modelling. *Neuroimage* 30, 1243–1254.

Logothetis, N. K., and Pfeuffer, J. (2004). On the nature of the BOLD fMRI contrast mechanism. *Magn. Reson. Imaging* 22, 1517–1531.

Marreiros, A. C., Kiebel, S. J., and Friston, K. J. (2008). Dynamic causal modelling for fMRI: a two-state model. *Neuroimage* 39, 269–278.

Marsh, L., Biglan, K., Gerstenhaber, M., and Williams, J. R. (2009). Atomoxetine for the treatment of executive dysfunction in Parkinson's disease: a pilot open-label study. *Mov. Disord.* 24, 277–282.

McIntosh, A., and Gonzalez-Lima, F. (1994). Structural equation modeling and its application to network analysis in functional brain imaging. *Hum. Brain Mapp.* 2, 2–22.

McIntosh, A. R., Bookstein, F. L., Haxby, J. V., and Grady, C. L. (1996). Spatial pattern analysis of functional brain images using partial least squares. *Neuroimage* 3, 143–157.

McIntosh, A. R., Chau, W. K., and Protzner, A. B. (2004). Spatiotemporal analysis of event-related fMRI data using partial least squares. *Neuroimage* 23, 764–775.

McIntosh, A. R., Grady, C. L., Ungerleider, L. G., Haxby, J. V., Rapoport, S. I., and Horwitz, B. (1994). Network analysis of cortical visual pathways mapped with PET. *J. Neurosci.* 14, 655–666.

McIntosh, A. R., and Lobaugh, N. J. (2004). Partial least squares analysis of neuroimaging data: applications and advances. *Neuroimage* 23(Suppl. 1), S250–S263.

McKeown, M. J., Makeig, S., Brown, G. G., Jung, T. P., Kindermann, S. S., Bell, A. J., and Sejnowski, T. J. (1998). Analysis of fMRI data by blind separation into independent spatial components. *Hum. Brain Mapp.* 6, 160–188.

Mechelli, A., Price, C. J., Noppeney, U., and Friston, K. J. (2003). A dynamic causal modeling study on category effects: bottom-up or top-down mediation? *J. Cogn. Neurosci.* 15, 925–934.

Mentis, M. J., Dhawan, V., Feigin, A., Delalot, D., Zgaljardic, D., Edwards, C., and Eidelberg, D. (2003). Early stage Parkinson's disease patients and normal volunteers: comparative mechanisms of sequence learning. *Hum. Brain Mapp.* 20, 246–258.

Morales, R., Estrada, L. D., Diaz-Espinoza, R., Morales-Scheihing, D., Jara, M. C., Castilla, J., and Soto, C. (2010). Molecular cross talk between misfolded proteins in animal models of Alzheimer's and prion diseases. *J. Neurosci.* 30, 4528–4535.

Mort, D. J., Malhotra, P., Mannan, S. K., Rorden, C., Pambakian, A., Kennard, C., and Husain, M. (2003). The anatomy of visual neglect. *Brain* 126, 1986–1997.

Mumford, J. A., and Nichols, T. E. (2008). Power calculation for group fMRI studies accounting for arbitrary design and temporal autocorrelation. *Neuroimage* 39, 261–268.

Murphy, K., and Garavan, H. (2004). An empirical investigation into the number of subjects required for an event-related fMRI study. *Neuroimage* 22, 879–885.

Palmer, S. J., Eigenraam, L., Hoque, T., McCaig, R. G., Troiano, A., and McKeown, M. J. (2009). Levodopa-sensitive, dynamic changes in effective connectivity during simultaneous movements in Parkinson's disease. *Neuroscience* 158, 693–704.

Passamonti, L., Rowe, J. B., Ewbank, M., Hampshire, A., Keane, J., and Calder, A. J. (2008). Connectivity from the ventral anterior cingulate to the amygdala is modulated by appetitive motivation in response to facial signals of aggression. *Neuroimage* 43, 562–570.

Passamonti, L., Rowe, J. B., Schwarzbauer, C., Ewbank, M. P., von dem Hagen, E., and Calder, A. J. (2009). Personality predicts the brain's response to viewing appetizing foods: the neural basis of a risk factor for overeating. *J. Neurosci.* 29, 43–51.

Penny, W. D., Stephan, K. E., Mechelli, A., and Friston, K. J. (2004a). Comparing dynamic causal models. *Neuroimage* 22, 1157–1172.

Penny, W. D., Stephan, K. E., Mechelli, A., and Friston, K. J. (2004b). Modelling functional integration: a comparison of structural equation and dynamic causal models. *Neuroimage* 23(Suppl. 1), S264–S274.

Pereira, J. M., Williams, G. B., Acosta-Cabronero, J., Pengas, G., Spillantini, M. G., Xuereb, J. H., Hodges, J. R., and Nestor, P. J. (2009). Atrophy patterns in histologic vs clinical groupings of frontotemporal lobar degeneration. *Neurology* 72, 1653–1660.

Price, C. J., Crinion, J., and Friston, K. J. (2006). Design and analysis of fMRI studies with neurologically impaired patients. *J. Magn. Reson. Imaging* 23, 816–826.

Price, C. J., and Friston, K. J. (1999). Scanning patients with tasks they can perform. *Hum. Brain Mapp.* 8, 102–108.

Ramnani, N., Behrens, T. E., Penny, W., and Matthews, P. M. (2004). New approaches for exploring anatomical and functional connectivity in the human brain. *Biol. Psychiatry* 56, 613–619.

Riera, J. J., Wan, X., Jimenez, J. C., and Kawashima, R. (2006). Nonlinear local electrovascular coupling. I: A theoretical model. *Hum. Brain. Mapp.* 27, 896–914.

Rodriguez-Oroz, M. C., Jahanshahi, M., Krack, P., Litvan, I., Macias, R., Bezard, E., and Obeso, J. A. (2009). Initial clinical manifestations of Parkinson's disease: features and pathophysiological mechanisms. *Lancet Neurol.* 8, 1128–1139.

Roebroeck, A., Formisano, E., and Goebel, R. (2005). Mapping directed influence over the brain using Granger causality and fMRI. *Neuroimage* 25, 230–242.

Roebroeck, A., Formisano, E., and Goebel, R. (2009a). The identification of interacting networks in the brain using fMRI: model selection, causality and deconvolution. *Neuroimage.* doi: 10.1016/j.neuroimage.2009.1009.1036.

Roebroeck, A., Formisano, E., and Goebel, R. (2009b). Reply to Friston and David after comments on: the identification of interacting networks in the brain using fMRI: model selection, causality and deconvolution. *Neuroimage.* doi: 10.1016/j.neuroimage.2009.1010.1077.

Rohrer, J. D., Ridgway, G. R., Modat, M., Ourselin, S., Mead, S., Fox, N. C., Rossor, M. N., and Warren, J. D. (2010). Distinct profiles of brain atrophy in frontotemporal lobar degeneration caused by progranulin and tau mutations. *Neuroimage* doi: 10.1016/j.neuroimage.2009.12.088.

Rowe, J., Friston, K., Frackowiak, R., and Passingham, R. (2002a). Attention to action: specific modulation of corticocortical interactions in humans. *Neuroimage* 17, 988–998.

Rowe, J., Stephan, K. E., Friston, K., Frackowiak, R., Lees, A., and Passingham, R. (2002b). Attention to action in Parkinson's disease: impaired effective connectivity among frontal cortical regions. *Brain* 125, 276–289.

Rowe, J. B., Eckstein, D., Braver, T., and Owen, A. M. (2008a). How does reward expectation influence cognition in the human brain? *J. Cogn. Neurosci.* 20, 1980–1992.

Rowe, J. B., Hughes, L., Ghosh, B. C., Eckstein, D., Williams-Gray, C. H., Fallon, S., Barker, R. A., and Owen, A. M. (2008b). Parkinson's disease and dopaminergic therapy – differential effects on movement, reward and cognition. *Brain* 131, 2094–2105

Rowe, J. B., Hughes, L., Williams-Gray, C. H., Bishop, S., Fallon, S., Barker, R. A., and Owen, A. M. (2008c). The val(158)met COMT polymorphism's effect on atrophy in healthy aging and Parkinson's disease. *Neurobiol. Aging.* 31, 1064–1068.

Rowe, J. B., Hughes, L. E., Barker, R. A., and Owen, A. M. (2010). Dynamic causal modelling of effective connectivity from fMRI: are results reproducible and sensitive to Parkinson's disease and its treatment? *Neuroimage* 31, 1064–1068.

Rowe, J. B., Sakai, K., Lund, T. E., Ramsoy, T., Christensen, M. S., Baare, W. F., Paulson, O. B., and Passingham, R. E. (2007). Is the prefrontal cortex necessary for establishing cognitive sets? *J. Neurosci.* 27, 13303–13310.

Rowe, J. B., Siebner, H., Filipovic, S. R., Cordivari, C., Gerschlager, W., Rothwell, J., and Frackowiak, R. (2006). Aging is associated with contrasting changes in local and distant cortical connectivity in the human motor system. *Neuroimage* 32, 747–760.

Sabatini, U., Boulanouar, K., Fabre, N., Martin, F., Carel, C., Colonnese, C., Bozzao, L., Berry, I., Montastruc, J. L., Chollet, F., Rascol, O. (2000). Cortical motor reorganization in akinetic patients with Parkinson's disease: a functional MRI study. *Brain* 123, 394–403.

Sakai, K., and Passingham, R. E. (2003). Prefrontal interactions reflect future task operations. *Nat. Neurosci.* 6, 75–81.

Sakai, K., and Passingham, R. E. (2006). Prefrontal set activity predicts rule-

specific neural processing during subsequent cognitive performance. *J. Neurosci.* 26, 1211–1218.

Sapir, A., Kaplan, J. B., He, B. J., and Corbetta, M. (2007). Anatomical correlates of directional hypokinesia in patients with hemispatial neglect. *J. Neurosci.* 27, 4045–4051.

Schuyler, B., Ollinger, J. M., Oakes, T. R., Johnstone, T., and Davidson, R. J. (2009). Dynamic causal modeling applied to fMRI data shows high reliability. *Neuroimage* 49, 603–611.

Seeley, W. W., Crawford, R. K., Zhou, J., Miller, B. L., and Greicius, M. D. (2009). Neurodegenerative diseases target large-scale human brain networks. *Neuron* 62, 42–52.

Sharma, N., Baron, J. C., and Rowe, J. B. (2009). Motor imagery after stroke: relating outcome to motor network connectivity. *Ann. Neurol.* 66, 604–616.

Smith, J. F., Pillai, A., Chen, K., and Horwitz, B. (2010a). Identification and validation of effective connectivity networks in functional magnetic resonance imaging using switching linear dynamic systems. *Neuroimage* 52, 1027–1040.

Smith, S., Woolrich, M., and Miller, K. (2010b). "Evaluation of network connectivity methods for resting fMRI timeseries," in *Poster presented at the 16th Annual Meeting of the Organization for Human Brain Mapping*, Barcelona (poster 1013).

Smith, S. M., Fox, P. T., Miller, K. L., Glahn, D. C., Fox, P. M., Mackay, C. E., Filippini, N., Watkins, K. E., Toro, R., Laird, A. R., Beckman, C. F. (2009). Correspondence of the brain's functional architecture during activation and rest. *Proc. Natl. Acad. Sci. U.S.A.* 106, 13040–13045.

Sonty, S. P., Mesulam, M. M., Weintraub, S., Johnson, N. A., Parrish, T. B., and Gitelman, D. R. (2007). Altered effective connectivity within the language network in primary progressive aphasia. *J. Neurosci.* 27, 1334–1345.

Soto, C., and Estrada, L. D. (2008). Protein misfolding and neurodegeneration. *Arch. Neurol.* 65, 184–189.

Stephan, K. E., Kamper, L., Bozkurt, A., Burns, G. A., Young, M. P., and Kotter, R. (2001). Advanced database methodology for the Collation of Connectivity data on the Macaque brain (CoCoMac). *Philos. Trans. R. Soc. Lond. B Biol. Sci.* 356, 1159–1186.

Stephan, K. E., Kasper, L., Harrison, L. M., Daunizeau, J., den Ouden, H. E., Breakspear, M., and Friston, K. J. (2008). Nonlinear dynamic causal models for fMRI. *Neuroimage* 42, 649–662.

Stephan, K. E., Penny, W. D., Daunizeau, J., Moran, R. J., and Friston, K. J. (2009a). Bayesian model selection for group studies. *Neuroimage* 46, 1004–1017.

Stephan, K. E., Tittgemeyer, M., Knosche, T. R., Moran, R. J., and Friston, K. J. (2009b). Tractography-based priors for dynamic causal models. *Neuroimage* 47, 1628–1638.

Stephan, K. E., Penny, W. D., Moran, R. J., den Ouden, H. E., Daunizeau, J., and Friston, K. J. (2010). Ten simple rules for dynamic causal modeling. *Neuroimage* 49, 3099–3109.

Supekar, K., Menon, V., Rubin, D., Musen, M., and Greicius, M. D. (2008). Network analysis of intrinsic functional brain connectivity in Alzheimer's disease. *PLoS Comput. Biol.* 4, e1000100. doi: 10.1371/journal.pcbi.1000100.

Verdon, V., Schwartz, S., Lovblad, K. O., Hauert, C. A., and Vuilleumier, P. (2010). Neuroanatomy of hemispatial neglect and its functional components: a study using voxel-based lesion-symptom mapping. *Brain* 133, 880–894.

Vincent, J. L., Patel, G. H., Fox, M. D., Snyder, A. Z., Baker, J. T., Van Essen, D. C., Zempel, J. M., Snyder, L. H., Corbetta, M., and Raichle, M. E. (2007). Intrinsic functional architecture in the anaesthetized monkey brain. *Nature* 447, 83–86.

Vul, E., Harris, C., Winkielman, P., and Pashler, H. (2009). Puzzlingly high correlations in fMRI studies of emotion, personality, and social cognition (The paper formerly known as "Voodoo correlations in social neuroscience"). *Perspect. Psychol. Sci.* 4, 274–290.

Witt, S. T., and Meyerand, M. E. (2009). The effects of computational method, data modeling, and TR on effective connectivity results. *Brain Imaging Behav.* 3, 220–231.

Wu, T., Wang, L., Chen, Y., Zhao, C., Li, K., and Chan, P. (2009). Changes of functional connectivity of the motor network in the resting state in Parkinson's disease. *Neurosci. Lett.* 460, 6–10.

Zhou, J., Greicius, M. D., Gennatas, E. D., Growdon, M. E., Jang, J. Y., Rabinovici, G. D., Kramer, J. H., Weiner, M., Miller, B. L., and Seeley, W. W. (2010). Divergent network connectivity changes in behavioural variant frontotemporal dementia and Alzheimer's disease. *Brain* 133, 1352–1367.

Conflict of Interest Statement: The author declares that the research was conducted in the absence of any commercial or financial relationships that could be construed as a potential conflict of interest.

Received: 16 July 2010; paper pending published: 11 August 2010; accepted: 27 August 2010; published online: 17 September 2010.

*Citation: Rowe JB (2010) Connectivity analysis is essential to understand neurological disorders. Front. Syst. Neurosci. **4**:144. doi:10.3389/fnsys.2010.00144*

Copyright © 2010 Rowe. This is an open-access article subject to an exclusive license agreement between the authors and the Frontiers Research Foundation, which permits unrestricted use, distribution, and reproduction in any medium, provided the original authors and source are credited.

frontiers in
SYSTEMS NEUROSCIENCE

REVIEW ARTICLE
published: 26 August 2010
doi: 10.3389/fnsys.2010.00142

Identifying abnormal connectivity in patients using dynamic causal modeling of fMRI responses

Mohamed L. Seghier[1]*, Peter Zeidman[1], Nicholas H. Neufeld[1], Alex P. Leff[2] and Cathy J. Price[1]

[1] *Wellcome Trust Centre for Neuroimaging, Institute of Neurology, University College London, London, UK*
[2] *Institute of Cognitive Neuroscience, Institute of Neurology, University College London, London, UK*

Edited by:
Barry Horwitz, National Institutes of Health, USA

Reviewed by:
Alumit Ishai, University of Zurich, Switzerland
Barry Horwitz, National Institutes of Health, USA

****Correspondence:***
Mohamed L. Seghier, Wellcome Trust Centre for Neuroimaging, Institute of Neurology, University College London, 12 Queen Square, London WC1N 3BG, UK.
e-mail: m.seghier@fil.ion.ucl.ac.uk

Functional imaging studies of brain damaged patients offer a unique opportunity to understand how sensorimotor and cognitive tasks can be carried out when parts of the neural system that support normal performance are no longer available. In addition to knowing which regions a patient activates, we also need to know how these regions interact with one another, and how these inter-regional interactions deviate from normal. Dynamic causal modeling (DCM) offers the opportunity to assess task-dependent interactions within a set of regions. Here we review its use in patients when the question of interest concerns the characterization of abnormal connectivity for a given pathology. We describe the currently available implementations of DCM for fMRI responses, varying from the deterministic bilinear models with one-state equation to the stochastic non-linear models with two-state equations. We also highlight the importance of the new Bayesian model selection and averaging tools that allow different plausible models to be compared at the single subject and group level. These procedures allow inferences to be made at different levels of model selection, from features (model families) to connectivity parameters. Following a critical review of previous DCM studies that investigated abnormal connectivity we propose a systematic procedure that will ensure more flexibility and efficiency when using DCM in patients. Finally, some practical and methodological issues crucial for interpreting or generalizing DCM findings in patients are discussed.

Keywords: dynamic causal modeling, effective connectivity, functional MRI, patients, abnormal connectivity, abnormal networks

INTRODUCTION

Accurate characterization of abnormalities in neural processing is important for understanding pathological conditions and recovery mechanisms. It may also contribute to the tailoring of efficient therapy and intervention procedures. A large fMRI literature has already investigated how pathological conditions change neural processing, usually in terms of activity or signal changes in a set of spatially segregated regions. However, several studies have shown that characterizing such abnormal processes in terms of activation differences in a set of distinct (isolated) brain regions is not enough to provide a comprehensive picture of the abnormal brain (Meyer-Lindenberg et al., 2001; Ween, 2008). This is due to the fact that the function of any brain region cannot be understood in isolation but only in conjunction with the regions it interacts with during active behavior (e.g., McIntosh, 2000; He et al., 2007; Bassett and Bullmore, 2009; Bressler and Menon, 2010; Guye et al., 2010), a principle known as functional integration (Friston, 1994, 2002b, 2007).

Functional integration refers to task-dependent processing that emerges from changes in interactions among brain regions. In this context, deficits in functional integration or connectivity are implied when the influence of one brain region on another is stronger or weaker in patients relative to control subjects (Price et al., 2006; Ween, 2008). There are several approaches that have been proposed to assess functional integration or connectivity (for a review see Ramnani et al., 2004; Harrison et al., 2007; Rogers et al., 2007; Li et al., 2009; Bressler and Menon, 2010), including structural equation modeling (McIntosh and Gonzalez-Lima, 1994), dynamic causal modeling (DCM) (Friston et al., 2003), Granger causality (Roebroeck et al., 2005), psycho-physiological interactions (Friston et al., 1997), dynamic Bayesian networks (Rajapakse and Zhou, 2007), multivariate autoregressive modeling (Harrison et al., 2003), partial correlation analysis (Marrelec et al., 2009), non-linear system identification (Li et al., 2010b), and switching linear dynamic systems (Smith et al., 2010). Each method has its advantages and weaknesses (e.g., see Penny et al., 2004; Ramnani et al., 2004; Witt and Meyerand, 2009) and its use should be motivated by the question of interest, level of inference, paradigm design, data acquisition and analysis.

Here, we consider the use of DCM as a flexible and robust tool for assessing effective connectivity (Friston et al., 2003). In contrast to functional connectivity, effective connectivity provides a mechanistic account of the cause of the inter-regional interactions that would explain the emergence of a particular functional pattern (see for more details Friston, 1994, 2002b, 2009b). DCM has been widely used across different imaging modalities, populations and tasks (for a review see Stephan et al., 2007, 2010; Friston, 2009a). For instance, many studies have used DCM of fMRI data to explore inter-regional interactions during different cognitive tasks in normal healthy subjects. This literature has provided interesting insights about how brain regions talk to each other in healthy populations during cognitive and motor processing (Grol et al., 2007; Kasess et al.,

2008), face processing (Fairhall and Ishai, 2007; Li et al., 2010a), word reading (Chow et al., 2008; Carreiras et al., 2009; Seghier and Price, 2010), speech perception (Leff et al., 2008; Eickhoff et al., 2009), semantic access (Heim et al., 2009; Fan et al., 2010; Seghier et al., submitted), spatial memory (Doeller et al., 2008), emotional processing (Ethofer et al., 2006; Smith et al., 2006), attentional control (Acs and Greenlee, 2008; Plailly et al., 2008; Wang et al., 2010), conflict monitoring (Fan et al., 2008), and decision making (Alexander and Brown, 2010; den Ouden et al., 2010).

In this review we highlight some of the issues that need to be considered when effective connectivity is assessed with DCM of patient data. The paper is divided into five sections. The first section provides some useful definitions that are important for interpreting abnormal functional integration in patients. The second succinctly presents the theoretical foundations of DCM including the effective connectivity parameters, the available frameworks, and the multiple levels of inference that DCM can provide. The third section reviews previous studies that used DCM of data from patients with focal or non-focal damage to characterize abnormal connectivity. The fourth section aims to describe some practical guidelines that we believe would improve the use of DCM of patient data. In this context, we provide a systematic and unbiased approach to reveal abnormal connectivity in patients. The fifth section is concerned with some critical methodological issues that need to be taken into account when interpreting DCM findings in patients.

DEFINITIONS AND PRINCIPLES

We need first to define some concepts used throughout this review. Our review of previous work indicates that different terms have been used across studies to refer to the same concept. First, the term "network" has been used to refer to a set of temporally and spatially segregated regions that interact and engage in multiple complex behaviors. A network is by definition dynamic, where nodes and interactions between these nodes change continuously in time and space across different cognitive processes. A network can also be referred to as a "system" or "circuit." A part of a network can be referred to as a "sub-network" or "subsystem." Second, the complex dynamics within the network have been described with different terms, including: inter-regional interactions, connectivity, coupling, interactivity, interdependency, and co-operative action. Here we refer to these complex dynamics as "inter-regional interactions." Third, when characterizing how inter-regional interactions differ in patients and controls, previous studies used the terms: altered, abnormal, disturbed, atypical, impaired, or dysfunctional. Throughout the review we will use the term of "abnormal" when referring to inter-regional interactions in patients that are outside the range of those observed in healthy controls.

Using these definitions, we tentatively summarize some of the implicit assumptions that motivate studies of functional integration in patients:

(i) local damage to a part of a network can propagate throughout the whole network (e.g., Alstott et al., 2009; Kim and Horwitz, 2009);
(ii) an abnormal network can be viewed as a "new" network and not simply the normal network minus the damaged parts (e.g., He et al., 2007);
(iii) an abnormal network can comprise sub-networks that correspond to those seen in healthy subjects and novel sub-networks that are not typically seen in healthy subjects;
(iv) abnormal behavior can be an indicator of abnormal inter-regional interactions, however an abnormal network may not necessarily produce abnormal behavior;
(v) an abnormal network is not fixed; it can evolve and change during the course of therapy and recovery; and
(vi) for a given pathology, an abnormal network can vary from patient to patient even within a relatively homogenous population.

WHAT IS DCM?

Dynamic causal modeling aims to explain, quantitatively and mechanistically, how observed fMRI responses are generated (Friston et al., 2003). The key features that make DCM the method of choice for estimating effective connectivity can be summarized as follows (see detailed description in page 3100 of Stephan et al., 2010): (i) DCM is dynamic, in the sense that it uses differential equations to model inter-regional interactions, (ii) DCM is causal as it aims to infer the directionality of the inter-regional interactions and their context-dependent modulations, (iii) DCM is a hypothesis-driven approach that can incorporate any known effect (e.g., stimuli and tasks) to test specific hypotheses that motivated the experimental design, (iv) DCM is Bayesian in all its aspects and uses a generative model to constrain effects by prior knowledge, (v) DCM explicitly uses an empirical forward model that links observed hemodynamic responses to the (hidden) neuronal dynamics, allowing inferences to be made at the neuronal level, (vi) DCM estimates a range of connectivity parameters that present parallels with neuro-physiological models, including psycho-physiological or physio-physiological interactions, (vii) the use of DCM with Bayesian model selection (BMS) and averaging tools enables inferences at different levels, from a set of plausible models (a family of models) to a specific connectivity parameter, and (viii) DCM inferences can be made both at the single subject and group level.

Fundamentally, DCM is only appropriate for describing responses (fMRI, MEG, ERP) that result from controlled external stimuli (Friston, 2009a; Stephan et al., 2010). This requires datasets that also include periods when external stimuli are both present and absent. DCM is therefore not currently suitable for uncontrolled continuous "natural" stimulations such as resting-states. It treats the human brain as a dynamic system that is subject to multiple inputs and produces multiple outputs. Thus, DCM characterizes task-dependent inter-regional interactions.

The starting point for DCM is the selection of a fixed set of regions and their possible connections. Each combination of experimentally modulated connections corresponds to a model, which can then be compared to other alternative models in order to identify which model(s) best predict(s) the data (see illustration in **Figure 1** for details of the practical steps). For a given model, DCM estimates three different sets of parameters: (i) input or extrinsic parameters that quantify how brain regions respond to external stimuli (i.e., the external inputs that perturb the model), (ii) endogenous or latent parameters that characterize context-independent (or average) inter-regional interactions, and (iii) modulatory parameters that measure changes in effective connectivity induced by the

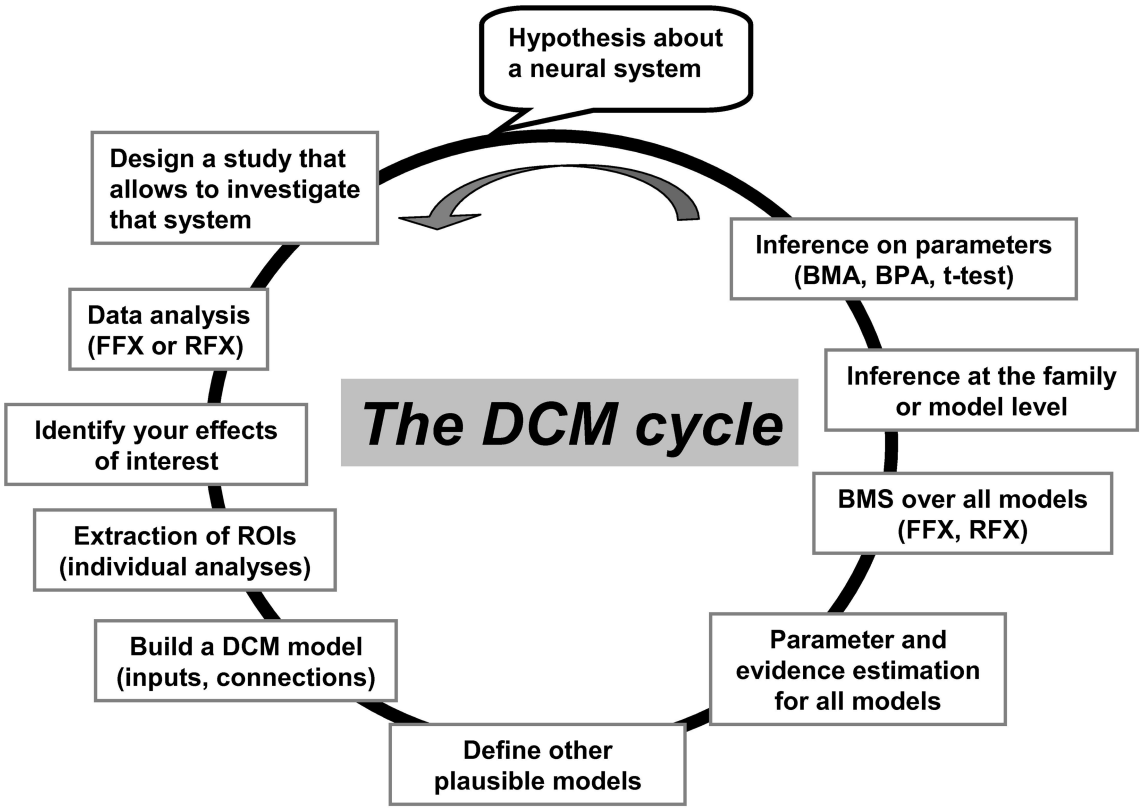


FIGURE 1 | An illustration of the "cycle" of practical steps in a typical DCM analysis. These steps have been made easy and flexible within the SPM software package. It starts with the selection of effects of interest (activated patterns) and the time-series extraction of the appropriate regions. Then, a predefined structure of the model is specified, including the driving inputs and where they enter the system, how the regions inter-connect, and where modulatory effects are specified. Additional alternative models can be specified and then all models can be compared. ROIs, regions of interest; FFX, fixed-effect analysis; RFX, random-effect analysis; BMS, Bayesian model selection; BMA, Bayesian model averaging; BPA, Bayesian parameter averaging. This figure has been adapted from a previous talk given by KE Stephan and L Harrison (during the ICN-SPM course in May 2005).

experimental conditions. These connectivity parameters are each expressed in Hz within the DCM framework. They are not necessarily constrained by mono-synaptic (i.e., direct) anatomical connections and can be either positive or negative. A positive parameter means that an increase in activity in one region results in increased rate of change in the activity of another region. Conversely, a negative parameter means that an increase in activity in one region results in a decreased rate of change in the activity of another region. Note that, due to the limited temporal resolution in fMRI, conduction delays in inputs and inter-regional interactions are ignored in DCM of fMRI responses, but not in DCM for EEG or MEG data (Friston et al., 2003). All DCM parameters and their posterior probabilities are assessed with Bayesian inversion by means of the expectation-maximization algorithm (Dempster et al., 1977; Friston, 2002a).

Below, we succinctly present the available implementations of DCM, how to compare alternative models, and the different levels of inference that can be made with DCM.

MULTIPLE IMPLEMENTATIONS

Since the seminal paper reported by Friston et al. (2003), there have been several extensions of the DCM algorithm to increase its flexibility. It is therefore necessary to consider which algorithms are most suitable for the question of interest. This section presents the extensions implemented for DCM of fMRI responses. By default, the most widely used DCM version corresponds to the bilinear and deterministic implementation with one-state equation per region (see below).

Bilinear vs. non-linear

The default implementation in DCM codes the rate change in neuronal activity according to the following bilinear evolution or state equation (Friston et al., 2003):

$$\frac{dz}{dt} = \left(A + \sum_{i=1}^{m} u_i B^{(i)} \right) z + Cu \qquad (1)$$

where z is the activity of the neuronal population, A is the first-order (endogenous, latent, or average) inter-regional interactions in the absence of inputs, B is the second-order interaction between activity and input (the modulatory effect), and C is the extrinsic effects of inputs "u" on activity. The bilinear term B is equivalent to the psycho-physiological interactions in the network that reflects how the inter-regional interactions are modulated by a given input/context. This fundamental equation in DCM has been extended

for the assessment of physio-physiological interactions in a given network. The extension, known as non-linear DCM (Stephan et al., 2008), is suitable for explicitly testing whether the activity in a given region gates or enables interactions between other regions. The state equation in non-linear DCM is given by:

$$\frac{dz}{dt} = \left(A + \sum_{i=1}^{m} u_i B^{(i)} + \sum_{j=1}^{n} z_j D^{(j)} \right) z + Cu \quad (2)$$

where the new term "D" is a quadratic quantity that represents the physio-physiological interactions in the model or the strength of the activity-dependent gating of connections.

This non-linear DCM equation can be helpful when modeling "neural gain control" mechanisms in short-term synaptic plasticity (Stephan et al., 2008) which are likely to be relevant for characterizing a given pathology. Such mechanisms are critical for various cognitive processes, including top-down modulation of attention and learning (see example in den Ouden et al., 2010).

One-state vs. two-state neuronal equations

Because each region is modeled by one neuronal state equation only (Eq. 1), it is not possible to assess selective changes in excitatory (e.g., glutamatergic) and inhibitory (e.g., GABAergic) subpopulations in each region of the DCM model. This is a very important issue that needs to be taken into account when, for instance, making inferences about potential inhibitory or excitatory mechanisms in DCM. To address this, an extended version of DCM exists that uses two-state neuronal equations (Marreiros et al., 2008) to model excitatory and inhibitory subpopulations in each region. This allows for an explicit description of intrinsic (between subpopulations) connectivity within a region. In other words, each region is modeled by two neuronal subpopulations and DCM can thus estimate the interactions between these two subpopulations. Interestingly, this parameterization confers dynamical stability on the system, enforces positivity constraints on the extrinsic connections, and enables context-dependent changes in the interactions to be modeled as a proportional increase or decrease in connection strength (Marreiros et al., 2008). The two-state DCM can be used, for instance, to specifically test whether patients and controls differ in the interactions between excitatory and inhibitory subpopulations.

Anatomical-based priors vs. default shrinkage priors

Different priors are embodied within the Bayesian framework of DCM. These include priors on the connectivity parameters (see for more details Friston et al., 2003) that are referred to as "shrinkage" priors because they tend to "shrink" posterior means to their prior expectation of zero, particularly when the data are noisy. These shrinkage priors make the detection of significant inter-regional interactions somewhat conservative. Thus only effects that have a significant likelihood with high precision are allowed to deviate from zero (i.e., when new data strongly support an existing effect). However, it has been shown that such priors can be modified (relaxed) to take into account an *a priori* knowledge about anatomical connectivity (Stephan et al., 2009b). The idea is to assign a stronger belief (i.e., by relaxing the shrinkage priors) to a particular interaction between two regions if one has strong evidence for an existing anatomical connection between the regions. These anatomically-based priors have been shown to provide stronger evidence for anatomically motivated models (Stephan et al., 2009b) and are particularly useful if tractography data (DTI) are available. They can also take advantage of the white matter tracts that are specified in recent atlases (e.g., Mori et al., 2005, 2008; Catani and Thiebaut de Schotten, 2008) and incorporate this information into the DCM when defining the appropriate model structure. In the context of the current paper, it is interesting to note that information about damaged tracts in a group of patients can be explicitly modeled. However, because of the deterministic nature of the current DCM implementation (see below), indirect influences on regions cannot be ruled out even if direct white matter tracts are missing.

Deterministic vs. stochastic

The default implementation of DCM in SPM is deterministic as only the explicitly modeled effects are allowed to influence the inter-regional interactions. Thus, DCM estimates the interactions between the spatially segregated regions that are temporally perturbed by the external inputs included in the model. However, it is obvious that this framework cannot rule out the influence of indirect effects, including interactions with regions not included in the DCM or temporal innovations not modeled in the inputs (see discussion in Smith et al., 2010). For instance, a connection can excite a group of neurons that inhibit another region thereby resulting in an overall effect of inhibition. An extended version, known as stochastic DCM (Daunizeau et al., 2009), allows such subtle indirect effects to be expressed. It extends the previous state equation to:

$$\frac{dz}{dt} = \left(A + \sum_{i=1}^{m} u_i B^{(i)} + \sum_{j=1}^{n} z_j D^{(j)} \right) z + Cu + \eta \quad (3)$$

where η is the state noise that models stochastic innovations in the system. The new term η is defined by Gaussian variables with a mean of zero and a covariance structure that can express any form of innovations. In other words, in this framework, all indirect effects are modeled as stochastic phenomena, thereby allowing the hidden-states causing the data and any non-controlled exogenous inputs to the system to be inferred (Daunizeau et al., 2009). This framework can be very useful because it provides more flexibility in modeling unknown or indirect pathologic effects in patients.

LEVELS OF INFERENCE WITH BAYESIAN MODEL SELECTION

One exciting tool in DCM is its BMS procedure. This procedure compares the evidence for different competing hypotheses. Because the exact mechanisms behind any fMRI responses are unknown, it might not be possible to have an *a priori* prediction about the "exact" model. Therefore, it is important to specify a range of alternative models and search for the best (most useful) model in the model space, e.g., Leff et al. (2008), Seghier and Price (2010), and Seghier et al. (submitted). This procedure increases the certainty of the best model by testing many other potential explanations of the data.

During the Bayesian inversion of the model, the probability of the data given the model, known as the model evidence, is approximated by the negative variational Free-energy (Friston et al., 2007;

Stephan et al., 2009a). This approximation, as a lower bound on the model evidence, points to the optimal compromise between the accuracy and complexity of a given model. It provides a better estimation for the complexity term, by taking into account the interdependency between the estimated parameters. Thus, model evidence is not an "absolute" measure of how good a model is; instead it is used in BMS to compare between alternative models. Moreover, by using the negative variational Free-energy as the optimal compromise between accuracy and complexity, the current implementation of DCM ensures that (i) model complexity will not increase if additional parameters are "redundant" to existing parameters and (ii) the parameter estimates of a good model are as precise and uncorrelated as possible. In short, BMS estimates the likelihood that a given model has generated the observed data.

Sampling the model space

The most critical step when using the BMS tool is the definition of the DCM model space (i.e., the set of specified models) because any inference at the model level depends on the way the model space has been defined (sampled). There are three principles that need to be considered: compatibility, size, and plausibility. First, compatibility between models is attained by ensuring that all models of a given subject have the same regions, that is, the models all contain the same data. Specifically, BMS cannot be applied to models that are fitted to different fMRI data. For group studies, a good practice is to ensure consistent regions between subjects since group BMS implicitly assumes functional compatibility of the modeled effects across subjects. Second, there are an infinite number of possibilities that can explain the data; it is impossible to sample all these possibilities and thus a practical limitation on the number of models (i.e., the size of the model space) is necessary. Third, plausibility reflects a systematic way of defining realistic and interpretable models according to *a priori* knowledge or some predefined criteria. This will automatically limit the size of the model space and crucially avoid including bad or unrealistic models.

Random-effects vs. fixed-effects

Once the model space has been defined and estimated in all subjects, BMS can be used to identify the best (most useful) models at the group level. There are two classic ways of achieving group BMS analyses: fixed-effects and random-effects (see Figure 1 in Stephan et al., 2010). The former assumes that the best models are comparable across subjects because subjects would reasonably perform the task in a similar way (e.g., identical cognitive strategies). The latter may be preferable when studying heterogeneous populations or using complex cognitive tasks where optimal models are likely to vary across subjects. Random-effects BMS is also preferable when outlier effects are suspected because the current implementation (in SPM8) of random-effects BMS uses a robust hierarchical Bayesian approach. It quantifies the likelihood that a specific model generated the data of a subject chosen at random, measured via two quantities: (i) the Dirichlet parameter estimates (alpha) represents a measure of the effective number of subjects in which a given model generated the observed data, and (ii) the "exceedance" probability (xp) describes the belief that a particular model is more likely than any other model given the group data (Stephan et al., 2009a). The exceedance probability "xp" is particularly intuitive as all exceedance probabilities sum to one over all tested models. Note also that there are two sampling schemes in random-effects BMS, the first uses a Variational Bayes method that is optimal and fast when the number of tested models is smaller than the number of subjects (Stephan et al., 2009a), and the second uses a Gibbs sampling method that is optimal and accurate when the number of models is larger than the number of subjects (Penny et al., 2010).

Inference at the family and the model level

When comparing models with BMS, the best model would be the winning model that has the most evidence (e.g., significant exceedance probability) compared to other models. However, it is commonly found that one single model does not dominate all other models, particularly when the number of models is very large with many connections shared between models. In this situation, one can look for any similarity in model structures that can better explain the data. To do this, a recent extension of BMS has introduced the ability to make inferences on a "family" of models (Penny et al., 2010). A family is a subset of models that share similar characteristics such as the same driving region or the same modulated connections (see Penny et al., 2010; Seghier and Price, 2010; Seghier et al., submitted). The formation of families should be motivated by the question of interest to ensure all models in the model space are partitioned into different families with no overlap. It is permissible to have different numbers of models in each family. BMS can then be used to compare these competing families and inferences can be made at the family level.

Inference at the connection level

The last level of inference assesses the significance of a particular connectivity parameter. Analysis of the connectivity parameters is conducted after comparing models or families because the posterior densities of such parameters are conditional on the particular model or family selected (Stephan et al., 2010). If a winning model has been identified, one can look at the consistency of effects across subjects using random-effects analysis (e.g., *t*-tests). Alternatively, fixed-effect approaches can be applied using Bayesian parameter averaging where the connectivity parameters are weighted by their precision during the computation of the mean across subjects or sessions. Significant effects at the group level are commonly reported at a corrected *p*-value (e.g., using a Bonferroni correction based on the number of tested connections, Sonty et al., 2007; Leff et al., 2008; Seghier and Price, 2010). If the inference has been made at the family level, it is possible to use the new Bayesian model averaging (BMA) method where the contribution of each model to the mean effect is weighted by its evidence (Penny et al., 2010).

PREVIOUS DCM STUDIES OF PATIENTS

In this section we review previous DCM studies of patients. We are particularly interested in the way DCM has been carried out in patients and how the differences between controls and patients have been statistically characterized both at the model and connection level. A PUBMED search was conducted with the following inclusion criteria: (i) fMRI studies, (ii) published in English that (ii) used DCM in (iv) patients with any disorder. A total of 28 studies were identified and are listed in **Tables 1 and 2** (Bird et al., 2006; Mechelli et al., 2007; Rocca et al., 2007a,b; Sonty et al.,

Table 1 | List of previous DCM studies of patients that used one single model (i.e., DCM model space = 1 model). Studies are listed in alphabetical order.

Study	Disorder	Np/Nc	Task	*R*	*M*	Findings
Abutalebi et al. (2009)	Bilingual Aphasia	1 pat., 0 con.	Picture naming (in L1 and L2); Longitudinal recovery study (3 sessions).	5	1	Increased connectivity after therapy between regions associated with "language control".
Agosta et al. (2010)	Alzheimer's disease	25 pat., 11 con. (with two groups of patients)	A simple motor task with the right hand.	6	1	Altered endogenous connectivity between patients and controls on the primary sensorimotor cortex.
Almeida et al. (2009b)	Major and bipolar depression	31 pat., 16 con.	Emotion labeling in happy vs. sad faces.	4	1	Abnormal connectivity between orbitofrontal and amygdala differentiated major from bipolar depressed patients.
Bird et al. (2006)	Autism spectrum disorder	16 pat., 16 con.	Attention modulation in faces and houses.	3	1	Reduced attentional modulation in patients compared to controls.
Cao et al. (2008)	Dyslexia	12 pat., 12 con. (children)	Rhyme judgment task.	4	1	Reduced connectivity modulation in dyslexics compared to controls between fusiform and parietal regions. Correlations between reading skills and connectivity in left parietal.
Crossley et al. (2009)	Schizophrenia	26 pat., 13 con. (with two groups of patients)	Working memory task.	5	1	Connectivity between superior temporal and middle frontal gyrus was negative in controls and positive in patients.
Eickhoff et al. (2008)	heterotopic hand replantation	2 pat., 14 con.	Motor (hand movement).	8	1	Abnormal inhibition from ipsilateral to contralateral M1.
Goulden et al. (2010)	Major depression	30 pat., 29 con.	Emotional face processing task.	4	1	Improved group differences on connectivity parameters when using permutation testing.
Grefkes et al. (2008)	Stroke patients (subcortical lesions)	12 pat., 12 con.	Motor (hand movement).	8	1	Reduced coupling between bilateral M1 during stroke-affected hand movements. Correlation between reduced connectivity and degree of impairment.
Mechelli et al. (2007)	Schizophrenia	21 pat., 10 con. (with two groups of patients)	Voice detection from spoken words task.	5	1	Abnormal connectivity between anterior cingulate and superior temporal gyrus, in particular in patients with verbal hallucinations.
Mintzopoulos et al. (2009)	Stroke patients	5 pat., 12 con.	Motor (squeezing a robotic device).	3	1	Reduced endogenous connectivity between M1 and cerebellum and increased connectivity between SMA and M1 in patients relative to controls.
Miyake et al. (2010)	Patients with eating disorders	36 pat., 12 con. (with 3 groups of patients)	Detection of negative vs. neutral words.	2	1	Significant group differences in the endogenous connectivity from medial frontal to the amygdala.
Rocca et al. (2007a)	Patients with multiple sclerosis	12 pat., 14 con.	A simple motor task with the right hand.	4	1	Stronger endogenous connectivity in patients than controls between right primary sensorimotor cortex and cerebellum.
Shannon et al. (2009)	Externalizing behavior disorder	21 pat., 11 con.	A reward and non-reward task.	2	1	Significant differences between controls and patients on both endogenous and non-reward modulatory effects, mainly on the caudate.

Np, number of patients; Nc, number of controls; R, number of regions; M, number of models.

2007; Cao et al., 2008; Eickhoff et al., 2008; Grefkes et al., 2008, 2010; Hamandi et al., 2008; Schlosser et al., 2008, 2010; Abutalebi et al., 2009; Almeida et al., 2009a,b; Benetti et al., 2009; Crossley et al., 2009; Dima et al., 2009; Fujii et al., 2009; Grezes et al., 2009; Mintzopoulos et al., 2009; Shannon et al., 2009; Vaudano et al., 2009; Agosta et al., 2010; Allen et al., 2010; Goulden et al., 2010; Miyake et al., 2010; Rowe et al., 2010). These studies have provided valuable insights into the abnormal connectivity in patients with

Table 2 | List of previous DCM studies of patients that used and compared more than one model (DCM model space ≥ 2 models).

Study	Disorder	Np/Nc	Task	R	M	Findings
Allen et al. (2010)	Schizophrenia	15 pat., 15 con.	Sentence completion task.	3	14	Best model identical in controls and patients. Increased endogenous connectivity between anterior cingulate and middle temporal regions in patients compared to controls.
Almeida et al. (2009a)	Bipolar disorder	21 pat., 25 con.	Emotion labeling in happy vs. neutral faces.	3	4	Best model identical in controls and patients. Abnormal increase in endogenous connectivity between parahippocampal and cingulate cortex in patients compared to controls.
Benetti et al. (2009)	Schizophrenia	26 pat., 14 con. (with two groups of patients)	Working memory task.	2	4	Models have different regions. Endogenous connectivity between right hippocampus and inferior frontal gyrus was stronger in controls than patients.
Dima et al. (2009)	Schizophrenia	13 pat., 16 con.	Perception of the hollow-mask illusion.	5	2	Best model identical in controls and patients (but not when using RFX analysis). No significant correlations between connectivity and symptoms.
Fujii et al. (2009)	Blind patients	15 pat., 24 con.	Tactile Braille discrimination task.	5	2	Model comparison done in patients, and the best model was then used in controls. Modulations between parietal and occipital regions were positive in patients and negative in controls. Early blind showed stronger connectivity than the late blind patients.
Grefkes et al. (2010)	Stroke patients (subcortical lesions)	11 pat., 0 con.	Motor (hand movement); interference with TMS.	6	4	TMS applied to the contralesional motor cortex. TMS enhanced endogenous connectivity between ipsilesional SMA and M1.
Grezes et al. (2009)	Autism spectrum disorder	12 pat., 12 con.	Perception of fearful or neutral actions (videos).	6	2	The connectivity parameters of both models were compared between patients and controls. Stronger connectivity in controls than patients during fearful compared to neutral context, in particular on the amygdala.
Hamandi et al. (2008)	Epileptic patients	1 pat., 0 con.	Interictal epileptiform discharges.	2	2	Onsets defined as spikes (visual monitoring in EEG); Increased connectivity from left parahippocampal to lingual gyrus during epileptic discharges.
Rocca et al. (2007b)	Patients with benign multiple sclerosis	15 pat., 19 con.	Stroop color-word task.	6	2	The best model of driving inputs in controls was then used in patients. Endogenous and modulatory effects were different in patients vs. controls, and they were correlated to the severity of the structural damage.
Rowe et al. (2010)	Parkinson's disease	16 pat., 17 con.	Action selection in finger-tapping task; Dopaminergic therapy.	4	48	Best model identical in controls and patients. Model selection is reproducible. Connectivity parameters are less reliable across sessions
Schlosser et al. (2008)	Major depression	16 pat., 16 con.	Stroop color-word task.	5	4	Best model identical in controls and patients. Higher endogenous connectivity between anterior cingulate regions in patients compared to controls.
Schlosser et al. (2010)	Obsessive Compulsive disorder	21 pat., 21 con.	Stroop color-word task.	6	5	Best model identical in controls and patients. Increased modulation between frontal and cingulate cortex in patients during incongruent trials.
Sonty et al. (2007)	Primary Progressive Aphasia	8 pat., 8 con.	Semantic word matching.	6	5	Best model identical in controls and patients. Reduced connectivity between Broca and Wernicke's area in patients compared to controls. Reduced connectivity was correlated with accuracy.
Vaudano et al. (2009)	Epileptic patients	7 pat., 0 con.	Generalized spike wave discharges.	3	3	Discharges used as driving inputs and enter the system at different regions. The best model showed spike wave discharges input on precuneus.

Np, number of patients; Nc, number of controls; R, number of regions; M, number of models.

a range of pathologies. However, the aim of our review is not to discuss the relevance of their findings. This would necessitate a separate review that considered the models tested, tasks and stimuli used, region selection, driving and modulatory inputs, and the relevance of the findings in light of previous neuropsychological and computational models. Instead, the current review considers the methodological approaches that have been used (see **Tables 1 and 2**) and we refer to these studies for illustrations of the methods.

Consistent with the most widely used implementation of DCM, all 28 studies were deterministic and used the bilinear one-state neuronal equation without anatomical-based priors. Matched groups of controls were included in all but four studies (Hamandi et al., 2008; Abutalebi et al., 2009; Vaudano et al., 2009; Grefkes et al., 2010). The driving inputs were specified in standard block or event-related designs in all but two studies (Hamandi et al., 2008; Vaudano et al., 2009) where internally generated epileptogenic wave discharges from the epileptic patients being studied were used as the driving inputs.

The models used varied in their complexity, from simple models with two regions (e.g., Benetti et al., 2009) to complex models with eight regions (e.g., Grefkes et al., 2008). All studies involved adult subjects except one study of dyslexic children (Cao et al., 2008). The tasks and stimuli varied extensively between the studies because they were purposely designed to maximize differences between patients and controls. For instance, working memory tasks were used in patients with schizophrenia (Benetti et al., 2009; Crossley et al., 2009), Stroop word-color tasks were used in patients with depression (Schlosser et al., 2008), and semantic tasks were used in aphasic patients (Sonty et al., 2007; Abutalebi et al., 2009). One critical difference between these studies concerns the level of inference made in both patients and controls. We thus divided the 28 studies into two sets: a set of 14 studies that tested one model only (**Table 1**) and therefore did not require the BMS procedure and a second set of 14 studies that used BMS to compare at least 2 models in patients and controls (**Table 2**).

STUDIES WITH ONE FIXED DCM MODEL

The 14 studies with only one DCM model in both patients and controls were exclusively interested in how connectivity parameters differed between groups. The same model (i.e., same regions, driving inputs, and modulatory inputs) was defined in patients and controls and the connectivity parameters of that model were compared between patients and controls on a connection by connection basis. The main motivation of such strong reliance on a single model is to ensure the same model is tested on both populations so that connectivity parameters can be compared. This avoids the case when the winning model is not the same in patients and controls. Because the parameters are conditional on the selected model the definition of one unique model can be problematic. Some studies have used a fully connected model because it allows all possible combinations of inter-regional connections to be estimated and tested (e.g., Bird et al., 2006; Mechelli et al., 2007; Rocca et al., 2007b; Cao et al., 2008; Agosta et al., 2010; Miyake et al., 2010). However, we argue that a fully connected model is by definition the most complex and may lead to over-fitting of the data. Moreover, it cannot guarantee that connectivity parameters are estimated within the best model structure given the data. Other studies have used a model that is less complex than the fully connected version when *a priori* hypotheses concerning the architecture of the optimal model are possible on the basis of previous structural and functional connectivity findings (e.g., Grefkes et al., 2008; Abutalebi et al., 2009; Crossley et al., 2009; Goulden et al., 2010). Irrespective of which model is selected, single model studies were more concerned about the differences in connectivity parameters and thus their findings do not address differences between patients and controls at the network level.

STUDIES WITH MULTIPLE COMPETING DCM MODELS

To avoid heavy reliance on a predefined model other studies have used BMS to identify the best model from competing alternatives (varying from 2 to 48 models, see **Table 2**). The comparison between connectivity parameters is then performed on the parameters of the best model. This procedure has the advantage of providing the opportunity to make inferences both at the model/system level and the parameter/connection level within the optimal structure. It is perfectly valid (and sufficient) to limit the inference to the system level, for instance by showing whether or not patients are using the same network as the controls (e.g., is the winning model identical in patients and controls?). That said, all previous studies were mainly interested in inferences at the connection level and the BMS was usually presented as an intermediate analysis step. To ensure the possibility of such inference, these studies used different methods to guarantee that the final selected model is the same between controls and patients. This conceptual limitation will be unnecessary when the new BMA tool for making comparisons across multiple models or families is implemented in SPM (see Penny et al., 2010).

Practically, three methodologies have been used to compare the best model in patients and controls. First, the majority of studies used BMS on the same set of alternative models and implemented this independently in patients and controls (e.g., Sonty et al., 2007; Schlosser et al., 2008, 2010; Almeida et al., 2009a; Allen et al., 2010; Rowe et al., 2010). All these studies showed the winning model to be identical in patients and controls. Note however that this similarity may depend on whether RFX or FFX methods are used; for instance, patient and control models were found to be identical with FFX analysis but different with RFX analysis (Dima et al., 2009). Second, an alternative approach used by Rocca et al. (2007b) in a study of patients with multiple sclerosis performing a Stroop task involved the use of BMS within controls only to find the best model in controls, followed by a comparison of the parameters of that model in patients and controls (Rocca et al., 2007b). For instance, when faced with the choice of where inputs enter the system, Rocca and colleagues defined two alternative models with two different driving regions. They then identified the best model and used the driving region of the winning model as a driving region for patients as well (Rocca et al., 2007b). The third procedure was used by Fujii et al. (2009) to study blind patients during tactile Braille discrimination tasks. It involved identification of the best model in patients and then used this model in comparison to controls (Fujii et al., 2009). Note that the last two procedures rely on the hypothesis that the best model of one group is identical to the best model in the second group.

DIFFERENCES IN CONNECTIVITY PARAMETERS

After defining the best model in both patients and controls, previous studies have tested whether the parameters of that model differ between the two groups. Some studies have limited this comparison to the endogenous connectivity (e.g., Rocca et al., 2007a; Benetti et al., 2009; Miyake et al., 2010), whereas other studies have looked at how patient connectivity differed in the context of stimulus or task changes (e.g., Bird et al., 2006). Abnormal connectivity in patients has been found to correspond to either a change in the strength of connectivity (stronger or weaker parameters than controls) or a change in polarity (positive vs. negative). For instance, Schlosser et al. (2008) found patients with major depression have stronger connectivity between anterior cingulate regions when compared to controls during a Stroop color-word task (Schlosser et al., 2008). Conversely, Sonty et al. (2007) illustrated reduced connectivity by showing that, relative to controls, patients with primary progressive aphasia have weaker connectivity between Broca and Wernicke's areas during semantic word matching tasks. An example of reversed polarity has also been shown with negative modulatory effects between parietal and occipital regions in controls compared to positive modulations in blind patients (Fujii et al., 2009).

Interestingly, a few studies have also investigated the correlations between abnormal connectivity and other behavioral or diagnostic measures in patients. For instance, Rocca et al. (2007b) showed a significant correlation between abnormal connectivity and the severity of structural damage in patients with multiple sclerosis. Cao et al. (2008) found that reduced modulations between the fusiform and parietal regions correlated with reading skills in dyslexic children (Cao et al., 2008). Another example is provided by Grefkes et al. (2008) who found a significant correlation between reduced connectivity in primary motor regions and the degree of motor impairment in stroke patients with subcortical lesions (Grefkes et al., 2008). Moreover, other studies have used connectivity parameters to distinguish between different pathological groups. For instance, Almeida et al. (2009b) found that the abnormal connectivity between the orbitofrontal cortex and the amygdala differentiated patients with major depression from patients with bipolar depression during a task of emotional labeling of happy vs. sad faces (Almeida et al., 2009b). Miyake et al. (2010) found that endogenous connectivity between the medial frontal gyrus and the amygdala during the detection of negative vs. neutral words showed variable patterns between three subgroups with different types of eating disorders (Miyake et al., 2010). Furthermore, two other studies illustrated how external interventions can be monitored with DCM in diseased populations. The first was a longitudinal study of a bilingual aphasic patient by Abutalebi et al. (2009) and assessed connectivity between five regions of interest during a picture naming task in two languages. Increased connectivity was found after therapy in regions associated with "language control," consistent with the patients' behavioral recovery (Abutalebi et al., 2009). The second study combined DCM and transcranial magnetic stimulation (TMS) (Grefkes et al., 2010) and focused on stroke patients with subcortical lesions during hand movement tasks. In their study, Grefkes et al. (2010) found that applying TMS to the contralesional motor cortex increased connectivity between ipsilesional motor regions (Grefkes et al., 2010).

A SYSTEMATIC PROCEDURE FOR DCM IN PATIENTS

The studies reviewed above have used a variety of procedures to assess effective connectivity in patients. This makes any meaningful comparison between their findings difficult. This diversity also illustrates the different procedures that have been used to address the methodological challenges that arise when DCM is used with patient data. In this section, we propose a practical procedure that can be used to compare effective connectivity in patients and controls. This involves the standard DCM procedures (see Definitions and Principles above) but with some specific modifications that are particularly relevant for patient studies. They relate to region selection, the definition of the driving regions, the definition of plausible models, identifying the best model or family of models, and the comparison of connectivity parameters in patients and controls. Note however we are not claiming this approach is the only correct way of using DCM in patients; the optimal approach should always be tailored to the specific questions, the selected effects of interest, and the definition of the model space.

REGION SELECTION

Models should, by definition, be comparable between patients and controls. This means models must have identical nodes. Accordingly, only commonly activated regions in patients and controls can be included in DCM. Thus, DCM in patients focuses on the characterization of abnormal connectivity in a common network of regions (see schematic illustration in **Figure 2**). A fuller characterization of patient data would therefore benefit from a report of abnormalities at the level of regions (areas that are more or less activated in patients than controls) in addition to a report of abnormal connectivity within the set of areas commonly activated in patients and controls. Second, there should be minimal inter-subject variability in the anatomical location of a given region. This is because large variability in region locations may result in the comparison of functionally different regions across patients and controls (for a similar rationale, see Seghier and Price, 2010; Seghier et al., submitted). This is particularly critical in regions where functional specialization may vary at a high spatial scale. As a general rule, the distance between corresponding regions in different individuals should correspond to the size of the spatial smoothing kernel. Third, the distance between different regions in the same individual needs to ensure that the data included in one region is not also entered into another region. Fourth, we also advocate the definition of proper F-contrasts of interest that can be used to adjust the extracted time-series and thus minimize the contribution of other confounds (e.g., session effect, head motion, incorrect trials).

DRIVING REGIONS

After extracting the ROIs, an important step in the construction of plausible models is the choice of driving regions (i.e., where the inputs enter the system). It is wise to specify primary sensory regions as driving regions if they are included in a model. However, for other regions, the motivation for selecting driving regions should be carefully based on prior anatomical or functional knowledge as all connectivity parameters depend on how the information flow is assumed to propagate from driving regions.

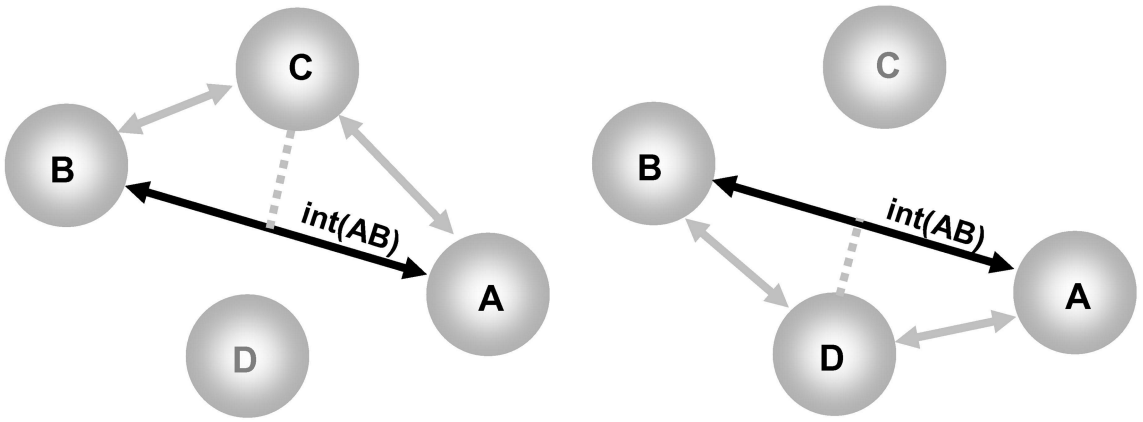


FIGURE 2 | Illustration of the problem of the "missing nodes" in DCM when comparing patients to controls. Regions A and B are activated in both groups, region D is damaged in patients but present in controls, and region C is a compensatory region that is only activated in patients. The deterministic DCM can assess the interactions between A and B [noted int(AB) on a solid black line], but would ignore the indirect effects of regions D and C (shown with gray lines). The interactions between A and B are thus a complex mixture of these effects [e.g., in patients = int(AB) in the context of C without D; in controls = int(AB) in the context of D without C].

In the absence of *a priori* knowledge, it is useful to perform a preliminary BMS procedure that systemically varies the site of driving regions across a set of candidate regions. This can be done by specifying all plausible models (in terms of endogenous and modulatory effects) and repeating them with each combination of driving regions (for a similar procedure, see Leff et al., 2008; Penny et al., 2010; Seghier et al., submitted). Then, by using a RFX BMS across patients and controls, the winning family represent the best driving regions.

PLAUSIBLE MODELS

This step should be *systematic* in the sense that it needs to explore a set of alternative *plausible* models for a given set of regions, particularly when prior knowledge of a network is uncertain. Even if the inference of interest is at the connection level, it is difficult to interpret and generalize differences in connectivity parameters in patients that have only been compared to controls in the context of one fixed model. Our concern is based on the fact that the connectivity parameters are conditional on the predefined model. Thus, evidence is stronger when it is known to be based on several competing models. It is also helpful (if possible) to classify models in a set of meaningful families that can then be compared with BMS. For instance, family categorization could be based on the existence of a commonality at the level of an endogenous connection, modulated connection, or driving input. Additional constraints help to limit the size of the DCM model space. This is necessary, since, for example, there are over one billion possible models in the model space of a fully connected DCM with six regions if it is searched in an unconstrained manner for the best modulated connections. Limiting the model space to the most plausible models limits the possibility of diluting evidence with the inclusion of bad or implausible models. It would also be helpful if authors detailed how they constrained the model space as this may aid in the design of future studies.

BMS FOR THE BEST MODEL OR FAMILY OF MODELS

First, it should be stressed that it is better to use the most recently available negative variational Free-energy model evidence measure instead of the suboptimal AIC or BIC measures (for more details see Stephan et al., 2009a). The problem with AIC and BIC (still used in some recent work) is that they may bias model selection toward more simplistic models and do not take into account the interdependency between connectivity parameters. Using the negative variational Free-energy measures, BMS can be run separately on patients and controls to identify the best family of models in patients and controls (assuming the same model space is defined in both groups). Family inference enables the investigator to test and report the evidence for an optimal class of models in patients or controls. If patients and controls show a different winning family or model then this is an interesting result to report, particularly in the context of a commonly activated set of regions (see previous section). This would mean that data from patients and controls cannot be adequately and sufficiently fitted by the same model structure (e.g., Horwitz et al., 1995), suggesting that the patterns of fMRI activation observed in patients have emerged from other alternative models that can be tested and identified with the BMS. Moreover, differences can be investigated at the level of inter-subject variability within and between patients and controls. For example, some patients may have similar winning models to controls and other patients may have different winning models. Inter-subject variability within groups can then be related to behavioral measures acquired in or out of the scanner. This is particularly interesting when the aim of the study is to predict performance at the individual subject level.

DIFFERENCES AT THE CONNECTION LEVEL

If inference is sought at the connection level it is important to only compare models that are tested within the same model space in both groups, including the same winning model or family of models. For the same winning model, two sample *t*-tests or ANOVAs can

be used to compare connectivity parameters between patients and controls. Alternative permutation testing (Goulden et al., 2010) can be used in studies with small samples. For the same family of models, the latest BMA procedure is more suitable (see illustration in Penny et al., 2010; Seghier et al., submitted) when the two groups differ in the distribution of model evidence across the model space (e.g., the posterior probabilities of plausible models are different in the two groups). Moreover, it is sometimes interesting to look for correlations between connectivity parameters in patients and their phenotype or genotype. This helps to interpret differences between patients and controls and to determine whether any connectivity pattern can serve as a biomarker for a particular deficit or signature of a particular reorganization mechanism.

CONCEPTUAL AND METHODOLOGICAL ISSUES

Other conceptual and methodological issues should be acknowledged when using DCM in patients (see for instance Daunizeau et al., 2010). We focus here on five issues that we believe are crucial for interpreting or generalizing DCM findings. All five warrant further systematic investigations, on both simulated and real data, in order to characterize their influences.

(1) Effective connectivity, like functional responses, varies across subjects. Although group effects are easy to report and important in showing the most consistent effects in a given population, variable connectivity patterns across patients can indicate different ways a given deficit can be expressed and the strategies that patients may be using to compensate for those deficits. It is also possible that variability may change with the level of inference, as shown recently in a group of patients with Parkinson's disease where inferences at the model level were more reliable and reproducible than inferences at the connection level (e.g., Rowe et al., 2010).

(2) The network of areas included in a DCM are typically only part of the complete and complex neural system that supports the task. Therefore, the inter-regional interactions within the selected sub-network are only a parsimonious model of the "true" system.

(3) The problem of missing nodes is crucial for DCM (see Smith et al., 2010). As highlighted above, the deterministic DCM will only test the differences in connectivity within the commonly activated network, ignoring the regional effects that are absent or novel in patients compared to controls. For this reason we have suggested that the abnormalities should be reported at the level of regions in addition to the level of connectivity.

(4) The remote effect of abnormal connectivity in another network. This problem concerns the influence of abnormal parts in a subsystem that may propagate to other networks causing "indirect" abnormal connectivity in the subsystem of interest. For instance, it is possible that damaged parts within one functional system manifest as abnormal connectivity that is not necessarily related to the main task/process of interest. This effect is linked to the more global problem of the missing nodes that can sometimes be sufficiently strong to invalidate DCM results of a given subsystem (see discussion in Daunizeau et al., 2010).

(5) How generalizable are conclusions concerning abnormal connectivity? This issue is particularly critical for studies that aim to define a biomarker for a given pathology. First, the results identified in a particular group of subjects can only be translated to other subjects that show significant effects in all the regions of interest. What then happens when patients have one or two missing nodes? Second, generalizability also depends on abnormalities that manifest outside the network of interest, because the effects could have indirect influences on the sub-network of interest. This problem concerns all levels of inference in the implementation of deterministic DCM and should be carefully considered when generalizations are made about abnormal connectivity. It is even more critical if one is interested in making inferences at the individual level (e.g., if abnormal connectivity is being used as a biomarker for distinguishing between patients and controls or for classifying new patients). Nevertheless, it should be noted that patient and control connectivity parameters represent the same thing and are directly comparable when the analysis of patient and control data is based on the identical model space with identical priors for the model parameters (including those for the forward hemodynamic model and those for neuronal coupling).

FUTURE DEVELOPMENTS

In addition to the methodological issues highlighted above that warrant further investigations, other developments can potentially add more flexibility to the use of DCM in patient studies. We focus here on four future developments: (1) quantify the vulnerability of a given network after damage, (2) sample the model space in an unconstrained manner, (3) include new computational models in DCM, and (4) combine DCM with other approaches.

(1) *Quantifying the vulnerability of the network to damage.* Parallels can be made with the increased interest in graph theory for complex brain network analysis (for review see Bassett and Bullmore, 2009; Bullmore and Sporns, 2009; Bressler and Menon, 2010; Guye et al., 2010). Using graph theory, previous studies have investigated connectivity changes that result from an insult to a given part of the network (e.g., Kaiser et al., 2007; Honey and Sporns, 2008; Alstott et al., 2009), for instance by using structural network properties of the lesion site to predict the functional (i.e., dynamic) consequences of the focal damage. This literature has yielded the development of different measures to quantify the "resilience" or the "vulnerability" of a given network after insult (see different coefficients in Rubinov and Sporns, 2010) and also proposed new statistical approaches for identifying differences in networks between patients and controls (see Zalesky et al., 2010). The translation of these sorts of measures to the DCM framework would be a valuable contribution for future studies of patients.

(2) *Sampling model space in an unconstrained manner.* Defining the model space in a comprehensive way is a challenging step (e.g., see critique in Tauchmanova and Hromcik, 2008), in particular when the number of nodes or inputs is relatively high. One exciting possibility is the ability to sparsely sample

the model space in order to produce an approximation of the best model structure. For instance, using Gaussian Processes, it has been shown that it is possible to identify the optimal model structure based on the selected subsample of models (for more details see Anderson and Lane, 2009). We believe this kind of future development will increase the robustness of DCM when exploring large model spaces and will allow the structure of complex models to be identified.

(3) *Including new computational models*. There is also an exciting opportunity to combine previous computational models with DCM (for detailed discussion see Friston and Dolan, 2010). For instance, previous models from computational neuroscience and theoretical neurobiology can be linked to a particular behavior or pathology (e.g., in patients with schizophrenia, Friston, 1996, or Alzheimer's disease, Hasselmo, 1997) that can then be tested with DCM. Previous theoretical models constitute an interesting source of hypotheses that can inform the formation of the model space in DCM.

(4) *Combining DCM with other approaches*. One crucial step in DCM is the identification of a subset of regions of interest that is usually based on an *a priori* knowledge. This hypothesis-driven step may leave several other activated regions unexplored. In this context, data-driven approaches can be used to explore the whole pattern and reduce it to a set of representative nodes that can then be incorporated into DCM (see de Marco et al., 2009). For instance, during a go/no-go task, a previous study has used independent component analysis to identify three response inhibition components and then DCM was used to assess the interactions between these components (Stevens et al., 2007). Recently, a new method called the switching linear dynamic systems was developed to identify important regions that might be left out during the specification of models (Smith et al., 2010). This method explicitly models the task factor as a Markov random variable and it aims to objectively measure the overall quality and sufficiency of an identified model (see illustration with a motor task in Smith et al., 2010).

CONCLUSION

We have succinctly reviewed the available DCM frameworks for fMRI responses that can be applied to characterize brain disorders at the level of networks and their dynamics. The previous literature has demonstrated the feasibility of DCM in diverse populations of patients and has provided valuable insights that characterize the dynamic signatures of focal and non-focal pathologies. We believe the growing use of DCM will shape the field of brain network dynamics and will have an important impact on the future development of theoretical neurobiology and clinical biomarkers.

ACKNOWLEDGMENTS

This work was funded by the Wellcome Trust and the James S. MacDonnell Foundation (conducted as part of the Brain Network Recovery Group initiative).

REFERENCES

Abutalebi, J., Rosa, P. A., Tettamanti, M., Green, D. W., and Cappa, S. F. (2009). Bilingual aphasia and language control: a follow-up fMRI and intrinsic connectivity study. *Brain Lang.* 109, 141–156.

Acs, F., and Greenlee, M. W. (2008). Connectivity modulation of early visual processing areas during covert and overt tracking tasks. *Neuroimage* 41, 380–388.

Agosta, F., Rocca, M. A., Pagani, E., Absinta, M., Magnani, G., Marcone, A., Falautano, M., Comi, G., Gorno-Tempini, M. L., and Filippi, M. (2010). Sensorimotor network rewiring in mild cognitive impairment and Alzheimer's disease. *Hum. Brain Mapp.* 31, 515–525.

Alexander, W. H., and Brown, J. W. (2010). Competition between learned reward and error outcome predictions in anterior cingulate cortex. *Neuroimage* 49, 3210–3218.

Allen, P., Stephan, K. E., Mechelli, A., Day, F., Ward, N., Dalton, J., Williams, S. C., and McGuire, P. (2010). Cingulate activity and fronto-temporal connectivity in people with prodromal signs of psychosis. *Neuroimage* 49, 947–955.

Almeida, J. R., Mechelli, A., Hassel, S., Versace, A., Kupfer, D. J., and Phillips, M. L. (2009a). Abnormally increased effective connectivity between parahippocampal gyrus and ventromedial prefrontal regions during emotion labeling in bipolar disorder. *Psychiatry Res* 174, 195–201.

Almeida, J. R., Versace, A., Mechelli, A., Hassel, S., Quevedo, K., Kupfer, D. J., and Phillips, M. L. (2009b). Abnormal amygdala-prefrontal effective connectivity to happy faces differentiates bipolar from major depression. *Biol. Psychiatry* 66, 451–459.

Alstott, J., Breakspear, M., Hagmann, P., Cammoun, L., and Sporns, O. (2009). Modeling the impact of lesions in the human brain. *PLoS Comput. Biol.* 5, e1000408. doi: 10.1371/journal.pcbi.1000408.

Anderson, B., and Lane, T., 2009. Fast Bayesian network structure search using Gaussian processes. Available at http://www.cs.unm.edu/~treport/tr/09-06/paper.pdf, 1–15.

Bassett, D. S., and Bullmore, E. T. (2009). Human brain networks in health and disease. *Curr. Opin. Neurol.* 22, 340–347.

Benetti, S., Mechelli, A., Picchioni, M., Broome, M., Williams, S., and McGuire, P. (2009). Functional integration between the posterior hippocampus and prefrontal cortex is impaired in both first episode schizophrenia and the at risk mental state. *Brain* 132, 2426–2436.

Bird, G., Catmur, C., Silani, G., Frith, C., and Frith, U. (2006). Attention does not modulate neural responses to social stimuli in autism spectrum disorders. *Neuroimage* 31, 1614–1624.

Bressler, S. L., and Menon, V. (2010). Large-scale brain networks in cognition: emerging methods and principles. *Trends Cogn. Sci. (Regul. Ed.)* 14, 277–290.

Bullmore, E., and Sporns, O. (2009). Complex brain networks: graph theoretical analysis of structural and functional systems. *Nat. Rev. Neurosci.* 10, 186–198.

Cao, F., Bitan, T., and Booth, J. R. (2008). Effective brain connectivity in children with reading difficulties during phonological processing. *Brain Lang.* 107, 91–101.

Carreiras, M., Seghier, M. L., Baquero, S., Estevez, A., Lozano, A., Devlin, J. T., and Price, C. J. (2009). An anatomical signature for literacy. *Nature* 461, 983–986.

Catani, M., and Thiebaut de Schotten, M. (2008). A diffusion tensor imaging tractography atlas for virtual in vivo dissections. *Cortex* 44, 1105–1132.

Chow, H. M., Kaup, P., Raabe, M., and Greenlee, M. W. (2008). Evidence of fronto-temporal interactions for strategic inference processes during language comprehension. *Neuroimage* 40, 940–954.

Crossley, N. A., Mechelli, A., Fusar-Poli, P., Broome, M. R., Matthiasson, P., Johns, L. C., Bramon, E., Valmaggia, L., Williams, S. C., and McGuire, P. K. (2009). Superior temporal lobe dysfunction and frontotemporal dysconnectivity in subjects at risk of psychosis and in first-episode psychosis. *Hum. Brain Mapp.* 30, 4129–4137.

Daunizeau, J., David, O., and Stephan, K. E. (2010). Dynamic causal modelling: a critical review of the biophysical and statistical foundations. *Neuroimage* doi: 10.1016/j.neuroimage.2009.11.062. (in press).

Daunizeau, J., Friston, K. J., and Kiebel, S. J. (2009). Variational Bayesian identification and prediction of stochastic nonlinear dynamic causal models. *Physica D* 238, 2089–2118.

de Marco, G., Devauchelle, B., and Berquin, P. (2009). Brain functional modeling, what do we measure with fMRI data? *Neurosci. Res.* 64, 12–19.

Dempster, A. P., Laird, N. M., and Rubin, D. B. (1977). Maximum Likelihood from Incomplete Data via the EM Algorithm. *J. R. Stat. Soc. Series B* 39, 1–38.

den Ouden, H. E., Daunizeau, J., Roiser, J., Friston, K. J., and Stephan, K. E. (2010). Striatal prediction error modulates

cortical coupling. *J. Neurosci.* 30, 3210–3219.

Dima, D., Roiser, J. P., Dietrich, D. E., Bonnemann, C., Lanfermann, H., Emrich, H. M., and Dillo, W. (2009). Understanding why patients with schizophrenia do not perceive the hollow-mask illusion using dynamic causal modelling. *Neuroimage* 46, 1180–1186.

Doeller, C. F., King, J. A., and Burgess, N. (2008). Parallel striatal and hippocampal systems for landmarks and boundaries in spatial memory. *Proc. Natl. Acad. Sci. U.S.A.* 105, 5915–5120.

Eickhoff, S. B., Dafotakis, M., Grefkes, C., Shah, N. J., Zilles, K., and Piza-Katzer, H. (2008). Central adaptation following heterotopic hand replantation probed by fMRI and effective connectivity analysis. *Exp. Neurol.* 212, 132–144.

Eickhoff, S. B., Heim, S., Zilles, K., and Amunts, K. (2009). A systems perspective on the effective connectivity of overt speech production. *Philos Transact A Math Phys Eng Sci* 367, 2399–2421.

Ethofer, T., Anders, S., Erb, M., Herbert, C., Wiethoff, S., Kissler, J., Grodd, W., and Wildgruber, D. (2006). Cerebral pathways in processing of affective prosody: a dynamic causal modeling study. *Neuroimage* 30, 580–587.

Fairhall, S. L., and Ishai, A. (2007). Effective connectivity within the distributed cortical network for face perception. *Cereb. Cortex* 17, 2400–2406.

Fan, J., Hof, P. R., Guise, K. G., Fossella, J. A., and Posner, M. I. (2008). The functional integration of the anterior cingulate cortex during conflict processing. *Cereb. Cortex* 18, 796–805.

Fan, L. Y., Lee, S. H., and Chou, T. L. (2010). Interaction between brain regions during semantic processing in Chinese adults. *Lang. Linguist.* 11, 159–182.

Friston, K. J. (1994). Functional and effective connectivity in neuroimaging: a synthesis. *Hum. Brain Mapp.* 2, 56–78.

Friston, K. J. (1996). Theoretical neurobiology and schizophrenia. *Br. Med. Bull.* 52, 644–655.

Friston, K. J. (2002a). Bayesian estimation of dynamical systems: an application to fMRI. *Neuroimage* 16, 513–530.

Friston, K. J. (2002b). Functional integration and inference in the brain. *Prog. Neurobiol.* 68, 113–143.

Friston, K. J. (2007). "Functional integration," in *Statistical Parametric Mapping: The Analysis of Functional Brain Images*, eds K. J. Friston, J. T. Ashburner, S. J. Kiebel, T. E. Nichols, and W. D. Penny (London: Elsevier), 471–491.

Friston, K. J. (2009a). Causal modelling and brain connectivity in functional magnetic resonance imaging. *PLoS Biol.* 7, e1000033. doi: 10.1371/journal.pbio.1000033.

Friston, K. J. (2009b). Modalities, modes, and models in functional neuroimaging. *Science* 326, 399–403.

Friston, K. J., Buechel, C., Fink, G. R., Morris, J., Rolls, E., and Dolan, R. J. (1997). Psychophysiological and modulatory interactions in neuroimaging. *Neuroimage* 6, 218–229.

Friston, K. J., and Dolan, R. J. (2010). Computational and dynamic models in neuroimaging. *Neuroimage* 52, 752–765.

Friston, K. J., Harrison, L., and Penny, W. (2003). Dynamic causal modelling. *Neuroimage* 19, 1273–1302.

Friston, K. J., Mattout, J., Trujillo-Barreto, N., Ashburner, J., and Penny, W.D. (2007). "Variational Bayes under the Laplace approximation," in *Statistical Parametric Mapping: The Analysis of Functional Brain Images*, eds K. J. Friston, J. T. Ashburner, S. J. Kiebel, T. E. Nichols, and W. D. Penny. (London: Elsevier), 606–618.

Fujii, T., Tanabe, H. C., Kochiyama, T., and Sadato, N. (2009). An investigation of cross-modal plasticity of effective connectivity in the blind by dynamic causal modeling of functional MRI data. *Neurosci. Res.* 65, 175–186.

Goulden, N., McKie, S., Suckling, J., Williams, S. R., Anderson, I. M., Deakin, J. F., and Elliott, R. (2010). A comparison of permutation and parametric testing for between group effective connectivity differences using DCM. *Neuroimage* 50, 509–515.

Grefkes, C., Nowak, D. A., Eickhoff, S. B., Dafotakis, M., Küst, J., Karbe, H., and Fink, G. R. (2008). Cortical connectivity after subcortical stroke assessed with functional magnetic resonance imaging. *Ann. Neurol.* 63, 236–246.

Grefkes, C., Nowak, D. A., Wang, L. E., Dafotakis, M., Eickhoff, S. B., and Fink, G. R. (2010). Modulating cortical connectivity in stroke patients by rTMS assessed with fMRI and dynamic causal modeling. *Neuroimage* 50, 233–242.

Grezes, J., WIcker, B., Berthoz, S., and de Gelder, B. (2009). A failure to grasp the affective meaning of actions in autism spectrum disorder subjects. *Neuropsychologia* 47, 1816–1825.

Grol, M. J., Majdandzić, J., Stephan, K. E., Verhagen, L., Dijkerman, H. C., Bekkering, H., Verstraten, F. A., and Toni, I. (2007). Parieto-frontal connectivity during visually guided grasping. *J. Neurosci.* 27, 11877–11887.

Guye, M., Bettus, G., Bartolomei, F., and Cozzone, P. J. (2010). Graph theoretical analysis of structural and functional connectivity MRI in normal and pathological brain networks. *MAGMA* doi: 10.1007/s10334-010-0205-z (in press).

Hamandi, K., Powell, H. W., Laufs, H., Symms, M. R., Barker, G. J., Parker, G. J., Lemieux, L., and Duncan, J. S. (2008). Combined EEG-fMRI and tractography to visualise propagation of epileptic activity. *J. Neurol. Neurosurg. Psychiatr.* 79, 594–597.

Harrison, L., Penny, W., and Friston, K. J. (2003). Multivariate autoregressive modeling of fMRI time series. *Neuroimage* 19, 1477–1491.

Harrison, L. M., Stephan, K. E., and Friston, K. J. (2007). "Effective connectivity," in *Statistical Parametric Mapping: The Analysis of Functional Brain Images*, eds K. J. Friston, J. T. Ashburner, S. J. Kiebel, T. E. Nichols, and W. D. Penny (London: Elsevier), 508–521.

Hasselmo, M. E. (1997). A computational model of the progression of Alzheimer's disease. *MD Comput.* 14, 181–191.

He, B. J., Shulman, G. L., Snyder, A. Z., and Corbetta, M. (2007). The role of impaired neuronal communication in neurological disorders. *Curr. Opin. Neurol.* 20, 655–660.

Heim, S., Eickhoff, S. B., Ischebeck, A. K., Friederici, A. D., Stephan, K. E., and Amunts, K. (2009). Effective connectivity of the left BA 44, BA 45, and inferior temporal gyrus during lexical and phonological decisions identified with DCM. *Hum. Brain Mapp.* 30, 392–402.

Honey, C. J., and Sporns, O. (2008). Dynamical consequences of lesions in cortical networks. *Hum. Brain Mapp.* 29, 802–809.

Horwitz, B., McIntosh, A. R., Haxby, J. V., Furey, M., Salerno, J. A., Schapiro, M. B., Rapoport, S. I., and Grady, C. L. (1995). Network analysis of PET-mapped visual pathways in Alzheimer type dementia. *Neuroreport* 6, 2287–2292.

Kaiser, M., Martin, R., Andras, P., and Young, M. P. (2007). Simulation of robustness against lesions of cortical networks. *Eur. J. Neurosci.* 25, 3185–3192.

Kasess, C. H., Windischberger, C., Cunnington, R., Lanzenberger, R., Pezawas, L., and Moser, E. (2008). The suppressive influence of SMA on M1 in motor imagery revealed by fMRI and dynamic causal modeling. *Neuroimage* 40, 828–837.

Kim, J., and Horwitz, B. (2009). How well does structural equation modeling reveal abnormal brain anatomical connections? An fMRI simulation study. *Neuroimage* 45, 1190–1198.

Leff, A. P., Schofield, T. M., Stephan, K. E., Crinion, J. T., Friston, K. J., and Price, C. J. (2008). The cortical dynamics of intelligible speech. *J. Neurosci.* 28, 13209–13215.

Li, J., Liu, J., Liang, J., Zhang, H., Zhao, J., Rieth, C. A., Huber, D. E., Li, W., Shi, G., Ai, L., Tian, J., and Lee, K. (2010a). Effective connectivities of cortical regions for top-down face processing: a dynamic causal modeling study. *Brain Res.* 1340, 40–51.

Li, X., Marrelec, G., Hess, R. F., and Benali, H. (2010b). A nonlinear identification method to study effective connectivity in functional MRI. *Med. Image Anal.* 14, 30–38.

Li, K., Guo, L., Nie, J., Li, G., and Liu, T. (2009). Review of methods for functional brain connectivity detection using fMRI. *Comput. Med. Imaging. Graph.* 33, 131–139.

Marreiros, A. C., Kiebel, S. J., and Friston, K. J. (2008). Dynamic causal modelling for fMRI: a two-state model. *Neuroimage* 39, 269–278.

Marrelec, G., Kim, J., Doyon, J., and Horwitz, B. (2009). Large-scale neural model validation of partial correlation analysis for effective connectivity investigation in functional MRI. *Hum. Brain Mapp.* 30, 941–950.

McIntosh, A. R. (2000). Towards a network theory of cognition. *Neural. Netw.* 13, 861–870.

McIntosh, A. R., and Gonzalez-Lima, F. (1994). Structural equation modeling and its application to network analysis in functional brain imaging. *Hum. Brain Mapp.* 2, 2–22.

Mechelli, A., Allen, P., Amaro, E. J., Fu, C. H., Williams, S. C., Brammer, M. J., Johns, L. C., and McGuire, P. K. (2007). Misattribution of speech and impaired connectivity in patients with auditory verbal hallucinations. *Hum. Brain Mapp.* 28, 1213–1222.

Meyer-Lindenberg, A., Poline, J. B., Kohn, P. D., Holt, J. L., Egan, M. F., Weinberger, D. R., and Berman, K. F. (2001). Evidence for abnormal cortical functional connectivity during working memory in schizophrenia. *Am. J. Psychiatry* 158, 1809–1817.

Mintzopoulos, D., Astrakas, L. G., Khanicheh, A., Konstas, A. A., Singhal, A., Moskowitz, M. A., Rosen, B. R., and Tzika, A. A. (2009). Connectivity alterations assessed by combining fMRI and MR-compatible hand robots in chronic stroke. *Neuroimage* 47, T90-T97.

Miyake, Y., Okamoto, Y., Onoda, K., Shirao, N., Okamoto, Y., Otagaki, Y., and Yamawaki, S. (2010). Neural processing of negative word stimuli concerning body image in patients with eating disorders: an fMRI study. *Neuroimage* 50, 1333–1339.

Mori, S., Oishi, K., Jiang, H., Jiang, L., Li, X., Akhter, K., Hua, K., Faria, A.

V., Mahmood, A., Woods, R., Toga, A. W., Pike, G. B., Neto, P. R., Evans, A., Zhang, J., Huang, H., Miller, M. I., van Zijl, P., and Mazziotta, J. (2008). Stereotaxic white matter atlas based on diffusion tensor imaging in an ICBM template. *Neuroimage* 40, 570–582.

Mori, S., Wakana, S., van Zijl, P. C. M., and Nagae-Poetscher, L. M. (2005). *MRI Atlas of Human White Matter*. Amsterdam Elsevier.

Penny, W. D., Stephan, K. E., Daunizeau, J., Rosa, M. J., Friston, K. J., Schofield, T. M., and Leff, A. P. (2010). Comparing families of dynamic causal models. *PLoS Comput. Biol.* 6, e1000709. doi: 10.1371/journal.pcbi.1000709.

Penny, W. D., Stephan, K. E., Mechelli, A., and Friston, K. J. (2004). Modelling functional integration: a comparison of structural equation and dynamic causal models. *Neuroimage* 23, S264–S274.

Plailly, J., Howard, J. D., Gitelman, D. R., and Gottfried, J. A. (2008). Attention to odor modulates thalamocortical connectivity in the human brain. *J. Neurosci.* 28, 5257–5267.

Price, C. J., Crinion, J., and Friston, K. J. (2006). Design and analysis of fMRI studies with neurologically impaired patients. *J. Magn. Reson. Imaging* 23, 816–826.

Rajapakse, J. C., and Zhou, J. (2007). Learning effective brain connectivity with dynamic Bayesian networks. *Neuroimage* 37, 749–760.

Ramnani, N., Behrens, T. E., Penny, W. D., and Matthews, P. M. (2004). New approaches for exploring anatomical and functional connectivity in the human brain. *Biol. Psychiatry* 56, 613–619.

Rocca, M. A., Pagani, E., Absinta, M., Valsasina, P., Falini, A., Scotti, G., Comi, G., and Filippi, M. (2007a). Altered functional and structural connectivities in patients with MS. *Neurology* 69, 2136–2145.

Rocca, M. A., Valsasina, P., Ceccarelli, A., Absinta, M., Ghezzi, A., Riccitelli, G., Pagani, E., Falini, A., Comi, G., Scotti, G., and Filippi, M. (2007b). Structural and functional MRI correlates of Stroop control in benign MS. *Hum. Brain Mapp.* 30, 276–290.

Roebroeck, A., Formisano, E., and Goebel, R. (2005). Mapping directed influence over the brain using Granger causality and fMRI. *Neuroimage* 25, 230–242.

Rogers, B. P., Morgan, V. L., Newton, A. T., and Gore, J. C. (2007). Assessing functional connectivity in the human brain by fMRI. *Magn. Reson. Imaging* 25, 1347–1357.

Rowe, J. B., Hughes, L. E., Barker, R. A., and Owen, A. M. (2010). Dynamic causal modelling of effective connectivity from fMRI: are results reproducible and sensitive to Parkinson's disease and its treatment? *Neuroimage* 52, 1015–1026.

Rubinov, M., and Sporns, O. (2010). Complex network measures of brain connectivity: uses and interpretations. *Neuroimage* 52, 1059–1069.

Schlosser, R. G., Wagner, G., Koch, K., Dahnke, R., Reichenbach, J. R., and Sauer, H. (2008). Fronto-cingulate effective connectivity in major depression: a study with fMRI and dynamic causal modeling. *Neuroimage* 43, 645–655.

Schlosser, R. G., Wagner, G., Schachtzabel, C., Peikert, G., Koch, K., Reichenbach, J. R., and Sauer, H. (2010). Fronto-cingulate effective connectivity in obsessive compulsive disorder: a study with fMRI and dynamic causal modeling. *Hum. Brain Mapp.* doi: 10.1002/hbm.20980 (in press).

Seghier, M. L., and Price, C. J. (2010). Reading aloud boosts connectivity through the putamen. *Cereb. Cortex* 20, 570–582.

Shannon, K. E., Sauder, C., Beachaine, T. P., and Gatzke-Kopp, L. M. (2009). Disrupted effective connectivity between the medial frontal cortex and the caudate in adolescent boys with externalizing behavior disorders. *Crim. Justice Behav.* 36, 1141–1157.

Smith, A. P., Stephan, K. E., Rugg, M. D., and Dolan, R. J. (2006). Task and content modulate amygdala-hippocampal connectivity in emotional retrieval. *Neuron* 49, 631–638.

Smith, J. F., Pillai, A., Chen, K., and Horwitz, B. (2010). Identification and validation of effective connectivity networks in functional magnetic resonance imaging using switching linear dynamic systems. *Neuroimage* 52, 1027–1040.

Sonty, S. P., Mesulam, M. M., Weintraub, S., Johnson, N. A., Parrish, T. B., and Gitelman, D. R. (2007). Altered effective connectivity within the language network in primary progressive aphasia. *J. Neurosci.* 27, 1334–1345.

Stephan, K. E., Harrison, L. M., Kiebel, S. J., David, O., Penny, W. D., and Friston, K. J. (2007). Dynamic causal models of neural system dynamics: current state and future extensions. *J. Biosci.* 32, 129–144.

Stephan, K. E., Kasper, L., Harrison, L. M., Daunizeau, J., den Ouden, H. E., Breakspear, M., and Friston, K. J. (2008). Nonlinear dynamic causal models for fMRI. *Neuroimage* 42, 649–662.

Stephan, K. E., Penny, W. D., Daunizeau, J., Moran, R. J., and Friston, K. J. (2009a). Bayesian model selection for group studies. *Neuroimage* 46, 1004–1017.

Stephan, K. E., Tittgemeyer, M., Knosche, T. R., Moran, R. J., and Friston, K. J. (2009b). Tractography-based priors for dynamic causal models. *Neuroimage* 47, 1628–1638.

Stephan, K. E., Penny, W. D., Moran, R. J., den Ouden, H. E., Daunizeau, J., and Friston, K. J. (2010). Ten simple rules for dynamic causal modeling. *Neuroimage* 49, 3099–3109.

Stevens, M. C., Kiehl, K. A., Pearlson, G. D., and Calhoun, V. D. (2007). Functional neural networks underlying response inhibition in adolescents and adults. *Behav. Brain Sci.* 181, 12–22.

Tauchmanova, J., and Hromcik, M. (2008). *Subspace Identification Methods and fMRI Analysis*. 30th Annual International IEEE EMBS Conference, Vancouver, 4427-4430.

Vaudano, A. E., Laufs, H., Kiebel, S. J., Carmichael, D. W., Hamandi, K., Guye, M., Thornton, R., Rodionov, R., Friston, K. J., Duncan, J. S., and Lemieux, L. (2009). Causal hierarchy within the thalamo-cortical network in spike and wave discharges. *PLoS ONE* 4, e6475. doi: 10.1371/journal.pone.0006475.

Wang, L., Liu, X., Guise, K. G., Knight, R. T., Ghajar, J., and Fan, J. (2010). Effective connectivity of the fronto-parietal network during attentional control. *J. Cogn. Neurosci.* 22, 543–553.

Ween, J. E. (2008). Functional imaging of stroke recovery: an ecological review from a neural network perspective with an emphasis on motor systems. *J. Neuroimaging* 18, 227–236.

Witt, S. T., and Meyerand, M. E. (2009). The effects of computational method, data modeling, and TR on effective connectivity results. *Brain Imaging Behav.* 3, 220–231.

Zalesky, A., Fornito, A., and Bullmore, E. T. (2010). Network-based statistic: identifying differences in brain networks. *Neuroimage* doi: 10.1016/j.neuroimage.2010.06.041 (in press).

Conflict of Interest Statement: The authors declare that the research was conducted in the absence of any commercial or financial relationships that could be construed as a potential conflict of interest.

Received: 21 June 2010; paper pending published: 27 July 2010; accepted: 12 August 2010; published online: 26 August 2010.
Citation: Seghier ML, Zeidman P, Neufeld NH, Leff AP and Price CJ (2010) Identifying abnormal connectivity in patients using dynamic causal modeling of fMRI responses. Front. Syst. Neurosci. ***4****:142. doi: 10.3389/fnsys.2010.00142*
Copyright © 2010 Seghier, Zeidman, Neufeld, Leff and Price. This is an open-access article subject to an exclusive license agreement between the authors and the Frontiers Research Foundation, which permits unrestricted use, distribution, and reproduction in any medium, provided the original authors and source are credited.

frontiers in
SYSTEMS NEUROSCIENCE

REVIEW ARTICLE
published: 12 August 2010
doi:10.3389/fnsys.2010.00040

Transcranial magnetic stimulation and connectivity mapping: tools for studying the neural bases of brain disorders

M. Hampson[1]* and R. E. Hoffman[2]

[1] *Department of Diagnostic Radiology, Yale University School of Medicine, New Haven, CT, USA*
[2] *Department of Psychiatry, Yale University School of Medicine, New Haven, CT, USA*

Edited by:
Silvina G. Horovitz, National Institutes of Health, USA

Reviewed by:
Daryl E. Bohning, Medical University of South Carolina, USA
Nik Sharma, National Institutes of Health, USA

****Correspondence:***
Michelle Hampson, Yale University, MRRC, TAC-N121, 300 Cedar Street, P. O. Box 208042, New Haven, CT 06520-8042, USA.
e-mail: michelle.hampson@yale.edu

There has been an increasing emphasis on characterizing pathophysiology underlying psychiatric and neurological disorders in terms of altered neural connectivity and network dynamics. Transcranial magnetic stimulation (TMS) provides a unique opportunity for investigating connectivity in the human brain. TMS allows researchers and clinicians to directly stimulate cortical regions accessible to electromagnetic coils positioned on the scalp. The induced activation can then propagate through long-range connections to other brain areas. Thus, by identifying distal regions activated during TMS, researchers can infer connectivity patterns in the healthy human brain and can examine how those patterns may be disrupted in patients with different brain disorders. Conversely, connectivity maps derived using neuroimaging methods can identify components of a dysfunctional network. Nodes in this dysfunctional network accessible as targets for TMS by virtue of their proximity to the scalp may then permit TMS-induced alterations of components of the network not directly accessible to TMS via propagated effects. Thus TMS can provide a portal for accessing and altering neural dynamics in networks that are widely distributed anatomically. Finally, when long-term modulation of network dynamics is induced by trains of repetitive TMS, changes in functional connectivity patterns can be studied in parallel with changes in patient symptoms. These correlational data can elucidate neural mechanisms underlying illness and recovery. In this review, we focus on the application of these approaches to the study of psychiatric and neurological illnesses.

Keywords: transcranial magnetic stimulation, connectivity, psychiatry, neurology, brain disorders, resting, stimulation

INTRODUCTION

Transcranial magnetic stimulation (TMS) allows focal, non-invasive stimulation of the human brain using very brief duration magnetic waves administered by an electromagnetic coil positioned on the scalp. Stimulation coils typically generate magnetic field pulses of approximately 1.5–2 T that pass relatively undistorted through the scalp and skull (George et al., 1999). Rapidly oscillating magnetic fields within the brain induce corresponding electrical fields, which stimulate underlying gray matter. A standard figure-8 configured coil achieves relatively focal direct stimulation with a 2–2.5 cm diameter spread at the cortical surface under the crossing of the figure-8, while a circular coil delivers a wider spread of stimulation (Cohen et al., 1990). Direct neural activation is achieved up to ~2 cm from the surface of the magnet (Rudiak and Marg, 1994), which is sufficient to reach the gray/white interface of cortex adjacent to skull. The exact nature of neural effects induced by TMS is not known, but complex, enduring changes in spontaneous and evoked activity and synchronization of neural firing have been shown to be induced when administered to the cat visual cortex (Allen et al., 2007). Overall, TMS has proved to be relatively safe with a few cases of seizures associated primarily with repetitive stimulation at higher frequencies (i.e., 10 Hz or above, Wassermann, 1998; Rossi et al., 2009). Although momentary virtual "lesions" can be induced by TMS that are detectable via neuropsychological methods (Walsh and Rushworth, 1999), sustained cognitive disturbances induced by TMS in humans have not been observed (Pascual-Leone et al., 1993; Rossi et al., 2009).

Excellent reviews of TMS from the perspectives of neuropsychology (Walsh and Rushworth, 1999), psychiatry (George et al., 1999) neurology (Rossini and Rossi, 2007) and safety (Rossi et al., 2009) have been published. In this review, we focus primarily on approaches in which connectivity mapping and TMS can be used in conjunction to study neurological and psychiatric disorders in order to provide a sense of the more common available techniques and examples of these approaches. By connectivity mapping, we mean imaging techniques that assess connectivity between distal brain areas, such as functional connectivity analyses and diffusion tensor imaging. Thus, we focus primarily on TMS studies of inter-regional, rather than intraregional, connectivity.

Another form of non-invasive brain stimulation, transcranial direct current stimulation, or tDCS, can produce changes in brain excitability that can persist for a period of time after stimulation (Priori, 2003). To date, this technology has been less extensively used in conjunction with connectivity mapping, and will not be covered in this review except to note that several recent papers have reported that tDCS may modulate distal brain areas via inter-regional connectivity (Boros et al., 2008; Galea et al., 2009; Stagg et al., 2009).

TYPES OF STIMULATION

There are two broad classes of stimulation paradigms for TMS: single/paired/triple-pulse paradigms, and repetitive stimulation paradigms.

SINGLE/PAIRED/TRIPLE-PULSE

Single pulse TMS can be used to interfere with activity in the stimulated region, and thus to act as a temporary lesion. By applying such pulses at different times and to different regions, and examining the behavioral consequences, the roles of different regions in a cognitive process, and their temporal dynamics, can be studied (Terao et al., 1998; Zangaladze et al., 1999). A single pulse does not always have an inhibitory effect on a region: in some cases, facilitatory effects have been reported (Grosbras and Paus, 2002). However, the temporal profile of such facilitatory effects can also be informative.

Paired-pulse paradigms can be used to investigate interactions between motor or visual regions of the brain. When applied to the primary motor cortex (M1), a single pulse can induce a motor evoked potential (and the corresponding body movement), and when applied to the primary visual cortex (V1), the perception of a phosphene can be induced. The response elicited by a single pulse (that is, the motor evoked potential or phosphene) can be modulated by the application of preceding pulses in the same, or a connected brain region in a manner dependent on the temporal relationship of the pulses. In this fashion, paired pulses, that is, a conditioning pulse followed by a test pulse, can be used to examine connectivity and cortical dynamics in the motor and visual systems.

More complex aspects of cortical dynamics can be studied with triple-pulse paradigms. The effect of a conditioning pulse on a subsequent test pulse can be altered by preceding them both with an earlier pulse. Paradigms like this have been used to investigate the possible cellular mechanisms underlying different forms of intracortical inhibition and facilitation (Sanger et al., 2001) and to investigate how intracortical dynamics affect interregional interactions (Koch et al., 2007).

REPETITIVE TMS

Repetitive stimulation typically involves short trains of high-frequency stimulation (≥5 Hz) or long trains of low-frequency stimulation (≤2 Hz) applied at a single site. Low-frequency stimulation typically results in depression of the target brain area for a period of time following stimulation, while high-frequency stimulation typically induces facilitation of the region (Pascual-Leone et al., 1994; Chen et al., 1997; Speer et al., 2000). However, one particular high-frequency stimulation paradigm, referred to as theta burst stimulation, can produce either inhibitory or facilitatory effects that extend for many minutes after stimulation (Huang et al., 2005). This paradigm involves short bursts of very high-frequency stimulation (3 pulses at 50 Hz) repeated at 200 ms interval (which corresponds to the 5 Hz theta frequency). If the stimulation pattern is applied continuously, facilitatory effects are produced, but when applied intermittently (2 s trains repeated every 10 s), inhibitory effects can result.

Repetitive TMS (rTMS) has been investigated as a treatment for a variety of psychiatric illnesses. By examining behavioral, clinical, or cognitive changes before and after rTMS, repetitive stimulation can also be used in basic research to study how perturbations in activity in a focal brain area affect the network function.

INVESTIGATING CONNECTIVITY WITH TMS ALONE

Single-pulse TMS paradigms can, in some scenarios, provide information regarding connectivity in the human brain. The excitability of the primary motor and visual cortices can vary depending on the cognitive context in which stimulation occurs, and this dependence on cognitive state provides a window into the connectivity between these areas and cognitive regions. For example, during some language tasks, the motor cortical hand area in the language dominant hemisphere of healthy subjects is more excitable, as reflected by larger motor evoked potentials recorded following TMS (Tokimura et al., 1996; Meister et al., 2003). This finding provides evidence of functional connectivity between the hand area of motor cortex and language areas in healthy subjects, and allows investigation of the integrity of these connections in patient groups. In patients with mild cognitive impairment, for example, language tasks were shown to have a reduced effect on motor cortex excitability, suggesting decreased connectivity between motor and language areas in this patient group (Bracco et al., 2009). In patients recovering from post-stroke aphasia due to a dominant hemisphere lesion, the motor cortical hand area in the right (non-dominant) hemisphere was found to be more excitable during reading aloud, suggesting a reorganization of language function with greater recruitment of right hemisphere circuitry (Meister et al., 2006).

Paired-pulse paradigms using two sequential pulses provide an alternative and more spatially focused approach to probing interregional connectivity. The first pulse is referred to as the conditioning stimulus, and the second is referred to as the test stimulus. The latter is applied to a region with an observable output response. Typically, primary motor cortex (M1) receives the test stimulus, and motor evoked potentials are recorded in the affected muscles. By applying a preceding conditioning stimulus to another motor area and measuring how it affects the motor potentials induced by the test stimulus, connectivity between the region receiving the conditioning stimulus and M1 can be probed (Civardi et al., 2001). Individual differences across subjects in specific connections to M1 can be estimated in this manner and correlated with subject variables such as personality dimensions (Hofman and Schutter, 2009) in order to gain greater insight into the role of those specific connections in mental function.

A variety of creative paradigms have been adopted using paired pulse stimulation to examine connectivity in the motor system and its role in behavior. For example, it has been reported that a conditioning stimulus to the ventral premotor cortex during grasp preparation facilitates motor evoked potentials (in response to M1 stimulation) in the muscles specific to the grasp prepared (Davare et al., 2009). This supports the view that ventral premotor cortex contains populations of neurons that exert grasp-specific facilitatory influences on M1. Another study examining excitation of the hand area of M1 during foot movements revealed that dorsal premotor cortex influenced the hand region of M1 in a manner that facilitated isodirectional hand and foot movements (Byblow et al., 2007). Paired-pulse paradigms have revealed aberrant patterns of connectivity to primary motor cortex associated with disorders that have long been hypothesized to involve dysfunctional connectivity, such as schizophrenia and epilepsy (Daskalakis et al., 2005; Loscher et al., 2007; Koch et al., 2008a; D'Argenzio et al., 2009).

Triple-pulse paradigms can probe more complex relationships. For example, a study of interactions between dorsal premotor cortex (which was stimulated with a pair of pulses) and contralateral M1 (which received a single pulse) in focal arm dystonia failed to reveal the usual pattern of interaction between pairs of premotor stimuli (Koch et al., 2008b). Thus, disrupted intraregional dynamics in premotor cortex may play a role in the aberrant influence premotor cortex exerts on M1 in this disorder.

To a lesser extent, connectivity in the visual system has also been probed using paired-pulse paradigms. For example, although in healthy subjects, a conditioning stimulus to MT/V5+ does not modulate the perception of phosphenes in contralateral V1, in a patient with a unilateral V1 lesion, a conditioning stimulus to MT/V5+ in the damaged hemisphere did modulate phosphenes induced by a test stimulus to V1 in the intact hemisphere (Silvanto et al., 2009). This finding was consistent with prior reports of increased connectivity between right and left MT/V5+ in that patient.

In summary, using a variety of experimental designs in which the context is modified, single, paired, and triple-pulse TMS paradigms can be effective tools for probing connectivity in the motor and visual systems in both healthy and patient populations. However, these paradigms are limited to studying connectivity to regions with overt responses (that is, M1 and V1). In order to study connectivity between other regions of the brain, paradigms combining TMS with other imaging modalities are utilized.

INVESTIGATING CONNECTIVITY PATTERNS BY COMBINING TMS WITH IMAGING

Transcranial magnetic stimulation can be used in conjunction with a variety of brain imaging technologies to map connectivity patterns in the human brain. A site is stimulated, and the subsequent activation occurring in distal areas is assessed. Such data can provide information on connectivity patterns. If propagated activation is assessed using electrophysiological methods, conduction delays can also be estimated. However, it is important to remember that physiological propagation of activation between brain regions under natural conditions may not be precisely reflected by the patterns elicited during TMS, which stimulates the brain in a highly unnatural manner. Despite this caveat, the combination of TMS with brain imaging can be very useful in probing brain systems.

Transcranial magnetic stimulation and imaging can be used together in a multitude of ways. They can be combined together in the same sessions, or used in alternate sessions. The first three subsections below describe approaches in which TMS is combined with different imaging modalities simultaneously. These studies are frequently used to examine patterns of connectivity between brain areas. In the final subsection, we discuss studies that use both TMS and imaging, but in different sessions. Such methods can be effective tools for examining changes in connectivity patterns induced by TMS.

TMS AND POSITRON EMISSION TOMOGRAPHY

The ability to examine interregional connectivity using simultaneous TMS and positron emission tomography (PET) was first demonstrated by two studies published in 1997 (Fox et al., 1997; Paus et al., 1997). Fox et al. (1997) stimulated M1 with TMS and reported that changes in blood flow in the stimulated region were positively correlated with changes in blood flow in ipsilateral somatosensory areas, lateral premotor cortex, and contralateral supplementary motor area (SMA), and negatively correlated with changes in blood flow in contralateral M1. Paus et al. (1997) stimulated the left frontal eye field (FEF) and detected blood flow increases in the superior parietal and medial parieto-occipital regions; level of propagated activation correlated with number of TMS pulses delivered. Patterns of distal effects in both studies conformed to expectations based on connectivity studies in non-human species, providing evidence that activity in the stimulated area was propagating to those distal areas via neural connections. Soon afterward, a study examining regional cerebral glucose consumption across the brain during rTMS of the left sensorimotor cortex was published (Siebner et al., 1998). A significant increase in glucose consumption in the SMA was identified during the repetitive stimulation of sensorimotor cortex, providing evidence of neural interaction between the two regions. A later PET study by Paus et al. (2001a) showed that repetitive rTMS delivered to the left mid-dorsolateral frontal cortex robustly modulated brain activity in a fronto-cingulate circuit, which was predicted by a parallel rat experiment using electrical stimulation and field-potential recordings. More recently, TMS of prefrontal and motor cortical areas was shown to activate subcortical regions via trans-synaptic connections using simultaneous PET (Ferrarelli et al., 2004).

In addition to measuring the net neural activity in different brain regions, PET can be used to measure the activity associated with specific neurotransmitter systems. This feature of PET is particularly exciting from a neuropsychiatric perspective, as it allows researchers to probe how specific neurotransmitter systems may be disrupted in different disorders, and thus how drugs that target particular neurotransmitters may influence the function of brain networks. Combined TMS–PET studies have reported changes in dopamine and serotonin activity in regions that are distal to the stimulation site (Strafella et al., 2001, 2005; Sibon et al., 2007; Ko et al., 2008; Cho and Strafella, 2009). For example, an [11C]raclopride study of dopamine activity following stimulation of the left dorsolateral prefrontal cortex reported changes in binding in the left dorsal caudate nucleus in healthy subjects (Strafella et al., 2001) and another [11C]raclopride study of dopamine activity following stimulation of left M1 reported changes in binding in the left putamen (Strafella et al., 2003). A follow-up study in patients with early Parkinson's disease and unilateral motor symptoms revealed that the TMS-induced dopamine release in the striatum following ipsilateral M1 stimulation was lower and more spatially diffuse in the symptomatic hemisphere (Strafella et al., 2005).

In addition to Parkinson's disease, simultaneous TMS–PET has been used to examine connectivity patterns in other patient groups. Chouinard et al. (2006) studied recovery of motor function following stroke, and detected complex shifts in cross-hemisphere and basal ganglia connectivity when stimulating ipsilateral and contralateral M1 using TMS. Another study compared early versus late blind subjects and sighted controls when rTMS was delivered over sensorimotor cortex. Only the early blind group showed significant activation of early visual areas during stimulation, which was significantly greater than in late blind subjects but not when compared to controls (Wittenberg et al., 2004). These data suggest that tactile information is transmitted to early visual

regions via cortico-cortical pathways in early blind subjects, possibly providing a mechanism for enhanced tactile processing in this population.

TMS AND ELECTROENCEPHALOGRAPHY

Combining TMS with electroencephalography (EEG) to characterize connectivity was first reported by Ilmoniemi et al. (1997). Ordinary EEG amplifiers are saturated by TMS pulses. However, this difficulty was overcome by using a sample-and-hold circuit that pinned the amplifier output to a constant level during the TMS pulse with amplifier recovery in just 100 μs. Using this methodology combined with signal averaging, single pulse stimulation of the left sensorimotor cortex produced a near immediate response at the stimulated site, with spread of activation to adjacent ipsilateral motor areas within 5–10 ms and to homologous regions in the opposite hemisphere within 20 ms. Similar activation patterns were generated by magnetic stimulation of the visual cortex. A variety of other systems have since been described for simultaneous EEG/TMS recording (Thut et al., 2003; Bonato et al., 2006), and analysis approaches have been introduced for minimizing artifacts (Litvak et al., 2007).

The effects of TMS on the EEG signal have been studied both in the time domain (Paus et al., 2001b; Iramina et al., 2002; Iwahashi et al., 2008; Lioumis et al., 2009; Casali et al., 2010) and the frequency domain (Paus et al., 2001b; Iramina et al., 2002; Fuggetta et al., 2005, 2008). Several studies have reported changes in coherence between electrodes associated with the stimulation (Fuggetta et al., 2005, 2008), suggesting a reorganization in interregional interaction associated with the stimulation.

Combined TMS–EEG has been used to examine a range of clinical conditions. A study of Alzheimer's disease patients found that TMS delivered to M1 was less effective in activating widespread regions in Alzheimer's patients compared with controls (Julkunen et al., 2008). In patients with schizophrenia, TMS delivered to a premotor area was found to be less effective at eliciting responses in the gamma range in fronto-central regions when compared to healthy controls (Ferrarelli et al., 2008). These data were interpreted as indicating deficient thalamocortical interactions in this patient group. Another study compared healthy controls and patients with schizophrenia when TMS was applied to the Cz electrode position (Levit-Binnun et al., 2010); the patient group failed to generate an early phase frontal negativity (detected in the control group ~29 ms after stimulation) and demonstrated reductions in coincident parietal positivity as well as abnormalities in subsequent peaks when compared to controls. A study of epilepsy patients and controls found that TMS-induced activation at various scalp sites elicited a late phase response in a majority of patients that was absent in healthy subjects (Valentin et al., 2008). Of interest is that this method detected abnormalities in some epilepsy patients where interictal EEG records were normal.

Electroencephalography has intrinsic limitations in terms of spatial resolution. Nonetheless the very high temporal resolution of EEG allows the possibility of detecting differential effects of brain disturbance on conduction time or frequency-specific interregional oscillations that could have wide applicability for characterizing the functional networks underlying pathological conditions.

TMS AND FUNCTIONAL MAGNETIC RESONANCE IMAGING

Functional MRI has superior spatial resolution to other functional imaging modalities and temporal resolution on a seconds timescale. Furthermore, it does not expose subjects to ionizing radiation as PET does. These features make it an extremely popular imaging technique. However there are daunting technical challenges inherent in combining functional magnetic resonance imaging (fMRI) and TMS related to interference between the magnetic field of the scanner and that of the stimulator, to imaging artifacts caused by the presence of even small amounts of metal in the scanner room, and to possible torquing of the TMS coil when used in the scanner field.

Despite these technical challenges, TMS and fMRI have been used together effectively by several research labs. The capability of collecting fMRI data interleaved with TMS stimulation was first demonstrated by Bohning et al. (1998). Soon after, it was reported that activity in areas distal to the stimulation site were detected using interleaved fMRI/TMS protocols, illustrating the promise of this technique for mapping patterns of connectivity between brain areas (Bohning et al., 1999; Nahas et al., 2001; Bestmann et al., 2004).

Combined fMRI/TMS has now been used to explore the functional architecture of many different brain systems, and in some cases, to identify the functional consequences of specific interregional interactions. For example, a study stimulating the FEF reported a distinctive pattern of activity changes in early visual areas: activity increased in regions representing the peripheral visual field and decreased in regions representing the central visual field (Ruff et al., 2006). Furthermore, a psychophysical experiment confirmed that FEF stimulation enhanced contrast perception in the peripheral visual field relative to central visual field. These findings suggest that the FEF exerts top–down effects on early visual cortex in a manner that enhances contrast of peripheral relative to central stimuli.

Most combined fMRI/TMS studies to date have examined brain systems in healthy individuals, although one exception is a study of the neural basis of the perception of phantom hand movements in an amputee patient that was found to be elicited by TMS applied to the contralateral motor cortex (Bestmann et al., 2006). In a novel experimental design, TMS trials producing phantom movements were compared to trials not producing these sensations that corresponded to the same TMS intensities. The experience of phantom movement was specifically associated with coactivation in the primary motor cortex, dorsal premotor cortex, anterior intraparietal sulcus, and caudal SMA.

At present, there is great deal of unexplored potential for clinical research using combined fMRI/TMS paradigms. However, accessibility to this technique is still limited, as not many sites have developed the technical capacity for using TMS in the MR scanner.

STUDIES USING TMS AND IMAGING IN SEPARATE SESSIONS

Studies using imaging and TMS in separate sessions have been used to study a variety of phenomena, such as the neural substrates enabling functional recovery after stroke (Lee et al., 2003; O'Shea et al., 2007; Conchou et al., 2009). For the purposes of this review, the most relevant studies have used imaging to examine changes in connectivity induced by TMS.

Protocols that examine EEG coherence before and after a session of rTMS have provided a window into the cortical reorganization induced by TMS (Jing and Takigawa, 2000; Strens et al., 2002; Oliviero et al., 2003). For example, high and low-frequency rTMS to left motor cortex induced decreasing and increasing alpha-band coherence, respectively, between the stimulated site and ipsilateral premotor cortex (Strens et al., 2002; Oliviero et al., 2003). The contrasting effects of high and low-frequency rTMS on connectivity are consistent with the opposite effects of these stimulation paradigms on motor cortical excitability.

As discussed above, PET can be used in conjunction with TMS to assess connectivity. Therefore, paradigms using combined PET–TMS before and after an rTMS session can potentially provide information regarding how the rTMS session modulates connectivity (Paus et al., 2001a). However, assessment of changes in connectivity based on differences (before and after rTMS) in the activity induced in distal sites in the combined PET–TMS sessions can become complicated when the region stimulated during the PET–TMS session has an altered response to stimulation after rTMS. In such a case, changes in activity in the distal regions could be due to differences in interregional connectivity, but they could also be due to a different amount of activation in the stimulated region propagating through an unchanged connection. Alternatively, PET on its own can be used to assess connectivity if a sufficient number of PET scans can be collected for each subject. Using this approach, effective connectivity in the motor system immediately after rTMS to M1 was shown to differ from the connectivity patterns after sham stimulation of the same region (Lee et al., 2003). The changes in connectivity were similar to those seen after stroke, suggesting rTMS could provide a reversible lesion with which to study acute plasticity in the brain following stroke.

A very promising approach for studying TMS-induced connectivity changes is the use of fMRI to assess connectivity before and after rTMS. Functional magnetic resonance imaging has recently become an extremely popular tool for assessing functional (Hampson et al., inpress) and effective (McIntosh and Gonzalez-Lima, 1994; Friston et al., 2003; Goebel et al., 2003; Marrelec et al., 2005) connectivity. To date, however, fMRI studies of functional/effective connectivity before and after rTMS have been limited. However, a recent paper using dynamic causal modeling to assess effective connectivity in the motor system before and after rTMS of contralesional M1 in stroke patients illustrates the potential of this approach (Grefkes et al., 2010). rTMS reduced transcallosal connectivity between homologous parts of M1 during motor task performance and enhanced intrinsic connectivity between M1 in the lesioned hemisphere and the SMA. These changes in connectivity were accompanied by, and possibly responsible for, an improvement in motor performance.

In addition to examining changes in connectivity changes induced by TMS, studies using TMS and connectivity mapping in separate sessions can provide other forms of information. For example, a recent diffusion tensor imaging study reported that connectivity patterns predicted TMS response in patients with post-stroke pain (Goto et al., 2008).

USING CONNECTIVITY MAPPING TO TARGET TMS STIMULATION

There is wide recognition that TMS is a powerful tool for studying and modulating connectivity in the human brain, but perhaps less awareness that connectivity mapping can be a useful tool for guiding TMS stimulation. For example, when brain areas with disrupted function are not accessible to TMS, connectivity mapping can identify connected regions to be stimulated, and the inaccessible regions may thus be influenced indirectly via propagated activity patterns. Or, if the precise locus of only one region in a network of interest is known, connectivity mapping can be used to identify other nodes of a functional network in a subject-specific manner; thus multiple targets for TMS can be identified that may prove clinically effective for disrupting a pathological process involving that network.

Both structural and functional connectivity mapping can be used to identify target sites for TMS. In a study investigating the role of the prefrontal cortex in suppressing irrelevant somatosensory information during working memory tasks, diffusion tensor imaging was used to identify regions of prefrontal cortex anatomically connected with the primary somatosensory cortex (S1) in each subject (Hannula et al., 2010). Stimulation of this specific site (but not other sites) in prefrontal cortex was then shown to suppress somatosensory evoked potentials and to facilitate working memory performance, consistent with the view that the connected prefrontal region was acting on S1 in a manner that suppressed processing of irrelevant sensory stimuli.

Functional connectivity mapping has also been used to identify target regions for TMS. An example of this is a study by our group in which TMS was used to probe the circuitry involved in auditory hallucinations of schizophrenic subjects (Hoffman et al., 2007). In each subject, three to six sites were selected for stimulation. For intermittent hallucinators, the target regions were identified by comparing brain activity during hallucinations to brain activity at rest and selecting peak areas in the resulting hallucination-related activation maps. However, a subgroup of the patients in the study had continuous hallucinations and thus no rest periods for comparison purposes. For these individuals, maps of functional connectivity to Wernicke's region were created, and peaks in those maps within classic language areas were targeted. Wernicke's area was selected as the seed region for functional connectivity maps given other studies showing activation in this region during auditory hallucinations (Shergill et al., 2000). Regions showing high functional connectivity with this seed region were then targeted with "suppressive" low-frequency TMS. rTMS positioned using these functional connectivity maps did not produce better clinical responses compared to targeting Wernicke's area itself. However, a noteworthy finding is that the level of Wernicke's seeded functional connectivity assessed relative to the right homologue of Broca's area strongly and negatively predicted the capacity of low-frequency rTMS to suppress auditory hallucinations. These data suggested that especially tight functional coupling incorporating these regions was able to override rTMS effects. Consistent with this finding is a recent fMRI study showing that right homologue of Broca's area corresponds to the most prominent site of cortical activation coincident with auditory hallucinations (Sommer et al., 2008).

FUTURE DIRECTIONS

The effects of TMS at a cellular level are not well understood, and the relationship between activity of different cell types in a region and the signals measured via PET, fMRI, or EEG are also not well understood. Efforts to bridge these gaps are needed. One approach is the development of large-scale neurobiologically realistic models. For example, a model of TMS applied to visual areas during a delayed-match-to-sample task reproduced both local and distal changes in regional cerebral blood flow associated with stimulation, and allowed investigation of the different patterns of blood flow changes associated with stimulating inhibitory versus excitatory units (Husain et al., 2002). Neurobiological models that span multiple spatial scales, from cellular to systems-level neuroscience, may be particularly enlightening for neural disorders in which certain populations of cells are hypothesized to be abnormal.

Modeling of the effective connectivity between regions is also a promising avenue for future work. One of the most exciting aspects of TMS is that brain activity in one region is directly induced and the propagation of that activity to other regions can thus provide information regarding causal interactions between areas. A study using exploratory structural equation modeling of PET/TMS data extracted a model of effective connectivity (that is, of causal interactions between brain areas) with an excellent fit to the data that was also highly consistent with known anatomical connectivity (Laird et al., 2008). This suggests that combining PET/TMS (or PET/fMRI) data with structural equation modeling is a promising approach to mapping out effective connectivity in the human brain.

From a clinical perspective, more studies are needed examining how specific interventions influence brain dynamics in patient populations. A study of the effects of l-dopa on the motor network in Parkinson's disease illustrates the potential of such approaches (Buhmann et al., 2004). Stimulation of premotor cortex decreased the excitability of ipsilateral M1 in untreated Parkinson's patients, which was the opposite effect that it had in control subjects. However, a single dose of l-dopa reversed this pattern in the patients, effectively normalizing the premotor–motor interaction in Parkinson's disease. Changes in connectivity patterns associated with long-term treatments, and their associations with symptom improvements or negative side effects, could also be informative.

SUMMARY

These studies, considered together, show how diverse neuroimaging methodologies used to characterize functional connectivity and coactivation can be usefully combined with TMS. Although methodological challenges remain, these approaches provide powerful tools for investigating the network basis of a range of brain disorders. Results to date have permitted characterization of broadly distributed disconnection and hyperconnection patterns associated with Alzheimer's disease, schizophrenia, and epilepsy, and have provided intriguing glimpses into alterations in neurocircuitry associated with clinical phenomena, such as recovery from stroke. Our expectation is that these integrated studies will permit more detailed characterizations of network dynamics and connectivity that do not rely on the cognitive or task performance that is likely to be variable across individual patients, especially in illness conditions. These methods may not only elucidate pathophysiology, but may assist in diagnosis and subtyping of illness, as well as in guiding rTMS as a treatment intervention.

ACKNOWLEDGMENTS

This work was supported by National Institute of Mental Health grants R01 MH073673 and R01 MH067073.

REFERENCES

Allen, E. A., Pasley, B. N., Duong, T., and Freeman, R. D. (2007). Transcranial magnetic stimulation elicits coupled neural and hemodynamic consequences. *Science* 317, 1918–1921.

Bestmann, S., Baudewig, J., Siebner, H. R., Rothwell, J. C., and Frahm, J. (2004). Functional MRI of the immediate impact of transcranial magnetic stimulation on cortical and subcortical motor circuits. *Eur. J. Neurosci.* 19, 1950–1962.

Bestmann, S., Oliviero, A., Voss, M., Dechent, P., Lopez-Dolado, E., Driver, J., and Baudewig, J. (2006). Cortical correlates of TMS-induced phantom hand movements revealed with concurrent TMS-fMRI. *Neuropsychologia* 44, 2959–2971.

Bohning, D. E., Shastri, A., McConnell, K. A., Nahas, Z., Lorberbaum, J. P., Roberts, D. R., Teneback, C., Vincent, D. J., and George, M. S. (1999). A combined TMS/fMRI study of intensity-dependent TMS over motor cortex. *Biol. Psychiatry* 45, 385–394.

Bohning, D. E., Shastri, A., Nahas, Z., Lorberbaum, J. P., Andersen, S. W., Dannels, W. R., Haxthausen, E. U., Vincent, D. J., and George, M. S. (1998). Echoplanar BOLD fMRI of brain activation induced by concurrent transcranial magnetic stimulation. *Invest. Radiol.* 33, 336–340.

Bonato, C., Miniussi, C., and Rossini, P. M. (2006). Transcranial magnetic stimulation and cortical evoked potentials: a TMS/EEG co-registration study. *Clin. Neurophysiol.* 117, 1699–1707.

Boros, K., Poreisz, C., Munchau, A., Paulus, W., and Nitsche, M. A. (2008). Premotor transcranial direct current stimulation (tDCS) affects primary motor excitability in humans. *Eur. J. Neurosci.* 27, 1292–1300.

Bracco, L., Giovannelli, F., Bessi, V., Borgheresi, A., Di Tullio, A., Sorbi, S., Zaccara, G., and Cincotta, M. (2009). Mild cognitive impairment: loss of linguistic task-induced changes in motor cortex excitability. *Neurology* 72, 928–934.

Buhmann, C., Gorsler, A., Baumer, T., Hidding, U., Demiralay, C., Hinkelmann, K., Weiller, C., Siebner, H. R., and Munchau, A. (2004). Abnormal excitability of premotor-motor connections in de novo Parkinson's disease. *Brain* 127, 2732–2746.

Byblow, W. D., Coxon, J. P., Stinear, C. M., Fleming, M. K., Williams, G., Muller, J. F., and Ziemann, U. (2007). Functional connectivity between secondary and primary motor areas underlying hand-foot coordination. *J. Neurophysiol.* 98, 414–422.

Casali, A. G., Casarotto, S., Rosanova, M., Mariotti, M., and Massimini, M. (2010). General indices to characterize the electrical response of the cerebral cortex to TMS. *Neuroimage* 49, 1459–1468.

Chen, R., Classen, J., Gerloff, C., Celnik, P., Wassermann, E. M., Hallett, M., and Cohen, L. G. (1997). Depression of motor cortex excitability by low-frequency transcranial magnetic stimulation. *Neurology* 48, 1398–1403.

Cho, S. S., and Strafella, A. P. (2009). rTMS of the left dorsolateral prefrontal cortex modulates dopamine release in the ipsilateral anterior cingulate cortex and orbitofrontal cortex. *PLoS ONE* 4, e6725. doi:10.1371/journal.pone.0006725.

Chouinard, P. A., Leonard, G., and Paus, T. (2006). Changes in effective connectivity of the primary motor cortex in stroke patients after rehabilitative therapy. *Exp. Neurol.* 201, 375–387.

Civardi, C., Cantello, R., Asselman, P., and Rothwell, J. C. (2001). Transcranial magnetic stimulation can be used to test connections to primary motor areas from frontal and medial cortex in humans. *Neuroimage* 14, 1444–1453.

Cohen, L. G., Roth, B. J., Nilsson, J., Dang, N., Panizza, M., Bandinelli, S., Friauf, W., and Hallett, M. (1990). Effects of coil design on delivery of focal magnetic stimulation. Technical con-

siderations. *Electroencephalogr. Clin. Neurophysiol.* 75, 350–357.

Conchou, F., Loubinoux, I., Castel-Lacanal, E., Le Tinnier, A., Gerdelat-Mas, A., Faure-Marie, N., Gros, H., Thalamas, C., Calvas, F., Berry, I., Chollet, F., and Simonetta Moreau, M. (2009). Neural substrates of low-frequency repetitive transcranial magnetic stimulation during movement in healthy subjects and acute stroke patients. A PET study. *Hum. Brain Mapp.* 30, 2542–2557.

D'Argenzio, L., Koch, G., Bombardieri, R., Mori, F., Moavero, R., Centonze, D., and Curatolo, P. (2009). Abnormal parieto-motor connectivity in Tuberous Sclerosis Complex. *Epilepsy Res.* 87, 102–105.

Daskalakis, Z. J., Christensen, B. K., Fitzgerald, P. B., Fountain, S. I., and Chen, R. (2005). Reduced cerebellar inhibition in schizophrenia: a preliminary study. *Am. J. Psychiatry* 162, 1203–1205.

Davare, M., Montague, K., Olivier, E., Rothwell, J. C., and Lemon, R. N. (2009). Ventral premotor to primary motor cortical interactions during object-driven grasp in humans. *Cortex* 45, 1050–1057.

Ferrarelli, F., Haraldsson, H. M., Barnhart, T. E., Roberts, A. D., Oakes, T. R., Massimini, M., Stone, C. K., Kalin, N. H., and Tononi, G. (2004). A [17F]-fluoromethane PET/TMS study of effective connectivity. *Brain Res. Bull.* 64, 103–113.

Ferrarelli, F., Massimini, M., Peterson, M. J., Riedner, B. A., Lazar, M., Murphy, M. J., Huber, R., Rosanova, M., Alexander, A. L., Kalin, N., and Tononi, G. (2008). Reduced evoked gamma oscillations in the frontal cortex in schizophrenia patients: a TMS/EEG study. *Am. J. Psychiatry* 165, 996–1005.

Fox, P., Ingham, R., George, M. S., Mayberg, H., Ingham, J., Roby, J., Martin, C., and Jerabek, P. (1997). Imaging human intra-cerebral connectivity by PET during TMS. *Neuroreport* 8, 2787–2791.

Friston, K. J., Harrison, L., and Penny, W. (2003). Dynamic causal modelling. *Neuroimage* 19, 1273–1302.

Fuggetta, G., Fiaschi, A., and Manganotti, P. (2005). Modulation of cortical oscillatory activities induced by varying single-pulse transcranial magnetic stimulation intensity over the left primary motor area: a combined EEG and TMS study. *Neuroimage* 27, 896–908.

Fuggetta, G., Pavone, E. F., Fiaschi, A., and Manganotti, P. (2008). Acute modulation of cortical oscillatory activities during short trains of high-frequency repetitive transcranial magnetic stimulation of the human motor cortex: a combined EEG and TMS study. *Hum. Brain Mapp.* 29, 1–13.

Galea, J. M., Jayaram, G., Ajagbe, L., and Celnik, P. (2009). Modulation of cerebellar excitability by polarity-specific noninvasive direct current stimulation. *J. Neurosci.* 29, 9115–9122.

George, M. S., Lisanby, S. H., and Sackeim, H. A. (1999). Transcranial magnetic stimulation: applications in neuropsychiatry. *Arch. Gen. Psychiatry* 56, 300–311.

Goebel, R., Roebroeck, A., Kim, D. S., and Formisano, E. (2003). Investigating directed cortical interactions in time-resolved fMRI data using vector autoregressive modeling and Granger causality mapping. *Magn. Reson. Imaging* 21, 1251–1261.

Goto, T., Saitoh, Y., Hashimoto, N., Hirata, M., Kishima, H., Oshino, S., Tani, N., Hosomi, K., Kakigi, R., and Yoshimine, T. (2008). Diffusion tensor fiber tracking in patients with central post-stroke pain; correlation with efficacy of repetitive transcranial magnetic stimulation. *Pain* 140, 509–518.

Grefkes, C., Nowak, D. A., Wang, L. E., Dafotakis, M., Eickhoff, S. B., and Fink, G. R. (2010). Modulating cortical connectivity in stroke patients by rTMS assessed with fMRI and dynamic causal modeling. *Neuroimage* 50, 233–242.

Grosbras, M. H., and Paus, T. (2002). Transcranial magnetic stimulation of the human frontal eye field: effects on visual perception and attention. *J. Cogn. Neurosci.* 14, 1109–1120.

Hampson, M., Shen, X., and Constable, R. T. (in press). "Functional connectivity MR imaging," in *Functional Neuroradiology: Principles and Clinical Applications*, eds S. Faro and F. Mohamed (New York, NY: Springer Science + Business Media, LLC).

Hannula, H., Neuvonen, T., Savolainen, P., Hiltunen, J., Ma, Y. Y., Antila, H., Salonen, O., Carlson, S., and Pertovaara, A. (2010). Increasing top-down suppression from prefrontal cortex facilitates tactile working memory. *Neuroimage* 49, 1091–1098.

Hoffman, R. E., Hampson, M., Wu, K., Anderson, A. W., Gore, J. C., Buchanan, R. J., Constable, R. T., Hawkins, K., Sahay, N., and Krystal, J. H. (2007). Probing the pathophysiology of auditory hallucinations by combining functional magnetic resonance imaging and transcranial magnetic stimulation. *Cereb. Cortex* 17, 2733–2743.

Hofman, D., and Schutter, D. J. (2009). Inside the wire: aggression and functional interhemispheric connectivity in the human brain. *Psychophysiology* 46, 1054–1058.

Huang, Y. Z., Edwards, M. J., Rounis, E., Bhatia, K. P., and Rothwell, J. C. (2005). Theta burst stimulation of the human motor cortex. *Neuron* 45, 201–206.

Husain, F. T., Nandipati, G., Braun, A. R., Cohen, L. G., Tagamets, M. A., and Horwitz, B. (2002). Simulating transcranial magnetic stimulation during PET with a large-scale neural network model of the prefrontal cortex and the visual system. *Neuroimage* 15, 58–73.

Ilmoniemi, R. J., Virtanen, J., Ruohonen, J., Karhu, J., Aronen, H. J., Naatanen, R., and Katila, T. (1997). Neuronal responses to magnetic stimulation reveal cortical reactivity and connectivity. *Neuroreport* 8, 3537–3540.

Iramina, K., Maeno, T., Kowatari, Y., and Ueno, S. (2002). Effects of transcranial magnetic stimulation on EEG activity. *IEEE Trans. Magn.* 38, 3347–3349.

Iwahashi, M., Arimatsu, T., Ueno, S., and Iramina, K. (2008). Differences in evoked EEG by transcranial magnetic stimulation at various stimulus points on the head. *Proceedings of International Conference of IEEE, Engineering in Medicine and Biology Society,* 2008, Vancouver, pp. 2570–2573.

Jing, H., and Takigawa, M. (2000). Observation of EEG coherence after repetitive transcranial magnetic stimulation. *Clin Neurophysiol* 111, 1620–1631.

Julkunen, P., Jauhiainen, A. M., Westeren-Punnonen, S., Pirinen, E., Soininen, H., Kononen, M., Paakkonen, A., Maatta, S., and Karhu, J. (2008). Navigated TMS combined with EEG in mild cognitive impairment and Alzheimer's disease: a pilot study. *J. Neurosci. Methods* 172, 270–276.

Ko, J. H., Monchi, O., Ptito, A., Bloomfield, P., Houle, S., and Strafella, A. P. (2008). Theta burst stimulation-induced inhibition of dorsolateral prefrontal cortex reveals hemispheric asymmetry in striatal dopamine release during a set-shifting task: a TMS-[(11)C]raclopride PET study. *Eur. J. Neurosci.* 28, 2147–2155.

Koch, G., Franca, M., Mochizuki, H., Marconi, B., Caltagirone, C., and Rothwell, J. C. (2007). Interactions between pairs of transcranial magnetic stimuli over the human left dorsal premotor cortex differ from those seen in primary motor cortex. *J. Physiol. (Lond.)* 578, 551–562.

Koch, G., Ribolsi, M., Mori, F., Sacchetti, L., Codeca, C., Rubino, I. A., Siracusano, A., Bernardi, G., and Centonze, D. (2008a). Connectivity between posterior parietal cortex and ipsilateral motor cortex is altered in schizophrenia. *Biol. Psychiatry* 64, 815–819.

Koch, G., Schneider, S., Baumer, T., Franca, M., Munchau, A., Cheeran, B., Fernandez del Olmo, M., Cordivari, C., Rounis, E., Caltagirone, C., Bhatia, K., and Rothwell, J. C. (2008b). Altered dorsal premotor-motor interhemispheric pathway activity in focal arm dystonia. *Mov. Disord.* 23, 660–668.

Laird, A. R., Robbins, J. M., Li, K., Price, L. R., Cykowski, M. D., Narayana, S., Laird, R. W., Franklin, C., and Fox, P. T. (2008). Modeling motor connectivity using TMS/PET and structural equation modeling. *Neuroimage* 41, 424–436.

Lee, L., Siebner, H. R., Rowe, J. B., Rizzo, V., Rothwell, J. C., Frackowiak, R. S., and Friston, K. J. (2003). Acute remapping within the motor system induced by low-frequency repetitive transcranial magnetic stimulation. *J. Neurosci.* 23, 5308–5318.

Levit-Binnun, N., Litvak, V., Pratt, H., Moses, E., Zaroor, M., and Peled, A. (2010). Differences in TMS-evoked responses between schizophrenia patients and healthy controls can be observed without a dedicated EEG system. *Clin. Neurophysiol.* 121, 332–339.

Lioumis, P., Kicic, D., Savolainen, P., Makela, J. P., and Kahkonen, S. (2009). Reproducibility of TMS-evoked EEG responses. *Hum. Brain Mapp.* 30, 1387–1396.

Litvak, V., Komssi, S., Scherg, M., Hoechstetter, K., Classen, J., Zaaroor, M., Pratt, H., and Kahkonen, S. (2007). Artifact correction and source analysis of early electroencephalographic responses evoked by transcranial magnetic stimulation over primary motor cortex. *Neuroimage* 37, 56–70.

Loscher, W. N., Dobesberger, J., Szubski, C., and Trinka, E. (2007). rTMS reveals premotor cortex dysfunction in frontal lobe epilepsy. *Epilepsia* 48, 359–365.

Marrelec, G., Daunizeau, J., Pélégrini-Issac, M., Doyon, J., and Benali, H. (2005). Conditional correlation as a measure of mediated interactivity in fMRI and MEG/EEG. *IEEE Trans. Signal Process* 53, 3505–3516.

McIntosh, A. R., and Gonzalez-Lima, F. (1994). Network interactions among limbic cortices, basal forebrain, and cerebellum differentiate a tone conditioned as a Pavlovian excitor or inhibitor: fluorodeoxyglucose mapping and covariance structural modeling. *J. Neurophysiol.* 72, 1717–1733.

Meister, I. G., Boroojerdi, B., Foltys, H., Sparing, R., Huber, W., and Topper, R. (2003). Motor cortex hand area and speech: implications for the development of language. *Neuropsychologia* 41, 401–406.

Meister, I. G., Sparing, R., Foltys, H., Gebert, D., Huber, W., Topper, R., and Boroojerdi, B. (2006). Functional

connectivity between cortical hand motor and language areas during recovery from aphasia. *J. Neurol. Sci.* 247, 165–168.

Nahas, Z., Lomarev, M., Roberts, D. R., Shastri, A., Lorberbaum, J. P., Teneback, C., McConnell, K., Vincent, D. J., Li, X., George, M. S., and Bohning, D. E. (2001). Unilateral left prefrontal transcranial magnetic stimulation (TMS) produces intensity-dependent bilateral effects as measured by interleaved BOLD fMRI. *Biol. Psychiatry* 50, 712–720.

Oliviero, A., Strens, L. H., Di Lazzaro, V., Tonali, P. A., and Brown, P. (2003). Persistent effects of high frequency repetitive TMS on the coupling between motor areas in the human. *Exp. Brain Res.* 149, 107–113.

O'Shea, J., Johansen-Berg, H., Trief, D., Gobel, S., and Rushworth, M. F. (2007). Functionally specific reorganization in human premotor cortex. *Neuron* 54, 479–490.

Pascual-Leone, A., Houser, C. M., Reese, K., Shotland, L. I., Grafman, J., Sato, S., Valls-Sole, J., Brasil-Neto, J. P., Wassermann, E. M., Cohen, L. G., Hallett, M. (1993). Safety of rapid-rate transcranial magnetic stimulation in normal volunteers. *Electroencephalogr Clin Neurophysiol* 89, 120–130.

Pascual-Leone, A., Valls-Sole, J., Wassermann, E. M., and Hallett, M. (1994). Responses to rapid-rate transcranial magnetic stimulation of the human motor cortex. *Brain* 117(Pt 4), 847–858.

Paus, T., Castro-Alamancos, M. A., and Petrides, M. (2001a). Cortico-cortical connectivity of the human mid-dorsolateral frontal cortex and its modulation by repetitive transcranial magnetic stimulation. *Eur. J. Neurosci.* 14, 1405–1411.

Paus, T., Sipila, P. K., and Strafella, A. P. (2001b). Synchronization of neuronal activity in the human primary motor cortex by transcranial magnetic stimulation: an EEG study. *J. Neurophysiol.* 86, 1983–1990.

Paus, T., Jech, R., Thompson, C. J., Comeau, R., Peters, T., and Evans, A. C. (1997). Transcranial magnetic stimulation during positron emission tomography: a new method for studying connectivity of the human cerebral cortex. *J. Neurosci.* 17, 3178–3184.

Priori, A. (2003). Brain polarization in humans: a reappraisal of an old tool for prolonged non-invasive modulation of brain excitability. *Clin Neurophysiol* 114, 589–595.

Rossi, S., Hallett, M., Rossini, P. M., and Pascual-Leone, A. (2009). Safety, ethical considerations, and application guidelines for the use of transcranial magnetic stimulation in clinical practice and research. *Clin Neurophysiol* 120, 2008–2039.

Rossini, P. M., and Rossi, S. (2007). Transcranial magnetic stimulation: diagnostic, therapeutic, and research potential. *Neurology* 68, 484–488.

Rudiak, D., and Marg, E. (1994). Finding the depth of magnetic brain stimulation: a re-evaluation. *Electroencephalogr Clin Neurophysiol* 93, 358–371.

Ruff, C. C., Blankenburg, F., Bjoertomt, O., Bestmann, S., Freeman, E., Haynes, J. D., Rees, G., Josephs, O., Deichmann, R., and Driver, J. (2006). Concurrent TMS-fMRI and psychophysics reveal frontal influences on human retinotopic visual cortex. *Curr. Biol.* 16, 1479–1488.

Sanger, T. D., Garg, R. R., and Chen, R. (2001). Interactions between two different inhibitory systems in the human motor cortex. *J. Physiol.* 530, 307–317.

Shergill, S. S., Brammer, M. J., Williams, S. C., Murray, R. M., and McGuire, P. K. (2000). Mapping auditory hallucinations in schizophrenia using functional magnetic resonance imaging. *Arch. Gen. Psychiatry* 57, 1033–1038.

Sibon, I., Strafella, A. P., Gravel, P., Ko, J. H., Booij, L., Soucy, J. P., Leyton, M., Diksic, M., and Benkelfat, C. (2007). Acute prefrontal cortex TMS in healthy volunteers: effects on brain 11C-alphaMtrp trapping. *Neuroimage* 34, 1658–1664.

Siebner, H. R., Willoch, F., Peller, M., Auer, C., Boecker, H., Conrad, B., and Bartenstein, P. (1998). Imaging brain activation induced by long trains of repetitive transcranial magnetic stimulation. *Neuroreport* 9, 943–948.

Silvanto, J., Walsh, V., and Cowey, A. (2009). Abnormal functional connectivity between ipsilesional V5/MT+ and contralesional striate cortex (V1) in blindsight. *Exp. Brain Res.* 193, 645–650.

Sommer, I. E., Diederen, K. M., Blom, J. D., Willems, A., Kushan, L., Slotema, K., Boks, M. P., Daalman, K., Hoek, H. W., Neggers, S. F., and Kahn, R. S. (2008). Auditory verbal hallucinations predominantly activate the right inferior frontal area. *Brain* 131, 3169–3177.

Speer, A. M., Kimbrell, T. A., Wassermann, E. M., J, D. R., Willis, M. W., Herscovitch, P., and Post, R. M. (2000). Opposite effects of high and low frequency rTMS on regional brain activity in depressed patients. *Biol. Psychiatry* 48, 1133–1141.

Stagg, C. J., O'Shea, J., Kincses, Z. T., Woolrich, M., Matthews, P. M., and Johansen-Berg, H. (2009). Modulation of movement-associated cortical activation by transcranial direct current stimulation. *Eur. J. Neurosci.* 30, 1412–1423.

Strafella, A. P., Ko, J. H., Grant, J., Fraraccio, M., and Monchi, O. (2005). Corticostriatal functional interactions in Parkinson's disease: a rTMS/[11C] raclopride PET study. *Eur. J. Neurosci.* 22, 2946–2952.

Strafella, A. P., Paus, T., Barrett, J., and Dagher, A. (2001). Repetitive transcranial magnetic stimulation of the human prefrontal cortex induces dopamine release in the caudate nucleus. *J. Neurosci.* 21, RC157.

Strafella, A. P., Paus, T., Fraraccio, M., and Dagher, A. (2003). Striatal dopamine release induced by repetitive transcranial magnetic stimulation of the human motor cortex. *Brain* 126, 2609–2615.

Strens, L. H., Oliviero, A., Bloem, B. R., Gerschlager, W., Rothwell, J. C., and Brown, P. (2002). The effects of subthreshold 1 Hz repetitive TMS on cortico-cortical and interhemispheric coherence. *Clin. Neurophysiol.* 113, 1279–1285.

Terao, Y., Fukuda, H., Ugawa, Y., Hikosaka, O., Hanajima, R., Furubayashi, T., Sakai, K., Miyauchi, S., Sasaki, Y., and Kanazawa, I. (1998). Visualization of the information flow through human oculomotor cortical regions by transcranial magnetic stimulation. *J. Neurophysiol.* 80, 936–946.

Thut, G., Northoff, G., Ives, J. R., Kamitani, Y., Pfennig, A., Kampmann, F., Schomer, D. L., and Pascual-Leone, A. (2003). Effects of single-pulse transcranial magnetic stimulation (TMS) on functional brain activity: a combined event-related TMS and evoked potential study. *Clin. Neurophysiol.* 114, 2071–2080.

Tokimura, H., Tokimura, Y., Oliviero, A., Asakura, T., and Rothwell, J. C. (1996). Speech-induced changes in corticospinal excitability. *Ann. Neurol.* 40, 628–634.

Valentin, A., Arunachalam, R., Mesquita-Rodrigues, A., Garcia Seoane, J. J., Richardson, M. P., Mills, K. R., and Alarcon, G. (2008). Late EEG responses triggered by transcranial magnetic stimulation (TMS) in the evaluation of focal epilepsy. *Epilepsia* 49, 470–480.

Walsh, V., and Rushworth, M. (1999). A primer of magnetic stimulation as a tool for neuropsychology. *Neuropsychologia* 37, 125–135.

Wassermann, E. M. (1998). Risk and safety of repetitive transcranial magnetic stimulation: report and suggested guidelines from the International Workshop on the Safety of Repetitive Transcranial Magnetic Stimulation, June 5–7, 1996. *Electroencephalogr. Clin. Neurophysiol.* 108, 1–16.

Wittenberg, G. F., Werhahn, K. J., Wassermann, E. M., Herscovitch, P., and Cohen, L. G. (2004). Functional connectivity between somatosensory and visual cortex in early blind humans. *Eur. J. Neurosci.* 20, 1923–1927.

Zangaladze, A., Epstein, C. M., Grafton, S. T., and Sathian, K. (1999). Involvement of visual cortex in tactile discrimination of orientation. *Nature* 401, 587–590.

Conflict of Interest Statement: The authors declare that the research was conducted in the absence of any commercial or financial relationships that could be construed as a potential conflict of interest.

Received: 18 May 2010; paper pending published: 15 June 2010; accepted: 23 July 2010; published online: 12 August 2010.

*Citation: Hampson M and Hoffman RE (2010). Transcranial magnetic stimulation and connectivity mapping: tools for studying the neural bases of brain disorders. Front. Syst. Neurosci. **4**:40. doi:10.3389/fnsys.2010.00040*

Copyright © 2010 Hampson and Hoffman. This is an open-access publication subject to an exclusive license agreement between the authors and the Frontiers Research Foundation, which permits unrestricted use, distribution, and reproduction in any medium, provided the original authors and source are credited.

frontiers in
SYSTEMS NEUROSCIENCE

REVIEW ARTICLE
published: 20 October 2010
doi: 10.3389/fnsys.2010.00148

Studying network mechanisms using intracranial stimulation in epileptic patients

***Olivier David*[1,2,3]*, *Julien Bastin*[1,2], *Stéphan Chabardès*[1,2,4], *Lorella Minotti*[1,2,5] and *Philippe Kahane*[1,2,5,6]**

[1] *INSERM U836, Grenoble Institut des Neurosciences, Grenoble, France*
[2] *Université Joseph Fourier, Grenoble, France*
[3] *Clinique Universitaire de Neuroradiologie et Unité IRM, Centre Hospitalier Universitaire, Grenoble, France*
[4] *Clinique Universitaire de Neurochirurgie, Centre Hospitalier Universitaire, Grenoble, France*
[5] *Laboratoire de Neurophysiopathologie de l'Epilepsie, Clinique Universitaire de Neurologie, Centre Hospitalier Universitaire, Grenoble, France*
[6] *CTRS-IDEE, Centre Hospitalier Universitaire, Lyon, France*

Edited by:
Barry Horwitz, National Institutes of Health, USA

Reviewed by:
Sacha van Albada, Research Center Jülich, Germany
Arpan Banerjee, Florida Atlantic University, USA

***Correspondence:**
Olivier David, Grenoble Institut des Neurosciences – INSERM U836, Chemin Fortuné Ferrini – Bât EJ Safra, 38700 La Tronche, France.
e-mail: olivier.david@ujf-grenoble.fr

Patients suffering from focal drug-resistant epilepsy who are explored using intracranial electrodes allow to obtain data of exceptional value for studying brain dynamics in correlation with pathophysiological and cognitive processes. Direct electrical stimulation (DES) of cortical regions and axonal tracts in those patients elicits a number of very specific perceptual or behavioral responses, but also abnormal responses due to specific configurations of epileptic networks. Here, we review how anatomo-functional brain connectivity and epilepsy network mechanisms can be assessed from DES responses measured in patients. After a brief summary of mechanisms of action of brain electrical stimulation, we recall the conceptual framework for interpreting DES results in the context of brain connectivity and review how DES can be used for the characterization of functional networks, the identification of the seizure onset zone, the study of brain plasticity mechanisms, and the anticipation of epileptic seizures. This pool of exceptional data may be underexploited by fundamental research on brain connectivity and leaves much to be learned.

Keywords: neurostimulation, epilepsy, connectivity, networks, cognition, plasticity, electroencephalography

INTRODUCTION

Epilepsy is a common chronic neurological disorder characterized by recurrent spontaneous seizures showing paroxysmal electrical activity. A cortical imbalance between excitation and inhibition within local and large-scale networks is likely to trigger abnormal brain electrical activity and, thus, to be the pathophysiological basis for epilepsy. In models of epilepsy, either *in vitro* or *in vivo*, such imbalance can be induced in several ways. For instance, status epilepticus, i.e., seizures lasting more than 30 min, can be initiated by blocking inhibition by injecting GABA receptors antagonists, e.g., bicuculline (Jefferys and Whittington, 1996). In the kindling model (Morimoto et al., 2004), permanent increases in seizure susceptibility can be provoked by repeated, although sparse, electrical stimulation of some brain sites.

Some patients with drug-resistant focal epilepsy in whom the epileptogenic zone cannot be defined with non-invasive measures are explored using depth electrodes (stereoelectroencephalography, SEEG) and/or subdural grids and strips (electrocorticography, ECoG) (Spencer et al., 2006). These techniques allow to obtain data of exceptional value for studying brain dynamics in correlation with pathophysiological (Jirsch et al., 2006) and cognitive (Jerbi et al., 2009) processes. In particular, they allow measuring intracranial functional responses to assess connectivity of the human brain beyond limitations of other techniques, such as post mortem dissections (Mesulam, 1979), diffusion tensor imaging (Jones, 2008), functional magnetic resonance imaging (Roebroeck et al., 2009), and combination of transcranial magnetic stimulation and neuroimaging (Paus et al., 1997).

Since the pioneering works of Penfield and Jasper (1954) performed during surgical interventions, it is also well known that direct electrical stimulation (DES) of cortical regions and axonal tracts allows a number of very specific perceptual or behavioral responses to be obtained. Despite the development of neuroimaging techniques, DES remains the gold standard for mapping brain functions, particularly regarding functional specialization whereas some interrogations remain when assessing functional integration (Mandonnet et al., 2010). For instance, DES of language areas performed during tumor resection induces very specific speech disturbances in awake patients (Duffau et al., 2008). Similarly, using subdural and/or depth electrodes implanted in epileptic patients for presurgical evaluations, various sensations, or behavioral effects elicited by DES have been reported (see below Section "Functional Mapping of the Eloquent Cortex Using DES"). In addition to these functional studies, several teams have used DES either to estimate functional anatomical connectivity (Buser and Bancaud, 1983; Matsumoto et al., 2004, 2007; Catenoix et al., 2005; Lacruz et al., 2007; Rosenberg et al., 2009), or to identify the epileptogenic area by searching for after-discharge thresholds (Cherlow et al., 1977; Engel et al., 1981; Chitoku et al., 2003) or abnormal brain responses (Valentin et al., 2002, 2005a,b; Flanagan et al., 2009), and by eliciting auras (Schulz et al., 1997) or complete seizures (Wieser et al., 1979; Bernier et al., 1987; Munari et al., 1993; David et al., 2008). These epileptic events induced by DES are likely to occur because epileptogenic networks may be particularly prone to short-term plasticity of synaptic weights induced by DES, at least in mesial temporal lobe epilepsy (Wilson et al., 1998; David et al., 2008).

Direct electrical stimulation is thus a very powerful technique to investigate network mechanisms in epilepsy. Here, we will review how brain connectivity can be assessed from responses obtained after electrical stimulation of cortical regions in epileptic patients implanted with depth or subdural grids. We will cover neither animal studies, nor therapeutic brain stimulation (for review, see Saillet et al., 2009). After a brief summary of mechanisms of action of brain electrical stimulation, we will first recall the conceptual framework that is classically used in imaging neuroscience to study brain connectivity. It appears that DES studies do not fit easily in this interpretational context, because electrical stimuli are non-physiological and elicit unusual neural responses. Second, we will briefly review studies that aimed at assessing the main brain functions using DES in epileptic patients. Third, abnormal responses to DES will be reviewed in the context of the identification of the seizure onset zone. Fourth, we will show how DES can be used to study brain plasticity. Finally, we will indicate how weak stimulation can also be tailored to anticipate seizures by using properties of brain responses to DES in relation to short-term structural changes of brain networks. From this review, we will conclude that this pool of exceptional data is underexploited by fundamental research on brain connectivity and leaves much to be learned.

MECHANISMS OF ACTION OF BRAIN ELECTRICAL STIMULATION

The effects of brain electrical stimulation within the central nervous system can be studied using neural modeling, neural recording, neurochemistry, and functional imaging (for review see McIntyre et al., 2004). Mechanisms of action of brain electrical stimulation are however not well understood because of the large number of intermingled processes that are initiated. Charge injection across the electrode/electrolyte (brain tissue) interface involves both capacitive and Faradaic mechanisms that interact and result in complex electrochemical reactions (Merrill et al., 2005). In view of this complexity, the choice of electrode material and geometry, and of stimulating patterns is crucial. One method that is commonly used for functional electrical stimulation of excitable tissue is the current-controlled method, in which a current source is attached between the working and counter electrode. Of considerable importance is the shape of current pulses. Specifically, it has been shown that monophasic pulses induce more tissue damage than biphasic pulses (Piallat et al., 2009), and should thus be avoided for long periods of stimulation. However, monophasic pulses are more efficient to initiate action potentials (Merrill et al., 2005), and are commonly used for short trains of stimulation in patients implanted with depth electrodes (Valentin et al., 2002, 2005a,b; Catenoix et al., 2005; Zumsteg et al., 2006a,b; David et al., 2008; Flanagan et al., 2009; Rosenberg et al., 2009). Biphasic pulses are nonetheless also used for acute stimulation by several teams (Wilson et al., 1990, 1998; Zangaladze et al., 2008; Jacobs et al., 2010).

It is now commonly accepted that the primary targets of intracerebral electrical stimulation are (large myelinated) axons, and not cell bodies (Nowak and Bullier, 1998a,b; Holsheimer et al., 2000; Kiss et al., 2003), and in particular that the initial segment of axons is the most excitable element recruited by electrical stimulation (Rattay, 1999). This has important implications for functional connectivity studies of DES responses. Indeed, both orthodromic and antidromic action potential propagation, which activates respectively the output and input structures of the stimulated area, can be observed. Also, one cannot completely exclude the activation of en passant fibers (axonal tracts), in particular when small deep nuclei are stimulated with strong currents. It is thus clear that localized microstimulation has remote effects, in addition to local ones. This is well documented from intracranial recordings that are specifically reviewed here, but also from functional imaging (Zonenshayn et al., 2000; Tolias et al., 2005; Canals et al., 2008).

Intracranial measurements of electrophysiological responses to DES are thought to capture mainly postsynaptic potentials resulting from indirect mono- or poly-synaptic cell activation (Jankowska et al., 1975) and thus provide a very interesting window on functional connectivity. However, there is an important limitation to this technique: DES delivers non-physiological stimuli and may activate pathways in an unusual way, e.g., antidromically. Therefore, because DES causes patterns of activation that may be different than natural neural activity, there will always be a potential indeterminacy in assessing true directionality of anatomo-functional connections identified with this technique. In other words, results of DES alone cannot be used to unequivocally establish that a given structure is naturally involved in a given function, despite DES of this structure has specific effects on that function. Empirically though, DES studies give invaluable insights into brain function and brain connectivity.

CONCEPTS OF BRAIN CONNECTIVITY IN THE CONTEXT OF DES STUDIES

Historically, behavioral consequences of localized brain lesions and biophysical measures of brain responses to various stimuli helped define what is now accepted as *functional specialization* of brain regions. This has led to localizationist theories of brain functions, but functional specialization is obviously not limited to location, because dense interregional connectivity makes any region of the brain part of an extended network (Sporns et al., 2005). Adhering to the principle of functional specialization thus does not necessarily imply that any function can be localized in a single area. Conversely, a single area may support different functions depending on its different connections.

For clarity, we will adopt the following definition:

Definition 1. A brain region participates in a brain function if a change in its activity is correlated to a change in that function, as assessed by subject's perception or behavior.

Note that this definition may be difficult to address experimentally if unconscious, or weakly observable, processes take place. In the context of DES studies, one could think of:

Corollary 1.1. A change in subject's perception or behavior induced by DES of a brain region indicates the functional specialization of that region.

This view of DES as a means to demonstrate functional specialization of specific brain regions predominates in the literature, and has proved to be very useful for functional neurosurgery of eloquent cortex. However, as perfectly reviewed in (Mandonnet et al., 2010), since each area responsive to stimulation is in fact an input gate into a large-scale network rather than an isolated discrete functional site, DES may lead to interpretations that a structure is crucial

because of the induction of a transient functional response when stimulated, whereas this effect is caused by the backward spreading of neuronal waves to another essential area. This might explain, at least in part, why apparently similar electrically induced symptoms can be elicited by distant areas (Mulak et al., 2008). An important modification to Corollary 1.1 is therefore required:

Corollary 1.2. A change in subject's perception or behavior induced by DES of a brain region indicates the functional specialization of *a large-scale network* of which that region either is an input/output or a part.

Though the physical effects of DES are very focal (<5 mm), "physiological" effects of DES clearly suggest that functional specialization is only meaningful in the context of functional integration. In DES experiments, the stimulated point is only an input gate into a large distributed network. As suggested by others (Mandonnet et al., 2010), one should forget about distinct localizationist and connectionist models and shift toward a theory that integrates these two when analyzing how DES works.

Functional integration is quantified using measures of *functional connectivity* which can be thought of as an extension of *functional specialization* in which the activity of a brain region is no longer correlated to an extrinsic measure (behavior or perception), but to the activity of one, or more, other brain regions:

Definition 2. Two regions are functionally connected if their activities co-vary.

In the context of mechanisms of action of DES, this can be rephrased as:

Corollary 2.1. Brain regions showing specific responses to DES of a brain region are functionally connected to it, *or* send axonal tracts passing through this region.

Corollary 2.1 clearly indicates that there is an inherent indeterminacy in the interpretation of connectivity results from DES experiments, which may not appear at first sight of the standard Definition 2 of functional connectivity. This has to be kept in mind for the following of this review.

Note also that, according to Definition 2, functional connectivity depends on how brain activity is defined (raw local field potentials, firing rate, etc.) and also on the measure of correlation, or covariation, of this activity. Therefore, there are as many measures of functional connectivity as ways of defining covariations between variables (for reviews see Quian Quiroga et al., 2002; David et al., 2004; Wendling et al., 2009). Approaches can rely on linear or non-linear metrics, can be bivariate (e.g., simple linear correlation) or multivariate (e.g., multivariate autoregressive models), and can account for time delays if necessary. An important distinction concerns statistical models versus biophysical models. Statistical models consider brain time series as any time-embedded process, and compute standard measures of interactions. Historically, they clearly predominate. Biophysical models are marginal and recent in comparison, but have the interesting feature to give access to variables that are neuronally interpretable (e.g., synaptic efficacy). This class of models includes dynamic causal models (DCM) (Friston et al., 2003; David et al., 2006a).

In theory, functional connectivity does not necessitate *anatomical connectivity*. For instance, it has been shown in rat hippocampal slices bathing in low-Ca^{2+} solution that extracellular diffusion, most probably of potassium, was sufficient to synchronize anatomically unconnected populations of neurons and propagate low-frequency epileptiform activity (Lian et al., 2001). However, in the context of cortical electrical stimulation, we will assume functional connectivity is implicitly supported by anatomical connectivity, by the means of direct or indirect pathways.

FUNCTIONAL MAPPING OF THE ELOQUENT CORTEX USING DES

Direct electrical stimulation has been extensively used in epilepsy, and a few other neurological disorders such as Parkinson's disease, for mapping of normal functions in the human brain. For epilepsy resective surgery, the main goal of DES is to identify the eloquent cortex, i.e., crucial functional regions to be spared by surgery.

One must be careful when assessing the effect of DES of epileptic cortices, because of possible structural changes that may have occurred in the lead-up or in response to repeated seizures. However, not every part of the brain studied by intracerebral or subdural electrodes is pathological (Lachaux et al., 2003), and DES results in epileptic patients have revealed the same somatotopic organization of the primary sensori-motor areas as in healthy brains, as well as congruent findings with those coming from functional magnetic resonance imaging studies in normal volunteers (Lobel et al., 2001). However the physiological significance of DES should be questioned when the stimulation is applied inside or at the vicinity of an epileptogenic lesion, or when it elicits after-discharges, i.e., electroencephalographic seizures evoked in response to cortical stimulation.

Largely for historical reasons, the commonly applied method of stimulation for functional mapping consists of using 3–20 s trains of constant current 50–60 Hz biphasic square wave pulses of 0.2–1 ms duration, at current intensity (~<10 mA) set below the threshold for evoking after-discharges (Penfield and Jasper, 1954; Luders et al., 1986). High frequency stimulation elicits both positive behavioral response (e.g., muscle contraction) and negative response (e.g., speech arrest). However, a number of brain areas seem to be "silent" after DES, which does not mean lack of function of those regions because subtle cognitive or behavioral changes can be missed. Recently, it has been demonstrated that stimulating at low frequencies (5–10 Hz) may be as effective for functional mapping, with the significant benefit of reducing the tendency of electrical stimulation to produce after-discharges (Zangaladze et al., 2008). In contradiction, DES at lower frequencies (1 Hz) would be of special interest for eliciting seizures (Munari et al., 1993). Whatever the frequency used, the electrical field produced by DES depends on other stimulation parameters such as the pulse duration and current intensity, and bipolar DES produces a more localized current distribution than unipolar stimulation (Nathan et al., 1993).

Below, we will briefly review DES assessment of sensorimotor and language processing, which are the systems most commonly investigated by DES. In principle, numerous other processes can be examined, such as verbal memory (Ojemann, 2003), spatial cognition, experiential auras, mental rotation (Thiebaut de Schotten et al., 2005), limbic responses (Elliott et al., 2009), out-of-body

experiences (Blanke et al., 2002), and dreamy state phenomena (Vignal et al., 2007). For completeness, note that an exhaustive review focused very recently on perceptual and behavioral phenomena induced by DES in human beings (Selimbeyoglu and Parvizi, 2010).

SENSORIMOTOR PROCESSING

The classic work of Penfield and Boldrey (1937) brought evidence in humans that cortical maps representing body parts (somatotopic maps) could be found in the primary motor and sensory cortices. In addition to body parts, it was proposed recently to map the motor cortex with DES as a function of behavioral repertoire (Graziano and Aflalo, 2007). The specific contribution to motor control of the different medial premotor areas was also evaluated using DES, including supplementary motor area (SMA), pre-SMA and cingulate motor area (CMA) (Lim et al., 1994; Luders et al., 1995; Chassagnon et al., 2008; Sumner et al., 2007). These studies particularly suggest that SMA and pre-SMA are strongly involved in motor inhibition. DES was also very useful to delineate human frontal eye fields in BA6 (Blanke et al., 2000; Lobel et al., 2001) and to examine cortico-spinal connectivity and muscle contraction during voluntary movement (Ikeda et al., 2002; Szelenyi et al., 2005).

Regarding sensory processing, early attempts discovered the possibility to obtain olfactory, gustatory, auditory, and somato-sensory responses to DES, Recently, the temporo-peri-Sylvian vestibular cortex was described in human from DES (Kahane et al., 2003) and DES of the insula was reported to be able to elicit pain (Afif et al., 2008). Visual responses to DES in the occipital lobe are common but vary according to stimulated areas and range from simple to complex visual form, color, and illusions (Lesser et al., 1998; Puce et al., 1999; Lee et al., 2000).

LANGUAGE PROCESSING

Direct electrical stimulation for language mapping in pharmacologically intractable epilepsy patients undergoing resection of epileptogenic cortex in the language dominant hemisphere has been widely and successfully used to diminish the probability of occurrence of language decline following the surgery. Because of response specificity, the tasks chosen to evaluate the effect of DES on language processing are critical. For instance, DES may induce speech arrest during counting in only 1/3 of all positive sites (i.e., sites where DES affected task performance) identified using other tasks such as naming or reading (Hamberger, 2007). It is therefore important to test in each patient several tasks, which incidentally makes DES very useful to identify individual components of language processing and their neural correlates. Hence, tasks such as visual or auditory object naming, automatic speech (e.g., counting), writing and reading were used to map language functions distributed in the frontal–temporal–parietal language network. Word retrieval was associated with posterior temporal lobe stimulated sites (Hamberger, 2007; Mani et al., 2008), whereas more anterior sites were involved in semantic processes *per se* (Sharp et al., 2004; Boatman and Miglioretti, 2005; Trebuchon-Da Fonseca et al., 2009) and speech production (Afif et al., 2010).

DES AS A TOOL FOR REVEALING NEUROANATOMICAL PATHWAYS

The vast majority of literature devoted to functional connectivity studies using cortical electrical stimulation in epileptic patients (Wilson et al., 1990; Catenoix et al., 2005; Lacruz et al., 2007; Rosenberg et al., 2009) considers DES as an efficient way to estimate which brain regions are anatomically connected to the site of stimulation. Responses to DES usually consist of a sharp deflection followed by a slow wave (Lacruz et al., 2007). Estimation of neuroanatomical pathways is performed by (i) the detection of sites showing such a response to the stimulation (by looking at amplitude variations above a threshold defined according to baseline level); (ii) the measure of first peak latency to estimate roughly whether anatomical connections are direct or indirect. Methodology is thus typically limited to quantifying amplitude and delay of DES-evoked responses. Our recent study, discussed in a following section (David et al., 2008), went beyond this by using biophysical modeling of intracranial data to assess brain connectivity from responses to DES.

Because patients suffering from mesial-temporal lobe epilepsy are good candidates for resective surgery, they are commonly explored with depth electrodes, located in temporal limbic regions and also in suspected regions of seizure propagation such as temporal, insular, and frontal neocortex. As a consequence, functional anatomical connectivity of the temporal and of the frontal lobes is extensively discussed in the DES literature.

In Wilson et al. (1990), connections within the human mesial temporal lobe were investigated using brief, single pulses of electric stimulation of 8 different limbic areas in 74 epileptic patients. Biphasic, rectangular pulses of 100 μs/phase duration were delivered at a rate of 0.1 Hz or less, with currents ranging from 0.25 to 5.0 mA. Specific measures included response probability, amplitude, latency (first peak detection) and conduction velocities (estimated distance between targeted stimulation and recording site divided by the onset response latency). Evoked responses were obtained in amygdala, entorhinal cortex, presubiculum, hippocampus, and parahippocampal gyrus. The authors were able to differentiate fast pathways (perforant path connecting entorhinal cortex to anterior hippocampus; 4.4 ms conduction delay and 3.64 m/s conduction speed) from slow pathways (connection between amygdala and middle hippocampus; 24.8 ms and 0.88 m/s). In addition, from the absence of contralateral responses to the stimulation of the mesial temporal structures, they did not find a functional contralimbic projection in the human brain, which appears consistent with reduced hippocampal commissural connections in lower primates as compared to lower animals.

In (Lacruz et al., 2007), functional anatomical connectivity between frontal (medial, lateral, and orbital) and temporal (entorhinal, medial, and lateral) lobes has been described extensively using brain responses to 1 ms single pulses, delivered every 10 s at current intensity ranging between 4 and 8 mA, obtained in 51 epileptic patients implanted with subdural and depth electrodes. The measured variables were the presence or absence of early responses at different recording sites when stimulating each location and the latency of contralateral responses. Anatomical functional connections were assessed by quantifying the number of

electrodes showing evoked responses. Contralateral temporal connections were found to be rare (<9% of stimulated hemispheres), as in (Wilson et al., 1990). This appeared distinct to interhemispheric frontal connections, which were faster and more common (>57% of stimulated hemispheres). Intralobar connections were frequent, either in the temporal (>67% of stimulated hemispheres) or in the frontal (>78% of stimulated hemispheres) cortices. In addition, ipsilateral connections from frontal toward temporal cortices were found to be more prominent than in the opposite direction. Because of limited spatial sampling, but also of physiological limitations such as attenuation of the signal in polysynaptic pathways and the recruitment of inhibition, these connectivity figures should be regarded as the lower limit of the true functional connectivity.

Using single pulses (3 mA current intensity, 1 ms duration, 0.2 Hz frequency), Catenoix et al. (2005) were the first to describe orbitofrontal cortex responses following electrical stimulation of temporomesial structures in humans, in a small group of three patients. They found a long latency of the main response (222 ms on average) that suggested a polysynaptic projection of the hippocampus to the orbitofrontal cortex. In the absence of strong hippocampal commissural pathway in humans (Wilson et al., 1990, 1991), these results strongly support the existence of a temporal frontal pathway for the interhemispheric propagation of mesial temporal seizures (Lieb et al., 1991).

Using the same stimulation protocol, this team recently published an extension of this work on temporal frontal connections, where the focus was on reciprocal thalamocortical connectivity of the medial pulvinar (PuM) estimated in seven epileptic patients implanted with thalamic and cortical electrodes (Rosenberg et al., 2009). Cortical-evoked potentials to PuM stimulation were recorded from all explored cortical regions, except striate cortex, anterior cingulate, and postcentral gyrus. Response rate was high, and ranged from 80% in temporal neocortex, temporoparietal junction, insula, and frontoparietal opercular cortex to 34% in mesial temporal regions. Reciprocally, PuM responses were observed following cortical stimulation, with response rate ranging from 14% (insula and frontoparietal opercular cortex) to 76–80% (temporal neocortex and mesial temporal regions). From these findings, it is clear that there exist functional pathways between thalamic medial pulvinar nucleus and numerous cortical regions, with preferential and fastest pathways that interconnect the PuM with the temporal neocortex, the temporoparietal junction and the insulo-opercular region. This explains why PuM is involved in most of temporal and insular lobe seizures (Rosenberg et al., 2006). These results agree with data gathered in non-human primates, except for the important connectivity between pulvinar and hippocampus in primates. Another important point is the unexpected imbalance between some reciprocal pathways (with the insula, notably), which could not be found using magnetic resonance tractography for instance (Behrens et al., 2003), whereas the connections between the major sensory thalamic relay nuclei and cortex are considered as "reciprocal" (Steriade et al., 1997).

DES AS A TOOL FOR REVEALING EPILEPTOGENIC NETWORKS

Single pulse (Valentin et al., 2002, 2005a,b; Flanagan et al., 2009), paired pulse (Wilson et al., 1998), and repetitive (i.e., trains of pulses) (Buser and Bancaud, 1983; Kahane et al., 1993, 2004; Landré et al., 2004; Kalitzin et al., 2005) stimulation have been shown to be useful in localizing the seizure onset zone in patients suffering from various forms of focal epilepsy.

EPILEPTIC RESPONSES TO SINGLE PULSES OR TO SHORT TRAINS OF PULSES

In a series of papers (Valentin et al., 2002, 2005a,b; Flanagan et al., 2009), Alarcón and colleagues classified responses to single pulses into three types: (i) "early responses" composed of a sharp wave often followed by a slow wave, which is ubiquitous and reflects normal processes. This is the type of response exploited for anatomical functional studies and discussed so far in this review; (ii) "delayed responses" that resembles an epileptiform discharge occurring later than 100 ms after stimulus, thus indicating polysynaptic processes. They are thought of as pathological responses generated by areas of seizure onset; (iii) "repetitive responses" that look like early responses, but with longer lasting oscillations which may be initiated by reverberating loops. In fact, they are similar to damped oscillations that can be obtained with neural mass models with connectivity parameters tuned so as to be just below the threshold of stability, e.g., with strong intrinsic excitatory efficacy or feedback connections (David et al., 2005).

Recently, Gotman and colleagues studied the effects of another standard type of stimulation, i.e., short trains of high frequency pulses, in patients having either mesiotemporal or neocortical seizure onset zones (Jacobs et al., 2010). They found that the sites showing interictal high frequency oscillations (HFOs – ripples, 80–250 Hz; fast ripples, 250–500 Hz), thought to be linked to seizure onset (Jirsch et al., 2006), were the same as those showing afterdischarges or seizures elicited by electrical stimulation (bipolar biphasic 60 Hz stimulus, pulse width = 0.5 ms, 3–4 s duration, electrical currents <2 mA in mesial temporal and <10 mA in neocortical regions), especially in neocortical regions.

PLASTICITY OF EPILEPTOGENIC NETWORKS INDUCED BY REPEATED ELECTRICAL STIMULATION

Delayed, repetitive and HFO responses directly point toward the idea that epileptogenic networks are hyperexcitable. In addition, there is evidence that epileptogenic networks are prone to exhibit fast structural modifications via the reorganization of synaptic weights: From *in vitro* and *in vivo* animal studies, it is well known that repeated electrical stimulation may induce massive reorganization of brain networks, particularly in the hippocampus (Bliss and Lomo, 1973). In humans, although long-term potentiation cannot be easily demonstrated because of lack of experimental possibilities, it has been possible to identify short-term plasticity effects.

The most standard, but not unique, paradigm of stimulation to study short-term plasticity is paired-pulse stimulation. Paired-pulse stimulation detects excitability changes on the assumption that the first (conditioning) stimulus acts to recruit recurrent excitatory or inhibitory activity, which affords detecting facilitatory or suppressive effect upon the response to the second (test) stimulus. Paired-pulse inhibition is thought to reflect changes of presynaptic release probability and the influence of recurrent inhibition (Zucker and Regehr, 2002). Analyzing the different patterns of paired-pulse facilitation and paired-pulse inhibition may also give

some insights for distinguishing neuronal drivers from neuronal modulators (Reichova and Sherman, 2004). In mesial temporal lobe epilepsy (MTLE), paired-pulse induced changes of synaptic and intrinsic excitability are usually more easily observed in the hippocampus than in the neocortex (Koch et al., 2005). *In vitro* experiments (Feng et al., 2003) allowed to gather more information about neuronal mechanisms involved. Modulation of NMDA or kainate receptors, the receptor type depending on the structures involved, was systematically found to be associated with electrically induced short-term plasticity in epilepsy. As shown by using trains of stimuli at different frequencies (Feng et al., 2003; Schiller and Bankirer, 2007), short-term plasticity is frequency-dependent and can be either inhibitory or excitatory. When repetitive stimulation has an anti-epileptic effect, this effect is mediated mainly by short-term synaptic depression of excitatory neurotransmission (Schiller and Bankirer, 2007).

In MTLE patients, *in vivo*, a significantly greater paired-pulse suppression has been observed in epileptic regions, by comparing the epileptic hemisphere to the contralateral intact hemisphere in 20 patients (Wilson et al., 1998). Hippocampal pathways and perforant path responses located in the epileptogenic lobe showed greater paired-pulse suppression of population post-synaptic potentials. These authors derived from these responses interesting hypotheses about adaptive enhanced inhibition to inhibit seizures produced by abnormal recurrent excitatory circuits. In other words, increased short-term plasticity has been interpreted as a functional consequence of the formation of abnormal recurrent inhibitory and excitatory pathways in the sclerotic hippocampus.

By analyzing the preictal modulation in time of the shape of responses evoked by 1 Hz stimulation in twenty MTLE patients, we have shown that the seizure onset zone was particularly likely to show fast changing evoked responses to DES, even of remote areas (David et al., 2008). In this study, we have first developed a pure data-driven analysis to illustrate that short-term plasticity could be quantified easily for clinical purposes. However, this type of data analysis, which is commonly used in DES studies, is very limited for the explanation of the underlying neural mechanisms. In a second step, we moved further and showed how synaptic plasticity could be explicitly modeled using generative models of local field potentials (David et al., 2005). We used dynamic causal modeling (DCM) (David et al., 2006a) and assumed different possible neural network configurations within the temporal lobe, with some connections expressing synaptic plasticity via a modulation of their weight between successive stimulations. After parameter estimation (intrinsic neural parameters and coupling between regions) from measured evoked responses and Bayesian model selection (Penny et al., 2004), we were able to estimate the general architecture of stimulated temporal networks, and to demonstrate that observed modification of the shape of evoked responses to DES was sufficiently explained by a modulation of excitatory efficacies within temporal lobe circuitry.

For instance, in two patients stimulated in the amygdala who showed a strong increase of the amplitude of responses in the anterior hippocampus a few stimulations before the seizure onset, an increase of effective connectivity between the temporal pole and the anterior hippocampus was found. This pathway is supported by human anatomical studies showing that the hippocampus receives afferents from all over the anterior temporal cortex and an amygdala-temporal fascicle that originates at the rostrolateral surface of the amygdala and specifically connects to the temporal pole (Klingler and Gloor, 1960; Chabardes et al., 2002). Furthermore, it is known from visual analysis of SEEG recordings that the temporal pole is a determinant structure, concomitantly with the hippocampus, during the onset of seizures in temporal lobe epilepsy in many patients (Kahane et al., 2002; Chabardes et al., 2005). The results obtained from this small DCM study call for an interpretation of the genesis of a certain type of mesial temporal lobe epilepsy as a preictal increase of the hippocampal afferents coming from the temporal pole, which could be triggered by the amygdala. This putative type of mesial temporal lobe epilepsy remains to be fully characterized.

It is important to develop further models of DES to better understand the network mechanisms of action of this type of stimulation. Among the different lines of research, a possibility is to extend the current DCM framework (Daunizeau et al., 2009) and, under due consideration of the limits of statistical inversion, represent different neurobiological mechanisms of synaptic plasticity more explicitly, such that their relative importance can be disambiguated by model selection. Since aberrant plasticity is a central pathological mechanism in many brain diseases, and particularly epilepsy, developing *plastic* DCMs that can distinguish between different aspects of synaptic plasticity has an interesting potential for establishing physiologically interpretable diagnostic markers. As an academic exercise, we have made an early attempt in this direction by proposing a reinterpretation of short-term plasticity induced by 1 Hz DES in the context of autopoietic theory (Varela et al., 1974; David, 2007). This deserves to be pursued.

ACTIVE ANTICIPATION OF SEIZURE USING DES

Brain networks are very complex and generate spontaneous brain dynamics that are difficult to understand fully. In the recent years, emphasis has been put on synchronous oscillations which have been proposed to support large scale integration during cognitive processes (Varela et al., 2001). Another interpretation of transient features of brain dynamics correlated to behavior, or thoughts, has generalized and extended frequency-specific synchronization using tools from non-linear physics that embed brain signals in a multidimensional "state space." Successive transient synchronization of brain activity may then be thought of as the evolution of the system through a temporal sequence of different local attractors segregated in that state space (Tsuda, 2001). This latter theoretical framework is interesting for reading epileptic signals because a seizure is characterized by hypersynchronous and non-linear oscillations, two properties that are well captured by the formalism of non-linear dynamics. Briefly, transient hypersynchronicity corresponds to the transition of the state of the system from a region of high-dimensional chaos toward a low-dimensional attractor, the shape of which depends on the kind of non-linearity of the signals. Thus a seizure can be interpreted as a transition of the brain states from a succession of high-dimensional "physiological" states toward a low-dimensional "epileptic" state. It is important to question what sorts of dynamics govern that transition.

In the previous sections, we have shown that repetitive stimulation using strong current intensity (>1 mA) was able to initiate after-discharges and complete seizures (David et al., 2008), possibly by the means of short-term plasticity mechanisms in brain networks. These seizures then represent transitions due to shifts in one or more parameters of the system. These parameters, e.g., synaptic efficacies, are structural in the sense that they govern dynamic responses of the brain, e.g., evoked responses to a brief stimulation (David et al., 2006b). If the preictal modifications of the parameters show a slow time evolution which can take several minutes, hours or days, analyzing dynamical properties of the brain to a stimulation is a way to reveal structural modifications. In principle, it can thus be used to anticipate seizures.

Stimulation-based seizure anticipation, reviewed in (Kalitzin et al., 2010), has been proposed by Lopes da Silva and colleagues. Early trials were based on photic stimulation in patients having photosensitive epilepsy (Kalitzin et al., 2002; Parra et al., 2003). This was followed by an experimental validation using intracerebral stimulation of the hippocampus in six patients (Kalitzin et al., 2005) and by simulations (Suffczynski et al., 2008). They used intermittent pulse stimulation (0.5–1 mA; 0.1 ms pulse width; trains of 5 s duration) in the frequency range 10–20 Hz and quantified the responsiveness of neural networks using a quantitative measure of spectral phase demodulation called the relative phase clustering index (rPCI). Although seizures could not be anticipated precisely, regions showing high interictal rPCI correlated with the seizure onset zone. Measurements of the modulation of neural synchronization of brain networks by the means of electrical stimulation are thus potentially an interesting approach for seizure anticipation techniques. More clinical trials are needed to better evaluate the specificity of such findings.

CONCLUSION

In this review, we have tried to show the multiple possibilities of DES to study network mechanisms in epilepsy. They mainly relate to the opportunity to identify, in the human brain, epileptogenic and plastic network properties, in addition to *oriented* neuroanatomical pathways, which is unique. Strikingly, these exceptional data have not yet been the object of many methodological studies, possibly, at least in part, because of ethical aspects that cannot be underestimated. This let us suppose that many interesting features regarding brain connectivity remain to be discovered from DES data, should adequate signal analysis techniques be applied to them, and experimental protocols be not deleterious for the patients.

Though we have not reviewed extensively this issue here, there are actually very few DES studies that combine direct stimulation and recordings of cortical activity during fluctuations of resting state, cognitive tasks and/or behavioral evaluations (e.g., Sinai et al., 2009; see for review Selimbeyoglu and Parvizi, 2010). Among them, an attempt was made to decipher brain connectivity in an epileptic patient during vivid memory recollection following perirhinal DES (Barbeau et al., 2005). This study showed that there was a widespread (between limbic and visual brain areas) theta synchronization quantified using cross-correlation analyzes. Another recent advance on DES mechanisms and their relationship to local physiological brain states was made (Lesser et al., 2008). These authors showed that spontaneous brain electrical activity at the moment of DES delivery could be predictive of an after-discharge occurrence that was often restricted to sites belonging to the same functional network (motor, sensory, or language) as the site of stimulation. Therefore, these authors speculated that similar rapid variations may occur during normal intracortical communication and may underlie changes in the cortical organization of functions. A potentially very interesting line of research for the coming years would thus be exploit further this hypothesis and to examine (i) how the perceptual and behavioral effects of DES may vary according to the undergoing cognitive task, (ii) how functional connectivity is affected after DES is applied during various cognitive tasks and (iii) how resting state connectivity at the moment of DES delivery might predict DES effects, both at the behavioral and electrophysiological levels.

Because they allow transient modifications of brain dynamics, DES studies can investigate short-term plastic network properties of several systems in a limited amount of time. Under the hypothesis that epileptogenic networks are hyperexcitable, and thus prone to exhibit short-term plasticity, plasticity analysis of DES responses is potentially a very powerful clinical tool to quickly identify epileptic foci (David et al., 2008). Thus, DES studies go well beyond lesion studies performed in animals or in stroke patients. However, they present some important limitations for connectivity analyses: though perceptual, behavioral, and epileptic phenomena can easily be induced by DES in human beings (Kahane et al., 2004; Selimbeyoglu and Parvizi, 2010), the use of macroelectrodes precludes the precise control of the mechanisms by which neurologists or neurosurgeons interact with patients' brain. For instance, it is difficult to evaluate in what exact proportions antidromic and orthodromic propagation take place, or if observed effects are mainly mediated by the activation of local neuronal populations, or by the stimulation of en passant fibers that target distributed remote regions. These experimental limitations are crucial regarding the key concepts of functional brain mapping that underlie the way we analyze recorded data (see above Section "Concepts of Brain Connectivity in the Context of DES Studies"). In that respect, DES studies differ from other functional studies because they elicit unusual brain responses mediated by the means of unusual input gates to the human brain. This is something that has to be kept in mind when anatomical, functional, or computational models of the brain are derived from the DES literature. In terms of biophysical modeling of DES responses, the experimental uncertainty summarized in Corollary 2.1, i.e., in a given experiment does DES target local neuronal populations or en passant fibers?, must be taken into account. For instance in the framework of DCM, this could correspond to loose priors on how DES input perturb the system, i.e., on the extrinsic connectivity matrix (David et al., 2008). Hopefully, in addition to these theoretical considerations, new data coming from the optogenetic literature in animals (Miesenbock, 2009) will shed new light on how one can model human brain connectivity from DES responses.

ACKNOWLEDGMENTS

This work was funded by INSERM, Agence Nationale pour la Recherche and Fondation pour la Recherche Médicale.

REFERENCES

Afif, A., Hoffmann, D., Minotti, L., Benabid, A. L., and Kahane, P. (2008). Middle short gyrus of the insula implicated in pain processing. *Pain* 138, 546–555.

Afif, A., Minotti, L., Kahane, P., and Hoffmann, D. (2010). Middle short gyrus of the insula implicated in speech production: intracerebral electric stimulation of patients with epilepsy. *Epilepsia* 51, 206–213.

Barbeau, E., Wendling, F., Regis, J., Duncan, R., Poncet, M., Chauvel, P., and Bartolomei, F. (2005). Recollection of vivid memories after perirhinal region stimulations: synchronization in the theta range of spatially distributed brain areas. *Neuropsychologia* 43, 1329–1337.

Behrens, T. E., Johansen-Berg, H., Woolrich, M. W., Smith, S. M., Wheeler-Kingshott, C. A., Boulby, P. A., Barker, G. J., Sillery, E. L., Sheehan, K., Ciccarelli, O., Thompson, A. J., Brady, J. M., and Matthews, P. M. (2003). Non-invasive mapping of connections between human thalamus and cortex using diffusion imaging. *Nat. Neurosci.* 6, 750–757.

Bernier, G. P., Saint-Hilaire, J. M., Giard, N., Bouvier, G., and Mercier, M. (1987). "Commentary: intracranial electrical stimulation," in *Surgical Treatment of the Epilepsies*, ed. J. Engel Jr. (New York: Raven Press), 323–334.

Blanke, O., Ortigue, S., Landis, T., and Seeck, M. (2002). Stimulating illusory own-body perceptions. *Nature* 419, 269–270.

Blanke, O., Spinelli, L., Thut, G., Michel, C. M., Perrig, S., Landis, T., and Seeck, M. (2000). Location of the human frontal eye field as defined by electrical cortical stimulation: anatomical, functional and electrophysiological characteristics. *Neuroreport* 11, 1907–1913.

Bliss, T. V., and Lomo, T. (1973). Long-lasting potentiation of synaptic transmission in the dentate area of the anaesthetized rabbit following stimulation of the perforant path. *J. Physiol.* 232, 331–356.

Boatman, D. F., and Miglioretti, D. L. (2005). Cortical sites critical for speech discrimination in normal and impaired listeners. *J. Neurosci.* 25, 5475–5480.

Buser, P., and Bancaud, J. (1983). Unilateral connections between amygdala and hippocampus in man. A study of epileptic patients with depth electrodes. *Electroencephalogr. Clin. Neurophysiol.* 55, 1–12.

Canals, S., Beyerlein, M., Murayama, Y., and Logothetis, N. K. (2008). Electric stimulation fMRI of the perforant pathway to the rat hippocampus. *Magn. Reson. Imaging* 26, 978–986.

Catenoix, H., Magnin, M., Guenot, M., Isnard, J., Mauguiere, F., and Ryvlin, P. (2005). Hippocampal-orbitofrontal connectivity in human: an electrical stimulation study. *Clin. Neurophysiol.* 116, 1779–1784.

Chabardes, S., Kahane, P., Minotti, L., Hoffmann, D., and Benabid, A. L. (2002). Anatomy of the temporal pole region. *Epileptic. Disord.* 4(Suppl. 1), S9–S15.

Chabardes, S., Kahane, P., Minotti, L., Tassi, L., Grand, S., Hoffmann, D., and Benabid, A. L. (2005). The temporopolar cortex plays a pivotal role in temporal lobe seizures. *Brain* 128, 1818–1831.

Chassagnon, S., Minotti, L., Kremer, S., Hoffmann, D., and Kahane, P. (2008). Somatosensory, motor, and reaching/grasping responses to direct electrical stimulation of the human cingulate motor areas. *J. Neurosurg.* 109, 593–604.

Cherlow, D. G., Dymond, A. M., Crandall, P. H., Walter, R. D., and Serafetinides, E. A. (1977). Evoked response and after-discharge thresholds to electrical stimulation in temporal lobe epilepsy. *Arch. Neurol.* 34, 527–531.

Chitoku, S., Otsubo, H., Harada, Y., Jay, V., Rutka, J. T., Weiss, S. K., Elliott, I., Ochi, A., Kitayama, M., and Snead, O. C. III (2003). Characteristics of prolonged afterdischarges in children with malformations of cortical development. *J. Child Neurol.* 18, 247–253.

Daunizeau, J., David, O., and Stephan, K. E. (2009). Dynamic causal modelling: a critical review of the biophysical and statistical foundations. *Neuroimage* doi: 10.1016/j.neuroimage.2009.11.062.

David, O. (2007). Dynamic causal models and autopoietic systems. *Biol. Res.* 40, 487–502.

David, O., Cosmelli, D., and Friston, K. J. (2004). Evaluation of different measures of functional connectivity using a neural mass model. *Neuroimage* 21, 659–673.

David, O., Harrison, L., and Friston, K. J. (2005). Modelling event-related responses in the brain. *Neuroimage* 25, 756–770.

David, O., Kiebel, S. J., Harrison, L. M., Mattout, J., Kilner, J. M., and Friston, K. J. (2006a). Dynamic causal modeling of evoked responses in EEG and MEG. *Neuroimage* 30, 1255–1272.

David, O., Kilner, J. M., and Friston, K. J. (2006b). Mechanisms of evoked and induced responses in MEG/EEG. *Neuroimage* 31, 1580–1591.

David, O., Wozniak, A., Minotti, L., and Kahane, P. (2008). Preictal short-term plasticity induced by intracerebral 1 Hz stimulation. *Neuroimage* 39, 1633–1646.

Duffau, H., Peggy Gatignol, S. T., Mandonnet, E., Capelle, L., and Taillandier, L. (2008). Intraoperative subcortical stimulation mapping of language pathways in a consecutive series of 115 patients with Grade II glioma in the left dominant hemisphere. *J. Neurosurg.* 109, 461–471.

Elliott, B., Joyce, E., and Shorvon, S. (2009). Delusions, illusions and hallucinations in epilepsy: 1. Elementary phenomena. *Epilepsy Res.* 85, 162–171.

Engel, J. Jr., Rausch, R., Lieb, J. P., Kuhl, D. E., and Crandall, P. H. (1981). Correlation of criteria used for localizing epileptic foci in patients considered for surgical therapy of epilepsy. *Ann. Neurol.* 9, 215–224.

Feng, L., Molnar, P., and Nadler, J. V. (2003). Short-term frequency-dependent plasticity at recurrent mossy fiber synapses of the epileptic brain. *J. Neurosci.* 23, 5381–5390.

Flanagan, D., Valentin, A., Garcia Seoane, J. J., Alarcon, G., and Boyd, S. G. (2009). Single-pulse electrical stimulation helps to identify epileptogenic cortex in children. *Epilepsia* 50, 1793–1803.

Friston, K. J., Harrison, L., and Penny, W. (2003). Dynamic causal modelling. *Neuroimage* 19, 1273–1302.

Graziano, M. S., and Aflalo, T. N. (2007). Mapping behavioral repertoire onto the cortex. *Neuron* 56, 239–251.

Hamberger, M. J. (2007). Cortical language mapping in epilepsy: a critical review. *Neuropsychol. Rev.* 17, 477–489.

Holsheimer, J., Demeulemeester, H., Nuttin, B., and de Sutter, P. (2000). Identification of the target neuronal elements in electrical deep brain stimulation. *Eur. J. Neurosci.* 12, 4573–4577.

Ikeda, A., Miyamoto, S., and Shibasaki, H. (2002). Cortical motor mapping in epilepsy patients: information from subdural electrodes in presurgical evaluation. *Epilepsia* 43(Suppl. 9), 56–60.

Jacobs, J., Zijlmans, M., Zelmann, R., Olivier, A., Hall, J., Gotman, J., and Dubeau, F. (2010). Value of electrical stimulation and high frequency oscillations (80-500 Hz) in identifying epileptogenic areas during intracranial EEG recordings. *Epilepsia* 51, 573–582.

Jankowska, E., Padel, Y., and Tanaka, R. (1975). The mode of activation of pyramidal tract cells by intracortical stimuli. *J. Physiol.* 249, 617–636.

Jefferys, J. G., and Whittington, M. A. (1996). Review of the role of inhibitory neurons in chronic epileptic foci induced by intracerebral tetanus toxin. *Epilepsy Res.* 26, 59–66.

Jerbi, K., Ossandon, T., Hamame, C. M., Senova, S., Dalal, S. S., Jung, J., Minotti, L., Bertrand, O., Berthoz, A., Kahane, P., and Lachaux, J. P. (2009). Task-related gamma-band dynamics from an intracerebral perspective: review and implications for surface EEG and MEG. *Hum. Brain Mapp.* 30, 1758–1771.

Jirsch, J. D., Urrestarazu, E., LeVan, P., Olivier, A., Dubeau, F., and Gotman, J. (2006). High-frequency oscillations during human focal seizures. *Brain* 129, 1593–1608.

Jones, D. K. (2008). Studying connections in the living human brain with diffusion MRI. *Cortex* 44, 936–952.

Kahane, P., Chabardes, S., Minotti, L., Hoffmann, D., Benabid, A. L., and Munari, C. (2002). The role of the temporal pole in the genesis of temporal lobe seizures. *Epileptic Disord.* 4(Suppl. 1), S51–S58.

Kahane, P., Hoffmann, D., Minotti, L., and Berthoz, A. (2003). Reappraisal of the human vestibular cortex by cortical electrical stimulation study. *Ann. Neurol.* 54, 615–624.

Kahane, P., Minotti, L., Hoffmann, D., Lachaux, J. P., Ryvlin, P., Rosenow, F., and Lüders, H. O. (2004). "Invasive EEG in the definition of the seizure onset zone: depth electrodes," in *Handbook of Clinical Neurophysiology,* Vol. 3 eds F. Rosenow and H. Luders (Amsterdam: Elsevier BV), 109–133.

Kahane, P., Tassi, L., Francione, S., Hoffmann, D., Lo, R. G., and Munari, C. (1993). Electroclinical manifestations elicited by intracerebral electric stimulation "shocks" in temporal lobe epilepsy. *Neurophysiol. Clin.* 23, 305–326.

Kalitzin, S., Parra, J., Velis, D. N., and Lopes da Silva, F. H. (2002). Enhancement of phase clustering in the EEG/MEG gamma frequency band anticipates transitions to paroxysmal epileptiform activity in epileptic patients with known visual sensitivity. *IEEE Trans. Biomed. Eng.* 49, 1279–1286.

Kalitzin, S., Velis, D., Suffczynski, P., Parra, J., and da Silva, F. L. (2005). Electrical brain-stimulation paradigm for estimating the seizure onset site and the time to ictal transition in temporal lobe epilepsy. *Clin. Neurophysiol.* 116, 718–728.

Kalitzin, S. N., Velis, D. N., and da Silva, F. H. (2010). Stimulation-based anticipation and control of state transitions in the epileptic brain. *Epilepsy Behav.* 17, 310–323.

Kiss, Z. H., Anderson, T., Hansen, T., Kirstein, D., Suchowersky, O., and Hu, B. (2003). Neural substrates of microstimulation-evoked tingling: a chronaxie study in human

somatosensory thalamus. *Eur. J. Neurosci.* 18, 728–732.

Klingler, J., and Gloor, P. (1960). The connections of the amygdala and of the anterior temporal cortex in the human brain. *J. Comp. Neurol.* 115, 333–369.

Koch, U. R., Musshoff, U., Pannek, H. W., Ebner, A., Wolf, P., Speckmann, E. J., and Kohling, R. (2005). Intrinsic excitability, synaptic potentials, and short-term plasticity in human epileptic neocortex. *J. Neurosci. Res.* 80, 715–726.

Lachaux, J. P., Rudrauf, D., and Kahane, P. (2003). Intracranial EEG and human brain mapping. *J. Physiol. Paris* 97, 613–628.

Lacruz, M. E., Garcia Seoane, J. J., Valentin, A., Selway, R., and Alarcon, G. (2007). Frontal and temporal functional connections of the living human brain. *Eur. J. Neurosci.* 26, 1357–1370.

Landré, E., Turak, B., Toussaint, D., and Trottier, S. (2004). Intérêt des stimulations électriques intracérébrales en stéréo-électroencéphalographie dans les épilepsies partielles. *Epilepsies* 16, 213–225.

Lee, H. W., Hong, S. B., Seo, D. W., Tae, W. S., and Hong, S. C. (2000). Mapping of functional organization in human visual cortex: electrical cortical stimulation. *Neurology* 54, 849–854.

Lesser, R. P., Arroyo, S., Crone, N., and Gordon, B. (1998). Motor and sensory mapping of the frontal and occipital lobes. *Epilepsia* 39(Suppl. 4), S69–S80.

Lesser, R. P., Lee, H. W., Webber, W. R., Prince, B., Crone, N. E., and Miglioretti, D. L. (2008). Short-term variations in response distribution to cortical stimulation. *Brain* 131, 1528–1539.

Lian, J., Bikson, M., Shuai, J., and Durand, D. M. (2001). Propagation of non-synaptic epileptiform activity across a lesion in rat hippocampal slices. *J. Physiol.* 537, 191–199.

Lieb, J. P., Dasheiff, R. M., and Engel, J. Jr. (1991). Role of the frontal lobes in the propagation of mesial temporal lobe seizures. *Epilepsia* 32, 822–837.

Lim, S. H., Dinner, D. S., Pillay, P. K., Luders, H., Morris, H. H., Klem, G., Wyllie, E., and Awad, I. A. (1994). Functional anatomy of the human supplementary sensorimotor area: results of extraoperative electrical stimulation. *Electroencephalogr. Clin. Neurophysiol.* 91, 179–193.

Lobel, E., Kahane, P., Leonards, U., Grosbras, M., Lehericy, S., Le Bihan, D., and Berthoz, A. (2001). Localization of human frontal eye fields: anatomical and functional findings of functional magnetic resonance imaging and intracerebral electrical stimulation. *J. Neurosurg.* 95, 804–815.

Luders, H., Lesser, R. P., Hahn, J., Dinner, D. S., Morris, H., Resor, S., and Harrison, M. (1986). Basal temporal language area demonstrated by electrical stimulation. *Neurology* 36, 505–510.

Luders, H. O., Dinner, D. S., Morris, H. H., Wyllie, E., and Comair, Y. G. (1995). Cortical electrical stimulation in humans. The negative motor areas. *Adv. Neurol.* 67, 115–129.

Mandonnet, E., Winkler, P. A., and Duffau, H. (2010). Direct electrical stimulation as an input gate into brain functional networks: principles, advantages and limitations. *Acta Neurochir. (Wien)* 152, 185–193.

Mani, J., Diehl, B., Piao, Z., Schuele, S. S., Lapresto, E., Liu, P., Nair, D. R., Dinner, D. S., and Luders, H. O. (2008). Evidence for a basal temporal visual language center: cortical stimulation producing pure alexia. *Neurology* 71, 1621–1627.

Matsumoto, R., Nair, D. R., LaPresto, E., Bingaman, W., Shibasaki, H., and Luders, H. O. (2007). Functional connectivity in human cortical motor system: a cortico-cortical evoked potential study. *Brain* 130, 181–197.

Matsumoto, R., Nair, D. R., LaPresto, E., Najm, I., Bingaman, W., Shibasaki, H., and Luders, H. O. (2004). Functional connectivity in the human language system: a cortico-cortical evoked potential study. *Brain* 127, 2316–2330.

McIntyre, C. C., Savasta, M., Kerkerian-Le, G. L., and Vitek, J. L. (2004). Uncovering the mechanism(s) of action of deep brain stimulation: activation, inhibition, or both. *Clin. Neurophysiol.* 115, 1239–1248.

Merrill, D. R., Bikson, M., and Jefferys, J. G. (2005). Electrical stimulation of excitable tissue: design of efficacious and safe protocols. *J. Neurosci. Methods* 141, 171–198.

Mesulam, M. M. (1979). Tracing neural connections of human brain with selective silver impregnation. Observations on geniculocalcarine, spinothalamic, and entorhinal pathways. *Arch. Neurol.* 36, 814–818.

Miesenbock, G. (2009). The optogenetic catechism. *Science* 326, 395–399.

Morimoto, K., Fahnestock, M., and Racine, R. J. (2004). Kindling and status epilepticus models of epilepsy: rewiring the brain. *Prog. Neurobiol.* 73, 1–60.

Mulak, A., Kahane, P., Hoffmann, D., Minotti, L., and Bonaz, B. (2008). Brain mapping of digestive sensations elicited by cortical electrical stimulations. *Neurogastroenterol. Motil.* 20, 588–596.

Munari, C., Kahane, P., Tassi, L., Francione, S., Hoffmann, D., Lo, R. G., and Benabid, A. L. (1993). Intracerebral low frequency electrical stimulation: a new tool for the definition of the "epileptogenic area"? *Acta Neurochir. Suppl. (Wien)* 58, 181–185.

Nathan, S. S., Sinha, S. R., Gordon, B., Lesser, R. P., and Thakor, N. V. (1993). Determination of current density distributions generated by electrical stimulation of the human cerebral cortex. *Electroencephalogr. Clin. Neurophysiol.* 86, 183–192.

Nowak, L. G., and Bullier, J. (1998a). Axons, but not cell bodies, are activated by electrical stimulation in cortical gray matter. I. Evidence from chronaxie measurements. *Exp. Brain Res.* 118, 477–488.

Nowak, L. G., and Bullier, J. (1998b). Axons, but not cell bodies, are activated by electrical stimulation in cortical gray matter. II. Evidence from selective inactivation of cell bodies and axon initial segments. *Exp. Brain Res.* 118, 489–500.

Ojemann, G. A. (2003). The neurobiology of language and verbal memory: observations from awake neurosurgery. *Int. J. Psychophysiol.* 48, 141–146.

Parra, J., Kalitzin, S. N., Iriarte, J., Blanes, W., Velis, D. N., and Lopes da Silva, F. H. (2003). Gamma-band phase clustering and photosensitivity: is there an underlying mechanism common to photosensitive epilepsy and visual perception? *Brain* 126, 1164–1172.

Paus, T., Jech, R., Thompson, C. J., Comeau, R., Peters, T., and Evans, A. C. (1997). Transcranial magnetic stimulation during positron emission tomography: a new method for studying connectivity of the human cerebral cortex. *J. Neurosci.* 17, 3178–3184.

Penfield, W., and Boldrey, E. (1937). Somatic motor and sensory representation in the cerebral cortex of man as studied by electrical stimulation. *Brain* 60, 389–443.

Penfield, W. G., and Jasper, H. H. (1954). *Epilepsy and the Functional Anatomy of the Human Brain.* Boston, MA: Little Brown & Co.

Penny, W. D., Stephan, K. E., Mechelli, A., and Friston, K. J. (2004). Comparing dynamic causal models. *Neuroimage* 22, 1157–1172.

Piallat, B., Chabardes, S., Devergnas, A., Torres, N., Allain, M., Barrat, E., and Benabid, A. L. (2009). Monophasic but not biphasic pulses induce brain tissue damage during monopolar high-frequency deep brain stimulation. *Neurosurgery* 64, 156–162; discussion 162–153.

Puce, A., Allison, T., and McCarthy, G. (1999). Electrophysiological studies of human face perception. III: effects of top-down processing on face-specific potentials. *Cereb. Cortex* 9, 445–458.

Quian Quiroga, R., Kraskov, A., Kreuz, T., and Grassberger, P. (2002). Performance of different synchronization measures in real data: a case study on electroencephalographic signals. *Phys. Rev. E* 65, 041903.

Rattay, F. (1999). The basic mechanism for the electrical stimulation of the nervous system. *Neuroscience* 89, 335–346.

Reichova, I., and Sherman, S. M. (2004). Somatosensory corticothalamic projections: distinguishing drivers from modulators. *J. Neurophysiol.* 92, 2185–2197.

Roebroeck, A., Formisano, E., and Goebel, R. (2009). The identification of interacting networks in the brain using fMRI: model selection, causality and deconvolution. *Neuroimage* doi: 10.1016/j.neuroimage.2009.1009.1036.

Rosenberg, D. S., Mauguiere, F., Catenoix, H., Faillenot, I., and Magnin, M. (2009). Reciprocal thalamocortical connectivity of the medial pulvinar: a depth stimulation and evoked potential study in human brain. *Cereb. Cortex* 19, 1462–1473.

Rosenberg, D. S., Mauguiere, F., Demarquay, G., Ryvlin, P., Isnard, J., Fischer, C., Guenot, M., and Magnin, M. (2006). Involvement of medial pulvinar thalamic nucleus in human temporal lobe seizures. *Epilepsia* 47, 98–107.

Saillet, S., Langlois, M., Feddersen, B., Minotti, L., Vercueil, L., Chabardes, S., David, O., Depaulis, A., Deransart, C., and Kahane, P. (2009). Manipulating the epileptic brain using stimulation: a review of experimental and clinical studies. *Epileptic Disord.* 11, 100–112.

Schiller, Y., and Bankirer, Y. (2007). Cellular mechanisms underlying antiepileptic effects of low- and high-frequency electrical stimulation in acute epilepsy in neocortical brain slices *in vitro*. *J. Neurophysiol.* 97, 1887–1902.

Schulz, R., Luders, H. O., Tuxhorn, I., Ebner, A., Holthausen, H., Hoppe, M., Noachtar, S., Pannek, H., May, T., and Wolf, P. (1997). Localization of epileptic auras induced on stimulation by subdural electrodes. *Epilepsia* 38, 1321–1329.

Selimbeyoglu, A., and Parvizi, J. (2010). Electrical stimulation of the human brain: perceptual and behavioral phenomena reported in the old and new literature. *Front. Hum. Neurosci.* 4:46. doi: 10.3389/fnhum.2010.00046.

Sharp, D. J., Scott, S. K., and Wise, R. J. (2004). Retrieving meaning after

temporal lobe infarction: the role of the basal language area. *Ann. Neurol.* 56, 836–846.

Sinai, A., Crone, N. E., Wied, H. M., Franaszczuk, P. J., Miglioretti, D., and Boatman-Reich, D. (2009). Intracranial mapping of auditory perception: event-related responses and electrocortical stimulation. *Clin. Neurophysiol.* 120, 140–149.

Spencer, S. S., Sperling, M. R., Shewmon, D. A., and Kahane, P. (2006). "Intracranial electrodes," in *Epilepsy: A Comprehensive Textbook*, eds J. Engel Jr. and T. A. Pedley (Philadelphia: Lippincott Williams & Wilkins), 1791–1815.

Sporns, O., Tononi, G., and Kotter, R. (2005). The human connectome: a structural description of the human brain. *PLoS Comput. Biol.* 1:e42. doi: 10.1371/journal.pcbi.0010042.

Steriade, M., Jones, E. G., and McCormick, D. A. (1997). *Thalamus Vol. I: Organisation and Function*. Amsterdam: Elsevier.

Suffczynski, P., Kalitzin, S., da Silva, F. L., Parra, J., Velis, D., and Wendling, F. (2008). Active paradigms of seizure anticipation: computer model evidence for necessity of stimulation. *Phys. Rev. E. Stat. Nonlin. Soft Matter Phys.* 78, 051917.

Sumner, P., Nachev, P., Morris, P., Peters, A. M., Jackson, S. R., Kennard, C., and Husain, M. (2007). Human medial frontal cortex mediates unconscious inhibition of voluntary action. *Neuron* 54, 697–711.

Szelenyi, A., Kothbauer, K., de Camargo, A. B., Langer, D., Flamm, E. S., and Deletis, V. (2005). Motor evoked potential monitoring during cerebral aneurysm surgery: technical aspects and comparison of transcranial and direct cortical stimulation. *Neurosurgery* 57, 331–338; discussion 331–338.

Thiebaut de Schotten, M., Urbanski, M., Duffau, H., Volle, E., Levy, R., Dubois, B., and Bartolomeo, P. (2005). Direct evidence for a parietal-frontal pathway subserving spatial awareness in humans. *Science* 309, 2226–2228.

Tolias, A. S., Sultan, F., Augath, M., Oeltermann, A., Tehovnik, E. J., Schiller, P. H., and Logothetis, N. K. (2005). Mapping cortical activity elicited with electrical microstimulation using FMRI in the macaque. *Neuron* 48, 901–911.

Trebuchon-Da Fonseca, A., Guedj, E., Alario, F. X., Laguitton, V., Mundler, O., Chauvel, P., and Liegeois-Chauvel, C. (2009). Brain regions underlying word finding difficulties in temporal lobe epilepsy. *Brain* 132, 2772–2784.

Tsuda, I. (2001). Toward an interpretation of dynamic neural activity in terms of chaotic dynamical systems. *Behav. Brain Sci.* 24, 793–810.

Valentin, A., Alarcon, G., Garcia-Seoane, J. J., Lacruz, M. E., Nayak, S. D., Honavar, M., Selway, R. P., Binnie, C. D., and Polkey, C. E. (2005a). Single-pulse electrical stimulation identifies epileptogenic frontal cortex in the human brain. *Neurology* 65, 426–435.

Valentin, A., Alarcon, G., Honavar, M., Garcia Seoane, J. J., Selway, R. P., Polkey, C. E., and Binnie, C. D. (2005b). Single pulse electrical stimulation for identification of structural abnormalities and prediction of seizure outcome after epilepsy surgery: a prospective study. *Lancet Neurol.* 4, 718–726.

Valentin, A., Anderson, M., Alarcon, G., Seoane, J. J., Selway, R., Binnie, C. D., and Polkey, C. E. (2002). Responses to single pulse electrical stimulation identify epileptogenesis in the human brain *in vivo*. *Brain* 125, 1709–1718.

Varela, F., Lachaux, J. P., Rodriguez, E., and Martinerie, J. (2001). The brainweb: phase synchronization and large-scale integration. *Nat. Rev. Neurosci.* 2, 229–239.

Varela, F. G., Maturana, H. R., and Uribe, R. (1974). Autopoiesis: the organization of living systems, its characterization and a model. *Curr. Mod. Biol.* 5, 187–196.

Vignal, J. P., Maillard, L., McGonigal, A., and Chauvel, P. (2007). The dreamy state: hallucinations of autobiographic memory evoked by temporal lobe stimulations and seizures. *Brain* 130, 88–99.

Wendling, F., Ansari-Asl, K., Bartolomei, F., and Senhadji, L. (2009). From EEG signals to brain connectivity: a model-based evaluation of interdependence measures. *J. Neurosci. Methods* 183, 9–18.

Wieser, H. G., Bancaud, J., Talairach, J., Bonis, A., and Szikla, G. (1979). Comparative value of spontaneous and chemically and electrically induced seizures in establishing the lateralization of temporal lobe seizures. *Epilepsia* 20, 47–59.

Wilson, C. L., Isokawa, M., Babb, T. L., and Crandall, P. H. (1990). Functional connections in the human temporal lobe. I. Analysis of limbic system pathways using neuronal responses evoked by electrical stimulation. *Exp. Brain Res.* 82, 279–292.

Wilson, C. L., Isokawa, M., Babb, T. L., Crandall, P. H., Levesque, M. F., and Engel, J. Jr. (1991). Functional connections in the human temporal lobe. II. Evidence for a loss of functional linkage between contralateral limbic structures. *Exp. Brain Res.* 85, 174–187.

Wilson, C. L., Khan, S. U., Engel, J. Jr., Isokawa, M., Babb, T. L., and Behnke, E. J. (1998). Paired pulse suppression and facilitation in human epileptogenic hippocampal formation. *Epilepsy Res.* 31, 211–230.

Zangaladze, A., Sharan, A., Evans, J., Wyeth, D. H., Wyeth, E. G., Tracy, J. I., Chervoneva, I., and Sperling, M. R. (2008). The effectiveness of low-frequency stimulation for mapping cortical function. *Epilepsia* 49, 481–487.

Zonenshayn, M., Mogilner, A. Y., and Rezai, A. R. (2000). Neurostimulation and functional brain imaging. *Neurol. Res.* 22, 318–325.

Zucker, R. S., and Regehr, W. G. (2002). Short-term synaptic plasticity. *Annu. Rev. Physiol.* 64, 355–405.

Zumsteg, D., Lozano, A. M., and Wennberg, R. A. (2006a). Depth electrode recorded cerebral responses with deep brain stimulation of the anterior thalamus for epilepsy. *Clin. Neurophysiol.* 117, 1602–1609.

Zumsteg, D., Lozano, A. M., Wieser, H. G., and Wennberg, R. A. (2006b). Cortical activation with deep brain stimulation of the anterior thalamus for epilepsy. *Clin. Neurophysiol.* 117, 192–207.

Conflict of Interest Statement: The authors declare that the research was conducted in the absence of any commercial or financial relationships that could be construed as a potential conflict of interest.

Received: 11 June 2010; accepted: 20 September 2010; published online: 20 October 2010.

Citation: David O, Bastin J, Chabardès S, Minotti L and Kahane P (2010) Studying network mechanisms using intracranial stimulation in epileptic patients. Front. Syst. Neurosci. ***4****:148. doi: 10.3389/fnsys.2010.00148*

Copyright © 2010 David, Bastin, Chabardès, Minotti and Kahane. This is an open-access article subject to an exclusive license agreement between the authors and the Frontiers Research Foundation, which permits unrestricted use, distribution, and reproduction in any medium, provided the original authors and source are credited.

frontiers in
SYSTEMS NEUROSCIENCE

ORIGINAL RESEARCH ARTICLE
published: 25 November 2010
doi: 10.3389/fnsys.2010.00154

From intracerebral EEG signals to brain connectivity: identification of epileptogenic networks in partial epilepsy

Fabrice Wendling[1,2]*, Patrick Chauvel[3,4], Arnaud Biraben[5] and Fabrice Bartolomei[3,4]

[1] *INSERM, U642, Rennes, F-35000, France*
[2] *Université de Rennes 1, LTSI, F-35000, Rennes, France*
[3] *INSERM, U751, Marseille, F-13000, France*
[4] *AP-HM, Hôpital de la Timone, Service de Neurophysiologie Clinique, Marseille, F-13000, France*
[5] *CHU Pontchaillou, Service de Neurologie, Rennes, F-35000, France*

Edited by:
Barry Horwitz, National Institutes of Health, USA

Reviwed by:
Arpan Banerjee, National Institutes of Health, USA
Olivier David, INSERM, France

****Correspondence:***
Fabrice Wendling, LTSI – Inserm U642, Université de Rennes 1, Campus de Beaulieu, Bat. 22, 35042 Rennes Cedex, France.
e-mail: fabrice.wendling@univ-rennes1.fr

Epilepsy is a complex neurological disorder characterized by recurring seizures. In 30% of patients, seizures are insufficiently reduced by anti-epileptic drugs. In the case where seizures originate from a relatively circumscribed region of the brain, epilepsy is said to be partial and surgery can be indicated. The success of epilepsy surgery depends on the accurate localization and delineation of the epileptogenic zone (which often involves several structures), responsible for seizures. It requires a comprehensive pre-surgical evaluation of patients that includes not only imaging data but also long-term monitoring of electrophysiological signals (scalp and intracerebral EEG). During the past decades, considerable effort has been devoted to the development of signal analysis techniques aimed at characterizing the functional connectivity among spatially distributed regions over interictal (outside seizures) or ictal (during seizures) periods from EEG data. Most of these methods rely on the measurement of statistical couplings among signals recorded from distinct brain sites. However, methods differ with respect to underlying theoretical principles (mostly coming from the field of statistics or the field of non-linear physics). The objectives of this paper are: (i) to provide an brief overview of methods aimed at characterizing functional brain connectivity from electrophysiological data, (ii) to provide concrete application examples in the context of drug-refractory partial epilepsies, and iii) to highlight some key points emerging from results obtained both on real intracerebral EEG signals and on signals simulated from physiologically plausible models in which the underlying connectivity patterns are known *a priori* (ground truth).

Keywords: connectivity, functional, effective, non-linear regression, neuronal population model, network, intracerebral EEG, epilepsy

INTRODUCTION

Epilepsies constitute a common neurological disorder that affects about 1% of the world population (Engel et al., 1993). Epilepsies are characterized by the repetitive seizures (called ictal periods), the frequency and duration of which is variable. In 20–30% of the cases, seizures remain drug-resistant and considerably affect the patient's quality of life. Drug-resistant epilepsies are often partial or focal, with an origin located in relatively circumscribed brain regions. For patients with partial epilepsy, a surgical treatment can be considered. The problem is then to determine which brain areas which must be removed such that seizures are suppressed under the constraint that post-surgical deficits (sensory-motor or cognitive) induced by surgery are limited. In other words, the epileptogenic zone (EZ) that is responsible for seizures must be defined from anatomo-functional observations acquired during pre-surgical evaluation (Bartolomei et al., 2002).

The delineation of the EZ is the essential diagnostic step, prior to surgery. As the epileptic seizure is a dynamic phenomenon, imaging techniques providing "static" images of the brain (MRI, PET scan) are frequently not the best tools to identify the EZ. About 20–30% of patients have either no lesion or some lesions but without any clear link with their epilepsy.

Electroencephalography is the technique most suited to capture the dynamical properties of a seizure. In some specialized Epilepsy Surgery Units, direct exploration of brain regions using intracerebral depth-electrodes is performed (Bancaud and Talairach, 1973; Chauvel et al., 1993, 1996; Guenot et al., 2001; Cossu et al., 2005; McGonigal et al., 2007). These depth-EEG recordings have long been considered as the "gold standard" for EZ identification. Although they allow for better definition of the EZ, the complete delineation of the EZ may remain elusive, such that suppression of seizures is not always obtained. The reason is that in most of the cases the organization of the EZ is quite complex. This organization corresponds to that of a network of neuronal populations (showing "hyperexcitabilty" and "hypersynchronization" properties) distributed in distinct and distant brain structures. This network is often referred to as the epileptogenic network (Spencer, 2002; Bartolomei et al., 2008b). Accurate identification of epileptogenic networks is the thus the central problem in drug-resistant epilepsies and novel methods have to be proposed to achieve this goal (Wendling et al., 2009). In particular, the demand is high for diagnostic methods allowing for better characterization and interpretation of depth-EEG signals, in terms of underlying neuronal networks and pathophysiological mechanisms taking place in these networks (Rampp and Stefan, 2006).

In this context, signal analysis techniques have considerably developed since the middle of the last century (Brazier and Casby, 1952; Barlow and Brazier, 1954). It is now admitted that signal analysis can provide relevant information regarding epileptic processes (either during interictal or ictal periods) when three conditions are met, at least: (i) signal processing methods are specifically adapted to phenomena under study, (ii) methods have been successfully evaluated on "control" datasets and (iii) the information conveyed by computed quantities is appropriately interpreted.

More specifically, methods aimed at quantifying interactions between recorded structures are of particular interest for identifying functional networks involving spatially distributed brain regions. Over the past decades, considerable effort has been devoted to the development of such methods allowing for characterization of functional and/or effective brain connectivity (Friston, 1994; Jirsa and McIntosh, 2007; Sporns, 2010). A consequence of this increasing interest is that now a plethora of methods is available, each method being based on specific assumptions about the underlying model of relationship between analyzed signals. The objective of this paper is not to provide a comprehensive review of all these methods but rather to focus on those aimed at quantifying functional connectivity from EEG signals. A particular attention is paid to a well-established method in the field of EEG signal processing, namely non-linear regression analysis. Over the past decade, this method has been extensively used in our group to analyze EEG signals recorded in epileptic patients. In this paper, its behavior is illustrated on a typical activity that has long been considered as a hallmark of the EZ: low-voltage rapid discharges observed in depth-EEG signals at the onset of partial seizures. Based on realistic models of coupled neuronal populations, it is showed that this method can provide relevant information on connectivity and can thus be used to interpret the behavior of brain structures involved at the onset of seizures. Finally, the advantages and the limitations of brain connectivity methods will be discussed in the context of the identification of epileptogenic networks from electrophysiological signals, which remains a difficult and still unsolved issue.

MATERIALS AND METHODS

FROM EEG SIGNALS TO BRAIN FUNCTIONAL CONNECTIVITY: A BRIEF OVERVIEW

The idea of extracting, from EEG recordings, some information about brain connectivity is not new. Research in this domain has been – and is still – very active (Uhlhaas and Singer, 2006) and novel methods (or improvement of existing ones) are continuously reported. The underlying assumption is quite simple: the temporal evolution of the cross-correlation (in a wide sense) between electrophysiological signals recorded (with appropriate time resolution) from spatially distributed brain regions is a reflection of the functional connectivity among these regions. The word "functional" here is important as it marks a difference with the concept of "anatomic connectivity" (the actual brain circuitry) and the concept of "effective connectivity" (the actual influence of one region over another one). Regarding functional connectivity, the first methods (Barlow and Brazier, 1954) were developed in the 50s, just after fast Fourier transform (FFT) algorithms were introduced (Cooley and Tukey, 1965). Authors made use of either the cross-correlation function in the time domain or the coherence function in the frequency domain. The first results about the propagation of interictal events as observed in human intracerebral EEG data were reported by Brazier (1972). A few years later, quantitative analysis of these events was performed on scalp-EEG data (Lopes da Silva et al., 1977). From 1980, with the fast development of computers and EEG digital systems, signal processing methods spread more and more rapidly in the field of neurophysiology (for both clinical and research purpose). In the context of epilepsy, Gotman (1987) made use of the averaged coherence function computed on signals recorded from both hemispheres to study the evolution of inter-hemispheric interactions over the entire duration of partial seizures. This coherence function was also used to reveal the possible existence of activities propagating over short- or long-range connection fibers (Thatcher et al., 1986) as well as synchronization mechanisms particularly at the onset of seizures (Duckrow and Spencer, 1992). A corollary study was the estimation of time delays from coherence values (Avoli et al., 1983; Ktonas and Mallart, 1991) as measured "latencies" can be related to the propagation of activity among distant structures. In this category of coherence-based methods, some attempts to use time-varying linear models (autoregressive models) were also reported. These parametric methods were used to measure the degree of synchronization of interictal and ictal EEG signals and to characterize the relationship between brain oscillations in the time and/or frequency domain (Haykin et al., 1996; Franaszczuk and Bergey, 1999).

It is noteworthy that the aforementioned methods are said to be linear. This means that they can only capture the linear component of the relationship between analyzed time series. However, it is commonly admitted that most of the mechanisms at the origin of the generation of EEG signals are non-linear. Therefore, research effort was also devoted to the development of so-called non-linear methods (Pikovsky et al., 2001). A first family of non-linear methods was introduced in the field of EEG about twenty years ago. It included mutual information (Mars and Lopes da Silva, 1983) and non-linear regression analysis (Pijn and Lopes da silva, 1993b; Wendling et al., 2001b). A second family developed later on, based on works related to the analysis of non-linear dynamical systems and chaos (Iasemidis, 2003; Lehnertz, 1999). Regarding this second family of methods, the number of variants is high. Basically, two groups have emerged: (i) phase synchronization methods (Bhattacharya, 2001; Rosenblum et al., 2004) which first estimate the instantaneous phase of each signal and then compute a quantity based on co-variation of extracted phases to determine the degree of relationship and (ii) generalized synchronization methods (Arnhold et al., 1999; Stam et al., 2002, 2003) which also proceed according to two steps. Firstly, state space trajectories are reconstructed from scalar time series signals. Secondly, a similarity index is computed to quantify the similarity between these trajectories.

As shown by this brief literature review the panel of methods that can be used to estimate functional connectivity is wide. In a recent comparative study, we have analyzed the performances of ten methods aimed at characterizing functional connectivity from EEG signals. These methods belonged to three families (linear and non-linear regression, phase synchronization, and generalized synchronization) and were evaluated according to a model-based methodology. In considered simulations, the underlying relationship was known *a priori* (ground truth). It could be controlled

using a parameter representing a degree of coupling in the three types of models (coupled stochastic signals, coupled non-linear dynamical systems, and coupled neuronal populations) that were used to generate output signals. Readers may refer to (Ansari-Asl et al., 2006; Wendling et al., 2009) for detailed results. In brief, the most salient findings of this study can be summarized as follows. First, we could demonstrate that some methods are insensitive to the coupling parameter in considered models (for instance, phase synchronization methods when the relationship between simulated signals only involves their envelope). Second, results showed strong dependence on the frequency distribution of signals (broad band versus narrow band). Third, we found that there is no "universal" method, i.e., none of the studied methods performed better than the other ones whatever the considered situation. Nevertheless, results revealed that methods belonging to the family of linear and non-linear regression analyses showed to be always sensitive to the coupling parameter in considered models. In particular, in the context of ictal activity simulated from coupled populations of neurons, the non-linear correlation coefficient h^2 showed good performances. The behavior of this method on simulated and on real depth-EEG signals is illustrated in section Application to the identification of epileptogenic networks in partial epilepsies. Theoretical aspects as well as basic principles of the modeling approach are summarized in the next two sections.

NON-LINEAR REGRESSION ANALYSIS: NON-LINEAR CORRELATION COEFFICIENT, TIME DELAY AND DIRECTION INDEX

Non-linear regression analysis was first introduced in the field of EEG analysis by Lopes da Silva et al. (1989) as a non-parametric method for characterizing the dependency of a signal Y on a signal X, from signal samples only and independently of the type of relation between the two signals. Readers may refer to (Pijn, 1990; Pijn et al., 1992; Pijn and Lopes Da Silva, 1993a; Kalitzin et al., 2007) for theoretical aspects of this method and to (Bartolomei et al., 2001; Wendling and Bartolomei, 2001; Wendling et al., 2001b) for practical application of this method in the context of epileptic activity analysis. In short, the dependency between considered signals is quantified by a normalized non-linear correlation coefficient h^2_{XY} given by

$$h^2_{XY}(\tau) = 1 - \frac{VAR\,[Y(t+\tau)/X(t)]}{VAR\,[Y(t+\tau)]} \quad (1)$$

where

$$VAR\left[Y(t+\tau)/X(t)\right] \triangleq \arg\min_{h}\left(E[Y(t+\tau) - h(X(t))]^2\right) \quad (2)$$

and where h is a non-linear fitting curve which approximates the statistical relationship between X and Y. In practice, this function h can be obtained from the piece-wise linear approximation between the samples of the two time series. Conceptually, h^2_{XY} quantifies the reduction of variance of signal Y that is obtained when Y samples are predicted for X samples. Indeed, as depicted from Eq. (1), $h^2_{XY} = 0$ when there exists no relationship between X and Y (i.e., the conditional variance $VAR[Y(t+\tau)/X(t)]$ is equal to the marginal variance $VAR[Y(t+\tau)]$). Conversely, signal Y is fully determined by signal X, the conditional variance $VAR[Y(t+\tau)/X(t)] = 0$ and $h^2_{XY} = 1$.

The h^2 coefficient is asymmetric (h^2_{XY} is different from the quantity h^2_{YX}). This asymmetry property was shown to provide insight into causality (Arnhold et al., 1999): if signals X and Y are of the same order of complexity and if Y is (at least partially) driven by X then the difference $h^2_{XY} - h^2_{YX}$ is positive. Finally, in Eq. (1), parameter τ corresponds to the time shift that maximizes the value of the h^2 coefficient. Due to the asymmetry property, this time shift can take two values (either τ_{XY} or τ_{YX}) depending on the way the computation of the h^2 coefficient is performed (from X to Y or vice versa). As a notation convention, we will consider that $\tau_{YX} > 0$ (resp. $\tau_{YX} < 0$) in the case where signal Y is delayed (resp. in advance) with respect to X. The time delay information corresponds to the notion of latency classically used in neurophysiology. It can also be related to causality as the delayed activity is more likely – caused by – rather than – causing – the preceding activity.

To end with this section on non-linear regression analysis, it is noteworthy that the asymmetry information and the time delay information were combined in single quantity named "direction index" D (Wendling and Bartolomei, 2001; Wendling et al., 2001a). This quantity allows for more reliable estimation of the direction of coupling between systems that generate signals, compared to the case where asymmetry information and time delay are considered separately. Briefly, the direction index D starts from the fact that the difference $\Delta h^2 = h^2_{XY} - h^2_{YX}$ and the difference $\Delta\tau = \tau_{YX} - \tau_{XY}$ are both positive when signal Y is dependent on – and is delayed with respect to – signal X. The idea is thus to make a conjoint use of the sign of Δh^2 and $\Delta\tau$ in order to provide a probabilistic information on the direction of coupling. A possible formula is $D = 1/2[\mathrm{sgn}(\Delta h^2) + \mathrm{sgn}(\Delta\tau)]$ when the same weighting coefficient is used for the asymmetry and delay information. In this case, $D = +1$ (respectively -1) denotes that Y (respectively X) is dependant on – and delayed with respect to – X (respectively Y). Conversely, $D = 0$ denotes either (i) a situation where there is a constant discrepancy between the information provided by the asymmetry (Δh^2) and by the time delay ($\Delta\tau$) or (ii) a situation where the sign of Δh^2 and the sign of $\Delta\tau$ continuously fluctuates, over the considered time window.

A MODEL OF DEPTH-EEG SIGNALS GENERATED FROM COUPLED NEURONAL POPULATIONS

A general scientific approach that has proven useful in the study of complex systems is to capture some essential properties in a formal description – a model – which allows for thorough analysis of possible behaviors based on parameters considered in the model. More particularly, in the field of epilepsy, computational neuroscience has developed quite rapidly over the three past decades (Soltesz and Staley, 2008). Besides experimental models, computational models have gained maturity. They are now considered as an efficient way of structuring the tremendous amount of data coming from neurobiological and neurophysiological research in order to interpret experimental findings and, in some cases, to generate hypotheses that can be tested experimentally (Suffczynski et al., 2006). Basically, two complementary approaches developed since the 1970s and led to either detailed (i.e., microscopic) or lumped (i.e., mesoscopic) models of neural systems involved in the generation of epileptic activity. Readers may refer to (Bartolomei et al., 2008b; Lytton, 2008; Ullah and Schiff, 2009) for recent reviews

on this topic. In this section, we focus on a mesoscopic model of coupled neuronal populations, illustrated in **Figure 1A**. This type of model has been described in previous reports (Wendling et al., 2000, 2002, 2005). It is intended to reproduce the activity of two (or more) populations of neurons interacting through excitatory synaptic connections. Each population contains different subsets of neurons, typically main cells, and local interneurons. **Figure 1A** shows a model of two bi-directionally coupled neuronal populations. Each population comprises a subset of excitatory pyramidal neurons (with collateral glutamatergic excitation) and two subsets of inhibitory interneurons which receive excitatory input (glutamatergic) from pyramidal cells and which, in turn, provide inhibition (GABAergic) to pyramidal cells. It is noteworthy that the mesoscopic approach provides a description of the "average" activity in the considered populations of neurons. This means that it does not require an explicit representation of single units and that it leads to "much smaller" sets of ordinary differential equations, especially when compared to high-dimensional networks in which each neuron is described using a multicompartmental model. Two main input–output functions are used at the level of each subset in order to describe the whole population activity. The first function transforms the average density of incoming action potentials (APs) into an average post-synaptic potential (PSP). This average PSP can be either excitatory (EPSP) or inhibitory (IPSP) depending on the nature of the considered subset of cells. The kinetics of PSPs (rise and decay times) are adjusted to match experimentally recorded PSPs. The second function changes the average PSP into an average density of APs fired by the subset. This function is non-linear and accounts for threshold and saturation effects classically observed in neuronal physiology. In addition to the specific input from population P2 (resp. P1), an input noise $p_1(t)$ (resp. $p_2(t)$) is used to describe the influence of non-specific afferences to population P1 (resp. P2). Both signals $p_1(t)$ and $p_2(t)$ represent a density of action potentials. They were chosen to have a Gaussian distribution (mean = 90, SD = 30). Finally, the model output that is usually chosen is the summation of EPSPs and IPSPs generated at the level of pyramidal cells. Indeed, it can be shown that these summated PSPs are the principal contribution to the local field potential (LFP, the signal that would be recorded by an extracellular electrode positioned in the vicinity of the neuronal population). Note that this output can be directly used as an estimate of the temporal dynamics of the LFP if one neglects the source-sensor transfer function (quasi-static assumption).

In the particular context of this study, two important aspects must be underlined. Firstly, this model corresponds to a network of coupled non-linear dynamical systems. Coupling parameters (degree, direction) corresponding to "inter-population" excitatory connections can be tuned. Second, in this network, the behavior of each "node" is governed by "intra-population" parameters, typically the efficacy of excitatory and inhibitory synaptic transmission among local subsets of neurons comprised in the population. These two aspects are illustrated in **Figure 1B**. In this example, two coupled populations are considered. Inside each population, the scenario is as follows: the excitatory synaptic efficacy is constant

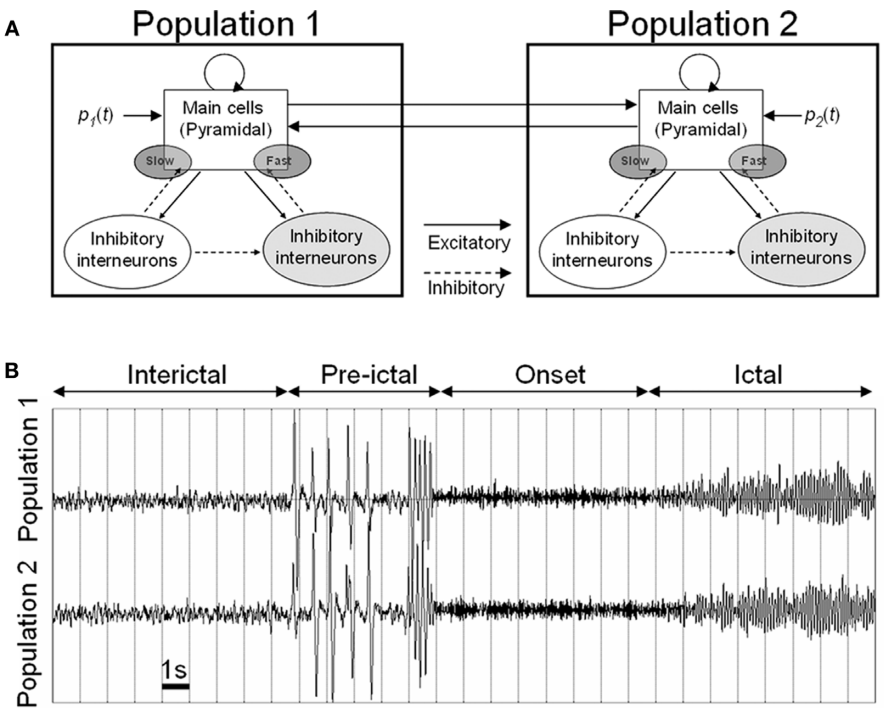


FIGURE 1 | (A) Mesoscopic model of coupled neuronal populations reproducing the activity of two (or more) populations of neurons interacting through excitatory synaptic connections. Each population contains pyramidal cells and local interneurons projecting either to the perisomatic or dendritic region of pyramidal cells. **(B)** Simulated signals obtained for gradual disinhibition in both neuronal populations (see text for details). This neuronal population model is available at: http://senselab.med.yale.edu/modeldb/showmodel.asp?model=97983.

but has been augmented with respect to "normal" value while the average IPSP on pyramidal cells is progressively decreased with time. This gradual disinhibition leads to dynamical changes in the system as reflected by simulated signals. Indeed, a first transition from background activity (interictal phase) to spikes (pre-ictal phase) is observed in this simulation. Spikes occur synchronously, they become more frequent and then an abrupt change to higher frequency activity happens (onset phase). This fast activity finally changes into higher-amplitude lower-frequency activity (ictal phase). Such dynamics and transitions match those occurring in depth-EEG signals recorded from limbic structures in temporal lobe epilepsy (TLE) as already reported in (Wendling et al., 2002, 2005) and as briefly described in the next section.

APPLICATION TO THE IDENTIFICATION OF EPILEPTOGENIC NETWORKS IN PARTIAL EPILEPSIES

STEREOELECTROENCEPHALOGRAPHY AS A PRESURGICAL EXPLORATION TECHNIQUE

Among pre-surgical evaluation methods, stereoelectroencephalography (SEEG) permits direct recording of electrical activity from brain structures that are potentially part of the epileptogenic zone. It provides electrophysiological markers of epileptic activities (interictal and ictal) in the form of time series signals with excellent temporal resolution (about 1 ms). The term "stereoelectroencephalography" was introduced by Bancaud et al. (1965) to emphasize the fact that recording of electrical activity is performed within the intracranial space (rather than from the surface) and that stereotaxic determination of the anatomical structures is necessary to "strategically" position intracerebral multi-contact electrodes (**Figure 2**). The positioning of electrodes is determined in each patient from available non-invasive information and hypotheses about the localization of his/her epileptogenic zone. Implantation accuracy is per-operatively controlled by telemetric X-ray imaging. A post-operative CT scan without contrast product is then used to verify both the absence of bleeding and the precise 3D location of each electrode contact. After SEEG exploration, intracerebral electrodes are removed and an MRI is performed on which the trajectory of each electrode remains visible. Finally, a CT scan/MRI data fusion is performed to anatomically locate each contact along each electrode trajectory. In practice, SEEG is carried out as part of normal clinical care of patients who give their informed consent about the use of data for research purposes.

TRANSITION TO ICTAL ACTIVITY IN TEMPORAL LOBE EPILEPSY (TLE): DESCRIPTION OF INTRACEREBRAL ELECTROPHYSIOLOGICAL SIGNALS

An example of intracerebral SEEG recording is given in **Figure 3**. In this example, the patient had mesial TLE. Signals were recorded on a 128-channel Deltamed™ system and were sampled at 256 Hz. The only filter present in the acquisition procedure is a hardware analog high-pass filter (cut-off frequency equal to 0.16 Hz) used to remove very low frequency variations of the baseline. For simplicity, only signals recorded from contacts located in the hippocampus (anterior and posterior parts), in the entorhinal cortex, in the amygdala and in the lateral temporal cortex (middle temporal gyrus) are represented in **Figure 3**. This electrophysiological pattern is very typical in TLE and reproducible in the various ictal episodes of a given patient (Wendling et al., 1996, 1997). Interictal and pre-ictal spikes (generally of higher amplitude) are usually observed in limbic structures (**Figure 3A**, before seizure onset). They are also observed in lateral structures of the temporal lobe relatively frequently (Wendling et al., 2003). Of particular interest is the activity observed at the onset of seizures. Indeed, in TLE (but not only), the onset of seizures is very often characterized by the appearance of a fast activity (also referred to as rapid discharge) in mesial structures (**Figure 3A**, seizure onset). This fast onset activity dramatically differs from interictal background activity recorded far from seizure (in time). The salient feature is a re-distribution of the energy of intracerebral EEG signals into higher frequency bands. Typically, in the temporal lobe, the dominant frequency ranges from 20 to 30 Hz (**Figure 3B**) which corresponds to the low gamma frequency band. The duration of the rapid discharge may vary from patient to patient. Generally, it lasts for 5 to 10 s. Then, as the seizure develops, the signal frequency gradually slows down and the amplitude progressively increases. The activity becomes more rhythmic and

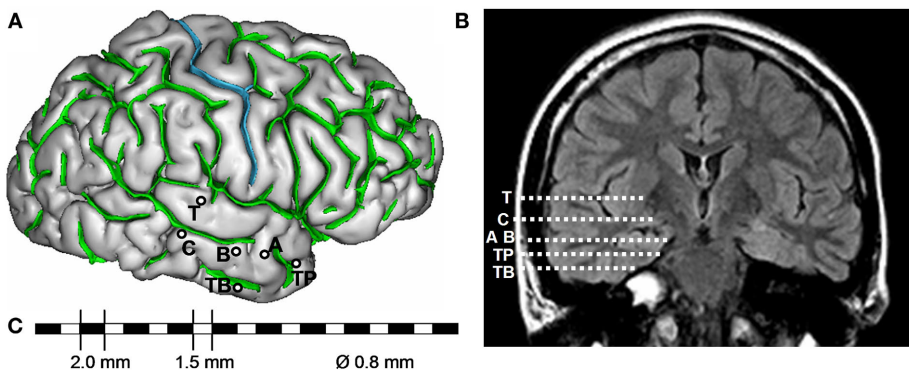


FIGURE 2 | Example of SEEG exploration in patient with mesial temporal lobe epilepsy. (A) Intracerebral implantation scheme. Electrodes are identified by one or two capital letters: A, B and C (medial contacts: amygdala, anterior part of hippocampus, posterior part of hippocampus; lateral contacts: middle temporal gyrus from anterior to posterior part), T (medial contacts, insula; lateral contacts, superior temporal gyrus), TB (medial contacts, entorhinal cortex; lateral contacts, temporo-basal cortex), TP (temporal pole). **(B)** Electrode trajectories reported on MRI data (coronal view). **(C)** Each intracerebral electrode is composed of 10–15 cylindrical contacts (length: 2 mm, diameter: 0.8 mm, 1.5 mm apart).

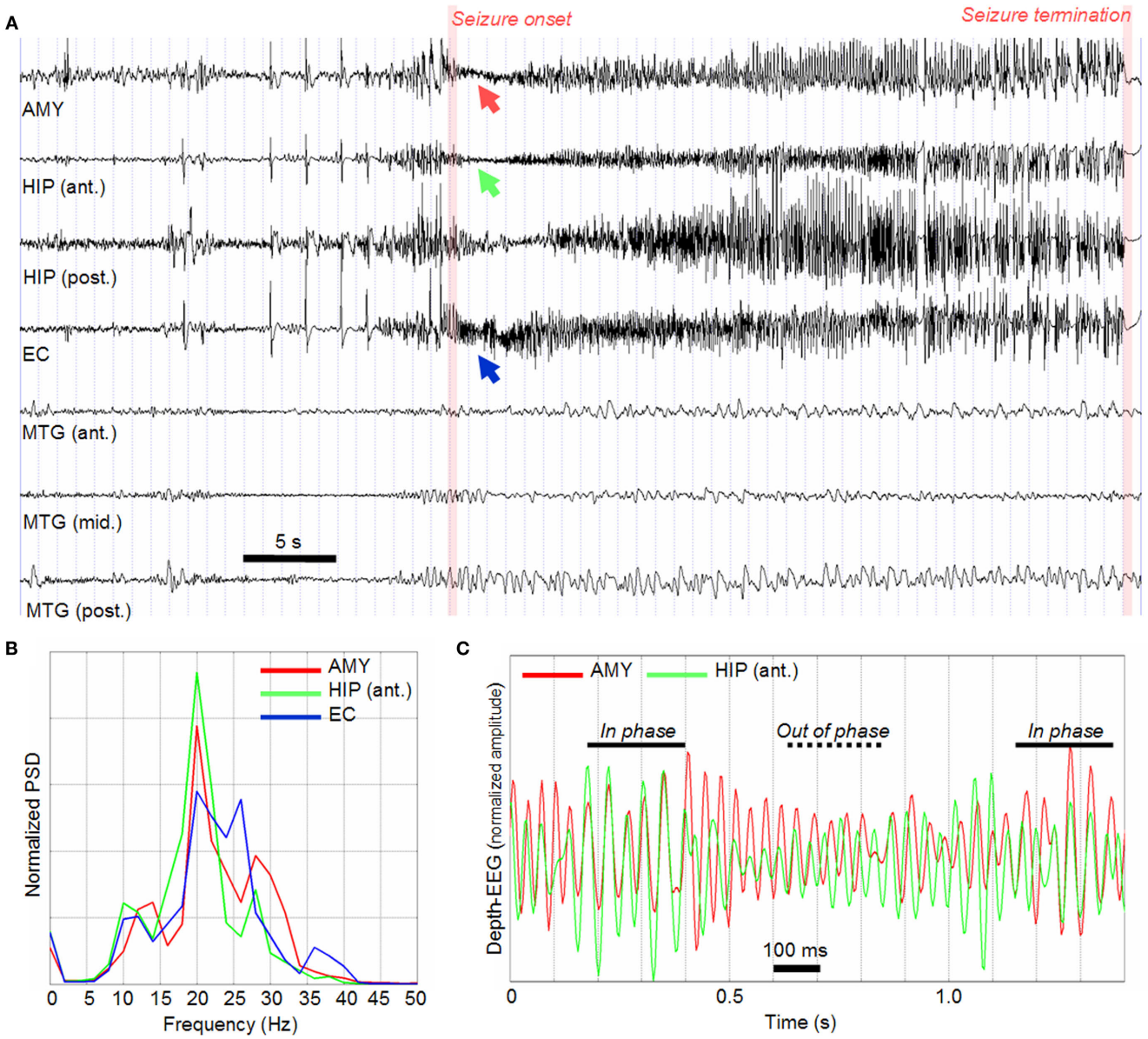


FIGURE 3 | (A) Example of SEEG recording (bipolar signals) performed during transition to seizure activity. Only signals recorded from mesial (AMY, HIP, EC) and lateral (MTG) structures in the temporal lobe are represented. AMY, amygdala; HIP (ant.), anterior part of hippocampus; HIP (post.), posterior part of hippocampus; EC, entorhinal cortex; MTG (ant., mid., post.), middle temporal gyrus from anterior to posterior part). **(B)** Normalized power spectral density (PSD) computed on the segment of SEEG signal corresponding to seizure onset and where a fast activity (about 25 Hz) is observed. **(C)** A zoom on the fast onset activity showing that a jitter is present: as time goes on, signals are either in phase or out of phase.

more synchronous across the recorded regions. Clinical symptoms generally occur during this "clonic" phase. Finally, seizure termination occurs after a few tens of seconds with respect to onset. A striking and reproducible feature is the "abrupt stop" of the ictal activity simultaneously observed on all channels.

The diversity of dynamics (and transitions of dynamics) observed at the level of depth-EEG signals shows that the epileptic seizure is a complex dynamical process. The seizure onset is particularly important in this dynamical process as it conveys key information about the EZ: what are the involved structures? Why and how are these structures engaged into the fast activity? What is the underlying network and how is it organized? Which "nodes" in this network should be removed in the aim to suppress ictal activity? These are typical questions faced by epileptologists as they analyze EEG recordings. From the signal processing viewpoint, these are particularly difficult questions. Indeed, the seizure onset phase is relatively short (a few seconds) and the number of seizures, in a given patient, is usually limited (typically in the order of 5–10 s). Therefore, statistical significance of computed quantities (whatever the quantity) is always a delicate issue. The close analysis of rapid discharges reveals that

they often start quasi-synchronously (**Figure 3A**). As far as limbic structures are concerned, their frequency content is quite similar, as depicted in **Figure 3B** which shows the power spectral density (PSD) of signals recorded from the amygdala, the hippocampus, and the entorhinal cortex during the fast onset activity. This PSD reveals that rapid discharges are quite narrow band (15–30 Hz) which is confirmed by the plot in **Figure 3C** where the "sinusoidal" nature and amplitude modulation of recorded signals can be easily observed. This plot also shows a striking feature of recorded signals: a jitter is present as shown by the alternation of epochs where signals are either in phase or out of phase. By "jitter," we mean a "phase shift" (between analyzed quasi-sinusoidal depth-EEG signals) that is continuously and randomly changing over the duration of the fast activity. This jitter makes the problem of interpreting the propagation of epileptic activity quite complicated. Indeed, from visual inspection, it cannot be determined whether one signal is in advance – or is delayed – with respect to the other signal.

APPLICATION OF NON-LINEAR REGRESSION ANALYSIS TO FAST ONSET ACTIVITY

This section illustrates the behavior of non-linear regression analysis as applied on the fast activity recorded at the onset of seizures (as described above). The non-linear correlation coefficient h^2, the time delay, and the direction index were computed on signals recorded from the amygdala (AMY), the anterior hippocampus (HIP, ant.) and the entorhinal cortex where rapid discharges could be observed (**Figure 3**). The three pair-wise combinations (AMY vs. HIP, AMY vs. EC, and AMY vs. HIP) were considered.

In order to assess the statistical significance of measured quantities, we compared the statistical distributions of the h^2 values, as computed over the seizure onset period and over the interictal period that precedes the seizure. As these distributions are not normal, a possible approach is to compare the means of Z-transformed variables via t-tests. Indeed, it can be shown that the variable $w = 1/2 \times \log((1 + r)/(1 - r))$ (Eq. 3, where r denotes the linear correlation coefficient) follows a Gaussian distribution. However, it is worth to mention that this transformation cannot be readily applied in the case of non-linear correlation values, as those computed in the example shown in **Figures 3 and 4**. Indeed, the r quantity takes values in the interval $[-1, 1]$ and is therefore mapped into the interval $]-\infty, +\infty[$. Conversely, the non-linear correlation coefficient h^2 is strictly positive (see Eq. 1). Therefore, using Eq. 3, it will be mapped into the $R + =]0, +\infty[$ interval and theoretically can never follow a normal distribution. To deal with this issue a solution is to set the variable r equal to $(2 \times h^2 - 1)$ in Eq. 3. This transformation is such that r takes values in the interval $[-1, 1]$ and that $w = 1/2 \times \log(h^2/(1 - h^2))$ takes values in $]-\infty, +\infty[$ with a distribution that can be assumed to be Gaussian (verified on empirical histograms). In addition, it worth mentioning that the time delay and direction index can only be interpreted in the situations where the h^2 coefficient is significantly high. Indeed, analyzing those quantities is meaningless when there is no relationship between recorded brain sites.

Results are summarized in **Figure 4** which shows the behavior of estimated quantities. Note that the h^2 coefficient and the time delay were computed according to the two possibilities: dependence

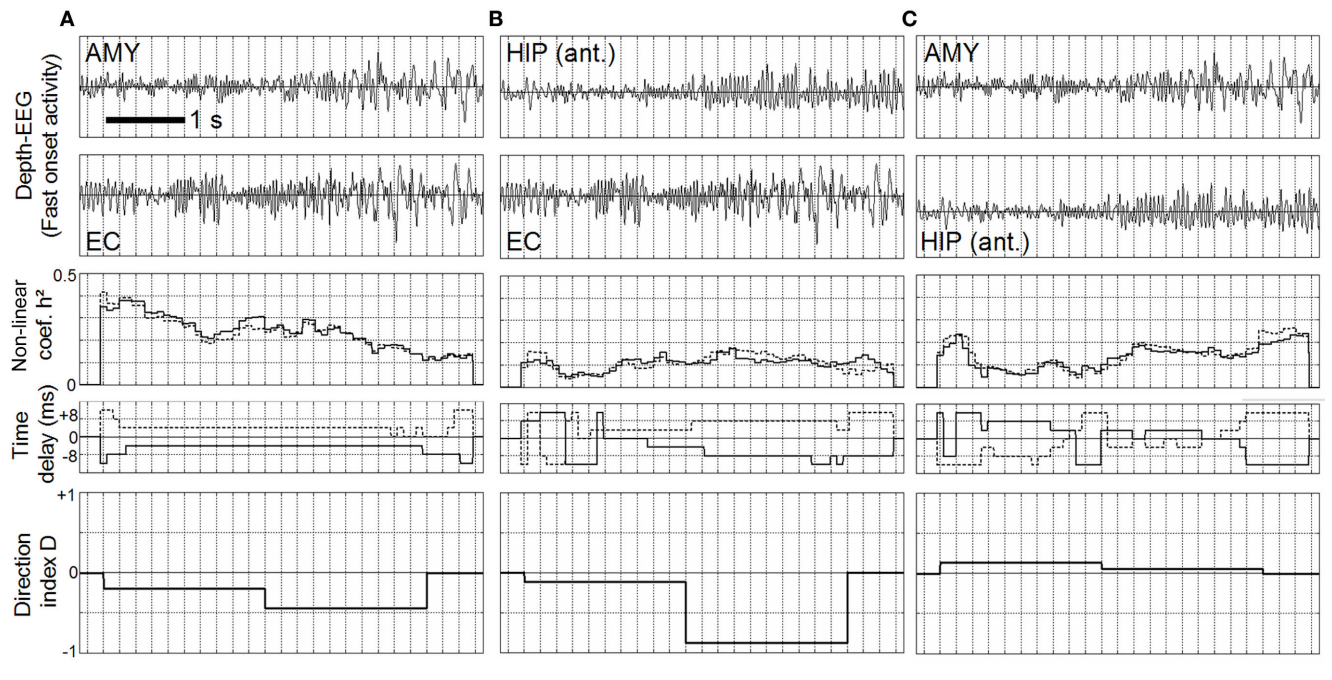


FIGURE 4 | Non-linear regression analysis applied on real EEG signals according to a pair-wise procedure (AMY vs. EC (A), HIP vs. EC **(B)**, AMY vs. HIP **(C))**, during the fast onset activity. Left, middle: h^2 coefficient values are significantly high (**) compared to values measured during interictal periods. Time delays (solid line: upper signal vs. lower, dotted line: lower signal vs. upper) are stable. Direction index is lower than 0 indicating that lower signal is driving the upper signal. Right: Time delays are unstable and direction index stays close to 0, providing no clues about the direction of coupling.

of the first signal on the second one (**Figure 4**, solid line) and vice versa (**Figure 4**, dash line). First, results showed that for the two first pairs (AMY vs. EC, **Figure 4A**) and (HIP vs. EC, **Figure 4B**), the behavior of computed quantities is similar. First, the h^2 values averaged over the duration of the fast discharge were found to be significantly higher (AMY vs. EC: p = 5.706e−3, HIP vs. EC: p = 8.743e−3) than those computed on interictal activity. Second, time delays were found to be relatively stable over this seizure onset period as the direction index that is negative in both cases, indicating that the direction of coupling was more likely to be from the EC toward the AMY (**Figure 4A**, fourth plot) and from the EC toward the HIP (**Figure 4B**, fourth plot). Results were quite different regarding the third pair (AMY vs. HIP, **Figure 4C**). The average h^2 values were not found to be different from those computed during interictal activity (AMY vs. HIP: p = 0.215). Second, time delays were found to be unstable as continuously varying from positive to negative value. This resulted in a direction index which stayed close to 0 and which was more difficult to interpret in term of effective connectivity.

This example (typical of mesial TLE) shows the difficulty of interpreting connectivity measures performed on intracerebral EEG data. Indeed, we are facing situations where computed quantities exhibit different behaviors. As described in the next section, data simulated from models in which (i) the excitability of neuronal populations and (ii) the underlying connectivity among these populations are known *a priori* may help this interpretation.

MODEL-BASED INTERPRETATION OF CONNECTIVITY MEASURES AT SEIZURE ONSET

In this section, we report results about the behavior of non-linear regression analysis (h^2, time delay and direction index measures) as applied on signals simulated from two coupled neuronal

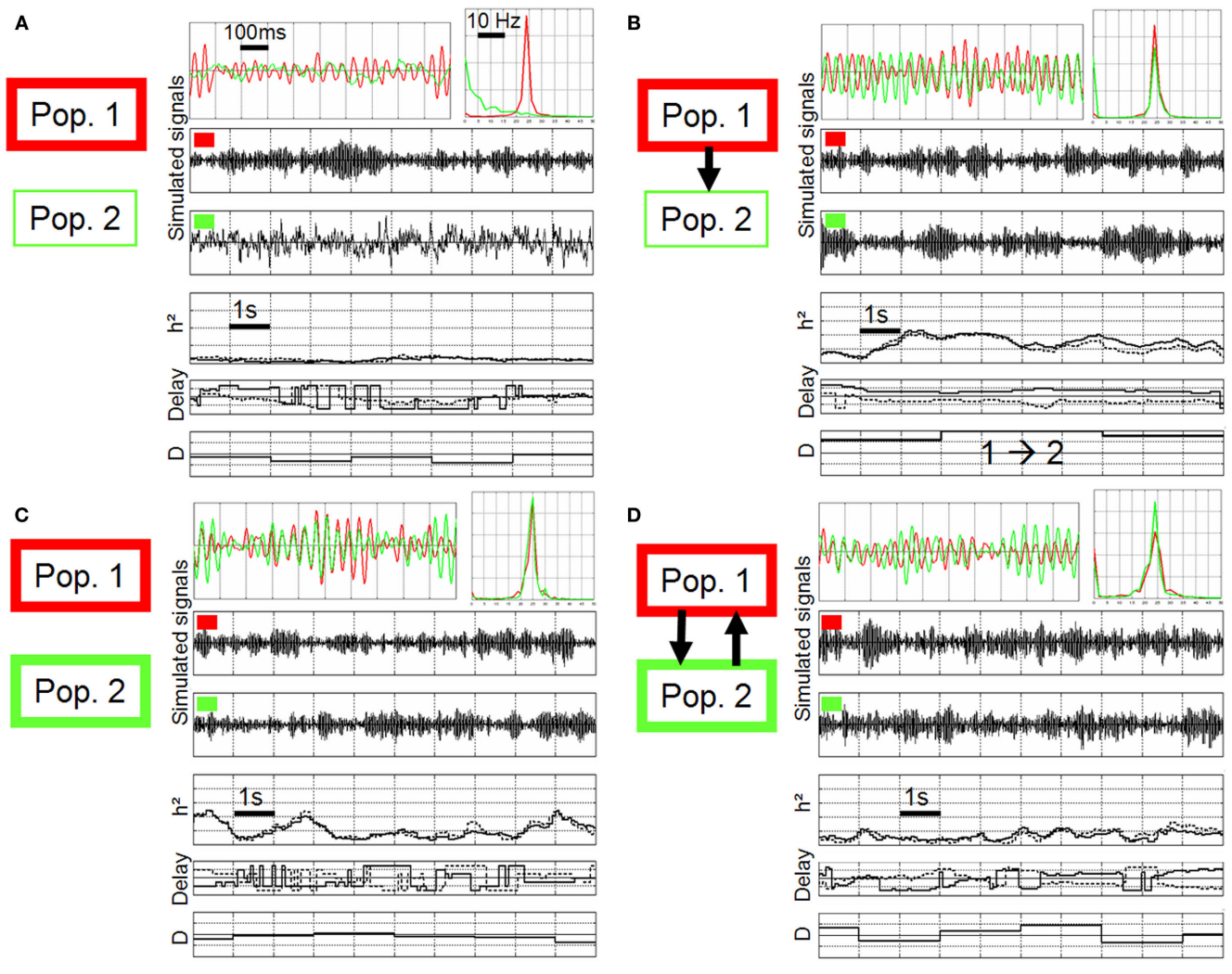


FIGURE 5 | Non-linear regression analysis applied on simulated signals, using the same method settings compared to Figure 4. (A) Different scenarios were considered regarding the intrinsic excitability of neuronal populations (thin line: excitability increased, thick line: excitability more strongly increased) and regarding the connectivity (no coupling, unidirectional coupling, bidirectional coupling). **(B–D)**: both populations generate a fast activity (about 25 Hz) and a jitter is observed between simulated signals (red vs. green) as in real signals. Note that the behavior of non-linear regression analysis (h^2 coefficient, time delays, direction index D) depends on the modeled situation (see text for details).

populations. Simulations were performed under two constraints: (i) the spectral content of simulated signals matches that of real signals and (ii) a jitter similar to that observed in real data is also present in simulated signals.

Results are reported in **Figure 5**. A first general result is that the model could generate a fast activity (about 25 Hz, as observed) at the level of both populations if, and only if, the ratio between excitation and inhibition was increased such that the populations of neurons become "more excitable." Note that this result is not new. It was already shown (Wendling et al., 2002, 2005) that decreased inhibition (at the level of GABAa,slow receptors on pyramidal cells) leads to a dramatic change in the model: the fast feedback inhibitory loop (involving GABAa,fast receptors on pyramidal cells) becomes very active and leads to the generation of fast IPSPs on pyramidal cells (GABAa,fast receptors). These IPSPs dramatically affect the LFP by adding higher-frequency components.

Starting from this "increased excitability" condition at both populations, we found three situations where the model could generate signals with the aforementioned constraints.

The first situation is displayed in **Figure 5B** where excitability was strongly increased in population 1 (thick red rectangle) and less strongly in population 2 (thin green rectangle) and where population 2 received excitatory input from population 1 (unidirectional arrow). Note that without this excitatory drive, population 2 did not generate a fast activity, as shown in **Figure 5A**. In other words, the fast discharge in population 2 "is caused by" the input from population 1. In this situation (**Figure 5B**), a significant increase of the h^2 value could be measured with respect to the uncoupled situation (**Figure 5A**). Time delays were found to be quite stable and symmetric. Finally, the direction index was strictly positive, clearly indicating an influence of population 1 on population 2.

The second situation is displayed in **Figure 5C**. Here, populations were uncoupled but excitability was strongly increased in both populations such that they both generated a fast activity "intrinsically". It can be depicted that the behavior of measured quantities is different compared to the previous situation. The h^2 values were lower and the variance strongly increased. Time delays were found to be very unstable, continuously reversing as time goes on. Conversely, the direction index D was more stable and centered around 0. It did not indicate a preferred direction in the coupling between population 1 and population 2.

The third situation is illustrated in **Figure 5D**. Here, excitability was increased and both populations mutually interacted. For each population, the excitatory input from the other population was such that it generated a fast activity. Again, and as the underlying scenario changed, measured quantities behaved in a different manner compared to previous situations. Strikingly, the h^2 values measured in a situation where neuronal populations are bi-directionally coupled were even lower compared to the previous uncoupled situation (**Figure 5C**). Time delays were also found to be very unstable. Finally, the direction index was also close to 0 but the variance was higher compared to the uncoupled situation. In order to assess the statistical significance of results, we generated long-duration simulated signals (400 s) from which we could evaluate the asymptotic behavior (mean and standard deviation) of measured quantities. Results are summarized in **Figure 6**. They corroborated those obtained on shorter duration segments. The most salient finding is that there was only one situation, among the three analyzed situations, for which measured quantities provided a non-ambiguous result. This situation is that presented in **Figure 5B** and corresponds to the case where population 2 generated a rapid discharge, due to the excitatory drive from population 1.

Therefore, according to the above simulation results, a possible interpretation of the underlying network organization in the example of real data show in **Figure 3** is as follows. In the three recorded structures (AMY, HIP, and EC), excitability would be increased with respect to normal condition. The disinhibition in the entorhinal cortex would lead to the generation of a fast activity. Then, measured h^2 values (functional connectivity), time delay and direction index (effective connectivity) would indicate that the EC is driving the fast activity observed in the two other structures (AMY and HIP).

DISCUSSION

High frequency oscillations occurring at the onset of epileptic seizures have long been considered as a potentially valuable marker of the epileptogenic zone (EZ), usually defined as the subset of brain structures involved in the generation of seizures. These oscillations, also referred to as "fast onset activity" or "rapid discharges" (Allen et al., 1992; Alarcon et al., 1995; Wendling et al., 2003) have been recognized to be one of the most characteristic electrophysiological patterns of the EZ in focal epilepsy (Bancaud et al., 1965). Several experimental (Traub et al., 2001; Uva et al., 2005; Gnatkovsky et al., 2008; de Curtis and Gnatkovsky, 2009) and computational modeling (Wendling et al., 2005) studies demonstrated the existence of a relationship between the epileptogenicity of the neuronal tissue and its propensity to generate fast oscillations at seizure onset. From clinical viewpoint, resection of regions with rapid discharges has also been found to favorably influence the surgical prognosis (Alarcon et al., 1995). A striking feature of rapid discharges is that they always involve distinct – and possibly distant – brain structures, either in a quasi-synchronous or a more delayed manner. Based on these observations, an index, called epileptogenicity index, was recently proposed (Bartolomei et al., 2008a). This index accounts for both spectral (occurrence of fast oscillations) and temporal (delay of occurrence with respect to seizure onset) properties of intracerebral EEG signals to quantify the epileptogenic nature of recorded neuronal systems.

However, the mechanisms of seizure generation and propagation remain elusive. A number of studies have used signal processing techniques (in particular those able to characterize the underlying connectivity) in order to characterize the seizure dynamics from intracerebral EEG data (Gotman, 1987; Lieb et al., 1987; Mormann et al., 2003; Schindler et al., 2007; Bartolomei and Wendling, 2009). The intent of this paper was to also address this issue with a particular focus on the mechanisms involved in the generation of fast activity at the onset of seizures. We assumed that the epileptogenic zone is organized as a network of distributed neuronal populations with altered excitability properties and then study how a simple computational model (two (un)coupled populations) could help us to better interpret connectivity (functional and effective) measures performed on real signals (intracerebral EEG). The main findings of this study are discussed hereafter.

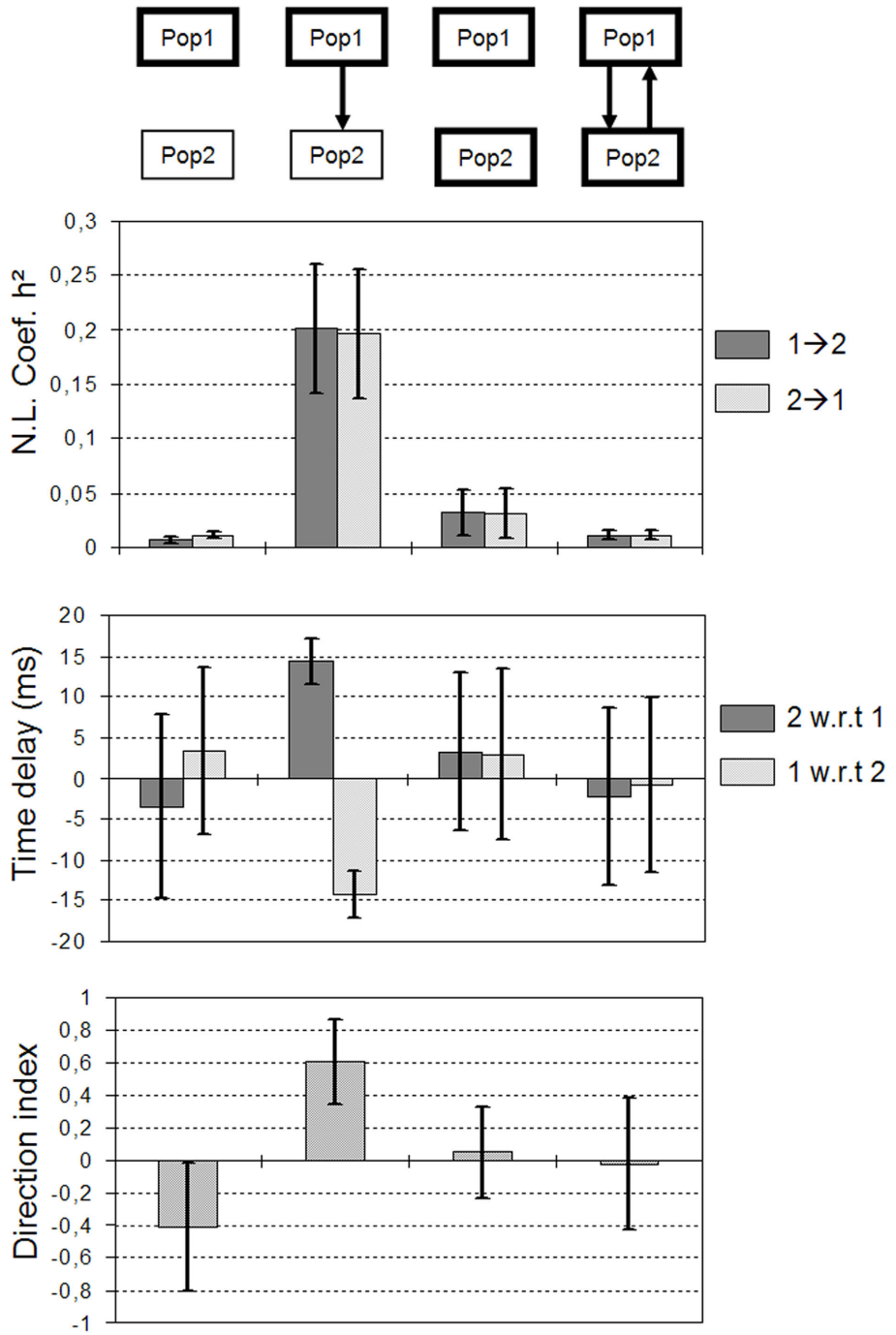


FIGURE 6 | Asymptotic behavior (mean and standard deviation computed over 500 s) of measured quantities in the four situations considered in Figure 5. For one situation measured quantities provide a non-ambiguous result. It corresponds to the case where population 2 generates a rapid discharge, due to the excitatory drive from population 1 (see also **Figure 5B**).

First, what do we learn from this apparently simple model? This question is always raised in any study involving modeling aspects. In the present work, the first insight is that rapid discharges with properties that are similar to those observed in real signals can be generated from different model configurations, in terms of level of excitability (moderate vs. major increase) in the two considered populations and connectivity pattern (no coupling, unidirectional coupling or bidirectional coupling). Indeed, we managed to generate signals that not only have a realistic spectral content but also in which a random phase jitter (instability of the phase difference between signals) is observed. The second insight is that the level of excitability is a crucial parameter. In the network, only the

"nodes" with decreased inhibition (i.e., increased excitability) can be involved in the fast onset activity. The tricky question is then related to the mode of involvement of neuronal populations into the fast run. This question leads to the third insight. Our model shows that there are basically two situations. According to the first situation, the level of excitability in one population is so high that this population "autonomously" generates a fast activity. Of course, this population can have excitatory connections to distant populations (typically on the sub-population of pyramidal cells). When the excitability in these "remote" populations is altered (i.e., also increased), the model shows that they can be "driven" into the fast activity mode. Formally, this "entrainment" would correspond to an external perturbation that continuously drives the target dynamical system away from its "normal" behavior. It is noteworthy that the driven neuronal population does not become unstable as the removal of the external input leads it to return back to "normal background activity". According to the second situation, the level of excitability in considered populations is such that they autonomously generate a fast activity. In this case, the influence of couplings is much more difficult to determine and would deserve, in itself, a detailed analysis.

Second, what do we learn from signal analysis methods aimed at characterizing the connectivity? It is difficult to answer this question as only one method, among the many methods presented in section "From EEG signals to brain functional connectivity: a brief overview", was applied on real and simulated signals. In the following we will thus emphasize results we obtained regarding non-linear regression analysis which could provide interpretable results in the first studied situation. A first interesting aspect in this method is that it does not require strong assumptions about the properties of analyzed signals (broadband vs. narrow band, for instance) nor about the nature of the relationship between these signals (linear, non-linear, phase, or amplitude). The only restriction is that the duration of the sliding window (which defines the number of independent (X,Y) pairs of amplitude values) is large enough to correctly estimate the non-linear fitting curve h in Eq. 2. A second interesting aspect is that this method was able to provide reliable results in a complicated situation where the phase difference between signals is continuously varying. On simulated signals, we could obtain statistically significant results regarding the mean non-linear correlation coefficient, time delays (as measured in both directions) and direction index values. Indeed, measured quantities could be related, without ambiguity, to the underlying organization (population 2 receives excitatory input from population 1). Nevertheless, this result also means that there exist some situations where this method cannot provide univocal interpretation of recorded signals. Two examples were presented in this study corresponding to two situations where both neuronal populations generate a fast activity. In this case, we could not determine, from measured quantities, whether or not the two populations are coupled. Therefore, these results show that one should be cautious with the interpretation of connectivity measures, as already mentioned in several studies (Horwitz, 2003; Wendling et al., 2009). In particular, they show that deriving relevant information regarding the underlying effective connectivity is particularly difficult in the situations where the non-linear correlation coefficient is low.

From the physiological viewpoint, these results also show that the notion of "propagation of rapid discharges" should be clarified. Indeed, in some cases, the fact that rapid discharges are observed at different brain sites, is not due to propagation but, instead, to quasi-synchronous involvement of neuronal populations. According to this view, an epileptogenic network would include two types of "nodes," both having a capacity to generate fast activity due to altered excitation- and/or inhibition-related mechanisms. Some nodes could spontaneously generate rapid discharges and could "drive" some other nodes which would act as "relays" of those rapid discharges. For instance, in real signals shown in this study, the entorhinal cortex would belong to the first category whereas the hippocampus and amygdala would go in the second. This latter point leads us to a frequently asked question: how are functional, effective and anatomical connectivity related one with another? This is still a challenging question that cannot be answered in this study. However, it can be noticed, in the chosen example, that the entorhinal cortex has direct anatomical projections (temporoamonic pathway) to the hippocampus (see, for instance, Witter and Wouterlood, 2002 for detailed description). Projections to the amygdala are less clear. Some detailed studies were performed in the cat using tract-tracing techniques (Russchen, 1982a,b; Witter and Groenewegen, 1986; Witter et al., 1986). As in the rat (Brothers and Finch, 1985; McDonald and Mascagni, 1997), results showed entorhinal–amygdala projections arising primarily from deep layers of the lateral entorhinal cortex. Although little is known about details of the projection of the entorhinal cortex to the amygdala in primates, such a pathway has been hypothesized in human based on neuronal responses evoked by electrical stimulation (Wilson et al., 1990, 1991). Besides these *in vivo* studies, functional connections as well as spread of epileptic activity were also studied *in vitro*, using slice preparations (rat brain) which preserve the connectivity between the hippocampus and the entorhinal cortex (Rafiq et al., 1993) and also with the amygdala (Stoop and Pralong, 2000). These studies confirmed the existence of reciprocal connections between hippocampus and entorhinal cortex. In addition, it was found that bursting epileptic activity could spread via two different pathways, either from entorhinal cortex or hippocampus and both toward the amygdala.

To end with this discussion, one should also mention the limitations of this study that lead, in fact, to open issues that should be addressed in the future. First, scenarios involving more than two coupled neuronal populations should be investigated, keeping in mind that the number of combinations becomes rapidly high with the number of populations and with the various ways of interconnecting populations. Second, an interesting issue would be to compare results obtained from "classical" methods (as used here) with those obtained with methods "dedicated" to the analysis of causality among time series like Granger causality, directed transfer function and partial directed coherence on simulated signals (Blinowska et al., 2004; Kus et al., 2004). One advantage of these methods is that they make use of multichannel estimates conversely to the method used in this study that proceeds according to a bivariate approach, often considered as less powerful. Nevertheless, for simulated data, most of the studies which analyze the performances of multivariate versus bivariate methods make us of a multivariate autoregressive model which may not be the most relevant model for

epileptic ictal-like activity. It would therefore be very informative to test aforementioned methods on signals generated with more "physiologically plausible" models of EEG (or LFP) generation, as the one used in this study and which can easily extended to multiple populations of neurons. A similar approach based on neural mass models was used to examine linear and non-linear methods for assessing functional connectivity (David et al., 2004). Finally, in the context of drug-resistant epilepsy, a nice – but difficult – perspective would be to investigate brain connectivity from both scalp-EEG and depth-EEG signals. This would allow us to assess the relationship between connectivity measures as obtained from global field potentials and from LFPs and to determine whether "finer" hypotheses about the epileptogenic zone could be establish on the basis on non-invasive electrophysiological data.

REFERENCES

Alarcon, G., Binnie, C. D., Elwes, R. D., and Polkey, C. E. (1995). Power spectrum and intracranial EEG patterns at seizure onset in partial epilepsy. *Electroencephalogr. Clin. Neurophysiol.* 94, 326–337.

Allen, P. J., Fish, D. R., and Smith, S. J. (1992). Very high-frequency rhythmic activity during SEEG suppression in frontal lobe epilepsy. *Electroencephalogr. Clin. Neurophysiol.* 82, 155–159.

Ansari-Asl, K., Senhadji, L., Bellanger, J. J., and Wendling, F. (2006). Quantitative evaluation of linear and nonlinear methods characterizing interdependencies between brain signals. *Phys. Rev. E. Stat. Nonlin. Soft Matter Phys.* 74(Pt 1), 031916.

Arnhold, J., Grassberger, P., Lenhertz, K., and Elger, C. (1999). A robust method for detecting interdependences: application to intracranially recorded EEG. *Physica D* 134, 419–430.

Avoli, M., Gloor, P., Kostopoulos, G., and Gotman, J. (1983). An analysis of penicillin-induced generalized spike and wave discharges using simultaneous recordings of cortical and thalamic single neurons. *J. Neurophysiol.* 50, 819–837.

Bancaud, J., and Talairach, J. (1973). [Methodology of stereo EEG exploration and surgical intervention in epilepsy]. *Rev. Otoneuroophtalmol.* 45, 315–328.

Bancaud, J., Talairach, J., Bonis, A., Schaub, C., Szikla, G., Morel, P., and Bordas-Ferrer, M. (1965). *La Stéréoélectroencéphalographie dans L'épilepsie: Informations Neurophysiopathologiques Apportées par L'investigation Fonctionnelle Stereotaxique*. Paris: Masson.

Barlow, J. S., and Brazier, M. A. (1954). A note on a correlator for electroencephalographic work. *Electroencephalogr. Clin. Neurophysiol.* 6, 321–325.

Bartolomei, F., Chauvel, P., and Wendling, F. (2008a). Epileptogenicity of brain structures in human temporal lobe epilepsy: a quantified study from intracerebral EEG. *Brain* 131, 1818–1830.

Bartolomei, F., Wendling, F., and Chauvel, P. (2008b). [The concept of an epileptogenic network in human partial epilepsies]. *Neurochirurgie* 54, 174–184.

Bartolomei, F., Guye, M., Gavaret, M., Regis, J., Wendling, F., Raybaud, C., and Chauvel, P. (2002). [The presurgical evaluation of epilepsies]. *Rev. Neurol. (Paris)* 158(Pt 2), 4S55–4S64.

Bartolomei, F., and Wendling, F. (2009). Synchrony in neural networks underlying seizure generation in human partial epilepsies in coordinated activity in the brain. *Springer Series Comput. Neurosci.* 2, 137–147.

Bartolomei, F., Wendling, F., Bellanger, J. J., Regis, J., and Chauvel, P. (2001). Neural networks involving the medial temporal structures in temporal lobe epilepsy. *Clin. Neurophysiol.* 112, 1746–1760.

Bhattacharya, J. (2001). Reduced degree of long-range phase synchrony in pathological human brain. *Acta Neurobiol. Exp. (Wars)* 61, 309–318.

Blinowska, K. J., Kus, R., and Kaminski, M. (2004). Granger causality and information flow in multivariate processes. *Phys. Rev. E. Stat. Nonlin. Soft Matter Phys.* 70(Pt 1), 050902.

Brazier, M. A. (1972). Spread of seizure discharges in epilepsy: anatomical and electrophysiological considerations. *Exp. Neurol.* 36, 263–272.

Brazier, M. A., and Casby, J. U. (1952). Cross-correlation and autocorrelation studies of electroencephalographic potentials. *Electroencephalogr. Clin. Neurophysiol.* 4, 201–211.

Brothers, L. A., and Finch, D. M. (1985). Physiological evidence for an excitatory pathway from entorhinal cortex to amygdala in the rat. *Brain Res.* 359, 10–20.

Chauvel, P., Landre, E., Trottier, S., Vignel, J. P., Biraben, A., Devaux, B., and Bancaud, J. (1993). Electrical stimulation with intracerebral electrodes to evoke seizures. *Adv. Neurol.* 63, 115–121.

Chauvel, P., Vignal, J., Biraben, A., Badier, J., and Scarabin, J. (1996). "Stereoelectroencephalography," in *Multimethodological Assessment of the Epileptic Forms*, eds G. Pawlik and H. Stefan (New York: Springer Verlag), 80–108.

Cooley, J. W., and Tukey, J. W. (1965). An algorithm for the machine calculation of complex Fourier series. *Math. Comput.* 19, 297–301.

Cossu, M., Cardinale, F., Castana, L., Citterio, A., Francione, S., Tassi, L., Benabid, A. L., and Lo Russo, G. (2005). Stereoelectroencephalography in the presurgical evaluation of focal epilepsy: a retrospective analysis of 215 procedures. *Neurosurgery* 57, 706–718; discussion 706–718.

David, O., Cosmelli, D., and Friston, K. J. (2004). Evaluation of different measures of functional connectivity using a neural mass model. *Neuroimage* 21, 659–673.

de Curtis, M., and Gnatkovsky, V. (2009). Reevaluating the mechanisms of focal ictogenesis: the role of low-voltage fast activity. *Epilepsia* 50, 2514–2525.

Duckrow, R. B., and Spencer, S. S. (1992). Regional coherence and the transfer of ictal activity during seizure onset in the medial temporal lobe. *Electroencephalogr. Clin. Neurophysiol.* 82, 415–422.

Engel, J., VanNess, P., Rasmussen, T., and Ojemann, L. (1993). "Outcome with respect to epileptic seizures," in *Surgical Treatment of the Epilepsies*, 2nd Edn, ed. J. Engel (New York: Raven Press), 609–622.

Franaszczuk, P. J., and Bergey, G. K. (1999). An autoregressive method for the measurement of synchronization of interictal and ictal EEG signals. *Biol. Cybern.* 81, 3–9.

Friston, K. (1994). Functional and effective connectivity in neuroimaging: A synthesis. *Hum. Brain Mapp.* 2, 56–78.

Gnatkovsky, V., Librizzi, L., Trombin, F., and de Curtis, M. (2008). Fast activity at seizure onset is mediated by inhibitory circuits in the entorhinal cortex in vitro. *Ann. Neurol.* 64, 674–686.

Gotman, J. (1987). Interhemispheric interactions in seizures of focal onset: data from human intracranial recordings. *Electroenceph. Clin. Neurophysiol.* 67, 120–133.

Guenot, M., Isnard, J., Ryvlin, P., Fischer, C., Ostrowsky, K., Mauguiere, F., and Sindou, M. (2001). Neurophysiological monitoring for epilepsy surgery: the Talairach SEEG method. StereoElectroEncephaloGraphy. Indications, results, complications and therapeutic applications in a series of 100 consecutive cases. *Stereotact. Funct. Neurosurg.* 77, 29–32.

Haykin, S., Racine, R. J., Xu, Y., and Chapman, C. A. (1996). Monitoring neural oscillation and signal transmission between cortical regions using time-frequency analysis of electroencephalographic activity. *Proc. IEEE* 84, 1295–1301.

Horwitz, B. (2003). The elusive concept of brain connectivity. *Neuroimage* 19(Pt 1), 466–470.

Iasemidis, L. D. (2003). Epileptic seizure prediction and control. *IEEE Trans. Biomed. Eng.* 50, 549–558.

Jirsa, V., and McIntosh, A. (Eds.). (2007). *Handbook of Brain Connectivity*. Berlin: Springer Verlag.

Kalitzin, S. N., Parra, J., Velis, D. N., and Lopes da Silva, F. H. (2007). Quantification of unidirectional nonlinear associations between multidimensional signals. *IEEE Trans. Biomed. Eng.* 54, 454–461.

Ktonas, P. Y., and Mallart, R. (1991). Estimation of time delay between EEG signals for epileptic focus localization: statistical error considerations. *Electroencephalogr. Clin. Neurophysiol.* 78, 105–110.

Kus, R., Kaminski, M., and Blinowska, K. J. (2004). Determination of EEG activity propagation: pair-wise versus multichannel estimate. *IEEE Trans. Biomed. Eng.* 51, 1501–1510.

Lehnertz, K. (1999). Non-linear time series analysis of intracranial EEG recordings in patients with epilepsy – an overview. *Int. J. Psychophysiol.* 34, 45–52.

Lieb, J. P., Hoque, K., Skomer, C. E., and Song, X. W. (1987). Inter-hemispheric propagation of human mesial temporal lobe seizures: a coherence/phase analysis. *Electroencephalogr. Clin. Neurophysiol.* 67, 101–119.

Lopes da Silva, F., Pijn, J. P., and Boeijinga, P. (1989). Interdependence of EEG signals: linear vs. nonlinear associations and the significance of time delays and phase shifts. *Brain Topogr.* 2, 9–18.

Lopes da Silva, F. H., van Hulten, K., Lommen, J. G., Storm van Leeuwen, W., van Veelen, C. W., and Vliegenthart, W. (1977). Automatic detection and localization of epileptic foci. *Electroencephalogr. Clin. Neurophysiol.* 43, 1–13.

Lytton, W. W. (2008). Computer modelling of epilepsy. *Nat. Rev. Neurosci.* 9, 626–637.

Mars, N., and Lopes da Silva, F. (1983). Propagation of seizure activity in kindled dogs. *Electroencephalogr. Clin. Neurophysiol.* 56, 194–209.

McDonald, A. J., and Mascagni, F. (1997). Projections of the lateral entorhinal cortex to the amygdala: a Phaseolus vulgaris leucoagglutinin study in the rat. *Neuroscience* 77, 445–459.

McGonigal, A., Bartolomei, F., Regis, J., Guye, M., Gavaret, M., Trebuchon-Da Fonseca, A., Dufour, H., Figarella-Branger, D., Girard, N., Peragut, J. C., and Chauvel, P. (2007). Stereoelectroencephalography in presurgical assessment of MRI-negative epilepsy. *Brain* 130(Pt 12), 3169–3183.

Mormann, F., Andrzejak, R. G., Kreuz, T., Rieke, C., David, P., Elger, C. E., and Lehnertz, K. (2003). Automated detection of a preseizure state based on a decrease in synchronization in intracranial electroencephalogram recordings from epilepsy patients. *Phys. Rev. E. Stat. Nonlin. Soft Matter Phys.* 67(Pt 1), 021912.

Pijn, J. (1990). *Quantitative Evaluation of EEG Signals in Epilepsy, Nonlinear Associations, Time Delays and Nonlinear Dynamics.* Ph.D. Thesis. Amsterdam: University of Amsterdam.

Pijn, J., and Lopes Da Silva, F. (1993a). "Propagation of electrical activity: nonlinear associations and time delays between EEG signals," in *Basic Mechanisms of the EEG*, eds S. Zschocke, E. J. Speckmann (Boston: Birkauser), 41–61.

Pijn, J., Velis, D. N., and Lopes da Silva, F. (1992). Measurement of interhemispheric time differences in generalised spike-and-wave. *Electroencephalogr. Clin. Neurophysiol.* 83, 169–171.

Pijn, J. P., and Lopes da silva, F. H. (1993b). "Propagation of electrical activity: nonlinear associations and time delays between EEG signals," in *Basic Mechanisms of the EEG, Brain Dynamics,* eds S. Zschocke and E. J. Speckmann (Boston: Birkhauser), 41–61.

Pikovsky, A., Rosenblum, M., and Kurths, J. (2001). *Synchronization: A Universal Concept in Nonlinear Sciences*. Cambridge: Cambridge University Press.

Rafiq, A., DeLorenzo, R. J., and Coulter, D. A. (1993). Generation and propagation of epileptiform discharges in a combined entorhinal cortex/hippocampal slice. *J. Neurophysiol.* 70, 1962–1974.

Rampp, S., and Stefan, H. (2006). Fast activity as a surrogate marker of epileptic network function? *Clin. Neurophysiol.* 117, 2111–2117.

Rosenblum, M., Pikovsky, A., and Kurths, J. (2004). Synchronization approach to analysis of biological signals. *Fluctuation Noise Lett.* 4, L53–L62.

Russchen, F. T. (1982a). Amygdalopetal projections in the cat. I. Cortical afferent connections. A study with retrograde and anterograde tracing techniques. *J. Comp. Neurol.* 206, 159–179.

Russchen, F. T. (1982b). Amygdalopetal projections in the cat. II. Subcortical afferent connections. A study with retrograde tracing techniques. *J. Comp. Neurol.* 207, 157–176.

Schindler, K., Leung, H., Elger, C. E., and Lehnertz, K. (2007). Assessing seizure dynamics by analysing the correlation structure of multichannel intracranial EEG. *Brain* 130(Pt 1), 65–77.

Soltesz, I., and Staley, K. J. (2008). *Computational Neuroscience in Epilepsy*. New York: Elsevier.

Spencer, S. S. (2002). Neural networks in human epilepsy: evidence of and implications for treatment. *Epilepsia* 43, 219–227.

Sporns, O. (2010). *Networks of the Brain*. Cambridge, MA: MIT Press.

Stam, C. J., Breakspear, M., van Cappellen van Walsum, A. M., and van Dijk, B. W. (2003). Nonlinear synchronization in EEG and whole-head MEG recordings of healthy subjects. *Hum. Brain Mapp.* 19, 63–78.

Stam, C. J., van Cappellen van Walsum, A. M., Pijnenburg, Y. A., Berendse, H. W., de Munck, J. C., Scheltens, P., and van Dijk, B. W. (2002). Generalized synchronization of MEG recordings in Alzheimer's Disease: evidence for involvement of the gamma band. *J. Clin. Neurophysiol.* 19, 562–574.

Stoop, R., and Pralong, E. (2000). Functional connections and epileptic spread between hippocampus, entorhinal cortex and amygdala in a modified horizontal slice preparation of the rat brain. *Eur. J. Neurosci.* 12, 3651–3663.

Suffczynski, P., Wendling, F., Bellanger, J., and Lopes Da Silva, F. (2006). Some insights into computational models of (patho)physiological brain activity. *Proc. IEEE* 94, 784–804.

Thatcher, R. W., Krause, P. J., and Hrybyk, M. (1986). Cortico-cortical associations and EEG coherence: a two-compartmental model. *Electroencephalogr. Clin. Neurophysiol.* 64, 123–143.

Traub, R., Whittington, M., Buhl, E., LeBeau, F., Bibbig, A., Boyd, S., Cross, H., and Baldeweg, T. (2001). A possible role for gap junctions in generation of very fast EEG oscillations preceding the onset of, and perhaps initiating, seizures. *Epilepsia* 42, 153–170.

Uhlhaas, P. J., and Singer, W. (2006). Neural synchrony in brain disorders: relevance for cognitive dysfunctions and pathophysiology. *Neuron* 52, 155–168.

Ullah, G., and Schiff, S. J. (2009). Models of epilepsy. Scholarpedia (http://www.scholarpedia.org/article/Models_of_epilepsy) 4, 1409.

Uva, L., Librizzi, L., Wendling, F., and de Curtis, M. (2005). Propagation dynamics of epileptiform activity acutely induced by bicuculline in the hippocampal-parahippocampal region of the isolated Guinea pig brain. *Epilepsia* 46, 1914–1925.

Wendling, F., Ansari-Asl, K., Bartolomei, F., and Senhadji, L. (2009). From EEG signals to brain connectivity: a model-based evaluation of interdependence measures. *J. Neurosci. Methods* 183, 9–18.

Wendling, F., Badier, J., Chauvel, P., and Coatrieux, J. (1997). A method to quantify invariant information in depth-recorded epileptic seizures. *Electroenceph. Clin. Neurophysiol.* 102, 472–485.

Wendling, F., and Bartolomei, F. (2001). Modeling EEG signals and interpreting measures of relationship during temporal-lobe seizures: an approach to the study of epileptogenic networks. *Epileptic Disord.* 3, 67–78.

Wendling, F., Bartolomei, F., Bellanger, J. J., Bourien, J., and Chauvel, P. (2003). Epileptic fast intracerebral EEG activity: evidence for spatial decorrelation at seizure onset. *Brain* 126(Pt 6), 1449–1459.

Wendling, F., Bartolomei, F., Bellanger, J. J., and Chauvel, P. (2002). Epileptic fast activity can be explained by a model of impaired GABAergic dendritic inhibition. *Eur. J. Neurosci.* 15, 1499–1508.

Wendling, F., Bartolomei, F., Bellanger, J. J., and Chauvel, P. (2001a). [Identification of epileptogenic networks from modeling and nonlinear analysis of SEEG signals]. *Neurophysiol. Clin.* 31, 139–151.

Wendling, F., Bartolomei, F., Bellanger, J. J., and Chauvel, P. (2001b). Interpretation of interdependencies in epileptic signals using a macroscopic physiological model of the EEG. *Clin. Neurophysiol.* 112, 1201–1218.

Wendling, F., Bellanger, J. J., Badier, J. M., and Coatrieux, J. L. (1996). Extraction of spatio-temporal signatures from depth EEG seizure signals based on objective matching in warped vectorial observations. *IEEE Trans. Biomed. Eng.* 43, 990–1000.

Wendling, F., Bellanger, J. J., Bartolomei, F., and Chauvel, P. (2000). Relevance of nonlinear lumped-parameter models in the analysis of depth-EEG epileptic signals. *Biol. Cybern.* 83, 367–378.

Wendling, F., Hernandez, A., Bellanger, J. J., Chauvel, P., and Bartolomei, F. (2005). Interictal to ictal transition in human temporal lobe epilepsy: insights from a computational model of intracerebral EEG. *J. Clin. Neurophysiol.* 22, 343–356.

Wilson, C. L., Isokawa, M., Babb, T. L., and Crandall, P. H. (1990). Functional connections in the human temporal lobe. I. Analysis of limbic system pathways using neuronal responses evoked by electrical stimulation. *Exp. Brain Res.* 82, 279–292.

Wilson, C. L., Isokawa, M., Babb, T. L., Crandall, P. H., Levesque, M. F., and Engel, J. Jr. (1991). Functional connections in the human temporal lobe. II. Evidence for a loss of functional linkage between contralateral limbic structures. *Exp. Brain Res.* 85, 174–187.

Witter, M., and Wouterlood, F. (2002). *The Parahippocampal Region: Organization and Role in Cognitive Function*. Oxford: Oxford University Press.

Witter, M. P., and Groenewegen, H. J. (1986). Connections of the parahippocampal cortex in the cat. IV. Subcortical efferents. *J. Comp. Neurol.* 252, 51–77.

Witter, M. P., Room, P., Groenewegen, H. J., and Lohman, A. H. (1986). Connections of the parahippocampal cortex in the cat. V. Intrinsic connections; comments on input/output connections with the hippocampus. *J. Comp. Neurol.* 252, 78–94.

Conflict of Interest Statement: The authors declare that the research was conducted in the absence of any commercial or financial relationships that could be construed as a potential conflict of interest.

Received: 14 June 2010; accepted: 03 November 2010; published online: 25 November 2010.

Citation: Wendling F, Chauvel P, Biraben A and Bartolomei F (2010) From intracerebral EEG signals to brain connectivity: identification of epileptogenic networks in partial epilepsy. Front. Syst. Neurosci. 4:154. doi: 10.3389/fnsys.2010.00154

Copyright © 2010 Wendling, Chauvel, Biraben and Bartolomei. This is an open-access article subject to an exclusive license agreement between the authors and the Frontiers Research Foundation, which permits unrestricted use, distribution, and reproduction in any medium, provided the original authors and source are credited.

frontiers in
SYSTEMS NEUROSCIENCE

REVIEW ARTICLE
published: 22 March 2011
doi: 10.3389/fnsys.2011.00012

Concepts of connectivity and human epileptic activity

***Louis Lemieux*[1,2]*, *Jean Daunizeau*[3] *and Matthew C. Walker*[1]**

[1] *Department of Clinical and Experimental Epilepsy, University College London Institute of Neurology, London, UK*
[2] *Magnetic Resonance Imaging Unit, National Society for Epilepsy, Buckinghamshire, UK*
[3] *Wellcome Trust Centre for Neuroimaging, University College London Institute of Neurology, London, UK*

Edited by:
Silvina G. Horovitz, National Institutes of Health, USA

Reviewed by:
Robert Turner, Max Planck Institute for Human Cognitive and Brain Sciences, Germany
Heiko J. Luhmann, Institute of Physiology and Pathophysiology, Germany

***Correspondence:**
Louis Lemieux, Department of Clinical and Experimental Epilepsy, University College London Institute of Neurology, Queen Square, London WC1N 3BG, UK.
e-mail: l.lemieux@ion.ucl.ac.uk

This review attempts to place the concept of connectivity from increasingly sophisticated neuroimaging data analysis methodologies within the field of epilepsy research. We introduce the more principled connectivity terminology developed recently in neuroimaging and review some of the key concepts related to the characterization of propagation of epileptic activity using what may be called traditional correlation-based studies based on EEG. We then show how essentially similar methodologies, and more recently models addressing causality, have been used to characterize whole-brain and regional networks using functional MRI data. Following a discussion of our current understanding of the neuronal system aspects of the onset and propagation of epileptic discharges and seizures, we discuss the most advanced and ambitious framework to attempt to fully characterize epileptic networks based on neuroimaging data.

Keywords: epilepsy, connectivity, neuroimaging, EEG, modeling

INTRODUCTION

The brain is essentially an electro-chemical network. Connectivity is at the center of the problem of Epilepsy since its defining element is the occurrence of seizures, which essentially are periods of abnormal inter-neuronal synchrony. Unanswered questions that are central to an improved understanding of the mechanisms of epilepsy include some which implicate connectivity directly, such as: Why does ictal activity spread? Why do seizures persist in some patients, following surgical resection? Why do focal insults often give rise to recurrent seizures, i.e., epilepsy? And some which do so less directly: Why do spike and wave discharges and seizures occur when they do? Why does the spatial relationship between the generators of interictal discharges and seizures vary between patients? Answers to these questions would fundamentally improve our ability to eliminate seizures.

The difficulty of pinning down the concept of brain connectivity has already been noted (Horwitz, 2003). Nonetheless at the macroscopic scale (brain) connectivity can be partitioned into three main concepts: (i) anatomical (or structural) connectivity measured in terms of physical (and chemical) connections between neuronal populations or individual neurons, (ii) "functional" connectivity by which we mean the statistical similarity between activities in distributed neuronal populations, and (iii) "effective" connectivity, which speaks to the directed influence the activity of one region exerts onto another region's activity in a given context (Sporns, 2010). This distinction is useful for our discussion in that the measurement instruments and data analytical tools at our disposal have mainly focused on each aspect separately (but see Guye et al., 2008).

Here we focus on connectivity of neuronal activity, reflected in electrophysiological (LFP, EEG, MEG) and hemodynamic (functional MRI, fMRI) signals measured in humans and animals, but with reference to structural connectivity when possible. In the following, we will focus on connectivity assessed in relation to events or to (transient) brain states.

We are motivated by the following two perceived needs: firstly, to relate the various measures of connectivity found in the field of epilepsy research to the more general language of functional and effective connectivity as used in neuroscience (neuroimaging) and secondly, to gage the potential benefits of applying state-of-the-art connectivity methods to answer scientific questions raised within the field of human epilepsy research.

We begin by reviewing basic principles of connectivity, followed by a description of connectivity measurement and quantification methodologies. We then review some of the main findings of basic studies of connectivity in epilepsy, focusing on human data but making essential links to animal studies. The last part of this review describes the latest developments in models of coupled (distributed) generators of EEG/MEG and fMRI signals, with the view of scrutinizing their possible role as a bridge between scales of understanding in epilepsy.

DEFINITIONS, PRINCIPLES, AND THE CHARACTERIZATION OF CONNECTIVITY IN EPILEPSY

Because of the history of brain connectivity analysis, the functional/effective dichotomy is a convenient starting point for our discussion. As we shall see, *a priori*, both forms of connectivity are aimed at identifying the presence and strength of connections between network nodes and, when possible, their directionality. However, a further ambition of effective connectivity is to allow the inference of (biophysical) mechanisms by which causal links are expressed in measured neuroimaging signals. The study of effective connectivity is, therefore, usually a more model-based (or hypothesis-driven) approach than that of functional connectivity. It is worth noting that the term functional connectivity is not commonly encountered in the field of epilepsy, particularly in relation to EEG data although its use has increased recently in view of growing interest in resting-state fMRI data.

EEG: PROPAGATION, SPREAD, SOURCE MAPPING, AND CONNECTIVITY

A key concept in epilepsy is propagation, which is usually understood to mean the observation of similar patterns or of signals with different patterns but all suspected of reflecting a common underlying phenomenon, on an increasing number of EEG recording channels. This is particularly relevant for seizure activity, where it can be commonly observed on intracranial EEG recordings (Brazier, 1972; Tao et al., 2007b). There does not seem to be a formal distinction between "spread" and "propagation" in the field of epilepsy, although the term spread can be seen as implying spatial contiguity and possibly a more passive process than propagation, which therefore may be more general. Propagation, and synchronization to take one of the commonly used measures of propagation, implies connectivity and therefore the various ways of characterizing propagation discussed below are connectivity measures. In the following, measures of functional connectivity dominate as there have been very few studies attempting to characterize effective connectivity in epilepsy.

Signal space connectivity

Continuing with the example of EEG recorded within the brain the problem of characterizing propagation is confounded by the fact that the most prominent feature may not necessarily reflect the driving source ("pacemaker"; Brazier, 1972; Pijn et al., 1990). Therefore, early efforts to address the specific problem of identifying the driving component focused on correlation and phase lag analysis in the temporal domain or coherence in the frequency domain (Walter, 1963). In general, the propagation velocity is expected to be large and therefore quantitative methods to detect and measure small inter-channel time differences were developed. In principle, methods based on spectral estimates such as coherence analysis may be best suited to study phenomena of sufficient duration, such as seizures, while correlation linear or non-linear may be applied to shorter epochs (Allen et al., 1992). Event coincidence analysis of icEEG data recorded in TLE has been used to identify sets of networks involved in interictal epileptiform discharge (IED) generation with good reproducibility (Bourien et al., 2005; Wendling et al., 2009b). For extended discharges (e.g., focal or generalized seizures) inter-channel phase difference analyses, evaluated for a specific frequency (Brazier, 1972) or over a range of frequencies showing a sufficiently high degree of coherence and linear relationship between phase difference and frequency (Gotman, 1983) have been used to characterize propagation. Relaxation of the assumption of linearity, which can be violated in epilepsy, has lead to the use of more general measures of association (e.g., mutual information and non-linear correlation ratio: h^2) to study seizure propagation (Pijn et al., 1990, 1992; Bartolomei et al., 2001; Wendling et al., 2001, 2009a; Guye et al., 2006). The ability to identify reliable pre- or early ictal connectivity patterns has obvious implications for our ability to predict seizures (Litt and Lehnertz, 2002; Mormann et al., 2007; see Hughes, 2008 for an interesting historical account).

Another application of the concept of connectivity in epilepsy has been the more recent attempts to identify syndrome-specific patterns in resting-state EEG data. For example, the concept of generalized synchronization has been used to identify functional connectivity differences in resting-state scalp EEG at the global level or regionally based on icEEG between patient groups with potential diagnostic value (Monto et al., 2007; Bettus et al., 2008; Douw et al., 2010). Below, we will discuss how the same approach has been used on fMRI data.

Scalp EEG and MEG source space connectivity

Changes in scalp EEG/MEG field topography reflect a combination of changes in source morphology and strength, and noise (Ebersole and Hawes-Ebersole, 2007). Although subjective, the interpretation of changes in scalp EEG patterns in terms of lobar localization, lateralization, and generalization forms an integral part of clinical practice. However, characterization of neural connectivity based on quantitative analyses of scalp EEG in signal space is particularly problematic because the signals result from propagation through the head and subject to fundamental ambiguities of source identification (Schoffelen and Gross, 2009). Furthermore, even for such simple events as focal spikes, propagation, or spread can result in severe violations of the modeling assumptions, such as synchronized activity over a relatively limited cortical area for the case of the single moving dipole. The demonstration that 10 cm^2 of synchronously active cortex is necessary to produce a visually recognizable spike on scalp EEG (Tao et al., 2005, 2007a) suggests that point dipole mapping may often break down. Nonetheless, source tracking has been used to characterize spike propagation within the brain, possibly down to the sub-lobar level although careful interpretation of any localizing information is required in view of the above caveats (Ebersole and Hawes-Ebersole, 2007). Ictal activity represents a much greater challenge due to the length and complexity of the events, with rare studies attempting to link the intracranial and scalp EEG representations of ictal spread (Tao et al., 2007b). The observed complex dynamic patterns of synchrony mean that we are even further from useful source-based analyses than for interictal discharges.

It is beyond the scope of this review to discuss the entire range of generator models available to the investigator and clinician, from the single moving equivalent current dipole (ECD) to distributed source models of cortical patches. However, these can be characterized as essentially static, and address the problem of estimating spatial activity profile under various spatial constraints at each time point. This can be taken to reflect a lag between our understanding of the biophysics of generator geometry (point dipole as a representation of EPSP and IPSP in the pyramidal neuron) versus that of generator dynamics. Although there have been recent efforts to incorporate the temporal dimension to source estimation, the use of such techniques to assess spread remains to be assessed (Daunizeau et al., 2006).

The spread of epileptiform activity, measured as the ratio of the regional MEG dipole source strength in a distributed model over the local noise level, has been mapped (statistically) at 2.5 ms intervals showing realistic patterns in a few children with focal epilepsy, comparing advantageously to the results of serial ECD fitting for interictal activity (Shiraishi et al., 2005a,b) and for discharges in the early ictal period (Tanaka et al., 2009).

In generalized epilepsy, EEG/MEG source phase synchrony analysis based on its surrogate measure, instantaneous narrowband frequency locking, has been used to study long-range cortical synchronization during 3-Hz generalized spike-wave discharges, allowing the identification of a consistent fronto-central network, in agreement with other localization studies (Amor et al., 2009).

Causality and effective connectivity

A number of generalized measures of signal synchrony possess asymmetry which has been used to infer "driver-response" relationships (Le Van Quyen et al., 1998; Quiroga et al., 2002). However, the causality inferred from these has been shown to be dubious in the presence of noise (Quiroga et al., 2000) although there are examples of agreement with clinical data (Le Van Quyen et al., 1998). Of note is the use of generalized synchrony on icEEG (inter-channel spike peak time delay measurements) to validate a model of effective connectivity during seizures based on fMRI data in a rat model of epilepsy [David et al., 2008a; see Section "Signal Generation and Effective Connectivity Modeling in Epilepsy" on dynamic causal modeling (DCM)].

Granger causality (GC, sometimes referred to as *Granger–Geweke* causality; see Kaminski et al., 2001) is based on the notion that one signal can be called causal with respect to another if the latter can be better predicted by using information from the former. The directed transfer function (DTF; Kaminski and Blinowska, 1991), which was subsequently shown to be a generalization of GC, has been used to study information flow on icEEG data recorded during epileptic seizures (Franaszczuk and Bergey, 1998). More recently, a dynamic form of GC has been proposed for the study of epileptic spike propagation measured with MEG (Lin et al., 2009). The method can be used to track changes in effective connectivity based in the temporal and frequency domains over sub-spike time scales.

Dynamic causal modeling is a model of effective connectivity based on a biophysically realistic generative model of the signals and there are versions of DCM for EEG, MEG, and fMRI (see Section "Signal Generation and Effective Connectivity Modeling in Epilepsy" for a more detailed discussion of DCM). DCM is a relatively novel approach that was introduced as a generic formalism for studying effective connectivity in a seminal paper by Friston et al. (2003). In brief, at the heart of DCM is a set of bilinear differential equations (of the same form as Newtonian motion equations) that relate the rate of change in regional neuronal activity in terms of linearly separable components that reflect the influence of other regional state variables (Friston et al., 2003). One of DCM's main claims is that it attempts to model neuronal states through generative models in contrast to other approaches to effective connectivity such as Granger causal modeling, which model the signals (Friston, 2009). DCM has been used to study plasticity in the human epileptic focus using evoked responses measured intracranially (David et al., 2008b).

FUNCTIONAL MRI: FUNCTIONAL AND EFFECTIVE CONNECTIVITY

Compared to EEG or even MEG, fMRI is a newcomer in the toolkit available to investigators interested in studying epileptic activity. Among the attractive aspects of the technique in comparison with EEG and MEG are: its capacity to image the entire brain more or less uniformly without the need to solve the inverse problem, its spatial resolution and the potentially complimentary nature of the information it provides (hemodynamic). The addition of simultaneous EEG recording means that one is able to correlate the fMRI time series data with subclinical (unpredictable and brief) events, such as IED, with the aim of mapping the associated hemodynamic changes.

Ictal events can also be studied, either fortuitously or intentionally, although the occurrence of seizures in the scanner poses a specific health hazard which requires special attention. Although *a priori* simultaneous EEG is not always necessary to study ictal events using fMRI in a given patient depending on clinical features it can be an important source of information. Without EEG and in absence of clinical manifestations or ictal trigger, fMRI can be used to study the resting-state brain hemodynamics without reference to any specific event, allowing comparing features of the fMRI signal such as inter-regional temporal correlation patterns (i.e., functional connectivity) across patient groups, for example (Guye et al., 2008, 2010).

There have now been more than 100 publications describing fMRI studies of epileptic activity in humans, mostly with simultaneous EEG recording and using a general linear modeling approach, which have revealed sometimes complex patterns of IED or seizure-related BOLD changes in a large proportion of the cases studied. Using this approach maps containing multiple significant BOLD clusters can be said to represent networks to the extent that the signals in those regions show a sufficient high degree of correlation with the modeled waveform. However, in the context of functional connectivity, it is worth remembering that the fact that two signals significantly correlated with a third (e.g., a modeled signal) does not imply that the former are significantly correlated with each other. Therefore, fMRI functional connectivity analyses are typically based on calculating inter-regional correlations directly from the data. For example, Waites et al. (2006) showed differences in resting-state functional connectivity patterns in the language network in patients with TLE compared to a group of healthy controls. Also in TLE, studies of resting-state fMRI connectivity have focused on identifying asymmetries with possible clinical implications (Bettus et al., 2009, 2010).

In the above studies, the characterization of networks is performed based on correlation analyses of time series data acquired over extended periods of rest, without reference to specific events, and do not address causality. There have been a few applications of DCM to fMRI data in epilepsy to study effective connectivity in networks associated with generalized spike-wave discharges (David et al., 2008a; Vaudano et al., 2009). The final section of this article focuses on DCM, in particular its possible role in elucidating the pathological mechanisms responsible for epileptic activity based on electrophysiological and hemodynamic data.

ELECTROPHYSIOLOGICAL MARKERS OF EPILEPSY: ICTAL AND INTERICTAL EPILEPTIFORM EEG PATTERNS

The *epileptiform* patterns commonly observed on scalp EEG recordings from patients with epilepsy can be categorized as arising focally or appearing simultaneously over a large region or propagating to many remote locations. The identification and characterization of these patterns form an important element of the patient's assessment and subsequent management. As for all types of brain activity neural interactions form a central element in the onset, continuation and cessation of epileptic activity. In this section we review the phenomenology of epileptic activity and the underlying neural interactions but with special emphasis on the aspects of connectivity that can be measured using human brain imaging and electrophysiology.

THE GENERATORS OF EPILEPTIFORM ACTIVITY

While our understanding of the basic neurophysiology of the generators of epileptic activity has been derived from studies at the microscopic level, we envisage increasingly direct links with phenomenology at higher scales and that these will be made through biophysically realistic models of whole-brain signals, such as DCM (to be discussed in Section "Signal Generation and Effective Connectivity Modeling in Epilepsy"). The possibility of identifying and characterizing the pathological substrate of whole-brain data within such a framework would rest on models capable of representing the neurophysiological excesses and deficiencies described below, be they node-specific or network-wide, at the appropriate scale.

Interictal discharges

Interictal epileptiform discharges include spikes, which are fast electrographic transients lasting less than 70 ms and sharp waves, which last 70–120 ms (de Curtis and Avanzini, 2001); these occur rarely (<1%) in healthy individuals (Gregory et al., 1993), and are strongly associated with epilepsy (Marsan and Zivin, 1970). IEDs are generated by the synchronous "activation" of a large numbers of neurons – in order to be detectable by scalp EEG, the synchronous activation of 10–20 cm^2 of gyral cortex is necessary (Tao et al., 2007a). Excitatory postsynaptic potentials following activation of glutamate receptors cause an influx of sodium into dendrites (current sink), and the consequent flow of sodium from the soma (current source). The intracellular correlate of the interictal spike is the paroxysmal depolarizing shift (Matsumoto and Marsan, 1964), a slow depolarizing potential with a high frequency (>200 Hz) burst of action potentials. A number of pathological mechanisms have been proposed to underlie the interictal spike, including changes in the intrinsic burst properties of neurons (increased neuronal excitability) and increased network excitability (secondary to changes in neurotransmission and/or neuronal connectivity).

Interictal epileptiform discharges are usually followed by a slow wave lasting hundreds of milliseconds. This depends upon the activation of hyperpolarizing GABA(A) and GABA(B) receptor-mediated currents and calcium-dependent potassium currents (de Curtis and Avanzini, 2001; McCormick and Contreras, 2001). Therefore, IEDs activate hyperpolarizing currents, resulting in a post-spike refractory period during which neuronal activity is inhibited (de Curtis and Avanzini, 2001). Increased interictal spiking occurs after seizures, raising the possibility that this is a compensatory antiepileptic response (de Curtis and Avanzini, 2001). Indeed, experiments in entorhinal cortex–hippocampal slice preparations have confirmed the antiepileptic potential of spikes. Spike discharges generated in the CA3 region inhibited epileptic activity in the entorhinal cortex, so that sectioning of part of the hippocampal circuitry, preventing invasion of the entorhinal cortex by these spikes, led to potentiation of entorhinal cortex seizure activity (Barbarosie and Avoli, 1997). This leads to two important conclusions: first, interictal spikes can have a lasting inhibitory effect; second, they can have this effect remote from where the spikes arise. This is critical for understanding cortico-cortical signal propagation as single spikes may disrupt propagation by, in effect, silencing cortical areas.

Fast oscillations

Ripple oscillations (100–200 Hz) are physiological phenomena that occur in relationship with hippocampal sharp waves. An observation in epileptic tissue is the presence of even higher frequency (250–500 Hz) oscillations, also termed fast ripples, which seem to be a marker of epileptogenicity (Bragin et al., 1999; Jacobs et al., 2009). These can occur in association with IEDs but also may precede seizures. It is likely that most high frequency oscillations are generated in and remain restricted to small areas of neocortex, but more rarely can occur over larger areas which may be more indicative of epileptogenic cortex (Schevon et al., 2009). There remains controversy about the mechanisms generating such high frequency oscillations. These have been proposed to be due either to a barrage of high frequency inhibitory postsynaptic potentials from fast spiking interneurons impinging on relatively depolarized principal cells (Trevelyan, 2009) or to the synchronous firing of principal neurons coupled through non-synaptic mechanisms such as gap junction (providing direct electrical coupling of neurons; Roopun et al., 2010).

Partial seizures

Spike discharges can precede a seizure with progressively less effective after-hyperpolarizations in mesial temporal lobe epilepsy (King and Spencer, 1995); however, the hallmark of seizure activity is the build up of fast activity that is usually initially spatially confined, and is distinct from IEDs. The mechanisms underlying this activity are unclear but it has been proposed to represent the excessive firing of a group of principal neurons, perhaps coupled through gap junctions (Traub et al., 2001). This pattern evolves to high amplitude spikes that occur at a lower frequency. Two questions concerning seizures arise: first, what is it that triggers a seizure? And second, what is it about an area of cortex that makes it epileptogenic? The first question is far from clear; there are conflicting data from analysis of preictal data (see Mormann et al., 2007) that suggest that there may be changes occurring minutes before the seizure (i.e., the seizure results as a critical point of network activity is reached). The transition from normal to epileptiform behavior is probably caused by greater spread and neuronal recruitment secondary to a combination of enhanced connectivity, enhanced excitatory transmission, a failure of inhibitory mechanisms, and changes in intrinsic neuronal properties. The second question is therefore easier to address as many of these changes have been described, but it is unclear which are most important (Walker et al., 2007). Indeed, it is likely that there is no unique process and that cortex can become epileptogenic via a variety of mechanisms, examples of which are given below.

During the development of epilepsy (epileptogenesis) changes have been documented in neuronal properties (Su et al., 2002), ion channel expression (Bernard et al., 2004; Shah et al., 2004), and GABAergic inhibition (Obenaus et al., 1993; Cossart et al., 2001). Moreover GABA(A) receptor potentials can and shift from hyperpolarizing to depolarizing (potentially excitatory; Cohen et al., 2002; and the effect of this on, for example, the BOLD response to GABAergic inhibition is not clear). Excitatory transmission is potentiated not only through changes in receptors (Lieberman and Mody, 1999; Porter et al., 2006), but also through sprouting of excitatory fibers (Tauck and Nadler, 1985). Sprouting has been

most clearly demonstrated in the dentate gyrus in which recurrent collaterals form between dentate granule cells, and this hyperconnectivity promotes the formation of local excitatory circuits and hyper-excitability. Importantly, however, the probability of a connection between any two granule cells is low and the observed hyper-excitability may be explained by non-random connectivity and the formation of a few, highly connected "hub" cells (Morgan and Soltesz, 2008), a feature of small-world networks. Epileptogenic insults are also associated with gliosis, altering the regulation of external potassium (Lux et al., 1986) and contributing to the release of neurotransmitters into the extracellular space (Tian et al., 2005). There are also changes in non-synaptic mechanisms involving increases in ephaptic transmission and the expression of gap junctions which may promote neuronal synchronization (Jefferys, 1995). Suggesting that the local spread of seizure activity can occur independent of axonal connections.

Some of these changes (e.g., excitatory fiber sprouting, gliosis, neuronal death) have an obvious anatomical correlate and can be easily quantified by microscopic and, on occasion, macroscopic tools. Moreover, pathologies leading to these changes such as stroke, tumors, cortical dysgenesis, traumatic brain injury are often clearly evident, and although the hallmark of these pathologies (e.g., brain damage) may not be the substrate for the epileptogenic process, they are an indicator of an epileptogenic process. However, these clear anatomical changes are not necessary for a network to become epileptogenic and certain changes (e.g., in ion channels and receptors) may only be apparent with functional investigation. Therefore, epileptogenic cortex may not always be discernible using anatomic techniques.

Absence seizures and 3 Hz spike-wave discharges

Absence seizures are generalized seizures which are generated within the thalamocortical loop. This depends upon the recruitment of reticular thalamic neurons by the neocortex. These in turn hyperpolarize (inhibit) thalamocortical neurons. This activates various ionic currents, resulting in the rebound burst firing of thalamocortical neurons which project onto and excite neocortical neurons and so the cycle repeats (McCormick and Contreras, 2001). Absences were originally believed to be generated subcortically, by thalamic neurons initially driving the recruitment of neocortical neurons. However, paroxysmal oscillations within thalamocortical loops in absence seizures in rats seem to originate in the somatosensory cortex rather than the thalamus, with synchronization mediated by rapid intracortical propagation of seizure activity (Meeren et al., 2002). This is supported by anatomical evidence in humans of subtle cortical structural abnormalities in some patients with absence seizures (Woermann et al., 1999). Indeed, this and the potential of focal pathological change in the medial frontal lobe to generate absence-like seizures have blurred the distinction between focal and generalized epilepsies.

PROPAGATION OF EPILEPTIC ACTIVITY: OBSERVATIONS AND MECHANISMS

Both IEDs and seizures propagate, by which we mean that the pathological EEG pattern spreads to distant brain areas, reflecting recruitment of neuronal activity in those areas. This occurs locally due to local connections and networks and at more distant sites through longer range connections. However, recruitment depends on not only connections between different brain regions but also the ease with which a brain region can be recruited (see below). In some situations the observed propagation pattern can be rationalized based on general anatomical knowledge and can be correlated with the evolution of clinical signs (in the case of seizures), however these can significantly vary from event to event and our general understanding of these patterns remains poor; studies comparing patient-specific structural connectivity (MRI tractography) with interictal and ictal propagation patterns are just beginning to emerge (Hamandi et al., 2007; Diehl et al., 2010).

Nonetheless, the mechanisms underlying propagation and recruitment at these different scales are probably quite similar, though may differ for interictal and ictal activity. An IED can be considered in three distinct mechanistic stages: initiation, propagation, and termination (Pinto et al., 2005). The threshold for initiation depends upon the balance of excitation and inhibition. However, propagation velocity depends solely upon excitation, probably because the delay between excitatory activity and the recruitment of inhibitory activity provides a window during which an IED can propagate unimpeded by inhibition. The termination of an IED is a complex process including depolarizing block and synaptic inhibition.

The propagation of seizures is more complex because, by necessity, these are longer lasting and so cannot depend on the short-lived delay between excitatory and inhibitory activity. Focal seizure activity recruits local inhibitory neurons which importantly provide a strong "surround" inhibition limiting the spread and time course of the abnormal activity (Prince and Wilder, 1967). This inhibitory constraint provides a mechanism that limits seizure activity in both temporal and spatial domains. Repeated seizure activity can however result in the breakdown of this constraint and seizure propagation. Moreover, the speed of propagation is dependent upon the strength of inhibition with faster propagation occurring with less powerful inhibitory constraint (Trevelyan et al., 2006, 2007a). Furthermore, the arrangement of synaptic inhibition (divergent) in which feed-forward inhibition will constrain a number of pyramidal cells results in a stepwise recruitment of groups of principal neurons as inhibition fails. The mechanisms underlying the breakdown of the inhibitory constraint are unclear and may not be unique.

Although propagation of seizure activity may be well-defined, the propagation of discharges that occur during seizure activity is less certain. Ictal activity is prolonged and so having propagated to a region, later repetitive discharges during the ictus will spread according to the pattern of the connections of that area and the strength of surrounding inhibition. It is therefore possible that later discharges during the ictus may back propagate to areas from which the seizure has spread (Trevelyan et al., 2007b). This is also observed with human recordings.

SIGNAL GENERATION AND EFFECTIVE CONNECTIVITY MODELING IN EPILEPSY

In this section we consider the scope for uni- and multi-modal data to be brought together in a biophysically realistic modeling and data statistical analysis framework, namely DCM.

WHY SHOULD WE ATTEMPT MODEL-BASED EFFECTIVE CONNECTIVITY ANALYSES TO STUDY EPILEPSY?

As can be abstracted from the previous sections, initiation, propagation, and termination of epileptiform activity are thought to result from the complex interplay between the natural balance of excitation and inhibition within the system and some pathological perturbations of various physiological processes, e.g., neuromodulatory activity (impacting upon neuronal excitability). This is most probably the reason why epilepsy expresses itself at so many different spatial and temporal scales of observation, from e.g., genetic disruptions of biomolecular neuronal properties (e.g., conformational change of ion channels, see Steinlein, 2004) to macroscopic structural abnormalities (e.g., cortical thickness in temporal lobe epilepsy, see Bernhardt et al., 2010), through impaired resting-state activity (e.g., phasic suspension of the attentional network; see Gotman et al., 2005; Hamandi et al., 2006; Laufs et al., 2007).

At first glance, it does not seem possible to embrace the diversity of these traits within a common comprehensive theoretical framework. However, it must be the case that adequately realistic models of brain dynamics, in conjunction with appropriate brain activity measurements, can reveal the link between these phenomena (Wendling, 2008). This is because whether or not a given trait is related to epilepsy has to do with the observed correlation between its occurrence and the presence of epileptiform brain activity, such as focal seizures or generalized spike-wave discharges. For example, if a model is able to account for basic cellular mechanisms such as the impact of neurotransmitter levels onto average ion channel dynamics, it might be able to link genetic observations to neuroimaging. If such a model was also able to account for the relative proportion of cell types in different cortical layers (e.g., pyramidal cells in layer IV and excitatory/inhibitory interneurons in layer VI), it might be able to predict dynamical changes resulting from sufficiently specified loss of gray matter. Finally, if it was based on the notion of a distributed brain network to capture observed transient and steady-state macroscopic dynamics, it might well be an appropriate tool to understand the large-scale structure of epileptogenic brain networks.

Having said this, the model alone, even if exquisitely realistic, cannot disambiguate between different candidate scenarios about, e.g., what is it that triggers, propagates and/or terminates an observed seizure. This is because the seizure etiology is expected to vary greatly across patients, or even within patients. In other words, the mechanisms that lead to the seizures are context-dependent. Hence, one cannot predict those *a priori*, on a patient-by-patient basis.

Taken together, this means that one wants to embed sophisticated biophysical models into the statistical data analysis, with the aim of exploiting the specificities of the observed (neuroimaging) data to identify the subject-specific relevant mechanisms underlying epileptiform activity. This is the basic idea behind DCM (Friston et al., 2003). The DCM framework has two main components: biophysical modeling and probabilistic statistical data analysis. Realistic neurobiological modeling is required to simulate observed brain network dynamics. However, context-dependent variables of these models cannot be known *a priori*, e.g., whether or not activity-dependent plasticity did occur. Therefore, statistical techniques (embedding the above biophysical models) are necessary for statistical inference on these context-dependent effects, which are the experimental questions of interest.

DCM: STATE-OF-THE-ART

Nevertheless, existing implementations of DCM restrict the application of this generic perspective to more specific questions that are limited either by the unavoidable simplifying assumptions of the underlying biophysical models and/or by the bounded efficiency of the associated statistical inference techniques. In brief, the validity of DCM relies upon a careful balance between the realism of the underlying biophysical models and the feasibility of the statistical treatment. This has motivated the development of many variants of DCM, focusing on either of the two DCM components. To date, about 30 DCM methodological articles have been published in the peer-reviewed literature (see Daunizeau et al., 2010 for a recent review).

The (Bayesian) statistical treatment of DCM eventually provides model parameter estimates (synaptic time constants, action potential thresholds, adaptation effects, etc…) and the model marginal likelihood. The latter quantity measures how likely is a model given the measured (neuroimaging) dataset, and is used to perform statistical model comparison. This statistical component of DCM is further described below (see DCM: Statistical Data Analysis). This can be useful to identify epileptogenic mechanisms that are *a priori* likely to underlie ictal or interictal epileptiform activity.

In brief, DCM for fMRI data includes a simple dynamical model of coupled brain regions as well as a model of neurovascular coupling, relating neural activity to BOLD time series. In addition, it comes in three flavors:

- whether or not distinct excitatory and inhibitory populations are considered within each region of the brain network
- whether or not one includes spontaneous (stochastic) fluctuations in the brain network dynamics
- whether or not (non-linear) gating effects, whereby activity in one area enables or disables a connection between two other areas, are assumed to underlie observed brain dynamics.

In its simplest form, Bayesian model comparison was used in Vaudano et al. (2009) to assess the structure of the epileptogenic network in terms of the role of three brain structures, namely thalamus, prefrontal cortex, and precuneus in seizure generation or facilitation using EEG–fMRI data in seven patients with idiopathic generalized epilepsy (IGE). The findings lead the authors to hypothesize a role for the precuneus as a form of modulator of generalized spike-wave activity, and by extension, of the occurrence of absence seizures, linking spontaneous fluctuations in brain state as reflected by the so-called Default-Mode Network of brain activity (Raichle et al., 2001) to the occurrence of epileptic discharges (Vaudano et al., 2009; Carney et al., 2010).

David et al. (2008a) performed concurrent fMRI and icEEG measurements to measure the spread of excitation in a genetically defined type of epilepsy in rodents. It is important to note that in these studies, the onset of EEG epileptic activity (back-shifted in time in the case of David et al., 2008a) was treated as the input (knowledge of which is required, except

– exceptionally – for stochastic DCMs) in families of models, where each model was distinguished by the choice of input node, for comparison to identify the best model. One may question the meaning of intrinsic activity being treated as an input in this context, given that DCM was conceived based on extrinsic inputs under experimental control. In fact, this can be interpreted as embodying the empirical assumption that the initial cause of the modeled effects corresponds to the time of GSW onset. It is worth remembering that the families of models considered and the DCM results are as good as the assumptions, which they are based on (Penny et al., 2004). Daunizeau et al. (2010) has used model comparison on stochastic DCMs for fMRI to provide evidence in favor of the existence of (nonlinear) thalamic gating effects onto the cortico-thalamic loop during interictal activity[1].

"Neural mass" models in DCMs for EEG/MEG/LFP data are typically considerably more complex than in DCMs for fMRI. This is because the temporal information on neural activity, which can be extracted from electrophysiological measurements, can only be captured by models that represent neurobiologically detailed mechanisms. Here, each region is assumed to be composed of three interacting subpopulations (pyramidal cells, spiny-stellate excitatory and inhibitory interneurons) whose (fixed) intrinsic connectivity was derived from an invariant meso-scale cortical structure (Jansen and Rit, 1995). The temporal dynamics of each subpopulation relies on two operators: a temporal convolution of the average presynaptic firing rate yielding the average postsynaptic membrane potential and an instantaneous sigmoidal mapping from membrane depolarization to firing rate (see **Figure 1**). This forms the basic building block of DCMs for EEG/MEG/LFP data, in the sense that it summarizes the activity within one brain region that composes the large-scale network. Such basic building block has already been extensively used in the context of epilepsy (see, e.g., Wendling, 2008).

Critically though, the qualitative nature of the network dynamics relates to the between-areas connectivity structure. In DCM for EEG/MEG/LFP data, three qualitatively different extrinsic (excitatory) connections types are considered (cf. Felleman and Van Essen, 1991): (i) bottom-up or forward connections that originate in agranular layers and terminate in layer IV, (ii) top-down or backward connections that connect agranular layers, and (iii) lateral connections that originate in agranular layers and target all layers. Lastly, the model can include the propagation of electromagnetic fields through head tissues to address the problem of spatial mixing of the respective contributions of cortically segregated sources in the measured scalp EEG/MEG data (see e.g., Mosher et al., 1999). Existing variants of DCM for EEG/MEG and LFP (local field potential data) are related to:

- which data features one wants to model, i.e., evoked responses in the time domain, steady-state responses in the frequency domain, induced responses in the time-frequency domain, oscillations in the (within-frequency band) phase domain, etc;
- whether or not voltage-dependent effects on membrane ion conductances are included in the model;
- whether local spatial propagation effects are considered, in relation to the size of the brain regions participating in the network.

The previously mentioned work by David (2007) is a first step toward understanding the gradual recruitment of the epileptogenic network that gives rise to epileptic discharges within the framework of DCM. Some of the critical pathological mechanisms discussed in the previous section can already be assessed through DCM analyses. This is because one can include these in terms of *a priori* beliefs onto model parameters (e.g., altered voltage-dependent sodium channel kinetic time constants) or even on model structure (e.g., anatomically localized cell type-specific neuronal death), and quantify how likely they are, given observed brain dynamics.

DCM: STATISTICAL DATA ANALYSIS

The need for neurobiological plausibility can make DCMs fairly complex, compared to conventional regression-based models of effective connectivity, such as structural equation modeling (SEM; McIntosh and Gonzalez-Lima, 1994; Büchel and Friston, 1997) or autoregressive models (Harrison et al., 2003; Roebroeck et al., 2005). This complexity induces potential non-identifiability problems, requiring novel sophisticated model inversion techniques that are typically cast within a Bayesian framework. For example, the non-linearities of the models, as well as the dimension of the dynamical systems involved, have necessitated the development of dedicated approximate inference schemes, namely variational Bayes (VB; see e.g., Beal, 2003). In brief, VB is an iterative algorithm that indirectly optimizes an approximation to both the model evidence (used for model comparison) and the posterior density (for parameter estimation), under simplifying assumptions about the form of the latter distribution (see, e.g., Friston et al., 2007). Furthermore, developments have been required to address Bayesian model comparison for group studies. Stephan et al. (2009) address random effects on models at the between-subjects level, i.e., accounting for group heterogeneity or outliers. This second-level analysis provides the so-called "exceedance probability," of one model being more likely than any other model, given the group data. It also introduced model space partitioning, which allows one to compare subsets of all models considered, integrating out uncertainty about any aspect of model structure other than the one of interest. This work was recently extended to allow for comparisons between model families of arbitrary size and for Bayesian model averaging within model families Penny et al. (2010). Allowing statistical inference at the level of families of model is important whenever the question of interest may correspond to more than one model within the comparison set (e.g., serial versus parallel connectivity structure).

Note that using the model evidence to compare models against each other means that the most likely model may not be the model "fitting best" the data. One should remember that measuring the fit

[1]Stochastic DCM refers to an extension of the DCM framework, whereby one assumes that activity within network nodes may by driven by unknown (random or stochastic) inputs, in addition to experimentally controlled inputs and influences from other areas. In other words, in addition to the usual DCM parameters, one has to estimate the trajectory of neural noise that may have distorted the response of the system to known inputs. The key idea here is that neural noise can extend the dynamical repertoire of the system in a non-trivial way. Besides, stochastic DCM reduces to deterministic DCM by *a priori* constraining the neural noise variance to 0.

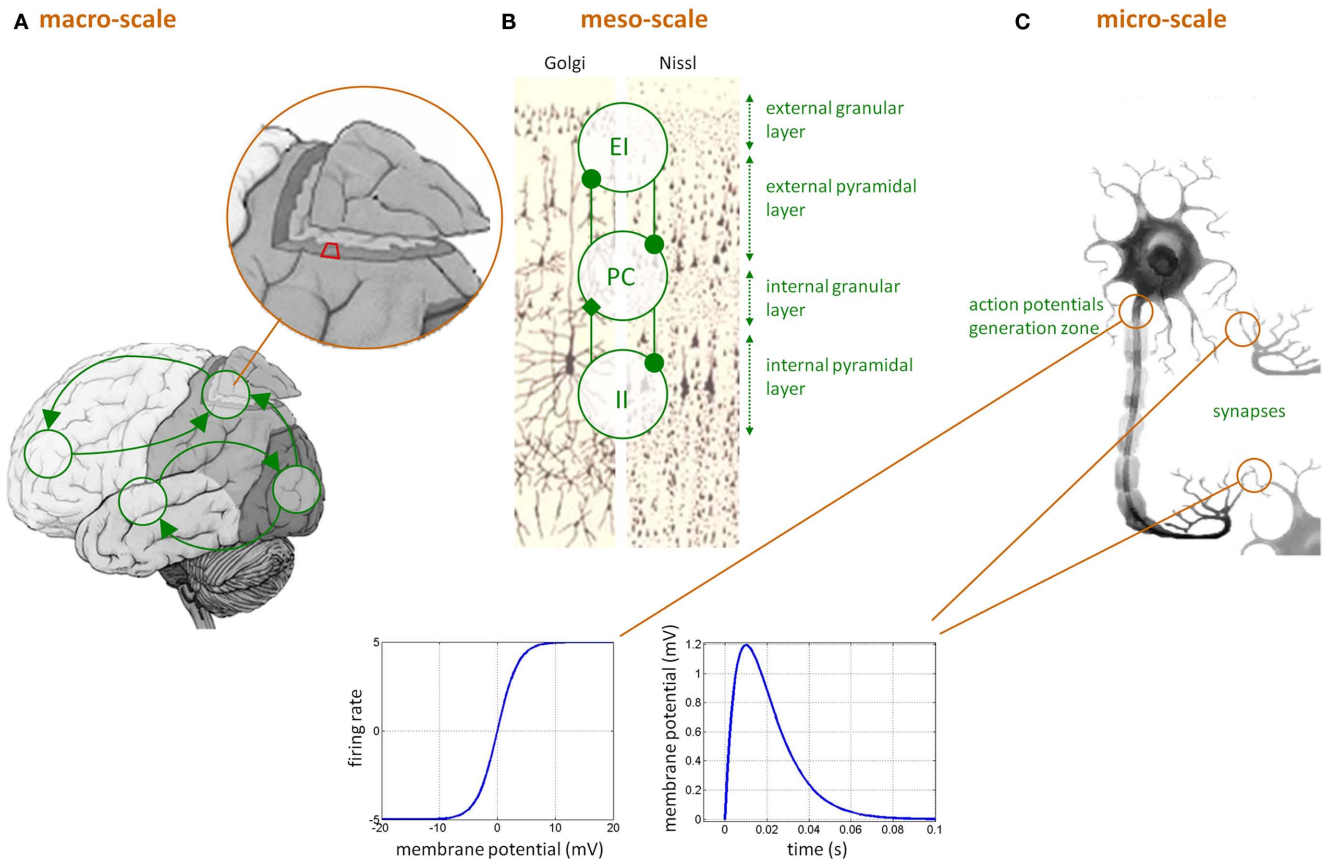


FIGURE 1 | Dynamic causal modeling for EEG/MEG data. (C) Neuronal features at the micro-scale that affect the level of the neural ensemble, i.e., at the meso-scale **(B)**: (i) sigmoidal transformation, describing how mean postsynaptic membrane potential is linked to mean presynaptic firing rate, and (ii) temporal convolution (kernel shown) of mean presynaptic firing rate yielding mean postsynaptic membrane depolarization. **(B)** The meso-scale properties that affect the macro-scale **(A)**, i.e., within-region invariant connectivity structure between pyramidal cells (PC), excitatory interneurons (EI), and inhibitory interneurons (II) subpopulations across cortical layers. **(A)** The macro-scale effective connectivity structure.

(e.g., percentage of variance explained) is not a very good measure for the quality of a model. This has to do with the fact that minimizing residuals can lead to severe lack of generalizability. Correcting the fit with complexity penalty terms is the hallmark of Bayesian inference schemes, which, as a consequence, do not try to minimize the residuals. Within a Bayesian framework, it is thus perfectly acceptable to reasonably compromise data fit, if this guaranties improved generalizability. Guessing whether or not this trade-off is optimal by looking at the fit itself is impossible without factoring in the complexity of the model. In other words, any optimal Bayesian inversion only explains in the data what is estimated to be generalizable, i.e., reproducible across repetitions of the same experiment, given the explanatory factors at hand.

Besides, we would like to further comment on the causal aspect of DCM. It is not because DCM relies upon a dynamical formulation that it assesses causal influences from evidence of temporal precedence (as, e.g., GC techniques do; see Valdes-Sosa et al., 2011 for a comprehensive discussion). Time is certainly an important dimension of causal influences, but definitely not the main component of DCM for fMRI, which, compared to the underlying neural events, is poorly temporally resolved. Causality can be inferred from non-symmetrical shared variance[2] (e.g., see Pearl, 2000). DCM was designed to capture these effects. The motivation for including the temporal dimension in DCM is actually to allow for feedback influences (loopy causal systems), rather than to detect temporal precedence. This is why DCM is more (though not entirely) immune to heterogeneous hemodynamic delays than, e.g., GC analyses (David et al., 2008a).

Finally, we would like to stress that DCM is ultimately not an exploratory analysis: it is meant to test/compare precise hypotheses about brain function. Furthermore, its mathematical form is explicitly based on generic assumptions about brain organization, e.g., that the brain enjoys a hierarchical structure. This means that DCM is optimally used to answer a specific class of questions, typically: whether or not feedback/feed-forward influences within the network vary as a function of experimental manipulations or perturbations (such as diseases). In the context of epilepsy, examples of DCM-relevant questions are: (i) whether ictal activity propagates from a region that triggers epileptiform activity, or rather

[2]Pearl takes the following example: one actually infers that rains causes the grass to be wet (and not the reverse), because it does not rain each time the grass is wet (due to other – independent – influences, e.g., the gardener), but the grass is wet each time it is raining.

that epileptiform activity emerges from self-excitatory influences throughout the network; or (ii) how does the system reconfigures itself (short-term plasticity) during the interictal to ictal transition. DCM is probably not the right data analysis tool to address more loosely defined questions about brain organization, e.g., can we get a global picture of the networks active during the fMRI data acquisition session?…

DCM: LIMITATIONS

Neuroanatomical and neurophysiological studies have been crucial in motivating the basic modeling assumptions that underlie DCMs for fMRI and electrophysiological data. However, one may question whether all neurobiological facts relevant for explaining neuronal population dynamics are represented in existing DCMs. This question is of particular importance for DCMs of electrophysiological data, from the healthy or diseased brain, which have much more fine-grained representations of neuronal mechanisms than DCM for fMRI.

For example, macro-scale propagation effects, mediated by distance-dependent lateral connections, have not yet been properly accounted for[3]. These effects can be thought of as wave propagation in a complex medium, leading to spatiotemporal pattern formation or self-organization. Since the early work by Amari (1977), much effort has been invested in developing a *neural field* theory (e.g., see Deco et al., 2008 and references therein); incorporating these ideas into the DCM framework may prove fruitful.

Also, it is well known that neurons are subject to internal (e.g., thermal) noise, which may still have an impact at the population scale (see e.g., Soula and Chow, 2007 for "finite size" effects). If this is the case, the neural ensemble dynamics would deviate from the mean-field theoretical treatment that underlies most current modeling efforts in macro-scale neural dynamics (including DCMs).

Perhaps most importantly, there are several neurophysiological processes at the micro-scale that have been neglected in existing DCMs, notably *activity-dependent plasticity*, i.e., continuously modified activity-dependent efficacy of synaptic transmission. This includes different forms of short-term plasticity, such as synaptic depression/facilitation or spike-timing dependent plasticity, and long-term plasticity, such as long-term potentiation (LTP) and depression (LTD). An important task for the future will be to evaluate whether the above processes are necessary for explaining, e.g., the transition from interictal to ictal activity, as observed with presently available recording techniques.

Concerning DCM for fMRI, the above phenomena are not explicitly modeled[4]. This may (or may not) be a lesser concern than for electrophysiological DCMs, since it is unlikely that these fine-grained mechanisms are accurately reflected in and can be inferred from BOLD data. Instead, physiological details of the neurovascular coupling are perhaps more important (see Stephan et al., 2004 for review). So far, it neglects the potential influence of inhibitory activity on the hemodynamic response, which is a likely explanation for deactivations (Shmuel et al., 2006; Sotero and Trujillo-Barreto, 2007). Furthermore, there is no realistic account of the metabolic cascade that relates synaptic activity and neuronal metabolism to the vasodilatation kinetics (Riera et al., 2006). This is mainly due to the simplistic account of neuronal activity in DCMs for fMRI, which does not disambiguate between, e.g., postsynaptic membrane depolarization and presynaptic firing rate. Also, DCM for fMRI has ignored the important role of glial cells (Takano et al., 2006; Iadecola and Nedergaard, 2007). We refer the interested reader to Rosa et al. (2010) for further reading on the current debate regarding the neurovascular coupling.

Many DCM validation studies have been conducted (see Daunizeau et al., 2010 for a review). Among these, the most far-reaching experimental assessment of the validity of DCM analyses so far was done by David et al. (2008a), who performed concurrent fMRI and intracerebral EEG measurements to measure the spread of excitation in a genetically rat model of absence epilepsy. In brief, this study (i) provides supportive evidence for the validity of DCM for inferring network structure from fMRI data and (ii) stresses the importance of having a realistic model of neurovascular coupling. Clearly, further validation studies will be needed. Further invasive *in vivo* measurements of electrical (e.g., implantable miniaturized probes or clinical electrodes (combined with fMRI: Vulliemoz et al., 2010) and optical (e.g., two-photon laser scanning microscopy) signals are likely to be very useful for such an experimental validation (Riera et al., 2008).

Criticisms have also been raised against the statistical component of DCM. Most of these are related to the generic properties of the VB algorithm, which is essentially an approximation scheme. We refer the reader to Daunizeau et al. (2010) for a comprehensive critical review of the biophysical, statistical and practical aspects of DCM. In addition, it has often been advocated that the computational complexity of DCM prevents any analysis of a large-scale brain network containing more than a handful of nodes/regions. This is supposed to be due to the fact that one may have to compare a number of models that is an exponentially increasing function of the number of nodes (curse of dimensionality). Also, it has been argued that the proportion of explained variance in the measured signals was "low," even for the "best" models within the comparison set (this has sometimes been referred to as a form of "underfitting"). However, recent developments in the statistical treatment of DCM render these claims irrelevant:

- The use of Savage–Dickey ratios within a Bayesian framework allows one to derive the model evidence of any model that can be derived as a reduction of a full "reference" model (i.e., the DCM corresponding to an entirely connected network)[5]. This means that one has to perform only one numerical inversion

[3]But see Daunizeau et al. (2009a) for a "standing wave" approximation to local propagation effects.

[4]But see David (2007), David et al. (2008b), and Stephan et al. (2008) for phenomenological accounts of activity-dependent plasticity effects.

[5]Savage–Dickey ratios rely upon simple conditional probability calculus to numerically derive the relative evidence of nested models from the divergence between prior and posterior distributions of the full model. Loosely speaking: if any hypothesis (e.g., $\theta = 0$) is more probable under the posterior than under the prior, then it means that the data affords evidence in favor of the hypothesis. It turns out that adding such hypotheses to the full model defines nested models, i.e., models with fixed (zero) connections in the network. We refer the interested reader to Friston et al. (2011) and references therein.

(that of the full model) in order to compare all other possible reduced models (i.e., networks lacking connections). This makes it possible to compare thousands of models in a few seconds (Friston et al., 2011).

- Following recent developments in probabilistic identification of stochastic systems (Friston et al., 2008; Daunizeau et al., 2009b), the first steps toward stochastic DCMs are now being taken (Daunizeau et al., 2011, submitted; Li et al., 2011). These models extend the current deterministic DCM framework by accounting for unspecific perturbations to the network dynamics. As a result, the proportion of explained variance drastically increases. Note that being a Bayesian scheme, stochastic DCM does not suffer from overfitting, which is the hallmark of frequentist statistical techniques.

Having said this, no increase in the sophistication of the statistical treatment of DCM can legitimately be said to guarantying the validity of the overall data analysis. This is already evident when considering the bounded realism of the underlying biophysical models (c.f. above comments). But more generally, the validity of DCM may well be context-dependent. Thus, the relevance of DCM within the context of epileptogenic networks has to be quantitatively assessed, by cross-validating the analyses with established results in the field. In addition, it may be necessary to extend the current DCM approach, in order to account for effects that may *a priori* be playing a key role when investigating the genesis, spread and termination of epileptic events using neuroimaging techniques. We will come to this in the next section.

DCM: RELEVANT POTENTIAL EXTENSIONS

Despite being so far the most far-reaching experimental assessment of the validity of fMRI DCM analyses so far, the study in David et al. (2008a) stressed the importance of having a model of neurovascular coupling. The concurrent use of two important neuroimaging modalities (i.e., EEG and fMRI data) raises the need for an integrated framework, whereby the same model is complementarily informed by the characteristic spatial and temporal resolutions of both datasets, beyond the use of EEG purely as a temporal event marker for fMRI modeling or DCM for example (Vaudano et al., 2009). This appears to be, despite a number of acknowledged theoretical and experimental concerns (see Daunizeau et al., 2009c for a review about EEG–fMRI information fusion), a promising future avenue for studying whole-brain, millisecond range, spontaneous or evoked paroxysmal activity and to characterize the underlying networks.

But more importantly, other potential extensions of the existing DCM framework can be considered to be relevant for studying epilepsy:

- *Field DCMs*: By incorporating elements of neural field theory (see Amari, 1977), field DCMs could account for local macroscale propagation effects. The basic idea here is to account for the distributed nature of brain activity (see Daunizeau et al., 2009a for a first step toward field DCMs). Among other phenomena, this could be helpful to assess within-region spread and boundaries of paroxysmal activity (e.g., inhibitory surrounding effects).
- *Stochastic DCMs*: Accounting for stochastic inputs to the network may be of particular importance for studying pathological resting-state data, whereby coherent activity within the network is not driven by experimentally controlled inputs to the system (which is usually the case in fMRI studies of epilepsy). In addition, provided that the probabilistic inversion schemes are properly extended (cf. Friston et al., 2008; Daunizeau et al., 2009b), this could also increase the stability of the statistical treatment of DCM (e.g., robustness to "missing regions").
- *Plastic DCMs*: Aberrant long- and short-term synaptic plasticity may play a key role in the gradual recruitment of regions within the epileptogenic network. An attractive goal is to extend the current DCM framework and, under due consideration of the limits of statistical inversion, represent different neurobiological mechanisms of synaptic plasticity more explicitly, such that their relative importance for explaining a patient-specific measurement of ictal and interictal activity can be disambiguated by model selection. Autonomous (activity-dependent) plastic effects may turn out to be particularly important to explain phase transition phenomena, e.g., transition from interictal to ictal activity (and back).

These modeling extensions could also benefit from the development of explicitly controlled experimental paradigms, provided that they can be undertaken ethically. For example, the use of seizure-inducing repetitive sensory or electrical stimulation might provide a statistically very powerful way of disclosing the properties of the epileptogenic network. Also, its interaction with non-pathological functional networks might be studied in the context of standard neuropsychological tasks. Lastly, trans-cranial magnetic stimulation (TMS) and/or deep-brain stimulation (DBS) could be used to causally interfere with parts of the network, providing exquisite information about the specific role of brain regions within a reciprocally connected network. Such experimental paradigms can easily be modeled with DCM, as is routinely done nowadays within the context of non-clinical neuropsychological research studies.

DISCUSSION AND CONCLUSION

The problem of characterizing the causal chains that give rise to and take place during epileptic events is central to our understanding of epilepsy, with vital consequences for the development of improved seizure management strategies. Following a period dedicated to the identification of regional abnormalities, we envisage that studies of epileptic activity and its substrate will focus increasingly on network aspects. We also believe that the long-term aim of developing non-invasive (whole-brain) neuroimaging techniques capable of solving the presurgical localization problem, by the very nature of the data they provide, goes hand in hand with this vision.

We have seen the progressively more sophisticated use of the various forms of data available to the investigator interested in studying epileptic networks, from scalp EEG to fMRI and alluded to increasingly sophisticated models. We have seen how the characterization of connectivity based on signal propagation relies on empirical rules mainly based on measures of association. This approach has been most rigorous and informative in relation to EEG signals measured intracranially. Access to hemodynamic brain signals

measured non-invasively during spontaneous epileptic activity in humans is a novel and potentially important avenue for the study of the temporal relationship between activities in different brain regions in a complementary way to electrophysiological study. For example, such studies may be able to reveal changes taking place over long time scales more easily than using electrophysiological techniques.

In the context of attempts to characterize the networks involved in seizure onset, propagation and cessation based on macroscopic measurements such as EEG/MEG and fMRI, the lack of a complete understanding, particularly in humans, of the underlying network dynamics poses a challenge and therefore an opportunity. This is because we do not really know what we are looking for with neuroimaging; the limitations of our gold standard (currently icEEG and post-surgical outcome) are clear to see. Therefore, we are still essentially at the stage of mapping hemodynamic changes based on temporal coincidence with scalp EEG and/or clinical manifestations. Even if we had a more complete electrophysiological description of such networks which for example could be used to devise more sophisticated GLMs, we do not yet fully understand the relationship between neuronal activity as measured using the most advanced electrophysiological techniques, such as depth EEG, and the BOLD signal (see Buzsaki et al., 2007; Logothetis, 2008). This makes the comparison of measures of connectivity based on the two types of data even more complex.

Nonetheless, the advent of models of effective connectivity such as DCM, incorporating increasingly sophisticated models of neuronal activity at various scales, combined with our improved understanding of the interictal and ictal states and the transition between them offers the opportunity for the first time to explore epileptic networks over the entire brain in a mechanistic, causal framework through model comparison. Efforts to tackle this challenge have already been made in relation to generalized spike-wave activity and absence seizures, due to the presence of a good rationale for a limited number of alternative models. The challenge is much greater in focal epilepsy where the phenomenology is much more varied. In addition, through our increasing understanding of the integrative aspects of brain activity derived from whole-brain cognitive neuroimaging studies this may help us answer questions such as: What is the interaction between fluctuations in connectivity associated with normal brain activity and the networks associated with paroxysmal events? Why do spikes and seizures occur when they do?

REFERENCES

Allen, P. J., Smith, S. J. M., and Scott, C. A. (1992). Measurement of interhemispheric time differences in generalised spike-and-wave. *Electroencephalogr. Clin. Neurophysiol.* 82, 81–84.

Amari, S. (1977). Dynamics of pattern formation in lateral inhibition type neural fields. *Biol. Cybern.* 27, 77–87.

Amor, F., Baillet, S., Navarro, V., Adam, C., Martinerie, J., and Le Van Quyen, M. (2009). Cortical local and long-range synchronization interplay in human absence seizure initiation. *Neuroimage* 45, 950–962.

Barbarosie, M., and Avoli, M. (1997). CA3-driven hippocampal-entorhinal loop controls rather than sustains in vitro limbic seizures. *J. Neurosci.* 17, 9308–9314.

Bartolomei, F., Wendling, F., Bellanger, J. J., Regis, J., and Chauvel, P. (2001). Neural networks involving the medial temporal structures in temporal lobe epilepsy. *Clin. Neurophysiol.* 112, 1746–1760.

Beal, M. (2003). *Variational Algorithms for Approximate Bayesian Inference*. Ph.D. thesis, Gatsby Computational Unit, University College London, London.

Bernard, C., Anderson, A., Becker, A., Poolos, N. P., Beck, H., and Johnston, D. (2004). Acquired dendritic channelopathy in temporal lobe epilepsy. *Science* 305, 532–535.

Bernhardt, B. C., Bernasconi, N., Concha, L., and Bernasconi, A. (2010). Cortical thickness in temporal lobe epilepsy. *Neurology* 74, 1776–1784.

Bettus, G., Bartolomei, F., Confort-Gouny, S., Guedj, E., Chauvel, P., Cozzone, P. J., Ranjeva, J. P., and Guye, M. (2010). Role of resting state functional connectivity MRI in presurgical investigation of mesial temporal lobe epilepsy. *J. Neurol. Neurosurg. Psychiatry*. 81, 1147–1154.

Bettus, G., Guedj, E., Joyeux, F., Confort-Gouny, S., Soulier, E., Laguitton, V., Cozzone, P. J., Chauvel, P., Ranjeva, J. P., Bartolomei, F., and Guye, M. (2009). Decreased basal fMRI functional connectivity in epileptogenic networks and contralateral compensatory mechanisms. *Hum. Brain Mapp.* 30, 1580–1591.

Bettus, G., Wendling, F., Guye, M., Valton, L., Regis, J., Chauvel, P., and Bartolomei, F. (2008). Enhanced EEG functional connectivity in mesial temporal lobe epilepsy. *Epilepsy Res.* 81, 58–68.

Bourien, J., Bartolomei, F., Bellanger, J. J., Gavaret, M., Chauvel, P., and Wendling, F. (2005). A method to identify reproducible subsets of co-activated structures during interictal spikes. Application to intracerebral EEG in temporal lobe epilepsy. *Clin. Neurophysiol.* 116, 443–455.

Bragin, A., Engel, J. Jr., Wilson, C. L., Fried, I., and Mathern, G. W. (1999). Hippocampal and entorhinal cortex high-frequency oscillations (100–500 Hz) in human epileptic brain and in kainic acid – treated rats with chronic seizures. *Epilepsia* 40, 127–137.

Brazier, M. A. (1972). Spread of seizure discharges in epilepsy: anatomical and electrophysiological considerations. *Exp. Neurol.* 36, 263–272.

Büchel, C., and Friston, K. J. (1997). Modulation of connectivity in visual pathways by attention: cortical interactions evaluated with structural equation modelling and fMRI. *Cereb Cortex* 7, 768–778.

Buzsaki, G., Kaila, K., and Raichle, M. (2007). Inhibition and Brain Work. *Neuron* 56, 771–783.

Carney, P. W., Masterton, R. A. J., Harvey, A. S., Scheffer, I. E., Berkovic, S. F., and Jackson, G. D. (2010). The core network in absence epilepsy – differences in cortical and thalamic BOLD response. *Neurology* 75, 904–911.

Cohen, I., Navarro, V., Clemenceau, S., Baulac, M., and Miles, R. (2002). On the origin of interictal activity in human temporal lobe epilepsy in vitro. *Science* 298, 1418–1421.

Cossart, R., Dinocourt, C., Hirsch, J. C., Merchan-Perez, A., De Felipe, J., Ben-Ari, Y., Esclapez, M., and Bernard, C. (2001). Dendritic but not somatic GABAergic inhibition is decreased in experimental epilepsy. *Nat. Neurosci.* 4, 52–62.

Daunizeau, J., David, O., and Stephan, K. E. (2010). Dynamic causal modelling: a critical review of the biophysical and statistical foundations. *Neuroimage* (in press).

Daunizeau, J., Kiebel, S. J., and Friston, K. J. (2009a). Dynamic causal modeling of distributed electromagnetic responses. *Neuroimage* 47, 590–601.

Daunizeau, J., Friston, K. J., and Kiebel, S. J. (2009b). Variational Bayesian identification and prediction of stochastic nonlinear dynamic causal models. *Physica D* 238, 2089–2118.

Daunizeau, J., Laufs, H., and Friston, K. J. (2009c). "EEG-fMRI information fusion: biophysics and data analysis," in *EEG-fMRI-Physiology, Technique and Applications*, eds C. Mulert and L. Lemieux (Heidelberg: Springer), 511–522.

Daunizeau, J., Mattout, J., Clonda, D., Goulard, B., Benali, H., and Lina, J. M. (2006). Bayesian spatio-temporal approach for EEG source reconstruction: conciliating ECD and distributed models. *IEEE Trans. Biomed. Eng.* 53, 503–516.

David, O. (2007). Dynamic causal models and autopoietic systems. *Biol. Res.* 40, 487–502.

David, O., Guillemain, I., Saillet, S., Reyt, S., Deransart, C., Segebarth, C., and Depaulis, A. (2008a). Identifying neural drivers with functional MRI: an electrophysiological validation. *PLoS Biol.* 6, 2683–2697. doi: 10.1371/journal.pbio.0060315

David, O., Wozniak, A., Minotti, L., and Kahane, P. (2008b). Precital short-term plasticity induced by 1 Hz stimulation. *Neuroimage* 39, 1633–1646.

de Curtis, M., and Avanzini, G. (2001). Interictal spikes in focal epileptogenesis. *Prog. Neurobiol.* 63, 541–567.

Deco, G., Jirsa, V. K., Robinson, P., Breakspear, M., and Friston K. J. (2008). The dynamic brain: from spiking neurons to neural masses and cortical fields. *Plos. Comput. Biol.* 4, e1000092. doi: 10.1371/journal.pcbi.1000092

Diehl, B., Tkach, J., Piao, Z., Ruggieri, P., LaPresto, E., Liu, P., Fisher, E., Bingaman, W., and Najm, I. (2010).

Diffusion tensor imaging in patients with focal epilepsy due to cortical dysplasia in the temporo-occipital region: electro-clinico-pathological correlations. *Epilepsy Res.* 90, 178–187.

Douw, L., de Groot, M., van Dellen, E., Heimans, J. J., Ronner, H. E., Stam, C. J., and Reijneveld, J. C. (2010). 'Functional connectivity' is a sensitive predictor of epilepsy diagnosis after the first seizure. *PLoS ONE* 5, e10839. doi: 10.1371/journal.pone.0010839

Ebersole, J. S., and Hawes-Ebersole, S. (2007). Clinical application of dipole models in the localization of epileptiform activity. *J. Clin. Neurophysiol.* 24, 120–129.

Felleman, D. J., and Van Essen, D. C. (1991). Distributed hierarchical processing in the primate cerebral cortex. *Cereb. Cortex* 1, 1–47.

Franaszczuk, P. J., and Bergey, G. K. (1998). Application of the directed transfer function method to mesial and lateral onset temporal lobe seizures. *Brain Topogr.* 11, 13–21.

Friston, K. (2009). Causal modelling and brain connectivity in functional magnetic resonance imaging. *PLoS Biol.* 7, e33. doi: 10.1371/journal.pbio.1000033

Friston, K. J., Harrison, L., and Penny, W. D. (2003). Dynamic causal modelling. *Neuroimage* 19, 1273–1302.

Friston, K. J., Li, B., Daunizeau, J., and Stephan K. E. (2011). Network discovery with DCM. *Neuroimage* (in press).

Friston, K. J., Mattout, J., Trujillo-Barreto, N. J., Ashburner, J., and Peeny, W. (2007). Variational free energy and the Laplace approximation. *Neuroimage* 34, 220–234.

Friston, K. J., Trujillo-Barreto, N. J., and Daunizeau, J. (2008). DEM: a variational treatment of dynamical systems. *Neuroimage* 42, 849–885.

Gotman, J. (1983). Measurement of small time differences between EEG channels: method and application to epileptic seizure propagation. *Electroencephalogr. Clin. Neurophysiol.* 56, 501–514.

Gotman, J., Grova, C., Bagshaw, A., Kobayashi, E., Aghakhani, Y., and Dubeau, F. (2005). Generalized epileptic discharges show thalamocortical activation and suspension of the default state of the brain. *Proc. Natl. Acad. Sci. U.S.A.* 102, 15236–15240.

Gregory, R. P., Oates, T., and Merry, R. T. (1993). Electroencephalogram epileptiform abnormalities in candidates for aircrew training. *Electroencephalogr. Clin. Neurophysiol.* 86, 75–77.

Guye, M., Bartolomei, F., and Ranjeva, J. P. (2008). Imaging structural and functional connectivity: towards a unified definition of human brain organization? *Curr. Opin. Neurol.* 21, 393–403.

Guye, M., Bettus, G., Bartolomei, F., and Cozzone, P. J. (2010). Graph theoretical analysis of structural and functional connectivity MRI in normal and pathological brain networks. *MAGMA* 23, 409–421.

Guye, M., Regis, J., Tamura, M., Wendling, F., McGonigal, A., Chauvel, P., and Bartolomei, F. (2006). The role of corticothalamic coupling in human temporal lobe epilepsy. *Brain* 129, 1917–1928.

Hamandi, K., Powell, H. W., Laufs, H., Symms, M. R., Barker, G. J., Parker, G. J., Lemieux, L., and Duncan, J. S. (2007). Combined EEG-fMRI and tractography to visualise propagation of epileptic activity. *J. Neurol. Neurosurg. Psychiatry* 79, 594–597.

Hamandi, K., Salek-Haddadi, A., Laufs, H., Liston, A., Friston, K., Fish, D. R., Duncan, J. S., and Lemieux, L. (2006). EEG-fMRI of idiopathic and secondarily generalized epilepsies. *Neuroimage* 31, 1700–1710.

Harrison, L., Penny, W. D., and Friston, K. (2003). Multivariate autoregressive modeling of fMRI time series. *Neuroimage* 19, 1477–1491.

Horwitz, B. (2003). The elusive concept of brain connectivity. *Neuroimage* 19, 466–470.

Hughes, J. R. (2008). Progress in predicting seizure episodes with nonlinear methods. *Epilepsy Behav.* 12, 128–135.

Iadecola, C., and Nedergaard, M. (2007). Glial regulation of the cerebral microvasculature. *Nat. Neurosci.* 10, 1369–1376.

Jacobs, J., Levan, P., Châtillon, C. E., Olivier, A., Dubeau, F., and Gotman, J. (2009). High frequency oscillations in intracranial EEGs mark epileptogenicity rather than lesion type. *Brain* 132(Pt 4), 1022–1037.

Jansen, B. H., and Rit, V. G. (1995). Electroencephalogram and visual evoked potential generation in a mathematical model of coupled cortical columns. *Biol. Cybern.* 73, 357–366.

Jefferys, J. G. (1995). Nonsynaptic modulation of neuronal activity in the brain: electric currents and extracellular ions. *Physiol. Rev.* 75, 689–723.

Kaminski, M., Ding, M., Truccolo, W. A., and Bressler, S. L. (2001). Evaluating causal relations in neural systems: Granger causality, directed transfer function and statistical assessment of significance. *Biol. Cybern.* 85, 145–157.

Kaminski, M. J., and Blinowska, K. J. (1991). A new method of the description of the information flow in the brain structures. *Biol. Cybern.* 65, 203–210.

King, D., and Spencer, S. (1995). Invasive electroencephalography in mesial temporal lobe epilepsy. *J. Clin. Neurophysiol.* 12, 32–45.

Laufs, H., Hamandi, K., Salek-Haddadi, A., Kleinschmidt, A. K., Duncan, J. S., and Lemieux, L. (2007). Temporal Lobe Interictal Epileptic Discharges Affect Cerebral Activity in "Default Mode". Brain Regions. *Human Brain Mapping* 28, 1023–1032.

Le Van Quyen, M., Adam, C., Baulac, M., Martinerie, J., and Varela, F. J. (1998). Nonlinear interdependencies of EEG signals in human intracranially recorded temporal lobe seizures. *Brain Res.* 792, 24–40.

Li, B., Daunizeau, J., Stephan, K. E., Penny, W., and Friston K. J. (2011). Stochastic DCM and generalized filtering. *Neuroimage* (in press).

Lieberman, D. N., and Mody, I. (1999). Properties of single NMDA receptor channels in human dentate gyrus granule cells. *J. Physiol.* 518(Pt 1), 55–70.

Lin, F. H., Hara, K., Solo, V., Vangel, M., Belliveau, J. W., Stufflebeam, S. M., and Hamalainen, M. S. (2009). Dynamic Granger–Geweke causality modeling with application to interictal spike propagation. *Hum. Brain Mapp.* 30, 1877–1886.

Litt, B., and Lehnertz, K. (2002). Seizure prediction and the preseizure period. *Curr. Opin. Neurol.* 15, 173–177.

Logothetis, N. K. (2008). What we can do and what we cannot do with fMRI. *Nature* 453, 869–878.

Lux, H. D., Heinemann, U., and Dietzel, I. (1986). Ionic changes and alterations in the size of the extracellular space during epileptic activity. *Adv. Neurol.* 44, 619–639.

Marsan, C. A., and Zivin, L. S. (1970). Factors related to the occurrence of typical paroxysmal abnormalities in the EEG records of epileptic patients. *Epilepsia* 11, 361–381.

Matsumoto, H., and Marsan, C. A. (1964). Cortical cellular phenomena in experimental epilepsy: interictal manifestations. *Exp. Neurol.* 9, 286–304.

McCormick, D. A., and Contreras, D. (2001). On the cellular and network bases of epileptic seizures. *Annu. Rev. Physiol.* 63, 815–846.

McIntosh, A. R., and Gonzalez-Lima, F. (1994). Structural equation modelling and its application to network analysis in functional brain imaging. *Hum. Brain Mapp.* 2, 2–22.

Meeren, H. K., Pijn, J. P., Van Luijtelaar, E. L., Coenen, A. M., and Lopes da Silva, F. H. (2002). Cortical focus drives widespread corticothalamic networks during spontaneous absence seizures in rats. *J. Neurosci.* 22, 1480–1495.

Monto, S., Vanhatalo, S., Holmes, M. D., and Palva, J. M. (2007). Epileptogenic neocortical networks are revealed by abnormal temporal dynamics in seizure-free subdural EEG. *Cereb. Cortex* 17, 1386–1393.

Morgan, R. J., and Soltesz, I. (2008). Nonrandom connectivity of the epileptic dentate gyrus predicts a major role for neuronal hubs in seizures. *Proc. Natl. Acad. Sci. U.S.A.* 105, 6179–6184.

Mormann, F., Andrzejak, R. G., Elger, C. E., and Lehnertz, K. (2007). Seizure prediction: the long and winding road. *Brain* 130(Pt 2), 314–333.

Mosher, J. C., Leahy, R. M., and Lewis, P. S. (1999). EEG and MEG: forward solutions for inverse methods. *IEEE Trans Biomed Eng.* 46, 245–259.

Obenaus, A., Esclapez, M., and Houser, C. R. (1993). Loss of glutamate decarboxylase mRNA-containing neurons in the rat dentate gyrus following pilocarpine-induced seizures. *J. Neurosci.* 13, 4470–4485.

Pearl, J. (2000). *Causality: Models, Reasoning, and Inference.* New York: Cambridge University Press.

Penny, W., Joao, M., Flandin, G., Daunizeau, J., Stephan, K. E., Friston, K. J., Schofield, T., and Leff, A. P. (2010). Comparing families of dynamic causal models. *Plos Comput. Biol.* 6, e1000709. doi: 10.1371/journal.pcbi.1000709

Penny, W. D., Stephan, K. E., Mechelli, A., and Friston, K. J. (2004). Comparing dynamic causal models. *Neuroimage* 22, 1157–1172.

Pijn, J. P., Velis, D. N., and Lopes da Silva, F. H. (1992). Measurement of interhemispheric time differences in generalised spike-and-wave. *Electroencephalogr. Clin. Neurophysiol.* 83, 169–171.

Pijn, J. P., Vijn, P. C., Lopes da Silva, F. H., Van Ende, B. W., and Blanes, W. (1990). Localization of epileptogenic foci using a new signal analytical approach. *Neurophysiol. Clin.* 20, 1–11.

Pinto, D. J., Patrick, S. L., Huang, W. C., and Connors, B. W. (2005). Initiation, propagation, and termination of epileptiform activity in rodent neocortex in vitro involve distinct mechanisms. 25, 8131–8140.

Porter, B. E., Cui, X. N., and Brooks-Kayal, A. R. (2006). Status epilepticus differentially alters AMPA and kainate receptor subunit expression in mature and immature dentate granule neurons. *Eur. J. Neurosci.* 23, 2857–2863.

Prince, D. A., and Wilder, B. J. (1967). Control mechanisms in cortical epileptogenic foci. *"Surround" inhibition. Arch Neurol.* 16, 194–202.

Quiroga, R. Q., Arnhold, J., and Grassberger, P. (2000). Learning driver-response relationships from synchronization patterns. *Phys. Rev. E* 61, 5142–5148.

Quiroga, R. Q., Kraskov, A., Kreuz, T., and Grassberge, P. (2002). Performance of

different synchronization measures in real data: a case study on electroencephalographic signals. *Phys. Rev. E* 65, 041903.

Raichle, M. E., MacLeod, A. M., Snyder, A. Z., Powers, W. J., Gusnard, D. A., and Shulman, G. L. (2001). A default mode of brain function. *Proc. Natl. Acad. Sci. U.S.A.* 98, 676–682.

Riera, J. J., Schousboe, A., Waagepetersen, H. S., Howarth, C., and Hyder, F. (2008). The micro-architecture of the cerebral cortex: functional neuroimaging models and metabolism. *Neuroimage* 40, 1436–1459.

Riera, J. J., Wan, X., Jimenez, J. C., and Kawashima, R. (2006). Nonlinear local electrovascular coupling. I: a theoretical model. *Hum. Brain Mapp.* 27, 896–914.

Roebroeck, A., Formisano, E., Goebel, R. (2005). Mapping directed influence over the brain using Granger causality and fMRI. *Neuroimage* 25, 230–242.

Roopun, A. K., Simonotto, J. D., Pierce, M. L., Jenkins, A., Nicholson, C., Schofield, I. S., Whittaker, R. G., Kaiser, M., Whittington, M. A., Traub, R. D., and Cunningham, M. O. (2010). A nonsynaptic mechanism underlying interictal discharges in human epileptic neocortex. *Proc. Natl. Acad. Sci. U.S.A.* 107, 338–343.

Rosa, M. J., Daunizeau, J., Friston, K. J. (2010). EEG-fMRI integration: a critical review of biophysical modelling and data analysis approaches. *J. Integr. Neurosci.* 9, 453–476.

Schevon, C. A., Trevelyan, A. J., Schroeder, C. E., Goodman, R. R., McKhann, G. Jr., and Emerson, R. G. (2009). Spatial characterization of interictal high frequency oscillations in epileptic neocortex. *Brain* 132(Pt 11), 3047–3059.

Schoffelen, J. M., and Gross, J. (2009). Source connectivity analysis with MEG and EEG. *Hum. Brain Mapp.* 30, 1857–1865.

Shah, M. M., Anderson, A. E., Leung, V., Lin, X., and Johnston, D. (2004). Seizure-induced plasticity of h channels in entorhinal cortical layer III pyramidal neurons. *Neuron* 44, 495–508.

Shiraishi, H., Ahlfors, S. P., Stufflebeam, S. M., Takano, K., Okajima, M., Knake, S., Hatanaka, K., Kohsaka, S., Saitoh, S., Dale, A. M., and Halgren, E. (2005a). Application of magnetoencephalography in epilepsy patients with widespread spike or slow-wave activity. *Epilepsia* 46, 1264–1272.

Shiraishi, H., Stufflebeam, S. M., Knake, S., Ahlfors, S. P., Sudo, A., Asahina, N., Egawa, K., Hatanaka, K., Kohsaka, S., Saitoh, S., Grant, P. E., Dale, A. M., and Halgren, E. (2005b). Dynamic statistical parametric mapping for analyzing the magnetoencephalographic epileptiform activity in patients with epilepsy. *J. Child Neurol.* 20, 363–369.

Shmuel, A., Augath, M., Oeltermann, A., and Logothetis, N. K. (2006). Negative functional MRI response correlates with decreases in neuronal activity in monkey visual area V1. *Nat Neurosci.* 9, 569–577.

Sotero, R. C., and Trujillo-Barreto, N. J. (2007). Biophysical model for integrating neuronal activity, EEG, fMRI and metabolism. *Neuroimage* 39, 290–309.

Soula, H., and Chow, C. C. (2007). Stochastic dynamics of a finite size spiking neural network. *Neural Comput.* 19, 3262–3292.

Sporns, O. (2010). *Networks of the Brain.* Cambridge, MA: MIT Press.

Steinlein, O. (2004). Genetic mechanisms that underlie epilepsy. *Nat. Rev. Neurosci.* 5, 400–408.

Stephan, K. E., Harrison, L. M., Penny, W. D., and Friston, K. J. (2004). Biophysical models of fMRI responses. *Curr. Opin. Neurobiol.* 14, 629–635.

Stephan, K. E., Kasper, L., Harrison, L., Daunizeau, J., Den Ouden, H., Breakspear, M., and Friston K. J. (2008). Nonlinear dynamic causal models for fMRI. *Neuroimage* 42, 649–662.

Stephan, K. E., Penny, W. D., Daunizeau, J., Moran, R., and Friston K. J. (2009). Bayesian model comparison for group studies. *Neuroimage* 46, 1004–1017.

Su, H., Sochivko, D., Becker, A., Chen, J., Jiang, Y., Yaari, Y., and Beck, H. (2002). Upregulation of a T-type Ca2+ channel causes a long-lasting modification of neuronal firing mode after status epilepticus. *J. Neurosci.* 22, 3645–3655.

Takano, T., Tian, G. F., Peng, W., Lou, N., Libionka, W., Han, X., and Nedergaard, M. (2006). Astrocyte-mediated control of cerebral blood flow. *Nat. Neurosci.* 9, 260–267.

Tanaka, N., Cole, A. J., von Pechmann, D., Wakeman, D. G., Hamalainen, M. S., Liu, H., Madsen, J. R., Bourgeois, B. F., and Stufflebeam, S. M. (2009). Dynamic statistical parametric mapping for analyzing ictal magnetoencephalographic spikes in patients with intractable frontal lobe epilepsy. *Epilepsy Res.* 85, 279–286.

Tao, J. X., Baldwin, M., Hawes-Ebersole, S., and Ebersole, J. S. (2007a). Cortical substrates of scalp EEG epileptiform discharges. *J. Clin. Neurophysiol.* 24, 96–100.

Tao, J. X., Baldwin, M., Ray, A., Hawes-Ebersole, S., and Ebersole, J. S. (2007b). The impact of cerebral source area and synchrony on recording scalp electroencephalography ictal patterns. *Epilepsia* 48, 2167–2176.

Tao, J. X., Ray, A., Hawes-Ebersole, S., and Ebersole, J. S. (2005). Intracranial EEG substrates of scalp EEG interictal spikes. *Epilepsia* 46, 669–676.

Tauck, D. L., and Nadler, J. V. (1985). Evidence of functional mossy fiber sprouting in hippocampal formation of kainic acid-treated rats. *J. Neurosci.* 5, 1016–1022.

Tian, G. F., Azmi, H., Takano, T., Xu, Q., Peng, W., Lin, J., Oberheim, N., Lou, N., Wang, X., Zielke, H. R., Kang, J., and Nedergaard, M. (2005). An astrocytic basis of epilepsy. *Nat Med.* 11, 973–981.

Traub, R. D., Whittington, M. A., Buhl, E. H., LeBeau, F. E., Bibbig, A., Boyd, S., Cross, H., and Baldeweg, T. (2001). A possible role for gap junctions in generation of very fast EEG oscillations preceding the onset of, and perhaps initiating, seizures. *Epilepsia* 42, 153–170.

Trevelyan, A. J. (2009). The direct relationship between inhibitory currents and local field potentials. *J. Neurosci.* 29, 15299–15307.

Trevelyan, A. J., Sussillo, D., and Yuste, R. (2007a). Feedforward inhibition contributes to the control of epileptiform propagation speed. *J. Neurosci.* 27, 3383–3387.

Trevelyan, A. J., Baldeweg, T., van Drongelen, W., Yuste, R., and Whittington, M. (2007b). The source of after discharge activity in neocortical tonic-clonic epilepsy. *J. Neurosci.* 27, 13513–13519.

Trevelyan, A. J., Sussillo, D., Watson, B. O., and Yuste, R. (2006). Modular propagation of epileptiform activity: evidence for an inhibitory veto in neocortex. *J. Neurosci.* 26, 12447–12455.

Vaudano, A. E., Laufs, H., Kiebel, S. J., Carmichael, D. W., Hamandi, K., Guye, M., Thornton, R., Rodionov, R., Friston, K. J., Duncan, J. S., and Lemieux, L. (2009). Causal hierarchy within the thalamo-cortical network in spike and wave discharges. *PLoS ONE* 4, e6475. doi: 10.1371/journal.pone.0006475

Vulliemoz, S., Carmichael, D. W., Rosenkranz, K., Diehl, B., Rodionov, R., Walker, M. C., McEvoy, A. W., and Lemieux, L. (2010). Simultaneous intracranial EEG and fMRI of interictal epileptic discharges in humans. *Neuroimage* 54, 182–190.

Waites, A. B., Briellmann, R. S., Saling, M. M., Abbott, D. F., and Jackson, G. D. (2006). Functional connectivity networks are disrupted in left temporal lobe epilepsy. *Ann. Neurol.* 59, 335–343.

Walker, M., Chan, D., and Thom, M. (2007). "Hippocampus and human disease," in *The Hippocampus Book*, eds P. Andersen, R. Morris, D. G. Amaral, T. Bliss, and J. O'Keefe (Oxford: Oxford University Press), 769–812.

Walter, D. O. (1963). Spectral analysis for electroencephalograms: mathematical determination of neurophysiological relationships from records of limited duration. *Exp. Neurol.* 8, 155–181.

Wendling, F. (2008). Computational models of epileptic activity: a bridge between observation and pathophysiological interpretation. *Expert Rev. Neurother.* 8, 889–896.

Wendling, F., Ansari-Asl, K., Bartolomei, F., and Senhadji, L. (2009a). From EEG signals to brain connectivity: a model-based evaluation of interdependence measures. *J. Neurosci. Methods* 183, 9–18.

Wendling, F., Bartolomei, F., and Senhadji, L. (2009b). Spatial analysis of intracerebral electroencephalographic signals in the time and frequency domain: identification of epileptogenic networks in partial epilepsy. *Philos. Trans. Math. Phys. Eng. Sci.* 367, 297–316.

Wendling, F., Bartolomei, F., Bellanger, J. J., and Chauvel, P. (2001). Interpretation of interdependencies in epileptic signals using a macroscopic physiological model of the EEG. *Clin. Neurophysiol.* 112, 1201–1218.

Woermann, F. G., Free, S. L., Koepp, M. J., Sisodiya, S. M., and Duncan, J. S. (1999). Abnormal cerebral structure in juvenile myoclonic epilepsy demonstrated with voxel-based analysis of MRI. *Brain* 122(Pt 11), 2101–2108.

Conflict of Interest Statement: The authors declare that the research was conducted in the absence of any commercial or financial relationships that could be construed as a potential conflict of interest.

Received: 05 August 2010; accepted: 24 February 2011; published online: 22 March 2011.

Citation: Lemieux L, Daunizeau J and Walker MC (2011) Concepts of connectivity and human epileptic activity. Front. Syst. Neurosci. ***5****:12. doi: 10.3389/fnsys.2011.00012*

Copyright © 2011 Lemieux, Daunizeau and Walker. This is an open-access article subject to an exclusive license agreement between the authors and Frontiers Media SA, which permits unrestricted use, distribution, and reproduction in any medium, provided the original authors and source are credited.

frontiers in
SYSTEMS NEUROSCIENCE

ORIGINAL RESEARCH ARTICLE
published: 08 October 2010
doi: 10.3389/fnsys.2010.00147

Disrupted modularity and local connectivity of brain functional networks in childhood-onset schizophrenia

Aaron F. Alexander-Bloch[1,2,3], Nitin Gogtay[2], David Meunier[1], Rasmus Birn[4], Liv Clasen[2], Francois Lalonde[2], Rhoshel Lenroot[5], Jay Giedd[2] and Edward T. Bullmore[1,6]*

[1] *Department of Psychiatry, Behavioural and Clinical Neuroscience Institute, University of Cambridge, Cambridge, UK*
[2] *Child Psychiatry Branch, National Institute of Mental Health, Bethesda, MD, USA*
[3] *David Geffen School of Medicine at University of California, Los Angeles, CA, USA*
[4] *Department of Psychiatry, University of Wisconsin School of Medicine and Public Health, Madison, WI, USA*
[5] *Prince of Wales Medical Research Institute, University of New South Wales, Sydney, NSW, Australia*
[6] *GlaxoSmithKline Clinical Unit Cambridge, Addenbrooke's Hospital, Cambridge, UK*

Edited by:
Silvina G. Horovitz, National Institutes of Health, USA

Reviewed by:
Barry Horwitz, National Institutes of Health, USA
Malle A. Tagamats, University of Maryland, USA

****Correspondence:***
Edward T. Bullmore, Department of Psychiatry, University of Cambridge, Herchel Smith Building, Cambridge Biomedical Campus, Cambridge CB2 0SZ, UK.
e-mail: etb23@cam.ac.uk

Modularity is a fundamental concept in systems neuroscience, referring to the formation of local cliques or modules of densely intra-connected nodes that are sparsely inter-connected with nodes in other modules. Topological modularity of brain functional networks can quantify theoretically anticipated abnormality of brain network community structure – so-called dysmodularity – in developmental disorders such as childhood-onset schizophrenia (COS). We used graph theory to investigate topology of networks derived from resting-state fMRI data on 13 COS patients and 19 healthy volunteers. We measured functional connectivity between each pair of 100 regional nodes, focusing on wavelet correlation in the frequency interval 0.05–0.1 Hz, then applied global and local thresholding rules to construct graphs from each individual association matrix over the full range of possible connection densities. We show how local thresholding based on the minimum spanning tree facilitates group comparisons of networks by forcing the connectedness of sparse graphs. Threshold-dependent graph theoretical results are compatible with the results of a k-means unsupervised learning algorithm and a multi-resolution (spin glass) approach to modularity, both of which also find community structure but do not require thresholding of the association matrix. In general modularity of brain functional networks was significantly reduced in COS, due to a relatively reduced density of intra-modular connections between neighboring regions. Other network measures of local organization such as clustering were also decreased, while complementary measures of global efficiency and robustness were increased, in the COS group. The group differences in complex network properties were mirrored by differences in simpler statistical properties of the data, such as the variability of the global time series and the internal homogeneity of the time series within anatomical regions of interest.

Keywords: graph theory, brain, network, modularity, schizophrenia, clustering, fMRI

INTRODUCTION

One of the most ubiquitous properties of complex systems, like large-scale functional brain networks, is that they generally have a modular community structure (Bullmore and Sporns, 2009). Using resting-state fMRI analysis, functional communities or modules can be broadly defined as groups of brain regions whose fMRI time series are similar to each other and dissimilar from other groups. How to partition the brain into such functional communities, and the related question of how to assess the quality of these partitions, are methodological issues that have been approached from the perspectives of both unsupervised learning and graph theory. In the context of unsupervised learning, where brain regions are considered as objects in n-dimensional functional space to be classified into their "natural" groups, hierarchical cluster analysis has been used to decompose the brain into a small number of functional modules that resemble known patterns of neural connectivity (Cordes et al., 2002; Salvador et al., 2005). In graph theory, on the other hand, brain regions are nodes (or vertices), functional connections between nodes are edges (or links), and modules are groups of nodes with many intra-modular links to each other but few inter-modular links to external groups (Newman and Girvan, 2004). Graph theoretical work has shown that human brain functional modules are hierarchically organized (Meunier et al., 2009b; Bassett et al., 2010), that their structure is altered in normal aging (Meunier et al., 2009a) and in adolescence (Fair et al., 2009), and that their structure is relatively consistent for fMRI and diffusion spectrum imaging (DSI) of the same subjects (Hagmann et al., 2008). The brain, at least the healthy brain, is a modular system.

Here we test the hypothesis that the normal modular community structure of functional brain networks might be somehow disrupted in neuropsychiatric disease, specifically in schizophrenia. There are theoretical reasons to posit that the brain's modularity is crucial in terms of its evolution and healthy neurodevelopment. Modularity may allow the brain to adapt to multiple, distinct selection criteria over time (Kashtan and Alon, 2005). Modules may also represent stable subcomponents of the brain, which facilitate the construction of a complex system from simple building blocks (Simon, 1962). In the context of the recent focus on the

developmental phenotypes of neuropsychiatric disease (e.g., Gogtay et al., 2008; Giedd et al., 2009), it makes sense to measure properties of neuroimaging data, such as modularity, that are theoretically linked to network development and that may provide sensitive markers of abnormal brain development in disorders such as schizophrenia. In fact, dysmodularity in schizophrenia has already been proposed as a neuropsychological theory, implying the breakdown of information encapsulation between brain systems that are specialized to carry out different tasks (Fodor, 1983; David, 1994). In the functional neuroanatomical context, possible examples might include pathological crosstalk between inner speech and auditory areas in the pathogenesis of hallucinations (Shapleske et al., 2002), or between left and right prefrontal cortex in working memory tasks (Lee et al., 2008). However, it is clear that this point can be argued from both sides: For example, patients seem to be more susceptible than controls to the Müller-Lyer illusion (Pessoa et al., 2008), a visual illusion that persists in spite of explicit knowledge about the nature of the illusion, which has been held up as an exemplar of perceptual modularity. At any rate, it is not obvious how to relate the notions of psychological modularity and topological modularity as it is quantified in complex systems, and the dysmodularity hypothesis has not yet been tested with any rigor in neuroimaging experiments.

There are methodological barriers to testing this hypothesis. As already noted there are a number of possible ways in which the community structure of functional networks can be described, and these alternatives have not been comparatively evaluated. Moreover it is non-trivial to make comparisons of modularity, however measured, between two groups of brain graphs with different topological properties. Even random graphs show complex properties including modularity to an extent that varies depending on the number of nodes and edges in the graphs (Bollobás, 1985; Anderson et al., 1999; Guimerà et al., 2004). Network properties can change dramatically around the percolation threshold where graphs become node-connected (Dorogovtsev et al., 2008), where "node-connected" means that none of the nodes is entirely isolated, each is linked by at least one edge to a single giant connected cluster. To ensure that statistical comparisons of brain network properties are meaningful, therefore, all of the graphs should ideally have the same number of nodes and edges, and they should all be node-connected. This last point is crucial because graphs constructed by global thresholding from data on different subjects may often show different degrees of node-connectedness, especially if the graphs are sparse. While differences in node-connectedness, e.g., as measured by percolation threshold, may be informative in their own right (Chen et al., 2007), they should ideally be controlled when considering group differences in other more edge-based network metrics such as degree. One conceptually simple way of doing this is to restrict evaluation of network metrics to a range of connection densities for which all graphs are node-connected (Bassett et al., 2008; Lynall et al., 2010). However, this approach may preclude comparative analysis of network properties at sparser connection densities where complex topological features such as modularity are typically most prominent.

We explore some of these methodological issues in the context of a preliminary investigation of the modularity and other properties of brain functional networks measured using fMRI in childhood-onset schizophrenia. We devise a way of applying a local threshold to construct brain graphs, which ensures that all of the graphs are node-connected at minimal densities, in contrast to the variability of node-connectedness that typically arises when graphs are constructed by a global threshold. We compare standard graph theoretical modularity results with the results of an unsupervised learning approach, using a generalization of the *k*-means algorithm known as partition around medoids (PAM), and a multi-resolution spin glass algorithm. In addition to modularity, we estimate several other properties of the graphs, most of which have previously been investigated in adult-onset schizophrenia (Liu et al., 2008; Rubinov et al., 2009; Lynall et al., 2010). Finally, we ground the complex network analysis by looking at simpler properties of the fMRI time series in these subjects, such as the variability of the time series and its internal homogeneity within anatomical regions of interest. We find evidence in support of network dysmodularity in COS, and explain this finding in the context of the other properties of the fMRI phenotype that we investigate. To our knowledge this is the first study to report less modular brain organization or abnormal community structure of brain functional networks in any human population.

MATERIALS AND METHODS

SAMPLE

Thirteen COS patients and 19 controls or "normal volunteers" (NV) were recruited as part of an ongoing National Institute of Mental Health study of COS and normal brain development (ClinicalTrials.gov Identifier: NCT00001246). All patients met the DSM-IV criteria for childhood-onset schizophrenia, and consent was acquired from both patients and their legal guardians. The populations did not differ significantly in terms of age (COS sample mean age = 18, standard deviation = 4; NV sample mean age = 19, standard deviation 4; *t*-test *p*-value = 0.29) or gender (8 female, 5 male COS; 10 female, 9 male, NV; chi squared test *p*-value = 0.89).

IMAGE ACQUISITION AND PREPROCESSING

All images were acquired using a 1.5T General Electric Signa MRI scanner located at the National Institutes of Health Clinical Center (Bethesda, MD). One anatomical T1-weighted fast spoiled gradient echo MRI volume was acquired: TE 5 ms; TR 24 ms; flip angle 45Â°; matrix 256 × 256 × 124; FOV 24 cm. In addition, two sequential 3 min EPI scans were acquired while subjects were lying quietly in the scanner with eyes closed: TR 2.3 s; TE 40 ms; voxel 3.75 mm × 3.75 mm × 5 mm; matrix size 64 × 64; FOV 240 mm × 240 mm; 27 interleaved slices. The first four volumes of each functional scan were discarded to allow for T1 equilibration effects. AFNI was used for slice time correction and for motion correction (Cox, 1996). In terms of motion, the maximum displacement of brain voxels due to motion did not differ significantly between the groups (sample mean COS maximum displacement = 2.45 mm; sample mean NV maximum displacement = 1.93 mm; *t*-test *p*-value = 0.41). FSL's FLIRT (Jenkinson and Smith, 2001; Jenkinson et al., 2002) was used to register each subject's functional scans to that subject's structural scan using a 6 degrees of freedom transformation, and to register the structural scan to MNI stereotactic standard space using a 12 degrees of freedom transformation. Although registering both pediatric and adult

brains to the MNI adult brain template image could result in some age-specific differences in spatial normalization, these differences are unlikely to affect fMRI results because of fMRI's relatively low spatial resolution (Burgund et al., 2002; Kang et al., 2003) and because functional activity is represented by regional mean time series averaged over multiple voxels comprising regions of the parcellation template image. Both these factors suggest that the scale of any possible age-related mis-registration is likely to be small in comparison to the relatively coarse-grained scale of functional network analysis applied to the data. We note that adult template images have previously been used as a basis for normalization of fMRI data on participants in similar and even younger age-ranges than our sample (Durston et al., 2003; Turkeltaub et al., 2003; Cantlon et al., 2006; Crone et al., 2006; Galvan et al., 2006).

WAVELET MEASURES OF VARIABILITY AND COVARIABILITY AT DIFFERENT SCALES

For each functional scan, 111 anatomical regions were defined using the combined cortical and subcortical Harvard-Oxford Probabilistic Atlas (Smith et al., 2004) thresholded at 25%. Because of low quality signal due to susceptibility artifacts in some regions, quantified as the majority of a region being absent from the EPIs of the majority of subjects, the brainstem and 5 bilateral cortical regions at the inferior frontotemporal junction were excluded, which resulted in a dataset of 100 regions for each functional scan. In addition to the voxel time series, 100 regional time series were estimated by averaging the voxels within each of the regions, while one global time series was estimated by averaging the voxels within all of the regions.

The maximal overlap discrete wavelet transform (MODWT) with a Daubechies 4 wavelet was used to band-pass filter the time series (Percival and Walden, 2006) and, in what follows, we will focus on the results obtained using the scale 2 frequency interval, 0.05–0.111 Hz. This frequency scale was chosen to minimize the impact of higher frequency physiological noise while maximizing the degrees of freedom available for wavelet correlation, as well as for consistency with previous work. Wavelet coefficients with boundary effects from the MODWT were excluded, and the coefficients of the sequential functional scans were concatenated to form a single series of 144 wavelet coefficients which was the basis for all further analyses of variability and covariability (e.g., see **Figures 2B,D**).

Variability of the global and regional signals

We quantified the variability of the low frequency MRI signal simply as the sample variance of the MODWT wavelet coefficients at scale 2. (To make comparisons between the variability of the signal at different temporal scales, the wavelet variances would have to be corrected for the redundancy of the MODWT, but we focus exclusively on differences between the clinical populations at the same scale.) Variability was estimated for each of the anatomical regions and also for the global signal.

Covariability between and within regions

The wavelet correlation, $-1 \le r_{i,j} \le +1$, was used as an estimate of the covariability between two time series i and j. For N anatomically defined regions, this value was found for all $(N^2 - N)/2$ pairs of regions. The regional strength of connectivity $s(i)$ for a region i was defined as the mean of the correlations with the $N-1$ other regions:

$$s(i) = \frac{\sum_{j \neq i} r_{i,j}}{N-1} \tag{1}$$

We also explored the covariability of the voxels within each anatomical region, treating each anatomical region as a distinct subnetwork. If x is a voxel within a region i, and K is the number of voxels within i, the average voxel connectivity strength $s(x)$ over all K is a measure of the internal homogeneity of the signal from region i. Although at a different spatial and temporal scale, this statistic is similar to so-called regional homogeneity (ReHo; Zang et al., 2004), which has been calculated between neighboring voxels. For greater consistency with this prior work, we also calculated Kendall's coefficient of concordance, $0 \le W(i) \le +1$, between the voxels in each region i:

$$W(i) = \frac{\sum \left(R_x\right)^2 - n(\bar{R})^2}{\frac{1}{12}K^2\left(n^3 - n\right)} \tag{2}$$

Here, K is the number of voxels in region i; n is the length of the time series; R_x is the sum of the ranks of the xth voxel; and $\bar{R}$ is the mean of R_x, over all K voxels. The numerator in Eq. 2 is the variance of the sums of the ranks, and the denominator is the maximum possible variance given the number of voxels and the length of the time series (Sheskin, 2007). The advantages of this statistic are that it is non-parametric and that it is defined for a region containing any number of voxels. The average regional concordance is the mean of W over all N regions.

GRAPH CONSTRUCTION

Note that R code used for graph construction is publicly available at http://brainnetworks.sourceforge.net, and the Appendix contains definitions of some commonly used graph theoretical terms. To make a graphical model of brain network connectivity, the usual approach is to generate a binary adjacency matrix A from a continuous association or connectivity matrix C. It is also possible to measure network properties by analysis of the connectivity matrix using tools which do not require a binary thresholding operation to generate an adjacency matrix. Here we explored two different (global and local) thresholding methods to construct an adjacency matrix from the 100×100 connectivity matrix, C, where $C_{i,j} = |r_{i,j}|$, the absolute wavelet correlation coefficient for a pair of regional time series i and j. We also investigated two complementary methods – the unsupervised learning algorithm "partition around medoids" (PAM) and the multi-resolution spin glass model of modularity – to measure network properties without thresholding the connectivity matrix.

Most human neuroimaging studies to date have used global thresholding to construct functional brain networks. Using this method, any $|r_{i,j}|$ of the functional connectivity matrix greater than a threshold, τ, implies an edge in the corresponding element of the adjacency matrix, A, meaning that $A_{i,j} = 1$. If $r_{i,j} < \tau$, then $A_{i,j} = 0$. Thresholding at a different value of τ creates a graph with a different edge density or cost, which is the number of edges in a graph

comprising N nodes, divided by the maximum number of possible edges, $(N^2 - N)/2$. A difficulty with global thresholding is that at sparse densities it can result in graphs that are not node-connected, i.e., there is not a finite path between every pair of nodes. Disconnectedness of the graphs affects the quantitative values of many network metrics. Therefore, comparisons of network metrics between different subjects may be biased if the network for one subject is connected at the chosen threshold, but the network for the other subject is fragmented or disconnected. We anticipated that this might be a significant challenge in making a fair comparison between networks estimated in healthy volunteers versus patients with COS.

To address the issue of disconnectedness that can arise as a result of global thresholding, we explored an alternative thresholding method that forces graphs to be connected even at sparse densities. To this end we made use of the standard graph theoretical concepts of the minimum spanning tree (MST; Kruskal, 1956; Prim, 1957) and the k nearest neighbor graph (k-NNG; Eppstein et al., 1992). The k-NNG is composed of those edges that link each node to the k nearest other nodes, where "nearest" in this case means highest functional connectivity. The MST is composed of those edges that node-connect the graph with the lowest possible number of edges and the highest possible functional connectivity. Put differently, an MST of a graph is a node-connected subgraph that includes the minimum total weight, and here we interpret the weight of an edge between two nodes as one minus the nodes' functional connectivity. Although in theory there could be more than one MST or k-NNG for a given network, in practice this does not occur in our data. Algorithmically, the MST can be found by starting with the 1-NNG, that is by including an edge between every node and its single nearest neighbor. If the 1-NNG is connected, then it is identical to the MST; if the 1-NNG is disconnected, including fragmented groups of nodes with no finite path between them, then additional edges are added to link these fragments. For a given graph with N nodes, the MST always has $N - 1$ edges, which include the edges of the 1-NNG as a subset.

Although the MST itself can be used as a sparse representation of the whole network, it is somewhat implausible biologically because the MST is by definition acyclic (no loops or triangles) and its edges do not form clusters or cliques. For example, the clustering coefficient (Watts and Strogatz, 1998) of an MST will always be zero. For this reason, it has been previously proposed to start with the MST as a minimal connected skeleton of the brain network and then grow the tree by adding extra edges according to a standard global thresholding rule (Hagmann et al., 2008). Alternatively, we developed a new method to grow the MST by adding extra edges according to a local thresholding rule. Specifically, we add the edges of the k-NNG in step-wise fashion, for higher and higher k. Since the MST is a connected superset of the 1-NNG, we generalize the concept to connected supersets of the k-NNG. See **Figure 1** for an illustration of these different graph construction methods, applied to a "toy" connectivity matrix composed of 11 of the 100 nodes of a typical subject.

A final alternative is to avoid thresholding altogether, using network measures that can be appropriately applied to the unthresholded connectivity matrix. This sidesteps the potentially arbitrary decision of how to threshold the connectivity matrix. However, the unthresholded graphs – also called "complete" graphs – will in general have lower signal-to-noise. In addition, there is less heterogeneity between the graphs of different subjects, as the adjacency matrices are identical and only the weights of the edges can differ. Finally, only some network measures, such as modularity (discussed below), have analogs that can be applied to weighted complete graphs.

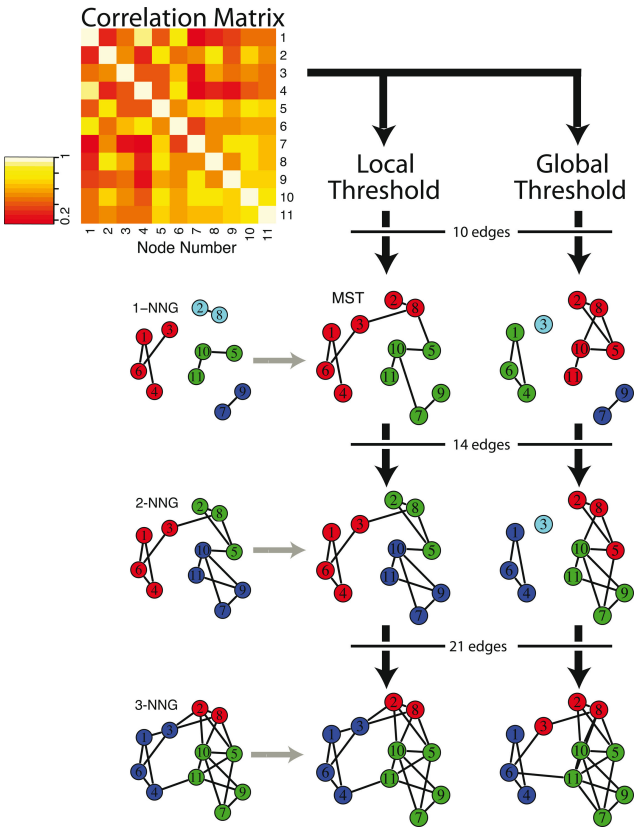


FIGURE 1 | Schematic illustrating local and global thresholding methods, and how these methods impact on the modular structure of graphs constructed from a correlation matrix. Starting with a model correlation matrix, which shows the functional connectivity between a subset of 11 brain regions for one subject, the two different thresholding methods are used to construct graphs with increasing numbers of edges. On the left, applying a local threshold produces connected supersets of the k nearest neighbor graph (k-NGG), which includes edges for each node's k highest functional connections, shown here for $k = 1, 2, 3$. The minimum spanning tree (MST) is a connected superset of the 1-NNG, and connects all 11 nodes with the lowest possible number of edges and the highest possible functional connectivity. On the right, applying a global threshold simply includes edges between the pairs of nodes with the highest functional connectivity in order. Nodes of the same color are in the same module, as determined by the fast greedy algorithm, showing the influence of graph construction and edge density on the modular partition.

GLOBAL NETWORK MEASURES

We report network properties over the whole of range of edge density or cost, from 0.02 to 0.98 at 0.02 intervals, for both globally and locally thresholded graphs. As a summary statistic, we also calculated the mean of each metric over the range of costs from 0.3 to 0.5. This range was chosen for several reasons: (1) most of the globally thresholded graphs become connected by a cost of

0.3; (2) previous work suggests that above a cost of 0.5 graphs become more random (Humphries et al., 2006) and less small-world; and (3) the network measures are relatively constant over this range. Statistics were calculated in R (R Development Core Team, 2009) using original code as well as the following packages: *wmtsa*, *brainwaver*, *cluster*, *MASS* (Venables and Ripley, 2002), and *igraph* (Csardi and Nepusz, 2006).

Randomized graphs

It is important to contrast the brain graphs with comparable random graphs (Watts and Strogatz, 1998). We used two procedures to construct such graphs. With one method, the edges of the graph were replaced by edges chosen completely at random, with every pair of nodes having an equal probability of being connected in the new graph. Thus the only constraint is that the random graphs have the same number of nodes and edges as the original graphs (Erdös and Rényi, 1959). Alternatively, the graphs were "rewired" so as to preserve the degree distribution of the original graph. This is accomplished by picking two edges at random, between nodes *A* and *B* and between nodes *C* and *D*, and replacing these with edges between nodes *A* and *C* and between nodes *B* and *D*. Enough iterations of this process ensure a randomized graph where every node still has the same degree as in the original graph (Milo et al., 2004). We also explored graphs that were only partially randomized, where some proportion of the edges had undergone one or the other randomization procedure.

Global efficiency

The global efficiency, $E(G)$, of a graph G is

$$E(G) = \frac{1}{N^2 - N} \sum_{i \neq j \in G} \frac{1}{L_{i,j}} \tag{3}$$

where $L_{i,j}$ is the minimum path length, or the minimum number of edges that must be traversed between regions i and j (Latora and Marchiori, 2001; Achard and Bullmore, 2007). Note that if there is not a finite path between nodes i and j, then $(1/L_{i,j}) = 0$. The regional or nodal efficiency of one brain region can also be calculated by averaging $1/L_{i,j}$ over each node separately. When calculating $L_{i,j}$ for weighted graphs, the edges themselves are treated as varying in length according to the weight matrix W, where $W_{k,l} = 1 - C_{k,l}$. For weighted graphs, the global efficiency at a given cost is normalized by dividing by the global efficiency of the unthresholded, complete graph. (Theoretically, this is the case for binary global efficiency as well, but the global efficiency of the complete graph is 1).

Local efficiency

The local efficiency, $E_{\text{loc}}(G, i)$, of a node i in a graph G is computed as:

$$E_{\text{loc}}(G,i) = E\left(G_i\right) \tag{4}$$

Here, G_i is the subgraph including only the neighbors of i (not i itself), and $E(G_i)$ is the global efficiency of G_i. The local efficiency of the graph is the average of the local efficiency of all of its nodes. This metric can be extended to weighted graphs in the same manner as global efficiency (Latora and Marchiori, 2001; Achard and Bullmore, 2007).

Clustering

The regional or nodal clustering coefficient, $C(G, i)$, of a node i in a graph G is the ratio of connected triangles, δ_v to connected triples, τ_v. In other words, it is the proportion of i's neighbors that are also neighbors of one another. For the graph as a whole, the clustering coefficient is:

$$C(G) = \frac{1}{|V'|} \sum_{v \in V'} \frac{\delta_v}{\tau_v} \tag{5}$$

where V' is the set of nodes with degree >2 (Watts and Strogatz, 1998; Schank and Wagner, 2004). Clustering is a measure of the locally aggregated structure in a graph.

Small-worldness

Small-world networks have high clustering, C, but low average minimum path length, L, compared to random networks. The small-worldness, $\sigma(G)$, of a graph G is calculated as:

$$\sigma(G) = \frac{\gamma(G)}{\lambda(G)} = \frac{\frac{C(G)}{C_R}}{\frac{L(G)}{L_R}} \tag{6}$$

Here, C_R is the clustering of random graph rewired so as to preserve the degree distribution of G, and L_R is the average minimum path length of such a random graph. For connected graphs, the average minimum path length is identical to the inverse of the (unweighted) global efficiency, so we can also write $\lambda(G) = E_R/E(G)$. For disconnected graphs, formally $\sigma(G)$ is undefined, but we can again substitute $\lambda(G) = E_R/E(G)$ to get a related quantity. A network is generally accepted as "small-world" if $\sigma > 1$ (Humphries et al., 2006).

Robustness

As a measure of robustness, we looked at the resistance of the network to fragmentation after removal of nodes either in random order or in decreasing order of their degree. Suppose that there are M fragments in the network, i.e., M subgraphs that are connected internally but disconnected from each other. Resistance to fragmentation is defined as:

$$R(G) = \frac{\sum_{j=1}^{M} N_j \left(N_j - 1\right)}{N(N-1)} \tag{7}$$

where N_j is the number of nodes in fragment j, and N is the number of nodes in the graph. $N - 1$ nodes are removed in order, and robustness is the mean of R over all of these smaller graphs (Chen et al., 2007).

MODULARITY

We explored modularity using three complementary methods from unsupervised learning and graph theory: partition around medoids (PAM), fast greedy optimization of thresholded graphs, and simulated annealing of a spin glass model. See **Figure 1** for an illustration of these methods, applied to a model network.

PAM

PAM, like the more widely known method of hierarchical clustering, is an unsupervised learning algorithm that does not require thresholding of the connectivity matrix (Kaufman and Rousseeuw, 1987). Modules are referred to as "clusters" in the unsupervised learning literature, but to avoid confusion we will use the graph theory terminology. PAM is a generalization of the *k*-means algorithm that is more robust to noise and outliers. It requires as inputs the number of expected modules and the dissimilarity between every pair of nodes *i* and *j*. For our purposes, the dissimilarity between *i* and *j* is defined as $1 - C_{i,j}$ for the connectivity matrix *C*. The algorithm finds each module a representative node (medoid), and assigns other nodes to modules so as to minimize their dissimilarity with these medoids. The silhouette width, *S*, can be used to assess the quality of this partition:

$$S_i = \frac{(A_i - B_i)}{\max(A_i, B_i)} \tag{8}$$

Here, *i* is a brain region, A_i is the mean dissimilarity between *i* and the other regions in its module, and B_i is the mean dissimilarity between i and the regions in the next nearest module. The silhouette width ranges from −1 to 1, and a high positive number means that *i* is well-classified. The mean silhouette width over every region provides a global measure of the quality of the partition. It is explored over a range of possible numbers of modules.

Graph theoretical modularity

The modularity, *Q*, of a graph *G* can be quantified as the proportion of *G*'s edges that fall within modules, subtracted by the proportion that would be expected due to random chance alone, for a given partition of nodes into modules. This can be written as (Newman and Girvan, 2004):

$$Q(G) = \frac{1}{2m}\sum_{i \neq j}(A_{ij} - P_{ij})\delta(M_i, M_j) \tag{9}$$

Here, *m* is the total number of edges; $A_{ij} = 1$ if an edge links *i* and *j* and 0 otherwise; $\delta(M_i, M_j)$ is 1 if *i* and *j* are in the same module and 0 otherwise, and ensures that only intra-modular edges are added to the sum; finally, P_{ij} is the probability that there would be an edge between *i* and *j*, given a random graph comparable to *G*. The value of P_{ij} depends on what counts as a "comparable" random graph, the so-called null model. We use

$$P_{ij} = \frac{k_i k_j}{2m} \tag{10}$$

where k_i is *i*'s degree, the number of other nodes to which *i* is linked by an edge. We include this information in the null model because it affects the expected proportion of intra-modular edges.

Weighted modularity is calculated analogously. In Eqs 9 and 10, the total number of edges, *m*, becomes the total weight of the edges. The degree, k_i, is replaced by *i*'s strength, which is the total weight of *i*'s edges. And finally the adjacency matrix, *A*, is replaced by the weight matrix, *W*; the ones in the adjacency matrix are replaced weights of the edges. P_{ij} can be understood as the expected weight between *i* and *j*. Note that an edge's weight in the weighted modularity calculation is actually one minus that edge's weight in the calculations of weighted global or local efficiency.

There are several known algorithms to assign nodes to modules so as to maximize *Q*. The principal benefits of the fast greedy algorithm that we use are its computational speed and the fact that it has been used in prior fMRI studies (e.g., Meunier et al., 2009a,b). This algorithm starts by assigning each node to its own module, and then agglomerates modules in a step-wise fashion, choosing the 2 modules whose combination results in the highest *Q*. The modularity value for the graph is then the highest *Q* that results throughout this step-wise process (Clauset et al., 2004). We applied this algorithm over the full cost range using a global threshold and a local threshold, for weighted and unweighted graphs.

Multi-resolution spin glass model

Finally, we employed a graph theoretical algorithm that looks at the modular structure at different resolutions. It has been shown that there is a resolution limit to modularity, in that modules smaller than a certain size are not found by traditional approaches (Fortunato and Barthélemy, 2007). Thus the modular structure is biased toward a certain scale, which is particularly problematic when considering a multi-scale system like the brain. This problem can be addressed by adding an additional parameter into the definition of modularity. One approach (Reichardt and Bornholdt, 2006) equates the problem of partitioning a graph with the problem of minimizing the energy of an infinite range Potts spin glass model, where the group indices become spin states. Groups of nodes with dense internal connections end up having parallel spins. The Hamiltonian, $\mathcal{H}$, of a graph *G* is:

$$\mathcal{H}(G) = -\sum_{i \neq j}(A_{ij} - \gamma P_{ij})\delta(M_i, M_j) \tag{11}$$

Here, $\gamma > 0$ is the additional, adjustable parameter. The γ parameter can be thought of as a resolution parameter, such that higher values result in higher number of modules, each of which has fewer members on average. To find the optimal partition at different resolutions, this quality function $\mathcal{H}$ is minimized for different values of γ, using a simulated annealing approach. When $\gamma = 1$, minimizing this function is equivalent to maximizing modularity as defined in Eq. 10. One of the virtues of the spin glass algorithm is that, although it can be applied to graphs with any cost, it can also be appropriately applied to the unthresholded connectivity matrix, so we do not have to set a threshold (Heimo et al., 2008). One drawback of the algorithm is that there is no obvious way to choose between the partitions found with different values of γ. A potential solution is to focus on partitions that are stable over a range of values of γ if a such a partition exists (Lambiotte, 2010). It is also informative to look at the pattern of how the modular structure changes with different values of γ.

RESULTS

VARIABILITY AND COVARIABILITY OF THE MRI TIME SERIES

There were clear differences between groups in terms of some statistically elementary properties of the images: global mean variability, strength of functional connectivity, and within-regional homogeneity. The global mean wavelet-filtered time series had significantly reduced variability in COS versus healthy volunteers (sample mean global variability NV = 2.08; COS = 0.95; permutation test $p = 0.007$; **Figures 2A,B**). There

was a similar but less obvious trend towards decreased variability at the regional level in the COS population (**Figures 2C,D**). The mean strength of between-regional functional connectivity was significantly reduced in COS versus healthy volunteers (sample mean pair-wise wavelet correlation NV = 0.37; COS = 0.26; permutation test $p = 0.001$). This finding extends to decreased strength of functional connectivity at the level of individual regions, if we consider each region's average wavelet correlation with all other regions of the brain (**Figure 2E**). The within-regional homogeneity of the fMRI signal was significantly reduced in COS versus healthy volunteers (sample mean regional concordance, Kendell's W, NV = 0.11; COS = 0.08; permutation test $p = 0.002$). This decreased regional concordance extends to almost every region considered individually (**Figure 2F**).

GRAPH THEORETICAL PROPERTIES

Comparing locally thresholded with globally thresholded graphs, both methods of network construction revealed a similar pattern of results. However, there were clear advantages to using locally thresholded networks, because differences in node-connectedness complicate group comparisons on other metrics at low costs. On average, using a global threshold, not all of the graphs become connected until a cost of 0.3, and the healthy volunteers generally become connected at higher costs than the patients (for some healthy subjects the minimum cost of node-connectedness >0.5). Another way of saying this is that the percolation threshold is set higher in healthy volunteers than in people with COS. On one level this difference is perhaps diagnostically interesting, but it is also

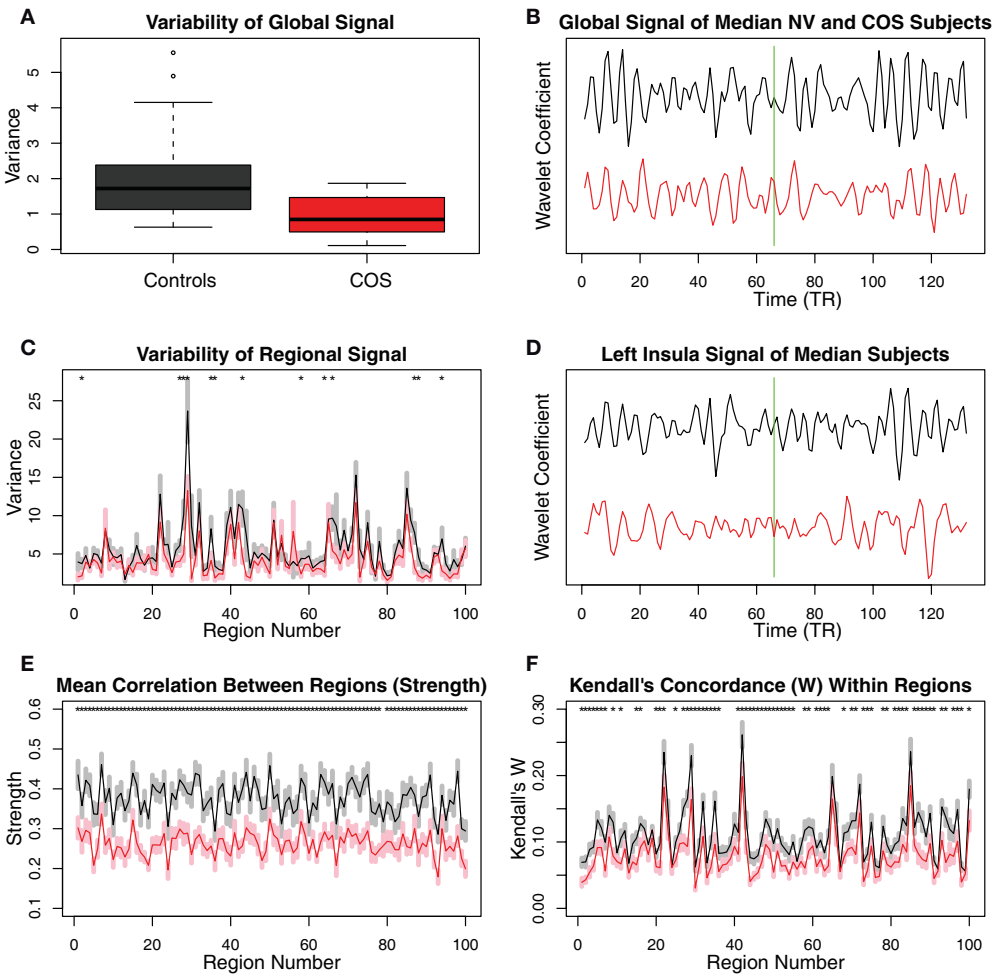


FIGURE 2 | Plots showing differences between the schizophrenic patients and the controls in terms of relatively simple, non-graph-theoretical properties of their MRI time series. (A) The variability in the scale 2 (0.05–0.111 Hz) global MR signal is higher in the controls than in the COS population. **(B)** The difference in the variability of the global MR signal is illustrated with the time series from the median subjects of each population. The green line shows the boundary between the successive scans, whose wavelet coefficients were concatenated. **(C)** There is a trend toward greater variability in the MR signal of anatomical regions, in the control population relative to the COS population. **(D)** The difference in the variability of the regional MR signals is illustrated with the time series from the median subjects of each population for one of the regions that shows a difference, the left insula. **(E)** Regional strength, the average wavelet correlation between each region and every other region, is decreased in the COS population. **(F)** Kendall's coefficient of concordance (W), a measure of the homogeneity of the signal within each anatomical region, is decreased in the COS population. Error bars are standard mean error, and asterisks signify $p < 0.05$ uncorrected p-value from a t-test.

methodologically inconvenient because comparison of any other network parameter between the two groups will be confounded if more of the networks are connected in one group than the other. For this reason we judged it was preferable to use a local thresholding method to compare graphs with low connection density.

For both types of thresholding, we found that simple binary functional networks on average showed decreased clustering and local efficiency in people with COS, relative to the healthy controls. These measures of reduced local connectivity in COS were associated with increased global efficiency and robustness, both implying relatively stronger global connectivity in COS (**Table 1**; **Figure 3**). Broadly speaking, the balance of global and local connectivity in functional brain networks was abnormally shifted toward the global end of the scale in childhood-onset schizophrenia. This can be quantified by a change in the small-worldness parameter σ. Although networks in both groups were small-world ($\sigma > 1$) over the whole cost range, indicating that they generally had greater-than-random clustering but near-random global efficiency, small-worldness was abnormally reduced because of the disproportionate reductions in local connectivity or clustering in the COS group.

The pattern of reduced local clustering and increased efficiency at a whole brain level was reflected by a convergent pattern of results at a regional level of analysis (**Figure 5**). Nineteen anatomical regions had significantly reduced clustering in COS relative to controls [permutation with 2000 tests, corrected for $N = 100$ multiple comparisons with false positive correction $p < (1/N) = 0.01$]. The cortical regions with abnormally reduced local connectivity included left and right superior temporal gyrus, left ventral occipital cortex, right cingulate, right insula, and right frontal operculum. In addition there were subcortical decreases of clustering bilaterally in the thalamus, caudate, and accumbens. The results for regional efficiency were less striking, but five anatomical regions had significantly increased efficiency in COS relative to the controls after correction for multiple comparisons. These increases were located in the right inferior parietal lobule, left ventral temporal cortex, bilateral frontal operculum, and right planum polare.

Another way of describing this pattern of global and regional topological abnormality is in terms of a relative randomization of network organization in childhood-onset schizophrenia. We found that we could quite accurately simulate the COS network data by

Table 1 | For 18 metrics, the mean value for the childhood-onset schizophrenia (COS) population, the mean value for the controls or "normal volunteers" (NV), and the *p*-value for a permutation test of the group difference. Tests were based on 2000 permutations.

	Mean COS	Mean NV	Permutation *p*-value
Global variability	0.95	2.08	0.007
Average regional variability	4.20	5.75	0.152
Average regional strength	0.26	0.37	0.001
Average regional concordance	0.08	0.11	0.002
Global efficiency, global threshold*	0.70	0.69	0.025
Local efficiency, global threshold*	0.80	0.83	0.002
Clustering, global threshold*	0.60	0.65	0.003
Robustness, global threshold*	0.90	0.85	0.044
Global efficiency, local threshold*	0.70	0.70	0.002
Local efficiency, local threshold*	0.77	0.80	0.001
Clustering, local threshold*	0.54	0.58	0.001
Robustness, local threshold*	0.96	0.94	0.11
Weighted global efficiency, local threshold*	0.92	0.94	0.003
Weighted local efficiency, local threshold*	0.93	0.96	0.001
Weighted modularity, local threshold*	0.24	0.26	0.027
Modularity, local threshold*	0.19	0.24	0.001
Modularity, global threshold*	0.17	0.19	0.041
PAM modularity**	0.14	0.18	0.005

**For the statistics based on thresholded graphs, the values are the mean over the cost range 0.3–0.5. **PAM modularity is summarized as the mean regional silhouette width, averaged over partitions with 2, 3, and 4 modules.*

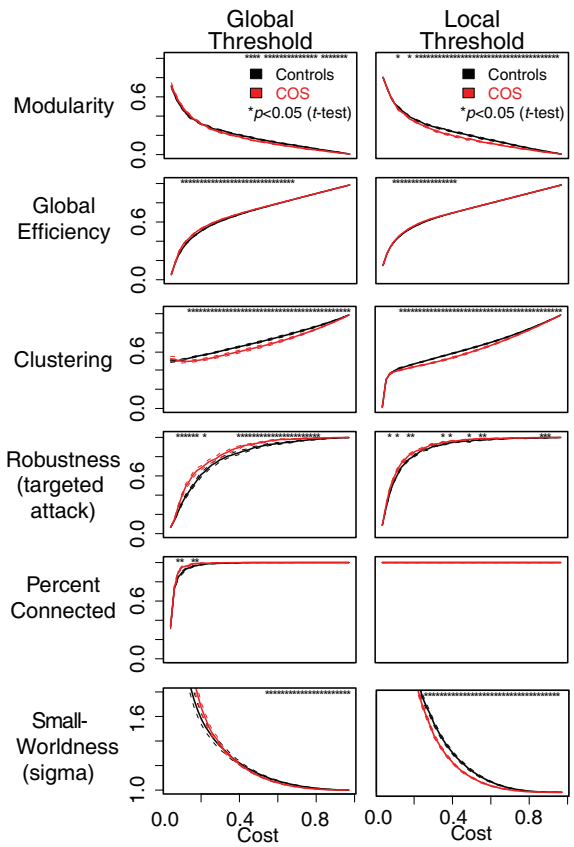


FIGURE 3 | Plots showing differences between the schizophrenic patients (red) and the controls (black) in terms of the graph theoretical properties of the brain networks, which have been constructed using local and global thresholding methods. The two methods produce a similar pattern of group differences. However, local thresholding ensures connected graphs and appears to be more sensitive to group differences in some complex network metrics. The six different graph theoretical measures are shown as a function of connection density or topological cost, which is the proportion of edges included. Error bars are standard mean error, and asterisks signify an uncorrected $p < 0.05$ for a *t*-test between the COS population and control population.

randomizing only 5% of the between-regional connections in the healthy volunteer networks (**Figure 4**). This is true whether the edges are randomized so as to preserve the degree distribution, or whether the degree distribution is allowed to change; and it is true across the range of cost densities, although a greater percent of edges must be randomized to simulate the COS data at higher densities.

The different global network measures are correlated with each other and with the non-graph theoretical measures, as shown in **Figure 8**. For example, binary global efficiency and robustness are correlated, as are local efficiency and clustering, for both locally and globally thresholded graphs. Weighted global network measures provide complementary results to the binary measures (not shown). Weighted local efficiency is decreased in the schizophrenia population, similar to binary local efficiency. However, weighted global efficiency was higher in the schizophrenic population than in the normal population, a reversal of the finding for binary global efficiency. In fact weighted global efficiency is correlated with weighted local efficiency, average regional strength, and clustering. This indicates that between-group differences in strength or weight of functional connectivity between pairs of regions, rather than differences in topology, are driving the difference in weighted global efficiency.

MODULARITY

The functional networks of both the patients and the controls have a modular community structure. All of the graphs were significantly more modular than random graphs with the same degree distributions, for the whole cost range of both globally and locally thresholded graphs (not shown). However, there were also quantitative differences in modularity between the groups. See **Figure 7** for a representative example of the modular structure of the brain networks and the difference between the groups.

Both the graph theoretical and unsupervised learning approaches provided evidence for relatively reduced modularity in COS networks. Decreased graph theoretical modularity implies that there are relatively less intra-modular edges and more inter-modular edges, compared to what would be expected by chance, in the COS population. For locally thresholded binary graphs, this decrease in modularity occurred at all costs >0.1. For weighted graphs and globally thresholded binary graphs, modularity was also lower in COS, but for a narrower range of costs (**Figures 3 and 6A,B**). Similar results were found with the unsupervised learning algorithm PAM, which projects brain regions into *n*-dimensional functional space and groups nearby nodes into the same module. The average silhouette width, which quantifies how well the modules are separated from each other, was lower in the COS population (**Figure 6C**).

Decreased modularity in the COS population is most clear when the networks are partitioned into fewer than 5 modules. For all the subjects, as more edges are included in the graphs at higher costs, the optimal partitions include fewer modules. On average, modularity is maximized with <5 modules for locally and globally thresholded graphs with costs >0.1 and >0.3 respectively. These are the same costs at which decreased modularity in COS emerges. Consistently, as quantified by decreased average silhouette width, the PAM algorithm finds less modular structure only when the networks are partitioned into less than 5 modules.

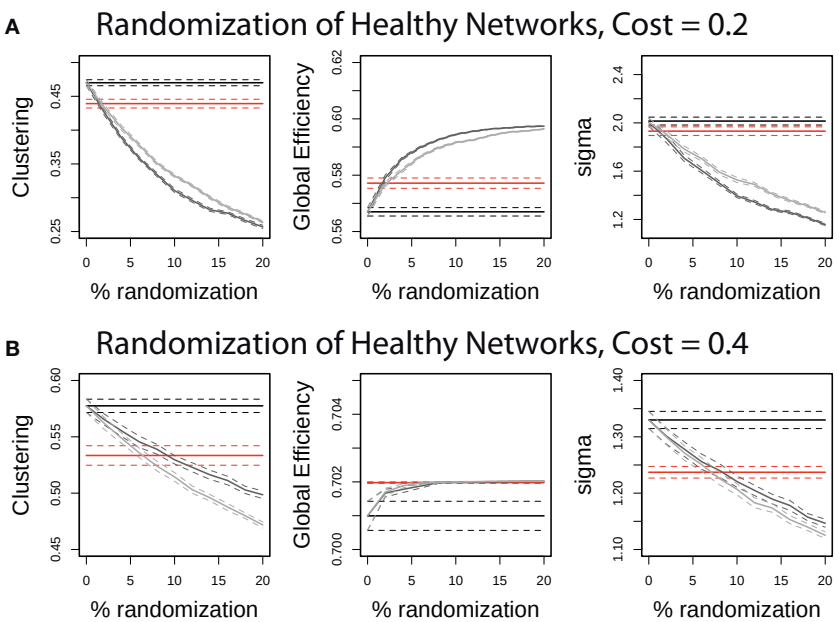


FIGURE 4 | The quantitative properties of the schizophrenic patients' brain networks can be approximated by randomizing a small proportion of the edges of the controls' brain networks. Illustrated on graphs with 0.2 topological cost **(A)** and on graphs with 0.4 topological cost **(B)**, the control networks have 0–20% of their edges randomized. The straight lines show the mean values of the controls (black) and patients (red) in clustering coefficient, global efficiency and small-worldness (sigma). The gray curves show the effect on these network properties of randomizing the control networks: The light gray curves result if the edges are rewired completely at random, whereas the dark gray curves result if the edges are rewired so as to preserve the degree distribution of the original graphs. See Section "Materials and Methods" for explanations of the network measures and the randomization procedures.

In terms of the multi-resolution structure of the graphs as explored with the spin glass algorithm, none of the brain graphs have a clear plateau in their structure, indicating that the modularity of the graphs is not specific to a certain scale. There is group difference in that the graphs of the healthy controls are on average more sensitive to changes in the γ parameter (**Figure 6D**), separating into a greater number of modules, each of which is composed of fewer nodes on average.

DISCUSSION

THE BALANCE BETWEEN GLOBAL AND LOCAL CONNECTIVITY IN SCHIZOPHRENIA

The data suggest the intriguing possibility that COS networks could be less effectively configured for topologically local communication, but better configured for global communication, relative to healthy adolescents, as evidenced by reduced clustering and modularity but greater connectedness, robustness, and global efficiency. Other resting-state fMRI studies of adult-onset schizophrenia have found decreased clustering (Liu et al., 2008) and increased robustness (Lynall et al., 2010). As far as the anatomical foci of the network differences are concerned (**Figure 5**), Lynall et al. (2010) also found decreased clustering in the superior temporal gyrus and anterior cingulate. Looking to the broader literature on task-activated fMRI, almost all of the brain areas that show decreased regional clustering or increased efficiency in COS – including the insula, the ventral occipital lobe, and the inferior parietal lobule – have been previous implicated in schizophrenia (Glahn et al., 2005; Minzenberg et al., 2009).

As small-world networks like the human brain are a balance between global and local efficiency (Watts and Strogatz, 1998; Achard et al., 2006), it could be argued that a global optimization process that is crucial for healthy neurodevelopment has been abnormally biased in schizophrenia. Decreased small-worldness, which has also been reported previously in adult-onset schizophrenia (Liu et al., 2008; Lynall et al., 2010), could result if the increase in global efficiency comes at the expense of a disproportionate decrease in clustering. Taken a speculative step further, if an intermediate phenotype with increased global efficiency were evolutionarily favored, this could help explain the persistence of schizophrenia as a disease (Lynall et al., 2010). Admittedly this argument is limited by the fact that while the increase in binary global efficiency is statistically significant, the absolute difference between the groups is quite small. Indeed while decreased clustering in schizophrenia has been replicated in other studies, the story for global efficiency is less clear (Liu et al., 2008; Bassett et al., 2009). Sibling studies will be crucial to better characterize potential intermediate phenotypes.

The shift in the balance between local and global efficiency is consistent with a process of randomization in COS. For all of the network measures that we investigated, the schizophrenic graphs were roughly equivalent to healthy graphs with 5% of the edges randomized (**Figures 4A,B**). This represents a quantification of what has been previously described as the "subtle randomization" of schizophrenia (Rubinov et al., 2009). Encouragingly it is also testable model for future experiments, because it predicts the direction of the change in schizophrenics relative to controls for any network measure. As network randomization or dedifferentiation has been suggested as an intermediate phenotype for a variety of diseases, it would be very informative to look at the specificity of network properties found in COS, e.g., relative to an ADHD cohort. Randomization of functional network topology is arguably consistent with various neurodevelopmental models of the pathogenesis of schizophrenia, including abnormal axonal growth, synaptic pruning (Feinberg, 1982) or white matter development (Davis et al., 2003). We cannot distinguish between these and other putative developmental mechanisms for abnormal brain network organization based solely on a cross-sectional study of fMRI networks in patients compared to healthy volunteers. However, one potential advantage of using graph theory to describe network organization empirically is that graphical models of network growth or development can be formulated computationally and used to test various competing hypotheses about growth mechanisms driving the formation of the observed network. A classic example of this approach was the demonstration that the observed scale-free degree distribution of the worldwide web could be plausibly explained by a simple growth rule based on preferential attachment (new nodes added to the network tend to become attached preferentially to existing nodes of high degree) (Barabasi and Albert, 1999). In future, it may be possible to use biologically more sophisticated

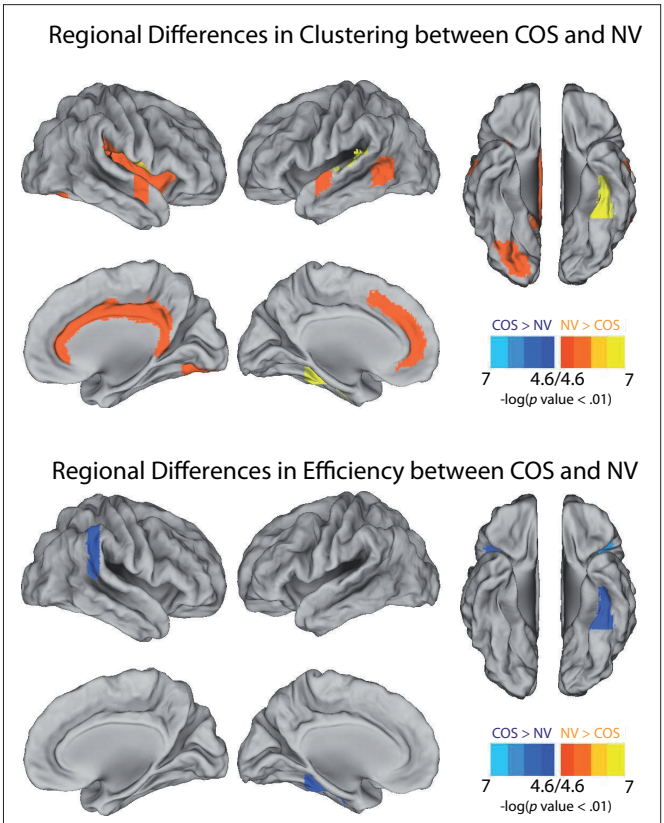


FIGURE 5 | Illustrations of the anatomical foci of decreased clustering and increased global efficiency in schizophrenic (COS) patients relative to controls (NV). At a local threshold of 0.3 topological cost, permutation tests estimated the significance of the differences in regional clustering and efficiency, which are calculated in the same way as the clustering coefficient and the global efficiency, but for each of the 100 nodes individually. Estimations of significance were based on 2000 permutations per region, with *p*-values corrected for 100 multiple comparisons using a false positive correction $p < 1/N = 0.01$ Surface representations were created using Caret (http://brainmap.wustl.edu/caret/).

growth models (Goh et al., 2006) to explain the generative developmental mechanisms driving formation of normal and abnormal brain networks.

MODULARITY

The convergence of our evidence from different methodological approaches points to a disrupted modular organization, with less community structure, in the brain networks of COS patients (**Figures 3, 6, and 7**). This finding makes sense in the context of a vast literature on the modularity of complex systems, the brain and the mind. As modularity is thought to lessen the potential for error in the construction of complex systems (Simon, 1962), decreased modularity may jeopardize the development of a functional brain network. In theory, a less modular brain would be less able to adapt to multiple and changing goals in the environment (Kashtan and Alon, 2005), predicting cognitive deficits. Decreased topological modularity is also consistent with David's neurocognitive (1994) hypothesis of dysmodularity in schizophrenia. Of course topological modularity in fMRI networks is not equivalent to neurocognitive modularity. For example, while the relationship between perceptual and attentional systems is crucial to most renditions of the thesis of psychological modularity (Fodor, 1983), our data is agnostic on this issue. David's account in particular implies that brain systems are hyperconnected in an absolute sense, whereas graph theoretical dysmodularity signifies increased inter-modular connectivity only *relative* to intra-modular connectivity, and is compatible with the absolute decrease in average connectivity that we also observe in this patient sample. Still, our results provide experimental support for the core prediction of a breakdown of the boundaries between specialized brain systems.

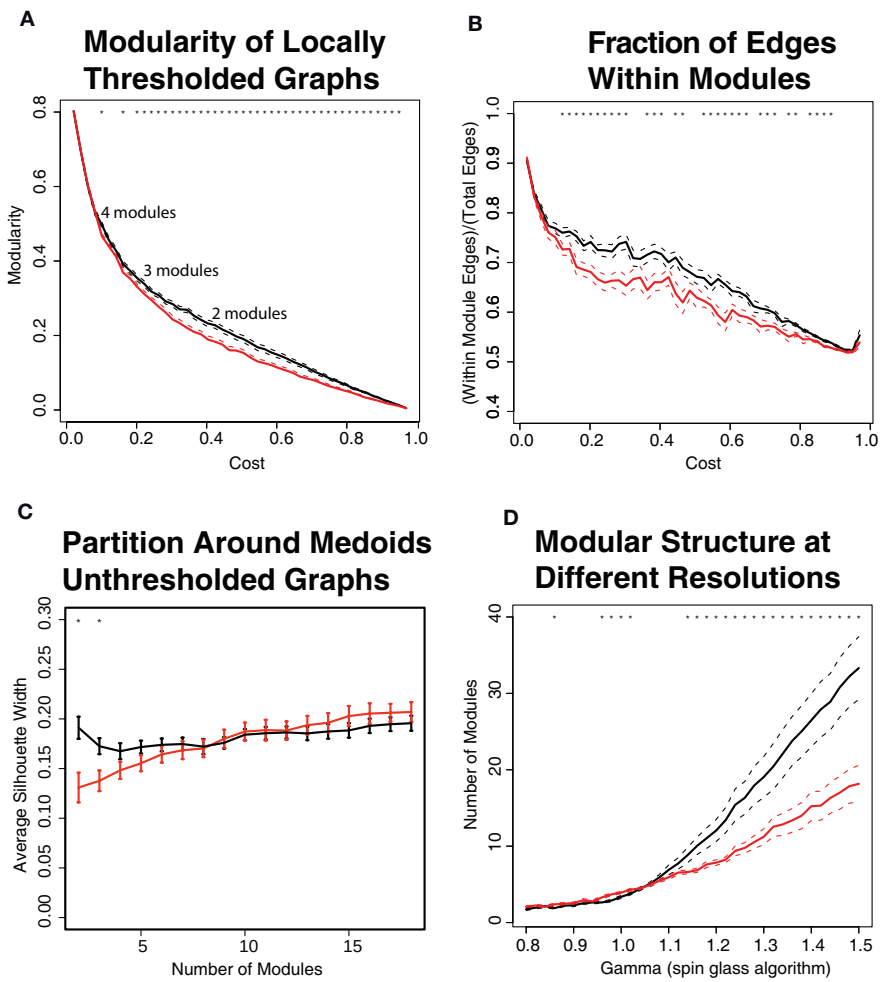


FIGURE 6 | The modular structure of brain networks is disturbed in the childhood-onset schizophrenia (COS) population (red) relative to the control population (black). (A) Modularity is calculated using the fast greedy algorithm on binary, locally thresholded graphs. The COS networks have lower modularity, especially in the range of topological costs where the networks are partitioned into less than 5 modules. **(B)** The fraction of intra-modular edges, which link nodes in the same module, is decreased in COS. This value is the same as modularity except not normalized by the *expected* fraction of intra-modular edges. **(C)** Using the unsupervised learning algorithm Partition Around Medoids (PAM), when the graphs are partitioned into less than 5 modules, the healthy controls have higher modularity as quantified by the average silhouette width. **(D)** Using a spin glass model with simulated annealing, which looks at the modular structure at different resolutions depending on the gamma parameter, the controls have a wider range of modular structure at different scales.

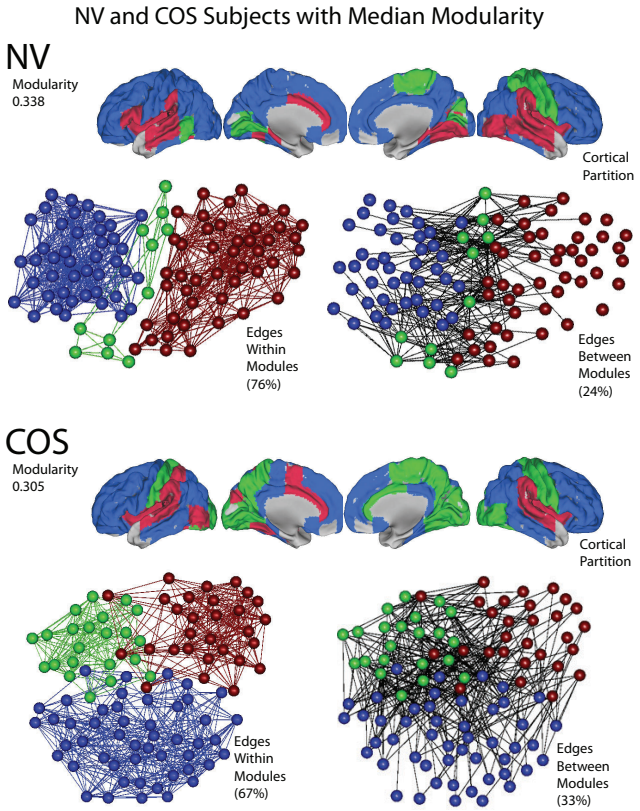


FIGURE 7 | An illustration of modularity, using representative brain networks from the childhood-onset schizophrenia (COS) population and the control (NV) population. At a local threshold of 0.22 topological cost, the modular partition is shown for the median NV subject (above) and the median COS subject (below), in terms of modularity estimated by the fast greedy algorithm. Each module is assigned a specific color, and the modular structure of each subject is illustrated in three different ways: the cortical partition shows the anatomical location of the modules; the left-hand topological plot shows the density of intra-modular edges, between nodes in the same module; and the right-hand topological plot shows the density of inter-modular edges, between nodes in different modules. The layouts of the topological plots are determined by a force-directed algorithm (Fruchterman and Reingold, 1991).

Although differences in modularity have not previously been reported in human brain networks, differences have been found in the modular partition itself, i.e., which brain regions are grouped together into functional communities. For example, Meunier et al. (2009a) found that the brains of a healthy aging population contained more functional modules than younger adults, and Fair et al. (2009) found that during adolescence modules are composed of brain regions that are further apart in physical space. We do not find strong evidence for a group difference in the physical dispersion of brain modules, but it is slightly greater in the controls (not shown). Although the finding that brain networks are modular at multiple resolutions is anticipated by their hierarchical modular organization (Meunier et al., 2009b; Bassett et al., 2010), this is the first study to define modularity across a continuous range of resolutions. Our results may suggest that the modular structure of the functional brain networks is more multi-scale in the healthy controls than the COS population, as reflected by greater sensitivity to the gamma parameter of the spin glass algorithm, but quantifying this hypothesis is an area for future work.

TIME SERIES STATISTICS

It is unsurprising that in counterpoint to the differences in the complex networks, simpler properties of the MRI time series also differ in COS. The COS population shows decreased internal homogeneity of the MRI signal within anatomical regions, decreased variability of the signal, and decreased average connectivity between anatomical brain regions. Although the exact metric is different, decreased homogeneity of the MRI signal within anatomical regions is consistent with decreased regional homogeneity (ReHo; Zang et al., 2004), which has been reported in some brain regions in an adult-onset schizophrenia population (Liu et al., 2006). The decreases reported with ReHo were for spatial volumes at the scale of a voxel and its nearest neighbors, between 7 and 27 voxels total, so our finding of a decrease of the homogeneity within regions hundreds of voxels in volume is a similar finding at a lower spatial resolution. Decreased regional homogeneity could also be interpreted as yet another aspect of decreased modularity, at a different spatial scale. As for the decreased variability of the global MRI signal, nothing similar has to our knowledge been reported in schizophrenia. A metric called the "resting state activity index" (RSAI), which is ReHo multiplied by the variance of the band-pass filtered time series of a voxel, has been reported as increased in some brain regions in an ADHD cohort (Tian et al., 2008). Our results indicate that this measure would be decreased in COS, although at a different spatial scale.

Finally, decreased average strength or connectivity between anatomical brain regions is a confirmation of a finding in two adult-onset samples (Liu et al., 2008; Lynall et al., 2010). There is a potential link between decreased average strength and topological randomness. Since the connectivity matrices of the graphs are composed of thresholded correlation coefficients, decreased overall connectivity implies that, at a given graph density, there is a lower signal-to-noise ratio in the COS graphs. Assuming that this increased noise is spread equally throughout the nodes, it would be expected to result in increased topological randomness. Topological randomness could also result from other processes, e.g., highly correlated regional time series could result in graphs with the same properties as random graphs. But since our study shows both decreased correlations and increased randomness, it seems likely that they are two sides of the same coin.

METHODOLOGICAL ISSUES

As the globally thresholded graphs show group differences in connectedness, it would not be implausible for this to drive the differences in other network metrics. The introduction of local thresholding ensures that the disparity between the COS and controls are not due simply to this issue. The known lack of uniformity in the quality of the MR signal from different anatomical regions also makes it reasonable to employ a local threshold, rather than apply the same threshold to regions with different signal-to-noise. The limitations of simply applying a

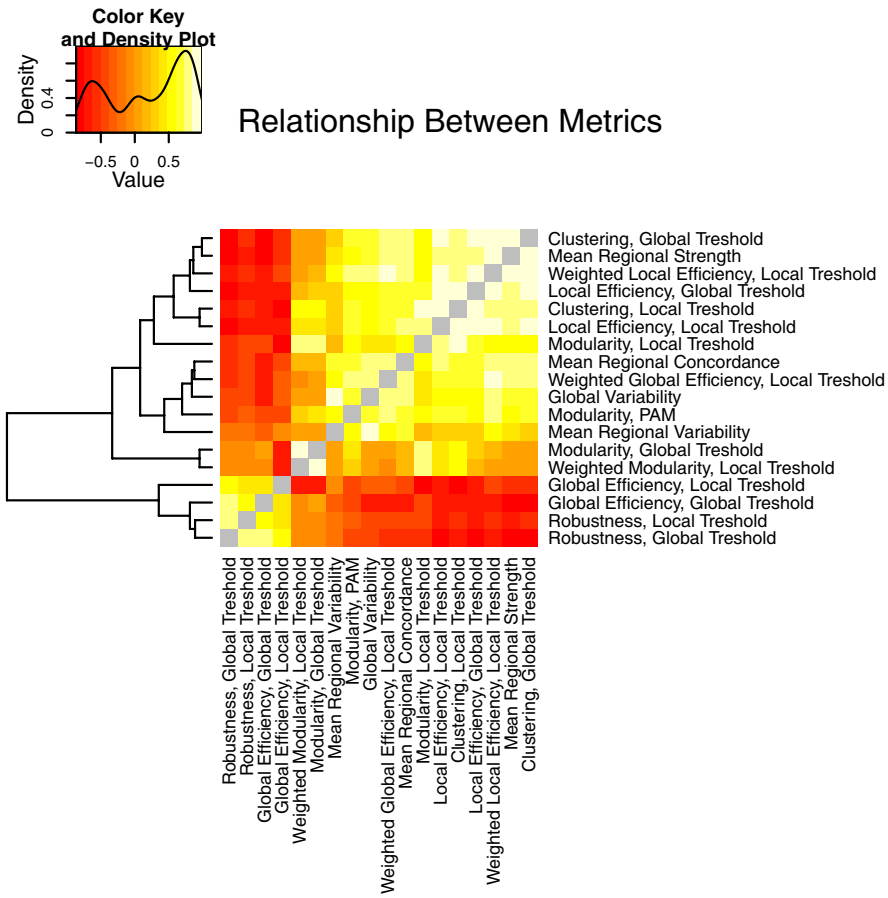


FIGURE 8 | An illustration of the relationship between the different properties of brain networks, including both graph theoretical and non-graph-theoretical metrics. The metrics from **Table 1** are correlated between all the subjects in the study and presented as a heat map, with the color value corresponding to the Pearson's correlation coefficient. The layout is organized by complete linkage hierarchical clustering, according to the dendrogram shown at the left of the figure.

global threshold to a correlation matrix have previously been documented in physics and economics, and several alternatives have been proposed (Onnela et al., 2002; Tumminello et al., 2005; Serrano et al., 2009). Our method is fast, simple, ensures connected graphs, and is defined over the whole cost range. Lacking knowledge of a "true" functional network to provide a gold standard for evaluation of results, it is inappropriate to be too assertive about which graph construction algorithm is best. From a statistical perspective on the individual pairs of time series, we have the most confidence that the edges in a globally thresholded network are genuine functional connections, but the locally thresholded networks have desirable topological constraints and facilitate group comparisons. Side by side contrasts – whether visually on small "model" networks (**Figure 1**) or in terms of statistical comparisons between groups (**Figure 3**) – reveal a high degree of similarity in the differently constructed graphs, with some divergence probably due to network fragmentation issues that arise with global thresholding. In addition, for both thresholding schemes, the patient trend in complex network properties is consistent with randomization of a small percentage of the edges in the control networks, as illustrated in **Figure 4** for locally thresholded graphs. In short, on the basis of current data, it seems likely that both global and local thresholding rules can be used to construct broadly consistent results but that the between-group comparisons based on local thresholding are simpler to interpret because these networks will all be node-connected by design even at low connection densities. Future studies should attempt to compare these and other methods of graph construction more rigorously using modeled data with known and biologically plausible properties.

Unsupervised learning and graph theoretical algorithms to quantify the community structure of a functional brain network have different strengths and weakness. In the context of fMRI networks, one strength of unsupervised learning algorithms such as partition around medoids (PAM) is that they deal with similarities between objects in *n*-dimensional space, while graph theory deals with relations between objects. Unsupervised learning methods are thus appropriate to the complete, unthresholded correlation matrix. In contrast graph theoretical approaches allow us to query the community structure of the same, thresholded graphs for which we discuss other network properties. Another difference is that graph theoretical algorithms naturally output an optimum number of

modules, which is non-trivial for unsupervised learning algorithms. With PAM, one solution is to maximize the silhouette width over a range of possibilities for the number of modules; this is a potential virtue of PAM compared to hierarchical clustering as it is generally implemented, where the dilemma becomes one of how to cut the dendrogram. In a sense the spin glass algorithm with simulated annealing is intermediate between the two other classes of methods. Similarly to PAM, it can be applied to the unthresholded, weighted graphs, but it also outputs an optimal number of modules, at least for a given value of the gamma parameter. However the inclusion of the gamma parameter, while allowing us to explore the multi-scale modular structure of the graphs, introduces the non-trivial question of which if any scale of description best captures the modular structure. Another serious drawback of the spin glass algorithm is that it is by far the slowest computationally of the 3.

This study is based on a small sample size with short MRI scans. With only 13 COS subjects included, the group differences that we have found will need to be verified in a larger study. In terms of the scans, concatenating two consecutive 3-min scans is probably inferior to having one 6-min scan; however, it would seem comparable to concatenating the interleaved rest blocks from a task-activation study, which has been suggested as acceptable data for a resting-state fMRI study (Fair et al., 2007). In our case, the short consecutive scans are unavoidable, because children and adolescents with severe neuropsychiatric disease often find it difficult to tolerate longer scans. The total acquisition time of 6 min is also quite short, but it has been argued that correlations between brain regions stabilize with even shorter acquisition times (Dijk et al., 2010). The short scanning time does prevent us from looking at very low frequency fluctuations (<0.05 Hz), as the statistical power starts to become quite low.

REFERENCES

Achard, S., and Bullmore, E. (2007). Efficiency and cost of economical brain functional networks. *PLoS Comput. Biol.* 3, e17. doi:10.1371/journal.pcbi.0030017.

Achard, S., Salvador, R., Whitcher, B., Suckling, J., and Bullmore, E. (2006). A resilient, low-frequency, small-world human brain functional network with highly connected association cortical hubs. *J. Neurosci.* 26, 63–72.

Anderson, B., Butts, C., and Carley, K. (1999). The interaction of size and density with graph-level indices. *Soc. Networks* 21, 239–267.

Barabasi, A., and Albert, R. (1999). Emergence of scaling in random networks. *Science* 286, 509–512.

Bassett, D. S., Bullmore, E., Verchinski, B. A., Mattay, V. S., Weinberger, D. R., and Meyer-Lindenberg, A. (2008). Hierarchical organization of human cortical networks in health and schizophrenia. *J. Neurosci.* 28, 9239–9248.

Bassett, D. S., Bullmore, E., Meyer-Lindenberg, A., Apud, J. A., Weinberger, D. R., and Coppola, R. (2009). Cognitive fitness of cost-efficient brain functional networks. *Proc. Natl. Acad. Sci. U.S.A.* 106, 11747–11752.

Bassett, D. S., Greenfield, D., Meyer-Lindenberg, A., Weinberger, D., Moore, S., and Bullmore, E. (2010). Efficient physical embedding of topologically complex information processing networks in brains and computer circuits. *PLoS Comput. Biol.* 6, e1000748. doi:10.1371/journal.pcbi.1000748.

Bollobás, B. (1985). *Random Graphs*. London: Academic.

Bullmore, E., and Sporns, O. (2009). Complex brain networks: graph theoretical analysis of structural and functional systems. *Nat. Rev. Neurosci.* 10, 1–13.

Burgund, E. D., Kang, H. C., Kelly, J. E., Buckner, R. L., Snyder, A. Z., Petersen, S. E., and Schlaggar, B. L. (2002). The feasibility of a common stereotactic space for children and adults in fMRI studies of development. *Neuroimage* 17, 184–200.

Cantlon, J. F., Brannon, E. M., Carter, E. J., and Pelphrey, K. A. (2006). Functional imaging of numerical processing in adults and 4-y-old children. *PLoS Biol.* 4, e125. doi: 10.1371/journal.pbio.0040125.

Chen, Y., Paul, G., Cohen, R., Havlin, S., Borgatti, S. P., Liljeros, F., and Stanley, H. E. (2007). Percolation theory applied to measures of fragmentation in social networks. *Phys. Rev. E. Stat. Nonlin. Soft Matter Phys.* 75, 046107.

Clauset, A., Newman, M. E. J., and Moore, C. (2004). Finding community structure in very large networks. *Phys. Rev. E. Stat. Nonlin. Soft Matter Phys.* 70, 066111.

Cordes, D., Haughton, V., Carew, J. D., Arfanakis, K., and Maravilla, K. (2002). Hierarchical clustering to measure connectivity in fMRI resting-state data. *Magn. Reson. Imaging* 20, 305–317.

Cox, R. W. (1996). AFNI: software for analysis and visualization of functional magnetic resonance neuroimages. *Comput. Biomed. Res.* 29, 162–173.

Crone, E. A., Wendelken, C., Donohue, S., van Leijenhorst, L., and Bunge, S. A. (2006). Neurocognitive development of the ability to manipulate information in working memory. *Proc. Natl. Acad. Sci. U.S.A.* 103, 9315–9320.

Csardi, G., and Nepusz, T. (2006). The igraph software package for complex network research. *InterJournal Complex Syst.* Article No. 1695.

David, A. S. (1994). Dysmodularity: a neurocognitive model for schizophrenia. *Schizophr. Bull.* 20, 249–255.

Davis, K. L., Stewart, D. G., Friedman, J. I., Buchsbaum, M., Harvey, P. D., Hof, P. R., Buxbaum, J., and Haroutunian, V. (2003). White matter changes in schizophrenia: evidence for myelin-related dysfunction. *Arch. Gen. Psychiatry* 60, 443–456.

Dijk, K. R. A. V., Hedden, T., Venkataraman, A., Evans, K. C., Lazar, S. W., and Buckner, R. L. (2010). Intrinsic functional connectivity as a tool for human connectomics: theory, properties, and optimization. *J. Neurophysiol.* 103, 297–321.

Dorogovtsev, S., Goltsev, A., and Mendes, J. (2008). Critical phenomena in complex networks. *Rev. Mod. Phys.* 80, 1275.

Durston, S., Tottenham, N. T., Thomas, K. M., Davidson, M. C., Eigsti, I. M., Yang, Y., Ulug, A. M., and Casey, B. J. (2003). Differential patterns of striatal activation in young children with and without ADHD. *Biol. Psychiatry* 53, 871–878.

Eppstein, D., Paterson, M., and Yao, F. (1992). On nearest-neighbor graphs. *Lect. Notes Comput. Sci.* 623, 416–426.

Erdös, P., and Rényi, A. (1959). On random graphs. *Publ. Math.* 6, 290–297.

Fair, D. A., Cohen, A. L., Power, J. D., Dosenbach, N. U. F., Church, J. A., Miezin, F. M., Schlaggar, B. L., and Petersen, S. E. (2009). Functional brain networks develop from a "local to distributed" organization. *PLoS Comput. Biol.* 5, e1000381. doi: 10.1371/journal.pcbi.1000381.

Fair, D. A., Schlaggar, B. L., Cohen, A. L., Miezin, F. M., Dosenbach, N. U. F., Wenger, K. K., Fox, M. D., Snyder, A. Z., Raichle, M. E., and Petersen, S. E. (2007). A method for using blocked and event-related fMRI data to study "resting state" functional connectivity. *Neuroimage* 35, 396–405.

Feinberg, I. (1982). Schizophrenia: caused by a fault in programmed synaptic elimination during adolescence? *J. Psychiatr. Res.* 17, 319–334.

Fodor, J. A. (1983). *The Modularity of Mind: An Essay on Faculty Psychology.* Cambridge, MA: MIT Press.

Fortunato, S., and Barthélemy, M. (2007). Resolution limit in community detection. *Proc. Natl. Acad. Sci. U.S.A.* 104, 36–41.

Fruchterman, T. M. J., and Reingold, E. M. (1991). Graph drawing by force-directed placement. *Softw. Pract. Exper.* 21, 1129–1164.

Galvan, A., Hare, T. A., Parra, C. E., Penn, J., Voss, H., Glover, G., and Casey, B. J. (2006). Earlier development of the accumbens relative to orbitofrontal cortex might underlie risk-taking behavior in adolescents. *J. Neurosci.* 26, 6885–6892.

Giedd, J. N., Lalonde, F. M., Celano, M. J., White, S. L., Wallace, G. L., Lee, N. R., and Lenroot, R. K. (2009). Anatomical brain magnetic resonance imaging of typically developing children and adolescents. *J. Am. Acad. Child Adolesc. Psychiatry* 48, 465–470.

Glahn, D. C., Ragland, J. D., Abramoff, A., Barrett, J., Laird, A. R., Bearden, C. E., and Velligan, D. I. (2005). Beyond hypofrontality: a quantitative meta-analysis of functional neuroimaging studies of working memory in schizophrenia. *Hum. Brain Mapp.* 25, 60–69.

Gogtay, N., Lu, A., Leow, A. D., Klunder, A. D., Lee, A. D., Chavez, A., Greenstein, D., Giedd, J. N., Toga, A. W., Rapoport, J. L., and Thompson, P. M. (2008). Three-dimensional brain growth abnormalities in childhood-onset schizophrenia visualized by using tensor-based morphometry. *Proc. Natl. Acad. Sci. U.S.A.* 105, 15979–15984.

Goh, K. I., Salvi, G., Kahng, B., and Kim, D. (2006). Skeleton and fractal scaling in complex networks. *Phys. Rev. Lett.* 96, 018701.

Guimerà, R., Sales-Pardo, M., and Amaral, L. A. N. (2004). Modularity from fluctuations in random graphs and complex networks. *Phys. Rev. E. Stat. Nonlin. Soft Matter Phys.* 70, 025101.

Hagmann, P., Cammoun, L., Gigandet, X., Meuli, R., Honey, C. J., Wedeen, V. J., and Sporns, O. (2008). Mapping the structural core of human cerebral cortex. *PLoS Biol.* 6, e159. doi:10.1371/journal.pbio.0060159.

Heimo, T., Kumpula, J., Kaski, K., and Saramaki, J. (2008). Detecting modules in dense weighted networks with the potts method. *J. Stat. Mech. Theory Exp.* 2008, 08007.

Humphries, M. D., Gurney, K., and Prescott, T. J. (2006). The brainstem reticular formation is a small-world, not scale-free, network. *Proc. Biol. Sci.* 273, 503–511.

Jenkinson, M., Bannister, P., Brady, M., and Smith, S. (2002). Improved optimization for the robust and accurate linear registration and motion correction of brain images. *Neuroimage* 17, 825–841.

Jenkinson, M., and Smith, S. (2001). A global optimisation method for robust affine registration of brain images. *Med. Image Anal.* 5, 143–156.

Kang, H. C., Burgund, E. D., Lugar, H. M., Petersen, S. E., and Schlaggar, B. L. (2003). Comparison of functional activation foci in children and adults using a common stereotactic space. *Neuroimage* 19, 16–28.

Kashtan, N., and Alon, U. (2005). Spontaneous evolution of modularity and network motifs. *Proc. Natl. Acad. Sci. U.S.A.* 102, 13773–13778.

Kaufman, L., and Rousseeuw, P. (1987). "Clustering by means of medoids," in *Statistical Data Analysis Based on the L1-Norm and Related Methods,* ed. Y. Dodge (Berlin: Birkhäuser), 405–416.

Kruskal, J. B. (1956). On the shortest spanning subtree of a graph and the traveling salesman problem. *Proc. Am. Math. Soc.* 7, 48–50.

Lambiotte, R. (2010). Multi-scale modularity in complex networks. arXiv:1004.4268.

Latora, V., and Marchiori, M. (2001). Efficient behavior of small-world networks. *Phys. Rev. Lett.* 87, 198701.

Lee, J., Folley, B. S., Gore, J., and Park, S. (2008). Origins of spatial working memory deficits in schizophrenia: an event-related fMRI and near-infrared spectroscopy study. *PLoS ONE* 3, e1760. doi:10.1371/journal.pone.0001760.

Liu, H., Liu, Z., Liang, M., Hao, Y., Tan, L., Kuang, F., Yi, Y., Xu, L., and Jiang, T. (2006). Decreased regional homogeneity in schizophrenia: a resting state functional magnetic resonance imaging study. *Neuroreport* 17, 19–22.

Liu, Y., Liang, M., Zhou, Y., He, Y., Hao, Y., Song, M., Yu, C., Liu, H., Liu, Z., and Jiang, T. (2008). Disrupted small-world networks in schizophrenia. *Brain* 131, 945–961.

Lynall, M.-E., Bassett, D. S., Kerwin, R., McKenna, P. J., Kitzbichler, M., Muller, U., and Bullmore, E. (2010). Functional connectivity and brain networks in schizophrenia. *J. Neurosci.* 30, 9477–9487.

Meunier, D., Achard, S., Morcom, A., and Bullmore, E. (2009a). Age-related changes in modular organization of human brain functional networks. *Neuroimage* 44, 715–723.

Meunier, D., Lambiotte, R., Fornito, A., Ersche, K. D., and Bullmore, E. (2009b). Hierarchical modularity in human brain functional networks. *Front. Neuroinformatics* 3:37. doi: 10.3389/neuro.11.037.2009.

Milo, R., Kashtan, N., Itzkovitz, S., Newman, M., and Alon, U. (2004). On the uniform generation of random graphs with prescribed degree sequences. arXiv:0312028v2.

Minzenberg, M. J., Laird, A. R., Thelen, S., Carter, C. S., and Glahn, D. C. (2009). Meta-analysis of 41 functional neuroimaging studies of executive function in schizophrenia. *Arch. Gen. Psychiatry* 66, 811–822.

Newman, M. E. J., and Girvan, M. (2004). Finding and evaluating community structure in networks. *Phys. Rev. E. Stat. Nonlin. Soft Matter Phys.* 69, 026113.

Onnela, J.-P., Chakraborti, A., Kaski, K., and Kertiész, J. (2002). Dynamic asset trees and portfolio analysis. *Eur. Phys. J. B.* 30, 285–288.

Percival, D. B., and Walden, A. T. (2006). *Wavelet Methods for Time Series Analysis.* Cambridge, UK: Cambridge University Press.

Pessoa, V. F., Monge-Fuentes, V., Simon, C. Y., Suganuma, E., and Tavares, M. C. H. (2008). The Müller-Lyer illusion as a tool for schizophrenia screening. *Rev. Neurosci.* 19, 91–100.

Prim, R. C. (1957). Shortest connection networks and some generalizations. *Bell Syst. Tech. J.* 36, 1389–1401.

R Development Core Team (2009). *R: A Language and Environment for Statistical Computing*. Vienna: R Foundation for Statistical Computing. Available at http://www.R-project.org.

Reichardt, J., and Bornholdt, S. (2006). Statistical mechanics of community detection. *Phys. Rev. E. Stat. Nonlin. Soft Matter Phys.* 74, 016110.

Rubinov, M., Knock, S. A., Stam, C. J., Micheloyannis, S., Harris, A. W. F., Williams, L. M., and Breakspear, M. (2009). Small-world properties of nonlinear brain activity in schizophrenia. *Hum. Brain Mapp.* 30, 403–416.

Salvador, R., Suckling, J., Coleman, M. R., Pickard, J. D., Menon, D., and Bullmore, E. (2005). Neurophysiological architecture of functional magnetic resonance images of human brain. *Cereb. Cortex* 15, 1332–1342.

Schank, T., and Wagner, D. (2004). Approximating clustering-coefficient and transitivity. *J. Graph Algorithms Appl.* 9, 265–275.

Serrano, M. A., Boguñá, M., and Vespignani, A. (2009). Extracting the multiscale backbone of complex weighted networks. *Proc. Natl. Acad. Sci. U.S.A.* 106, 6483–6488.

Shapleske, J., Rossell, S. L., Chitnis, X. A., Suckling, J., Simmons, A., Bullmore, E. T., Woodruff, P. W. R., and David, A. S. (2002). A computational morphometric MRI study of schizophrenia: effects of hallucinations. *Cereb. Cortex* 12, 1331–1341.

Sheskin, D. J. (2007). *Handbook of Parametric and Nonparametric Statistical Procedures,* 4th Edn. Boca Raton, FL: CRC Press.

Simon, H. (1962). The architecture of complexity. *Proc. Amer. Philos. Soc.* 106, 467–482.

Smith, S. M., Jenkinson, M., Woolrich, M. W., Beckmann, C. F., Behrens, T. E. J., Johansen-Berg, H., Bannister, P. R., Luca, M. D., Drobnjak, I., Flitney, D. E., Niazy, R. K., Saunders, J., Vickers, J., Zhang, Y., Stefano, N. D., Brady, J. M., and Matthews, P. M. (2004). Advances in functional and structural MR image analysis and implementation as FSL. *Neuroimage* 23(Suppl. 1), S208–S219.

Tian, L., Jiang, T., Liang, M., Zang, Y., He, Y., Sui, M., and Wang, Y. (2008). Enhanced resting-state brain activities in ADHD patients: a fMRI study. *Brain Dev.* 30, 342–348.

Tumminello, M., Aste, T., Matteo, T. D., and Mantegna, R. N. (2005). A tool for filtering information in complex systems. *Proc. Natl. Acad. Sci. U.S.A.* 102, 10421–10426.

Turkeltaub, P. E., Gareau, L., Flowers, D. L., Zeffiro, T. A., and Eden, G. F. (2003). Development of neural mechanisms for reading. *Nat. Neurosci.* 6, 767–773.

Venables, W. N., and Ripley, B. D. (2002). *Modern Applied Statistics with S*, 4th Edn. New York: Springer.

Watts, D. J., and Strogatz, S. H. (1998). Collective dynamics of "small-world" networks. *Nature* 393, 440–442.

Zang, Y., Jiang, T., Lu, Y., He, Y., and Tian, L. (2004). Regional homogeneity approach to fMRI data analysis. *Neuroimage*, 22, 394–400.

Conflict of Interest Statement: Edward Bullmore is employed half-time by GlaxoSmithKline and half-time by University of Cambridge.

Received: 14 June 2010; paper pending published: 25 July 2010; accepted: 10 September 2010; published online: 08 October 2010.

*Citation: Alexander-Bloch AF, Gogtay N, Meunier D, Birn R, Clasen L, Lalonde F, Lenroot R, Giedd J and Bullmore ET (2010) Disrupted modularity and local connectivity of brain functional networks in childhood-onset schizophrenia. Front. Syst. Neurosci. **4**:147. doi: 10.3389/fnsys.2010.00147*

Copyright © 2010 Alexander-Bloch, Gogtay, Meunier, Birn, Clasen, Lalonde, Lenroot, Giedd and Bullmore. This is an open-access article subject to an exclusive license agreement between the authors and the Frontiers Research Foundation, which

permits unrestricted use, distribution, and reproduction in any medium, provided the original authors and source are credited.

APPENDIX

GRAPH THEORY TERMS

Clustering coefficient: A measure of cliquishness, or the extent to which edges are locally agglomerated, which can be defined for a graph as a whole or for each node individually.

Complete graph: A graph where every node is linked by an edge to every other node.

Connected or node-connected graph: A graph in which each node is linked by a finite number of edges to every other node, i.e., all nodes are part of a giant connected component. A disconnected graph is also called "fragmented."

Connection density or topological cost: The number of edges in a graph, divided by the number of edges in a complete graph with the same number of nodes.

Degree: The degree of a node is its number of edges.

Edge or link: An interaction between nodes in a graph, usually illustrated as a straight line.

Gamma (γ): See Modularity.

Global efficiency: A measure of global integration, which can be defined for a graph as a whole or for each node individually, for weighted or unweighted (binary) graphs.

Graph: A group of elements and their interactions, represented as nodes and edges.

***k* Nearest Neighbors Graph** (*k*-NNG)**:** For a weighted graph, the *k*-NNG includes edges linking each node to its *k* nearest neighbors, where the weight of an edge is interpreted as the distance between the nodes.

Local efficiency: Conceptually similar to the clustering coefficient, a measure of the local agglomeration of edges, which can be defined for weighted or unweighted (binary) graphs.

Minimum spanning tree (MST): For a weighted graph, an MST is composed of the edges that connect all of the nodes of the graph while including the lowest possible total weight.

Modularity: A measure of the community structure of a graph, based on an optimal partition of the nodes into distinct communities or modules, which can be defined for weighted or unweighted graphs. There are many different approaches to this problem. In the multi-resolution spin glass model, the gamma (γ) parameter adjusts the resolution of the modular partition.

Network: See Graph.

Node or vertex: An object in a graph, usually illustrated as a circle.

Path length: The shortest path length between two nodes is the length of the shortest sequence of edges that links the nodes. The characteristic path length of a graph is the average shortest path length between every pair of nodes.

Random graph: A random graph is generated by a set of rules with minimal topological constraints. For example, each edge could occur independently with some probability. Different methods of generating random graphs result in different topological properties.

Sigma (σ)**:** See Small-world.

Small-world: A small-world graph has a high clustering coefficient and a low characteristic path length, compared to random graphs. The extent to which a graph is small-world is captured by the quantity sigma (σ).

Strength: The strength of a node is the sum of the weights of all of its edges. Depending on the context, "strength" can also refer to the average functional connectivity of a brain region

Weighted graph: A graph where each edge is assigned a quantitative value, which could for example reflect how strongly the nodes interact. Depending on the context, it can be convenient to assign higher weights either to stronger interactions or to weaker interactions. An unweighted graph is also called a "binary" graph.

frontiers in
SYSTEMS NEUROSCIENCE

REVIEW ARTICLE
published: 22 February 2011
doi: 10.3389/fnsys.2011.00010

Inter-regional brain communication and its disturbance in autism

Sarah E. Schipul*, Timothy A. Keller and Marcel Adam Just

Center for Cognitive Brain Imaging, Department of Psychology, Carnegie Mellon University, Pittsburgh, PA, USA

Edited by:
Barry Horwitz, National Institutes of Health, USA

Reviewed by:
Susan Whitfield-Gabrieli, Massachusetts Institute of Technology, USA
John Suckling, University of Cambridge, UK

****Correspondence:***
Sarah E. Schipul, Center for Cognitive Brain Imaging, Department of Psychology, Carnegie Mellon University, Pittsburgh, PA 15213, USA.
e-mail: schipul@cmu.edu

In this review article, we summarize recent progress toward understanding disturbances in functional and anatomical brain connectivity in autism. Autism is a neurodevelopmental disorder affecting language, social interaction, and repetitive behaviors. Recent studies have suggested that limitations of frontal–posterior brain connectivity in autism underlie the varied set of deficits associated with this disorder. Specifically, the underconnectivity theory of autism postulates that individuals with autism have a reduced communication bandwidth between frontal and posterior cortical areas, which constrains the psychological processes that rely on the integrated functioning of frontal and posterior brain networks. This review summarizes the recent findings of reduced frontal–posterior functional connectivity (synchronization) in autism in a wide variety of high-level tasks, focusing on data from functional magnetic resonance imaging studies. It also summarizes the findings of disordered anatomical connectivity in autism, as measured by a variety of techniques, including distribution of white matter volumes and diffusion tensor imaging. We conclude with a discussion of the implications of these findings for autism and future directions for this line of research.

Keywords: autism, brain connectivity, fMRI, DTI

INTRODUCTION

The diagnosis of autism is currently based on observed behavioral characteristics, without the aid of biological markers. The triad of behavioral impairments that characterize this neurodevelopmental disorder consists of seemingly diverse types of deficits: social reciprocity, language skills, and restricted repetitive and stereotyped patterns of behavior (American Psychiatric Association [APA], 2000). Individuals with autism also often show intact (if not enhanced) perceptual functioning (Mottron et al., 2006). Autism is a spectrum disorder, such that individuals who meet the diagnosis can have a wide range of severity of impairment in these three areas (Frith, 1989). Language impairments can vary widely, ranging from near absence of language or gestures in cases of low-functioning autism to the near normal language in high-functioning autism, but with persistent pragmatic communication difficulties (Frith and Happé, 1994). Social impairments include a lack of seeking to share enjoyment with others, a lack of emotional reciprocity, and marked impairment in the use of non-verbal behaviors such as eye-to-eye gaze (APA, 2000). Restricted repetitive and stereotyped patterns of behavior include repetitive motor mannerisms and inflexible adherence to specific routines (APA, 2000). As awareness about autism has increased dramatically in the past decade, so has research into the behavioral and biological characteristics of autism. This diverse set of behavioral impairments in autism provides a formidable research challenge, namely, to identify a biological mechanism that can explain all of them in a unified way.

The influential theory of autism known as "weak central coherence" (Frith, 1989) aimed to explain an extended set of behavioral characteristics of autism in behavioral terms. The theory proposed that underlying the distinct behavioral impairments of autism is a general deficit in the ability to integrate multiple information sources into a unified whole. This hypothesized integration deficit thus provided an account that can be applied to all three areas of impairments in autism. For example, impairments in social interactions can be attributed by weak central coherence theory to inadequate integration of many types of concurrent social information, such as the content and context of the dialog, the speaker's tone of voice, the speaker's facial expression and body language, the speaker's relationship with the listener, etc. Moreover, the sparing of certain behaviors can be explained in terms of the spared domains relying less on multiple information sources. Although the weak central coherence theory provides a compelling conceptual description that explains the clinical symptoms of autism, it does not indicate what specific cognitive or biological mechanism may underlie this general integration deficit. Several other cognitive-level theories of autism have also been proposed, including Theory of Mind disruption (Baron-Cohen et al., 1985), executive processing dysfunction (Ozonoff et al., 1991), complex information processing disorder (Minshew et al., 1997), and enhanced perceptual functioning (Mottron and Burack, 2001). While each of these theories accounts for some aspects of the behavioral symptoms of autism, neuroimaging research has the potential to identify a biological mechanism underlying and explaining the behavioral manifestations of this disorder in a unified account.

Since the advent of neuroimaging, autism researchers have attempted to use imaging methods to identify atypical characteristics of brain function and brain structure in autism. Magnetic resonance imaging (MRI) studies can be used to measure the size and properties of various gray and white matter structures in the brain. Functional MRI (fMRI) studies measure the brain activation in gray matter regions during the performance of various tasks. Furthermore, the synchronization of the activation between brain

regions has been used as a measure of inter-regional coordination or functional connectivity. Recently, new techniques have been developed to measure the integrity of white matter pathways in the brain, providing a more precise characterization of anatomical connectivity. These neuroimaging techniques have explored differences between individuals with autism and neurotypical control individuals to investigate the possibility of localized deficits in specific areas of the brain in autism as well as network-wide disruptions throughout the brain.

What a number of fMRI studies examining brain activation in a diverse set of tasks collectively show is that the diverse behavioral symptoms of autism are not underpinned by the activity of any single brain area. Instead, these studies indicate that many different sets of brain areas are involved in the performance of tasks that show behavioral abnormalities in autism (see Di Martino et al., 2009 for a recent meta-analysis). This outcome suggests that the disturbance underlying autism is more likely a non-localized disruption. Recent neuroimaging findings have led to the hypothesis that a network-wide disruption in brain connectivity may explain the varied set of behavioral impairments in autism.

Based on neuroimaging evidence of anatomical and functional connectivity disruptions in autism, Just et al. (2004, 2007) proposed the underconnectivity theory of autism. This theory suggests that the behavioral markers of autism are directly or indirectly caused by limitations of the communication between frontal and posterior brain regions, and predicts that these limitations will impact those tasks that require extensive coordinated functioning of frontal and posterior processing centers. For example, in both language comprehension and social interaction processes, fMRI studies have shown that extensive, coordinated activity between frontal and posterior brain areas is involved. The theory accounts for restricted repetitive and stereotyped patterns of behavior in terms of the inability of the frontal executive system to exert control over posterior processing centers. The theory characterizes spared behaviors as those that do not require extensive frontal–posterior coordination, such as some perceptual processes. Thus the theory posits a biological mechanism, frontal–posterior underconnectivity, which may be able to explain the full set of diverse impairments that characterize autism.

Neuroimaging studies have demonstrated that coordinated functioning of frontal and posterior processing centers is critical for the types of behavior in which individuals with autism are impaired. Language comprehension and production require the coordinated functioning of at least the inferior frontal gyrus (Broca's area, in the left hemisphere) and the posterior superior temporal gyrus (Wernicke's area, in the left hemisphere). Similarly, social processing requires the coordinated functioning of at least medial frontal areas and posterior (right-hemisphere dominant) areas, such as the temporo-parietal junction (associated with Theory of Mind processing), the superior temporal sulcus (associated with processing biological motion), and the fusiform gyrus (associated with face processing). Restricted repetitive and stereotyped patterns of behavior may arise as a result of poor coordination between frontal executive systems that guide attention through suppression or focus and posterior systems that execute the repeated behavior. The sparing of certain visuospatial abilities in autism may be due to these processes being less reliant on the participation of frontal systems and more reliant on posterior (parietal and occipital) systems. Thus, the full set of behavioral impairments that characterize autism may be explainable by impaired integration of frontal and posterior brain systems, caused by frontal–posterior underconnectivity.

Below we review different sources of evidence of underconnectivity in autism, including measures of both functional [positron emission tomography (PET), fMRI, and electroencephalography (EEG)] and anatomical connectivity (T1-weighted structural imaging, DTI, and histological analyses). Importantly, as pointed out by Horwitz (2003), we note that methodological factors in measuring connectivity affect the inferences that can be drawn, and that because of this, the conclusions may differ depending on the particular way that connectivity is measured. Most neuroimaging studies only include high-functioning individuals (IQs in the normal range), and the majority of the studies reported here include only high-functioning individuals with autism spectrum disorders (ASD). One exception is that several structural imaging studies of children under 5 years of age do not restrict their ASD group based on IQ. We also consider the growing evidence of the relations between measures of connectivity and behavior. Finally, we discuss the implications of these findings for the treatment of autism and future directions for this area of research.

FUNCTIONAL CONNECTIVITY IN AUTISM

In a groundbreaking paper in autism neuroimaging, Horwitz et al. (1988) provided the first evidence that disrupted coordination among brain regions might be an important factor underpinning the behavioral manifestations of the disorder. This evidence was based on cross-participant, between-region correlations of regional cerebral glucose metabolism during rest, measured with PET. The striking finding from this study was that a group of adult males with autism showed a lower than normal degree of correlation between the level of metabolic activity in various activated brain regions, particularly when considering correlations between frontal and parietal regions. Interestingly, this study also found reduced across-subject correlations in autism for frontal–subcortical correlations of metabolic rates, but not for inter-hemispheric, homologous regions. It took over a decade for the next breakthrough to occur, a period of time during which fMRI methods were developed, which allowed for even more fine-grained, repeated measurement of task-related activation within the same participant. These new methods made it possible to extract a time series of the activation in each area and measure the correlations of the time series across areas within participants, rather than just within groups. In recent years, a variety of methods have been used to assess how functional connectivity compares between individuals with and without autism. Across many tasks and paradigms, the vast majority of studies of brain activity have reported converging findings of disrupted synchronization of brain activation in autism.

Functional connectivity is a measure of the synchronization, or covariance, of activation among different brain regions, and it is often interpreted as an indirect measure of the communication or coordination of processing between the regions. In fMRI studies, functional connectivity is typically measured by calculating the simple Pearson correlation coefficient between two time courses of activation measured in different regions. Moreover, the measurement of dyadic coordination rather than coordination

among larger numbers of areas is simply a matter of convenience. Where appropriate, higher-order measures of coordination among a larger set of areas can be informative, showing for example, that the groupings of areas are different and smaller in autism in some tasks (Koshino et al., 2005). The more general issue concerns impaired communication between the frontal and posterior brain areas that concurrently perform a given task. If two brain areas show synchronized patterns of activation, it implies that they are performing their functions within some coordinated, coherent system, possibly involving dyadic communication and coordination between them; a better term for "functional connectivity" may have been *informational connectivity*. Measurements of functional connectivity can be used to examine how the communication between distinct brain areas differs between individuals with autism and neurotypical individuals.

Despite the fact that all studies of functional connectivity somehow measure inter-regional covariance of activation levels, the particular techniques used to assess this covariance can differ substantially across imaging modalities, laboratories, and studies. At the most basic level, the choice of imaging modality will determine the spatial and temporal resolution at which such covariance can be measured. As noted above, early PET studies (e.g., Horwitz et al., 1988) lacked the temporal resolution to evaluate functional connectivity within individual subjects, and later PET studies could only evaluate such connectivity at the temporal resolution of lengthy (e.g., 45-s) blocks of data acquisition (Castelli et al., 2002). With the advent of fMRI, these limitations on temporal resolution were removed, but different techniques resulted in functional connectivity being measured at different spatial resolutions.

One approach that is well-suited to fMRI measurement of the coordination of information processing involves averaging the activation time course of all the voxels in each region which have been shown to be activated in the task at hand. The analyses then examine the correlations among all pairs of these averaged time series in a given task (e.g., Just et al., 2004). Alternatively, voxel-based analyses can measure the synchronization between one seed region [based on a single voxel or an average of all voxels in a predefined region of interest (ROI)] and all the remaining voxels throughout the brain. This latter method focuses on measuring the synchronization between the activation in a specific brain structure and the rest of the brain, rather than examining connectivity between all possible pairs of regions, but allows group differences in this connectivity with a single region to be assessed in each voxel over the entire brain.

In the measurement of functional connectivity in fMRI, it is important to note which range of frequencies is being included in the measurement and with what rationale. The majority of fMRI studies of functional connectivity correlate activation measurements that occur once every second or 2 s during task performance. These studies focus on the synchronization of activation that is assumed to reflect conjoint modulations of the information processing activity in each of two regions. By contrast, a few fMRI studies of functional connectivity have instead examined only the slow activation changes (occurring over the course of 10 s or more) that are independent of task performance. (This is done by removing frequencies above 0.1 Hz.) This approach assesses whether the functional connectivity differences in autism are present in slower-changing biological activity unrelated to cognition. This review focuses on the findings of task-dependent functional connectivity differences in autism related to cognitive processing, but also includes the findings of task-independent functional connectivity.

FRONTAL–POSTERIOR FUNCTIONAL CONNECTIVITY IN AUTISM

The most consistent finding of functional connectivity differences in autism is a pattern of lower frontal–posterior functional connectivity relative to neurotypical individuals. Many studies have found decreased synchronization between whatever frontal and posterior regions are recruited for a given task. For example, in a task designed to require the integration of spatial processing and language comprehension, decreased functional connectivity was found in autism[1] between frontal language regions and parietal spatial processing regions (Kana et al., 2006). Participants had to judge sentences such as the following as true or false: *The number 8 when rotated 90° looks like a pair of eyeglasses*. Similarly, in a working memory task where participants were asked to judge whether a face they were viewing was the same as one seen previously, decreased functional connectivity was found in autism between frontal executive regions and the fusiform gyrus, an area involved in face processing (Koshino et al., 2008). This latter study illustrates that what is impaired in autism is not just the functioning of a particular brain area (although the activation in the fusiform gyrus was in a slightly offset location in autism), but that, in addition, the functional connectivity between the fusiform gyrus and frontal regions was abnormally low. Furthermore, this pair of studies illustrates the point that functional underconnectivity emerges between whatever frontal and posterior regions are centrally involved in the task. Almost all complex language, social, and executive tasks, precisely where behavioral deficits are typically found in autism, would be expected to show frontal–posterior functional underconnectivity. (An example of a task that might be expected not to draw heavily on frontal regions is a perceptual task that can be performed without strategic control, and this is also the type of task where one might expect sparing in autism. It will be interesting to learn about the functional connectivities among posterior regions in autism in such tasks, which have not yet been reported).

Similar findings of lower functional connectivity in autism in relevant frontal and posterior areas have been reported in a wide variety of cognitive tasks. For example, in a passage comprehension task in which participants had to make inferences about the characters' intentions, decreased functional connectivity in autism was found between frontal and parietal Theory of Mind areas, as well as between frontal language areas and parietal Theory of Mind areas (Mason et al., 2008). **Figure 1** depicts the frontal–posterior underconnectivity in autism during this task (where line width corresponds to the group difference in functional connectivity). In a Tower of London task, decreased functional connectivity in autism was found between frontal and parietal working memory areas (Just et al., 2007). In a task which required participants to make inferences about the intentions of computer-animated geometric

[1]As we report findings, we use either autism or autism spectrum disorders (ASD) to reflect the author's use. The two terms generally have different qualifications, with ASD typically being a superordinate category that may include autism, Asperger's syndrome, and pervasive developmental disorder.

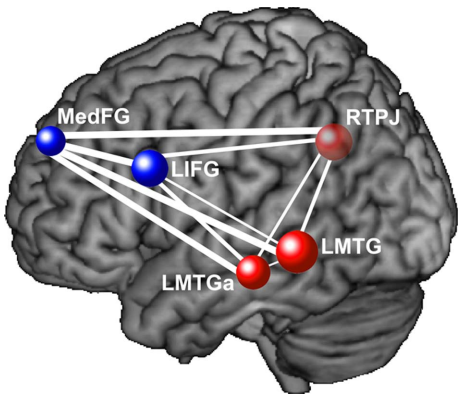


FIGURE 1 | This diagram depicts functional underconnectivity, specifically between frontal and posterior areas, in autism during an inferential text comprehension task. The *width* of each connecting line represents the *t*-value of the *difference in functional connectivity* between the participants with autism and the neurotypical participants. Blue nodes are frontal regions and red nodes are posterior regions. The widest lines (reflecting the greatest group differences) are those connecting frontal and posterior regions. Data from Mason et al. (2008), with permission. MedFG, medial frontal gyrus; LIFG, left inferior frontal gyrus; RTPJ, right temporo-parietal junction; LMTG, left middle temporal gyrus; LMTGa, anterior left middle temporal gyrus.

figures, individuals with autism had lower functional connectivity between frontal and posterior Theory of Mind areas (Kana et al., 2009). In a reading comprehension task with sentences of varying complexity, underconnectivity was found in autism between frontal and posterior areas involved in language comprehension and working memory (Just et al., 2004). In a working memory task with alphabetic characters, lower functional connectivity was reported between frontal and parietal working memory areas (Koshino et al., 2005). In a complex inhibition task, functional connectivity was lower in autism between the frontal inhibition network and the inferior parietal lobe (Kana et al., 2007). In a cognitive control task, lower functional connectivity was reported in ASD between the frontal executive system and several posterior regions in the brain, including parietal working memory areas and the visual cortex (Solomon et al., 2009). In the context of a working memory task with faces and houses (similar to that of Koshino et al., 2008, described above), lowered functional connectivity was found in ASD between the fusiform gyrus and the amygdala (both related to face processing), as well as between the fusiform gyrus and the posterior cingulate (Kleinhans et al., 2008). These studies collectively illustrate that functional underconnectivity has been observed in autism in a wide variety of frontal–posterior pairs. The communication between the members of each of these pairs is necessary for the integration of the multiple cognitive processes required for a given task. These findings support the underconnectivity theory's claim that decreased frontal–posterior connectivity in autism specifically affects behaviors that require the extensive coordinated functioning of frontal and posterior processing centers.

Findings of underconnectivity in autism have also been reported in the absence of task performance, while participants are at rest. Such "resting state" studies offer the advantage of measuring the functional connectivity between different brain regions in spontaneous, naturally occurring patterns of brain activity. Studies of resting state in autism have revealed a "default network" of areas (very similar to the neurotypical default network), which includes the medial prefrontal cortex, anterior and posterior cingulate cortex, the precuneus, and the inferior parietal cortex (Cherkassky et al., 2006). The majority of resting state studies have found decreased functional connectivity in autism in both frontal–posterior pairs and other pairs. Decreased functional connectivity in autism during rest was found in 94% of possible pairs among the default network ROIs, including between the anterior cingulate and the posterior cingulate and precuneus (Cherkassky et al., 2006). In another study, decreased functional connectivity in ASD was found within the task-negative network (medial prefrontal cortex, posterior cingulate, and angular gyrus), but not in the task-positive network (intraparietal sulcus, superior precentral sulcus, and middle temporal gyrus; Kennedy and Courchesne, 2008). Functional connectivity was also found to be lower in ASD between the superior frontal gyrus and the posterior cingulate (Monk et al., 2009). Notably, Monk et al. (2009) found that among posterior regions (involving posterior cingulate, temporal lobe, and parahippocampal gyrus), the functional connectivity was *higher* in ASD, providing a suggestion that connectivity among posterior regions may not only be unaffected in autism, but that there may be compensatory posterior overconnectivity. Decreased functional connectivity was also found in adolescents with ASD between the posterior cingulate and 9 of the 11 other default network regions, including medial prefrontal and superior frontal (Weng et al., 2010). These studies show decreased functional connectivity within the default network in autism while participants are at rest, suggesting that functional underconnectivity in autism is not necessarily dependent on the performance of overt complex cognitive tasks.

As mentioned above, task-independent functional connectivity has also been examined in autism. This method focuses on the synchronization of the task-independent, very low-frequency activation fluctuations that are not related to cognitive processing. It is unclear how this task-independent measure of synchronization is related to disruption of thought in autism. Nevertheless, several such studies have also found functional connectivity differences in autism between frontal and posterior areas. Functional underconnectivity in autism has been reported between the visual cortex and several frontal regions (Villalobos et al., 2005), and lower frontal–posterior connectivity was found in ASD both with and without regressing out task effects in an overt verbal fluency task (Jones et al., 2010). However, there have also been findings of increased frontal–posterior functional connectivity in ASD using this method (Noonan et al., 2009). The findings of atypical task-independent functional connectivity in autism may suggest that even at the biological level, differences are present in this disorder.

FUNCTIONAL CONNECTIVITY IN AUTISM IN PAIRS OTHER THAN FRONTAL–POSTERIOR

Disturbances of functional connectivity in autism have also been reported between pairs of regions other than frontal–posterior pairs, but the findings in such pairs have been less consistent across studies, as shown in **Table 1**. For example, lower functional connectivity in ASD has been reported between the amygdala and temporal and frontal regions (Monk et al., 2010), between the anterior cingulate

Table 1 | Summary of fMRI functional connectivity results.

Task	Pairs of regions	Functional underconnectivity in autism
Task performance	Frontal–posterior pairs	Just et al. (2004, 2007), Koshino et al. (2005, 2008), Kana et al. (2006, 2007, 2009), Kleinhans et al. (2008), Mason et al. (2008), Solomon et al. (2009)
Task performance	Other pairs	Kleinhans et al. (2008), Mostofsky et al. (2009), Agam et al. (2010), Lombardo et al. (2010), Monk et al. (2010)
Resting state	Frontal–posterior pairs	Cherkassky et al. (2006), Kennedy and Courchesne (2008), Monk et al. (2009), Weng et al. (2010)

and frontal eye fields (Agam et al., 2010), within a motor network consisting of primary and supplementary motor areas, anterior cerebellum, and the thalamus (Mostofsky et al., 2009), between the prefrontal cortex and premotor and somatosensory cortices (Lombardo et al., 2010), and between the fusiform gyrus and the amygdala, the posterior cingulate and the cuneus (Kleinhans et al., 2008). Based on activation results, Silk et al. (2006) proposed a disruption in the frontostriatal network in ASD. While these studies all report functional underconnectivity in autism in non-frontal–posterior pairs, the findings vary across a wide variety of pairs of regions and across a large range of tasks, making it difficult to isolate a specific pattern of disturbance. Furthermore, the fact that two studies have reported *increased* functional connectivity in ASD in non-frontal–posterior pairs of areas (Welchew et al., 2005; Monk et al., 2010) further illustrates the variability of functional connectivity findings in autism for pairs of regions other than frontal–posterior pairs.

Functional MRI studies of task-independent functional connectivity have also found group differences in other pairs of areas, often focusing on subcortical regions. Although decreased functional connectivity in autism was reported between the visual cortex and the thalamus and cerebellum (Villalobos et al., 2005), and between the superior frontal gyrus and the caudate (Turner et al., 2006), studies have also found increased connectivity in autism in many pairs involving subcortical regions. Increased functional connectivity in autism was reported between the thalamus and several areas throughout the cortex (Mizuno et al., 2006), as well as between the caudate and many other regions, including frontal regions, the cingulate, and the cuneus (Turner et al., 2006). Increased task-independent functional connectivity in ASD was also reported in frontal–frontal and posterior–posterior pairs (Noonan et al., 2009). The most consistent finding of increased task-independent functional connectivity in autism is in subcortico-cortical pairs. Because this method measures task-independent synchronization, it remains unclear how these findings may be related to the integration of cognitive processes during task performance, although they may suggest differences in autism even at the biological level.

As this section has illustrated, functional connectivity differences in autism have also been found in pairs of areas that are not frontal–posterior, in both task-dependent and task-independent measures. While the majority of studies report lower functional connectivity in autism in these other pairs, some studies have reported increased functional connectivity in autism, most often in subcortico-cortical pairs. It should be noted that all findings of overconnectivity in ASD come from studies using non-standard methods, such as psychophysiological interaction connectivity analysis (Monk et al., 2010), multidimensional scaling (Welchew et al., 2005), and task-independent functional connectivity analyses (Mizuno et al., 2006; Turner et al., 2006; Noonan et al., 2009), and, with the exception of Noonan et al. (2009), all of these studies reported differences in pairs involving the amygdala or subcortical structures. Further research is necessary to determine if these findings of increased functional connectivity in autism reflect unique properties of subcortico-cortical connections in autism. In addition, several studies reported decreased functional connectivity in autism in non-frontal–posterior pairs, but this varied set of findings has yet to illustrate a clear pattern of disturbance. Future research in this area should be able to produce a more complete account of functional connectivity disturbances in autism, using a variety of tasks and measurement methods. It is possible that whatever biological mechanisms lead to frontal–posterior underconnectivity in autism may have also affected other connections, but to a lesser degree or less consistently. It may be that frontal–posterior connections are most strongly affected by the biological disturbance underlying autism, but functional connectivity differences may occasionally appear in any number of other connections.

ALTERNATIVE METHODS OF ASSESSING FUNCTIONAL CONNECTIVITY

Functional connectivity in fMRI data has also been measured with various other techniques. For example, independent component analysis (ICA) identifies temporally coherent networks by selecting spatially independent brain areas whose hemodynamic time courses closely co-vary. ICA is a data-driven method which does not rely on *a priori* ROIs or the performance of a cognitive task. An ICA examination of resting state fMRI data revealed that individuals with ASD had decreased strength of functional connectivity between both the precuneus and the anterior cingulate cortex and a default network consisting of the posterior cingulate cortex, the inferior parietal lobule, and the medial prefrontal cortex (Assaf et al., 2010). Thus, ICA is a novel technique which is producing findings in accordance with previous reports of functional underconnectivity in ASD during resting state (Cherkassky et al., 2006; Kennedy and Courchesne, 2008; Weng et al., 2010).

Another data-driven approach to measuring functional connectivity is the measurement of regional homogeneity (ReHo), which tests for local correlations in fMRI time series. This technique calculates the Kendall's coefficient of concordance (KCC) for each voxel with its neighboring voxels, thereby estimating the local connectivity of every voxel in the brain. While the two existing studies of ReHo in ASD have somewhat divergent results, both find decreased ReHo in young adolescents with ASD in the frontal lobe (Paakki et al., 2010; Shukla et al., 2010). However, while Shukla et al. (2010) also found decreased ReHo in the superior parietal lobule and increased ReHo in the temporal lobe, Paakki et al. (2010) instead found decreased ReHo in right superior temporal sulcus and cerebellum with increased ReHo in the right thalamus, left inferior frontal gyrus/subcallosal gyrus, and cerebellum. These divergent results may stem from methodological differences:

Shukla et al. (2010) calculated ReHo as the KCC of each voxel and its six neighboring voxels, while Paakki et al. (2010) used 27 neighboring voxels. Thus, the two studies may be examining different levels of neuronal organization. Nevertheless, this method may provide new insight into local functional connectivity in ASD, although it is at yet unclear how this measure would relate to long-distance inter-regional functional connectivity. Graph theory is another tool now being used to characterize both functional and anatomical networks in the neurotypical brain (see Bullmore and Sporns, 2009, for a review), and future research may apply these techniques to the investigation of underconnectivity in autism. Many novel techniques are being used to examine characteristics of brain connectivity and have the potential to further illuminate the characteristic properties of the brains of individuals with autism.

Yet another measure that has also shown differences in ASD is effective connectivity (Wicker et al., 2008), a measure that attempts to assess the influence of the activation in one region on the activation in another region (Friston, 1994). Wicker et al. (2008) used structural equation modeling to assess effective connectivity in the BOLD response in a dynamic face processing task. The resulting findings of weaker path coefficients in ASD in many connections with the prefrontal cortex converge with Koshino et al.'s (2008) findings of decreased frontal–posterior functional connectivity in a working memory task with faces, discussed above. A potential contribution of effective connectivity measures seems most likely in cases where there might be a group difference in the inter-regional control relations. However, the activity among association areas may be too interactive to allow detection of differences in inter-regional influence.

Finally, functional connectivity differences in ASD have also been found through other imaging methods, including PET (Castelli et al., 2002), EEG (Murias et al., 2007), and magnetoencephalography (MEG; Coskun et al., 2009). While fMRI and PET measure the blood flow in the brain on the order of seconds, EEG and MEG measure electrical and magnetic signals of neuron firing on the order of milliseconds and, therefore, may reflect properties of brain function that are distinct from those revealed by fMRI data. However, EEG studies have also found reduced long-range coherence in ASD between frontal and posterior areas in both the alpha band (Murias et al., 2007) and the delta band (Barttfeld et al., 2011), as well as elevated short-range coherence in both the theta band (Murias et al., 2007) and the delta band (Barttfeld et al., 2011). Furthermore, Barttfeld et al. (2011) used graph theory metrics to determine that the network of activated brain regions is less well organized in ASD, as reflected by longer path lengths, less clustering, and increased modularity. While the focus of this review is on functional connectivity as measured in fMRI data, current work in EEG is also providing insights into the characteristics of brain connectivity in autism.

ANATOMICAL CONNECTIVITY IN AUTISM

The lower frontal–posterior functional connectivity in autism might be attributable to an impairment in anatomical connectivity. (It is also logically possible for the functional connectivity between two areas to be poor because of the communication protocols rather than the carrier anatomical link.) The anatomical evidence that is most relevant to underconnectivity is that by adulthood, individuals with autism tend to have more poorly developed white matter pathways relative to neurotypical individuals, as described below. Evidence from several neuroimaging methods has also revealed an atypical developmental pattern of cortical connectivity in autism. Individuals with autism show a large increase in white matter growth in very early childhood, followed by a period of relatively slowed growth. There are several sources of evidence of white matter abnormalities in autism that can affect connectivity.

VOLUME MEASUREMENTS OF WHITE MATTER IN AUTISM

Infants who are later diagnosed with ASD show typical brain characteristics at birth, but shortly thereafter show atypically fast brain growth. Based on measurements of head circumference (a rough estimate of brain size), newborns with ASD had slightly smaller head circumferences than typical infants, but then showed an atypically large increase in head size within the first 6–14 months of age, resulting in atypically large head circumferences (Courchesne et al., 2003). Structural MRI measurements of brain volumes have revealed converging evidence of increased volumes in children with autism between the ages of 2 and 4 years in both cerebral gray and white matter. Ninety percent of 2- to 4-year-olds with autism had increased brain volumes in gray and white matter relative to neurotypical children (Courchesne et al., 2001). Greater brain volumes in 2- to 4-year-olds with autism were more pronounced in the frontal lobe, with no differences in the occipital lobe (Carper et al., 2002). Together, these findings suggest that children with autism show atypically rapid increases in frontal gray and white matter in the first 2 years of life.

The pattern of rapid brain growth in autism reverses around age 4, such that children with autism then show a decreased rate of brain growth in white matter from ages 3 to 12 (Courchesne et al., 2001). Neurotypical children showed a 59% increase in white matter volume during this time period, while children with autism showed only a 10% increase. Greater volume of white matter was found, particularly in frontal radiate white matter in 5- to 11-year-olds with autism, as well as volumetric increases and decreases in a number of other regions, indicating the disruption of the white matter (Herbert et al., 2004). The period of slowed growth eventually results in a smaller volume of white matter in adolescents with autism relative to neurotypical adolescents (Courchesne et al., 2001). A similar pattern was found in cortical gray matter. Thus, brain volume measurements have revealed that the rate of brain growth in autism slows after age 4, leading to a decreased volume of white matter in adolescents with autism relative to neurotypical adolescents. Given that white matter is the medium which is used for inter-regional brain communication, it seems incontrovertible that brain connectivity is disrupted in autism.

The presence of a temporary excess of white matter in children with autism does not necessarily denote superior connectivity. These data simply indicate that white matter in the frontal lobe is increasing in volume earlier in children with autism than in neurotypical children. However, the white matter may not be developing properly during its rapid growth in autism. Therefore, it is useful to also examine the quality of white matter in individuals with autism using diffusion tensor imaging.

DIFFUSION TENSOR IMAGING ASSESSMENT OF WHITE MATTER IN AUTISM

Diffusion tensor imaging methods can be used to examine the integrity of white matter tracts in the brain. This technique measures the movement of water molecules as they diffuse along white matter tracts, reflecting characteristics of white matter architecture. An increasing number of studies are finding areas of lower structural integrity in autism.

Children with autism show areas of decreased white matter integrity relative to typically developing children, similar to the developmental pattern reflected in volume measurements of white matter. Fractional anisotropy (FA) is a measure of the coherence of diffusion directionality, such that lower FA suggests decreased white matter integrity. FA was found to be reduced in children and adolescents with autism in white matter adjacent to the prefrontal cortex, the anterior cingulate, and the temporo-parietal junctions (Barnea-Goraly et al., 2004). Lower FA has also been reported in adolescents with autism in frontal–temporal pathways (Sahyoun et al., 2010). Decreased white matter integrity was found in both adolescents and children with ASD in the arcuate fasciculus, which connects frontal and posterior language regions (Fletcher et al., 2010; Kumar et al., 2010). FA was lower in short- but not long-range fibers in the frontal lobe in individuals with ASD as young as 5 (Sundaram et al., 2008). Thus, many studies have shown that older children and adolescents with autism show reduced white matter integrity in the frontal lobe, relative to typically developing children.

However, several studies involving children with ASD of varying age ranges have found areas of not only decreased but also increased FA in ASD (ages 1–3 years old: Ben Bashat et al., 2007; ages 6–14 years old: Cheung et al., 2009; Ke et al., 2009; ages 10–18 years old: Cheng et al., 2010). Such heterogeneous findings might arise because of large variance due to rapid developmental changes in the integrity of white matter in autism during this period of childhood. Despite the inconsistencies of DTI findings in such young children with autism, older children and adolescents with autism consistently show decreased white matter integrity relative to their neurotypical peers.

Decreased white matter integrity in autism has been found to persist into adulthood. Several clusters of decreased FA near the corpus callosum in the frontal and temporal lobes were reported in autism participants between the ages of 10 and 35 (Keller et al., 2007). Lower FA was also reported in individuals with ASD from ages 7 to 33 in the corpus callosum (Alexander et al., 2007) and in the temporal lobe (Lee et al., 2007). Thus, decreased white matter integrity persists into adulthood, possibly constituting the biological basis of the decreased functional connectivity in adults with autism.

It is as yet undetermined how early brain overgrowth in autism may be related to decreased white matter integrity in adulthood. It is noteworthy that early brain overgrowth is greatest in the frontal lobe, while impaired functional connectivity later in life is most prevalent in synchronizations between the frontal lobe and more posterior regions. Evidence of smaller and more numerous cortical minicolumns in autism in the frontal and temporal lobes (Casanova et al., 2002) may suggest an increased formation of short-range connections within these lobes. Such increased short-range connectivity may be the cause or consequence of poor inter-regional connectivity. Future investigation of the molecular origins underlying brain connectivity differences in autism may further illuminate the connectivity phenomena.

RELATING FUNCTIONAL CONNECTIVITY, ANATOMICAL CONNECTIVITY, AND BEHAVIOR IN AUTISM

The underconnectivity theory of autism proposes that anatomical and functional connectivity are related, and that both of these measures should be related to behavior. Findings of correlations across subjects between functional connectivity, anatomical connectivity, and behavior provide support for this hypothesis. In fact, neuroimaging studies have shown evidence of such relations between each of these measures of connectivity and behavior.

RELATING FUNCTIONAL CONNECTIVITY AND BEHAVIOR IN AUTISM

If decreased functional connectivity is truly a neural mechanism underlying behavioral impairments of autism as proposed, one would expect functional connectivity measurements to be related to behavioral markers of autism. Several studies have found a relation between functional connectivity measures and measures of autism characteristics as measured by the Autism Diagnostic Observation Schedule (ADOS) and the Autism Diagnostic Interview-Revised (ADI-R). The ADOS and ADI-R are diagnostic tools that measure behavioral characteristics of autism. The ADOS has subscores for social behavior and communication, which are combined into a total score. The ADI-R has three separate scores for reciprocal social interaction, communication and language, and restricted and repetitive, stereotyped interests and behaviors. Although these measures were developed to optimize their diagnostic rather than their psychometric properties (e.g., the range of scores on these tests is fairly low among people with high-functioning autism), they nevertheless produce sensible correlations with functional and anatomical connectivity measures. One study found that high-functioning individuals with more severe cases of autism (higher total ADOS score) had lower frontal–parietal functional connectivity (Just et al., 2007). Other studies have also shown that individuals with ASD with poorer social functioning (high ADI-R social score) have lower functional connectivity between the superior frontal gyrus and posterior cingulate (Monk et al., 2009; Weng et al., 2010). Lower functional connectivity between frontal structures and the posterior cingulate was found in participants with more severe repetitive behaviors (Weng et al., 2010). These findings suggest that impaired frontal–posterior functional connectivity may be directly related to more severe autistic traits in language, social functioning, and repetitive behaviors.

There have also been reports of increased functional connectivity in non-frontal–posterior pairs in individuals with more severe autistic traits. The higher functional connectivity between posterior regions may develop in some people with autism in compensation for decreased connectivity between frontal and posterior areas, with more such compensation in cases with poorer frontal–posterior connectivity. Adolescents with ASD who had higher functional connectivities within various areas of the default network during rest had lower abilities in both verbal and non-verbal communication (Weng et al., 2010). Higher functional connectivity between the posterior cingulate and the parahippocampal gyrus was associated with more severe repetitive behaviors (Monk et al., 2009), as was higher functional connectivity between the anterior cingulate and the frontal eye fields (Agam et al., 2010).

Individuals with autism with the most impaired inter-regional communication between frontal and posterior areas also show larger behavioral deficits. Thus, if an intervention were able to facilitate the

communication between frontal and posterior processing centers in individuals with autism, this may result in improvements in the behavioral impairments associated with autism.

RELATING ANATOMICAL CONNECTIVITY AND BEHAVIOR IN AUTISM

Studies have also found relations between anatomical connectivity and behavioral markers of autism. Lower FA (lower white matter integrity) was related to more severe disruptions manifested in social function, communication, and repetitive behaviors (as measured by ADI-R scores; Cheung et al., 2009). This finding suggests that decreased anatomical connectivity may lead to greater behavioral impairments in autism. Specifically, decreased integrity in fronto-striato-temporal pathways was related to more impaired social functioning and communication abilities, while decreased integrity in more anterior and posterior pathways, including the splenium of the corpus callosum, was related to more severe repetitive behaviors. Lower FA (specifically in the white matter underlying the anterior cingulate cortex) was also associated with more severe ADI-R repetitive behavior scores (Thakkar et al., 2008). The majority of findings have shown that decreased integrity in white matter tracts is associated with more severe autistic behaviors, suggesting that impaired anatomical connectivity may underlie the behavioral characteristics of autism.

RELATING FUNCTIONAL AND ANATOMICAL CONNECTIVITY IN AUTISM

Several studies have reported correlations between functional connectivity and corpus callosum area measurements in autism. The corpus callosum is a major white matter tract connecting the two hemispheres, and many studies have reported smaller corpus callosum sizes in ASD (Vidal et al., 2006; Hardan et al., 2009; Keary et al., 2009). Although this effect has not always been found at lower magnetic field strengths (0.5–1.5 T: Gaffney et al., 1987; Rice et al., 2005; Tepest et al., 2010), two meta-analyses found that smaller corpus callosum size in ASD is significant across MRI studies (Stanfield et al., 2008; Frazier and Hardan, 2009). Furthermore, magnetic field strength was shown to be a marginally significant predictor of group differences, such that stronger magnets show larger discrepancies in corpus callosum size between ASD and neurotypical participants (Frazier and Hardan, 2009). Because the corpus callosum is such a critical pathway in the brain and is often found to be smaller in autism, corpus callosum size is sometimes used as an index of general anatomical connectivity in the brain. Several studies have found measures of functional connectivity to be positively correlated with corpus callosum size in autism (Cherkassky et al., 2006; Kana et al., 2006; Just et al., 2007; Mason et al., 2008), as illustrated in **Figure 2**. Furthermore, in all of the above studies, this correlation was not found in the control group, suggesting that only in autism is communication between distinct brain areas constrained by impaired anatomical connectivity.

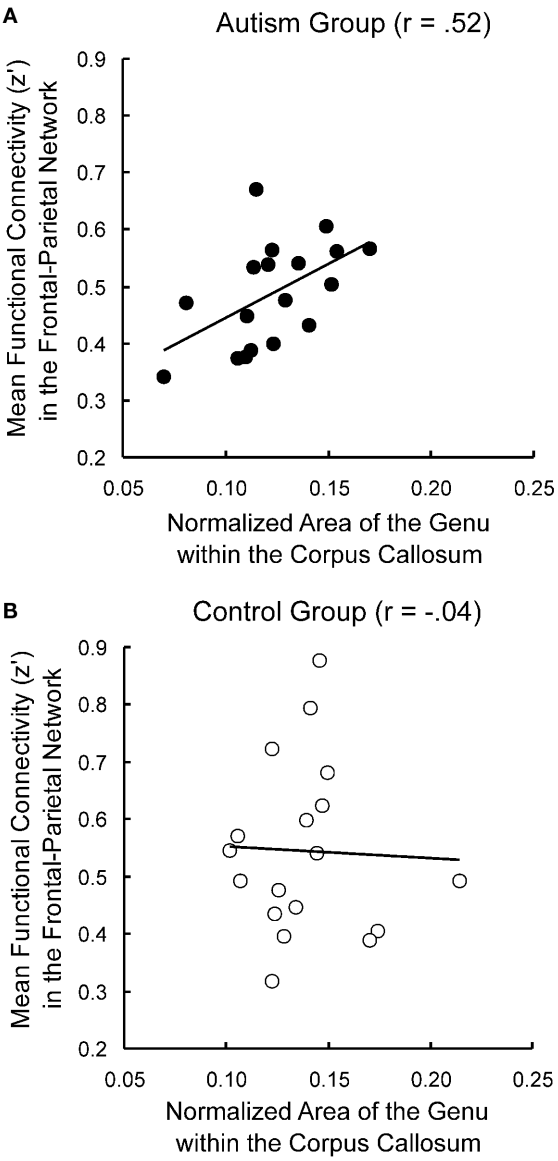


FIGURE 2 | Correlations between functional and anatomical connectivity. Functional connectivity is correlated with corpus callosum size in autism participants **(A)** but not control participants **(B)**. Adapted from Just et al. (2007).

IMPLICATIONS FOR THE TREATMENT OF AUTISM

The body of work described in this article provides substantial evidence that behavioral impairments in autism may be caused by limitations in brain connectivity. These findings suggest that it may be fruitful to develop intervention methods that aim to improve inter-regional communication in the brain in individuals with autism.

Functional MRI evidence has shown that it is possible to observe increases in functional connectivity through learning over a very short time period in neurotypical participants (Büchel et al., 1999). Schipul et al. (2008) examined functional connectivity during learning in autism: participants both with and without autism learned to discriminate between lying and truth-telling avatars (animations of human-like speakers) over the course of a 20-min experiment. The results showed that the functional connectivity increased in both the autism and control groups as they learned to perform the task, but the control participants showed a much larger increase in functional connectivity than the autism participants throughout the brain. These findings suggest that as participants practice a task and learn new strategies, inter-regional communication may increase, perhaps

contributing to improved behavioral performance. Therefore, autism intervention methods that incorporate guided repetition of tasks involving frontal–posterior coordination may be able to temporarily or permanently improve inter-regional brain communication.

White matter connectivity has been shown to be amenable to such intervention. A study of children with impaired reading ability found that after 100 h of intensive remedial instruction in reading, the structural integrity increased in the specific white matter structure that was previously impaired in these children (Keller and Just, 2009). Moreover, the degree of white matter improvement was correlated with the degree of reading improvement. This finding suggests that it is possible to improve the wiring of the brain through behavioral training. Therefore, it may be possible to design intervention methods for autism which will improve the anatomical connectivity and inter-regional communication in the brain, which may lead to improvements in behaviors that are often impaired in autism.

RELATION TO OTHER DISORDERS

Altered functional connectivity has also been found in other disorders, including schizophrenia (Meyer-Lindenberg et al., 2001), attention deficit hyperactivity disorder (Tian et al., 2006), multiple sclerosis (Au Duong et al., 2005), and dyslexia (Pugh et al., 2000). These findings suggest that disordered brain connectivity may underlie a variety of cognitive impairments. While autism is primarily associated with frontal–posterior underconnectivity, preliminary evidence suggests that these other disorders are linked with impairments in other types of connections (Pugh et al., 2000; Meyer-Lindenberg et al., 2001; Au Duong et al., 2005; Tian et al., 2006). Therefore, the location of the impaired connections may be specific to the associated cognitive impairments. For example, dyslexia, which impairs reading, has been associated with underconnectivity between the angular gyrus, an area implicated in reading, and occipital and temporal regions (Pugh et al., 2000). Furthermore, the disordered functional connectivity associated with each of these disorders may arise for different reasons and may be either a cause or a consequence of the disorder. Moreover, the disordered functional connectivity can arise at different times in development: whereas disordered brain connectivity appears in childhood in autism, it may not arise until later in disorders such as schizophrenia, whose symptoms first appear at a much later age than autism. The impairments associated with the various psychiatric disorders include hallucinations, disorganized speech, attention problems, hyperactivity, and reading difficulties, illustrating the wide range of effects that may be associated with disordered brain connectivity. Thus, assessments of functional and anatomical connectivity may be able to provide useful insights into a number of neurological and psychiatric illnesses, but the basis of any connectivity disorder may vary from illness to illness. But regardless of its basis, disordered brain connectivity can give rise to a wide variety of behavioral impairments, indicating the centrality of brain connectivity to all types of cognition.

FUTURE DIRECTIONS

The majority of the functional connectivity studies reviewed above involved adult participants with high-functioning autism. In order to fully explain this disorder, especially in light of the anatomical findings of the atypical development of white matter, it is necessary to examine functional connectivity throughout development. Furthermore, it is also important to include participants with autism across all IQ levels. While it is difficult to collect functional imaging data in the context of complex task performance in young children and individuals with low IQs, it is feasible to collect resting state fMRI data in these populations. It is important that future research determine to what degree underconnectivity applies to different age and IQ ranges within the autism population.

It will also be important for future research to explore the links between functional connectivity and diffusion tensor imaging measures of white matter integrity. Biologically realistic neural models also have great potential to examine the relationship between functional connectivity and anatomical connectivity (Horwitz et al., 2005).

CONCLUSION

Recent findings of atypical patterns in both functional and anatomical connectivity in autism have established that autism is a not a localized neurological disorder, but one that affects many parts of the brain in many types of thinking tasks. fMRI studies repeatedly find evidence of decreased coordination between frontal and posterior brain regions in autism, as measured by functional connectivity. Furthermore, neuroimaging studies have also shown evidence of an atypical pattern of frontal white matter development in autism. These findings indicate that limitations of brain connectivity give rise to the varied behavioral deficits found in autism. As research continues to explore these biological mechanisms, new intervention methods may be developed to help improve brain connectivity and overcome the behavioral impairments of autism.

ACKNOWLEDGMENTS

This work was supported by the Autism Centers of Excellence Grant (HD055748) from the National Institute of Child Health and Human Development; and by the National Institute of Mental Health (Training Grant T32MH019983-11 to Sarah E. Schipul).

REFERENCES

Agam, Y., Joseph, R. M., Barton, J. J., and Manoach, D. S. (2010). Reduced cognitive control of response inhibition by the anterior cingulate cortex in autism spectrum disorders. *Neuroimage* 52, 336–347.

Alexander, A. L., Lee, J. E., Lazar, M., Boudos, R., DuBray, M. B., Oakes, T. R., Miller, J. N., Lu, J., Jeong, E. K., McMahon, W. M., Bigler, E. D., and Lainhart, J. E. (2007). Diffusion tensor imaging of the corpus callosum in autism. *Neuroimage* 34, 61–73.

American Psychiatric Association. (2000). *Diagnostic and Statistical Manual of Mental Disorders*, 4th Edn. Washington, DC: American Psychiatric Association.

Assaf, M., Jagannathan, K., Calhoun, V. D., Miller, L., Stevens, M. C., Sahl, R., O'Boyle, J. G., Schultz, R. T., and Pearlson, G. D. (2010). Abnormal functional connectivity of default mode sub-networks in autism spectrum disorder patients. *Neuroimage* 53, 247–256.

Au Duong, M. V., Audoin, B., Boulanouar, K., Ibarrola, D., Malikova, I., Confort-Gouny, S., Celsis, P., Pelletier, J., Cozzone, P. J., and Ranjeva, J. P. (2005). Altered functional connectivity related to white matter changes inside the working memory network at the very early stage of MS. *J. Cereb. Blood Flow Metab.* 25, 1245–1253.

Barnea-Goraly, N., Kwon, H., Menon, V., Eliez, S., Lotspeich, L., and Reiss, A. L. (2004). White matter structure in autism: preliminary evidence from diffusion tensor imaging. *Biol. Psychiatry* 55, 323–326.

Baron-Cohen, S., Leslie, A. M., and Frith, U. (1985). Does the autistic child have a "theory of mind"? *Cognition* 21, 37–46.

Barttfeld, P., Wicker, B., Cukier, S., Navarta, S., Lew, S., and Sigman, M. (2011).

A big-world network in ASD: dynamical connectivity analysis reflects a deficit in long-range connections and an excess of short-range connections. *Neuropsychologia* 49, 254–263.

Ben Bashat, D., Kronfeld-Duenias, V., Zachor, D. A., Ekstein, P. M., Hendler, T., Tarrasch, R., Even, A., Levy, Y., and Ben Sira, L. (2007). Accelerated maturation of white matter in young children with autism: a high b value DWI study. *Neuroimage* 37, 40–47.

Büchel, C., Coull, J. T., and Friston, K. J. (1999). The predictive value of changes in effective connectivity for human learning. *Science* 283, 1538–1541.

Bullmore, E., and Sporns, O. (2009). Complex brain networks: graph theoretical analysis of structural and functional systems. *Nat. Rev. Neurosci.* 10, 186–198.

Carper, R. A., Moses, P., Tigue, Z. D., and Courchesne, E. (2002). Cerebral lobes in autism: early hyperplasia and abnormal age effects. *Neuroimage* 16, 1038–1051.

Casanova, M. F., Buxhoeveden, D. P., Switala, A. E., and Roy, E. (2002). Minicolumnar pathology in autism. *Neurology* 58, 428–432.

Castelli, F., Frith, C., Happé, F., and Frith, U. (2002). Autism, Asperger syndrome and brain mechanisms for the attribution of mental states to animated shapes. *Brain* 125, 1839–1849.

Cheng, Y., Chou, K. H., Chen, I. Y., Fan, Y. T., Decety, J., and Lin, C. P. (2010). Atypical development of white matter microstructure in adolescents with autism spectrum disorders. *Neuroimage* 50, 873–882.

Cherkassky, V. L., Kana, R. K., Keller, T. A., and Just, M. A. (2006). Functional connectivity in a baseline resting-state network in autism. *Neuroreport* 17, 1687–1690.

Cheung, C., Chua, S. E., Cheung, V., Khong, P. L., Tai, K. S., Wong, T. K., Ho, T. P., and McAlonan, G. M. (2009). White matter fractional anisotrophy differences and correlates of diagnostic symptoms in autism. *J. Child Psychol. Psychiatry* 50, 1102–1112.

Coskun, M. A., Varghese, L., Reddoch, S., Castillo, E. M., Pearson, D. A., Loveland, K. A., Papanicolaou, A. C., and Sheth, B. R. (2009). Increased response variability in autistic brains? *Neuroreport* 20, 1543–1548.

Courchesne, E., Carper, R., and Akshoomoff, N. (2003). Evidence of brain overgrowth in the first year of life in autism. *JAMA* 290, 337–344.

Courchesne, E., Karns, C. M., Davis, H. R., Ziccardi, R., Carper, R. A., Tigue, Z. D., Chisum, H. J., Moses, P., Pierce, K., Lord, C., Lincoln, A. J., Pizzo, S., Schreibman, L., Haas, R. H., Akshoomoff, N. A., and Courchesne, R. Y. (2001). Unusual brain growth patterns in early life in patients with autistic disorder: an MRI study. *Neurology* 57, 245–254.

Di Martino, A., Ross, K., Uddin, L. Q., Sklar, A. B., Castellanos, F. X., and Milham, M. P. (2009). Functional brain correlates of social and nonsocial processes in autism spectrum disorders: an activation likelihood estimation meta-analysis. *Biol. Psychiatry* 65, 63–74.

Fletcher, P. T., Whitaker, R. T., Tao, R., DuBray, M. B., Froehlich, A., Ravichandran, C., Alexander, A. L., Bigler, E. D., Lange, N., and Lainhart, J. E. (2010). Microstructural connectivity of the arcuate fasciculus in adolescents with high-functioning autism. *Neuroimage* 51, 1117–1125.

Frazier, T. W., and Hardan, A. Y. (2009). A meta-analysis of the corpus callosum in autism. *Biol. Psychiatry* 66, 935–941.

Friston, K. J. (1994). Functional and effective connectivity in neuroimaging: a synthesis. *Hum. Brain Mapp.* 2, 56–78.

Frith, U. (1989). *Autism: Explaining the Enigma*. Oxford: Blackwell.

Frith, U., and Happé, F. (1994). Language and communication in autistic disorders. *Philos. Trans. R. Soc. Lond., B, Biol. Sci.* 346, 97–104.

Gaffney, G. R., Kuperman, S., Tsai, L. Y., Minchin, S., and Hassanein, K. M. (1987). Midsagittal magnetic resonance imaging of autism. *Br. J. Psychiatry* 151, 831–833.

Hardan, A. Y., Pabalan, M., Gupta, N., Bansal, R., Melhem, N. M., Fedorov, S., Keshavan, M. S., and Minshew, N. J. (2009). Corpus callosum volume in children with autism. *Psychiatry Res.* 174, 57–61.

Herbert, M. R., Ziegler, D. A., Makris, N., Filipek, P. A., Kemper, T. L., Normandin, J. J., Sanders, H. A., Kennedy, D. N., and Caviness, V. S. Jr. (2004). Localization of white matter volume increase in autism and developmental language disorder. *Ann. Neurol.* 55, 530–540.

Horwitz, B. (2003). The elusive concept of brain connectivity. *Neuroimage* 19, 466–470.

Horwitz, B., Rumsey, J. M., Grady, C. L., and Rapoport, S. I. (1988). The cerebral metabolic landscape in autism: intercorrelations of regional glucose utilization. *Arch. Neurol.* 45, 749–755.

Horwitz, B., Warner, B., Fitzer, J., Tagamets, M. A., Husain, F. T., and Long, T. W. (2005). Investigating the neural basis for functional and effective connectivity. Application to fMRI. *Philos. Trans. R. Soc. Lond., B, Biol. Sci.* 360, 1093–1108.

Jones, T. B., Bandettini, P. A., Kenworthy, L., Case, L. K., Milleville, S. C., Martin, A., and Birn, R. M. (2010). Sources of group differences in functional connectivity: an investigation applied to autism spectrum disorder. *Neuroimage* 49, 401–414.

Just, M. A., Cherkassky, V. L., Keller, T. A., Kana, R. K., and Minshew, N. J. (2007). Functional and anatomical cortical underconnectivity in autism: evidence from an FMRI study of an executive function task and corpus callosum morphometry. *Cereb. Cortex* 17, 951–961.

Just, M. A., Cherkassky, V. L., Keller, T. A., and Minshew, N. J. (2004). Cortical activation and synchronization during sentence comprehension in high-functioning autism: evidence of underconnectivity. *Brain* 127, 1811–1821.

Kana, R. K., Keller, T. A., Cherkassky, V. L., Minshew, N. J., and Just, M. A. (2006). Sentence comprehension in autism: thinking in pictures with decreased functional connectivity. *Brain* 129, 2484–2493.

Kana, R. K., Keller, T. A., Cherkassky, V. L., Minshew, N. J., and Just, M. A. (2009). Atypical frontal–posterior synchronization of theory of mind regions in autism during mental state attribution. *Soc. Neurosci.* 4, 135–152.

Kana, R. K., Keller, T. A., Minshew, N. J., and Just, M. A. (2007). Inhibitory control in high-functioning autism: decreased activation and underconnectivity in inhibition networks. *Biol. Psychiatry* 62, 198–206.

Ke, X., Tang, T., Hong, S., Hang, Y., Zou, B., Li, H., Zhou, Z., Ruan, Z., Lu, Z., Tao, G., and Liu, Y. (2009). White matter impairments in autism, evidence from voxel-based morphometry and diffusion tensor imaging. *Brain Res.* 1265, 171–177.

Keary, C. J., Minshew, N. J., Bansal, R., Goradia, D., Fedorov, S., Keshavan, M. S., and Hardan, A. Y. (2009). Corpus callosum volume and neurocognition in autism. *J. Autism Dev. Disord.* 39, 834–841.

Keller, T. A., and Just, M. A. (2009). Altering cortical connectivity: remediation-induced changes in the white matter of poor readers. *Neuron* 64, 624–631.

Keller, T. A., Kana, R. K., and Just, M. A. (2007). A developmental study of the structural integrity of white matter in autism. *Neuroreport* 18, 23–27.

Kennedy, D. P., and Courchesne, E. (2008). The intrinsic functional organization of the brain is altered in autism. *Neuroimage* 39, 1877–1885.

Kleinhans, N. M., Richards, T., Sterling, L., Stegbauer, K. C., Mahurin, R., Johnson, L. C., Greenson, J., Dawson, G., and Aylward, E. (2008). Abnormal functional connectivity in autism spectrum disorders during face processing. *Brain* 131, 1000–1012.

Koshino, H., Carpenter, P. A., Minshew, N. J., Cherkassky, V. L., Keller, T. A., and Just, M. A. (2005). Functional connectivity in an fMRI working memory task in high-functioning autism. *Neuroimage* 24, 810–821.

Koshino, H., Kana, R. K., Keller, T. A., Cherkassky, V. L., Minshew, N. J., and Just, M. A. (2008). fMRI investigation of working memory for faces in autism: visual coding and underconnectivity with frontal areas. *Cereb. Cortex* 18, 289–300.

Kumar, A., Sundaram, S. K., Sivaswamy, L., Behen, M. E., Makki, M. I., Ager, J., Janisse, J., Chugani, H. T., and Chugani, D. C. (2010). Alterations in frontal lobe tracts and corpus callosum in young children with autism spectrum disorder. *Cereb. Cortex* 20, 2103–2113.

Lee, J. E., Bigler, E. D., Alexander, A. L., Lazar, M., DuBray, M. B., Chung, M. K., Johnson, M., Morgan, J., Miller, J. N., McMahon, W. M., Lu, J., Jeong, E. K., and Lainhart, J. E. (2007). Diffusion tensor imaging of white matter in the superior temporal gyrus and temporal stem in autism. *Neurosci. Lett.* 424, 127–132.

Lombardo, M. V., Chakrabarti, B., Bullmore, E. T., Sadek, S. A., Pasco, G., Wheelwright, S. J., Suckling, J., and Baron-Cohen, S. (2010). Atypical neural self-representation in autism. *Brain* 133, 611–624.

Mason, R. A., Williams, D. L., Kana, R. K., Minshew, N., and Just, M. A. (2008). Theory of mind disruption and recruitment of the right hemisphere during narrative comprehension in autism. *Neuropsychologia* 46, 269–280.

Meyer-Lindenberg, A., Poline, J. B., Kohn, P. D., Holt, J. L., Egan, M. F., Weinberger, D. R., and Berman, K. F. (2001). Evidence for abnormal cortical functional connectivity during working memory in schizophrenia. *Am. J. Psychiatry* 158, 1809–1817.

Minshew, N. J., Goldstein, G., and Siegel, D. J. (1997). Neuropsychologic functioning in autism: profile of a complex information processing disorder. *J. Int. Neuropsychol. Soc.* 3, 303–316.

Mizuno, A., Villalobos, M. E., Davies, M. M., Dahl, B. C., and Muller, R. A. (2006). Partially enhanced thalamocortical functional connectivity in autism. *Brain Res.* 1104, 160–174.

Monk, C. S., Peltier, S. J., Wiggins, J. L., Weng, S. J., Carrasco, M., Risi, S., and Lord, C. (2009). Abnormalities of intrinsic functional connectivity in autism spectrum disorders. *Neuroimage* 47, 764–772.

Monk, C. S., Weng, S. J., Wiggins, J. L., Kurapati, N., Louro, H. M., Carrasco, M., Maslowsky, J., Risi, S., and Lord, C. (2010). Neural circuitry of emotional face processing in autism spectrum disorders. *J. Psychiatry Neurosci.* 35, 105–114.

Mostofsky, S. H., Powell, S. K., Simmonds, D. J., Goldberg, M. C., Caffo, B., and Pekar, J. J. (2009). Decreased connectivity and cerebellar activity in autism during motor task performance. *Brain* 132, 2413–2425.

Mottron, L., and Burack, J. (2001). "Enhanced perceptual functioning in the development of autism," in *The Development of Autism: Perspectives from Theory and Research,* eds J. A. Burack, T. Charman, N. Yirmiya, and P. R. Zelazo (Mahwah, NJ: Erlbaum), 131–148.

Mottron, L., Dawson, M., Soulieres, I., Hubert, B., and Burack, J. A. (2006). Enhanced perceptual functioning in autism: an update, and eight principles of autistic perception. *J. Autism Dev. Disord.* 36, 27–43.

Murias, M., Webb, S. J., Greenson, J., and Dawson, G. (2007). Resting state cortical connectivity reflected in EEG coherence in individuals with autism. *Biol. Psychiatry* 62, 270–273.

Noonan, S. K., Haist, F., and Muller, R. A. (2009). Aberrant functional connectivity in autism: evidence from low-frequency BOLD signal fluctuations. *Brain Res.* 1262, 48–63.

Ozonoff, S., Pennington, B., and Rogers, S. J. (1991). Executive function deficits in high-functioning autistic individuals: relationship to theory of mind. *J. Child Psychol. Psychiatry* 32, 1081–1105.

Paakki, J. J., Rahko, J., Long, X., Moilanen, I., Tervonen, O., Nikkinen, J., Starck, T., Remes, J., Hurtig, T., Haapsamo, H., Jussila, K., Kuusikko-Gauffin, S., Mattila, M. L., Zang, Y., and Kiviniemi, V. (2010). Alterations in regional homogeneity of resting-state brain activity in autism spectrum disorders. *Brain Res.* 1321, 169–179.

Pugh, K. R., Mencl, W. E., Shaywitz, B. A., Shaywitz, S. E., Fulbright, R. K., Constable, R. T., Skudlarski, P., Marchione, K. E., Jenner, A. R., Fletcher, J. M., Liberman, A. M., Shankweiler, D. P., Katz, L., Lacadie, C., and Gore, J. C. (2000). The angular gyrus in developmental dyslexia: task-specific differences in functional connectivity within posterior cortex. *Psychol. Sci.* 11, 51–56.

Rice, S. A., Bigler, E. D., Cleavinger, H. B., Tate, D. F., Sayer, J., McMahon, W., Ozonoff, S., Lu, J., and Lainhart, J. E. (2005). Macrocephaly, corpus callosum morphology, and autism. *J. Child Neurol.* 20, 34–41.

Sahyoun, C. P., Belliveau, J. W., Soulieres, I., Schwartz, S., and Mody, M. (2010). Neuroimaging of the functional and structural networks underlying visuospatial vs. linguistic reasoning in high-functioning autism. *Neuropsychologia* 48, 86–95.

Schipul, S. E., Williams, D. L., Keller, T. A., Kana, R. K., Minshew, N. J., and Just, M. A. (2008). "Learning to detect lies in autism," in *Poster Presented at the International Meeting for Autism Research*, London, UK.

Shukla, D. K., Keehn, B., and Muller, R. A. (2010). Regional homogeneity of fMRI time series in autism spectrum disorders. *Neurosci. Lett.* 476, 46–51.

Silk, T. J., Rinehart, N., Bradshaw, J. L., Tonge, B., Egan, G., O'Boyle, M. W., and Cunnington, R. (2006). Visuospatial processing and the function of prefrontal–parietal networks in autism spectrum disorders: a functional MRI study. *Am. J. Psychiatry* 163, 1440–1443.

Solomon, M., Ozonoff, S. J., Ursu, S., Ravizza, S., Cummings, N., Ly, S., and Carter, C. S. (2009). The neural substrates of cognitive control deficits in autism spectrum disorders. *Neuropsychologia* 47, 2515–2526.

Stanfield, A. C., McIntosh, A. M., Spencer, M. D., Philip, R., Gaur, S., and Lawrie, S. M. (2008). Towards a neuroanatomy of autism: a systematic review and meta-analysis of structural magnetic resonance imaging studies. *Eur. Psychiatry* 23, 289–299.

Sundaram, S. K., Kumar, A., Makki, M. I., Behen, M. E., Chugani, H. T., and Chugani, D. C. (2008). Diffusion tensor imaging of frontal lobe in autism spectrum disorder. *Cereb. Cortex* 18, 2659–2665.

Tepest, R., Jacobi, E., Gawronski, A., Krug, B., Moller-Hartmann, W., Lehnhardt, F. G., and Vogeley, K. (2010). Corpus callosum size in adults with high-functioning autism and the relevance of gender. *Psychiatry Res.* 183, 38–43.

Thakkar, K. N., Polli, F. E., Joseph, R. M., Tuch, D. S., Hadjikhani, N., Barton, J. J., and Manoach, D. S. (2008). Response monitoring, repetitive behaviour and anterior cingulate abnormalities in autism spectrum disorders (ASD). *Brain* 131, 2464–2478.

Tian, L., Jiang, T., Wang, Y., Zang, Y., He, Y., Liang, M., Sui, M., Cao, Q., Hu, S., Peng, M., and Zhuo, Y. (2006). Altered resting-state functional connectivity patterns of anterior cingulate cortex in adolescents with attention deficit hyperactivity disorder. *Neurosci. Lett.* 400, 39–43.

Turner, K. C., Frost, L., Linsenbardt, D., McIlroy, J. R., and Müller, R. A. (2006). Atypically diffuse functional connectivity between caudate nuclei and cerebral cortex in autism. *Behav. Brain Funct.* 2, 34.

Vidal, C. N., Nicolson, R., DeVito, T. J., Hayashi, K. M., Geaga, J. A., Drost, D. J., Williamson, P. C., Rajakumar, N., Sui, Y., Dutton, R. A., Toga, A. W., and Thompson, P. M. (2006). Mapping corpus callosum deficits in autism: an index of aberrant cortical connectivity. *Biol. Psychiatry* 60, 218–225.

Villalobos, M. E., Mizuno, A., Dahl, B. C., Kemmotsu, N., and Muller, R. A. (2005). Reduced functional connectivity between V1 and inferior frontal cortex associated with visuomotor performance in autism. *Neuroimage* 25, 916–925.

Welchew, D. E., Ashwin, C., Berkouk, K., Salvador, R., Suckling, J., Baron-Cohen, S., and Bullmore, E. (2005). Functional disconnectivity of the medial temporal lobe in Asperger's syndrome. *Biol. Psychiatry* 57, 991–998.

Weng, S. J., Wiggins, J. L., Peltier, S. J., Carrasco, M., Risi, S., Lord, C., and Monk, C. S. (2010). Alterations of resting state functional connectivity in the default network in adolescents with autism spectrum disorders. *Brain Res.* 1313, 202–214.

Wicker, B., Fonlupt, P., Hubert, B., Tardif, C., Gepner, B., and Deruelle, C. (2008). Abnormal cerebral effective connectivity during explicit emotional processing in adults with autism spectrum disorder. *Soc. Cogn. Affect. Neurosci.* 3, 135–143.

Conflict of Interest Statement: The authors declare that the research was conducted in the absence of any commercial or financial relationships that could be construed as a potential conflict of interest.

Received: 24 August 2010; accepted: 08 February 2011; published online: 22 February 2011.

Citation: Schipul SE, Keller TA and Just MA (2011) Inter-regional brain communication and its disturbance in autism. Front. Syst. Neurosci. ***5****:10. doi: 10.3389/fnsys.2011.00010*

Copyright © 2011 Schipul, Keller and Just. This is an open-access article subject to an exclusive license agreement between the authors and Frontiers Media SA, which permits unrestricted use, distribution, and reproduction in any medium, provided the original authors and source are credited.

frontiers in
SYSTEMS NEUROSCIENCE

REVIEW ARTICLE
published: 20 December 2010
doi: 10.3389/fnsys.2010.00160

Brain connectivity in pathological and pharmacological coma

Quentin Noirhomme[1*†], Andrea Soddu[1†], Rémy Lehembre[1,2], Audrey Vanhaudenhuyse[1], Pierre Boveroux[1,3], Mélanie Boly[1] and Steven Laureys[1]

[1] *Coma Science Group, Cyclotron Research Centre and Neurology Department, University and University Hospital of Liège, Liège, Belgium*
[2] *Communications and Remote Sensing Laboratory, School of Engineering, Université Catholique de Louvain, Louvain-la-Neuve, Belgium*
[3] *Department of Anesthesiology, University Hospital of Liège, Liège, Belgium*

Edited by:
Silvina G. Horovitz, National Institutes of Health, USA

Reviewed by:
Silvina G. Horovitz, National Institutes of Health, USA
Allen R. Braun, National Institutes of Health, USA

****Correspondence:***
Quentin Noirhomme, Cyclotron Research Centre, University of Liège, Bat B30, Allée du 6 août 8, 4000 Liège, Belgium.
e-mail: quentin.noirhomme@ulg.ac.be

[†]Quentin Noirhomme and Andrea Soddu contributed equally to this work.

Recent studies in patients with disorders of consciousness (DOC) tend to support the view that awareness is not related to activity in a single brain region but to thalamo-cortical connectivity in the frontoparietal network. Functional neuroimaging studies have shown preserved albeit disconnected low-level cortical activation in response to external stimulation in patients in a "vegetative state" or unresponsive wakefulness syndrome. While activation of these "primary" sensory cortices does not necessarily reflect conscious awareness, activation in higher-order associative cortices in minimally conscious state patients seems to herald some residual perceptual awareness. PET studies have identified a metabolic dysfunction in a widespread frontoparietal "global neuronal workspace" in DOC patients including the midline default mode network ("intrinsic" system) and the lateral frontoparietal cortices or "extrinsic system." Recent studies have investigated the relation of awareness to the functional connectivity within intrinsic and extrinsic networks, and with the thalami in both pathological and pharmacological coma. In brain damaged patients, connectivity in all default network areas was found to be non-linearly correlated with the degree of clinical consciousness impairment, ranging from healthy controls and locked-in syndrome to minimally conscious, vegetative, coma, and brain dead patients. Anesthesia-induced loss of consciousness was also shown to correlate with a global decrease in cortico-cortical and thalamo-cortical connectivity in both intrinsic and extrinsic networks, but not in auditory, or visual networks. In anesthesia, unconsciousness was also associated with a loss of cross-modal interactions between networks. These results suggest that conscious awareness critically depends on the functional integrity of thalamo-cortical and cortico-cortical frontoparietal connectivity within and between "intrinsic" and "extrinsic" brain networks.

Keywords: disorders of consciousness, connectivity, anesthesia, fMRI, PET, coma, default mode network, consciousness

INTRODUCTION

Functional brain imaging and particularly fMRI and PET is increasingly showing its interest in the diagnosis (Laureys et al., 2000a; Hirsch, 2005; Schiff et al., 2005; Phillips et al., 2010) and prognosis (Di et al., 2008; Coleman et al., 2009) of patients with disorders of consciousness (DOC). Active paradigms are now enabling to probe patients' awareness and communication by identifying command following independent of muscle activity (Monti et al., 2010). However, besides some exceptional cases, in the absence of a full understanding of the neural correlates of consciousness, even a near-to-normal activation in response to passive stimulation (e.g., auditory, visual, or somatosensory) can be difficult to interpret in terms of unequivocal proofs of consciousness. All that can be inferred is that a specific brain region is, to some degree, still able to activate and process relevant sensory stimuli. Studies on pharmacological coma, i.e., general anesthesia, can help us better understand residual brain functional integration and perception in patients with DOC. Healthy volunteers studied under anesthesia may show residual activation of segregated cortical islands in response to external stimuli (auditory, visual, or somatosensory) encompassing the brainstem, thalamus, and "low-level" primary cortices, similar to findings obtained in unconscious DOC patients. Higher-order areas encompassing lateral and midline frontoparietal networks show no activation in either volunteers under deep anesthesia or in patients in a "vegetative state." At the opposite, patients in minimally conscious state can show activation of the higher-order areas sometimes similar to healthy control subjects (Laureys, 2005).

A common finding of studies on both pathological and pharmacological coma is an impairment in the activity of a widespread cortical network, encompassing bilateral frontoparietal associative cortices, but not of "lower level" sensory cortices (Baars et al., 2003; Alkire and Miller, 2005; Laureys, 2005). As we will see, a decrease in regional activation seems not sufficient to loose awareness but also requires a functional disconnection within that network and with the thalami, in line with a number of current theoretical views on consciousness (Tononi, 2004; Dehaene et al., 2006; Seth et al., 2006).

ALTERED STATES OF CONSCIOUSNESS

Altered states of consciousness here refer to an alteration in the level and content of conscious awareness during to sleep, general anesthesia, seizure or coma, and related states. In the latter case, they are coined DOC and encompass a spectrum of clinical conditions

involving profound disruption in wakefulness and/or awareness due to severe brain lesions (Giacino et al., 2002; Laureys et al., 2004; Bernat, 2006; Schiff, 2006). The clinical definition of consciousness distinguishes between two components, namely wakefulness and awareness (Laureys, 2005). Patients in coma are unconscious because they cannot be awakened (i.e., the never open the eyes). Following coma, some patients may "awaken" (meaning they open the eyes) but remain unaware. This condition is called the "vegetative state" (Jennett and Plum, 1972) recently renamed "unresponsive wakefulness syndrome" (Laureys et al., 2010).

Minimally conscious state refers to patients who are unable to reliably communicate but show reproducible albeit fluctuating behavioral evidence of awareness (i.e., non-reflex movements or command following; Giacino et al., 2002). Locked-in syndrome patients (Plum and Posner, 1972) are fully conscious but are completely paralyzed except for small movements of the eyes or eyelids.

Pharmacologically induced unconscious states are commonly named deep sedation or general anesthesia. All sedative anesthetic agents do not act on the brain in the same way. They can be separated into three main categories: (i) classic anesthetic agents (e.g., propofol, midazolam, halothane, isoflurane, or sevoflurane) are able to induce graded states of sedation and combine alterations of wakefulness and awareness; (ii) dissociative anesthetic agents (e.g., ketamine or nitrous oxide), are able to blunt out conscious processes while maintaining signs of wakefulness; and (iii) minimally sedative agents induce graded alterations of wakefulness while preserving several cognitive brain functions (Boveroux et al., 2008). At low-sedative doses anesthetic agents may cause a state similar to drunkenness and subjects may present an increased sleepiness distorted time perception and depersonalization (Alkire et al., 2008b). Furthermore, they show a reduced response to pain and loss of memory. Next, when the anesthetic dose is increased, the subject will fail to move in response to commands and is therefore considered unconscious. During surgery, higher anesthetic doses are used to prevent movement and response to painful stimulation, also ensuring stable hemodynamic function.

DISCONNECTED ISLANDS OF SENSORY "LOW-LEVEL" CORTICAL ACTIVATION

In response to external stimulation, islands of activation can be observed in the brain of patients with DOC (Laureys et al., 2004; Laureys, 2005; Boly et al., 2008a; Owen and Coleman, 2008), or anesthetized healthy subjects (Alkire and Miller, 2005; Ramani and Wardhan, 2008). Few studies looked at the functional connectivity between these cortical islands and the rest of the brain. PET H_2O^{15} activation studies on auditory processing in patients with DOC using psychophysiological interaction analyses (Friston et al., 1997), showed a higher functional connectivity between auditory sensory cortex and a widespread network of "higher-order" frontotemporoparietal areas in normal volunteers (Laureys et al., 2000a, 2002) and in patients in a minimally conscious state (Boly et al., 2004) as compared to patients in a vegetative/unresponsive state. Similar psychophysiological interaction analyses of noxious processing revealed preserved modulation between primary somatosensory cortex and a large set of associative areas, again including frontoparietal associative areas, in patients in minimally conscious state (Boly et al., 2008a) that was not observed in patients in a vegetative/unresponsive state (Laureys et al., 2002). Compared with healthy controls, patients in minimally conscious state had impaired connectivity between sensory cortex and anterior and posterior midline cortices (Boly et al., 2008a).

Resting state fMRI studies with pharmacologically induced loss of consciousness have shown contrasting results. In a study using midazolam sedation (Greicius et al., 2008), independent component analysis (McKeown and Sejnowski, 1998) was used to isolate sensory-motor, mid-cingulate, and supplementary motor networks. At low-sedative dose without loss of consciousness, the network was still covering both hemispheres and increased connectivity was found in the mid-cingulate area. These results are in line with an fMRI resting state study (Kiviniemi et al., 2005) employing correlation analyses showing increased correlation at low-sedative dose in "low-level" sensory areas. However, a PET study (White and Alkire, 2003) employing higher sedation dose with either halothane or isoflurane leading to loss of consciousness demonstrated (using psychophysiological interaction analyses) a decreased *functional* connectivity between the thalamus and primary motor cortex, and between the thalamus and supplemental motor area. In the same study, a structural equation modeling (assessing *effective* connectivity; McIntosh and Lobaugh, 2004) showed disconnections between supplementary motor and thalamic areas and between the former and primary motor cortex. A fMRI resting state study using sevoflurane anesthesia (again leading to loss of consciousness) and a seed-voxel cross-correlation analysis also showed a decreased connectivity of the primary motor cortex (Peltier et al., 2005). In this study, the activity of the seed region in the primary motor cortex in the awake state correlated with bilateral sensorimotor and supplementary motor areas. When sevoflurane was given upto the point of loss of consciousness, the seed exhibited reduced connectivity with the opposite hemisphere. At higher even doses of the anesthetic, functional connectivity was virtually absent. We recently assessed functional connectivity in auditory and visual networks by means of both independent component and seed-correlation analyses during induced propofol anesthesia using resting state fMRI (Boveroux et al., 2010). When comparing deep sedation to wakefulness, no significant differences in cortico-cortical and thalamo-cortical connectivity could be identified in early visual and auditory networks. On the other hand, we found a linear decrease in cortico-cortical connectivity with the level of sedation of "higher-order" associative areas. Finally, Alkire et al. (2008a), studied the influence of emotion on memory during light sedation with structural equation modeling. During 0.25% sevoflurane anesthesia (a subanesthetic dose), the connections between right hippocampus and amygdala and between right hippocampus and nucleus basalis of Meynert were suppressed, as compared to normal wakefulness.

"HIGHER-ORDER" FRONTOPARIETAL ACTIVATION

A large frontoparietal network encompassing bilateral frontal and temporo-parietal associative cortices has its activity commonly impaired during altered states of consciousness (Baars et al., 2003; Alkire and Miller, 2005; Laureys, 2005) (**Figure 1**). This network can be divided into several parts with distinct functions (Boly et al., 2008b,c; Vanhaudenhuyse et al., 2010a). In particular, a distinction can be made between a network involved in the awareness of

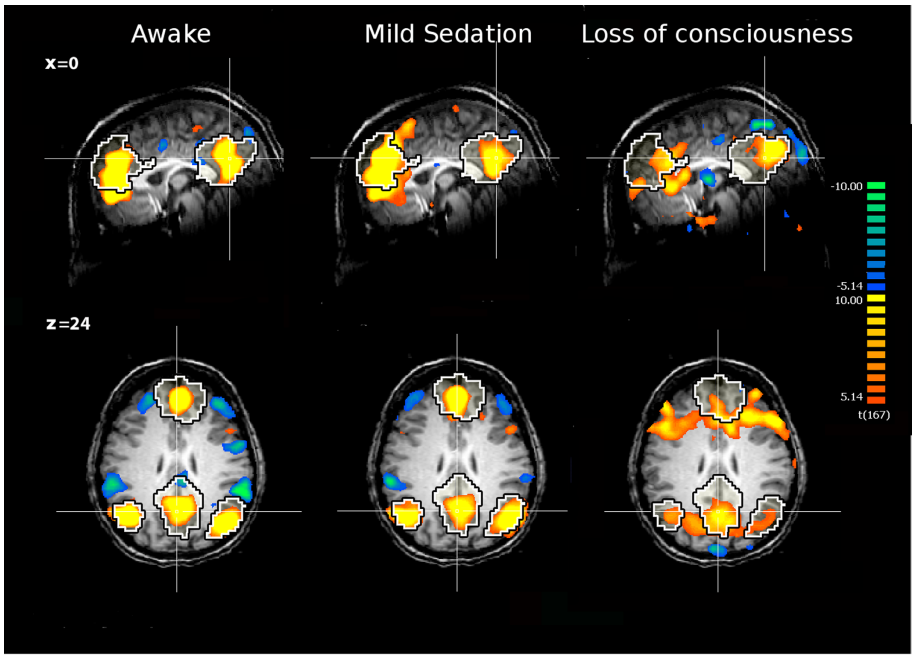


FIGURE 1 | The internal network of a healthy subject awake, under mild sedation and after loss of consciousness. The network was extracted with ICA. The black and white contour represents a template of the internal network extracted from 11 awake healthy subjects with ICA. Yellow and orange colors represent the areas which activities positively correlate with the time course of the internal network. The green and blue colors represent the areas which activities are anticorrelated with activities of the internal network, i.e., the external network. The anticorrelation disappears during deep sedation. The figure is based on data from Boveroux et al. (2010).

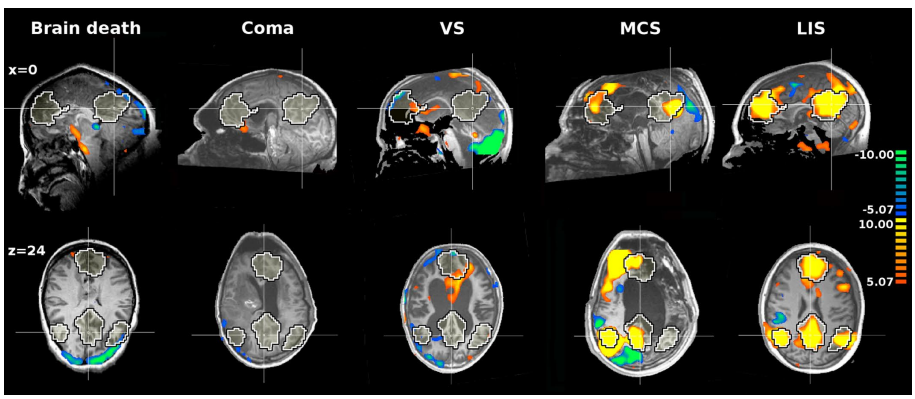


FIGURE 2 | The internal network of patients with brain death, coma, vegetative state (VS), minimally conscious state (MCS), and Locked-in syndrome (LIS). The network was extracted with ICA. The black and white contour represents a template of the internal network extracted from 11 awake healthy subjects with ICA. Yellow and orange colors represent the areas which activities positively correlate with the time course of the internal network. The figure is based on data from Boly et al. (2009) and Vanhaudenhuyse et al. (2010b).

self (the "internal" midline default mode network) encompassing precuneus/posterior cingulate, mesas-frontal/anterior cingulate, and temporo-parietal cortices (Gusnard and Raichle, 2001; Mason et al., 2007) and an "external" more lateral and dorsal frontoparietal network involved in the awareness of environment (Boly et al., 2008b). Activities of both internal and external networks are anticorrelated.

Functional connectivity studies with PET and psychophysiological interaction analyses identified a disturbed cortico-cortical connectivity within the frontoparietal network in patients in vegetative/unresponsive state (Laureys et al., 1999). More recently, fMRI studies on the default/internal network confirmed a decreased cortico-cortical connectivity in patients with DOC (Boly et al., 2009; Cauda et al., 2009; Vanhaudenhuyse et al., 2010b) and an absence of connectivity in brain death (Boly et al., 2009) (**Figure 2**). Paralleling clinical experience, a non-linear correlation was found between this default/"internal" network connectivity and the level of consciousness ranging from healthy volunteers and pseudocoma/locked-in syndrome, to minimally conscious, vegetative/unresponsive, and comatose patients (Vanhaudenhuyse et al., 2010b).

Furthermore, precuneus connectivity was found to be significantly stronger in minimally conscious patients compared to vegetative/unresponsive state patients, while locked-in syndrome patients' default/"internal" network connectivity was shown not to be significantly different from healthy control subjects. Finally, thalamo-cortical connectivity with the higher-order frontoparietal network was only studied in patients in vegetative/unresponsive state with H_2O^{15} PET (Laureys et al., 2000b) where it shown to be severely disturbed and recovered near normal modulation after recovery of consciousness.

Functional connectivity studies during anesthesia reported decreased cortico-cortical connectivity in "internal" (Greicius et al., 2008; Boveroux et al., 2010) and "external" (Boveroux et al., 2010) networks in healthy volunteers during light sedation with either midazolam or propofol. During deep sedation with propofol inducing clinical unconsciousness, partially preserved residual functional connectivity could be identified both in the internal and external networks (**Figure 1**). Across sedation states, functional connectivity strength in key nodes of both networks and in thalamo-cortical connectivity with internal and external networks showed a linear correlation with decreasing consciousness (Boveroux et al., 2010). Finally, anticorrelations between internal and external networks also showed a linear trend and could not be identified during loss of consciousness.

FUTURE DIRECTIONS

In conclusion, PET and fMRI connectivity studies on pathological and pharmacological coma emphasize the two different kinds of brain function that can be encountered during unconsciousness. On one hand, the functional connectivity in "low-level" sensory networks (i.e., auditory, somatosensory, visual, and motor) seems independent of the level and content of consciousness. On the other hand, the connectivity between these primary cortices and "higher-order" associative cortices as well as connectivity inside the nodes of the default/"internal" network show a correlation decreasing consciousness in both coma and anesthesia. Thalamo-cortical connectivity follows the same distinction with preserved connectivity between the thalamus and primary cortices, and impaired connectivity between the thalamus and the default/"internal" and perceptual/"external" networks during states of altered consciousness.

Even when consciousness vanishes, i.e., in vegetative/unresponsive state or anesthesia, residual functional connectivity can be identified in both networks. These results are in line with recent findings in anesthetized monkey (Vincent et al., 2007), and in humans during light and slow wave sleep (Horovitz et al., 2008, 2009). During light sleep, the functional connectivity of the default/"internal" network is partially preserved, while during slow wave sleep, there is a functional disconnection between frontal and parietal nodes of the networks. The preservation of functional connectivity in the absence of consciousness could be seen as reflecting preserved anatomical/structural connections with some degree of basal functional connectivity dissociated from higher cognitive functions as they disappear in brain death (Boly et al., 2009).

Taken together, these findings suggest a two-layer view of resting state fMRI "internal" and "external" network connectivity: one part of the connectivity would persist independently of the level or content of consciousness, and possibly be related to underlying anatomical connectivity (Vincent et al., 2007; Greicius et al., 2009), and the other part being more tightly related to the presence of conscious cognitive processes (Vanhaudenhuyse et al., 2010a,b). fMRI connectivity studies in patients with DOC need to deal with major methodological issues (Soddu et al., 2010). When studying non-collaborative patients, especially patients that show a significantly reduced neuronal activity, the first issue is the possible contamination by artifact and noise sources. Major confounds in fMRI acquisitions and analyses are movement, pulse, and respiration artifacts. Furthermore, patients with pathological alterations of consciousness often suffer from severe diffuse brain injuries leading to extreme brain atrophy and secondary ex-vacuo hydrocephalus (i.e., dilated ventricles) or from major focal lesions resulting in a largely deformed brain. This implies that a spatial normalization procedure is difficult to apply, and the selection of the regions under study becomes difficult and requires visual inspection of an expert eye.

In studies on general anesthesia, a potential bias may be that most studies use relatively low sedation levels. Indeed, most if not all studies use just enough sedative agent to reach unconsciousness. Deeper sedation levels as those used in the operating room probably would result in much more profound functional cerebral disconnections. The use of classical anesthesia as a model for studying human consciousness can also be discussed. Indeed, classical sedative anesthetic agents, as all the ones reviewed in the present paper, decrease both wakefulness and awareness while DOC may present a dissociation between both (e.g., the vegetative or unresponsive syndrome). Dissociative agents have some properties more similar to the latter but also some disadvantages related to the induction of confusion and motor agitation making their use in a scientific setting more difficult. Further studies should investigate brain connectivity changes under these different yet challenging dissociative anesthetic agents such as ketamine or xenon.

From a methodological point of view, most presented studies rely on functional connectivity which measures temporal correlation between cerebral activities in distinct brain areas but cannot infer causality. Effective connectivity methods which can infer causality have been proposed but seldom used in studies on consciousness. They suffer from their higher complexity and from the difficulty to assess causality from the low pass filtered hemodynamic signal in fMRI studies. A more straightforward approach would rely on transcranial magnetic stimulation coupled to electroencephalography (TMS–EEG) to infer effective connectivity from the brain response to a TMS pulse. This perturbation approach has shown promising results in sleep (Massimini et al., 2005) and anesthesia (Ferrarelli et al., 2010). Methods specifically developed to measure consciousness based on the information integration theory (Tononi, 2004) like causal density (Seth, 2005) also used connectivity information but remain difficult to measure (Seth et al., 2008) and have never been applied in these contexts. In our view, the upcoming challenges are to apply effective connectivity approaches to altered states of consciousness aiming to infer causality between brain areas, to integrate hemodynamic and electromagnetic information, and to explain empirical data with theoretical models using specific measures of consciousness.

ACKNOWLEDGMENT

Steven Laureys is Senior Research Associate; Andrea Soddu, Mélanie Boly, Audrey Vanhaudenhuyse, and Quentin Noirhomme are Postdoctoral Fellows at the Fonds de la Recherche Scientifique (FRS). Audrey Vanhaudenhuyse was also funded by French Speaking Community Concerted Research Action (ARC 06/11-340). This work was supported by European Commission (DISCOS, Mindbridge, DECODER, COST), McDonnell Foundation, Mind Science Foundation, FRS, Reine Elisabeth Medical Foundation and University and University Hospital of Liège. The text reflects solely the views of its authors. The European Commission is not liable for any use that may be made of the information contained therein.

REFERENCES

Alkire, M. T., Gruver, R., Miller, J., McReynolds, J. R., Hahn, E. L., and Cahill, L. (2008a). Neuroimaging analysis of an anesthetic gas that blocks human emotional memory. *Proc. Natl. Acad. Sci. U.S.A.* 105, 1722–1727.

Alkire, M. T., Hudetz, A. G., and Tononi, G. (2008b). Consciousness and anesthesia. *Science* 322, 876–880.

Alkire, M. T., and Miller, J. (2005). General anesthesia and the neural correlates of consciousness. *Prog. Brain Res.* 150, 229–244.

Baars, B. J., Ramsoy, T. Z., and Laureys, S. (2003). Brain, conscious experience and the observing self. *Trends Neurosci.* 26, 671–675.

Bernat, J. L. (2006). Chronic disorders of consciousness. *Lancet* 367, 1181–1192.

Boly, M., Faymonville, M. E., Peigneux, P., Lambermont, B., Damas, P., Del Fiore, G., Degueldre, C., Franck, G., Luxen, A., Lamy, M., Moonen, G., Maquet, P., and Laureys, S. (2004). Auditory processing in severely brain injured patients: differences between the minimally conscious state and the persistent vegetative state. *Arch. Neurol.* 61, 233–238.

Boly, M., Faymonville, M. E., Schnakers, C., Peigneux, P., Lambermont, B., Phillips, C., Lancellotti, P., Luxen, A., Lamy, M., Moonen, G., Maquet, P., and Laureys, S. (2008a). Perception of pain in the minimally conscious state with PET activation: an observational study. *Lancet Neurol.* 7, 1013–1020.

Boly, M., Phillips, C., Balteau, E., Schnakers, C., Degueldre, C., Moonen, G., Luxen, A., Peigneux, P., Faymonville, M. E., Maquet, P., and Laureys, S. (2008b). Consciousness and cerebral baseline activity fluctuations. *Hum. Brain Mapp.* 29, 868–874.

Boly, M., Phillips, C., Tshibanda, L., Vanhaudenhuyse, A., Schabus, M., Dang-Vu, T. T., Moonen, G., Hustinx, R., Maquet, P., and Laureys, S. (2008c). Intrinsic brain activity in altered states of consciousness: how conscious is the default mode of brain function? *Ann. N. Y. Acad. Sci.* 1129, 119–129.

Boly, M., Tshibanda, L., Vanhaudenhuyse, A., Noirhomme, Q., Schnakers, C., Ledoux, D., Boveroux, P., Garweg, C., Lambermont, B., Phillips, C., Luxen, A., Moonen, G., Bassetti, C., Maquet, P., and Laureys, S. (2009). Functional connectivity in the default network during resting state is preserved in a vegetative but not in a brain dead patient. *Hum. Brain Mapp.* 30, 2393–2400.

Boveroux, P., Bonhomme, V., Boly, M., Vanhaudenhuyse, A., Maquet, P., and Laureys, S. (2008). Brain function in physiologically, pharmacologically, and pathologically altered states of consciousness. *Int. Anesthesiol. Clin.* 46, 131–146.

Boveroux, P., Vanhaudenhuyse, A., Bruno, M. A., Noirhomme, Q., Lauwick, S., Luxen, A., Degueldre, C., Plenevaux, A., Schnakers, C., Phillips, C., Brichant, J. F., Bonhomme, V., Maquet, P., Greicius, M. D., Laureys, S., and Boly, M. (2010). Breakdown of within- and between-network resting state functional magnetic resonance imaging connectivity during propofol-induced loss of consciousness. *Anesthesiology* 113, 1038–1053.

Cauda, F., Micon, B. M., Sacco, K., Duca, S., D'Agata, F., Geminiani, G., and Canavero, S. (2009). Disrupted intrinsic functional connectivity in the vegetative state. *J. Neurol. Neurosurg. Psychiatr.* 80, 429–431.

Coleman, M. R., Bekinschtein, T., Monti, M. M., Owen, A. M., and Pickard, J. D. (2009). A multimodal approach to the assessment of patients with disorders of consciousness. *Prog. Brain Res.* 177, 231–248.

Dehaene, S., Changeux, J. P., Naccache, L., Sackur, J., and Sergent, C. (2006). Conscious, preconscious, and subliminal processing: a testable taxonomy. *Trends Cogn. Sci.* 10, 204–211.

Di, H., Boly, M., Weng, X., Ledoux, D., and Laureys, S. (2008). Neuroimaging activation studies in the vegetative state: predictors of recovery? *Clin. Med.* 8, 502–507.

Ferrarelli, F., Massimini, M., Sarasso, S., Casali, A., Riedner, B. A., Angelini, G., Tononi, G., and Pearce, R. A. (2010). Breakdown in cortical effective connectivity during midazolam-induced loss of consciousness. *Proc. Natl. Acad. Sci. U.S.A.* 107, 2681–2686.

Friston, K. J., Buechel, C., Fink, G. R., Morris, J., Rolls, E., and Dolan, R. J. (1997). Psychophysiological and modulatory interactions in neuroimaging. *Neuroimage* 6, 218–229.

Giacino, J. T., Ashwal, S., Childs, N., Cranford, R., Jennett, B., Katz, D. I., Kelly, J. P., Rosenberg, J. H., Whyte, J., Zafonte, R. D., and Zasler, N. D. (2002). The minimally conscious state: definition and diagnostic criteria. *Neurology* 58, 349–353.

Greicius, M. D., Kiviniemi, V., Tervonen, O., Vainionpaa, V., Alahuhta, S., Reiss, A. L., and Menon, V. (2008). Persistent default-mode network connectivity during light sedation. *Hum. Brain Mapp.* 29, 839–847.

Greicius, M. D., Supekar, K., Menon, V., and Dougherty, R. F. (2009). Resting-state functional connectivity reflects structural connectivity in the default mode network. *Cereb Cortex* 19, 72–78.

Gusnard, D. A., and Raichle, M. E. (2001). Searching for a baseline: functional imaging and the resting human brain. *Nat. Rev. Neurosci.* 2, 685–694.

Hirsch, J. (2005). Functional neuroimaging during altered states of consciousness: how and what do we measure? *Prog. Brain Res.* 150, 25–43.

Horovitz, S. G., Braun, A. R., Carr, W. S., Picchioni, D., Balkin, T. J., Fukunaga, M., and Duyn, J. H. (2009). Decoupling of the brain's default mode network during deep sleep. *Proc. Natl. Acad. Sci. U.S.A.* 106, 11376–11381.

Horovitz, S. G., Fukunaga, M., de Zwart, J. A., van Gelderen, P., Fulton, S. C., Balkin, T. J., and Duyn, J. H. (2008). Low frequency BOLD fluctuations during resting wakefulness and light sleep: a simultaneous EEG-fMRI study. *Hum. Brain Mapp.* 29, 671–682.

Jennett, B., and Plum, F. (1972). Persistent vegetative state after brain damage. *Lancet* 299, 734–737. (*RN* 35:ICU1-4).

Kiviniemi, V. J., Haanpaa, H., Kantola, J. H., Jauhiainen, J., Vainionpaa, V., Alahuhta, S., and Tervonen, O. (2005). Midazolam sedation increases fluctuation and synchrony of the resting brain BOLD signal. *Magn. Reson. Imaging* 23, 531–537.

Laureys, S. (2005). The neural correlate of (un)awareness: lessons from the vegetative state. *Trends Cogn. Sci.* 9, 556–559.

Laureys, S., Celesia, G. G., Cohadon, F., Lavrijsen, J., León-Carrión, J., Sannita, W. G., Sazbon, L., Schmutzhard, E., von Wild, K. R., Zeman, A., and Dolce, G.; Consciousness tETFoDo. (2010). Unresponsive wakefulness syndrome: a new name for the vegetative state or apallic syndrome. *BMC Med.* 8, 68. doi: 10.1186/1741-7015-8-68

Laureys, S., Faymonville, M. E., Degueldre, C., Fiore, G. D., Damas, P., Lambermont, B., Janssens, N., Aerts, J., Franck, G., Luxen, A., Moonen, G., Lamy, M., and Maquet, P. (2000a). Auditory processing in the vegetative state. *Brain* 123(Pt 8), 1589–1601.

Laureys, S., Faymonville, M. E., Luxen, A., Lamy, M., Franck, G., and Maquet, P. (2000b). Restoration of thalamocortical connectivity after recovery from persistent vegetative state. *Lancet* 355, 1790–1791.

Laureys, S., Faymonville, M. E., Peigneux, P., Damas, P., Lambermont, B., Del Fiore, G., Degueldre, C., Aerts, J., Luxen, A., Franck, G., Lamy, M., Moonen, G., and Maquet, P. (2002). Cortical processing of noxious somatosensory stimuli in the persistent vegetative state. *Neuroimage* 17, 732–741.

Laureys, S., Goldman, S., Phillips, C., Van Bogaert, P., Aerts, J., Luxen, A., Franck, G., and Maquet, P. (1999). Impaired effective cortical connectivity in vegetative state: preliminary investigation using PET. *Neuroimage* 9, 377–382.

Laureys, S., Owen, A. M., and Schiff, N. D. (2004). Brain function in coma, vegetative state, and related disorders. *Lancet Neurol.* 3, 537–546.

Mason, M. F., Norton, M. I., Van Horn, J. D., Wegner, D. M., Grafton, S. T., and Macrae, C. N. (2007). Wandering minds: the default network and stimulus-independent thought. *Science* 315, 393–395.

Massimini, M., Ferrarelli, F., Huber, R., Esser, S. K., Singh, H., and Tononi, G. (2005). Breakdown of cortical effective connectivity during sleep. *Science* 309, 2228–2232.

McIntosh, A. R., and Lobaugh, N. J. (2004). Partial least squares analysis of neuroimaging data: applications and advances. *Neuroimage* 23(Suppl. 1), S250–S263.

McKeown, M. J., and Sejnowski, T. J. (1998). Independent component analysis of fMRI data: examining the assumptions. *Hum. Brain Mapp.* 6, 368–372.

Monti, M. M., Vanhaudenhuyse, A., Coleman, M. R., Boly, M., Pickard, J. D., Tshibanda, L., Owen, A. M., and Laureys, S. (2010). Willful modulation of brain activity in disorders of consciousness. *N. Engl. J. Med.* 362, 579–589.

Owen, A. M., and Coleman, M. R. (2008). Functional neuroimaging of the vegetative state. *Nat. Rev. Neurosci.* 9, 235–243.

Peltier, S. J., Kerssens, C., Hamann, S. B., Sebel, P. S., Byas-Smith, M., and Hu, X. P. (2005). Functional connectivity changes with concentration of sevoflurane anesthesia. *Neuroreport* 16, 285–288.

Phillips, C. L., Bruno, M. A., Maquet, P., Boly, M., Noirhomme, Q., Schnakers, C., Vanhaudenhuyse, A., Bonjean, M., Hustinx, R., Moonen, G., Luxen, A., and Laureys, S. (2010). "Relevance vector machine" consciousness classifier applied to cerebral metabolism of vegetative and locked-in patients. *Neuroimage.* (in press).

Plum, F., and Posner, J. B. (1972). The diagnosis of stupor and coma. *Contemp. Neurol. Ser.* 10, 1–286.

Ramani, R., and Wardhan, R. (2008). Understanding anesthesia through functional imaging. *Curr. Opin. Anaesthesiol.* 21, 530–536.

Schiff, N. D. (2006). Multimodal neuroimaging approaches to disorders of consciousness. *J. Head Trauma Rehabil.* 21, 388–397.

Schiff, N. D., Rodriguez-Moreno, D., Kamal, A., Kim, K. H., Giacino, J. T., Plum, F., and Hirsch, J. (2005). fMRI reveals large-scale network activation in minimally conscious patients. *Neurology* 64, 514–523.

Seth, A. K. (2005). Causal connectivity of evolved neural networks during behavior. *Network* 16, 35–54.

Seth, A. K., Dienes, Z., Cleeremans, A., Overgaard, M., and Pessoa, L. (2008). Measuring consciousness: relating behavioural and neurophysiological approaches. *Trends Cogn. Sci.* 12, 314–321.

Seth, A. K., Izhikevich, E., Reeke, G. N., and Edelman, G. M. (2006). Theories and measures of consciousness: an extended framework. *Proc. Natl. Acad. Sci. U.S.A.* 103, 10799–10804.

Soddu, A., Vanhaudenhuyse, A., Demertzi, A., Bruno, M. A., Tshibanda, L., Di, H., Boly, M., Laureys, S., and Noirhomme, Q. (2010). Resting state activity in patients with disorders of consciousness. *Funct. Neurol.* (in press).

Tononi, G. (2004). An information integration theory of consciousness. *BMC Neurosci.* 5, 42. doi: 10.1186/1471-2202-5-42

Vanhaudenhuyse, A., Demertzi, A., Schabus, M., Noirhomme, Q., Bredart, S., Boly, M., Phillips, C., Soddu, A., Luxen, A., Moonen, G., and Laureys, S. (2010a). Two distinct neuronal networks mediate the awareness of environment and of self. *J. Cogn. Neurosci.* 23, 570–578.

Vanhaudenhuyse, A., Noirhomme, Q., Tshibanda, L. J., Bruno, M. A., Boveroux, P., Schnakers, C., Soddu, A., Perlbarg, V., Ledoux, D., Brichant, J. F., Moonen, G., Maquet, P., Greicius, M. D., Laureys, S., and Boly, M. (2010b). Default network connectivity reflects the level of consciousness in non-communicative brain-damaged patients. *Brain* 133, 161–171.

Vincent, J. L., Patel, G. H., Fox, M. D., Snyder, A. Z., Baker, J. T., Van Essen, D. C., Zempel, J. M., Snyder, L. H., Corbetta, M., and Raichle, M. E. (2007). Intrinsic functional architecture in the anaesthetized monkey brain. *Nature* 447, 83–86.

White, N. S., and Alkire, M. T. (2003). Impaired thalamocortical connectivity in humans during general-anesthetic-induced unconsciousness. *Neuroimage* 19, 402–411.

Conflict of Interest Statement: The authors declare that the research was conducted in the absence of any commercial or financial relationships that could be construed as a potential conflict of interest.

Received: 11 June 2010; accepted: 07 December 2010; published online: 20 December 2010.

Citation: Noirhomme Q, Soddu A, Lehembre R, Vanhaudenhuyse A, Boveroux P, Boly M and Laureys S (2010) Brain connectivity in pathological and pharmacological coma. Front. Syst. Neurosci. ***4****:160. doi: 10.3389/fnsys.2010.00160*

Copyright © 2010 Noirhomme, Soddu, Lehembre, Vanhaudenhuyse, Boveroux, Boly and Laureys. This is an open-access article subject to an exclusive license agreement between the authors and the Frontiers Research Foundation, which permits unrestricted use, distribution, and reproduction in any medium, provided the original authors and source are credited.

frontiers in
SYSTEMS NEUROSCIENCE

REVIEW ARTICLE
published: 16 March 2011
doi: 10.3389/fnsys.2011.00008

Functional connectivity in relation to motor performance and recovery after stroke

Kelly P. Westlake and Srikantan S. Nagarajan*

Biomagnetic Imaging Laboratory, Department of Radiology and Biomedical Imaging, University of California San Francisco, CA, USA

Edited by:
Barry Horwitz, National Institutes of Health, USA

Reviewed by:
Christian Gerloff, University Medical Center Hamburg-Eppendorf, Germany
Cecile Gallea, Hôpital de la Pitié Salpétrière, France

***Correspondence:**
Srikantan S. Nagarajan, Biomagnetic Imaging Laboratory, Department of Radiology and Biomedical Imaging, University of California San Francisco, 513 Parnassus Avenue Suite S362, Box 0628, San Francisco, CA 94143, USA.
e-mail: sri@radiology.ucsf.edu

Plasticity after stroke has traditionally been studied by observing changes only in the spatial distribution and laterality of focal brain activation during affected limb movement. However, neural reorganization is multifaceted and our understanding may be enhanced by examining dynamics of activity within large-scale networks involved in sensorimotor control of the limbs. Here, we review functional connectivity as a promising means of assessing the consequences of a stroke lesion on the transfer of activity within large-scale neural networks. We first provide a brief overview of techniques used to assess functional connectivity in subjects with stroke. Next, we review task-related and resting-state functional connectivity studies that demonstrate a lesion-induced disruption of neural networks, the relationship of the extent of this disruption with motor performance, and the potential for network reorganization in the presence of a stroke lesion. We conclude with suggestions for future research and theories that may enhance the interpretation of changing functional connectivity. Overall findings suggest that a network level assessment provides a useful framework to examine brain reorganization and to potentially better predict behavioral outcomes following stroke.

Keywords: stroke, functional connectivity, brain, recovery of function, neuroimaging, neuroplasticity

INTRODUCTION

Stroke lesions cause neural dysfunction both at the lesion site and in remote brain regions. Historically, reduced neural function of distant, structurally intact regions was thought to be due to edema and increased pressure on the remaining neurons. It was not until 1914 when Constantin von Monakow coined the term diaschisis that disruption in the transfer of information between connected brain regions became more widely acknowledged. He described *diaschisis associative* – cortical dysfunction due to lesions of connected areas within the ipsilesional hemisphere, and *diaschisis commissuralis* – cortical dysfunction due to lesions of the interconnections to the contralesional hemisphere (Von Monakow, 1914). Years later, Geschwind (1965a,b), echoing the ideas of Wernicke (1874), provided further theoretical support for non-local effects of brain lesions with a thorough account of "disconnection syndromes." He contended that the various forms of aphasia, apraxia, and agnosia were the result of anatomical disconnections caused by white matter lesions or lesions of association cortices (i.e., posterior sensory areas). Nevertheless, with a lack of empirical evidence supporting these principles, the prevailing belief for many years was that a reasonable symptomatic explanation could be obtained merely by defining the locus of a lesion, which inversely confirmed the function of that region. Even with the advent of functional neuroimaging, regional shifts of activity have come to define plasticity following stroke and yet still do not sufficiently capture the widely variable recovery of motor function. Therefore, in order to comprehend and treat persistent motor impairments, it appears crucial to move beyond segregated perspectives of brain function and characterize the lesioned brain as an integrated and reorganized functional network.

Recently, the creation of anatomically connected network maps in healthy brains has led to a conceptualization of the impact of lesions in brains affected by stroke. To a certain extent, these models have shown that the unpredictability in functional outcomes may indeed be due to the lesion location (Alstott et al., 2009). However, the reasons extend beyond the localized function of the region and emphasize the importance of whether the lesion occurred at a node of a large-scale brain network and whether it has caused dysfunction at other nodes in the network (Kaiser and Hilgetag, 2004; Honey and Sporns, 2008; Alstott et al., 2009). If at a centralized location, symptoms may be more severe and reflect distributed effects than when the lesion is less centralized, in which case the effects may be largely attributed to the specialized function of the ischemic area (Alstott et al., 2009). Accordingly, recovery of function may depend on the repair and redistribution of activity in structurally intact, yet functionally disconnected nodes of a task-relevant network.

In this review, we aim to explore the subject of functional connectivity, defined as temporal correlations between neural or hemodynamic signals arising from distinct brain regions. We focus on functional connectivity in relation to motor recovery after stroke by providing a synthesis of findings that highlight three important points. First, an ischemic stroke lesion causes disruptions in functional connections to areas remote to the site of the lesion. Second, the intrinsic architecture of the residual functional connections reflects the behavioral consequences of stroke. Third, reorganization within a functional network is possible and plays a key role in the recovery of motor function. We begin with a description of current analysis techniques used to assess functional connectivity after stroke. We then discuss functional networks in a stroke population

as they relate to anatomical substrates, motor task performance, and resting-state paradigms. The final sections shed some light on concerns specific to the relationship of functional connectivity with motor recovery after stroke as well as suggestions for future research. Because motor recovery of the upper extremity is most commonly evaluated in neuroimaging studies, we focus here on the recovery of sensorimotor arm and hand function.

TECHNIQUES FOR ASSESSMENT OF FUNCTIONAL CONNECTIVITY

The synchronous firing of transient neural signals is what functionally binds widely distributed sets of neurons (Singer, 1999). Currently, there is no consensus on the most accurate method of assessing functional connectivity, but in many respects, the temporal resolution (milliseconds) of electroencephalography (EEG) and magnetoencephalography (MEG) is optimal for non-invasively capturing the precise timing of this activity. Changes in the electromagnetic field related to neuronal activity can be acquired over a broad frequency spectrum and spectrally decomposed into distinct frequency bands. Measurements of "coherence" or "phase synchronization" are two techniques that are specific to these two modalities and may be employed to depict the functional coupling between neural populations. Coherence is a technique that evaluates the covariance of the phase and amplitude of oscillations while phase synchronization assesses the precision of neuronal discharges independent of amplitude. Functional connectivity analyses of EEG and MEG data is sometimes performed at the level of sensor correlations which can be difficult to interpret in terms of the underlying brain structures involved. More recently, studies have examined correlations between inferred brain activity obtained by solving the MEG/EEG inverse problem. While these studies allow us to interpret the functional connectivity of underlying brain structures involved, caution must be placed on these findings due to potential confounding effects resulting from the reconstruction algorithms used.

Evaluations of coordinated neural activity have also been derived from covariations of the amplitude and latencies of hemodynamic signals arising from distinct brain regions. Techniques such as fMRI and PET make indirect inferences about neural activity through recordings of alterations in blood oxygen level dependent (BOLD) signals or metabolic activity. In an ischemic brain, the hemodynamic underpinnings of these signals may be confounded and must be cautiously interpreted and appropriately modeled through advanced statistical techniques. Still, in many cases it is possible to define functionally connected nodes within a widespread neural network located remote to the site of the lesion.

The two most commonly applied techniques to measure functional connectivity following stroke are seed-based correlation and component analysis, which can capture both resting and task-based activity in the brain. Seed-based approaches were first introduced by Biswal et al. (1995), who correlated the mean time course of the BOLD signal within a region of interest (in this case, left motor cortex) with the time courses of all other brain voxels. The results indicated correlated brain activity between bihemispheric primary and secondary sensory and motor areas and supplementary cortex even in a resting brain state. To explain this phenomenon, Biswal proposed that the fluctuations in blood oxygenation or flow is a result of functional connectivity between these regions (Biswal et al., 1995). A limitation of this technique, however, is that *a priori* data assumptions are required to define the seed region, which may introduce selection bias. This point becomes particularly relevant following stroke when the focal lesion may cause widespread network changes that can no longer be defined by expected normal distributions. As an alternative to seed-based connectivity, independent component and principal component analysis techniques have been applied (Friston et al., 1993; Calhoun et al., 2001; Beckmann et al., 2005). These statistical approaches evaluate the extent of signal covariance between all voxel (volume element) pairs for the entire voxel matrix of brain space. The resulting set of components account for independent (orthogonal) amounts of variance in the observed data. In terms of functional connectivity, each component represents a spatially distinct functional neural network that is highly intercorrelated.

Other, more advanced techniques that are gaining recognition as a meaningful indices of connectivity are based on graph theory. Within this framework, information processing and propagation is topographically represented by a set of nodes (i.e., brain regions) and links between the nodes (i.e., functional connections; Bullmore and Sporns, 2009). A variety of metrics have been proposed to quantify network structure based on graph theoretic criteria (Gerloff and Hallett, 2010). For instance, networks can be described as either regular, small world, or random based on the number of local connections at each node and the path length between nodes. In general, a small world may be considered optimally efficient, having a high clustering coefficient (i.e., number of local connections) with some long-range connections. On the other hand, a random network demonstrates less clustering and more long-range connections. Thus, by virtue of the distance in which most information must travel, random networks are considered relatively inefficient. The degree of efficiency is one metric that has been used to quantify brain networks and is defined by an inverse relationship with path length (i.e., distance required to go from one network node to another) and a positive relationship to clustering coefficients. By this measure, brain networks are found to be small world. Another popular graph theoretic metric is the degree of centrality. Nodes with a high degree of connections linking it to other nodes of the network are referred to as having high centrality, which elevates the importance of the hub within the overall network. Graph theoretic methods allow us to quantify network structure. While currently many of these measures describe global properties in brain networks, more efforts should be aimed at quantifying localized metrics as a means of probing local network structure.

Techniques described thus far represent *functional connectivity* and must be distinguished from a more recently applied subset of techniques known as *effective connectivity*. While functional connectivity represents two connected regions, effective connectivity depicts the intrinsic or task dependent influences that a particular area exerts over another. Two statistical methods of effective connectivity have been employed to evaluate the impact of stroke lesion and subsequent reorganization patterns (Penny et al., 2004). Dynamic causal modeling is one approach, whereby the brain is treated as a deterministic system in which known external inputs cause changes in neural activity (Marreiros et al., 2008). Accordingly,

neuronal activity is explicitly modeled using direction and timing information. Structural equation modeling is the second technique and is similar in approach to dynamic causal modeling in that it confirms how well a model fits the data, but structural equation modeling assumes that the interactions are instantaneous or driven by an unknown source (Penny et al., 2004). Because only a select number of regions can be included for either dynamic causal modeling or structural equation modeling, it is important to keep in mind that changes may exist in regions outside of the pre-defined model (Mechelli et al., 2002).

Finally, while not considered a measure of functional connectivity *per se*, transcranial magnetic stimulation (TMS) approaches have been employed to probe intra- and intercortical physiology and causal changes in the intrinsic circuits in the brain (Reis et al., 2008). In a stroke population, recent attention has been directed toward the notion of interhemispheric inhibition (IHI) leading from the contralesional to the ipsilesional motor cortex (Dimyan and Cohen, 2010). Within this context, a paired pulse technique is used, whereby a test stimulus over the ipsilesional cortex is preceded by a suprathreshold conditioning stimulus to the contralesional motor cortex. Electromyographic (EMG) electrodes over the muscle of interest then record the resulting modulation of, what is known as, a motor evoked potential (MEP). Another approach used to assess connectivity is known as "jamming" or "virtual lesion," in which trains of repetitive TMS (rTMS) can used to inhibit activity arising from a pre-defined region, such as contralesional M1 or premotor cortex (Johansen-Berg et al., 2002; Lotze et al., 2006). The behavioral effects are simultaneously measured during motor task performance. Therefore, rather than a direct measure of connectivity, inferences about the influential state of cortical connections may be evaluated using TMS. One limitation, however, is that since current is reduced as a function of distance from the TMS stimulation coil, resulting brain stimulation and subsequent IHI or regional inhibition is generally restricted to the cortical level. Also, as with structural equation modeling and seed-based functional connectivity, interpretation of TMS observations only go as far as the pre-defined areas of stimulation/inhibition. By incorporating a thorough understanding of the anatomical underpinnings and important nodes of a functional network, TMS offers an immense potential to provide further insight into brain connectivity and to better guide rehabilitation efforts following stroke.

ANATOMICAL SUBSTRATES OF FUNCTIONAL CONNECTIVITY

It is widely assumed that, for the most part, functional connections reflect neuro-anatomical substrates (Fransson, 2005; Greicius et al., 2009; Honey et al., 2009; van den Heuvel et al., 2009). The strongest correlations of oscillating neural signals are thought to exist between structurally connected regions, while weaker functional ties reflect indirect structural connections (Honey et al., 2009). However, one crucial point to keep in mind is that the nature of the relationship between functional and structural connectivity is far from clear. Current methods used to quantify disrupted neural connections are anatomical tracings such as diffusion tensor imaging (DTI) in conjunction with tractography and high angular resolution diffusion imaging (HARDI) with residual bootstrap q-ball fiber tracking (Stinear et al., 2007; Berman et al., 2008; Schaechter et al., 2009). These techniques provide information about the passive diffusivity of water molecules, which preferentially travel parallel to white matter axonal fiber bundles. Despite the remarkable contribution of these approaches to the recreation of axonal networks within the brain, an ongoing limitation is the uncertainly by which a tract can be delineated (Chung et al., 2006). Water molecules inevitably encounter crossing, merging, or kissing fibers throughout the brain, thereby leading to false positives and false negatives when defining the principal diffusion direction of a given fiber tract. This limitation is particularly true with DTI fiber tracking techniques as opposed to q-ball deterministic or probabilistic tracking that specifically accounts for crossing fibers. Moreover, a common assumption in attempting to predict functional from structural connections is that the relationship will be one to one. Certainly, a direct relationship is possible, but functional connections may also be characterized as one to many or even many to one, which are very difficult to structurally resolve considering that many of these connections involve small and difficult to discern intra- and intercortical connections. Also, because tractography assesses the probability of finding a tract rather than the strength of the connection, results cannot be directly compared to the resulting functional connections, which are defined by strength. Nonetheless, while acknowledging these limitations, there still exists a pronounced need for more directed studies aimed at resolving the implied structure–function relationship in an integrated, multimodal approach. In subjects with stroke, these techniques have mostly been assessed in parallel, which underscores the difficulty in linking the two modes of neural connectivity as a comprehensive depiction of recovery.

To support and understand interhemispheric functional connections apart from DTI techniques, studies of the corpus callosum – the largest connective structure in the brain – provide evidence of a feasible anatomical substrate. While there has been considerable debate on whether the interhemispheric transfer of information is excitatory or inhibitory in healthy controls, the general consensus is that most connections between the two primary motor cortices are inhibitory to maximize the segregation of cross-cortical activity (Ferbert et al., 1992). Another intriguing postulate is that the inhibitory and facilitatory nature of the transcallosal connections may differ depending on the particular dynamics of the task demand. For example, TMS studies of healthy controls found motor preparation to initially be accompanied by inhibition, followed by facilitation immediately prior to movement onset (Murase et al., 2004). Following stroke, the interhemispheric balance may be altered, such that both movement preparation and execution are accompanied by an abnormal persistence of intracortical inhibition on ipsilesional M1 (Murase et al., 2004; Hummel et al., 2009). One question currently being pursued is whether these inhibitory mechanisms are interfering with recovery rather than helping it as was found in some patients with subcortical lesions and moderate to good recovery (Murase et al., 2004; Hummel et al., 2009). As an alternative hypothesis, the contralesional M1 and premotor cortex may be a potentially relevant substrate for recovery. Using single pulse TMS, Johansen-Berg et al. (2002) demonstrated the importance of contralesional premotor cortex in people with profound motor impairments performing a simple reaction time task. As an extension to these findings, Lotze and colleagues used rTMS and a "virtual lesion" approach to demonstrate that the control complex

sequential finger movements in well-recovered subjects relies on the contribution of the contralesional premotor and primary motor cortex. Nevertheless, since TMS studies present a coarse perspective of network function, a better understanding the underlying of functional architecture may enhance interpretation and provide direction as to the most important regions of stimulation.

TASK-BASED CONNECTIVITY

To date, theories of the brain's response to a stroke lesion emphasize extensive changes in localized functional activation patterns during a motor task compared to that of a healthy control population. In general, the response to affected limb movement initially includes a bilateral overactivation in primary and secondary sensorimotor regions. During the process of recovery, a reduction in activation is observed that can either persist in a bilateral distribution or become lateralized toward the perilesional tissue and motor regions of the lesioned hemisphere (Calautti et al., 2001; Ward et al., 2003). Presumably, these changes represent an attempt to maximize the residual cortical output, but the involvement of multiple areas is generally inversely related to recovery. In the event that the ipsilesional primary motor cortex is no longer capable of functional contributions, secondary regions gain importance, and perhaps become a necessary component to sustain further, albeit incomplete, recovery. In this case, cortico-cortico and corticospinal tract are the two primary connections, although the specific contribution of each pathway to motor recovery is still unknown. While the identification of these localized activation patterns has been informative with respect to the recovery process, we now have the analysis tools to deepen the understanding of the underlying neural integration. That is, spatial reorganization implies an underlying network of activity, but the analysis fails to explicitly identify functional connections and, more importantly, the evolution of these connections as a process of recovery.

FUNCTIONAL CONNECTIVITY

Moving beyond investigations of the reorganization of localized neural activations, Seitz et al. (1999) was the first to probe functional network changes induced by a stroke lesion. PET data was collected in seven subjects in the chronic (~6 months) stage after infarction. Subjects were scanned at rest and during performance of finger movement sequences as accurately and fast as possible. Using principal component analysis, results indicated that of the eight principal components representing 80% of PET data variance, two were differentially expressed in controls and subjects with stroke. The first component, deemed, the "lesion-affected" network, was expressed in the absence of task and supported the widespread abnormalities occurring in regions remote to the ischemic core. Specific changes included the ischemic core and perilesional area, as well as contralesional and subcortical structures. The second component was expressed during finger movement and correlated with motor scores acquired within a few days of stroke. Consequently, the authors deemed this component a "recovery-related" network. Of particular interest was the spatial overlay of the lesion-affected and recovery-related networks, which demonstrated similar areas of connectivity in the thalamus and visual association areas. Because the thalamus is an area of visual processing, it is not surprising that these regions fall within an integrated network, but why they are involved in both networks remains unanswered. One intriguing explanation is that remote resting network changes induced by the lesion may, in fact, facilitate motor recovery. However, a relationship between either of these networks and motor performance at the time of imaging (i.e., chronic stage) was not demonstrated, leaving questions as to the relevancy of these connectivity patterns to motor impairments and the process of recovery. Nevertheless, this early study highlighted the potential usefulness of a functional network approach, beyond localization theories, to identify disrupted brain activity following stroke.

Electroencephalography coherence studies during affected hand movement have also shown changes in the patterns of cortical interactions compared to healthy controls, yet still with limited relationship with motor performance. For instance, Strens et al. (2004) recorded brain activity from nine electrodes in 25 subjects in the chronic (1–6 years) post-stroke stage during a 25% maximal handgrip task. Corticocortical coherence was determined in the combined alpha and low beta-frequency bands (9–25 Hz) and averaged across six connectivity groupings: left lateral frontal (three electrode pairs), right lateral frontal (three electrode pairs), left mesiolateral (nine electrode pairs), right mesiolateral (nine electrode pairs), mesial (three electrode pairs), and interhemispheric (nine electrode pairs). Of these regions, coherence was greater in subjects with stroke compared with control subjects during task execution in three connectivity patterns, namely, between ipsilesional mesial (SMA) and lateral frontal region (sensorimotor cortex), over contralesional lateral frontal region (sensorimotor cortex), and over contralesional mesial motor region (SMA). The authors speculated that increased connectivity of mesial and lateral frontal regions related to increased attention to task that, in cases of incomplete recovery, represented a compensatory mechanism. Also of note was that the group differences appear specific to the task execution since no differences were identified during the task preparation phase (Strens et al., 2004). Although these changes were interesting from a connectivity perspective, there was again a general lack of association with motor performance, which may merely reflect the limitations in the EEG coherence metric used to identify cortical changes. Specifically, the authors considered a "hand difference score" representing asymmetries in cortical coherence obtained during affected and unaffected hand movement. Therefore, group differences in the degree of asymmetry may have partially been driven by reorganization of cortical networks during unaffected hand movement as may have arisen through compensatory overuse of this hand. Consequently, interpretation of these results was somewhat confounded and required further research to isolate changes of the affected hand.

Apart from the relatively unknown association with motor performance, one particularly surprising finding of the previous study was the lack of change in interhemispheric connectivity. Given that the commonly observed increased activity of ipsilesional sensorimotor cortex is suggestive of increased output from this region, the authors conducted a follow-up study to further evaluate the interhemispheric coupling (Serrien et al., 2004). Within this study, they also chose to disentangle changes due to movement of the unaffected from those of the affected hand. Using a directed coherence approach, it was observed that, in the low beta-frequency band, information flowed from the contralesional

to the ipsilesional sensorimotor cortex during affected hand movement in less recovered subjects. Directed information flow was also found from mesial to contralesional sensorimotor cortex, again highlighting the importance of SMA as part of a larger network. Thus, in patients with incomplete recovery, the importance of connectivity in the contralesional sensorimotor cortex, possibly acting under the influence of mesial areas is supported in this study. However, whether these integrative effects are facilitatory or inhibitory remained blurred and have since become an important focus of TMS research (Dimyan and Cohen, 2010). Also, it should be kept in mind that the inclusion criteria were primarily based on motor impairment status (i.e., weakness of wrist and finger extensors). As a result, differences in lesion location (cortical, subcortical, left, right), lesion type (ischemic, hemorrhagic), and initial level of severity may have introduced important confounding variables to the connectivity patterns and data interpretation.

In an effort to further clarify network contribution of contralesional primary motor cortex to motor recovery in a very specific patient cohort, Gerloff et al. (2006) employed a multimodal analysis. Eleven subjects with chronic ischemic lesions (1–9 years post-stroke onset) of the left internal capsule and mild to moderate extremity impairments were included. Functional connectivity was assessed using EEG corticocortical coherence during affected finger extension and interpreted using TMS MEP of ipsilesional and contralesional M1. An increase in functional coupling was observed between contralesional motor/premotor cortex and SMA in all frequency bands tested (low alpha 8–10 Hz; high alpha 11–13 Hz; low beta 16–20 Hz, high beta 22–26 Hz) compared to healthy controls. In contrast, reduced connectivity was found between links of ipsilesional motor/premotor cortex with SMA and contralesional motor/premotor cortex in the low beta band. These results largely corroborate findings of Serrien et al. (2004), supporting key connections between SMA and contralesional M1 in subjects with residual motor deficits. Interestingly, TMS applied to contralesional M1 did not induce a motor response of the affected hand, essentially refuting the possibility of compensation through corticospinal commands from this hemisphere, at least in subjects with mild impairments. Gerloff et al. (2006) additionally tested the localization of functional activation using PET during affected hand movement. Without any insight other than a bilateral activation response pattern, the advantages of assessing functional connections over local activations to understand neural changes after stroke were clear. However, although there are benefits to using a multimodal approach to better inform EEG and fMRI functional connectivity, interpretation may be enhanced by considering the directionality of information flow using measures of effective connectivity.

EFFECTIVE CONNECTIVITY

Grefkes and colleagues used fMRI and dynamic causal modeling to identify the impact of subcortical stroke lesions on neural networks during whole hand flexion/extension. Subjects were assessed in the subacute (5–32 weeks) stage of recovery and each demonstrated mild weakness of their hand. During affected hand movement, inhibitory influences from contralesional to ipsilesional M1 were observed that related to the extent of motor impairment (**Figure 1**). Bilateral hand movements were also included and resulted in a reduction in the facilitatory drive leading from ipsilesional M1 to contralesional M1 compared to healthy controls. Moreover, a reduced facilitation was demonstrated from ipsilesional SMA to contralesional M1 that correlated with bilateral hand motor deficit. Even in the absence of task performance, differences in interhemispheric coupling between both SMAs and ipsilesional coupling between SMA and M1 were identified and were suggested as further mechanisms underlying hand motor impairment (Grefkes et al., 2008). While these results corroborated previous TMS studies of IHI during a unimanual motor task, dynamic causal modeling enabled the assessment of the motor network beyond M1. As stated by the authors, these findings may have important implications for treatment. If bilateral arm activities can improve the facilitatory effect of SMA, then promoting activity of contralesional M1 may, in turn, facilitate ipsilesional M1 as seen in healthy controls. Presumably, the facilitatory effect would extend to unimanual movements of the affected hand. Further longitudinal interventions are required to support these hypotheses.

In addition to effective connectivity analysis of the classical motor network, the inclusion of cognitive regions revealed new areas of connectivity after stroke during a bilateral hand task (Walsh et al., 2008). Using fMRI and structural equation modeling, interhemispheric connectivity of prefrontal cortex with ipsilesional SMA was observed in subjects with stroke that was not apparent in healthy controls, suggesting that attention to action or explicit learning may be a key compensatory mechanism following stroke. Clinical implications may initially include the promotion of this mechanism to facilitate SMA and, through interhemispheric connectivity, ipsilesional M1. Later, as recovery ensues, movement may become more implicit such that the activation is again limited to the classical motor network, in the absence of prefrontal input.

Recognizing a need to identify whether pathological changes in connectivity may be reversed through targeted TMS interventions, Grefkes et al. (2010) assessed subjects using fMRI and effective connectivity analysis immediately before and after paired pulse TMS stimulation. Dynamic causal modeling revealed that TMS did indeed induce interhemispheric network changes resulting in reduced suppression from contralesional to ipsilesional M1 during a unimanual affected hand task. These network changes were observed in relation to enhanced motor performance. A bilateral task was additionally evaluated, but because of an overall positive coupling between all motor regions during a bilateral task, network changes during bimanual movements were not observed. In other words, a suppression of contralesional M1 was not indicated in this model and therefore, was not expected to induce changes (Grefkes et al., 2010).

Effective connectivity changes within an extended motor network have also been revealed during motor imagery following stroke. Sharma et al. (2009) evaluated the extent to which motor recovery is associated with network reorganization induced by motor imagery compared to motor execution. fMRI and structural equation modeling were assessed in subjects who were 1 week to 2 years post-stroke. Results revealed differential connectivity patterns in motor imagery and execution networks between subjects with stroke and controls. Specifically, a reduction in the connectivity between ipsilesional SMA and premotor cortex was found in both networks, while only during motor imagery was increased coupling observed between ipsilesional

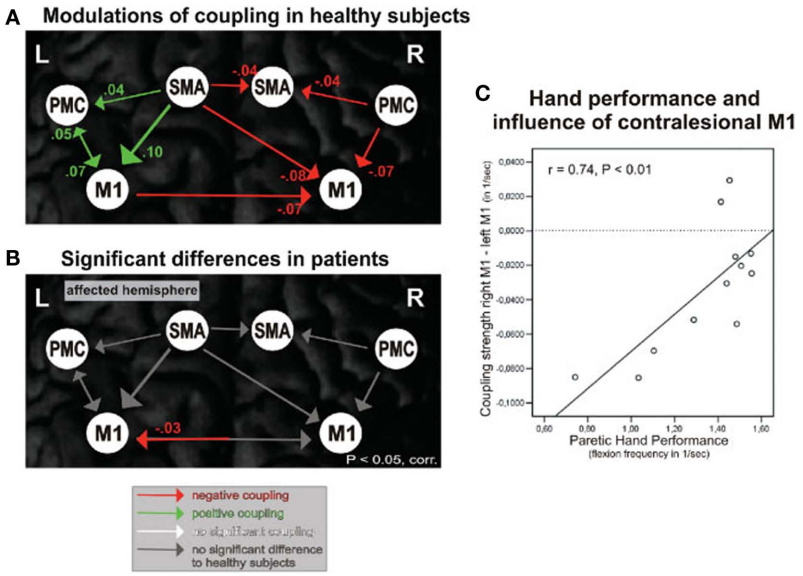


FIGURE 1 | Effective connectivity of motor network during unimanual hand movements. (A) Functional coupling in healthy control subjects during right hand movement. **(B)** Significant differences in functional coupling during affected (right) hand movement between healthy control subjects and subjects with stroke. **(C)** Significant correlation between rate of affected hand movement and strength of inhibitory connections from contralesional M1 to ipsilesional M1. SMA, supplementary motor area; PMC, premotor cortex; M1, Primary motor cortex. Reproduced with permission from Grefkes et al. (2008).

prefrontal and both premotor cortex and SMA. These results are in line with previous work demonstrating the importance of premotor cortex to stroke recovery (Johansen-Berg et al., 2002) and the inhibitory coupling between SMA and M1 in healthy controls (Solodkin et al., 2004). In terms of motor performance, only connectivity within the motor imagery network, and not the motor execution network, was relevant. That is, positive correlations were observed between hand function (assessed following motor imagery) and connectivity from contralesional prefrontal cortex to SMA as well as from ipsilesional prefrontal cortex to premotor cortex. Therefore, increased connectivity with prefrontal cortex may have also facilitated recovery. Negative correlations were identified with connectivity between ipsilesional SMA and premotor cortex. The authors contend that abnormal integration of the prefrontal cortex within the motor network in patients with stroke is due to the important role of this region in motor preparation and planning. In particular, the cognitive rehearsal of the motor planning program that inevitably takes place during motor imagery may be the reason for the increased connectivity in this population. Once again, it should be mentioned that differences between subjects with stroke and controls were not observed using classical analysis of changes in localized functional activations for either task (motor imagery or execution), thereby reinforcing the importance of evaluating motor network changes (Sharma et al., 2009).

In general, the interpretation of the combined findings of these studies is that lesions in one hemisphere cause dysfunctional connections with contralesional motor regions that appear to mediate unimanual and bimanual impairments during hand motor tasks. Evidence is in support of the importance of secondary motor regions, particularly SMA, that influence ipsilesional M1, either directly or indirectly through contralesional motor cortex or ipsilesional premotor cortex. Whether the influence of this region is compensatory due to enhanced attention to task mechanisms or marks true reorganization of the motor network has yet to be resolved.

Despite the potential usefulness of task-based activation studies, at least two important limitations must be considered. First, subjects are typically selected because they are able to perform a standardized task, thereby limiting the generalizability of findings to the function of the particular task and to subjects with moderate to good motor recovery (Dong et al., 2006; Calautti et al., 2007). Second, mirror movements and increased effort are two common occurrences during affected limb movement leading to exaggerated activation of the unaffected hemisphere (Wittenberg et al., 2000; Ward et al., 2007). Although it is clear that lesions induce broad changes within a cortical network or activity, the dependency on task performance in the previously mentioned studies leaves critical uncertainties of the behavioral link. Are these network changes representative of the recovery process and cortical reorganization after stroke or are they merely an epiphenomenon?

RESTING-STATE CONNECTIVITY

Resting-state functional connectivity represents a reliable and promising means of assessing the intrinsic transfer of neural information within a network while avoiding many task-based confounds (Damoiseaux et al., 2006). Although the physiological source of spontaneous activity is unclear, validation studies using fMRI and EEG identified a spectral profile of rhythmic neural activity within a number of functionally relevant networks. For example, neural oscillations within a combination of primarily low frequency bands was found to contribute to the BOLD signal contributing to a sensorimotor network (Mantini et al., 2007; Nir et al., 2008). Moreover, using MEG, regions identified as having the highest density of functional

connections in the alpha "idling" frequency band reflected the high functional demands placed on these regions during daily tasks including somatosensory, visual, and language cortices (Guggisberg et al., 2008). Clearly, because this testing paradigm is not induced by an active task, it allows for an assessment of functional connectivity within multiple neural networks collected during a single experimental session. Equally important is the possibility to overcome many of the limitations of task-based paradigms, particularly as they relate to stroke as mentioned in the previous section. Such intrinsically connected networks have also been proposed as useful biomarkers of sensorimotor impaired brain states such as Parkinson's disease (Stoffers et al., 2008; Wu et al., 2009), amyotrophic lateral sclerosis (Mohammadi et al., 2009), multiple sclerosis (Lowe et al., 2002; Cover et al., 2006), and brain tumors (Guggisberg et al., 2008). Because the concept of resting-state networks as they apply to neurological conditions is still relatively new, only a handful of studies have employed this method to assess the influence of stroke. However, the consensus within these studies is that resting-state connectivity is indeed disturbed by a stroke lesion and the resulting spatial patterns of connectivity are related to functional outcomes.

The sensorimotor resting network, in particular, has proven to be important in understanding motor deficits. Carter et al. (2009) used seed regions within an attention and motor network to evaluate interhemispheric and intrahemispheric connectivity in relation to clinical motor deficits in an acute (9–31 days) stage after stroke. Regions of the motor network included bilateral sensorimotor cortex, SMA, secondary somatosensory cortex, putamen, thalamus, and cerebellum. Results revealed a disruption to interhemispheric functional connectivity of homologous pairs within both networks that correlated with upper extremity impairment. Remarkably, intrahemispheric connectivity, even within the lesioned hemisphere, did not relate to behavioral outcomes. Also, although the focus of this review is on upper extremity impairments, it is worth mentioning that lower extremity deficits and gait impairment were most highly correlated with the attention network rather than the sensorimotor network. This finding is well in line with the clinical observation of the marked difficulty in attending to a secondary task while walking. Thus, the critical point in this study was that the strength of cross-cortical functional connections assessed in the resting brain are related to motor tasks. Equally important is that these results could not be explained by structural damage, since for the most part, the attention and motor networks were outside of the lesion core (Carter et al., 2009).

While the strength of connectivity is one characterizing feature of resting-state functional connectivity, pathological changes may also be quantified by the degree of efficiency in which information flows between connected regions. In a recent longitudinal study, Wang et al. (2010) described dynamic changes in network efficiency using a graph theoretical approach. fMRI data was collected at five post-stroke time points (1 week, 2 weeks, 1 month, 3 months, and 1 year). The primary finding was that changes occurring within a motor network, defined by 21 brain regions, progress toward a random, less optimized network (**Figures 2A,B**). That is, nodes tend to become less clustered and information must travel over longer distances as more time passes from the stroke event. Interestingly, the degree of randomization positively related motor recovery. Though the underlying mechanisms of this process remain unclear, the authors site the possibility of changes occurring on a cellular level that are known to include a random outgrowth of new axonal connections (Kaiser et al., 2009). Regardless of the cause, however, a shift toward random networks is not new to brain pathology and has been shown before in the presence of brain tumors (Bartolomei et al., 2006), Alzheimer's disease (de Haan et al., 2009; Stam et al., 2009), epilepsy (van Dellen et al., 2009), and traumatic brain injury (Nakamura et al., 2009). Therefore, as the authors of this study state, network randomization may represent a final common pathway for many brain pathologies when normal connections are impaired. Further investigations are required to better understand this phenomenon and whether randomization is indeed facilitating recovery or merely hindering the potential for further recovery.

Along with network efficiency changes, the emergence of asymmetries in the importance of centralized "hubs" of connectivity within a motor network appear to be related to the recovery process after stroke. As time post-stroke progresses, Wang and colleagues also report that the greater the degree of centralization within ipsilesional M1 and contralesional cerebellum (dentate nucleus), the better the clinical outcomes, while the inverse was true of the ipsilesional cerebellum and thalamus (**Figure 2C**). Compared to controls, specific regions to which ipsilesional motor cortex demonstrated increased connectivity included contralesional motor cortex, post-central gyrus, and ventrolateral premotor cortex, as well as bilateral dorsolateral premotor cortex. Contralesional cerebellum revealed increased connectivity with ipsilesional ventrolateral premotor cortex. In contrast, regions to which ipsilesional thalamus demonstrated reduced connectivity included bilateral dorsolateral premotor cortex and basal ganglia as well as contralesional SMA. Ipsilesional cerebellum was less connected with contralesional cerebellum and bilateral basal ganglia. Importantly, the notion of increased connectivity within key regions may have critical implications for prognosis and treatment (Wang et al., 2010).

Lesions identified within the above-mentioned centralized hubs of connectivity create models in which lesion location is of high importance and may offer a good predictor of recovery potential. In a sophisticated computational model of known structural connections, Alstott et al. (2009) deleted nodes based on centrality within the theoretical network and effectively predicted non-local brain effects. For example, deletion of nodes within regions of the frontal cortex resulted in particularly large and widespread effects, whereas lesions directly over primary sensory or motor cortices induced smaller, but primarily interhemispheric as opposed to intrahemispheric, disruptions (**Figures 3A,B**). One consideration in employing a network model to predict recovery is the time in which connectivity changes develop, which may depend on the delayed spread of local neural disruption from the lesion site. For instance, the randomization noted by Wang et al. (2010) did not begin to emerge until 10–14 days after stroke, suggesting that a certain amount of time must elapse before the deterioration and reorganization of connections leading to and from remote regions may be statistically captured and used to predict outcomes. This timeline is in contrast to previous stroke predictive markers based on early identification of penumbral size and the extent of Wallerian degeneration of the corticospinal tract (Witte et al., 2000; DeVetten et al., 2010). Since it is well known that early stroke deficits are not

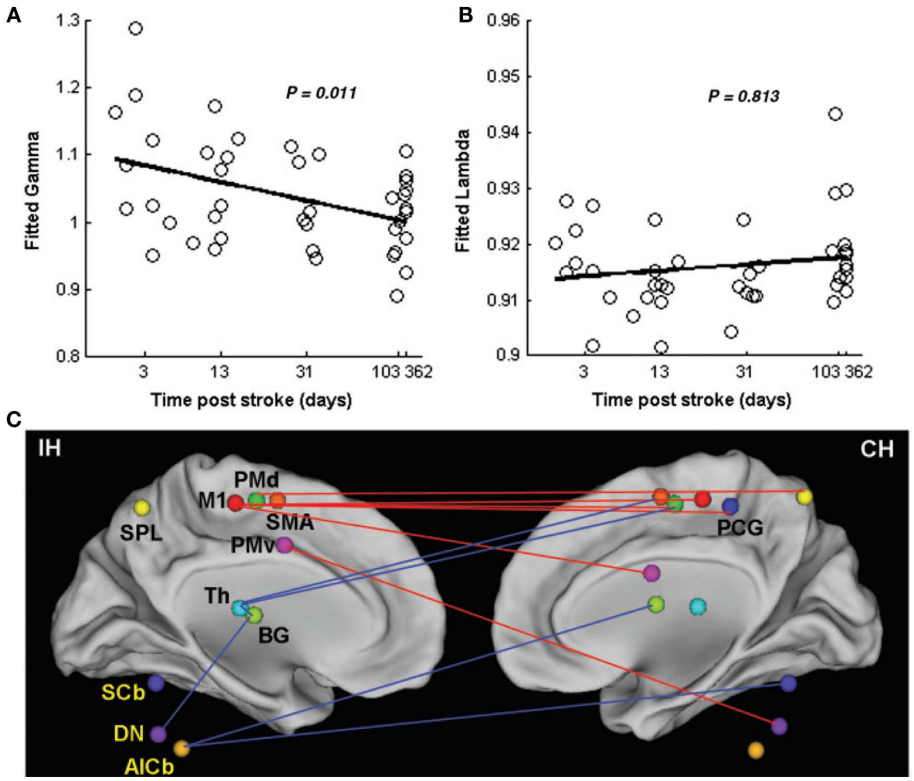


FIGURE 2 | Changes in network efficiency over time post-stroke. (A) Significant negative correlation between clustering coefficients (fitted gamma) and time post-stroke represents shift toward a random network configuration. **(B)** Non-significant positive correlation between the shortest path length (fitted lambda) and time post-stroke **(C)** Connectivity parameters between nodes of the motor network. Increased connectivity (red lines) are primarily seen as interhemispheric connections between M1 and contralesional sensorimotor regions. Reduced connectivity (blue lines) is mainly found in ipsilesional subcortical areas and cerebellum. IH, ipsilesional hemisphere; CH, contralesional hemisphere; M1, primary motor cortex; PCG, post-central gyrus; PMd, dorsolateral premotor cortex; PMv, ventrolateral premotor cortex; SMA, supplementary motor area; Th, thalamus; BG, basal ganglia; SPL, superior parietal lobule; SCb, superior cerebellum; DN, dentate nucleus; AICb, anterior inferior cerebellum. Reprinted with permission (Wang et al., 2010).

representative of eventual outcomes, it may be that the delays in network changes are at least one of the mechanisms accounting for further damage or repair.

Because functional resting-state networks appear to represent the foundation of neural activity, the possibility to induce change through rehabilitation is an intriguing concept. In a recent study, James et al. (2009) used fMRI and structural equation modeling to assess whether a novel intervention could alter the driving influences of connectivity within a resting motor network in subjects in the subacute stage (34–55 days) after stroke (**Figure 4**). The intervention followed a task specific training protocol including repetitive, goal-directed movements of the affected upper extremity at a dose of 2 h per day, 5 days per week, for 3 weeks. The structural equation modeling analysis included anatomically defined regions of bilateral primary motor cortices, lateral dorsal premotor cortices, and SMA. Following treatment, an increased influence of ipsilesional premotor cortex on contralesional premotor cortex was observed that positively related to improvements in motor performance. In contrast, a control subject with stroke who did not receive the intervention, demonstrated the reverse pattern: contralesional premotor cortex influenced ipsilesional premotor cortex. An intrahemispheric influence of ipsilesional premotor on M1 was also found in four subjects within the intervention group. Interestingly, the two subjects who improved the most as a result of the intervention were the only subjects to demonstrate an increased influence of SMA on ipsilesional premotor cortex, which then indirectly influenced ipsilesional M1. Although the different types and location of stroke included in this study may have confounded the results, these findings highlight the potential for asymmetrical reorganization to occur in relation to recovery after stroke rather than a return to the symmetrical connections seen in healthy controls (James et al., 2009).

As with task-based paradigms, limitations in resting-state approaches also exist. For example, recent TMS data with simultaneous motor task suggest that network activity is modulated from rest to executed movement. At this point, it remains unclear whether these changes are comparable between subjects with stroke and healthy controls. For resting-state analyses, these findings open several questions that have yet to be resolved. That is, precisely what information can we gain from resting-state activity that extends beyond knowledge of structural anatomy? How is "resting-state" defined? What is the consistent set of instructions that should be provided to all subjects (i.e., "Be free of thought?" "Eyes open or closed?"). Until a consensus is reached on the resting-state paradigm, comparisons across studies must be cautiously interpreted.

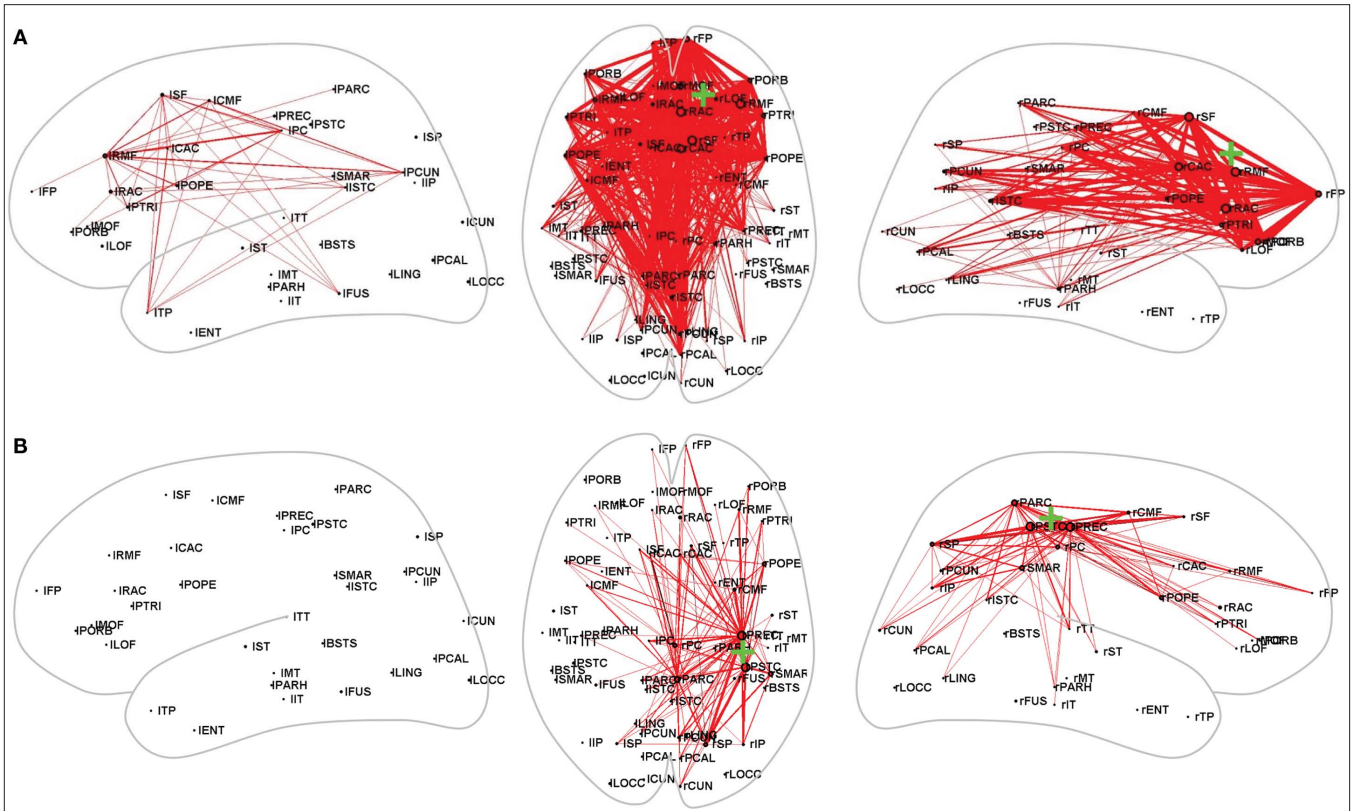


FIGURE 3 | Computational modulations in connectivity resulting from lesions in (A) Frontal cortex and (B) Sensorimotor cortex. Red lines indicate increased strength in connectivity. Note the widespread disruption caused by a lesion in the prefrontal cortex compared with the relatively constrained, intrahemispheric changes resulting from a lesion of the sensorimotor cortex. Reproduced with permission from Alstott et al. (2009).

NOTES ON MEASUREMENT OF RECOVERY

One of the surprisingly understated considerations in any study of the neural substrates of stroke recovery is the definition of recovery. Clearly, the choice of the clinical outcome by which recovery is judged and, in turn, used to interpret changes in brain connectivity patterns is tremendously important. Unfortunately, a familiar limitation of clinical outcome scales is that they often do not capture true motor recovery inasmuch as they capture compensatory changes at the behavioral level (Levin et al., 2009). To overcome these limitations and to generate an overall impression of recovery, it is recommended that either a composite score based on several outcome measures (Ward et al., 2003) or kinematic and kinetic variables should be employed. Moreover, since hemiparesis is generally more severe in the distal musculature, and less severe in the proximal musculature (Colebatch and Gandevia, 1989), evaluation of recovery should consider hand movement in isolation (i.e., grip) and in combination with proximal upper extremity movement (i.e., reach). In doing so, differential recovery of both grasp and reaching, if present, will be captured. If clinical scales are used, redundancy can be avoided by including data reduction techniques such as principal component analysis (Strens et al., 2004; Chouinard et al., 2006). For example, Strens et al. (2004) assessed subjects using a range of eight outcome measures. A principle component factor analysis revealed that only two principal components were required to adequately describe 82% of the total variance. The first component was evenly distributed across the eight outcome measures, reflecting global disability. The second component was found to reflect scores describing hand and upper limb function (Strens et al., 2004). In general, during these early investigations of stroke-related recovery patterns, the challenge will be to adequately model motor performance to best derive meaning from the relationship with functional connectivity. Just because behavioral correlations of a selected group of outcomes did not correlate does not mean a behavioral relationship does not exists with other, potentially more meaningful motor outcomes.

Loss of motor control of the so-called "unaffected" upper or lower extremity should also be considered. Given that a lesion may affect a bilaterally distributed motor network, it seems plausible that the ipsilateral limb may be affected. A handful of studies have evaluated this possibility with kinetic and kinematic measures and demonstrated bilateral impairment in grasp following unilateral subcortical stroke (Quaney et al., 2005; Nowak et al., 2007). At least two possible mechanisms account for these bilateral deficits. The first is that a subcortical lesion may damage the small percentage of ipsilesional descending corticospinal tract fibers. The second possibility is that a unilateral lesion-affected the inhibitory balance between the two homologous motor cortices. Consequently, these deficits must be taken into account when evaluating and interpreting the behavioral correlates of changes in widespread brain networks.

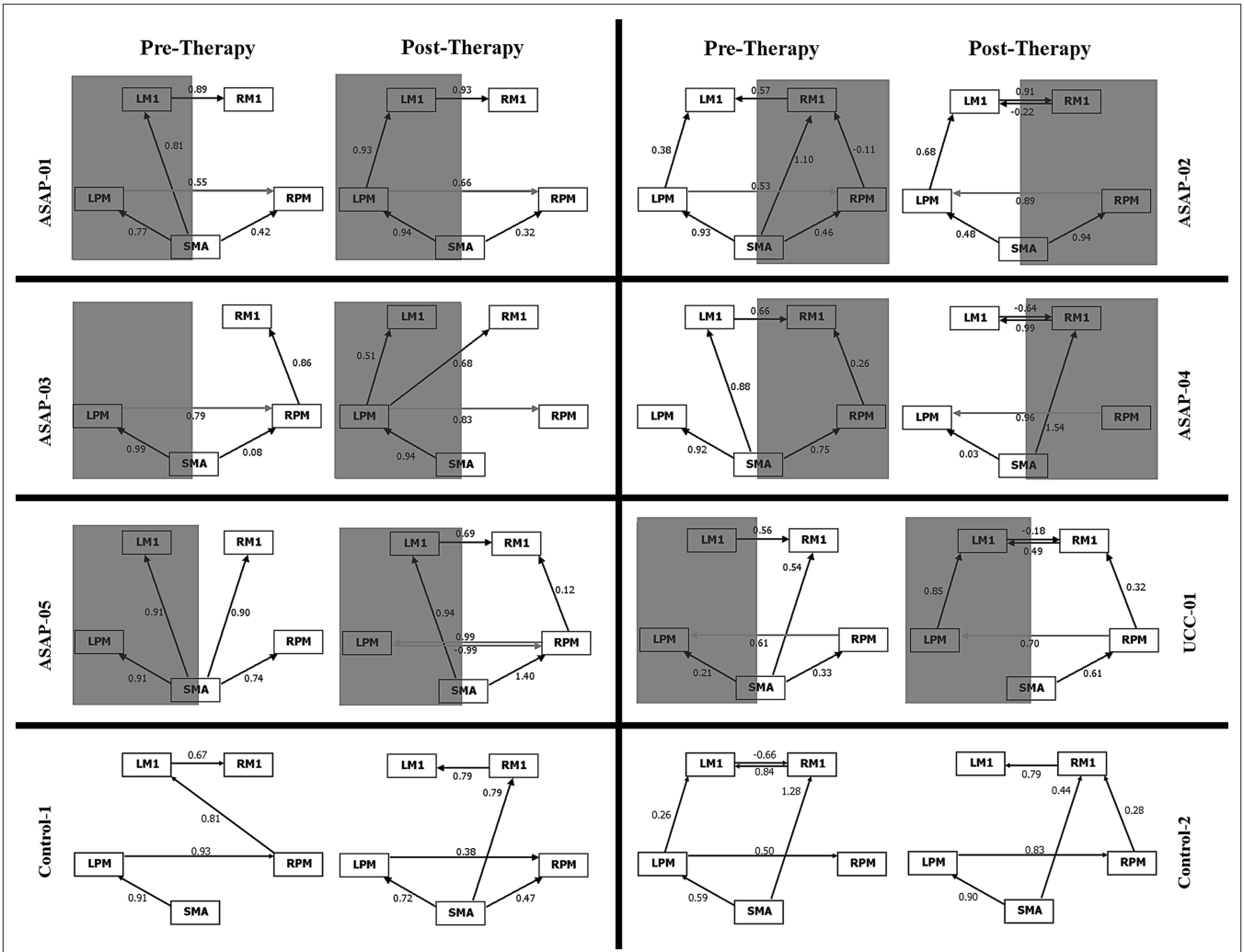


FIGURE 4 | Effective connectivity within the motor network pre and post TMS intervention. Gray shading indicates lesioned hemisphere. Numbers above each line correspond to the strength of the path coefficient. ASAP, training group; UCC, usual care subject; Control, healthy control; LM1, left primary motor cortex; RM1, right primary motor cortex; LPM, left premotor cortex; RPM, premotor cortex; SMA, supplementary motor area. Reproduced with permission from James et al. (2009). Thomas Land Publishers, Inc.

Besides adequately defining clinical outcome, capturing motor recovery also necessitates that a change in motor skill is measured. Therefore, while cross sectional designs are useful to determine the association between patterns of neural connectivity and the extent of motor control, only a longitudinal assessment will truly define the changes in neural connectivity associated with recovery. This point has been made clear in studies evaluating focal activation data (Ward et al., 2003) and now needs to be applied to connectivity data.

Finally, when evaluating functional networks during task performance across a group of subjects or at sequential time points, it is essential to control the amount of effort exerted during the task. For example, asking patients and control populations to reproduce a small percent of their maximal effort will help to match the initial performance level of all subjects. Otherwise, a fixed maximal level of exertion will inevitably overestimate changes associated with recovery (Ward et al., 2007).

WHAT IS NEXT?

The distributed impairments of connected neural systems after a stroke lesion will likely have widespread implications for clinical neuroscience. Clearly, with the relatively sparse number of studies evaluating stroke recovery from a neural network perspective, more research is needed. At this point, it remains unclear whether differences in functional connectivity between control subjects and subjects with stroke are related to adaptive or maladaptive brain reorganization, motor performance compensation, or if they are merely an epiphenomenon such as the release of the contralesional hemisphere from suppression of the ipsilesional hemisphere (Strens et al., 2004).

Overall, with a growing body of literature to support a functional connectivity approach, it is crucial that future research continue to expand the understanding of the spectrum of changes occurring in the brain after stroke. In this capacity, investigations of lesion-induced network plasticity are anticipated to challenge current

frameworks of post-stroke rehabilitation such that patient stratification may be enhanced to maximize motor performance. Current models of stroke intervention are primarily based on behavioral status. Within the proposed recovery framework, predictions of a patient's capacity to achieve motor gains after stroke will instead be based on a more precise understanding of the neurophysiological underpinnings and, in turn, present a more accurate portrait of recovery. Unique advantages and limitations of individual imaging approaches suggest a multimodal assessment of functional connectivity as the best approach to assess this framework. Findings may then be integrated with results of structural connectivity analysis, and even genetic factors of motor learning such as BDNF and COMT, to create a powerful combination of complementary techniques to best depict the interruption and subsequent reorganization of neural networks after stroke.

In summary, neurological deficits after a focal stroke lesion not only reflect local dysfunction at the site of injury, but are also determined by the distributed impairment of connected neural systems. To a large extent, the evidence in support of functional and effective connectivity underlying clinical symptoms enables the reconciliation of previous localized neuroimaging findings with known anatomical connections of sensorimotor function. The notion of hemispheric competition and the potentially negative influence of the contralesional motor cortex on ipsilesional cortex requires further investigation within this framework. Nonetheless, evaluations of the positive and negative influences acting upon each node of an extended motor network is emerging as an essential technique in the study of motor recovery. Modulation of neural interactions, either through TMS, physical therapy, or pharmacological interventions, may then be directly targeted so that increasingly favorable outcomes may ensue.

ACKNOWLEDGMENTS

Funded by NIH grants RO1 DC4855, DC6435, DC10145, NS67962, NS64060, and by NSF grant BCS-0926196 (Srikantan S. Nagarajan); American Heart Association (Kelly P. Westlake); and Canadian Institutes of Health Research (postdoctoral fellowship to Kelly P. Westlake).

REFERENCES

Alstott, J., Breakspear, M., Hagmann, P., Cammoun, L., and Sporns, O. (2009). Modeling the impact of lesions in the human brain. *PLoS Comput. Biol.* 5, e1000408. doi: 10.1371/journal.pcbi.1000408

Bartolomei, F., Bosma, I., Klein, M., Baayen, J. C., Reijneveld, J. C., Postma, T. J., Heimans, J. J., van Dijk, B. W., de Munck, J. C., de Jongh, A., Cover, K. S., and Stam, C. J. (2006). Disturbed functional connectivity in brain tumour patients: evaluation by graph analysis of synchronization matrices. *Clin. Neurophysiol.* 117, 2039–2049.

Beckmann, C. F., DeLuca, M., Devlin, J. T., and Smith, S. M. (2005). Investigations into resting-state connectivity using independent component analysis. *Philos. Trans. R. Soc. Lond. B Biol. Sci.* 360, 1001–1013.

Berman, J. I., Chung, S., Mukherjee, P., Hess, C. P., Han, E. T., and Henry, R. G. (2008). Probabilistic streamline q-ball tractography using the residual bootstrap. *Neuroimage* 39, 215–222.

Biswal, B., Yetkin, F. Z., Haughton, V. M., and Hyde, J. S. (1995). Functional connectivity in the motor cortex of resting human brain using echo-planar MRI. *Magn. Reson. Med.* 34, 537–541.

Bullmore, E., and Sporns, O. (2009). Complex brain networks: graph theoretical analysis of structural and functional systems. *Nat. Rev. Neurosci.* 10, 186–198.

Calautti, C., Leroy, F., Guincestre, J. Y., Marie, R. M., and Baron, J. C. (2001). Sequential activation brain mapping after subcortical stroke: changes in hemispheric balance and recovery. *Neuroreport* 12, 3883–3886.

Calautti, C., Naccarato, M., Jones, P. S., Sharma, N., Day, D. D., Carpenter, A. T., Bullmore, E. T., Warburton, E. A., and Baron, J. C. (2007). The relationship between motor deficit and hemisphere activation balance after stroke: a 3T fMRI study. *Neuroimage* 34, 322–331.

Calhoun, V. D., Adali, T., Pearlson, G. D., and Pekar, J. J. (2001). Spatial and temporal independent component analysis of functional MRI data containing a pair of task-related waveforms. *Hum. Brain Mapp.* 13, 43–53.

Carter, A., S. V., A., Lang, C. E., Connor , L. T., Rengachary, J., Strube, M. J., Pope, D. L., Shulman, G. L., and Corbett, M. (2009). Resting state inter-hemispheric fMRI connectivity predicts performance after stroke. *Ann. Neurol.* 67, 365–375.

Chouinard, P. A., Leonard, G., and Paus, T. (2006). Changes in effective connectivity of the primary motor cortex in stroke patients after rehabilitative therapy. *Exp. Neurol.* 201, 375–387.

Chung, S., Lu, Y., and Henry, R. G. (2006). Comparison of bootstrap approaches for estimation of uncertainties of DTI parameters. *Neuroimage* 33, 531–541.

Colebatch, J. G., and Gandevia, S. C. (1989). The distribution of muscular weakness in upper motor neuron lesions affecting the arm. *Brain* 112(Pt 3), 749–763.

Cover, K. S., Vrenken, H., Geurts, J. J., van Oosten, B. W., Jelles, B., Polman, C. H., Stam, C. J., and van Dijk, B. W. (2006). Multiple sclerosis patients show a highly significant decrease in alpha band interhemispheric synchronization measured using MEG. *Neuroimage* 29, 783–788.

Damoiseaux, J. S., Rombouts, S. A., Barkhof, F., Scheltens, P., Stam, C. J., Smith, S. M., and Beckmann, C. F. (2006). Consistent resting-state networks across healthy subjects. *Proc. Natl. Acad. Sci. U.S.A.* 103, 13848–13853.

de Haan, W., Pijnenburg, Y. A., Strijers, R. L., van der Made, Y., van der Flier, W. M., Scheltens, P., and Stam, C. J. (2009). Functional neural network analysis in frontotemporal dementia and Alzheimer's disease using EEG and graph theory. *BMC Neurosci.* 10, 101. doi: 10.1186/1471-2202-10-101

DeVetten, G., Coutts, S. B., Hill, M. D., Goyal, M., Eesa, M., O'Brien, B., Demchuk, A. M., and Kirton, A. (2010). Acute corticospinal tract Wallerian degeneration is associated with stroke outcome. *Stroke* 41, 751–756.

Dimyan, M. A., and Cohen, L. G. (2010). Contribution of transcranial magnetic stimulation to the understanding of functional recovery mechanisms after stroke. *Neurorehabil. Neural Repair* 24, 125–135.

Dong, Y., Dobkin, B. H., Cen, S. Y., Wu, A. D., and Winstein, C. J. (2006). Motor cortex activation during treatment may predict therapeutic gains in paretic hand function after stroke. *Stroke* 37, 1552–1555.

Ferbert, A., Priori, A., Rothwell, J. C., Day, B. L., Colebatch, J. G., and Marsden, C. D. (1992). Interhemispheric inhibition of the human motor cortex. *J. Physiol.* 453, 525–546.

Fransson, P. (2005). Spontaneous low-frequency BOLD signal fluctuations: an fMRI investigation of the resting-state default mode of brain function hypothesis. *Hum. Brain Mapp.* 26, 15–29.

Friston, K. J., Frith, C. D., Liddle, P. F., and Frackowiak, R. S. (1993). Functional connectivity: the principal-component analysis of large (PET) data sets. *J. Cereb. Blood Flow Metab.* 13, 5–14.

Gerloff, C., Bushara, K., Sailer, A., Wassermann, E. M., Chen, R., Matsuoka, T., Waldvogel, D., Wittenberg, G. F., Ishii, K., Cohen, L. G., and Hallett, M. (2006). Multimodal imaging of brain reorganization in motor areas of the contralesional hemisphere of well recovered patients after capsular stroke. *Brain* 129(Pt 3), 791–808.

Gerloff, C., and Hallett, M. (2010). Big news from small world networks after stroke. *Brain* 133(Pt 4), 952–955.

Geschwind, N. (1965a). Disconnexion syndromes in animals and man. I. *Brain* 88, 237–294.

Geschwind, N. (1965b). Disconnexion syndromes in animals and man. II. *Brain* 88, 585–544.

Grefkes, C., Nowak, D.A. , Eickhoff, S. B., Dafotakis, M., Kust, J., Karbe, H., and Fink, G. R. (2008). Cortical connectivity after subcortical stroke assessed with functional magnetic resonance imaging. *Ann. Neurol.* 63, 236–246.

Grefkes, C., Nowak, D. A., Wang, L. E., Dafotakis, M., Eickhoff, S. B., and Fink, G. R. (2010). Modulating cortical connectivity in stroke patients by rTMS assessed with fMRI and dynamic causal modeling. *Neuroimage* 50, 233–242.

Greicius, M. D., Supekar, K., Menon, V., and Dougherty, R. F. (2009). Resting-state functional connectivity reflects structural connectivity in the default mode network. *Cereb. Cortex* 19, 72–78.

Guggisberg, A. G ., Honma, S. M., Findlay, A. M., Dalal, S. S., Kirsch, H. E., Berger, M. S., and Nagarajan, S. S (2008). Mapping functional connectivity in patients with brain lesions. *Ann. Neurol.* 63, 193–203.

Honey, C. J., and Sporns, O. (2008). Dynamical consequences of lesions in cortical networks. *Hum. Brain Mapp.* 29, 802–809.

Honey, C. J., Sporns, O., Cammoun, L., Gigandet, X., Thiran, J. P., Meuli, R., and Hagmann, P. (2009). Predicting human resting-state functional connectivity from structural connectivity. *Proc. Natl. Acad. Sci. U.S.A.* 106, 2035–2040.

Hummel, F. C., Steven, B., Hoppe, J., Heise, K., Thomalla, G., Cohen, L. G., and Gerloff, C. (2009). Deficient intracortical inhibition (SICI) during movement preparation after chronic stroke. *Neurology* 72, 1766–1772.

James, G. A., Lu, Z. L., VanMeter, J. W., Sathian, K., Hu, X. P., and Butler, A. J. (2009). Changes in resting state effective connectivity in the motor network following rehabilitation of upper extremity poststroke paresis. *Top. Stroke. Rehabil.* 16, 270–281.

Johansen-Berg, H., Rushworth, M. F., Bogdanovic, M. D., Kischka, U., Wimalaratna, S., and Matthews, P. M. (2002). The role of ipsilateral premotor cortex in hand movement after stroke. *Proc. Natl. Acad. Sci. U.S.A.* 99, 14518–14523.

Kaiser, M., and Hilgetag, C. C. (2004). Edge vulnerability in neural and metabolic networks. *Biol. Cybern.* 90, 311–317.

Kaiser, M., Hilgetag, C. C., and van Ooyen, A. (2009). A simple rule for axon outgrowth and synaptic competition generates realistic connection lengths and filling fractions. *Cereb. Cortex* 19, 3001–3010.

Levin, M. F., Kleim, J. A., and Wolf, S. L. (2009). What do motor "recovery" and "compensation" mean in patients following stroke? *Neurorehabil. Neural Repair* 23, 313–319.

Lotze, M., Markert, J., Sauseng, P., Hoppe, J., Plewnia, C., and Gerloff, C. (2006). The role of multiple contralesional motor areas for complex hand movements after internal capsular lesion. *J. Neurosci.* 26, 6096–6102.

Lowe, M. J., Phillips, M. D., Lurito, J. T., Mattson, D., Dzemidzic, M., and Mathews, V. P. (2002). Multiple sclerosis: low-frequency temporal blood oxygen level-dependent fluctuations indicate reduced functional connectivity initial results. *Radiology* 224, 184–192.

Mantini, D., Perrucci, M. G., Del Gratta, C., Romani, G. L., and Corbetta, M. (2007). Electrophysiological signatures of resting state networks in the human brain. *Proc. Natl. Acad. Sci. U.S.A.* 104, 13170–13175.

Marreiros, A. C., Kiebel, S. J., and Friston, K. J. (2008). Dynamic causal modelling for fMRI: a two-state model. *Neuroimage* 39, 269–278.

Mechelli, A., Penny, W. D., Price, C. J., Gitelman, D. R., and Friston, K. J. (2002). Effective connectivity and intersubject variability: using a multisubject network to test differences and commonalities. *Neuroimage* 17, 1459–1469.

Mohammadi, B., Kollewe, K., Samii, A., Krampfl, K., Dengler, R., and Munte, T. F. (2009). Changes of resting state brain networks in amyotrophic lateral sclerosis. *Exp. Neurol.* 217, 147–153.

Murase, N., Duque, J., Mazzocchio, R., and Cohen, L. G. (2004). Influence of interhemispheric interactions on motor function in chronic stroke. *Ann. Neurol.* 55, 400–409.

Nakamura, T., Hillary, F. G., and Biswal, B. B. (2009). Resting network plasticity following brain injury. *PLoS ONE* 4, e8220. doi: 10.1371/journal.pone.0008220

Nir, Y., Mukamel, R., Dinstein, I., Privman, E., Harel, M., Fisch, L., Gelbard-Sagiv, H., Kipervasser, S., Andelman, F., Neufeld, M. Y., Kramer, U., Arieli, A., Fried, I., and Malach, R. (2008). Interhemispheric correlations of slow spontaneous neuronal fluctuations revealed in human sensory cortex. *Nat. Neurosci.* 11, 1100–1108.

Nowak, D. A., Grefkes, C., Dafotakis, M., Kust, J., Karbe, H., and Fink, G. R. (2007). Dexterity is impaired at both hands following unilateral subcortical middle cerebral artery stroke. *Eur. J. Neurosci.* 25, 3173–3184.

Penny, W. D., Stephan, K. E., Mechelli, A., and Friston, K. J. (2004). Modelling functional integration: a comparison of structural equation and dynamic causal models. *Neuroimage* 23(Suppl. 1), S264–S274.

Quaney, B. M., Perera, S., Maletsky, R., Luchies, C. W., and Nudo, R. J. (2005). Impaired grip force modulation in the ipsilesional hand after unilateral middle cerebral artery stroke. *Neurorehabil. Neural Repair* 19, 338–349.

Reis, J., Swayne, O.B ., Vandermeeren, Y., Camus, M., Dimyan, M. A., Harris-Love, M., Perez, M. A., Ragert, P., Rothwell, J. C., and Cohen, L. G. (2008). Contribution of transcranial magnetic stimulation to the understanding of cortical mechanisms involved in motor control. *J. Physiol.* 586, 325–351.

Schaechter, J. D., Fricker, Z. P., Perdue, K. L., Helmer, K. G., Vangel, M. G., Greve, D. N., and Makris, N. (2009). Microstructural status of ipsilesional and contralesional corticospinal tract correlates with motor skill in chronic stroke patients. *Hum. Brain Mapp.* 30, 3461–3474.

Seitz, R. J., Azari, N. P., Knorr, U., Binkofski, F., Herzog, H., and Freund, H. J. (1999). The role of diaschisis in stroke recovery. *Stroke* 30, 1844–1850.

Serrien, D. J., Strens, L. H., Cassidy, M. J., Thompson, A. J., and Brown, P. (2004). Functional significance of the ipsilateral hemisphere during movement of the affected hand after stroke. *Exp. Neurol.* 190, 425–432.

Sharma, N., Baron, J. C., and Rowe, J. B. (2009). Motor imagery after stroke: relating outcome to motor network connectivity. *Ann. Neurol.* 66, 604–616.

Singer, W. (1999). Neuronal synchrony: a versatile code for the definition of relations? *Neuron* 24, 49–65, 111–125.

Solodkin, A., Hlustik, P., Chen, E. E., and Small, S. L. (2004). Fine modulation in network activation during motor execution and motor imagery. *Cereb. Cortex* 14, 1246–1255.

Stam, C. J ., de Haan, W., Daffertshofer, A., Jones, B. F., Manshanden, I., van Cappellen van Walsum, A. M., Montez, T., Verbunt, J. P., de Munck, J. C., van Dijk, B. W., Berendse, H. W., and Scheltens, P. (2009). Graph theoretical analysis of magnetoencephalographic functional connectivity in Alzheimer's disease. *Brain* 132(Pt 1), 213–224.

Stinear, C. M., Barber, P. A., Smale, P. R., Coxon, J. P., Fleming, M. K., and Byblow, W. D. (2007). Functional potential in chronic stroke patients depends on corticospinal tract integrity. *Brain* 130(Pt 1), 170–180.

Stoffers, D., Bosboom, J. L., Deijen, J. B., Wolters, E., Stam, C. J., and Berendse, H.W. (2008). Increased cortico-cortical functional connectivity in early-stage Parkinson's disease: an MEG study. *Neuroimage* 41, 212–222.

Strens, L. H., Asselman, P., Pogosyan, A., Loukas, C., Thompson, A. J., and Brown, P. (2004). Corticocortical coupling in chronic stroke: its relevance to recovery. *Neurology* 63, 475–484.

van Dellen, E., Douw, L., Baayen, J. C., Heimans, J. J., Ponten, S. C., Vandertop, W. P., Velis, D. N., Stam, C. J., and Reijneveld, J. C. (2009). Long-term effects of temporal lobe epilepsy on local neural networks: a graph theoretical analysis of corticography recordings. *PLoS ONE* 4, e8081. doi: 10.1371/journal.pone.0008081

van den Heuvel, M. P., Mandl, R. C., Kahn, R. S., and Hulshoff Pol, H. E. (2009). Functionally linked resting-state networks reflect the underlying structural connectivity architecture of the human brain. *Hum. Brain Mapp.* 30, 3127–3141.

Von Monakow, C. (1914). "Die lokalisation im Grosshirn und der Abbau der Funktion durch kortikale Herde Wiesbaden: Bergmann 1914," (Transl. G Harris) in *Brain and Behavior I: Mood States and Mind*, ed. K. Pribam (Baltimore: Penguin), 27–36.

Walsh, R. R., Small, S. L., Chen, E. E., and Solodkin, A. (2008). Network activation during bimanual movements in humans. *Neuroimage* 43, 540–553.

Wang, L., Yu, C., Chen, H., Qin, W., He, Y., Fan, F., Zhang, Y., Wang, M., Li, K., Zang, Y., Woodward, T. S., and Zhu, C. (2010). Dynamic functional reorganization of the motor execution network after stroke. *Brain* 133(Pt 4), 1224–1238.

Ward, N. S., Brown, M. M., Thompson, A. J., and Frackowiak, R. S. (2003). Neural correlates of motor recovery after stroke: a longitudinal fMRI study. *Brain* 126(Pt 11), 2476–2496.

Ward, N. S., Newton, J. M., Swayne, O. B., Lee, L., Frackowiak, R. S., Thompson, A. J., Greenwood, R. J., and Rothwell, J. C. (2007). The relationship between brain activity and peak grip force is modulated by corticospinal system integrity after subcortical stroke. *Eur. J. Neurosci.* 25, 1865–1873.

Wernicke, C. (1874). *Der aphasische Symptomenkomplex: eine psychologische Studie auf anatomomischer Basis.* Breslau: Cohn and Weigert.

Witte, O. W., Bidmon, H. J., Schiene, K., Redecker, C., and Hagemann, G. (2000). Functional differentiation of multiple perilesional zones after focal cerebral ischemia. *J. Cereb. Blood Flow Metab.* 20, 1149–1165.

Wittenberg, G. F., Bastian, A. J., Dromerick, A. W., Thach, W. T., and Powers, W. J. (2000). Mirror movements complicate interpretation of cerebral activation changes during recovery from subcortical infarction. *Neurorehabil. Neural Repair* 14, 213–221.

Wu, T., Wang, L., Chen, Y., Zhao, C., Li, K., and Chan, P. (2009). Changes of functional connectivity of the motor network in the resting state in Parkinson's disease. *Neurosci. Lett.* 460, 6–10.

Conflict of Interest Statement: The authors declare that the research was conducted in the absence of any commercial or financial relationships that could be construed as a potential conflict of interest.

Received: 19 August 2010; accepted: 08 February 2011; published online: 16 March 2011.

Citation: Westlake KP and Nagarajan SS (2011) Functional connectivity in relation to motor performance and recovery after stroke. Front. Syst. Neurosci. 5:8. doi: 10.3389/fnsys.2011.00008

Copyright © 2011 Westlake and Nagarajan. This is an open-access article subject to an exclusive license agreement between the authors and Frontiers Media SA, which permits unrestricted use, distribution, and reproduction in any medium, provided the original authors and source are credited.

frontiers in
SYSTEMS NEUROSCIENCE

REVIEW ARTICLE
published: 02 November 2010
doi: 10.3389/fnsys.2010.00146

Relevance of structural brain connectivity to learning and recovery from stroke

Heidi Johansen-Berg*, Jan Scholz and Charlotte J. Stagg

Department of Clinical Neurology, University of Oxford, Oxford, UK

Edited by:
Silvina G. Horovitz, National Institutes of Health, USA

Reviewed by:
Douglas Fields, National Institutes of Health, USA
Christian Beaulieu, University of Alberta, Canada

****Correspondence:***
Heidi Johansen-Berg, Oxford Centre for Functional MRI of the Brain, John Radcliffe Hospital, Headington, Oxford OX3 9DU, UK.
e-mail: heidi@fmrib.ox.ac.uk

The physical structure of white matter fiber bundles constrains their function. Any behavior that relies on transmission of signals along a particular pathway will therefore be influenced by the structural condition of that pathway. Diffusion-weighted magnetic resonance imaging provides localized measures that are sensitive to white matter microstructure. In this review, we discuss imaging evidence on the relevance of white matter microstructure to behavior. We focus in particular on motor behavior and learning in healthy individuals and in individuals who have suffered a stroke. We provide examples of ways in which imaging measures of structural brain connectivity can inform our study of motor behavior and effects of motor training in three different domains: (1) to assess network degeneration or damage with healthy aging and following stroke, (2) to identify a structural basis for individual differences in behavioral responses, and (3) to test for dynamic changes in structural connectivity with learning or recovery.

Keywords: MRI, diffusion imaging, white matter, stroke, recovery, motor learning, human

INTRODUCTION

White matter fiber pathways form the brain's communication network. The physical condition of a given pathway will influence how effectively it can be used to transmit signals between brain regions and might thereby influence performance of behaviors that rely on that pathway (Fields, 2008). Individual differences in white matter structure may therefore be expected to correlate with variations in behavioral performance (Scholz et al., 2009b; Johansen-Berg, 2010). In addition, *changes* in white matter structure over time might accompany behavioral decrements or gains in performance due to disease, recovery or learning. This review considers evidence that an individual's movement abilities are determined in part by white matter microstructure both in the healthy brain and following stroke.

White matter microstructure can be interrogated non-invasively using diffusion-weighted magnetic resonance imaging (DWI). This imaging method probes tissue structure by measuring restrictions to local water diffusion. It has been suggested that cell membranes, myelin sheaths and the cytoskeleton, might hinder water diffusion (Beaulieu, 2002). If, due to the presence of cellular structures, water diffusion is no longer uniform in space, diffusion is called anisotropic (i.e., directionally dependent). In tissue with well-aligned structure, such as axons in white matter, this anisotropy reflects the underlying tissue structure. Here, diffusion is hindered by physical barriers, predominantly the axon membranes, in the direction perpendicular to the axons and relatively unrestricted parallel to it. Fractional anisotropy (FA) is a DWI-derived measure that quantifies the degree of anisotropy. FA is high (i.e., closer to 1) in highly organized white matter bundles, such as the corpus callosum and the corticospinal tract and low (i.e., closer to 0) in brain regions with little or no directional structure, such as cerebrospinal fluid within the ventricles.

Damage to the brain, such as stroke, often disrupts white matter pathways, either directly (Stys, 2004) or through secondary degeneration (Kuhn et al., 1988). The "disconnection" that results from such damage can have significant functional consequences (Catani and ffytche, 2005) and recent studies have exploited DWI and tractography to relate damage to specific white matter pathways to particular impairments such as neglect or aphasia (Bird et al., 2006; Catani and Mesulam, 2008). Motor impairment is particularly common following stroke, affecting about 80% of patients, many of whom are left with a persistent disability (Jorgensen et al., 1995). This review will consider whether assessment of structural brain connectivity can offer valuable insights into motor impairment, recovery and rehabilitation. Although impairment can be reduced through rehabilitative interventions (Winstein et al., 2004; Stewart et al., 2006; Wolf et al., 2006), outcomes for individual patients are highly variable. It is likely that some of this variation is due to variation in residual brain anatomy. Imaging measures of white matter microstructure (potentially in combination with functional measures; Stinear et al., 2007) could be used to predict responses to an intervention in order to allow for individual tailoring of therapeutic interventions to optimize outcomes (Dobkin, 2004; Ward and Cohen, 2004). In addition, longitudinal imaging of patients could provide insights into putative substrates for rehabilitation-mediated improvements in performance.

Repetitive motor task practice is a key component of many effective neurorehabilitation interventions (Langhorne et al., 2009). At a neuronal level, response to rehabilitation is thought to depend on brain systems typically employed for learning of novel motor skills (Karni and Bertini, 1997; Krakauer, 2006). Motor skill learning has therefore been used as an experimental model for rehabilitation following stroke (Pohl et al., 2001; Boyd and Winstein, 2003; Orrell et al., 2006; Stinear et al., 2007) and we propose that studying the systems involved in motor learning and practice in the healthy brain will help shed light on processes involved in motor recovery and rehabilitation following stroke. We will address similar questions in the healthy brain to those posed above for the damaged brain. Specifically, do individual

differences in structural connectivity correlate with variations in behavior and can changes in structural connectivity be induced by training?

We will focus on the degree to which imaging measures of structural brain connectivity can inform our study of motor behavior and motor training in the healthy brain and following stroke in three different domains: (1) to assess network degeneration with healthy aging and following stroke, (2) to identify a structural basis for individual differences in behavioral responses, and (3) to test for dynamic changes in structural connectivity with learning or recovery.

STRUCTURAL NETWORK DEGENERATION

Many physiological and pathological changes occur during the healthy aging process, but a particularly consistent change is a gradual decrease over time in the number of neurons as they die and are not replaced. Neuronal death is followed by a gradual degeneration of the proximal axons; a process known as Wallerian degeneration (Waller, 1850). As the axons degenerate, the surrounding structures and myelin sheaths are also lost, resulting, theoretically at least, in a greater overall decrease in total white matter volume than in gray matter volume.

Post-mortem studies have reported a gradual decline in brain weight after the age of 60 (Mrak et al., 1997) and have shown that this is primarily caused by significant loss of white matter volume (Meier-Ruge et al., 1992; Mrak et al., 1997). However, the results from conventional *in vivo* MRI studies are not entirely consistent with these post-mortem findings. A number of MRI studies have shown a gradual loss of the gray matter specifically from young adulthood onwards (Ge et al., 2002; Sowell et al., 2003; Walhovd et al., 2005; Lehmbeck et al., 2006), but have also described a concomitant non-linear *increase* in white matter volume until the end of the fifth decade before a gradual decline with advancing age (Bartzokis et al., 2001; Ge et al., 2002; Sowell et al., 2003; Walhovd et al., 2005).

Studies using DWI to assess age related white matter change have demonstrated that FA is potentially a more sensitive metric to assess microstructural degeneration of brain networks than conventional structural MR, with decreases in FA observed from young (23–40 years) to middle (41–59 years) adulthood (Salat et al., 2005; Ardekani et al., 2007; Giorgio et al., 2010), at a time when the total volume of white matter in the same subjects was relatively stable (Giorgio et al., 2010) (**Figure 1**). Decreases in FA continue to occur after this time, even in healthy aging in people without atypical cortical atrophy or a large number of white matter lesions (O'Sullivan et al., 2001; Head et al., 2004; Madden et al., 2004; Giorgio et al., 2010; Michielse et al., 2010).

Although structural changes with age are diffuse and widespread across the white matter, regional differences in the rate of decline in FA have been reported, with greater decreases in FA (and therefore greater inferred disruption in the white matter structure) in frontal areas, with temporal and posterior areas relatively preserved until later stages of aging (Abe et al., 2002; Salat et al., 2005; Ota et al., 2006; Sullivan et al., 2006; Michielse et al., 2010), though the

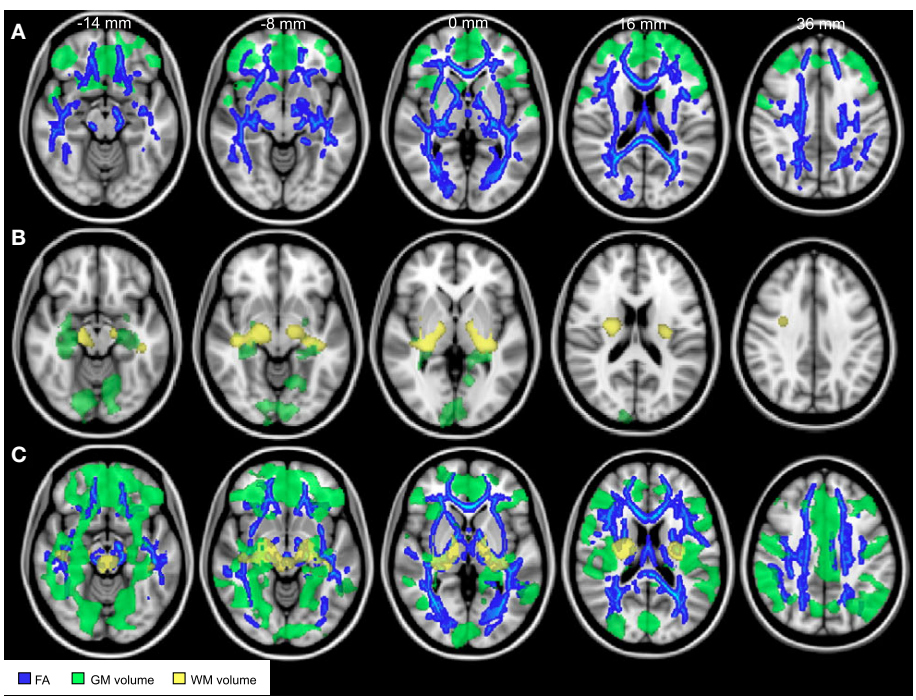


FIGURE 1 | Structural brain changes with age. Comparisons of fractional anisotropy (blue), gray matter volume (green), and white matter volume (yellow) between young (aged 23–40 years), middle-aged (aged 41–60 years), and older (aged 60–82 years) adults. **(A)** Comparisons between the young and middle-aged groups revealed widespread reductions in fractional anisotropy and reductions in GM density predominantly in frontal lobe. **(B)** Comparisons between middle and older aged adults revealed later reductions in white matter and gray matter volume. **(C)** Comparisons between young and older adults revealed widespread reductions in all measures. Adapted from Giorgio et al. (2010) with permission.

degree to which this differential is evident varies between studies (Giorgio et al., 2010). While the preferential loss of prefrontal white matter integrity has been demonstrated with aging even in highly functioning older people (Pfefferbaum et al., 2005), reduced FA in frontal white matter have been found to correlate with poor performance on a test executive function in healthy elderly adults with normal structural MRI scans (O'Sullivan et al., 2001). However, when compared with age-matched healthy adults, patients with early stage dementia did *not* have significantly greater white matter abnormalities within frontal regions but did have greater disruption to posterior white matter (Head et al., 2004).

These findings, in groups of individuals in whom conventional structural imaging is likely to be normal, highlight the sensitivity of diffusion imaging as a technique for investigating subtle changes in network structure, and its potential not only to identify disruption in white matter tracts over time with healthy aging, but as a tool to distinguish pathological processes from normal aging.

In addition, changes in white matter metrics over time may allow investigation of the relationship between white matter deterioration and cognitive decline. One study has investigated the relationship between FA and response times in a visual detection task. In young adults (19–25 years) response times correlated with FA in the splenium of the corpus callosum whereas for older adults (60–70 years) response times were best correlated with FA in the anterior limb of the internal capsule. This distinction between age groups suggests that there is an alteration in cortical networks required to perform a task with increasing age (Madden et al., 2004).

In the clinic, diffusion MRI has a well-established role in detecting acute stroke pathology, and is a more sensitive and specific imaging modality than conventional MRI or CT for detection of early ischemic signs in the hyperacute setting (Saur et al., 2003). Both gray and white matter are vulnerable to primary ischemic damage (Stys, 2004) and, following the acute stage, slowly evolving secondary degeneration of white matter can occur. DWI can detect these patterns of anterograde (Wallerian) and retrograde white matter tract degeneration in the days and months following stroke (Werring et al., 2000; Pierpaoli et al., 2001; Thomalla et al., 2004; Liang et al., 2007) (**Figure 2**). In the acute phase, reductions in FA have been observed within 16 days of stroke within distant regions within the corticospinal tract, at a time when conventional MRI was normal in this area (Thomalla et al., 2004). This decrease in FA is in line with the temporal evolution of Wallerian degeneration in these tracts, which has been demonstrated to occur as early as 2–7 days after experimental ischemic lesions in rat models (Iizuka et al., 1990). In a study by Thomalla et al. (2004), the degree of FA decrease was correlated with the patient's clinical score at the time of the MRI (**Figure 2G**), suggesting that these changes may have functional importance, but despite this cross-section relationship the FA decrease in the acute phase did not predict clinical outcome 3 months later.

Structural studies in the chronic stages of stroke recovery have tended to highlight damage or degeneration of pathways in the stroke-affected hemisphere but studies of remote *functional* change following stroke have identified the phenomenon of transhemispheric diaschisis (Andrews, 1991), raising the possibility that more remote interconnected regions, even in the contralesional hemisphere, undergo alterations following stroke. However, the fact that white matter microstructural changes in the contralesional hemisphere are not typically found in MRI studies (Liang et al., 2007), suggests that, if present, such changes are subtle or variable in spatial distribution.

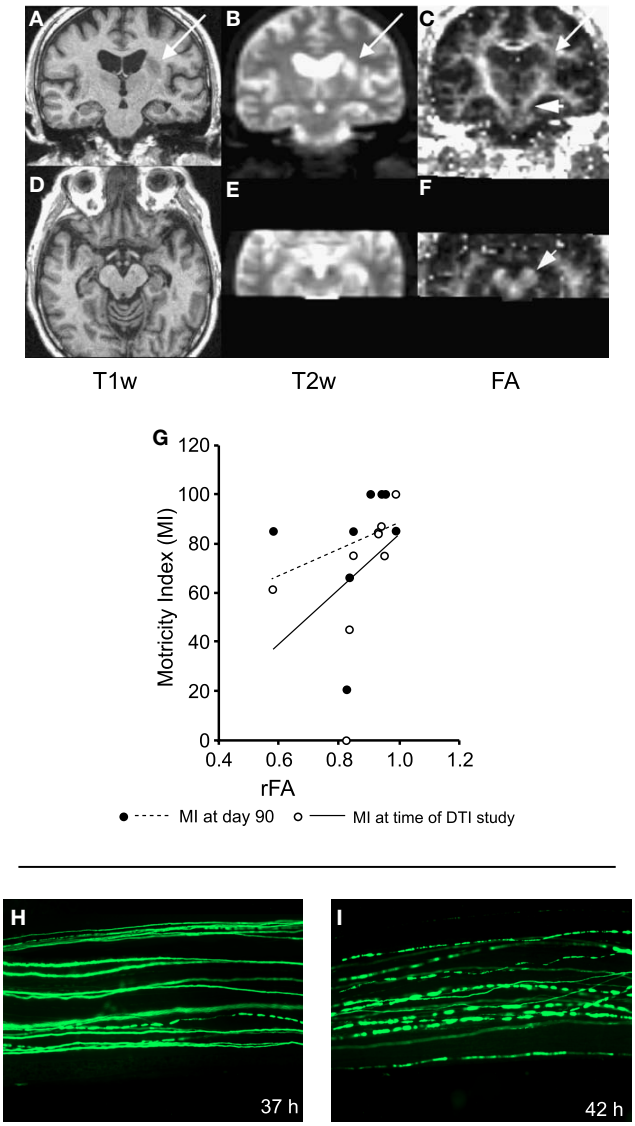


FIGURE 2 | White matter degeneration following damage. (A–G) Effects of stroke. **(A–F)** Coronal (top row) and axial (bottom row) MR sections taken in a patient with left striatocapsular infarction, 12 days after onset. The lesion area can be localized on T1- **(A,D)** and T2- **(B,E)** weighted scans. Fractional anisotropy (FA) is not only reduced in the lesion area, but also further along the pyramidal tract **(C)** and in the cerebral peduncle (**F**, short arrows). **(G)** The fractional anisotropy ratio between affected and unaffected side (rFA) for the cerebral peduncle correlates with the Motricity Index. Individuals with a more symmetric fractional anisotropy distribution had better motor performance. **(H,I)** Example of Wallerian degeneration in the peripheral nervous system. The example shows Wallerian degeneration in a mouse peripheral nerve after cut injury. **(H)** Thirty-seven hours after cut injury with few individual fluorescent axons are broken into fragments. **(I)** Forty-two hours after cut injury most labeled axons appear fragmented. **(A–G)** Adapted with permission from Thomalla et al. (2004). **(H,I)** Adapted with permission from Beirowski et al. (2005).

One promising approach for detecting subtle or spatially variable changes in structural connectivity is to use complex network analysis methods. These are a class of techniques that have been employed to interrogate network structure in a variety of contexts such as protein interactions, social networks or the internet (Barabasi, 2009), and that have proved powerful in exploring the network structure of the brain (Bullmore and Sporns, 2009). We recently used a novel network measure of weighted communicability (Estrada and Hatano, 2008; Crofts and Higham, 2009) to assess differences in structural connectivity between stroke patients and age-matched healthy controls using probabilistic tractography on diffusion data to generate estimates of structural connectivity between brain regions (Crofts et al., 2010). Communicability measures the ease with which information can travel between brain regions by considering not only the direct path between them but also all possible indirect paths. We used clustering methods to test whether or not this measure could differentiate between structural brain networks of chronic stroke patients and controls. When considering data from the stroke hemisphere (**Figure 3A**) we found a clear separation between patients and controls – as expected given the presence of a lesion and widespread degeneration in this hemisphere (Werring et al., 2000; Pierpaoli et al., 2001). However, more surprisingly, we also found that clustering differentiated between patients and controls even when considering only the structural connections of the *contralesional* hemisphere (**Figure 3B**). This suggests that subtle changes in structural connectivity, that are not apparent on conventional MRI or maps of FA (Liang et al., 2007), are present bilaterally following stroke and potentially provide a structural correlate of transhemispheric diaschisis (Andrews, 1991). The separation between groups depended on communicability changes in a few brain regions (**Figure 3C**). Our patients all had left hemisphere subcortical strokes around the basal ganglia/internal capsule and regions of reduced communicability clustered around this area in the stroke hemisphere and around remote, but interconnected, mirror locations in the contralesional hemisphere. This pattern of change is consistent with the idea that, in addition to direct ischemic damage to white matter, secondary degeneration occurs along distributed white matter pathways.

RELATIONSHIPS BETWEEN STRUCTURAL CONNECTIVITY AND BEHAVIOR IN HEALTH AND DISEASE

To what extent do changes in structural connectivity following stroke have functional consequences? It is well-established that the functional (Rapisarda et al., 1996; Delvaux et al., 2003; Brouwer and Schryburt-Brown, 2006) or structural (Jang et al., 2005; Jang et al., 2008) integrity of the corticospinal tract in the lesioned hemisphere is a major determinant of motor recovery following stroke. Recent studies, however, suggest that motor performance following stroke may have a more complex dependence on widespread pathways, not limited to primary corticospinal outputs from the lesioned hemisphere. For example, Schaechter et al. (2009) reported that a motor skill measure (a composite score based on pegboard performance and index finger tapping speed) correlated with *bilateral* clusters in the posterior limb of the internal capsule. *Post hoc* analysis suggested that while poorly recovered patients had reduced FA relative to controls in the contralesional posterior limb of the internal capsule, well-recovered patients had elevated FA relative to controls. The authors therefore suggest that motor performance following stroke depends on the net effect of degeneration and remodeling of motor related pathways in both hemispheres.

The fact that we can find such brain–behavior relationships raises the possibility that imaging measures of structural connectivity could be used to *predict* how an individual might behave

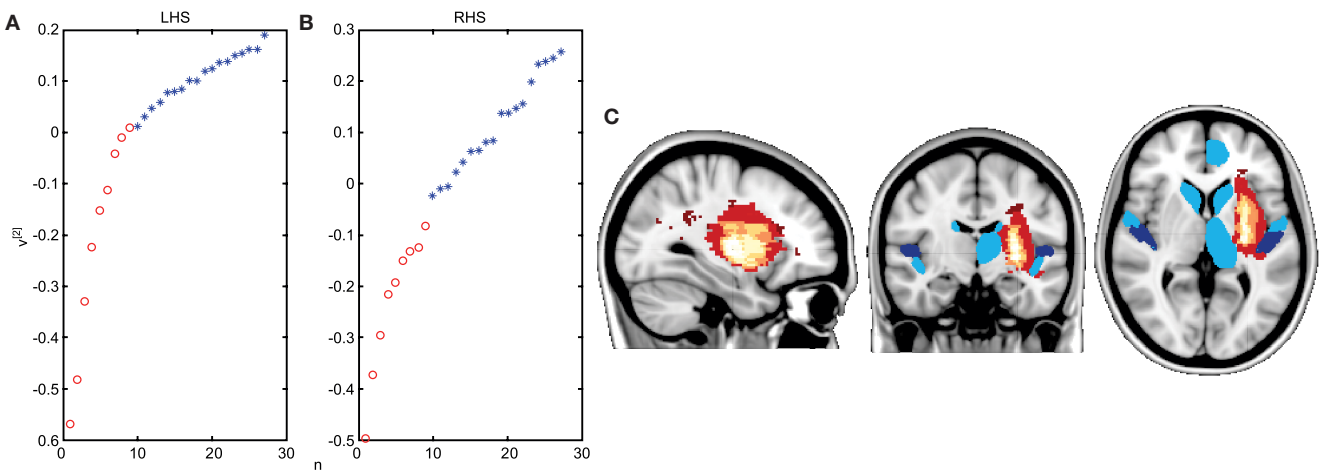


FIGURE 3 | Network analysis detects changes in contralesional structural connectivity following stroke. (A,B) Results of reordering of participants using structural connectivity data. Chronic stroke patients are indicated by red circles and age-matched healthy controls by blue stars. Ordering of participants is achieved using spectral reordering and is based on the right singular vector, v[2], which is plotted on the *y*-axis (see Crofts et al., 2010 for details). Individuals are ordered along the *x*-axis based on increasing values of [v]2. Clear separation between patients and controls is apparent when using communicability information from both the lesioned **(A)** and the contralesional hemisphere **(B)**. **(C)** Areas driving the separation between patients and controls are shown in blue. These regions have significantly lower communicability in patients compared to controls. They tend to be clustered around the lesion location (overlap map of lesions is shown in red to yellow). Based on data presented in Crofts et al. (2010).

in a particular scenario. From a clinical perspective this suggests opportunities to define imaging biomarkers that could be used to predict behavioral responses to a therapeutic intervention.

A previous study has attempted to define baseline measures able to predict response to a subsequent training intervention by assessing the structural and functional integrity of the corticospinal tract in chronic stroke patients who went on to receive a 30-day program of motor training (Stinear et al., 2007). For the subgroup of patients with poor residual functional connectivity in the affected corticospinal tract (as defined by the absence of an identifiable muscle response to transcranial magnetic stimulation of the affected motor cortex), the response to training depended on the structural integrity of the corticospinal tract: those with lower structural integrity of the affected corticospinal tract (measured using FA) showed no functional improvements (Stinear et al., 2007).

In the healthy brain, significant relationships have been detected between white matter microstructure and behavior across a broad range of cognitive tasks (**Figure 4**) (Johansen-Berg, 2010). These findings suggest that even in healthy subjects, subtle variations in brain anatomy have consequences for behavior. For example, better performance on a bimanual co-ordination task is associated with increased white matter integrity in the body of the corpus callosum, suggesting that callosal connections between medial wall areas are most critical in bimanual motor co-ordination (Johansen-Berg et al., 2007) (**Figure 4A**). In the majority of published studies, correlations between behavioral performance and FA within task-relevant pathways is positive – such that better performance is associated with higher FA. This is intuitively attractive as higher FA is associated with anatomical properties, such as increased myelination, that we might expect to speed conduction time, and so enhance performance (Fields, 2008). However, one study reports the opposite pattern: slower performance on a simple choice reaction time task is associated with higher FA in the right optic radiation, which might sub-serve the visuospatial component of the task (Tuch et al., 2005) (**Figure 4B**). This result does not fit the simple-minded idea that "bigger is better" when it comes to FA. However, FA is a complex measure that does not always relate in a straightforward way to fiber architecture. One explanation of the observed relationship, for example, is the complex crossing fiber architecture in this specific region, where increased myelination or axonal coherence of *one* fiber population could lead to an overall *decrease* in FA within a voxel.

Not only general motor performance, but also *changes* in motor performance that occur during learning are related to white matter microstructure. For example, the rate of adaptation in a visuo-motor tracking task correlated with FA in the cerebellum (Della-Maggiore et al., 2009). Some of these structurally correlating regions have also been found to be functionally more active in individuals who are faster at learning a similar task (Della-Maggiore and McIntosh, 2005). Microstructural variation in cerebellar white matter, as well as white matter underlying dorsal premotor cortex, has also been related to variation in performance on visuo-motor tracking task in which individuals learn a sequence of repeating hand grip forces (Tomassini et al., 2010). Taken together, this evidence suggests that the cellular features associated with increased FA in the cerebellum might support

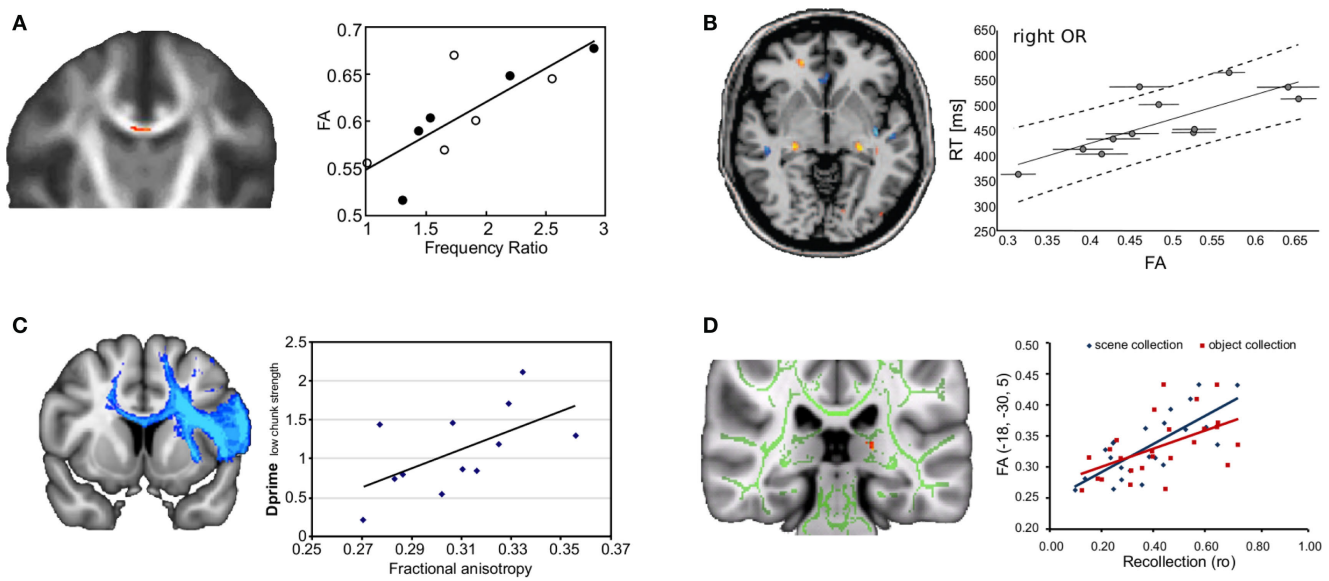


FIGURE 4 | Relationship between fractional anisotropy (FA) and behavioral indices for a range of different tasks. Brain images show voxels where a significant correlation was found. Scatter plots illustrate spread of behavioral and fractional anisotropy values across subjects. **(A)** Individuals with higher callosal fractional anisotropy performed better at an asynchronous bimanual finger-tapping task (closed circles represent males, open circles females). **(B)** Counter-intuitively, individuals with higher fractional anisotropy in the right optic radiation (OR) performed worse on a choice reaction time task (i.e., had higher reaction times). **(C)** Individuals with higher fractional anisotropy averaged over tracts arising from Broca's area were better at implicitly extracting grammatical rules from artificial grammars. **(D)** Higher fractional anisotropy in the fornix tail was found to be associated with significantly better recollection memory. **(A)** Adapted from Johansen-Berg et al. (2007) with permission; **(B)** adapted from Tuch et al. (2005) with permission; **(C)** adapted from Floel et al. (2009) with permission; **(D)** adapted from Rudebeck et al. (2009) with permission.

more efficient communication between cerebellar regions and other cortical and subcortical regions important for visuo-motor adaptation.

Correlations between learning-related behavioral change and brain structure have been found in other domains such as language. Individuals who were better at learning an artificial grammar had higher FA in white matter integrity surrounding Broca's area, and within cortico-cortical fibers arising from this area. This suggests that rule-based grammar learning might rely on and potentially benefit from increased connectivity of Broca's area (Floel et al., 2009) (**Figure 4C**).

A number of recent studies have shown that variations in performance of specific aspects of memory can also be related to structural variation in particular white matter pathways. For example, microstructure of white matter within the left uncinate fasciculus was related to auditory–verbal memory in children and adolescents (Mabbott et al., 2009). Further, inter-individual differences in the white matter microstructure in the fornix, the main link between episodic-memory regions of the medial temporal lobe and medial diencephalon, were found to reflect variations in recollection memory performance (Rudebeck et al., 2009) (**Figure 4D**). Finally, inter-individual differences in true and false memory retrieval has been associated with differences in FA in inferior and superior longitudinal fascicles respectively (Fuentemilla et al., 2009).

DYNAMIC CHANGES IN BRAIN STRUCTURAL CONNECTIVITY WITH LEARNING AND WITH RECOVERY FROM STROKE

The results of cross-sectional studies of behavior–structure correlations, such as those discussed above, need to be interpreted carefully. Inter-individual differences in brain structure might be the result of variations in life experience or of different genetic predispositions. In other words, greater white matter integrity might reflect cellular changes caused by experience. Alternatively, an individual might have been born with a white matter pathway that supports a particular skill. These two scenarios illustrate the fact that it is difficult to distinguish genetic, epigenetic, and experience-related factors with cross-sectional paradigms, a shortcoming that can only be addressed with longitudinal imaging.

The prospect that brain structures can change in response to experience, training or practice even in adults holds promise for patients recovering from injury or disease. Recent imaging studies provide evidence in both healthy individuals and stroke patients that dynamic changes in white matter microstructure can be induced by experience.

For example, a recent study showed an increase in FA in children (8–10 years) with poor reading skills who underwent 100 h of intensive reading training over a 6-month period (Keller and Just, 2009). The increase in FA in the left anterior centrum semiovale correlated with improvement in phonological decoding ability. This suggests that, at least in the young brain, targeted behavioral intervention can bring about changes in task-specific cortico-cortical white matter tracts.

It might be the case that white matter is only malleable during the first two decades of life, when ongoing maturation takes place (Casey et al., 2005). However, we recently found evidence that white matter continues to be susceptible to structural change even in adulthood (Scholz et al., 2009a). In response to 6 weeks of juggling training FA changed in white matter underlying the intraparietal sulcus of previously naïve adults (21–32 years) (**Figure 5**). These white matter changes were accompanied by structural changes in overlying gray matter regions. This suggests that brain matter continues to be malleable during adulthood and that learning might rely on reorganization of specific brain regions and their connections.

To what extent can such remodeling be harnessed in response to damage? There is currently little direct evidence from human studies for white matter remodeling after stroke. As discussed above, cross-sectional studies have demonstrated that the FA within the contralesional internal capsule correlates with residual function in the paretic hand (Schaechter et al., 2009). However, by their cross-sectional nature, such studies are not able to determine what these

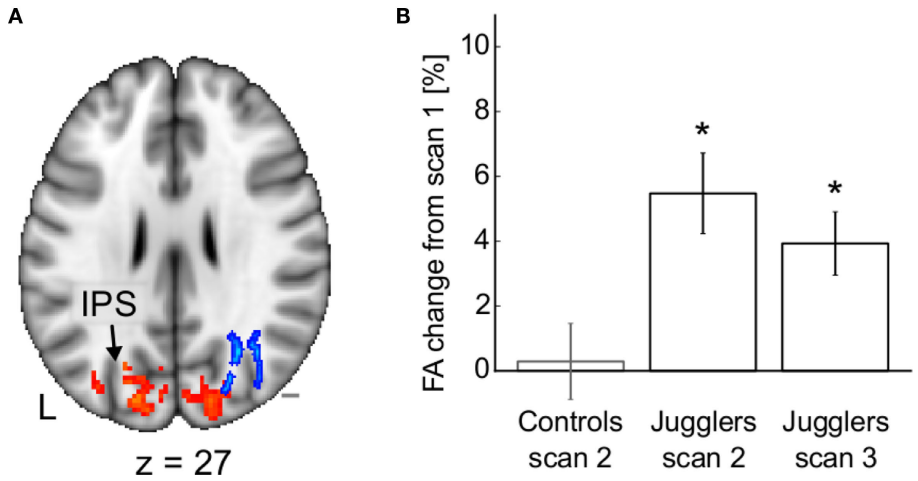


FIGURE 5 | Structural changes after juggling training. (A) Fractional anisotropy (blue) and gray mater density (red) increase in occipito-parietal areas following the training period. **(B)** Mean fractional anisotropy change from scan 1 in the cluster shown in **(A)**. Adapted from Scholz et al. (2009a) with permission.

brain–behavior relationships reflect. The observed relationships between motor performance and structural integrity could be due to pre-existing differences in white matter structure between the patients in these areas, to the effects of ischemic damage or secondary degeneration or to positive remodeling of the tracts during recovery. One observation from the study by Schaechter et al. (2009) supports that notion that white matter remodeling may occur at least in some patients. They found that patients who had made a poorer functional recovery had lower FA in the contralesional corticospinal tract than age-matched healthy controls. However, patients who had made a better recovery had *higher* FA than healthy controls within the contralesional corticospinal tract, although this was in a more inferior region than that demonstrating the correlation with behavior (Schaechter et al., 2009).

One recent study has sought to answer the question of causality directly using a longitudinal study design. Schlaug et al. (2009) investigated the strength of the arcuate fasciculus; the white matter connection between the two major language centers, Broca's area and Wernicke's area, in six stroke patients with chronic aphasia, before and after a intensive period of 75–80 daily sessions of intonation-based speech therapy. All patients' speech improved after training and there was an increased number of tractography-derived "fibers" in the arcuate fasciculus in the right hemisphere after therapy, a finding the authors suggest represents an increased recruitment of the homologues of the speech areas within the right hemisphere. This finding was specific to the right arcuate fasciculus and was not seen in the corticospinal tract. In addition, for these six patients, a relationship was observed between increase in number of fibers and improvement in clinical score, such that patients who demonstrated the greatest speech improvements also had the greatest increase in fiber number. Although the study is limited by the relatively small number of patients, these initial findings suggest that, in line with animal models, remodeling of white matter may occur in regions distant to the lesion after stroke. However, although it is tempting to interpret tractography-derived fiber number as a measure of density of axonal projections between two regions, there are numerous other factors that will influence such the performance of a tractography algorithm (such as tract geometry, length, data quality etc) (Johansen-Berg and Behrens, 2006). It would be useful to test the effects of such an intervention on a range of diffusion and other structural measures in order to gain a better understanding of potential biological events that underlie the observed change.

More generally, understanding the biological basis of changes in diffusion parameters is challenging. What do observed changes in MR measures of white matter signify in terms of cellular changes? Here animal studies of white matter plasticity can give clues to the most likely underlying structural changes. *In vitro* experiments have shown that myelination can be positively and negatively regulated by increasing and decreasing the firing rate of neurons with neurotoxins (Demerens et al., 1996). Alterations in white matter microstructure have also been observed in studies of behaving animals with training or recovery from damage (Johansen-Berg, 2007). In macaque monkeys that were trained for 2 weeks to retrieve food with a rake, tracers revealed more connections between the temporo-parietal junction and the intraparietal sulcus compared to a control group (Hihara et al., 2006), suggesting that the experience of training had led to cortico-cortical rewiring. Such rewiring has also been observed in response to brain damage; in squirrel monkeys that had received a lesion to the primary motor cortex, axons originating in the ventral premotor cortex were found to grow around the lesioned area to innervate somatosensory cortex (Dancause et al., 2005). Because somatosensory cortex projects directly to the spinal cord, this re-routing might provide an alternative route for premotor cortex to innervate the spinal cord following motor cortex damage.

Therefore, animal studies have identified potential mechanisms for observed patterns of white matter microstructural change with learning or recovery. Future studies could aim to perform imaging and histological analyses in parallel in order to test more directly hypotheses on their correspondence. For example, it has been suggested that changes in FA observed in the songbird brain are correlated with changes in myelination observed with histology (De Groof et al., 2008). The songbird brain undergoes dramatic structural changes in a seasonal cycle. It is possible that these changes involve both the creation of new axons or axon collaterals as well as the modification of existing circuitry by changes in myelination. In the context of disease, a recent study in a rat model found that, after an initial decrease in FA in the area surrounding an experimental lesion, FA increased over 6 weeks. Subsequent histological investigations suggested that the increased FA reflected increasing axon density with recovery (Ding et al., 2008).

CONCLUSIONS AND FUTURE DIRECTIONS

The physical structure of white matter pathways influences behavior both in healthy individuals and following stroke. Damage or degeneration of pathways with healthy aging (Salat et al., 2005; Ardekani et al., 2007; Giorgio et al., 2010) or following stroke (Werring et al., 2000; Pierpaoli et al., 2001; Thomalla et al., 2004) can be detected using diffusion MRI and has consequences for behavior (O'Sullivan et al., 2001; Madden et al., 2004). Measures of white matter microstructure in specific pathways related to motor execution and motor learning can be used to predict recovery following stroke (Jang et al., 2008) or response to intervention (Stinear et al., 2007) across groups of individuals. Future studies should assess the degree to which such measures could be used to design targeted interventions for individual patients. It is likely that combination of multi-modal structural imaging measures, along with measures of functional connectivity provided by imaging or electrophysiology (Stinear et al., 2007), will be most powerful in predicting individual responses. Even in healthy individuals, inter-individual variations in white matter microstructure of task-relevant pathways can predict variation in behavioral performance in motor, cognitive and learning domains (Scholz et al., 2009b; Johansen-Berg, 2010). Finally, recent evidence suggests that white matter microstructure may be susceptible to experience-dependent modification (Keller and Just, 2009; Scholz et al., 2009a). Future studies should test whether such changes can be detected in response to rehabilitation following stroke (Schlaug et al., 2009) and, if so, whether they can be used to identify potential therapeutic targets. However, the clinical relevance of such observations is currently limited by the challenge of interpreting changes in diffusion MRI measures

in biological terms (Beaulieu, 2009). Further studies in animal models, in which imaging and histological measures can be taken in the same individuals, will be useful to probe the biological basis of such changes.

ACKNOWLEDGMENTS

We are grateful for financial support from the Wellcome Trust (Heidi Johansen-Berg and Jan Scholz) and NIHR Biomedical Research Centre, Oxford (Heidi Johansen-Berg and Charlotte J. Stagg).

REFERENCES

Abe, O., Aoki, S., Hayashi, N., Yamada, H., Kunimatsu, A., Mori, H., Yoshikawa, T., Okubo, T., and Ohtomo, K. (2002). Normal aging in the central nervous system: quantitative MR diffusion-tensor analysis. *Neurobiol. Aging* 23, 433–441.

Andrews, R. J. (1991). Transhemispheric diaschisis. A review and comment. *Stroke* 22, 943–949.

Ardekani, S., Kumar, A., Bartzokis, G., and Sinha, U. (2007). Exploratory voxel-based analysis of diffusion indices, and hemispheric asymmetry in normal aging. *Magn. Reson. Imaging* 25, 154–167.

Barabasi, A. L. (2009). Scale-free networks: a decade, and beyond. *Science* 325, 412–413.

Bartzokis, G., Beckson, M., Lu, P. H., Nuechterlein, K. H., Edwards, N., and Mintz, J. (2001). Age-related changes in frontal, and temporal lobe volumes in men: a magnetic resonance imaging study. *Arch. Gen. Psychiatry* 58, 461–465.

Beaulieu, C. (2002). The basis of anisotropic water diffusion in the nervous system – a technical review. *NMR. Biomed.* 15, 435–455.

Beaulieu, C. (2009). "The biological basis of diffusion anisotropy," in *Diffusion MRI: From Quantitative Measurement to In-vivo Neuroanatomy*, eds H. Johansen-Berg and T. E. J. Behrens (London: Elsevier), 105–126.

Beirowski, B., Adalbert, R., Wagner, D., Grumme, D. S., Addicks, K., Ribchester, R. R., and Coleman, M. P. (2005). The progressive nature of Wallerian degeneration in wild-type, and slow Wallerian degeneration (WldS) nerves. *BMC Neurosci.* 6, 6.

Bird, C. M., Malhotra, P., Parton, A., Coulthard, E., Rushworth, M. F., and Husain, M. (2006). Visual neglect after right posterior cerebral artery infarction. *J. Neurol. Neurosurg. Psychiatry* 77, 1008–1012.

Boyd, L. A., and Winstein, C. J. (2003). Impact of explicit information on implicit motor-sequence learning following middle cerebral artery stroke. *Phys. Ther.* 83, 976–989.

Brouwer, B. J., and Schryburt-Brown, K. (2006). Hand function, and motor cortical output poststroke: are they related? *Arch. Phys. Med. Rehabil.* 87, 627–634.

Bullmore, E., and Sporns, O. (2009). Complex brain networks: graph theoretical analysis of structural, and functional systems. *Nat. Rev. Neurosci.* 10, 186–198.

Casey, B. J., Tottenham, N., Liston, C., and Durston, S. (2005). Imaging the developing brain: what have we learned about cognitive development? *Trends Cogn. Sci.* 9, 104–110.

Catani, M., and ffytche, D. H. (2005). The rises, and falls of disconnection syndromes. *Brain* 128(Pt 10), 2224–2239.

Catani, M., and Mesulam, M. (2008). The arcuate fasciculus, and the disconnection theme in language, and aphasia: history, and current state. *Cortex* 44, 953–961.

Crofts, J. J., and Higham, D. J. (2009). A weighted communicability measure applied to complex brain networks. *J. R. Soc. Interface* 6, 411–414.

Crofts, J. J., Higham, D. J., Bosnell, R., Jbabdi, S., Matthews, P. M., Behrens, T. E. J., and Johansen-Berg, H. (2010). Network analysis detects changes in the contralesional hemisphere following stroke. *Neuroimage* doi: 10.1016/j.neuroimage.2010.08.032. [Epub ahead of print].

Dancause, N., Barbay, S., Frost, S. B., Plautz, E. J., Chen, D., Zoubina, E. V., Stowe, A. M., and Nudo, R. J. (2005). Extensive cortical rewiring after brain injury. *J. Neurosci.* 25, 10167–10179.

De Groof, G., Verhoye, M., Van Meir, V., Balthazart, J., and Van der Linden, A. (2008). Seasonal rewiring of the songbird brain: an in vivo MRI study. *Eur. J. Neurosci.* 28, 2475–2485; discussion 4.

Della-Maggiore, V., and McIntosh, A. R. (2005). Time course of changes in brain activity, and functional connectivity associated with long-term adaptation to a rotational transformation. *J. Neurophysiol.* 93, 2254–2262.

Della-Maggiore, V., Scholz, J., Johansen-Berg, H., and Paus, T. (2009). The rate of visuomotor adaptation correlates with cerebellar white-matter microstructure. *Hum. Brain Mapp.* [Epub ahead of print].

Delvaux, V., Alagona, G., Gerard, P., De Pasqua, V., Pennisi, G., and de Noordhout, A. M. (2003). Post-stroke reorganization of hand motor area: a 1-year prospective follow-up with focal transcranial magnetic stimulation. *Clin. Neurophysiol.* 114, 1217–1225.

Demerens, C., Stankoff, B., Logak, M., Anglade, P., Allinquant, B., Couraud, F., Zalc, B., and Lubetzki, C. (1996). Induction of myelination in the central nervous system by electrical activity. *Proc. Natl. Acad. Sci. U.S.A.* 93, 9887–9892.

Ding, G., Jiang, Q., Li, L., Zhang, L., Zhang, Z. G., Ledbetter, K. A., Panda, S., Davarani, S. P. N., Athiraman, H., Li, Q., Ewing, J. R., and Chopp, M. (2008). Magnetic resonance imaging investigation of axonal remodeling, and angiogenesis after embolic stroke in sildenafil-treated rats. *J. Cereb. Blood Flow Metab.* 28, 1440–1448.

Dobkin, B. H. (2004). Strategies for stroke rehabilitation. *Lancet Neurol.* 3, 528–536.

Estrada, E., and Hatano, N. (2008). Communicability in complex networks. *Phys. Rev. E. Stat. Nonlin. Soft Matter Phys.* 77(Pt 2), 036111.

Fields, R. D. (2008). White matter in learning, cognition, and psychiatric disorders. *Trends Neurosci.* 31, 361–370.

Floel, A., de Vries, M. H., Scholz, J., Breitenstein, C., and Johansen-Berg, H. (2009). White matter integrity in the vicinity of Broca's area predicts grammar learning success. *Neuroimage* 47, 1974–1981.

Fuentemilla, L., Camara, E., Munte, T. F., Kramer, U. M., Cunillera, T., Marco-Pallares, J., Tempelmann, C., and Rodriguez-Fornells, A. (2009). Individual differences in true, and false memory retrieval are related to white matter brain microstructure. *J. Neurosci.* 29, 8698–8703.

Ge, Y., Grossman, R. I., Babb, J. S., Rabin, M. L., Mannon, L. J., and Kolson, D. L. (2002). Age-related total gray matter, and white matter changes in normal adult brain. Part I: volumetric MR imaging analysis. *AJNR Am. J. Neuroradiol.* 23, 1327–1333.

Giorgio, A., Santelli, L., Tomassini, V., Bosnell, R., Smith, S., De Stefano, N., and Johansen-Berg, H. (2010). Age-related changes in grey, and white matter structure throughout adulthood. *Neuroimage* 51, 943–951.

Head, D., Buckner, R., Shimony, J., Williams, L., Akbudak, E., Conturo, T., McAvoy, M., Morris, J. C., and Snyder, A. Z. (2004). Differential vulnerability of anterior white matter in nondemented aging with minimal acceleration in dementia of the Alzheimer type: evidence from diffusion tensor imaging. *Cereb. Cortex* 14, 410.

Hihara, S., Notoya, T., Tanaka, M., Ichinose, S., Ojima, H., Obayashi, S., Fujii, N., and Iriki, A. (2006). Extension of corticocortical afferents into the anterior bank of the intraparietal sulcus by tool-use training in adult monkeys. *Neuropsychologia* 44, 2636–2646.

Iizuka, H., Sakatani, K., and Young W. (1990). Neural damage in the rat thalamus after cortical infarcts. *Stroke* 21, 790–794.

Jang, S. H., Bai, D., Son, S. M., Lee, J., Kim, D. S., Sakong, J., Kim, D. G., and Yang, D. S. (2008). Motor outcome prediction using diffusion tensor tractography in pontine infarct. *Ann. Neurol.* 64, 460–465.

Jang, S. H., Cho, S. H., Kim, Y. H., Han, B. S., Byun, W. M., Son, S. M., Kim, S. H., and Lee, S. J. (2005). Diffusion anisotrophy in the early stages of stroke can predict motor outcome. *Restor. Neurol. Neurosci.* 23, 11–17.

Johansen-Berg, H. (2007). Structural plasticity: rewiring the brain. *Curr. Biol.* 17, R141–R144.

Johansen-Berg, H. (2010). Behavioural relevance of variation in white matter microstructure. *Curr. Opin. Neurol.* 23, 351–358.

Johansen-Berg, H., and Behrens, T. E. (2006). Just pretty pictures? What diffusion tractography can add in clinical neuroscience. *Curr. Opin. Neurol.* 19, 379–385.

Johansen-Berg, H., Della-Maggiore, V., Behrens, T. E., Smith, S. M., and Paus, T. (2007). Integrity of white matter in the corpus callosum correlates with bimanual co-ordination skills. *Neuroimage* 36(Suppl. 2), T16–T21.

Jorgensen, H. S., Nakayama, H., Raaschou, H. O., Vive-Larsen, J., Stoier, M., and Olsen, T. S. (1995). Outcome, and time course of recovery in stroke. Part I: Outcome. The Copenhagen Stroke Study. *Arch. Phys. Med. Rehabil.* 76, 399–405.

Karni, A., and Bertini, G. (1997). Learning perceptual skills: behavioral probes into adult cortical plasticity. *Curr. Opin. Neurobiol.* 7, 530–535.

Keller, T. A., and Just, M. A. (2009). Altering cortical connectivity: remediation-induced changes in the white matter of poor readers. *Neuron* 64, 624–631.

Krakauer, J. W. (2006). Motor learning: its relevance to stroke recovery, and neurorehabilitation. *Curr. Opin. Neurol.* 19, 84–90.

Kuhn, M. J., Johnson, K. A., and Davis, K. R. (1988). Wallerian degeneration: evaluation with MR imaging. *Radiology* 168, 199–202.

Langhorne, P., Coupar, F., and Pollock, A. (2009). Motor recovery after stroke: a systematic review. *Lancet Neurol.* 8, 741–754.

Lehmbeck, J. T., Brassen, S., Weber-Fahr, W., and Braus, D. F. (2006). Combining voxel-based morphometry, and diffusion tensor imaging to detect age-related brain changes. *Neuroreport* 17, 467–470.

Liang, Z., Zeng, J., Liu, S., Ling, X., Xu, A., Yu, J., and Ling, L. (2007). A prospective study of secondary degeneration following subcortical infarction using diffusion tensor imaging. *J. Neurol. Neurosurg. Psychiatry* 78, 581–586.

Mabbott, D. J., Rovet, J., Noseworthy, M. D., Smith, M. L., and Rockel, C. (2009). The relations between white matter, and declarative memory in older children, and adolescents. *Brain Res.* 1294, 80–90.

Madden, D. J., Whiting, W. L., Huettel, S. A., White, L. E., MacFall, J. R., and Provenzale, J. M. (2004). Diffusion tensor imaging of adult age differences in cerebral white matter: relation to response time. *Neuroimage* 21, 1174.

Meier-Ruge, W., Ulrich, J., Brühlmann, M., and Meier, E. (1992). Age-related white matter atrophy in the human brain. *Ann. N. Y. Acad. Sci.* 673, 260–269.

Michielse, S., Coupland, N., Camicioli, R., Carter, R., Seres, P., Sabino, J., and Malykhin, N. (2010). Selective effects of aging on brain white matter microstructure: a diffusion tensor imaging tractography study. *Neuroimage* 52, 1190–1201.

Mrak, R. E., Griffin, S. T., and Graham, D. I. (1997). Aging-associated changes in human brain. *J. Neuropathol. Exp. Neurol.* 56, 1269–1275.

Orrell, A. J., Eves, F. F., and Masters, R. S. (2006). Motor learning of a dynamic balancing task after stroke: implicit implications for stroke rehabilitation. *Phys. Ther.* 86, 369–380.

O'Sullivan, M., Jones, D. K., Summers, P. E., Morris, R. G., Williams, S. C., and Markus, H. S. (2001). Evidence for cortical "disconnection" as a mechanism of age-related cognitive decline. *Neurology* 57, 632–638.

Ota, M., Obata, T., Akine, Y., Ito, H., Ikehira, H., Asada, T., and Suhara, T. (2006). Age-related degeneration of corpus callosum measured with diffusion tensor imaging. *Neuroimage* 31, 1445–1452.

Pfefferbaum, A., Adalsteinsson, E., and Sullivan, E. (2005). Frontal circuitry degradation marks healthy adult aging: evidence from diffusion tensor imaging. *Neuroimage* 26, 891–899.

Pierpaoli, C., Barnett, A., Pajevic, S., Chen, R., Penix, L. R., Virta, A., and Basser, P. (2001). Water diffusion changes in Wallerian degeneration, and their dependence on white matter architecture. *Neuroimage* 13(Pt 1), 1174.

Pohl, P. S., McDowd, J. M., Filion, D. L., Richards, L. G., and Stiers, W. (2001). Implicit learning of a perceptual-motor skill after stroke. *Phys. Ther.* 81, 1780–1789.

Rapisarda, G., Bastings, E., de Noordhout, A. M., Pennisi, G., and Delwaide, P. J. (1996). Can motor recovery in stroke patients be predicted by early transcranial magnetic stimulation? *Stroke* 27, 2191–2196.

Rudebeck, S. R., Scholz, J., Millington, R., Rohenkohl, G., Johansen-Berg, H., and Lee, A. C. (2009). Fornix microstructure correlates with recollection but not familiarity memory. *J. Neurosci.* 29, 14987–14992.

Salat, D. H., Tuch, D. S., Greve, D. N., van der Kouwe, A. J., Hevelone, N. D., Zaleta, A. K., Rosen, B. R., Fischl, B., Corkin, S., Rosas, H. D., and Dale, A. M. (2005). Age-related alterations in white matter microstructure measured by diffusion tensor imaging. *Neurobiol. Aging* 26, 1215–1227.

Saur, D., Kucinski, T., Grzyska, U., Eckert, B., Eggers, C., Niesen, W., Schoder, V., Zeumer, H., Weiller, C., and Röther, J. (2003). Sensitivity, and interrater agreement of CT, and diffusion-weighted MR imaging in hyperacute stroke. *AJNR Am. J. Neuroradiol.* 24, 878–885.

Schaechter, J. D., Fricker, Z. P., Perdue, K. L., Helmer, K. G., Vangel, M. G., Greve, D. N., and Makris, N. (2009). Microstructural status of ipsilesional, and contralesional corticospinal tract correlates with motor skill in chronic stroke patients. *Hum. Brain Mapp.* 30, 3461–3474.

Schlaug, G., Marchina, S., and Norton, A. (2009). Evidence for plasticity in white-matter tracts of patients with chronic Broca's aphasia undergoing intense intonation-based speech therapy. *Ann. N. Y. Acad. Sci.* 1169, 385–394.

Scholz, J., Klein, M. C., Behrens, T. E., and Johansen-Berg, H. (2009a). Training induces changes in white-matter architecture. *Nat. Neurosci.* 12, 1370–1371.

Scholz, J., Tomassini, V., and Johansen-Berg, H. (2009b). "Individual differences in white matter microstructure in the healthy human brain," in *Diffusion MRI: From Quantitative Measurement to In Vivo Neuroanatomy*, eds T. Behrens and H. Johansen-Berg (Oxford: Elsevier), 237–250.

Sowell, E. R., Peterson, B. S., Thompson, P. M., Welcome, S. E., Henkenius, A. L., and Toga, A. W. (2003). Mapping cortical change across the human life span. *Nat. Neurosci.* 6, 309–315.

Stewart, K. C., Cauraugh, J. H., and Summers, J. J. (2006). Bilateral movement training, and stroke rehabilitation: a systematic review, and meta-analysis. *J. Neurol. Sci.* 15, 244, 89–95.

Stinear, C. M., Barber, P. A., Smale, P. R., Coxon, J. P., Fleming, M. K., and Byblow, W. D. (2007). Functional potential in chronic stroke patients depends on corticospinal tract integrity. *Brain* 130(Pt 1), 170–180.

Stys, P. K. (2004). White matter injury mechanisms. *Curr. Mol. Med.* 4, 113–130.

Sullivan, E., Adalsteinsson, E., and Pfefferbaum, A. (2006). Selective age-related degradation of anterior callosal fiber bundles quantified in vivo with fiber tracking. *Cereb. Cortex* 16, 1030.

Thomalla, G., Glauche, V., Koch, M. A., Beaulieu, C., Weiller, C., and Rother, J. (2004). Diffusion tensor imaging detects early Wallerian degeneration of the pyramidal tract after ischemic stroke. *Neuroimage* 22, 1767–1774.

Tomassini, V., Jbabdi, S., Kincses, T., Bosnell, R., Douaud, G., Pozzilli, C, Matthews, P. M., and Johansen-Berg, H. (2010). Structural, and functional bases of individual difference in motor learning. *Hum. Brain Mapp.* doi: 10.1002/hbm.21037. [Epub ahead of print].

Tuch, D. S., Salat, D. H., Wisco, J. J., Zaleta, A. K., Hevelone, N. D., and Rosas, H. D. (2005). Choice reaction time performance correlates with diffusion anisotropy in white matter pathways supporting visuospatial attention. *Proc. Natl. Acad. Sci. U.S.A.* 102, 12212–12217.

Walhovd, K. B., Fjell, A. M., Reinvang, I., Lundervold, A., Dale, A. M., Eilertsen, D. E., Quinn, B. T., Salat, D., Makris, N., and Fischl, B. (2005). Effects of age on volumes of cortex, white matter, and subcortical structures. *Neurobiol. Aging* 26, 1261–1268.

Waller, A. (1850). Experiments on the section of the glossopharyngeal, and hypoglossal nerves of the frog, and observations of the alterations produced thereby in the structure of their primitive fibres. *Philos. Trans. R. Soc. Lond., B, Biol. Sci.* 140, 423–429.

Ward, N. S., and Cohen, L. G. (2004). Mechanisms underlying recovery of motor function after stroke. *Arch. Neurol.* 61, 1844–1848.

Werring, D. J., Toosy, A. T., Clark, C. A., Parker, G. J., Barker, G. J., Miller, D. H., and Thompson, A. J. (2000). Diffusion tensor imaging can detect, and quantify corticospinal tract degeneration after stroke. *J. Neurol. Neurosurg. Psychiatry* 69, 269–272.

Winstein, C. J., Rose, D. K., Tan, S. M., Lewthwaite, R., Chui, H. C., and Azen, S. P. (2004). A randomized controlled comparison of upper-extremity rehabilitation strategies in acute stroke: a pilot study of immediate, and long-term outcomes. *Arch. Phys. Med. Rehabil.* 85, 620–628.

Wolf, S. L., Winstein, C. J., Miller, J. P., Taub, E., Uswatte, G., Morris, D., Giuliani, C., Light, K. E., and Nichols-Larsen, D., E. X. C. I. T. E. Investigators. (2006). Effect of constraint-induced movement therapy on upper extremity function 3 to 9 months after stroke: the EXCITE randomized clinical trial. *JAMA* 296, 2095–2104.

Conflict of Interest Statement: The authors declare that the research was conducted in the absence of any commercial or financial relationships that could be construed as a potential conflict of interest.

Received: 31 May 2010; paper pending published: 25 July 2010; accepted: 10 September 2010; published online: 02 November 2010.

*Citation: Johansen-Berg H, Scholz J and Stagg CJ (2010) Relevance of structural brain connectivity to learning and recovery from stroke. Front. Syst. Neurosci. **4**:146. doi: 10.3389/fnsys.2010.00146*

Copyright © 2010 Johansen-Berg, Scholz and Stagg. This is an open-access article subject to an exclusive license agreement between the authors and the Frontiers Research Foundation, which permits unrestricted use, distribution, and reproduction in any medium, provided the original authors and source are credited.

frontiers in
SYSTEMS NEUROSCIENCE

EDITORIAL
published: 13 February 2012
doi: 10.3389/fnsys.2012.00004

Introduction to research topic – Brain connectivity analysis: investigating brain disorders. Part 2: original research articles

Silvina G. Horovitz[1]* and Barry Horwitz[2]

[1] *Human Motor Control Section, National Institute of Neurological Disorders and Stroke, National Institutes of Health, Bethesda, MD, USA*
[2] *Brain Imaging and Modeling Section, National Institute on Deafness and Other Communication Disorders, National Institutes of Health, Bethesda, MD, USA*
**Correspondence: horovits@mail.nih.gov*

Although the review articles discussed in part 1 (Introduction to research topic – Brain connectivity analysis: investigating brain disorders. Part 1: the review articles) give a nice overview of the scope of brain connectivity analysis as applied to brain disorders, the original research papers included in this collection enable the reader to see how one actually goes about employing such analyses on real data sets. In these articles we see the specific steps that are necessary to perform each particular connectivity analysis. We believe that these articles will be especially useful as guides for other researchers attempting brain connectivity analyses.

Several articles focus on normal brain function, but these papers are included because the subject groups that are investigated experience changing patterns of brain connectivity, and as such, share some of the conceptual difficulties that occur when studying brain disorders. Karunanayaka et al. (2011) evaluate the developmental trajectories of fMRI effective connectivity using linear structural equation modeling (SEM) during the verb-generate task in a large group of children whose ages ranged between 5 and 18 years. Allen et al. (2011) present an independent component analysis (ICA) of the effects of healthy aging (12–71 years) and gender on resting state fMRI networks. As with the previous paper, the study population is quite large (over 600 subjects). Both studies provide results that can act as baselines for future investigations. A much smaller-scale study by Beauchamp et al. (2010) employs fMRI–SEM to examine the interaction of sensory systems (visual and tactile) during multisensory integration. This is an important issue, especially in aged populations where deterioration of peripheral sensory systems is common.

Language processing is the topic addressed by three of the original research connectivity articles. Turken and Dronkers (2011) used both DTI tractography and resting state fMRI functional connectivity to investigate in healthy subjects the structural and functional connectivity of white matter pathways between left hemisphere brain regions critical for language comprehension. These critical regions were identified in an earlier voxel-based lesion–symptom mapping analysis of data from aphasic patients (Dronkers et al., 2004). Reading is the issue examined in the other two articles. Frye et al. (2010) compared young adult normal and dyslexic readers. They used Granger causality applied to MEG data to investigate the relation between effective connectivity between left inferior frontal gyrus and other brain areas and phonological decoding. The work of Davis et al. (2010) is interesting in that it shows how neuroimaging may impact education. They present DTI data analyzed using probabilistic tractography that were acquired from first-grade children who differed in their levels of responsiveness to reading instruction.

One of the most challenging aspects of studying the brain is its amazing adaptive capabilities. It often reorganizes itself in response to occurrences in the external world; that is why we are able to remember past events, why we are able to learn new skills, and why we send our children to school. But, the brain also can reorganize to changes within the brain itself, including disease. Thus, an important set of issues for understanding brain disorders is to determine which changes are compensatory and which are maladaptive. Three articles presented here investigate connectivity changes accompanying reorganization. Turner et al. (2011) report on an fMRI study of traumatic brain injury (TBI) patients. By combining brain–behavior and functional connectivity analyses, they sought to determine whether the compensatory brain changes they found in the patients represented functional reorganization (novel brain region recruitment) or altered functional engagement (differential recruitment of similar brain regions between patients and controls based on task demands). The other two articles focus on developmental changes in the visual system following loss of vision. The paper by Sani et al. (2010) used fMRI to investigate motion processing in sighted and blind (loss of vision from birth or before 2 years of age) adults. They compared the differences between the two groups in functional connectivity of the human middle temporal complex (hMT+), parts of which are activated in sighted subjects by visual motion and parts of which can be activated by non-visual motion. The third paper in this group, by Bock et al. (2010), is unique in that its study population consists of ferrets, thus allowing one to compare neuroimaging results with detailed histopathological data. The question they addressed relates to understanding the neural basis of the changes observed in DTI data following early bilateral enucleation of the eyes.

The remaining articles present connectivity analyses of data from patients with specific neurological and psychiatric disorders. Amyotrophic lateral sclerosis (ALS), a progressive neurodegerative disorder affecting motor neurons, is the topic of the article by Jelsone-Swain et al. (2010). They studied this disorder using resting state functional connectivity analysis, focusing on early stage ALS and directing their analysis to the connectivity changes of motor cortex. Another neurodegenerative disorder, Parkinson's disease (PD), was addressed by Kwak et al. (2010). They also employed resting state fMRI functional connectivity analysis, applying it to data acquired from PD patients as well as healthy controls. An interesting feature of this paper was the fact that the PD patients were studied in both the ON and OFF L-DOPA medication states (a drug used to treat the symptoms of PD). The psychiatric disorders examined by the remaining papers were depression and social phobia. Resting state fMRI connectivity analysis of depression was covered in the article by Veer et al. (2010), who applied ICA to their

resting state fMRI data and identified thirteen relevant networks. In the paper by Danti et al. (2010), fMRI data obtained during a face perception task were analyzed using functional connectivity analysis in patients with social phobia and in control subjects, with the goal of examining communication between sensory and emotional processing brain areas.

ACKNOWLEDGMENTS

This work was supported by the Intramural Research Programs of NINDS (Silvina G. Horovitz) and NIDCD (Barry Horwitz).

REFERENCES

Allen, E. A., Erhardt, E. B., Damaraju, E., Gruner, W., Segall, J. M., Silva, R. F., Havlicek, M., Rachakonda, S., Fries, J., Kalyanam, R., Michael, A. M., Caprihan, A., Turner, J. A., Eichele, T., Adelsheim, S., Bryan, A. D., Bustillo, J., Clark, V. P., Feldstein Ewing, S. W., Filbey, F., Ford, C. C., Hutchison, K., Jung, R. E., Kiehl, K. A., Kodituwakku, P., Komesu, Y. M., Mayer, A. R., Pearlson, G. D., Phillips, J. P., Sadek, J. R., Stevens, M., Teuscher, U., Thoma, R. J., and Calhoun, V. D. (2011). A baseline for the multivariate comparison of resting-state networks. *Front. Syst. Neurosci.* 5:2. doi: 10.3389/fnsys.2011.00002

Beauchamp, M. S., Pasalar, S., and Ro, T. (2010). Neural substrates of reliability-weighted visual-tactile multisensory integration. *Front. Syst. Neurosci.* 4:25. doi: 10.3389/fnsys.2010.00025

Bock, A. S., Olavarria, J. F., Leigland, L. A., Taber, E. N., Jespersen, S. N., and Kroenke, C. D. (2010). Diffusion tensor imaging detects early cerebral cortex abnormalities in neuronal architecture induced by bilateral neonatal enucleation: an experimental model in the ferret. *Front. Syst. Neurosci.* 4:149. doi: 10.3389/fnsys.2010.00149

Danti, S., Ricciardi, E., Gentili, C., Gobbini, M. I., Pietrini, P., and Guazzelli, M. (2010). Is social phobia a "mis-communication" disorder? Brain functional connectivity during face perception differs between patients with social phobia and healthy control subjects. *Front. Syst. Neurosci.* 4:152. doi: 10.3389/fnsys.2010.00152

Davis, N., Fan, Q., Compton, D. L., Fuchs, D., Fuchs, L. S., Cutting, L. E., Gore, J. C., and Anderson, A. W. (2010). Influences of neural pathway integrity on children's response to reading instruction. *Front. Syst. Neurosci.* 4:150. doi: 10.3389/fnsys.2010.00150

Dronkers, N. F., Wilkins, D. P., Van Valin, R. D. Jr., Redfern, B. B., and Jaeger, J. J. (2004). Lesion analysis of the brain areas involved in language comprehension. *Cognition* 92, 145–177.

Frye, R. E., Wu, M. H., Liederman, J., and Fisher, J. M. (2010). Greater pre-stimulus effective connectivity from the left inferior frontal area to other areas is associated with better phonological decoding in dyslexic readers. *Front. Syst. Neurosci.* 4:156. doi: 10.3389/fnsys.2010.00156

Jelsone-Swain, L. M., Fling, B. W., Seidler, R. D., Hovatter, R., Gruis, K., and Welsh, R. C. (2010). Reduced interhemispheric functional connectivity in the motor cortex during rest in limb-onset amyotrophic lateral sclerosis. *Front. Syst. Neurosci.* 4:158. doi: 10.3389/fnsys.2010.00158

Karunanayaka, P., Schmithorst, V. J., Vannest, J., Szaflarski, J. P., Plante, E., and Holland, S. K. (2011). A linear structural equation model for covert verb generation based on independent component analysis of FMRI data from children and adolescents. *Front. Syst. Neurosci.* 5:29. doi: 10.3389/fnsys.2011.00029

Kwak, Y., Peltier, S., Bohnen, N. I., Muller, M. L., Dayalu, P., and Seidler, R. D. (2010). Altered resting state cortico-striatal connectivity in mild to moderate stage Parkinson's disease. *Front. Syst. Neurosci.* 4:143. doi: 10.3389/fnsys.2010.00143

Sani, L., Ricciardi, E., Gentili, C., Vanello, N., Haxby, J. V., and Pietrini, P. (2010). Effects of visual experience on the human MT+ functional connectivity networks: an fMRI study of motion perception in sighted and congenitally blind individuals. *Front. Syst. Neurosci.* 4:159. doi: 10.3389/fnsys.2010.00159

Turken, A. U., and Dronkers, N. F. (2011). The neural architecture of the language comprehension network: converging evidence from lesion and connectivity analyses. *Front. Syst. Neurosci.* 5:1. doi: 10.3389/fnsys.2011.00001

Turner, G. R., McIntosh, A. R., and Levine, B. (2011). Prefrontal compensatory engagement in TBI is due to altered functional engagement of existing networks and not functional reorganization. *Front. Syst. Neurosci.* 5:9. doi: 10.3389/fnsys.2011.00009

Veer, I. M., Beckmann, C. F., van Tol, M. J., Ferrarini, L., Milles, J., Veltman, D. J., Aleman, A., van Buchem, M. A., van der Wee, N. J., and Rombouts, S. A. (2010). Whole brain resting-state analysis reveals decreased functional connectivity in major depression. *Front. Syst. Neurosci.* 4:41. doi: 10.3389/fnsys.2010.00041

Received: 25 January 2012; accepted: 27 January 2012; published online: 13 February 2012. Citation: Horovitz SG and Horwitz B (2012) Introduction to research topic – Brain connectivity analysis: investigating brain disorders. Part 2: original research articles. Front. Syst. Neurosci. ***6****:4. doi: 10.3389/fnsys.2012.00004*

Copyright © 2012 Horovitz and Horwitz. This is an open-access article distributed under the terms of the Creative Commons Attribution Non Commercial License, which permits non-commercial use, distribution, and reproduction in other forums, provided the original authors and source are credited.

frontiers in
SYSTEMS NEUROSCIENCE

ORIGINAL RESEARCH ARTICLE
published: 01 June 2011
doi: 10.3389/fnsys.2011.00029

A linear structural equation model for covert verb generation based on independent component analysis of fMRI data from children and adolescents

Prasanna Karunanayaka[1], Vincent J. Schmithorst[2], Jennifer Vannest[2], Jerzy P. Szaflarski[2,3], Elena Plante[4] and Scott K. Holland[2]*

[1] *Center for NMR Research, Department of Radiology, The Milton S. Hershey Medical Center, The Pennsylvania State University College of Medicine, Hershey, PA, USA*
[2] *Pediatric NeuroImaging Research Consortium, Cincinnati Children's Hospital Medical Center, Cincinnati, OH, USA*
[3] *Center for Imaging Research, Department of Neurology, University of Cincinnati, Cincinnati, OH, USA*
[4] *Department of Speech and Hearing Sciences, University of Arizona, Tucson, AZ, USA*

Edited by:
Silvina G. Horovitz, National Institutes of Health, USA

Reviewed by:
Vince D. Calhoun, University of New Mexico, USA

****Correspondence:***
Scott K. Holland, Pediatric NeuroImaging Research Consortium, Children's Hospital Medical Center, 3333 Burnet Avenue, ML 5033, Cincinnati, OH 45229, USA.
e-mail: scott.holland@cchmc.org

Human language is a complex and protean cognitive ability. Young children, following well defined developmental patterns learn language rapidly and effortlessly producing full sentences by the age of 3 years. However, the language circuitry continues to undergo significant neuroplastic changes extending well into teenage years. Evidence suggests that the developing brain adheres to two rudimentary principles of functional organization: functional integration and functional specialization. At a neurobiological level, this distinction can be identified with *progressive specialization* or *focalization* reflecting consolidation and synaptic reinforcement of a network (Lenneberg, 1967; Muller et al., 1998; Berl et al., 2006). In this paper, we used group independent component analysis and linear structural equation modeling (McIntosh and Gonzalez-Lima, 1994; Karunanayaka et al., 2007) to tease out the developmental trajectories of the language circuitry based on fMRI data from 336 children ages 5–18 years performing a blocked, covert verb generation task. The results are analyzed and presented in the framework of theoretical models for neurocognitive brain development. This study highlights the advantages of combining both modular and connectionist approaches to cognitive functions; from a methodological perspective, it demonstrates the feasibility of combining data-driven and hypothesis driven techniques to investigate the developmental shifts in the semantic network.

Keywords: brain development, functional neuroimaging, language, pediatric, child, fMRI

INTRODUCTION

Functional brain imaging methods have recently emerged as means of investigating connectivity and the dynamic flow of information across neural networks sub-serving cognitive functions (McIntosh and Gonzalez-Lima, 1994; McIntosh et al., 1994; Friston et al., 2003; Penny et al., 2004a,b). These methods measure, e.g., the generated electrical/magnetic fields (EEG/MEG) or the hemodynamic response associated with neural activity (fMRI). The functional data analysis methods frequently focus on identifying areas of activation under different behavioral conditions with less attention paid to the behavior of the underlying network (Friston et al., 1995).

Until recently, fMRI studies have employed model-based approaches predicated upon *a priori* knowledge of an applied stimulus and the brain's response [*hemodynamic response function* (*HRF*)] to the stimulus (Bandettini et al., 1993; Worsley and Friston, 1995). Such models are typically based on canonical forms for the HRF and do not reflect individual variations or account for differences between individuals of different age, sex, or pathologies. We have *previously* discussed that this statistical approach may not capture the complexity of brain networks supporting a language task such as covert verb generation (Karunanayaka et al., 2010). Several methods have been proposed to circumvent this drawback by avoiding assumptions about the shape of the HRF (Ollinger et al., 2001). Moreover, *a priori* model testing based on fewer free parameters presents significant challenges for an investigation that deals with the developmental trajectories of skills sub-serving verb generation. In particular, such limitations significantly impact our ability to test specific models (e.g., regionally weighted or focal network models) of language development using neuroimage data as input to connectionist approaches for neurocognitive modeling. In the connectionist approaches a system behavior is captured by adjusting the weights on connections between elements in the network to investigate how the statistical structure of inputs influences the behavior of the network (Plaut et al., 1996). Therefore, with more parameters (degrees of freedom) one is better positioned to capture any development shifts in neurocognitive modeling.

The utility of independent component analysis (ICA) for examining changes in brain networks associated with age and brain development has recently been demonstrated in the context of resting state (Stevens et al., 2009a) as well as active neurocognitive processes (Stevens et al., 2009a,b) such as language function (Schmithorst et al., 2006; Karunanayaka et al., 2007, 2010, 2011; Kim et al., 2011). Unlike model-based approaches, ICA is a data-driven technique capable of detecting additional task-related neural networks that exhibit activity with different temporal behavior (Calhoun et al., 2001a). This approach has significant advantages

when compared to the model-based methods that may not identify brain areas with temporal behavior that is not correlated with the experimental design matrix. However, ICA generates a considerable number of components that may not necessarily be part of the studied network (Calhoun et al., 2001b). To address this issue, we have incorporated several additional steps in our ICA method that make the results of our study more targeted and objective (Karunanayaka et al., 2010). In particular, we have adopted a theory-driven focus based on the Wernicke–Geschwind model of the language network with the aim of investigating developmental shifts in the verb generation circuitry in children from 5 to 18 years of age (Geschwind, 1965a; Anderson et al., 1999). Inclusion of such a focus yields a biologically plausible network model for covert verb generation predicted by the methods proposed here, which is more inclusive and specific in comparison to models extracted using general linear modeling (Yuan et al., 2006; Holland et al., 2007).

In the present paper, we explore the age dependency of the connections between the nodes of the language network that sub-serve the verb generation task. The verb generation model discussed here is based on nodes generated from a group ICA of fMRI data obtained from 336 children ranging in age from 5 to 18 years: which has been discussed in detail in one of our previous publications (Karunanayaka et al., 2010). The current analysis takes the previously described ICA analysis further by investigating interactions within the identified verb generation network using linear structural equation modeling (LSEM). The initial investigation of verb data using group ICA specifically dealt with: (1) ICA decomposition of verb data; (2) age effects in the task-relatedness of each individual IC map (at individual network level) using an *a priori* criterion (e.g., correlation with the task reference) and Bayesian formalism; (3) brief description of the steps leading to the present model (Karunanayaka et al., 2010). In the current analysis, the previously described model is further expanded with input functions (processing of presented nouns) and output functions (retrieval and covert verb production) together with hypothesized connections within and between them. In addition, a theory-driven focus has been proposed taking the biological plausibility of the verb model into account; evaluated against the literature with the focus on the language circuitry. Thus, the current investigation provides an elegant methodology capable of providing unique insight into the framework of neurocognitive brain development in children: by combining and extending previously published ICA results (Karunanayaka et al., 2010) with some of the figures reproduced in this paper for convenience and completeness. Thus, in the present work the emphasis is placed on the neurocognitive brain development and on estimating the age dependency of inter- and intra-network connectivity predicted using LSEM and correlation analysis.

The verb generation task begins with an auditory presentation of a noun: requires the listener to process the noun's phonological form, and attach meaning to that form (Hickok and Poeppel, 2004). Based on our previous description, this process begins with an input via the superior temporal gyrus (Karunanayaka et al., 2010). Processing in this area extends posteriorly from primary auditory cortex, as the act of accessing word's meaning is presumed to activate a broader network (Levelt et al., 1999; Pulvermuller, 2001). The posterior superior temporal cortex is known to be structurally asymmetric from the prenatal period (Wada et al., 1975; Chi et al., 1977), which suggests a structural basis for early left hemisphere lateralization of related functions (Foundas et al., 1994). While functional asymmetries are not present at birth (Kotilahti et al., 2010) the anatomical asymmetries, in association with genetic factors, may underlie later development of functional asymmetries (Szaflarski et al., 2002; Francks et al., 2007). In fact, previous reports from the parent project that generated this data set (Szaflarski et al., 2006a,b; Holland et al., 2007) and others (Wood et al., 2004; Chou et al., 2006) have indicated that the initial left lateralization in this area strengthens with age with maximum left lateralization achieved around the age of 20–25 years followed by gradual decrease in the observed asymmetries with increasing age (Szaflarski et al., 2002, 2006a). Therefore, in this study we expected to confirm the age-related changes in the networks (inter and intra) that sub-serve verbal abilities.

Because the noun must be held in working memory as the verbs are generated, we expect that the temporal cortex must be connected to a fronto-parietal network that is routinely activated in studies involving working memory (Chein et al., 2003). This includes activation of the inferior frontal gyrus, dorsolateral prefrontal cortex, and parietal cortex. More specifically, the superior temporal cortex is functionally connected to the inferior frontal gyrus (through the arcuate fasciculus) as the anatomical connections between these two regions are well established (Catani et al., 2005). The dorsolateral prefrontal (executive control) and parietal (sustained attention to words) cortices modulate activity in this region through either the superior branch of the arcuate fasciculus (Catani et al., 2005) or the superior longitudinal fasciculus. Because working memory shows age-related improvement, we would expect that the associated neural regions will also show age-related changes. Furthermore, the protracted period of development of the frontal lobes (Giedd et al., 1999; Schmithorst et al., 2002; Giedd, 2004; including connections with Brodmann's areas 17, 18, 31, and 32) may make the associated cognitive functions, the underlying regions, and the connections with these regions particularly dynamic through the course of childhood.

To generate a verb that is plausibly related to the noun, the child must select semantic concepts that are associated with the meaning of the noun. On the output side, semantic retrieval is likely to engage the middle and inferior temporal regions (semantic knowledge) and the hippocampi (information retrieval). The semantic concepts must be coded into phonological form, typically thought of as the second stage of the word retrieval process (Binder et al., 2008). Because semantic associations refine over the course of childhood (McDonald, 1997; McGregor et al., 2002; Beitchman et al., 2008), it is likely that activation in both of these areas will change with age. The phonological form is further coded into subvocal speech (Thompson-Schill et al., 1997). This suggests a second activation by inferior frontal gyrus for subvocal phonological encoding as well as contributions by the insula for speech coordination in subvocal naming. In the covert verb generation task the speech motor network is still engaged but must be inhibited so that words are not spoken overtly (Skipper et al., 2005). We would also expect age-related changes in the neural networks supporting these cognitive components and the connections between them.

There is evidence to suggest that the developing brain adheres to two rudimentary principles of organization: functional integration and functional specialization (Berl et al., 2006). At a neurobiological

level, this distinction can be identified with *progressive specialization* or *focalization* reflecting the consolidation of synaptic reinforcement of a network (Lenneberg, 1967; Muller et al., 1998; Berl et al., 2006). In this paper, we present a unified framework and examine the developmental trajectories in the language circuitry based on fMRI data using complementary modeling approaches. As previously (Karunanayaka et al., 2010), we employ ICA, a data-driven method, to identify spatially coherent activation patterns. In the current investigation, we extend these analyses by applying correlation analysis and LSEM to model connectivity between these spatial distributions. Several, other approaches have previously been proposed to investigate network interactions following ICA analyses. Stevens et al.'s (2007) used dynamic causal modeling (DCM) to search for the presence of a meaningful causal structure among selected IC time courses in an event related fMRI study of visual Go/No–Go task. Another study examined the functional network connectivity (FNC) between schizophrenia patients and healthy controls based on the temporal dependency among ICA components (Jafri et al., 2008). Demirci et al. (2009) extended this analysis one step further by incorporating Granger causality test (GCT) to investigate causal relationships between brain activation networks; we also have recently implemented Granger causality analysis to investigate the connections within the epileptic network (Szaflarski et al., 2010). Several, other investigations have further highlighted the usefulness of combining ICA with Granger causality on simulated, single subject and group data (Londei et al., 2006, 2007, 2010). Some of the above mentioned methods are relatively sophisticated and more suitable for investigating specific group differences between healthy and patient populations. However, the emphasis of the current analysis is on investigating the overall developmental trends associated with the language circuitry and presenting the findings in the framework of a theoretical model for neurocognitive brain development. Thus, given the large sample size, the simplicity of the proposed partially data-driven approach can be considered more suitable for understanding the global network structure (including connectivity) associated with complex verbal language tasks in general, and verbal fluency tasks in particular.

MATERIALS AND METHODS

SUBJECTS

One hundred sixty-five boys and 171 girls took part in the study following Cincinnati Children's Hospital Institutional Review Board approval. Informed consent was obtained from parent or guardian, an assent was also obtained from subjects 8 years and older. Exclusion criteria were: previous neurological illness; learning disability; head trauma with loss of consciousness; current or past use of psychostimulant medication; pregnancy; birth at 37 weeks gestational age or earlier; or abnormal findings at a routine neurological examination performed by an experienced pediatric neurologist. All subjects were considered *healthy* based on neurological, psychological, and structural measures (Holland et al., 2007). Subjects included in this report were also included in our previous studies focusing on verb generation in children (Holland et al., 2001, 2007; Karunanayaka et al., 2010) and adults (Szaflarski et al., 2006a). While this report includes fMRI data from the same subjects, it describes an entirely new analysis of connectivity (causality) associated with covert verb generation networks extending the finding of our previous study (Karunanayaka et al., 2010). The previously described group ICA provides a complete recipe of the prerequisite steps involved in ICA decomposition to identify the key elements underlying a biologically plausible neural network that sub-serve a specific neurocognitive task (Schmithorst and Brown, 2004; Schmithorst et al., 2006; Karunanayaka et al., 2010, 2011; Kim et al., 2011). A complete age and sex breakdown of the included subjects (native, monolingual, English speakers) is detailed in **Table 1**. Based on the Edinburgh Handedness Inventory (Oldfield, 1971), 311 subjects were right-handed, 24 left-handed, and 1 ambidextrous. All subjects were prescreened for any conditions which would prevent an MRI scan from being acquired (Karunanayaka et al., 2010). Out of 336 subjects, 331 received the Wechsler Preschool and Primary Scale of Intelligence (WPPSI-R, ages below 6) or the Wechsler Intelligence Scale for Children [Third Edition (WISC–III, ages 6–16 years); Wechsler, 1991] or the Wechsler Adult Intelligence Scale, Third Edition (WAIS–III, ages 17 and 18 years; Wechsler, 1997). Similarly, 330 subjects received the Oral and Written Language Scales (Carrow-Woolfolk, 1996). The age range for all subjects was 4.92–18.92 years; Mean Wechsler Full-scale IQ = 111.6 ± 13.84 (range = 70–147); Mean OWLS = 107.7 ± 14.3 (range = 66–151).

FUNCTIONAL IMAGING

All images were acquired using a Bruker 3T Medspec (Bruker Medizintechnik, Karlsruhe, Germany) imaging system. An MRI-compatible audiovisual system was used for presentation of the stimuli. Details of the techniques used to obtain fMRI data from younger children are discussed elsewhere (Byars et al., 2002). EPI–fMRI scan parameters were: TR/TE = 3000/38 ms; 125 kHz; FOV = 25.6 cm × 25.6 cm; matrix = 64 × 64; slice thickness = 5 mm. Twenty-four slices were acquired, covering the entire cerebrum. One hundred ten whole-brain volumes were acquired (with the first 10 being dummy scans) in 5 min 30 s. Techniques detailed elsewhere (Byars et al., 2002) were used to acclimatize the subjects to the MRI procedure and make them comfortable inside the scanner. A whole-brain T1 weighted MP-RAGE scan was also acquired for anatomical co-registration.

VERB GENERATION TASK

The fMRI paradigm of silent verb generation (Holland et al., 2001, 2007) is a 30-s on–off block design. All stimuli were presented using MacStim (White Ant Software, Melbourne, VIC, Australia) at a rate of one noun every 5 s, for six stimuli during each 30 s epoch. During the active epochs, the subjects silently generated

Table 1 | Age and gender breakdown of the study population (165 boys and 171 girls).

Age in years	5	6	7	8	9	10	11	12	13	14	15	16	17	18
SEX														
M	9	8	9	17	14	12	17	18	17	9	10	9	13	3
F	7*	12	17	10	11	12	11	15	21	11	11	10	12	11

**Includes one girl 4 years 11 months. The ethnic background of the subjects was: 302 Caucasian, 21 African–American, 2 Asian, 3 Hispanic, 1 Native American, 2 Asian/European, and 5 Multi-Ethnic.*

appropriate verbs such as *drink* or *fill*, to aurally presented nouns such as *cup*. Subjects were asked to tap their fingers in response to a modulated tone presented at 5 s intervals during the control epochs. The control task was specifically designed to control for sublexical auditory processing and also to divert subjects to stop generating verbs into the control epochs. The fMRI task was selected such that children as young as 5 years old would be readily able to perform the task without any difficulty.

GROUP ICA

A complete description of the group ICA methodology for verb generation fMRI data has been discussed in detail elsewhere (McKeown et al., 1998; Calhoun et al., 2001a; Schmithorst et al., 2006; Karunanayaka et al., 2010). Basic steps involved in ICA decomposition are briefly mentioned here for the purpose of completeness. ICA is a data-driven analysis technique that does not rely on any prior knowledge of the task performed and is capable of identifying spatially independent components that have similar time courses. The power of group ICA in making statistical inferences from fMRI data has been presented in several investigations (Calhoun et al., 2001a; Schmithorst and Brown, 2004; Schmithorst and Holland, 2006; Karunanayaka et al., 2010).

The ICA decomposition entails several preprocessing steps [normalizing (mean centering) and 40 retained principal components (PCA)] at the single subject level. The data from all subjects are then concatenated into a single dataset before a second PCA reduction resulting in 50 retained components. Finally, 25 runs of the Fast ICA algorithm (Hyvarinen, 1999b) are combined with hierarchical agglomerative clustering (Himberg et al., 2004) to estimate and validate the independent component maps sub-serving covert verb generation. Performing multiple runs (when combined with hierarchical agglomerative clustering) ensures that our analysis resulted in the most reliable components even after taking into account the stochastic nature of the Fast ICA algorithm. Although, ICA can be used to remove motion-related artifacts, individual motion has been fully characterized before performing the ICA decomposition. A detailed analysis of motion (including task-related movement) related to this task is discussed elsewhere (Yuan et al., 2009).

The task-relatedness of each IC map is then investigated using the associated IC time course by examining the spectral power at the task frequency and the phase of the IC time course relative to the task reference function as detailed previously (Karunanayaka et al., 2010). It should be noted that, by definition, spatial ICA requires independence only in the spatial domain and not in the time domain. Thus, an analysis performed in one domain (e.g., time) can be followed by analysis in another domain (e.g., spatial) without adding any undue bias to subsequent statistical manipulations. Finally, a voxel-wise random effects analysis (one-sample *t* test) is performed on selected individual IC maps in the spatial domain to determine the cortical regions active in the entire cohort. To further clarify this step, if one were to reverse the domains of the preceding analysis (e.g., spatial followed by time), the end result would be the same because of the above mentioned symmetry. An assumption inherent in this approach is that the structural components of the network for verb generation are in place by the age of the youngest subjects in our cohort (5 years) and continue to get fine tuned to form the structural basis for completion of the task through the age of the oldest subjects (18 years). By concatenating the data from the entire cohort and searching for the components (or networks) that are common across the age group, we are able to identify the persistent structural elements (network nodes) underlying the fMRI verb generation task consisting of seven IC networks and shown in **Figure 1**. **Table 2** contains a summary of the respective activation foci for each of the components. Coordinates listed for each IC correspond to the center of mass of each individual spatial element contained in the IC map.

To summarize, the selection of IC maps is based on three criteria: (1) power spectral analysis at the task frequency; (2) phase and (3) relevance of the spatial maps to the theoretical model of verb generation. Thus, by following the above mentioned criteria, the results of this ICA analysis can be replicated by other researchers in the field.

From this point on, we focus on estimating the changes in connectivity between elements of the model identified by ICA using LSEM which is a unique contribution of this work.

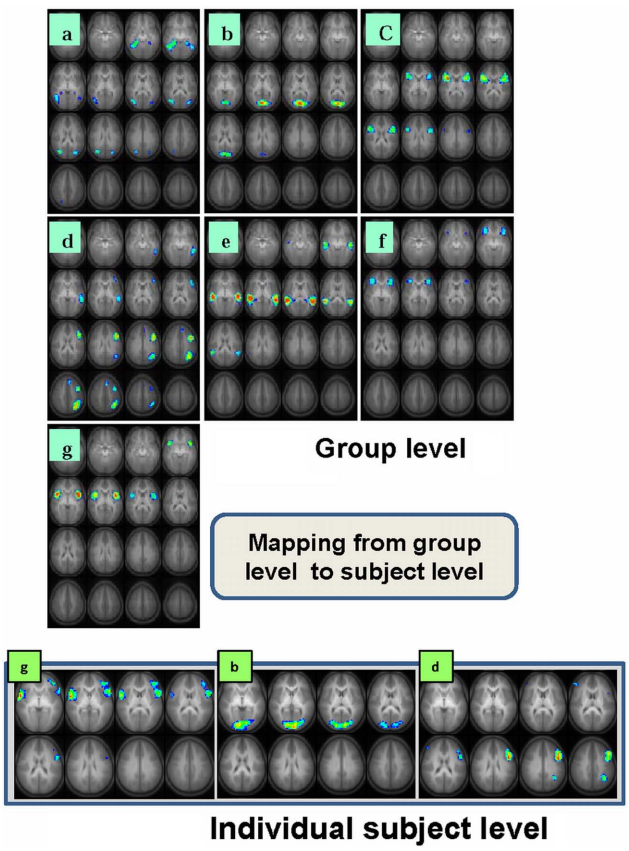


FIGURE 1 | Seven task-related spatial independent components maps are shown in panels a-g. These ICs are computed using group ICA analysis of 336 children ages 5–18 performing the task of covert verb generation (Karunanayaka et al., 2010). Slice range: Z = −25 to +50 mm (Talairach coordinates). Three corresponding single subject IC maps are shown at bottom (**g, b, d**). These individual spatial maps and the associated time courses (**Figure 2B**) are estimated using a back propagation algorithm following the ICA decomposition at the group level and used in the subsequent LSEM analysis. All images are in radiologic orientation.

Table 2 | Activation foci (Talairach coordinates) for the ICA components displayed in Figure 1.

Anatomical region	BA	Talairach		
		X,	*Y,*	*Z*
A				
R. parahippocampal gyrus	30/35	22,	–41,	–5
L. parahippocampal gyrus	30/35	–26,	–41,	–5
R. inferior temporal gyrus	19/37	42,	–57,	–5
L. inferior temporal gyrus	19/37	–46,	–57,	–5
R. medial temporal gyrus	19/39	34,	–69,	20
L. medial temporal gyrus	19/39	–26,	–73,	25
B				
Cuneus	17	2,	–77,	10
C				
R. inferior frontal gyrus	44	34,	11,	10
L. inferior frontal gyrus	44	–34,	11,	10
D				
L. medial temporal gyrus	21	–54,	–41,	–5
L. inferior frontal gyrus	45/46	–46,	27,	15
L. inferior/medial frontal gyrus	44/9	–42,	7,	35
L. middle frontal gyrus	6/8	–6,	23,	45
L. angular gyrus/inferior parietal lobule	39/40	–30,	–65,	40
E				
R. superior temporal gyrus	22	50,	–29,	5
L. superior temporal gyrus	22	–54,	–45,	10
F				
R. inferior frontal gyrus	45/47	30,	31,	0
L. Inferior frontal gyrus	45/47	–38,	23,	0
G				
R. insula	Insula	38,	11,	0
L. insula		–38,	11,	0

LINEAR STRUCTURAL EQUATION MODELING

Linear Structural Equation Modeling is a statistical method mainly used for hypothesis testing regarding causal influences among measured or latent variables. In addition, SEM is capable of statistically testing a variety of theoretical models that hypothesize how sets of variables define constructs and how these constructs are related to each other. In terms of neuroimaging, SEM relates to effective connectivity that captures causal relationships (directionality) in terms of path coefficients in the model. This approach differs from a typical functional connectivity analysis that can only determine the degree to which two brain regions co-vary (Friston et al., 1997). As mentioned elsewhere, our group ICA decomposition is based on the methods developed by Calhoun et al. (2001b) and is designed to evaluate individual IC maps and corresponding time courses based on group results. In other words, in this method individual IC time courses are estimated using a back propagation method which is followed by the ICA decomposition at the group level. In this paper, we use these individual IC time courses as input to estimate LSEM(s) at the subject level in order to examine the effective connectivity within the network model for verb generation.

A second level, intra-network functional connectivity analysis was also performed using representative real signal intensity average time courses from ROIs defined based on the spatial distribution of each group IC map (Karunanayaka et al., 2007). Specifically, representative average time courses were extracted from the functional data set (i.e., real signal intensities) based on these functionally defined ROIs. It is important to remember that ROIs derived from spatial IC maps often include multiple anatomical brain areas, as outlined in **Table 2**. For all of the IC maps shown in **Figure 1**, except for IC d, ROIs were defined separately for the left and right hemisphere components of the IC. Based on these ROIs, as mentioned earlier, extracted real signal time courses from the functional data set were then used for the between hemispheres intra-network connectivity computations.

A variety of models can be tested in SEM to capture relationships among variables and can provide a quantitative test for a hypothesized theoretical model. SEM takes the entire variance–covariance structure into consideration when evaluating models. Furthermore, SEM is a generalization of regression, path and confirmatory factor models that have been extensively used in psychology, economics and other social sciences. The model estimation in SEM involves minimizing the difference between the observed variance–covariance structure and the one predicted by the implied model. However, when using SEM to model brain activity no distinction is made between the neuronal and the hemodynamic levels (Penny et al., 2004b) which can be considered a drawback of the method.

In the presented model, which is based on **Figure 1**, we only evaluated the feed-forward connections. As noted above, representative time courses for each of the components (*elements*) in the LSEM are comprised of individual IC time courses from the previously performed ICA decomposition. The individual LSEM(s) were then solved for optimal path coefficients using the Amos software (Arbuckle, 1989) which utilizes an iterative maximum likelihood method. These optimal path coefficients (connection strengths) correspond to the solution of the structural equations where the difference between the observed and the predicted covariance matrix is a minimum. Finally, we evaluated the goodness of fit between the predicted and the implied covariance matrices using the χ^2 distribution with $m\ (m+1) - n$ degrees of freedom (m corresponds to the number of elements and n corresponds to the number of coefficients in the LSEM respectively). The details of LSEM implementation for fMRI data have been discussed elsewhere (McIntosh and Gonzalez-Lima, 1994; Solodkin et al., 2004; Karunanayaka et al., 2007; Dick et al., 2010). The LSEM itself was used (constrained by the proposed verb generation model discussed in the introduction) in a semi-exploratory manner when selecting the final LSEM. Advantages of alternative methods for brain activity modeling (such as DCM) have also been discussed by other authors (Friston et al., 2003; Penny et al., 2004b). Recently, an extended version of SEM called unified structural equation modeling (uSEM; Smith et al., 2010) has been proposed capable of estimating contemporaneous as well as lagged effects simultaneously (Stoeckel et al., 2009). An automatic search procedure has also been proposed to uSEM making it entirely data-driven by increasing its flexibility substantially (Kim and Horwitz, 2009). However, DCM is still appears to be the most statistically sophisticated approach that incorporates neuronal hemodynamic relationship into a dynamic model of BOLD activities using Bayesian estimation (Friston et al., 2003; Friston and Stephan, 2007; Sarty, 2007). Thus, given the fact that the relationship between BOLD signal and neuronal activity

is poorly understood (de Marco et al., 2009), LSEM may be a very effective method for making inferences about changes in the causal structure from fMRI time series data.

In addition, several methods have been employed to obtain representative time courses for the components included in a SEM analysis: one popular method being the maximum active voxel representation (Jennings et al., 1998; Goncalves et al., 2001) which we employed previously to investigate developmental trends associated with the narrative story comprehension in children (Karunanayaka et al., 2007). However, in the current analysis, IC time courses were used to evaluate individual LSEMs to investigate the verb generation task in children. A brief description of the differences between the two methods are included in the section below and also in the Section "Discussion."

BIOLOGICAL CONSTRAINTS

Several principles have guided the process of constructing a biologically plausible linear structural equation model for verb generation. As the first step (described above), ICA was used as a data-driven descriptor of neural elements involved in performing the fMRI paradigm. The second step involved a Fourier method in the time domain to determine which ICs were most task-related by testing the correlation between the fundamental frequency of each IC time course and the task frequency. The third step involved constructing a biologically plausible LSEM using the knowledge of the sequence of neurocognitive functions involved in the task with IC modules as building blocks (Karunanayaka et al., 2007). The IC maps require only independence in the spatial domain allowing highly correlated temporal structures to form the theoretical basis for the current SEM analysis. Finally, the phase of the Fourier transform of the associated IC time courses and the known neuroanatomical constraints were also taken into consideration when imposing connections between the model elements.

Some individual ICs out of the seven selected, contain more than one Brodmann's area even though the representative time course for the IC represents all of the voxels included in the spatial map. This is because ICA reveals a set of chronoarchitectonically identified areas (Bartels and Zeki, 2004) or functionally connected regions that may span several Brodmann's areas. If a given cognitive task recruits only one of the observed regions in a given map, then there will be another component separated out by ICA containing only that region. However, if two distinct cognitive functions have very similar time course, they may well be grouped into a single ICA component. This is a limitation of correlational analysis. Still, under certain minimal assumptions, the spatial independence of IC maps can be equated with their modularity, establishing a correspondence between the IC component and a specific cognitive task (Duann et al., 2002; Calhoun et al., 2004). A limitation of this assumption is our inability to determine spatial independence of components with absolute certainty due to the finite number of voxels in fMRI experiments. However, this limitation may have only a minimal effect on the current investigation because of the excellent signal to noise ratio provided by the large number of subjects in the study. Therefore, we argue that it is reasonable to assume that each IC map constitutes a module (a cognitive functional unit) in the proposed LSEM. Depending on the spatial distribution of the IC (activation), a specific language function can be assigned to each IC based on known functional neuroanatomy (*knowledge-base*) ascribed to each Brodmann's area encompassed by the component. As mentioned previously, a theory-driven focus (Geschwind, 1965a; Anderson et al., 1999) complements data-driven methods such as ICA by way of corroborating prior hypotheses about cognitive functions sub-serving the verb generation fMRI task.

Depending on the modularity (or function), IC modules are then connected to one another to form the LSEM. In this study, LSEM is directly derived from the covert verb generation model as discussed in the Section "Introduction". For studies of developmental changes within a network, LSEM of an fMRI task can investigate what changes in functional connectivity explain the neural basis of development in language networks. This physiological approach should be guided by the weak constraint that anatomical proximity and connectivity of brain regions are incorporated in the model (Karunanayaka et al., 2007). Alternatively, a cognitive approach can also be implemented to investigate how functional/effective connectivity changes are related to cognitive development. The emphasis of the current analysis is inline with the latter approach where the effective connectivity changes between IC modules subserving covert verb generation are investigated.

Finally, a second level Pearson correlation analysis was performed on path coefficients in the LSEM to investigate any age effects associated with the proposed cognitive model for covert verb generation.

RESULTS

Six out of the seven IC maps shown in **Figure 1** were detected in all 25 IC runs while the component shown in **Figure 1a** was detected in 17 IC runs assuring high reliability (Karunanayaka et al., 2010) and defines the covert verb generation network for each subject included in the study. The maps in the lower row (individual subject level) of **Figure 1** shows three corresponding individual subject level IC maps with corresponding IC time courses: estimated following the ICA decomposition at the group level and used in the subsequent subject level LSEM analysis. **Figure 2A** shows two of the corresponding average time courses for IC maps shown in **Figures 1a,d**. **Figure 2B** shows the individual IC time courses for these networks in two subjects: used as the input to the LSEM computations. The phase progression of the average time courses from leading to lagging the task reference time course (indicated by dark and light gray background) is clearly visualized in **Figure 2A**.

The developmental trajectories, network behavior (lateralization, task-relatedness, etc.) and the language functions attributed to each IC have been discussed in detail elsewhere (Karunanayaka et al., 2010). The highly left-lateralized IC map shown in **Figure 1d** (with lateralization index equal to 1) was identified previously as capturing most of the left-dominance observed in a standard GLM analysis for the covert verb generation task (Holland et al., 2007). To perform the intra-network connectivity analysis for this left-lateralized network, four separate ROIs were defined in the left hemisphere as shown and labeled in **Figure 3**. As explained above, only the real signal time courses from activated regions (refer to **Table 2** for further details) inside the colored circles are included in the ROI analysis. The connection between (1) left middle temporal gyrus (LMTG) $\rightarrow$ (3) left middle inferior frontal gyrus (LMIFG) showed significant age dependent connectivity changes ($r = 0.15$,

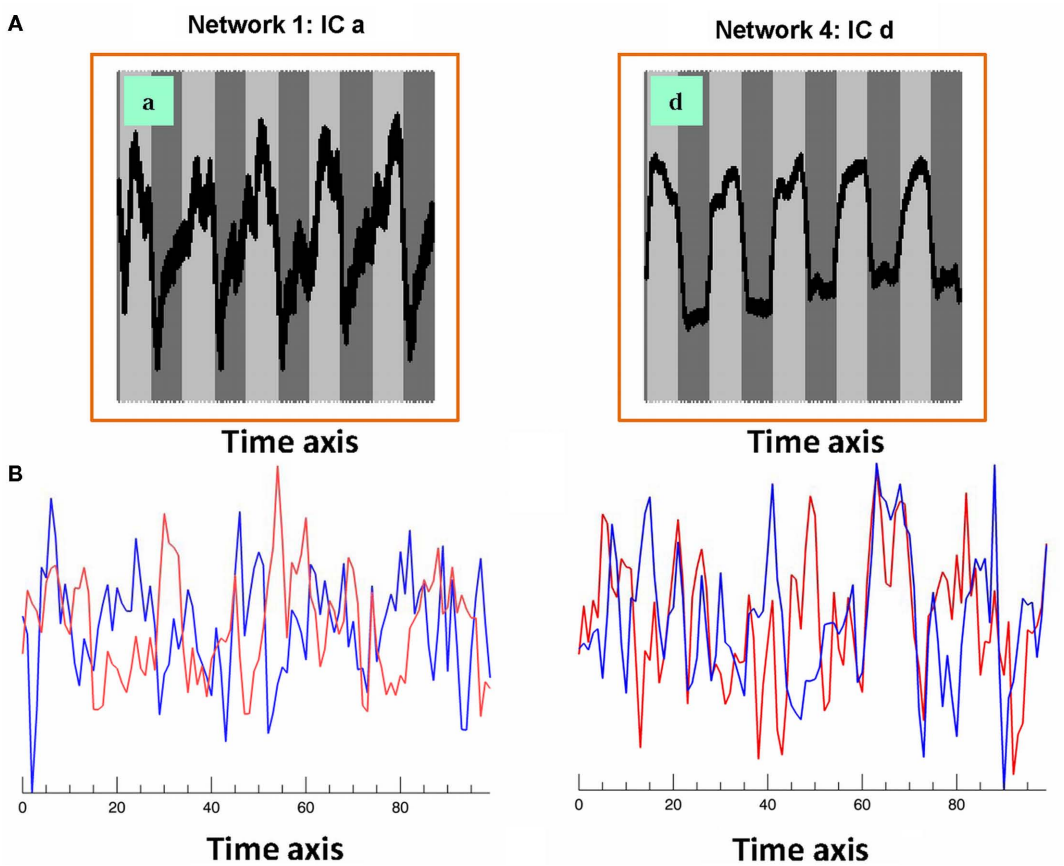


FIGURE 2 | (A) Associated averaged time courses from two group IC networks shown in **Figure 1**. Horizontal axis is *time* and the vertical axis is *intensity* (*pseudo*). Gray and white background indicates the timing of the task reference function; **(B)** associated IC time courses from two subjects (red and blue) corresponding to **Figures 1a,d** networks. These IC time courses correspond to similar individual subject networks as shown in the lower row (individual subject level) of **Figure 1.** These IC time courses are used in subject level LSEM evaluations.

$p = 0.007$). The Functional connectivity between (1) LMTG → (4) left angular gyrus (LANG) showed no significant age effects. Similarly, the functional connectivity between (4) LANG → (2) left inferior frontal gyrus (LIFG) showed significant age effects ($r = 0.143$, $p = 0.0089$) while the functional connectivity between (4) LANG → (3) LMIFG did not. Finally, the functional connectivity between (3) LMIFG → (2) LIFG showed a highly significant age effect ($r = 0.18$, $p = 0.002$).

Similarly, we also examined the inter-hemispheric functional connectivity based on individual spatial IC maps. The IC map shown in **Figure 1c** showed a highly significant age effect ($r = -0.3$, $p = 2.457e - 008$) in the connectivity between the hemispheres (**Figure 4**). Similarly, the IC map shown in **Figure 1f** also showed significant age effect ($r = -0.132$, $p = 0.015$) in inter-hemispheric connectivity. However, the IC shown in **Figure 1e** (bilateral superior temporal gyri; BA 22) did not exhibit significant age effects in functional connectivity between the left and right hemispheres (**Figure 4**). Similarly, IC modules a, b, and g also did not exhibit any age-related inter-hemispheric functional connectivity changes. Thus, for these components, we have not included the results of the above mentioned inter-hemispheric functional connectivity analysis.

As described in the Section "Materials and Methods," an LSEM was constructed using the functional IC maps with reference to the literature for prior knowledge (i.e., knowledge-base) about the known neuroanatomy of the brain regions involved in the language circuitry. This LSEM was further refined based on the hypothesized cognitive functions associated with the brain regions encompassed within each spatial IC map, forming the basis for the proposed theoretical cognitive model for covert verb generation as shown in **Figure 5**. Of note is that the connections between brain regions may not be explicitly included in the proposed model if they are implied by inclusion within a single IC. For example, IC d includes frontal, temporal, and parietal regions. The cartoon in **Figure 5** demonstrates this aspect of the model by using an extended ROI spanning these lobes to illustrate the spatial extent of IC d.

Table 3 shows the average value of each standardized path coefficient and the age-related changes in path coefficients computed for the LSEM shown in **Figure 5**. A similar figure (model) was included in a previous study by Karunanayaka et al. (2010); though that diagram did not include the path coefficients computed here as a parameter expressing brain connectivity. As mentioned earlier, the focus of the present analysis is on developmental changes in connectivity within the neural circuitry of language; therefore, we

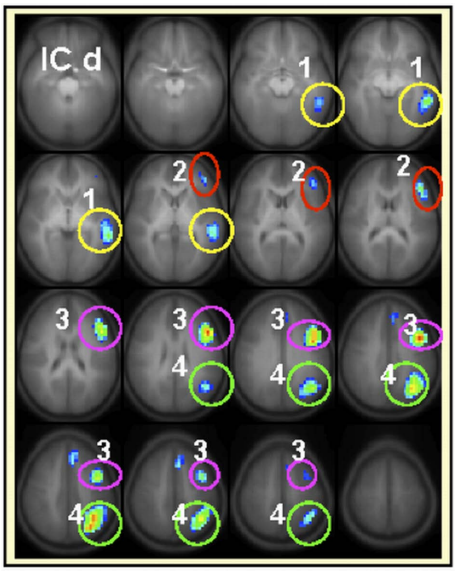


FIGURE 3 | Regions included (only the active areas) in the intra-component functional connectivity analysis for IC d are [1]medial temporal gyrus (LMTG), [2]inferior frontal gyrus (LIFG), [3]middle inferior frontal gyrus (LMIFG), [4]angular gyrus (LANG). Each brain region will be represented by the average activation within that ROI across time. Slice range: $Z = -25$ to +50 mm (Talairach coordinates). All images are in radiologic orientation (left in the picture is right in the brain).

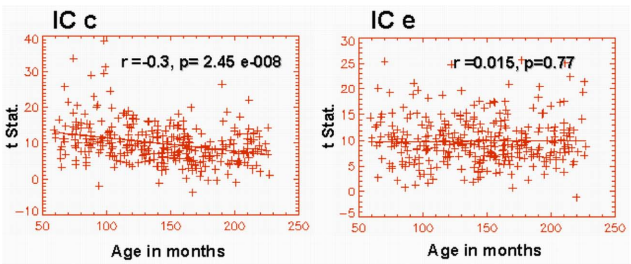


FIGURE 4 | Graphical representation of the age dependence of functional connectivity between left and right hemispheres corresponding to IC maps shown in Figures 1C,E. IC c exhibits a highly significant functional connectivity between the left and the right inferior frontal gyrus.

examined changes in the path coefficients estimated by the LSEM as a function of age. The following path coefficients exhibited age-related changes: The path coefficient between IC e → IC f showed an increase in connectivity with age ($r = 0.13$, $p < 0.017$). The path coefficient between IC e → IC d showed a modest (identified with a trend) age-related connectivity decrease ($r = -0.111$, $p < 0.044$). However, the path coefficient between IC f → IC d exhibited a highly significant age-related increase in connectivity ($r = 0.18$, $p < 0.00088$). **Figure 6** graphically displays the corresponding standardized path coefficients that showed statistically significant age-related changes. These values are italicized in **Table 3**.

For the group of children included in this study, subject age was significantly correlated with the full-scale IQ (Spearman's $r = -0.18$, $p < 0.0008$). This small but significant negative correlation is mainly attributed to the youngest subjects having higher than average IQ (Karunanayaka et al., 2010). To be more specific, when the children between the ages 5 and 8 years were excluded, the weak correlation between age an IQ did not reach significance and consequently we have not included IQ as a covariate in the analysis.

DISCUSSION

Methods for network connectivity analysis based on functional neuroimaging data are developing rapidly as a means of expanding our understanding of neurocognitive function beyond what the neo-phrenology or functional blobology of fMRI have been able to reveal (Friston et al., 2003; Schmithorst and Holland, 2007; Schmithorst et al., 2007; Rajapakse et al., 2008; Dick et al., 2010). ICA is an ideal preliminary step for network connectivity analysis because it is able to detect areas that exhibit task-related behavior which might not correlate highly with an *a priori* model or reference function. In the present analysis, we began with ICA of verb generation data which detected activations in multiple networks with different temporal signatures. Multiple activation time courses detected in the same brain regions (specifically frontal and temporal cortex) provide direct evidence of their participation in multiple cognitive aspects of the verb generation task. ICA provided the basis for construction of a LSEM for the network that sub-serves verb generation task and allowed us to use this standard statistical methodology to explore the age dependency of the relationships among cognitive modules revealed by the ICA analysis (Karunanayaka et al., 2007).

The theoretical framework guiding this research focuses on investigating the developing brain from a network perspective and lays the foundation for deciphering any developmental trends as interactions between underlying networks. Starting with the Wernicke–Geschwind model for the language network, we used a data-driven approach to analyze results from an fMRI experiment in a large sample of children over a wide age range in order to extract key network elements supporting verb generation. This classical model guided our thinking about how to connect modules identified by group ICA results as having a strong correlation with the task behavior. We then examined the network structure to identify developmental trajectories that correlate with age and ability of children to think and reason at increasing levels of maturity (Schmithorst et al., 2006, 2007). We have shown elsewhere, how ICA can be used to explore developmental changes in brain activation patterns associated with individual neural networks supporting covert verb generation (Karunanayaka et al., 2010). The current analysis takes this approach one step further by incorporating LSEM to the investigations of the theories of brain development using the regionally weighted or focal network models (Berl et al., 2006). Although, these hypothesized brain developmental models draw support from current neuroimaging literature, our analysis seems to favor the regionally weighted model of normal language development.

Independent component analysis by itself is not capable of revealing the precise cognitive correlates of the identified components (Schmithorst et al., 2006). Instead, this data-driven method must be utilized to identify spatial distributions (IC maps) from fMRI data. As with GLM-based analyses, the function of the detected regions must be inferred and should be constrained by prior knowledge of

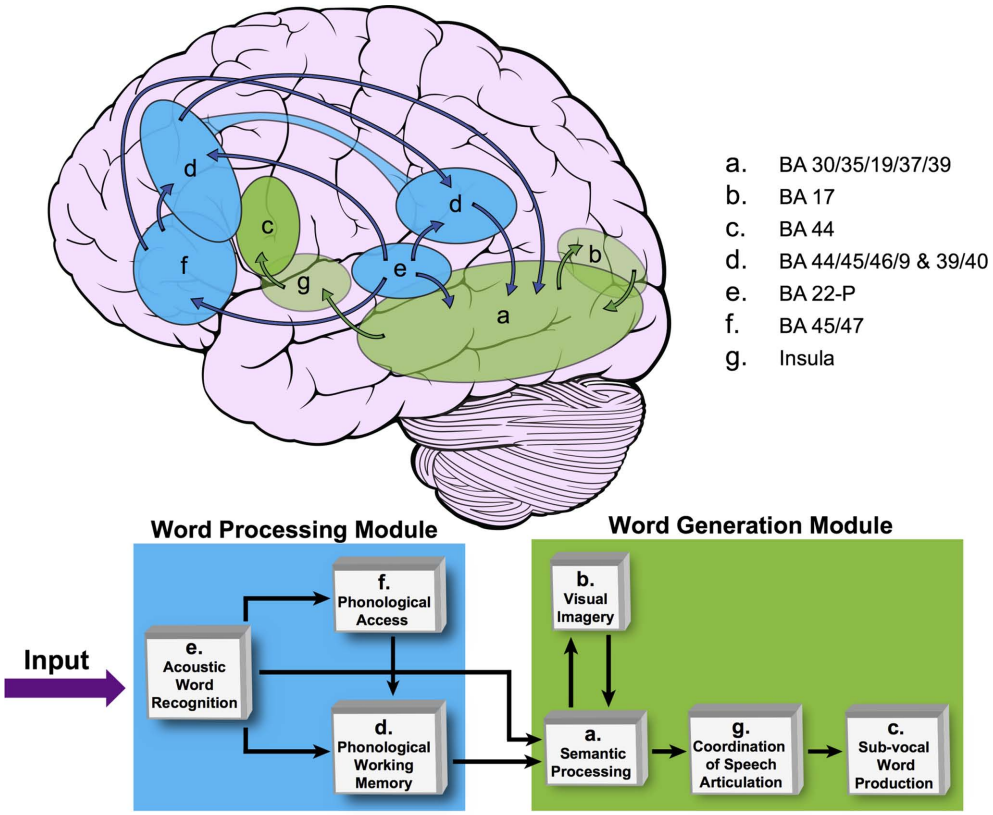


FIGURE 5 | The proposed covert verb generation model based on group ICA maps shown in Figure 1. This model is based on our previous publication (Karunanayaka et al., 2010; **Figure 4**). The brain cartoon shows the approximate locations of each IC map from **Figure 1**. Transparent ellipses indicate regions located medially within the brain and not visible from the lateral surface whereas opaque ellipses correspond to regions that are mainly located on the lateral surface of the brain. IC d is represented in both frontal and temporal–parietal regions as reflected in the distributed nature of this left-lateralized network. The network is divided into *word processing* (shown in blue) and *word generation* modules (shown in green). The SEM block diagram at bottom shows how these brain networks are graphically connected forming the basis for the cognitive model for the covert verb generation task. Only the Feed Forward Connections are evaluated.

Table 3 | The age-related changes in the standardized path coefficients (r and p value) for the SEM shown in Figure 5 are shown in column 2 as Pearson correlations between the path coefficient and age. Column 3 shows the average value of each standardized path coefficient for the entire age range of 5–18 years included in the analysis. Path coeffiences with a significant age correlations are highlighted in bold font.

Connection	*r* value, *p* value	Avg. value of Std. path coefficient
IC e → IC f	**0.1295, 0.0175**	0.31
IC e → IC a	–0.0429, 0.4326	0.16
IC e → IC d	**0.1804, 0.0444**	0.27
IC f → IC d	**0.1804, 0.000888**	0.33
IC d → IC a	–0.07917, 0.1475	0.17
IC a → IC b	–0.1036, 0.0577	0.36
IC a → IC g	–0.0232, 0.6660	0.23
IC g → IC c	–0.0385, 0.4807	0.57

the functional neuroanatomy. However, once the spatial distributions are known, depending on the complexity either a physiological or a cognitive approach can be employed for the connectivity analysis (Karunanayaka et al., 2010). Given the limitations [(Wright's rules; Write, 1934) and the number of nodes in the model] in evaluating LSEM(s), a careful consideration must be given before selecting either approach. In general, any theoretical model for language related cognitive functions will be a compromise between the complexity of the neural system sub-serving language comprehension and the interpretability of the resulting models. Complex models can account for intricate dependencies (both anatomical and functional) but the interpretability of the resulting models would be severely compromised (McIntosh and Gonzalez-Lima, 1994; Dick et al., 2010).

As suggested by Dick et al. (2010), one approach would be to use the hypotheses being tested as guiding the constraining aspects of the model development. An alternative, more appealing approach would be to model brain functions in terms of interactions between underlying sub-networks, inline with the method we have proposed in this paper. To circumvent inherent drawbacks of the second approach, in addition to the theory-driven focus, we incorporated a secondary correlation analysis specifically to investigate the within network behavior sub-serving covert verb generation in children (Friston et al., 1997).

The functional connectivity results of IC d revealed unique features related to semantic processing circuitry in children. Several studies have implicated activation in the middle temporal gyrus

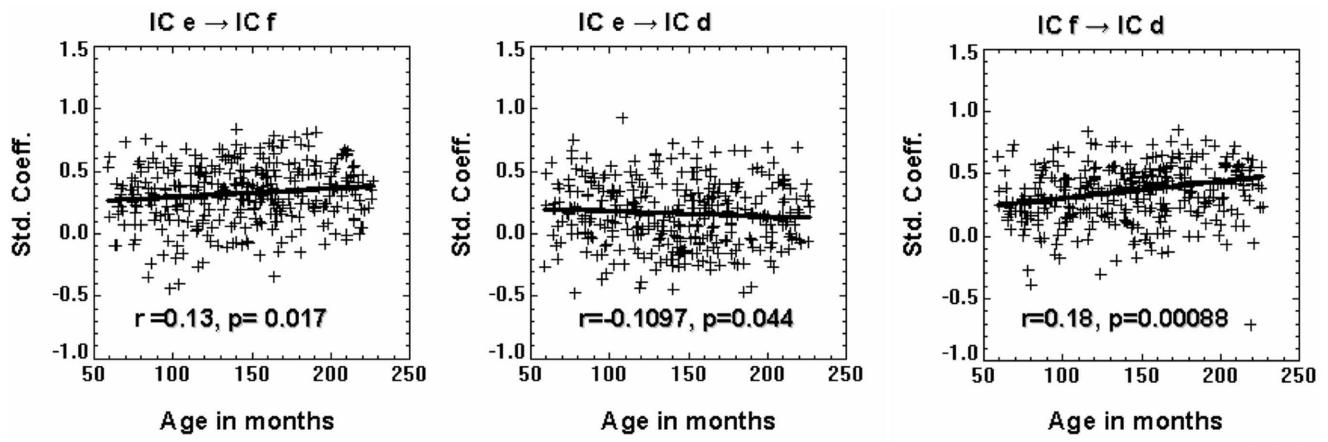


FIGURE 6 | Standardized path coefficients corresponding to the SEM shown in Figure 5 that showed significant changes with age are plotted as a function of age in months.

in the acquisition of semantic representations (Blumenfeld et al., 2006; Booth et al., 2007). Similarly, research in adults suggests that more activation in the inferior frontal cortex is associated with more effortful retrieval or greater selection demands (Seger et al., 2000; Gurd et al., 2002; Whatmough et al., 2002; Booth et al., 2007). Age effects seen in the functional connectivity between these two regions suggest that the selection demands imposed on the inferior frontal gyrus increase with age. This may be due to the fact that the present verb generation task does not impose restriction on the number of verbs a subject can generate for a given noun. Evidence suggests that this design is successful in minimizing the amount of variance attributable to performance (Gaillard et al., 2003).

The functional connectivity between LMTG → LANG showed no significant age effects. The inferior parietal cortex has been implicated in feature integration and semantic categorization to form a coherent concept so that semantic relationships between words can be determined (Grossman et al., 2003; Karunanayaka et al., 2010). The demand for such processes may be at a minimum for this task (ceiling effect) since we developed this fMRI task in such a manner that even the youngest children in our study can perform this task easily. Nevertheless, Booth et al. (2007) have suggested that the inferior parietal lobule may have distinct areas for processing semantic versus phonological information. This may explain observed age effects in functional connectivity: between LANG → LMIFG with no age effects and between LMIFG → LIFG with highly significant age effects.

The significant decrease in functional connectivity with age between right and left hemisphere elements of IC c implies a substantial change in the degree to which the left and right brain regions (inferior frontal gyrus) co-vary. Note that structural and functional asymmetries have also been found in the prenatal and early postnatal brain (Wada et al., 1975; Chi et al., 1977; Dehaene-Lambertz et al., 2002) suggesting a bias for left hemisphere language lateralization very early in life. The anatomical data suggest that early brain development may lead to an underlying architecture that preferentially supports language within the left hemisphere: a normal variant of the focal network model (Berl et al., 2006). This neuroanatomical bias is hypothesized to be related to functional lateralization and localization over the course of language development (Ahmad et al., 2003; Gaillard et al., 2003). Our previous findings of increasing left lateralization of IFG activation with age for the verb generation task in children are consistent with the functional connectivity findings showing decreasing left–right connectivity with age suggesting that the left hemisphere is able to act more autonomously in support of word generation as the brain matures (Holland et al., 2007). This interpretation is also consistent with the regionally weighted model of normal language development. Further, this finding alone can explain the differences between young and old subjects in language recovery after left-hemispheric injury with the ability of the language functions to shift to the right hemisphere in the early (prenatal and early postnatal injury) but dependence on the left-hemispheric regions for aphasia recovery in late life stroke (Tillema et al., 2008; Saur et al., 2010).

The inter-hemispheric functional connectivity between the posterior aspects of superior temporal gyrus (IC e) showed no age effects. The time courses for IC e and IC c described above have shown the highest increase in task-relatedness (developmental trend) as detailed in a previous study involving the same subject population (Karunanayaka et al., 2010). However, the age dependence of these networks differs in terms of the inter-hemispheric connectivity as seen in **Figure 4**, with no significant age trend found in the posterior network encompassed by IC e (BA22).

Although the relationship between structural maturation and functional activation is rather complex, the present functional connectivity data provides additional evidence in support of language lateralization being dominated by the inferior frontal brain regions. While one recent study did not observe any asymmetries in language lateralization in newborns (Kotilahti et al., 2010), this study also found a more uniform involvement of the left hemisphere in speech processing indicating that left-hemispheric specialization for language processing may already be present at birth. Dehaene-Lambertz et al. (2002) also found that left lateralization of language function was present in posterior brain regions in infants as young as 3 months of age. These findings are inline with previously reported left lateralization of language functions noted in 6- to

12-month-old children (Minagawa-Kawai et al., 2007) and later studies of language lateralization in older children, adolescents and young adults (Holland et al., 2001; Szaflarski et al., 2006a).

The proposed LSEM for verb generation is hypothesized to support both word processing and word generation. However, only the networks included in the word processing module exhibited age dependent effective connectivity changes. Each of these networks represents a unique spatial distribution with corresponding time course that sub-serves specific functions of the network (e.g., working memory, visual imagery, or acoustic word recognition). As mentioned earlier, although the spatial distributions of IC maps are independent, the corresponding time courses are allowed to have highly correlated temporal structures.

According to the focal network theory, the underlying neural network structure for language processing is generally well established by the age of 5 (Ahmad et al., 2003) with first evidence of network structure seen already in newborns (Kotilahti et al., 2010). Therefore, it is reasonable to assume that interactions between functions such as coordination of speech articulation, subvocal word production, and visual imagery at network level are well established for this group of children. However, based on our results, there is ample evidence to suggest that the within network (intra-network) behavior is undergoing a continuous process of dynamic change. As discussed in detail elsewhere (Karunanayaka et al., 2010), the areas of a distributed network can change the degree of engagement making it a more efficient component of the normally developing network. This forms the basis for the regionally weighted model and the differences in weights may account for the observed normal variations in cognitive skill level, use of different cognitive strategies and changes in the biological substrate for a function (Berl et al., 2006). This picture is consistent with the intra-component functional connectivity results observed for IC c, d, and e. (Karunanayaka et al., 2010).

As mentioned above, module IC d is the most left-lateralized part of the network for this task and is presumed to be associated with semantic representations of the nouns that are being heard (Karunanayaka et al., 2010). All connections to this module are age dependent. This module may also sub-serve working memory required by the verb generation task. Several studies have reported age-dependent BOLD signal and connectivity changes mainly in the frontal areas of the brain (Gaillard et al., 2000; Schlaggar et al., 2002; Schmithorst et al., 2002; Schapiro et al., 2004). We suggest that these later aspects of development are captured by the observed connectivity changes within the word processing module in our proposed model. Finally, in terms of the regionally weighted model, these changes can be interpreted as increasing the participation of this left-lateralized network supporting phonological and semantic expressive functions as part of covert verb generation.

The biological relevance of the model derives from two sources. First, the highly task-related elements of the model are selected based on the data-driven ICA results. Secondly, the biological plausibility originated with the close correspondence to the Wernicke–Geschwind model and has been evaluated against the literature for the neural circuitry of language; especially for the semantic processing network (Kim et al., 2011). These biological underpinnings for our model give us confidence that the proposed model is indeed relevant to the cognitive and biological processes taking place during verb generation in the developing brain. As mentioned previously, compared to DCM, the current investigation only models contemporaneous connections without taking into account the neuronal hemodynamic relationships explicitly (Penny et al., 2004b). The emphasis is, therefore, on the overall network behavior confirming or facilitating the generation of new hypothesis. The current investigation focused on the overall connectivity pattern shedding more insight into several networks that need further investigations using more sophisticated methods like uSEM, DCM, or Granger causality (Stevens et al., 2007; Jafri et al., 2008; Demirci et al., 2009; Londei et al., 2010; Smith et al., 2010). SEM is useful in this regard in that it provides a quantitative measure of overall model fit which allows the optimum set of path coefficients to be identified objectively. These coefficients can then be examined as a function of age to determine how connection strengths change with brain development. Finally, LSEM was also used as an exploratory tool in the proposed theoretical model in a highly restrictive manner. By introducing a theory-driven focus we partially avoided evaluating models of different structures. However, model selection (or identifying the true network structure) is a challenging statistical problem that has received increased attention in the neuroimaging community in recent times (Zheng and Rajapakse, 2006; Rajapakse and Zhou, 2007). We have already developed a Spectral Bayesian Network method (based on Model Averaging) to identify the most plausible models based on fMRI data, which is inline with our long-term objective of developing statistical methods capable of confirming (or rejecting) existing theoretical models for cognitive development.

LIMITATIONS

Study limitations inherent in covert verb generation task have been discussed in detail elsewhere (Szaflarski et al., 2006a,b; Karunanayaka et al., 2010). Therefore, we will only review additional limitations pertaining to the analyses employed in this paper.

In this study, we have only focused our attention on task-related networks even though considerable amount of intrinsic fluctuations are typically inherent in fMRI time courses. ICA, in general, tends to over specify the problem imposing severe limitations on our computational ability for connectivity analysis. Implementing objective methods to select non-task-related components to be included in the connectivity analysis is non-trivial. On the other hand, including such components is very subjective making interpretations difficult. The SEM should also be limited to a reasonable number of nodes (maximum of 10~15) as any data set can be fitted to models with increasing complexity. Thus, we have adopted a theory-driven focus coupled with proper selection processes to guide the analysis and interpretations circumventing above mentioned drawbacks. Therefore, we had no option but to limit the analysis to task-related components. However, if one can overcome the computational (and methodological) limitations, DCM might be more suitable to investigate intrinsic connectivity that is affected by the context of the task in ways which do not show up as a strictly task-related modulation of the time course.

As previously mentioned, ICA is a data-driven technique and, therefore, its use obviates conventional statistical approaches to hypothesis testing. Consequently, one extension of this data analysis method would be to incorporate constraints at the ICA

decomposition step to guide the analysis and increase the predictive power (Lu and Rajapakse, 2005). Finally, the verb generation task utilized here was not specifically designed to acquire in-scanner performance data. Consequently, performance effects on the connectivity coefficients cannot be completely discounted even though the fMRI task design enabled the youngest children in the study to complete the task without any difficulty. Since, performance can be related to IQ, including IQ as a covariate can produce overcorrected, anomalous, and counterintuitive findings about neurocognitive functions (Dennis et al., 2009). It has also been shown that IQ should only be used as a covariate in those rare circumstances where selection bias has produced problems of non-representativeness in the sample (Dennis et al., 2009). Clearly, such a condition was not present here although we observed a small negative correlation between age and IQ. This was mainly due to our youngest subjects having higher than average IQ scores. Furthermore, in one of our previous connectivity studies (narrative story comprehension) with the same population, the effects of the age × IQ interaction term were investigated using a multivariate regression model and were found not to confound the age-related tendencies associated with SEM path coefficients (Karunanayaka et al., 2007). This performance-related limitation can be addressed in the future by collecting intra-scanner performance data using either sparse fMRI data collection (Schmithorst and Holland, 2004) or block-design task with forced responses (Szaflarski et al., 2002). Such a design will also allow real-time performance on the task to be monitored and potentially included as a covariate in the analysis of age dependence in connectivity. Recently we have shown that brain activation during covert verb generation correlates with the number of verbs generated during an overt phase of verb generation during the same task (Vannest et al., 2010). While both overt and covert verb generation produced similar patterns of activation, the correlation with performance suggests that performance could also be related to connectivity in the language networks sub-serving the tasks. This question could be specifically addressed with a modified overt verb generation task in which the number of responses is explicitly controlled as a design parameter.

CONCLUSION

A theoretical model for covert verb generation was investigated using fMRI data from a large cohort of children and adolescents between the ages 5–18 years undergoing fMRI study with such a task. Previously identified, spatially independent and task-related networks (IC maps) were combined with SEM to investigate age dependent changes in network connectivity. Connections between networks such as word recognition, phonological working memory and semantic processing exhibited age dependent connectivity changes to varying degrees. We also highlighted the importance of combining network analysis at both the local and global levels.

The intra-network connectivity analysis of the highly left-lateralized network (IC d) provided convincing evidence for ongoing within network connectivity changes. These changes highlight the importance of the degree of engagement of each brain region within a network and can be considered a part of normal development. The results show the capacity of ICA to detect additional task-related spatial modules and their developmental trajectories. Age dependence found in both the path coefficients and in the task-relatedness of this network support the idea that this network will be used increasingly for covert verb generation as children mature. Combined with the results of our previous investigations, the current analysis further endorses the regionally weighted model for neurocognitive development that highlights the importance of interactions between brain regions within a network.

The main emphasis of the current analysis was on investigating the age dependent *connectivity* trends in language networks in the developing brain using functional neuroimaging data and an inferential statistical method capable of testing hypothesis based upon existing theoretical models for cognitive functions. Modeling cognitive functions will always be a compromise between the complexity of the underlying neural systems and the interpretability of proposed models. However, by carefully selecting appropriate analysis methods *in an incremental manner of complexity*, theories of cognitive development can be investigated in detail. This new approach to network modeling reveals a more complex developmental trajectory than proposed by models currently in use, e.g., the Wernicke–Lichtheim–Geschwind theory (Geschwind, 1965a,b) and has the potential to lead to a deeper understanding of developmental changes in cognitive function.

ACKNOWLEDGMENTS

The study was supported by a grant from the U.S. National Institute of Child Health and Development, R01-HD38578. The authors acknowledge the assistance of Dr. Anna Byars, Ph.D., in the administration of the Wechsler IQ tests, and Drs. Richard Strawsburg, M.D. and Mark Schapiro, M.D., for performing the neurological examinations. Dr. Szaflarski is currently supported by NINDS K23 NS052468. Thanks to Meghan O'Connell for applying her medical illustration skills to Figure 5.

REFERENCES

Ahmad, Z., Balsamo, L. M., Sachs, B. C., Xu, B., and Gaillard, W. D. (2003). Auditory comprehension of language in young children: neural networks identified with fMRI. *Neurology* 60, 1598–1605.

Anderson, J. M., Gilmore, R., Roper, S., Crosson, B., Bauer, R. M., Nadeau, S., Beversdorf, D. Q., Cibula, J., Rogish, M. III, Kortencamp, S., Hughes, J. D., Gonzalez Rothi, L. J., and Heilman, K. M. (1999). Conduction aphasia and the arcuate fasciculus: a reexamination of the Wernicke-Geschwind model. *Brain Lang.* 70, 1–12.

Arbuckle, J. (1989). Analysis of moment structures. *Am. Stat.* 43, 66–67.

Bandettini, P. A., Jesmanowicz, A., Wong, E. C., and Hyde, J. S. (1993). Processing strategies for time-course data sets in functional MRI of the human brain. *Magn. Reson. Med.* 30, 161–173.

Bartels, A., and Zeki, S. (2004). The chronoarchitecture of the human brain-natural viewing conditions reveal a time-based anatomy of the brain. *Neuroimage* 22, 419–433.

Beitchman, J. H., Jiang, H., Koyama, E., Johnson, C. J., Escobar, M., Atkinson, L., Brownlie, E. B., and Vida, R. (2008). Models and determinants of vocabulary growth from kindergarten to adulthood. *J. Child. Psychol. Psychiatry* 49, 626–634.

Berl, M. M., Vaidya, C. J., and Gaillard, W. D. (2006). Functional imaging of developmental and adaptive changes in neurocognition. *Neuroimage* 30, 679–691.

Binder, J. R., Swanson, S. J., Hammeke, T. A., and Sabsevitz, D. S. (2008). A comparison of five fMRI protocols for mapping speech comprehension systems. *Epilepsia* 49, 1980–1997.

Blumenfeld, H. K., Booth, J. R., and Burman, D. D. (2006). Differential prefrontal-temporal neural correlates of semantic processing in children. *Brain Lang.* 99, 226–235.

Booth, J. R., Bebko, G., Burman, D. D., and Bitan, T. (2007). Children with reading disorder show modality independent brain abnormalities during semantic tasks. *Neuropsychologia* 45, 775–783.

Byars, A. W., Holland, S. K., Strawsburg, R. H., Bommer, W., Dunn, R. S., Schmithorst, V. J., and Plante, E. (2002). Practical aspects of conducting large-scale functional magnetic resonance imaging studies in children. *J. Child Neurol.* 17, 885–890.

Calhoun, V. D., Adali, T., McGinty, V. B., Pekar, J. J., Watson, T. D., and Pearlson, G. D. (2001a). fMRI activation in a visual-perception task: network of areas detected using the general linear model and independent components analysis. *Neuroimage* 14, 1080–1088.

Calhoun, V. D., Adali, T., Pearlson, G. D., and Pekar, J. J. (2001b). A method for making group inferences from functional MRI data using independent component analysis. *Hum. Brain Mapp.* 14, 140–151.

Calhoun, V. D., Pekar, J. J., and Pearlson, G. D. (2004). Alcohol intoxication effects on simulated driving: exploring alcohol-dose effects on brain activation using functional MRI. *Neuropsychopharmacology* 29, 2097–2017.

Carrow-Woolfolk, E. (1996). *Oral and Written Language Scales*. Circle Pines, MN: American Guidance Service.

Catani, M., Jones, D. K., and Ffytche, D. H. (2005). Perisylvian language networks of the human brain. *Ann. Neurol.* 57, 8–16.

Chein, J. M., Ravizza, S. M., and Fiez, J. A. (2003). Using neuroimaging to evaluate models of working memory and their implications for language processing. *J. Neurolinguistics* 16, 315–339.

Chi, J. G., Dooling, E. C., and Gilles, F. H. (1977). Left-right asymmetries of the temporal speech areas of the human fetus. *Arch. Neurol.* 34, 346–348.

Chou, T. L., Booth, J. R., Burman, D. D., Bitan, T., Bigio, J. D., Lu, D., and Cone, N. E. (2006). Developmental changes in the neural correlates of semantic processing. *Neuroimage* 29, 1141–1149.

Dehaene-Lambertz, G., Dehaene, S., and Hertz-Pannier, L. (2002). Functional neuroimaging of speech perception in infants. *Science* 298, 2013–2015.

de Marco, G., Devauchelle, B., and Berquin, P. (2009). Brain functional modeling, what do we measure with fMRI data? *Neurosci. Res.* 64, 12–19.

Demirci, O., Stevens, M. C., Andreasen, N. C., Michael, A., Liu, J., White, T., Pearlson, G. D., Clark, V. P., and Calhoun, V. D. (2009). Investigation of relationships between fMRI brain networks in the spectral domain using ICA and Granger causality reveals distinct differences between schizophrenia patients and healthy controls. *Neuroimage* 46, 419–431.

Dennis, M., Francis, D. J., Cirino, P. T., Schachar, R., Barnes, M. A., and Fletcher, J. M. (2009). Why IQ is not a covariate in cognitive studies of neurodevelopmental disorders. *J. Int. Neuropsychol. Soc.* 15, 331–343.

Dick, A. S., Solodkin, A., and Small, S. L. (2010). Neural development of networks for audiovisual speech comprehension. *Brain Lang.* 114, 101–114.

Duann, J. R., Jung, T. P., Kuo, W.-J., Yeh, T.-C., Makeig, S., Hsieh, J.-C., and Sejnowski, T. J. (2002). Single-trial variability in event-related BOLD signals. *Neuroimage* 15, 823–835.

Foundas, A. L., Leonard, C. M., lmore, R., Fennell, E., and Heilman, K. M. (1994). Planum temporale asymmetry and language dominance. *Neuropsychologia* 32, 1225–1231.

Francks, C., Maegawa, S., Laurén, J., Abrahams, B. S., Velayos-Baeza, A., Medland, S. E., Colella, S., Groszer, M., McAuley, E. Z., Caffrey, T. M., Timmusk, T., Pruunsild, P., Koppel, I., Lind, P. A., Matsumoto-Itaba, N., Nicod, J., Xiong, L., Joober, R., Enard, W., Krinsky, B., Nanba, E., Richardson, A. J., Riley, B. P., Martin, N. G., Strittmatter, S. M., Möller, H. J., Rujescu, D., St Clair, D., Muglia, P., Roos, J. L., Fisher, S. E., Wade-Martins, R., Rouleau, G. A., Stein, J. F., Karayiorgou, M., Geschwind, D. H., Ragoussis, J., Kendler, K. S., Airaksinen, M. S., Oshimura, M., DeLisi, L. E., and Monaco, A. P. (2007). LRRTM1 on chromosome 2p12 is a maternally suppressed gene that is associated paternally with handedness and schizophrenia. *Mol. Psychiatry* 12, 1129–1139.

Friston, K. J., Buechel, C., Fink, G. R., Morris, J., Rolls, E., and Dolan, R. J. (1997). Psychophysiological and modulatory interactions in neuroimaging. *Neuroimage* 6, 218–229.

Friston, K. J., Harrison, L., and Penny, W. (2003). Dynamic causal modelling. *Neuroimage* 19, 1273–1302.

Friston, K. J., Holmes, A. P., Poline, J. B., Grasby, P. J., Williams, S. C., Frackowiak, R. S., and Turner, R. (1995). Analysis of fMRI time-series revisited. *Neuroimage* 2, 45–53.

Friston, K. J., and Stephan, K. E. (2007). S*tatistical Parametric Mapping: The Analysis of Functional Brain Images*, eds K. J. Friston, J. T. Ashburner, S. J. Kiebel, T. E. Nichols, and W. D. Penny (Amsterdam: Academic Press).

Gaillard, W. D., Hertz-Pannier, L., Mott, S. H., Barnett, A. S., LeBihan, D., and Theodore, W. H. (2000). Functional anatomy of cognitive development: fMRI of verbal fluency in children and adults. *Neurology* 54, 180–185.

Gaillard, W. D., Sachs, B. C., Whitnah, J. R., Ahmad, Z., Balsamo, L. M., Petrella, J. R., Braniecki, S. H., McKinney, C. M., Hunter, K., Xu, B., and Grandin, C. B. (2003). Developmental aspects of language processing: fMRI of verbal fluency in children and adults. *Hum. Brain Mapp.* 18, 176–185.

Geschwind, N. (1965a). Disconnexion syndromes in animals and man. I. *Brain* 88, 237–294.

Geschwind, N. (1965b). Disconnexion syndromes in animals and man. II. *Brain* 88, 585–644.

Giedd, J. N. (2004). Structural magnetic resonance imaging of the adolescent brain. *Ann. N. Y. Acad. Sci.* 1021, 77–85.

Giedd, J. N., Blumenthal, J., Jeffries, N. O., Castellanos, F. X., Liu, H., Zijdenbos, A., Paus, T., Evans, A. C., and Rapoport, J. L. (1999). Brain development during childhood and adolescence: a longitudinal MRI study. *Nat. Neurosci.* 2, 861–863.

Goncalves, M. S., Hall, D. A., Johnsrude, I. S., and Haggard, M. P. (2001). Can meaningful effective connectivities be obtained between auditory cortical regions? *Neuroimage* 14, 1353–1360.

Grossman, M., Koenig, P., Glosser, G., DeVita, C., Moore, P., Rhee, J., Detre, J., Alsop, D., Gee, J., and fMRI Study, Functional Magnetic Resonance Imaging. (2003). Neural basis for semantic memory difficulty in Alzheimer's disease: an fMRI study. *Brain* 126(Pt 2), 292–311.

Gurd, J. M., Amunts, K., Weiss, P. H., Zafiris, O., Zilles, K., Marshall, J. C., and Fink, G. R. (2002). Posterior parietal cortex is implicated in continuous switching between verbal fluency tasks: an fMRI study with clinical implications. *Brain* 125(Pt 5), 1024–1038.

Hickok, G., and Poeppel, D. (2004). Dorsal and ventral streams: a framework for understanding aspects of the functional anatomy of language. *Cognition* 92, 67–99.

Himberg, J., Hyvarinen, A., and Esposito, F. (2004). Validating the independent components of neuroimaging time series via clustering and visualization. *Neuroimage* 22, 1214–1222.

Holland, S. K., Plante, E., Weber Byars, A., Strawsburg, R. H., Schmithorst, V. J., and Ball, W. S. Jr. (2001). Normal fMRI brain activation patterns in children performing a verb generation task. *Neuroimage* 14, 837–843.

Holland, S. K., Vannest, J., Mecoli, M., Jacola, L. M., Tillema, J. M., Karunanayaka, P. R., Schmithorst, V. J., Yuan, W., Plante, E., and Byars, A. W. (2007). Functional MRI of language lateralization during development in children. *Int. J. Audiol.* 46, 533–551.

Hyvarinen, A. (1999a). Fast and robust fixed-point algorithms for independent component analysis. *IEEE Trans. Neural Netw.* 10, 626–634.

Hyvarinen, A. (1999b). Sparse code shrinkage: denoising of nongaussian data by maximum likelihood estimation. *Neural Comput.* 11, 1739–1768.

Jafri, M. J., Pearlson, G. D., Stevens, M., and Calhoun, V. D. (2008). A method for functional network connectivity among spatially independent resting-state components in schizophrenia. *Neuroimage* 39, 1666–1681.

Jennings, J. M., McIntosh, A. R., and Kapur, S. (1998). Mapping neural interactivity onto regional activity: an analysis of semantic processing and response mode interactions. *Neuroimage* 7, 244–254.

Karunanayaka, P., Kim, K. K., Holland, S. K., and Szaflarski, J. P. (2011). The effects of left or right hemispheric epilepsy on language networks investigated with semantic decision fMRI task and independent component analysis. *Epilepsy Behav.* 20, 623–632.

Karunanayaka, P., Schmithorst, V. J., Vannest, J., Szaflarski, J. P., Plante, E., and Holland, S. K. (2010). A group independent component analysis of covert verb generation in children: a functional magnetic resonance imaging study. *Neuroimage* 51, 472–487.

Karunanayaka, P. R., Holland, S. K., Schmithorst, V. J., Solodkin, A., Chen, E. E., Szaflarski, J. P., and Plante, E. (2007). Age-related connectivity changes in fMRI data from children listening to stories. *Neuroimage* 34, 349–360.

Kim, J., and Horwitz, B. (2009). How well does structural equation modeling reveal abnormal brain anatomical connections? An fMRI simulation study. *Neuroimage* 45, 1190–1198.

Kim, K. K., Karunanayaka, P., Privitera, M. D., Holland, S. K., and Szaflarski, J. P. (2011). Semantic association investigated with functional MRI and independent component analysis. *Epilepsy Behav.* 20, 613–622.

Kotilahti, K., Nissila, I., Näsi, T., Lipiäinen, L., Noponen, T., Meriläinen, P., Huotilainen, M., and Fellman, V. (2010). Hemodynamic responses to speech and music in newborn infants. *Hum. Brain Mapp.* 31, 595–603.

Lenneberg, E. H. (1967). *Biological Foundations of Language*. New York: Wiley.

Levelt, W. J., Roelofs, A., and Meyer, A. S. (1999). A theory of lexical access in speech production. *Behav. Brain Sci.* 22, 1–38; discussion 38–75.

Londei, A., D'Ausilio, A., Basso, D., and Belardinelli, M. O. (2006). A new method for detecting causality in fMRI data of cognitive processing. *Cogn. Process.* 7, 42–52.

Londei, A., D'Ausilio, A., Basso, D., Sestieri, C., Del Gratta, C., Romani, G. L., and Olivetti Belardinelli, M.

(2007). Brain network for passive word listening as evaluated with ICA and Granger causality. *Brain Res. Bull.* 72, 284–292.

Londei, A., D'Ausilio, A., and Basso, D., Sestieri, C., Gratta, C. D., Romani, G. L., and Belardinelli, M. O. (2010). Sensory-motor brain network connectivity for speech comprehension. *Hum. Brain Mapp.* 31, 567–580.

Lu, W., and Rajapakse, J. C. (2005). Approach and applications of constrained ICA. *IEEE Trans. Neural Netw.* 16, 203–212.

McDonald, J. L. (1997). Language acquisition: the acquisition of linguistic structure in normal and special populations. *Annu. Rev. Psychol.* 48, 215–241.

McGregor, K. K., Friedman, R. M., Reilly, R. M., and Newman, R. M. (2002). Semantic representation and naming in young children. *J. Speech Lang. Hear. Res.* 45, 332–346.

McIntosh, A. R., and Gonzalez-Lima, F. (1994). Structural equation modeling and its application to network analysis in functional brain imaging. *Hum. Brain Mapp.* 2, 22.

McIntosh, A. R., Grady, C. L., Ungerleider, L. G., Haxby, J. V., Rapoport, S. I., and Horwitz, B. (1994). Network analysis of cortical visual pathways mapped with PET. *J. Neurosci.* 14, 655–666.

McKeown, M. J., Makeig, S., Brown, G. G., Jung, T. P., Kindermann, S. S., Bell, A. J., and Sejnowski, T. J. (1998). Analysis of fMRI data by blind separation into independent spatial components. *Hum. Brain Mapp.* 6, 160–188.

Minagawa-Kawai, Y., Mori, K., Naoi, N., and Kojima, S. (2007). Neural attunement processes in infants during the acquisition of a language-specific phonemic contrast. *J. Neurosci.* 27, 315–321.

Muller, R. A., Rothermel, R. D., Behen, M. E., Muzik, O., Mangner, T. J., and Chugani, H. T. (1998). Developmental changes of cortical and cerebellar motor control: a clinical positron emission tomography study with children and adults. *J. Child Neurol.* 13, 550–556.

Oldfield, R. C. (1971). The assessment and analysis of handedness: the Edinburgh inventory. *Neuropsychologia* 9, 97–113.

Ollinger, J. M., Corbetta, M., and Corbetta, M. (2001). Separating processes within a trial in event-related functional MRI. *Neuroimage* 13, 218–229.

Penny, W. D., Stephan, K. E., Mechelli, A., and Friston, K. J. (2004a). Comparing dynamic causal models. *Neuroimage* 22, 1157–1172.

Penny, W. D., Stephan, K. E., Mechelli, A., and Friston, K. J. (2004b). Modelling functional integration: a comparison of structural equation and dynamic causal models. *Neuroimage* 23(Suppl. 1), S264–S274.

Plaut, D. C., McClelland, J. L., Seidenberg, M. S., and Patterson, K. (1996). Understanding normal and impaired word reading: computational principles in quasi-regular domains. *Psychol. Rev.* 103, 56–115.

Pulvermuller, F. (2001). Brain reflections of words and their meaning. *Trends Cogn. Sci. (Regul. Ed.)* 5, 517–524.

Rajapakse, J. C., Wang, Y., Zheng, X., and Zhou, J. (2008). Probabilistic framework for brain connectivity from functional MR images. *IEEE Trans. Med. Imaging* 27, 825–833.

Rajapakse, J. C., and Zhou, J. (2007). Learning effective brain connectivity with dynamic Bayesian networks. *Neuroimage* 37, 749–760.

Sarty, G. E. (2007). *Computational brain activity maps from fMRI time-series images*. New York: Cambridge University Press.

Saur, D., Ronneberger, O., Kümmerer, D., Mader, I., Weiller, C., and Klöppel, S. (2010). Early functional magnetic resonance imaging activations predict language outcome after stroke. *Brain* 133(Pt 4), 1252–1264.

Schapiro, M. B., Schmithorst, V. J., Wilke, M., Byars, A. W., Strawsburg, R. H., and Holland, S. K. (2004). BOLD fMRI signal increases with age in selected brain regions in children. *Neuroreport* 15, 2575–2578.

Schlaggar, B. L., Brown, T. T., Lugar, H. M., Visscher, K. M., Miezin, F. M., and Petersen, S. E. (2002). Functional neuroanatomical differences between adults and school-age children in the processing of single words. *Science* 296, 1476–1479.

Schmithorst, V. J., and Brown, R. D. (2004). Empirical validation of the triple-code model of numerical processing for complex math operations using functional MRI and group independent component analysis of the mental addition and subtraction of fractions. *Neuroimage* 22, 1414–1420.

Schmithorst, V. J., and Holland, S. K. (2004). Event-related fMRI technique for auditory processing with hemodynamics unrelated to acoustic gradient noise. *Magn. Reson. Med.* 51, 399–402.

Schmithorst, V. J., and Holland, S. K. (2006). Functional MRI evidence for disparate developmental processes underlying intelligence in boys and girls. *Neuroimage* 31, 1366–1379.

Schmithorst, V. J., and Holland, S. K. (2007). Sex differences in the development of neuroanatomical functional connectivity underlying intelligence found using Bayesian connectivity analysis. *Neuroimage* 35, 406–419.

Schmithorst, V. J., Holland, S. K., and Plante, E. (2006). Cognitive modules utilized for narrative comprehension in children: a functional magnetic resonance imaging study. *Neuroimage* 29, 254–266.

Schmithorst, V. J., Holland, S. K., and Plante, E. (2007a). Development of effective connectivity for narrative comprehension in children. *Neuroreport* 18, 1411–1415.

Schmithorst, V. J., Holland, S. K., and Plante, E. (2007b). Object identification and lexical/semantic access in children: a functional magnetic resonance imaging study of word-picture matching. *Hum. Brain Mapp.* 28, 1060–1074.

Schmithorst, V. J., Wilke, M., Dardzinski, B. J., and Holland, S. K. (2002). Correlation of white matter diffusivity and anisotropy changes with age during childhood: a cross-sectional diffusion tensor imaging study. *Radiology* 222, 212–218.

Seger, C. A., Desmond, J. E., Glover, G. H., and Gabrieli, J. D. (2000). Functional magnetic resonance imaging evidence for right-hemisphere involvement in processing unusual semantic relationships. *Neuropsychology* 14, 361–369.

Skipper, J. I., Nusbaum, H. C., and Small, S. L. (2005). Listening to talking faces: motor cortical activation during speech perception. *Neuroimage* 25, 76–89.

Smith, J. F., Alexander, G. E., Chen, K., Husain, F. T., Kim, J., Pajor, N., and Horwitz, B. (2010). Imaging systems level consolidation of novel associate memories: a longitudinal neuroimaging study. *Neuroimage* 50, 826–836.

Solodkin, A., Hlustik, P. E., Chen, E., and Small, S. L. (2004). Fine modulation in network activation during motor execution and motor imagery. *Cereb. Cortex* 14, 1246–1255.

Stevens, M. C., Kiehl, K. A., Pearlson, G. D., and Calhoun, V. D. (2007). Functional neural networks underlying response inhibition in adolescents and adults. *Behav. Brain Res.* 181, 12–22.

Stevens, M. C., Pearlson, G. D., and Calhoun, V. D. (2009a). Changes in the interaction of resting-state neural networks from adolescence to adulthood. *Hum. Brain Mapp.* 30, 2356–2366.

Stevens, M. C., Skudlarski, P., Pearlson, G. D., and Calhoun, V. D. (2009b). Age-related cognitive gains are mediated by the effects of white matter development on brain network integration. *Neuroimage* 48, 738–746.

Stoeckel, L. E., Kim, J., Weller, R. E., Cox, J. E., and Cook, E. W. III, Horwitz, B. (2009). Effective connectivity of a reward network in obese women. *Brain Res. Bull.* 79, 388–395.

Szaflarski, J. P., Binder, J. R., Possing, E. T., McKiernan, K. A., Ward, B. D., and Hammeke, T. A. (2002). Language lateralization in left-handed and ambidextrous people: fMRI data. *Neurology* 59, 238–244.

Szaflarski, J. P., DiFrancesco, M., Hirschauer, T., Banks, C., Privitera, M. D., Gotman, J., and Holland, S. K. (2010). Cortical and subcortical contributions to absence seizure onset examined with EEG/fMRI. *Epilepsy Behav.* 18, 404–413.

Szaflarski, J. P., Holland, S. K., Schmithorst, V. J., and Byars, A. W. (2006a). fMRI study of language lateralization in children and adults. *Hum. Brain Mapp.* 27, 202–212.

Szaflarski, J. P., Schmithorst, V. J., Altaye, M., Byars, A. W., Ret, J., Plante, E., and Holland, S. K. (2006b). A longitudinal functional magnetic resonance imaging study of language development in children 5 to 11 years old. *Ann. Neurol.* 59, 796–807.

Thompson-Schill, S. L., D'Esposito, M., Aguirre, G. K., and Farah, M. J. (1997). Role of left inferior prefrontal cortex in retrieval of semantic knowledge: a reevaluation. *Proc. Natl. Acad. Sci. U.S.A.* 94, 14792–14797.

Tillema, J. M., Byars, A. W., Jacola, L. M., Schapiro, M. B., Schmithorst, V. J., Szaflarski, J. P., and Holland, S. K. (2008). Cortical reorganization of language functioning following perinatal left MCA stroke. *Brain Lang.* 105, 99–111.

Vannest, J., Rasmussen, J. M., Eaton, K. P., Patel, K., Schmithorst, V., Karunanayaka, P., Plante, E., Byars, A., and Holland, S. (2010). fMRI Activation in language areas reflects children's verb generation performance. *Neuropediatrics* 2010 (neuped-04-2010-0577-SC). 41, 235–239.

Wada, J. A., Clarke, R., and Hamm, A. (1975). Cerebral hemispheric asymmetry in humans. Cortical speech zones in 100 adults and 100 infant brains. *Arch. Neurol.* 32, 239–246.

Wechsler, D. (1991). *Wechsler Intelligence Scale for Children*, 3rd Edn. San Antonio, TX: The Psychological Corporation.

Wechsler, D. (1997). *Wechsler Adult Intlelligence Scale*, 3rd Edn. San Antonio, TX: The Psychological Corporation.

Whatmough, C., Chertkow, H., Murtha, S., and Hanratty, K. (2002). Dissociable brain regions process object meaning and object structure during picture naming. *Neuropsychologia* 40, 174–186.

Wood, A. G., Harvey, A. S., Wellard, R. M., Abbott, D. F., Anderson, V., Kean, M., Saling, M. M., and Jackson, G. D. (2004). Language cortex activation in normal children. *Neurology* 63, 1035–1044.

Worsley, K. J., and Friston, K. J. (1995). Analysis of fMRI time-series revisited-again. *Neuroimage* 2, 173–181.

Write, S. (1934). The method of path coefficients. *Ann. Math. Stat.* 5, 161–215.
Yuan, W., Altaye, M., Ret, J., Schmithorst, V., Byars, A. W., Plante, E., and Holland, S. K. (2009). Quantification of head motion in children during various fMRI language tasks. *Hum. Brain Mapp.* 30, 1481–1489.
Yuan, W., Holland, S. K., Cecil, K. M., Dietrich, K. N., Wessel, S. D., Altaye, M., Hornung, R. W., Ris, M. D., Egelhoff, J. C., and Lanphear, B. P. (2006). The impact of early childhood lead exposure on brain organization: a functional magnetic resonance imaging study of language function. *Pediatrics* 118, 971–977.
Zheng, X., and Rajapakse, J. C. (2006). Learning functional structure from fMR images. *Neuroimage* 31, 1601–1613.

Conflict of Interest Statement: The authors declare that the research was conducted in the absence of any commercial or financial relationships that could be construed as a potential conflict of interest.

Received: 24 May 2010; accepted: 29 April 2011; published online: 01 June 2011.
Citation: Karunanayaka P, Schmithorst VJ, Vannest J, Szaflarski JP, Plante E and Holland SK (2011) A linear structural equation model for covert verb generation based on independent component analysis of fMRI data from children and adolescents. Front. Syst. Neurosci. ***5****:29. doi: 10.3389/fnsys.2011.00029*
Copyright © 2011 Karunanayaka, Schmithorst, Vannest, Szaflarski, Plante and Holland. This is an open-access article subject to a non-exclusive license between the authors and Frontiers Media SA, which permits use, distribution and reproduction in other forums, provided the original authors and source are credited and other Frontiers conditions are complied with.

frontiers in
SYSTEMS NEUROSCIENCE

ORIGINAL RESEARCH ARTICLE
published: 04 February 2011
doi: 10.3389/fnsys.2011.00002

A baseline for the multivariate comparison of resting-state networks

Elena A. Allen[1]*, Erik B. Erhardt[1], Eswar Damaraju[1], William Gruner[1,2], Judith M. Segall[1,3], Rogers F. Silva[1,2], Martin Havlicek[1,2], Srinivas Rachakonda[1], Jill Fries[1], Ravi Kalyanam[1,2], Andrew M. Michael[1], Arvind Caprihan[1], Jessica A. Turner[1,4], Tom Eichele[5], Steven Adelsheim[4], Angela D. Bryan[1,6,7], Juan Bustillo[4,8], Vincent P. Clark[1,6,8], Sarah W. Feldstein Ewing[1], Francesca Filbey[1,9], Corey C. Ford[10], Kent Hutchison[1,6,8], Rex E. Jung[1,11], Kent A. Kiehl[1,6,8], Piyadasa Kodituwakku[12], Yuko M. Komesu[13], Andrew R. Mayer[1,10], Godfrey D. Pearlson[14,15,16], John P. Phillips[1,10], Joseph R. Sadek[4,17], Michael Stevens[14,15], Ursina Teuscher[1,6], Robert J. Thoma[1,4,6] and Vince D. Calhoun[1,2,4,8,15]

[1] *The Mind Research Network, Albuquerque, NM, USA*
[2] *Department of Electrical and Computer Engineering, University of New Mexico, Albuquerque, NM, USA*
[3] *Department of Family and Community Medicine, University of New Mexico, Albuquerque, NM, USA*
[4] *Department of Psychiatry, University of New Mexico, Albuquerque, NM, USA*
[5] *Department of Biological and Medical Psychology, Faculty of Psychology, University of Bergen, Bergen, Norway*
[6] *Department of Psychology, University of New Mexico, Albuquerque, NM, USA*
[7] *Center on Alcoholism Substance Abuse and Addiction, University of New Mexico, Albuquerque, NM, USA*
[8] *Department of Neuroscience, University of New Mexico, Albuquerque, NM, USA*
[9] *Center for BrainHealth, School of Behavioral and Brain Sciences, University of Texas at Dallas, Dallas, TX, USA*
[10] *Department of Neurology, University of New Mexico, Albuquerque, NM, USA*
[11] *Department of Neurosurgery, University of New Mexico, Albuquerque, NM, USA*
[12] *Center for Development and Disability, University of New Mexico, Albuquerque, NM, USA*
[13] *Department Obstetrics and Gynecology, University of New Mexico, Albuquerque, NM, USA*
[14] *Olin Neuropsychiatry Research Center, The Institute of Living, Hartford, CT, USA*
[15] *Department of Psychiatry, Yale University, New Haven, CT, USA*
[16] *Department of Neurobiology, Yale University, New Haven, CT, USA*
[17] *Behavioral Health Care Line, New Mexico VA Health Care System, Albuquerque, NM, USA*

Edited by:
Silvina G. Horovitz, National Institutes of Health, USA

Reviewed by:
Scott K. Holland, Cincinnati Children's Research Foundation, USA

****Correspondence:***
Elena A. Allen, The Mind Research Network, 1101 Yale Boulevard NE, Albuquerque, NM 87106, USA.
e-mail: eallen@mrn.org

As the size of functional and structural MRI datasets expands, it becomes increasingly important to establish a baseline from which diagnostic relevance may be determined, a processing strategy that efficiently prepares data for analysis, and a statistical approach that identifies important effects in a manner that is both robust and reproducible. In this paper, we introduce a multivariate analytic approach that optimizes sensitivity and reduces unnecessary testing. We demonstrate the utility of this mega-analytic approach by identifying the effects of age and gender on the resting-state networks (RSNs) of 603 healthy adolescents and adults (mean age: 23.4 years, range: 12–71 years). Data were collected on the same scanner, preprocessed using an automated analysis pipeline based in SPM, and studied using group independent component analysis. RSNs were identified and evaluated in terms of three primary outcome measures: time course spectral power, spatial map intensity, and functional network connectivity. Results revealed robust effects of age on all three outcome measures, largely indicating decreases in network coherence and connectivity with increasing age. Gender effects were of smaller magnitude but suggested stronger intra-network connectivity in females and more inter-network connectivity in males, particularly with regard to sensorimotor networks. These findings, along with the analysis approach and statistical framework described here, provide a useful baseline for future investigations of brain networks in health and disease.

Keywords: fMRI, functional connectivity, resting-state, independent component analysis, connectome

1 INTRODUCTION

Measurement of the blood oxygen level-dependent (BOLD) signal with functional magnetic resonance imaging (fMRI) has become a powerful tool for studying large-scale *in vivo* brain function. Following the seminal discovery by Biswal et al. (1995) that distinct brain regions exhibit synchronous fluctuations in intrinsic activity, our understanding of so-called functional connectivity has grown substantially. Several different methods have successfully delineated a large number of temporally coherent networks that subserve critical functions such as vision, audition, motor planning, and directing attention (Calhoun et al., 2002a; Beckmann et al., 2005; Damoiseaux et al., 2006; Smith et al., 2009). These networks show surprisingly consistent, though not identical, patterns of activation in the presence or absence of a particular task (Calhoun et al., 2008a; Harrison et al., 2008; Laird et al., 2009; Smith et al., 2009), and are often acquired while subjects are at rest. Despite evaluation during a relatively unconstrained state, resting-state networks (RSNs) exhibit high reproducibility (Damoiseaux et al., 2006) and

moderate to high test-retest reliability (Franco et al., 2009; Shehzad et al., 2009; Zuo et al., 2010), suggesting a robust examination of the intrinsic functional architecture, or "connectome," of the human brain (Biswal et al., 2010).

Because functional connectivity between regions is believed to characterize large-scale system integrity (Van Dijk et al., 2010), there is great interest in understanding the variability of these networks in normal development and clinical contexts. Studies of the default-mode network (DMN), a set of brain regions preferentially active when subjects are not focused on the external environment (Raichle et al., 2001; Buckner et al., 2008), have established that this network not only shows a high degree of heritability (Glahn et al., 2010), but also shows alterations in a number of different neurological disorders (see Greicius, 2008 and Broyd et al., 2009 for recent reviews). For example, in autism, functional connectivity between DMN regions is substantially reduced, though coactivation within the dorsal attention network, a set of brain regions implicated in directing attention during cognitively demanding tasks, appears relatively unaffected (Kennedy and Courchesne, 2008). The parallel between altered connectivity (specific to regions associated with internal, self-referential processes) and symptoms that characterize autism suggests that straightforward investigations into functional connectivity can elucidate the etiology of complex disorders. Similar success has been found with regard to schizophrenia, where impaired modulation of the DMN has been observed in schizophrenia patients as well as their first-degree relatives, identifying an endophenotype based on large-scale connectivity (Whitfield-Gabrieli et al., 2009; Abbott et al., 2010). Furthermore, increased connectivity between particular DMN regions is associated with the severity of positive symptoms, suggesting a correspondence between specific "hyperconnectivity" and psychosis (Garrity et al., 2007; Whitfield-Gabrieli et al., 2009). The spectral properties of network activation in schizophrenia have also been explored, revealing a signature of reduced low frequency power and increased high frequency power in the DMN as well as many other RSNs (Garrity et al., 2007; Calhoun et al., 2008b, 2009).

While multiple aspects of intrinsic functional connectivity show potential for clinical applications, the utility of network evaluation as a reliable diagnostic tool depends on the ability to interpret aberrant findings in the presence of an appropriate baseline. Fundamental factors, such as age and gender, are expected to exert large influences on functional connectivity based on their strong associations with underlying anatomy. For instance, most cortical regions show rapid gray matter loss as the brain matures through adolescence, followed by more gradual reductions in adulthood and advanced aging (Good et al., 2001; Sowell et al., 2003; Tamnes et al., 2010), though this trend is heterogeneous across structures and particularly variable in subcortical regions (Østby et al., 2009). White matter shows a different developmental trajectory, with volume and tract integrity peaking in adulthood (approximately 25–35 years of age) then declining slowly with age (Sowell et al., 2003; Sullivan and Pfefferbaum, 2006; Tamnes et al., 2010). Structural differences are also observed between genders; effects are smaller and some findings lack consistency, however studies concur that females show modest increases in gray matter volume localized to frontal, temporal, and parietal cortices and basal ganglia (BG) structures (Good et al., 2001; Luders et al., 2005, 2009; Sowell et al., 2007).

As anticipated, recent investigations have identified effects of age and gender on functional connectivity. With regard to age, reports suggest network maturation in childhood (Szaflarski et al., 2006; Karunanayaka et al., 2007; Fair et al., 2008), progressive decreases in network mutual influences throughout adolescences into adulthood (Stevens et al., 2009), followed by decreases in functional connectivity and coherence in middle and late adulthood (Andrews-Hanna et al., 2007; Damoiseaux et al., 2008; Esposito et al., 2008; Koch et al., 2009; Biswal et al., 2010). Gender-related differences have received less attention but there appears to be some consensus of slightly greater connectivity in females localized to the precuneus and posterior cingulate cortex (Bluhm et al., 2008; Biswal et al., 2010). While these studies establish the influence of age and gender on functional connectivity, most unfortunately limit their investigations to the DMN, creating a dearth of reported effects with regard to other regions. In part, this bias reflects the unique function of the DMN related to internal mental processes and the desire to explicitly explore the "cognitive baseline" (Raichle et al., 2001). However, the relatively narrow scope of prior studies may also reflect the difficulty and somewhat overwhelming nature of investigations of full brain connectivity (Bullmore and Sporns, 2009). As the dimensions of data increase, so do the challenges associated with each analysis step, extending from data collection and processing to interpretation and visualization (Biswal et al., 2010; Costafreda, 2010).

Given the need for a more comprehensive understanding of functional connectivity and the methodological challenges associated with such a pursuit, the current study has two primary goals. First, we aim to present a statistical framework optimized for the analysis of large datasets that can be easily applied to investigations in other areas. We advocate a hierarchical approach where multivariate models are used first to identify important covariates, reducing the number of subsequent univariate tests and decreasing the risk of spurious findings. For multivariate analyses, we exploit the autoregressive structure common to many types of data and recommend appropriate dimension reduction of response variables to enhance the sensitivity and specificity of model estimation.

Our second goal is to apply this statistical framework in a detailed and careful investigation of the effects of age and gender on large-scale resting-state functional connectivity throughout the brain. To this end, we focus our analysis on data from a large number of healthy subjects ($M = 603$) collected on a single instrument, and employ group independent components analysis (GICA) to identify a set of robust and reliable RSNs (Calhoun et al., 2001). We examine the effects of age and gender on three ICA-derived outcome variables describing distinct but complementary facets of functional connectivity. These include (1) the power spectra of RSN time course (TCs), related to level of coherent activity within a network; (2) the intensities of RSN spatial map (SMs), related to the connectivity and degree of coactivation within a network; and (3) the functional network connectivity (FNC; Jafri et al., 2008), related to the connectivity between networks. Furthermore, we consider these outcome measures as a function of local gray matter concentration (GMC) to determine the extent to which functional changes reflect those observed in the structural domain (Damoiseaux et al., 2008; Glahn et al., 2010).

Using the described statistical approach, we identify numerous effects of age and gender on different aspects of functional connectivity throughout cortical and subcortical structures. Our results corroborate previous observations and provide novel findings that motivate future in-depth investigations.

2 MATERIALS AND METHODS

2.1 PARTICIPANTS

This analysis combines existing data from 603 subjects scanned on the same scanner and spread across 34 studies and 18 principal investigators at the Mind Research Network (MRN). Informed consent was obtained from all subjects according to institutional guidelines at the University of New Mexico (UNM) and all data were anonymized prior to group analysis. None of the participants were taking psychoactive medications at the time of the scan or had a history of neurological or psychiatric disorders. Subjects were excluded from analysis if their functional scans showed extreme motion (maximum translation >6 mm, roughly two voxels) or showed poor spatial normalization to the EPI template (see below). Subjects were also excluded if they maintained high levels of substance use (smoking an average of 11 or more cigarettes per day; drinking 2.5 or more drinks per day).

Table 1 provides characteristics of the participants under investigation. The sample is nearly balanced on gender (305 females), and the age distributions for genders are very similar. Because the sample is overwhelmingly right-handed (46 ambidextrous or left-handed individuals) and preliminary tests showed no handedness effects, we do not consider handedness from this point forward. Similarly, because participants in the white racial category are over-represented, and some studies did not collect racial information, we do not consider race from this point forward. Age is right skewed with only seven people older than 50 and the majority of individuals in adolescence or young adulthood (80% of subjects between 13 and 30 years old). We therefore use a normalizing transformation, log(age), to reduce the leverage of older subjects in regression analyses (**Figure 2A**).

Table 1 | Demographic information. Distributions for primary variables gender and age, as well as secondary variables handedness and race.

	N	%				N	%
Gender	603	100		**Handedness***			
Male	298	49.4		Right		508	91.7
Female	305	50.6		Left and ambi		46	8.3
	Mean	**SD**	**Min.**	**25%**	**50%**	**75%**	**Max.**
Age (years)	23.4	9.2	12	17	21	27	71
Male	23.8	9.1	12	17	21	26	71
Female	23.1	9.3	12	16	21	27	55
Race*	LTN	AI	ASN	NH	AA	WH	MOR
N	14	26	12	1	27	276	20
%	4	7	3	0.3	7	73	5

LTN, Latino; AI, American Indian/Alaska native; ASN, Asian; NH, native Hawaiian or other Pacific islander; AA, Black or African American; WH, White; MOR, more than one race.

**Race and handedness frequencies and percentages do not account for missing values.*

2.2 DATA ACQUISITION

All images were collected on a 3-Tesla Siemens Trio scanner with a 12-channel radio frequency coil. High resolution T1-weighted structural images were acquired with a five-echo MPRAGE sequence with TE = 1.64, 3.5, 5.36, 7.22, 9.08 ms, TR = 2.53 s, TI = 1.2 s, flip angle = 7°, number of excitations = 1, slice thickness = 1 mm, field of view = 256 mm, resolution = 256 × 256. $T2^*$-weighted functional images were acquired using a gradient-echo EPI sequence with TE = 29 ms, TR = 2 s, flip angle = 75°, slice thickness = 3.5 mm, slice gap = 1.05 mm, field of view 240 mm, matrix size = 64 × 64, voxel size = 3.75 mm × 3.75 mm × 4.55 mm. Resting-state scans were a minimum of 5 min, 4 s in duration (152 volumes). Any additional volumes were discarded to match data quantity across participants. Subjects were instructed to keep their eyes open during the scan and stare passively at a foveally presented fixation cross, as this is suggested to facilitate network delineation compared to eyes-closed conditions (Van Dijk et al., 2010).

2.3 DATA PREPROCESSING

Functional and structural MRI data were preprocessed using an automated preprocessing pipeline and neuroinformatics system (**Figure 1**, step 1) developed at MRN (Bockholt et al., 2009) and based around SPM5[1]. Following the completion of a scan, data are automatically archived and copied to an analysis directory where preprocessing is performed. In the functional data pipeline, the first four volumes are discarded to remove T1 equilibration effects, images are realigned using INRIALIGN, and slice-timing correction is applied using the middle slice as the reference frame. Data are then spatially normalized into the standard Montreal Neurological Institute (MNI) space (Friston et al., 1995), resliced to 3 mm × 3 mm × 3 mm voxels, and smoothed using a Gaussian kernel with a full-width at half-maximum (FWHM) of 10 mm. To ensure quality and consistency of spatial normalization across subjects we calculate the spatial correlation between each subjects normalized data and the EPI template, as well as the degree of intersection between the EPI mask (determined by retaining voxels greater than the mean of the distribution) and the subject mask (determined by the same criteria). For the analysis presented here, these two metrics flagged datasets from 35 subjects, three of which were uncorrectable due to incomplete brain coverage and one that was unusable due to large signal dropout. The remaining 31 scans were corrected by manually reorienting the original images (shift in the yaw direction), then were re-preprocessed through the pipeline. Subsequent to automated preprocessing, the data were intensity-normalized to improve the accuracy and test-retest reliability of independent components analysis (ICA) output (Allen et al., 2010). Intensity normalization divides the time series of each voxel by its average intensity, converting data to percent signal change units.

For the structural data pipeline, tissue classification, bias correction, image registration, and spatial normalization were automatically performed using voxel-based morphometry (VBM) in

[1]http://www.fil.ion.ucl.ac.uk/spm/software/spm5

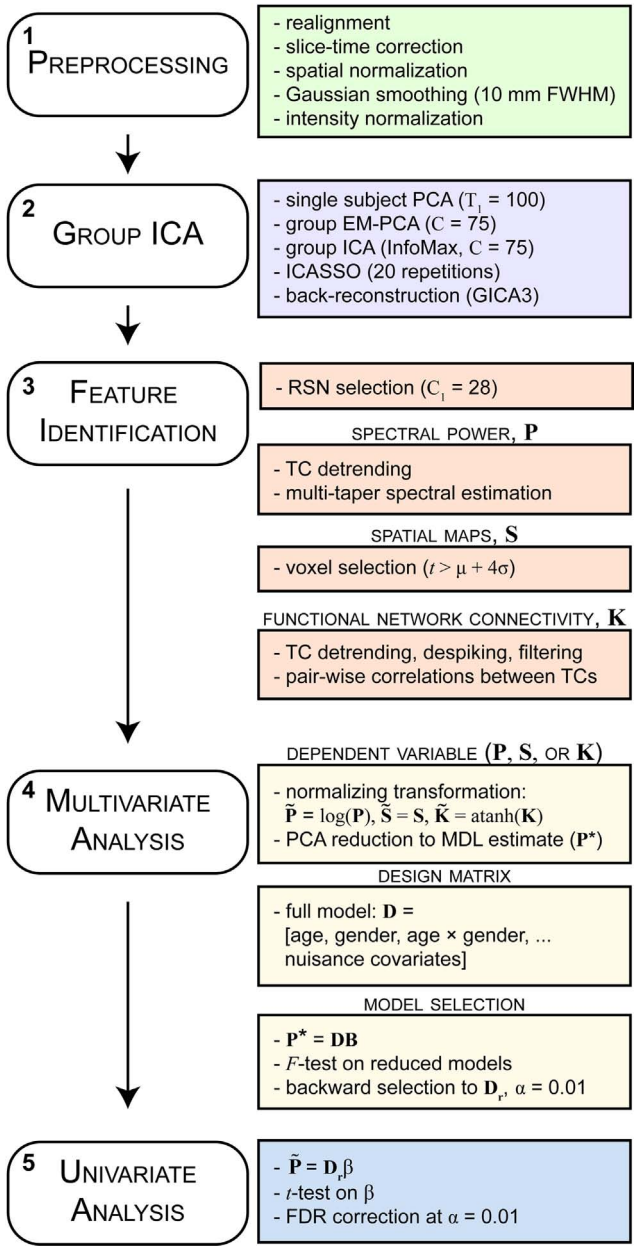


FIGURE 1 | Schematic of the analysis pipeline. Boxes on the left indicate general steps potentially applicable to a variety of data and analysis types; boxes on the right indicate particular choices made for the data and analysis presented here. See Section 2 for details and abbreviations.

SPM5, wherein the above steps are integrated into a unified model (Ashburner and Friston, 2005). Unmodulated gray matter images, estimating local GMC were then smoothed using a Gaussian kernel with a FWHM of 10 mm and resliced to 3 mm × 3 mm × 3 mm to match the functional image dimensions. Our choice of unmodulated rather than modulated images is based on a previous study showing that modulated images confer greater inter-subject variability and thus reduced sensitivity to detect differences between groups (see Figure 2 of Meda et al., 2008). For the analyses presented here, modulated data, i.e., gray matter volume (GMV), yielded similar findings to those found with GMC, and the choice of GMC or GMV would have little impact on our general results or interpretation.

2.4 GROUP INDEPENDENT COMPONENT ANALYSIS

Data were decomposed into functional networks using spatial ICA. Spatial ICA applied to fMRI data identifies temporally coherent networks by estimating maximally independent spatial sources, referred to as SMs, from their linearly mixed fMRI signals, referred to as TCs (**Figure 1**, step 2). We use ICA, rather than seed-based approaches, to identify networks as this multivariate data-driven method eliminates the somewhat arbitrary choice of seed regions and simultaneously takes into account the relationships between all voxels (as opposed to simple pairwise correlations). Furthermore, compared to seed-based methods, ICA may provide increased sensitivity to detect subtle differences between subjects (Koch et al., 2009).

A detailed description of the GICA implemented in this study is provided in Appendix A. Here, we describe the choices we made to prioritize detailed and reliable ICA outcome measures, as well as a processing strategy to accommodate our large dataset and resource-intensive analysis.

Group independent components analysis was performed using the GIFT toolbox[2]. We chose relatively high model order ICA (number of components, $C = 75$) as previous studies have demonstrated that such models yield refined components that correspond to known anatomical and functional segmentations (Kiviniemi et al., 2009; Smith et al., 2009; Abou-Elseoud et al., 2010; Ystad et al., 2010). Subject-specific data reduction principal components analysis (PCA) retained $T_1 = 100$ principal components (PCs) using a standard economy-size decomposition. The relatively large number of subject-specific PCs has been shown to stabilize subsequent back-reconstruction (Erhardt et al., 2010). Group data reduction retained $C = 75$ PCs using the expectation-maximization (EM) algorithm, included in GIFT, to avoid otherwise prohibitive memory requirements (Roweis, 1998). The Infomax ICA algorithm (Bell and Sejnowski, 1995) was repeated 20 times in Icasso[3] and resulting components were clustered to estimate the reliability of the decomposition (Himberg et al., 2004). The quality of component clusters was quantified using the index I_q, which ranges from 0 to 1 and reflects the difference between intra-cluster and extra-cluster similarity (Himberg et al., 2004). Aggregate SMs were estimated as the centrotypes of component clusters to reduce sensitivity to initial algorithm parameters. Subject-specific SMs and TCs were estimated using the recently developed GICA3 back-reconstruction method based on PCA compression and projection (Calhoun et al., 2001, 2002b; Erhardt et al., 2010). There are desirable properties in GICA3 not available in other methods, including that the aggregate SM is the sum of the subject-specific SMs, analogous to a random effects model where the subject-specific effects are zero-mean distributed deviations from the group mean effect. Compared with dual regression, a least-squares alternative to back-reconstruction (Filippini et al., 2009), evidence suggests that noise-free PCA with noise-free ICA using GICA3 provides more robust results with a more intuitive and natural interpretation (Erhardt et al., 2010).

[2]http://icatb.sourceforge.net/groupica.htm

[3]http://www.cis.hut.fi/projects/ica/icasso

2.5 FEATURE IDENTIFICATION

2.5.1 RSN selection

We identified a subset of C_1 components considered to be RSNs (as opposed to physiological artifacts) by inspecting the aggregate SMs and average power spectra (see below; **Figure 1**, step 3). Four viewers rated the components from 0 (definite artifact) to 1 (certain RSN) based on expectations that RSNs should exhibit peak activations in gray matter, low spatial overlap with known vascular, ventricular, motion, and susceptibility artifacts, and TCs dominated by low frequency fluctuations (Cordes et al., 2000). To facilitate evaluation, spectra were characterized with two metrics used previously to classify components (Robinson et al., 2009): dynamic range, the difference between the peak power and minimum power at frequencies to the right of the peak, and low frequency to high frequency power ratio, the ratio of the integral of spectral power below 0.10 Hz to the integral of power between 0.15 and 0.25 Hz (**Figure 3**). Tallied votes from the four raters were used to separate components into three broad classes: artifact (score equal to zero), mixed (score between zero and three), and RSN (score of three or greater and no votes equal to zero). This classification scheme constitutes somewhat conservative selection criteria for RSNs, though we feel it is appropriate given our larger goal of discovering associations with gender and age.

2.5.2 Outcome measures

For the set of selected RSNs, we considered three outcome variables: (1) component power spectra, (2) component SMs, and (3) between component connectivity (FNC).

Spectra were estimated on the detrended subject-specific TCs (involving removal of the mean, slope, and period π and 2π sines and cosines over each TC) using the multi-taper approach as implemented in Chronux[4], with the time-bandwidth product set to 3 and the number of tapers set to 5 (Mitra and Bokil, 2008).

Component SMs were thresholded to focus our analysis on the subset of voxels most representative of each network. Thresholding was based on the distribution of voxelwise *t*-statistics to identify voxels with strong and consistent activation across subjects, as explained in Appendix B (**Figure A1**). From this point forward, descriptions of component SMs refer to the thresholded maps, which include regions most associated with component TCs.

Functional network connectivity was estimated as the Pearson's correlation coefficient between pairs of TCs (Jafri et al., 2008). Subject-specific TCs were detrended and despiked using 3dDespike[5], then filtered using a fifth-order Butterworth low-pass filter with a high frequency cutoff of 0.15 Hz. Pairwise correlations were computed between RSN TCs, resulting in a symmetric $C_1 \times C_1$ correlation matrix for each subject. For all FNC analyses, correlations were transformed to *z*-scores using Fisher's transformation, $z = \text{atanh}(k)$, where k is the correlation between two component TCs.

2.6 STATISTICAL ANALYSIS

2.6.1 Overview

Our primary aim is to develop a statistical approach optimized for the large dimensions of the three ICA-derived outcome measures. We propose a multivariate model selection strategy to reduce the total number of statistical tests performed and facilitate testing predictors on the response matrices as a whole (**Figure 1**, step 4). Analogous to a standard ANOVA *F*-test with subsequent pairwise univariate contrasts, our strategy performs backward selection by testing whether each predictor in our model explains variability in the multivariate response using a multivariate analysis of covariance (MANCOVA), and for the reduced model of significant predictors proceeds to perform univariate tests corrected for multiple comparisons.

2.6.2 Design matrix

The design matrix, **D**, includes gender (coded as one for female and zero for male) and age as covariates of interest, as well as a gender by age interaction. In addition, we include three nuisance predictors related to motion and spatial normalization. Although spatial ICA successfully identifies motion-related sources which are removed from analysis (McKeown et al., 2003; Kochiyama et al., 2005), residual motion-related variance may also be present in RSNs. Thus we incorporate motion covariates, defined as the average scan-to-scan rotation and translation from INRIAlign motion estimates, to improve our evaluation of age and gender effects. Similarly, we include a measure of spatial normalization accuracy, defined as the Spearman correlation between the warped T2*-weighted image and the EPI template. We apply normalizing transformations to all continuous variables to improve symmetry and reduce disproportionate influence (leverage) of outlying values on the model fit. Age, rotation, and translation are log-transformed, while spatial correlation is Fisher-transformed. The distributions of these variables and effects of transformation are displayed in **Figure 2**.

In general, covariates of interest were not strongly associated with nuisance predictors. No significant correlations were observed between (transformed) age and translation ($r = -0.02$; $p > 0.69$), rotation ($r = -0.04$; $p > 0.27$), or spatial normalization ($r = 0.01$; $p > 0.80$). Genders did not show a difference in translation ($t_{601} = 1.25$; $p > 0.20$) or rotation ($t_{601} = 1.22$; $p > 0.20$), but showed a slight difference in spatial normalization ($t_{601} = 2.53$; $p < 0.01$), with females having higher correlations to the EPI template than males. Accurate estimation of model coefficients is unlikely to be affected by the relatively low correlation between these columns in the design matrix ($r = 0.10$).

In follow-up analyses, we also considered GMC (averaged over each component region) as a predictor variable. However, because GMC and age were highly negatively correlated over all regions ($r \approx -0.7$, **Figure A2A**), we used a modified approach to disambiguate the predictive power of these covariates (see Appendix C) and did not include GMC in our standard design matrix.

2.6.3 Response variables

For each of $i = 1, \ldots, M$ subjects, we have $c = 1, \ldots, C_1$ power spectra ($\mathbf{P}_{ic}$), $c = 1, \ldots, C_1$ SMs ($\mathbf{S}_{ic}$), and a single vector of FNC correlations ($\mathbf{K}_i$). Each of these response variables is modeled separately. Prior to modeling, response variables are transformed and dimension-reduced, as simulations suggest that these steps optimize model selection (see Appendix D and **Figure A3**). Spectra are element-wise log-transformed, which is useful because it normalizes the highly skewed power distribution and facilitates dimension estimation with minimum description length (MDL) in the next step. Similarly, FNC correlations are Fisher-transformed [$z = \text{atanh}(k)$]. Response matrices are then formed by concatenation of the subject response vectors: $\tilde{\mathbf{P}}_c = [1\log(\mathbf{P}_{1c}^{\mathrm{T}}), \ldots, \log(\mathbf{P}_{Mc}^{\mathrm{T}})]^{\mathrm{T}}$, $\tilde{\mathbf{S}}_c = [\mathbf{S}_{1c}^{\mathrm{T}}, \ldots, \mathbf{S}_{Mc}^{\mathrm{T}}]^{\mathrm{T}}$, and $\tilde{\mathbf{K}} = [\text{atanh}(\mathbf{K}_1^{\mathrm{T}}), \ldots, \text{atanh}(\mathbf{K}_M^{\mathrm{T}})]^{\mathrm{T}}$.

[4]http://chronux.org

[5]http://afni.nimh.nih.gov/afni

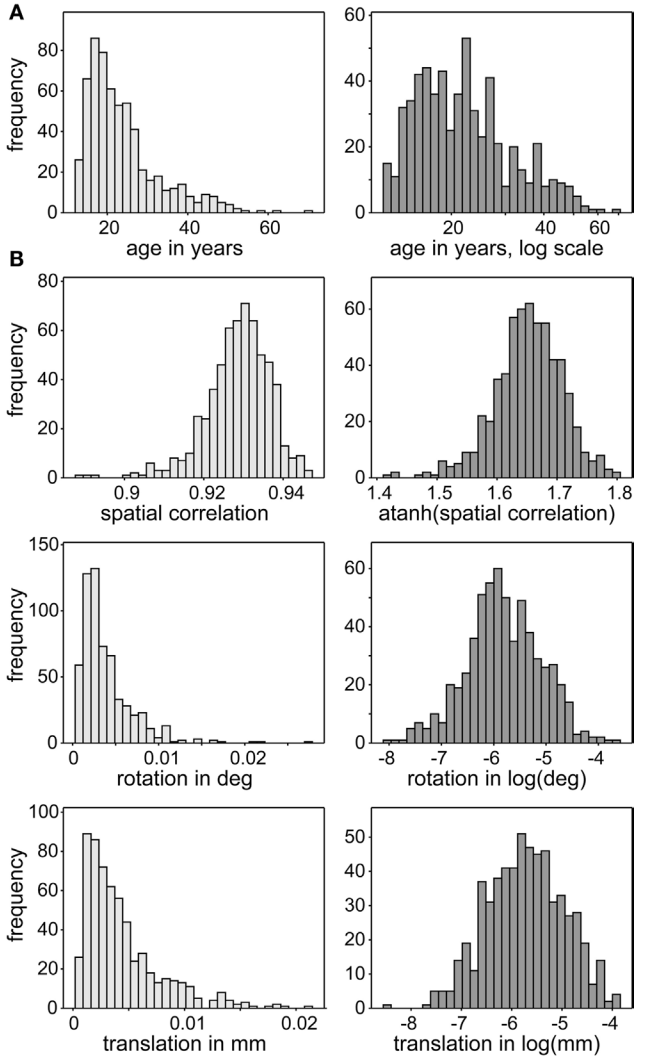


FIGURE 2 | Distributions of continuous covariates of interest (A) and nuisance predictors (B). Distributions of covariates are skewed (light gray, left panels) so are transformed to have more symmetric distributions (dark gray, right panels). This reduces disproportionate influence of more extreme observations on the MANCOVA and univariate model fits.

Because of the large number of columns of each response matrix, and because of autoregressive correlation structure between columns, we perform a PCA dimension reduction on each matrix. For dimension reduction, we use MDL to estimate the "true" number of dimensions, u. Let $\mathbf{P}_c^*$ be the dimension-reduced matrix of power spectra, keeping the first u PCs, with $\mathbf{S}_c^*$ and $\mathbf{K}^*$ defined similarly. Over the C_1 components, spectra with 129 frequency bins were reduced to a range of 25–27 dimensions. SMs with 2000–6000 voxels were reduced to 10–25 dimensions, and the FNC matrix with 378 pairwise correlations was reduced to 31 dimensions.

2.6.4 Backward selection

In this section, we describe model selection in terms of the spectra; the procedure is identical for SM and FNC response matrices. For each of the C_1 components, the MANCOVA model predicting spectral power is $\mathbf{P}_c^* = \mathbf{DB} + \mathbf{E}$, where $\mathbf{P}_c^*$ is the $M \times u$ response matrix, $\mathbf{D}$ is the design matrix, $\mathbf{B}$ is the matrix of regression coefficients, and $\mathbf{E}$ is the matrix of errors. Backward selection is implemented in mStepwise from the MANCOVAN toolbox[6]. Each step performs an F-test using the Wilks' Lambda likelihood ratio test statistic (Christensen, 2001) comparing the current full model with each reduced model, defined by removing one column of the current $\mathbf{D}$ and the associated interactions, if present. The F-test evaluates whether the associated row(s) of $\mathbf{B}$ are simultaneously equal to zero. When all reduced models have been assessed, the term associated with the least significant reduced model (largest p-value) is removed from the design matrix, and this reduced model becomes our full model in the next iteration. The final reduced model, $\mathbf{D}_f$, has all terms not associated with higher-order interactions significant at $\alpha = 0.01$. Note that reduced models are independently selected for each response matrix, i.e., $\mathbf{P}_c^*$ and $\mathbf{S}_c^*$, for $c = 1, \ldots, C_1$, and $\mathbf{K}^*$.

There are criticisms of stepwise selection methods, including that redundant (or correlated) predictors can adversely affect model selection and that resulting models have an inflated risk of capturing chance features of the data (Mantel, 1970; Henderson and Velleman, 1981; Judd et al., 1989; Derksen and Keselman, 1992). We minimize the potential negative impact a stepwise procedure can have on a resulting model by carefully considering a small full model (for example, not blindly including all pairwise interactions or higher-order terms), by performing only backward selection for the fewest model comparisons, and by not including highly correlated predictors of interest (see Appendix C and **Figure A2**). Simulations evaluating the performance of backward selection on spectra-like data show that it typically identifies the correct model (see Appendix D and **Figure A3**) suggesting that backward selection of a well-considered full model is an effective heuristic for model selection.

2.6.5 Univariate tests

At last, we wish to discover which spectral bins, SM voxels, or FNC correlations are associated with gender and age. Given the reduced model terms, univariate models are fit to the original (not dimension-reduced) response data, $\tilde{\mathbf{P}}_c$, $\tilde{\mathbf{S}}_c$, $c = 1, \ldots, C_1$, and $\tilde{\mathbf{K}}$, to test the association with gender and age (**Figure 1**, step 5). Associations are visualized by plotting the log of the p-value with the sign of the associated t-statistic, $-\text{sign}(t)\log_{10}(p)$, which provides information on both the directionally and statistical strength of the result. Univariate tests were corrected for multiple comparisons at an $\alpha = 0.01$ significance level using false discovery rate (FDR; Genovese et al., 2002). We calculate partial correlation coefficients to measure the strength of the linear relationship between two variables [e.g., log(power) and log(age)] after adjusting for other predictors (the remaining regressors in the model). This is calculated as the correlation between the residualized variables, obtained by fitting models between the remaining predictors and each of the variables as response vectors (Christensen, 1996). For visualization, scatter plots display the response adjusted for nuisance predictors, where the fitted nuisance terms of the model are subtracted from the response vector.

[6]http://www.mathworks.com/matlabcentral/fileexchange/27014-mancovan

3 RESULTS

We performed a 75-component GICA using resting-state fMRI data from 603 healthy participants. Demographic information for these subjects is provided in **Table 1**. Each of the 75-components had a cluster quality index greater than 0.8, indicating a highly stable ICA decomposition. Based on visual inspection of SMs and power spectra, we identified 35 components as ventricular, vascular, susceptibility or motion-related artifacts, 28 components as RSNs, and 12 components as mixed, representing a mixture of RSNs and artifactual sources (see **Figure 3** and Section 2 for details). The set of mixed components is composed of networks with activation in subcortical regions (e.g., thalamus and caudate) that extends into neighboring ventricles, cerebellar components showing spatial overlap with sinuses, and components at frontal and occipital poles contaminated by motion. To reduce the likelihood of spurious results, only components classified as RSNs are considered further.

3.1 RESTING-STATE NETWORKS

Spatial maps of the 28 selected RSNs are shown in **Figure 4A**. Coordinates of their peak activations are provided in **Table 2**. The observed networks are similar to those identified previously with low model order ICA (roughly 20 components; Beckmann et al., 2005; Damoiseaux et al., 2006; Calhoun et al., 2008a; Smith et al., 2009) and nearly identical to those identified using high model order (roughly 70 components; Kiviniemi et al., 2009; Smith et al., 2009; Abou-Elseoud et al., 2010). For this reason, we describe the RSNs only briefly here, and provide citations to more comprehensive references.

Resting-state networks are grouped by their anatomical and functional properties. The BG are represented by a single component (IC 21) with activation focused in the putamen and pallidum (Robinson et al., 2009; Ystad et al., 2010). IC 17 forms a rather prototypical representation of the large parts of the auditory system (AUD), including bilateral activation of the superior temporal gyrus, superior temporal sulcus, and middle temporal gyrus (Seifritz et al., 2002; Specht and Reul, 2003). Motor and somatosensory functions (MOT) are captured by six components (ICs 7, 23, 24, 38, 56, and 29) situated in the vicinity of the central sulcus. Similar to previous studies (Krienen and Buckner, 2009; Abou-Elseoud et al., 2010), we find corresponding cerebellar coactivation in bilateral and lateralized networks. The visual system (VIS) is also represented by six components (ICs 46, 64, 67, 48, 39, and 59) in good agreement with the anatomical and functional delineations of occipital cortex (Grill-Spector and Malach, 2004). The DMN is captured in four components, separating the full map reported initially by Raichle et al. (2001) along the anterior-posterior and inferior-superior axes (Buckner et al., 2008; Harrison et al., 2008). We classify several RSNs known to be involved in directing and monitoring behavior as attentional networks (ATTN). These include lateralized fronto-parietal networks (IC 34 and 60) similar to the ventral attention network (Corbetta and Shulman, 2002; Vincent et al., 2008), a parietal and frontal-eye field network (IC 52) reminiscent of the dorsal attention network (Corbetta and Shulman, 2002), a component centered in the central and anterior precuneus (IC 72) which is implicated in directing attention (Cavanna and Trimble, 2006; Margulies et al., 2009), a bilateral component focused at the temporo-parietal junction (IC 71) and overlapping the alerting system (Fan et al., 2005), and an anterior cingulate and insular network (IC 55) observed to activate during demanding tasks and conflict processing (Ridderinkhof et al., 2004; Klein et al., 2007; Eichele et al., 2008). Finally, we observe a number of frontal networks (FRONT; ICs 42, 20, 47, and 49) known to mediate executive as well as memory and language functions (Koechlin et al., 2003; Koechlin and Summerfield, 2007). Consistent with previous findings (Krienen and Buckner, 2009), we observe coactivation between medial prefrontal cortex and the contralateral cerebellum (IC 49). We note that a similar fronto-cerebellar network was observed as the bilateral homologue of IC 49, however this component (IC 18) was not classified as an RSN due to contamination with motion.

Functional connectivity between RSNs is presented in **Figure 4B**. Correlations between component TCs reveal patterns of connectivity highly consistent with known functional relationships. For example, clusters of positive correlations correspond to greater connectivity within functional domains, and negative correlations between DMN components and sensory-related networks reflect the natural opposition of these systems as attention drifts between external and internal mental states (Buckner et al., 2008).

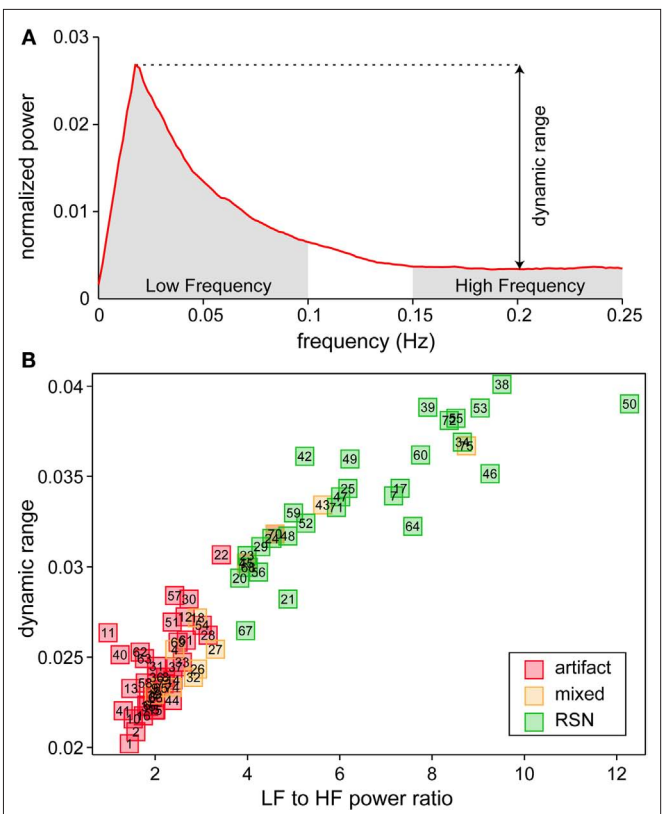


FIGURE 3 | Spectral characteristics of component TCs. (A) Average power spectrum of independent component (IC) 52 illustrating the features used to compute dynamic range and low frequency (LF) to high frequency (HF) power ratio. **(B)** Scatter plot of LF to HF power ratio versus dynamic range for all components. Along with spectral characteristics, SMs were used to categorize components as RSNs (green), artifacts (red) or mixture of the two (yellow).

3.2 MULTIVARIATE RESULTS

We applied a multivariate model selection strategy to determine the effects of age and gender on RSN power spectra, SMs, and FNC while accounting for variance associated with nuisance regressors. Results from the multivariate analysis are displayed in **Figure 5**, which provides the significance of model terms gender, log(age), their interaction, and several nuisance parameters related to motion and spatial normalization in predicting response vari-

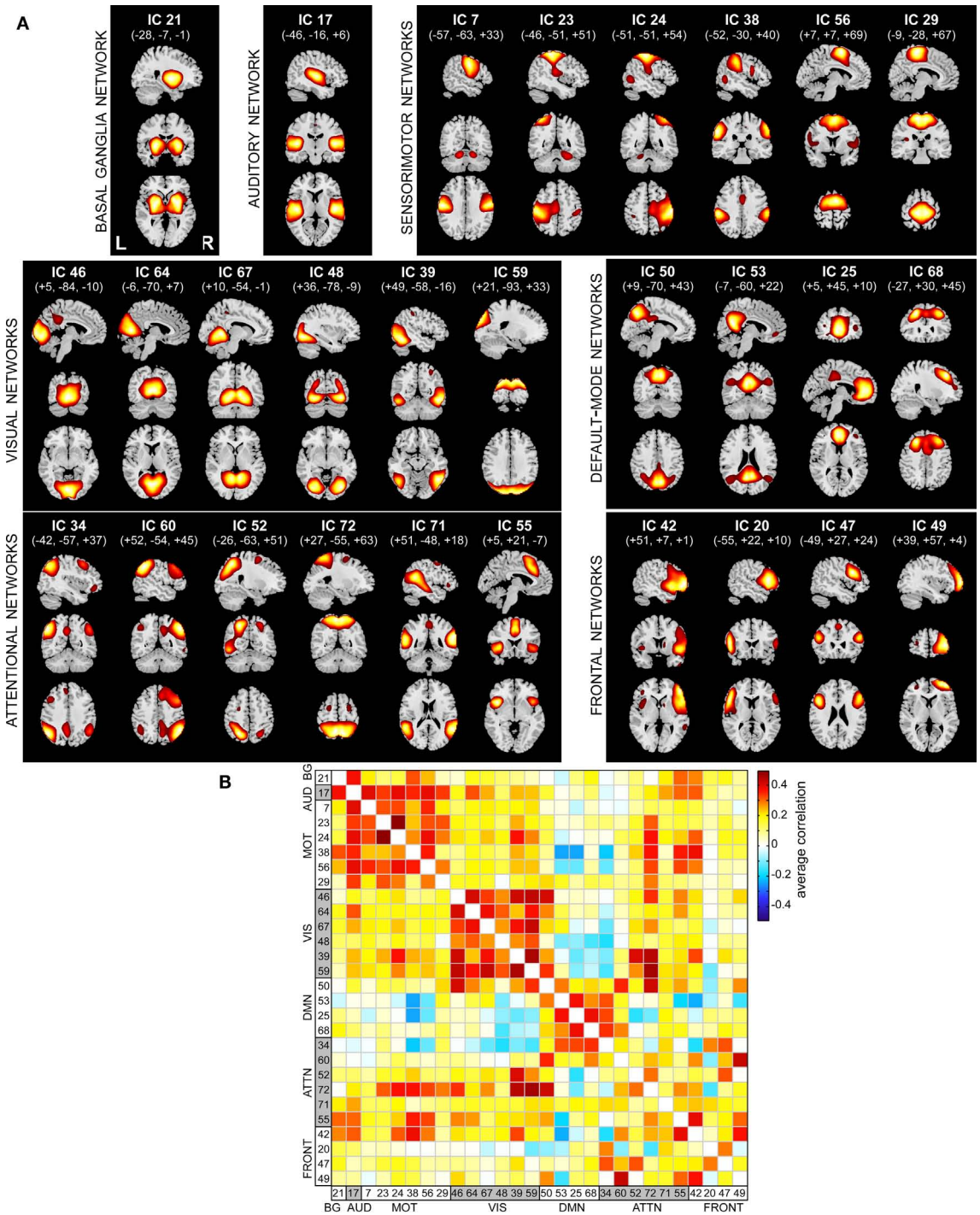


FIGURE 4 | Functional connectivity within and between RSNs. **(A)** SMs of the 28 components identified as RSNs. SMs are plotted as *t*-statistics, thresholded at $t_c > \mu_c + 4\sigma_c$ (see Appendix B), and are displayed at the three most informative slices. RSNs are divided into groups based on their anatomical and functional properties and include basal ganglia (BG), auditory (AUD), sensorimotor (MOT), visual (VIS), default-mode (DMN), attentional (ATTN), and frontal (FRONT) networks. **(B)** Functional network connectivity matrix. Pairwise correlations between RSN TCs were Fisher *z*-transformed and averaged across subjects, then inverse *z*-transformed for display.

Table 2 | Peak activations of RSN SMs. The quality index (I_q) associated with each RSN is listed in parentheses adjacent to the component number. BA, Brodmann area; V_ℓ, number of voxels in each cluster; t_{max}, maximum t-statistic in each cluster; Coordinate, coordinate (in mm) of t_{max} in MNI space, following LPI convention.

	BA	V_ℓ	t_{max}	Coordinate
BASAL GANGLIA NETWORK				
IC 21 (0.98)				
R putamen		1454	108.7	25, –1, 0
L putamen		1407	108.7	–25, –3, 0
AUDITORY NETWORK				
IC 17 (0.98)				
L superior temporal gyrus	22	2374	107.0	–51, –18, 7
R superior temporal gyrus	22	2257	108.3	52, –15, 5
R middle cingulate cortex	24	165	42.8	2, –4, 49
SENSORIMOTOR NETWORKS				
IC 07 (0.98)				
L precentral gyrus	6	1814	81.0	–52, –9, 31
R precentral gyrus	6	1694	78.3	52, –7, 29
L cerebellum (declive)		116	45.5	–16, –63, –22
R cerebellum (declive)		84	40.9	17, –63, –21
IC 23 (0.98)				
L precentral gyrus	4	3623	86.8	–35, –27, 54
R cerebellum		342	40.3	24, –52, –23
R postcentral gyrus		252	35.6	44, –28, 56
R inferior frontal gyrus	45	79	23.7	54, 29, 0
R precuneus		76	26.7	8, –62, 32
IC 24 (0.98)				
R precentral gyrus	4	3882	83.3	37, –25, 53
R middle temporal gyrus		165	36.1	50, –64, –2
L cerebellum		99	26.1	–20, –53, –24
L middle temporal gyrus		63	23.5	–61, –28, –8
L middle temporal gyrus		44	24.5	–51, –70, 4
IC 29 (0.98)				
Bi paracentral lobule	6	3199	100.9	1, –28, 61
L insula	13	44	40.1	–35, –24, 15
IC 38 (0.98)				
L supramarginal gyrus	2	1377	110.5	–55, –34, 37
R supramarginal gyrus	2	963	96.2	56, –32, 40
L inferior frontal gyrus	44	207	58.6	–48, 5, 18
Bi middle cingulate cortex	24	189	51.5	1, 7, 38
L middle temporal gyrus	37	128	54.4	–57, –60, –2
IC 56 (0.97)				
Bi supplementary motor area	6	3770	122.7	1, –3, 61
R superior temporal gyrus	22	193	48.2	50, 8, 4
L inferior frontal gyrus	44	149	42.7	–53, 5, 14
R inferior parietal lobule	40	61	41.1	58, –29, 24
L inferior parietal lobule	40	26	35.9	–58, –32, 23
VISUAL NETWORKS				
IC 46 (0.96)				
Bi lingual gyrus	17, 18	3654	87.3	1, –87, –2
Bi middle cingulate cortex	31	230	34.1	1, –45, 32
IC 64 (0.90)				
Bi calcarine gyrus	17, 18	3694	117.9	1, –71, 13
IC 67 (0.89)				
R lingual gyrus	18	1740	97.7	17, –55, –9
L lingual gyrus	18	1820	94.8	–15, –56, –8
IC 48 (0.96)				
R lingual gyrus	18, 19	1367	86.5	29, –76, –8
L lingual gyrus	18, 19	1324	83.6	–29, –76, –7
L inferior parietal lobule	40	43	41.0	–49, –55, 42
IC 39 (0.97)				
R inferior temporal gyrus	37	1800	91.9	48, –63, –8
L inferior temporal gyrus	37	667	80.7	–47, –63, –14
R inferior parietal lobule	40	33	46.2	42, –39, 50
IC 59 (0.92)				
Bi cuneus	19	3079	113.7	2, –84, 28
DEFAULT-MODE NETWORKS				
IC 50 (0.96)				
Bi precuneus	7	2902	102.5	1, –64, 43
IC 53 (0.95)				
Bi posterior cingulate cortex	23	2387	139.6	0, –52, 22
L angular gyrus	39	332	71.5	–43, –69, 33
R angular gyrus	39	194	59.8	47, –66, 32
Bi medial frontal gyrus	10	61	50.7	–1, 45, –9
IC 25 (0.98)				
Bi anterior cingulate cortex	32	3126	114.5	0, 41, 4
Bi middle cingulate cortex	31	358	53.6	1, –30, 41
R inferior frontal gyrus		93	48.2	32, 22, –15
R middle frontal gyrus	46	63	37.8	40, 43, 8
IC 68 (0.85)				
L middle frontal gyrus	8	1490	95.2	–26, 26, 42
R middle frontal gyrus	8	1210	87.9	26, 33, 41
Bi middle cingulate cortex	32	450	67.6	0, 21, 40
ATTENTIONAL NETWORKS				
IC 34 (0.98)				
L inferior parietal lobule	40	1383	124.6	–47, –57, 39
L middle frontal gyrus	8	1000	76.3	–27, 24, 49
R inferior parietal lobule	40	482	75.3	49, –54, 39
L precuneus	31	373	63.4	–6, –52, 37
L middle temporal gyrus	21	233	75.3	–62, –37, –12
R superior temporal gyrus	22	124	44.1	56, 0, 2
IC 60 (0.93)				
R inferior parietal lobule	40	2480	120.8	42, –56, 42
R middle frontal gyrus	8	2137	87.3	34, 24, 44
L superior temporal gyrus	22	318	46.9	–61, –2, 0
R middle temporal gyrus	21	249	58.7	64, –39, –11
L inferior parietal lobule	40	163	45.7	–45, –53, 45
IC 52 (0.96)				
L angular gyrus	39	2841	100.6	–33, –64, 31
L inferior frontal gyrus	45	295	54.2	–43, 24, 21
R superior parietal lobule	7	283	57.8	27, –65, 44
L middle frontal gyrus	6	119	52.3	–25, 1, 60
L superior temporal gyrus	22	24	40.4	–50, –5, –4
IC 72 (0.93)				
Bi precuneus	7	3283	105.2	0, –53, 61
L superior frontal gyrus	9	111	35.8	–32, 38, 39

(Continued)

Table 2 | Continued

	BA	V_ℓ	t_{max}	Coordinate
R middle frontal gyrus	6	85	32.4	26, 0, 60
L middle frontal gyrus	6	80	32.4	–23, 0, 63
R superior frontal gyrus	9	53	30.3	33, 39, 35
IC 71 (0.88)				
R superior temporal gyrus	22	1775	95.0	57, –44, 11
L superior temporal gyrus	22	1337	89.0	–56, –48, 18
Bi precuneus	7	123	51.0	1, –51, 51
R precentral gyrus	6	44	50.0	51, 2, 50
IC 55 (0.95)				
Bi cingulate gyrus	32	1210	92.8	0, 22, 45
L insula	47	670	103.1	–46, 15, –5
R insula	47	331	80.8	45, 18, –6
L middle frontal gyrus	10	217	65.4	–32, 53, 21
FRONTAL NETWORKS				
IC 42 (0.98)				
R inferior frontal gyrus	45	3371	105.7	50, 23, 2
L insula	44	132	40.0	–41, 10, –2
L inferior frontal gyrus	45	70	35.3	–42, 39, 5
R supramarginal gyrus	2	65	35.5	58, –36, 36
R middle temporal gyrus		56	33.0	63, –45, 0
L inferior parietal lobule	40	37	31.9	–58, –40, 49
R caudate nucleus		31	33.5	12, 8, 5
IC 20 (0.98)				
L inferior frontal gyrus	44, 45	1781	103.2	–55, 22, 7
R inferior frontal gyrus	45	252	50.7	56, 26, 4
IC 47 (0.95)				
L middle frontal gyrus	9	1020	110.8	–48, 17, 29
R middle frontal gyrus	9, 46	885	97.1	49, 22, 25
Bi superior medial gyrus	8	259	64.1	–1, 32, 46
R superior parietal lobule	7	38	49.3	33, –60, 49
IC 49 (0.97)				
R middle frontal gyrus	10	1661	84.3	31, 55, 7
L pyramis		144	42.2	–39, –66, –44
L middle frontal gyrus	10	64	33.4	–31, 52, 8

ables for all RSNs. Darker colors correspond to more significant effects, while white squares indicate terms that were not retained in the backward selection process ($\alpha = 0.01$). Gender was found to be mildly significant for a few of the spectra and slightly more significant for some of the SMs. Age was found to be highly significant in all models. Interestingly, the interaction term between age and gender was never retained in the backward selection process, suggesting that the effects of age are somewhat equivalent between genders for the age range and response variables investigated here. It should also be noted that either translation or rotation were retained in most models, meaning that these terms consistently accounted for significant variability in the outcome measures. This indicates considerable motion contamination of RSN SMs and, particularly, TCs, and strongly supports the incorporation of motion-related regressors to improve the estimates related to the covariates of interest.

3.3 UNIVARIATE RESULTS

The strength of a multivariate selection process is its ability to identify which covariates are important when each separate response vector (power spectrum, SM, or FNC matrix) is considered as a whole. The multivariate results of dimension-reduced responses, however, are difficult to interpret. Thus, we performed univariate tests on each of the covariates of interest retained in the final model to understand the nature and extent of the relationship between these variables and RSN properties.

3.3.1 Power spectra

Univariate results summarizing the effects of age on RSN power spectra are shown in **Figure 6A**. We observe a decrease in low frequency power with age across all RSNs (**Figure 6A1**). Significant effects are found primarily between 0 and 0.15 Hz, consistent with the frequency range over which synchronous fluctuations between brain regions are detected (Cordes et al., 2000; Sun et al., 2004). Age-related reductions in spectral power are slightly more significant in attentional and DMN components, however the rate of decrease is fairly consistent over networks (**Figure 6A2**), suggesting that a single process underlies these somewhat global trends.

Given the profound structural changes that occur with age (Good et al., 2001; Sowell et al., 2003; Østby et al., 2009; Tamnes et al., 2010), we performed additional analyses to address the extent to which decreases in low frequency power could be explained by decreases in GMC (see Appendix C). These analyses demonstrated that age has more explanatory power over and above that of GMC than GMC has over and above that of age (**Figure A2B**), meaning that age is a better predictor of spectral power than GMC. While this could be due to the error associated with measuring and computing local GMC, it may also imply that age includes information related not only to gray matter but also other factors, such as vascular compliance or degree of neural activation, that are related to differences in RSN spectral power.

Information regarding the effects of gender on spectral power is displayed in **Figure 6B**. Gender differences are found in only a few sensorimotor and attention-related RSNs and indicate slightly greater spectral power in males than females at very low frequencies (<0.05 Hz). Effects of gender are considerably smaller than those observed for age, both in terms of the test statistics at individual frequency bins and the fraction of the spectrum showing significant effects (**Figures 6B1,B2**).

Typical examples of the relationships between spectral power and the covariates of interest are shown in the rightmost panels of **Figure 6**. IC 53, representing the "core" of the posterior DMN, shows no difference with regard to gender (**Figure 6A3**, as expected from the multivariate results in **Figure 5**), and a fairly linear relationship between log(age) and log(power; **Figure 6A4**). The partial correlation coefficient, $r_p = -0.38$, is related to the variance accounted for by log(age) that is not accounted for by other regressors and indicates modest explanatory power. IC 72, composed largely of the central and anterior precuneus, shows a similar relationship with age and an additional gender effect (**Figures 6B3,B4**). Though the gender difference is statistically significant, distributions of power for males and females are highly overlapping and the gender term accounts for a relatively small portion of the response variance (**Figure 6B4**, right panel, $r_p = -0.19$). For both IC 53 and IC 72, close

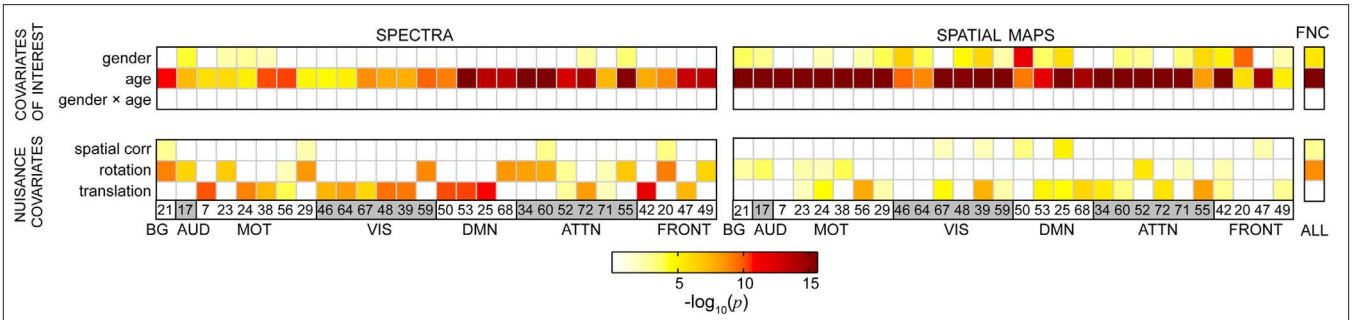


FIGURE 5 | Results from the reduced MANCOVA models, depicting the significance of covariates of interest (top) and nuisance predictors (bottom) for power spectra (left), SMs (middle), and the FNC matrix (right) in $\log_{10}(p)$ units. White cells indicate terms that were removed from the full model during backward selection process. Note that the term labels refer to continuous covariates following normalizing transformations (e.g., log(age); see **Figure 2**). Also note that the range of $\log_{10}(p)$ is limited by computational precision. In our analysis, epsilon is 2^{-52}, which corresponds to a maximal $-\log_{10}(p)$ value of 15.65.

inspection of the scatter plots between log(age) and log(power) reveals that decreases in power do not begin until roughly 15 or 16 years of age, with power staying approximately constant or possibly showing a slight increase between 12 and 15 years. This trend, which was observed in additional RSNs, suggests a more complex relationship between age and spectral power during development (see Section 4).

3.3.2 Spatial maps

The effects of age on SM intensities are summarized in **Figure 7A**. Significant age-related decreases were observed in all RSNs and extend across large areas of cortex. Decreases were particularly pronounced (with regard to significance and rate of change) in several motor networks, frontal regions, and the precuneus (**Figures 7A1,A2**). Increases in SM intensity with age were found in a few sensory-related components, however only the BG network (IC 21) showed this effect in large clusters comprising a substantial portion of the component. Additional analyses investigating the contribution of GMC to the changes in SM intensities again suggested that age has more explanatory power than GMC (**Figure A2C**).

In **Figure 7A**, right panels, we show examples of regions with age-related decreases (IC 25, centered in anterior cingulate cortex) and increases (IC 21, putamen) in SM intensity. Note that both these regions also showed slight gender effects, seen in the different intercepts of the regression lines for males and females. For IC 25, the relationship between log(age) and intensity (**Figure 7A3**) is approximately linear and the partial correlation coefficient ($r_p = -0.45$) indicates moderate explanatory ability. For IC 21, the scatter plot (**Figure 7A4**) suggests a positive linear relationship between log(age) and intensity at younger ages (roughly 12–27 years) that flattens or even decreases after 30 years of age. This pattern again implies the presence of more complex relationships between age and functional connectivity that should be investigated in future studies.

Figure 7B describes differences in SMs with regard to gender. Similar to the results for power spectra, gender effects are weaker and more sparse than those observed for age. We find evidence of gender effects in both directions (i.e., males > females and males < females), however the majority of regions passing significance and those with the largest spatial extents show greater intensity in females (**Figures 7B1,B2**). Examples of the most pronounced gender effects are shown in **Figures 7B3,B4**, indicating slightly greater SM intensity in females than in males centered within the bilateral globus pallidus (IC 21) and left IFG (IC 20). As before, the distributions of intensity largely overlap between genders and the partial correlation coefficients ($r_p = 0.22$ and $r_p = 0.31$ for IC 21 and IC 20, respectively) suggest relatively low explanatory power.

3.3.3 Functional network connectivity

Figure 8 shows differences in FNC related to age and gender. The majority of between-network correlations decrease with age, and significant reductions appear to largely involve motor and attention networks (**Figure 8A1**). In particular, the supplementary motor area (IC 56) and precuneus (IC 72), two of the brain's most interconnected regions (Hagmann et al., 2008; Gong et al., 2009), exhibit decreased correlations with a large number of other RSNs as a function of age. Gender-related differences in FNC are less significant than those observed for age, but show a consistent pattern of slightly greater correlations in males than females for connections involving motor networks (**Figure 8B1**). This is true for correlations between components *within* the motor system, for example IC 24 (right sensorimotor cortex) and IC 7 (bilateral precentral gyri), and *between* motor RSN and other sensory-related networks, for example IC 24 and IC 17 (auditory cortex). Examples of age and gender effects on FNC correlations are displayed in **Figures 8A2,B2**. Correlation magnitude between IC 38 (bilateral postcentral gyri) and IC 56 (supplementary motor area) decreases very slightly with age ($r_p = -0.20$), and shows no difference with regard to gender (**Figure 8A2**). Correlations between IC 24 (right sensorimotor cortex) and IC 72 (precuneus) reveal a similar trend with age ($r_p = -0.19$) and a very modest gender difference with males showing slightly stronger correlations than females ($r_p = -0.15$) (**Figure 8B2**). These effects are noticeably weaker than those found in spectra and SMs (see **Figures 6 and 7**), suggesting that functional connectivity between regions may be less affected by age and gender than connectivity within regions.

4 DISCUSSION

In the present study, we used a high model order ICA decomposition of resting-state functional imaging data to delineate a set of RSNs on a very large sample ($n = 603$). We outlined a framework

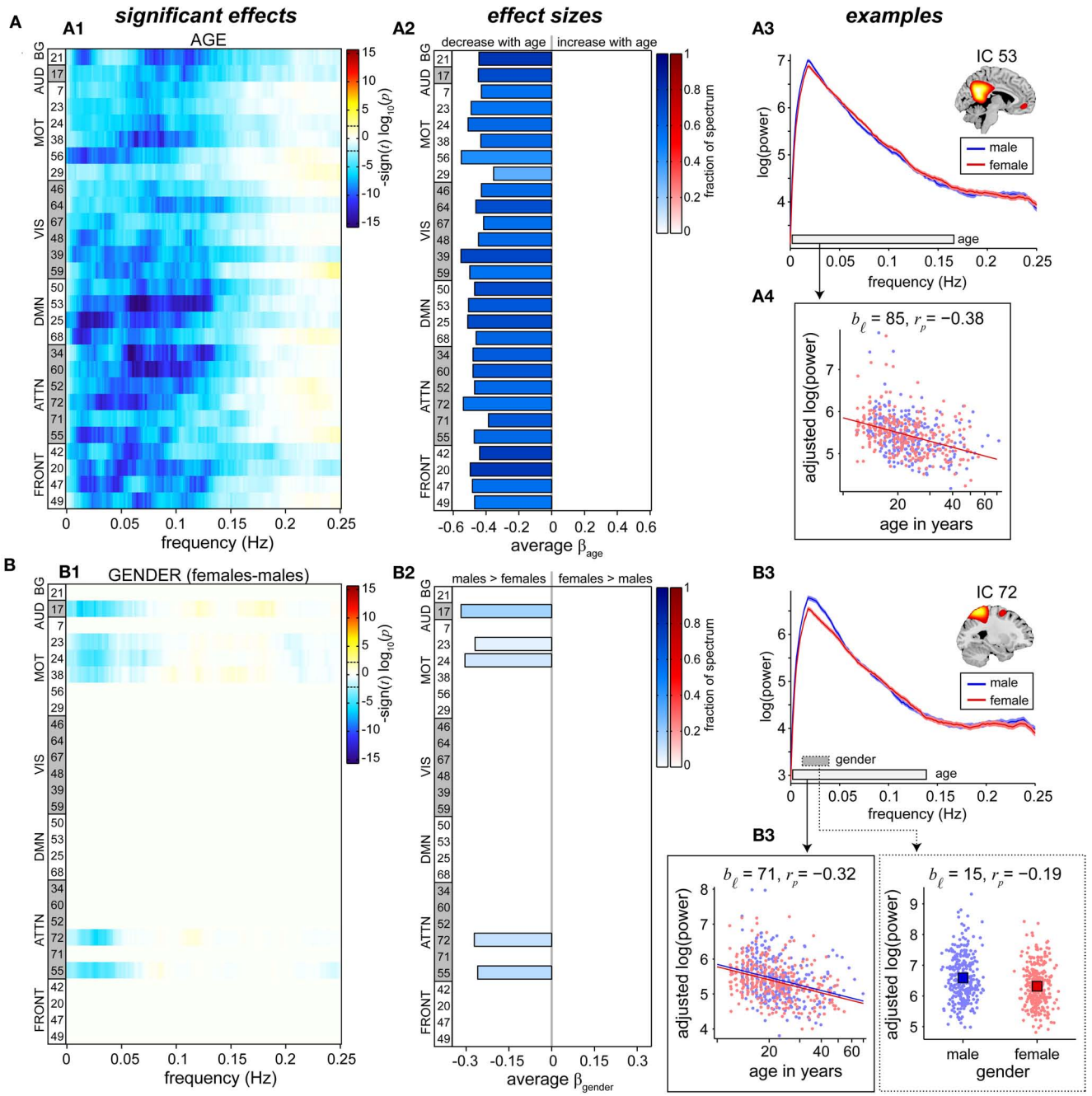


FIGURE 6 | Univariate test results showing the effects of age (A) and gender (B) on power spectra. Univariate tests were performed only on covariates of interest retained in the reduced MANCOVA model (**Figure 5**). Left panels **(A1,B1)** depict the significance and direction of age **(A)** and gender **(B)** terms as a function of frequency for each component, displayed as the $-\text{sign}(t)\log_{10}(p)$. Dashed horizontal lines on the colorbar designate the FDR-corrected threshold ($\alpha = 0.01$). Middle panels **(A2,B2)** show bar plots of the average β-values for age **(A)** and gender **(B)** terms. β-Values were averaged over frequency bands with effects of the same directionality where test statistics exceeded the FDR threshold. The color of the bar is proportional to the fraction of contributing frequency bins; the absence of a bar indicates that univariate tests were not performed or test statistics were not significant. Right panels show examples of components with a sole age effect (**A**, IC 53, posterior DMN) and both age and gender effects (**B**, IC 72, precuneus). Line plots of the power spectra **(A3,B3)** show the mean log(power) ± 1 SE for males (blue) and females (red). Horizontal bars on the frequency axis denote bands with significant effects for age (white bar, solid line) and gender (gray bar, dotted line), and correspond to the range over which log(power) was averaged in the scatter plots. Scatter plots **(A4, B4)** show the covariate of interest versus log(power) after adjusting for nuisance regressors and age (for gender effects). The model fit is shown by colored lines and squares for age and gender, respectively. We indicate the number of frequency bins contributing to the data displayed (b_ℓ) and the partial correlation coefficient (r_p) between the covariate of interest and log(power).

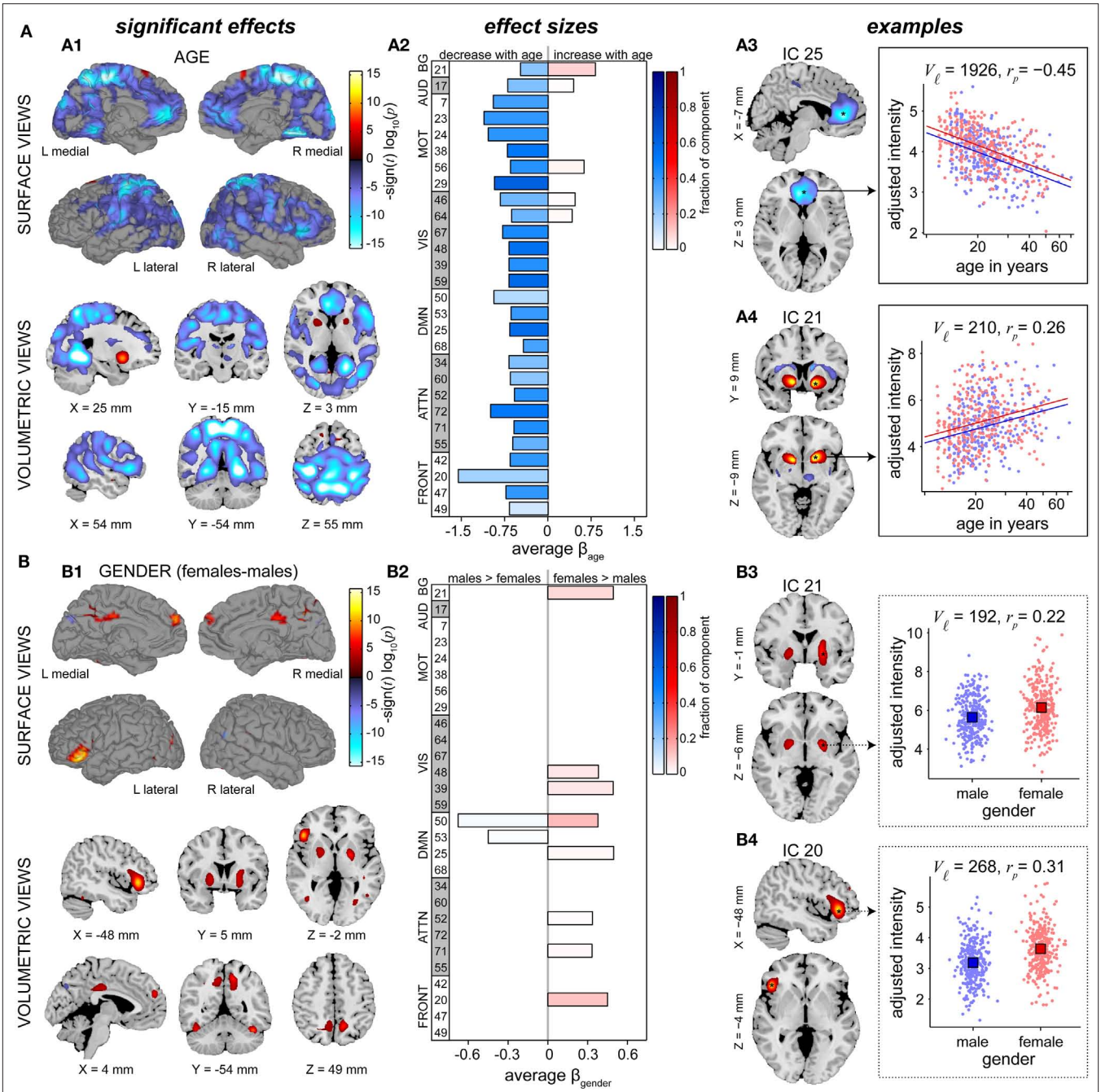


FIGURE 7 | Univariate test results showing the effects age (A) and gender (B) on SMs, in a similar format to Figure 6. Left panels **(A1,B1)** show surface and volumetric maps depicting composite renderings of significant effects over all RSNs, displayed as the $-\text{sign}(t)\log_{10}(p)$. Effects are considered significant if test statistics exceeded the FDR threshold ($\alpha = 0.01$) with a cluster extent of at least 27 contiguous voxels. Middle panels **(A2,B2)** show bar plots of the average β-values for the age **(A2)** and gender **(B2)** terms. β-Values were averaged over significant clusters with effects of the same directionality and the color of the bar is proportional to the fraction of component voxels contributing to each effect. Right panels show examples of components with age effects (**A3**: IC 25, anterior DMN, and **A4**: IC 21, basal ganglia,) and gender effects (**B3**: IC 21, basal ganglia, and B4: IC 20, left IFG). Scatter plots show the effects for a single significant cluster (indicated by asterisks in the $-\text{sign}(t)\log_{10}(p)$ maps), with the number of contributing voxels indicated on each plot (V_ℓ).

to systematically analyze such high-dimensional datasets and estimated the effects of age and gender on the connectivity properties of RSNs. We discuss the findings of each of these steps and their relevance to the current literature in turn.

4.1 RESTING-STATE NETWORKS

Similar to recent reports, we found that high model order ICA yielded extremely stable sources with sufficient spatial segregation of functional regions (Kiviniemi et al., 2009; Smith et al., 2009;

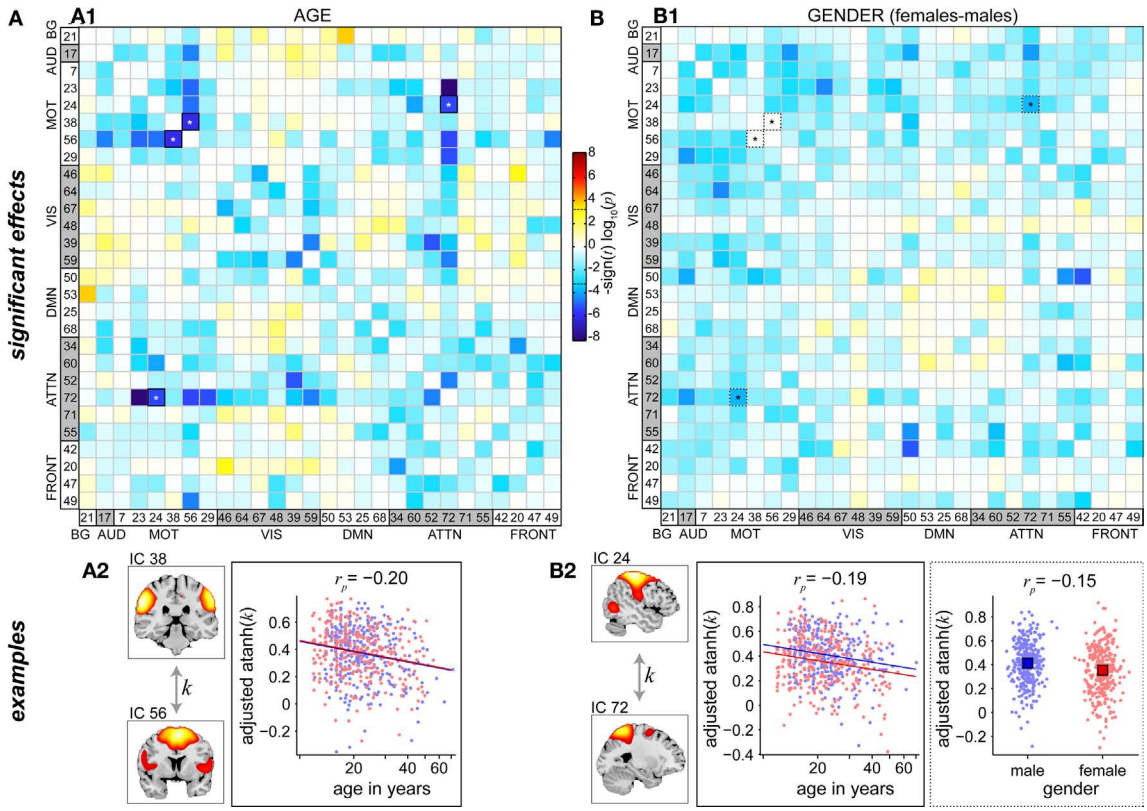


FIGURE 8 | Univariate test results showing the effects age (A) and gender (B) on FNC, in a similar format to Figure 6. Top panels depict the significance and direction of age **(A1)** and gender **(B1)** terms for each pairwise correlation, displayed as the $-\text{sign}(t)\log_{10}(p)$. Dashed horizontal lines on the colorbar designate the FDR-corrected threshold ($\alpha = 0.01$). Bottom panels show examples of age effects (**A2**, temporal correlation (k) between motor RSNs IC 38 and IC 56) and both age and gender effects (**B2**, between motor RSN IC 24 and precuneus RSN IC 72). FNC examples are highlighted in panels **(A1,B1)** by asterisks.

Abou-Elseoud et al., 2010; Ystad et al., 2010). From 75 components, we identified 28 RSNs whose peak activation clusters were confined to cortical gray matter that describe direct cortico-cortical axonal pathways, indirect polysynaptic connections, and common feed-forward projections among cortical, subcortical, and cerebellar structures. These components are highly reminiscent of those described in previous studies regardless of the method of determination (e.g., spatial ICA, tensor ICA, or seed-based correlation), suggesting that they are fundamental components of the human connectome (Damoiseaux et al., 2006; Kiviniemi et al., 2009; Smith et al., 2009; Abou-Elseoud et al., 2010; Van Dijk et al., 2010). An important limitation of the set of RSNs is their breadth. Due to contamination of putative RSNs and artifacts (see **Figure 3**), we lack "full coverage" of all brain regions. This is particularly problematic for areas neighboring known susceptibility artifacts (orbitofrontal cortex), motion edges (frontal/occipital poles), and ventricles (subcortical nuclei). Future analyses could employ preprocessing steps optimized for subcortical regions (e.g., masking areas not of interest, using a smaller Gaussian smoothing kernel) or potentially use higher model order to better separate artifactual sources. An alternative method to increase coverage is to be less conservative with regard to component selection. Though this is a reasonable approach for a primary analysis identifying and characterizing networks, our ultimate goal is a secondary association analysis thus we chose to err on the side of caution using highly selective criteria.

For the set of RSNs, we further characterized large-scale functional connectivity by computing temporal correlations between networks. Our examination of a large sample of healthy subjects may provide the best estimate of FNC to date, and the structure of the correlation matrix identifies a number of interesting features (see **Figure 4**). As would be expected, there is strong clustering within functional domains (e.g., VIS, MOT, and DMN), and components within the DMN are anti-correlated with other systems. Note that negative correlations are observed without the application of global mean regression in preprocessing (Murphy et al., 2009; Fox et al., 2009), supporting the interpretation that temporally anti-correlated networks subserve opposing functions (Fox et al., 2005; Fox and Raichle, 2007). We also observe that the precuneus (IC 72) exhibits heterogeneous functional connectivity with numerous components in motor, visual, and attentional systems. This is consistent with recent reports implicating the precuneus as a central core in the cortical anatomical network (Hagmann et al., 2008; Bullmore and Sporns, 2009; Gong et al., 2009; Margulies et al., 2009). Another notable feature is the distinction in connectivity between the left and right fronto-parietal networks (IC 34 and 60, respectively). The left network is positively correlated with the DMNs and anti-correlated with visual and motor networks. In contrast, the right fronto-parietal network shows weak *positive* correlations with visual and motor components. Disparate behavior of these lateralized networks has been noted previously (Calhoun et al., 2008a; Smith et al., 2009) and

corresponds well with task-based findings, which demonstrate that the ventral attentional system involved in stimulus-driven orienting is right-lateralized (Corbetta and Shulman, 2002; He et al., 2007; Vincent et al., 2008), whereas the left fronto-parietal network is more implicated in explicit memory retrieval (Iidaka et al., 2006). Overall, these findings suggest highly distinct functional roles for these networks in a variety of mental states.

4.2 AGE AND GENDER EFFECTS

For our sample of healthy controls largely composed of adolescents and young adults, age accounted for 10–20% of the variance in all investigated properties of resting-state functional connectivity. With the exception of the BG (see below), age-related decreases were observed across all RSNs. These findings are consistent with previous studies focusing on DMN regions, though our examination of a large complement of RSNs suggests that age-related changes are most prominent in motor and attentional networks (Andrews-Hanna et al., 2007; Damoiseaux et al., 2008; Esposito et al., 2008; Koch et al., 2009; Biswal et al., 2010). A near-ubiquitous decrease in functional connectivity across cortex may appear at odds with Biswal et al. (2010), who in a large multi-site investigation report both age-related increases and decreases in connectivity. However, it should be noted that the cortical areas showing increases with age also exhibited negative SM loadings, i.e., were anti-correlated with seed regions or the component TC (e.g., see their **Figure 2**). Therefore, age-related increases in Biswal et al. (2010) correspond to *reductions* in the magnitude of anti-correlation, consistent with the notion that network activity decreases with age. In the current study, we confined analysis only to voxels with positive SM loadings, thus the directionality of age-related effects have an unambiguous interpretation.

In our analysis only the bilateral putamen (IC 21) showed pronounced age-related increases in functional connectivity (see **Figure 7A**). The etiology of this distinction is unclear and certainly warrants future in-depth investigation. It is interesting to note that gray matter volumes in subcortical regions show very different age-related trajectories from those found in cortex (Østby et al., 2009), suggesting that were they evaluated, additional BG and thalamic components would show changes with age that are distinct from the cortical trends. As the methodology to delineate these structures improves, so can investigations into the development of subcortical networks and cortical-subcortical interactions (Robinson et al., 2009; Fair et al., 2010; Ystad et al., 2010).

The specific relationship between age and measures of functional connectivity warrants special attention. As mentioned in the Section 3, inspection of the scatter plots for spectra and SMs suggest that reductions with age in cortical RSNs do not typically start until mid to late adolescence. Furthermore, the relatively linear relationships between log(age) and connectivity measures following adolescence indicate more rapid changes in young adulthood than in late adulthood. These trends are somewhat reminiscent of developmental changes in cortical gray matter (Good et al., 2001; Sowell et al., 2003; Østby et al., 2009; Tamnes et al., 2010), consistent with the notion that structural substrates underlie function (Hagmann et al., 2008). However, as indicated in previous studies and our own analysis (see **Figure A2**), alterations in functional connectivity cannot be explained by differences in gray matter alone (Damoiseaux et al., 2008; Glahn et al., 2010), and may be better predicted when including changes in white matter tracts and possible interactions. Future studies should examine changes in functional connectivity while considering the underlying structure and be designed specifically to probe developmental and transitional periods. Regression models might also incorporate higher-order age terms to capture curvature and non-monotonic trends which have been found previously (Szaflarski et al., 2006; Kelly et al., 2009; Stevens et al., 2009). It is also important to note that cross-sectional analyses, such as those used here, can reduce sensitivity to estimate trajectories and may increase bias; future studies should consider a longitudinal approach to alleviate these issues (Kraemer et al., 2000).

An important consideration for interpreting age-related effects in functional connectivity measures, particularly power spectra, is the influence of non-neural factors. Changes in the BOLD signal are a function of complex metabolic and vascular reactions and are only indirectly related to changes in resting-state neural activity (Schölvinck et al., 2010). The magnitude of spontaneous fluctuations and stimulus-evoked responses is affected by a multitude of physiological variables (e.g., baseline levels of blood flow, vascular compliance, cardiac and respiratory rhythms) that are known to change with age and therefore preclude a full interpretation of age-related findings (D'Esposito et al., 2003; Birn et al., 2006, 2008; Ances et al., 2009). In our analysis, the influence of non-neural factors may be mitigated by the use of an ICA framework, which appears to partially separate physiological noise sources at higher model orders (Birn et al., 2008; Beall and Lowe, 2010; Starck et al., 2010), however there is almost certainly some remaining contribution of non-neural variables to the age-related trends in functional connectivity measures. In an effort to assess the magnitude of this contribution, we performed additional statistical analyses on the power spectra and SMs of vascular, ventricular and white matter regions, as detailed in Appendix E. As expected, age was found to be a significant predictor for nearly all vascular compartments and tissue types, but based on the size of the observed effects these results suggest at least a partial neural origin for age-related findings in power spectra and a likely neural origin in SMs. Note, however, that without direct measurements or the concurrent use of additional non-invasive techniques such as EEG (Whitford et al., 2007), NIRS (Huppert et al., 2006), or calibrated-fMRI (Ances et al., 2009), it is generally not feasible to fully dissociate neural from confounding physiological factors. We further note that regardless of their etiology, our study demonstrates robust age-related effects in functional connectivity measures that must be considered in future analyses, even when the age range across subjects is relatively narrow (e.g., 20–30 years).

Compared to age, gender differences in functional connectivity were smaller (accounting for between 5 and 15 percent of response variance) and confined to fewer areas. Despite relatively small effects, we note that the inclusion of gender and appropriate interaction terms in regression models may be critical for discovering and interpreting the effects of other covariates, particularly when investigating complex phenotypes such as general intelligence (Haier et al., 2005; Schmithorst and Holland, 2006, 2007). Similar to previous studies, we found evidence for greater connectivity in females versus males within DMN regions (Bluhm et al., 2008; Biswal et al., 2010), though these effects were not nearly as pronounced as those in the left IFG or bilateral BG. Gender differences in the left IFG (Broca's area) are consistent with earlier

reports showing increased GMC in the same region for females (Good et al., 2001; Luders et al., 2005). Given the importance of the left IFG in various aspects of speech generation (for review see Bookheimer, 2002), the difference likely reflects gender distinctions in the use or organization of language networks at rest. It is possible that the observed increases in GMC and functional connectivity relate to a slight enhancement of language skills in adult females (Weiss et al., 2003), though the existence and extent of this gender difference is debated (Wallentin, 2009). Regardless, our results motivate further investigation into the relationship between verbal fluency and resting-state activity in language networks (Hampson et al., 2002, 2006). Gender differences in the BG centered at the pallidum appear to be a novel finding and it is not clear why this network might be more coherent in females. Sexual dimorphisms in the structural aspects of the BG are found throughout development (Good et al., 2001; Luders et al., 2009), and further examination of gender-specific function in these regions is warranted. Gender differences were also observed in FNC and spectral power within the motor and sensory systems, where males showed increases relative to females. A greater level of basal activity in motor networks, as well as greater coactivation between different networks, may be related to increased use and coordination between these systems, as suggested by recent studies of motor learning and functional connectivity (Albert et al., 2009; Xiong et al., 2009). Alternatively, this distinction may reflect an inherent gender difference in sensorimotor connectivity, possibly related to the enhancement of motor and visuospatial skills in males (Weiss et al., 2003; Hamilton, 2008).

4.3 STATISTICAL APPROACH

Investigations of resting-state functional connectivity provide an exciting and potentially rich look into intrinsic architecture of the human brain, however this approach brings with it some methodological challenges that must be acknowledged. Unlike analysis of task-related data, which typically involves a limited number of predefined contrasts and is often constrained to regions of interest, analysis of intrinsic connectivity presents an overwhelming number of possible comparisons to be made within and between regions. To avoid mass univariate testing with inherent multiple comparison correction problems, we propose a hierarchical framework to focus analysis and effectively reduce the number of tests performed. At the initial level, we adopt a multivariate approach with backward selection on a carefully selected set of predictors which refines the model and limits the number of statistical tests performed. Using power spectra as an example, the full spectrum is PCA compressed over frequency bins and used as a single multivariate response for model selection. Only when relevant regressors are retained (age and/or gender) are univariate regressions performed, saving many tests in the case of gender (see **Figures 5 and 6B1**). Note that the use of ICA has also greatly refined the testing procedure by initially delineating relevant features: power spectra are evaluated for a relatively small number of select components (here, $C_1 = 28$), rather than the comparatively large number of voxels (here, $V \approx 67000$) that might be tested in a seed-based coherence approach. Simulations indicate that the MANCOVA results are robust to false positives and that sensitivity is optimized by PCA reduction of response variables to the MDL estimate (see **Figure A3**). There are, of course, limitations to this method, chiefly that the effects of interest must be captured in the retained principal components. Thus it is possible that age or gender-related differences in functional connectivity were not identified in the current analysis if the relevant features contributed a small fraction of variance to the response. To avoid this limitation, one could use alternative multivariate approaches such as discriminatory PCA (Caprihan et al., 2008) or coefficient-constrained ICA (Sui et al., 2009) that "optimize" dimension reduction based on the desired contrast. Though such approaches can improve feature identification and classification, we opt to use PCA on the response vectors *independently* of predictors to retain statistical tests and interpretations that are unbiased by an optimization procedure.

Regarding model selection, it is interesting to note that in most cases at least one of the motion-related nuisance regressors was retained as a predictor (see **Figure 5**). This indicates mild contamination of motion-related variance in nearly all ICA outcome measures and suggests that covariates summarizing motion should generally be included in design matrices to improve estimates for predictors of interest. Ideally, one would include additional nuisance regressors, such as average heart rate or variability in respiration depth, as these variables also contribute to variance in ICA, TCs, and SMs (Birn et al., 2008; Beall and Lowe, 2010; Starck et al., 2010). Though cardiac and respiratory measures were unfortunately not acquired for the group of subjects studied here, their inclusion would almost certainly improve estimation and inference of gender and age effects.

As a final note on the statistical approach described here, we comment on its broad applicability. The proposed method can be used to investigate the effects of numerous covariates on functional connectivity, and we anticipate that it will enhance the ability to detect differences related to neuropsychiatric disorders while controlling for demographic and other factors. Perhaps more importantly, this method is easily applied to a variety of datasets where response variables have high dimensionality but show considerable collinearity. These include outcome measures estimating functional and effective connectivity with various techniques (Sun et al., 2004; Karunanayaka et al., 2007; Deshpande et al., 2009), multidimensional parameters summarizing full brain network topology (Gong et al., 2009), as well as large-scale structural datasets such as those describing cortical thickness or white matter integrity. Though this multivariate framework provides a relatively minor departure from the mass univariate approach typically used, we feel it represents an important step toward the development of more sophisticated statistical and inferential methods that are necessary to comprehend increasingly large and complex data (Costafreda, 2010).

ACKNOWLEDGMENTS

This research was supported by NIH 1R01-EB006841, NIH 1R01-EB005846, NIH 2R01-EB000840, NIH 1 P20 RR021938-01, and DOE DE-FG02-08ER64581 (PI: Calhoun). Support for data collection by NIMH 1R01-MH072681-01 (PI: Kiehl); John Templeton Foundation Grant #12456 (PI: Jung); NRC Bilatgrunn (PI: Eichele); NIH 1P20 AA017068 (PI: Kodituwakku); NIH R21NS064464, NIH 1 R03 DA022435-01A1, and NIH 1 R03 DA024212-01A1 (PI: Mayer); NIH KO1-DA021632-02 (PI: Filbey).

REFERENCES

Abbott, C., Kim, D., Sponheim, S. R., Bustillo, J., and Calhoun, V. D. (2010). Decreased default mode neural modulation with age in schizophrenia. *Am. J. Geriatr. Psychiatry* 18, 897–907.

Abou-Elseoud, A., Starck, T., Remes, J., Nikkinen, J., Tervonen, O., and Kiviniemi, V. (2010). The effect of model order selection in group PICA. *Hum. Brain Mapp.* 31, 1207–1216.

Albert, N., Robertson, E., and Miall, R. (2009). The resting human brain and motor learning. *Curr. Biol.* 19, 1023–1027.

Allen, E., Erhardt, E., Eichele, T., Mayer, A. R., and Calhoun, V. D. (2010). "Comparison of pre-normalization methods on the accuracy of group ICA results", in *16th Annual Meeting of the Organization for Human Brain Mapping*, 6–10 June, Barcelona, Spain.

Ances, B., Liang, C., Leontiev, O., Perthen, J., Fleisher, A., Lansing, A., and Buxton, R. (2009). Effects of aging on cerebral blood flow, oxygen metabolism, and blood oxygenation level dependent responses to visual stimulation. *Hum. Brain Mapp.* 30, 1120–1132.

Andrews-Hanna, J., Snyder, A., Vincent, J., Lustig, C., Head, D., Raichle, M., and Buckner, R. (2007). Disruption of large-scale brain systems in advanced aging. *Neuron* 56, 924–935.

Ashburner, J., and Friston, K. J. (2005). Unified segmentation. *Neuroimage* 26, 839–851.

Barron, S., Jacobs, L., and Kinkel, W. (1976). Changes in size of normal lateral ventricles during aging determined by computerized tomography. *Neurology* 26, 1011–1013.

Beall, E., and Lowe, M. (2010). The non-separability of physiologic noise in functional connectivity MRI with spatial ICA at 3T. *J. Neurosci. Methods* 191, 263–276.

Beckmann, C. F., DeLuca, M., Devlin, J. T., and Smith, S. M. (2005). Investigations into resting-state connectivity using independent component analysis. *Philos. Trans. R. Soc. Lond. B Biol. Sci.* 360, 1001–1013.

Bell, A. J., and Sejnowski, T. (1995). An information-maximization approach to blind separation and blind deconvolution. *Neural. Comput.* 7, 1129–1159.

Birn, R., Diamond, J., Smith, M., and Bandettini, P. (2006). Separating respiratory-variation-related fluctuations from neuronal-activity-related fluctuations in fMRI. *Neuroimage* 31, 1536–1548.

Birn, R., Murphy, K., and Bandettini, P. (2008). The effect of respiration variations on independent component analysis results of resting state functional connectivity. *Hum. Brain Mapp.* 29, 740–750.

Biswal, B. B., Mennes, M., Zuo, X. N., Gohel, S., Kelly, C., Smith, S. M., Beckmann, C. F., Adelstein, J. S., Buckner, R. L., Colcombe, S., Dogonowski, A. M., Ernst, M., Fair, D., Hampson, M., Hoptman, M. J., Hyde, J. S., Kiviniemi, V. J., Kötter, R., Li, S. J., Lin, C. P., Lowe, M. J., Mackay, C., Madden, D. J., Madsen, K. H., Margulies, D. S., Mayberg, H. S., McMahon, K., Monk, C. S., Mostofsky, S. H., Nagel, B. J., Pekar, J. J., Peltier, S. J., Petersen, S. E., Riedl, V., Rombouts, S. A., Rypma, B., Schlaggar, B. L., Schmidt, S., Seidler, R. D., Siegle, G. J., Sorg, C., Teng, G. J., Veijola, J., Villringer, A., Walter, M., Wang, L., Weng, X.C., Whitfield-Gabrieli, S., Williamson, P., Windischberger, C., Zang, Y. F., Zhang, H. Y., Castellanos, F. X., and Milham, M. P. (2010). Toward discovery science of human brain function. *Proc. Natl. Acad. Sci. U.S.A.* 107, 4734–4739.

Biswal, B., Yetkin, F., Haughton, V., and Hyde, J. (1995). Functional connectivity in the motor cortex of resting human brain using echo-planar MRI. *Magn. Reson. Med.* 34, 537–541.

Bluhm, R. L., Osuch, E. A., Lanius, R. A., Boksman, K., Neufeld, R. W. J., Théberge, J., and Williamson, P. (2008). Default mode network connectivity: effects of age, sex, and analytic approach. *Neuroreport* 19, 887–891.

Bockholt, H. J., Scully, M., Courtney, W., Rachakonda, S., Scott, A., Caprihan, A., Fries, J., Kalyanam, R., Segall, J., dela Garza, R., Lane, S., and Calhoun, V. D. (2009). Mining the mind research network: a novel framework for exploring large scale, heterogeneous translational neuroscience research data sources. *Front. Neuroinformatics* 3:36. doi: 10.3389/neuro.11.036.2009

Bookheimer, S. (2002). Functional MRI of language: new approaches to understanding the cortical organization of semantic processing. *Annu. Rev. Neurosci.* 25, 151–188.

Broyd, S., Demanuele, C., Debener, S., Helps, S. K., James, C. J., and Sonuga-Barke, E. J. S. (2009). Default-mode brain dysfunction in mental disorders: a systematic review. *Neurosci. Biobehav. Rev.* 33, 279–296.

Buckner, R., Andrews-Hanna, J., and Schacter, D. (2008). The brain's default network. *Ann. N. Y. Acad. Sci.* 1124, 1–38.

Bullmore, E., and Sporns, O. (2009). Complex brain networks: graph theoretical analysis of structural and functional systems. *Nat. Rev. Neurosci.* 10, 186–198.

Calhoun, V. D., Adali, T., Pearlson, G. D., and Pekar, J. J. (2001). A method for making group inferences from functional MRI data using independent component analysis. *Hum. Brain Mapp.* 14, 140–151.

Calhoun, V. D., Adali, T., Pearlson, G. D., and Pekar, J. J. (2002a). Erratum: a method for making group inferences from functional MRI data using independent component analysis. *Hum. Brain Mapp.* 16, 131.

Calhoun, V., Pekar, J., McGinty, V., Adali, T., Watson, T., and Pearlson, G. (2002b). Different activation dynamics in multiple neural systems during simulated driving. *Hum. Brain Mapp.* 16, 158–167.

Calhoun, V. D., Eichele, T., and Pearlson, G. (2009). Functional brain networks in schizophrenia: a review. *Front. Hum. Neurosci.* 3:17. doi: 10.3389/neuro.09.017.2009

Calhoun, V. D., Kiehl, K. A., and Pearlson, G. D. (2008a). Modulation of temporally coherent brain networks estimated using ICA at rest and during cognitive tasks. *Hum. Brain Mapp.* 29, 828–838.

Calhoun, V. D., Maciejewski, P. K., Pearlson, G. D., and Kiehl, K. A. (2008b). Temporal lobe and "default" hemodynamic brain modes discriminate between schizophrenia and bipolar disorder. *Hum. Brain Mapp.* 29, 1265–1275.

Caprihan, A., Pearlson, G., and Calhoun, V. (2008). Application of principal component analysis to distinguish patients with schizophrenia from healthy controls based on fractional anisotropy measurements. *Neuroimage* 42, 675–682.

Cavanna, A., and Trimble, M. (2006). The precuneus: a review of its functional anatomy and behavioural correlates. *Brain* 1293, 564–583.

Christensen, R. (1996). *Analysis of Variance, Design and Regression: Applied Statistical Methods*. New York: Chapman and Hall/CRC.

Christensen, R. (2001). *Advanced Linear Modeling: Multivariate, Time Series, and Spatial Data; Nonparametric Regression and Response Surface Maximization*. New York: Springer Verlag.

Corbetta, M., and Shulman, G. (2002). Control of goal-directed and stimulus-driven attention in the brain. *Nat. Rev. Neurosci.* 3, 201–215.

Cordes, D., Haughton, V. M., Arfanakis, K., Wendt, G. J., Turski, P. A., Moritz, C. H., Quigley, M. A., and Meyerand, M. E. (2000). Mapping functionally related regions of brain with functional connectivity MR imaging. *Am. J. Neuroradiol.* 21, 1636–1644.

Costafreda, S. G. (2010). Pooling fMRI data: meta-analysis, mega-analysis and multi-center studies. *Front. Neuroinformatics* 3:33. doi: 10.3389/neuro.11.033.2009

Damoiseaux, J. S., Beckmann, C. F., Arigita, E. J., Barkhof, F., Scheltens, P., Stam, C. J., Smith, S. M., and Rombouts, S. (2008). Reduced resting-state brain activity in the "default network" in normal aging. *Cereb. Cortex* 18, 1856–1864.

Damoiseaux, J. S., Rombouts, S., Barkhof, F., Scheltens, P., Stam, C. J., Smith, S. M., and Beckmann, C. F. (2006). Consistent resting-state networks across healthy subjects. *Proc. Natl. Acad. Sci. U.S.A.* 103, 13848–13853.

Derksen, S., and Keselman, H. J. (1992). Backward, forward and stepwise automated subset selection algorithms: frequency of obtaining authentic and noise variables. *Br. J. Math. Stat. Psychol.* 45, 265–282.

Deshpande, G., LaConte, S., James, G., Peltier, S., and Hu, X. (2009). Multivariate granger causality analysis of fMRI data. *Hum. Brain Mapp.* 30, 1361–1373.

D'Esposito, M., Deouell, L. Y., and Gazzaley, A. (2003). Alterations in the BOLD fMRI signal with ageing and disease: a challenge for neuroimaging. *Nat. Rev. Neurosci.* 4, 863–872.

Eichele, T., Debener, S., Calhoun, V. D., Specht, K., Engel, A. K., Hugdahl, K., VonCramon, D. Y., and Ullsperger, M. (2008). Prediction of human errors by maladaptive changes in event-related brain networks. *Proc. Natl. Acad. Sci. U.S.A.* 105, 6173–6178.

Erhardt, E. B., Rachakonda, S., Bedrick, E. J., Allen, E. A., Adali, T., and Calhoun, V. D. (2010). Comparison of multi-subject ICA methods for analysis of fMRI data. *Hum. Brain Mapp*. doi: 10.1002/hbm.21170. [Epub ahead of print].

Esposito, F., Aragri, A., Pesaresi, I., Cirillo, S., Tedeschi, G., Marciano, E., Goebel, R., and DiSalle, F. (2008). Independent component model of the default-mode brain function: combining individual-level and population-level analyses in resting-state fMRI. *Magn. Reson. Imaging* 26, 905–913.

Fair, D. A., Bathula, D., Mills, K. L., Dias, T. G. C., Blythe, M. S., Zhang, D., Snyder, A. Z., Raichle, M. E., Stevens, A. A., Nigg, J. T., and Nagel, B. J. (2010). Maturing thalamocortical functional connectivity across development. *Front. Syst. Neurosci.* 4:10. doi: 10.3389/fnsys.2010.00010

Fair, D. A., Cohen, A. L., Dosenbach, N. U., Church, J. A., Miezin, F. M., Barch, D. M., Raichle, M. E., Petersen, S. E., and Schlaggar, B. L. (2008). The maturing architecture of the brain's default network. *Proc. Natl. Acad. Sci. U.S.A.* 105, 4028–4032.

Fan, J., McCandliss, B. D., Fossella, J., Flombaum, J. I., and Posner, M. I. (2005). The activation of attentional networks. *Neuroimage* 26, 471–479.

Filippini, N., MacIntosh, B. J., Hough, M. G., Goodwin, G. M., Frisoni, G. B., Smith, S. M., Matthews, P. M.,

Beckmann, C. F., and Mackay, C. E. (2009). Distinct patterns of brain activity in young carriers of the APOE-4 allele. *Proc. Natl. Acad. Sci. U.S.A.* 106, 7209–7214.

Fox, M. D., and Raichle, M. E. (2007). Spontaneous fluctuations in brain activity observed with functional magnetic resonance imaging. *Nat. Rev. Neurosci.* 8, 700–711.

Fox, M., Snyder, A., Vincent, J., Corbetta, M., Van Essen, D., and Raichle, M., (2005). The human brain is intrinsically organized into dynamic, anticorrelated functional networks. *Proc. Natl. Acad. Sci. U.S.A.* 102, 9673.

Fox, M., Zhang, D., Snyder, A., and Raichle, M., (2009). The global signal and observed anticorrelated resting state brain networks. *J. Neurophysiology* 101, 3270.

Franco, A. R., Pritchard, A., Calhoun, V. D., and Mayer, A. R. (2009). Interrater and intermethod reliability of default mode network selection. *Hum. Brain Mapp.* 30, 2293–2303.

Friston, K. J., Holmes, A. P., Worsley, K. J., Poline, J. B., Frith, C. D., and Frackowiak, R. S. J. (1995). Statistical parametric maps in functional imaging: a general linear approach. *Hum. Brain Mapp.* 2, 189–210.

Garrity, A. G., Pearlson, G. D., McKiernan, K., Lloyd, D., Kiehl, K. A., and Calhoun, V. D. (2007). Aberrant "default mode" functional connectivity in schizophrenia. *Am. J. Psychiatry* 164, 450–457.

Genovese, C. R., Lazar, N. A., and Nichols, T. (2002). Thresholding of statistical maps in functional neuroimaging using the false discovery rate. *Neuroimage* 15, 870–878.

Glahn, D., Winkler, A., Kochunov, P., Almasy, L., Duggirala, R., Carless, M., Curran, J., Olvera, R., Laird, A., Smith, S., Beckmann, C. F., Fox, P. T., and Blangerod, J. (2010). Genetic control over the resting brain. *Proc. Natl. Acad. Sci. U.S.A.* 107, 1223–1228.

Gong, G., Rosa-Neto, P., Carbonell, F., Chen, Z. J., He, Y., and Evans, A. C. (2009). Age- and gender-related differences in the cortical anatomical network. *J. Neurosci.* 29, 15684–15693.

Good, C., Johnsrude, I., Ashburner, J., Henson, R., Friston, K., and Frackowiak, R. (2001). Cerebral asymmetry and the effects of sex and handedness on brain structure: a voxel-based morphometric analysis of 465 normal adult human brains. *Neuroimage* 14, 685–700.

Greicius, M. (2008). Resting-state functional connectivity in neuropsychiatric disorders. *Curr. Opin. Neurol.* 21, 424–430.

Grill-Spector, K., and Malach, R. (2004). The human visual cortex. *Annu. Rev. Neurosci.* 27, 649–677.

Hagmann, P., Cammoun, L., Gigandet, X., Meuli, R., Honey, C. J., Wedeen, V. J., and Sporns, O. (2008). Mapping the structural core of human cerebral cortex. *PLoS Biol.* 6, e159. doi: 10.1371/journal.pbio.0060159

Haier, R., Jung, R., Yeo, R., Head, K., and Alkire, M. (2005). The neuroanatomy of general intelligence: sex matters. *Neuroimage* 25, 320–327.

Hamilton, C. (2008). *Cognition and Sex Differences*. New York: Palgrave Macmillan.

Hampson, M., Peterson, B., Skudlarski, P., Gatenby, J., and Gore, J. (2002). Detection of functional connectivity using temporal correlations in MR images. *Hum. Brain Mapp.* 15, 247–262.

Hampson, M., Tokoglu, F., Sun, Z., Schafer, R., Skudlarski, P., Gore, J., and Constable, R. (2006). Connectivity-behavior analysis reveals that functional connectivity between left BA39 and Broca's area varies with reading ability. *Neuroimage* 31, 513–519.

Harrison, B. J., Pujol, J., López-Solà, M., Hernández-Ribas, R., Deus, J., Ortiz, H., Soriano-Mas, C., Yücel, M., Pantelis, C., and Cardoner, N. (2008). Consistency and functional specialization in the default mode brain network. *Proc. Natl. Acad. Sci. U.S.A.* 105, 9781–9786.

He, B. J., Snyder, A. Z., Vincent, J. L., Epstein, A., Shulman, G. L., and Corbetta, M. (2007). Breakdown of functional connectivity in frontoparietal networks underlies behavioral deficits in spatial neglect. *Neuron* 53, 905–918.

Henderson, H. V., and Velleman, P. F. (1981). Building multiple regression models interactively. *Biometrics* 37, 391–411.

Himberg, J., Hyvärinen, A., and Esposito, F. (2004). Validating the independent components of neuroimaging time series via clustering and visualization. *Neuroimage* 22, 1214–1222.

Huppert, T., Hoge, R., Diamond, S., Franceschini, M., and Boas, D. (2006). A temporal comparison of BOLD, ASL, and NIRS hemodynamic responses to motor stimuli in adult humans. *Neuroimage* 29, 368–382.

Hyvärinen, A., Karhunen, J., and Oja, E. (2001). *Independent Component Analysis, Adaptive and Learning Systems for Signal Processing, Communications, and Control*. New York: John Wiley and Sons.

Iidaka, T., Matsumoto, A., Nogawa, J., Yamamoto, Y., and Sadato, N. (2006). Frontoparietal network involved in successful retrieval from episodic memory: spatial and temporal analyses using fMRI and ERP. *Cereb. Cortex* 16, 1349–1360.

Jafri, M. J., Pearlson, G. D., Stevens, M., and Calhoun, V. D. (2008). A method for functional network connectivity among spatially independent resting-state components in schizophrenia. *Neuroimage* 39, 1666–1681.

Judd, C. M., McClelland, G. H., and Ryan, C. S. (1989). *Data Analysis: A Model-Comparison Approach*. San Diego: Harcourt Brace Jovanovich.

Karunanayaka, P., Holland, S., Schmithorst, V., Solodkin, A., Chen, E., Szaflarski, J., and Plante, E. (2007). Age-related connectivity changes in fMRI data from children listening to stories. *Neuroimage* 34, 349–360.

Kelly, A. M., Di Martino, A., Uddin, L. Q., Shehzad, Z., Gee, D. G., Reiss, P. T., Margulies, D. S., Castellanos, F. X., and Milham, M. P. (2009). Development of anterior cingulate functional connectivity from late childhood to early adulthood. *Cereb. Cortex* 19, 640–657.

Kennedy, D. P., and Courchesne, E. (2008). The intrinsic functional organization of the brain is altered in autism. *Neuroimage* 39, 1877–1885.

Kiviniemi, V., Starck, T., Remes, J., Long, X., Nikkinen, J., Haapea, M., Veijola, J., Moilanen, I., Isohanni, M., Zang, Y. F., and Tervonen, O. (2009). Functional segmentation of the brain cortex using high model order group PICA. *Hum. Brain Mapp.* 30, 3865–3886.

Klein, T. A., Endrass, T., Kathmann, N., Neumann, J., Von Cramon, D. Y., and Ullsperger, M. (2007). Neural correlates of error awareness. *Neuroimage* 34, 1774–1781.

Koch, W., Teipel, S., Mueller, S., Buerger, K., Bokde, A. L. W., Hampel, H., Coates, U., Reiser, M., and Meindl, T. (2009). Effects of aging on default mode network activity in resting state fMRI: does the method of analysis matter? *Neuroimage* 51, 280–287.

Kochiyama, T., Morita, T., Okada, T., Yonekura, Y., Matsumura, M., and Sadato, N. (2005). Removing the effects of task-related motion using independent-component analysis. *Neuroimage* 25, 802–814.

Koechlin, E., Ody, C., and Kouneiher, F. (2003). The architecture of cognitive control in the human prefrontal cortex. *Science* 302, 1181–1185.

Koechlin, E., and Summerfield, C. (2007). An information theoretical approach to prefrontal executive function. *Trends Cogn. Sci.* 11, 229–235.

Kraemer, H., Yesavage, J., Taylor, J., and Kupfer, D. (2000). How can we learn about developmental processes from cross-sectional studies, or can we? *Am. J. Psychiatry* 157, 163–171.

Krienen, F., and Buckner, R. (2009). Segregated fronto-cerebellar circuits revealed by intrinsic functional connectivity. *Cereb. Cortex* 19, 2485–2497.

Laird, A. R., Eickhoff, S. B., Li, K., Robin, D. A., Glahn, D. C., and Fox, P. T. (2009). Investigating the functional heterogeneity of the default mode network using coordinate-based meta-analytic modeling. *J. Neurosci.* 29, 14496–14505.

Luders, E., Gaser, C., Narr, K. L., and Toga, A. W. (2009). Why sex matters: brain size independent differences in gray matter distributions between men and women. *J. Neurosci.* 29, 14265–14270.

Luders, E., Narr, K., Thompson, P., Woods, R., Rex, D., Jancke, L., Steinmetz, H., and Toga, A. (2005). Mapping cortical gray matter in the young adult brain: effects of gender. *Neuroimage* 26, 493–501.

Mantel, N. (1970). Why stepdown procedures in variable selection. *Technometrics* 12, 621–625.

Margulies, D. S., Vincent, J. L., Kelly, C., Lohmann, G., Uddin, L. Q., Biswal, B. B., Villringer, A., Castellanos, F. X., Milham, M. P., and Petrides, M. (2009). Precuneus shares intrinsic functional architecture in humans and monkeys. *Proc. Natl. Acad. Sci. U.S.A.* 106, 20069–20074.

McKeown, M. J., Hansen, L. K., and Sejnowsk, T. J. (2003). Independent component analysis of functional MRI: what is signal and what is noise? *Curr. Opin. Neurobiol.* 13, 620–629.

Meda, S., Giuliani, N., Calhoun, V., Jagannathan, K., Schretlen, D., Pulver, A., Cascella, N., Keshavan, M., Kates, W., Buchanan, R., Sharma, T., and Pearlson, G. D. (2008). A large scale (n= 400) investigation of gray matter differences in schizophrenia using optimized voxel-based morphometry. *Schizophrenia Research* 101, 95–105.

Mitra, P., and Bokil, H. (2008). *Observed Brain Dynamics*. New York: Oxford University Press.

Murphy, K., Birn, R., Handwerker, D., Jones, T., and Bandettini, P., (2009). The impact of global signal regression on resting state correlations: are anti-correlated networks introduced? *NeuroImage* 44, 893–905.

Murphy, K., Birn, R., Handwerker, D., Jones, T., Bandettini, P., 2009. The impact of global signal regression on resting state correlations: Are anti-correlated networks introduced? *NeuroImage* 1041 44 (3), 893–905.

Østby, Y., Tamnes, C., Fjell, A., Westlye, L., Due-Tønnessen, P., and Walhovd, K. (2009). Heterogeneity in subcortical brain development: a structural magnetic resonance imaging study of brain maturation from 8 to 30 years. *J. Neurosci.* 29, 11772–11782.

Raichle, M. E., MacLeod, A. M., Snyder, A. Z., Powers, W. J., Gusnard, D. A., and Shulman, G. L. (2001). A default mode of brain function. *Proc. Natl. Acad. Sci. U.S.A.* 98, 676–682.

Ridderinkhof, K. R., Ullsperger, M., Crone, E. A., and Nieuwenhuis, S.

(2004). The role of the medial frontal cortex in cognitive control. *Science* 306, 443–447.

Robinson, S., Basso, G., Soldati, N., Sailer, U., Jovicich, J., Bruzzone, L., Kryspin-Exner, I., Bauer, H., and Moser, E. (2009). A resting state network in the motor control circuit of the basal ganglia. *BMC Neurosci.* 10, 137. doi: 10.1186/1471-2202-10-137

Roweis, S. (1998). EM algorithms for PCA and SPCA. *Adv. Neural Inf. Process Syst.* 626–632.

Schmithorst, V., and Holland, S. (2006). Functional MRI evidence for disparate developmental processes underlying intelligence in boys and girls. *Neuroimage* 31, 1366–1379.

Schmithorst, V., and Holland, S. (2007). Sex differences in the development of neuroanatomical functional connectivity underlying intelligence found using Bayesian connectivity analysis. *Neuroimage* 35, 406–419.

Schölvinck, M., Maier, A., Ye, F., Duyn, J., and Leopold, D. (2010). Neural basis of global resting-state fMRI activity. *Proc. Natl. Acad. Sci. U.S.A.* 107, 10238–10243.

Seifritz, E., Esposito, F., Hennel, F., Mustovic, H., Neuhoff, J., Bilecen, D., Tedeschi, G., Scheffler, K., and Di Salle, F. (2002). Spatiotemporal pattern of neural processing in the human auditory cortex. *Science* 297, 1706–1708.

Shehzad, Z., Kelly, A., Reiss, P., Gee, D., Gotimer, K., Uddin, L., Lee, S., Margulies, D., Roy, A., Biswal, B., Petkova, E., Castellanos, F. X., and Milham, M. P. (2009). The resting brain: unconstrained yet reliable. *Cereb. Cortex* 19, 2209–2229.

Smith, S. M., Fox, P. T., Miller, K. L., Glahn, D. C., Fox, P. M., Mackay, C. E., Filippini, N., Watkins, K. E., Toro, R., Laird, A. R., and Beckmann, C. F. (2009). Correspondence of the brain's functional architecture during activation and rest. *Proc. Natl. Acad. Sci. U.S.A.* 106, 13040–13045.

Sowell, E., Peterson, B., Kan, E., Woods, R., Yoshii, J., Bansal, R., Xu, D., Zhu, H., Thompson, P., and Toga, A. (2007). Sex differences in cortical thickness mapped in 176 healthy individuals between 7 and 87 years of age. *Cereb. Cortex* 17, 1550–1560.

Sowell, E., Peterson, B., Thompson, P., Welcome, S., Henkenius, A., and Toga, A. (2003). Mapping cortical change across the human life span. *Nat. Neurosci.* 6, 309–315.

Specht, K., and Reul, J. (2003). Functional segregation of the temporal lobes into highly differentiated subsystems for auditory perception: an auditory rapid event-related fMRI-task. *Neuroimage* 20, 1944–1954.

Starck, T., Remes, J., Nikkinen, J., Tervonen, O., and Kiviniemi, V. (2010). Correction of low-frequency physiological noise from the resting state BOLD fMRI–effect on ICA default mode analysis at 1.5 T. *J. Neurosci. Methods* 186, 179–185.

Stevens, M. C., Pearlson, G. D., and Calhoun, V. D. (2009). Changes in the interaction of resting-state neural networks from adolescence to adulthood. *Hum. Brain Mapp.* 30, 2356–2366.

Sui, J., Adali, T., Pearlson, G. D., and Calhoun, V. D. (2009). An ICA-based method for the identification of optimal fMRI features and components using combined group-discriminative techniques. *Neuroimage* 46, 73–86.

Sullivan, E. V., and Pfefferbaum, A. (2006). Diffusion tensor imaging and aging. *Neurosci. Biobehav. Rev.* 30, 749–761.

Sun, F., Miller, L., and D'Esposito, M. (2004). Measuring interregional functional connectivity using coherence and partial coherence analyses of fMRI data. *Neuroimage* 21, 647–658.

Szaflarski, J., Holland, S., Schmithorst, V., and Byars, A. (2006). fMRI study of language lateralization in children and adults. *Hum. Brain Mapp.* 27, 202–212.

Tamnes, C. K., Ostby, Y., Fjell, A. M., Westlye, L. T., Due-Tønnessen, P., and Walhovd, K. B. (2010). Brain maturation in adolescence and young adulthood: regional age-related changes in cortical thickness and white matter volume and microstructure. *Cereb. Cortex* 20, 534–548.

Van Dijk, K. R. A., Hedden, T., Venkataraman, A., Evans, K. C., Lazar, S. W., and Buckner, R. L. (2010). Intrinsic functional connectivity as a tool for human connectomics: theory, properties, and optimization. *J. Neurophysiol.* 103, 297–321.

Vincent, J., Kahn, I., Snyder, A., Raichle, M., and Buckner, R. (2008). Evidence for a frontoparietal control system revealed by intrinsic functional connectivity. *J. Neurophysiol.* 100, 3328–3342.

Wallentin, M. (2009). Putative sex differences in verbal abilities and language cortex: a critical review. *Brain Lang.* 108, 175–183.

Weiss, E. M., Kemmler, G., Deisenhammer, E. A., Fleischhacker, W. W., and Delazer, M. (2003). Sex differences in cognitive functions. *Pers. Individ. Dif.* 35, 863–875.

Whitfield-Gabrieli, S., Thermenos, H., Milanovic, S., Tsuang, M., Faraone, S., McCarley, R., Shenton, M., Green, A., Nieto-Castanon, A., LaViolette, P., Wojcik, J., Gabrieli, J. D. E., and Seidman, L. J. (2009). Hyperactivity and hyperconnectivity of the default network in schizophrenia and in first-degree relatives of persons with schizophrenia. *Proc. Natl. Acad. Sci. U.S.A.* 106, 1279–1284.

Whitford, T., Rennie, C., Grieve, S., Clark, C., Gordon, E., and Williams, L. (2007). Brain maturation in adolescence: concurrent changes in neuroanatomy and neurophysiology. *Hum. Brain Mapp.* 28, 228–237.

Xiong, J., Ma, L., Wang, B., Narayana, S., Duff, E., Egan, G., and Fox, P. (2009). Long-term motor training induced changes in regional cerebral blood flow in both task and resting states. *Neuroimage* 45, 75–82.

Ystad, M., Eichele, T., Lundervold, A. J., and Lundervold, A. (2010). Subcortical functional connectivity and verbal episodic memory in healthy elderly-a resting state fMRI study. *Neuroimage* 52, 379–388.

Zuo, X. N., Di Martino, A., Kelly, C., Shehzad, Z. E., Gee, D. G., Klein, D. F., Castellanos, F. X., Biswal, B. B., and Milham, M. P. (2010). The oscillating brain: complex and reliable. *Neuroimage* 49, 1432–1445.

Conflicts of Interest Statement: The authors declare that the research was conducted in the absence of any commercial or financial relationships that could be construed as a potential conflict of interest.

Received: 16 June 2010; accepted: 03 January 2011; published online: 04 February 2011.

*Citation: Allen EA, Erhardt EB, Damaraju E, Gruner W, Segall JM, Silva RF, Havlicek M, Rachakonda S, Fries J, Kalyanam R, Michael AM, Caprihan A, Turner JA, Eichele T, Adelsheim S, Bryan AD, Bustillo J, Clark VP, Feldstein Ewing SW, Filbey F, Ford CC, Hutchison K, Jung RE, Kiehl KA, Kodituwakku P, Komesu YM, Mayer AR, Pearlson GD, Phillips JP, Sadek JR, Stevens M, Teuscher U, Thoma RJ and Calhoun VD (2011) A baseline for the multivariate comparison of resting-state networks. Front. Syst. Neurosci. **5**:2. doi: 10.3389/fnsys.2011.00002*

Copyright © 2011 Allen, Erhardt, Damaraju, Gruner, Segall, Silva, Havlicek, Rachakonda, Fries, Kalyanam, Michael, Caprihan, Turner, Eichele, Adelsheim, Bryan, Bustillo, Clark, Feldstein Ewing, Filbey, Ford, Hutchison, Jung, Kiehl, Kodituwakku, Komesu, Mayer, Pearlson, Phillips, Sadek, Stevens, Teuscher, Thoma and Calhoun. This is an open-access article subject to an exclusive license agreement between the authors and Frontiers Media SA, which permits unrestricted use, distribution, and reproduction in any medium, provided the original authors and source are credited.

APPENDIX

A. GROUP INDEPENDENT COMPONENT ANALYSIS

Let $\mathbf{Y}_i$ be the $T \times V$ preprocessed and intensity-normalized functional imaging data matrix for subject i, where T time points over V voxels are collected on M subjects. For GICA, the data first undergo reduction and whitening at the subject and group levels using principal component analysis (PCA). Let $\mathbf{Y}_i^* = \mathbf{F}_i^- \mathbf{Y}_i$ be the $T_1 \times V$ PCA-reduced data for subject i, where $\mathbf{F}_i^- = \mathbf{F}_i^{\mathrm{T}}$ is the $T_1 \times T$ standardized reducing matrix and T_1 is the number of principal components retained for each subject. Note that $\mathbf{Y}_i$ has rows of zero mean (we remove the mean across space for each time point) to improve conditioning of the covariance matrix, however this step has no affect on the PCA reduction or GICA decomposition. Let $\mathbf{Y}^* = [\mathbf{Y}_1^{*\mathrm{T}}, \ldots, \mathbf{Y}_M^{*\mathrm{T}}]^{\mathrm{T}}$ be the $MT_1 \times V$ time-concatenated aggregate data (Calhoun et al., 2001, 2002b). Group-level PCA is required to reduce the dimension of the data to the number of components to be estimated with ICA. Let the $T_2 \times V$ PCA-reduced aggregate data be $\mathbf{X} \equiv \mathbf{G}^- \mathbf{Y}^* = [\mathbf{G}_1^{\mathrm{T}}, \ldots, \mathbf{G}_M^{\mathrm{T}}][(\mathbf{F}_1^- \mathbf{Y}_1)^{\mathrm{T}}, \ldots, (\mathbf{F}_M^- \mathbf{Y}_M)^{\mathrm{T}}]^{\mathrm{T}} = \sum_{i=1}^{M} \mathbf{G}_i^{\mathrm{T}} \mathbf{F}_i^{\mathrm{T}} \mathbf{Y}_i = \sum_{i=1}^{M} \mathbf{X}_i$, where $\mathbf{G}^-$ is the $T_2 \times MT_1$ standardized reducing matrix. Following square noise-free spatial ICA estimation (Hyvärinen et al., 2001), we can write $\mathbf{X} = \hat{\mathbf{A}}\hat{\mathbf{S}}$ where the generative linear latent variables $\hat{\mathbf{A}}$ and $\hat{\mathbf{S}}$ are the $T_2 \times T_2$ mixing matrix related to subject TCs and the $T_2 \times V$ aggregate SM, respectively.

To estimate subject-specific SMs and TCs, we use the recently developed GICA3 back-reconstruction method based on PCA compression and projection (Calhoun et al., 2001, 2002b; Erhardt et al., 2010). In GICA3, the subject-specific SM is defined as $\tilde{\mathbf{S}}_i \equiv \hat{\mathbf{A}}^- \mathbf{G}_i^{\mathrm{T}} \mathbf{F}_i^{\mathrm{T}} \mathbf{Y}_i$ which yields exactly that the aggregate SM is the sum of the subject-specific SMs, $\hat{\mathbf{S}} \equiv \sum_{i=1}^{M} \tilde{\mathbf{S}}_i$. This is analogous to a random effects model where the subject-specific effects are zero-mean distributed deviations from the group mean effect. The natural estimator of subject-specific TCs is $\tilde{\mathbf{R}}_i \equiv \mathbf{F}_i (\mathbf{G}_i^{\mathrm{T}})^- \hat{\mathbf{A}}$. The product of each subject-specific TC and SM is a perpendicular projection of the data onto the PCA column space, $\tilde{\mathbf{Y}}_i \equiv \tilde{\mathbf{R}}_i \tilde{\mathbf{S}}_i = P_{C(\mathbf{F}_i \mathbf{G}_i)} \mathbf{Y}_i$. The PCA compressed fitted values are exactly the PCA compressed data $\mathbf{X}$, that is, the fitted values and data agree in the PCA space. The fitted compressed values, $\tilde{\mathbf{X}}_i \equiv \hat{\mathbf{A}}\tilde{\mathbf{S}}_i = \mathbf{X}_i$, are a product of the subject-specific TC and SM, and similarly for the mean fitted compressed value, $\tilde{\mathbf{X}} \equiv \sum_{i=1}^{M} \tilde{\mathbf{X}}_i = \mathbf{X}$. Thus, it is the amount of information retained in the PCA steps that largely determines the subject-specific TC and SM estimates. Compared with dual regression (Filippini et al., 2009), GICA3 provides more robust and accurate estimates of subject-specific components (Erhardt et al., 2010).

B. FEATURE SELECTION WITH MIXTURE MODEL

We developed a model to identify the subset of voxels most representative of each component. We considered the distribution of voxelwise t-statistics in a SM as a mixture of three distributions. In particular, we assumed t-statistics for the voxels not associated with the component to be normally distributed and activation to be gamma-distributed at positive or negative values. While extreme values will not be estimated well by this mixture model, the relatively sparse points at the tails will not strongly affect model fit and are always included in the thresholded component. Thus, for each component, the distribution of the $V \times 1$ vector of observed t-statistics, $\mathbf{t}_c$, is fit by a normal-gamma-gamma (NGG) mixture model,

$$p_{c1}\mathcal{N}(\mathbf{t}_c \mid \mu_c, \sigma_c) + p_{c2}\mathcal{G}(\mathbf{t}_c - \mu_c \mid \alpha_{c1}, \beta_{c1}) + (1 - p_{c1} - p_{c2})\mathcal{G}(-\mathbf{t}_c - \mu_c \mid \alpha_{c2}, \beta_{c2}),$$

where $N(\cdot)$ and $\mathcal{G}(\cdot)$ indicate normal and gamma distributions. The six distribution parameters $(\mu_c, \sigma_c, \alpha_{c1}, \beta_{c1}, \alpha_{c2}, \beta_{c2})$ and the two proportions (p_{c1} and p_{c2}) were estimated by minimizing the residual sum of squares using the LSQNONLIN function in Matlab with the trust-region-reflective Newton algorithm. Conditional on the fit of the Gaussian parameters, component-related voxels were determined as those more extreme than the threshold $\mu_c \pm 4\sigma_c$. Because the distributions of t-statistics for RSNs are typically skewed with more extreme positive values, we further limit our statistical analyses to voxels exceeding the threshold on the right tail: $t > \mu + 4\sigma$. This strategy provided results consistent with what had previously been selected by eye and provides an excellent fit to the center of the voxel distribution (**Figure A1**).

C. GRAY MATTER CONCENTRATION AND AGE

Age is a highly significant predictor of RSN connectivity (see e.g., Figure 5), however given the profound structural changes that accompany age (Good et al., 2001; Sowell et al., 2003; Tamnes et al., 2010; Ostby et al., 2009), we ask whether gray matter concentration (GMC) might be a better predictor. Because age and GMC were highly correlated (**Figure A2A**), the inclusion of both terms in a full model for variable selection would lead to reduced models that sometimes include one or the other as a strong effect, or both predictors together weakly. It is difficult to interpret and make inferences from such reduced models, thus we instead assess the *additional* contributions of each variable over the other to determine which predictor has more explanatory power for the power spectra and SMs.

To determine their explanatory power, we first orthogonalize age and GMC by fitting two linear regressions, GMC onto age to obtain residualized GMC (GMC_r, GMC information not explained by log(age)) and residualized age (age_r, log(age) information not

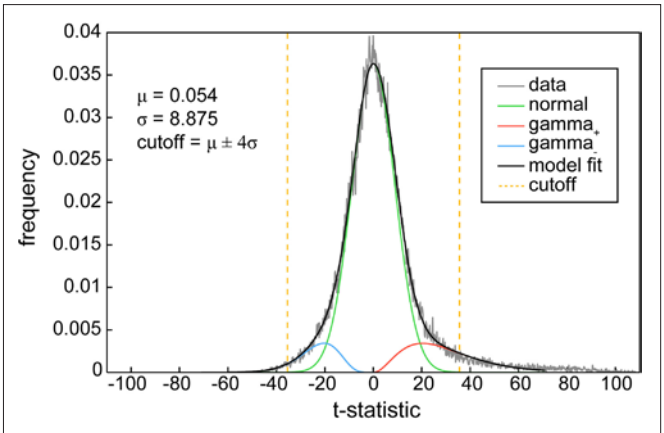


FIGURE A1 | A typical example of the normal-gamma-gamma (NGGs) model, fit to the distribution of *t*-statistics for IC 38. The distribution (gray) is relatively well described by a mixture of a normal (green), positive gamma (red), and negative gamma (blue). The full model fit is shown in black, and cutoffs ($\mu \pm 4\sigma$) are determined from the estimated mean (μ) and SD (σ) of the normal. Thresholded SMs include only voxels with positive t-statistics: $t > \mu + 4\sigma$.

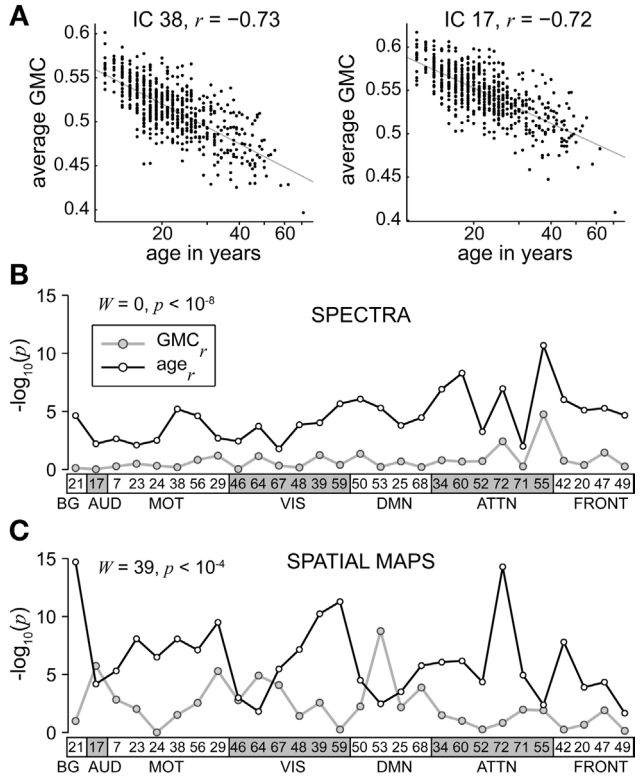


FIGURE A2 | Evaluation of age and gray matter concentration as predictors. (A) Typical examples of the relationship between log(age) and GMC (averaged over voxels in the thresholded SM). **(B,C)** Significance of the residualized GMC (GMC_r, gray) and residualized log(age; age_r, black) terms in models predicting spectral power **(B)** and SM intensity **(C)** for each RSN. Wilcoxon signed-rank statistics (*W*), based on the difference between $-\log_{10}(p)$ values, are displayed on each plot.

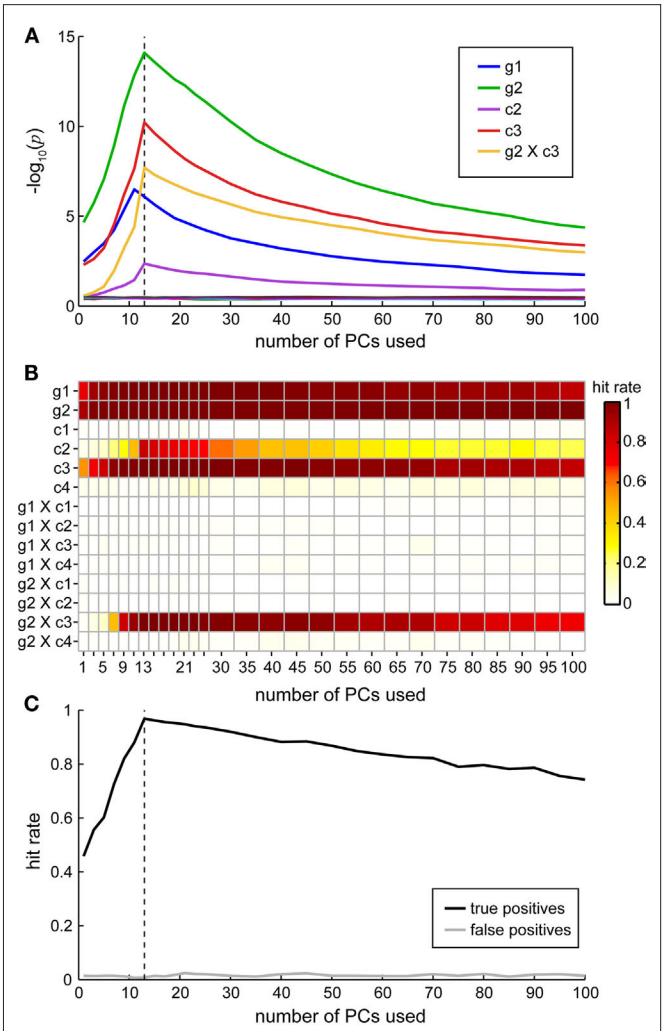


FIGURE A3 | Simulations showing benefits of dimension reduction using the MDL estimate. (A) Average *p*-values from the MANCOVA *F*-test for each model term over different number of components used, ranging from 1 to 100. Dashed black line shows the true number of dimensions estimated correctly as 13 by MDL for all 100 simulations. **(B)** Hit rate (fraction of times each model term appeared in the reduced model, following backward selection) as a function of components used. **(C)** True positives (average hit rate for true effects) and false positives (average hit rate for false effects) as a function of components used. Though difficult to see given the scale, the false positive rate was lowest at 11 and 13 components (0.0067 and 0.0078, respectively), and never rose above 0.024 (21 components).

explained by GMC). We then consider two models: model M_1 which includes age as a predictor and M_2 which includes GMC in place of age. Similar to our main approach, backward selection is performed on each model to select a reduced model. We next add GMC_r to the reduced model M_1 and add age_r to reduced model M_2 and test for significance of the added variables in each model,

$$M_1 : \mathbf{P}_c^* = \beta_0 + \beta_1 \text{age} + \beta_2 \text{GMC}_r + \cdots \quad \text{and}$$
$$M_2 : \mathbf{P}_c^* = \beta_0 + \beta_1 \text{GMC} + \beta_2 \text{age}_r + \cdots.$$

The *F*-statistics and associated *p*-values indicate the variability in the response explained by the residualized predictor, for example in M_1, by GMC not explained by age.

This process is performed for the spectra and SMs of each RSN. **Figures A2B,C** show the $-\log_{10}(p)$ values for the addition of GMC_r in model M_1 and age_r in model M_2 over all components. With the exception of a few component SMs, age_r almost always contributes over GMC alone while GMC_r rarely contributes over age alone. These model comparisons demonstrate that while age can often account for GMC-related changes component spectra and SMs, GMC is not sufficient to account for age-related effects. This result also justifies the inclusion of age and omission of GMC in the primary design matrix used for model selection.

D. BACKWARD SELECTION AND COLLINEARITY SIMULATION

To investigate the effects of backward selection and highly collinear data on model estimation, we created a simulation approximately matching the size and properties of our data. We begin with 600 subjects and 3000 response "bins," but only 13 true Gaussian sources uniformly spaced and with moderate overlap over the bins. Our design matrix includes two grouping predictors (g_1, g_2) each with two levels, four continuous predictors (c_1, c_2, c_3, c_4) normally distributed, and all group-covariate interactions as predictors, yielding 15 model terms including the constant. Gaussian

sources are related to the covariates in the following way: source 1 is $q_{1i} = 0.6c_{3i}g_{2i} + e_{1i}$, source 6 is $q_{6i} = 0.7g_{1i} + e_{2i}$, source 7 is $q_{7i} = 0.25c_{3i} + 0.8g_{2i} + e_{7i}$, source 13 is $q_{13i} = 0.21c_{2i} + e_{13i}$, and the remaining sources are Gaussian noise. Thus, subject response vectors are associated with covariates g_1, g_2, c_2, c_3, and a g_2-by-c_3 interaction. The 13 sources are linearly mixed by addition, Gaussian noise is added, and subject data are concatenated for **Q**. A PCA is performed resulting in $\mathbf{Q}^*$, and the number of PCs retained is varied from 1 to 100. MANCOVA backward selection is performed to determine a reduced model and the *p*-value for each term in that reduced model is retained. Simulations were repeated 100 times, randomizing the predictors and noise. MDL correctly estimates the dimension as 13 for all 100 simulations.

Results from the simulations are displayed in **Figure A3**. **Figure A3A** illustrates that predictors are most significant (as determined from the average *p*-value) when the correct number of dimensions are used, but significance is not greatly sensitive to this variable, even with collinear data. With respect to the observed level of significance, the simulation is similar to what we observe for component spectra. **Figure A3B** shows that over the 100 simulations, the correct reduced model was often selected for a range of dimensions from 13 to 25 PCs, and the four strongest predictor effects were well estimated over a wide range of dimensions. **Figure A3C** emphasizes the same point by showing that the reduced model correctly included the important predictors most often when the correct dimension was estimated, with a slow decline in true positive model reduction with an overestimate of dimension. Incorrectly including non-important predictors, false positives, was rare for the full range of PCs retained.

E. EFFECTS OF AGE ON NON-RSN COMPONENTS

To examine the effects of age on non-neural signals, we identified components with peak activations overlapping large arterial vessels (**Figure A4A**, left panel) and the ventricular system (**Figure A4A**, middle panel), where physiological noise sources should be most prominent (e.g., see Figure 5 of Beall and Lowe, 2010). The selected components approximately capture the basilar artery (IC 3), vertebral arteries (IC 6), fourth ventricle and neighboring cisterns (IC 16), and lateral ventricles (IC 44). Effects of age on the component spectra and SMs were then determined using the MANCOVA model with backward selection, identical to the approach used for RSNs (see Section 2.6.4).

In addition, we examined the spectra of time series from white matter (WM) and cerebrospinal fluid (CSF) regions, as defined by anatomical segmentations of the T1-weighted images. To compute the regional time series, we began with the spatially normalized, unsmoothed group averages of WM and CSF segmentations from the VBM analysis (see Section 2.3), resliced to the 3-mm isotropic EPI grid. We conservatively thresholded the WM and CSF images at probabilities of 0.99 and 0.87, respectively, and spatially restricted the CSF mask to the lateral ventricles to maximize temporal coherence across voxels. **Figure A4A** (right panel) displays the WM and CSF masks comprising 3350 and 329 voxels, respectively. We averaged the time series of masked voxels from each subject/s EPI data to obtain a representative WM and CSF time course. Power spectra were then estimated from the time courses and multivariate model selection was performed using the procedures detailed in Sections 2.6.3 and 2.6.4.

Multivariate results for the power spectra and SMs are displayed in **Figures A4B,C**. The $-\log_{10}(p)$ values in each plot indicate the significance of age in predicting the power spectra (**Figure A4B**) and SMs (**Figure A4C**) of RSNs (gray circles; same data as shown in **Figure 5**) and non-RSNs (orange squares). As discussed in the main text, age accounts for a significant portion of response variance in all RSN spectra and SMs. Age is also a significant covariate for non-RSN spectra and SMs, though, notably, age is not retained in the models predicting the spectra of IC 16 or the SM of IC 3. Furthermore, the significance of the age terms for non-RSN spectra are largely equivalent to or less than the significance level observed for RSN power spectra. Because contributions of vascular, cardiac and respiratory signals should be maximal in non-RSN power spectra, we can infer that the larger age-related effects in RSN spectra result from additional (putatively neural) sources. For SMs, three of the four examined components show little or no effect of age; no voxel clusters from ICs 6 or 16 passed FDR correction. In contrast, age is a highly significant predictor for IC 44 (lateral ventricles). This result is expected given the known increase in ventricular volume over the lifespan (Barron et al., 1976), as demonstrated in **Figure A4D**. With age, the component distribution appears to expand more posteriorly, increasing SM intensity in the trigone of the lateral ventricles and decreasing intensity in the frontal horns. These results suggest that age-related effects in SMs reflect changes in the spatial distributions of activity, whether due to putative alterations in neural connectivity or large-scale morphological changes.

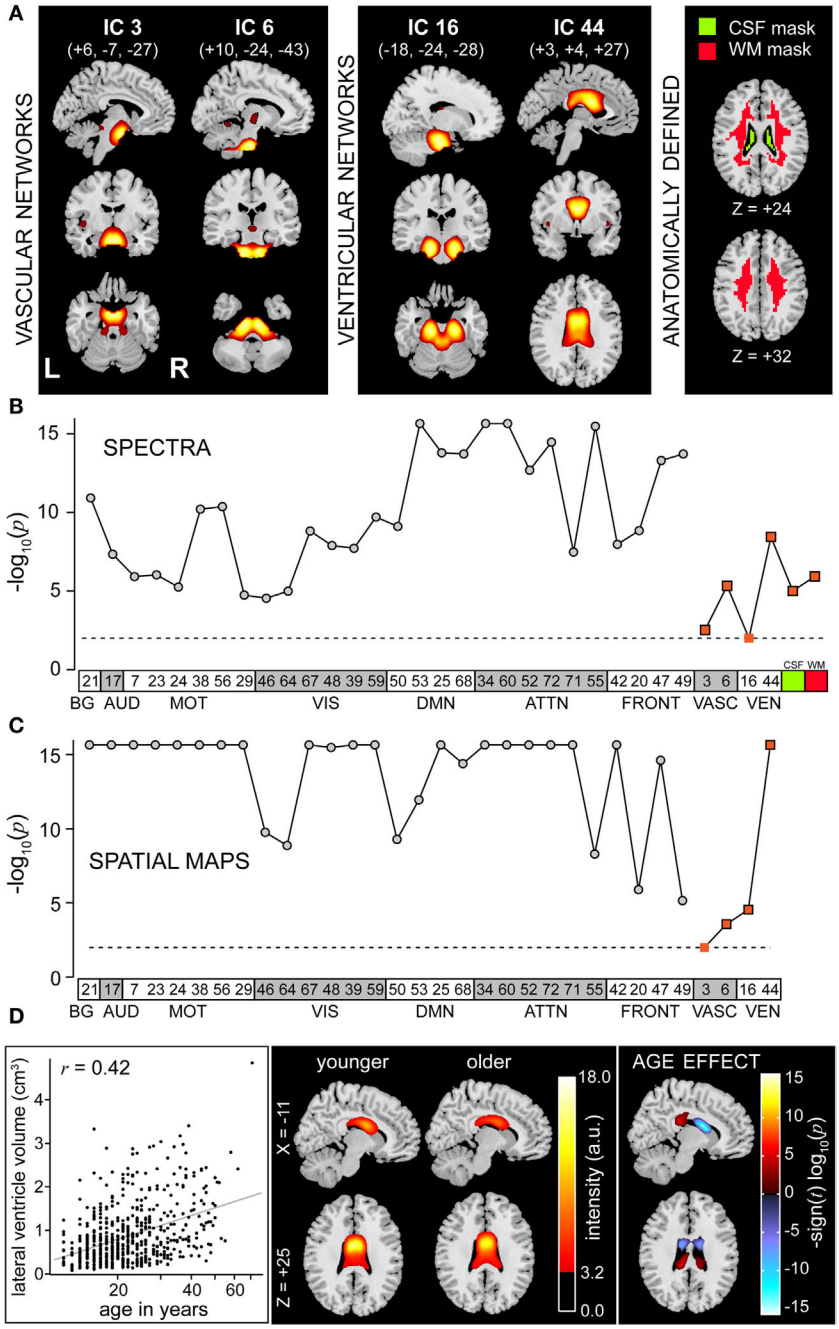


FIGURE A4 | Comparison of age effects in RSN and non-RSN components. (A) SMs of components representing vascular (VASC, left panel) and ventricular (VENT, middle panel) networks. SMs are plotted as *t*-statistics following the format of **Figure 4**. Right panel shows the CSF (green) and WM (red) masks used to determine the ROI time series; see text for details. **(B,C)** *F*-test results of log(age) from the reduced MANCOVA models. $-\log_{10}(p)$ values indicate the significance of age in predicting power spectra **(B)** and SMs **(C)** of RSNs (gray circles) and non-RSNs (orange squares). Note that for power spectra, non-RSNs comprise manually identified components (ICs 3, 6, 16, 44) as well as anatomically defined CSF (green) and WM (red) regions. When the log(age) was removed from the model during backward selection, the symbol is displayed at the significance threshold ($\alpha = 0.01$, dashed line; IC 16 spectra; IC 3 SM). Note that the saturation of $-\log_{10}(p)$ values is due to limited computational precision; for our analysis, epsilon is 2^{-52} thus $-\log_{10}(p)$ is maximally 15.65. **(D)** Origin of significant age effect for the SM of IC 44 (lateral ventricles). Left panel: scatter plot of age versus lateral ventricular volume, as determined from the CSF segmented images with a probability threshold of 0.95. Middle panel: SMs of IC 44, averaged over the youngest quartile (<17 years, $n = 134$) and oldest quartile (>28 years, $n = 137$) of subjects. Right panel: statistical map of univariate results for IC 44 following the format of **Figure 7**. With age, the component distribution expands more posteriorly, increasing SM intensity in the trigone of the lateral ventricles and decreasing intensity in the frontal horns.

frontiers in
SYSTEMS NEUROSCIENCE

ORIGINAL RESEARCH ARTICLE
published: 23 June 2010
doi: 10.3389/fnsys.2010.00025

Neural substrates of reliability-weighted visual-tactile multisensory integration

Michael S. Beauchamp[1]*, Siavash Pasalar[1] and Tony Ro[2]

[1] *Department of Neurobiology and Anatomy, University of Texas Health Science Center at Houston, Houston, TX, USA*
[2] *Department of Psychology and Program in Cognitive Neuroscience, The City College of the City University of New York, New York, NY, USA*

Edited by:
Barry Horwitz, National Institutes of Health, USA

Reviewed by:
Gregory C. DeAngelis, University of Rochester, USA
Randy McIntosh, Rotman Research Institute, Canada

****Correspondence:***
Michael S. Beauchamp, Department of Neurobiology and Anatomy, University of Texas Health Science Center at Houston, 6431 Fannin St Suite G.550G, Houston, TX 77030, USA.
e-mail: michael.s.beauchamp@uth.tmc.edu

As sensory systems deteriorate in aging or disease, the brain must relearn the appropriate weights to assign each modality during multisensory integration. Using blood-oxygen level dependent functional magnetic resonance imaging of human subjects, we tested a model for the neural mechanisms of sensory weighting, termed "weighted connections." This model holds that the connection weights between early and late areas vary depending on the reliability of the modality, independent of the level of early sensory cortex activity. When subjects detected viewed and felt touches to the hand, a network of brain areas was active, including visual areas in lateral occipital cortex, somatosensory areas in inferior parietal lobe, and multisensory areas in the intraparietal sulcus (IPS). In agreement with the weighted connection model, the connection weight measured with structural equation modeling between somatosensory cortex and IPS increased for somatosensory-reliable stimuli, and the connection weight between visual cortex and IPS increased for visual-reliable stimuli. This double dissociation of connection strengths was similar to the pattern of behavioral responses during incongruent multisensory stimulation, suggesting that weighted connections may be a neural mechanism for behavioral reliability weighting.

Keywords: effective connectivity, intraparietal cortex, BOLD fMRI, structural equation modeling, weighted connections, area MT

INTRODUCTION

Integrating information from different sensory modalities is critical for obtaining an accurate representation of the environment. On a windy day, it may be more accurate to rely on the visual modality to determine if an insect has landed on one's arm because the somatosensory stimulation of the skin by the breeze renders the somatosensory modality unreliable, while on a calm day the somatosensory modality may be more reliable. Behavioral experiments show that neurologically normal subjects take reliability into account when making behavioral decisions, weighting each modality by its reliability (Ernst and Banks, 2002; Alais and Burr, 2004). A better understanding of the neural mechanisms for reliability-weighted multisensory integration may help in the development of treatment and rehabilitation strategies for the many disorders in which the information from a sensory modality is degraded, such as vision loss due to macular degeneration.

Computational modeling studies have suggested that reliability weighting could occur by a simple linear summation of neuronal responses (Ma et al., 2006; Ma and Pouget, 2008). This model, which we term the "linear summation" model, predicts that increasing stimulus reliability scales the responses of neurons in sensory cortex ("early" areas) that respond to that stimulus. An explicit prediction of this model is that connection weights between early and late areas should not change (Ma et al., 2006). In an alternative model, which we term the "weighted connections" model, the connection weights between early and late areas change depending on the reliability of the stimulus (and are independent of the level of activity in early areas). This model receives some support from a recent electrophysiological study of visual-vestibular multisensory integration in macaque monkeys. Morgan et al. (2008) found that the effective weight of visual inputs into area MST decreased when the visual stimulus was made less reliable. However, Morgan et al., derived these weights from response measurements within a single area without directly measuring connection strengths between areas.

In order to better understand the neural substrates of reliability-weighted multisensory integration, we measured activity in both early and late areas using blood-oxygen level dependent functional magnetic resonance imaging (BOLD fMRI). Subjects detected viewed and felt touches delivered to the right index finger. The reliability of each sensory modality was adjusted by varying the signal-to-noise ratio (SNR) of the stimulus.

We used the average BOLD signal change to assess the neural activity associated with visual and somatosensory processing within early sensory areas. To measure connection strengths between early sensory areas and later multisensory ones, we used structural equation modeling, a validated technique for examining the effective connectivity between different brain areas (McIntosh et al., 1994; Horwitz et al., 1995; Buchel and Friston, 2001; Stein et al., 2007). The weighted connections model predicts that connection weights should be modulated by reliability, independent of the level of activity in early sensory areas.

MATERIALS AND METHODS

Experiments were conducted in accordance with the Institutional Review Boards of the University of Texas Health Science Center at Houston and the City University of New York. Written informed consent was obtained from each subject prior to experimentation.

SENSORY STIMULI AND TASK

Subjects performed a two-alternative forced choice task, deciding whether a touch was delivered to the index finger of the right hand or not. Visual stimuli consisted of a 1.5 s video of an animated triangular probe approaching the tip of the index finger of a photograph of an actor's hand (**Figure 1**). On "visual touch" trials, the probe contacted the finger at $t = 1.0$ s and then withdrew. On "visual no-touch" trials, the probe stopped just short of the fingertip at $t = 1.0$ s and then withdrew.

The reliability of the visual stimulus was manipulated by adjusting the transparency of the dynamic noise. First, the digital video of the probe approaching the finger was generated using Apple FinalCut software. Next, single video frames containing white noise (i.e., dynamic random black and white bit maps) were generated using Matlab and overlaid on the video. Finally, Neurobehavioral Systems Presentation software was used to combine each frame of the probe video and a randomly-selected white noise frame using the alpha-channel compositing method (Porter and Duff, 1984). Every pixel in the image was assigned the same alpha-channel transparency value, which was then used to combine the two images, with lower values indicating more transparency of the white noise frame and high values indicating more opacity of the white noise frame. Transparency of the noise made it easy to discriminate the touch and no-touch stimuli (reliable); opacity of the noise made it difficult to discriminate the stimuli (unreliable).

Somatosensory stimuli were delivered using piezoelectric benders attached to the tip of the index finger of the subject's right hand. The somatosensory stimulus consisted of a small deflection of the piezoelectric benders that was perceived as a faint tap. The deflection was created by a 150 ms Gaussian-modulated sine wave delivered to the benders under computer control at $t = 1.0$ s, precisely synchronized with the visual touch during multisensory trials.

On multisensory trials, subjects perceived the visual probe touching the index finger shown on screen as "causing" the tap delivered by the bender to their index finger, an inference familiar to those who have played video games that provide tactile feedback.

To adjust the reliability of the somatosensory stimulus, a 100 Hz background oscillation of variable amplitude was introduced into the piezoelectric benders throughout the entire 1.5 s stimulus period, analogous to the dynamic noise in the visual stimulus. This background noise was perceived as a tactile hum, and was distinct from the "tap" percept produced by the Gaussian monopulse. A low amplitude of the background noise resulted in the tap being easily detectable above the background (reliable); high-amplitude noise made it difficult to detect the tap (unreliable). On "somatosensory touch" trials, taps were delivered; on "somatosensory no-touch" trials, no tap was delivered (only background noise).

BEHAVIORAL EXPERIMENT

In the first experiment, 21 subjects participated in a behavioral experiment of visual-somatosensory multisensory integration. Subjects always performed the same touch/no-touch judgment. Subjects viewed the video on a 21″ CRT display placed 42 cm from the face. The right hand was placed out-of-sight on a table in a palm up position, corresponding to the posture of the viewed right hand on the display. Subjects responded verbally as to whether or not they saw or felt a tap; each response was entered into the computer by an experimenter. In the first part of the experiment, subjects performed a staircase level-setting procedure to find the stimulus reliability level (adjusted by manipulating the SNR of the stimulus) that produced 70% correct performance on each of the modalities in isolation. Then, subjects viewed and felt unisensory visual touches, unisensory somatosensory touches, and congruent and incongruent multisensory touches. In congruent multisensory trials, a touch stimulus was presented in both modalities or a no-touch stimulus was presented in both modalities. In incongruent trials, a touch stimulus was presented in one modality (e.g., tactile tap) and a no-touch stimulus was presented in the other modality (e.g., a video showing the probe missing the finger). In the neuroimaging experiment, only congruent touches were presented.

During unisensory somatosensory touches, subjects viewed a fixation crosshairs that changed intensity to signal the beginning of each trial. Subjects were presented with the somatosensory stimulus. Then, the fixation crosshairs changed intensity again, signaling subjects to respond. During unisensory visual touches, subjects viewed the stimulus video until it was replaced by fixation crosshairs, signaling them to respond. During multisensory trials, the somatosensory and visual stimuli commenced at the same time, and trial offset was signaled by the return to fixation crosshairs. Congruent and incongruent multisensory trials were equally distributed and randomly intermixed, with 40 of each type.

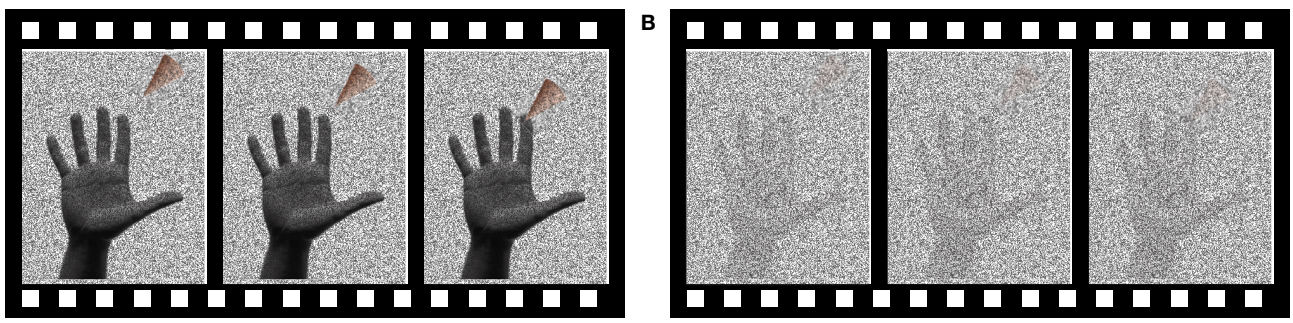


FIGURE 1 | The visual stimulus. The visual stimulus consisted of a video of an animated probe (triangular shape) approaching the image of a hand. Three frames of the video are shown. **(A)** Reliable visual stimulus. Dynamic random noise was overlaid on the visual stimulus. During reliable visual stimulation, the dynamic noise was transparent. **(B)** Unreliable visual stimulus. During unreliable visual stimulation, the dynamic noise was opaque.

Visual-somatosensory stimuli can produce changes in response criteria in addition to true changes in sensitivity (Johnson et al., 2006). Therefore, our primary behavioral measure was d', a measure of sensitivity independent of response biases.

NEUROIMAGING EXPERIMENT

In the second experiment, nine subjects participated in an fMRI experiment (data from one subject was discarded due to sleepiness). An MR-compatible eye-tracking system (Applied Science Laboratories, Bedford, MA, USA) was used to monitor fixation and behavioral state. The visual display was projected into the bore of the MR scanner using an LCD projector but was otherwise identical to the visual stimuli in the behavioral experiment. The right hand was placed out-of-sight at the side of the subject in the palm up position, corresponding to the posture of the viewed hand. Subjects responded with an fMRI compatible button box (Current Designs, Philadelphia, PA, USA) held in the left hand. Before scanning commenced, the same level-setting procedure as in the behavioral experiment was used to find the appropriate dynamic noise level for each modality.

ANATOMICAL MRI

Anatomical MRI scans were obtained from each subject using a 3 T whole-body MR scanner (Phillips Medical Systems, Bothell, WA, USA). Images were collected using a magnetization-prepared 180° radio-frequency pulses and rapid gradient-echo (MP-RAGE) sequence optimized for gray–white matter contrast with 1 mm thick sagittal slices and an in-plane resolution of 0.938 mm × 0.938 mm. AFNI software (Cox, 1996) was used to analyze MRI data. 3D cortical surface models were created with FreeSurfer (Fischl et al., 1999a) and visualized in SUMA (Argall et al., 2006). Surface averages were created using the FreeSurfer template (Fischl et al., 1999b) and volume averages were created using the N27 template brain (Mazziotta et al., 2001).

fMRI EXPERIMENTAL DESIGN AND DATA ANALYSIS

Functional images were collected using a gradient-recalled-echo echo-planar-imaging sequence sensitive to the BOLD signal. Thirty-three axial slices were collected with a repetition time (TR) of 2000 ms, an echo time of 30 ms and a flip angle of 90°. Slice thickness was 3 mm and in-plane resolution was 2.75 mm × 2.75 mm. Each scan series contained 150 scans. Following motion correction and slice timing correction, data were smoothed with a spatial Gaussian filter with root-mean-square deviation of 3 mm.

EXPERIMENTAL CONDITIONS AND REGION OF INTEREST CREATION

A block design was used in all scan series. Each block contained 10 trials with total duration of 20 s followed by 10 s of fixation baseline in which no stimulus was presented. Each trial within a block consisted of the presentation of a 1.5 s stimulus, followed by a 0.5 s response window for total trial duration of 2.0 s.

There were nine block types: unisensory visual (reliable and unreliable); unisensory somatosensory (reliable and unreliable); multisensory visual + somatosensory (both modalities reliable or both modalities unreliable); multisensory visual + somatosensory (visual-reliable/somatosensory-unreliable and visual-unreliable/somatosensory-reliable); and passive tactile stimulation (touches only, with no behavioral task). The multisensory stimuli were always congruent and touch and no-touch trials were randomly intermixed within each block.

We had strong *a priori* hypotheses about three brain regions: the secondary somatosensory cortex, lateral occipital cortex, and anterior intraparietal sulcus (IPS). In previous studies using piezoelectric benders, we have observed robust activity in inferior parietal lobe and the parietal operculum (Beauchamp et al., 2007, 2009), the location of secondary somatosensory cortex and associated areas (Disbrow et al., 2000; Francis et al., 2000; Ruben et al., 2001; Beauchamp et al., 2007, 2009; Eickhoff et al., 2007, 2008; Burton et al., 2008). fMRI studies using visual motion stimuli (such as the moving probe) and biological stimuli (such as the image of the hand) the strongest activity was observed in lateral occipital cortex (Tootell et al., 1995; Beauchamp et al., 1997, 2002, 2003; Downing et al., 2001; Wheaton et al., 2004; Pelphrey et al., 2005). Examinations of visual-somatosensory interactions have implicated the anterior IPS for visual-somatosensory integration, at the junction with the postcentral sulcus (Grefkes and Fink, 2005; Culham and Valyear, 2006; Stilla and Sathian, 2008; Pasalar et al., 2010). The somatosensory stimulus was delivered to the right hand, evoking somatosensory-related responses in the left, contralateral hemisphere, while the behavioral response was made with the left hand, resulting in motor-related responses in the right hemisphere. In order to maximize the contribution of the somatosensory stimulus and minimize the contribution of the motor response to the observed activity, ROIs were formed only in the left hemisphere. Independent data from each subject was used to create the ROIs and perform the comparisons of interest (BOLD amplitude between reliable and unreliable stimulation) to prevent bias (Simmons et al., 2007; Vul et al., 2009).

BOLD AMPLITUDE MEASURES

We used the 3dREMLfit program in the AFNI package (Cox, 1996) to account for serial correlations in the fMRI data by fitting an autoregressive moving average model with one autoregressive term and one moving average term separately to each voxel. The time series data were analyzed with the general linear model; the motion correction estimates were used as regressors of no interest. A separate regressor of interest was used for each block type. The beta-weight of the regressor for each block type was converted to percent signal change and used as a measure of response amplitude. The full F (omnibus) statistic from only reliable stimuli was thresholded at $p < 0.001$ corrected for false discovery rate (Genovese et al., 2002) to identify voxels that responded significantly.

STRUCTURAL EQUATION MODELING

In BOLD fMRI, measures of activity correlation can be used to derive the connection strength between areas (Buchel and Friston, 2001; Stein et al., 2007). For each subject and each ROI, a normalized time series was constructed by subtracting the amplitude of the mean response to each condition from the average time series, preventing the high-amplitude block onset and offset from artificially inflating the correlation between ROIs (Buchel and Friston, 1997). We used the 1ddot program in AFNI to calculate the correlation matrix between the ROI time series. Two separate matrices were constructed, one for the time series during each of two block types:

visual-reliable/somatosensory-unreliable and visual-unreliable/somatosensory-reliable. The correlation weights were calculated independently for each subject and then averaged.

RESULTS

BEHAVIORAL EXPERIMENT: MULTISENSORY INCREASES IN SENSITIVITY

For reliable unisensory stimuli, subjects were able to determine with near perfect accuracy whether or not a visual or somatosensory touch occurred. For unreliable unisensory stimuli, performance decreased to 68 ± 5% SEM for visual and 58 ± 5% for somatosensory. When unreliable stimuli were presented in both modalities simultaneously, performance improved to 79 ± 3% for visual-somatosensory (**Figure 2A**). As measured with d', a criterion-independent measure of performance, there was a significant benefit of multisensory stimulation, demonstrating that the visual-somatosensory stimulus successfully induced multisensory integration [d' = 1.98 ± 0.17 for visual-somatosensory vs. d' = 1.44 ± 0.19 for visual and d' = 1.34 ± 0.13 for somatosensory, $F(2,40) = 12.41$; $p = 6e\text{-}5$]. There were no differences in criterion between the conditions [mean $c = 0.31$, $F(2,40) = 1.78$; $p = 0.18$].

RELIABILITY WEIGHTING

In order to study the effectiveness of each modality in driving behavior, we presented incongruent multisensory stimuli in which a touch occurred in one modality but not the other. The reliability-weighting literature predicts that subjects should weight the more reliable modality more heavily in their judgment (Ernst and Banks, 2002; Alais and Burr, 2004). As predicted, subjects were much more likely to report that a touch occurred when a touch was presented in the more reliable modality (**Figure 2B**). This effect was significant for both visual and somatosensory modalities as measured with a paired *t*-test (visual-reliable: 70 ± 3% visual wins vs. 30 ± 3% somatosensory wins, $p < 1e-6$; Somatosensory reliable: 24 ± 4% visual wins vs. 76 ± 4% somatosensory wins, $p < 1e-6$).

LOCALIZERS: ACTIVE BRAIN AREAS

When subjects viewed and felt touches, the largest clusters of activity were observed in extrastriate visual areas in lateral occipital cortex, in inferior parietal lobe in the location of secondary somatosensory cortex and associated areas, and in anterior IPS near the junction with postcentral sulcus (see **Figure 3** and **Table 1** for a list of all active regions). We measured BOLD fMRI activity in three regions of interest (visual, somatosensory, and IPS) in order to test the two competing models of multisensory integration (see **Figure 3** for the average time series from each ROI for each stimulus condition). As shown in **Figure 4**, the response to unreliable stimuli was slightly *greater* than the response to reliable stimuli (0.92% vs. 0.76% for somatosensory, 2.7% vs. 2.3% for visual, $p = 0.06$ in a paired *t*-test). We examined the connectivity between visual cortex, somatosensory cortex and IPS during presentation of multisensory stimuli with varying stimulus reliability (**Figure 5**). The connection weight, measured as a

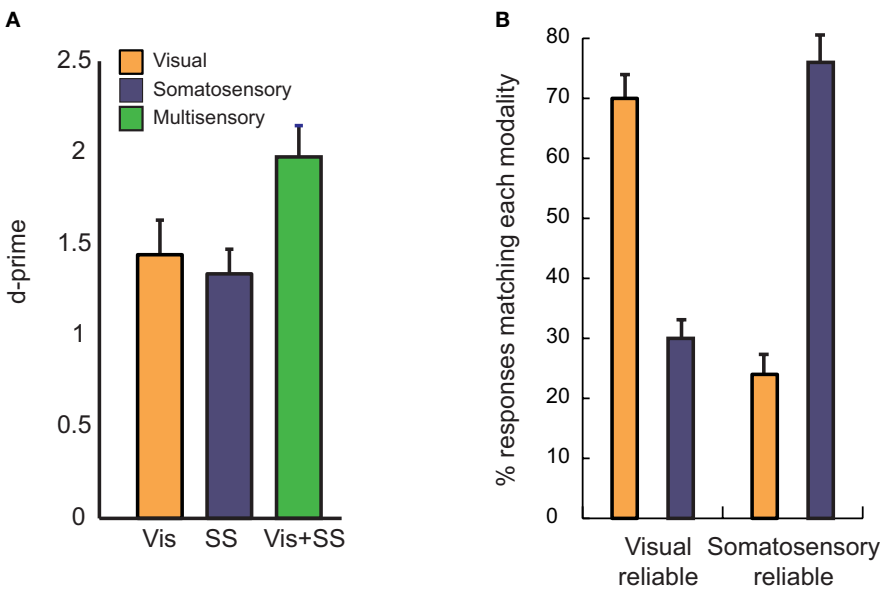


FIGURE 2 | Behavioral measures of visual-somatosensory multisensory integration. (A) In the visual condition (Vis, orange), subjects made a touch/no-touch judgment, discriminating between noisy movies of a probe touching or just missing the finger (see **Figure 1**). In the somatosensory condition (SS, blue) a touch/no-touch judgment was performed on a background vibration delivered to the finger with or without an additional touch. In the congruent multisensory condition (Vis + SS, green) the touch/no-touch judgment was performed on a touch that was both seen and felt, or neither seen nor felt. The error bars show the SEM ($n = 21$ subjects). **(B)** In the incongruent multisensory condition, subjects made a touch/no-touch judgment for stimuli which were reliable in one modality but not the other (e.g., probe clearly missed the finger in the video but a barely detectable touch was delivered in the somatosensory modality). The orange bars show the percentage of responses that corresponded to the visual stimulus; the blue bars show the percentage of responses that corresponded to the somatosensory stimulus, collapsed across touch and no-touch conditions. Subjects responses usually matched the stimulus presented in the more reliable modality, with responses corresponding to the visual modality in the visual-reliable condition (left bars) and the somatosensory modality in the somatosensory-reliable condition (right bars).

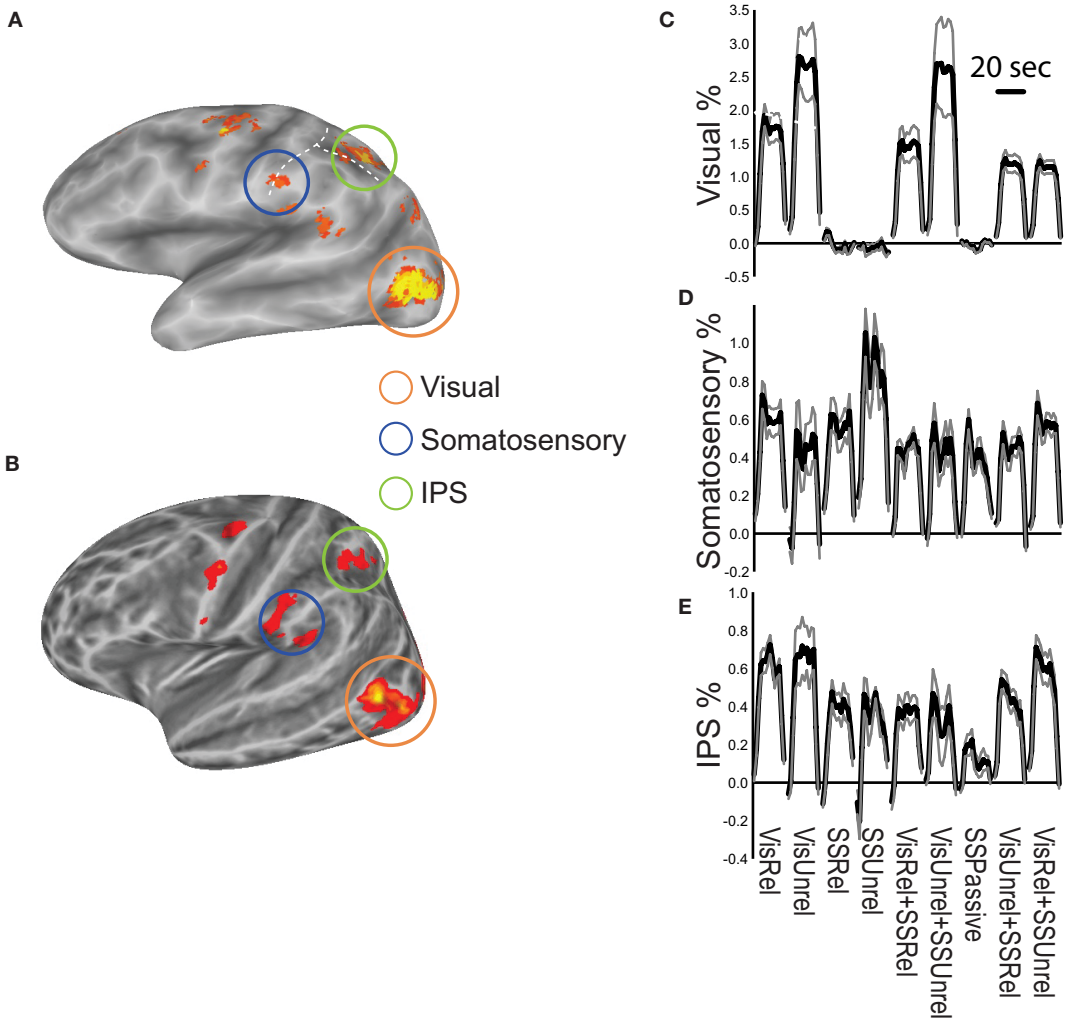


FIGURE 3 | Summary of fMRI activations. (A) Activation during performance of the multisensory touch detection task shown on an inflated average cortical surface model (left hemisphere, single subject). The orange circle highlights active visual areas in lateral occipital cortex. The blue circle highlights active areas in inferior parietal lobe, the location of secondary somatosensory cortex. The green circle highlights active areas in and around the intraparietal sulcus (IPS). The horizontal dashed white line shows the intraparietal sulcus, vertical dashed white line shows the postcentral sulcus. **(B)** Group activation map from $n = 8$ subjects. **(C)** Time course of the BOLD response in the visual cortex ROI during 20 s stimulation blocks of each experimental condition, averaged across blocks and subjects (black lines show the mean percent signal change, gray lines show + -SEM). **(D)** Time course of the somatosensory cortex response. **(E)** Time course of the IPS response.

correlation coefficient, between somatosensory cortex and IPS was lower during somatosensory-unreliable stimulation than during somatosensory-reliable stimulation (0.24 vs. 0.38, $p = 0.002$ in a paired t-test), even though somatosensory cortex was slightly more activated in the unreliable condition. Similarly, the connection weight between visual cortex and IPS was lower during visual-unreliable stimulation than during visual-reliable stimulation (0.23 vs. 0.32, $p = 0.001$), even though visual cortex was slightly more activated in the unreliable condition. As predicted by the weighted connections model, the connection weights were higher for the reliable stimulus modality despite there being less activity in the unisensory cortices for the reliable as compared to the unreliable conditions. The connection weight changes (higher for reliable stimuli) were in the opposite direction as the mean BOLD signal change (lower for reliable stimuli). The connection weight between visual cortex and somatosensory cortex was unaffected by reliability (0.11 vs. 0.15, $p = 0.3$).

DISCUSSION

We found that a somatosensory tap to the finger in combination with a video showing a finger touch produced behavioral visual-somatosensory multisensory integration. Behavioral studies have shown that vision can enhance touch perception, especially for touches to the hand (Kennett et al., 2001; Ro et al., 2004; Haggard et al., 2007 for a review see Maravita et al., 2003). While it might seem surprising that a video of an actor's hand being touched by an artificial probe could result in multisensory integration, it is consistent with previous results that a video feed of the subject's

Table 1 | Summary table showing all active brain areas during the localizer scan series using the contrast of multisensory touch vs. fixation baseline. Constructed from the group average volume activation map (n = 8 subjects). The active brain areas are ordered by the size of the active region, as shown in the first column, followed by the location of the peak activation within the active region, and the t-statistic of the peak activation. The center of the coordinate system is the anterior commissure, with left, posterior, and inferior the negative direction and right, anterior and superior the positive direction. The final column shows the anatomical description.

Volume (ml)	Standard coordinates of peak			Peak-statistic	Anatomical/functional description
	x	*y*	*z*		
LEFT HEMISPHERE					
15.33	–53	–27	30	9.5	Somatosensory cortex and intraparietal sulcus
3.34	–45	–61	6	5.3	Lateral occipital visual areas
2.41	–25	7	32	9.1	Inferior frontal gyrus
2.10	–51	1	26	7.0	Premotor cortex
1.09	–31	27	12	8.6	Anterior insular cortex
0.99	–9	–1	20	6.8	Caudate nucleus
RIGHT HEMISPHERE AND MIDLINE AREAS					
11.10	11	–87	8	7.8	Primary and secondary visual cortex
5.46	55	–1	32	9.3	Premotor cortex
5.38	31	–23	48	9.0	Motor cortex
5.06	47	–39	48	6.6	Parietal cortex
4.34	–3	–5	54	14.7	Supplementary motor cortex
2.66	21	–25	6	8.6	Thalamus
2.33	39	–65	0	6.7	Lateral occipital visual areas
0.94	49	–53	34	4.3	Supramarginal gyrus

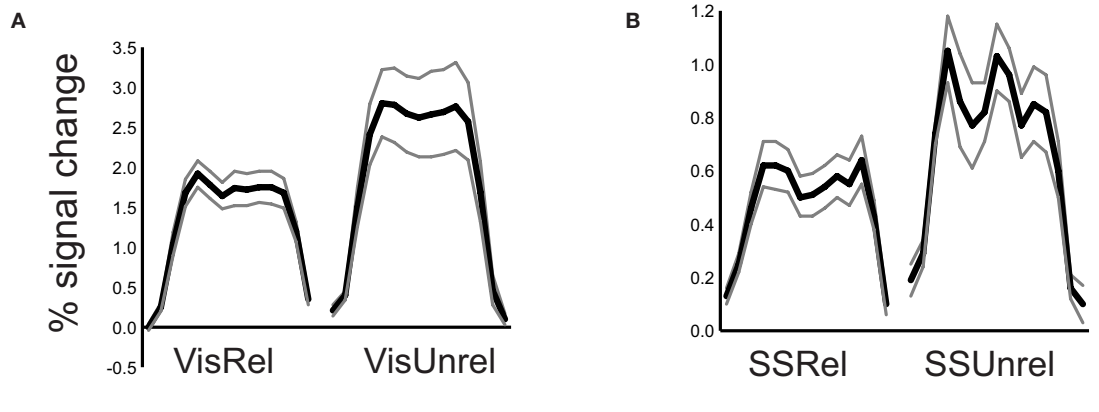


FIGURE 4 | Response to reliable and unreliable unisensory stimuli. (A) The average BOLD signal change in the visual cortex ROI during 20 s stimulation blocks of unisensory visual-reliable stimulation (left plot) and visual-unreliable unisensory stimulation (right plot). Black line shows mean response, gray lines shows ±SEM (n = 8 subjects). **(B)** The average BOLD signal change in the somatosensory cortex ROI during unisensory somatosensory-reliable stimulation blocks (left plot) and somatosensory-unreliable stimulation blocks (right plot).

own hand (Tipper et al., 1998), a flash of light near the subject's hand (Johnson et al., 2006), or an image or line drawing of a hand (Schaefer et al., 2005; Igarashi et al., 2008) can result in multisensory integration. Multisensory enhancements are even noted at the end of tools that serve to artificially extend the hand (Farne et al., 2007; Holmes et al., 2007). The behavioral multisensory integration that occurred during a touch to the finger was reliability weighted, with the more reliable modality receiving a stronger behavioral weighting. Reliability weighting during multisensory integration makes intuitive sense as an adaptation to cope with changes in sensation: as we age or in some diseases, the sensitivity of different modalities deteriorates at different rates and the brain must compensate. Ernst and Banks (2002) made the important discovery that behavioral reliability weighting of visual and somatosensory stimuli is statistically optimal. By artificially adjusting the amount of noise in the visual stimulus, they showed that we weight visual stimuli in inverse proportion to their variance. This finding has been extended to other visual-somatosensory tasks (Helbig and Ernst, 2007) and other modality combinations (Alais and Burr, 2004). The ubiquitous nature of reliability weighting suggests that it may be a fundamental building block of multisensory integration.

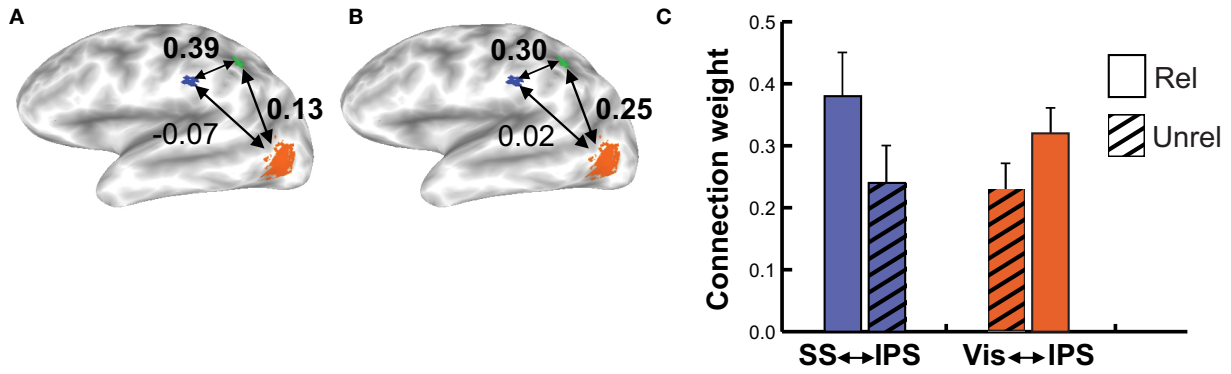


FIGURE 5 | Connection weights during reliable and unreliable stimulation. (A) Connectivity in the multisensory somatosensory-reliable/visual-unreliable condition in an individual subject, viewed on that subject's inflated cortical surface. Colored regions show areas with a significant fMRI response during the localizer scan used to create the regions of interest, with a different color for each region of interest (orange for visual, blue for somatosensory, green for IPS). The numbers adjacent to each arrow show the weights between that pair of ROIs, as derived from the structural equation model. **(B)** Connectivity in the multisensory somatosensory-unreliable/visual-reliable condition in the same subject. **(C)** Group data showing connection strengths across subjects during multisensory reliable and unreliable stimulation (n = 8 subjects). The blue bars show the connection strength from somatosensory cortex to the IPS, the orange bars show the connection strength from the visual ROI to the IPS ROI. The solid bar in each pair represents the reliable condition for that modality; the hatched bar in each pair is the unreliable condition.

To study the neural mechanisms of reliability weighting, we performed BOLD fMRI experiments of human subjects detecting a touch to the index finger of the hand. Consistent with previous studies of visual-somatosensory integration, brain activity was observed in a network of brain areas. These areas were subdivided into three regions of interest: visual, somatosensory, and multisensory. The visual ROI contained a group of visual areas in lateral occipito-temporal cortex, centered on posterior middle temporal gyrus and inferior temporal sulcus, which corresponds to areas that respond strongly to moving objects and pictures or videos of hands and hand-held manipulable objects (Downing et al., 2001; Beauchamp et al., 2002, 2003; Wheaton et al., 2004; Pelphrey et al., 2005). While these areas are located in classical visual cortex, they are also responsive to touch (Amedi et al., 2001, 2002; Hagen et al., 2002; James et al., 2002; Prather et al., 2004; Beauchamp et al., 2007; Summers et al., 2009). The somatosensory ROI contained a group of areas in the inferior parietal lobe that respond to hand stimulation that have been labeled S2+ (Disbrow et al., 2000; McGlone et al., 2002; Burton et al., 2004, 2008; Beauchamp et al., 2007; Eickhoff et al., 2007, 2008). For reasons that are not fully clear, in fMRI studies that stimulate the hand, especially with vibrotactile stimuli like those used in the present study, S2+ activation is much stronger than S1 activation (Ruben et al., 2001; Gizewski et al., 2005; Beauchamp et al., 2007, 2009). S2+ is also active during observation of touch (Keysers et al., 2004; Blakemore et al., 2005; Schaefer et al., 2006). The multisensory ROI contained association areas in and around the IPS thought to be critical for the integration of vision and touch (Grefkes and Fink, 2005). Although many studies have used fMRI to show that the IPS responds to visual and somatosensory stimulation (Bremmer et al., 2001; Saito et al., 2003; Makin et al., 2007; Peltier et al., 2007; Nakashita et al., 2008; Stilla and Sathian, 2008; Tal and Amedi, 2009) this does not demonstrate the necessity of the IPS for behavioral multisensory integration. We recently conducted a transcranial magnetic stimulation (TMS) study that disrupted activity in the IPS while subjects performed a touch/no-touch discrimination task using visual and somatosensory stimuli similar to those used in the present study (Pasalar et al., 2010). Without TMS, a significant behavioral improvement for multisensory compared with unisensory stimuli was observed. However, when activity in the IPS was disrupted with TMS, multisensory behavioral improvement was eliminated. Unisensory discrimination performance was not affected, illustrating that the effect was specific to multisensory integration. Furthermore, TMS of a control brain location did not interfere with multisensory integration, illustrating that the effect could not be attributed to non-specific effects of TMS, such as the auditory click produced by each TMS pulse.

We classified the visual and somatosensory ROIs as "early" and the IPS ROI as "late," based on their location in the cortical processing hierarchy (Felleman and Van Essen, 1991). Early areas responded more to less reliable sensory stimuli. While this is contrary to the predictions of the linear summation model (Ma et al., 2006; Ma and Pouget, 2008) it is likely to be a result of our method of creating unreliable stimuli, and therefore does not disconfirm the linear summation model. In our experiments, we determined the threshold for visual and tactile stimulation, and then decreased the reliability of the stimuli by adding noise. This added noise is likely to evoke neural activity in a broad population of neurons in the sensory cortex, causing the observed increases in the BOLD fMRI signal. However, the linear summation model hypothesizes only that the neurons carrying information about the sensory stimulus (in this case, the touch vs. no-touch distinction) show decreased activity with decreasing reliability. With BOLD fMRI, we cannot easily distinguish the neural activity of the relatively small population of neurons in a voxel that carry information about the sensory stimulus (and presumably show a decreased response with increasing noise)

from other neurons in the voxel that do not carry information about the sensory stimulus (and show an increased response to the dynamic noise present in the unreliable condition). In future experiments, it may be possible to create a better test of the linear summation model by using fMRI adaptation to measure activity in only those neurons that carry information about the sensory stimulus, or by manipulating reliability in other ways, such as decreasing the signal strength by making the visual and tactile stimuli weaker.

Unlike the linear summation model, the weighted connections model makes no predictions about the response amplitude of early sensory areas. Instead, it predicts that the connection strength between early and late areas should be proportional to reliability. To test this prediction, structural equation modeling was used to assess the connection strengths. During presentation of reliable visual stimuli, the connection strength between visual cortex and IPS was high; during presentation of unreliable visual stimuli, this connection strength decreased. Conversely, during presentation of reliable somatosensory stimuli, the connection strength between somatosensory cortex and IPS was high, and during presentation of unreliable somatosensory stimuli, this connection strength was low. These findings match the predictions of the weighted connections model.

The double dissociation of connection strengths between the IPS and somatosensory and visual cortex in the two conditions mirrored the pattern of behavioral responses observed during incongruent multisensory stimulation, in which the reliable modality was more effective at driving behavior. The correspondence between the neural connection strengths and behavior substantiates the notion that connection weight changes underlie behavioral reliability weighting.

Two recent studies in non-human primates examined visual-vestibular integration (Morgan et al., 2008; Fetsch et al., 2009). Responses in single MST neurons were a function of the weighted sum of visual and vestibular responses: the weight of the visual modality decreased as the visual stimulus was degraded, while the strength of the vestibular responses increased. This converging evidence from two different modality combinations (visual-vestibular and visual-somatosensory) and techniques (electrophysiology and BOLD fMRI) supports the weighted connections model. However, the electrophysiological data might also be consistent with a modified version of the linear-sum model (Morgan et al., 2008; Fetsch et al., 2010).

We considered the possibility that the weighted connections model could be more parsimoniously explained by visual attention. Attention to the visual modality increases the connection weights between early visual cortex and parietal regions (Buchel and Friston, 1997). In the attention scenario, if subjects attended more to the visual modality in the visual-reliable stimulus condition, the visual-to-IPS connection weights would increase (as predicted by the weighted connections model) but the weight change would be mediated by top-down visual attention and not by reliability. However, in addition to changing weights, visual attention also increases the response in early visual areas, including lateral occipital areas such as area MT (Beauchamp et al., 1997; Buchel et al., 1998; Kastner et al., 1998; Saenz et al., 2002). In the attention scenario, visual-reliable stimuli attract more attention and thus should evoke a *larger* response in visual areas. We saw the opposite pattern, with a trend towards reliable stimuli evoking *smaller* responses in visual areas (although this may have been a consequence of the visual noise that we added to make the stimuli less reliable). Conversely, if we suppose that subjects attended more to the unreliable visual stimuli because it was harder to see, the connection weight between visual cortex and IPS should increase for the unreliable visual condition (Buchel and Friston, 1997), which is the opposite of the observed weight change. Therefore, our BOLD fMRI data is incompatible with a simple effect of top-down visual attention, and consistent with behavioral studies showing that reliability weighting is independent of attention (Helbig and Ernst, 2008).

An caveat to the reliability-weighting model is that effective and functional connectivity methods applied to BOLD fMRI data do not necessarily correspond to direct axonal projections from one area to another (Buchel and Friston, 2001). Information may instead flow through a third area that is not modeled, such as thalamic nuclei in the "porpoise model" of Sherman (2007). However, there is anatomical evidence for direct connections between IPS, somatosensory cortex and visual cortex. Tracer-injection studies in macaque monkeys have shown that area VIP in anterior IPS receives strong inputs from extrastriate visual areas including area MST and weak or absent connections from primary visual cortex, V1, and area VIP and nearby areas also receive direct projections from the upper-body representation of secondary somatosensory cortex (Boussaoud et al., 1990; Lewis and Van Essen, 2000). Diffusion tensor imaging tractography studies in humans have shown comparable results, with anterior IPS showing the strongest anatomical connectivity with the superior longitudinal fasciculus connecting temporal, parietal, and frontal regions (Rushworth et al., 2006).

The results of the present study suggest a number of promising avenues for future exploration. In the influential behavioral experiments of Ernst and Banks (2002) and Alais and Burr (2004), subjects made quantitative estimates about stimulus properties using different sensory modalities. When discrepancies between the modalities were introduced, the quantitative weight given to each modality in the sensory judgment could be measured experimentally. However, in our behavioral experiment, the judgment was qualitative (touch vs. no-touch) rather than quantitative, so we were unable to precisely measure the weights of different modalities. Multidimensional scaling could be used to extend optimal integration to situations in which perceptual judgments are qualitative instead of quantitative, such as word perception (Ma et al., 2009).

By introducing incongruent stimulation (even though the judgments were qualitative), our behavioral experiment demonstrates that subjects gave more weight to the more reliable modality in their perceptual decision. However, in our neuroimaging experiment, all of the stimuli were congruent. Therefore, we were unable to measure the perceptual reliability-weighting or compare the percept on each trial with the BOLD fMRI data from the different ROIs for that trial. The neural connection strengths could be compared with the percepts for incongruent stimuli on a trial by trial basis to ascertain the relationship between neural connection strengths and perception.

There has been a burst of interest in the use of multi-voxel pattern analysis (MVPA) to decode the sensory stimulus presented to the subject from the observed BOLD fMRI response (Norman et al., 2006). Recently, we demonstrated that MVPA could be used to decode the location of somatosensory stimulation from the fMRI signal across the whole brain or in somatosensory cortex (Beauchamp et al., 2009). An extension of the present study would be to determine the effects of stimulus reliability on MVPA decoding performance.

A further avenue for exploration will be examining connectivity changes in patients with sensory loss. For instance, macular degeneration causes the visual stimulus to be constantly degraded, as in our dynamic noise condition. Our results predict that in patients with macular degeneration, the connectivity weight between visual cortex and IPS should be low, regardless of the amplitude of the BOLD amplitude of the response in visual cortex to a given stimulus. However, it may be possible to increase this decreased connectivity through attention or other top-down mechanisms, counteracting the effects of the disease. Similarly, patients who are blinded at an early age may suffer from reduced connectivity between visual cortex and other brain areas because of the lack of normal input. Restoration of the retinal image in adulthood in these patients does not allow them to regain the visual abilities critical for daily function (Levin et al., 2010). A better understanding of how reliability weighting adjusts connection strengths between sensory cortex and other brain areas may help in the rehabilitation of these patients (Ro and Rafal, 2006).

In summary, our experiments suggest that changes in the BOLD signal amplitude and changes in connection weights between early and late areas may both be important for behavioral reliability-weighting in visual-somatosensory multisensory integration. Because reliability-weighting is a ubiquitous phenomenon across many modality combinations (Witten and Knudsen, 2005), in future experiments it will be necessary to test the connection weights model in a variety of modality combinations and behavioral conditions, and to investigate the synaptic and physiological mechanisms underlying changes in connection weights. Our findings suggest that particularly dramatic weight changes should be observed following brain damage affecting one sensory system (Ro et al., 2007).

ACKNOWLEDGMENTS

This research was supported by National Science Foundation Cognitive Neuroscience Initiative Research Grants 0642532 to MSB and 0847607 to TR and NIH NS065395 to MSB. SP was supported by NIH T32HD049350. NIH S10 RR19186 provided partial funding for the purchase of the 3T scanner. We thank Vips Patel for assistance with MR data collection and Kyung Hwa Kim and Olivia Plante for assistance with behavioral data collection.

REFERENCES

Alais, D., and Burr, D. (2004). The ventriloquist effect results from near-optimal bimodal integration. *Curr. Biol.* 14, 257–262.

Amedi, A., Jacobson, G., Hendler, T., Malach, R., and Zohary, E. (2002). Convergence of visual and tactile shape processing in the human lateral occipital complex. *Cereb. Cortex* 12, 1202–1212.

Amedi, A., Malach, R., Hendler, T., Peled, S., and Zohary, E. (2001). Visuo-haptic object-related activation in the ventral visual pathway. *Nat. Neurosci.* 4, 324–330.

Argall, B. D., Saad, Z. S., and Beauchamp, M. S. (2006). Simplified intersubject averaging on the cortical surface using SUMA. *Hum. Brain Mapp.* 27, 14–27.

Beauchamp, M. S., Cox, R. W., and DeYoe, E. A. (1997). Graded effects of spatial and featural attention on human area MT and associated motion processing areas. *J. Neurophysiol.* 77, 516–520.

Beauchamp, M. S., Laconte, S., and Yasar, N. (2009). Distributed representation of single touches in somatosensory and visual cortex. *Hum. Brain Mapp.* 30, 3163–3171.

Beauchamp, M. S., Lee, K. E., Haxby, J. V., and Martin, A. (2002). Parallel visual motion processing streams for manipulable objects and human movements. *Neuron* 34, 149–159.

Beauchamp, M. S., Lee, K. E., Haxby, J. V., and Martin, A. (2003). fMRI responses to video and point-light displays of moving humans and manipulable objects. *J. Cogn. Neurosci.* 15, 991–1001.

Beauchamp, M. S., Yasar, N. E., Kishan, N., and Ro, T. (2007). Human MST but not MT responds to tactile stimulation. *J. Neurosci.* 27, 8261–8267.

Blakemore, S. J., Bristow, D., Bird, G., Frith, C., and Ward, J. (2005). Somatosensory activations during the observation of touch and a case of vision-touch synaesthesia. *Brain* 128, 1571–1583.

Boussaoud, D., Ungerleider, L. G., and Desimone, R. (1990). Pathways for motion analysis: cortical connections of the middle superior temporal and fundus of the superior temporal visual areas in the macaque. *J. Comp. Neurol.* 296, 462–495.

Bremmer, F., Schlack, A., Shah, N. J., Zafiris, O., Kubischik, M., Hoffmann, K., Zilles, K., and Fink, G. R. (2001). Polymodal motion processing in posterior parietal and premotor cortex: a human fMRI study strongly implies equivalencies between humans and monkeys. *Neuron* 29, 287–296.

Buchel, C., and Friston, K. (2001). Interactions among neuronal systems assessed with functional neuroimaging. *Rev. Neurol. (Paris)* 157, 807–815.

Buchel, C., and Friston, K. J. (1997). Modulation of connectivity in visual pathways by attention: cortical interactions evaluated with structural equation modelling and fMRI. *Cereb. Cortex* 7, 768–778.

Buchel, C., Josephs, O., Rees, G., Turner, R., Frith, C. D., and Friston, K. J. (1998). The functional anatomy of attention to visual motion. A functional MRI study. *Brain* 121, 1281–1294.

Burton, H., Sinclair, R. J., and McLaren, D. G. (2004). Cortical activity to vibrotactile stimulation: an fMRI study in blind and sighted individuals. *Hum. Brain Mapp.* 23, 210.

Burton, H., Sinclair, R. J., Wingert, J. R., and Dierker, D. L. (2008). Multiple parietal operculum subdivisions in humans: tactile activation maps. *Somatosens. Mot. Res.* 25, 149–162.

Cox, R. W. (1996). AFNI: software for analysis and visualization of functional magnetic resonance neuroimages. *Comput. Biomed. Res.* 29, 162–173.

Culham, J. C., and Valyear, K. F. (2006). Human parietal cortex in action. *Curr. Opin. Neurobiol.* 16, 205–212.

Disbrow, E., Roberts, T., and Krubitzer, L. (2000). Somatotopic organization of cortical fields in the lateral sulcus of *Homo sapiens*: evidence for SII and PV. *J. Comp. Neurol.* 418, 1–21.

Downing, P. E., Jiang, Y., Shuman, M., and Kanwisher, N. (2001). A cortical area selective for visual processing of the human body. *Science* 293, 2470–2473.

Eickhoff, S. B., Grefkes, C., Fink, G. R., and Zilles, K. (2008). Functional lateralization of face, hand, and trunk representation in anatomically defined human somatosensory areas. *Cereb. Cortex.* 18, 2820–2830.

Eickhoff, S. B., Grefkes, C., Zilles, K., and Fink, G. R. (2007). The somatotopic organization of cytoarchitectonic areas on the human parietal operculum. *Cereb. Cortex* 17, 1800–1811.

Ernst, M. O., and Banks, M. S. (2002). Humans integrate visual and haptic information in a statistically optimal fashion. *Nature* 415, 429–433.

Farne, A., Serino, A., and Ladavas, E. (2007). Dynamic size-change of peri-hand space following tool-use: determinants and spatial characteristics revealed through cross-modal extinction. *Cortex* 43, 436–443.

Felleman, D. J., and Van Essen, D. C. (1991). Distributed hierarchical processing in the primate cerebral cortex. *Cereb. Cortex* 1, 1–47.

Fetsch, C. R., Deangelis, G. C., and Angelaki, D. E. (2010) Neural correlates of dynamic sensory cue reweighting in macaque area MSTd. *Comput. Syst. Neurosci.* doi: 10.3389/conf.fnins.2010.03.00299.

Fetsch, C. R., Turner, A. H., DeAngelis, G. C., and Angelaki, D. E. (2009). Dynamic reweighting of visual and vestibular cues during self-motion perception. *J. Neurosci.* 29, 15601–15612.

Fischl, B., Sereno, M. I., and Dale, A. M. (1999a). Cortical surface-based analysis. II: inflation, flattening, and a surface-based coordinate system. *Neuroimage* 9, 195–207.

Fischl, B., Sereno, M. I., Tootell, R. B., and Dale, A. M. (1999b). High-resolution intersubject averaging and a coordinate system for the cortical surface. *Hum. Brain Mapp.* 8, 272–284.

Francis, S. T., Kelly, E. F., Bowtell, R., Dunseath, W. J., Folger, S. E., and McGlone, F. (2000). fMRI of the responses to vibratory stimulation of digit tips. *Neuroimage* 11, 188–202.

Genovese, C. R., Lazar, N. A., and Nichols, T. (2002). Thresholding of statistical maps in functional neuroimaging using the false discovery rate. *Neuroimage* 15, 870–878.

Gizewski, E. R., Koeze, O., Uffmann, K., de Greiff, A., Ladd, M. E., and Forsting, M. (2005). Cerebral activation using a MR-compatible piezoelectric actuator with adjustable vibration frequencies and *in vivo* wave propagation control. *Neuroimage* 24, 723–730.

Grefkes, C., and Fink, G. R. (2005). The functional organization of the intraparietal sulcus in humans and monkeys. *J. Anat.* 207, 3–17.

Hagen, M. C., Franzen, O., McGlone, F., Essick, G., Dancer, C., and Pardo, J. V. (2002). Tactile motion activates the human middle temporal/V5 (MT/V5) complex. *Eur. J. Neurosci.* 16, 957–964.

Haggard, P., Christakou, A., and Serino, A. (2007). Viewing the body modulates tactile receptive fields. *Exp. Brain Res.* 180, 187–193.

Helbig, H. B., and Ernst, M. O. (2007). Optimal integration of shape information from vision and touch. *Exp. Brain Res.* 179, 595–606.

Helbig, H. B., and Ernst, M. O. (2008). Visual-haptic cue weighting is independent of modality-specific attention. *J. Vis.* 8, 1–16.

Holmes, N. P., Calvert, G. A., and Spence, C. (2007). Tool use changes multisensory interactions in seconds: evidence from the crossmodal congruency task. *Exp. Brain Res.* 183, 465–476.

Horwitz, B., McIntosh, A. R., Haxby, J. V., and Grady, C. L. (1995). Network analysis of brain cognitive function using metabolic and blood flow data. *Behav. Brain Res.* 66, 187–193.

Igarashi, Y., Kimura, Y., Spence, C., and Ichihara, S. (2008). The selective effect of the image of a hand on visuotactile interactions as assessed by performance on the crossmodal congruency task. *Exp. Brain Res.* 184, 31–38.

James, T. W., Humphrey, G. K., Gati, J. S., Servos, P., Menon, R. S., and Goodale, M. A. (2002). Haptic study of three-dimensional objects activates extrastriate visual areas. *Neuropsychologia* 40, 1706–1714.

Johnson, R. M., Burton, P. C., and Ro, T. (2006). Visually induced feelings of touch. *Brain Res.* 16, 398–406.

Kastner, S., De Weerd, P., Desimone, R., and Ungerleider, L. G. (1998). Mechanisms of directed attention in the human extrastriate cortex as revealed by functional MRI [see comments]. *Science* 282, 108–111.

Kennett, S., Taylor-Clarke, M., and Haggard, P. (2001). Noninformative vision improves the spatial resolution of touch in humans. *Curr. Biol.* 11, 1188–1191.

Keysers, C., Wicker, B., Gazzola, V., Anton, J. L., Fogassi, L., and Gallese, V. (2004). A touching sight: SII/PV activation during the observation and experience of touch. *Neuron* 42, 335–346.

Levin, N., Dumoulin, S. O., Winawer, J., Dougherty, R. F., and Wandell, B. A. (2010). Cortical maps and white matter tracts following long period of visual deprivation and retinal image restoration. *Neuron* 65, 21–31.

Lewis, J. W., and Van Essen, D. C. (2000). Corticocortical connections of visual, sensorimotor, and multimodal processing areas in the parietal lobe of the macaque monkey. *J. Comp. Neurol.* 428, 112–137.

Ma, W. J., Beck, J. M., Latham, P. E., and Pouget, A. (2006). Bayesian inference with probabilistic population codes. *Nat. Neurosci.* 9, 1432–1438.

Ma, W. J., and Pouget, A. (2008). Linking neurons to behavior in multisensory perception: a computational review. *Exp. Brain Res.* 1242, 4–12.

Ma, W. J., Zhou, X., Ross, L. A., Foxe, J. J., and Parra, L. C. (2009). Lip-reading aids word recognition most in moderate noise: a Bayesian explanation using high-dimensional feature space. *PLoS ONE* 4, e4638. doi: 10.1371/journal.pone.0004638.

Makin, T. R., Holmes, N. P., and Zohary, E. (2007). Is that near my hand? Multisensory representation of peripersonal space in human intraparietal sulcus. *J. Neurosci.* 27, 731–740.

Maravita, A., Spence, C., and Driver, J. (2003). Multisensory integration and the body schema: close to hand and within reach. *Curr. Biol.* 13:R531–539.

Mazziotta, J., Toga, A., Evans, A., Fox, P., Lancaster, J., Zilles, K., Woods, R., Paus, T., Simpson, G., Pike, B., Holmes, C., Collins, L., Thompson, P., MacDonald, D., Iacoboni, M., Schormann, T., Amunts, K., Palomero-Gallagher, N., Geyer, S., Parsons, L., Narr, K., Kabani, N., Le Goualher, G., Boomsma, D., Cannon, T., Kawashima, R., and Mazoyer, B. (2001). A probabilistic atlas and reference system for the human brain: international consortium for brain mapping (ICBM). *Philos. Trans. R. Soc. Lond., B, Biol. Sci.* 356, 1293–1322.

McGlone, F., Kelly, E. F., Trulsson, M., Francis, S. T., Westling, G., and Bowtell, R. (2002). Functional neuroimaging studies of human somatosensory cortex. *Behav. Brain Res.* 135, 147–158.

McIntosh, A. R., Grady, C. L., Ungerleider, L. G., Haxby, J. V., Rapoport, S. I., and Horwitz, B. (1994). Network analysis of cortical visual pathways mapped with PET. *J. Neurosci.* 14, 655–666.

Morgan, M. L., Deangelis, G. C., and Angelaki, D. E. (2008). Multisensory integration in macaque visual cortex depends on cue reliability. *Neuron* 59, 662–673.

Nakashita, S., Saito, D. N., Kochiyama, T., Honda, M., Tanabe, H. C., and Sadato, N. (2008). Tactile-visual integration in the posterior parietal cortex: a functional magnetic resonance imaging study. *Brain Res. Bull.* 75, 513–525.

Norman, K. A., Polyn, S. M., Detre, G. J., and Haxby, J. V. (2006). Beyond mind-reading: multi-voxel pattern analysis of fMRI data. *Trends Cogn. Sci. (Regul. Ed.)* 10, 424–430.

Pasalar, S., Ro, T., Beauchamp, M. S. (2010). TMS of posterior parietal cortex disrupts visual tactile multisensory integration. *Eur. J. Neurosci.* 31, 1783–1790.

Pelphrey, K. A., Morris, J. P., Michelich, C. R., Allison, T., and McCarthy, G. (2005). Functional anatomy of biological motion perception in posterior temporal cortex: an fMRI study of eye, mouth and hand movements. *Cereb. Cortex.* 15, 1866–1876.

Peltier, S., Stilla, R., Mariola, E., LaConte, S., Hu, X., and Sathian, K. (2007). Activity and effective connectivity of parietal and occipital cortical regions during haptic shape perception. *Neuropsychologia* 45, 476–483.

Porter, T., and Duff, T. (1984). Compositing Digital Images. *Comput. Graph. (ACM)* 18, 253–259.

Prather, S. C., Votaw, J. R., and Sathian, K. (2004). Task-specific recruitment of dorsal and ventral visual areas during tactile perception. *Neuropsychologia* 42, 1079–1087.

Ro, T., Farne, A., Johnson, R. M., Wedeen, V., Chu, Z., Wang, Z. J., Hunter, J. V., and Beauchamp, M. S. (2007). Feeling sounds after a thalamic lesion. *Ann. Neurol.* 62, 433–441.

Ro, T., and Rafal, R. (2006). Visual restoration in cortical blindness: insights from natural and TMS-induced blindsight. *Neuropsychol. Rehabil.* 16, 377–396.

Ro, T., Wallace, R., Hagedorn, J., Farne, A., and Pienkos, E. (2004). Visual enhancing of tactile perception in the posterior parietal cortex. *J. Cogn. Neurosci.* 16, 24–30.

Ruben, J., Schwiemann, J., Deuchert, M., Meyer, R., Krause, T., Curio, G., Villringer, K., Kurth, R., and Villringer, A. (2001). Somatotopic organization of human secondary somatosensory cortex. *Cereb. Cortex* 11, 463–473.

Rushworth, M. F., Behrens, T. E., and Johansen-Berg, H. (2006). Connection patterns distinguish 3 regions of human parietal cortex. *Cereb. Cortex* 16, 1418–1430.

Saenz, M., Buracas, G. T., and Boynton, G. M. (2002). Global effects of feature-based attention in human visual cortex. *Nat. Neurosci.* 5, 631–632.

Saito, D. N., Okada, T., Morita, Y., Yonekura, Y., and Sadato, N. (2003). Tactile-visual cross-modal shape matching: a functional MRI study. *Brain Res. Cogn. Brain Res.* 17, 14–25.

Schaefer, M., Flor, H., Heinze, H. J., and Rotte, M. (2006). Dynamic modulation of the primary somatosensory cortex during seeing and feeling a touched hand. *Neuroimage* 29, 587–592.

Schaefer, M., Heinze, H. J., and Rotte, M. (2005). Seeing the hand being touched modulates the primary somatosensory cortex. *Neuroreport* 16, 1101–1105.

Sherman, S. M. (2007). The thalamus is more than just a relay. *Curr. Opin. Neurobiol.* 17, 417–422.

Simmons, W. K., Bellgowan, P. S., and Martin, A. (2007). Measuring selectivity in fMRI data. *Nat. Neurosci.* 10, 4–5.

Stein, J. L., Wiedholz, L. M., Bassett, D. S., Weinberger, D. R., Zink, C. F., Mattay, V. S., and Meyer-Lindenberg, A. (2007). A validated network of effective amygdala connectivity. *Neuroimage* 36, 736–745.

Stilla, R., and Sathian, K. (2008). Selective visuo-haptic processing of shape and texture. *Hum. Brain Mapp.* 29, 1123–1138.

Summers, I. R., Francis, S. T., Bowtell, R. W., McGlone, F. P., and Clemence, M. (2009). A functional-magnetic-resonance-imaging investigation of cortical activation from moving vibrotactile stimuli on the fingertip. *J. Acoust. Soc. Am.* 125, 1033–1039.

Tal, N., and Amedi, A. (2009). Multisensory visual-tactile object related network in humans: insights gained using a novel crossmodal adaptation approach. *Exp. Brain Res.* 198, 165–182.

Tipper, S., Lloyd, D., Shorland, B., Dancer, C., Howard, L., and McGlone, F. (1998). Vision influences tactile per-

ception without proprioceptive orienting. *Neuroreport* 9, 1741–1744.
Tootell, R. B., Reppas, J. B., Kwong, K. K., Malach, R., Born, R. T., Brady, T. J., Rosen, B. R., and Belliveau, J. W. (1995). Functional analysis of human MT and related visual cortical areas using magnetic resonance imaging. *J. Neurosci.* 15, 3215–3230.
Vul, E., Harris, C., Winkielman, P., and Pashler, H. (2009). Puzzlingly high correlations in fMRI studies of emotion, personality and social cognition. *Perspect. Psychol. Sci.* 4, 274–290.
Wheaton, K. J., Thompson, J. C., Syngeniotis, A., Abbott, D. F., and Puce, A. (2004). Viewing the motion of human body parts activates different regions of premotor, temporal, and parietal cortex. *Neuroimage* 22, 277–288.
Witten, I. B., and Knudsen, E. I. (2005). Why seeing is believing: merging auditory and visual worlds. *Neuron* 48, 489–496.

Conflict of Interest Statement: The authors declare that the research was conducted in the absence of any commercial or financial relationships that could be construed as a potential conflict of interest.

Received: 03 March 2010; paper pending published: 31 March 2010; accepted: 25 May 2010; published online: 23 June 2010.
Citation: Beauchamp MS, Pasalar S and Ro T (2010) Neural substrates of reliability-weighted visual-tactile multisensory integration. Front. Syst. Neurosci. ***4****:25. doi: 10.3389/fnsys.2010.00025*
Copyright © 2010 Beauchamp, Pasalar and Ro. This is an open-access article subject to an exclusive license agreement between the authors and the Frontiers Research Foundation, which permits unrestricted use, distribution, and reproduction in any medium, provided the original authors and source are credited.

frontiers in
SYSTEMS NEUROSCIENCE

ORIGINAL RESEARCH ARTICLE
published: 10 February 2011
doi: 10.3389/fnsys.2011.00001

The neural architecture of the language comprehension network: converging evidence from lesion and connectivity analyses

And U. Turken[1]* and Nina F. Dronkers[1,2]*

[1] *Department of Veterans Affairs Northern California Health Care System, Center for Aphasia and Related Disorders, Martinez, CA, USA*
[2] *Neurology Department, University of California Davis, Davis, CA, USA*

Edited by:
Barry Horwitz,
National Institutes of Health, USA

Reviewed by:
Jeffrey R. Binder,
Medical College of Wisconsin, USA
Soo-Eun Chang, Michigan State University, USA

****Correspondence:***
And U. Turken,
Veterans Affairs Northern California Health Care System, Research Service R4 151/MTZ, 150 Muir Road, Martinez, CA 94553, USA.
e-mail: and.turken@va.gov;
Nina F. Dronkers,
Veterans Affairs Northern California Health Care System, Center for Aphasia and Related Disorders (126R), 150 Muir Road, Martinez, CA 94553, USA.
e-mail: dronkers@ucdavis.edu

While traditional models of language comprehension have focused on the left posterior temporal cortex as the neurological basis for language comprehension, lesion and functional imaging studies indicate the involvement of an extensive network of cortical regions. However, the full extent of this network and the white matter pathways that contribute to it remain to be characterized. In an earlier voxel-based lesion-symptom mapping analysis of data from aphasic patients (Dronkers et al., 2004), several brain regions in the left hemisphere were found to be critical for language comprehension: the left posterior middle temporal gyrus, the anterior part of Brodmann's area 22 in the superior temporal gyrus (anterior STG/BA22), the posterior superior temporal sulcus (STS) extending into Brodmann's area 39 (STS/BA39), the orbital part of the inferior frontal gyrus (BA47), and the middle frontal gyrus (BA46). Here, we investigated the white matter pathways associated with these regions using diffusion tensor imaging from healthy subjects. We also used resting-state functional magnetic resonance imaging data to assess the functional connectivity profiles of these regions. Fiber tractography and functional connectivity analyses indicated that the left MTG, anterior STG/BA22, STS/BA39, and BA47 are part of a richly interconnected network that extends to additional frontal, parietal, and temporal regions in the two hemispheres. The inferior occipito-frontal fasciculus, the arcuate fasciculus, and the middle and inferior longitudinal fasciculi, as well as transcallosal projections via the tapetum were found to be the most prominent white matter pathways bridging the regions important for language comprehension. The left MTG showed a particularly extensive structural and functional connectivity pattern which is consistent with the severity of the impairments associated with MTG lesions and which suggests a central role for this region in language comprehension.

Keywords: aphasia, language comprehension, language network, structural connectivity, fiber tracts, resting-state functional connectivity, disconnection, middle temporal gyrus

INTRODUCTION

The brain regions that subserve verbal comprehension are traditionally associated with Wernicke's and, to some extent, Broca's areas. Following the seminal work of Wernicke (1874), who described neurological patients with trouble understanding spoken language, it has been assumed that the posterior superior temporal cortex in the left hemisphere is primarily responsible for language comprehension (Geschwind, 1970, 1972; Goodglass, 1993). Broca's area has also been implicated in sentence comprehension in that patients with Broca's aphasia have difficulty processing the syntactic rules that affect sentence meaning. However, this position is gradually giving way to a network perspective, which emphasizes the contribution of several brain regions organized into a large-scale network via long-distance association pathways (Mesulam, 1990; Damasio, 1991). Lesion–deficit correlation findings with aphasic patients have led to an appreciation of how several other brain regions within and outside the left temporal lobe also contribute to language comprehension. It has been shown in several studies that language comprehension deficits can be produced by lesions in several posterior and frontal cortical areas and subcortical structures (Kertesz et al., 1979, 1982, 1993; Naeser et al., 1982, 1987; Alexander et al., 1989; Damasio, 1992; Dronkers et al., 1994, 2000b, 2004; Caplan et al., 1996, 2007; Damasio and Damasio, 2002; Bates et al., 2003; Binder, 2003; Tyler and Marslen-Wilson, 2008). Functional neuroimaging investigations have also highlighted distributed activation patterns in the healthy brain during the performance of tasks that involve language comprehension and the processing of lexical-semantic information (Demonet et al., 1992; Demb et al., 1995; Binder et al., 1997, 2009; Price, 2000, 2010; Bookheimer, 2002; Friederici, 2002; Vigneau et al., 2006; Ferstl et al., 2008).

Thus, an extensive left-lateralized network for language comprehension is indicated by both lesion–symptom correlations in aphasia and functional imaging findings in the healthy brain. This network is distributed throughout association areas in the left perisylvian cortex and neighboring regions, including parts of the posterior middle temporal gyrus (MTG), inferior temporal regions, the inferior parietal lobe (IPL), inferior frontal gyrus (IFG), as well as other frontal regions not directly involved in language but facilitating comprehension through working memory and cognitive control operations (Dronkers et al., 2004). The anatomical

extent of this network is consistent with the notion that language comprehension is a complex process which, like other complex behaviors, is the product of the coordinated activity of several brain regions, each contributing to several subprocesses of comprehension. The functioning of the overall network can be disrupted by brain lesions damaging different cortical nodes and disconnecting the white matter (WM) pathways that subserve their interactions. Better understanding of the functional anatomy of the language comprehension network and its disorders requires a detailed characterization of the underlying connectional architecture that allows the functional integration of the brain structures that comprise the language network.

The specific contributions of individual brain regions to the large-scale networks specialized for different aspects of cognition are determined by their connectivity patterns (Mesulam, 1990, 1998, 2005; Schmahmann and Pandya, 2008). Each brain region acquires its particular function in a brain network by virtue of how it interacts with other regions in the brain. This highlights the need to delineate the WM pathways that interconnect distinct components of the language network in order to elucidate how each part is functionally integrated to the overall network and makes specific contributions to language processing, and to understanding why lesions in different brain regions cause the particular symptoms observed in aphasic patients. Behavioral deficits can also be produced by WM lesions that disconnect healthy brain regions, and the resulting deficits can be as severe as those produced by damage to the areas that subserve cortical information processing (Lichtheim, 1885; Geschwind, 1965a,b; Catani and Mesulam, 2008a,b). Reorganization of the architecture of functional networks is a key factor for the recovery of function following neurological injury, and this process might be mediated by the connections that allow intact regions to acquire new functions and enable the surviving sections of damaged regions to be reintegrated into functional networks (Heiss et al., 2003; Dancause et al., 2005; Ward, 2005; Marsh and Hillis, 2006; Murphy and Corbett, 2009). Thus, better knowledge of the connectional anatomy of the language network is essential for understanding the consequences of the disruption of WM pathways due to brain injury, and the contributions of these pathways to functional recovery.

While the arcuate fasciculus (AF) has traditionally been viewed as the single critical WM pathway that provides the scaffolding for the language network (Dronkers et al., 2000a; Catani and Mesulam, 2008a; Friederici, 2009), the growing knowledge of WM anatomy indicates that the language network is subserved by a richer network of fiber systems than originally appreciated. The arcuate itself has been shown to be composed not of a single arc, but at least three segments, including a direct pathway between temporal and frontal regions, and an indirect segment involving inferior parietal regions (Catani et al., 2005). Histological tracing studies of the homologues of human language areas in the monkey brain have shown the existence of a distinct parieto-temporal pathway, the middle longitudinal fasciculus (MdLF), that interconnects the superior temporal and inferior parietal cortices (Seltzer and Pandya, 1984, 1994; Schmahmann et al., 2007), and long fibers that pass through the extreme capsule (EmC) to link posterior superior temporal regions with the IFG (Petrides and Pandya, 1988, 2009). These connections have also been characterized in the human brain using *in vivo* imaging techniques (Frey et al., 2008; Makris and Pandya, 2009; Makris et al., 2009). The inferior occipito-frontal fasciculus, a major pathway extending from frontal cortex to temporal, parietal, and occipital cortices, has been implicated in semantic processing by subcortical stimulation data from neurosurgical patients (Duffau et al., 2005, 2008). It has also been proposed, on anatomical grounds, that semantic processing might be subserved by a two-step pathway involving the inferior longitudinal fasciculus (ILF), which runs along the whole length of the temporal lobe, and the uncinate fasciculus (UF), which connects the temporal pole with the inferior frontal regions (Vigneau et al., 2006). It is important to examine these new findings in relation to the lesion anatomy in aphasia in order to appreciate the functional contributions of these pathways.

Here, we investigated the structural and functional connectivity of the brain regions found to be critical for auditory sentence comprehension in an earlier investigation from our laboratory (Dronkers et al., 2004). Sentence comprehension is a complex function that engages many components of the language network and other brain regions that support language, such as working memory and cognitive control systems (Friederici, 2002; Dronkers et al., 2004). Thus, sentence comprehension is an ideal task for exploring the language comprehension network. In our previous investigation, auditory sentence comprehension deficits were analyzed in relation to lesion anatomy in 64 chronic stage aphasic patients who had suffered focal left hemisphere damage due to stroke. Sentence comprehension was assessed by the Curtiss-Yamada Comprehensive Language Evaluation, Receptive Language Test (CYCLE-R; Curtiss and Yamada, 1988). Lesions that significantly alter sentence comprehension performance were mapped on a standard template using voxel-based lesion-symptom mapping (VLSM, Bates et al., 2003). Subgroups of patients whose lesions encompassed each of these regions were also examined separately, using their scores on each CYCLE-R subtest, and their performance on the Western Aphasia Battery (WAB; Kertesz, 1982). Five brain regions were highlighted in this analysis as being critical for language comprehension: the MTG and underlying WM (hereafter referred to as "MTG"), the anterior superior temporal gyrus ("anterior STG/BA22"), a region including parts of the posterior superior temporal sulcus (STS) and the angular gyrus ("STS/BA39"), Brodmann's area 47 in pars orbitalis of the IFG ("BA47"), and a part of Brodmann's area 46 in the middle frontal gyrus ("BA46"; **Figures 1,2**).

Patients with lesions in MTG and adjacent white matter, including those classified with a severe Wernicke's aphasia, were impaired in all but the simplest sentences, indicating a word-level deficit, which was also confirmed by data from the WAB Auditory Comprehension subtests. Lesions in other areas affected sentence level processing as difficulty level increased (Dronkers et al., 2004, Figure 5), suggesting higher-level contributions to language comprehension. For example, the performance of patients with anterior STG/BA22 lesions declined when the syntactic structure of test items influenced the interpretation of the sentence, suggesting a role for this region in basic morphosyntactic processing. Patients with lesions in frontal regions BA46 and BA47 were impaired only for the most complex sentence structures. The BA47 finding was interpreted as reflecting the impairment of a working memory system for semantic information, whereas the BA46 involvement was attributed to deficits in general cognitive control processes. Finally, posterior STS/BA39 involvement was attributed to auditory short-term memory impairments, as patients with lesions in this region were most

impaired on items that relied on auditory rehearsal. Patients whose lesions spared all of these regions showed only minor deficits on the most difficult items. Critically, lesions in the two regions which have traditionally been considered to be at the core of language functioning in the brain, Broca's area (IFG pars opercularis and pars triangularis) and posterior superior temporal gyrus, the cortical zone commonly attributed to Wernicke's area, were not found to be associated with significant language comprehension deficits in this investigation. A small WM region medial to the posterior STS was also identified as being critical for sentence comprehension, suggesting that not only cortical damage but a disconnection produced by a lesion in WM adjacent to posterior STG and MTG might also produce language comprehension deficits.

In order to investigate how the above brain regions might participate in a larger network of interconnected areas, we analyzed brain imaging data from healthy subjects using two new magnetic resonance imaging (MRI) techniques. The first, diffusion tensor imaging (DT-MRI), examines the fiber pathways that structurally link brain regions to each other (Basser et al., 1994; Pierpaoli et al., 1996). We used this technique to determine which pathways were associated with the regions found to be critical for auditory sentence comprehension from our previous lesion analysis. The second technique, resting-state functional MRI (RS-fMRI), reveals functional brain networks by correlating blood oxygenation levels across brain regions over time to identify which parts of the brain are simultaneously active (Lowe et al., 1998; Greicius et al., 2003; Biswal et al., 2010; Van Dijk et al., 2010). We applied the second method to identify brain areas that were functionally connected with each of the regions critical for auditory sentence comprehension. We used these two approaches, described below, with data from healthy subjects to examine the structural and functional architecture of the brain regions associated with sentence comprehension deficits as previously found in aphasic patients.

Diffusion tensor magnetic resonance imaging shows the microstructural organization of white matter in the living brain. With this information, it is possible to perform tractography analysis and determine the trajectories of long-distance pathways by tracing the dominant orientation of fiber groups at different points in brain white matter (Conturo et al., 1999; Basser et al., 2000; Catani et al., 2002; Mori et al., 2002). DT-MRI tractography has been used to examine the anatomical organization of the pathways that support language in the brain, to determine which pathways interconnect specific brain regions, and to interpret the functions subserved by individual pathways based on their cortical termination patterns (Catani et al., 2005, 2007; Croxson et al., 2005; Makris et al., 2005, 2009; Parker et al., 2005; Anwander et al., 2007; Vernooij et al., 2007; Frey et al., 2008; Glasser and Rilling, 2008; Saur et al., 2008; Makris and Pandya, 2009; Kaplan et al., 2010; Brauer et al., 2010). In this investigation, we used the regions of interest (ROIs) from the lesion findings which were described earlier to constrain whole-brain streamline tractography results, in order to isolate the fiber pathways associated with the WM contained in each ROI. We then identified the major WM structures associated with these fibers using digital WM atlases (Wakana et al., 2004; Burgel et al., 2006; Catani and Thiebaut de Schotten, 2008; Mori et al., 2008).

The analysis of interregional correlations in RS-fMRI data is another technique for mapping the connectivity profiles of individual brain regions as well as complete functional circuits (Biswal et al., 1995, 2010; Lowe et al., 1998; Greicius et al., 2003; Damoiseaux et al., 2006; Buckner et al., 2009; Van Dijk et al., 2010). Correlated fluctuations of spontaneous brain activity, as assessed by the blood oxygenation-level dependent (BOLD) functional magnetic resonance imaging (fMRI) signal, provide information about which regions are physiologically coupled, either via direct structural connections, or indirect polysynaptic links. Thus, high correlations between the amount of oxygen consumed simultaneously by multiple regions are believed to mirror which brain areas typically interact with each other. Several investigations have shown that the functional organization of large-scale brain networks can be assessed by mapping with this approach the regions that show coherent resting-state activity (Fox et al., 2005; Damoiseaux et al., 2006; Dosenbach et al., 2007; He et al., 2007; Vincent et al., 2007; Buckner et al., 2009; Biswal et al., 2010), including those that may be related to language (other than comprehension; Hampson et al., 2002; Kelly et al., 2010; Koyama et al., 2010; Xiang et al., 2010). In order to examine the language comprehension network, we used the cortical ROIs derived from the previous lesion analysis findings and computed whole-brain correlation maps for each ROI.

By combining the information from these two connectivity analyses, we sought to determine the relationships among the brain regions identified as being important for auditory sentence comprehension in our previous lesion analysis with aphasic patients (Dronkers et al., 2004). This was achieved by identifying in the healthy brain (1) the major pathways associated with these regions, and (2) the functional connectivity of these regions with other cortical areas.

In this way we explored how these regions might fit into a network that supports language comprehension. We also examined the implications of our findings in the context of the lesion anatomy of comprehension deficits in aphasia.

MATERIALS AND METHODS

Structural and functional connectivity patterns of the regions that were found to be critical for language comprehension in our brain lesion analysis were investigated using diffusion tensor imaging and fMRI data. Streamline tractography was applied to the DTI data from 25 healthy subjects to trace the principal WM pathways associated with each of the regions. The functional connectivity profile for each region was assessed using resting-state fMRI data from another group of 25 healthy subjects. These data processing and analysis steps are described in detail in the following sections.

DEFINITION OF REGIONS OF INTEREST FOR THE LANGUAGE COMPREHENSION NETWORK ANALYSIS

The regions identified by the VLSM analysis of sentence comprehension deficits (**Figure 1**; Dronkers et al., 2004) were transformed from the DeArmond et al. (1989) atlas space, in which the original results were produced, to the Montreal Neurological Institute (MNI) space. A mapping from the DeArmond et al. atlas space to the MNI space was determined by the following steps. The MNI anatomical template was aligned to the atlas plates by a 7° rotation of the axial plane. Eleven slices were identified on the re-oriented MNI template that best match the axial photographic images of the brain in the DeArmond et al. atlas. The corresponding anatomical landmarks were marked by manually selecting several control points on each

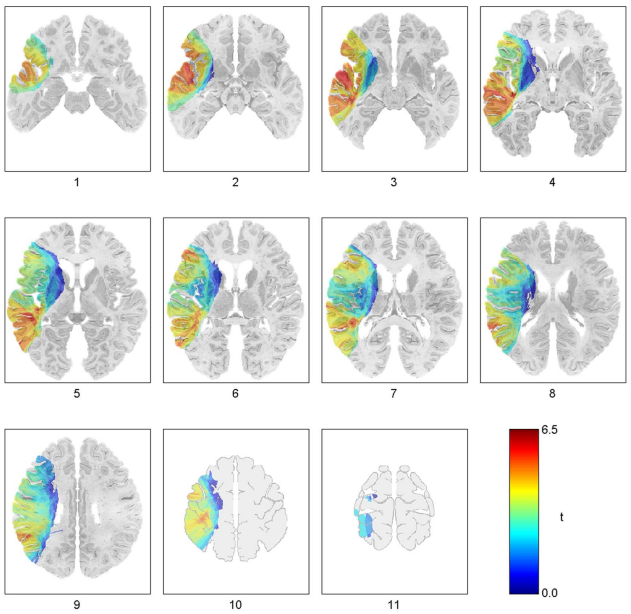


FIGURE 1 | Voxel-based lesion-symptom mapping findings for the regions critical for auditory sentence comprehension, as assessed by the CYCLE-R. The *t*-map is visualized on 11 slices from the DeArmond et al. (1989) brain atlas, which was used as the template for lesion reconstructions. Significant voxels from this map comprised five distinct regions, each associated with a different pattern of performance (see text). (Reprinted with permission from Dronkers et al., 2004).

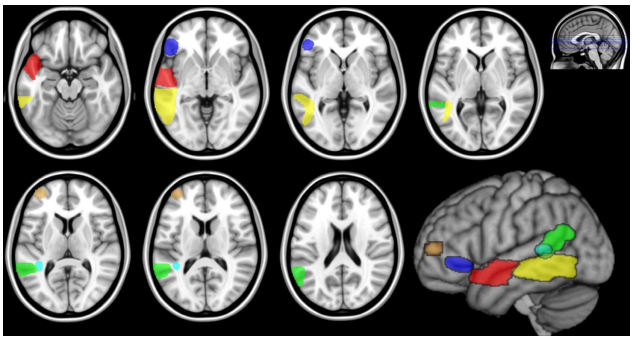


FIGURE 2 | Regions of interest in MNI space based on the lesion-symptom mapping findings for the posterior MTG (■), anterior STG/BA22 (■), BA47 (■), BA46 (■), STS/BA39 (■), and white matter underlying the STS (■). Slice positions are marked on a mid-sagittal view of the MNI template on the upper right side.

slice and used for 2D non-linear warping of the DeArmond et al. slices to MNI template slices using the Image Processing Toolbox for MATLAB[1]. The DeArmond et al. atlas slices were then realigned to the MNI space orientation and linearly interpolated to obtain a 2-mm inter-slice distance. A software implementation of this atlas transformation is included as part of the VLSM 1.6 package for MATLAB[2].

Region of interests in MNI space were then obtained from the VLSM results for the lesion–symptom analysis in DeArmond et al. (1989) atlas space (**Figure 1**; Dronkers et al., 2004, Figures 3 and 4) using the same procedure. A smoothing filter (8 mm FWHM Gaussian) was applied to each ROI in order to compensate for registration errors and the residual anatomical variability that remains after the spatial normalization of the healthy subject datasets to MNI space. These ROIs for the MTG, anterior STG/BA22, BA47, BA46, STS/BA39, and the WM subjacent to the STS were saved as binary mask images for the subsequent analyses (**Figure 2**). It should be noted that the VLSM findings include WM regions as well as the cortical areas listed in Table 3 of Dronkers et al. (2004). Tractography analysis of structural connectivity revealed the WM pathways associated with each ROI, while the functional connectivity analysis was restricted to the cortical gray matter (GM) contained within each ROI.

ASSESSMENT OF STRUCTURAL CONNECTIVITY WITH DIFFUSION IMAGING TRACTOGRAPHY

Diffusion tensor imaging data

Diffusion tensor imaging datasets from 25 healthy subjects were randomly selected from the publicly-available ICBM DTI-81 database[3,4], which includes diffusion imaging data from young and middle-aged healthy right-handed subjects (Oishi et al., 2008). The subject demographics, data acquisition protocols and the probabilistic maps of major pathways developed using these data have been described in publications by the ICBM researchers (Hua et al., 2009; Mori et al., 2008; Oishi et al., 2008; Zhang et al., 2008). The diffusion imaging data were acquired on Siemens 1.5T MRI scanners at the MNI and University of California Los Angeles using single-shot echo-planar imaging (EPI) sequences with sensitivity encoding and a parallel imaging factor of 2.0, 96×96 imaging matrix, field of view (FOV) = 240 mm × 240 mm, 60 transverse sections (2.5 mm slice thickness) parallel to the anterior commissure–posterior commissure line (AC–PC), two repetitions of a sequence of five images with minimal diffusion weighting and 30 diffusion-weighted (1000 s/mm^2) images with 30 gradient orientations (Mori et al., 2008).

DTI post-processing

First, an anatomical reference image was produced from the EPI images with minimal diffusion weighting (B0 images) by correcting for head motion by rigid-body alignment in SPM8, and averaging over the realigned scans. All diffusion-weighted images were co-registered to this reference image. Using SPM8, a brain mask was derived from the reference image by applying a tissue segmentation algorithm and then applied to the other scans to exclude non-brain tissue. The reference image was also normalized to MNI space for the ROI-based analyses. The diffusion datasets were resampled to 2.0 mm^3 resolution and averaged over the repeated series to improve signal-to-noise ratio. Using the methods implemented in the MedInria software package[5] (Fillard et al., 2007), the diffusion

[1]www.mathworks.com

[2]http://crl.ucsd.edu/vlsm

[3]http://www.loni.ucla.edu/ICBM

[4]https://www.mristudio.org

[5]http://www-sop.inria.fr/asclepios/software/MedINRIA

tensor was computed (Basser, 1995), and streamline tractography was applied to derive fiber pathways following the principal diffusion direction at each voxel. The default settings in MedInria were used for this analysis. The tractography results were then imported into the TrackVis package[6] (Wang et al., 2007) for visualization and the isolation of WM tracts for the structural connectivity analyses.

The ROIs described in the preceding section were transformed to each subject's native dataset space for isolating the tractography-defined fibers associated with each ROI. For this purpose, the deformation fields produced by the normalization of the reference (mean B0) image were inverted using the Deformations utility in SPM8, and the resulting reverse mapping was applied to each ROI defined in MNI space to identify the corresponding regions in each subject's brain. The fiber groups intersecting these reverse-normalized ROIs were isolated and manually segmented into fiber bundles corresponding to known anatomy and published diffusion imaging atlases (Wakana et al., 2004; Burgel et al., 2006; Catani and Thiebaut de Schotten, 2008; Hua et al., 2009; Lawes et al., 2008; Mori et al., 2008; Oishi et al., 2008). For this purpose, additional ROIs were used to delineate several major pathways, consistent with the published guidelines for identifying and isolating fiber bundles using the multiple-ROI approach (Wakana et al., 2007; Catani and Thiebaut de Schotten, 2008; Hua et al., 2008). These additional ROIs for isolating individual pathways were first drawn in MNI space on a color-coded principal diffusion direction map derived from the ICBM DTI-81 group-averaged tensor map. They were then reverse-normalized to native space datasets for tract identification. Custom MATLAB code was used to extract the fiber groups associated with the ROIs. The extracted bundles were compared against the ICBM DTI-81 probabilistic maps and tractography publications to verify their identity. The two authors independently completed this process. Fiber tract findings are reported in the results section if at least 10 tractography streamlines were found in at least 20 (80%) of the 25 subjects.

ASSESSMENT OF FUNCTIONAL CONNECTIVITY WITH RESTING-STATE fMRI DATA

Functional magnetic resonance imaging

Resting-state fMRI data from 25 healthy subjects were acquired from a publicly available database of functional and structural imaging data[7] (Biswal et al., 2010). We chose to use the NYU Test Retest Reliability dataset from the 1000 Functional Connectomes Project database, as the subjects in this study were scanned on three different dates and the stability of the functional connectivity patterns have been demonstrated (Shehzad et al., 2009). The image acquisition protocol (NYU Test Retest Reliability dataset, as described in previous publications that presented findings from these data (Margulies et al., 2009; Shehzad et al., 2009; Kelly et al., 2010), was: EPI on a Siemens Allegra 3.0 Tesla scanner with repetition time (TR) = 2000 ms, echo time (TE) = 25 ms; flip angle = 90°, matrix = 64 × 64; FOV = 192 mm; voxel size = 3 mm × 3 mm × 3 mm, 39 axial slices, 197 functional volumes, and a high-resolution T1-weighted anatomical image (magnetization-prepared gradient echo sequence with 1 mm × 1 mm × 1 mm resolution). During each functional imaging session, subjects were instructed to rest with their eyes open. Signed informed consent, approved by the institutional review boards of the New York University School of Medicine and New York University, was obtained from each subject prior to participation.

fMRI data pre-processing

Functional magnetic resonance imaging datasets were pre-processed using the standard SPM8[8] protocol which includes slice-timing correction, correction for head movements using rigid-body realignment to the mean EPI image from each session, co-registration of EPI data to the anatomical scan for each subject, tissue segmentation and normalization of anatomical scans to standard (MNI) space with the unified segmentation and normalization algorithm implemented in SPM8 (Ashburner and Friston, 2005). The EPI datasets were transformed to standard space using the normalization parameters for anatomical scans, with a final spatial resolution of 2.5 mm^3 isotropic voxels. A Gaussian smoothing filter (6.125 mm full width at half maximum) was applied to enhance the signal-to-noise ratio. Tissue segmentation of the anatomical images isolated the GM, WM, and cerebrospinal fluid (CSF) compartments, which were used in the functional connectivity analysis described below.

Resting-state functional connectivity analysis

The Functional Connectivity Toolbox[9] for SPM8 was used for deriving the functional connectivity maps for each ROI. The BOLD time-series for each of the ROIs was extracted, averaging over the GM voxels (derived from the tissue segmentation of anatomical images) included in the ROI. Resting fMRI data need to be corrected for artifacts of non-neural origin associated with physiological (respiratory and cardiac) events, instrument noise, and head movements, which can induce spurious correlations into the connectivity analysis. Confounding signals were estimated from the WM and CSF segments using the CompCor method (Behzadi et al., 2007). These signals together with movement-related covariates were removed from the fMRI data using regression. Next, the residual BOLD time-series were band-pass filtered over a low-frequency window of interest ($0.008\ Hz < f < 0.08\ Hz$). Correlation maps for each ROI in each session and each subject were then produced by computing the Pearson's correlation coefficients between the ROI time-series and the time courses for all brain voxels. The correlation maps for all subjects were converted to normally-distributed scores using Fischer's transform and submitted to one-sample *t*-tests to compute the group-level maps of functional connectivity for each ROI. Only positive correlations were mapped for this investigation. The resultant statistical parametric maps after testing for statistical significance using a voxel-wise threshold of $p < 0.01$, corrected for multiple comparisons (family-wise error rate across all brain voxels), and a cluster extent threshold of 100 mm^3 (40 contiguous voxels). Only the cortical extents of these maps are reported in the present manuscript. The anatomical distributions for the functional connectivity maps were assessed in relation to digital atlases for

[6]http://www.trackvis.org

[7]http://www.nitrc.org/projects/fcon_1000

[8]http://www.fil.ion.ucl.ac.uk/spm/

[9]http://www.nitrc.org/projects/conn

cortical areas and gyral anatomy (Harvard–Oxford probabilistic atlas, Desikan et al., 2006; AAL atlas, Tzourio-Mazoyer et al., 2002), distributed with the FSL[10] and MRICron[11] software packages.

In addition to the whole-brain resting-state functional connectivity maps for the five cortical ROIs, the pair-wise interregional correlations between these regions were also examined. The mean BOLD time-series for all the GM voxels contained in each ROI was obtained, after performing band-pass filtering and artifact correction as described above. Pearson's correlation coefficients were computed for each pair of ROIs in each subject, and analyzed across subjects with one-sample *t*-tests ($p < 0.01$, corrected for multiple comparisons).

RESULTS

In the following sections, the structural and functional connectivity patterns associated with each of the five ROIs are reported, followed by a summary of the findings. The structural connectivity findings are illustrated in figures for two representative subjects, showing the distinct fiber pathways associated with each ROI. Each pathway was reliably traced in at least 80% (20 out of 25) of the DTI datasets. Functional connectivity maps have been rendered on a semi-inflated view of the single-subject cortical surface reconstruction provided in SPM8.

POSTERIOR MIDDLE TEMPORAL GYRUS (MTG ROI)

Structural connectivity

Streamline tractography revealed that the white matter contained within the MTG ROI contains fibers from several major pathways, which were consistently identified in at least 80% of subjects (**Figure 3**). These pathways were: the direct (temporo-frontal) and indirect (temporo-parietal) segments of the AF; the IOFF; the MdLF; the ILF; and posterior corpus callosum fibers, consistent with the temporo-temporal interhemispheric connections through the tapetum.

As for the fiber bundles linking the MTG ROI with the other ROIs (**Figure 4**), those passing through the MTG ROI and reaching the BA47 ROI were identified as being part of the IOFF. Short fibers connecting the MTG with the STS/BA39 ROI were identified as fibers of the indirect segment of the AF. Those passing adjacent to the MTG and reaching the anterior STG/BA22 ROI were recognized as MdLF fibers, based on their trajectory[12]. Connections with the BA46 ROI could not be consistently traced, for reasons further discussed in the section entitled Anterior Middle Frontal Gyrus (BA46 ROI).

Resting-state functional connectivity

The whole-brain resting functional connectivity map for the MTG ROI revealed an extensive network of cortical association areas, importantly, several peri-sylvian and neighboring regions that have been implicated in language, and their right hemisphere homologues (**Figure 5**). Because of the broad extent of this map, we also identified the regions that show the strongest correlations at a more stringent threshold ($t > 12.13$, cluster extent > 62.5 mm^3), which are reported in **Table 1**. In the left lateral temporal lobe, we identified a zone running from the temporal pole to the temporo-parietal and temporo-occipital regions, extending into the inferior temporal cortex (BA 20 and BA 37), the STS, and parts of the STG (BA 22), but excluding the primary auditory cortex (BA 41 and

[10]www.fmrib.ox.ac.uk/fsl

[11]www.nitrc.org/projects/mricron

[12]It should be noted that while the MdLF has been shown to interconnect inferior parietal regions with the multimodal areas of the STG in the monkey brain Schmahmann et al. (2007), it is still unknown how this fiber bundle relates to the MTG in the human brain.

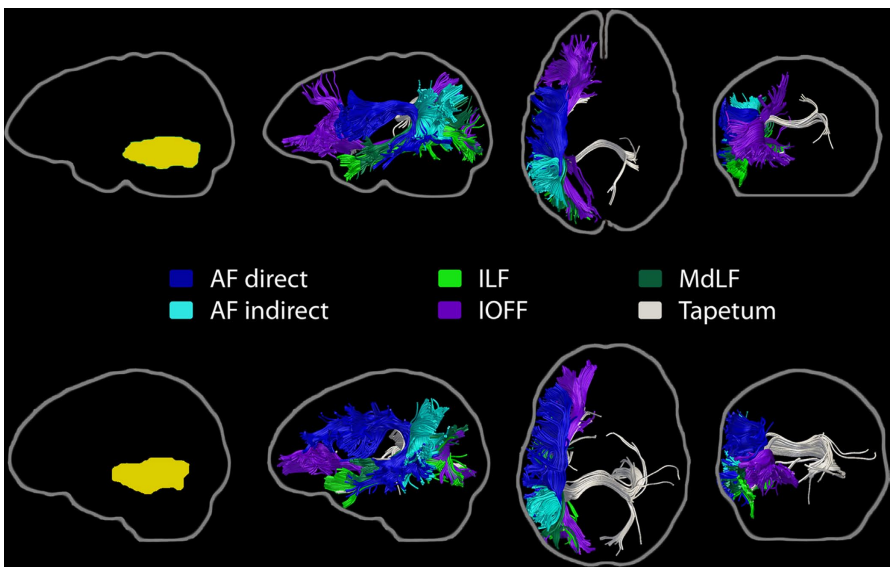


FIGURE 3 | Major pathways associated with the left MTG region of interest. Streamline tractography results from two subjects are presented as exemplars. Each row depicts the individual subject's ROI warped to their own native space (left, yellow), followed by sagittal, axial, and coronal perspectives of the fiber bundles involved. The direct and indirect segments of the arcuate fasciculus, the inferior occipito-frontal fasciculus, the middle longitudinal fasciculus, the inferior longitudinal fasciculus, and transcallosal projections, consistent with the tapetum, are shown.

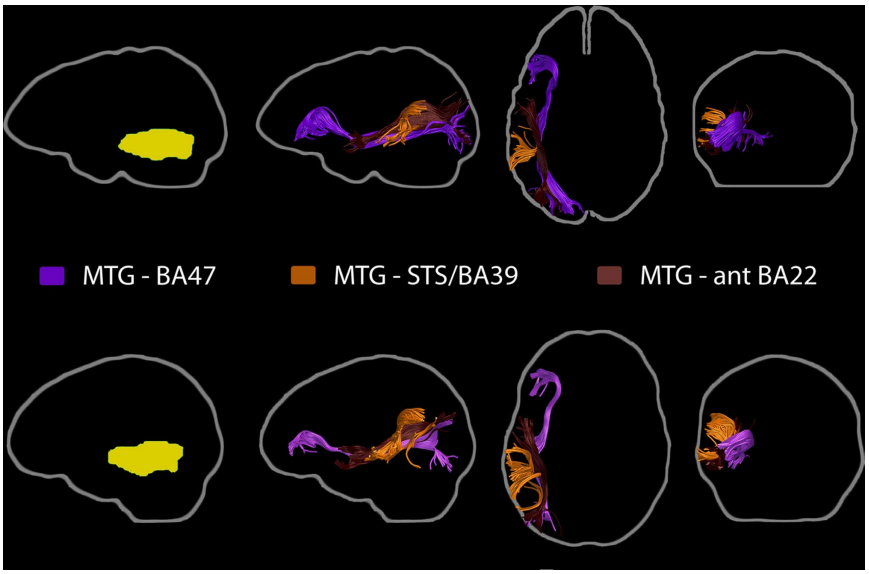


FIGURE 4 | Pathways linking the posterior MTG region of interest with the other ROIs: BA47, STS/BA39, and anterior STG/BA22. Each row again depicts the findings for each sampled individual, with the ROI and fiber bundles depicted in the subject's native space (left, yellow). Fibers passing between the MTG and BA47 were identified as part of the IOFF. Those connecting MTG with STS/BA39 were consistent with fibers of the indirect segment of the AF. The pathway likely to connect the MTG ROI with the anterior STG/BA22 ROI was identified as the MdLF.

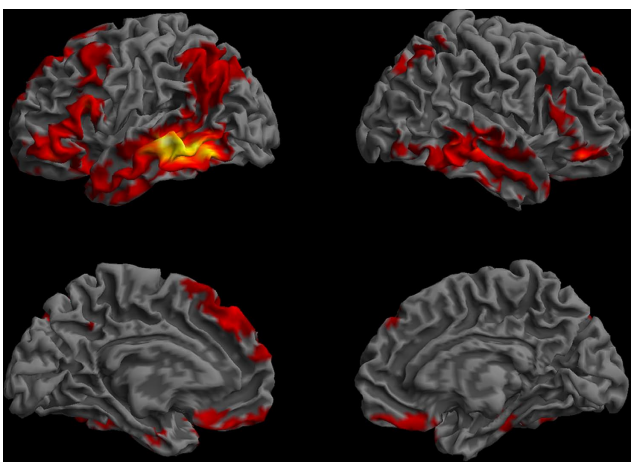


FIGURE 5 | Functional connectivity profile of the left posterior middle temporal region that was previously found to be critical for the core processes supporting sentence comprehension (Dronkers et al., 2004). The regions that showed highly correlated ($p < 0.01$, corrected, cluster extent > 100 mm^3) spontaneous activity with the left MTG seed are shown on a semi-inflated view of the cortical surface. The left and right hemispheres are shown on the left and right columns, respectively. The upper row shows the lateral surface, and the lower row, the medial surface of the cerebrum. Colors indicate *t*-values (dark red = lowest, yellow-white = highest, with the voxels within the ROI showing the highest correlation).

42), which was mirrored in the right temporal lobe. The parietal regions showing the strongest correlations with the MTG were the left angular gyrus (BA 39) and superior parietal lobe (BA 7). A medial posterior parietal region was also functionally connected with the MTG. Frontal lobe functional connectivity was bilateral (more extensive in the left hemisphere) and comprised three zones: a broad cortical swath running along the superior–inferior direction on the lateral prefrontal cortex, including parts of the middle frontal gyrus and the precentral gyrus dorsally, continuing through the pars opercularis (BA44) and pars triangularis (BA45) of the IFG and ending inferiorly into the pars orbitalis (BA47); a dorso-medial zone including parts of BA6, BA8, BA9, and BA 32; and the gyrus rectus (BA11) in the ventromedial frontal cortex. Regions of interest that showed functional connectivity with the MTG included STS/BA39, BA47, and parts of anterior STG/BA 22, but not BA46.

ANTERIOR BRODMANN'S AREA 22 IN THE SUPERIOR TEMPORAL GYRUS (ANTERIOR STG/BA22 ROI)

Structural connectivity

The middle longitudinal fasciculus and UF fibers were associated with the anterior STG/BA22 ROI in all subjects (**Figure 6**). Fibers passing adjacent to this ROI and the MTG ROI were identified as belonging to the MdLF. Pathways between the anterior STG/BA22 and STS/BA39, BA47, and BA46 ROIs could not be found consistently across subjects.

Resting-state functional connectivity

The functional connectivity map for the anterior STG/BA22 ROI included the whole extent of the superior temporal gyrus and neighboring sections of the MTG, BA 37, the temporal pole, the rolandic operculum, IFG pars orbitalis (BA 47) and the anterior cingulate cortex (BA 24), the supplementary motor area, the precentral gyrus (BA 6), and the insula (**Figure 7**). All of these regions were identified in both hemispheres. Other ROIs that showed functional connectivity with the anterior STG/BA22 ROI were parts of the MTG and BA47.

Table 1 | Cortical areas found to be functionally connected to the left MTG seed region at a stringent threshold for significance ($t > 12.13$, cluster extent > 62.5 mm^3).

Hemisphere and lobe where cluster is found	Cluster size (voxels)	Maximum *t* value	Peak coordinates *x*, *y*, *z* (mm)			Anatomical label (AAL atlas)
Left temporal	1327	35.39	–63	–31	–5	Middle temporal gyrus (BA 21)
		29.55	–55	–61	–12	Inferior temporal gyrus (BA 37)
		13.96	–45	–49	–15	Inferior temporal gyrus (BA 20)
Right temporal	233	21.89	70	–41	–10	Inferior temporal gyrus (BA 20)
		16.85	70	–26	–7	Middle temporal gyrus (BA 21)
		13.91	63	–51	–17	Inferior temporal gyrus (BA 37)
Left frontal	234	18.8	–50	42	–15	IFG pars orbitalis
		17.09	–40	37	–17	IFG pars orbitalis
		14.85	–55	34	3	IFG pars triangularis
Left frontal	190	18.42	–50	14	26	IFG pars triangularis
		15.24	–55	17	8	IFG pars opercularis
		14.26	–48	7	38	Precentral gyrus (BA 6)
Right frontal	28	16.73	43	39	–15	IFG orbitalis (BA 47)
Left parietal	47	14.73	–35	–59	48	IPL (BA 7)
Left parietal	35	14.34	–43	–56	31	AG (BA 39)

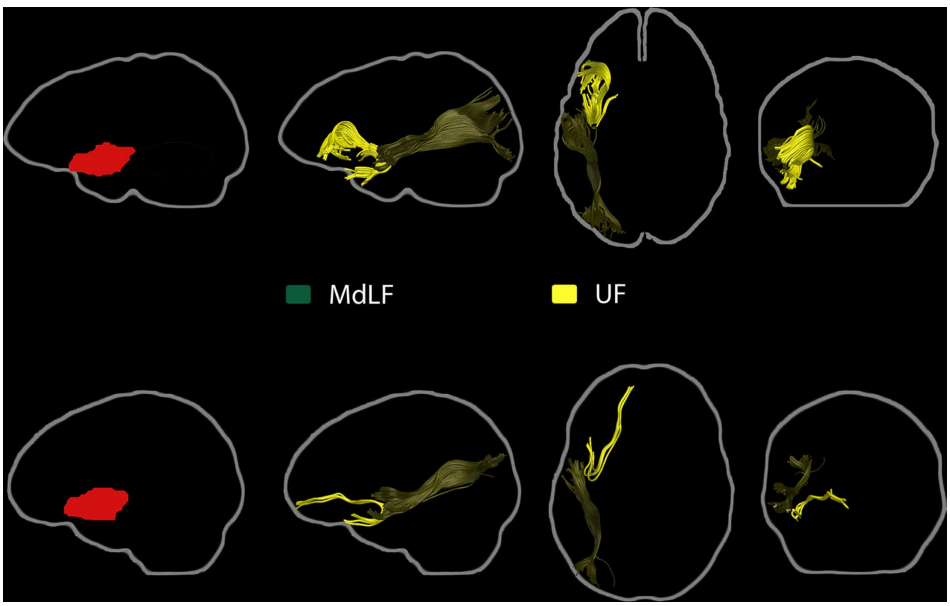


FIGURE 6 | Pathways associated with the anterior STG/BA22 region of interest (left, red). Streamline tractography results from two subjects are presented as exemplars. The middle longitudinal fasciculus and the uncinate fasciculus were found to be associated with this ROI.

PARS ORBITALIS OF THE INFERIOR FRONTAL GYRUS (BA47 ROI)

Structural connectivity

The BA47 ROI was consistently found to be associated with the inferior occipito-frontal fasciculus (**Figure 8**). In all subjects, streamlines consistent with the IOFF passed through both the BA47 and MTG ROIs.

Resting-state functional connectivity

The functional connectivity map for BA47 consisted of six clusters (**Figure 9**). The largest cluster was centered in the IFG, extending to pars opercularis (BA 44), inferior precentral gyrus (BA 6), and the temporal pole (BA 38). Other clusters were in the MTG bilaterally, the right IFG, a left posterior region which included parts of the left angular gyrus (BA 39) and the superior temporal gyrus (BA 22, but not anterior STG/BA22), and the left medial frontal cortex (SMA, BA 6, 8, and 9).

ANTERIOR MIDDLE FRONTAL GYRUS (BA46 ROI)

Structural connectivity

Tractography analysis of the BA46 ROI did not reveal a consistent pattern across subjects, possibly due to the smaller size of this ROI, intersubject anatomical variability that affected registration

accuracy, and/or limitations of streamline tractography. It is important to note the BA46 ROI does not cover the entire extent of Brodmann's area 46 and that an analysis of the entire region would undoubtedly reveal an extensive connectivity pattern.

Resting-state functional connectivity

The functional connectivity map for the BA46 ROI included bilateral middle frontal gyri, small sections of the supramarginal gyrus (SMG), and anterior cingulate cortex (BA 24, 32) as well as the left anterior insula (**Figure 10**).

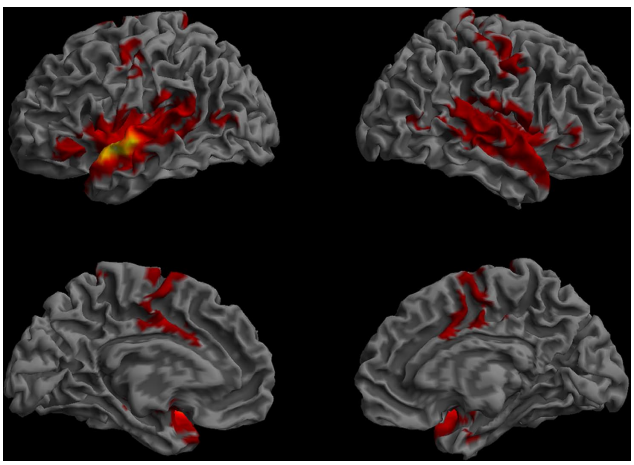


FIGURE 7 | Resting-state functional connectivity of the left anterior STG/BA22 ROI. (Lateral and medial views of the left and right hemispheres, $p < 0.01$, corrected, cluster extent > 100 mm^3, colors indicate *t*-values, dark red = lowest, yellow-white = highest, with the voxels within the ROI showing the highest correlation).

POSTERIOR SUPERIOR TEMPORAL SULCUS AND BRODMANN'S AREA 39 (STS/BA39 ROI)

Structural connectivity

Fibers associated with the direct and indirect segments of the AF were found to pass through the WM region included in the posterior STS/BA39 ROI (**Figure 11**). Short, vertically-oriented fibers interconnecting the MTG and STS/BA39 ROIs were also found in all subjects. Also of note was a robust bundle of short fibers connecting the STS/BA39 ROI with other parts of the angular gyrus. Fibers between STS/BA39 and BA47 or anterior STG/BA22 could not be consistently identified across subjects.

Resting-state functional connectivity

The functional connectivity pattern of the STS/BA39 ROI included two large clusters running along the MTG bilaterally, forming a bridge between the temporal pole and the angular gyrus, and extending into the superior and inferior temporal gyri (**Figure 12**). Other functionally-connected regions were in the left lateral prefrontal cortex, including the pars orbitalis (BA 47) and pars triangularis, the left middle frontal gyrus, bilateral dorso-medial frontal regions, right BA 47, the gyrus rectus, mid-cingulate cortex, and the medial posterior parietal cortex, bilaterally. Other ROIs that showed functional connectivity with the STS/BA39 ROI included parts of the MTG, BA47, and anterior STG/BA22 ROIs, but not the BA46 ROI.

WHITE MATTER UNDERLYING THE SUPERIOR TEMPORAL SULCUS (STS WM ROI)

The fiber composition of a WM region subjacent to the STS was also analyzed. This region was reported in our lesion–symptom mapping analysis as part of the STS/BA39 ROI (Dronkers et al., 2004), but it was also noted that it could represent a distinct func-

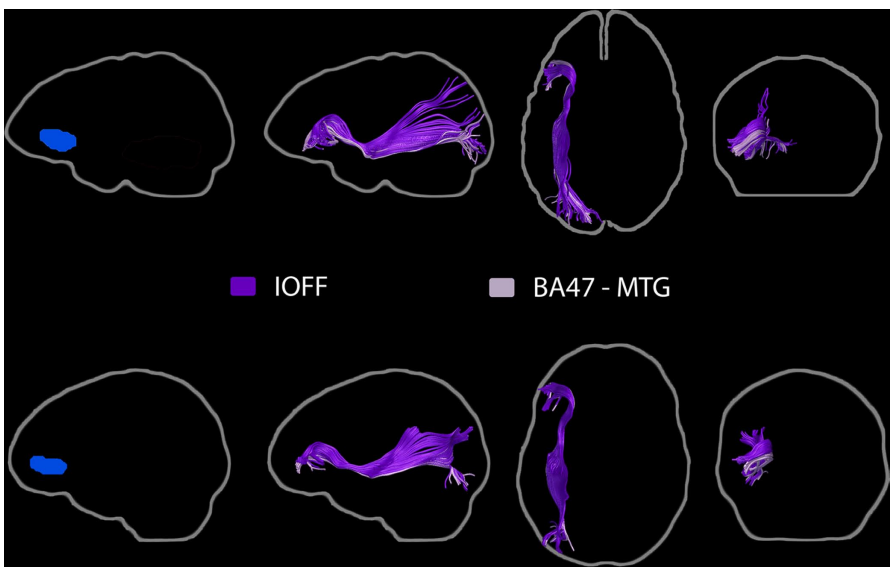


FIGURE 8 | Pathways associated with the BA47 ROI (left, blue). Streamline tractography results from two subjects are presented as exemplars. The inferior occipito-frontal fasciculus as well as a group of IOFF fibers associated with the posterior MTG ROI were identified.

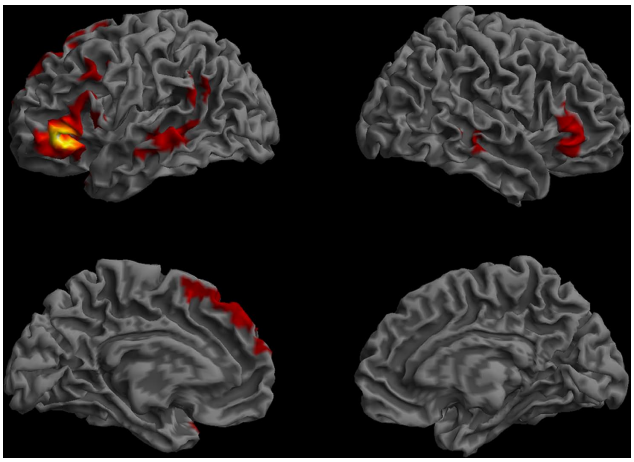


FIGURE 9 | Resting-state functional connectivity map of the BA 47 region of interest. (Lateral and medial views of the left and right hemispheres, $p < 0.01$, corrected, cluster extent > 100 mm^3, colors indicate *t*-values, dark red = lowest, yellow-white = highest, with the voxels within the ROI showing the highest correlation).

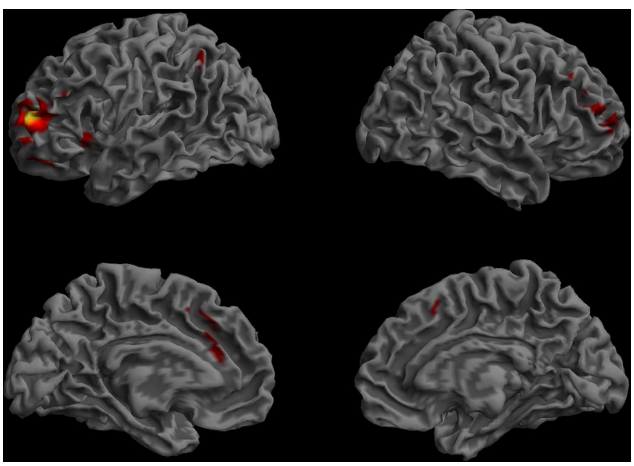


FIGURE 10 | Functional connectivity of the BA46 ROI. (Lateral and medial views of the left and right hemispheres, $p < 0.01$, corrected, cluster extent > 100 mm^3, colors indicate *t*-values, dark red = lowest, yellow-white = highest, with the voxels within the ROI showing the highest correlation).

tional unit on its own (Dronkers et al., 2004, p. 159, Figure 4, slice 7, footnote 2). This small region was found to contain fibers associated with five fiber systems: the direct (temporo-frontal) and indirect (temporo-parietal) segments of the AF, the IOFF, the MdLF, and transcallosal fibers consistent with the tapetum (**Figure 13**).

ADDITIONAL ANALYSES

Subdivisions of the posterior MTG

The extensive connectivity pattern of the MTG ROI was a surprising result. It is possible that ROI size, rather than location, may have contributed to this novel finding, as this ROI covers the whole extent of the MTG along the anterior–posterior axis ($y = -18$ to -70 mm) and also goes deeply into WM. For this reason, we subdivided the MTG ROI into subregions of equal length along the anterior–posterior axis, and analyzed their connectional anatomy patterns. Resting functional connectivity maps revealed an anterior-to-posterior gradient, with the compartments in the anterior half of the MTG showing more widely distributed functional connectivity patterns than those in the posterior half (**Figure 14**). The second quarter of the MTG showed a distribution that best matched the extent of the original MTG functional connectivity profile. This subregion is consistent with the main MTG termination of the ascending section of the AF, and the STS WM ROI [the subsection entitled White Matter Underlying the Superior Temporal Sulcus (STS WM ROI)] is situated superior to this section of the MTG. The IOFF, AF, MdLF, ILF and fibers of the tapetum all course through the WM underlying this segment of the MTG, so that a lesion in this region alone can affect all five fiber systems.

"Wernicke's area"

Although Wernicke's area has traditionally been associated with language comprehension, our 2004 lesion–symptom mapping results did not associate this region with language comprehension impairments. To test if functional connectivity analysis could offer additional information regarding the role of this area in the language network, Harvard–Oxford atlas-based ROIs were used. The functional connectivity maps for the planum temporale and the posterior SMG – regions associated with Wernicke's area in some models (Geschwind, 1972; Bogen and Bogen, 1976) – showed distinctly different patterns compared to our MTG map, suggesting that these regions belong to separate networks (**Figure 15**).

STRUCTURAL AND FUNCTIONAL CONNECTIONS LINKING THE REGIONS OF INTEREST: SUMMARY OF FINDINGS

Table 2 summarizes the structural and functional connectivity patterns for the five cortical regions of interest. The MTG ROI was linked with the anterior STG/BA22 and STS/BA39 and BA47 ROIs via several major pathways, although cortical terminations could not be ascertained in each case. In addition, the MdLF fibers associated with the anterior STG/BA22 ROI were found pass through a WM region subjacent to the STS, and course medially to the STS/BA39 ROI, suggesting that these two ROIs could be linked via the MdLF. Functional connectivity analysis of the ROI-to-ROI correlations were found to be significant for all pair-wise combinations of the MTG, anterior STG/BA22 and STS/BA39 and BA47 ROIs, whereas the BA46 ROI was only correlated with the MTG ROI ($p < 0.01$, corrected).

DISCUSSION

Our analysis of the structural and functional connectivity of the key regions implicated in auditory sentence comprehension by our previous work (Dronkers et al., 2004) revealed a bilateral temporo-parieto-frontal network supported by numerous WM pathways and interacting with several other brain regions outside the traditionally-recognized language areas.

The structural connectivity analyses revealed that six long-distance fiber pathways were associated with these regions: the AF, the IOFF, the ILF, the MdLF, the UF, and the tapetum.

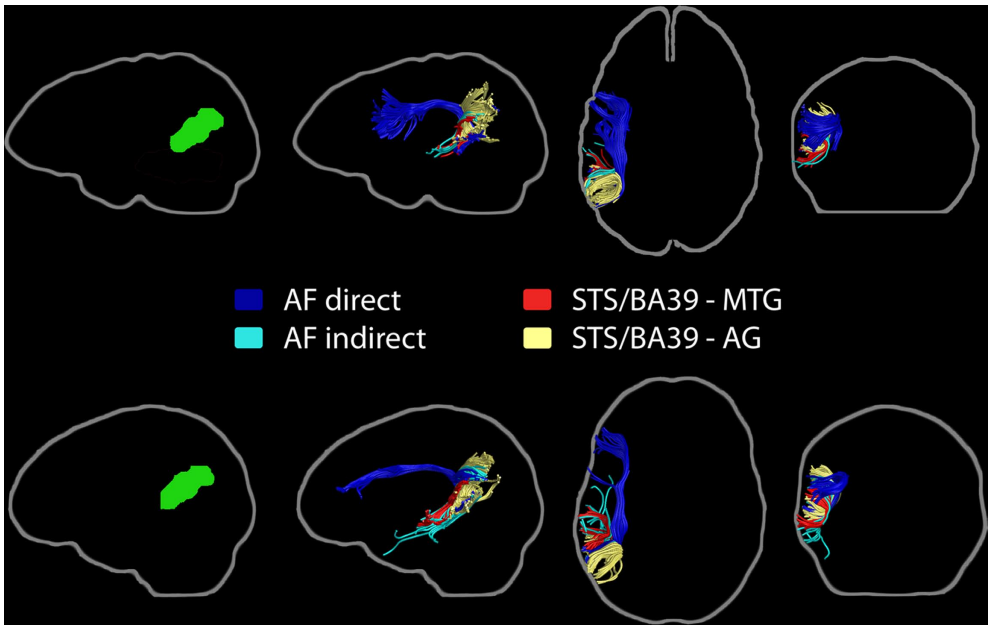


FIGURE 11 | Pathways associated with the left STS/BA39 region of interest (left, green). Streamline tractography results from two subjects are presented as exemplars. The primary fiber pathway associated with this ROI is the arcuate fasciculus, with its direct and indirect compartments shown. Short fiber bundles connecting this ROI to the MTG ROI and the angular gyrus are also represented.

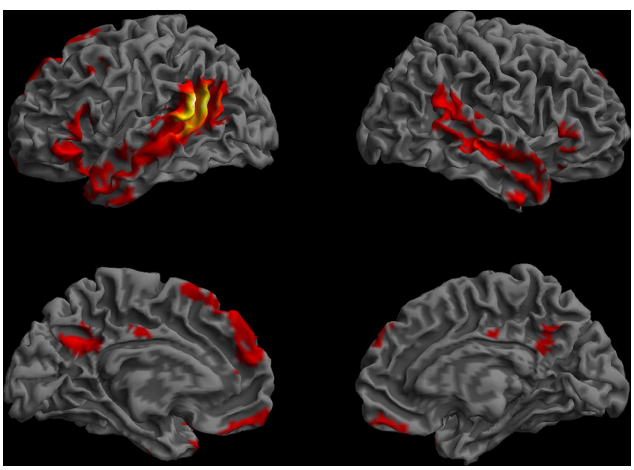


FIGURE 12 | Resting-state functional connectivity pattern for the posterior STS/BA39 region of interest. (Lateral and medial views of the left and right hemispheres, $p < 0.01$, corrected, cluster extent > 100 mm^3, colors indicate *t*-values, dark red = lowest, yellow-white = highest, with the voxels within the ROI showing the highest correlation).

Functional connectivity analyses revealed an extensive network of cortical association areas within the left hemisphere, extending to homologous regions of the right hemisphere. The extent of this network is consistent with the notion that a complex process such as understanding spoken sentences is not mediated by a single region or pathway alone, but requires the integrated functioning of a broadly-distributed constellation of regions interacting via multiple routes within and outside the language areas (Mesulam, 1998; Dronkers, 2000; Dronkers et al., 2000a; Damasio and Damasio, 2002).

One important implication of the present findings is that the left MTG holds a key position within this network for language comprehension, indicated by the richness of its structural and functional connectivity as described here. This region appears to function as a focal point with no less than five major fiber pathways passing beneath it and a broadly distributed set of cortical association areas functionally connected with it. It is not surprising that injury to this region, rich in connections, results in severe and persisting language comprehension impairments. This observation also highlights an important notion. Regions such as the MTG and its underlying white matter, where multiple fiber pathways converge, could serve as the backbone of a complex network, but such regions also become the most vulnerable part of the whole network when neurological damage occurs.

Another major finding supports the proposal (Duffau et al., 2005) that the IOFF, a pathway that is not part of the canonical language network, might play an important role in the comprehension and production of meaningful speech. We found that the IOFF fibers pass through the temporal white matter region highlighted in our lesion analysis, providing a bridge between the middle temporal region and inferior prefrontal area 47, which has been implicated in high-level language comprehension by several findings, including our lesion analysis (Bookheimer, 2002; Dronkers et al., 2004; Hagoort et al., 2004; Binder et al., 2009). Our functional connectivity findings also support a direct link between the MTG and BA47 that is mediated by the fibers that travel along the IOFF.

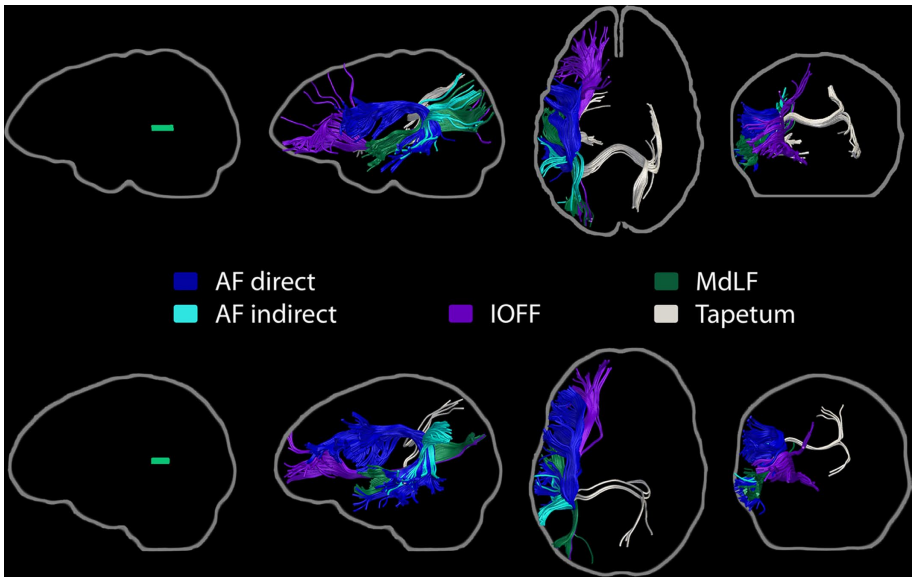


FIGURE 13 | Fiber pathways passing through the white matter underlying the superior temporal sulcus. Five different fiber bundles were found to contribute fibers to this small white matter region (left, green). Direct and indirect segments of the arcuate fasciculus, the inferior occipito-frontal fasciculus, the middle longitudinal fasciculus, and the tapetum are shown for the two subjects chosen as exemplars.

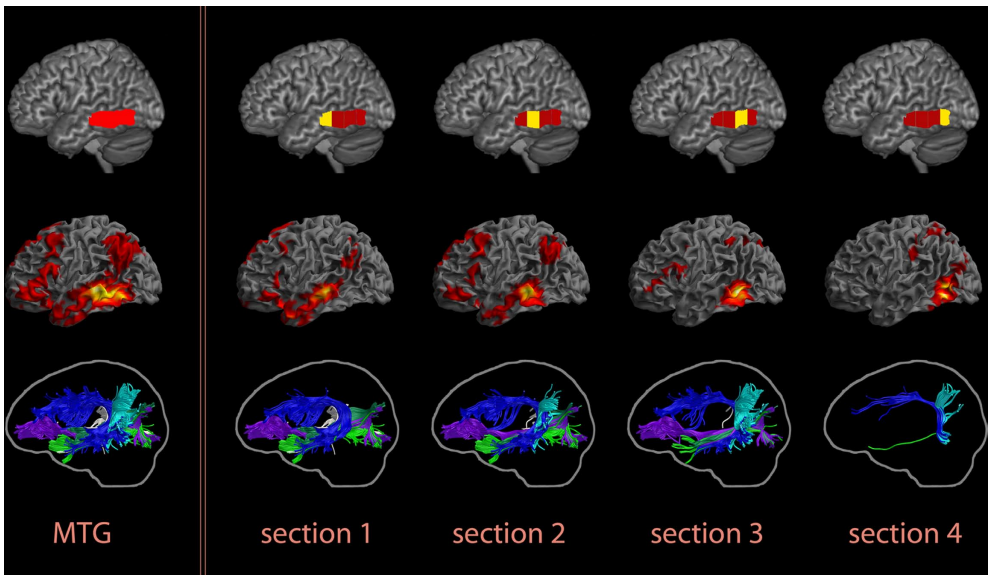


FIGURE 14 | Resting functional and structural connectivity profiles of subregions of the posterior MTG, divided into four parts of equal length along its anterior–posterior extent (*y* = −18 to −70 mm). An anterior-to-posterior gradient was observed in these maps, with the two anterior subregions showing more widely-distributed functional connectivity and richer structural connectivity patterns. The individual compartments are indicated on the top row, functional connectivity maps are presented in the middle row, and tractography results for one subject chosen as an exemplar are in the bottom row. The results for the whole MTG ROI are shown in the first column, followed by the findings for the individual subregions. In the functional connectivity maps, colors indicate *t*-values (dark red = lowest, yellow-white = highest, with the voxels within the ROI showing the highest correlation).

Finally, the AF was found to have extensive connections within the MTG, consistent with other recent findings (Powell et al., 2006; Glasser and Rilling, 2008; Rilling et al., 2008). Traditional models of language processing have previously considered this tract to connect the posterior superior temporal gyrus with inferior frontal regions. However it is important to remember that the terminations of this tract are not restricted to the superior temporal gyrus but reach the MTG as well. Thus, future models of language processing must also take into account the vast connections of this important fiber pathway including those that extend into the MTG.

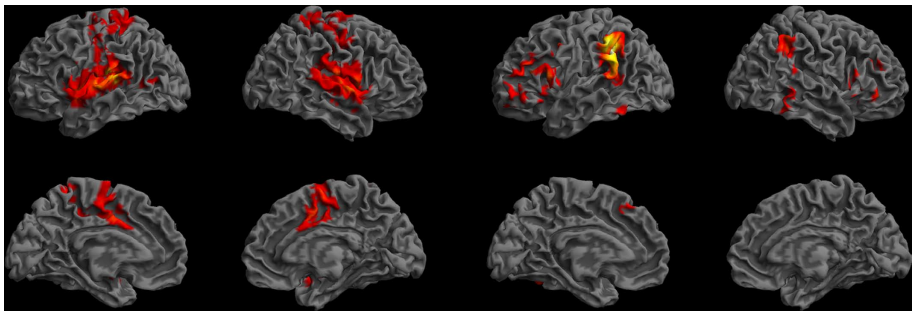


FIGURE 15 | Resting-state functional connectivity maps for the left planum temporale (left) and the left posterior supramarginal gyrus (right) according to the Harvard–Oxford cortical atlas. These maps suggest that the network associated with the posterior MTG is distinct from the networks that include the planum temporale and the posterior SMG. Colors indicate *t*-values (dark red = lowest, yellow-white = highest, with the voxels within the ROI showing the highest correlation).

Table 2 | Summary of the structural and functional connectivity findings for each region of interest in relation to the other ROIs.

ROI	Functional connectivity	Structural connectivity
MTG	STS/BA39 Anterior STG/BA22 BA47 BA46	STS/BA39 via the AF indirect, anterior STG/BA22 via the MdLF*, BA47 via the IOFF*
STS/BA39	MTG Anterior STG/BA22 BA47	MTG via the AF indirect, anterior STG/BA22 via the MdLF^
Anterior STG/BA22	MTG STS/BA39 BA47	MTG via the MdLF*, STS/BA39 via the MdLF^
BA47	MTG STS/BA39 Anterior STG/BA22	MTG via the IOFF*
BA46	MTG	

**It must be noted that the fiber pathways implicated here cannot be confirmed with the streamline tractography technique currently utilized. While these fibers do pass through both regions of interest, they cannot be traced to their cortical terminations as these would intermix with the ascending fibers of the arcuate fasciculus that run close to the cortical surface in this region.*
^Though MdLF fibers were not specifically seen to enter the STS/BA39 ROI, current knowledge of the anatomy of this tract is that it does traverse beneath the STG toward Brodmann's area 39, and thus would be the likely pathway to connect the Anterior BA22 ROI with the STS/BA39 ROI.

The present findings and their implications for understanding comprehension impairments in aphasia are discussed in more detail in the following sections.

THE EXTENDED NETWORK FOR LANGUAGE COMPREHENSION

The present findings indicate the involvement of a large-scale network in language comprehension, including the left MTG, anterior STG/BA22, BA47, and STS/BA39, which had been identified in our earlier lesion analysis findings (Dronkers et al., 2004). Several long-distance white matter pathways are associated with the lesion-symptom mapping findings: the direct and indirect segments of the AF, the IOFF, the ILF, the MdLF, the UF, and the tapetum. The left MTG, with the most extensive structural and functional connectivity profile, emerged as a central component of the language comprehension network. Of the six major pathways implicated in the present study, only the UF was not associated with the MTG. Regions of functional connectivity for the MTG included large territories in temporal, parietal, and frontal cortices in the two hemispheres. The anterior STG/BA22 ROI included fibers from the MdLF, consistent with its functional connectivity pattern extending posteriorly along the superior temporal gyrus toward the supramarginal and angular gyri, as well as fibers of the UF, which link anterior sections of the temporal lobe with the IFG. However, direct pathways linking this region with the MTG, STS/BA39, and BA47 could not be consistently identified. The STS/BA39 ROI was associated with fibers from the AF and had a functional connectivity pattern that bridged the middle temporal and the angular gyri. The structural and functional connectivity findings for the BA46 ROI did not link this area with the other regions of interest, which could be due to the technical limitations of the small ROI size and high inter-individual anatomical variability in this location. BA47 was found to be part of a lateral and dorso-medial prefrontal network, as indicated by its functional connectivity pattern, and was structurally connected to posterior brain regions via the IOFF.

The overall pattern is remarkably consistent with a recent characterization of the functional anatomy of the verbal semantic system based on a meta-analysis of 120 functional neuroimaging investigations (Binder et al., 2009). The congruence between the two sets of findings, as seen in **Figure 16**, provides further support for the notion that language comprehension is subserved by an extensive network of regions distributed throughout the left hemisphere.

STRUCTURAL AND FUNCTIONAL CONNECTIVITY OF THE LEFT MIDDLE TEMPORAL GYRUS: IMPLICATIONS FOR UNDERSTANDING THE ROLE OF THE MTG IN LANGUAGE AND OF MTG LESIONS IN APHASIA

The left MTG's rich pattern of structural and functional connectivity suggests a core function in the language comprehension network. This pattern can also help explain the severe nature of the comprehension deficits produced by lesions affecting the MTG and underlying white matter (Dronkers et al., 1995, 2004; Binder et al., 2003). We found that fibers from five major pathways are

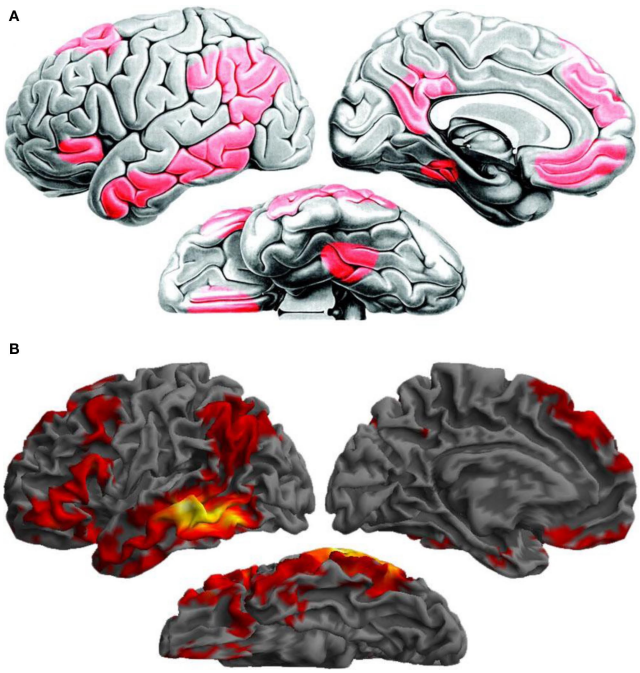


FIGURE 16 | (A) A large-scale network for verbal semantic processing identified by a meta-analysis of 120 functional neuroimaging studies, and the underlying structural connections inferred from tracing studies of the homologous regions in the macaque from (Reprinted with permission from Binder et al., 2009, page 2779, Figure 7). **(B)** Resting functional connectivity pattern for the left posterior MTG ROI, assessed in the present investigation, is largely consistent with the meta-analysis findings.

included in the white matter adjacent to the MTG. These pathways, the inferior occipito-frontal fasciculus, the AF, the inferior and middle longitudinal fasciculi, and the tapetum, mediate long-distance interactions between temporal, parietal and frontal regions and temporo-temporal interhemispheric communication. Consistent with its structural connectivity pattern, the functional connectivity profile of the MTG includes a broad network of left peri-sylvian association cortical areas known to be involved in language, homologous regions in the right hemisphere, as well as several association areas that extend beyond the classical canonical language network. This extensive functional connectivity pattern also accords with a resting-state functional connectivity mapping study of the brain regions involved in reading, which found the left MTG as a common node in a conjunction analysis of six different networks investigated (Koyama et al., 2010). A recent resting-state fMRI found that the MTG is among the most highly connected regions in the cerebral cortex ("cortical hubs"; Buckner et al., 2009). The left MTG peak reported by Buckner and colleagues (−62, −38, −12 mm, Buckner et al., 2009, Table 3) is also consistent with the MTG subdivision we have found to have the most extensive functional connectivity profile (**Figure 14**; second section of the MTG ROI).

It is perhaps not surprising that a region that supports core lexical-semantic processes should be highly integrated with broadly distributed brain networks. That the MTG is involved even in word-level comprehension is indicated by our previous lesion-symptom mapping analysis (Dronkers et al., 2004). Other investigations on the effects of brain lesions (Hart and Gordon, 1990; Hillis et al., 1999; Boatman et al., 2000; Bates et al., 2003) and functional neuroimaging findings with healthy individuals also support this conclusion (Binder et al., 1997, 2009; Bookheimer, 2002; Vigneau et al., 2006; Price, 2010). Binder (2003) has also reviewed the neurological evidence implicating the MTG in comprehension deficits in Wernicke's aphasia. Mapping lexical representations to their concepts relies upon extensive links between distributed representations throughout the cerebrum, including regions that support sensory and motor experiences, such that associations can be formed between words and their meanings.

The extensive connectivity of the left MTG also suggests a role that Mesulam (1990, 1998) describes as a neural epicenter. Mesulam introduced a framework for thinking about large-scale functional networks which are widely distributed but also include core regions that serve as transmodal gateways. This concept also finds a parallel in Damasio's convergence zones model positing that highly connected brain regions serve to bind together distributed representations (Damasio, 1989). Mesulam further predicted that lesions affecting such gateways would produce multiple disconnections, disrupting upstream, and downstream network functions. For the language network, the MTG could be such a critical neural epicenter.

A brain lesion affecting the MTG and underlying white matter would disrupt the functionally and structurally connected network that we found here in the healthy brain. For example, such a lesion could produce a disconnection between left temporal and frontal regions, as both the AF and the inferior occipito-frontal fasciculus would be affected. Communication across the length of the temporal lobe would be disrupted because of damage to the ILF. Lateral temporal and inferior parietal regions would be disconnected because of damage to the indirect segment of the AF and the MdLF. Temporo-temporal interhemispheric communication would also be affected by the loss of tapetum fibers. Thus, even a small lesion in a strategic place such as the MTG would have far more serious ramifications than a comparable lesion elsewhere in the network.

A SEMANTIC WORKING MEMORY PATHWAY VIA THE INFERIOR OCCIPITO-FRONTAL FASCICULUS?

We found that the left MTG and BA47 were functionally connected, and that their interaction was most likely to be mediated through a direct pathway via the IOFF. It has been proposed that the larger Brodmann's area 47, together with parts of the adjacent BA 45, might support higher-level processes in comprehension that are required only when processing demands are high (Bookheimer, 2002; Friederici, 2002; Dronkers et al., 2004). Proposals for BA 47 functions include working memory for semantic features and thematic structure (Friederici, 2002), the unification of individual semantic features into an overall representation at the multi-word level, and the controlled aspects of the retrieval, selection, and evaluation of semantic information (Thompson-Schill et al., 1997; Gabrieli et al., 1998; Poldrack et al., 1999). In our earlier lesion-symptom mapping investigation, patients whose lesions included BA47 were only impaired when

presented with the most syntactically-complex sentences. This finding is consistent the view that BA 47 is engaged only when successful performance depends on the ability to keep track of several pieces of information and to resolve between the alternative interpretations of sentence components. This could be achieved by reciprocal interactions between BA 47 and the MTG, so that the appropriate lexical-semantic representations can be selected, sustained in short-term memory throughout sentence processing, and integrated into the overall context. The structural substrate for these functional interactions could be provided by a direct connection between the two regions via the IOFF.

Evidence for a direct link between BA 47 and mid-lateral temporal cortex comes from tract tracing work in the monkey brain (Petrides and Pandya, 1988, 2006; Schmahmann et al., 2007). Walker's area 12, the monkey homolog of BA 47, was found to connect to the STS and adjacent dorsal inferotemporal cortex, the likely evolutionary precursor of the MTG (Rilling and Seligman, 2002). In our investigation, streamline tractography revealed a pathway with terminations in BA47, running toward posterior regions via the white matter underlying the MTG. This pattern was consistent with the trajectory of the inferior occipito-frontal fasciculus as identified in other diffusion imaging tractography investigations (Catani et al., 2002; Mori et al., 2002, 2008; Catani and Thiebaut de Schotten, 2008). Even though its existence has been disputed in the monkey brain (Schmahmann and Pandya, 2007), several recent post-mortem investigations have described this tract in the human brain (Ture et al., 2000; Kier et al., 2004; Burgel et al., 2006; Fernandez-Miranda et al., 2008; Lawes et al., 2008; Martino et al., 2010). While streamline tractography did not show IOFF terminations in the MTG, we did observe that IOFF fibers approached within a centimeter of the MTG cortex. It is possible that streamline tractography failed to resolve IOFF fibers entering the MTG by crossing the other major pathways in this region; high-angular resolution diffusion imaging techniques designed to trace fibers through regions with complex fiber architecture might be best suited for this task (Wedeen et al., 2008). Thus, it will be important to better characterize the relationship between the IOFF and the MTG in future investigations using new techniques.

A role for the IOFF in language has also been proposed by Duffau and colleagues (Duffau et al., 2005; Duffau, 2008) after finding that semantic paraphasias could be induced by electrical stimulation of the IOFF while patients undergoing neurosurgery performed a picture naming task. Their interpretation of this finding is that the IOFF may serve as the principal pathway for a ventral semantic system. We propose an extension of this idea. It is possible that the top-down control signals from BA 47 that modulate temporal lobe semantic selection processes are disrupted during IOFF stimulation, causing the semantic misnaming errors observed by Duffau and colleagues. Others have reported comprehension deficits in patients with thalamic infarcts that affect the temporal isthmus and adjacent peri-ventricular white matter (Naeser et al., 1982, 1987; Alexander et al., 1989). An interesting possibility, which can be tested with diffusion imaging data from patients with focal white matter lesions, is that the IOFF is affected as well in such cases, since IOFF fibers pass through the temporal isthmus, between the acoustic and optic radiations (Burgel et al., 2006).

Before reaching the frontal lobe, the IOFF passes between the insula and the putamen at the inferior level of the extreme and external capsules (Kier et al., 2004; Burgel et al., 2006; Fernandez-Miranda et al., 2008; Martino et al., 2010). Histological tracing studies in the monkey brain have revealed a pathway between the posterior superior temporal gyrus and monkey homologues of BA 44 and BA 45 in the IFG (Schmahmann and Pandya, 2006). These were later traced in the human brain with high-angular resolution diffusion imaging (Frey et al., 2008). Makris and Pandya (2009) also examined the trajectory of the frontal–posterior long association fibers through the extreme capsule in the human brain with streamline tractography, and found fibers extending to temporal, parietal, and occipital regions (Makris and Pandya, 2009, Figures 1C, 3 and 4). Saur et al. (2008, 2010) used probabilistic tractography to show a pathway through the EmC that links BA 47 and BA 45 with the most posterior extension of the MTG. These studies all describe fiber systems connecting temporal and frontal regions via an inferior pathway, which may contribute to language processing, Though they may not have been labeled as such, we believe all of the above investigations may have demonstrated fibers consistent with the IOFF, as their shape and trajectory are consistent with numerous fiber atlases and post-mortem examinations of the human brain (Ture et al., 2000; Catani et al., 2002; Mori et al., 2002, 2008; Kier et al., 2004; Burgel et al., 2006; Catani and Thiebaut de Schotten, 2008; Fernandez-Miranda et al., 2008; Lawes et al., 2008; Martino et al., 2010).

THE ARCUATE FASCICULUS AND LANGUAGE COMPREHENSION

The AF fibers that we found to be associated with the MTG are consistent with the emerging knowledge of this tract's anatomy; diffusion imaging investigations of the human brain indicate a considerably more complex architecture than traditional language models presume. In the temporal lobe, AF fibers have been found not only in the superior temporal gyrus but in the MTG as well (Powell et al., 2006; Glasser and Rilling, 2008; Rilling et al., 2008). Temporal projections to and from the parietal lobe have been identified via an indirect AF segment (Catani et al., 2005). Frontal terminations have extended beyond BA 44 and 45 into BA 47, BA 9, BA 46, and BA 6 (Rilling et al., 2008). Traditional language models that only consider the AF as connecting Broca's and Wernicke's areas overlook the other possible ways in which AF fibers could support language and related cognitive processes.

One of these alternative functions could fall in the realm of semantic integration. In our previous study, lesions in the MTG and underlying white matter were associated with severe lexical comprehension impairments (Dronkers et al., 2004). In the present study, the MTG ROI was found to include the AF, specifically the direct and indirect segments as described by Catani et al. (2005). Whether these middle temporal AF fibers are critical for lexical comprehension cannot be determined from the existing data. However, the present findings do suggest that fibers of this tract connecting to the MTG could support the integration of lexical-semantics with other cognitive and linguistic mechanisms that are also involved in language comprehension. Lexical–semantic integration is certainly not the only function of this tract. Among other functions, the AF has been proposed as a dorsal route for auditory-motor mapping (Saur et al., 2008, 2010) in accordance with a dual-stream model

which segregates phonological and semantic processing (Hickok and Poeppel, 2004). Most likely, the AF is a composite structure with multiple compartments specializing in transmitting different types of information. Whether this hypothesis is true is a question for future investigations.

OTHER OBSERVATIONS AND SOME QUESTIONS FOR FUTURE RESEARCH

The present study identified numerous major fiber pathways and functional connections that may form the backbone of the language comprehension network. Some of these structural and functional pathways and the cortical regions associated with them might be uniquely dedicated to auditory sentence comprehension. Another possibility is that each component of the language comprehension network might play multiple roles in the large-scale distributed neural systems that support different aspects of language and cognition. This possibility is suggested by the overlapping but distinct connectivity profiles that we found for each of the regions of interest.

What is specific to language comprehension might be the coordinated recruitment of these components to form a functional network to process verbal information. Thus, there are two important questions to be addressed in future investigations. One question is the precise delineation of the functional roles of individual fiber pathways and cortical regions in the language comprehension process. The other question is the characterization of the organizing principles that shape the overall architecture of the language comprehension network.

While several white matter pathways and cortical regions were found to be associated with the regions identified as being critical for comprehension by our earlier lesion-symptom analysis (Dronkers et al., 2004), the present findings do not establish which of these play essential roles. For instance, our findings suggest the involvement of the MdLF and the UF in language comprehension. However, surgical removal of parts of these pathways does not appear to elicit permanent language deficits (Duffau et al., 2009; De Witt Hamer et al., 2010). The fact that these structures were associated with our regions of interest does not necessarily mean that they support language comprehension *per se*. More information regarding the roles of these pathways may come from studies involving neurological patients.

Our functional connectivity findings implicate the right hemisphere homologues of key left hemisphere areas in the language comprehension network. Our tractography findings indicate that left hemisphere lesions that produce comprehension deficits affect temporo-temporal interhemispheric connections via the tapetum. Right hemisphere involvement in the language comprehension network (Just et al., 1996; Jung-Beeman, 2005) is another important question for future investigations.

Detailed analysis of neurological patient data with advanced imaging protocols will provide important clues as to the organization of this system, how it is affected by well-circumscribed lesions to its cortical and WM components, and the specific roles of each of these components in the overall functioning of the network. Combined analysis of data from healthy subjects and neurological patients will also play an important role (Turken et al., 2008). Further insights will also be gained by computer simulations of the effects of lesions in different parts of the language network to predict the functional impact of well-circumscribed brain lesions and to examine where the network might be most vulnerable to neurological damage (Achard et al., 2006; Kaiser et al., 2007; Nomura et al., 2010). Finally, better characterization of the language network and the relationship between lesion anatomy and behavioral disturbances will also allow a better characterization of patterns of recovery in aphasia, which is one of the key questions in behavioral neurology (Price, 2010).

LIMITATIONS

Each of the methods presented here naturally has its own limitations. The regions of interest that served as our starting point reflect the lesion-symptom mapping findings from only one study. While this study included a large a number of aphasic patients, there are certainly other lesion analyses and functional neuroimaging studies that can be used to identify and further refine regions of interest. The lesion findings were also restricted to the vascular territories affected in stroke. Therefore, cortical areas that emerged from the functional connectivity analysis, such as the dorso-medial frontal regions, would not have been identified in the patient findings. Structural and functional connectivity measures derived from *in vivo* magnetic resonance imaging data need to be interpreted with caution until they are fully validated with histological measures (Mesulam, 2009). While streamline tractography with DTI provides information on the trajectories of the core sections of major tracts, it cannot determine their cortical terminations with certainty (Hagmann et al., 2006). The utilization of established streamline tractography protocols in this investigation allowed us to identify the pathways associated with our earlier lesion findings in relation to DTI-based WM atlases (Catani and Thiebaut de Schotten, 2008; Mori et al., 2008), and to make predictions about the cortical destinations. Future investigations using high-angular resolution diffusion imaging protocols (Hagmann et al., 2008) and probabilistic tractography algorithms (Frey et al., 2008) can provide more precise mapping of these pathways. Resting-state functional connectivity reveals which regions exhibit coherent activity patterns, but cannot distinguish between monosynaptic and polysynaptic connections (Kelly et al., 2010). Despite such limitations, combining findings from neurological patients, with the newly available tools for assessing connectional anatomy of the brain, is a step in the right direction, both for understanding how language is organized in the brain, and for understanding the disorders that are caused by a disruption within the language network.

CONCLUSION

In this research, we analyzed the structural and functional connectivity of the brain regions found in our earlier investigation with aphasic patients to be critical for sentence comprehension. This analysis revealed a broadly distributed network of peri-sylvian and neighboring cortical association areas residing primarily, but not exclusively, in the left hemisphere and supported by numerous long-distance white matter pathways. These tracts span temporal, parietal, and frontal association cortices and provide a structural backbone for the language comprehension network, integrating the neural computations carried out by key cortical nodes. The additional finding of an extensive connectivity pattern underlying the left MTG answered an earlier question as to why lesions affecting these structures pro-

duce such severe and persisting comprehension deficits. The unique trajectories of the IOFF and the MTG compartment of the AF were also seen as novel additions to the network that supports language comprehension. Through the integration of three different methodologies – lesion analysis, white matter tractography, and resting state functional MRI – a vast network supporting language comprehension emerged, one far more extensive than previously thought, and one that may more accurately reflect the complexity of human language.

ACKNOWLEDGMENTS

This investigation was supported by a Department of Veterans Affairs CSR&D Career Development Award to And U. Turken, a CSR&D Research Career Scientist award to Nina F. Dronkers, and a grant from VA CSR&D Merit Review Program to Nina F. Dronkers and And U. Turken. We would like to thank the International Consortium for Brain Mapping (ICBM) and the Neuroimaging Informatics Tools and Resources Clearinghouse (NITRC) for making the diffusion and fMRI datasets that we have used in this research publicly available. We thank Susan Whitfield-Gabrieli for making the Functional Connectivity Toolbox available and for providing assistance in its use. Finally, we would like to thank members of the Center for Aphasia and Related Disorders, including Juliana Baldo, Shira Katseff, Carl Ludy, David Wilkins, Tim Justus, Analia Aravelo, and Janet Patterson for their input during the preparation of this manuscript, and Drs. Jeffrey R. Binder and Soo-Eun Chang for their insightful comments as reviewers.

REFERENCES

Achard, S., Salvador, R., Whitcher, B., Suckling, J., and Bullmore, E. (2006). A resilient, low-frequency, small-world human brain functional network with highly connected association cortical hubs. *J. Neurosci.* 26, 63–72.

Alexander, M. P., Hiltbrunner, B., and Fischer, R. S. (1989). Distributed anatomy of transcortical sensory aphasia. *Arch. Neurol.* 46, 885–892.

Anwander, A., Tittgemeyer, M., von Cramon, D. Y., Friederici, A. D., and Knosche, T. R. (2007). Connectivity-based parcellation of Broca's area. *Cereb. Cortex* 17, 816–825.

Ashburner, J., and Friston, K. J. (2005). Unified segmentation. *Neuroimage* 26, 839–851.

Basser, P. J. (1995). Inferring microstructural features and the physiological state of tissues from diffusion-weighted images. *NMR Biomed.* 8, 333–344.

Basser, P. J., Mattiello, J., and LeBihan, D. (1994). MR diffusion tensor spectroscopy and imaging. *Biophys. J.* 66, 259–267.

Basser, P. J., Pajevic, S., Pierpaoli, C., Duda, J., and Aldroubi, A. (2000). In vivo fiber tractography using DT-MRI data. *Magn. Reson. Med.* 44, 625–632.

Bates, E., Wilson, S. M., Saygin, A. P., Dick, F., Sereno, M. I., Knight, R. T., and Dronkers, N. F. (2003). Voxel-based lesion-symptom mapping. *Nat. Neurosci.* 6, 448–450.

Behzadi, Y., Restom, K., Liau, J., and Liu, T. T. (2007). A component based noise correction method (CompCor) for BOLD and perfusion based fMRI. *Neuroimage* 37, 90–101.

Binder, J. R. (2003). "Wernicke aphasia: a disorder of central language processing', in *Neurological Foundations of Cognitive Neuroscience*, ed. M. E. D'Esposito (Cambridge: The MIT Press), 75–238.

Binder, J. R., Desai, R. H., Graves, W. W., and Conant, L. L. (2009). Where is the semantic system? A critical review and meta-analysis of 120 functional neuroimaging studies. *Cereb. Cortex* 19, 2767–2796.

Binder, J. R., Frost, J. A., Hammeke, T. A., Cox, R. W., Rao, S. M., and Prieto, T. (1997). Human brain language areas identified by functional magnetic resonance imaging. *J. Neurosci.* 17, 353–362.

Biswal, B., Yetkin, F. Z., Haughton, V. M., and Hyde, J. S. (1995). Functional connectivity in the motor cortex of resting human brain using echo-planar MRI. *Magn. Reson. Med.* 34, 537–541.

Biswal, B. B., Mennes, M., Zuo, X. N., Gohel, S., Kelly, C., Smith, S. M., Beckmann, C. F., Adelstein, J. S., Buckner, R. L., Colcombe, S., Dogonowski, A. M., Ernst, M., Fair, D., Hampson, M., Hoptman, M. J., Hyde, J. S., Kiviniemi, V. J., Kotter, R., Li, S. J., Lin, C. P., Lowe, M. J., Mackay, C., Madden, D. J., Madsen, K. H., Margulies, D. S., Mayberg, H. S., McMahon, K., Monk, C. S., Mostofsky, S. H., Nagel, B. J., Pekar, J. J., Peltier, S. J., Petersen, S. E., Riedl, V., Rombouts, S. A., Rypma, B., Schlaggar, B. L., Schmidt, S., Seidler, R. D., Siegle, G. J., Sorg, C., Teng, G. J., Veijola, J., Villringer, A., Walter, M., Wang, L., Weng, X. C., Whitfield-Gabrieli, S., Williamson, P., Windischberger, C., Zang, Y. F., Zhang, H. Y., Castellanos, F. X., and Milham, M. P. (2010). Toward discovery science of human brain function. *Proc. Natl. Acad. Sci. U.S.A.* 107, 4734–4739.

Boatman, D., Gordon, B., Hart, J., Selnes, O., Miglioretti, D., and Lenz, F. (2000). Transcortical sensory aphasia: revisited and revised. *Brain* 123(Pt 8), 1634–1642.

Bogen, J. E., and Bogen, G. M. (1976). Wernicke's region-where is it? *Ann. N. Y. Acad. Sci.* 280, 834–843.

Bookheimer, S. (2002). Functional MRI of language: new approaches to understanding the cortical organization of semantic processing. *Annu. Rev. Neurosci.* 25, 151–188.

Brauer, J., Anwander, A., and Friederici, A. D. (2010). Neuroanatomical prerequisites for language functions in the maturing brain. *Cereb. Cortex* 41, 1484–1492.

Buckner, R. L., Sepulcre, J., Talukdar, T., Krienen, F. M., Liu, H., Hedden, T., Andrews-Hanna, J. R., Sperling, R. A., and Johnson, K. A. (2009). Cortical hubs revealed by intrinsic functional connectivity: mapping, assessment of stability, and relation to Alzheimer's disease. *J. Neurosci.* 29, 1860–1873.

Burgel, U., Amunts, K., Hoemke, L., Mohlberg, H., Gilsbach, J. M., and Zilles, K. (2006). White matter fiber tracts of the human brain: three-dimensional mapping at microscopic resolution, topography and intersubject variability. *Neuroimage* 29, 1092–1105.

Caplan, D., Hildebrandt, N., and Makris, N. (1996). Location of lesions in stroke patients with deficits in syntactic processing in sentence comprehension. *Brain* 119(Pt 3), 933–949.

Caplan, D., Waters, G., Kennedy, D., Alpert, N., Makris, N., Dede, G., Michaud, J., and Reddy, A. (2007). A study of syntactic processing in aphasia II: neurological aspects. *Brain Lang.* 101, 151–177.

Catani, M., Allin, M. P., Husain, M., Pugliese, L., Mesulam, M. M., Murray, R. M., and Jones, D. K. (2007). Symmetries in human brain language pathways correlate with verbal recall. *Proc. Natl. Acad. Sci. U.S.A.* 104, 17163–17168.

Catani, M., Howard, R. J., Pajevic, S., and Jones, D. K. (2002). Virtual in vivo interactive dissection of white matter fasciculi in the human brain. *Neuroimage* 17, 77–94.

Catani, M., Jones, D. K., and ffytche, D. H. (2005). Perisylvian language networks of the human brain. *Ann. Neurol.* 57, 8–16.

Catani, M., and Mesulam, M. (2008a). The arcuate fasciculus and the disconnection theme in language and aphasia: history and current state. *Cortex* 44, 953–961.

Catani, M., and Mesulam, M. (2008b). What is a disconnection syndrome? *Cortex* 44, 911–913.

Catani, M., and Thiebaut de Schotten, M. (2008). A diffusion tensor imaging tractography atlas for virtual in vivo dissections. *Cortex* 44, 1105–1132.

Conturo, T. E., Lori, N. F., Cull, T. S., Akbudak, E., Snyder, A. Z., Shimony, J. S., McKinstry, R. C., Burton, H., and Raichle, M. E. (1999). Tracking neuronal fiber pathways in the living human brain. *Proc. Natl. Acad. Sci. U.S.A.* 96, 10422–10427.

Croxson, P. L., Johansen-Berg, H., Behrens, T. E., Robson, M. D., Pinsk, M. A., Gross, C. G., Richter, W., Richter, M. C., Kastner, S., and Rushworth, M. F. (2005). Quantitative investigation of connections of the prefrontal cortex in the human and macaque using probabilistic diffusion tractography. *J. Neurosci.* 25, 8854–8866.

Curtiss, S., and Yamada, J. (1988). *Curtiss–Yamada Comprehensive Language Evaluation.* Unpublished test, UCLA.

Damasio, A. R. (1989). Time-locked multiregional retroactivation: a systems-level proposal for the neural substrates of recall and recognition. *Cognition* 33, 25–62.

Damasio, A. R. (1991). "Signs of aphasia," in *Acquired Aphasia*, 2nd Edn. ed. M. T. Sarno (San Diego, CA: Academic Press), 27–43.

Damasio, A. R. (1992). Aphasia. *N. Engl. J. Med.* 326, 531–539.

Damasio, A. R., and Damasio, H. (2002). *Principles of Behavioral and Cognitive Neurology*, 2nd Edn. New York: Oxford University Press.

Damoiseaux, J. S., Rombouts, S. A., Barkhof, F., Scheltens, P., Stam, C. J., Smith, S. M., and Beckmann, C. F. (2006). Consistent resting-state

networks across healthy subjects. *Proc. Natl. Acad. Sci. U.S.A.* 103, 13848–13853.

Dancause, N., Barbay, S., Frost, S. B., Plautz, E. J., Chen, D., Zoubina, E. V., Stowe, A. M., and Nudo, R. J. (2005). Extensive cortical rewiring after brain injury. *J. Neurosci.* 25, 10167–10179.

De Witt Hamer, P. C., Moritz-Gasser, S., Gatignol, P., and Duffau, H. (2010). Is the human left middle longitudinal fascicle essential for language? A brain electrostimulation study. *Hum. Brain Mapp.*

DeArmond, S. J., Fusco, M. M., and Dewey, M. M. (1989). *Structure of the Human Brain: A Photographic Atlas.* New York: Oxford University Press.

Demb, J. B., Desmond, J. E., Wagner, A. D., Vaidya, C. J., Glover, G. H., and Gabrieli, J. D. (1995). Semantic encoding and retrieval in the left inferior prefrontal cortex: a functional MRI study of task difficulty and process specificity. *J. Neurosci.* 15, 5870–5878.

Demonet, J. F., Chollet, F., Ramsay, S., Cardebat, D., Nespoulous, J. L., Wise, R., Rascol, A., and Frackowiak, R. (1992). The anatomy of phonological and semantic processing in normal subjects. *Brain* 115(Pt 6), 1753–1768.

Desikan, R. S., Segonne, F., Fischl, B., Quinn, B. T., Dickerson, B. C., Blacker, D., Buckner, R. L., Dale, A. M., Maguire, R. P., Hyman, B. T., Albert, M. S., and Killiany, R. J. (2006). An automated labeling system for subdividing the human cerebral cortex on MRI scans into gyral based regions of interest. *Neuroimage* 31, 968–980.

Dosenbach, N. U., Fair, D. A., Miezin, F. M., Cohen, A. L., Wenger, K. K., Dosenbach, R. A., Fox, M. D., Snyder, A. Z., Vincent, J. L., Raichle, M. E., Schlaggar, B. L., and Petersen, S. E. (2007). Distinct brain networks for adaptive and stable task control in humans. *Proc. Natl. Acad. Sci. U.S.A.* 104, 11073–11078.

Dronkers, N. F. (2000). The pursuit of brain–language relationships. *Brain Lang.* 71, 59–61.

Dronkers, N., Pinker, S., and Damasio, A. R., (2000a). "Language and the aphasias," in *Principles in Neural Science*, 4th Edn. eds E. R. Kandel, J. Schwartz, and T. Jessell (New York: McGraw-Hill), 1169–1187.

Dronkers, N. F., Redfern, B. B., and Knight, R. T., (2000b). "The neural architecture of language disorders," in *The New Cognitive Neurosciences*, ed. M. S. Gazzaniga (Cambridge: The MIT Press), 949–958.

Dronkers, N. F., Redfern, B. B., and Ludy, C. A. (1995). Lesion localization in chronic Wernicke's aphasia. *Brain Lang.* 51, 62–65.

Dronkers, N. F., Wilkins, D. P., Van Valin, R. D. J., Redfern, B. B., and Jaeger, J. J. (1994). A reconsideration of the brain areas involved in the disruption of morphosyntactic comprehension. *Brain Lang.* 47, 461–463.

Dronkers, N. F., Wilkins, D. P., Van Valin, R. D. Jr., Redfern, B. B., and Jaeger, J. J. (2004). Lesion analysis of the brain areas involved in language comprehension. *Cognition* 92, 145–177.

Duffau, H. (2008). The anatomo-functional connectivity of language revisited. New insights provided by electrostimulation and tractography. *Neuropsychologia* 46, 927–934.

Duffau, H., Gatignol, P., Mandonnet, E., Peruzzi, P., Tzourio-Mazoyer, N., and Capelle, L. (2005). New insights into the anatomo-functional connectivity of the semantic system: a study using cortico-subcortical electrostimulations. *Brain* 128, 797–810.

Duffau, H., Gatignol, P., Moritz-Gasser, S., and Mandonnet, E. (2009). Is the left uncinate fasciculus essential for language? A cerebral stimulation study. *J. Neurol.* 256, 382–389.

Duffau, H., Peggy Gatignol, S. T., Mandonnet, E., Capelle, L., and Taillandier, L. (2008). Intraoperative subcortical stimulation mapping of language pathways in a consecutive series of 115 patients with grade II glioma in the left dominant hemisphere. *J. Neurosurg.* 109, 461–471.

Fernandez-Miranda, J. C., Rhoton, A. L., Jr., Alvarez-Linera, J., Kakizawa, Y., Choi, C., and de Oliveira, E. P. (2008). Three-dimensional microsurgical and tractographic anatomy of the white matter of the human brain. *Neurosurgery* 62, 989–1026; discussion 1026–1028.

Ferstl, E. C., Neumann, J., Bogler, C., and von Cramon, D. Y. (2008). The extended language network: a meta-analysis of neuroimaging studies on text comprehension. *Hum. Brain Mapp.* 29, 581–593.

Fillard, P., Pennec, X., Arsigny, V., and Ayache, N. (2007). Clinical DT-MRI estimation, smoothing, and fiber tracking with log-Euclidean metrics. *IEEE Trans. Med. Imaging* 26, 1472–1482.

Fox, M. D., Snyder, A. Z., Vincent, J. L., Corbetta, M., Van Essen, D. C., and Raichle, M. E. (2005). The human brain is intrinsically organized into dynamic, anticorrelated functional networks. *Proc. Natl. Acad. Sci. U.S.A.* 102, 9673–9678.

Frey, S., Campbell, J. S., Pike, G. B., and Petrides, M. (2008). Dissociating the human language pathways with high angular resolution diffusion fiber tractography. *J. Neurosci.* 28, 11435–11444.

Friederici, A. D. (2002). Towards a neural basis of auditory sentence processing. *Trends Cogn. Sci.* 6, 78–84.

Friederici, A. D. (2009). Pathways to language: fiber tracts in the human brain. *Trends Cogn. Sci.* 13, 175–181.

Gabrieli, J. D., Poldrack, R. A., and Desmond, J. E. (1998). The role of left prefrontal cortex in language and memory. *Proc. Natl. Acad. Sci. U.S.A.* 95, 906–913.

Geschwind, N. (1965a). Disconnexion syndromes in animals and man. I. *Brain* 88, 237–294.

Geschwind, N. (1965b). Disconnexion syndromes in animals and man. II. *Brain* 88, 585–644.

Geschwind, N. (1970). The organization of language and the brain. *Science* 170, 940–944.

Geschwind, N. (1972). Language and the brain. *Sci. Am.* 226, 76–83.

Glasser, M. F., and Rilling, J. K. (2008). DTI tractography of the human brain's language pathways. *Cereb. Cortex* 18, 2471–2482.

Goodglass, H. (1993). *Understanding Aphasia.* San Diego: Academic Press.

Greicius, M. D., Krasnow, B., Reiss, A. L., and Menon, V. (2003). Functional connectivity in the resting brain: a network analysis of the default mode hypothesis. *Proc. Natl. Acad. Sci. U.S.A.* 100, 253–258.

Hagmann, P., Cammoun, L., Gigandet, X., Meuli, R., Honey, C. J., Wedeen, V. J., and Sporns, O. (2008). Mapping the structural core of human cerebral cortex. *PLoS Biol.* 6, e159. doi:10.1371/journal.pbio.0060159

Hagmann, P., Jonasson, L., Maeder, P., Thiran, J. P., Wedeen, V. J., and Meuli, R. (2006). Understanding diffusion MR imaging techniques: from scalar diffusion-weighted imaging to diffusion tensor imaging and beyond. *Radiographics* 26(Suppl. 1), S205–S223.

Hagoort, P., Hald, L., Bastiaansen, M., and Petersson, K. M. (2004). Integration of word meaning and world knowledge in language comprehension. *Science* 304, 438–441.

Hampson, M., Peterson, B. S., Skudlarski, P., Gatenby, J. C., and Gore, J. C. (2002). Detection of functional connectivity using temporal correlations in MR images. *Hum. Brain Mapp.* 15, 247–262.

Hart, J. Jr., and Gordon, B. (1990). Delineation of single-word semantic comprehension deficits in aphasia, with anatomical correlation. *Ann. Neurol.* 27, 226–231.

He, B. J., Snyder, A. Z., Vincent, J. L., Epstein, A., Shulman, G. L., and Corbetta, M. (2007). Breakdown of functional connectivity in frontoparietal networks underlies behavioral deficits in spatial neglect. *Neuron* 53, 905–918.

Heiss, W. D., Thiel, A., Kessler, J., and Herholz, K. (2003). Disturbance and recovery of language function: correlates in PET activation studies. *Neuroimage* 20(Suppl. 1), S42–S49.

Hickok, G., and Poeppel, D. (2004). Dorsal and ventral streams: a framework for understanding aspects of the functional anatomy of language. *Cognition* 92, 67–99.

Hillis, A. E., Boatman, D., Hart, J., and Gordon, B. (1999). Making sense out of jargon: a neurolinguistic and computational account of jargon aphasia. *Neurology* 53, 1813–1824.

Hua, K., Oishi, K., Zhang, J., Wakana, S., Yoshioka, T., Zhang, W., Akhter, K. D., Li, X., Huang, H., Jiang, H., van Zijl, P., and Mori, S. (2009). Mapping of functional areas in the human cortex based on connectivity through association fibers. *Cereb. Cortex* 19, 1889–1895.

Hua, K., Zhang, J., Wakana, S., Jiang, H., Li, X., Reich, D. S., Calabresi, P. A., Pekar, J. J., van Zijl, P. C., and Mori, S. (2008). Tract probability maps in stereotaxic spaces: analyses of white matter anatomy and tract-specific quantification. *Neuroimage* 39, 336–347.

Jung-Beeman, M. (2005). Bilateral brain processes for comprehending natural language. *Trends Cogn. Sci.* 9, 512–518.

Just, M. A., Carpenter, P. A., Keller, T. A., Eddy, W. F., and Thulborn, K. R. (1996). Brain activation modulated by sentence comprehension. *Science* 274, 114–116.

Kaiser, M., Martin, R., Andras, P., and Young, M. P. (2007). Simulation of robustness against lesions of cortical networks. *Eur. J. Neurosci.* 25, 3185–3192.

Kaplan, E., Naeser, M. A., Martin, P. I., Ho, M., Wang, Y., Baker, E., and Pascual-Leone, A. (2010). Horizontal portion of arcuate fasciculus fibers track to pars opercularis, not pars triangularis, in right and left hemispheres: a DTI study. *Neuroimage* 52, 436–444.

Kelly, C., Uddin, L. Q., Shehzad, Z., Margulies, D. S., Castellanos, F. X., Milham, M. P., and Petrides, M. (2010). Broca's region: linking human brain functional connectivity data and non-human primate tracing anatomy studies. *Eur. J. Neurosci.* 32, 383–398.

Kertesz, A. (1982). *Western Aphasia Battery.* New York: Grune and Stratton.

Kertesz, A., Harlock, W., and Coates, R. (1979). Computer tomographic localization, lesion size, and prognosis in aphasia and nonverbal impairment. *Brain Lang.* 8, 34–50.

Kertesz, A., Lau, W. K., and Polk, M. (1993). The structural determinants of

recovery in Wernicke's aphasia. *Brain Lang.* 44, 153–164.
Kertesz, A., Sheppard, A., and MacKenzie, R. (1982). Localization in transcortical sensory aphasia. *Arch. Neurol.* 39, 475–478.
Kier, E. L., Staib, L. H., Davis, L. M., and Bronen, R. A. (2004). MR imaging of the temporal stem: anatomic dissection tractography of the uncinate fasciculus, inferior occipitofrontal fasciculus, and Meyer's loop of the optic radiation. *AJNR Am. J. Neuroradiol.* 25, 677–691.
Koyama, M. S., Kelly, C., Shehzad, Z., Penesetti, D., Castellanos, F. X., and Milham, M. P. (2010). Reading networks at rest. *Cereb. Cortex* 10, 2549–2559.
Lawes, I. N., Barrick, T. R., Murugam, V., Spierings, N., Evans, D. R., Song, M., and Clark, C. A. (2008). Atlas-based segmentation of white matter tracts of the human brain using diffusion tensor tractography and comparison with classical dissection. *Neuroimage* 39, 62–79.
Lichtheim, L. (1885). On aphasia. *Brain* 7, 433–484.
Lowe, M. J., Mock, B. J., and Sorenson, J. A. (1998). Functional connectivity in single and multislice echoplanar imaging using resting-state fluctuations. *Neuroimage* 7, 119–132.
Makris, N., Kennedy, D. N., McInerney, S., Sorensen, A. G., Wang, R., Caviness, V. S., Jr., and Pandya, D. N. (2005). Segmentation of subcomponents within the superior longitudinal fascicle in humans: a quantitative, in vivo, DT-MRI study. *Cereb. Cortex* 15, 854–869.
Makris, N., and Pandya, D. N. (2009). The extreme capsule in humans and rethinking of the language circuitry. *Brain Struct. Funct.* 213, 343–358.
Makris, N., Papadimitriou, G. M., Kaiser, J. R., Sorg, S., Kennedy, D. N., and Pandya, D. N. (2009). Delineation of the middle longitudinal fascicle in humans: a quantitative, in vivo, DT-MRI study. *Cereb. Cortex* 19, 777–785.
Margulies, D. S., Vincent, J. L., Kelly, C., Lohmann, G., Uddin, L. Q., Biswal, B. B., Villringer, A., Castellanos, F. X., Milham, M. P., and Petrides, M. (2009). Precuneus shares intrinsic functional architecture in humans and monkeys. *Proc. Natl. Acad. Sci. U.S.A.* 106, 20069–20074.
Marsh, E. B., and Hillis, A. E. (2006). Recovery from aphasia following brain injury: the role of reorganization. *Prog. Brain Res.* 157, 143–156.
Martino, J., Brogna, C., Robles, S. G., Vergani, F., and Duffau, H. (2010). Anatomic dissection of the inferior fronto-occipital fasciculus revisited in the lights of brain stimulation data. *Cortex* 46, 691–699.
Mesulam, M. (2005). Imaging connectivity in the human cerebral cortex: the next frontier? *Ann. Neurol.* 57, 5–7.
Mesulam, M. (2009). Defining neurocognitive networks in the BOLD new world of computed connectivity. *Neuron* 62, 1–3.
Mesulam, M. M. (1990). Large-scale neurocognitive networks and distributed processing for attention, language, and memory. *Ann. Neurol.* 28, 597–613.
Mesulam, M. M. (1998). From sensation to cognition. *Brain* 121(Pt 6), 1013–1052.
Mori, S., Kaufmann, W. E., Davatzikos, C., Stieltjes, B., Amodei, L., Fredericksen, K., Pearlson, G. D., Melhem, E. R., Solaiyappan, M., Raymond, G. V., Moser, H. W., and van Zijl, P. C. (2002). Imaging cortical association tracts in the human brain using diffusion-tensor-based axonal tracking. *Magn. Reson. Med.* 47, 215–223.
Mori, S., Oishi, K., Jiang, H., Jiang, L., Li, X., Akhter, K., Hua, K., Faria, A. V., Mahmood, A., Woods, R., Toga, A. W., Pike, G. B., Neto, P. R., Evans, A., Zhang, J., Huang, H., Miller, M. I., van Zijl, P., and Mazziotta, J. (2008). Stereotaxic white matter atlas based on diffusion tensor imaging in an ICBM template. *Neuroimage* 40, 570–582.
Murphy, T. H., and Corbett, D. (2009). Plasticity during stroke recovery: from synapse to behaviour. *Nat. Rev. Neurosci.* 10, 861–872.
Naeser, M. A., Alexander, M. P., Helm-Estabrooks, N., Levine, H. L., Laughlin, S. A., and Geschwind, N. (1982). Aphasia with predominantly subcortical lesion sites: description of three capsular/putaminal aphasia syndromes. *Arch. Neurol.* 39, 2–14.
Naeser, M. A., Helm-Estabrooks, N., Haas, G., Auerbach, S., and Srinivasan, M. (1987). Relationship between lesion extent in "Wernicke's area" on computed tomographic scan and predicting recovery of comprehension in Wernicke's aphasia. *Arch. Neurol.* 44, 73–82.
Nomura, E. M., Gratton, C., Visser, R. M., Kayser, A., Perez, F., and D'Esposito, M. (2010). Double dissociation of two cognitive control networks in patients with focal brain lesions. *Proc. Natl. Acad. Sci. U.S.A.* 107, 12017–12022.
Oishi, K., Zilles, K., Amunts, K., Faria, A., Jiang, H., Li, X., Akhter, K., Hua, K., Woods, R., Toga, A. W., Pike, G. B., Rosa-Neto, P., Evans, A., Zhang, J., Huang, H., Miller, M. I., van Zijl, P. C., Mazziotta, J., and Mori, S. (2008). Human brain white matter atlas: identification and assignment of common anatomical structures in superficial white matter. *Neuroimage* 43, 447–457.
Parker, G. J., Luzzi, S., Alexander, D. C., Wheeler-Kingshott, C. A., Ciccarelli, O., and Lambon Ralph, M. A. (2005). Lateralization of ventral and dorsal auditory-language pathways in the human brain. *Neuroimage* 24, 656–666.
Petrides, M., and Pandya, D. N. (1988). Association fiber pathways to the frontal cortex from the superior temporal region in the rhesus monkey. *J. Comp. Neurol.* 273, 52–66.
Petrides, M., and Pandya, D. N. (2006). Efferent association pathways originating in the caudal prefrontal cortex in the macaque monkey. *J. Comp. Neurol.* 498, 227–251.
Petrides, M., and Pandya, D. N. (2009). Distinct parietal and temporal pathways to the homologues of Broca's area in the monkey. *PLoS Biol.* 7, e1000170. doi: 10.1371/journal.pbio.1000170
Pierpaoli, C., Jezzard, P., Basser, P. J., Barnett, A., and Di Chiro, G. (1996). Diffusion tensor MR imaging of the human brain. *Radiology* 201, 637–648.
Poldrack, R. A., Wagner, A. D., Prull, M. W., Desmond, J. E., Glover, G. H., and Gabrieli, J. D. (1999). Functional specialization for semantic and phonological processing in the left inferior prefrontal cortex. *Neuroimage* 10, 15–35.
Powell, H. W., Parker, G. J., Alexander, D. C., Symms, M. R., Boulby, P. A., Wheeler-Kingshott, C. A., Barker, G. J., Noppeney, U., Koepp, M. J., and Duncan, J. S. (2006). Hemispheric asymmetries in language-related pathways: a combined functional MRI and tractography study. *Neuroimage* 32, 388–399.
Price, C. J. (2000). The anatomy of language: contributions from functional neuroimaging. *J. Anat.* 197(Pt 3), 335–359.
Price, C. J. (2010). The anatomy of language: a review of 100 fMRI studies published in 2009. *Ann. N. Y. Acad. Sci.* 1191, 62–88.
Rilling, J. K., Glasser, M. F., Preuss, T. M., Ma, X., Zhao, T., Hu, X., and Behrens, T. E. (2008). The evolution of the arcuate fasciculus revealed with comparative DTI. *Nat. Neurosci.* 11, 426–428.
Rilling, J. K., and Seligman, R. A. (2002). A quantitative morphometric comparative analysis of the primate temporal lobe. *J. Hum. Evol.* 42, 505–533.
Saur, D., Kreher, B. W., Schnell, S., Kummerer, D., Kellmeyer, P., Vry, M. S., Umarova, R., Musso, M., Glauche, V., Abel, S., Huber, W., Rijntjes, M., Hennig, J., and Weiller, C. (2008). Ventral and dorsal pathways for language. *Proc. Natl. Acad. Sci. U.S.A.* 105, 18035–18040.
Saur, D., Schelter, B., Schnell, S., Kratochvil, D., Kupper, H., Kellmeyer, P., Kummerer, D., Kloppel, S., Glauche, V., Lange, R., Mader, W., Feess, D., Timmer, J., and Weiller, C. (2010). Combining functional and anatomical connectivity reveals brain networks for auditory language comprehension. *Neuroimage* 49, 3187–3197.
Schmahmann, J. D., and Pandya, D. N. (2006). *Fiber Pathways of the Brain.* Oxford; NY: Oxford University Press.
Schmahmann, J. D., and Pandya, D. N. (2007). Cerebral white matter-historical evolution of facts and notions concerning the organization of the fiber pathways of the brain. *J. Hist. Neurosci.* 16, 237–267.
Schmahmann, J. D., and Pandya, D. N. (2008). Disconnection syndromes of basal ganglia, thalamus, and cerebrocerebellar systems. *Cortex* 44, 1037–1066.
Schmahmann, J. D., Pandya, D. N., Wang, R., Dai, G., D'Arceuil, H. E., de Crespigny, A. J., and Wedeen, V. J. (2007). Association fibre pathways of the brain: parallel observations from diffusion spectrum imaging and autoradiography. *Brain* 130, 630–653.
Seltzer, B., and Pandya, D. N. (1984). Further observations on parieto-temporal connections in the rhesus monkey. *Exp. Brain Res.* 55, 301–312.
Seltzer, B., and Pandya, D. N. (1994). Parietal, temporal, and occipital projections to cortex of the superior temporal sulcus in the rhesus monkey: a retrograde tracer study. *J. Comp. Neurol.* 343, 445–463.
Shehzad, Z., Kelly, A. M., Reiss, P. T., Gee, D. G., Gotimer, K., Uddin, L. Q., Lee, S. H., Margulies, D. S., Roy, A. K., Biswal, B. B., Petkova, E., Castellanos, F. X., and Milham, M. P. (2009). The resting brain: unconstrained yet reliable. *Cereb. Cortex* 19, 2209–2229.
Thompson-Schill, S. L., D'Esposito, M., Aguirre, G. K., and Farah, M. J. (1997). Role of left inferior prefrontal cortex in retrieval of semantic knowledge: a reevaluation. *Proc. Natl. Acad. Sci. U.S.A.* 94, 14792–14797.
Ture, U., Yasargil, M. G., Friedman, A. H., and Al-Mefty, O. (2000). Fiber dissection technique: lateral aspect of the brain. *Neurosurgery* 47, 417–426; discussion 426–417.
Turken, A., Whitfield-Gabrieli, S., Bammer, R., Baldo, J. V., Dronkers, N. F., and Gabrieli, J. D. (2008). Cognitive processing speed and the structure of white matter pathways: convergent evidence from normal variation and lesion studies. *Neuroimage* 42, 1032–1044.

Tyler, L. K., and Marslen-Wilson, W. (2008). Fronto-temporal brain systems supporting spoken language comprehension. *Philos. Trans. R. Soc. Lond., B, Biol. Sci.* 363, 1037–1054.

Tzourio-Mazoyer, N., Landeau, B., Papathanassiou, D., Crivello, F., Etard, O., Delcroix, N., Mazoyer, B., and Joliot, M. (2002). Automated anatomical labeling of activations in SPM using a macroscopic anatomical parcellation of the MNI MRI single-subject brain. *Neuroimage* 15, 273–289.

Van Dijk, K. R., Hedden, T., Venkataraman, A., Evans, K. C., Lazar, S. W., and Buckner, R. L. (2010). Intrinsic functional connectivity as a tool for human connectomics: theory, properties, and optimization. *J. Neurophysiol.* 103, 297–321.

Vernooij, M. W., Smits, M., Wielopolski, P. A., Houston, G. C., Krestin, G. P., and van der Lugt, A. (2007). Fiber density asymmetry of the arcuate fasciculus in relation to functional hemispheric language lateralization in both right- and left-handed healthy subjects: a combined fMRI and DTI study. *Neuroimage* 35, 1064–1076.

Vigneau, M., Beaucousin, V., Herve, P. Y., Duffau, H., Crivello, F., Houde, O., Mazoyer, B., and Tzourio-Mazoyer, N. (2006). Meta-analyzing left hemisphere language areas: phonology, semantics, and sentence processing. *Neuroimage* 30, 1414–1432.

Vincent, J. L., Patel, G. H., Fox, M. D., Snyder, A. Z., Baker, J. T., Van Essen, D. C., Zempel, J. M., Snyder, L. H., Corbetta, M., and Raichle, M. E. (2007). Intrinsic functional architecture in the anaesthetized monkey brain. *Nature* 447, 83–86.

Wakana, S., Caprihan, A., Panzenboeck, M. M., Fallon, J. H., Perry, M., Gollub, R. L., Hua, K., Zhang, J., Jiang, H., Dubey, P., Blitz, A., van Zijl, P., and Mori, S. (2007). Reproducibility of quantitative tractography methods applied to cerebral white matter. *Neuroimage* 36, 630–644.

Wakana, S., Jiang, H., Nagae-Poetscher, L. M., van Zijl, P. C., and Mori, S. (2004). Fiber tract-based atlas of human white matter anatomy. *Radiology* 230, 77–87.

Wang, R., Benner, T., Sorensen, A. G., and Weeden, V. J. (2007). "Diffusion toolkit: a software package for diffusion imaging data processing and Ttactography," in *Annual Meeting of the International Society for Magnetic Resonance Medicine*, Berlin.

Ward, N. S. (2005). Plasticity and the functional reorganization of the human brain. *Int. J. Psychophysiol.* 58, 158–161.

Wedeen, V. J., Wang, R. P., Schmahmann, J. D., Benner, T., Tseng, W. Y., Dai, G., Pandya, D. N., Hagmann, P., D'Arceuil, H., and de Crespigny, A. J. (2008). Diffusion spectrum magnetic resonance imaging (DSI) tractography of crossing fibers. *Neuroimage* 41, 1267–1277.

Wernicke, C. (1874). *Der aphasische Symptomenkomplex.* Breslau: Cohn and Weigert.

Xiang, H. D., Fonteijn, H. M., Norris, D. G., and Hagoort, P. (2010). Topographical functional connectivity pattern in the perisylvian language networks. *Cereb. Cortex* 20, 549–560.

Zhang, W., Olivi, A., Hertig, S. J., van Zijl, P., and Mori, S. (2008). Automated fiber tracking of human brain white matter using diffusion tensor imaging. *Neuroimage* 42, 771–777.

Conflict of Interest Statement: The authors declare that the research was conducted in the absence of any commercial or financial relationships that could be construed as a potential conflict of interest.

Received: 03 November 2010; accepted: 03 January 2011; published online: 10 February 2011.

Citation: Turken AU and Dronkers NF (2011) The neural architecture of the language comprehension network: converging evidence from lesion and connectivity analyses. Front. Syst. Neurosci. ***5****:1. doi: 10.3389/fnsys.2011.00001*

Copyright © 2011 Turken and Dronkers. This is an open-access article subject to an exclusive license agreement between the authors and Frontiers Media SA, which permits unrestricted use, distribution, and reproduction in any medium, provided the original authors and source are credited.

frontiers in
SYSTEMS NEUROSCIENCE

ORIGINAL RESEARCH ARTICLE
published: 02 December 2010
doi: 10.3389/fnsys.2010.00156

Greater pre-stimulus effective connectivity *from* the left inferior frontal area to other areas is associated with better phonological decoding in dyslexic readers

Richard E. Frye[1]*, Meng-Hung Wu[2], Jacqueline Liederman[3] and Janet McGraw Fisher[4]

[1] *Department of Pediatrics, Division of Child and Adolescent Neurology and the Children's Learning Institute, University of Texas Health Science Center, Houston, TX, USA*
[2] *Department of Computer Science, University of Houston, Houston, TX, USA*
[3] *Department of Psychology, Boston University, Boston, MA, USA*
[4] *Department of Psychology, State University of New York Westchester County, Westchester, NY, USA*

Edited by:
Barry Horwitz, National Institutes of Health, USA

Reviewed by:
Ben Xu, National Institutes of Health, USA
Jason Smith, National Institutes of Health, USA

***Correspondence:**
Richard E. Frye, Department of Pediatrics, University of Texas Health Science Center, 7000 Fannin—UCT 2478, Houston, TX 77030, USA
e-mail: richard.e.frye@uth.tmc.edu

Functional neuroimaging studies suggest that neural networks that subserve reading are organized differently in dyslexic readers (DRs) and typical readers (TRs), yet the hierarchical structure of these networks has not been well studied. We used Granger causality to examine the effective connectivity of the preparatory network that occurs prior to viewing a non-word stimulus that requires phonological decoding in 7 DRs and 10 TRs who were young adults. The neuromagnetic activity that occurred 500 ms prior to each rhyme trial was analyzed from sensors overlying the left and right inferior frontal areas (IFA), temporoparietal areas, and ventral occipital–temporal areas within the low, medium, and high beta and gamma sub-bands. A mixed-model analysis determined whether connectivity to or from the left and right IFAs differed across connectivity direction (into vs. out of the IFAs), brain areas, reading group, and/or performance. Results indicated that greater connectivity in the low beta sub-band *from* the left IFA *to* other cortical areas was significantly related to better non-word rhyme discrimination in DRs but not TRs. This suggests that the left IFA is an important cortical area involved in compensating for poor phonological function in DRs. We suggest that the left IFA activates a wider-than usual network prior to each trial in the service of supporting otherwise effortful phonological decoding in DRs. The fact that the left IFA provides top-down activation to both posterior left hemispheres areas used by TRs for phonological decoding and homologous right hemisphere areas is discussed. In contrast, within the high gamma sub-band, *better* performance was associated with *decreased* connectivity between the left IFA and other brain areas, in both reading groups. Overly strong gamma connectivity during the pre-stimulus period may interfere with subsequent transient activation and deactivation of sub-networks once the non-word appears.

Keywords: Granger causality, effective connectivity, magnetoencephalography, reading, dyslexia, top-down, compensatory mechanisms

INTRODUCTION

Developmental dyslexia is the most common learning disorder worldwide, affecting both children and adults with a prevalence ranging up to 17.5% (Shaywitz, 1998). Dyslexia is a lifelong disorder with a wide variability in prognosis regardless of the quality of remediation. Reading disability may be represented on a continuum of severity with multiple genetic and environmental risk factors interacting to result in the phenotype known as dyslexia (Pennington and Lefly, 2001; Snowling, 2008). Individuals with developmental dyslexia have atypical patterns of cortical folding and migrational anomalies, both of which are consistent with a prenatal origin of dyslexia (Galaburda et al., 1985; Kaufmann and Galaburda, 1989; Humphreys et al., 1990; Frye et al., 2010a). Many neuroimaging studies have compared patterns of functional activation between dyslexic readers (DRs) and typical readers (TRs). Three regions of the brain that are often atypically activated in DRs as compared to TRs, include the inferior frontal areas (IFAs), the temporoparietal areas (TPAs) and the ventral occipital–temporal areas (VOTAs; Pugh et al., 2000a). This study will focus on the IFAs and its connection to these other two brain areas.

FUNCTIONAL ACTIVATION OF THE INFERIOR FRONTAL AREA IN DYSLEXIC READERS

The IFA has been reported to have abnormal activation in DRs as compared to TRs in several studies. However, differences in IFA activation between DRs and TRs during phonological word decoding tasks are not consistent across studies. Functional magnetic resonance imaging (fMRI) studies have reported over-activation of the left IFA (Hoeft et al., 2007; MacSweeney et al., 2009), the right IFA (Shaywitz et al., 2003), or neither IFA (Eden et al., 2004; Hoeft et al., 2006; Richards et al., 2007; MacSweeney et al., 2009) in DRs as compare to TRs during phonological word decoding tasks. Other fMRI studies have found underactivation of the IFA in DRs as compared to TRs during phonological word decoding tasks (Aylward et al., 2003; Cao et al., 2006). In fact, two meta-analyses

of fMRI studies have not verified a consistent increase or decrease in activation of either the left or right IFAs (Maisog et al., 2008; Richlan et al., 2009).

In contrast to fMRI studies, magnetoencephalography (MEG) studies have suggested that it is not the amount of activation *per se* that is different between DRs and TRs, but the timing of the activation. For example, the onset of TPA activity preceded the onset of IFA activity for TRs while the onset of activity for the IFA and TPA were not different for DRs before an intervention (Simos et al., 2007).

The inconsistent findings for IFA activation may be related to variation in the characteristics of the participants, in particular, the level of remediation. Indeed, it has been repeatedly reported in fMRI studies that IFA activity increases following remediation (Richards et al., 2002; Temple et al., 2003; Eden et al., 2004). This could suggest that IFA activity has a key role in enabling better phonological function in DRs. In addition, fMRI studies have shown that IFA activity increases from childhood to adulthood for DRs but not TRs, suggesting that the maturation of the IFA occurs along a different trajectory in DRs and TRs (Brunswick et al., 1999; Shaywitz et al., 2007). It is noteworthy that the developmental increase in IFA activity from childhood through adolescence into adulthood for DRs corresponds to the course of phonological skill development for DRs that succeed in developing adequate phonological decoding skills (Miller-Shaul, 2005; Svensson and Jacobson, 2006). Thus, improvement in phonological across this time period might be related to IFA maturation.

Timing of the onset of IFA activity may also be related to remediation. In DRs, the onset of activity for the IFA and TPA were not different before remediation. After remediation TPA activity preceded IFA activity in DRs the way it usually does in TRs (Simos et al., 2006, 2007). However, the number of dipoles, the MEG measure of functional activation, in the IFA did not change after remediation for those participants that responded to the remediation therapy (Simos et al., 2006, 2007). These studies suggest that the IFA plays an integral role in phonological function, especially in the improvement of phonological function over time and with remediation, in DRs. However, there also appear to be discrepancies in functional activation between fMRI and MEG studies.

The involvement of the IFA in DRs may also be important since it subserves several aspects of executive function including inhibition and switching (Kenner et al., 2010), analogical reasoning (Hampshire et al., 2010), and updating (Tamnes et al., 2010). This is of special interest because several lines of evidence point to problems with executive function in DRs. For example, deficits in working memory (Willcutt et al., 2001; Gioia et al., 2002), planning and organization (Gioia et al., 2002), set shifting and organization (Narhi et al., 1997), inhibition (Willcutt et al., 2005), sequencing (Brosnan et al., 2002), and problem solving (Lazar and Frank, 1998) have been documented in DRs. In fact, dysfunction of the executive attentional system has recently been implicated in relation to reading ability in DRs (Shaywitz and Shaywitz, 2008). Interestingly, the IFA may have an executive role specific to language as it has been shown to be involved in regulating language networks and word learning (Pugh et al., 2000a; Aron and Poldrack, 2005). Moreover, recent studies have shown that top-down regulation of the language system from the IFA develops during childhood in TRs (Bitan et al., 2009).

FUNCTIONAL CONNECTIVITY IN NORMAL AND DYSLEXIC READERS

As opposed to just studying regions of activation and deactivation, functional connectivity has been used to illuminate how subsystems interact to enable reading. One landmark study used positron emission tomography (PET) during single word reading of exception words or pseudowords. Correlational analyses were computed within task, between regions, and across subjects (Horwitz et al., 1998). Adult DRs as compared to TRs had weaker connectivity between the left fusiform gyrus and the left angular gyrus (Horwitz et al., 1998). This finding was similar to that reported by Pugh et al. (2000b) who used fMRI to determine functional connectivity between cortical areas. Pugh et al. (2000b) concluded that adult DRs as compared to TRs had weaker connectivity in the left hemisphere between the extrastriate cortex and left angular gyrus. In the right hemisphere, however, DRs as compared to TRs had stronger connectivity between these structures. Recently Koyama et al. (2010) examined fMRI functional connectivity between key brain regions consistently implicated in reading during the resting state. Conjunction analysis identified the posterior part of the left IFA and the posterior part of the left middle temporal gyrus as loci of functional interactions with the majority of the other cortical regions involved in reading.

Newer effective connectivity techniques measure causal connectivity. Structural equation modeling and dynamic causal modeling are the two effective connectivity techniques that have been applied to reading. These techniques require the experimenter to set up a restricted number of causal models. Free parameters are estimated and then the model's fit to the data is assessed. Such effective connectivity techniques have been used in limited studies on reading in TRs (Bitan et al., 2009; Levy et al., 2009) and DRs (Cao et al., 2008; Quaglino et al., 2008). These studies have provided insight into the relationship among key areas involved in reading for DRs. A recent study using structural equation modeling applied to fMRI data obtained during a pseudoword reading task found that causal connectivity between the left supramarginal cortex and the left IFA was *absent* in DRs but present in TRs matched for age or reading level. In contrast, in the same study, causal connectivity between the left supramarginal cortex and the left VOTA was *intact* for DRs and both groups of TRs (Quaglino et al., 2008). These data imply a specific lack of connectivity between the left IFA and left TPA in DRs. Similarly, using fMRI and dynamic causal modeling, other researchers showed that the top-down influence from the left IFA to the left TPA found in TRs was absent in DRs (Cao et al., 2008). These studies provide support for the idea that interactions with IFA and posterior brain regions are abnormal in DRs. However, these model-driven techniques restrict the number of possible causal hypotheses. Consequently, some studies on reading have only evaluated one direction of coupling (e.g., feedforward; Levy et al., 2009) or analyzed only the left hemisphere (Cao et al., 2008; Quaglino et al., 2008; Bitan et al., 2009).

USING GRANGER CAUSALITY TO MEASURE EFFECTIVE CONNECTIVITY

In contrast to these *model-driven* techniques, Granger causality (GC) is a *data-driven* technique that empirically calculates the direction and strength of connectivity with minimal assumptions about the structure of the neural network. Unlike previous studies using effective connectivity techniques to study reading which have used fMRI and *model-driven* techniques, the current study uses GC to analyze MEG data. MEG has more than 100 times the temporal resolution of fMRI, thus providing the ability to resolve brain connectivity at

multiple brain frequencies. However, the higher temporal resolution also allows connectivity to potentially change within the sampling window selected for analysis, thereby potentially resulting in a non-stationary signal. Using a short window can mitigate this issue, but guidelines for choosing the window size have not been investigated in MEG (Ding et al., 2000; Frye and Wu, in press). For this reason, we analyzed effective connectivity before the onset of the experimental trial, just before presentation of the stimulus. During this pre-stimulus period, brain activity reflects a relatively static preparatory state (Liang et al., 2002), allowing the assumption of stationarity with respect to brain connectivity (and the first and second moment of the signal).

HYPOTHESIZED COMPENSATORY ROLE OF GREATER TOP-DOWN INFLUENCE OF THE LEFT INFERIOR FRONTAL AREA IN DYSLEXIC READERS

One characteristic that is pervasive among DRs is a lack of automaticity in the phonological decoding systems. This has led some authors to describe DRs as having "effortful" word processing and suggest that the increased IFA activation in DRs represents this increased effort (Shaywitz and Shaywitz, 2005). However, despite this hypothesis, there is little evidence to specifically link the IFA to increased effort. Here we hypothesis that, indeed, the IFA is involved in compensating for this lack of automaticity by activating the language system though top-down influence. The optimal time to activate the language network would be prior to the onset of the stimulus, during the pre-stimulus periods.

Our main hypothesis is that the left IFA will demonstrate increased top-down influence on the posterior language brain areas (i.e., left TPA and left VOTA) for DRs but not TRs (since engagement of the language network is automatic in TRs). Moreover we predict that a greater degree of top-down activation from left IFA to these posterior areas will be associated with better phonological decoding only in DRs.

To test this hypothesis, MEG data were extracted from each trial during the period just before the first non-word was presented on the display. We used GC to measure effective connectivity between key regions implicated in the brain networks responsible for phonological word decoding and compared this connectivity between TRs and DRs. We also tested whether task performance correlated with effective connectivity during the pre-stimulus period.

EXAMINING FREQUENCY BANDS TO FURTHER UNDERSTAND THE ROLE OF THE INFERIOR FRONTAL AREA

In MEG, electroencephalogram (EEG), and intracranial studies, activity within the beta and gamma frequency sub-bands have been linked to phonological and orthographic processes required for reading (Duncan Milne et al., 2003; Mainy et al., 2008; Matsumoto and Iidaka, 2008; Cornelissen et al., 2009; Trebuchon-Da Fonseca et al., 2009; Penolazzi et al., 2010) and beta and gamma sub-bands have been reported to be different in TRs and DRs (Ortiz et al., 1992; Ackerman et al., 1994; Klimesch et al., 2001). Since beta band activity has been linked to large-scale integration of brain activity such as long range synchronization of the frontal, parietal, temporal, and occipital areas (Gross et al., 2004, 2006) and multimodal integration between cortical lobes (von Stein et al., 1999), it is hypothesized that activity within the beta frequency band will be related to large-scale inter-regional integration such as top-down control of frontal areas on posterior brain areas. In contrast to beta band activity, gamma band activity has been linked to local feature integration (Fries, 2007) and the transient coupling and uncoupling of local neural networks (Lachaux et al., 2008). Thus, we hypothesize that the gamma band activity will not be related to inter-regional integration signals like the beta-band activity.

MATERIALS AND METHODS

PARTICIPANTS

We examined 10 TRs and 7 DRs native English speakers between the ages of 18 and 45 years, with normal or corrected vision, normal hearing, and no history of severe psychiatric or neurological illnesses or attention defects. DRs reported a childhood diagnosis of dyslexia and were either referred from the Office of Disability Services at Boston University or recruited from Curry College in Milton, MA, USA.

Reading performance composite was calculated by averaging the percentile ranks of reading rate and comprehension of the Nelson–Denny Reading Test. DRs scored below and TRs scored above the 25th percentile. All participants scored greater than or equal to 80 on the Wechsler Adult Intelligence Scale as estimated from vocabulary and block design subtests (Wechsler, 1997) and subtest scores were equivalent for DRs and TRs (**Table 1**). Right-handedness was confirmed by a score greater than 50 on the Edinburgh Handedness Inventory (Dragovic, 2004). Written informed consent was obtained in accordance with our Institutional Review Board regulations. Participants underwent an MEG and MRI scan as described below and received $20 per hour.

NON-WORD RHYME TASK

Since equating difficulty across reading groups can be a confounding factor, a non-word rhyming task that could be manipulated to provide equivalent performance across reading groups was developed (McGraw Fisher et al., in press). The visual stimuli were projected by a Panasonic DLP projector (Model No. PT-D7500U) through an aperture in the chamber onto the back of a non-magnetic screen located 1.5 m in front of the participant. Non-word target items were presented for 400 ms each, and then the non-word test item appeared for 400 ms. The total time from trial onset to the onset of the test item remained constant at 1650 ms. Depending on the block, one, two, or three target items were presented sequentially before the test item. The participant's task was to indicate if any of the target non-word(s) rhymed with the test non-word. A keypad press with the right index or middle finger indicated a rhyme or non-rhyme, respectively. The inter-trial interval was 2000 ms. Each testing block consisted of 60 randomly presented novel trials. TRs completed six blocks: four with one target item, one with two target items, and one with three target items. DRs completed five blocks:

Table 1 | Participant characteristics [mean (standard deviation)].

Characteristic	Typical readers	Dyslexic readers
Age	21.9 (3.1)	25.0 (6.3)
Male:female	5:5	3:4
Handedness	77.8 (17.2)	87.1 (11.1)
Nelson–Denny rate	35% (21%)	6% (6%)
Nelson–Denny comprehension	65% (32%)	12% (13%)
Nelson–Denny average	50% (21%)	11% (8%)
Vocabulary subtest	12.6 (2.6)	13.6 (3.4)
Block design subtest	12.7 (1.6)	11.4 (2.0)

four with one target item and one with two target items. The block with three target items was not given to the DRs since they were found in preliminary studies to perform at about chance with such a difficult phonological task. In addition, this experimental design was found to provide equivalent performance across these two reading groups (McGraw Fisher et al., in press).

PERFORMANCE MEASUREMENTS

A signal detection paradigm was used to obtain a measurement of performance without response bias. Rhyme trials were considered signal + noise trials while non-rhyme trials were considered noise trials. Sensitivity (*d*-prime) was calculated from the hit and false alarm rates assuming an equal variance model [i.e., *z* (hit rate) − *z* (false alarm rate)].

MAGNETIC RESONANCE IMAGING

After the MEG session, a high-resolution, 3D, T1-weighted structural MRI of the brain was acquired. Using FreeSurfer software, the MRI images were segmented and the cortical surface was reconstructed (Dale et al., 1999; Fischl et al., 1999). These images were used to ensure that the MEG sensors selected were located above the true regions of interest.

MAGNETOENCEPHALOGRAPHY ACQUISITION

Participant preparation

Four head position indicator coils were placed on both sides of the forehead and behind the ears. These coils were used to determine the relative position of the head while in the scanner. The coils' positions were measured using a low-intensity magnetic field generated by each coil at the start of each run. The positions of the coils, the nasion, and auricular points were recorded with a Polhemus Fastrack (Colchester, VT, USA) 3-D digitizer (Hämäläinen et al., 1993) and about 70 points on the scalp were marked with the digitizer. Electro-oculography (EOG) electrodes were placed at each temple and above and below the left eye, with the ground on the left lower cheek. Vertical and horizontal EOG was recorded to detect blinks and large eye movements.

MEG recording

Magnetoencephalography recordings were performed at the Massachusetts General Hospital Athinoula A. Martinos Center for Biomedical Imaging using a whole-head VectorView™ system (Elekta Neuromag Oy, Finland) inside a high performance magnetically shielded room (Imedco AG, Switzerland; Cohen et al., 2002). The device has 306 SQUID (superconducting quantum interference device) sensors arranged in 102 locations within a helmet-shaped array. Each location contained a longitudinal and latitudinal planar gradiometers and a magnetometer. Signals were filtered at 0.1–172 Hz and sampled at 601 Hz.

MEG data processing

Blinking and other artifacts were excluded by removing epochs with EOG amplitudes exceeding 150 μV or gradiometer signals exceeding 3000 fT/cm. Typically, one or two MEG channels were excluded for each participant due to artifacts. To examine the preparatory state activity, the neural activity was extracted from 500 to 0 ms before the onset of the first stimulus from each trial. Approximately 300 trials were extracted for each participant. To reduce the number of channels, the signal amplitude at each location was derived from the longitudinal and latitudinal planar gradiometers as given in Eq. 1.

$$\text{Signal amplitude} = \sqrt{\text{longitudinal amplitude}^2 + \text{latitudinal amplitude}^2} \quad (1)$$

Signals were filtered into low (12–14 Hz), medium (15–19 Hz), and high (20–29 Hz) beta and low (30–59 Hz), medium (60–89 Hz), and high (90–120 Hz) gamma sub-bands using low-order bidirectional Butterworth filters to prevent frequency and phase distortion. The signal was down-sampled by a factor of 2.

Region of interest selection

Data was selected from 24 sensor locations overlying the right and left IFA, TPA, and VOTA. A viewer depicting the exact position of the selected sensors over the 3D model for each participant was used to ensure that the position of the sensors corresponded to the regions of interest for each participant. The average Talairach coordinates of the cortex underlying the center of the groups of sensors for each region of interest are as follows: left IFA −54.2, 22.4, 1.71; left TPA −62.5, −51.1, 30.4; left VOTA −42.8, −62.4, −13.2; right IFA 57.7, 26.7, 7.1; right TPA 58.0, −54.4, 35.8; right VOTA 39.2, −55.1, −14.4.

GRANGER CAUSALITY ANALYSIS

The interaction between multiple brain regions were processed using an implementation of GC we recently developed – Dynamic Autoregressive Neuromagnetic Causal Imaging (DANCI). DANCI uses least-squares linear regression (LSLR) to model the interactions between a large number of MEG sensors or sources (Frye and Wu, in press). To calculate GC, a system of autoregressive (AR) models was constructed to represent the mutual influence of S sensors on one another. The MEG signal from a set of sensors $[1 \ldots S]$, where $S = 24$, with time points $[1 \ldots T]$, where $T = 20$ (see below), is given in time series $A = [a_s(t):s = 1 \ldots S, t = 1 \ldots T]$. A system of AR models of order P (see Eq. 2) was used to model the time series. The model order determines the number of coefficients that are used to model each sensor–sensor interaction.

$$\begin{aligned}
a_1(t) &= \sum_{j=1}^{p} c_{1,1,j} a_1(t-j) + \sum_{j=1}^{p} c_{1,2,j} a_2(t-j) + \ldots \\
&\quad + \sum_{j=1}^{p} c_{1,S,j} a_S(t-j) + e_{1|1\ldots S}(t) \\
a_2(t) &= \sum_{j=1}^{p} c_{2,1,j} a_1(t-j) + \sum_{j=1}^{p} c_{2,2,j} a_2(t-j) + \ldots \\
&\quad + \sum_{j=1}^{p} c_{2,S,j} a_S(t-j) + e_{2|1\ldots S}(t) \\
&\ldots \\
&\ldots \\
a_S(t) &= \sum_{j=1}^{p} c_{S,1,j} a_1(t-j) + \sum_{j=1}^{p} c_{S,2,j} a_2(t-j) + \ldots \\
&\quad + \sum_{j=1}^{p} c_{S,S,j} a_S(t-j) + e_{S|1\ldots S}(t)
\end{aligned} \quad (2)$$

In (2) each equation represents a signal $a_s(t)$ at time t that is predicted by previous values of itself and all other signals. For example, in (2), coefficients $c_{1,1,j}$ $(j = 1 \ldots P)$ quantitatively describe the influence of the activity of $a_1(t)$ on itself, coefficients $c_{1,2,j}$ $(j = 1 \ldots P)$ quantitatively describe the influence of the activity of $a_2(t)$ on $a_1(t)$, and coefficients $c_{1,s,j}$ $(j = 1 \ldots P)$ quantitatively describe the influence of signal $a_s(t)$ on $a_1(t)$, etc. Likewise, coefficients $c_{s,1,j}$ $(j = 1 \ldots P)$ describe the quantitative influence of signal $a_1(t)$ on signal $a_s(t)$.

To maintain stationarity, a brief "snapshot" of the signal was extracted using the short-window approach (Ding et al., 2000). To derive observations for the AR model, the data window was set at 20 data points and was incrementally moved across the 500 ms data epoch. The epoch length was 150 data points after down-sampling and these 150 data points fit 131 20-point windows. Thus, this yielded 131 observations per trial. Given that about 300 data trials were recorded from each participant, approximately 39,300 (i.e., 300×131) observations were produced for each participant. The signal was normalized with respect to both the individual trial and ensemble amplitude and variation by detrending each trial, normalizing by the trial mean and standard deviation, and then normalizing by the ensemble mean and standard deviation in a point-by-point manner (Ding et al., 2000; Frye and Wu, in press). Stationarity was verified by examining the unit roots using the Dickey–Fuller test. The details of calculating GC from the AR models are provided in Section "Calculations of Granger Causality Using Least-Squares Linear Regression" in Appendix. To insure that the LSLR algorithm performed adequately, we examined diagnostic residual plots, the leverage values and the condition index to eliminate the possibility of an ill-condition design matrix, bias, or systematic autocorrelations.

The optimal model order is typically chosen by estimating several AR model with different orders and determining which model order optimizes two standard information criteria, the Akaike information criterion (AIC) and the Bayesian information criterion (BIC). Since there is no specific criterion to guide the choice of model orders to test, we selected a wide range of model orders, including 8, 12, and 16. AIC and BIC were optimized with an order of 16 for all models.

Using the approach above, we constructed a matrix of GC values to represent the influence of each MEG sensor on every other MEG sensor. We then evaluated the significance of each GC value in order to consider only the connections which represented significant connectivity. The same measure of error that is used to calculate GC can also be used in a partial F-test in order to calculate the significance of the GC value. Equation 3 outlines the calculation of this F-distributed value which has P and $O \times T - S \times P - 1$ degrees of freedom in the numerator and denominator, respectively. Granger used the same symptom "F" to signify GC, making the notation confusing.

$$F^{2\to s}_{P,O\times T-S\times P-1} = \frac{\dfrac{O\cdot(\mathrm{MSE}_{s|1,3\ldots S} - \mathrm{MSE}_{s|1\ldots S})}{P}}{\dfrac{O\cdot \mathrm{MSE}_{s|1\ldots S}}{O\cdot T - S\cdot P - 1}} \quad (3)$$

Granger causality values with a corresponding F-value that was significant to $p \leq 10^{-4}$ were used further. The average GC values between language areas were calculated by averaging the significant GC values between language areas. This whole process was performed for each frequency band separately.

STATISTICAL ANALYSIS

In order to quantitatively analyze GC values, we constructed a linear mixed-model similar to models in our recent studies (Frye et al., 2007, 2008, 2009, 2010a,b). In our previous studies we investigated the relation between performance and anatomic connectivity. In these studies we found that this relation was not necessarily the same for both reading groups (i.e., DRs, TRs). Thus, our previous models contained the fixed effects of reading group (TRs vs. DRs), a covariate for performance, and the interaction between these effects. In the current study we examine effective connectivity to/from the IFA. Since there are two directions of connectivity for each connection (in vs. out) an additional fixed effect of connectivity direction is included in the models. Since the IFA is connected to five other areas (i.e., right and left TPA, right and left VOTA, and the contralateral IFA) an additional fixed effect which represented brain area was included in the model. Thus, the final model for this study had fixed effects of area (five levels), reading group (TRs vs. DRs), and connectivity direction (in vs. out) with a covariate representing performance, which in this case is d-prime (i.e., sensitivity). The "mixed" procedure of SAS 9.1 (SAS Institute Inc., Cary, NC, USA; see Section "Linear Mixed-Model Used for Statistical Analysis" in Appendix) was used to evaluation the model. Participant, cortical area and connectivity direction were entered as random effects in the mixed-model.

This model provides the ability to test the specific hypothesis of this study. Specifically, it was hypothesized that DRs would have greater top-down connectivity from the left IFA (i.e., outward) to the left hemisphere language areas (TPA, VOTA) as compared to TRs, with this connectivity proportional to performance on the non-word rhyme task. Thus, a four-way interaction was predicted, specifically, a reading group by connectivity direction by performance by area interaction, such that the DRs, but not the TRs, would manifest a relation between performance and outward connectivity from the IFA to the left VOTA and left TPA but not to their right sided homologs.

Each left and right IFA and frequency sub-band was analyzed with a separate mixed-model. For each analysis, all effects along with their interactions were examined for significance. In order to mitigate the effects of inflated alpha due to performing multiple statistical models, we corrected the alpha for the full model using the Bonferroni method. Since there are six frequency bands examined and two IFAs (i.e., left and right) we use an alpha of $0.05/12 = 0.004$ for the overall analysis. All follow-up statistical tests used an alpha of 0.05. Model interactions were analyzed by first breaking down the model by reading group and then breaking down the model by connectivity direction. Differences in connectivity between areas were analyzed using orthogonal contrasts. The relationship between performance and connectivity was additionally analyzed using two-tailed Pearson correlations.

RESULTS

BETA FREQUENCY SUB-BANDS

Low beta (12–14 Hz)

Left IFA. Left IFA connectivity was influenced by a three-way interaction (i.e., performance by connectivity direction by reading group) [$F(1,52) = 15.30$, $p < 0.001$]. To investigate the three-way interaction in more detail each reading group was analyzed separately. The DRs, but not the TRs, were found to demonstrate a performance by connectivity direction interaction [$F(1,56) = 57.63$, $p < 0.0001$]. **Figure 1A** depicts the correlation between performance and the difference between inward and outward connectivity. **Figure 1A** demonstrates that better performance was associated with greater outward as compared to inward connectivity from the left IFA to other brain areas for DRs ($r = -0.96$, $p < 0.01$). The relationship between performance and difference between inward and outward connectivity was not significant for TRs ($r = 0.54$, $p > 0.05$).

To examine this performance by connectivity direction in more detail for the DRs, the relation between performance and connectivity was examined for each connectivity direction separately for DRs. Outward, but not inward, connectivity was associated with performance for DRs [$F(1,28) = 8.82$, $p < 0.01$] such that greater outward connectivity from the left IFA to the other cortical areas (right and left TPA, right and left VOTA, right IFA) was associated with better performance. **Figure 1B** demonstrates that the correlation between outward connectivity and performance for DRs was significant ($r = 0.80$, $p < 0.05$). The correlation between inward connectivity and performance for DRs was not significant ($r = -0.34$, $p > 0.05$). These findings suggest that the relationship between the balance in inward and outward connectivity and performance was primarily driven by outward connectivity from the left IFA to other brain regions.

Right IFA. Connectivity between the right IFA and the other cortical areas differed depending on the cortical area [$F(4,60) = 5.62$, $p < 0.001$]. Planned *post hoc* contrast demonstrated that across reading groups connectivity between the right IFA and the right TPA was higher than connectivity between the right IFA and the other cortical areas [$t(60) = 4.62$, $p < 0.0001$; **Figure 1C**].

Middle beta (15–19 Hz) and high beta (20–29 Hz)

Connectivity of the left IFA or right IFA with the other brain areas was not influenced by performance, connectivity direction, cortical area or reading group for the middle or high beta sub-bands.

GAMMA FREQUENCY SUB-BANDS

Low gamma (30–59 Hz)

Connectivity between the left IFA and the other cortical areas differed depending on the cortical areas [$F(4,60) = 4.47$, $p < 0.004$]. Planned *post hoc* contrasts demonstrated that connectivity between the left IFA and the left TPA [$t(60) = 2.85$, $p < 0.01$] and the right TPA [$t(60) = 3.45$, $p = 0.001$] was higher than connectivity between the left IFA and the other cortical areas, and connectivity between the left IFA and the left VOTA [$t(60) = 3.26$, $p < 0.002$], right IFA [$t(60) = 3.24$, $p < 0.002$], and the right VOTA [$t(60) = 2.63$, $p = 0.01$] was lower than connectivity between the left IFA and other cortical regions (**Figure 2A**).

Connectivity between the right IFA and the other brain areas was not influenced by performance, connectivity direction, cortical area, or reading group.

Medium gamma (60–89 Hz)

Connectivity between the left IFA and the other brain areas was not influenced by performance, connectivity direction, cortical area, or reading group.

Connectivity between the right IFA and the other cortical areas differed depending on the cortical area [$F(4,60) = 5.32$, $p = 0.001$]. Planned *post hoc* contrasts demonstrated that connectivity between the right IFA and the left TPA [$t(60) = 3.07$, $p = 0.003$] and the right TPA [$t(60) = 2.77$, $p < 0.01$] was higher than connectivity between the right IFA and the other cortical areas, and connectivity between the right IFA and the left IFA [$t(60) = 2.46$, $p = 0.02$], left VOTA [$t(60) = 3.42$, $p = 0.001$], and the right VOTA [$t(60) = 2.76$, $p < 0.01$] was lower than connectivity between the right IFA and other cortical areas (**Figure 2B**).

High gamma (90–120 Hz)

The relationship between connectivity between the left IFA and the other cortical areas was related to performance but this relationship differed by cortical area (i.e., a performance by cortical

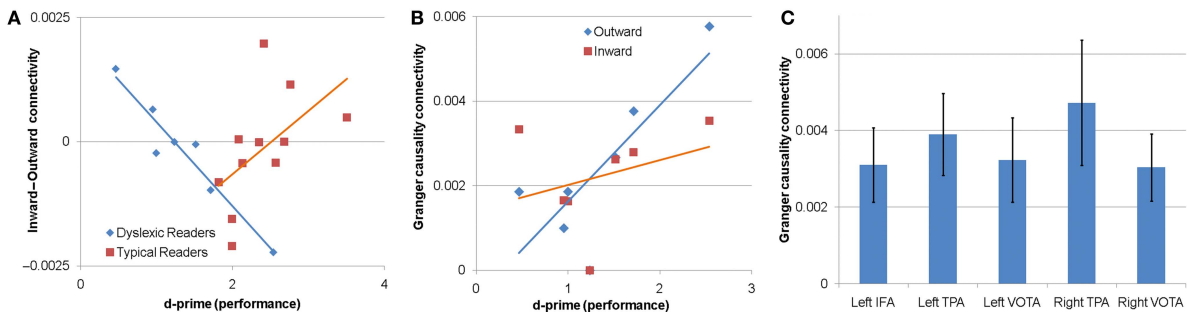


FIGURE 1 | Granger causality connectivity for the *low beta sub-band*. (A,B) The relationship between performance on the non-word phonological decoding task and Granger causality connectivity for the *left* inferior frontal area (IFA). **(A)** The relationship between performance and the difference between inward and outward connectivity. The relationship was only significant for DRs, for which greater outward connectivity (as compared to inward connectivity) from the IFA to other areas was associated with better non-word rhyme discrimination performance (d-prime). **(B)** The relationship between performance and inward and outward connectivity individually for DRs. Greater outward connectivity from the IFA to other areas was associated with better performance in DRs. **(C)** Connectivity between the *right* IFA and the other cortical areas investigated. TPA, temporoparietal area; VOTA, ventral occipital–temporal areas.

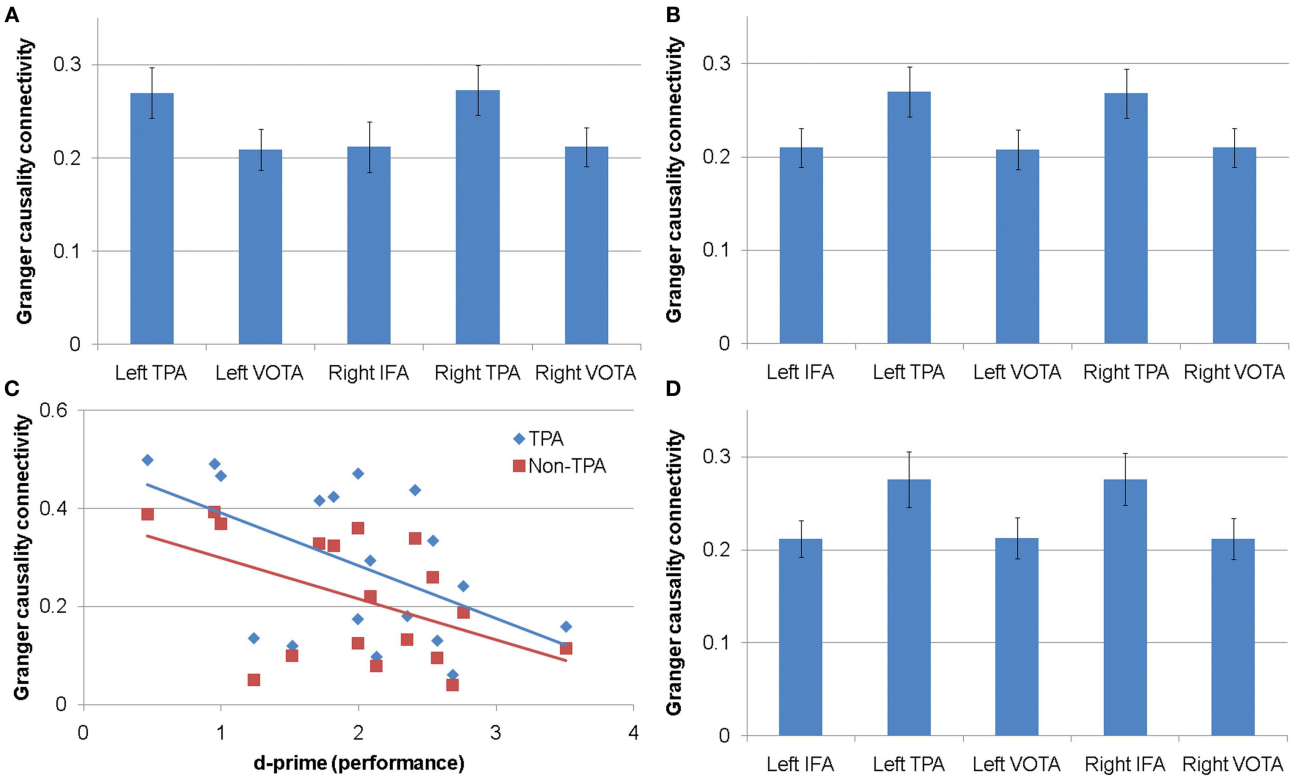


FIGURE 2 | Connectivity for *gamma frequency* sub-bands. (A) Connectivity between the *left* inferior frontal area (IFA) and other cortical areas in the *low gamma* sub-band. **(B)** Connectivity between the right IFA and other cortical area in the *medium gamma* sub-band. **(C)** Relationship between performance and connectivity between the *left* IFA and temporoparietal (TPA) and non-temporoparietal (non-TPA) areas for the *high gamma* sub-band. **(D)** Connectivity between the *right* IFA and other cortical areas for the *high gamma* sub-band. VOTA, ventral occipital–temporal areas.

area interaction) [$F(4,52) = 5.35, p = 0.001$]. Reading group membership had no influence on this interaction. Better performance was related to lower gamma connectivity with this relationship being steeper for connectivity between the left IFA and both the left TPA [$t(52) = 4.68, p < 0.0001$] and the right TPA [$t(52) = 4.02, p < 0.001$] than connectivity between the left IFA and other cortical areas. In addition, this relationship was less steep for connectivity between the left IFA and the left VOTA [$t(52) = 4.05, p < 0.001$], right IFA [$t(52) = 3.92, p < 0.001$], and the right VOTA [$t(52) = 4.98, p < 0.0001$] than connectivity between the left IFA and remaining brain areas. **Figure 2C** depicts the relationship between performance and the left IFA connectivity to TPAs and the non-TPAs separately. A significant correlation was found for connectivity between the left IFA and TPAs ($r = -0.51, p < 0.05$) and between the left IFA and non-TPA regions ($r = -0.49, p < 0.05$).

Connectivity between the right IFA and the other cortical areas differed depending on the cortical area [$F(4,60) = 5.49, p < 0.001$]. Planned *post hoc* contrasts demonstrated that connectivity between the right IFA and both the left TPA [$t(60) = 3.38, p = 0.001$] and the right TPA [$t(60) = 3.01, p = 0.004$] was higher than connectivity between the right IFA and the other cortical areas. In addition, connectivity between the right IFA and the left IFA [$t(60) = 2.74, p < 0.01$], left VOTA [$t(60) = 2.81, p < 0.01$], and the right VOTA [$t(60) = 3.89, p < 0.001$] was lower than connectivity between the right IFA and other cortical areas (**Figure 2D**).

DISCUSSION

This is the first study to compare effective neuromagnetic connectivity between DRs and TRs and one of the first studies to examine effective connectivity during the pre-stimulus period. In this study, we compared IFA connectivity to and from other brain areas known to be essential for reading (left and right IFA, TPA, and VOTA) in low, medium, and high beta and low, medium, and high gamma frequency sub-bands. One aspect of our hypothesis was that greater top-down connectivity *from* the left IFA to other cortical regions might serve in a compensatory manner in DRs to facilitate phonological decoding. This hypothesis was confirmed within the low beta sub-band. As predicted, this effect was observed in DRs but not TRs. In Section "Greater Connectivity *from* the Left IFA *to* Other Cortical Regions is Associated with Better phonological decoding performance in DRs, but not TRs: Does this reflect a compensatory mechanism in DRs?" we will examine the implications of this finding. In Section "Greater Top-Down Connectivity *from* the left IFA is not Restricted to Left Hemisphere Reading-Related Structures but Instead Includes Their Right Hemisphere homologs," we will discuss the other aspect of our hypothesis wherein it was predicted that the relationship between IFA connectivity and improved performance would be limited to connections between IFA and left-sided structures used by TRs during phonological decoding. This aspect of the hypothesis was not confirmed since greater left IFA connectivity between both left and right sided homologous structures was

associated with better phonological decoding performance in DRs. We will discuss the implications of increased bilateral influence of the IFA upon posterior cortical areas. In Section "Greater Gamma Band Effective Connectivity Between Left IFA and Other Regions was Associated with Worse Phonological Decoding Performance in Both Reading Groups" we will discuss our finding that greater effective connectivity in the gamma sub-band was associated with worse phonological decoding. In Section "Different Roles for Beta and the Gamma Preparatory Activity," we will comment on why greater beta connectivity from IFA to other cortical regions was associated with better performance and greater gamma connectivity from IFA to other regions was associated with worse performance. In Section "Future Studies to Examine the Generalizability of These Findings," we will discuss ways to test the generalizability of our findings.

GREATER CONNECTIVITY *FROM* THE LEFT IFA *TO* OTHER CORTICAL REGIONS IS ASSOCIATED WITH BETTER PHONOLOGICAL DECODING PERFORMANCE IN DRs, BUT NOT TRs: DOES THIS REFLECT A COMPENSATORY MECHANISM IN DRs?

During the pre-stimulus period, within the low beta sub-band, greater top-down effective connectivity *from* the left IFA to bilateral cortical areas was associated with better phonological decoding performance in DRs, but not TRs. The fact that the changes in effective connectivity were limited to DRs suggests that they might be associated with brain reorganization related to the development of dyslexia as a child. This would be consistent with fMRI studies that have reported over-activation of the left IFA (Hoeft et al., 2007; MacSweeney et al., 2009) in DRs. The fact that outward connectivity from the IFA was associated with performance suggests that such connectivity could be associated with compensatory reorganization. This is consistent with fMRI studies that have shown that left IFA activity increases following remediation (Richards et al., 2002; Temple et al., 2003; Eden et al., 2004). The relationship between the left IFA and improved phonological performance in DRs is also consistent with anatomic connectivity studies. For example, recent diffusion tensor imaging (DTI) studies have demonstrated that phonological performance is related to microstructure of the superior longitudinal fasciculus in DRs (Frye et al., 2010b).

A possible developmental sequence could explain the role that the left IFA has in compensation for the phonological deficit in DRs. Over-activation of the left IFA in preparation for a reading task or during a reading task could represent increased top-down activation of key cortical regions involved in neural language networks for word processing. Remediation training could reinforce the individual's ability to activate language networks in the context of tasks that require word processing. Over time, repeated top-down activation of the posterior language regions by the left IFA could cumulatively strengthen the connectivity between the left IFA and the posterior language areas during development. This is compatible with a recent DTI study that has shown that training therapies for reading change white matter microstructure of pathways in the reading circuit (Keller and Just, 2009). Thus cumulative use of the increased top-down left IFA influence could change white matter microstructure in the pathways connecting the left IFA and posterior language areas and would be compatible with the hypothesis and results of the current study. Of course, a longitudinal study would be needed to test this hypothesized developmental sequence.

GREATER TOP-DOWN CONNECTIVITY *FROM* THE LEFT IFA IS NOT RESTRICTED TO LEFT HEMISPHERE READING-RELATED STRUCTURES BUT INSTEAD INCLUDES THEIR RIGHT HEMISPHERE HOMOLOGS

Although others have recently demonstrated differences in top-down activation from the IFA to other brain regions between DRs and TRs (Cao et al., 2008) this study expands these findings by demonstrating that top-down modulatory activity can be related to phonological task performance on a continuum in DRs. In the current experiment, it was hypothesized that, in DRs, performance would be related to top-down connectivity from the left IFA to the other left-sided posterior language areas typically involved in word processing in TRs. Instead, the performance-related top-down connectivity from the left IFA influenced not only the left, but also the right-sided homologs of the cortical areas typically involved in word processing.

Our results are consistent with the majority of functional imaging studies on DRs which have demonstrated increased right hemisphere activation in DRs as compared to TRs (Simos et al., 2000; Temple, 2002; Heim and Keil, 2004). It is also consistent with studies which have reported increased activation of both left and right hemisphere TPA areas after remediation (Shaywitz et al., 2003; Temple et al., 2003). This pattern of connectivity may explain why many individuals with a history of dyslexia require so many years to develop adequate phonological decoding skills and often continue to have residual problems with reading-related skills well into adulthood. For example, activation of the left TPA and left VOTA by the left IFA in DRs could represent a positive compensatory strategy to activate appropriate posterior language networks. However, concurrent activation of the homologous right hemispheric regions could be somewhat counterproductive and inhibit the occurrence of the necessary neuroplastic changes for specific activation of left hemisphere language networks by leading to the formation of atypical neural networks for reading. Developmental of such atypical language networks could result an extended periods of time (i.e., decades vs. years) for accurate reading skills to develop. Clearly hemispheric asymmetries are important in the development of phonological function, even in individuals without a history of dyslexia. For example, the findings of a recent paper suggest that an intrinsic individual difference in the degree of asymmetry of microstructure of the arcuate fasciculus, a key cortico-cortical pathway involved in connection of anterior and posterior language regions, may predict phonological ability (Lebel and Beaulieu, 2009). Since these asymmetries were found to be age-invariant, these findings could suggest that part of the basis for over-involvement of the right hemispheric decoding network and individual variation in DRs may have to do with the wiring of the arcuate fasciculus from early in life.

GREATER GAMMA BAND EFFECTIVE CONNECTIVITY BETWEEN LEFT IFA AND OTHER REGIONS WAS ASSOCIATED WITH WORSE PHONOLOGICAL DECODING PERFORMANCE IN BOTH READING GROUPS

This study found that greater gamma band effective connectivity between left IFA and other regions was associated with worse nonword rhyme task performance as measured by *d*-prime within the high gamma sub-band. This relationship was steeper for the left and right TPAs as compared to the other brain areas (i.e., right and left VOTA, right IFA). Therefore during the pre-stimulus period a relatively reduced degree of gamma sub-band effective connectivity between left

IFA and other areas may be optimal. This is consistent with intracranial EEG data which shown transient desynchronization of gamma activity during a reading task in the left IFA (Lachaux et al., 2008).

DIFFERENT ROLES FOR BETA AND THE GAMMA PREPARATORY ACTIVITY

The association between better phonological decoding performance and increased outward connectivity between the left IFA and other brain regions was present in the beta (as opposed to the gamma) frequency band. This was predicted because beta activity is thought to operate on an inter-regional spatial scale (Gross et al., 2004, 2006). This may be an example of an advantage of MEG compared to fMRI in terms of GC analysis. Using MEG we were able to break down the connectivity analyses into different frequency sub-bands and the differential effects of increased connectivity in these sub-bands confirms the importance of analyzing the data within narrow frequency bands.

In contrast to beta band activity, gamma band synchronization has been proposed as a mechanism for facilitating communication between neighboring neurons participating in the formation of transient neural networks (Fries, 2007). In fact, transient desynchronization of gamma activity has been shown to occur during a reading task by means of intracranial EEG in the left IFA (Lachaux et al., 2008). Therefore, one interpretation of our findings is that within this high gamma sub-band, strong coupling between the nodes of the neural network during the pre-stimulus period may reduce the ability of the network to decouple and reorganize into large-scale cognitive networks during the performance of the actual task. In particular, tighter intercortical connectivity between the two TPAs during the pre-stimulus period may interfere with a necessary shift toward left TPA ascendency. We suggest that this may result in slower and less automatic pseudoword phonological decoding.

FUTURE STUDIES TO EXAMINE THE GENERALIZABILITY OF THESE FINDINGS

This study examines connectivity between language regions during the pre-stimulus period of a non-word phonological decoding task. Other word stimuli such as regular and irregular words may be processed through different neural networks as compared to non-words. It is not known whether the patterns of cortical connectivity identified in this study will also occur during the pre-stimulus period of tasks requiring processing of other word types. In fact, it is very possible that the patterns of cortical connectivity identified may not be word or language specific at all. For example, we expected top-down activity from the IFA to have a significant influence on the posterior language networks that subserve reading which are left hemisphere lateralized. What we found is that the IFA appeared to have equal top-down influence on all brain regions examined, suggesting that this influence is not word specific. In future studies, the pre-stimulus period associated with a non-word task should be compared to the pre-stimulus period associated with tasks requiring the processing of other types of word features including tasks focusing on orthographic and semantic word properties and stimuli other than words. Such studies will provide an understanding of whether the pattern of pre-stimulus connectivity found in this study is specific to phonological non-word decoding, word decoding or represents a more general pattern of pre-stimulus preparatory connectivity. Future studies should also incorporate additional participants, to afford the possibility of examining differences in brain connectivity attributable to gender.

CONCLUSION

This study has demonstrated that pre-stimulus preparatory networks are reorganized in DRs and that network structure is directly associated with non-word rhyme performance. Reorganization of the pre-stimulus network associated with DRs was found in the beta frequency band. Although preliminary, this finding of a performance-related relationship with IFA effective connectivity sheds light on previous functional neuroimaging findings of over-activation of the left IFA in DRs as compared to TRs. Over-activation of the left IFA in DRs during reading tasks may in fact reflect increased top-down influence of the left IFA. The relationship of IFA function to more general cognitive abnormalities associated with dyslexia is not clear, but given the number of studies demonstrating subtle deficits in executive function in DRs (Narhi et al., 1997; Lazar and Frank, 1998; Willcutt et al., 2001, 2005; Brosnan et al., 2002; Gioia et al., 2002), further investigation of the IFA in DRs may be fruitful.

Additionally, across reading groups, phonological decoding performance diminished in proportion to the strength of the inter-regional gamma connectivity during the pre-stimulus period. Therefore, individual differences in gamma frequency band activity affected rhyme task performance in a continuous manner across both DRs and TRs.

This combination of results demonstrates the importance of considering direction in connectivity analysis and suggests that analyses based on GC can help uncover the typical and atypical architecture of neural networks that underlie cognition. Future studies should attempt to analyze source localized MEG activation rather than sensor localized activation in order to more accurately examine cortical location. In the future, experimental paradigms which combine MEG and fMRI may also help better spatially localize these cognitive networks and help understand the discrepancies in the findings of these two imaging modalities in DRs. This will no doubt provide a more in-depth understanding of the neural networks that subserve reading in DRs. Such an understanding will help guide the development of innovative remediation programs and allow DRs to develop the ability to accurately read at a younger age.

ACKNOWLEDGMENTS

This study was supported by grant NS046565 to Dr. Richard E. Frye and in part by CELEST, an NSF Science of Learning Center (SBE-0354378), Jacqueline Liederman, Investigator.

REFERENCES

Ackerman, P. T., Dykman, R. A., Oglesby, D. M., and Newton, J. E. (1994). EEG power spectra of children with dyslexia, slow learners, and normally reading children with add during verbal processing. *J. Learn. Disabil.* 27, 619–630.

Aron, A. R., and Poldrack, R. A. (2005). The cognitive neuroscience of response inhibition: relevance for genetic research in attention-deficit/hyperactivity disorder. *Biol. Psychiatry* 57, 1285–1292.

Aylward, E. H., Richards, T. L., Berninger, V. W., Nagy, W. E., Field, K. M., Grimme, A. C., Richards, A. L., Thomson, J. B., and Cramer, S. C. (2003). Instructional treatment associated with changes in brain activation in children with dyslexia. *Neurology* 61, 212–219.

Bitan, T., Cheon, J., Lu, D., Burman, D. D., and Booth, J. R. (2009). Developmental increase in top-down and bottom-up

processing in a phonological task: an effective connectivity, fMRI study. *J. Cogn. Neurosci.* 21, 1135–1145.

Brosnan, M., Demetre, J., Hamill, S., Robson, K., Shepherd, H., and Cody, G. (2002). Executive functioning in adults and children with developmental dyslexia. *Neuropsychologia* 40, 2144–2155.

Brunswick, N., McCrory, E., Price, C. J., Frith, C. D., and Frith, U. (1999). Explicit and implicit processing of words and pseudowords by adult developmental dyslexics: a search for Wernicke's Wortschatz? *Brain* 122, 1901–1917.

Cao, F., Bitan, T., and Booth, J. R. (2008). Effective brain connectivity in children with reading difficulties during phonological processing. *Brain Lang.* 107, 91–101.

Cao, F., Bitan, T., Chou, T. L., Burman, D. D., and Booth, J. R. (2006). Deficient orthographic and phonological representations in children with dyslexia revealed by brain activation patterns. *J. Child. Psychol. Psychiatry* 47, 1041–1050.

Cohen, D., Schalpfer, U., Ahlfors, S., Hamalainen, M., and Halgren, E. (2002). New six-layer magnetically shielded room for MEG. *Biomag Proceed.*

Cornelissen, P. L., Kringelbach, M. L., Ellis, A. W., Whitney, C., Holliday, I. E., and Hansen, P. C. (2009). Activation of the left inferior frontal gyrus in the first 200 ms of reading: evidence from magnetoencephalography (MEG). *PLoS ONE* 4, e5359. doi: 10.1371/journal.pone.0005359.

Dale, A. M., Fischl, B., and Sereno, M. I. (1999). Cortical surface-based analysis. I. Segmentation and surface reconstruction. *Neuroimage* 9, 179–194.

Ding, M., Bressler, S. L., Yang, W., and Liang, H. (2000). Short-window spectral analysis of cortical event-related potentials by adaptive multivariate autoregressive modeling: data preprocessing, model validation, and variability assessment. *Biol. Cybern.* 83, 35–45.

Ding, M., Chen, Y., and Bressler, S. L. (2006). "Granger causality: basic theory and application to neuroscience," in *Handbook of Time Series Analysis*, eds B. Schelter, M. Winterhalder, and J. Timmer (Berlin: Wiley-VCH), 451–474.

Dragovic, M. (2004). Categorization and validation of handedness using latent class analysis. *Acta Neuropsychiatr.* 16, 212–218.

Duncan Milne, R., Hamm, J. P., Kirk, I. J., and Corballis, M. C. (2003). Anterior–posterior beta asymmetries in dyslexia during lexical decisions. *Brain Lang.* 84, 309–317.

Eden, G. F., Jones, K. M., Cappell, K., Gareau, L., Wood, F. B., Zeffiro, T. A., Dietz, N. A., Agnew, J. A., and Flowers, D. L. (2004). Neural changes following remediation in adult developmental dyslexia. *Neuron* 44, 411–422.

Fischl, B., Sereno, M. I., and Dale, A. (1999). Cortical surface-based analysis. II: inflation, flattening, and a surface-based coordinate system. *Neuroimage* 9, 195–207.

Fries, P. (2007). A mechanism for cognitive dynamics: neuronal communication through neuronal coherence. *Trends Cogn. Sci.* 9, 474–480.

Frye, R. E., Fisher, J. M., Coty, A., Zarella, M., Liederman, J., and Halgren, E. (2007). Linear coding of voice onset time. *J. Cogn. Neurosci.* 19, 1476–1487.

Frye, R. E., Fisher, J. M., Witzel, T., Ahlfors, S. P., Swank, P., Liederman, J., and Halgren, E. (2008). Objective phonological and subjective perceptual characteristics of syllables modulate spatiotemporal patterns of superior temporal gyrus activity. *Neuroimage* 40, 1888–1901.

Frye, R. E., Hasan, K., Xue, L., Strickland, D., Malmberg, B., Liederman, J., and Papanicolaou, A. C. (2009). Splenium microstructure is related to two dimensions of reading skill. *Neuroreport* 19, 1627–1631.

Frye, R. E., Liederman, J., Malmberg, B., McLean, J., Strickland, D., and Beauchamp, M. S. (2010a). Surface area accounts for the relation of gray matter volume to reading-related skills and history of dyslexia. *Cereb. Cortex.* 20, 2625–2635.

Frye, R. E., Liederman, J., Hasan, K. M., Lincoln, A., Malmberg, B., deSouza, L., McLean, J., and Papanicolaou, A. (2010b). Diffusion tensor quantification of the relations between microstructural and macrostructural indices of white matter and reading. *Hum. Brain Mapp.* doi: 10.1002/hbm.21103

Frye, R. E., and Wu, M.-H. (in press). Multichannel least-squares linear regression provides a fast, accurate, unbiased and robust estimation of Granger causality for neurophysiological data. *Comput. Biol. Med.*

Galaburda, A. M., Sherman, G. F., Rosen, G. D., Aboitiz, F., and Geschwind, N. (1985). Developmental dyslexia: four consecutive patients with cortical anomalies. *Ann. Neurol.* 18, 222–233.

Gioia, G. A., Isquith, P. K., Kenworthy, L., and Barton, R. M. (2002). Profiles of everyday executive function in acquired and developmental disorders. *Child Neuropsychol.* 8, 121–137.

Granger, C. W. J. (1969). Investigating causal relations by econometric models and cross-spectral methods. *Econometrica* 37, 424–438.

Gross, J., Schmitz, F., Schnitzler, I., Kessler, K., Shapiro, K., Hommel, B., and Schnitzler, A. (2004). Modulation of long-range neural synchrony reflects temporal limitations of visual attention in humans. *Proc. Natl. Acad. Sci. U.S.A.* 101, 13050–13055.

Gross, J., Schmitz, F., Schnitzler, I., Kessler, K., Shapiro, K., Hommel, B., and Schnitzler, A. (2006). Anticipatory control of long-range phase synchronization. *Eur. J. Neurosci.* 24, 2057–2060.

Hämäläinen, M., Hari, R., Ilmoniemi, R., Knuutila, J., and Lounasmaa, O. (1993). Magnetoencephalography – theory, instrumentation, and applications to noninvasive studies of the working human brain. *Rev. Mod. Phys.* 65, 1–93.

Hampshire, A., Thompson, R., Duncan, J., and Owen, A. M. (2010). Lateral prefrontal cortex subregions make dissociable contributions during fluid reasoning. *Cereb. Cortex.* doi: 10.1093/cercor/bhq085

Heim, S., and Keil, A. (2004). Large-scale neural correlates of developmental dyslexia. *Eur. Child Adolesc. Psychiatry* 13, 125–140.

Hoeft, F., Hernandez, A., McMillon, G., Taylor-Hill, H., Martindale, J. L., Meyler, A., Keller, T. A., Siok, W. T., Deutsch, G. K., Just, M. A., Whitfield-Gabrieli, S., and Gabrieli, J. D. (2006). Neural basis of dyslexia: a comparison between dyslexic and nondyslexic children equated for reading ability. *J. Neurosci.* 26, 10700–10708.

Hoeft, F., Meyler, A., Hernandez, A., Juel, C., Taylor-Hill, H., Martindale, J. L., McMillon, G., Kolchugina, G., Black, J. M., Faizi, A., Deutsch, G. K., Siok, W. T., Reiss, A. L., Whitfield-Gabrieli, S., and Gabrieli, J. D. (2007). Functional and morphometric brain dissociation between dyslexia and reading ability. *Proc. Natl. Acad. Sci. U.S.A.* 104, 4234–4239.

Horwitz, B., Rumsey, J. M., and Donohue, B. C. (1998). Functional connectivity of the angular gyrus in normal reading and dyslexia. *Proc. Natl. Acad. Sci. U.S.A.* 95, 8939–8944.

Humphreys, P., Kaufmann, W. E., and Galaburda, A. M. (1990). Developmental dyslexia in women: neuropathological findings in three patients. *Ann. Neurol.* 28, 727–738.

Kaufmann, W. E., and Galaburda, A. M. (1989). Cerebrocortical microdysgenesis in neurologically normal subjects: a histopathologic study. *Neurology* 39, 238–244.

Keller, T. A., and Just, M. A. (2009). Altering cortical connectivity. *Neuron* 64, 624–631.

Kenner, N. M., Mumford, J. A., Hommer, R. E., Skup, M., Leibenluft, E., and Poldrack, R. A. (2010). Inhibitory motor control in response stopping and response switching. *J. Neurosci.* 30, 8512–8518.

Klimesch, W., Doppelmayr, M., Wimmer, H., Gruber, W., Rohm, D., Schwaiger, J., and Hutzler, F. (2001). Alpha and beta band power changes in normal and dyslexic children. *Clin. Neurophysiol.* 112, 1186–1195.

Koyama, M. S., Kelly, C., Shehzad, Z., Penesetti, D., Castellanos, F. X., and Milham, M. P. (2010). Reading networks at rest. *Cereb. Cortex* 20, 2549–2559.

Lachaux, J. P., Jung, J., Mainy, N., Dreher, J. C., Bertrand, O., Baciu, M., Minotti, L., Hoffmann, D., and Kahane, P. (2008). Silence is golden: transient neural deactivation in the prefrontal cortex during attentive reading. *Cereb. Cortex* 18, 443–450.

Lazar, W., and Frank, Y. (1998). Frontal systems dysfunction in children with attention-deficit/hyperactivity disorder and learning disabilities. *J. Neuropsychiatry Clin. Neurosci.* 10, 160–167.

Lebel, C., and Beaulieu, C. (2009). Lateralization of the arcuate fasciculus from childhood to adulthood and its relation to cognitive abilities in children. *Hum. Brain Mapp.* 30, 3563–3573.

Levy, J., Pernet, C., Treserras, S., Boulanouar, K., Aubry, F., Demonet, J. F., and Celsis, P. (2009). Testing for the dual-route cascade reading model in the brain: an fMRI effective connectivity account of an efficient reading style. *PLoS ONE* 4, e6675. doi: 10.1371/journal.pone.0006675.

Liang, H., Bressler, S. L., Ding, M., Truccolo, W. A., and Nakamura, R. (2002). Synchronized activity in prefrontal cortex during anticipation of visuomotor processing. *Neuroreport* 13, 2011–2015.

MacSweeney, M., Brammer, M. J., Waters, D., and Goswami, U. (2009). Enhanced activation of the left inferior frontal gyrus in deaf and dyslexic adults during rhyming. *Brain* 132, 1928–1940.

Mainy, N., Jung, J., Baciu, M., Kahane, P., Schoendorff, B., Minotti, L., Hoffmann, D., Bertrand, O., and Lachaux, J. P. (2008). Cortical dynamics of word recognition. *Hum. Brain Mapp.* 29, 1215–1230.

Maisog, J. M., Einbinder, E. R., Flowers, D. L., Turkeltaub, P. E., and Eden, G. F. (2008). A meta-analysis of functional neuroimaging studies of dyslexia. *Ann. N. Y. Acad. Sci.* 1145, 237–259.

Matsumoto, A., and Iidaka, T. (2008). Gamma band synchronization and the formation of representations in visual word processing: evidence from repetition and homophone priming. *J. Cogn. Neurosci.* 20, 2088–2096.

McGraw Fisher, J., Liederman, J., Johnson, J., Lincoln, A., and Frye, R. (in press). A demonstration that task difficulty can confound the interpretation of lateral differences in brain activation between typical and dyslexic readers. *Laterality.*

Miller-Shaul S. (2005). The characteristics of young and adult dyslexic readers on reading and reading related cognitive tasks as compared to normal readers. *Dyslexia* 11, 132–151.

Narhi, V., Rasanen, P., Mesapelto, R. L., and Ahonen, T. (1997). Trail making test in assessing children with reading disabilities: a test of executive functions or content information. *Percept. Mot. Skills* 84, 1355–1362.

Ortiz, T., Exposito, F. J., Miguel, F., Martin-Loeches, M., and Rubia, F. J. (1992). Brain mapping in dysphonemic dyslexia: in resting and phonemic discrimination conditions. *Brain Lang.* 42, 270–285.

Pennington, B. F., and Lefly, D. L. (2001). Early reading development in children at family risk for dyslexia. *Child Dev.* 72, 816–833.

Penolazzi, B., Spironelli, C., Vio, C., and Angrilli, A. (2010). Brain plasticity in developmental dyslexia after phonological treatment: a beta EEG band study. *Behav. Brain Res.* 209, 179–182.

Pugh, K. R., Mencl, W. E., Jenner, A. R., Katz, L., Frost, S. J., Lee, J. R., Shaywitz, S. E., and Shaywitz, B. A. (2000a). Functional neuroimaging studies of reading and reading disability (developmental dyslexia). *Ment. Retard. Dev. Disabil. Res. Rev.* 6, 207–213.

Pugh, K. R., Mencl, W. E., Shaywitz, B. A., Shaywitz, S. E., Fulbright, R. K., Constable, R. T., Skudlarski, P., Marchione, K. E., Jenner, A. R., Fletcher, J. M., Liberman, A. M., Shankweiler, D. P., Katz, L., Lacadie, C., and Gore, J. C. (2000b). The angular gyrus in developmental dyslexia: task-specific differences in functional connectivity within posterior cortex. *Psychol. Sci.* 11, 51–56.

Quaglino, V., Bourdin, B., Czternasty, G., Vrignaud, P., Fall, S., Meyer, M. E., Berquin, P., Devauchelle, B., and de Marco, G. (2008). Differences in effective connectivity between dyslexic children and normal readers during a pseudoword reading task: an fMRI study. *Neurophysiol. Clin.* 38, 73–82.

Richards, T., Berninger, V., Winn, W., Stock, P., Wagner, R., Muse, A., and Maravilla, K. (2007). Functional MRI activation in children with and without dyslexia during pseudoword aural repeat and visual decode: before and after treatment. *Neuropsychology* 21, 732–741.

Richards, T. L., Berninger, V. W., Aylward, E. H., Richards, A. L., Thomson, J. B., Nagy, W. E., Carlisle, J. F., Dager, S. R., and Abbott, R. D. (2002). Reproducibility of proton MR spectroscopic imaging (PEPSI): comparison of dyslexic and normal-reading children and effects of treatment on brain lactate levels during language tasks. *AJNR Am. J. Neuroradiol.* 23, 1678–1685.

Richlan, F., Kronbichler, M., and Wimmer, H. (2009). Functional abnormalities in the dyslexic brain: a quantitative meta-analysis of neuroimaging studies. *Hum. Brain Mapp.* 30, 3299–3308.

Shaywitz, B. A., Skudlarski, P., Holahan, J. M., Marchione, K. E., Constable, R. T., Fulbright, R. K., Zelterman, D., Lacadie, C., and Shaywitz, S. E. (2007). Age-related changes in reading systems of dyslexic children. *Ann. Neurol.* 61, 363–370.

Shaywitz, S. E. (1998). Dyslexia. *N. Engl. J. Med.* 338, 307–312.

Shaywitz, S. E., and Shaywitz, B. A. (2005). Dyslexia (specific reading disability). *Biol. Psychiatry* 57, 1301–1309.

Shaywitz, S. E., and Shaywitz, B. A. (2008). Paying attention to reading: the neurobiology of reading and dyslexia. *Dev. Psychopathol.* 20, 1329–1349.

Shaywitz, S. E., Shaywitz, B. A., Fulbright, R. K., Skudlarski, P., Mencl, W. E., Constable, R. T., Pugh, K. R., Holahan, J. M., Marchione, K. E., Fletcher, J. M., Lyon, G. R., and Gore, J. C. (2003). Neural systems for compensation and persistence: young adult outcome of childhood reading disability. *Biol. Psychiatry* 54, 25–33.

Simos, P. G., Breier, J. I., Fletcher, J. M., Bergman, E., and Papanicolaou, A. C. (2000). Cerebral mechanisms involved in word reading in dyslexic children: a magnetic source imaging approach. *Cereb. Cortex* 10, 809–816.

Simos, P. G., Fletcher, J. M., Denton, C., Sarkari, S., Billingsley-Marshall, R., and Papanicolaou, A. C. (2006). Magnetic source imaging studies of dyslexia intervention. *Dev. Neuropsychol.* 30, 591–611.

Simos, P. G., Fletcher, J. M., Sarkari, S., Billingsley, R. L., Denton, C., and Papanicolaou, A. C. (2007). Altering the brain circuits for reading through intervention: a magnetic source imaging study. *Neuropsychology* 21, 485–496.

Snowling, M. J. (2008). Specific disorders and broader phenotypes: the case of dyslexia. *Q. J. Exp. Psychol. (Colchester)* 61, 142–156.

Spironelli, C., Penolazzi, B., and Angrilli, A. (2008). Dysfunctional hemispheric asymmetry of theta and beta EEG activity during linguistic tasks in developmental dyslexia. *Biol. Psychol.* 77, 123–131.

Svensson, I., and Jacobson, C. (2006). How persistent are phonological difficulties? A longitudinal study of reading retarded children. *Dyslexia* 12, 3–20.

Tamnes, C. K., Østby, Y., Walhovd, K. B., Westlye, L. T., Due-Tønnessen, P., and Fjell, A. M. (2010). Neuroanatomical correlates of executive functions in children and adolescents: a magnetic resonance imaging (MRI) study of cortical thickness. *Neuropsychologia* 48, 2496–2508.

Temple, E. (2002). Brain mechanisms in normal and dyslexic readers. *Curr. Opin. Neurobiol.* 12, 178–183.

Temple, E., Deutsch, G. K., Poldrack, R. A., Miller, S. L., Tallal, P., Merzenich, M. M., and Gabrieli, J. D. (2003). Neural deficits in children with dyslexia ameliorated by behavioral remediation: evidence from functional MRI. *Proc. Natl. Acad. Sci. U.S.A.* 100, 2860–2865.

Trebuchon-Da Fonseca, A., Benar, C. G., Bartolomei, F., Regis, J., Demonet, J. F., Chauvel, P., and Liegeois-Chauvel, C. (2009). Electrophysiological study of the basal temporal language area: a convergence zone between language perception and production networks. *Clin. Neurophysiol.* 120, 539–550.

von Stein, A., Rappelsberger, P., Sarnthein, J., and Petsche, H. (1999). Synchronization between temporal and parietal cortex during multimodal object processing in man. *Cereb. Cortex* 9, 137–150.

Wechsler, D. (1997). *Wechsler Adult Intelligence Scale-III (WAIS-III)*. New York: Psychological Corporation.

Willcutt, E. G., Pennington, B. F., Boada, R., Ogline, J. S., Tunick, R. A., Chhabildas, N. A., and Olson, R. K. (2001). A comparison of the cognitive deficits in reading disability and attention-deficit/hyperactivity disorder. *J. Abnorm. Psychol.* 110, 157–172.

Willcutt, E. G., Pennington, B. F., Olson, R. K., Chhabildas, N., and Hulslander, J. (2005). Neuropsychological analyses of comorbidity between reading disability and attention deficit hyperactivity disorder: in search of the common deficit. *Dev. Neuropsychol.* 27, 35–78.

Conflict of Interest Statement: The authors declare that the research was conducted in the absence of any commercial or financial relationships that could be construed as a potential conflict of interest.

Received: 15 June 2010; accepted: 08 November 2010; published online: 02 December 2010.

*Citation: Frye RE, Wu M-H, Liederman J and McGraw Fisher J (2010) Greater prestimulus effective connectivity from the left inferior frontal area to other areas is associated with better phonological decoding in dyslexic readers. Front. Syst. Neurosci. **4**:156. doi: 10.3389/fnsys.2010.00156*

Copyright © 2010 Frye, Wu, Liederman and McGraw Fisher. This is an open-access article subject to an exclusive license agreement between the authors and the Frontiers Research Foundation, which permits unrestricted use, distribution, and reproduction in any medium, provided the original authors and source are credited.

APPENDIX

CALCULATIONS OF GRANGER CAUSALITY USING LEAST-SQUARES LINEAR REGRESSION

In order to formulate this problem for LSLR we define matrix X^o for one data observation o as (A.1). The design matrix (A.2) is then defined for all observations from (A.1). The dependent matrix (A.3) is then defined from a series of O observations for each signal *s*. The coefficients for the above set of equations can then be solved for each signal s using the X and Y_s (A.4). The coefficients derived with (A.4) are the same coefficients outlined in Eq. 2. For each signal *s*, Eq. A.4 derives a coefficient matrix with coefficients $[c_{s,1,1}\ldots c_{s,1,P}.\ldots\ldots c_{s,S,1}\ldots c_{s,S,P}]$. Using the coefficients, the error of the AR for each source can be calculated using (A.5). The variance of the model error, also known as the mean squared error (MSE) for signal *s* is shown in Eq. A.6.

$$X^o = \left[a_1^o(t-1)\ldots a_1^o(t-P)\ a_2^o(t-1)\ldots a_2^o(t-P)\ldots a_S^o(t-1)\ldots a_S^o(t-P)\right] \quad (A.1)$$

$$X = \left[X^1\ldots X^o\right]' \quad (A.2)$$

$$Y_s = \left[a_s^1(t)\ldots a_s^o(t)\right] \quad (A.3)$$

$$c_s = (X'X)^{-1}(X'Y_s) \quad (A.4)$$

$$e_{s|1\ldots S} = Xc_s - Y_s \quad (A.5)$$

$$MSE_{s|1\ldots S} = \frac{\sum_{i=1}^{O} e_{s|1\ldots S}^2}{O} \quad (A.6)$$

Granger causality is a measure of the influence of one signal on another signal. This measure is based on the relative change in the model error when an independent signal is added to the AR model to improve the prediction of the dependent signal (Granger, 1969). For example, the signal $A = [a(t)\colon 1\ldots T]$ can be predicted by itself using as AR model as given in (A.7).

$$a(t) = \sum_{j=1}^{p} c_{a,j} \times a(t-j) + e_{a|a}(t) \quad (A.7)$$

In a similar manner, signal *A* can also be predicted by signal $B = [b(t)\colon 1\ldots T]$ as represented by (A.8).

$$a(t) = \sum_{j=1}^{p} c_{b,j} \times b(t-j) + e_{a|b}(t) \quad (A.8)$$

Similar to the equations provided in (2), signal *A* can also be predicted by itself, *A*, and another signal, *B*, as presented in (A.9).

$$a(t) = \sum_{j=1}^{p} c_{a,j} \times a(t-j) + \sum_{k=1}^{p} c_{b,j} \times b(t-k) + e_{a|ab}(t) \quad (A.9)$$

Granger causality (Ding et al., 2006) is calculated as the ratio of the variance of the model error before and after the addition of a new signal. We can calculate the GC of signal *B* on signal *A* using (A.10).

$$F_{b\to a} = \ln \frac{\mathrm{Var}(e_{a|a})}{\mathrm{Var}(e_{a|ab})} \quad (A.10)$$

We can apply the same calculation to the system of AR models presented in (2). The AR models for a signal *s* in (2) already accounts for the influence of all of signals, similar to (A.9) in the example above. We can now eliminate the signal of interest by reconstructing the matrix X^o leaving out the signal of interest. For example, if we were interested in the influence of signal 2 on any other signal *s*, we would reformulate X^o as demonstrated in (A.11), recalculate the LSLR and derive the error vector $e_{s|1,3\ldots S}$. Granger causality of the influence of signal 2 on signal *s* given all of the other signals 1 to *S* (expect for 2) would be calculated with (A.12).

$$X^o = \left[a_1^o(t-1)\ldots a_1^o(t-P)\ a_3^o(t-1)\ldots a_3^o(t-P)\ \ldots\ a_S^o(t-1)\ldots a_S^o(t-P)\right] \quad (A.11)$$

$$F_{2\to s} = \ln \frac{MSE_{s|1,3\ldots S}}{MSE_{s|1\ldots S}} \quad (A.12)$$

LINEAR MIXED-MODEL USED FOR STATISTICAL ANALYSIS

The general mixed-model is in the matrix form:

$$y = X\beta + Z\gamma + \varepsilon \quad (A.13)$$

where *y* is the dependent variable, which in this case is connectivity between two cortical regions, X is the design matrix for the fixed effects and covariate, β is a vector containing the parameters of the fixed effects and covariate, Z is the design matrix for the random effects, γ contains the parameters of the random effects and ε is the variance–covariance matrix of the model error. The key assumption of the mixed model are that both γ and ε have the expected value of 0 (i.e., $E(\gamma) = 0$ and $E(\varepsilon) = 0$) and known covariance structure given by the matrixes Var(γ) and Var(ε). The values for each row of the design matrix X are given by:

$$x(t,v,h,a_{p,v}) = \begin{bmatrix} c\ \mathrm{area}_1\ \mathrm{area}_2\ \mathrm{area}_3\ \mathrm{area}_4\ \mathrm{area}_5\ \mathrm{inout}\ \mathrm{read} \\ d_p(\mathrm{area}_1 \times \mathrm{inout})\ldots(\mathrm{area}_5 \times \mathrm{inout}) \\ (\mathrm{area}_1 \times \mathrm{read})\ldots(\mathrm{area}_5 \times \mathrm{read})\ldots(\mathrm{area}_1 \times d_p)\ldots \\ (\mathrm{area}_5 \times d_p)\ (\mathrm{inout} \times \mathrm{read}) \\ (\mathrm{inout} \times d_p)\ (\mathrm{read} \times d_p)\ (\mathrm{area}_1 \times \mathrm{inout} \times \mathrm{read})\ldots \\ (\mathrm{area}_5 \times \mathrm{inout} \times \mathrm{read}) \\ (\mathrm{area}_1 \times \mathrm{inout} \times d_p)\cdots(\mathrm{area}_5 \times \mathrm{inout} \times d_p) \\ (\mathrm{area}_1 \times \mathrm{read} \times d_p)\ldots(\mathrm{area}_5 \times \mathrm{read} \times d_p) \\ (\mathrm{inout} \times \mathrm{read} \times d_p)(\mathrm{area}_1 \times \mathrm{inout} \times \mathrm{read} \times d_p)\ldots \\ (\mathrm{area}_5 \times \mathrm{inout} \times \mathrm{read} \times d_p) \end{bmatrix} \quad (A.14)$$

where *c* is the constant with value 1, area is the cortical area represented by the five dummy variables $\mathrm{area}_1\ldots\ \mathrm{area}_5$ (i.e., for analysis of the left frontal region, dummy variables would be set up to represent the other cortical regions that the left frontal region is connected

to, for example $area_1 = 1$ for left TPA and 0 otherwise, $area_2 = 1$ for left occipital and 0 otherwise, etc.), inout is connectivity direction represented by a dummy variable (i.e., inward = 0, outward = 1), read is reading group as represented by a dummy variable (i.e., dyslexia = 1, typical = 0) and d_p is the centered *d*-prime value for the particular participant, *p*. The values for each row of the random-effects design matrix Z are given by

$$z(p, \text{area}, \text{inout}) = \left[p_1 \ldots p_{17}\ \text{area}_1\ \text{area}_2\ \text{area}_3\ \text{area}_4\ \text{area}_5\ \text{inout}\right] \quad \text{(A.15)}$$

where *p* is the participant where p_i is 1 for participant *i* and 0 otherwise. The mixed-model was calculated using the restricted maximum likelihood method.

frontiers in
SYSTEMS NEUROSCIENCE

ORIGINAL RESEARCH ARTICLE
published: 29 October 2010
doi: 10.3389/fnsys.2010.00150

Influences of neural pathway integrity on children's response to reading instruction

Nicole Davis[1,2,3]*, Qiuyun Fan[2,4], Donald L. Compton[1,5], Doug Fuchs[1,5], Lynn S. Fuchs[1,5], Laurie E. Cutting[1,2,3,5], John C. Gore[1,2,3,4] and Adam W. Anderson[1,2,3,4]

[1] *Vanderbilt University Kennedy Center for Research on Human Development, Nashville, TN, USA*
[2] *Vanderbilt University Institute of Imaging Science, Nashville, TN, USA*
[3] *Department of Radiology and Radiological Sciences, Vanderbilt University, Nashville, TN, USA*
[4] *Department of Biomedical Engineering, School of Engineering, Vanderbilt University, Nashville, TN, USA*
[5] *Vanderbilt Peabody, Department of Special Education, Vanderbilt University, Nashville, TN, USA*

Edited by:
Barry Horwitz, National Institutes of Health, USA

Reviewed by:
Kristina Simonyan, Mount Sinai School of Medicine, USA
Mohamed L. Seghier, University College London, UK

***Correspondence:**
Nicole Davis, Vanderbilt University, Peabody Box 328, 230 Appleton Place, Nashville, TN 37203, USA.
e-mail: nikki.davis@vanderbilt.edu

As the education field moves toward using responsiveness to intervention to identify students with disabilities, an important question is the degree to which this classification can be connected to a student's neurobiological characteristics. A few functional neuroimaging studies have reported a relationship between activation and response to instruction; however, whether a similar correlation exists with white matter (WM) is not clear. To investigate this issue, we acquired high angular resolution diffusion images from a group of first grade children who differed in their levels of responsiveness to a year-long reading intervention. Using probabilistic tractography, we calculated the strength of WM connections among nine cortical regions of interest and correlated these estimates with participants' scores on four standardized reading measures. We found eight significant correlations, four of which were connections between the insular cortex and angular gyrus. In each of the correlations, a relationship with children's response to intervention was evident.

Keywords: diffusion tensor imaging; probabilistic tractography, reading disability, response to intervention, connectivity, magnetic resonance imaging, children

INTRODUCTION

Cognitive tasks engage a set of distributed cortical areas that work together toward accomplishing a desired goal. Each neural center has its own specialization; activation is synchronized across participating areas. In regard to reading ability, the neural network can be generally associated with neuroanatomical areas within the left perisylvian region. Areas within this region have their own cognitive specialization and vary in their importance to reading ability (Shaywitz et al., 2004).

In terms of functional neuroimaging, an abundant literature links poor word recognition skill to differences in the neuronal functioning of three neuroanatomical areas within the perisylvian network: occipito-temporal cortex (OTC), temporo-parietal cortex (TPC), and inferior frontal gyrus (IFG). A variety of studies have shown that the neural signature of brain function in individuals with reading disability (RD) is characterized by decreased activity in the left OTC (Brunswick et al., 1999; Paulesu et al., 2001) and left TPC (Rumsey et al., 1997; Horwitz et al., 1998; Brunswick et al., 1999) and increased activity in right TPC (Shaywitz and Shaywitz, 2003) region. However, this functional pattern of RD is malleable: Children with RD who respond to intervention exhibit significantly increased activation of left hemisphere TPC and decreased activation of right hemisphere TPC (Simos et al., 2002, 2006; Aylward et al., 2003; Shaywitz et al., 2004). Such differences in functional activation serve to elucidate the neurobiological phenotype for responsiveness to intervention (RTI). This is an important point because under the new Federal educational policy enacted in the reauthorization of the Individuals with Disabilities Education Act (IDEA; P.L. 108-446; IDEA, 2004), RTI may be used to identify students with disabilities. An important question is the degree to which this classification can be connected to, and in a sense validated by, anomalous neurobiological characteristics.

While functional MRI (fMRI) studies have provided information about neuronal response to word stimuli, coordinated transfer of information between brain regions within a network is also an important component of information processing. White matter (WM) tracts connecting different brain regions support communication between brain regions, though these have been less frequently investigated in imaging studies. Until recently, the *in vivo* investigation of WM integrity was not possible. Now, with the advent of diffusion tensor imaging (DTI) WM integrity can be evaluated in adults and children. DTI is a technique that examines the structure of WM in the brain by measuring the molecular diffusion of water. Cell membranes and myelin hinder the diffusive movement of water perpendicular to those membranes. Hence diffusion rates are higher parallel to axons than perpendicular to them. Information on the directional preference of diffusion is used to perform fiber tracking and estimate connectivity (Conturo et al., 1999; Jones et al., 1999; Mori et al., 1999; Basser et al., 2000).

How highly connected gray matter regions are to one another appears to be associated with reading ability. In fact, several studies comparing children with reading difficulty to normal readers have reported significant differences in WM integrity in and between the temporal-parietal regions (Klingberg et al.,

2000; Beaulieu et al., 2005; Deutsch et al., 2005; Niogi and McCandliss, 2006). While differences between the WM of good and poor readers have been shown, the relationship between WM connectivity and intervention has only recently been investigated (Keller and Just, 2009). Using a voxel-based analysis of diffusion tensor parameters, Keller and Just (2009) showed changes in left medial superior frontal WM in 8–10 year olds after 100 h of tutoring. But, they did not examine WM architecture and connectivity as related to an individual's classification as a responder or non-responder to intervention. It should be noted that a few neuroimaging studies actually have addressed this issue, but *only* using functional neuroimaging (Simos et al., 2006; Odegard et al., 2008; Davis et al., in press). Whether a similar correlation exists between responsiveness to instruction and WM brain structures is not clear. Use of a complementary neuroimaging modality that captures WM connectivity thus can provide important and unique information.

The purpose of the current study was to investigate the potential relationship between WM connectivity and responsiveness to classroom based instruction in a group of children in the first grade, using voxel based analysis of diffusion tensor magnetic resonance imaging data. To investigate the relationship between WM connectivity and responsiveness to instruction, we identified nine cortical regions of interest that have strong theoretical justification for playing a part in reading skill (**Table 1**). Each region is involved with several different processes; therefore, we list in **Table 1** only the behaviors of interest to the current study. We calculated the connectivity strength (defined below) between these gray matter regions and correlated the strength estimate with participants' scores on reading measures. We hypothesized that we would replicate previous findings of differences in WM related to reading skill. In addition, we anticipated that children's responsiveness to reading intervention would provide additional information. To our knowledge, this is the first cortical connectivity study with children who differ in their response to a year-long reading intervention. However, this is an exploratory study with a small sample size and further studies with a larger sample size are needed.

MATERIALS AND METHODS

PARTICIPANTS

Imaging data were acquired on 15 children with a mean age of 7.5 years (SD = .43). All participants were recruited from a sample of first graders in Nashville participating in a federally funded randomized control trial (RCT). The RCT explores the effectiveness of response to intervention (RTI) as a means of identifying and preventing RD. All participants, including control participants, were screened and determined to be at-risk for reading difficulties at the beginning of first grade. Children with brain injury, other physical disabilities, severe emotional problems, uncorrected sensory disorders, ADHD, or an IQ < 80 were excluded during recruitment for this neuroimaging portion of the project. No child who was defined as having limited proficiency in English participated in the imaging study. No restriction was made for gender, ethnicity, or socioeconomic status. This study was approved by the Vanderbilt University Institutional Review Board. Written informed consent was obtained from the children's guardians. Written assent was obtained from the children.

Of the 15 datasets, four were not included due to severe head motion that rendered the tractography data unreliable. The remaining 11 participants were placed into groups based upon RCT categorization (described in Behavioral Measures and Responsiveness section below). As such, classroom controls (C; $n = 4$) were defined as children who were initially identified as at risk in the fall of first grade but benefited from classroom-based tier 1 instruction and therefore did not qualify for small-group tier 2 reading intervention. Treatment responders (R; $n = 2$) were defined as children who did not benefit from tier 1 instruction, were eligible for small-group tier 2 reading intervention, and achieved adequate results on behavioral measures indicating response to intervention. Treatment non-responders (NR; $n = 4$) were children who did not benefit from tier 1 instruction, were eligible for small-group tier 2 reading intervention, and did not achieve adequate results on behavioral measures, indicating a failure to respond to intervention.

Table 1 | Regions of interest.

Anatomical name	Acronym	Behavior of interest	L Vol* (cm)^3	R Vol* (cm)^3
Angular gyrus	ANG	Active during numerous verbal and written tasks	7.0 (1.3)	7.4 (1.5)
Fusiform	FUS	Related to the automatic recognition of written words	8.5 (2.3)	6.9 (1.9)
Inferior frontal sulcus	IFS	Active during naming tasks	2.5 (0.6)	2.4 (0.7)
Insula	INS	Supports phonological processing, particularly sublexical spelling to sound translation	2.5 (0.5)	2.1 (0.4)
Pars opercularis	OPE	Subregion of Broca's area mainly related to phonological processing but also syntactic processing	4.9 (1.2)	4.0 (1.0)
Planum temporale	PLA	Integration of orthographic with phonological and lexical features of printed words	2.2 (0.8)	1.6 (0.3)
Superior temporal cortex	STC	Associated with linking letters to corresponding phonemes	11.9 (3.0)	11.5 (3.1)
Thalamus	THA	Related to reading words out of context	7.1 (0.7)	7.0 (0.8)
Pars triangularis	TRI	Subregion of Broca's area mainly related to syntactic but also semantic and phonological processing	4.1 (1.0)	4.7 (0.9)

**L Vol, left hemisphere volume; R Vol, right hemisphere volume*

BEHAVIORAL MEASURES AND RESPONSIVENESS

Within the RCT, children's response to the instruction was estimated with a measure of word identification fluency (WIF; Fuchs et al., 2004; Compton et al., 2010), which was administered weekly. Growth modeling of WIF over 6 weeks at the beginning of the school year indicated each child's responsiveness to the general classroom instruction (prior to small-group tier 2 intervention). Children identified as unresponsive to general classroom instruction were assigned to small-group tier 2 intervention (tier 2), in which trained research assistants provided a prescribed reading intervention 3 days/week for 17 weeks. For participants receiving tier 2 intervention, weekly progress monitoring using WIF continued throughout the course of intervention. Upon conclusion of the intervention, responsiveness was determined using WIF intercept and slope over the duration of the intervention.

It is important to note that for the imaging study, limitations in sample size necessitated ranking participants by WIF intercept and slope and dividing participants to designate equal groups of responders and non-responders. These designations of responders and non-responders were used in all subsequent analyses.

Measures

Pre- and post-test behavioral measures were administered to all participants receiving tier 2 intervention. As stated above, the WIF growth was used to identify the participants' group membership. The pre- and post-test measures listed below were correlated with DTI data.

Word identification fluency. WIF consists of single-page lists of 100 high-frequency words randomly sampled from the Dolch preprimer, primer, and first-grade level lists (Fuchs et al., 2004). The task is to read as many words as possible in 1 min.

Untimed word identification skill. The Woodcock Reading Mastery Test – R/NU: Word Identification (WRMT-R: WID, Woodcock, 1998) is a norm-referenced test in which subjects read individual words ordered in difficulty until six sequential incorrect responses occur.

Untimed decoding skill. The Woodcock Reading Mastery Test – R/NU: Word Attack (WRMT-R: WAT, Woodcock, 1998) is a norm-referenced test that requires subjects to pronounce decodable pseudowords presented in ordered difficulty until a ceiling of six sequential incorrect responses is reached.

Sight word reading efficiency. The Test of Sight Word Reading Efficiency (TOWRE: SWE, Torgesen et al., 1997) is a norm-referenced measure of sight word reading accuracy and fluency in which participants read a list of words of increasing difficulty for 45 s.

Phonemic decoding efficiency. The Test of Phonemic Decoding Efficiency (TOWRE: PDE, Torgesen et al., 1997) is a norm-referenced measure of decoding accuracy and fluency that requires participants to read a list of decodable pseudowords of increasing difficulty for 45 s.

Intake procedure

In May, letters were sent to the parents of children who had successfully completed the RCT research protocol (including R, NR, and C participants) and met our recruitment criteria. All participants attended a single imaging session, in which each child was acclimated to the lab and received a child-oriented explanation of the study procedures. A play tunnel and a mock scanner were used to practice the tasks and prepare the child for the scanning environment.

Imaging and analysis

All imaging was performed on a research-dedicated Philips Achieva 3T MR scanner.

Structural imaging. High resolution 3D T1-weighted anatomical images were acquired (in a sagittal orientation) in just under 6 min. This was an inversion-prepared turbo field echo sequence (IR-TFE) with TI = 916 ms, TR = 7.9 ms, TE = 3.6 ms, SENSE acceleration factor of 2, matrix size 256 × 256 × 170, and FOV 170 mm × 256 mm × 256 mm for isotropic 1 mm^3 resolution. These images were used for subsequent scan prescription and for cortical parcellation.

Diffusion imaging. To measure brain tissue microstructure, we acquired high angular resolution diffusion images using a pulsed-gradient spin echo, echo planar imaging (single shot EPI) pulse sequence to image the entire brain at 2.5 mm isotropic resolution (50 slices, 96 × 96 matrix, TE = 65 ms, TR = 8.5 s, SENSE acceleration factor 2). We acquired 10 non-diffusion weighted and 92 diffusion weighted image volumes (92 directions at b = 1600 s/mm^2).

Field map. To correct for EPI distortions, we acquired a field map (1.875 mm × 1.875 mm × 4.934 mm voxels, TE = 2.9 and 3.9 ms, TR = 173 ms, scan time 28 s).

IMAGE ANALYSIS

The image analysis procedure performed for each participant is shown in **Figure 1**. As shown, diffusion weighted images were corrected for image distortions due to both eddy current (Netsch and van Muiswinkel, 2004) and static magnetic field errors (Jezzard and Balaban, 1995), the latter using the acquired field maps and FSL software[1]. Cortical reconstruction and volumetric segmentation was performed with the Freesurfer image analysis suite to identify the cortical and subcortical gray matter regions of interest (**Figure 2**) on the T_1-weighted structural scan. Briefly, this automated process includes motion correction, removal of non-brain tissue (Segonne et al., 2004), segmentation of the subcortical WM and deep gray matter volumetric structures (Fischl et al., 2002, 2004), intensity normalization (Sled et al., 1998), tessellation of the gray matter WM boundary, automated topology correction (Fischl et al., 2001; Segonne et al., 2007), and surface deformation (Dale and Sereno, 1993; Dale et al., 1999; Fischl and Dale, 2000). Information on Freesurfer is freely available online[2]. Regions were registered to the diffusion image space using a 12-parameter affine transformation calculated in FSL.

[1]www.fmrib.ox.ac.uk/fsl

[2]surfer.nmr.mgh.harvard.edu

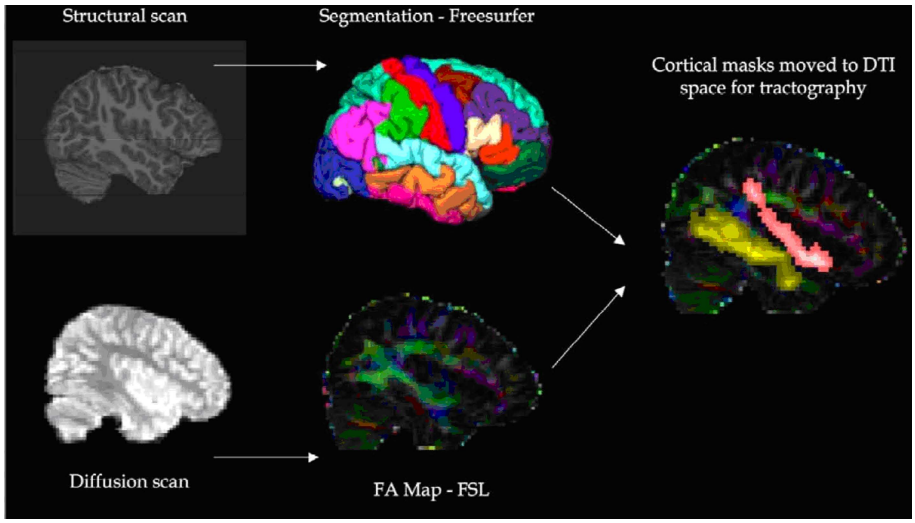


FIGURE 1 | Procedure used for imaging analysis.

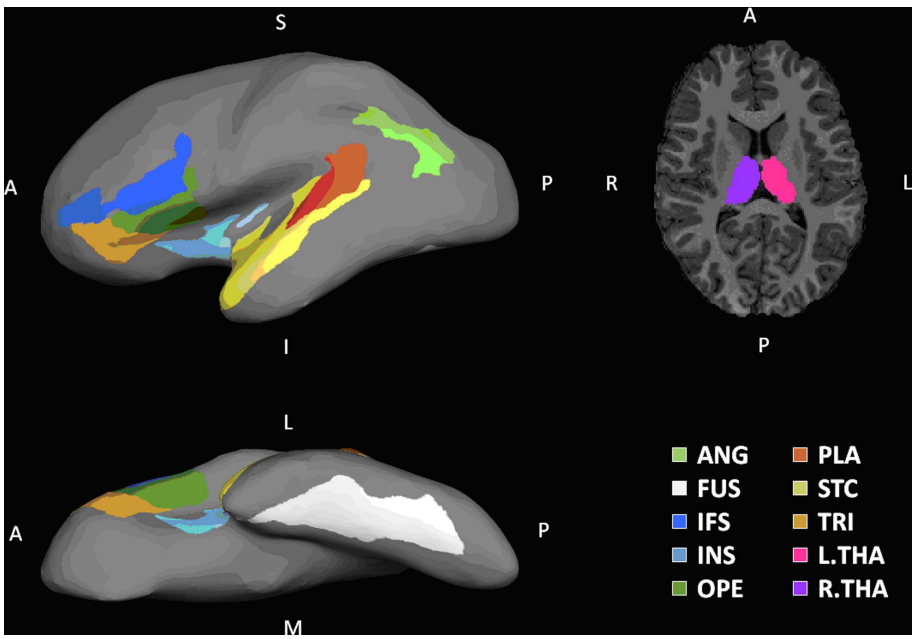


FIGURE 2 | Regions of interest. Shown on the left column are lateral and inferior views of ROIs rendered on the inflated surface of a left hemispherical brain. On the right column is a transverse slice of brain showing THA. Eighteen ROIs identified in this paper are labeled in the following manner: a prefix for cerebral hemisphere (L, left hemisphere; R, right hemisphere), a dot following the prefix, and one of the designators: ANG, angular gyrus; FUS, fusiform; IFS, inferior frontal sulcus; INS, insula; OPE, pars opercularis; PLA, planum temporale; STC, superior temporal gyrus; THA, thalamus; TRI, pars triangularis.

A probabilistic tractography algorithm (Behrens et al., 2003a,b, 2007), implemented in FSL, was then used to quantify the connectivity among these gray matter regions. Each of the 18 gray matter ROIs was used as a seed region, with the other 8 ROIs in the same hemisphere serving as possible termination regions. WM was used as a waypoint mask (i.e., all paths had to pass through the WM). Streamline tractography was initiated 10,000 times within each voxel of the seed region. The streamlines were propagated along directions sampled from the distribution characterizing the estimated uncertainty in the primary diffusion direction. A pathway is comprised of all the streamlines found connecting seed and target regions. In the current study we were only interested in direct pathways connecting region A to region B. Therefore, paths passing through the thalamus were excluded except when the thalamus was the seed or target region. For each pairing of seed and target regions, the number of connecting streamlines was calculated automatically by FSL. We divided this number by the number of seed voxels in A and used it to quantify the one-way connection ratio, $r(A- > B)$.

The same procedure was done for $r(B->A)$. The connectivity, or connection strength, between regions A and B was defined as the symmetrized connection ratio, c (A,B) = (r(A– > B) + r(B– > A)) /2. For each participant, we calculated the volume of each region of interest (**Table 1**). Because volume varied across participants, we calculated the correlation between region volume and the different behavioral measures. Connectivity was calculated for each of the possible 72 pairs of regions. **Figure 3** shows the result of these steps, a connectivity matrix, for one of the C participants in the study. An individual connectivity value that deviated from the original sample mean by two standard deviations or more was defined as an outlier and removed from the associated correlation analysis.

RESULTS

To test the hypothesis that reading performance was correlated with connectivity of key gray matter regions, we correlated each element of the connectivity matrix with the participants' scores on standardized tests of reading proficiency. **Figure 4** is a visual representation of the correlations between participants' connectivity estimates and their performance on each of the standardized measures. Within these matrices, left hemisphere connections are in the bottom triangle and right hemisphere connections are in the top triangle. The gray scale denotes significance level, with lighter colors indicating more significant correlations. Because of the small sample size, significant correlations were reported at $p < 0.05$ uncorrected. Connections with significant correlation at the $p < 0.05$ level are starred. We investigated age and gender influences on the behavioral and imaging results using two separate one way ANOVAs. Results showed a single significant effect: The left TRI to IFS pathway had a significant gender effect, in which girls had a significantly greater number of WM fibers connecting these regions. In addition, we correlated participant's performance on the behavioral tasks with the volume of each region. We found a positive correlation between the PDE subtest of the TOWRE and the left planum temporal ($p = 0.02$) and the left superior temporal cortex ($p = 0.03$).

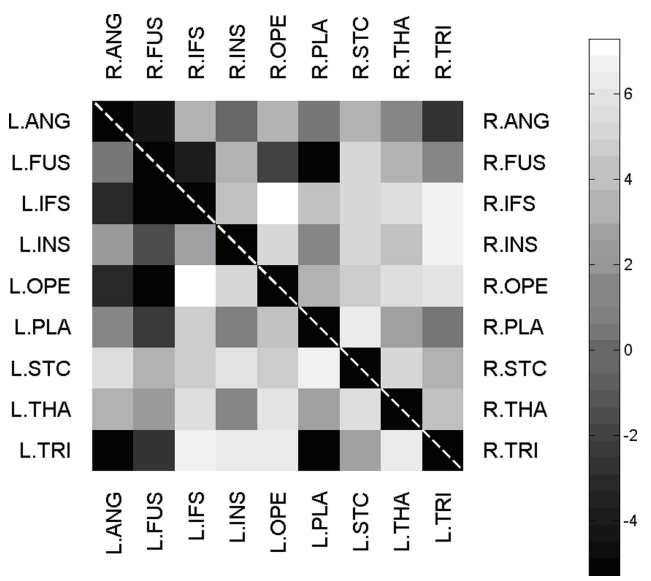


FIGURE 3 | Connectivity matrix. Matrix of connectivity between all intra-hemispherical pairs of $n = 18$ ROIs. Pairs within left-hemisphere are displayed in the lower left half, pairs within right-hemisphere in the upper right half. All connectivity strengths are displayed with a logarithmic grayscale map.

To facilitate interpretation of the significant connections, scatterplots for each finding are shown in **Figures 5 and 6**. These scatterplots also represent the relationship with response to instruction. In these plots, the NR participants are red, R participants are blue, and C participants are green.

As shown in **Figure 5**, increased reading score on each of the reading measures is related to greater connectivity between the left ANG and INS; the NR participants generally have lower connectivity than R or C participants. Similarly, performance on the WAT subtest correlated positively with connectivity values between TRI to STC (**Figure 6**). Scatterplots of this correlation showed that NR participants had lower connectivity than R or C participants (although only one R dataset survived outlier rejection). Alternatively, three negative correlations were found in which poorer readers, and more particularly, NR participants, had a greater magnitude of connectivity between brain regions than the other two groups. Two correlations involve connections to the THAL, yet in different hemispheres of the brain: the first was right THAL to right TRI and the second was left THAL to left STC. The third remaining region was also in the right hemisphere – TRI to STC.

DISCUSSION

Reading relies on a diffuse network of brain regions spread throughout the entire brain (Pugh et al., 2001). Reading skill is likely a result of the level of integration (and potentially segregation) of different gray matter regions within a network. Previous studies converge on the finding that good and poor readers have significantly different FA scores in a left hemisphere temporo-parietal region within this network (Klingberg et al., 2000; Beaulieu et al., 2005; Deutsch et al., 2005; Niogi and McCandliss, 2006; Rimrodt et al., 2010). From these results, the field has gained critical information on the structural relationship that exists between the brain and reading skill. However, the previous studies provide information on the contribution of a single tract to reading, effectively ignoring the connections between gray matter regions which are ultimately responsible for the functional processes that underlie reading skill. It may be that these findings are the critical pieces of the connectivity network that differs in good and poor reading. The present study attempted to clarify this issue by investigating connectivity strength between gray matter regions critical to reading, thus examining more directly than the previous studies the putative relationship between gray matter (function) and WM (structure).

Specifically, in the current study we used probabilistic tractography to calculate the strength of WM connections and investigate the potential relationship between WM connectivity and reading skill in the first grade. Results demonstrated that eight connectivity probability estimates correlated with participants' reading skill, four of which were connectivity estimates between the angular gyrus and insula. We are confident that these results are not attributable to differences in participants' gender or age. Furthermore, although we found evidence of a correlation between variability in the volume of the brain regions and participants' behavioral scores, these findings involved different regions than the connectivity findings. Our

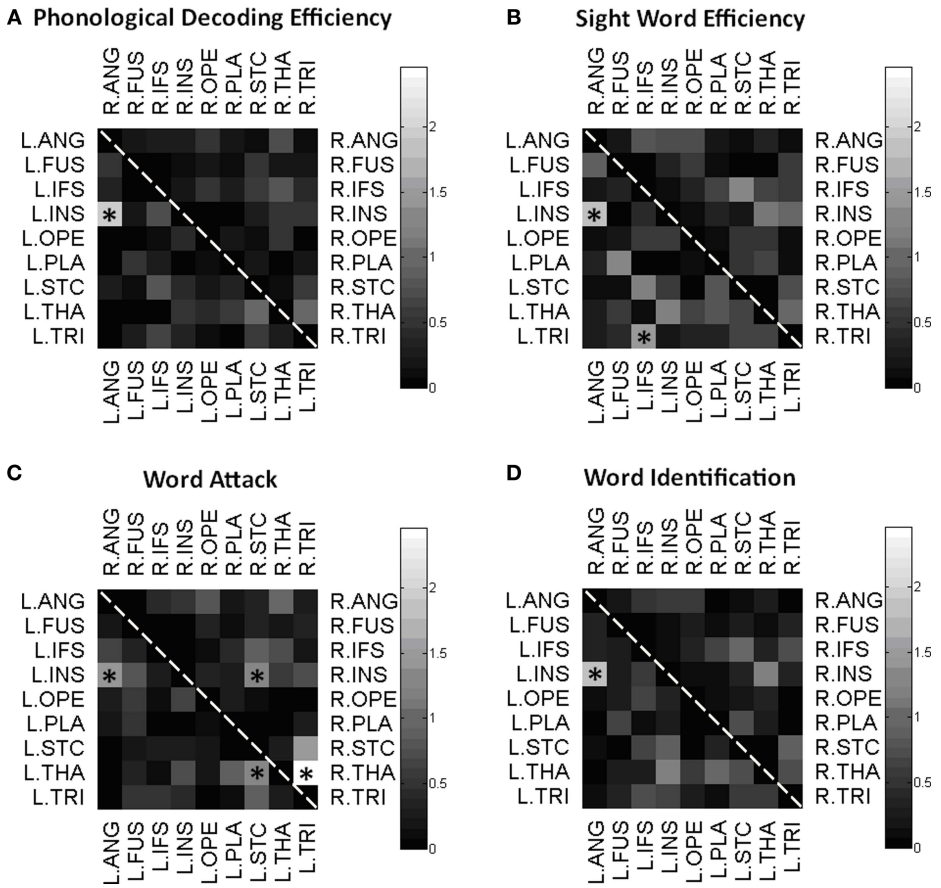


FIGURE 4 | Correlation matrices. Matrix of correlations between intra-hemispherical pairs of gray matter regions. Connectivity between each pair of ROIs is correlated with Phonological Decoding Efficiency **(A)**, Sight Word Efficiency **(B)**, Word Attack **(C)**, and Word Identification **(D)**, and the significance level of the correlation is displayed on a logarithmic scale. Significant correlations were marked by a star (*$p < 0.05$, uncorrected).

results extend the previous findings of WM differences related to reading skill to identify specific connections between gray matter regions. In particular, we propose that our findings of connectivity differences between insular cortex to angular gyrus in the left hemisphere corresponds to the temporo-parietal WM region reported in previous papers (Klingberg et al., 2000; Beaulieu et al., 2005; Deutsch et al., 2005; Niogi and McCandliss, 2006; Rimrodt et al., 2010).

Connectivity between left insula and angular gyrus correlated with all four reading tasks, indicating that better readers in general had greater connectivity estimates between these two brain regions on both timed and untimed reading tasks. Related to this, relative to the other two groups, NR had the fewest fiber pathways connecting these two regions. Despite the small sample size in the current study, the redundancy of findings across different measures of word reading skill is promising. However, interpretation of the findings is challenging, as the insula and the angular gyrus have very different roles. Within the cognitive domain, functional activation occurs in the left insula during language, speech, working memory, and attention tasks. Evidence exists that the left insula plays an integrative role between purely cognitive and other systems, including sensorimotor, social-emotional, and olfacto-gustatory systems (Dolan, 2002; Johansen-Berg and Matthews, 2002; Chen et al., 2007; Frith and Singer, 2008). By contrast, several studies have concluded that the left angular gyrus is important for the lexical processes that occur when reading words (e.g., Binder et al., 2009); though, it is possible that the angular gyrus is involved in phonological processing, especially in early years, as inferior parietal lobe is often associated with mapping phonological representations to their orthographic representations (Pugh et al., 2000). These results may indicate that connectivity between these two brain regions is a crucial aspect of the neural network that supports word recognition skill.

Alternatively, it may be that the insula and/or angular gyrus are simply acting as way stations (or relay stations), connecting the gray matter regions that are actually performing the domain specific tasks such as phonological processing and sight word recognition. For example, WM tracts traveling from planum temporale (Wernicke's area) in the superior temporal cortex to Broca's area in the frontal cortex are critical for speech development and normal reading (Hickok et al., 2003). These WM tracts may interact with the insula as they travel past on their way to frontal cortex. Related to this, it is possible that our results would change if a more liberal fiber tracking method were used. In the current study, WM tracts were counted if they connected a pair of gray matter regions and

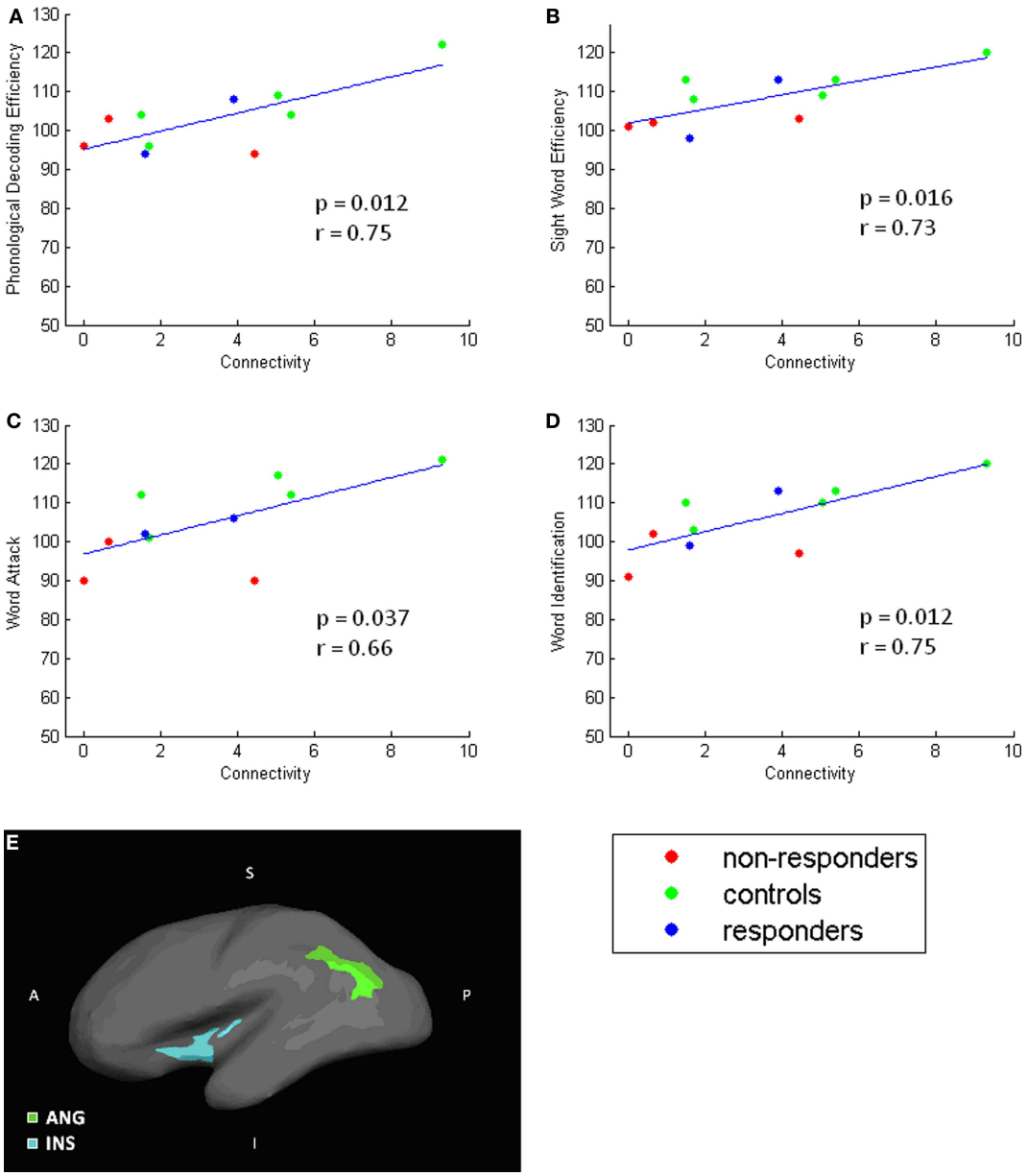


FIGURE 5 | Angular to insula scatterplots. Correlation scatterplots for L.INS and L.ANG. **(A–D)** Scatterplots showing detailed relationship between connectivity and specific test performances. **(E)** Locations of L.INS and L.ANG. A single NR participant was identified as an outlier and excluded from this analysis.

did not touch additional gray matter regions. This method was used because connectivity between two regions cannot be established with a high degree of reliability once the WM tract passes through additional gray matter region(s). Therefore, it would be fruitful for future imaging studies on reading skill to investigate both the direct connection between the insula and angular gyrus, while also considering the indirect role these regions play in the larger perisylvian language network. Additionally, in the current study, the entire insula was used as the seed region. However, insular cortex is often divided into separate regions with distinct functions (Dolan, 2002; Dupont et al., 2003; Kurth et al., 2010). Future connectivity studies with the insula would benefit from dividing it based on its functional differentiation.

In addition, a finding of interest that was unexpected was two negative correlations with thalamic connectivity estimates and the WAT subtest, a measure of pseudoword reading skill, in which NR participants had increased connectivity values compared to both R and C participants. Because the thalamus acts as an information processing way station for the brain, relaying sensation and motor signals and contributing to the regulation of arousal (Portas et al.,

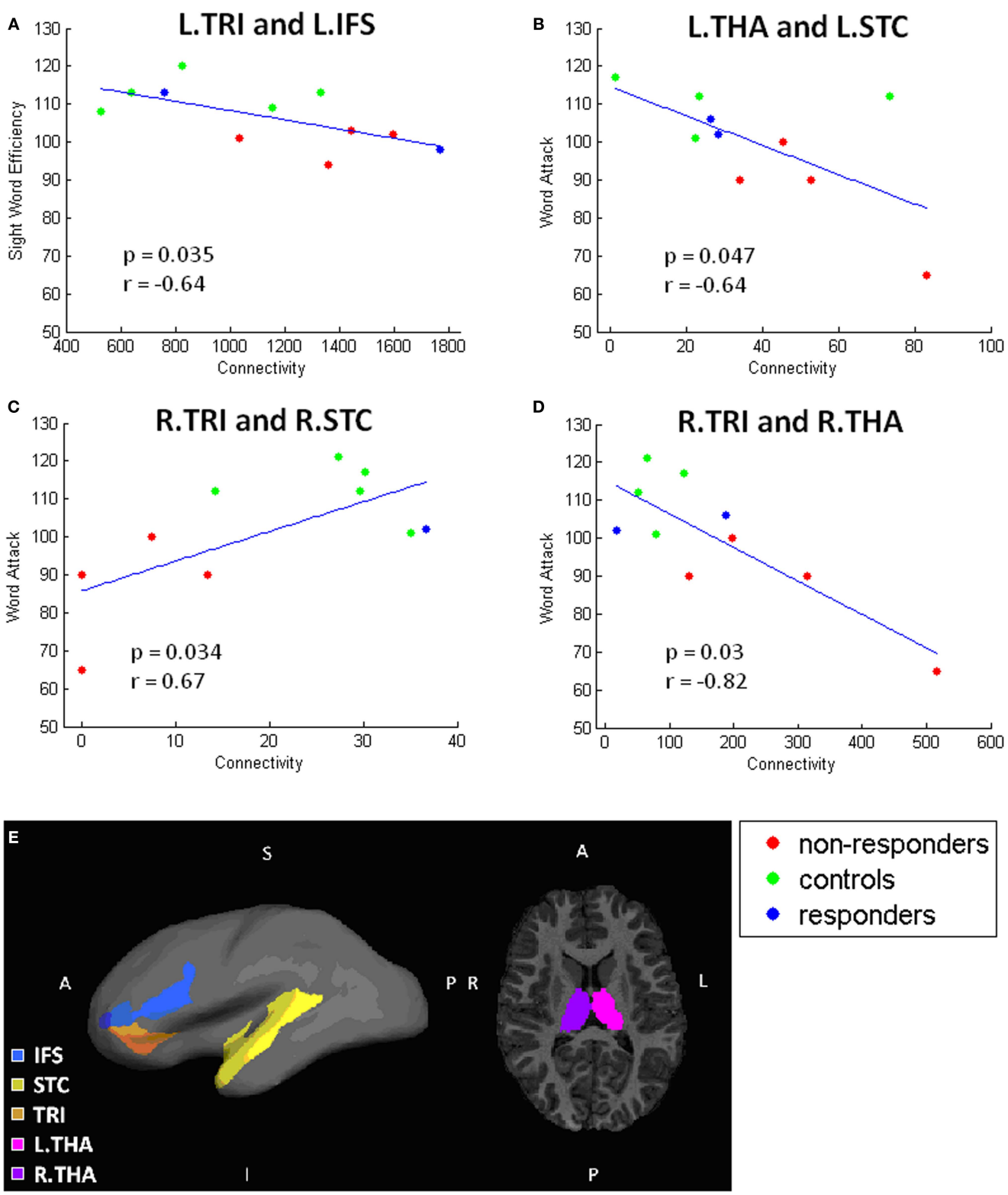


FIGURE 6 | Remaining significant correlations. Scatterplots showing correlations between connectivity and behavioral test performance. Each scatterplot corresponds to one pair of gray matter regions: **(A)** L.TRI and L.IFS, **(B)** L.THA and L.STC, **(C)** R.STC and R.TRI, **(D)** R.THA and R.TRI. Locations of these regions are illustrated in **(E)**.

1998), it is logical that there would be connections between the thalamus and reading related areas (STG and IFG). In fact, previous studies have reported individual variability in functional (Price et al., 1994; Fiebach et al., 2002; Turkeltaub et al., 2002) and structural (e.g., Galaburda and Eidelberg, 1982) aspects of the thalamus that relate to differences in reading skills, suggesting linkages between the thalamus and reading ability. For people who are poor at reading, thalamocortical connections may be more strongly related to reading ability than good readers because poor readers rely on these connections to a greater extent than those who are skilled. This would explain a negative correlation between strength of connection and reading skill (i.e., poorer reading = more connections). Although the sample size in the current study is small, these negative correlations, coupled with previous negative correlation findings and thalamic findings, are intriguing and suggest a need for further exploration. This finding requires follow up studies with larger numbers of participants to fully interpret its meaning. Other studies have also shown negative correlations between reading skill and neuroimaging findings (Brunswick et al., 1999; Sarkari et al., 2002; Shaywitz et al., 2002, 2003; Turkeltaub et al., 2003; Brem et al., 2009), which has been interpreted as utilization of alternative pathways. However, the exact meaning of these negative correlations is not known. It may be that they demonstrate that poor readers implement a compensatory strategy via the use of an alternative pathway (e.g., rely on memory for sight word reading; articulation based word decoding, etc.), or further investigations may reveal that they are in fact a result of error in measurement (e.g., multiple comparisons; performance differences between ability groups, etc.). For this reason, further investigation of this topic is needed to fully understand it.

An additional finding worth noting is that the scatterplots for each of the significant correlations showed a potential trend between participants' brain connectivity and their level of responsiveness to instruction. Although each correlation showed group differences in WM connectivity, the strength of the connections varied with the pair of regions under investigation. In other words, compared to children who responded to intervention (both R and C groups), the NR group had increased connectivity in some regions and decreased connectivity in others. Although caution is warranted when interpreting these results as the study was based on a small sample size, this is a promising finding, which demonstrates the importance of considering responsiveness to instruction in future studies of RD.

LIMITATIONS

Limitations in the study design hinder the interpretation of the results. In particular, the current study lacks a scan prior to intervention. Future studies would benefit from a longitudinal design, in which imaging data is acquired before and after intervention. This would provide data to investigate whether the group differences found in this study are a cause or a result of children's responsiveness to instruction. Large WM tracts are well within place by 9 months of age; however, a selective change in connectivity occurs at cortical and subcortical levels through the late second decade of life (O'Leary and Stanfield, 1989; Luo and O'Leary, 2005). Therefore, it is possible that WM is sculpted by life experiences. At our current level of understanding, it is not possible to determine the causal relationship between gray and WM deficits. It is possible that fiber pathways are abnormal in RD due to a deficit in the number of neurons in one reading-related region projecting along the fiber to other regions. On the other hand, deficits in myelination along a fiber could impact the efficiency and timing of information transfer between regions, which would cause reductions in activation. A longitudinal design in which functional, structural, and diffusion data were acquired would be useful to study this issue. Related to this, it is not clear how best to use fiber tractography to quantify pathway differences. In this study, we used a symmetrized measure of connectivity strength. In an attempt to minimize the variability in one way fiber measurements, more sensitive and specific connectivity methods may improve the correlations between DTI and behavior in future studies. In addition to a longitudinal design, more participants would increase the power of our study, allowing us to do more refined analyses of the data. In particular, due to the small sample size, conventional statistics were not used to test the significance of the results. Thus, replication and expansion of the current study's design with a larger sample size would be fruitful.

ACKNOWLEDGMENTS

This work was supported in part by the Vanderbilt Kennedy Center Hobbs Discovery grant, Grant R324G060036 from the U.S. Department of Education, Institute of Education Sciences, and the National Institutes of Health through the Biomedical MRI and MRS Training Program T32EB001628.

REFERENCES

Aylward, E. H., Richards, T. L., Berninger, V. W., Nagy, W. E., Field, K. M., Grimme, A. C., Richards, A. L., Thomson, J. B., and Cramer, S. C. (2003). Instructional treatment associated with changes in brain activation in children with dyslexia. *Neurology* 61, 212–219.

Basser, P. J., Pajevic, S., Pierpaoli, C., Duda, J., and Aldroubi, A. (2000). In vivo fiber tractography using DT-MRI data. *Magn. Reson. Med.* 44, 625–632.

Beaulieu, C., Plewes, C., Paulson, L. A., Roy, D., Snook, L., Concha, L., and Phillips, L. (2005). Imaging brain connectivity in children with diverse reading ability. *Neuroimage* 25, 1266–1271.

Behrens, T. E., Berg, H. J., Jbabdi, S., Rushworth, M. F., and Woolrich, M. W. (2007). Probabilistic diffusion tractography with multiple fibre orientations: what can we gain? *Neuroimage* 34, 144–155.

Behrens, T. E., Johansen-Berg, H., Woolrich, M. W., Smith, S. M., Wheeler-Kingshott, C. A., Boulby, P. A., Barker, G. J., Sillery, E. L., Sheehan, K., Ciccarelli, O., Thompson, A. J., Brady, J. M., and Matthews, P. M. (2003a). Non-invasive mapping of connections between human thalamus and cortex using diffusion imaging. *Nat. Neurosci.* 6, 750–757.

Behrens, T. E., Woolrich, M. W., Jenkinson, M., Johansen-Berg, H., Nunes, R. G., Clare, S., Matthews, P. M., Brady, J. M., and Smith, S. M. (2003b). Characterization and propagation of uncertainty in diffusion-weighted MR imaging. *Magn. Reson. Med.* 50, 1077–1088.

Binder, J. R., Desai, R. H., Graves, W. W., and Conant, L. L. (2009). Where is the semantic system? A critical review and meta-analysis of functional neuroimaging studies. *Cereb. Cortex* 19, 2767–2796.

Brem, S., Hadler, P., Bucher, K., Summers, P., Martin, E., and Brandeis, D. (2009). Tuning of the visual word processing system: distinct developmental ERP and fMRI effects. *Hum. Brain Mapp.* 30, 1833–1844.

Brunswick, N., McCrory, E., Price, C. J., Frith, C. D., and Frith, U. (1999). Explicit and implicit processing of words and pseudowords by adult developmental dyslexics: a search for Wernicke's Wortschatz? *Brain* 122, 1901–1917.

Chen, C. H., Ridler, K., Suckling, J., Williams, S., Fu, C. H., Merlo-Pich, E., and Bullmore, E. (2007). Brain

imaging correlates of depressive symptom severity and predictors of symptom improvement after antidepressant treatment. *Biol. Psychiatry* 62, 407–414.

Compton, D. L., Fuchs, D., Fuchs, L. S., Bouton, B., Gilbert, J. K., Barquero, L. A., Cho, E., and Crouch, R. C. (2010). Selecting at-risk first-grade readers for early intervention: eliminating false positives and exploring the promise of a two-stage gated screening process. *J. Educ. Psychol.* 102, 327–340.

Conturo, T. E., Lori, N. F., Cull, T. S., Akbudak, E., Snyder, A. Z., Shimony, J. S., McKinstry, R. C., Burton, H., and Raichle, M. E. (1999). Tracking neuronal fiber pathways in the living human brain. *Proc. Natl. Acad. Sci. U.S.A.* 96, 10422–10427.

Dale, A. M., Fischl, B., and Sereno, M. I. (1999). Cortical surface-based analysis. I. Segmentation and surface reconstruction. *Neuroimage* 9, 179–194.

Dale, A. M., and Sereno, M. I. (1993). Improved localization of cortical activity by combining EEG and MEG with MRI cortical surface reconstruction: a linear approach. *J. Cogn. Neurosci.* 5, 162–176.

Davis, N., Barquero, L., Compton, D., Fuchs, L. S., Fuchs, D., Gore, J., and Anderson, A. (in press). Functional correlates of children's responsiveness to intervention. *Dev. Neuropsychol.*.

Deutsch, G. K., Dougherty, R. F., Bammer, R., Siok, W. T., Gabrieli, J. D., and Wandell, B. (2005). Children's reading performance is correlated with white matter structure measured by diffusion tensor imaging. *Cortex* 41, 354–363.

Dolan, R. J. (2002). Emotion, cognition, and behavior. *Science* 298,1191–1194.

Dupont, S., Bouilleret, V., Hasboun, D., Semah, F., and Baulac, M. (2003). Functional anatomy of the insula: new insights from imaging. *Surg. Radiol. Anat.* 25, 113–119.

Fiebach, C. J., Friederici, A. D., Muller, K., and von Cramon, D. Y. (2002). fMRI evidence for dual routes to the mental lexicon in visual word recognition. *J. Cogn. Neurosci.* 14, 11–23.

Fischl, B., and Dale, A. M. (2000). Measuring the thickness of the human cerebral cortex from magnetic resonance images. *Proc. Natl. Acad. Sci. U.S.A.* 97, 11050–11055.

Fischl, B., Liu, A., and Dale, A. M. (2001). Automated manifold surgery: constructing geometrically accurate and topologically correct models of the human cerebral cortex. *IEEE Trans. Med. Imaging* 20, 70–80.

Fischl, B., Salat, D. H., Busa, E., Albert, M., Dieterich, M., Haselgrove, C., van der Kouwe, A., Killiany, R., Kennedy, D., Klaveness, S., Montillo, A., Makris, N., Rosen, B., and Dale, A. M. (2002). Whole brain segmentation: automated labeling of neuroanatomical structures in the human brain. *Neuron* 33, 341–355.

Fischl, B., Salat, D. H., van der Kouwe, A. J., Makris, N., Segonne, F., Quinn, B. T., and Dale, A. M. (2004). Sequence-independent segmentation of magnetic resonance images. *Neuroimage* 23(Suppl. 1), S69–S84.

Frith, C. D., and Singer, T. (2008). The role of social cognition in decision making. *Philos. Trans. R. Soc. Lond., B, Biol. Sci.* 363, 3875–3886.

Fuchs, L. S., Fuchs, D., and Compton, D. L. (2004). Monitoring early reading development in first grade: word identification fluency versus nonsense word fluency. *Except. Child.* 7–21.

Galaburda, A. M., and Eidelberg, D. (1982). Symmetry and asymmetry in the human posterior thalamus. Thalamic lesions in a case of developmental dyslexia. *Arch. Neurol.* 39, 333–336.

Hickok, G., Buchsbaum, B., Humphries, C., and Muftuler, T. (2003). Auditory-motor interaction revealed by fMRI: speech, music, and working memory in area Spt. *J. Cogn. Neurosci.* 15, 673–682.

Horwitz, B., Rumsey, J. M., and Donohue, B. C. (1998). Functional connectivity of the angular gyrus in normal reading and dyslexia. *Proc. Natl. Acad. Sci. U.S.A.* 95, 8939–8944.

IDEA, Public Law 108–446 (2004), 118 STAT. 2647, 2657–2658.

Jezzard, P., and Balaban, R. S. (1995). Correction for geometric distortion in echo planar images from B0 field variations. *Magn. Reson. Med.* 34, 65–73.

Johansen-Berg, H., and Matthews, P. M. (2002). Attention to movement modulates activity in sensori-motor areas, including primary motor cortex. *Exp. Brain Res.* 142, 13–24.

Keller, T. A., and Just, M. A. (2009). Altering cortical connectivity: remediation-induced changes in the white matter of poor readers. *Neuron* 64, 624–631.

Klingberg, T., Hedenhus, M., Temple, E., Salz, T., Gabrieli, J. D., Moseley, M. E., and Poldrack, R. A. (2000). Microstructure of temporoparietal white matter as a basis for reading ability: evidence from diffusion tensor magnetic resonance imaging. *Neuron* 25, 493–500.

Kurth, F., Ziles, K., Fox, P. T., Laird, A. R., and Eickhoff, S. B. (2010). A link between the systems: functional differentiation and integration within the human insula revealed by meta-analysis. *Brain Struct. Funct.* 214, 519–534.

Luo, L., and O'Leary, D. D. (2005). Axon retraction and degeneration in development and disease. *Annu. Rev. Neurosci.* 28, 127–156.

Mori, S., Crain, B. J., Chacko, V. P., and van Zijl, P. C. (1999). Three-dimensional tracking of axonal projections in the brain by magnetic resonance imaging. *Ann. Neurol.* 45, 265–269.

Netsch, T., and van Muiswinkel, A. (2004). Quantitative evaluation of image-based distortion correction in diffusion tensor imaging. *IEEE Trans. Med. Imaging* 23, 789–798.

Niogi, S. N., and McCandliss, B. D. (2006). Left lateralized white matter microstructure accounts for individual differences in reading ability and disability. *Neuropsychologia* 44, 2178–2188.

Odegard, T. N., Ring, J., Smith, S., Biggan, J., and Black, J. (2008). Differentiating the neural response to intervention in children with developmental dyslexia. *Ann. Dyslexia* 58, 1–14.

O'Leary, D. D., and Stanfield, B. B. (1989). Selective elimination of axons extended by developing cortical neurons is dependent on regional locale: experiments utilizing fetal cortical transplants. *J. Neurosci.* 9, 2230–2246.

Paulesu, E., Demonet, J. F., Fazio, F., McCrory, E., Chanoine, V., Brunswick, N., Cappa, S. F., Cossu, S. F., Habib, M., Frith, C. D., and Frith U. (2001). Dyslexia: cultural diversity and biological unity. *Science* 291, 2165–2167.

Portas, C. M., Rees, G., Howseman, A. M., Josephs, O., Turner, R., and Frith, C. D. (1998). A specific role for the thalamus in mediating the interaction of attention, and arousal in humans. *J. Neurosci.* 18, 8979–8989.

Price, C. J., Wise, R. J., Watson, J. D., Patterson, K., Howard, D., and Frackowiak, R. S. (1994). Brain activity during reading. The effects of exposure duration and task. *Brain* 117, 1255–1269.

Pugh, K. R., Mencl, W. E., Jenner, A. R., Katz, L., Frost, S. J., and Lee, J. R., Shaywitz, S. E., and Shaywitz, B. A. (2001). Neurobiological studies of reading and reading disability. *J. Commun. Disord.* 34, 479–492.

Pugh, K. R., Mencl, W. E., Shaywitz, B. A., Shaywitz, S. E., Fulbright, R. K., Constable, R. T., Skudarski, P., Marchione, K. E., Jenner, A. R., Fletcher, J. M., Liberman, A. M., Shankweiler, D. P., Katz, L., Lacadie, C., and Gore, J. C. (2000). The angular gyrus in developmental dyslexia. *Psychol. Sci.* 11, 51–56.

Rimrodt, S. L., Peterson, D. J., Denckla, M. B., Kaufmann, W. E., and Cutting, L. E. (2010). White matter microstructural differences linked to left perisylvian language network in children with dyslexia. *Cortex* 46, 739–749.

Rumsey, J. M., Nace, K., Donohue, B., Wise, D., Maisog, J. M., and Andreason, P. (1997). A positron emission tomographic study of impaired word recognition and phonological processing in dyslexic men. *Arch. Neurol.* 54, 562–573

Sarkari, S., Simos, P. G., Fletcher, J. M., Catillo, E. M., Brieier, J. I., and Papanicolaou, A. C. (2002). Contributions of magnetic source imaging to the understanding of dyslexia. *Semin. Pediatr. Neurol.* 9, 229–238.

Segonne, F., Dale, A. M., Busa, E., Glessner, M., Salat, D., Hahn, H. K., and Fischl, B. (2004). A hybrid approach to the skull stripping problem in MRI. *Neuroimage* 22, 1060–1075.

Segonne, F., Pacheco, J., and Fischl, B. (2007). Geometrically accurate topology-correction of cortical surfaces using nonseparating loops. *IEEE Trans. Med. Imaging* 26, 518–529.

Shaywitz, B. A., Shaywitz, S. E., Blachman, B. A., Pugh, K. R., Fulbright, R. K., Skudlarski, P., Mencl, W. E., Constable, R. T., Holahan, J. M., Marchione, K. E., Fletcher, J. M., Lyon, G. R., and Gore, J. C. (2004). Development of left occipitotemporal systems for skilled reading in children after a phonologically-based intervention. *Biol. Psychiatry* 55, 926–933.

Shaywitz, S. E., and Shaywitz, B. A. (2003). Dyslexia (specific reading disability). *Pediatr. Rev.* 24, 147–153.

Shaywitz, S. E., Shaywitz, B. A., Fulbright, R. K., Skudlarski, P., Mencl, W. E., Constable, R. T., Pugh, K. R., Holahan, J. M., Marchione, K. E., Fletcher, J. M., Lyon, G. R., and Gore, J. C. (2003). Neural systems for compensation and persistence: young adult outcome of childhood reading disability. *Biol. Psychiatry* 1, 25–33.

Shaywitz, B. A., Shaywitz, S. E., Pugh, K. R., Mencl, W. E., Fulbright, R. K., Skudlarski, P., Constable, R. T., Marchione, K. E., Fletcher, J. M., Lyon, G. R., and Gore, J. C. (2002). Disruption of posterior brain systems for reading in children with developmental dyslexia. *Biol. Psychiatry* 52, 101–110.

Simos, P. G., Fletcher, J. M., Bergman, E., Breier, J. I., Foorman, B. R., Castillo, E.

M., Davis, R. N., Fitzgerald, M., and Papanicolaou, A.C. (2002). Dyslexia-specific brain activation profile becomes normal following successful remedial training. *Neurology* 58, 1203–1213.

Simos, P. G., Fletcher, J. M., Denton, C., Sarkari, S., Billingsley-Marshall, R., and Papanicolaou, A. C. (2006). Magnetic source imaging studies of dyslexia interventions. *Dev. Neuropsychol.* 30, 591–611.

Sled, J. G., Zijdenbos, A. P., and Evans, A. C. (1998). A nonparametric method for automatic correction of intensity nonuniformity in MRI data. *IEEE Trans. Med. Imaging* 17, 87–97.

Torgesen, J. K., Wagner, R. K., and Rashotte, C. A. (1997). *Test of Word Reading Efficiency*. Austin, Tx: Pro:Ed.

Turkeltaub, P. E., Eden, G. F., Jones, K. M., and Zeffiro, T. A. (2002). Meta-analysis of the functional neuroanatomy of single-word reading: method and validation. *Neuroimage* 16, 765–780.

Turkeltaub, P. E., Gareau, L., Flowers, D. L., Zeffiro, T. A., and Eden, G. F. (2003). Development of neural mechanisms for reading. *Nat. Neurosci.* 6, 767–773.

Woodcock, R. W. (1998). *Woodcock Reading Mastery Test-Revised/Normative Update*. Circle Pines, MN: AGS.

Conflict of Interest Statement: The authors declare that the research was conducted in the absence of any commercial or financial relationships that could be construed as a potential conflict of interest.

Received: 14 June 2010; accepted: 01 October 2010; published online: 29 October 2010.

Citation: Davis N, Fan Q, Compton DL, Fuchs D, Fuchs LS, Cutting LE, Gore JC and Anderson AW (2010) Influences of neural pathway integrity in children's response to reading instruction. Front. Syst. Neurosci. ***4****:150. doi: 10.3389/fnsys.2010.00150*

Copyright: © 2010 Davis, Fan, Compton, Fuchs, Fuchs, Cutting, Gore and Anderson. This is an open-access article subject to an exclusive license agreement between the authors and the Frontiers Research Foundation, which permits unrestricted use, distribution, and reproduction in any medium, provided the original authors and source are credited.

frontiers in
SYSTEMS NEUROSCIENCE

ORIGINAL RESEARCH ARTICLE
published: 24 February 2011
doi: 10.3389/fnsys.2011.00009

Prefrontal compensatory engagement in TBI is due to altered functional engagement of existing networks and not functional reorganization

***Gary R. Turner*[1,2,3]*, *Anthony R. McIntosh*[3] *and Brian Levine*[3,4,5]**

[1] *Centre for Stroke Recovery, Sunnybrook Health Sciences Centre, Heart and Stroke Foundation, Toronto, ON, Canada*
[2] *Department of Occupational and Rehabilitation Sciences, Faculty of Medicine, University of Toronto, Toronto, ON, Canada*
[3] *Department of Psychology, University of Toronto, Toronto, ON, Canada*
[4] *Department of Neurology, Faculty of Medicine, University of Toronto, Toronto, ON, Canada*
[5] *Baycrest Center for Geriatric Care, Rotman Research Institute, Toronto, ON, Canada*

Edited by:
Barry Horwitz, National Institutes of Health, USA

Reviewed by:
Marco Atzori, University of Texas at Dallas, USA
Allison Carol Nugent, National Institute of Mental Health, USA

***Correspondence:**
Gary R. Turner, Centre for Stroke Recovery, Sunnybrook Health Sciences Centre, Heart and Stroke Foundation, 2075 Bayview Avenue, Room A447, Toronto, ON M4N 3M5, Canada.
e-mail: gary.turner@sunnybrook.ca

Functional neuroimaging studies of traumatic brain injury (TBI) have demonstrated altered neural recruitment, specifically within prefrontal cortex (PFC). This is manifest typically as increased recruitment of homologous regions of PFC (e.g., right ventrolateral PFC during performance of a verbal working memory task, possibly in response to damage involving the left PFC). The behavioral correlates of these functional changes are poorly understood. We used fMRI and multivariate analytic methods to investigate changes in spatially distributed activity patterns and their behavioral correlates in a sample of TBI patients with diffuse axonal injury (DAI, but without focal injury) and matched healthy controls. Participants performed working memory tasks with varying memory load and executive demand. We identified networks within left and right PFC that uniquely and positively correlated with performance in our control and TBI samples respectively, providing evidence of compensatory functional recruitment. Next we combined brain–behavior and functional connectivity analyses to investigate whether compensatory brain changes were facilitated by functional reorganization (i.e., recruitment of brain regions not engaged by our control sample) or altered functional engagement (i.e., differential recruitment of similar brain regions between the two groups based on task demands). In other words, does altered recruitment represent the instantiation of novel neural networks to support working memory performance after injury or the unmasking of extant, but behaviorally latent, functional connectivity? Our results support an altered functional engagement hypothesis. Areas within PFC that are normally coactivated during working memory are behaviorally relevant at an earlier stage of difficulty for TBI patients as compared to controls. This altered functional engagement, also evident in the aging literature, is attributable to distributed changes owing to significant DAI.

Keywords: traumatic brain injury, fMRI, working memory, functional connectivity, partial least squares, diffuse axonal injury

INTRODUCTION

Traumatic brain injury (TBI) is associated with altered patterns of neural recruitment during working memory (McAllister et al., 1999; Turner and Levine, 2008). This is typically manifest as increased activity in homologous regions of prefrontal cortex (PFC) or more spatially dispersed activity adjacent to areas implicated in non-injured controls (Christodoulou et al., 2001). Yet the cognitive implications of this altered recruitment are poorly understood. Altered functional brain response during working memory in TBI has been observed in the context of both poorer (e.g., Christodoulou et al., 2001) and equivalent task performance (e.g., Turner and Levine, 2008; Newsome et al., 2009). A recent review of functional neuroimaging studies in TBI reported similarly equivocal findings (Levine et al., 2006). To date, few studies have directly correlated brain activity and working memory performance. Perlstein et al. (2004) observed positive correlations between performance on an N-back working memory task and activity in left PFC in patients with mild and moderate TBI. Similar findings were also observed during N-back performance in a sample of more severely injured subjects, however, positive correlations were limited to posterior brain regions (Newsome et al., 2007). Thus it remains an open question as to whether these brain changes are compensatory, deleterious, or incidental to task performance following TBI. While the presence of functional brain changes in the context of preserved behavior suggests that such changes are unlikely to be deleterious, these data do not directly address whether these changes are compensatory.

Traumatic brain injury is associated with widespread disruptions in cerebral microvasculature and metabolic changes (Povlishock and Katz, 2005), thus altered functional recruitment may reflect physiological or systemic brain changes that, while co-occurring with working memory processing, are incidental to behavioral

performance. Functional brain changes may also be secondary to strategy differences between TBI and control subjects as has recently been demonstrated in healthy aging (Paxton et al., 2008). Previous studies have reported patterns of increased activity in homologous regions of lateral PFC or more spatially dispersed recruitment of adjacent brain regions in TBI relative to non-injured controls. A similar pattern of decreased lateralized response has also recently been observed in an electrophysiological investigation of sustained attention performance following TBI (Molteni et al., 2009). If these altered brain activity patterns are positively associated with task performance, this would provide evidence for compensatory functional brain changes. Here we used multivariate analysis (spatial–temporal partial least squares, PLS; McIntosh and Lobaugh, 2004) to identify brain–behavior correlations simultaneously across the whole-brain. The emphasis is on those brain regions that are correlated with task-behavior in healthy control subjects and whether these brain–behavior correlations are altered following TBI.

Characterizing the contribution of functional brain changes to behavioral performance following TBI has been hindered by heterogeneity in the severity of injury, chronicity, and neuropathology [e.g., focal lesions versus diffuse axonal injury (DAI)] as well as differences in task demand (Levine et al., 2006). Moreover, variability in behavioral performance is considered a hallmark of TBI (Stuss et al., 1989, 1994) and likely impedes detection of consistent brain–behavior correlations in this population. The current study directly investigates the relationship between altered functional brain response and behavioral performance during verbal working memory following TBI. To address the challenges identified in these earlier reports here we restricted recruitment to participants who had sustained a moderate to severe TBI but who had evidence of DAI on neuroradiological report but without evidence of focal brain damage (see Materials and Methods). In addition, the task paradigm varied load and executive demands (EDs) within working memory independently, allowing us to identify patterns of functional brain changes related to both maintenance and executive control processing separately.

We previously reported enhanced right PFC activity associated with increased ED within working memory following TBI (Turner and Levine, 2008). Here we examine whether functional changes in *distributed brain regions* following brain injury correlate with verbal working memory performance using behavioral PLS (bPLS) analyses (McIntosh et al., 2004). Unlike earlier studies that have correlated voxel-wise univariate changes in brain response with behavior, bPLS identifies whole-brain patterns of activity that are predictive of task-performance. Additionally, we examine whether functional connectivity amongst those network nodes demonstrating the most reliable brain and behavior correlations from the bPLS analysis are modulated by working memory task demands. Specifically, we ask whether functional brain changes observed in these participants reflect a pattern of altered functional engagement (i.e., recruitment of similar brain regions at lower levels of task demand than controls) or functional reorganization (i.e., recruitment of novel brain regions not engaged by controls). In other words, does the altered recruitment observed during working memory tasks following TBI represent the instantiation of novel neural networks to support working memory performance after injury or the unmasking of extant, but behaviorally latent, functional connectivity.

MATERIALS AND METHODS

PARTICIPANTS

All subjects were part of the Toronto TBI study (Levine et al., 2008) and were recruited based upon consecutive admissions to a level 1 trauma center. All subjects were right-handed, native English speakers and were screened for previous neurologic injury, major medical conditions affecting cognition, history of psychiatric illness, and the use of medications affecting cognition. Further details with respect to the patient demographics, injury characteristics, and recruitment inclusion and exclusion criteria of the larger sample have been reported elsewhere (Levine et al., 2008). Demographic and injury characteristics for the subset of patients included in the present report have been described in Turner and Levine (2008) and are only briefly reviewed here. We recognize that variability is a hallmark of TBI and we have addressed this variability in several ways. First, all subjects had sustained a closed head injury as a result of a motor vehicle accident. All were in the chronic stage of recovery at the time of study participation. The injury severity profile of the group included moderate and severe TBI participants as determined by trauma Glasgow Coma Score (GCS, Teasdale and Jennett, 1974), loss of consciousness and extent of post-traumatic amnesia. All participants underwent extensive behavioral testing as part of the larger Toronto TBI Study and data are reported in the earlier paper (Turner and Levine, 2008; **Table 1**). Neuropsychologically, participants had preserved neuropsychological performance on standardized testing and good functional recovery (return to previous level of work or school). All TBI participants in the current study had evidence of DAI-related neuropathology (hemosiderin deposits) on neuroradiological report. Moreover, patients were excluded from participation if they had evidence of focal lesions greater than 3 mm in diameter based on high resolution structural MRI, resulting in a final sample of relatively "pure" DAI participants. Other exclusion criteria included previous head injury, significant psychiatric history, or evidence of current or recent alcohol and drug abuse. Following screening a total sample of eight TBI participants (six male) were recruited for the study. Twelve neurologically normal participants (eight males) were also recruited. TBI and control participants were matched on age [$t(18) = 0.785$ ($p > 0.05$; NS)] and education [$t(18) = -1.99$ ($p > 0.05$; NS)]. All control participants were right-handed, native English speakers, and were screened for previous neurological injury, history of psychiatric illness, or drug use.

BEHAVIORAL TASK

In the present study we employed a modified version of the Alphaspan protocol described by Postle et al. (1999) and based on earlier work by Craik (1986). For each task trial, participants were required to study a letter set consisting of either three or five consonant letter strings (set size or "load" manipulation). For the ED manipulation, participants were asked to either hold the letter set in mind in it's original sequence ("MAINTAIN" condition) or to order the consonants alphabetically and maintain the new sequence over a brief delay period ("ALPHABETIZE" condition). At the end of the delay, a probe was presented consisting of a letter and an ordinal position (e.g., L-4? – "Was 'L' the fourth letter in the set?"). On Maintain trials, the probe referred to the ordinal position in the original letter set while on Alphabetize trials the probe referred to the letter position following

Table 1 | Cluster maxima from the behavior PLS (bPLS) analysis for the two-group analysis (LV 1).

Lag	x	y	z	Lat.	Anat.	BA	BSR	Clust.
0	–4	21	36	L	GFd	32	5.71	11
0	40	10	40	R	GFm	9	6.25	13
0	–20	–82	–13	L	GL	18	8.56	119
0	–8	–46	6	L	CG	29	7.40	78
0	0	–21	–36		B. stem		6.34	25
0	–8	–29	–29	L	B. stem		4.91	22
0	16	–33	–35	R	B. stem		4.64	13
0	16	–59	–14	R	Cereb		6.05	24
0	4	–83	–26	R	Cereb		7.11	80
1	8	52	27	R	GFs	9	5.86	11
1	–20	22	58	L	GFs	6	5.90	14
1	–51	–36	53	L	LPi	40	5.28	11
1	–28	–52	54	L	LPs/LPi	7/40	9.53	18
1	–24	–82	–13	L	GF	18	9.02	143
1	–44	–85	15	L	GOm	19	7.06	11
1	20	–86	–13	R	GL	18	12.10	66
1	–8	21	32	L	GC	32	5.66	22
1	–4	–50	6	L	CG	30	6.34	20
1	0	–25	–32		B. stem		6.65	62
1	24	–63	–14	R	Cereb		6.10	28
2	24	52	38	R	GFs	8	5.54	15
2	–48	51	12	L	GFm	10/46	5.82	16
2	44	47	16	R	GFm	46	13.75	38
2	40	16	18	R	GFi	44/45	5.91	25
2	–20	11	62	L	GFs	6	6.04	13
2	–32	–51	–14	L	GF	37	6.42	24
2	48	18	–21	R	GTs	38	6.22	13
2	–24	–53	21	L	GTm	39	5.61	22
2	16	–39	76	R	LPc	7	7.90	14
2	–16	–64	44	L	PCu	7	7.56	82
2	24	–86	–13	R	GF	18	10.65	51
2	–44	–88	23	L	GO	19	5.86	11
2	–44	–90	–9	L	GOi	18	7.67	53
2	0	–46	13		GC	30	6.97	41
2	–20	–25	–39	L	B. stem		6.58	81
2	28	–63	–17	R	Cereb		6.64	22
3	40	47	16	R	GFm	46	9.90	18
3	28	–46	21	R	GTm	39	5.74	18
3	–28	–50	14	L	GTm	39	5.75	19
3	–24	–59	58	L	PCu	7	6.31	69
3	24	–63	58	R	PCu	7	5.77	12
3	24	–90	–16	R	GF	18	9.49	54
3	16	–33	–39	R	B. stem		7.32	11
3	32	–55	–21	R	Cereb		5.72	27
4	–16	–83	–26	L	Cereb		5.18	11
4	20	–86	–19	R	Cereb		5.70	24

*This collection of brain regions demonstrated a positive correlation with task accuracy differentially across group and condition indicated in **Figure 1.** Cluster thresholds (i.e., how reliably each brain region expressed the LV) was determined using a bootstrapping procedure (see Materials and Methods). Here we report BSR's >4.0 (corresponding approximately to $p < 0.0001$) with a minimum spatial extent of 10 voxels. Lag refers to the temporal window with lag 0 corresponding to 2–4 s after stimulus onset. Each lag represents a 2-s time window (see Materials and Methods for details). Voxel coordinates are reported in Talairach coordinates.*

Lat, laterality; Anat., anatomical region; abbreviations consistent with the atlas (see below). BA, Brodmann area; BSR, bootstrap ratio; Clust., cluster size (in voxels); GFd, medial frontal gyrus; GFm, middle frontal gyrus; GL, lingual gyrus; CG, cingulate gyrus; B. stem, brain stem; Cereb, cerebellum; GFs, superior frontal gyrus; LPs, superior parietal lobule; LPi, inferior parietal lobule; GF, fusiform gyrus; GOm, middle occipital gyrus; GFi, inferior frontal gyrus; GTs, superior temporal gyrus; GTm, middle temporal gyrus; LPc, paracentral lobule; PCu, precuneus; GO, orbital frontal gyrus; GOi, inferior occipital gyrus..

alphabetization of the list. Probability of a correct probe was set at 0.5 for all trials in all conditions. Prior to scanning, each participant completed a training session consisting of step-by-step instructions for each task condition. Once there were no further questions for the administrator, all subjects completed 20 further trials (five trials in each of the four conditions) immediately prior to entering the MR scanner. During scanning, participants completed 28 trials of each of the four task conditions (Alphabetize three- and five-letter sets, Maintain three- and five-letter sets) during a single scanning session. Within each session a total of four individual scans were acquired. Trials were grouped by ED with two blocks of seven trials at each level of ED presented during a single scan acquisition. Total stimulus onset asynchrony was 18000 ms (three-letter trials) or 19000 ms (five-letter trials). Each individual scan acquisition was 12 min in duration (see Turner and Levine, 2008 for a full trial schematic).

fMRI SCANNING AND ANALYSES

Scanning was performed at Sunnybrook Health Sciences Centre on a research-dedicated whole-body 3.0 T MRI system (Signa 3T94 hardware, VH3M3 software; General Electric Healthcare, Waukesha, WI, USA) with a standard quadrature bird-cage head coil. Participants were placed in the scanner in supine position, with their head firmly placed in a vacuum pillow to minimize head movement. Earplugs were provided to reduce the noise from the scanner. A volumetric anatomical MRI was performed before functional scanning, using standard high-resolution 3D T1-weighted fast spoiled gradient echo (FSPGR) images (TR/TE = 7.2/3.1 ms, inversion-recovery prepared T1 = 300 ms, flip angle 15°, 256 × 192 acquisition matrix, 124 axial slices 1.4 mm thick, voxel size = 0.86 cm × 0.86 cm, FOV = 22 cm × 16.5 cm). Functional imaging was performed to measure the blood oxygenation level dependent (BOLD) effect (Ogawa et al., 1990). Scans were obtained using a single-shot T2*-weighted pulse with spiral in-out, achieving 26 slices, each 5 mm thick (TR/TE = 2000/30 ms, flip angle 70°, 64 × 64 acquisition matrix, 26 axial slices 5 mm thick, voxel size = 3.125 mm × 3.125 mm, slice spacing = 0, FOV = 20 cm × 20 cm). Data pre-processing was performed using Analysis of Functional NeuroImages software (Cox and Hyde, 1997). At the beginning of each scan, stimulus presentation was synchronized with the start of image acquisition through a triggering pulse input from the scanner to the E-prime presentation software. The initial 10 time points from each functional image volume were excluded from the analyses to allow for stabilization

of the magnetic field gradients. Time-series data were spatially co-registered (aligned volumetrically to a reference image within the run, using the 3dvolreg program in AFNI) to correct for small head motion using a 3-D Fourier transform interpolation, and the linear trends were removed. Uncorrected head motion (spikes) was identified through visual inspection and reduced through averaging the two surrounding time points. Physiological motion (respiration and heart beat) was also removed through linear filtering. Finally, slice timing correction was carried out to account for the time dependent discrepancy between the initial and final slice acquisitions. Images were then spatially transformed to an fMRI spiral scan template generated from 30 subjects scanned locally. This template was registered to the MNI305 template. The transformation of each subject to the spiral template was achieved using a 12-parameter affine transform with sinc interpolation as implemented in SPM99 (http://www.fil.ion.ucl.ac.uk/spm; Friston et al., 1995). Images were smoothed with an 8-mm isotropic Gaussian filter before analysis. For each subject, "brain" voxels in a specific image were defined as voxels with an intensity greater than 15% of the maximum value in that image. The union of masks was used for group analyses as described below.

PARTIAL LEAST SQUARES ANALYSES

Primary fMRI data analysis was carried out using spatiotemporal PLS (McIntosh et al., 1996; and for a full review of the method see McIntosh et al., 2004). In brief, PLS computes an optimal least squares fit to the "cross-block" correlation between the exogenous and dependent measures. Limiting the analysis to this part of a correlation or covariance matrix distinguishes PLS from principal components analysis (PCA) as solutions are constrained to the part of the covariance structure that is attributable to experimental manipulations or related to behavior. PLS is particularly suitable for neuroimaging data where measures are highly correlated as items within a block are not adjusted for these correlations. PLS operates on the entire data structure at once with one data matrix for each group. Within group, condition blocks are stacked, and each subject has a row of data within each block. With n subjects and k conditions, there are $n\,b \times k$ rows in the group matrix. Columns contain the hemodynamic response (HRF) signal intensity measure at each voxel at each time point. To account for the lag in hemodynamic response, the lag window is 6 (TR = 2; 12 s), beginning at trial onset −1 TR. The HRF for each trial is expressed as the intensity difference from trial onset. The first column has intensity for the first voxel at the first time point, the second column has the intensity for the first voxel at the second time point etc. With m voxels and t time points, there are $m \times t$ columns in the matrix.

Singular value decomposition (SVD) is applied to re-express the matrix as a set of orthogonal singular vectors or latent variables (LVs). LVs are analogous to eigenvectors in PCA and account for the matrix in decreasing order of magnitude. Each LV contains a pair of vectors relating brain activity and experimental design. Singular values are used to calculate the proportion of the matrix accounted for by each LV. Statistical assessment of the LVs is done using permutation tests (500 permutations) and bootstrap estimation (100 estimations) of standard errors for the voxel saliences. The permutation test assesses whether the effect represented in a given LV is sufficiently strong, in a statistical sense, to be different from random noise. Permutations were carried out using sampling without replacement to reassign the order of conditions for each subject. PLS is recalculated for each new sample, and the probability of the permuted exceeding observed is determined. To determine the stability of the voxel saliences for the LVs retained, bootstrap estimates are calculated using sampling with replacement and PLS is rerun keeping the assignment of experimental conditions fixed for all subjects. No corrections for multiple comparisons are necessary because the voxel saliences are calculated in a single mathematical step on the whole brain. The ratio of the salience to the bootstrap standard error is approximately equivalent to a z-score and is used assess the reliability of the individual voxel saliences. Two forms of PLS were performed. The first, bPLS, was the primary analysis to investigate group differences in brain–behavior correlations for the working memory tasks. bPLS is a variant of PLS that identifies LVs that capture task- and group-dependent patterns of brain–behavior correlations (McIntosh et al., 2004). The correlation of behavior measures and the fMRI signal is computed across subjects within each task, producing within-task brain–behavior correlations for each of the four task conditions and groups. The strength and reliability of the LVs for bPLS is carried out as described above. For these analyses an LV was considered "significant" if the probability of the observed singular value for the LV given permutation testing was less than 0.01. Effects were considered to be reliable if the ratio of observed to estimated effects on bootstrap testing was greater than 4. This corresponds to a probability of approximately $p < 0.0001$ assuming bootstrap estimates were normally distributed (**Figure 1**; **Table 1**). This addressed the fundamental question as to whether those regions correlating most strongly with behavior differed between our two groups. From this analysis we identified seed regions of interest (ROI) to be used in the combined behavior and functional connectivity analysis.

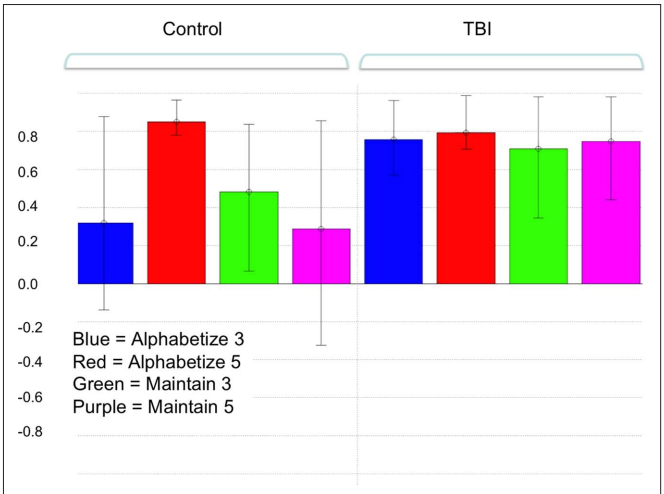


FIGURE 1 | Pattern of brain and behavioral correlations for the first latent variable (LV) in the combined group analysis. This LV accounted for the greatest magnitude of matrix variance (LV 1, $p < 0.01$). Colored bars denote the extent to which the experimental conditions relate to the differences in voxel signals represented in the LV (i.e., the design saliences). Error bars denote confidence intervals defined by the standard error of the bootstrap estimates. Error bars crossing zero reflect a non-significant contribution of that experimental condition to the LV pattern. Significant voxel clusters associated with this LV are presented in **Table 1**.

This second analysis used a behavior–seed PLS (sPLS) technique (McIntosh et al., 2004) to address the question of whether the behavioral relevance of regions demonstrating reliable brain–behavior correlations would depend upon their functional connectivity to other brain regions and whether these connectivity patterns varied between our two groups. sPLS identifies LVs that capture task- and group-dependent changes in functional connectivity between the seed ROI and the rest of the brain (i.e., brain–seed correlations). The correlation of the fMRI signal for the seed and for the rest of the brain is computed across subjects within groups within each task, resulting in a matrix of within group and within-task brain–seed correlation maps. SVD of the brain–seed correlation matrix produces three new matrices: the singular image of voxel saliences, singular values, and task saliences. The variation across the task saliences indicates whether a given LV represents a similarity or difference in the brain–seed correlation across tasks. This can also be shown by calculation of correlation between the brain scores (dot-product of the voxel salience and fMRI data) and seed fMRI signal for each task. The voxel saliences give the corresponding spatiotemporal activity pattern. Statistical assessment is identical to that used for bPLS.

RESULTS

BEHAVIOR

Full behavioral analyses are presented in Turner and Levine (2008), and only the between group results relevant to the current study are described here. As we were investigating brain and behavioral correlates at different levels of working memory task demand, task accuracy provided the best assay as it is less susceptible than reaction time measures to processing demands unrelated to working memory (e.g., scanning, retrieval, motor speed). One TBI patient was identified as an outlier for accuracy (TBI # 8). Trial-wise analysis for this patient revealed a consistent pattern of timing out on Alphabetize trials, greater for five- than for three-letter sets sizes. On those trials where responses were recorded, performance was within the average range of the TBI group for both three- and five-letter sets (78 and 67% respectively). This pattern is indicative of a task-specific decrement at response as opposed to disengagement or poor arousal. As we were interested in neural response during encoding and delay trial epochs, and not at probe, we did not exclude this patient's data. For the purposes of statistically assessing group effects on task performance, we used a winsorizing procedure by which the outlier values for this subject's accuracy on Alphabetize 3/5 trials were trimmed to 2 SD below the true mean of the sample (i.e., exclusive of the outlier). To confirm that our results were not unduly influenced by this outlier correction we ran all analyses with this subject's original data. There was a marginal but insignificant impact of the correction on the robustness of the bPLS output (see bPLS Results below). There was no impact on the behavioral results. Statistical analysis was carried out using a two group (control versus TBI) × 2 (ED) × 2 (set size) repeated measures ANOVA. There was a significant main effect of ED and set size (Set) [$F(1) = 18.51$ (ED); $F(1) = 11.42$ (Set), $p < 0.01$ for both comparisons] with poorer performance observed during the Alphabetize and set size five conditions. There was no main effect of group [$F(1) = 2.54$; NS] and no group × ED [$F(1) = 0.094$, NS] or group × Set [$F(1) = 0.182$, NS] interactions, indicating that the main effects of condition were stable across both the control and TBI groups. *Post hoc* analyses revealed that there were no group differences on any of the tasks ($p > 0.05$, all comparisons).

fMRI

Behavior PLS (brain and behavior)

A two-group bPLS with accuracy as the behavioral measure identified one significant LV ($p < 0.01$) reflecting brain and behavior correlations for all tasks in the TBI group but only for the Alphabetize 5 task in controls[1] (**Figure 1**). Positive saliences for this LV (**Table 1**) were observed in areas commonly implicated in neuroimaging studies of working memory (Wager and Smith, 2003). These task-related differences in brain–behavior correlations between our two groups suggests that TBI subjects were engaging this network, which included lateral aspects of PFC bilaterally, to support behavioral performance at lower levels of task demand than controls. That is, whereas controls engaged the network at the highest level of ED, Alphabetize 5, TBI patients did so at all levels.

We next conducted bPLS analyses for the control and TBI groups separately. For the control group analysis, one significant LV emerged ($p < 0.01$). This LV reflected positive brain and behavior correlations for all tasks (**Figure 2A**; **Table 2**). Brain regions demonstrating the highest salience for this LV included two regions of left lateral PFC [inferior frontal gyrus (GFi) and middle frontal gyrus (GFm)] as well as in posterior parietal and visual association cortices. For the TBI group, one LV approached statistical significance ($p < 0.058$). As with the control group, this LV reflected positive brain and behavior correlations for all tasks. However, in contrast to the control data, the highest salience for this LV occurred in regions of right lateral PFC (**Figure 2B**; **Table 3**) in addition to posterior parietal regions. These data extend the results of the combined group analysis and highlight the role of right lateral PFC in supporting working memory performance following TBI, particularly at lower levels of task demand.

Seed PLS (brain, behavior, and functional connectivity)

The results of the bPLS analyses supported our prediction that right frontal recruitment during working memory performance was compensatory for TBI participants. Next we asked whether this right PFC activity represented the instantiation of novel PFC networks to support working memory performance (functional reorganization) or the engagement of existing functional connections to support performance as load or executive control demands within working memory increase (altered functional engagement). For this analysis, we entered the four cluster maxima within PFC from the bPLS results (see **Figure 2**, i–iv; **Tables 2 and 3**) into a combined behavior and functional connectivity PLS analysis (Grady et al., 2003). Specifically, we investigated within a single PLS analysis: (i) how these regions functionally connect with other brain areas, in particular the other frontal ROIs, and how connectivity is altered by task demand (sPLS) (ii) whether these patterns of functional connectivity were related to task performance (bPLS)

[1]The brain and behavior correlation (r = 0.48) was also reliable for M3 in controls based on bootstrap estimates of standard error. However, this likely reflects near-ceiling performance on this task [mean = 0.96(0.03)] and is not discussed further here.

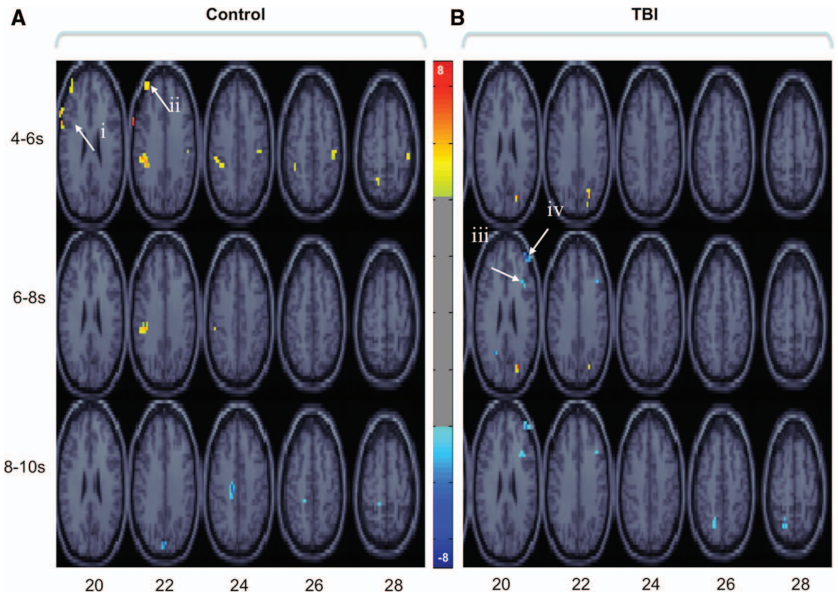


FIGURE 2 | Brain regions showing significant salience for the first LV in each group-wise bPLS analyses [i.e., those brain regions demonstrating positive correlations between brain response and task accuracy in control (A) and TBI (B) groups for all tasks]. Voxel salience reliabilities were determined by bootstrap ratios (BSR; range is indicated by the color bar). For these images BSR was set at 4 ($p < 10^{-4}$, corresponding approximately to a $p < 0.0001$) and cluster size was >10 voxels. Roman numerals indicate PFC regions with the most reliable and positive brain and behavior correlations across all tasks. Talairach coordinates (*x, y, z*) of cluster maxima: (i) left inferior frontal gyrus (GFi: –67, 9, 29); (ii) left middle frontal gyri (GFm: –40, 48, 23); (iii) right posterior middle frontal gyrus (pGFm: 36, 21, 25); (iv) right anterior middle frontal gyrus (aGFm: 40, 47, 16). These voxels are used as seed regions in subsequent seed and behavior PLS analyses (see text and **Figures 3 and 4)**.

and (iii) whether these patterns were different for our two groups. We present the behavioral and functional connectivity results from each of the four ROI seeds individually below.

Left inferior frontal gyrus (BA 44/6)

Latent variable 1 ($p < 0.001$) demonstrated reliable and positive behavior and seed correlations for the A3, A5, and M3 tasks in control participants. In contrast, only positive seed correlations were reliable in the TBI group (**Figure 3Ai**). Brain regions demonstrating reliable and positive saliences for this LV included left GFm and right inferior parietal lobule as well left occipital cortex and bilateral cerebellar cortices (**Figure 3Ai**).

Left middle frontal gyrus (BA 46)

Latent variable 1 ($p < 0.001$) demonstrated reliable and positive behavior and seed correlations for both the Alphabetize tasks (**Figure 3Aii**) in the control group. As with left GFi, only seed correlations were reliable for all tasks in the TBI group. Brain regions demonstrating positive saliences included left GFi, left inferior parietal lobule, bilateral superior parietal lobule, and bilateral temporal occipital junction (**Figure 3Aii**).

Right posterior middle frontal gyrus (BA 46/44)

Latent variable 1 ($p < 0.001$) demonstrated reliable and positive behavior and seed correlations for the Alphabetize and Maintain 5 conditions for the TBI group. In contrast to the left PFC ROIs, only the seed correlations were reliable for controls (**Figure 3Aiii**), with the exception of the Maintain 5 condition, where activity in this voxel was negatively correlated with behavior. Brain regions reflecting this pattern included bilateral anterior GFm (aGFm) (BA 46/10), left posterior cingulate gyrus, left precuneus (BA 7), and left posterior middle temporal gyrus (BA 39; **Figure 3Aiii**).

Right anterior middle frontal gyrus (BA 46/10)

Latent variable 1 ($p < 0.001$) demonstrated reliable and positive behavior and seed correlations for both groups. For the control group, positive correlations with behavior and activity in the seed region were reliable for Alphabetize 5 and, to a lesser extent, the Maintain 3 task (see note 1 above). In contrast, this pattern was reliable for both Alphabetize 3 and 5 as well as the Maintain 5 tasks in the TBI group (**Figure 3Aiv**). Positive saliences were observed in right posterior GFm (pGFm), left aGFm, posterior cingulate gyrus, left superior parietal lobule and the inferior occipital cortex and temporal–occipital junction bilaterally (**Figure 3Aiv**).

In sum, these results suggest a differential pattern of stepwise functional recruitment of right PFC regions between our two groups as working memory task demands increased. It is important to note here that the seed voxels selected for the functional connectivity analyses, derived from the bPLS results, were different for our two groups (**Figure 2**; **Tables 2 and 3**). We cannot rule out that the differential patterns of functional connectivity reported here may be, in part, attributable to the selection of these different seed ROIs for our two groups. Critically, however, the group differences in functional connectivity were task-dependent – and this pattern is not compatible with a biased-selection account. The pattern of task-dependent changes in functional connectivity between the Control and TBI groups is illustrated in **Figure 3B**. Bilateral functional connectivity within PFC is evident during working memory performance

Table 2 | Cluster maxima from the behavior PLS (bPLS) analysis for the control group (LV 1, see Figure 2A).

Lag	*x*	*y*	*z*	Lat.	Anat.	BA	BSR	Clust.	ROI
0	–44	44	16	L	GFm	46	5.22	12	
0	28	6	44	R	GFm	6	6.17	12	
0	24	–67	–13	R	GF	19	7.16	54	
0	–36	–78	–10	L	GOm	19	7.89	58	
1	–40	48	23	L	GFm	9/46	6.60	22	ii
1	–67	9	29	L	GFi	44/6	8.06	20	i
1	28	6	48	R	GFm	6	5.44	11	
1	–63	–46	10	L	GTs	22	6.34	18	
1	44	–28	53	R	LPi	40	5.27	30	
1	–51	–30	31	L	Gsm	40	6.67	44	
1	32	–48	50	R	LPs	7	4.84	12	
1	–24	–55	58	L	LPs	7	5.42	27	
1	–24	–78	–13	L	GF/GL	18	7.49	108	
1	28	–78	–13	R	GF/GL	18	6.44	75	
2	–44	26	–18	L	GTs	38	6.78	21	
2	–51	–29	35	L	LPi	40	6.00	24	
2	32	–56	54	R	LPs	7	6.10	15	
2	–24	–59	62	L	PCu	7	8.14	17	
2	8	–63	66	R	PCu	7	5.21	11	
2	–48	–63	–10	L	GOm	37/19	6.17	28	
3	–40	–66	–3	L	GOm	19	6.33	11	
2	–44	–84	23	L	GO	19	6.44	26	
2	28	–90	–16	R	GF	18	6.81	91	
2	–8	–98	–9	L	GL	18	6.07	11	
3	48	–64	–27	R	Cereb		7.44	58	

These regions demonstrated a positive correlation with task accuracy. Cluster threshold (BSR) was >4, corresponding approximately to p < 0.0001, with minimum size of 10 voxels. All column headings and abbreviations as in ***Table 1.***

ROI, region of interest (roman numerals correspond to regions highlighted in ***Figure 2****).*

whenever load is increased or when EDs are present. However, the threshold at which this expanded right PFC network is functionally necessary for working memory performance is reduced following TBI, consistent with an altered functional engagement hypothesis.

DISCUSSION

Traumatic brain injury is associated with altered functional recruitment during the performance of cognitively demanding tasks. We have recently demonstrated this in the context of working memory performance using fMRI methods (Turner and Levine, 2008), These functional brain changes have been reported in other cognitive domains (e.g., sustained attention; Dockree et al., 2004; and see Levine et al., 2006 for a review of functional neuroimaging and TBI) and with other imaging modalities (e.g., electrophysiology; Dockree et al., 2004; Molteni et al., 2009; see Duncan et al., 2005 for a review). However, the behavioral implications of this altered neural activity have been poorly characterized. Here we investigated whether altered patterns of neural recruitment observed following TBI are compensatory and, if so, do they represent the instantiation of novel neural networks (i.e., true functional reorganization) or enervation of functional networks that are behaviorally latent in the undamaged or under-challenged brain (i.e., altered functional engagement).

In the first analysis, we used bPLS to investigate whether the altered functional recruitment of brain regions observed during working memory performance was related to task accuracy. We hypothesized, based on previous reports from the functional neuroimaging literature (e.g., McAllister et al., 1999; Perlstein et al., 2004), that over-recruitment of areas within right PFC which we had reported previously in this TBI sample would be positively correlated with task accuracy (i.e., compensatory). These data provide strong support for our hypothesis. Activity in a right lateralized network, including two distinct regions of right lateral PFC in the vicinity of the aGFm on the border of BA 10/46 and a more dorsal region of GFm on the border of BA 44/45 was correlated with working memory task accuracy in our TBI group (**Figure 2B**; **Table 3**). Similar regions of right lateral PFC were observed by Perlstein et al. (2004) to track positively with working memory load in their TBI sample. This region has also been implicated in supra-span working memory performance in non-injured participants (e.g., Rypma et al., 1999) and during working memory performance in healthy aging (Erickson et al., 2007). However, these data represent the first time that activity in this region has been directly and positively correlated with performance on a working memory task, specifically taxing executive control processes, in a TBI sample.

In contrast to the right lateralized brain and behavior correlations observed in our TBI sample, task accuracy in the control sample during all tasks was predominantly associated with activity in a network of left lateralized brain regions, including GFi and GFm (BA 46/44; **Figure 2A**; **Table 2**), although this network expanded to include right lateral PFC during Alphabetize 5 trials (**Figure 1**; **Table 1**). This pattern replicates many previous reports implicating lateral PFC in working memory tasks involving a significant executive control component (Curtis and D'Esposito, 2003; see Cabeza and Nyberg, 2000 for a review). These results provide strong support for our original hypothesis that recruitment of right lateral PFC during cognitively demanding tasks, as has now been reported in several studies, is compensatory. Moreover, a similar finding from our laboratory using a feature integration task suggests that this pattern of compensatory neural recruitment following TBI is not specific to working memory but may represent a domain-general response to increased cognitive challenge.

Few reports to date have directly correlated brain and behavior measures in a TBI sample. Our findings are consistent with those of McAllister et al. (1999) who observed positive correlations between activity in left GFi and accuracy on a working memory task in patients with mild TBI; a pattern we also observed in our healthy controls (they did not report group-specific correlations). However, our data are not consistent with those of Newsome et al. (2007) who failed to observe significant correlations between brain response and performance during the 2-back condition of an N-back working memory task. This task is similar to that used by McAllister et al. (1999), where *maximal* brain response during the 2-back condition was observed in their sample of mild TBI patients. We suggest that patient heterogeneity in the sample of Newsome et al. (2007) may have limited their ability to detect

Table 3 | Cluster maxima from the behavior PLS (bPLS) analysis for the TBI group (see Figure 2B).

Lag	*x*	*y*	*z*	Lat.	Anat.	BA	BSR	Clust.	ROI
0	–20	–82	–13	L	GL	18	–6.25	12	
0	8	–82	–13	R	GL	17/18	–5.80	18	
0	0	–35	2	R	Pulvinar		–5.47	24	
0	–20	–25	–29	L	B. stem		–6.98	15	
1	20	–86	–13	R	GL/GF	18	–7.19	22	
1	0	–25	–32		B. stem		–10.13	16	
1	–20	–86	–19	L	Cereb		–6.47	19	
2	40	47	16	R	GFm	46	–11.98	28	iii
2	36	21	25	R	GFm/GFi	46/44	–7.89	12	iv
2	–28	–57	25	L	GTm	39	–7.69	14	
2	24	–86	–13	R	GF	18	–6.41	13	
2	–20	–29	–36	L	B. stem		–7.56	16	
2	12	–29	–39	R	B. stem		–6.25	19	
3	44	47	16	R	GFm	46	–9.99	16	iii
3	36	21	25	R	GFm/GFi	46/44	–6.01	13	iv
3	–28	–50	17	L	GTm	39	–5.08	14	
3	–24	–56	54	L	LPs	7	–7.13	18	
4	–16	–83	–26		Cereb		–5.23	14	

Cluster thresholding criteria as in ***Table 2****. All abbreviations as in* ***Tables 1 and 2****.*

significant correlations. While other reports examining functional brain changes during working memory performance following TBI did not report direct brain and behavior correlations (Christodoulou et al., 2001; Perlstein et al., 2004), these studies reported recruitment of right lateral PFC regions during working memory task performance, consistent with our findings. Moreover, Perlstein et al. (2004) also reported a group by laterality interaction whereby increased working memory load was associated with increased activity in left lateral PFC for controls and right lateral PFC for TBI consistent with our data (**Figure 2**).

We were particularly interested in questions of functional connectivity as our TBI sample was carefully screened for evidence of focal brain pathology, providing us with a sample of patients with relatively "pure" DAI. Higher cognition is increasingly understood to be an emergent property of brain activity within large scale neural networks anchored by nodes within PFC (McIntosh, 1999; Grady et al., 2003). Given that working memory is disrupted following TBI (e.g., D'Esposito et al., 2006), we surmised that such networks subserving working memory might be particularly sensitive to DAI. Moreover, data from our first analysis suggested that compensatory functional recruitment of right PFC following TBI was replicated in controls, but only at the highest level of ED within working memory. Consistent with recent reports in healthy aging (Lustig et al., 2009), these data suggested that this pattern of right lateralized recruitment may reflect a pattern of task-dependent altered functional engagement rather than functional reorganization *per se*.

To test this hypothesis, we employed multivariate methods (combined bPLS and sPLS) to examine the functional connectivity and behavioral relevance of networks anchored by four PFC "seed" regions, identified in the bPLS analysis as being highly correlated with performance on our working memory tasks. The results were consistent with an altered functional engagement hypothesis. Lateral regions of PFC including aGFm bilaterally, left GFi and the border zone of right GFi and GFm, were functionally connected in both groups. Their *behavioral* relevance, however was differentially altered both by task demands and by brain injury (see **Figure 4** for an overview of these results within PFC). Increasing either load or ED above baseline (Maintain 3) resulted in recruitment of right anterior PFC into the baseline left lateralized PFC network. Activity in this expanded network was only sufficient to support behavioral performance in controls. TBI patients required additional recruitment of right posterior lateral PFC to support performance at this level of task demand (Maintain 5, Alphabetize 3). Control performance was correlated with activity in this broader bilateral PFC network only when both ED and load increased (Alphabetize 5). Thus the stepwise pattern of behaviorally relevant functional recruitment observed in our controls as working memory demands increased was truncated for TBIs where right PFC brain–behavior correlation was observed with any increase in task demand.

When interpreting functional brain changes in neurological populations it is critical to consider the potential contribution of injury-related changes in the microvasculature, and thus BOLD signals, to observed group differences (see D'Esposito et al., 2003 for a review). We cannot directly rule out the impact of TBI-related vascular changes in our results. However, we observed robust lateralization and task-related differences in both brain and behavior correlations (**Figure 2**; and **Figure A1** in Appendix) as well as task-dependent differences in patterns of network connectivity (**Figure 3**) between our groups. This pattern of group-wise, task-dependent changes in localized brain regions could not be explained by a more generalized account of altered BOLD signaling following TBI.

In summary, these results support the altered functional engagement hypothesis following TBI. Existing PFC nodes that are normally coactivated during working memory task performance are behaviorally relevant at an earlier stage of difficulty for TBI patients as compared to controls. This finding is inconsistent with the notion of reorganization whereby new network nodes not previously engaged by the task are related to task performance. This would not have been apparent had we not included a functional connectivity analysis (sPLS) to assess extant, but latent PFC networks. Without such analysis, brain–behavior correlations may be misinterpreted as reflecting reorganization when in fact they reflect altered functional engagement. It is important to note that the controls' behaviorally relevant left-lateralized network indicated frontoparietal connectivity classically associated with working memory (Postle, 2006), whereas the TBI patients' right-lateralized network also included midline posterior regions not present for controls, consistent with previous reports (Levine et al., 2006). As this paper focuses on functional changes within PFC related to executive control within working memory, we cannot rule out that the inclusion of these midline posterior regions in the TBI patients reflects functional reorganization. However, we did not examine this directly here.

In a review of activation functional imaging in TBI, Levine et al. (2006) concluded that brain activity is more widely dispersed and weaker in PFC relative to non-injured controls. However, they cautioned that confirmation of these functional brain changes in TBI would have to await studies of TBI subjects with more homogenous neuropathology, well-validated

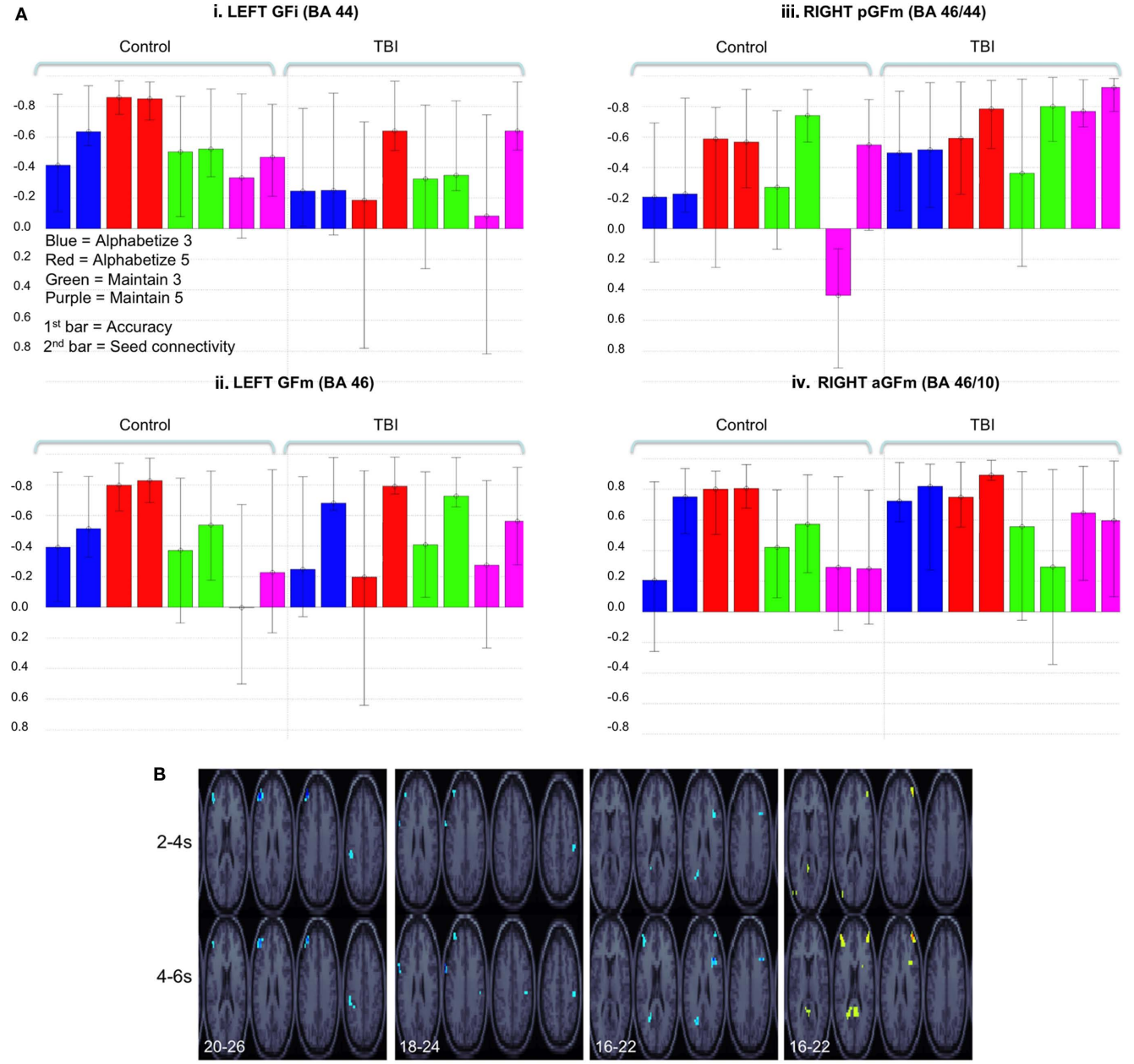


FIGURE 3 | (A) Behavioral and seed LVs (LV 1 all analyses) for the four PFC ROIs indicated in Figure 2. Legend in **(Ai)** applies to all histograms. For consistency of presentation, correlation values are reversed on the *x*-axis for **(Ai–iii)**. Significant brain saliences for these LVs were negative (**B**), thus indicating a positive behavior and seed correlation. Error bars represent confidence intervals defined by the standard error of the bootstrap estimates (as in **Figure 1**). **(B)** BSRs for each of the LVs represented in **(A)**. Slice coordinate in Talairach space (*z*) are indicated in bottom-left (step = 2). Time lags (either 2–4 or 4–6 s post stimulus onset) are indicated on the left of the images. BSR was set at 4 ($p < 10^{-4}$, corresponding approximately to a $p < 0.0001$) and cluster size was >5 voxels for all images. As noted above, the sign of the correlation and voxel saliences was reversed between images **(Ai–iv)**. This is reflected in the voxel color coding in **(Aiv)**. However, this does not affect interpretation; all brain–behavior correlations were positive.

experimental paradigms and matched behavioral performance. Our investigation meet these criteria and extend their conclusions in two important ways. First, we demonstrate that the pattern of spatially dispersed activity in TBI positively correlates with task performance – i.e., these functional brain changes in this population are compensatory. Secondly, the pattern of altered functional recruitment we observed in this sample of TBI participants mirrored that observed in healthy controls – but at lower levels of task challenge. In other words, TBI was associated with poor regulation of functional brain activity in response to increasing task demand.

The neuropathological profile of our patient sample is similar to that reported in studies of healthy aging where diffuse white matter pathology and generalized reductions in gray and white matter

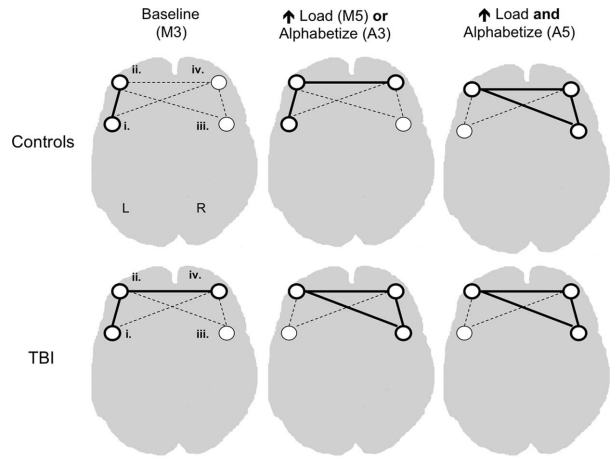


FIGURE 4 | Conceptual representation of combined behavioral and seed partial least squares analysis. Dashed lines connecting seed regions represent functional connectivity between these regions. Solid lines signify both functional connectivity and correlations between activity in the network and task accuracy. Roman numerals signify seed regions as defined in **Figure 1**.

have been observed (e.g., Tisserand et al., 2002; Raz et al., 2005). Interestingly, studies examining the functional neuroanatomy of working memory in healthy aging (e.g., Rypma and D'Esposito, 2000; Erickson et al., 2007; see Lustig et al., 2009 for a review), also report similar patterns of *compensatory* right prefrontal recruitment as we observed in our TBI sample. This convergence of neuropathology and functional recruitment patterns suggests that healthy aging may in part mimic DAI, at least with respect to the functional neuroanatomy of higher cognition.

Finally, we have previously reported that our TBI patients have evidence of DAI on neuroradiological report. Moreover, there were significant group-wise differences in cerebral white and gray matter in this TBI group relative to healthy age- and education-matched controls (Turner and Levine, 2008). An important next step in understanding the neural and behavioral sequelae of moderate to severe TBI will be to relate these structural brain changes to the pattern of functional brain changes reported here. Work is currently underway in our laboratory to examine this question using diffusion imaging techniques to characterize the structural integrity of white matter pathways in this population.

REFERENCES

Cabeza, R., and Nyberg, L. (2000). Imaging cognition II: an empirical review of 275 PET and fMRI studies. *J. Cogn. Neurosci.* 12, 1–47.

Christodoulou, C., DeLuca, J., Ricker, J. H., Madigan, N. K., Bly, B. M., Lange, G., Kalnin, A. J., Liu, W.-C., Steffener, J., Diamond, B. J., and Ni, A. C. (2001). Functional magnetic resonance imaging of working memory impairment after traumatic brain injury. *J. Neurol. Neurosurg. Psychiatry,* 71, 161–168.

Cox, R. W., and Hyde, J. S. (1997). Software tools for analysis, and visualization of fMRI data. *NMR Biomed.* 10, 171–178.

Craik, F. I. M. (1986). "A functional account of age differences in memory," in *Human Memory and Cognitive Capabilities, Mechanisms and Performances*, eds F. Klix and H. Hagendorf (New York: Elsevier Science), 409–422.

Curtis, C. E., and D'Esposito, M. (2003). Persistent activity in the prefrontal cortex during working memory. *Trends Cogn. Sci.* 7, 415–423.

D'Esposito, M., Cooney, J. W., Gazzaley, A., Gibbs, S. E., and Postle, B. R. (2006). Is the prefrontal cortex necessary for delay task performance? Evidence from lesion and FMRI data. *J. Int. Neuropsychol. Soc.* 12, 248–260.

D'Esposito, M., Deouell, L. Y., and Gazzaley, A. (2003). Alterations in the bold fMRI signal with ageing and disease: a challenge for neuroimaging. *Nat. Rev. Neurosci.* 4, 863–872.

Dockree, P. M., Kelly, S. P., Roche, R. A. P., Hogan, M. J., Reilly, R. B., and Robertson, I. H. (2004). Behavioural and physiological impairments of sustained attention after traumatic brain injury. *Cogn. Brain Res.* 20, 403–414.

Duncan, C. C., Kosmidis, M. H., and Mirsky, A. F. (2005). Closed head injury-related information processing deficits: an event-related potential analysis. *Int. J. Psychophysiol.* 58, 133–157.

Erickson, K. I., Colcombe, S. J., Wadhwa, R., Bherer, L., Peterson, M. S., Scalf, P. E., Kim, J. S., Alvarado, M., and Kramer, A. F. (2007). Training-induced plasticity in older adults: effects of training on hemispheric asymmetry. *Neurobiol. Aging* 28, 272–283.

Friston, K. J., Holmes, K. J., Worsley, J.-P., Poline, C. D., Frith, C. D., and Frackowiak, R. S. J. (1995). Statistical parametric maps in functional neuroimaging: a general linear approach. *Hum. Brain Mapp.* 2, 189–210.

Grady, C. L., McIntosh, A. R., Beig, S., Keightley, M. L., Burian, H., and Black, S. E. (2003). Evidence from functional neuroimaging of a compensatory prefrontal network in Alzheimer's disease. *J. Neurosci.* 23, 986–993.

Levine, B., Fujiwara, E., O'Connor, C., Richard, N., Kovacevic, N., Mandic, M., Restagno, A., Easdon, C., Robertson, I. H., Graham, S. J., Cheung, G. K., Gao, F. H., Schwartz, M. L., and Black, S. E. (2006). In vivo characterization of traumatic brain injury neuropathology with structural and functional neuroimaging. *J. Neurotrauma* 23, 1396–1411.

Levine, B., Kovacevic, N., Nica, I., Cheung, G., Schwartz, M. L., and Black, S. E. (2008). Toronto traumatic brain injury study: injury severity and quantified MRI. *Neurology* 70, 771–778.

Lustig, C., Shah, P., Seidler, R., and Reuter-Lorenz, P. (2009). Aging, training and the brain: a review and future directions. *Neuropsychol. Rev.* 19, 504–522.

McAllister, T. W., Saykin, A. J., Flashman, L. A., Sparling, M. B., Johnson, S. C., Guerin, S. J., Mamourian, A. C., Weaver, J. B., and Yanofsky, N. (1999). Brain activation during working memory 1 month after mild traumatic brain injury: a functional MRI study. *Neurology* 53, 1300–1308.

McIntosh, A. R. (1999). Mapping cognition to the brain through neural interactions. *Memory* 7, 523–548.

McIntosh, A. R., Bookstein, F. L., Haxby, J. V., and Grady, C. L. (1996). Spatial pattern analysis of functional brain images using partial least squares. *Neuroimage* 3, 143–157.

McIntosh, A. R., Chau, W. K., and Protzner, A. B. (2004). Spatiotemporal analysis of event-related fMRI data using partial least squares. *Neuroimage* 23, 764–775.

McIntosh, A. R., and Lobaugh, N. J. (2004). Partial least squares analysis of neuroimaging data: applications and advances. *Neuroimage* 23 (Suppl. 1), S250–S263.

Molteni, E., Baselli, G., Bianchi, A. M., Caffmi, M., Contint, D., Spinelli, L., Torricelli, A., Cerutti, S., and Cubeddu, R. (2009). Frontal brain activation during a working memory task: a time-domain fNIRS study. *Prog. Biomed. Opt. Imaging Proc. SPIE* 7161, Art. No. 71613N.

Newsome, M. R., Scheibel, R. S., Seignourel, P. J., Steinberg, J. L., Troyanskaya, M., Li, X., and Levin, H. S. (2009). Effects of methylphenidate on working memory in traumatic brain injury: a preliminary fMRI investigation. *Brain Imaging Behav.* 3, 298–305.

Newsome, M. R., Scheibel, R. S., Steinberg, J. L., Troyanskaya, M., Sharma, R. G., Rauch, R. A., Li, X., and Levin, H. S. (2007). Working memory brain activation following severe traumatic brain injury. *Cortex* 43, 95–111.

Ogawa, S., Lee, T. M., Kay, A. R., and Tank, D. W. (1990). Brain magnetic-resonance-imaging with contrast dependent on blood oxygenation. *Proc. Natl. Acad. Sci. U.S.A.* 87, 9868–9872.

Paxton, J. L., Barch, D. M., Racine, C. A., and Braver, T. S. (2008). Cognitive control, goal maintenance, and prefrontal function in healthy aging. *Cereb. Cortex* 18, 1010–1028.

Perlstein, W. M., Cole, M. A., Demery, J. A., Seignourel, P. J., Dixit, N. K., Larson, M. J., and Briggs, R. W. (2004). Parametric manipulation of working memory load in traumatic brain injury: behavioral and neural correlates. *J. Int. Neuropsychol. Soc.* 10, 724–741.

Postle, B. R. (2006). Working memory as an emergent property of the mind and brain. *Neuroscience* 139, 23–38.

Postle, B. R., Berger, J. S., and D'Esposito, M. (1999). Functional neuroanatomical double dissociation of mnemonic and executive control processes

contributing to working memory performance. *Proc. Natl. Acad. Sci. U.S.A.* 96, 12959–12964.

Povlishock, J. T., and Katz, D. I. (2005). Update of neuropathology and neurological recovery after traumatic brain injury. *J. Head Trauma Rehabil.* 20, 76–94.

Raz, N., Lindenberger, U., Rodrigue, K. M., Kennedy, K. M., Head, D., Williamson, A., Dahle, C., Gerstorf, D., and Acker, J. D. (2005). Regional brain changes in aging healthy adults: general trends, individual differences and modifiers. *Cereb. Cortex* 15, 1676–1689.

Rypma, B., and D'Esposito, M. (2000). Isolating the neural mechanisms of age-related changes in human working memory. *Nat. Neurosci.* 3, 509–515.

Rypma, B., Prabhakaran, V., Desmond, J. E., Glover, G. H., and Gabrieli, J. D. (1999). Load-dependent roles of frontal brain regions in the maintenance of working memory. *Neuroimage* 9, 216–226.

Stuss, D. T., Pogue, J., Buckle, L., and Bondar, J. (1994). Characterization of stability of performance in patients with traumatic brain injury: variability and consistency on reaction time tests. *Neuropsychology* 8, 316–324.

Stuss, D. T., Stethem, L. L., Hugenholtz, H., Picton, T., Pivik, J., and Richard, M. T. (1989). Reaction time after traumatic brain injury: fatigue, divided and focused attention, and consistency of performance. *J. Neurol. Neurosurg Psychiatry* 52, 742–748.

Teasdale, G., and Jennett, B. (1974). Assessment of coma and impaired consciousness. A practical scale. *Lancet* 2, 81–84.

Tisserand, D. J., Pruessner, J. C., Sanz Arigita, E. J., van Boxtel, M. P. J., Evans, A. C., Jolles, J., and Uylings, H. B. M. (2002). Regional frontal cortical volumes decrease differentially in aging: an MRI study to compare volumetric approaches and voxel-based morphometry. *Neuroimage* 17, 657–669.

Turner, G. R., and Levine, B. (2008). Augmented neural activity during executive control processing following diffuse axonal injury. *Neurology* 71, 812–818.

Wager, T. D., and Smith, E. E. (2003). Neuroimaging studies of working memory: A meta-analysis. Cognitive, Affective and Behavioral Neuroscience, 3, 255–274.

Conflict of Interest Statement: The authors declare that the research was conducted in the absence of any commercial or financial relationships that could be construed as a potential conflict of interest.

Received: 06 August 2010; accepted: 08 February 2011; published online: 24 February 2011.

*Citation: Turner GR, McIntosh AR and Levine B (2011) Prefrontal compensatory engagement in TBI is due to altered functional engagement of existing networks and not functional reorganization. Front. Syst. Neurosci. **5**:9. doi: 10.3389/fnsys.2011.00009*

Copyright © 2011 Turner, McIntosh and Levine. This is an open-access article subject to an exclusive license agreement between the authors and Frontiers Media SA, which permits unrestricted use, distribution, and reproduction in any medium, provided the original authors and source are credited.

APPENDIX

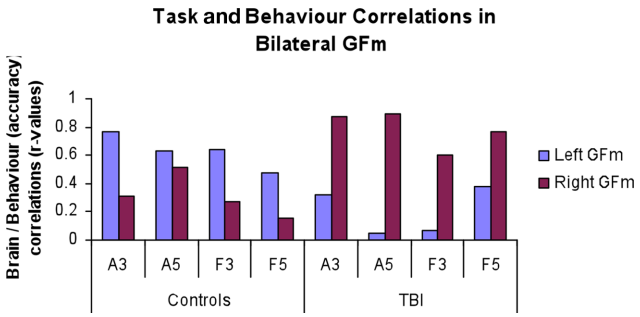


FIGURE A1 | Correlations between brain activity in anterior middle frontal gyrus seed regions (highlighted in Figure 3A). Talairach coordinate of left middle frontal gyrus (GFm): –40, 48, 23; right GFm: 40, 47, 16.

frontiers in
SYSTEMS NEUROSCIENCE

ORIGINAL RESEARCH ARTICLE
published: 20 December 2010
doi: 10.3389/fnsys.2010.00159

Effects of visual experience on the human MT+ functional connectivity networks: an fMRI study of motion perception in sighted and congenitally blind individuals

Lorenzo Sani[1,2], Emiliano Ricciardi[1,3], Claudio Gentili[3,4], Nicola Vanello[3,5], James V. Haxby[6] and Pietro Pietrini[1,2]*

[1] *Laboratory of Clinical Biochemistry and Molecular Biology, University of Pisa, Pisa, Italy*
[2] *Department of Laboratory Medicine and Molecular Diagnostics, Azienda Ospedaliero Universitaria Pisana, Pisa, Italy*
[3] *MRI Laboratory, Fondazione CNR/Regione Toscana Gabriele Monasterio, Pisa, Italy*
[4] *Clinical Psychology Unit, Department of Psychiatry, University of Pisa, Pisa, Italy*
[5] *Department of Information Engineering, University of Pisa, Pisa, Italy*
[6] *Department of Psychological and Brain Sciences, Dartmouth College, Hanover, VA, USA*

Edited by:
Silvina G. Horovitz, National Institutes of Health, USA

Reviewed by:
Victor Hugo de Lafuente Flores, University of Washington School of Medicine, USA
George Wittenberg, University of Maryland School of Medicine, USA

****Correspondence:***
Pietro Pietrini, Department of Laboratory Medicine and Molecular Diagnostics, University of Pisa Medical School, Via Roma, 67 I-56126 Pisa, Italy.
e-mail: pietro.pietrini@med.unipi.it

Human middle temporal complex (hMT+) responds also to the perception of non-visual motion in both sighted and early blind individuals, indicating a supramodal organization. Visual experience, however, leads to a segregation of hMT+ into a more anterior subregion, involved in the supramodal representation of motion, and a posterior subregion that processes visual motion only. In contrast, in congenitally blind subjects tactile motion activates the full extent of hMT+. Here, we used fMRI to investigate brain areas functionally connected with the two hMT+ subregions (seeds) during visual and tactile motion in sighted and blind individuals. A common functional connectivity network for motion processing, including bilateral ventral and dorsal extrastriate, inferior frontal, middle and inferior temporal areas, correlated with the two hMT+ seeds both in sighted and blind individuals during either visual or tactile motion, independently from the sensory modality through which the information was acquired. Moreover, ventral premotor, somatosensory, and posterior parietal areas correlated only with the anterior but not with the posterior portion of hMT+ in sighted subjects, and with both hMT+ seeds in blind subjects. Furthermore, a correlation between middle temporal and occipital areas with primary somatosensory seeds was demonstrated across conditions in both sighted and blind individuals, suggesting a cortico-cortical pathway that conveys non-visual information from somatosensory cortex, through posterior parietal regions, to ventral extrastriate cortex. These findings expand our knowledge about the development of the functional organization within hMT+ by showing that distinct patterns of brain functional correlations originate from the anterior and posterior hMT+ subregions as a result of visual experience.

Keywords: human middle temporal complex, supramodality, visual motion, tactile motion, blindness, functional connectivity, fMRI

INTRODUCTION

Visual perception of motion in humans activates specific areas of the temporo-occipital cortex that classically includes the human middle temporal complex, hMT+ (Watson et al., 1993; Zeki et al., 1993; Tootell et al., 1995). This extrastriate area is activated also during apparent and illusory visual motion, and mental imagery of movement (Tootell et al., 1995; Goebel et al., 1998; Kourtzi and Kanwisher, 2000; Mather et al., 2008). Moreover, hMT+ responds to the perception of auditory and tactile motion in sighted (Hagen et al., 2002; Ricciardi et al., 2007; Ptito et al., 2009; Summers et al., 2009), as well as in congenitally blind individuals (Poirier et al., 2006; Ricciardi et al., 2007). These latter findings indicate that hMT+ also processes non-visual sensory inputs of motion, and that visual experience is not a prerequisite for the development of the functional organization of this motion-responsive area. In addition, these results extend to motion-responsive temporo-occipital areas the supramodal functional organization that has been previously demonstrated for other "visual" ventral and dorsal extrastriate cortical areas (Amedi et al., 2001, 2005; Pietrini et al., 2004; Ricciardi et al., 2006, 2009; Bonino et al., 2008).

Visual experience, however, does lead to a functional segregation within hMT+ (Ricciardi et al., 2007). Indeed, tactile motion perception in sighted subjects activated the more anterior portion of visual motion-responsive regions but deactivated the more posterior subregion that was activated by visual motion only. By contrast, perception of tactile motion in congenitally blind subjects activated the full extent of hMT+, including the more posterior part. In line with these findings, Beauchamp et al. (2007) using fMRI to localize functional responses to visual and tactile stimuli within hMT+ demonstrated that the anterior and dorsal middle-superior temporal area (MST), but not the remaining portion, responded to simple vibrotactile stimuli.

Recently, repetitive transcranial magnetic stimulation (rTMS) was used to determine whether this more anterior portion of hMT+ truly plays a functional role in tactile motion processing.

In blindfolded sighted individuals who were asked to detect tactilely changes in the velocity of a random Braille-like dot pattern with the tip of their index and middle fingers, accuracy, and reaction times were significantly impaired only when rTMS was applied on the more anterior part of hMT+, but not on a control parieto-occipital area (Ricciardi et al., 2010). These results indicate that hMT+ recruitment is not an epiphenomenon but is truly necessary for tactile processing of motion, and provide additional evidence to the hypothesis of a "supramodal" functional organization for the more anterior part of this sensory motion processing area.

Over the last several years, increasing attention has been devoted to exploring interregional connectivity during a specific task, defined as "functional connectivity" (Friston et al., 1993; Horwitz, 2003; Horwitz et al., 2005). To characterize neural interactions across the whole brain, functional connectivity analyses select a voxel, or a group of voxels, as a reference (the so-called *seed* region of interest – seed-ROI), and cross-correlate the seed-ROI time course with the whole brain to identify functionally connected sites, i.e., brain regions showing high temporal coherence during a specific task or condition.

The present study was designed to examine the functional correlations between the more anterior "supramodal" and the posterior "visual" portions of hMT+ and the whole brain during visual and tactile processing of motion and the effects of visual experience and, conversely, of the lack of visual experience, on the development of these correlations. Based on our previous findings discussed above (Ricciardi et al., 2007), we hypothesized that the more anterior "supramodal" portion of hMT+ would show correlations not only within visual occipital areas but also with non-visual sensory brain area, or areas of visuo-tactile integration, such as sensorimotor and posterior parietal regions (Bremmer et al., 2001; Grefkes et al., 2002), independently from the specific motion detection task and from the occurrence of any visual experience. In contrast, we postulated that in sighted subjects the posterior part of hMT+ would show a wide pattern of correlation only within visual occipital areas. Finally, because perception of tactile motion in congenitally blind subjects engaged the full extent of hMT+, we predicted that the absence of visual experience would lead posterior hMT+ subregion to develop a pattern of functional connectivity similar to that shown by the more anterior hMT+ portion.

MATERIALS AND METHODS

SUBJECTS

For this study, we analyzed brain functional data obtained in a previously reported fMRI experiment (Ricciardi et al., 2007). In brief, we studied seven sighted (one female, 27 ± 2 years) and four blind (one female, 37 ± 14 years) right-handed healthy volunteers. Three subjects were blind from birth, and one became blind at the age of 2 years and had no recollection of any visual experience (causes of blindness: two congenital glaucoma, retinopathy of prematurity, and congenital optic atrophy). All subjects received medical, neurological and psychiatric examinations, and laboratory testing, including a structural brain MRI scan exam, to rule out history or presence of any disorder (other than blindness in the congenitally blind group) that could affect brain function and development. No subject was taking any psychotropic medication. All participants gave their written informed consent after the study procedures and potential risks had been explained. The study was conducted under a protocol approved by the Ethical Committee at the University of Pisa Medical School (Protocol n. 020850). All participants retained the right to withdraw from the study at any moment.

IMAGE ACQUISITION

fMRI images were acquired using a gradient echo echoplanar (GRE-EPI) sequence with a GE Signa 1.5 Tesla scanner (General Electric, Milwaukee, WI, USA). A scan cycle (repetition time, TR = 3000 ms) was composed of 22–26 contiguous axial slices [5 mm thickness, field of view (FOV) = 24 cm, echo time (TE) = 40 ms, flip angle = 90°, image in plane resolution = 64 × 64 pixels], and voxels dimensions were 3.75 mm × 3.75 mm × 5 mm. We obtained 3–7 time series of 79 brain volumes (237 s) in all subjects while they perceived tactile motion stimuli and, in sighted subjects only, also 2–4 time series while they perceived visual motion stimuli.

High-resolution T1-weighted spoiled gradient recall (SPGR) images were obtained for each subject to provide detailed brain anatomy during structural image acquisition.

EXPERIMENTAL TASK AND STIMULI

Tactile stimuli were administered using an MR compatible device (Ricciardi et al., 2007) on a polystyrene table placed over the subjects' legs. Subjects' hands lay on the table with the index and middle fingers touching a plastic surface with dot patterns at the same time. Tactile stimuli were moving or static Braille-like dot (average ∅: 1–1.5 mm; height: 0.5–1 mm) random patterns presented on a plastic flat surface (a 30-mm wide band). Horizontal translation (left-to-right and right-to-left; density 1 dot/cm^2, average distance: 9 mm; speed: 2.2 cm/s) and rotation (clockwise and counterclockwise; density 2 dot/cm^2, average distance: 6 mm; speed: 93.5°/s) motion were used. For the visual tasks, participants were asked to fixate a central static white cross (0.15°× 0.15°) while moving or static white dots were presented on a black background (dot radius: 0.06°, luminance about 20 cd/m^2). The same two types of motion as for the tactile motion task were used in the visual task: horizontal translation (1.8°/s) and rotation (9°/s). Visual stimuli were presented on a rear projection screen viewed through a mirror (visual field: 25° wide and 20° high).

Moving stimuli were presented in 8–40 s blocks separated by intervals with static stimuli of varying duration (11 ± 10 s). Each time series began and ended with 30 s of static stimuli. Participants were asked to fixate the central cross during the visual task, and to keep their eyes closed during the tactile tasks. Sensory modality (tactile or visual), type of movement, direction of movement, and hand of stimulation (left or right) were constant for each time series, and were presented in a pseudo-random sequence counterbalanced within and across subjects.

DATA ANALYSIS

The AFNI and SUMA software package was used to analyze functional imaging data (http://afni.nimh.nih.gov/afni, Cox, 1996). Based on the local maxima of group *Z* maps in sighted subjects during the tactile motion perception task (Ricciardi et al., 2007), the ROIs to be used as the seeds for the whole brain functional connectivity correlation analysis in tactile runs were identified bilaterally in a more anterior (aMT in **Figure 1**; Talairach atlas coordinates: $X = 44$, $Y = -48$, $Z = -5$;

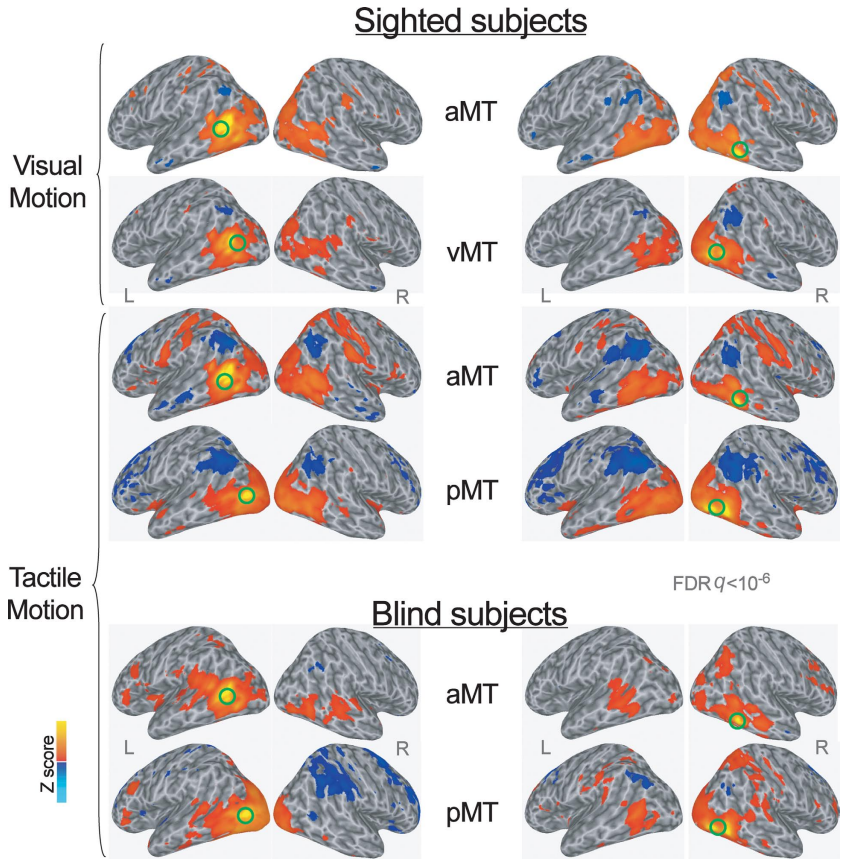


FIGURE 1 | Group averaged *Z* map showing brain regions significantly correlated with the average time series extracted from the left and right more anterior and more posterior subregions of the hMT+ during visual and tactile motion perception in sighted subjects, and during tactile motion perception in blind subjects (FDR corrected $q < 10^{-6}$).

Spatially normalized activations are projected onto a single-subject cortical surface template in the Talairach–Tournoux standard space. Lateral views of the inflated right and left hemispheres are shown. Green circles identify the seed-ROIs used for the functional connectivity correlation analysis.

$X = -49$, $Y = -62$, $Z = 5$) and a more posterior (pMT in **Figure 1**; Talairach atlas coordinates: $X = 44$, $Y = -70$, $Z = -4$; $X = -46$, $Y = -77$, $Z = 2$) subregion of hMT+ (**Figure 1**). Tactile motion perception task in sighted subjects activated the more anterior portion of hMT+, but deactivated the more posterior subregion that, in contrast, was activated by visual motion only (Ricciardi et al., 2007).

Similarly, based on the local maxima of group *Z* maps in sighted subjects during the visual motion perception task (Ricciardi et al., 2007), the local maxima of hMT+ (vMT in **Figure 1**; Talairach atlas coordinates: $X = 43$, $Y = -73$, $Z = 7$; $X = -46$, $Y = -62$, $Z = 7$) was used as the seed-ROI in visual runs. This visual seed-ROI almost overlapped with the more posterior subregion of hMT+ (pMT) as defined during the tactile motion task. The anterior hMT+ subregion (aMT) was used as a seed-ROI for the whole brain functional connectivity correlation analysis also for the visual runs.

Consistently, since blind individuals activated the whole extent of hMT+ during tactile motion perception (Ricciardi et al., 2007), for the functional connectivity analysis we located two seed-ROIs on the same coordinates for the anterior (aMT) and posterior (pMT) subregions of hMT+, as defined during the tactile motion perception task in the sighted subjects (see above).

Finally, to explore the hypothesis of a cortico-cortical pathway that from primary somatosensory cortex, through posterior parietal regions, would convey non-visual (tactile, in this case) information to the supramodal extrastriate cortex (Kupers et al., 2006; Peltier et al., 2007; Fujii et al., 2009; Matteau et al., 2010), we selected seed-ROIs also within the primary somatosensory (S1) regions (Talairach atlas coordinates- sighted, tactile runs: $X = 44$, $Y = -29$, $Z = 49$, $X = -43$, $Y = -28$, $Z = 54$; sighted, visual runs: $X = 51$, $Y = -29$, $Z = 44$, $X = -51$, $Y = -20$, $Z = 46$; blind, tactile runs: tactile runs: $X = 47$, $Y = -24$, $Z = 47$, $X = -42$, $Y = -37$, $Z = 60$). Definition of the seed-ROI in somatosensory cortex (S1) was based on the local maxima for each condition group *Z* maps for sighted and blind individuals, respectively (Ricciardi et al., 2007). As explained below, significant voxels ($p < 0.0005$; *Z*-score > 3.48) falling within 5 mm-radius spheres centered at local peak values for the selected ROIs were used to extract individual averaged time series. All raw volumes from the different runs were concatenated and coregistered, temporally aligned, and spatially smoothed (isotropic Gaussian filter, $\sigma = 3.4$ mm). Individual runs data were normalized by calculating the mean intensity value for each voxel, and by dividing the value within

each voxel by its mean to estimate the percent signal change at each time point. Effects of no interest (baseline shifts and linear/quadratic drifts) were removed from the pre-processed EPI time series of each individual run, and a low-pass filtering (filter cut-off frequency = 0.1 Hz) was performed on the signal time series of each voxel to eliminate high-frequency noises (Fox et al., 2005; Liang et al., 2006). Individual time series were then spatially transformed into the standard Talairach and Tournoux Atlas (Talairach and Tournoux, 1988) coordinate system, resampled to 1 mm^3 voxels, and averaged across all voxels of a seed-ROI to derive a reference signal time course for each visual or tactile run. The extracted time series were used as regressors of interest in a whole brain multiple regression analysis. For each subject, the global signal (averaged signal across whole brain voxels) and the six movement parameters derived from the volume spatial registration in each scan series were included in the correlation analysis as covariates (i.e., regressors of no interest), in order to factor out signal changes due respectively to physiological noise (e.g., cardiac or respiratory artifacts; Cordes et al., 2001; Birn et al., 2006) or head movements (Jiang et al., 1995; Lowe et al., 1998). The task-related regressor (tactile or visual moving stimuli) of each run was also included as an additional regressor of no interest in the correlation analysis in order to minimize the effect of the specific tasks (Whalley et al., 2005). For each subject, output maps of the correlation coefficients represented the functional connectivity maps of the considered seed-ROI with the whole brain. In order to run group analyses, to reduce skewness and improve the normality of the distribution of the correlation coefficients, correlation coefficients were converted to *Z*-scores using Fisher's *Z* transformation formula. For each ROI, individual and group *Z*-score correlation coefficient maps were computed by multiplying in two different steps the across runs and across subjects average *Z* correlation coefficient values by the square root of the number of runs, respectively. Significant correlations were defined by a false discovery rate (FDR) corrected $q < 10^{-6}$. Conjunction maps were created by overlapping significant correlations maps for each group and each task condition, in order to improve the description of the common network for motion processing functionally connected with both subregions of hMT+, and the distinctive patterns of functional correlations of the more anterior and posterior subregions of hMT+.

RESULTS

FUNCTIONAL CONNECTIVITY OF ANTERIOR AND POSTERIOR hMT+ SUBREGIONS IN SIGHTED INDIVIDUALS

During the visual motion perception task in sighted subjects, both the anterior "supramodal" and posterior "visual" seed-ROIs within hMT+ (respectively, aMT and vMT in **Figure 1**; yellow clusters in **Figure 2**, top row) showed correlations bilaterally, with a larger ipsilateral extension, with ventral extrastriate areas, including middle temporal, middle occipital and fusiform regions, and dorsal-occipital cortex. However, while the more anterior "supramodal" seed-ROI within hMT+ correlated bilaterally also with precentral and postcentral cortex, inferior and superior parietal areas, intraparietal cortex, dorsal premotor (BA6), dorsal (BA9) and anterior (BA46) middle frontal regions (aMT in **Figure 1**; red clusters in **Figure 2**, top row), the posterior "visual" hMT+ subregion showed additional

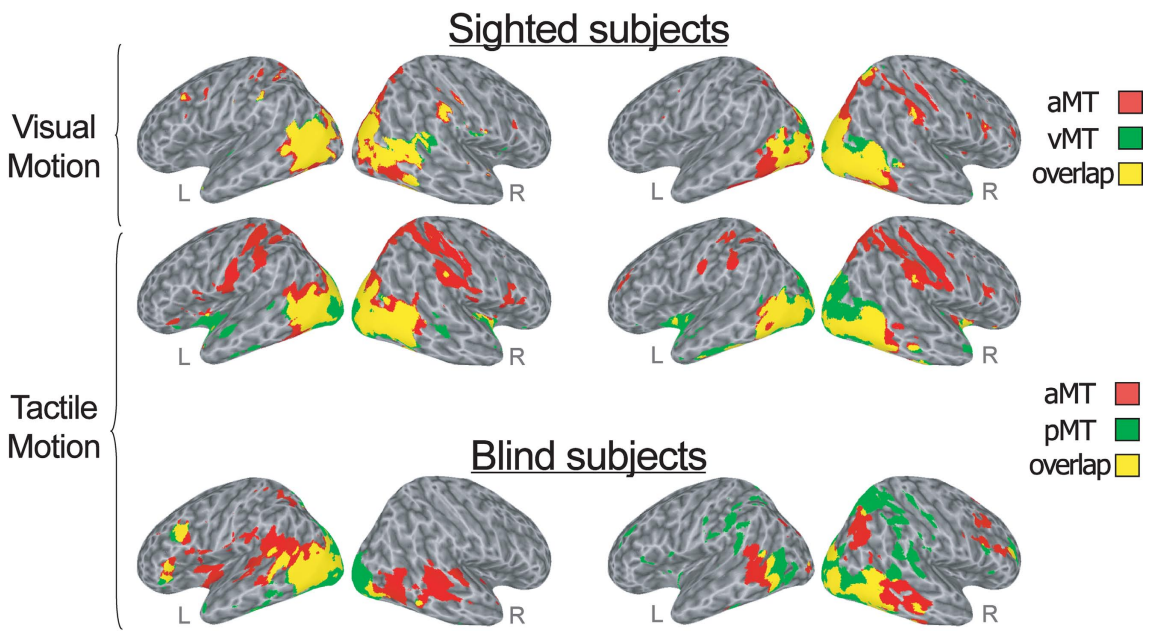


FIGURE 2 | Conjunction analysis (logical AND) created by overlapping significant (FDR corrected $q < 10^{-6}$) correlations maps for each group and each task condition. The overlap map shows the areas correlated with both the more anterior and the more posterior subregion of bilateral hMT+ (shown in yellow), as well as the areas correlated only with the anterior (red) and the posterior (green) hMT+ seed-ROIs during visual (top row) and tactile (middle row) motion runs in sighted subjects, and during tactile (bottom row) motion runs in congenitally blind subjects. Lateral views of the inflated right and left hemispheres are shown. Right and left sides of the figure show the areas correlated respectively with the right and left hMT+ seed-ROIs.

correlations only with ipsilateral precuneus and middle prefrontal cortex, and with small clusters in bilateral temporo-parietal cortex (vMT in **Figure 1**; green clusters in **Figure 2**, top row).

During the tactile motion perception runs in sighted subjects, both the anterior and posterior subregions of left and right hMT+ showed positive correlations extensively in bilateral striate and in ventral and dorsal extrastriate regions, including fusiform, parahippocampal and lingual gyri, middle and inferior temporal areas (aMT and pMT in **Figure 1**; yellow clusters in **Figure 2**, mid row). Clusters of correlations for both hMT+ seed-ROIs were also found in inferior frontal/insular areas and subcortical structures, such as the thalamus and putamen. As also was the case during visual motion perception, while the more anterior "supramodal" seed-ROIs significantly correlated with bilateral precentral and postcentral cortex, inferior and superior parietal areas, intraparietal cortex, dorsal premotor (BA6), middle (BA9) and inferior frontal (BA44) regions (aMT in **Figure 1**; red clusters in **Figure 2**, mid row), the posterior "visual" subregion of hMT+ showed additional positive correlations only with the cuneus and anterior temporal regions (pMT in **Figure 1**; green clusters in **Figure 2**, mid row).

FUNCTIONAL CONNECTIVITY OF ANTERIOR AND POSTERIOR hMT+ SUBREGIONS IN CONGENITALLY BLIND INDIVIDUALS

In the congenitally blind group, both the anterior and posterior seed-ROIs showed similar patterns of functional correlations bilaterally, with a larger ipsilateral extension, in middle temporal and middle occipital cortex, dorsal occipital and superior parietal areas, postcentral somatosensory cortex, temporo-parietal, ventral premotor, and anterior middle frontal clusters (aMT and pMT in **Figures 1 and 2**, bottom row). While the anterior seed-ROIs of hMT+ showed a broader correlation with bilateral middle and superior temporal cortex and a more distributed connection with insular and anterior prefrontal areas (aMT in **Figure 1**; red clusters in **Figure 2**, bottom row), the posterior seed-ROIs of hMT+ presented a significant functional connection also with medial occipital areas, such as lingual gyri and cuneus (pMT in **Figure 1**; green clusters in **Figure 2**, bottom row).

FUNCTIONAL CONNECTIVITY OF S1 DURING TACTILE AND VISUAL MOTION PERCEPTION

During the tactile motion perception task in both sighted and congenitally blind individuals, the somatosensory seed-ROIs showed extensive bilateral connections with contiguous paracentral cortex, ventral and dorsal premotor areas, supplementary motor, posterior parietal and intraparietal regions, anterior middle, and superior frontal clusters (**Figure 3**). Furthermore, both the left and right S1 seed-ROIs were functionally connected with bilateral middle temporal and lateral occipital areas, thus including also supramodal ventral and motion-responsive extrastriate regions.

A similar pattern was also described for the somatosensory seed-ROIs during visual motion perception in sighted subjects, including the connection with motion-responsive extrastriate regions.

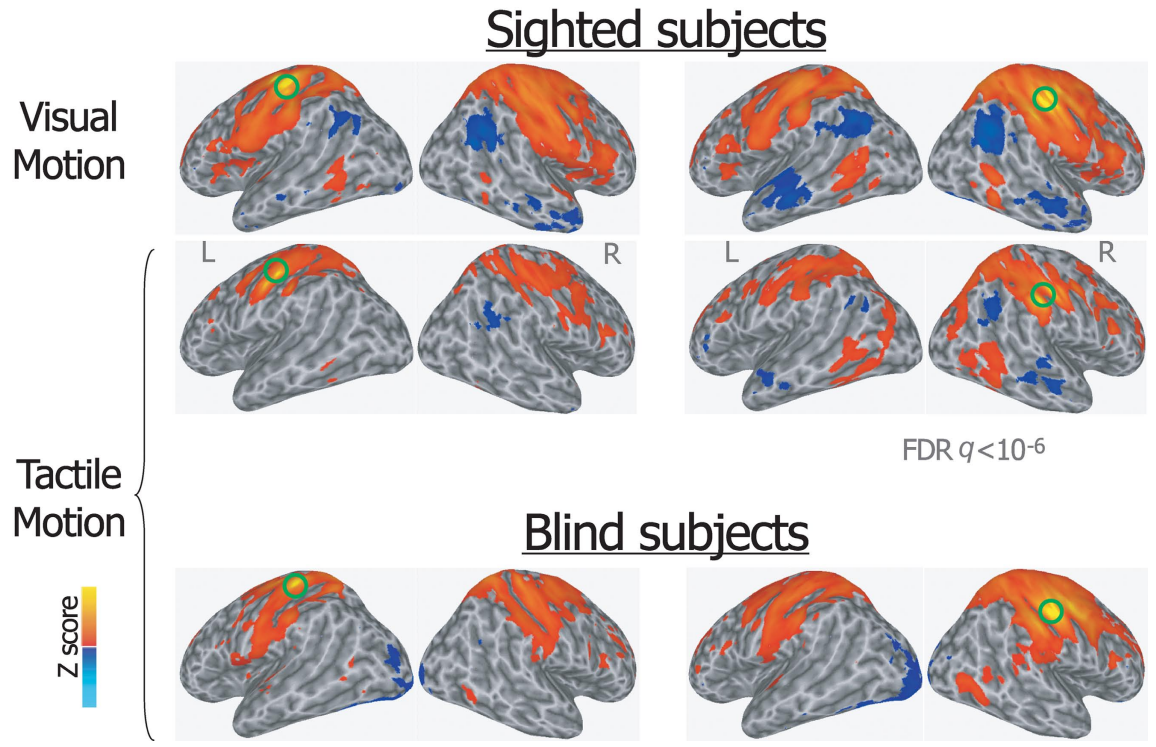


FIGURE 3 | Group averaged *Z* map showing brain regions significantly correlated with the average time series extracted from the left and right primary somatosensory seed-ROIs during visual and tactile motion perception in sighted subjects, and during tactile motion perception in blind subjects (FDR corrected $q < 10^{-6}$). Spatially normalized activations are projected onto a single-subject cortical surface template in the Talairach–Tournoux standard space. Lateral views of the inflated right and left hemispheres are shown. Green circles identify the seed-ROIs used for the functional connectivity correlation analysis.

DISTRIBUTION OF NEGATIVE FUNCTIONAL CONNECTIVITY CORRELATIONS COEFFICIENTS

In addition to the positive correlations, significant negative correlations were found both in sighted subjects during visual and tactile motion perception and in blind subjects during tactile motion perception. Specifically, the bilateral seed-ROIs in both hMT+ and primary somatosensory cortex showed bilateral significant negative correlations with the temporoparietal junction, anterior cingulate and medial prefrontal areas, posterior cingulate, and precuneus (**Figures 1 and 3**).

DISCUSSION

The aim of the present study was to explore the functional correlations between hMT+ and the rest of the brain during visual and tactile motion processing tasks and the effects of visual experience and, conversely, of lack of visual experience, on the development of these correlations. Specifically, we wished to determine patterns of functional correlations between the more anterior "supramodal" and the posterior "visual" subregions of hMT+, respectively, and the other brain areas during visual and tactile perception of moving dot patterns in both sighted and congenitally blind individuals.

A COMMON NETWORK FOR MOTION PROCESSING FUNCTIONALLY CONNECTED WITH BOTH SUBREGIONS OF hMT+

Overall, we found that, both in sighted and congenitally blind subjects, a common set of bilateral brain areas, including ventral and dorsal extrastriate regions – such as the fusiform, parahippocampal and lingual cortex – middle and inferior temporal areas, and inferior frontal areas were positively correlated with both seed-ROIs in the anterior and posterior subregions of hMT+, during either the visual or tactile motion perception runs. This network is consistent with other brain functional studies that have reported hMT+ to be mutually activated along with many of these visual motion processing regions (Watson et al., 1993; Zeki et al., 1993; Tootell et al., 1995; Shulman et al., 1998; Hampson et al., 2004).

Therefore, these brain areas have developed a common network for motion processing that is functionally correlated with the whole hMT+, does not depend from the sensory modality through which the information is acquired and does not require visual experience to form (Poirier et al., 2006; Ricciardi et al., 2007, 2010; Ptito et al., 2009). Interestingly, the observation that similar functional connectivity networks obtained using the hMT+ seed-ROIs are present also in congenitally blind subjects during tactile motion perception indicates that the involvement of hMT+ in non-visual motion detection cannot be interpreted merely as a consequence of visual imagery (Beauchamp et al., 2007; Ricciardi et al., 2007; Matteau et al., 2010). Altogether, these results are consistent with and extend to the hMT+ connectivity networks the supramodal functional organization that has been shown both in the ventral and dorsal "visual" cortical pathways in relation to object recognition and motion and spatial discrimination (Pietrini et al., 2004; Amedi et al., 2005; Ricciardi et al., 2006, 2007; Beauchamp et al., 2008; Cattaneo et al., 2008; Mahon et al., 2009; Matteau et al., 2010), and in other prefrontal and parietal cortical areas in relation to higher-order cognitive functions, such as mental imagery, working memory, and action recognition (Bonino et al., 2008; Cattaneo et al., 2008; Ricciardi et al., 2009). As a whole, the results of the above studies indicate that visual experience is not a mandatory prerequisite for the brain to develop its morphological and functional architecture (Pietrini et al., 2004, 2009).

A NEGATIVE FUNCTIONAL CORRELATIONS

In sighted subjects during visual and tactile motion perception and in blind subjects during tactile motion perception, the bilateral seed-ROIs of both hMT+ and primary sensorimotor cortex showed significant negative correlations in the bilateral temporoparietal junction, bilateral posterior cingulate and bilateral anterior cingulate. Interestingly, these brain regions belong to the so-called default mode network (Raichle et al., 2001; Greicius and Menon 2003). Since functional connectivity is a measure of the spatiotemporal synchrony, or correlation, of the fMRI signal between anatomically distinct brain regions within the cerebral cortex (Friston et al., 1993; Biswal et al., 1995), these negative correlations may likely indicate that the hMT+ and S1 seed-ROIs (that are "task responsive") are significantly anti-correlated with the default mode network regions (that are "rest responsive"). Even if negative correlations may be sometimes an artifact of global signal regression techniques, including those applied here (Chang and Glover, 2009; Murphy et al., 2009), these findings reflect the expected anticorrelation with brain regions that commonly exhibit activity decreases during the performance of various goal-directed tasks, and that have been previously reported as anticorrelated to brain regions routinely activated during goal-directed task performance (Raichle et al., 2001; Greicius and Menon, 2004; Fox et al., 2005). The neurophysiological meaning of fMRI negative correlations, which remains yet to be fully understood, falls much outside of the specific aim of this study.

DISTINCTIVE PATTERNS OF FUNCTIONAL CORRELATIONS OF THE MORE ANTERIOR AND POSTERIOR SUBREGIONS OF hMT+

In addition to this common network of brain regions for motion processing, however, differences between the patterns of functional correlations for the anterior and posterior hMT+ subregions were identified in the two groups.

In the sighted subjects, the functional connectivity network obtained using the bilateral anterior "supramodal" seeds of hMT+ differed from the set of brain regions connected to the posterior "visual" seed of this motion-responsive area during both visual and tactile motion perception. As hypothesized, in sighted subjects the posterior part of hMT+ showed a wider pattern of correlation within visual occipital areas, while the more anterior portion of hMT+ revealed correlations also with non-visual sensory brain area, or areas of visuo-tactile integration, such as somatosensory and posterior parietal cortex, independently from the specific motion detection task. Specifically, premotor and somatosensory regions, inferior and superior parietal areas, intraparietal, dorsal premotor (BA6), middle (BA9), and inferior frontal (BA44) cortex were functionally correlated with the anterior "supramodal" subregion of hMT+, but not with the posterior "visual" one.

In the congenitally blind subjects, during the tactile motion perception tasks both the anterior and the posterior part of bilateral hMT+ revealed a pattern of functional correlations with the anterior middle frontal, ventral premotor, somatosensory and posterior parietal areas, that was similar to the network identified using the anterior "supramodal" subregion in the sighted subjects.

Thus, these findings show that the anterior subregion of the motion-responsive occipito-temporal cortex develops functional correlation networks that do not depend on visual experience and that are equally elicited by both visual and tactile motion processing, extending previous findings on the supramodal nature of this cortical region to its connectivity networks (Poirier et al., 2006; Beauchamp et al., 2007; Ricciardi et al., 2007; Summers et al., 2009; Matteau et al., 2010). In contrast, the posterior subregion, that in sighted subjects processes visual motion only, develops patterns of functional regional correlations across the brain that differ between sighted and congenitally blind individuals. Moreover, the similarity between the anterior and posterior hMT+ subregion-related functional networks in congenitally blind individuals suggests that in the absence of visual experience the functional development of the more "visual" motion-responsive region and its related functional connectivity proceed toward the representation of non-visual motion (Wittenberg et al., 2004; Ricciardi et al., 2007; Fujii et al., 2009). As a result, in people lacking of visual experience since birth, the posterior "visual" part of hMT+ that in sighted individuals correlates more with related visual occipital areas, extends its functional connections also to areas of multisensory integration, such as somatosensory and posterior parietal cortex.

A CORTICO-CORTICAL PATHWAY MAY SUBSERVE SUPRAMODAL RESPONSES IN THE VISUAL CORTEX

Which mechanisms subserve these supramodal responses in the "visual" motion sensitive cortex of both sighted and congenitally blind individuals? Which neural pathways mediate the functional correlation between extrastriate motion-responsive regions and somatosensory and posterior parietal cortex both in sighted and blind individuals? Interestingly, in both experimental groups, when considering S1-seeded functional networks, somatosensory areas showed extensive bilateral connections with contiguous posterior parietal and intraparietal regions, and with middle temporal and lateral occipital areas. Similarly, the anterior supramodal subregion of hMT+ in sighted individuals, and both the anterior and posterior portions of hMT+ in congenitally blind subjects, showed a functional correlation with ventral premotor, sensorimotor, and posterior parietal areas. Thus, our data support a cortico-cortical pathway from primary somatosensory cortex through posterior parietal regions to the supramodal extrastriate areas, in line also with previous anatomical and functional studies (Kupers et al., 2006; Peltier et al., 2007; Fujii et al., 2009; Matteau et al., 2010). A concomitant involvement of a subcortical loop between the two sensory cortical areas also has been proposed (Cowey, 2010). In this respect, a functional and effective connectivity fMRI study recently indicated a direct functional connection between the thalamus and hMT+, that would enable motion information to reach hMT+ directly from the thalamus bypassing V1 (Gaglianese et al., 2010).

These anatomical connections, viable also in physiological conditions as demonstrated in the brain of blindfolded sighted subjects who perform object, spatial, and motion discrimination tasks through the tactile or auditory modality (Pietrini et al., 2004, 2009; Amedi et al., 2005; Ricciardi et al., 2006; Bonino et al., 2008), may then undergo a cross-modal plastic reorganization and become more robust in those individuals who lose sight at birth or in the early post-natal period (Wittenberg et al., 2004; Ptito and Kupers, 2005; Kupers et al., 2006, 2010; Ptito et al., 2008; Pietrini et al., 2009).

LIMITATIONS OF THE STUDY

The present study of brain regional functional correlations suffers from some methodological limitations. In the first place, the number of subjects recruited into the study is relatively small, especially for the blind group. While this issue may limit the generability of the findings, it should be kept in mind that congenitally blind individuals represent an exceptionally rare population, and even more so when strict medical selection criteria are adopted as in this study. As a matter of facts, several recently published brain imaging studies on congenitally blind individuals examined a similar or even smaller sample of subjects (Mahon et al., 2009, 2010).

Another limitation of this study is the lack of functional localizers and the relatively low field strength to properly ensure that the seed-ROIs may not overlap, even in part, with neighbor supramodal areas in lateral occipital cortex (LOtv – Amedi et al., 2001), or superior temporal sulcus (multisensory STSms – Beauchamp et al., 2008). However, the localization of the anterior seed-ROIs of hMT+ is sufficiently distant from the more dorsal and anterior STSms center-of-mass (x: −44, y: −35, z: 13) and the more ventral LOtv localization (x: −45 ± 5, y: −62 ± 6, z: −9 ± 3).

Finally, here we evaluated functional correlations of the distinct hMT+ subregions across different task conditions without having a resting-state condition, that would have been the optimal paradigm to assess the distinctive functional role of the two hMT+ subregions in the two experimental groups. However, modeling of the experimental paradigm in our analysis as a regressor of no interest contributes to mitigate the task-associated changes in BOLD responses (Whalley et al., 2005). The attempt to "subtract" task-related effects should enhance the specific functional features of the connectivity patterns in the two experimental groups, independently from task-related changes in regional activity, as indicated by the similarity of functional correlation maps during the different tasks in the sighted group. Indeed, the correlations between BOLD variations at rest have been found to reflect patterns of known connectivity in different cognitive operations (Hampson et al., 2004; Mennes et al., 2010).

In summary, these findings expand our previous results on the development of the functional organization of hMT+ by showing that distinct patterns of brain functional correlations originate from the anterior and posterior hMT+ subregions, and that these functional correlation patterns are differentially affected by visual experience. As a matter of facts, in congenitally blind subjects both the anterior and the posterior part of bilateral hMT+ revealed similar patterns of functional correlations, thus indicating that in the absence of visual experience brain regions responsive to visual motion develop toward processing of non-visual inputs. Along with previous studies by our and other laboratories, these findings provide a new perspective on how the human brain develops its functional organization in relation to the presence or absence of visual experience.

ACKNOWLEDGMENTS

The authors wish to thank all the volunteers who took part in the study, and the Unione Italiana Ciechi for its invaluable support to this project; the MRI Laboratory at the Fondazione Regione Toscana/C.N.R. "G. Monasterio" (Pisa, Italy), coordinated by Massimo Lombardi. We also thank Giacomo Handjaras for his advice on data analysis. This research was supported by the European Union (Grant IST-2001-38040 to Pietro Pietrini) and by the Italian Ministero dell'Istruzione, dell'Università e della Ricerca (Grant RBNE018ET9-003 and Grant 2004118414 to Pietro Pietrini).

REFERENCES

Amedi, A., Malach, R., Hendler, T., Peled, S., and Zohary, E. (2001). Visuo-haptic object-related activation in the ventral visual pathway. *Nat. Neurosci.* 4, 324–330.

Amedi, A., von Kriegstein, K., van Atteveldt, N. M., Beauchamp, M. S., and Naumer, M. J. (2005). Functional imaging of human crossmodal identification and object recognition. *Exp. Brain Res.* 166, 559–571.

Beauchamp, M. S., Yasar, N. E., Frye, R. E., and Ro, T. (2008). Touch, sound and vision in human superior temporal sulcus. *Neuroimage* 41, 1011–1020.

Beauchamp, M. S., Yasar, N. E., Kishan, N., and Ro, T. (2007). Human MST but not MT responds to tactile stimulation. *J. Neurosci.* 27, 8261–8267.

Birn, R. M., Diamond, J. B., Smith, M. A., and Bandettini, P. A. (2006). Separating respiratory-variation-related fluctuations from neuronal-activity-related fluctuations in fMRI. *Neuroimage* 31, 1536–1548.

Biswal, B., Yetkin, F. Z., Haughton, V. M., and Hyde, J. S. (1995). Functional connectivity in the motor cortex of resting human brain using echo-planar MRI. *Magn. Reson. Med.* 34, 537–541.

Bonino, D., Ricciardi, E., Sani, L., Gentili, C., Vanello, N., Guazzelli, M., Vecchi, T., and Pietrini, P. (2008). Tactile spatial working memory activates the dorsal extrastriate cortical pathway in congenitally blind individuals. *Arch. Ital. Biol.* 146, 133–146.

Bremmer, F., Schlack, A., Shah, N. J., Zafiris, O., Kubischik, M., Hoffmann, K., Zilles, K., and Fink, G. R. (2001). Polymodal motion processing in posterior parietal and premotor cortex: a human fMRI study strongly implies equivalencies between humans and monkeys. *Neuron* 29, 287–296.

Cattaneo, Z., Vecchi, T., Cornoldi, C., Mammarella, I., Bonino, D., Ricciardi, E., and Pietrini, P. (2008). Imagery and spatial processes in blindness and visual impairment. *Neurosci. Biobehav. Rev.* 32, 1346–1360.

Chang, C., and Glover, G. H. (2009). Effects of model-based physiological noise correction on default mode network anti-correlations and correlations. *Neuroimage* 47, 1448–1459.

Cordes, D., Haughton, V. M., Arfanakis, K., Carew, J. D., Turski, P. A., Moritz, C. H., Quigley, M. A., and Meyerand, M. E. (2001). Frequencies contributing to functional connectivity in the cerebral cortex in resting-state data. *AJNR Am. J. Neuroradiol.* 22, 1326–1333.

Cowey, A. (2010). The blindsight saga. *Exp. Brain Res.* 200, 3–24.

Cox, R. W. (1996). AFNI: software for analysis and visualization of functional magnetic resonance neuroimages. *Comput. Biomed. Res.* 29, 162–173.

Fox, M. D., Snyder, A. Z., Vincent, J. L., Corbetta, M., Van Essen, D. C., and Raichle, M. E. (2005). The human brain is intrinsically organized into dynamic, anticorrelated functional networks. *Proc. Natl. Acad. Sci. U.S.A.* 102, 9673–9678.

Friston, K. J., Frith, C. D., Liddle, P. F., and Frackowiak, R. S. J. (1993). Functional connectivity: the principal-component analysis of large (PET) data sets. *J. Cereb. Blood Flow Metab.* 13, 5–14.

Fujii, T., Tanabe, H. C., Kochiyama, T., and Sadato, N. (2009). An investigation of cross-modal plasticity of effective connectivity in the blind by dynamic causal modeling of functional MRI data. *Neurosci. Res.* 65, 175–186.

Gaglianese, A., Sani, L., Roebroeck, A., Handjaras, G., Bernardi, G., Costagli, M., Ricciardi, E., and Pietrini, P. (2010). *fMRI Functional and Effective Connectivity in Humans Supports a Direct Pathway from Thalamus to hMT+*. Presented at the 16th Annual Meeting of the Organization for Human Brain Mapping, Barcelona.

Goebel, R., Khorram-Sefat, D., Muckli, L., Hacker, H., and Singer, W. (1998). The constructive nature of vision: direct evidence from functional magnetic resonance imaging studies of apparent motion and motion imagery. *Eur. J. Neurosci.* 10, 1563–1573.

Grefkes, C., Weiss, P. H., Zilles, K., and Fink, G. R. (2002). Crossmodal processing of object features in human anterior intraparietal cortex: an fMRI study implies equivalencies between humans and monkeys. *Neuron* 35, 173–184.

Greicius, M. D., Krasnow, B., Reiss, A. L., and Menon, V. (2003). Functional connectivity in the resting brain: a network analysis of the default mode hypothesis. *Proc. Natl. Acad. Sci. U.S.A.* 100, 253–258.

Hagen, M. C., Franzen, O., McGlone, F., Essick, G., Dancer, C., and Pardo, J. V. (2002). Tactile motion activates the human middle temporal/V5 (MT/V5) complex. *Eur. J. Neurosci.* 16, 957–964.

Hampson, M., Olson, I. R., Leung, H. C., Skudlarski, P., and Gore, J. C. (2004). Changes in functional connectivity of human MT/V5 with visual motion input. *Neuroreport* 15, 1315–1319.

Horwitz, B. (2003). The elusive concept of brain connectivity. *Neuroimage* 19, 466–470.

Horwitz, B., Warner, B., Fitzer, J., Tagamets, M. A., Husain, F. T., and Long, T. W. (2005). Investigating the neural basis for functional and effective connectivity. Application to fMRI. *Philos. Trans. R. Soc. Lond., B, Biol. Sci.* 360, 1093–1108.

Jiang, A., Kennedy, D. N., Baker, J. R., Weisskoff, R. M., Tootell, B. H., Woods, R. P., Benson, R. R., Kwong, K. K., Brady, T. J., Rosen, B. R., and Belliveau, J. W. (1995). Motion detection and correction in functional MR imaging. *Hum. Brain Mapp.* 3, 224–235.

Kourtzi, Z., and Kanwisher, N. (2000). Activation in human MT/MST by static images with implied motion. *J. Cogn. Neurosci.* 12, 48–55.

Kupers, R., Chebat, D. R., Madsen, K. H., Paulson, O. B., and Ptito, M. (2010). Neural correlates of virtual route recognition in congenital blindness. *Proc. Natl. Acad. Sci. U.S.A.* 107, 12716–12721.

Kupers, R., Fumal, A., Maertens de Noordhout, A., Gjedde, A., Schoenen, J., and Ptito, M. (2006). Transcranial magnetic stimulation of the visual cortex induces somatotopically organized qualia in blind subjects. *Proc. Natl. Acad. Sci. U.S.A.* 103, 13256–13260.

Liang, M., Zhou, Y., Jiang, T., Liu, Z., Tian, L., Liu, H., and Hao, Y. (2006). Widespread functional disconnectivity in schizophrenia with resting-state functional magnetic resonance imaging. *Neuroreport* 17, 209–213.

Lowe, M. J., Mock, B. J., and Sorenson, J. A. (1998). Functional connectivity in single and multislice echo planar imaging using resting state fluctuations. *Neuroimage* 7, 119–132.

Mahon, B. Z., Anzellotti, S., Schwarzbach, J., Zampini, M., and Caramazza, A. (2009). Category-specific organization in the human brain does not require visual experience. *Neuron* 63, 397–405.

Mahon, B. Z., Schwarzbach, J., and Caramazza, A. (2010). The representation of tools in left parietal cortex is independent of visual experience. *Psychol. Sci.* 21,764–771.

Mather, G., Pavan, A., Campana, G., and Casco, C. (2008). The motion aftereffect reloaded. *Trends Cogn. Sci.* 12, 481–487.

Matteau, I., Kupers, R., Ricciardi, E., Pietrini, P., and Ptito, M. (2010). Beyond visual, aural and haptic movement perception: hMT+ is activated by electrotactile motion stimulation of the tongue in sighted and in congenitally blind individuals. *Brain Res. Bull.* 82, 264–270.

Mennes, M., Kelly, C., Zuo, X. N., Di Martino, A., Biswal, B. B., Castellanos, F. X., and Milham, M. P. (2010). Inter-individual differences in resting-state functional connectivity predict task-induced BOLD activity. *Neuroimage* 50, 1690–1701.

Murphy, K., Birn, R. M., Handwerker, D. A., Jones, T. B., and Bandettini, P. A. (2009). The impact of global signal regression on resting state correlations: are anti-correlated networks introduced? *Neuroimage* 44, 893–905.

Peltier, S., Stilla, R., Mariola, E., LaConte, S., Hu, X., and Sathian, K. (2007). Activity and effective connectivity of parietal and occipital cortical regions during haptic shape perception. *Neuropsychologia* 45, 476–483.

Pietrini, P., Furey, M. L., Ricciardi, E., Gobbini, M. I., Wu, W. H., Cohen, L., Guazzelli, M., and Haxby, J. V. (2004). Beyond sensory images: object-based representation in the human ventral pathway. *Proc. Natl. Acad. Sci. U.S.A.* 101, 5658–5663.

Pietrini, P., Ptito, M., and Kupers, R. (2009). "Blindness and consciousness: new light from the dark," in *The Neurology of Consciousness*, eds S. Laureys and G. Tononi (Amsterdam: Academic Press), 360–374.

Poirier, C., Collignon, O., Scheiber, C., Renier, L., Vanlierde, A., Tranduy, D., Veraart, C., and De Volder, A. G. (2006). Auditory motion perception activates visual motion areas in early blind subjects. *Neuroimage* 31, 279–285.

Ptito, M., Fumal, A., de Noordhout, A. M., Schoenen, J., Gjedde, A., and Kupers, R. (2008). TMS of the occipital cortex induces tactile sensations in the fingers of blind Braille readers. *Exp. Brain Res.* 184, 193–200.

Ptito, M., and Kupers, R. (2005). Cross-modal plasticity in early blindness. *J. Integr. Neurosci.* 4, 479–488.

Ptito, M., Matteau, I., Gjedde, A., and Kupers, R. (2009). Recruitment of the middle temporal area by tactile motion in congenital blindness. *Neuroreport* 20, 543–547.

Raichle, M. E., MacLeod, A. M., Snyder, A. Z., Powers, W. J., Gusnard, D. A., and Shulman, G.L. (2001). A default mode of brain function. *Proc. Natl. Acad. Sci. U.S.A.* 98, 676–682.

Ricciardi, E., Basso, D., Bonino, D., Sani, L., Guazzelli, M., Vecchi, T., Pietrini, P., and Miniussi, C. (2010). Functional inhibition of the human middle temporal cortex affects non-visual motion perception: a repetitive transcranial magnetic stimulation study during tactile speed discrimination. *Exp. Biol. Med. (Maywood)* doi: 10.1258/ebm.2010.010230.

Ricciardi, E., Bonino, D., Gentili, C., Sani, L., Pietrini, P., and Vecchi, T. (2006). Neural correlates of spatial working memory in humans: a functional magnetic resonance imaging study comparing visual and tactile processes. *Neuroscience* 139, 339–349.

Ricciardi, E., Bonino, D., Sani, L., Vecchi, T., Guazzelli, M., Haxby, J. V., Fadiga, L., and Pietrini, P. (2009). Do we really need vision? How blind people "see" the actions of others. *J. Neurosci.* 29, 9719–9724.

Ricciardi, E., Vanello, N., Sani, L., Gentili, C., Scilingo, E. P., Landini, L., Guazzelli, M., Bicchi, A., Haxby, J. V., and Pietrini, P. (2007). The effect of visual experience on the development of functional architecture in hMT+. *Cereb. Cortex* 17, 2933–2939.

Shulman, G. L., Schwarz, J., Miezin, F. M., and Petersen, S. E. (1998). Effect of motion contrast on human cortical responses to moving stimuli. *J. Neurophysiol.* 79, 2794–2803.

Summers, I. R., Francis, S. T., Bowtell, R. W., McGlone, F. P., and Clemence, M. (2009). A functional-magnetic-resonance-imaging investigation of cortical activation from moving vibrotactile stimuli on the fingertip. *J. Acoust. Soc. Am.* 125, 1033–1039.

Talairach, J., and Tournoux, P. (1988). *Co-Planar Stereotaxic Atlas of the Human Brain*. New York: Thieme Classics.

Tootell, R. B., Reppas, J. B., Dale, A. M., Look, R. B., Sereno, M. I., Malach, R., Brady, T. J., and Rosen, B. R. (1995). Visual motion aftereffect in human cortical area MT revealed by functional magnetic resonance imaging. *Nature* 375, 139–141.

Watson, J. D., Myers, R., Frackowiak, R. S., Hajnal, J. V., Woods, R. P., Mazziota, J. C., Shipp, S., and Zeki, S. (1993). Area V5 of the human brain: evidence from a combined study using positron emission tomography and magnetic resonance imaging. *Cereb. Cortex* 3, 79–94.

Whalley, H. C., Simonotto, E., Marshall, I., Owens, D. G., Goddard, N. H., Johnstone, E. C., and Lawrie, S. M. (2005). Functional disconnectivity in subjects at high genetic risk of schizophrenia. *Brain* 128, 2097–2108.

Wittenberg, G. F., Werhahn, K. J., Wassermann, E. M., Herscovitch, P., and Cohen, L. G. (2004). Functional connectivity between somatosensory and visual cortex in early blind humans. *Eur. J. Neurosci.* 20, 1923–1927.

Zeki, S., Watson, J. D., and Frackowiak, R. S. (1993). Going beyond the information given: the relation of illusory visual motion to brain activity. *Proc. Biol. Sci.* 252, 215–222.

Conflict of Interest Statement: The authors declare that the research was conducted in the absence of any commercial or financial relationships that could be construed as a potential conflict of interest.

Received: 21 July 2010; accepted: 07 December 2010; published online: 20 December 2010.

*Citation: Sani L, Ricciardi E, Gentili C, Vanello N, Haxby JV and Pietrini P (2010) Effects of visual experience on the human MT+ functional connectivity networks: an fMRI study of motion perception in sighted and congenitally blind individuals. Front. Syst. Neurosci. **4**:159. doi: 10.3389/fnsys.2010.00159*

Copyright © 2010 Sani, Ricciardi, Gentili, Vanello, Haxby and Pietrini. This is an open-access article subject to an exclusive license agreement between the authors and the Frontiers Research Foundation, which permits unrestricted use, distribution, and reproduction in any medium, provided the original authors and source are credited.

frontiers in
SYSTEMS NEUROSCIENCE

ORIGINAL RESEARCH ARTICLE
published: 15 October 2010
doi: 10.3389/fnsys.2010.00149

Diffusion tensor imaging detects early cerebral cortex abnormalities in neuronal architecture induced by bilateral neonatal enucleation: an experimental model in the ferret

Andrew S. Bock[1], Jaime F. Olavarria[1], Lindsey A. Leigland[2,3], Erin N. Taber[2], Sune N. Jespersen[4] and Christopher D. Kroenke[2,3,5]*

[1] *Department of Psychology, University of Washington, Seattle, WA, USA*
[2] *Advanced Imaging Research Center, Oregon Health and Science University, Portland, OR, USA*
[3] *Department of Behavioral Neuroscience, Oregon Health and Science University, Portland, OR, USA*
[4] *Center of Functionally Integrative Neuroscience, Aarhus University, Aarhus, Denmark*
[5] *Oregon National Primate Research Center, Oregon Health and Science University, Portland, OR, USA*

Edited by:
Silvina G. Horovitz, National Institutes of Health, USA

Reviewed by:
Adam W. Anderson, Vanderbilt University, USA
Petra Huppi, University of Geneva, Switzerland

****Correspondence:***
Christopher D. Kroenke, Advanced Imaging Research Center, Oregon Health and Science University, 3181 SW Sam Jackson Park Road, Portland, OR 97239, USA.
e-mail: kroenkec@ohsu.edu

Diffusion tensor imaging (DTI) is a technique that non-invasively provides quantitative measures of water translational diffusion, including fractional anisotropy (FA), that are sensitive to the shape and orientation of cellular elements, such as axons, dendrites and cell somas. For several neurodevelopmental disorders, histopathological investigations have identified abnormalities in the architecture of pyramidal neurons at early stages of cerebral cortex development. To assess the potential capability of DTI to detect neuromorphological abnormalities within the developing cerebral cortex, we compare changes in cortical FA with changes in neuronal architecture and connectivity induced by bilateral enucleation at postnatal day 7 (BEP7) in ferrets. We show here that the visual callosal pattern in BEP7 ferrets is more irregular and occupies a significantly greater cortical area compared to controls at adulthood. To determine whether development of the cerebral cortex is altered in BEP7 ferrets in a manner detectable by DTI, cortical FA was compared in control and BEP7 animals on postnatal day 31. Visual cortex, but not rostrally adjacent non-visual cortex, exhibits higher FA than control animals, consistent with BEP7 animals possessing axonal and dendritic arbors of reduced complexity than age-matched controls. Subsequent to DTI, Golgi-staining and analysis methods were used to identify regions, restricted to visual areas, in which the orientation distribution of neuronal processes is significantly more concentrated than in control ferrets. Together, these findings suggest that DTI can be of utility for detecting abnormalities associated with neurodevelopmental disorders at early stages of cerebral cortical development, and that the neonatally enucleated ferret is a useful animal model system for systematically assessing the potential of this new diagnostic strategy.

Keywords: diffusion tensor imaging, magnetic resonance imaging, ferret, enucleation, interhemispheric callosal connections, Golgi, brain, visual system

INTRODUCTION

Diffusion tensor imaging (DTI) studies have shown that in several neurological disorders, affected individuals possess white matter (WM) that is characterized by abnormally low fractional anisotropy (FA) in water diffusion (see reviews by Lim and Helpern, 2002; White et al., 2008). In WM of mature normal individuals, water diffusion is anisotropic because it is preferentially hindered or otherwise obstructed in directions perpendicular to an axonal fiber tract, but less so in directions parallel to the tract. The degree of anisotropy in water diffusion is commonly quantified in terms of FA (Basser and Pierpaoli, 1996), which ranges from 0 (isotropic diffusion) to 1 (maximally anisotropic diffusion). Several reports have shown that behavioral and/or sensory impairment correlates with a reduction in WM FA, and suggest that this reduction is a manifestation of abnormal axonal organization within the tract, or abnormal myelin structure. Although DTI provides a unique approach for studying the biological basis of neurological disorders, the abnormalities in WM identified using this strategy likely reflect an endpoint of disease because plasticity in the CNS typically decreases after critical/sensitive periods (Katz and Crowley, 2002; Olavarria and Hiroi, 2003; Innocenti and Price, 2005; Fields, 2008).

A potential way to extend the DTI approach to the developing brain is to monitor changes in water diffusion anisotropy within the cerebral cortex at the time in which neurons undergo morphological differentiation. In the immature cerebral cortex, water diffusion is highly anisotropic due to the influence of a different set of cellular structures (e.g., apical dendrites, undifferentiated dendrites, and axons) than those that influence water diffusion within WM at maturity (e.g., myelinated axons). Apical dendrites of pyramidal neurons are aligned perpendicular to the pial surface, and these selectively impose restrictions in directions parallel to the pial surface (Neil et al., 1998; McKinstry et al., 2002). However, as the brain matures, diffusion within cortex becomes increasingly restricted in all directions, causing fractional anisotropy of water diffusion to become progressively smaller, although still measurable in the mature brain (McNab et al., 2009). Immediately after pyramidal

neurons of the isocortex migrate from germinal zones to the cortical plate, the neuropil, consisting primarily of neuronal and glial processes and the associated extracellular space, begins to differentiate (Rakic, 1995). Dendrites and axons begin as simple elongated structures, oriented perpendicular to the pial surface, and then gain structural complexity as they arborize to form interconnected, functional neural circuits (Conel, 1939). It has previously been proposed that the reduction in FA associated with development of the cerebral cortex arises from morphological differentiation of the neuropil (McKinstry et al., 2002). This idea is supported by the fact that the age-related decreases in cerebral cortical FA coincide with developmental changes in neuropil morphology. Indeed, the progressive reduction of cortical diffusion anisotropy with age has been quantified for several mammalian species (see Leigland and Kroenke, 2010 for review), and in each case the period of cortical diffusion anisotropy loss occurs immediately following the genesis and subsequent migration of pyramidal neurons from ventricular/subventricular zones to the cortical plate (Kroenke et al., 2009). In addition, the neuropil represents 70–80% of the cortical volume fraction (Miller and Potempa, 1990; Granger et al., 1995), which is significantly greater than the volume fraction of other elements such as glial and neuron cell somas (3.6% and 22%, respectively, Miller and Potempa, 1990).

It has been established that certain neurodevelopmental disorders are associated with abnormal morphological differentiation of the cerebral cortical neuropil (e.g., Rett syndrome, Armstrong et al., 1995) and fetal alcohol spectrum disorder (Davies and Smith, 1981). Determining whether neurological disorders affecting development of the cortical neuropil lead to measurable changes in cortical FA would be of significant value because it would provide a means of detecting and monitoring the deleterious effects of pathological insults on cortical development, as well as allow for therapeutic interventions while the brain is still plastic. Here we describe an animal model designed to explore the potential of DTI techniques for detecting abnormal morphological development of the cerebral cortex.

Ferrets are recognized as an ideal model system for studies of brain development (Jackson and Hickey, 1985), and they have been utilized in numerous studies of visual system plasticity (see review by Katz and Crowley, 2002). We chose blindness induced by early enucleation as an experimental perturbation because there is a vast literature indicating that blindness induced by neonatal enucleation or other forms of visual deprivation can alter intracortical cellular morphology, as well as the patterns of cortico–cortical connectivity in visual areas. For example, in humans, early blindness has been shown to be associated with reductions in visual WM FA at adulthood (Shimony et al., 2006). Golgi studies of animals that have been dark-reared (Coleman and Riesen, 1968; Borges and Berry, 1978), stripe-reared (Tieman and Hirsch, 1982), or binocularly enucleated (Ryugo et al., 1975; Heumann and Rabinowicz, 1982) have documented effects on several aspects of dendritic development in the isocortex, including abnormalities in dendritic fields of pyramidal cells, and reductions in the number of dendritic spines. Moreover, neonatal enucleation induces massive changes in the distribution and topography of the interhemispheric connections through the corpus callosum (Berman, 1991; Olavarria and Li, 1995; Zufferey et al., 1999; Olavarria and Hiroi, 2003; Innocenti and Price, 2005; Olavarria and Safaeian, 2006). At the cellular level, enucleation increases the length of callosal axon branches and total length of arbors, without major effects on the number of branch tips (Olavarria et al., 2008), and reduces the proportion of multiple synaptic boutons in the visual callosal projection (Sorensen et al., 2003).

Due to the widespread distribution of callosal connections in the brain, the overall cortical area affected by enucleation can be readily estimated by determining which regions contain abnormal callosal patterns. In turn, this greatly facilitates the identification of areas to be analyzed with DTI methods. To test whether DTI methods are capable of detecting abnormal neuropil development, we compared measurements of FA in visual cortex of control and enucleated ferrets at P31, a stage in which neuronal morphological differentiation is still underway. We further asked whether changes in the organization of dendrites induced by enucleation are linked to abnormal changes in cortical FA. To address this question, we examined the effect of enucleation on dendrite morphology in Golgi-stained sections, and correlated the changes observed with abnormal changes in cortical FA. Our data indicate that enucleation causes morphological changes in the visual system that can be detected with DTI methods at early stages of cerebral cortical development. Moreover, our Golgi data suggest that abnormalities in the development of dendrites may underlie, at least in part, the abnormal changes in cortical FA that we observed in visual cortex of enucleated ferrets at early developmental stages.

MATERIALS AND METHODS

ANIMAL HANDLING AND PROCEDURES

Animal care

Our study is based on data obtained from a total of 10 ferrets (*Mustela putorius furo*) purchased from Marshall Bioresources (North Rose, NY, USA) and delivered to the Oregon Health & Science University (OHSU) Department of Comparative Medicine on postnatal day 5 (P5). This study, and all procedures involved, were approved by the OHSU and University of Washington Institutional Animal Care and Use Committees, and were carried out in accordance with the NIH "Guide for the Care and Use of Laboratory Animals" (NIH publication no. 86-23, revised 1987).

Enucleations

Ferrets were binocularly enucleated on postnatal day 7 (BEP7). Animals were placed under 2% isoflurane anesthesia, and arterial pulse oxygenation, pulse rate, respiration rate, and core body temperature were monitored throughout surgical *in vivo* procedures. Under aseptic conditions, slits were cut in both eyelids, the eyes were removed with iridectomy scissors, and the eyelids sutured closed. Topical bupivacaine was administered intra-operatively in the orbital cavity immediately after removing the eyes. After full recovery from anesthesia, animals were returned to their mothers.

Tracer injections

Anatomical tracer injections were performed on six animals (three controls and three animals binocularly enucleated on P7, BEP7) at adulthood (P120 or older). Animals were placed under 2% isoflurane anesthesia, intubated, and arterial pulse oxygenation, pulse rate, respiration rate, end-tidal pCO_2, and core body temperature

were monitored throughout surgical procedures. A 1 cm × 2 cm craniotomy was performed over the occipital and parietal lobes using a hand-held bone drill. Multiple 0.01–0.02 μl injections of the anatomical tracer horseradish peroxidase (HRP, 20% in saline), separated by 200–300 μm, were administered through glass micropipettes (50–100 μm tip diameter) 600–800 μm below the dura throughout the exposed cortex of one hemisphere. Following injections, the bone chip was replaced and the muscle and skin layers were sutured closed.

HISTOLOGICAL ANALYSES

Tissue collection

After a survival period of 2 days, animals were injected with 0.5 mL euthasol (i.p.) and previously described fixation procedures to unfold and flatten the cortical mantle were followed (Olavarria and Van Sluyters, 1985). Heparinized phosphate-buffered saline (PBS) was injected into the left cardiac ventricle until the fluid of the right atria was clear. Phosphate-buffered paraformaldehyde (2% for brains to undergo cortical unfolding and flattening, 4% for remaining brains, pH 7.4) was perfused through the left ventricle for 8 min. Brains were removed from the skull and those fixed in 2% paraformaldehyde were placed in PBS at 4°C, and brains fixed with 4% paraformaldehyde were post-fixed for 24 h (in 4% paraformaldehyde), and then transferred to PBS and allowed to equilibrate for at least 48 h prior to DTI experiments.

Callosal connectivity pattern

The hemisphere contralateral to tracer injections was unfolded and flattened according to procedures described previously (Olavarria and Van Sluyters, 1985, 1995). The patterns of retrogradely labeled somas and anterogradely labeled axon terminals in the contralateral hemisphere were revealed with standard HRP protocols (Olavarria et al., 1987) in histological sections (70-μm thick) cut tangentially to the cortical surface. The surface area occupied by callosal connections was calculated from thresholded versions of the patterns reconstructed using Adobe Photoshop CS2. The same parameters for image analysis were applied to all control and BE animals. Differences in the percent of area occupied by callosal connections were analyzed statistically using *t*-tests with the level of significance set at 0.05.

Golgi staining

Four animals (two controls and two BEP7) euthanized on P31 were used for Golgi staining and analysis following DTI experiments. Golgi staining was performed using the Rapid GolgiStain kit (FD NeuroTechnologies, Inc., Ellicott City, MD, USA). Tissue samples were frozen in Tissue Tek OCT (optimal cutting temperature) compound (Ted Pella, Inc., Redding, CA, USA) using a dry-ice slurry, 150-μm thick coronal slices were cut using a rotary microtome. Right hemispheres from two animals (herein termed Cntrl-1 and BEP7-1) were sectioned in the coronal plane, and hemispheres from the remaining two animals (Cntrl-2, left and BEP7-2, right) were sectioned in the axial plane. The left hemisphere of Cntrl-2 was analyzed here because the right hemisphere of this animal was used in a prior study (Kroenke et al., 2009, see below). Tissue sections were directly mounted onto Gelatin subbed slides and left to dry and then coverslipped. Photographic montages of entire coronal sections taken from Cntrl-1 and BEP7-1 were prepared from light microscope images captured at 2.5× magnification (e.g., see **Figure 2B**). Subsequent steps in the analyses of Golgi-stained tissue were performed using images captured at 10× magnification.

Quantification of orientation distributions of neuronal processes

Each of the 10× images was stored to disk as a 512 pixel × 512 pixel tif image (each pixel represents a 3 × 3 μm area), and a series of initial image processing operations were performed using ImageJ software (http://rsbweb.nih.gov/ij/). First, binarized images of Golgi-stained neurons and neuronal processes were generated by applying a threshold operation to each 10× image. These images were stored to disk and denoted "somas + processes". Second, neuronal processes were removed from the binary images by applying an erosion operation, followed by a dilation operation. The resulting images were stored to disk and denoted "somas". Third, difference images were constructed between the "somas + processes" and "somas" images to generate binary images of only neuronal processes. Last, a skeletonization operation was applied to the images of neuronal processes, and the output of this operation was stored to disk and denoted "skeletons".

Binary 2D skeletons representing the set of neuronal process were then approximated as a set of linear segments. To accomplish this, skeleton images were imported into the Matlab programming environment (The MathWorks, Boston, MA, USA) for further processing using a series of custom-built image processing macros. First, the length (e.g., the number of connected non-zero pixels) of each fragment of the skeletonized image was determined, and fragments of less than 10 pixels were removed from subsequent analysis (by setting the pixel values to 0). Second, a region within the cerebral cortex was identified within each image. This operation prevented contamination of Golgi-stained white matter. In addition, this operation enabled the analysis to be focused on cortical areas that have minimal curvature, thus minimizing the effect that macroscopic structure of the cerebral cortex may have on the orientation of cortical axons and dendrites (e.g., see **Figure 4**). Third, each skeleton fragment within the identified cerebral cortical region of interest was approximated using the equation for a line. Last, the set of slope parameters were converted to polar angles, θ, ranging from $-\frac{\theta}{2}$ to $\frac{\theta}{2}$, using the relation $\theta = \tan^{-1}(\text{slope})$.

To facilitate comparisons between sets of axon and dendrite orientations derived from the various images of Golgi-stained tissue, the orientation distribution was modeled using the von Mises-type axial distribution (Fisher, 1993)

$$P(\theta) = \frac{\exp\left[\kappa \cos\left(2(\theta - \alpha)\right)\right]}{\left(\pi I_0(k)\right)},$$

in which $I_0(k)$ is the modified Bessel function of order zero, and $P(\theta)$ is the observed distribution of angles θ in a region of interest. The factor of 2 in the cos argument differs from the expression given by Fisher (1993) because the distribution considered herein is undirected rather than directed (see Mardia et al., 1979). Such modeling is standard in the analysis of circular data; the von Mises parameters that provide quantitative characterizations of the mean and width of a set of angles are the mean angle, α, and the concentration parameter, κ, respectively. The parameter κ can be interpreted as the precision of the mean direction, and is

somewhat analogous to the inverse of the standard deviation of a Gaussian distribution of linear data; larger κ reflects *less* variability in the set of angles comprising the distribution (a larger standard deviation in a Gaussian distribution corresponds to *more* variability). A maximum likelihood approach for estimating parameters in the von Mises distribution was implemented in Matlab using the property that the distribution of 2θ follows the standard (unimodal) von Mises distribution with parameters κ and 2α.

Orientation distributions were measured for a total of 14 (seven control/BEP7 pairs) of cortical locations, including five in coronal sections from cases Cntrl-1 and BEP7-1, and two in axial sections from cases Cntrl-2 and BEP7-2 (see **Figure 5**). For the control cortical locations, a mean ± standard deviation of 216 ± 80 linear segments representing neuronal processes were used to estimate κ; and for the BEP7 locations, the number of line segments was 202 ± 153. Analysis of simulated data was performed to confirm accuracy of the procedure for estimating κ, and to ensure that bias in numerical procedures used to estimate κ is negligible for the sample sizes used. To estimate 95% confidence intervals for each of the 14 κ estimates, a bootstrap procedure (Fisher, 1993), using the "bootstrp" Matlab function, was utilized. For a cortical location with N line elements, this involved estimating the von Mises distribution parameters 1000 times, each time using a random sampling of the N values of θ. The 95% confidence interval for κ is estimated to range from the 26th to the 975th smallest κ value. A pair of κ values was interpreted to be significantly different if their associated 95% confidence intervals did not overlap.

DIFFUSION TENSOR IMAGING AND CORTICAL SURFACE CALCULATIONS

Post mortem DTI procedures

Diffusion tensor imaging was performed on the same P31 brains analyzed by Golgi. Each brain was sectioned along the midline prior to DTI measurements. For all cases except one control brain (Cntrl-2), the right hemisphere was analyzed. For the animal in which the left hemisphere was characterized, it's right hemisphere was included in a previously published study (brain P31b in Kroenke et al., 2009), and no differences between the left and right hemispheres for this animal were observed (data not shown). A 2-cm diameter single-turn solenoidal coil was utilized for radiofrequency transmission and reception. Experiments were performed using a 11.7 T magnet interfaced with a 9-cm inner diameter magnetic field gradient coil (Bruker, Rheinstetten, Germany). A Stejskal–Tanner multi-slice spin-echo pulse sequence with parameters $\delta = 12$ ms, $\Delta = 21$ ms, and $G = 27.3$ G/cm (resulting in $b = 2.7$ ms/μm^2) was used to perform DTI measurements. Diffusion anisotropy measurements were made using a 25-direction, icosahedral sampling scheme (Batchelor et al., 2003). Other pulse sequence settings were TR > 5 s, TE = 42 ms, and image resolution was isotropic voxels of dimensions (0.25 mm)^3. Fractional anisotropy was calculated from diffusion-weighted images following standard procedures (Basser and Pierpaoli, 1996). To facilitate FA comparisons between animals at corresponding coronal planes, FA parameter maps for each hemisphere were registered to one another using the FMRIB non-linear registration tool (FNIRT) (Smith et al., 2006; Klein et al., 2009).

Cortical diffusion anisotropy

For each right hemisphere, surface models were constructed of inner (white matter to subplate or layer VI) and outer (layer I to the pial surface) boundaries of the cortex (olfactory bulbs were omitted at the lateral olfactory tract in all analyses) using the CARET software package (Van Essen et al., 2001). Previously described procedures (Kroenke et al., 2009) were followed to project cortical FA values onto cortical surface models, and to register surfaces to a common atlas.

RESULTS

The distribution of labeled cell bodies and axon terminals was charted in flattened contralateral hemispheres of control ($N = 3$) and BEP7 ($N = 3$) adult ferrets following injection of HRP into the visual cortex of one hemisphere (**Figure 1**). Previous physiological studies have mapped the locations of visual areas relative to anatomical landmarks such as gyri and sulci (see green shaded areas in **Figures 1A,B**) (Manger et al., 2002, 2004). **Figure 1D** illustrates the overall callosal pattern demonstrated following multiple HRP injections into the contralateral visual cortex of a control animal, while **Figure 1F** shows the callosal pattern from a BEP7 ferret. In normal animals, the callosal pattern consists of a series of densely HRP-labeled bands and patches within extrastriate cortex, outlined in green on the flattened cortex (**Figure 1C**). These patterns were compared across animals by using several landmarks as reference, including the series of red dots that were drawn along the crown of the suprasylvian and ectosylvian gyri, and along the dorsal/caudal edge of the occipital lobe (**Figure 1**). Similar arrangement of labeled and unlabeled areas was observed in all three control ferrets studied, providing evidence that the callosal pattern in normal animals is consistent from animal to animal. Moreover, callosal labeling at the 17/18 border of the hemisphere contralateral to injection was sparse in all three control animals studied in spite of the fact that, in the injected hemisphere, the region of the 17/18 border was densely infiltrated with HRP, as confirmed by inspection of the cortex and thalamus in the injected hemisphere (data not shown). The approximate location of the representation of the horizontal meridian is shown as a blue line in **Figure 1**. In adult BEP7 ferrets the visual callosal pattern is more irregular and occupies a significantly greater cortical area compared to controls. As illustrated in **Figures 1F,G,** the callosal pattern in BEP7 ferrets consists of smaller patches of labeled cells and axon terminations compared to controls, and these patches often occupy regions that are relatively free of callosal labeling in control animals. This is particularly striking throughout visual areas 18, 19, and 21 (**Figures 1F,G**). Comparison of thresholded renderings (**Figures 1E,G**) of the patterns in **Figure 1D,F** reveals that the percent area occupied by callosal connections is significantly ($p < 0.05$) greater in BEP7 than control ferrets (**Figure 1H**).

Abnormalities in the callosal pattern induced by neonatal enucleation have been shown in other species to be present at early stages of development (Olavarria and Safaeian, 2006; Olavarria et al., 2008). Therefore, the abnormal distribution of labeling in mature BEP7 ferrets suggests that DTI measurements of cortical FA may provide a strategy for detecting developmental abnormalities early in life by characterizing morphological differentiation of cerebral cortical neurons. **Figure 2A** shows a coronal view of

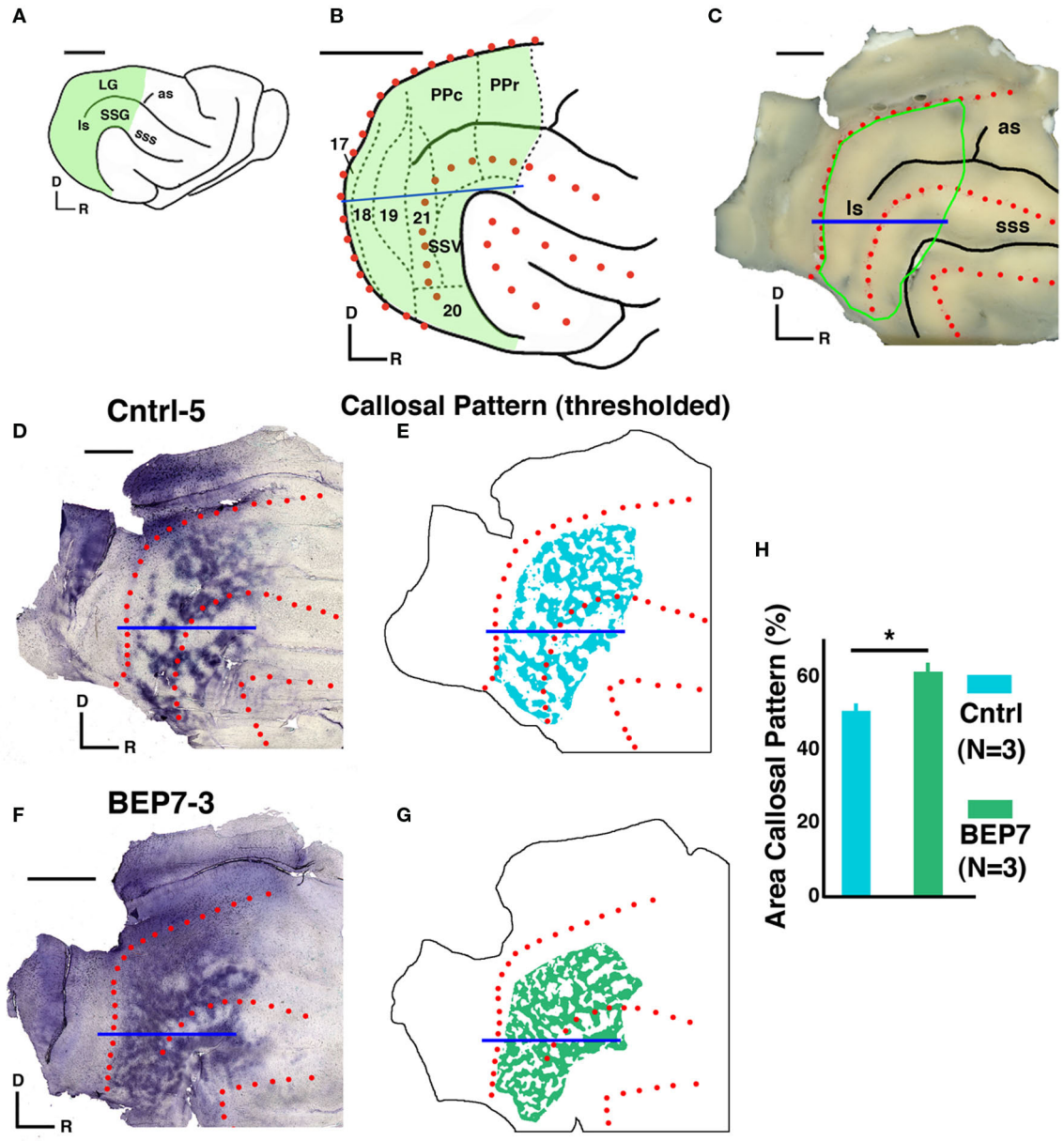


FIGURE 1 | Effect of bilateral enucleation on postnatal day 7 (BEP7) on the distribution of interhemispheric visual callosal connections in the ferret. The distribution of callosal connections in one hemisphere of adult BEP7 and control ferrets were studied following multiple intracortical injections of the tracer HRP in the contralateral hemisphere. Green areas in **(A)** and **(B)** include regions of visual cortex analyzed. Approximate locations of visual areas described in previous reports are indicated in **(B)**; the blue line marks the representation of the horizontal meridian. Red dots indicate the crown of the suprasylvian and ectosylvian and gyri, and the dorsal/caudal edge of the occipital lobe, which were marked directly on the brains before flattening. **(C)** Flattened brain before sectioning, area outlined by green line contains visual areas analyzed. Labeled callosal connections (labeled somas and axon terminations) appear as dark areas in **(D)** and **(F)**; and as colored areas in the thresholded versions **(E, G)**. The percent area occupied by callosal connections was significantly ($p < 0.05$) greater in BEP7 ferrets than in Control ferrets **(H)**. LG, lateral gyrus; PPc, posterior parietal caudal area; PPr, posterior parietal rostral area; SSG, suprasylvian gyrus; SSV, suprasylvian visual areas; as, ansate sulcus; ls, lateral sulcus, sss; suprasylvian sulcus. Scale = 5 mm.

DTI data obtained from a P31 BEP7 animal (case BEP7-1), following tissue fixation. The grayscale underlay in **Figure 2A** is a diffusion-weighted image, and the overlaying red line segments indicate principal eigenvector orientations for each voxel, which are parallel to the direction of least restricted diffusion. The length of each primary eigenvector displayed in **Figure 2A** is scaled by FA so that longer line segments overlap voxels with larger FA. Subsequent to acquiring DTI data, the tissue was stained using the rapid Golgi method, and sectioned in the coronal plane. **Figure 2B** is a montage of images acquired at 2.5× magnification from a section taken at a rostrocaudal level corresponding to that for **Figure 2A** (this level of the brain is indicated by the segmented line in the inset).

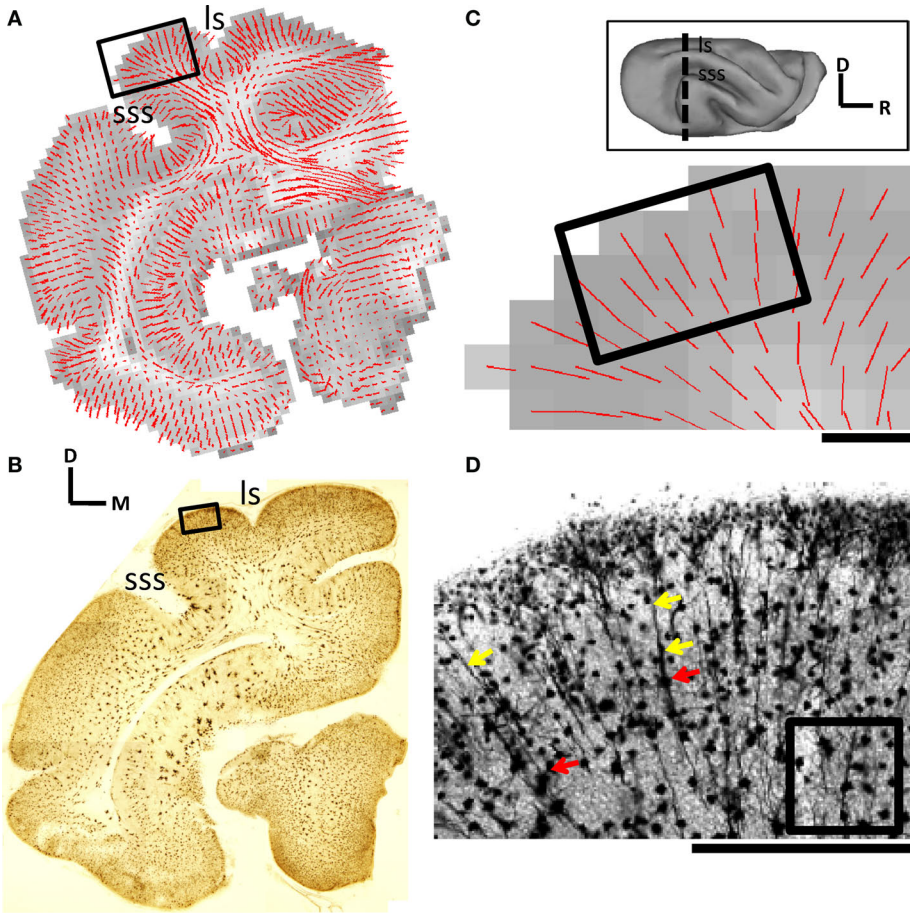


FIGURE 2 | Anisotropy in water diffusion within the developing cerebral cortex is oriented parallel to apical dendrites of pyramidal neurons. Corresponding coronal views of DTI data **(A)** and Golgi-stained tissue **(B)** obtained from brain BEP7-1. The rostrocaudal level of the coronal plane is represented by the dashed line in the inset. **(C,D)** Close-up views of the region of the suprasylvian gyrus indicated by the rectangles in **A** and **B,** respectively. Diffusion tensor primary eigenvector **(C)** and apical dendrites **(D)** are both oriented perpendicular to the pial surface. In **(D)**, yellow arrows indicate two apical dendrites, and red arrows indicate the associated cell bodies. The approximate size of the field in **(D)** is shown as a rectangle in **(C)**. The size of an individual DTI voxel is illustrated as a square in **(D)**. Abbreviations are as in **Figure 1**. Scale bars = 0.5 mm in panels **(C)** and **(D)**.

Figures 2C,D illustrate the close similarity between the orientations of water diffusion tensor primary eigenvectors (**Figures 2A,C**) and apical dendrites (**Figure 2D**). The rectangle in **Figure 2C** indicates the size and approximate location of the region shown in **Figure 2D**. The square in **Figure 2D** illustrates the size of a single DTI voxel. As indicated in **Figure 2D**, the P31 cerebral cortex contains incompletely differentiated pyramidal neurons with dendritic arbors that consist primarily of apical dendrites not yet ramified with oblique collaterals. Basal dendritic arbors are nascent at this developmental stage. As a result, cortical diffusion anisotropy at P31 is significant (Kroenke et al., 2009) and exhibits a radial orientation (**Figures 2A,C**).

To examine whether potential morphological differences between neurons of BEP7 and control animals can be detected through cortical diffusion anisotropy measurements at P31, cortical FA was compared between two BEP7 animals and two control animals, as shown in **Figure 3**. **Figure 3A** shows coronal views of FA parameter maps obtained at a rostrocaudal level (white segmented line in **Figure 3B**) running through visual cortical areas that are sensitive to visual deprivation (cf. **Figure 1**). Light colored regions, indicative of higher FA (gray-tone scale), occupy larger areas in the two BEP7 ferrets as compared to control ferrets, suggesting that cortical FA in the two BEP7 animals is increased relative to control at this position. To characterize diffusion anisotropy throughout the entire cerebral cortex, cortical FA was projected onto surface models of cerebral cortices for each of the four hemispheres. FA values are encoded by the yellow/high, red/low colormap shown in **Figure 3**. A surface region of interest (ROI) corresponding approximately to the green shading in **Figures 1A,B** was drawn, and its boundary is indicated by black dots in **Figure 3**, while the blue dots indicate the approximate representation of the horizontal meridian of the visual field. A rostrally located control area is also identified, outlined by blue-green dots (**Figure 3B**). Increased cortical diffusion anisotropy in visual areas of BEP7 animals is evident in the more extensive yellow pattern in the BEP7 brain compared to control. This difference is quantified for all four animals in **Figure 3C**. Increased cortical FA is observed within visual cortical areas (**Figure 3C**), but not within the rostral control area (**Figure 3D**), of BEP7 animals.

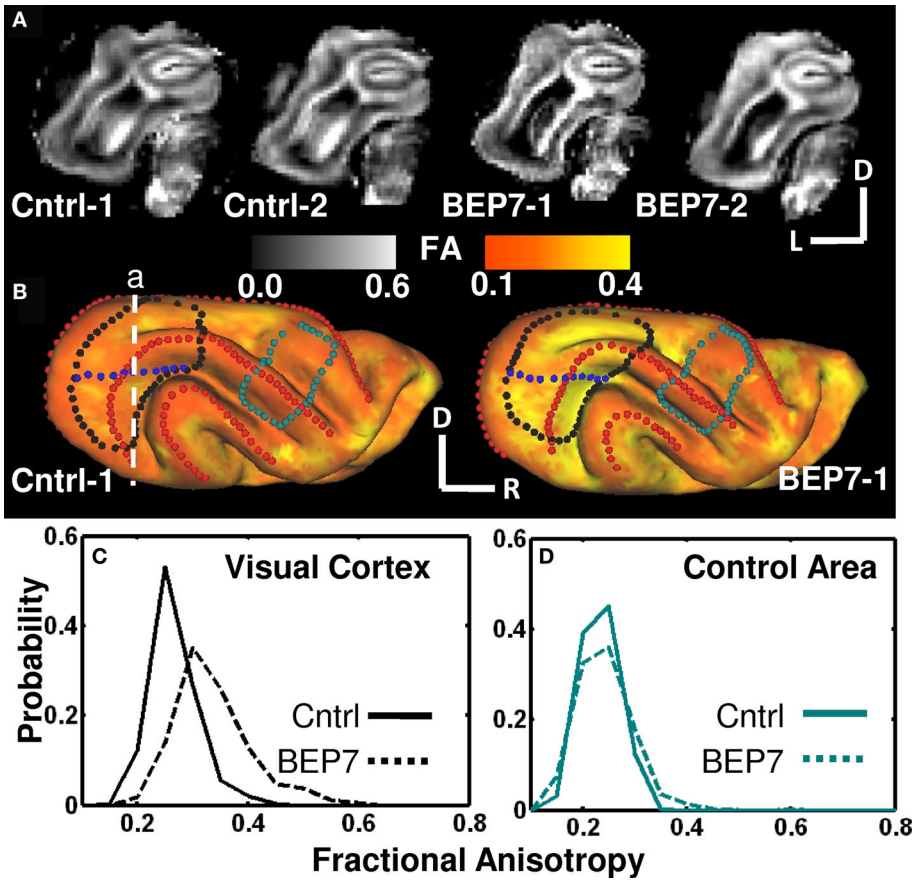


FIGURE 3 | Post mortem DTI measurements of two BEP7 hemispheres show increased visual cortical FA relative to two control hemispheres at P31. Coronal views of FA parameter maps are shown in **(A)** for two control animals (left) and two BEP7 animals (right) according to the gray color scale. In **(B)**, cortical FA is presented on cortical surface models for animals Cntrl-1 and BEP7-1, according to the red/yellow color scale. In **A** and **B**, increased FA is evident in visual areas of BEP7 animals compared to controls. Blue dots in **(B)** indicate the approximate location of the representation of the horizontal meridian (see **Figure 1** for comparison). Red dots indicate crown of gyri, as in **Figure 1**. Histograms reflecting data from all four animals are shown in **(C)** for visual cortex [encircled by black dots in **(B)**] and a rostrally located control area in **(D)** [encircled by blue-green dots in **(B)**].

The difference in mean values of cortical FA distributions between BEP7 and control animals was 0.07 in visual areas, but only 0.01 in the rostrally located non-visual area.

The cortical FA pattern evident in **Figure 3** suggests that the neuropil of BEP7 animals is less differentiated in the extrastriate visual cortex of P31 animals than in controls. This was further investigated by comparing Golgi-stained tissue from BEP7 animals to corresponding data from control animals. **Figure 4** illustrates the method used to quantify differentiation of the cerebral cortex, as reflected in the differential distribution of neuronal process orientations measured in Golgi-stained tissue. **Figure 4A** shows a region of the extrastriate visual cortex in Cntrl-1 visualized at 10× magnification (Region 3 in **Figure 5**, described below). The **Figure 4B** underlay is a skeleton image of neuronal processes, with skeleton elements of less than 10 image pixels in length removed. For a region of cerebral cortex within the **Figure 4B** field, the set of skeleton elements are approximated as lines, which are overlaid on the skeletonized image in **Figure 4B** and the original image in **Figure 4C** (red lines). **Figure 4D** shows an image/overlay obtained from a similar location within extrastriate visual cortex of BEP7-1. To characterize the orientation distribution of line segments within a region of cerebral cortex, the slope of each line segment is converted to an angle, θ, and the distribution in the set of angles is characterized by the von Mises mean α and concentration κ parameters. As shown in **Figure 4E**, the set of neuronal processes in the control animal (black) is distributed over a broader range than for the BEP7 animal (red), and hence the concentration parameter calculated from this data is smaller for the control ($\kappa = 1.41$) than for the BEP7 animal ($\kappa = 2.08$). To assess whether the difference in κ values achieved statistical significance, 95% confidence intervals in κ were determined using a bootstrap procedure. **Figure 4F** shows the distributions of κ values obtained from 1000 random samples from the Cntrl-1 (black) and BEP7-1 (red) polar angles. The means of the distributions are the values of κ used for the solid lines in **Figure 4E**, and as can be observed in the **Figure 4F** histograms, the 95% confidence ranges for the Cntrl-1 and BEP7-1 estimates of κ do not overlap, and therefore the BEP7-1 distribution is considered to be significantly more concentrated than Cntrl-1 for location 3 in **Figure 5** (see below).

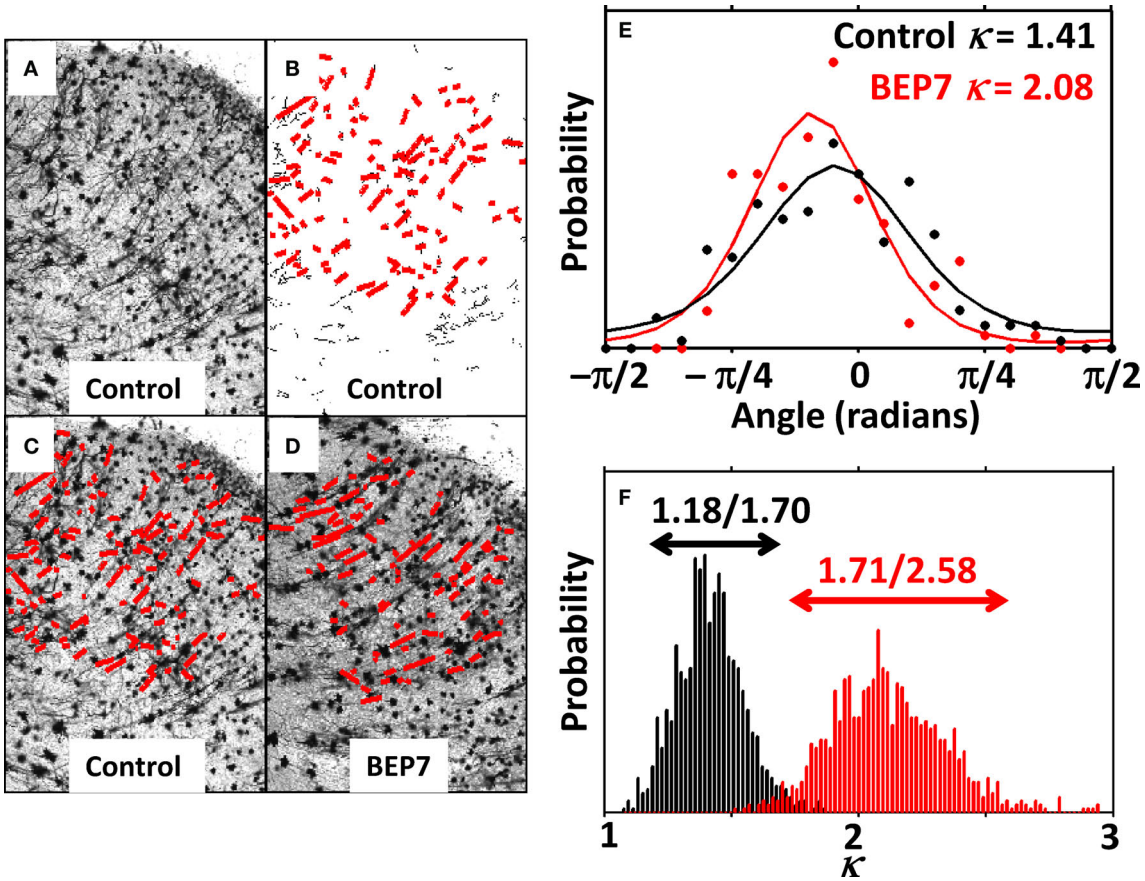


FIGURE 4 | Characterization of the distributions of neuronal process orientations. Golgi-stained tissue visualized at 10× magnification from the Cntrl-1 hemisphere is shown in **(A)**. Line segments (red) representing neuronal processes throughout a region of the cerebral cortex (corresponding to location 3 in **Figure 5**) are overlaid on the skeletonized image and original image in **(B)** and **(C)**, respectively. Line segments derived from the corresponding location in BEP7-1 are overlaid on the Golgi image in **(D)**. The polar angle for each line segment was determined as described in the text, and in **(E)**, histograms representing the distribution of polar angles are shown for the Cntrl-1 (black data points) and BEP7-1 (red data points) Golgi fields. Solid lines in **(E)** represent the results of approximating the data points as a von Mises distribution. To estimate 95% confidence intervals κ, a bootstrap procedure was used in which κ was determined 1000 times from randomly sampled subsets of the measured polar angles for each field. Histograms, with associated 95% confidence regions, of the resulting κ values are shown in **(F)** for the set of angles derived from Cntrl-1 (black) and BEP7-1 (red).

Figure 5 summarizes measurements of the orientation distribution widths (expressed as κ values) of neuronal processes obtained from five visual cortical locations and two non-visual locations. The position of each cortical location is indicated on the **Figure 5A** surface model. Five locations were analyzed within coronal slices obtained from corresponding positions in cases Cntrl-1 and BEP7-1 (filled bars in **Figure 5C**; black/gray indicates data from Cntrl-1 for visual/non-visual locations, respectively; red/orange indicates data from BEP7-1 for visual/non-visual locations, respectively). The five locations obtained from coronal sections are illustrated on the montage images in **Figure 5B**. In addition, two locations were analyzed within axial slices obtained from corresponding positions in cases Cntrl-2 and BEP7-2 (open bars in **Figure 5C**; black/gray indicates data from Cntrl-2 for visual/non-visual locations, respectively; red/orange indicates data from BEP7-2 for visual/non-visual locations, respectively). Concentration parameters reflecting the distribution of neuronal process orientations, with associated 95% confidence regions, are given for BEP7 brains (red/orange) and control animals (black/gray) in **Figure 5C**. For all visual regions analyzed, κ is larger in BEP7 subjects than in controls. In three of these, the difference is sufficient to separate 95% confidence intervals (asterisks, **Figure 5C**). In contrast, neuronal process orientation κ measured within one non-visual cortical region is slightly lower within BEP7-1 than for Cntrl-1, and the non-visual region characterized in BEP7-2 and Cntrl-2 exhibits nearly identical κ values. For both non-visual regions, there is a large amount of overlap in the 95% confidence intervals for κ. These findings indicate that in the visual cortex, neuronal process arborizations are less elaborate in the BEP7 brain than in the control.

DISCUSSION

We found that bilateral enucleation at P7 induces marked changes in the overall distribution of callosal connections in visual cortex. Cortical areas affected by these structural changes were associated with increases in cerebral cortical FA measured at P31. At the cellular level we observed that neuronal process arbors were less

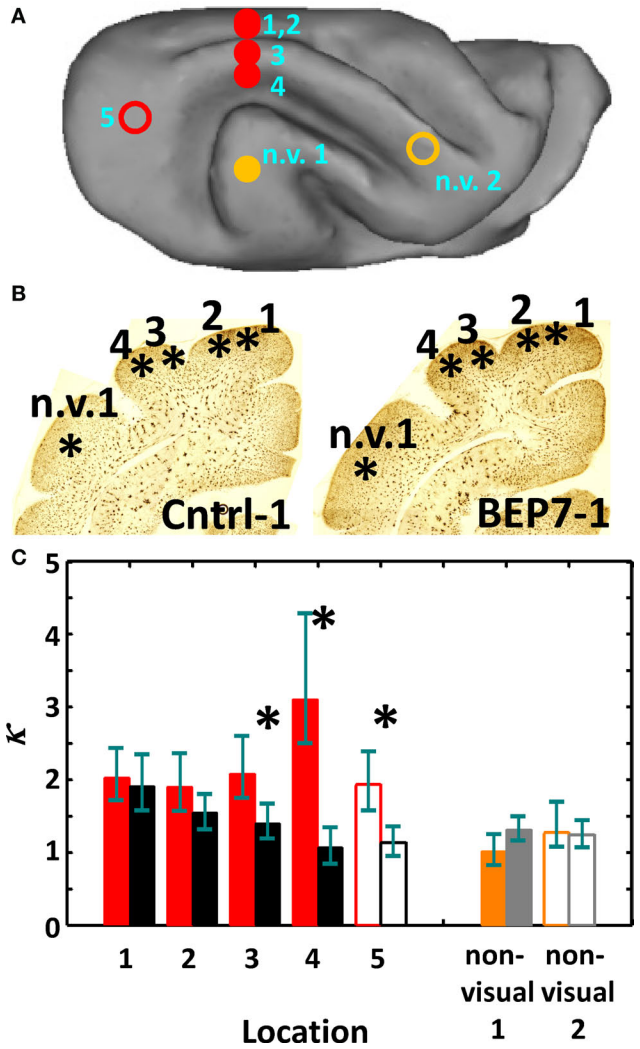


FIGURE 5 | Comparison of the distributions of orientations of neuronal processes in visual and non-visual areas of BEP7 and control ferrets at P31. The value of the parameter κ decreases as the distribution of orientations broadens (less concentrated). In **(A)**, filled circles represent locations of regions analyzed in coronal sections of Cntrl-1 and BEP7-1, with red indicating visual cortical areas, and orange a non-visual area. Open circles represent locations of regions analyzed in axial sections of Cntrl-2 and BEP7-2, with red and orange indicating visual and non-visual areas, respectively. **(B)** Cortical locations 1–4 and non-visual area 1 are shown in montages of Golgi sections **(C)** Concentration parameters, κ, of von Mises distributions associated with the sets of neuronal process orientations are shown for case BEP7-1 (visual locations, red filled bars; non-visual location, filled orange bar) and case Cntrl-1 (visual locations, black filled bars; non-visual location, filled gray bar), and case BEP7-2 (visual location, red open bar; non-visual location, open orange bar) and case Cntrl-2 (visual location, black open bar; non-visual location, open gray bar). Error bars represent 95% confidence intervals for κ. For visual locations indicated with asterisks, 95% confidence intervals for BEP7 and control regions do not overlap.

differentiated in Golgi-stained visual neurons from BEP7 animals on postnatal day 31 compared to age-matched controls. These results suggest that DTI measurements at early developmental stages are capable of detecting abnormalities in neuropil development induced by neonatal enucleation.

In agreement with previous studies in the rat (Cusick and Lund, 1982; Olavarria et al., 1987; Olavarria and Li, 1995; Olavarria and Hiroi, 2003; Olavarria and Safaeian, 2006), the cat (Innocenti and Frost, 1980; Berman, 1991; Olavarria, 1995; Olavarria and Van Sluyters, 1995), and the macaque (Dehay et al., 1989), neonatal enucleation in the ferret leads to abnormal development of callosal connections. Within visual cortex, we found that the area occupied by callosal connections in enucleated ferrets was significantly larger than in control ferrets. Based on previous physiological subdivisions of ferret visual cortex (Manger et al., 2002, 2004), our data indicate that regions showing abnormal patterns of callosal connectivity encompassed many visual areas, including areas 18, 19, and 21.

In BEP7 animals, cortical visual areas exhibiting differences in callosal connectivity at adulthood were spatially correlated with regions exhibiting altered cortical FA at P31. Water diffusion anisotropy in these visual areas was larger than controls in BEP7 animals at P31, while no differences in FA were found between BEP7 animals and controls in a more rostrally located non-visual area. This provides further evidence that binocular enucleation perturbs the normal development of visual cortex, and supports the notion that DTI is capable of detecting changes in connectivity associated with binocular enucleation at early stages of brain development. It is important to note that, in addition to the abnormalities induced on callosal connections, enucleation at P7 in the ferret likely affects several other visual connection systems, including thalamocortical and ipsilateral cortico–cortical projections (Berman, 1991; Ankaoua and Malach, 1993; Ruthazer and Stryker, 1996; Toldi et al., 1996; Karlen et al., 2006). It is therefore possible that the effect on FA within cerebral cortical gray matter we observed over much of visual cortex of BEP7 ferrets reflects the effect of enucleation in multiple pathways that either terminate or originate in visual cortex.

In order to directly examine the cellular-level determinants of the differences between control and BEP7 animals observed by DTI, a procedure was developed to quantitatively characterize orientation distributions of neuronal processes within Golgi-stained cerebral cortical tissue. For a subset of cortical locations, Golgi-stained neurons in visual cortex of BEP7 ferrets were found to possess less differentiated neuronal processes on postnatal day 31, and among these, radially oriented apical dendrites appear to be a dominant structure. Control animals were found to have more obliquely oriented collaterals of apical dendrites and basilar dendrites, contributing to a more complex and less organized neuropil than BEP7 animals. Although it is possible that the effect of binocular enucleation on cortical FA is mediated by cellular elements not detectable by Golgi staining, the findings reported here are consistent with a study in the rat (Olavarria et al., 2008), which showed that bilateral enucleation increased the length of axon branches and arbors without changing the number of branches, as well as a study in the mouse (Heumann and Rabinowicz, 1982) that showed a reduction in the number of spines on apical dendrites of pyramids in bilaterally enucleated animals. The possibility that enucleation delays the development of radial glial elements into astrocytes is unlikely because studies in other species have shown that enucleation does not affect the timing of other developmental milestones, such as the formation of topographically organized cortico–cortical

projections (Olavarria et al., 1987; Olavarria and Safaeian, 2006). Together, these results suggest that bilateral enucleation affects the differentiation of axonal and dendritic arbors in visual cortex.

Our approach builds upon previous comparisons between DTI and immunohistochemical studies related to cerebral cortical microarchitecture in the neonatal rat brain (Sizonenko et al., 2007), in which cortical FA was compared to indices reflecting the quantity of neuronal and glial fibers oriented approximately parallel to apical dendrites. Since radial glial cells have differentiated into astrocytes by P21 (Voigt, 1989), it is unlikely that they contribute significantly to cortical FA at the age we performed our analysis (P31). Therefore, Golgi-staining procedures were used here to estimate the orientation distribution of neuronal processes. Leergaard et al. (2010) have conducted an analysis similar to the approach presented here, in which diffusion MRI data were subsequently quantitatively validated with histological measurements. However, in the study by Leergaard and co-workers, white matter fibers in mature rat brain were compared to myelin-stained histological images. Though the purpose of the experiments presented herein differ from those of Leergaard et al., their study demonstrates the utility of performing morphological analysis of tissue to validate DTI measurements.

While our data provide evidence that neonatal bilateral enucleation induces alterations of neuronal processes that can be detected by DTI at early stages of development, a number of issues remain that must be addressed in future studies. First, the developmental trajectory of the difference between normal and bilaterally enucleated ferrets must be measured by examining brains at postnatal ages other than P31, and sample sizes for DTI and Golgi data must be increased. Such extensions of the approach described here will enable robust delineation of the cortical areas affected by enucleation, and identification of the developmental stage in which DTI is most sensitive for detecting abnormal morphological development of cerebral cortical neurons. Second, DTI methods characterize the three-dimensional properties of water diffusion, whereas the Golgi analysis employed herein was restricted to two dimensions. For the results presented here, care was taken to analyze sections at locations where gyri are approximately orthogonal to the section plane. However to address this issue more generally, work is currently underway in our laboratories to extend the analysis of Golgi data to a three-dimensional approach utilizing confocal microscopic data acquisition. Last, while DTI has sufficient sensitivity to detect changes in neuronal morphology using post-mortem tissue, it is possible that this sensitivity may be lost in an *in vivo* setting. Future studies involving DTI measurements of live ferrets and incorporating rapid image acquisition techniques such as echo-planar imaging will be needed to address this issue.

The data presented here indicate that the developmental trajectory produced by neonatal binocular enucleation in the ferret is an ideal experimental model for investigating the sensitivity of DTI for detecting abnormalities in neuronal architecture. Specifically, the system described here is amenable for systematically investigating water diffusion anisotropy patterns within the cerebral cortex associated with early stages of development. Such studies will be useful for understanding the morphological factors underlying the DTI findings in human studies of developmental disorders of the CNS. By avoiding potential confounds related to *in utero* manipulations or preterm birth, the use of newborn ferrets greatly facilitates DTI analysis of changes in diffusion anisotropy at stages of brain development that in primate species occur before birth. The strategy outlined here will thus potentially provide a means for using DTI to identify abnormalities early in brain development, thereby enabling therapeutic intervention before reduction of brain plasticity occurs.

ACKNOWLEDGMENTS

Financial support from National Institutes of Health grants R01NS070022 (Christopher D. Kroenke and Jaime F. Olavarria), P51RR000163 (Christopher D. Kroenke), and a grant from the Foundation for Alcohol Research (Christopher D. Kroenke). Sune N. Jespersen acknowledges financial support from The Danish National Research Foundation (CFIN), and Korning's fund. Lindsey A. Leigland was partially supported by T32AA007468. High-field MRI instrumentation used in this work was purchased with support from the W.M. Keck Foundation.

REFERENCES

Ankaoua, D., and Malach, R. (1993). Evidence for plasticity of intrinsic horizontal connections in area 17 of the rat. *Isr. J. Med. Sci.* 29, 555–569.

Armstrong, D., Dunn, J. K., Antalffy, B., and Trivedi, R. (1995). Selective dendritic alterations in the cortex of Rett syndrome. *J. Neuropathol. Exp. Neurol.* 54, 195–201.

Basser, P. J., and Pierpaoli, C. (1996). Microstructural and physiological features of tissues elucidated by quantitative-diffusion-tensor MRI. *J. Magn. Reson. B* 111, 209–219.

Batchelor, P. G., Atkinson, D., Hill, D. L., Calamante, F., and Connelly, A. (2003). Anisotropic noise propagation in diffusion tensor MRI sampling schemes. *Magn. Reson. Med.* 49, 1143–1151.

Berman, N. (1991). Alterations of visual cortical connections in cats following early removal of retinal input. *Brain Res. Dev. Brain Res.* 63, 163–180.

Borges, S., and Berry, M. (1978). The effects of dark rearing on the development of the visual cortex of the rat. *J. Comp. Neurol.* 180, 277–300.

Coleman, P. D., and Riesen, A. H. (1968). Evironmental effects on cortical dendritic fields. I. Rearing in the dark. *J. Anat.* 102(Pt 3), 363–374.

Conel, J. L. (1939). *The Postnatal Development of the Human Cerebral Cortex*. Cambridge, MA: Harvard University Press.

Cusick, C. G., and Lund, R. D. (1982). Modification of visual callosal projections in rats. *J. Comp. Neurol.* 212, 385–398.

Davies, D. L., and Smith, D. E. (1981). A Golgi study of mouse hippocampal CA1 pyramidal neurons following perinatal ethanol exposure. *Neurosci. Lett.* 26, 49–54.

Dehay, C., Horsburgh, G., Berland, M., Killackey, H., and Kennedy, H. (1989). Maturation and connectivity of the visual cortex in monkey is altered by prenatal removal of retinal input. *Nature* 337, 265–267.

Fields, R. D. (2008). White matter in learning, cognition and psychiatric disorders. *Trends Neurosci.* 31, 361–370.

Fisher, N. I. (1993). *Statistical Analysis of Circular Data*. Cambridge, UK: Cambridge University Press, 277 p.

Granger, B., Tekaia, F., Le Sourd, A. M., Rakic, P., and Bourgeois, J. P. (1995). Tempo of neurogenesis and synaptogenesis in the primate cingulate mesocortex: comparison with the neocortex. *J. Comp. Neurol.* 360, 363–376.

Heumann, D., and Rabinowicz, T. (1982). Postnatal development of the visual cortex of the mouse after enucleation at birth. *Exp. Brain Res.* 46, 99–106.

Innocenti, G. M., and Frost, D. O. (1980). The postnatal development of visual callosal connections in the absence of visual experience or of the eyes. *Exp. Brain Res.* 39, 365–375.

Innocenti, G. M., and Price, D. J. (2005). Exuberance in the development of cortical networks. *Nat. Rev. Neurosci.* 6, 955–965.

Jackson, C. A., and Hickey, T. L. (1985). Use of ferrets in studies of the visual system. *Lab. Anim. Sci.* 35, 211–215.

Karlen, S. J., Kahn, D. M., and Krubitzer, L. (2006). Early blindness results in

abnormal corticocortical and thalamocortical connections. *Neuroscience* 142, 843–858.

Katz, L. C., and Crowley, J. C. (2002). Development of cortical circuits: lessons from ocular dominance columns. *Nat. Rev. Neurosci.* 3, 34–42.

Klein, A., Andersson, J., Ardekani, B. A., Ashburner, J., Avants, B., Chiang, M. C., Christensen, G. E., Collins, D. L., Gee, J., Hellier, P., Song, J. H., Jenkinson, M., Lepage, C., Rueckert, D., Thompson, P., Vercauteren, T., Woods, R. P., Mann, J. J., and Parsey, R. V. (2009). Evaluation of 14 nonlinear deformation algorithms applied to human brain MRI registration. *NeuroImage* 46, 786–802.

Kroenke, C. D., Taber, E. N., Leigland, L. A., Knutsen, A. K., and Bayly, P. V. (2009). Regional patterns of cerebral cortical differentiation determined by diffusion tensor MRI. *Cereb Cortex* 19, 2916–2929.

Leergaard, T. B., White, N. S., de Crespigny, A., Bolstad, I., D'Arceuil, H., Bjaalie, J. G., and Dale, A. M. (2010). Quantitative histological validation of diffusion MRI fiber orientation distributions in the rat brain. *PloS One* 5(1), e8595. doi: 10.1371/journal.pone.0008595.

Leigland, L. A., and Kroenke, C. D. (2010). "A comparative analysis of cellular morphological differentiation within the cerebral cortex using diffusion tensor imaging (Chapter 13)," in *Neuromethods: Animal Models of Behavioral Analysis*, Vol. 50, ed J. Raber (Berlin: Springer).

Lim, K. O., and Helpern, J. A. (2002). Neuropsychiatric applications of DTI – a review. *NMR Biomed.* 15, 587–593.

Manger, P. R., Kiper, D., Masiello, I., Murillo, L., Tettoni, L., Hunyadi, Z., and Innocenti, G. M. (2002). The representation of the visual field in three extrastriate areas of the ferret (*Mustela putorius*) and the relationship of retinotopy and field boundaries to callosal connectivity. *Cereb Cortex* 12, 423–437.

Manger, P. R., Nakamura, H., Valentiniene, S., and Innocenti, G. M. (2004). Visual areas in the lateral temporal cortex of the ferret (*Mustela putorius*). *Cereb. Cortex* 14, 676–689.

Mardia, K. V., Kent, J. T., and Bibby, J. M. (1979). *Multivariate Analysis (Probability and Mathematical Statistics)*. London: Academic Press, 518 p.

McKinstry, R. C., Mathur, A., Miller, J. H., Ozcan, A., Snyder, A. Z., Schefft, G. L., Almli, C. R., Shiran, S. I., Conturo, T. E., and Neil, J. J. (2002). Radial organization of developing preterm human cerebral cortex revealed by non-invasive water diffusion anisotropy MRI. *Cereb Cortex* 12, 1237–1243.

McNab, J. A., Jbabdi, S., Deoni, S. C., Douaud, G., Behrens, T. E., and Miller, K. L. (2009). High resolution diffusion-weighted imaging in fixed human brain using diffusion-weighted steady state free precession. *NeuroImage* 46, 775–785.

Miller, M. W., and Potempa, G. (1990). Numbers of neurons and glia in mature rat somatosensory cortex: effects of prenatal exposure to ethanol. *J. Comp. Neurol.* 293, 92–102.

Neil, J. J., Shiran, S. I., McKinstry, R. C., Schefft, G. L., Snyder, A. Z., Almli, C. R., Akbudak, E., Aronovitz, J. A., Miller, J. P., Lee, B. C., and Conturo, T. E. (1998). Normal brain in human newborns: apparent diffusion coefficient and diffusion anisotropy measured by using diffusion tensor MR imaging. *Radiology* 209, 57–66.

Olavarria, J., Malach, R., and Van Sluyters, R. C. (1987). Development of visual callosal connections in neonatally enucleated rats. *J. Comp. Neurol.* 260, 321–348.

Olavarria, J., and Van Sluyters, R. C. (1985). Unfolding and flattening the cortex of gyrencephalic brains. *J. Neurosci. Methods* 15, 191–202.

Olavarria, J. F. (1995). The effect of visual deprivation on the number of callosal cells in the cat is less pronounced in extrastriate cortex than in the 17/18 border region. *Neurosci. Lett.* 195, 147–150.

Olavarria, J. F., and Hiroi, R. (2003). Retinal influences specify corticocortical maps by postnatal day six in rats and mice. *J. Comp. Neurol.* 459, 156–172.

Olavarria, J. F., Laing, R., Hiroi, R., and Lasiene, J. (2008). Topography and axon arbor architecture in the visual callosal pathway: effects of deafferentation and blockade of N-methyl-D-aspartate receptors. *Biol. Res.* 41, 413–424.

Olavarria, J. F., and Li, C. P. (1995). Effects of neonatal enucleation on the organization of callosal linkages in striate cortex of the rat. *J. Comp. Neurol.* 361, 138–151.

Olavarria, J. F., and Safaeian, P. (2006). Development of callosal topography in visual cortex of normal and enucleated rats. *J. Comp. Neurol.* 496, 495–512.

Olavarria, J. F., and Van Sluyters, R. C. (1995). Overall pattern of callosal connections in visual cortex of normal and enucleated cats. *J. Comp. Neurol.* 363, 161–176.

Rakic, P. (1995). A small step for the cell, a giant leap for mankind: a hypothesis of neocortical expansion during evolution. *Trends Neurosci.* 18, 383–388.

Ruthazer, E. S., and Stryker, M. P. (1996). The role of activity in the development of long-range horizontal connections in area 17 of the ferret. *J. Neurosci.* 16, 7253–7269.

Ryugo, R., Ryugo, D. K., and Killackey, H. P. (1975). Differential effect of enucleation on two populations of layer V pyramidal cells. *Brain Res.* 88, 554–559.

Shimony, J. S., Burton, H., Epstein, A. A., McLaren, D. G., Sun, S. W., and Snyder, A. Z. (2006). Diffusion tensor imaging reveals white matter reorganization in early blind humans. *Cereb Cortex* 16, 1653–1661.

Sizonenko, S. V., Camm, E. J., Garbow, J. R., Maier, S. E., Inder, T. E., Williams, C. E., Neil, J. J., and Huppi, P. S. (2007). Developmental changes and injury induced disruption of the radial organization of the cortex in the immature rat brain revealed by in vivo diffusion tensor MRI. *Cereb Cortex* 17, 2609–2617.

Smith, S. M., Jenkinson, M., Johansen-Berg, H., Rueckert, D., Nichols, T. E., Mackay, C. E., Watkins, K. E., Ciccarelli, O., Cader, M. Z., Matthews, P. M., and Behrens, T. E. (2006). Tract-based spatial statistics: voxelwise analysis of multi-subject diffusion data. *NeuroImage* 31, 1487–1505.

Sorensen, S. A., Jones, T. A., and Olavarria, J. F. (2003). Neonatal enucleation reduces the proportion of callosal boutons forming multiple synaptic contacts in rat striate cortex. *Neurosci. Lett.* 351, 17–20.

Tieman, S. B., and Hirsch, H. V. (1982). Exposure to lines of only one orientation modifies dendritic morphology of cells in the visual cortex of the cat. *J. Comp. Neurol.* 211, 353–362.

Toldi, J., Feher, O., and Wolff, J. R. (1996). Neuronal plasticity induced by neonatal monocular (and binocular) enucleation. *Prog. Neurobiol.* 48, 191–218.

Van Essen, D. C., Drury, H. A., Dickson, J., Harwell, J., Hanlon, D., and Anderson, C. H. (2001). An integrated software suite for surface-based analyses of cerebral cortex. *J. Am. Med. Inform. Assoc.* 8, 443–459.

Voigt, T. (1989). Development of glial cells in the cerebral wall of ferrets: direct tracing of their transformation from radial glia into astrocytes. *J. Comp. Neurol.* 289, 74–88.

White, T., Nelson, M., and Lim, K. O. (2008). Diffusion tensor imaging in psychiatric disorders. *Top. Magn. Reson. Imaging* 19, 97–109.

Zufferey, P. D., Jin, F., Nakamura, H., Tettoni, L., and Innocenti, G. M. (1999). The role of pattern vision in the development of cortico-cortical connections. *Eur. J. Neurosci.* 11, 2669–2688.

Conflict of Interest Statement: The authors declare that the research was conducted in the absence of any commercial or financial relationships that could be construed as a potential conflict of interest.

Received: 16 June 2010; accepted: 21 September 2010; published online: 15 October 2010.

Citation: Bock AS, Olavarria JF, Leigland LA, Taber EN, Jespersen SN and Kroenke CD (2010) Diffusion tensor imaging detects early cerebral cortex abnormalities in neuronal architecture induced by bilateral neonatal enucleation: an experimental model in the ferret. Front. Syst. Neurosci. 4:149. doi: 10.3389/fnsys.2010.00149

Copyright © 2010 Bock, Olavarria, Leigland, Taber, Jespersen and Kroenke. This is an open-access article subject to an exclusive license agreement between the authors and the Frontiers Research Foundation, which permits unrestricted use, distribution, and reproduction in any medium, provided the original authors and source are credited.

frontiers in
SYSTEMS NEUROSCIENCE

ORIGINAL RESEARCH ARTICLE
published: 31 December 2010
doi: 10.3389/fnsys.2010.00158

Reduced interhemispheric functional connectivity in the motor cortex during rest in limb-onset amyotrophic lateral sclerosis

Laura M. Jelsone-Swain[1], Brett W. Fling[2], Rachael D. Seidler[2,3], Rebecca Hovatter[1], Kirsten Gruis[4] and Robert C. Welsh[1,5]*

[1] *Department of Radiology, Basic Radiological Sciences, University of Michigan, Ann Arbor, MI, USA*
[2] *School of Kinesiology, University of Michigan, Ann Arbor, MI, USA*
[3] *Department of Psychology, University of Michigan, Ann Arbor, MI, USA*
[4] *Department of Neurology, University of Michigan, Ann Arbor, MI, USA*
[5] *Department of Psychiatry, University of Michigan, Ann Arbor, MI, USA*

Edited by:
Silvina G. Horovitz, National Institutes of Health, USA

Reviewed by:
Rasmus Birn, University of Wisconsin, USA
Brian D. Berman, University of Colorado at Denver Health Sciences Center, USA

****Correspondence:***
Robert C. Welsh,
Departments of Radiology and Psychiatry, 3208B Med Sci 1 5667, 1336 Catherine Street,
University of Michigan, Ann Arbor, MI 48109, USA.
e-mail: rcwelsh@med.umich.edu

Amyotrophic lateral sclerosis (ALS) is a progressive neurodegenerative disorder of motor neurons that leads to paralysis and eventually death. There is evidence that atrophy occurs in the primary motor cortex (M1), but it is unclear how the disease affects the intrinsic connectivity of this structure. Thus, the goal of this study was to examine interhemispheric coupling of low frequency blood-oxygen-level dependent (BOLD) signal fluctuations in M1 using functional connectivity magnetic resonance imaging during rest. Because disease progression is rapid, high-functioning patients were recruited to assess neural changes in the relatively early stages of ALS. Twenty patients with limb-onset ALS participated in this study. A parceling technique was employed to segment both precentral gyri into multiple regions of interest (ROI), thus increasing sensitivity to detect changes that exist along discretely localized regions of the motor cortex. We report an overall systemic decrease in functional connectivity between right and left motor cortices in patients with limb-onset ALS. Additionally, we observed a pronounced disconnection between dorsal ROI pairs in the ALS group compared to the healthy control group. Furthermore, measures of limb functioning correlated with the connectivity data from dorsal ROI pairs in the ALS group, suggesting a symptomatic relationship with interhemispheric M1 connectivity.

Keywords: ALS, fcMRI, resting-state, primary motor cortex

INTRODUCTION

Amyotrophic lateral sclerosis (ALS) is the most common adult motor neuron disease with a lifetime risk of approximately 1 in 2000 (Bruijn et al., 2004). Yet, the etiology of 90–95% of all ALS cases remains unknown. It is reported in the literature an 80% mortality rate within 5 years of symptom onset (del Aguila et al., 2003). One of the most notable features of ALS is its rapid development of motor impairments. ALS progresses from initial muscle weakness to complete loss of muscle function resulting in death from respiratory failure. Disease progression is associated with dysfunction of both upper and lower motor neurons; however, it is unclear as to which are more directly affected (van der Graaff et al., 2009). Seeley et al. (2009) have shown a direct and potentially unique correlation between disease and affected brain networks, and thus suggest that disease state can be characterized by quantitative descriptors of network metrics such as functional connectivity.

Resting-state functional connectivity magnetic resonance imaging (fcMRI) is a useful method for assessing neural-network connectivity (Biswal et al., 1995). It has been widely used to examine clinical populations, and is currently a method of interest in determining disease-specific neural biomarkers (Grady et al., 2001; Lowe et al., 2002; Koshino et al., 2005; Cao et al., 2006; Cherkassky et al., 2006; Tian et al., 2006; Waites et al., 2006; Wang et al., 2006a,b; Greicius et al., 2007; He et al., 2007; Welsh et al., 2008; Monk et al., 2009). Additionally, resting-state fcMRI eliminates the interpretation of task effort or demand, which can pose limitations on task-based fMRI studies. This is partly because resting-state fcMRI does not require patients to engage in any specific task (such as motor movements), which may confound BOLD signal interpretation as a result of task difficulty effects.

Ten prominent resting-state networks have been previously identified (Damoiseaux et al., 2006). Mohammadi et al. (2009) examined five of these, including the default mode, sensorimotor, parietal–temporo-frontal, posterior, and ventral networks, using independent component analysis (ICA) in patients with ALS. Of relevance to the present study, sensorimotor network differences were observed, showing decreased functional connectivity in the premotor cortex. These authors (Mohammadi et al., 2009) examined whole-brain voxel-wise effects. In the current study a seed-based analysis was used to examine more subtle and systemic changes that might occur in the network involving M1 connections.

The primary goal of the current study was to investigate coupling of interhemispheric low frequency BOLD signal fluctuations in the primary motor cortices (M1) using fcMRI during rest in patients with ALS. This structure within the sensorimotor network was of interest for several reasons. First, it is well established that interhemispheric connections between M1 exist. Even during rest it has been demonstrated that the left and right motor

cortices exhibit temporally correlated BOLD signal fluctuations (Biswal et al., 1997). Second, M1 is a large and somatotopically organized structure (Penfield and Boldrey, 1937). By examining the entire M1 we might be more sensitive to localize changes related to symptom presentation. Last, seminal work (Lawyer and Netsky, 1953; Smith, 1960; Brownell et al., 1970) described postmortem precentral gyrus nerve fiber degeneration in ALS, which suggests this deterioration occurs during the natural disease process. Therefore we hypothesized that a systemic decrease in functional connectivity across hemispheres would be observed. Specifically, we expected that the precentral gyri would show overall less correlated interhemispheric time-series fluctuations in the ALS group compared to controls.

In the present study, a parceling technique was employed that segmented the primary motor cortices into multiple regions of interest (ROIs). This was done to better delineate changes that might exist along the entire motor strip, thus increasing analysis sensitivity to discretely localized regions of this cortex. This investigation focused on the analysis of limb-only onset ALS patients to control for any potential differences in disease progression between limb and bulbar onset patients. Limb-onset ALS is most common, with the affected limb becoming progressively weaker as the disorder spreads to nearby myotomes. Finally, to identify whether systemic changes occur in M1 prior to moderate-severe symptom presentation, high-functioning and/or early disease stage patients were recruited.

MATERIALS AND METHODS

PARTICIPANTS AND BEHAVIORAL DATA

All ALS participants were recruited through the Department of Neurology, were diagnosed by a neuromuscular physician using the El Escorial criteria, and were followed in the Motor Neuron Disease Clinic at the University of Michigan. Healthy controls were recruited from the surrounding area through community advertisements (flyers and web-pages). All participants gave written consent to participate and the Institutional Review Board (IRB) at the University of Michigan approved this study. Twenty patients with limb-onset ALS (13 males, mean age 58.3 years) within 24 months of symptom onset, and 20 sex-matched healthy volunteers (13 males, mean age 57.5 years) were recruited to participate in this study. Participants between groups were matched as best as possible to age.

Several measurements of behavioral and cognitive functioning were taken prior to each participant's scanning session. Physical ability of ALS patients was assessed using the ALS functional rating scale, revised version (ALSFRS-r; Cedarbaum and Stambler, 1997). The ALSFRS-r is a validated rating instrument of ALS patients' functional abilities and has been demonstrated to correlate with physiological measures of the disease (Cedarbaum and Stambler, 1997). The ALSFRS-r instrument is comprised of 12 questions, each measuring the level of impairment for different behaviors, such as handwriting and walking. Each question is scored between four and zero points based on ability level, with a maximum total score of 48 points. The ALS cognitive behavioral screen (ALS-CBS; Woolley-Levine, 2006) was administered to assess general cognitive functioning. Because the CBS was not incorporated until after project initiation, 10 ALS patients and no healthy volunteers were tested. Hand dominance was determined by the Edinburgh Inventory (Oldfield, 1971), and hand strength was measured with a hand-grip dynamometer. The mean of three trials with the dynamometer per right and left hand were calculated to determine each participant's hand strength. These measures are presented in **Tables 1 and 2**.

A goal of our study was to examine neural changes in high-functioning patients that may take place in the early disease stage of ALS. Currently there are no standardized criteria to define disease stage. Therefore we defined our high-functioning ALS subjects as early in his or her disease course such that patients were within 24 months of symptom onset at the time of their scan. In addition, only patients who were ambulatory, without hemiplegia, were able to write, had a negative psychiatric evaluation, did not have dysphasia or breathing problems and were not on a ventilator, and were without other complicating mental disorders or disease were only included in the study.

IMAGE ACQUISITION

All scanning was performed at the University of Michigan's Functional MRI Laboratory on a GE 3T Excite 2 (General Electric, Milwaukee, WI, USA). During each participant's session, medium-resolution spin-echo, and high-resolution spoiled-gradient recall (SPGR) anatomic images (T_1-Overlay and T_1-SPGR respectively) were collected in the axial plane. T_2^* time-series data were acquired in the axial plane (aligned to the anterior–posterior commissure) using a reverse-spiral k-space readout. A total of 180 T_2^*-weighted volumes were collected for each participant during each scanning session (repetition time TR = 2 s, 40-slice volumes at 3 mm slice thickness and no skip, echo-time TE = 30 ms, 64 × 64 matrix, field-of-view, FOV = 220 mm). Four T_2^* volumes at the beginning of each time-series acquisition were excited but not

Table 1 | Group average (mean) demographic information for ALS patients and healthy participants. Range for age, hand strength, ALSFRS-r and CBS scores, and months since onset are also presented. Handedness is based on the Edinburgh Inventory (Oldfield, 1971).

Subject	Age (years)	Gender	Dominant hand	Dominant H.S.(kg)	Non-dominant H.S.(kg)	ALSFRS-r	CBS	M.S.O.
ALS (*n* = 20),	58.35 (46–67)	*n* = 13M, 7F	*n* = 15R, 5L	20.60 (0–50.75)	11.94 (0–42.42)	39.6 (29–46)	13.1 (7–19)	17.25 (8–24)
HC (*n* = 20),	57.51 (47–64)	*n* = 13M, 7F	*n* = 19R, 1L	32.99 (11.21–62.12)	30.62 (8.33–54.84)	NA	NA	NA

H.S., hand strength; CBS, cognitive behavioral screening test; ALSFRS-r, ALS functional rating scale, revised version; M.S.O., months between symptom onset and testing date.

Table 2 | Individual ALS patient demographic information.

ALS subject	Age (months)	Gender	Dominant hand	Onset location	H.S.D. (kg)	ALSFRS-r	CBS	M.S.O.	ALSFRS-r #4	ALSFRS-r #8
1	708	M	R	Hands	19.33	43	NA	08	3	3
2	576	F	L*	Right upper extremity	19.83	42	NA	23	1	4
3	709	F	R	Left upper extremity	25.16	39	NA	22	3	3
4	649	M	R	Hands	18.34	43	NA	18	3	4
5	721	F	L*	Right upper extremity	19.00	44	NA	24	3	4
6	553	M	R	Right leg	12.67	39	NA	21	3	2
7	780	F	R	Hands	0.06	29	NA	12	2	2
8	721	M	R	Left foot	14.39	46	NA	23	4	3
9	673	F	R	Left foot	2.27	33	NA	10	3	2
10	708	M	R	Hands	1.21	39	7	12	3	4
11	600	M	L	Left foot	3.04	43	17	21	3	3
12	757	M	L	Hands	1.82	38	NA	17	3	2
13	732	F	R	All four limbs	10.06	42	9	12	4	3
14	661	M	R	Right hand	9.09	43	19	14	3	4
15	780	F	R	Left leg	7.42	33	15	18	3	2
16	804	M	R	Legs	3.00	40	7	11	4	2
17	624	M	R	Left upper extremity	12.87	31	13	12	3	2
18	778	M	R	Right leg	0.00	45	15	23	4	2
19	699	M	R	Right Hand	10.06	46	17	23	4	4
20	765	M	L*	Upper extremities	0.00	33	12	21	3	4

*H.S.D., hand strength disparity; CBS, cognitive behavioral screening test; ALSFRS-r, ALS functional rating scale, revised version; M.S.O., months between symptom onset and testing date; ALSFRS-r #8, question number 8 on the questionnaire, which pertains to ambulation; ALSFRS-r #4, question number 4 on the questionnaire, which pertains to handwriting. Maximum score for these questions is 4 and minimum is 0. *Patients 2, 5, and 20 reported right hand dominance before symptom onset, however they were restricted to using the left hand due to weakness in their right hand at the time of their scan. These patients were considered as left handed based on results from the Edinburgh Inventory (Oldfield, 1971).*

recorded in order to achieve thermal equilibrium of magnetization. In addition, physiological recording took place during the scanning session (cardiac and respiratory cycles) using a MRI vendor supplied pulse oximeter and respiratory belt. These data were collected in order to correct for cardiac and respiratory influence on the resting-state signal. Medium-resolution anatomic images (T_1-Overlay) were acquired in the same-slice locations as the T_2^* volumes, however at a higher in-plane resolution (256×256 matrix, 220 mm FOV). The T_1-SPGR high-resolution images were collected with a 256×256 matrix, 220 mm FOV, and with 1.2 mm slice thickness.

RESTING-STATE TASK

Resting-state activity was collected over a period of 8 min for each scanning session. During this time, participants were instructed to view a white crosshair fixed on a black background. This image was projected onto a screen at the head of the scanner bore and viewed with a back-projected mirror, placed on the head coil. Participants were asked to keep their eyes open and to not think about anything in particular to elicit resting-state metabolism (Fox et al., 2005).

fcMRI PREPROCESSING

In order to reduce noise and artifact, several preprocessing steps were conducted. Using a custom code written in MATAB (Mathworks, Natick, MA, USA; Noll et al., 1991), raw fMRI data were reconstructed offline. Physiological correction of time-series data was implemented in the image domain (Hu et al., 1995; Pfeuffer et al., 2002). This was done because cardiac cycle and respiration give rise to correlated spatial and temporal variance during task execution in fMRI experiments, hence contributing to residual noise and overall decreased statistical power. Removal of physiological confounds is especially important during resting-state acquisition since no overt task is being executed, otherwise presenting the complication of masking true functional connectivity signals or falsely giving rise to functional networks (Lund, 2001; Peltier et al., 2003).

Using FSL's MCFLIRT and SLICETIMER within the fMRI analysis package[1], motion and slice timing were corrected for, respectively. Realigned images were used for the connectivity analysis, and movement was checked to assure that no more than 0.4 mm

[1]http://www.fmrib.ox.ac.uk/fsl/slicetier/index.html

translational and 0.1° rotational movement occurred, thereby minimizing motion-induced spatial–temporal correlations. Using Statistical Parametric Mapping, version 2 (SPM2; Wellcome Trust Center for Neuroimaging[2]), each participant's T_1-Overlay volume was co-registered to the time-series data; the T_1-SPGR was then co-registered to the co-registered T_1-overlay image. Spatial normalization to the Montreal Neurological Institute (MNI 152) template of the resulting co-registered T_1-SPGR image was then performed using SPM2. The resulting normalization matrix was applied to the slice-time-corrected, physiologically corrected time-series data. These normalized T_2^* time-series data were subsequently spatially smoothed with a 5-mm Gaussian kernel. The resulting T_2^* images had 3 mm isotropic voxels.

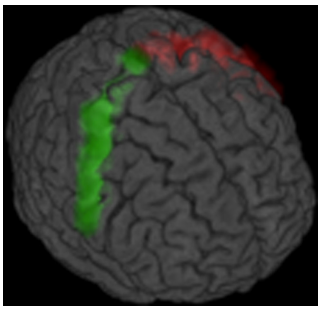


FIGURE 1 | Group average precentral gyrus masks in left and right hemispheres.

REGIONS OF INTEREST

The primary goal of this study was to examine relationships between the primary motor cortices in ALS and to identify the spectrum of changes that may be taking place. Normalized T_1 high-resolution images were used to manually create precentral gyrus gray matter masks in both hemispheres for each participant (using the mean location of the hand knob area as an anatomical anchor). A group anatomical ROI mask was constructed for each hemisphere from voxels shared by ≥10 participants. The ROI group masks were parceled along both motor cortices into 41 and 40 individual 6 mm ROI cubes in the left and right hemisphere, thus allowing for connectivity analyses between localized anatomical regions. The motor cortex is a large structure that is somatotopically organized (Penfield and Boldrey, 1937). Therefore by segmenting this strip into small ROIs we have increased our sensitivity to delineating functional connectivity changes along this cortex, rather than obscuring what is known about the detailed somatotopic organization of M1 (by using large ROIs, for example; Craddock et al., 2010).

The ventral and dorsal-most ROI cube locations correspond to MNI coordinates (x, y, z in mm) −60.8, −5.7, 26.0: −13.6, −29.3, 74.1 and 65.3, 0.6, 19.7: 5.4, −29.3, 78.6 in the left and right hemispheres, respectively. Because precentral gyrus masks were created from shared voxels in the participant group, coordinate locations of left and right ventral/dorsal-most ROI cubes are not perfectly symmetrical. The average precentral gyri masks are shown in **Figure 1**.

M1 ROI COUPLING CORRELATION ANALYSIS

The T_2^* time-series were detrended to remove slow drift. Additionally, the global volume intensity was regressed from the time-series. To remove any residual physiological nuisance, the global white matter and cerebral spinal fluid (CSF) temporal signals were sequentially regressed from the T_2^* time-series. (Fox et al., 2009). Additionally, motion parameters were treated as nuisance and removed via regression. Mean time-series data were extracted from these ROIs and correlated with each cube in the opposite hemisphere, resulting in an *r*-coefficient correlation-gram for each individual. In order to examine global group differences, the *r*-coefficient correlation-grams by group were then compared using the two sample non-parametric Kolmogorov–Smirnov (K–S) goodness-of-fit test (Chakravarti et al., 1967). Because we expected a systemic change in the distribution of connectivity between the ALS and healthy control groups, the K–S test was well suited to evaluate our hypothesis. Correlation-grams were further evaluated by comparing only near-homologous and homologous-interhemispheric ROIs to assure that differences observed between groups were not due to off-diagonal correlations. In other words, ROI pair correlations that may correspond to non-homologous body regions, such as the foot and face, were removed from this second analysis. A mask was created to only include these homologous- and near-homologous ROIs, which is represented in **Figure 2A**. Two additional correlation-gram masks were created, which divided the homologous/near-homologous ROIs into ventral (**Figure 2B**) and dorsal regions (**Figure 2C**), in order to systemically examine somatotopic subdivisions. Specifically, the dorsal motor cortex is functionally localized to control limb and trunk regions, whereas the ventral cortex corresponds to face regions (Penfield and Boldrey, 1937). Correlation-grams per group were averaged and are presented in **Figures 3 and 4**. Coordinates along the axes of this map represent ROIs in left and right hemispheres, moving from ventral to dorsal locations.

BEHAVIORAL ANALYSIS

To examine the possible brain–behavior relationship with limb functioning in the ALS group, behavioral test data were compared with resting-state functional connectivity. Linear regression tests between imaging and limb functioning data were separated into three different analyses based on the average functional connectivity correlation coefficients from (A) diagonal-only; (B) ventral–ventral; (C) and dorsal–dorsal ROI pairs (refer to **Figure 2**). Functional connectivity measures from these pairs were entered into each regression analysis as the dependent variable. In the ALSFRS-r, questions 4 and 8 pertain to upper and lower limb functioning. These questions assess the ability to write and walk, respectively. Therefore participant scores for these questions were entered into the regression analysis as independent variables. Total scores from the ALSFRS-r were not used because abilities other than limb functioning are measured in this questionnaire, such as breathing. Additionally, hand strength disparity was considered a factor of limb functioning and was entered as a third independent variable into the analysis. Hand strength disparity was calculated as the absolute value of strength difference between the right and left hands.

[2]http://www.fil.ion.ucl.ac.uk/spm

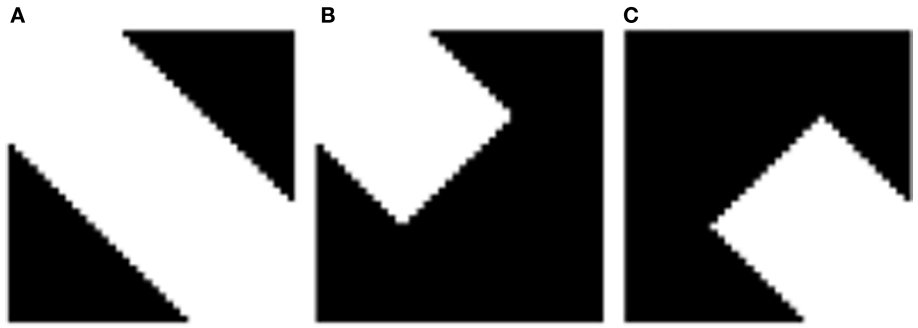


FIGURE 2 | Masks applied to correlation-grams after initial analysis of all ROI pairs. (A) diagonal-only mask; **(B)** ventral mask; **(C)** dorsal mask.

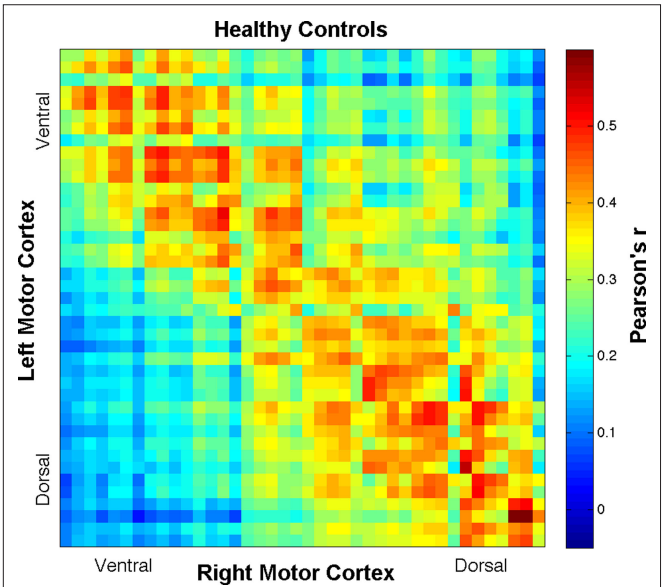


FIGURE 3 | Correlation-gram displaying all ROI Pearson's *r*-correlation coefficient means for the healthy control group. Coordinates along the axes of this map represent ROIs in left and right hemispheres, moving from ventral to dorsal locations.

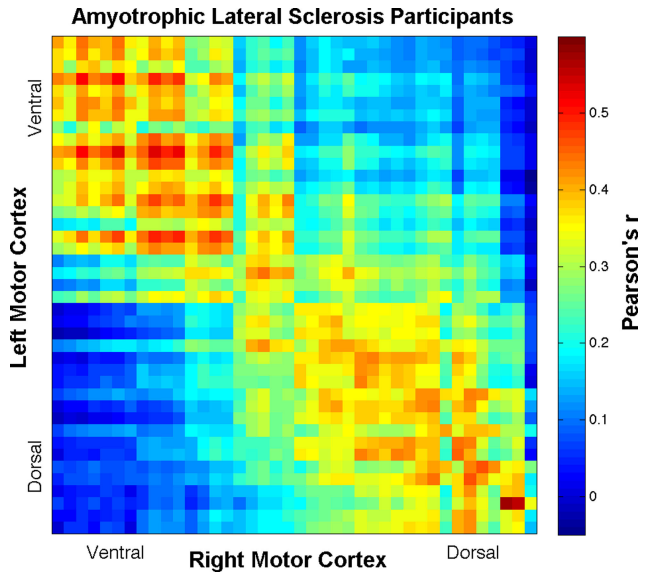


FIGURE 4 | Correlation-gram displaying all ROI Pearson's *r*-correlation coefficient means for the ALS patient group. Coordinates along the axes of this map represent ROIs in left and right hemispheres, moving from ventral to dorsal locations.

Bivariate correlation analyses were also conducted, using Pearson's correlation coefficient (two-tailed). In the healthy control group, hand strength disparity was correlated with (A) diagonal-only; (B) ventral–ventral; (C) and dorsal–dorsal ROI pairs. Hand strength disparity, months since onset, ALSFRS-r and CBS scores from the ALS group were entered into a separate correlation analysis. All behavioral analyses were conducted in SPSS, v.17.

RESULTS

GROUP PHYSICAL AND COGNITIVE BEHAVIORAL DATA

Group averages for demographic data and behavioral measures are shown in **Table 1**, and individual patient data are shown in **Table 2**. According to the ALSFRS-r, the ALS participants as a group were relatively high functioning (mean = 39.23, SD = 5.06). All patients were ambulatory, as shown by ALSFRS-r question #8 (mean = 2.95, SD = 0.88). In addition, ALSFRS-r question #4 showed that all but one of the patients could use their hand to write (mean = 3.1, SD = 0.72). Only one patient reported that they were unable to write, which was due to weakness in their dominant right hand and the resulting ineffective adaptation of writing with the left hand.

RESTING-STATE FUNCTIONAL CONNECTIVITY

Group comparisons of interhemispheric motor cortex BOLD signal *r*-coefficients, including all ROI pairs, resulted in highly significant K–S differences (D) between ALS and healthy participants ($D = 0.19$, $p < 7 \times 10^{-26}$) with ALS being less connected overall than healthy controls (see **Figures 3 and 4**). To control for more homologous correspondence, the K–S test was performed along the diagonal of the correlation-grams such that mainly homologous regions were included while those regions between which no functional connectivity was expected were excluded. That is, by only including the homologous- and near-homologous regions, we removed any potential for observed statistical difference being driven by negative correlations (Fox et al., 2009). The K–S difference was still found

to be statistically significant ($D = 0.14$, $p < 9 \times 10^{-9}$) and not driven solely by the off-diagonal components of the correlation-grams. Further, separating the gyri into ventral (first 20 ROI cubes) and dorsal (remaining ROI cubes) regions, a large effect was observed in the dorsal half ($D = 0.23$, $p < 3 \times 10^{-12}$), corresponding to limb and trunk locations of the motor homunculus. The ventral half still showed a significant decrease in connectivity, but not to the same extent ($D = 0.11$, $p < 0.005$).

Participant movement while scanning could potentially present confounded functional connectivity results, especially if one group moved more than the other. We tested this possible confound by running independent *post hoc t*-tests between groups on the standard deviations of the motion parameters. These results were null, $p > 0.05$, indicating no differences in movement between the ALS and healthy control group.

BEHAVIORAL CORRELATION RESULTS

The relationship between limb functioning and dorsal motor cortex connectivity in the ALS group was further examined in a regression analysis, with ALSFRS-r questions 4 and 8 and hand strength disparity as predictors of dorsal–dorsal M1 connectivity. This regression analysis was significant, $F(3, 19) = 3.35$, $p = 0.045$ ($R = 0.62$). In this model, hand strength disparity significantly predicted dorsal ROI connectivity, $t(19) = -2.22$, $p = 0.04$, and question 4 reached near significance, $t(19) = 1.81$, $p = 0.08$. Hand strength disparity and question 4 also significantly correlated with dorsal–dorsal M1 connectivity, $r = -0.51$, $p = 0.01$ and $r = 0.44$, $p = 0.03$, respectively. Question 8 was insignificant in this model, $t(19) = 0.44$, $p = 0.67$; $r = -0.13$, $p = 0.29$. Both remaining regression analyses conducted examining diagonal-diagonal and ventral–ventral M1 connectivity in the ALS patients yielded null results. The healthy control group did not show a significant correlation with hand strength disparity and functional connectivity for any of the three analyses: (A) diagonal–diagonal; (B) ventral–ventral; and (C) dorsal–dorsal pairs. **Figure 5** depicts the relationship between dorsal ROI connectivity and hand strength disparity for both ALS and healthy control groups.

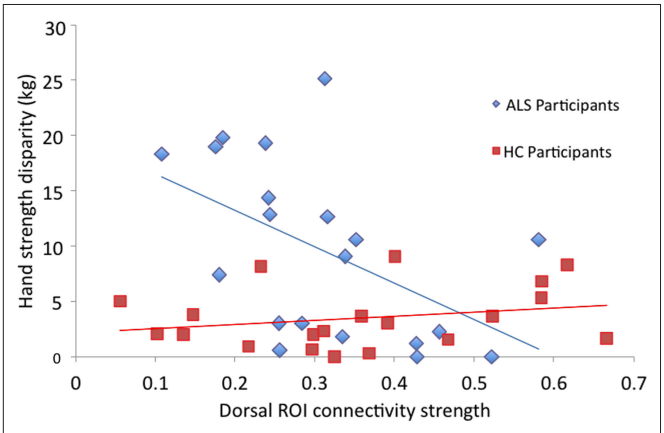


FIGURE 5 | Scatter-plot showing the correlation between average dorsal ROI interhemispheric connectivity per individual and hand strength disparity, across groups. Only results from the ALS group are significantly (inversely) correlated.

Hand strength disparity did not significantly correlate with months since onset, ALSFRS-r or CBS scores in the ALS group. Additionally, ALSFRS-r and CBS scores did not correlate. There was a trend toward significance between months since onset and ALSFRS-r scores ($r = 0.41$, $p = 0.07$) and an even stronger trend between months since onset and CBS scores ($r = 0.62$, $p = 0.058$).

DISCUSSION

GENERAL DISCUSSION

The current study provides new evidence for M1 network impairment in ALS, importantly showing for the first time an interhemispheric disconnect. We observed a decrease in overall functional connectivity between parceled motor cortices in the ALS group, as shown by less correlated resting-state low frequency BOLD signal fluctuations across hemispheres. Importantly, this decrease was seen within the first 24 months of ALS symptoms while patients were still in the early disease stage. Additionally, a pronounced difference was observed between groups in the dorsal half of the motor cortex – the half that corresponds to limb and trunk body regions of the homunculus. Dorsal M1 connectivity in the ALS group correlated with limb functioning, suggesting a brain–behavior relationship between these measures. It was found that the greater the disparity between right and left hand strength, the less functionally connected ROIs were in the dorsal motor cortex. This effect was not found in the healthy control group. Also, increased connectivity in the dorsal motor cortex was associated with better handwriting ability in those with ALS.

Results from the current study corroborate converging lines of evidence that intrinsic M1 functioning is altered in ALS. In a PET study, regional cerebral blood flow (rCBF) in M1 was reduced at rest in ALS patients compared to healthy participants. However, this reduction was not observed in lower motor neuron disease patients, implying upper motor neuron dysfunction in M1 (Kew et al., 1994). In an fMRI study, decreased blood oxygenated level dependent (BOLD) signal activity was found in contralateral M1 of ALS patients while performing a continuous unimanual button-pressing task (Schoenfeld et al., 2005). In this particular study task difficulty effects were observed, and the authors suggested that decreased motor neurons in M1 contribute to sequential movement impairments. The present study provides new evidence for primary motor cortex changes between right and left cortices, importantly showing for the first time an interhemispheric disconnect (as shown by seed-based fcMRI) that is present even when participants were not performing a motor task.

Decreased interhemispheric connectivity in the primary motor cortex is consistent with recent findings from diffusion tensor imaging (DTI) work as well. For example, several studies have examined microstructural integrity within the corpus callosum, which include interhemispheric M1 projections. Reduced fractional anisotropy (FA), a measure of white matter microstructure, was found within the corpus callosum in ALS patients (Senda et al., 2009; Metwalli et al., 2010). These studies suggest that interhemispheric structural connectivity is compromised in those with ALS. In addition, Bartels et al. (2008) found that FA values in the corpus callosum correlated with behavioral measurements, specifically with the Contralateral Co-Movement Test, in patients with ALS.

The only ALS resting-state fcMRI study to date demonstrated reduced functional connections between the premotor cortex and other sensorimotor regions during rest (Mohammadi et al., 2009). This may indicate that the sensorimotor network is becoming disconnected in ALS. Additionally, reduced functional connectivity was found in the prefrontal cortex, posterior/ventral-anterior areas of the cingulate cortex, and bilateral inferior parietal cortices, hence demonstrating decreased functional connectivity between core regions of the default mode network. Therefore, it is possible that regional increases in BOLD activity are related to neural-network breakdown in ALS.

There is a clinical need to establish biomarkers for those who will become diagnosed with ALS, and neuroimaging methodology may be well suited to identify these biomarkers (Agosta et al., 2010). This is important given the pronounced duration that occurs between symptom onset and diagnosis; for some people diagnosis is not established until years after symptoms present (Kraemer et al., 2010). This is especially true for those with limb onset, as symptoms often mimic other diseases (Leigh et al., 2003). Currently, the only reliable measurement used to diagnosis ALS is when a patient demonstrates progressive upper and lower motor neuron involvement (Turner et al., 2009). Results from the current study indicate that cortical neural changes are taking place in the early stages of ALS while patients are still highly functioning. Also, these changes are primarily occurring in the cortical regions that correspond to limb movement. Results from this study may be clinically relevant as a biomarker for limb-onset patients who have "suspected" or "probable" ALS. Identifying biomarkers specific to ALS will help increase the accuracy of diagnosis, decrease the duration between symptoms and diagnosis, and most importantly allow for initiation of early treatment (Turner et al., 2009; Ganesalingam and Bowser, 2010).

LIMITATIONS AND FUTURE DIRECTIONS

An important limitation in the current study is the lack of causal interpretation from our results. For example, this study emphasizes that interhemispheric M1 connectivity breakdown is more pronounced in the dorsal than ventral half between groups. Although the dorsal half corresponds to limb and trunk motor functioning, we cannot directly explain this relationship with the present findings. This is partially because it cannot be discerned whether our results reflect upper or lower motor neuron atrophy. Specifically, atrophy in lower motor neurons could give rise to M1 neural changes due to the decrease in afferent signals being received by M1. It could also be speculated that this area is more susceptible to the ALS disease process, or that it is an initial target of neurodegeneration. Another interpretation limitation is that we cannot differentiate whether these results are ALS-specific, or reflective of motor neuron disease processes in general. For example, neural atrophy has been identified in the primary motor cortex of patients with primary lateral sclerosis (Tartaglia et al., 2009), which may also give rise to functional connectivity changes. However, this hypothesis has yet to be tested and was beyond the scope of this current investigation. The specificity between motor neuron diseases will need to be further tested.

Context of using resting-state fcMRI must also be considered. It is assumed that temporally correlated signal fluctuations in brain regions imply functional connectivity. Therefore the interpretation that connections between right and left M1 are decreasing in ALS is based on this assumption. Furthermore, it is not known if this decrease in connectivity implies an axonal pathway impairment or gray matter loss within M1. Integrating other methods, such as DTI, would increase the effectiveness of addressing how the ALS disease process affects cortical networks.

Longitudinal methods are needed in order to clarify functional connectivity alterations in ALS. Results from the current study were from a single time point in the early stage of disease, yet it is suggested that these changes are progressive. Therefore we anticipate comparing results with data collected at subsequent sessions within the same participant group.

A fourth limitation is that the present results are only representative of ALS patients with limb-onset. There are both advantages and disadvantages to assessing neural changes in a homogenous patient group. This is advantageous in that disease processes specific to limb-onset ALS may be better described due to reduced variance by exclusion of a heterogeneous population. Also, a homogenous group increases our ability to control for any potential differences in disease progression between limb and bulbar onset patients. Through redefinition of inclusion criteria however, such as disease subtypes or individual behavioral symptoms, results may become more generalized to all disease processes. It could be potentially helpful for future studies to compare subtypes to disentangle pathological differences.

CONCLUSIONS

Results from the current study indicate that functional connections between the two primary motor cortices are decreased in ALS, and that this disconnect between hemispheres may be more specific to dorsal versus ventral M1. Dorsal M1 interhemispheric connectivity was related to metrics of upper limb functioning, specifically handwriting, and hand strength disparity. These brain–behavior correlations may have important clinical applications. Furthermore, neuroimaging methodology may be utilized for those with "possible" or "suspected" ALS by identifying reliable neural biomarkers.

ACKNOWLEDGMENTS

We greatly appreciate all participants who volunteered and gave their time for this study. We also thank Tom Nichols and Tim Johnson for statistical consultation, Scott Peltier for discussions and advice on functional connectivity methodology, and Pooja Modi for organizing the graph and tables. This work is supported by NIH/NINDS R01- NS052514 and Department of Radiology/ University of Michigan BRS Award.

REFERENCES

Agosta, F., Chio, A., Cosottini, M., De Stefano, N., Falini, A., Mascalchi, M., Rocca, M. A., Silani, V., Tedeschi, G., and Filippi, M. (2010). The present and future of neuroimaging in amyotrophic lateral sclerosis. *Am. J. Radiol.* 31, 1769–1777.

Bartels, C., Mertens, N., Hofer, S., Merboldt, K. D., Dietrich, J., Frahm, J., and Ehrenreich, H. (2008). Callosal dysfunction in amytrophic lateral sclerosis correlates with diffusion tensor imaging of the central motor system. *Neuromuscul. Disord.* 18, 398–407.

Biswal, B. B., Van Kylen, J., and Hyde, J. S. (1997). Simultaneous assessment of flow and BOLD signals in resting-state functional connectivity maps. *NMR Biomed.* 10, 165–170.

Biswal, B. B., Yetkin, F. Z., Haughton, V. M., and Hyde, J. S. (1995). Functional connectivity in the motor cortex of resting human brain using echo-planar MRI. *Magn. Reson. Med.* 34, 537–541.

Brownell, B., Oppenheimer, D. R., and Hughes, J. T. (1970). The central nervous system in motor neurone disease.

J. Neurol. Neurosurg. Psychiatr. 33, 338–357.

Bruijn, L. I., Miller, T. M., and Cleveland, D. W. (2004). Unraveling the mechanisms involved in motor neuron degeneration in ALS. *Annu. Rev. Neurosci.* 27, 723–749.

Cao, Q., Zang, Y., Sun, L., Sui, M., Long, X., Zou, Q., and Wang, Y. (2006). Abnormal neural activity in children with attention deficit hyperactivity disorder: a resting-state functional magnetic resonance imaging study. *Neuroreport* 17, 1033–1036.

Cedarbaum, J. M., and Stambler, N. (1997). Performance of the amyotrophic lateral sclerosis functional rating scale (ALSFRS) in multicenter clinical trials. *J. Neurol. Sci.* 152(Suppl. 1), s1–s9.

Chakravarti, I. M., Laha, R. G., and Roy, J. (1967). *Handbook of Methods of Applied Statistics (I)*. New York: John Wiley and Sons.

Cherkassky, V. L., Kana, R. K., Keller, T. A., and Just, M. A. (2006). Functional connectivity in a baseline resting-state network in autism. *Neuroreport* 17, 1687–1690.

Craddock, R. C., James, G. A., Holtzheimer, P. E., Hu, X. P., and Mayberg, H. S. (2010). "A whole brain fMRI atlas generated via spatially constrained spectral clustering: Part I, Method," in *Proceedings of the 16th Annual Meeting of the Organization for Human Brain Mapping,* Barcelona, Spain, 89.

Damoiseaux, J. S., Rombouts, S. A. R. B., Barkhof, F., Scheltens, P., Stam, C. J., Smith, S. M., and Beckmann, C. F. (2006). Consistent resting-state networks across healthy subjects. *Proc. Natl. Acad. Sci. U.S.A.* 103, 13848–13853.

del Aguila, M. A., Longstreth, W. T. J., McGuire, V., Koepsell, T. D., and van Belle, G. (2003). Prognosis in amyotrophic lateral sclerosis: a population-based study. *Neurology* 60, 813–819.

Fox, M. D., Snyder, A. Z., Vincent, J. L., Corbetta, M., Van Essen, D. C., and Raichle, M. E. (2005). The human brain is intrinsically organized into dynamic, anticorrelated functional networks. *Proc. Natl. Acad. Sci. U.S.A.* 102, 9673–9678.

Fox, M. D., Zhang, D., Snyder, A. Z., and Raichle, M. E. (2009). The global signal and observed anticorrelated resting state brain networks. *J. Neurophysiol.* 101, 3270–3283.

Ganesalingam, J., and Bowser, R. (2010). The application of biomarkers in clinical trials for motor neuron disease. *Biomark. Med.* 4, 281–297.

Grady, C. L., Furey, M. L., Pietrini, P., Horwitz, B., and Rapoport, S. I. (2001). Altered brain functional connectivity and impaired short-term memory in Alzheimer's disease. *Brain* 124, 739–756.

Greicius, M. D., Flores, B. H., Menon, V., Glover, G. H., Solvason, H. B., Kenna, H., Reiss, A. L., and Schatzberg, A. F. (2007). Resting-state functional connectivity in major depression: abnormally increased contributions from subgenual cingulate cortex and thalamus. *Biol. Psychiatry* 62, 429–437.

He, B. J., Snyder, A. Z., Vincent, J. L., Epstein, A., Shulman, G. L., and Corbetta, M. (2007). Breakdown of functional connectivity in frontoparietal networks underlies behavioral deficits in spatial neglect. *Neuron* 53, 905–918.

Hu, X., Le, T. H., Parrish, T., and Erhard, P. (1995). Retrospective estimation and correction of physiological fluctuations in functional MRI. *Magn. Reson. Med.* 34, 201–212.

Kew, J. J. M., Brooks, D. J., Passingham, R. E., Rothwell, J. C., Frackowiak, R. S. J., and Leigh, P. N. (1994). Cortical function in progressive lower motor neuron disorders and amyotrophic lateral sclerosis: a comparative PET study. *Neurology* 44, 1101–1110.

Koshino, H., Carpenter, P. A., Minshew, N. J., Cherkassky, V. L., Keller, T. A., and Just, M. A. (2005). Functional connectivity in an fMRI working memory task in high-functioning autism. *Neuroimage* 24, 810–821.

Kraemer, M., Buerger, M., and Berlit, P. (2010). Diagnostic problems and delay of diagnosis in amyotrophic lateral sclerosis. *Clin. Neurol. Neurosurg.* 112, 103–105.

Lawyer, T., and Netsky, M. G. (1953). Amyotrophic lateral sclerosis: a clinicoanatomic study of fifty-three cases. *AMA Arch. Neurol. Psychiatry* 69, 171–192.

Leigh, P. N., Abrahams, S., Al-Chalabi, A., Ampong, M. A., Goldstein, L. H., Johnson, J., Lyall, R., Moxham, J., Mustfa, N., Rio, A., Shaw, C., and Willey, E. (2003). The management of motor neurone disease. *J. Neurol. Neurosurg. Psychiatr.* 74(Suppl. 4), iv32–iv47.

Lowe, M. J., Phillips, M. D., Lurito, J. T., Mattson, D., Dzemidzic, M., and Mathews, V. P. (2002). Multiple sclerosis: low-frequency temporal blood oxygen level-dependent fluctuations indicate reduced functional connectivity – initial results. *Radiology* 224, 184–192.

Lund, T. E. (2001). fcMRI--mapping functional connectivity or correlating cardiac-induced noise? *Magn. Reson. Med.* 46, 628–629.

Metwalli, N. S., Benatar, M., Nair, G., Usher, S., Hu, X., and Carew, J. D. (2010). Utility of axial and radial diffusivity from diffusion tensor MRI as markers of neurodegeneration in amyotrophic lateral sclerosis. *Brain Res.* 1348, 156–164.

Mohammadi, B., Kollewe, K., Samii, A., Krampfl, K., Dengler, R., and Munte, T. F. (2009). Changes of resting state brain networks in amyotrophic lateral sclerosis. *Exp. Neurol.* 217, 147–153.

Monk, C. S., Peltier, S. J., Wiggins, J. L., Weng, S. J., Carrasco, M., Risi, S., and Lord, C. (2009). Abnormalities of intrinsic functional connectivity in autism spectrum disorders. *Neuroimage* 47, 764–772.

Noll, D. C., Meyer, C. H., Pauly, J. M., Nishimura, D. G., and Macovski, A. (1991). A homogeneity correction method for magnetic resonance imaging with time-varying gradients. *IEEE Trans. Med. Imaging* 10, 629–637.

Oldfield, R. C. (1971). The assessment and analysis of handedness; the Edinburgh inventory. *Neuropsychology* 9, 97–113.

Peltier, S. J., Polk, T. A., and Noll, D. C. (2003). Detecting low-frequency functional connectivity in fMRI using a self-organizing map (SOM) algorithm. *Hum. Brain Mapp.* 20, 220–226.

Penfield, W., and Boldrey, E. (1937). Somatic motor and sensory representation in the cerebral cortex of man as studied by electrical stimulation. *Brain* 60, 389–443.

Pfeuffer, J., Van De Moortele, P. F., Ugurbil, K., Hu, X., and Glover, G. H. (2002). Correction of physiologically induced global off-resonance effects in dynamic echo-planar and spiral functional imaging. *Magn. Reson. Med.* 47, 344–353.

Schoenfeld, M. A., Tempelmann, C., Gaul, C., Kühnel, G. R., Düzel, E., Hopf, J.-M., Feistner, H., Zierz, S., Heinze, H. J., and Vielhaber, S. (2005). Functional motor compensation in amyotrophic lateral sclerosis. *J. Neurol.* 252, 944–952.

Seeley, W. W., Crawford, R. K., Zhou, J., Miller, B. L., and Greicius, M. D. (2009). Neurodegenerative diseases target large-scale human brain networks. *Neuron* 62, 42–52.

Senda, J., Ito, M., Watanabe, H., Atsuta, N., Kawai, Y., Katsuno, M., Tanaka, F., Naganawa, S., Fukatsu, H., and Sobue, G. (2009). Correlation between pyramidal tract degeneration and widespread white matter involvement in amyotrophic lateral sclerosis: a study with tractography and diffusion-tensor imaging. *Amyotroph. Lateral Scler.* 10, 288–294.

Smith, M. C. (1960). Nerve fiber degeneration in the brain in amyotrophic lateral sclerosis. *J. Neurol. Neurosurg. Psychiatr.* 23, 269–282.

Tartaglia, M. C., Laluze, V., Rowe, A., Findlater, K., Lee, D. H., Kennedy., K., Kramer, J. H., and Strong, M. J. (2009). Brain atrophy in primary lateral sclerosis. *Neurology* 72, 1236–1241.

Tian, L., Jiang, T., Wang, Y., Zang, Y., He, Y., Liang, M., Sui, M., Cao, Q., Hu, S., Peng, M., and Zhuo, Y. (2006). Altered resting-state functional connectivity patterns of anterior cingulate cortex in adolescents with attention deficit hyperactivity disorder. *Neurosci. Lett.* 400, 39–43.

Turner, M. R., Kiernan, M. C., Leigh, P. N., and Talbot, K. (2009). Biomarkers in amyotrophic lateral sclerosis. *Lancet Neurol.* 8, 94–109.

van der Graaff, M. M., de Jong, J. M. B. V., Baas, F., and de Visser, M. (2009). Upper motor neuron and extra-motor neuron involvement in amyotrophic lateral sclerosis: a clinical and brain imaging review. *Neuromuscul. Disord.* 19, 53–58.

Waites, A. B., Briellmann, R. S., Saling, M. M., Abbott, D. F., and Jackson, G. D. (2006). Functional connectivity networks are disrupted in left temporal lobe epilepsy. *Ann. Neurol.* 59, 335–343.

Wang, K., Jiang, T., Liang, M., Wang, L., Tian, L., Zhang, X., Li, K., and Liu, Z. (2006a). Discriminative analysis of early Alzheimer's disease based on two intrinsically anti-correlated networks with resting-state fMRI. *Med. Image Comput. Comput. Assist. Interv.* 9, 340–347.

Wang, L., Zang, Y., He, Y., Liang, M., Zhang, X., Tian, L., Wu, T., Jiang, T., and Li, K. (2006b). Changes in hippocampal connectivity in the early stages of Alzheimer's disease: evidence from resting state fMRI. *Neuroimage* 31, 496–504.

Welsh, R. C., Chen, A. C., and Taylor, S. F. (2008). Low-frequency BOLD fluctuations demonstrate altered thalamocortical connectivity in schizophrenia. *Schizophr. Bull.* 36, 713–722.

Woolley-Levine, S. (2006). *ALS Cognitive Behavioral Screen*. San Francisco: California Pacific Medical Center.

Conflict of Interest Statement: The authors declare that the research was conducted in the absence of any commercial or financial relationships that could be construed as a potential conflict of interest.

Received: 01 July 2010; accepted: 06 December 2010; published online: 31 December 2010.

Citation: Jelsone-Swain LM, Fling BW, Seidler RD, Hovatter R, Gruis K and Welsh RC (2010) Reduced interhemispheric functional connectivity in the motor cortex during rest in limb-onset amyotrophic lateral sclerosis. Front. Syst. Neurosci. ***4****:158. doi: 10.3389/fnsys.2010.00158*

Copyright © 2010 Jelsone-Swain, Fling, Seidler, Hovatter, Gruis and Welsh. This is an open-access article subject to an exclusive license agreement between the authors and the Frontiers Research Foundation, which permits unrestricted use, distribution, and reproduction in any medium, provided the original authors and source are credited.

frontiers in
SYSTEMS NEUROSCIENCE

ORIGINAL RESEARCH ARTICLE
published: 15 September 2010
doi: 10.3389/fnsys.2010.00143

Altered resting state cortico-striatal connectivity in mild to moderate stage Parkinson's disease

Youngbin Kwak[1], Scott Peltier[2], Nicolaas I. Bohnen[3,4], Martijn L. T. M. Müller[3], Praveen Dayalu[4] and Rachael D. Seidler[1,5,6,7]*

[1] *Neuroscience Program, University of Michigan, Ann Arbor, MI, USA*
[2] *Department of Biomedical Engineering, University of Michigan, Ann Arbor, MI, USA*
[3] *Department of Radiology, University of Michigan, Ann Arbor, MI, USA*
[4] *Department of Neurology, University of Michigan, Ann Arbor, MI, USA*
[5] *School of Kinesiology, University of Michigan, Ann Arbor, MI, USA*
[6] *Department of Psychology, University of Michigan, Ann Arbor, MI, USA*
[7] *Institute of Gerontology, University of Michigan, Ann Arbor, MI, USA*

Edited by:
Barry Horwitz, National Institutes of Health, USA

Reviewed by:
Bruno B. Averbeck, National Institute of Mental Health, USA
Michelle Hampson, Yale University, USA

****Correspondence:***
Rachael D. Seidler, 401 Washtenaw Ave., Ann Arbor, MI 48109-2214, USA.
e-mail: rseidler@umich.edu

Parkinson's disease (PD) is a progressive neurodegenerative disorder that is characterized by dopamine depletion in the striatum. One consistent pathophysiological hallmark of PD is an increase in spontaneous oscillatory activity in the basal ganglia thalamocortical networks. We evaluated these effects using resting state functional connectivity MRI in mild to moderate stage Parkinson's patients on and off L-DOPA and age-matched controls using six different striatal seed regions. We observed an overall increase in the strength of cortico-striatal functional connectivity in PD patients off L-DOPA compared to controls. This enhanced connectivity was down-regulated by L-DOPA as shown by an overall decrease in connectivity strength, particularly within motor cortical regions. We also performed a frequency content analysis of the BOLD signal time course extracted from the six striatal seed regions. PD off L-DOPA exhibited increased power in the frequency band 0.02–0.05 Hz compared to controls and to PD on L-DOPA. The L-DOPA associated decrease in the power of this frequency range modulated the L-DOPA associated decrease in connectivity strength between striatal seeds and the thalamus. In addition, the L-DOPA associated decrease in power in this frequency band correlated with the L-DOPA associated improvement in cognitive performance. Our results demonstrate that PD and L-DOPA modulate striatal resting state BOLD signal oscillations and cortico-striatal network coherence.

Keywords: dopamine, Parkinson's disease, fMRI, functional connectivity, striatum, neural oscillation

INTRODUCTION

Parkinson's disease (PD) is a progressive neurodegenerative disorder associated with predominantly motor symptoms such as tremor, slowness of movement, rigidity, and difficulties with gait and balance, although cognitive and affective symptoms also occur (Shohamy et al., 2006; Caballol et al., 2007). The Braak staging system describes PD as a schema of ascending pathology, beginning in the lower brain stem and anterior olfactory structures, progressing to the basal mid- and forebrain nuclei, and then to the cortex (Braak et al., 2003, 2006). In stage 3 of the Braak system, when motor symptoms first begin to appear, the neuropathology of PD is characterized by a loss of dopaminergic neurons in the substantia nigra pars compacta and the ventral tegmental area with degeneration of the striatal nerve terminals (Braak et al., 2006).

One consistent pathophysiological hallmark of PD is an increase in spontaneous oscillatory activity in the basal ganglia thalamocortical networks (Gatev et al., 2006; Hammond et al., 2007). This increase in neural oscillatory activity is most prominent in the 10–35 Hz range (beta frequency band) and is often observed in local field potential recordings from the subthalamic nucleus (STN) (Kuhn et al., 2004, 2006; Foffani et al., 2005). Dopaminergic treatment suppresses this abnormally heightened oscillatory neural activity (Brown et al., 2001; Levy et al., 2002). Recently, EEG and MEG studies have shown that the increase in subcortical oscillatory activity is associated with increased intracortical coupling of neural activity, which is correlated with disease severity (Williams et al., 2002; Silberstein et al., 2005; Stoffers et al., 2008; Stam, 2010). For example, Stoffers et al. (2008) used MEG to explore how resting state cortical functional connectivity evolves over the course of PD. They found that even in recently diagnosed drug-naïve patients, there was an increase in correlations between time series in the alpha 1 frequency band measured by synchronization likelihood. Moreover, disease severity was correlated with theta and beta band synchronization (Stoffers et al., 2008). Silberstein et al. (2005) also found that EEG coherence in the 10–35 Hz range correlated with PD symptom severity (as measured via UPDRS). Treatments such as L-DOPA or DBS reduce this coherence, and the degree of reduction is correlated with clinical improvement (Silberstein et al., 2005).

Resting state functional connectivity MRI (fcMRI) is a non-invasive imaging technique with good spatial resolution. It identifies brain regions exhibiting correlated patterns of spontaneously occurring, slow changes in brain activity. Brain regions with similar functions and known anatomical connections have shown strong correlations in the low frequency blood oxygen level dependent

(BOLD) signal when participants are at rest (Fox and Raichle, 2007; Rogers et al., 2007; Vincent et al., 2007). Given its non-invasive nature, it can be used to study network functional connectivity in mild to moderate stage PD patients, as opposed to the intra-operative recordings that are restricted to more advanced stage PD patients. Examples of functional networks that have been identified with fcMRI in healthy individuals include motor cortical networks (Biswal et al., 1995; Peltier et al., 2005), cortico-striatal networks (Di Martino et al., 2008; Kelly et al., 2009), and the default mode network (Greicius et al., 2008, 2009). Resting state connectivity networks exhibit stability across data sets collected from different participants using differing acquisition parameters, locations, and scanners (Biswal et al., 2010) making the approach well-suited for future large scale clinical studies.

A recent fcMRI study identified distinctive cognitive, motor, and reward cortico-striatal circuitries (based on connectivity between individual striatal seed regions and their cortical projection targets) in healthy young adults (Di Martino et al., 2008). A follow-up study by the same group documented that these connectivity patterns are modulated by L-DOPA administration in healthy young adults (Kelly et al., 2009). In their study, functional connectivity between the putamen and cerebellum and between the inferior ventral striatum and the ventrolateral prefrontal cortex increased with L-DOPA administration, whereas ventral striatum and dorsal caudate connectivity with the default mode network decreased. This group interpreted that L-DOPA significantly changes the motor and cognitive networks of the cortico-striatal pathways.

Cortico-striatal networks have also been examined in PD using fcMRI (Wu et al., 2009; Helmich et al., 2010). Both studies found that compared to controls, PD patients showed increased functional connectivity in some cortico-striatal networks, and decreased connectivity in others. However, these studies only compared PD patients in the OFF medication state to controls and did not examine changes in connectivity patterns with dopaminergic medication.

In the current study, we investigated differences in cortico-striatal functional connectivity networks between PD patients and age matched controls, using the seed regions employed by Di Martino et al. (2008) and Kelly et al. (2009). Considering the abnormal coherence of cortico-striatal oscillatory activity reported in studies that used EEG and/or local field potential recordings (Williams et al., 2002; Kuhn et al., 2004, 2006; Foffani et al., 2005; Silberstein et al., 2005; Stoffers et al., 2008; Stam, 2010), we hypothesized that PD patients would exhibit hyperconnectivity of cortico-striatal networks in comparison to controls, and that a clinically relevant dose of L-DOPA would alleviate this hyperconnectivity. Given that PD patients exhibit increased oscillatory neural activity primarily in the alpha and beta frequency bands when off medication (Priori et al., 2004), we analyzed the frequency content of the resting state BOLD signal in the striatal seed regions. Recent work using simultaneous EEG-fMRI demonstrates that changes in the alpha and beta frequency content of neuronal activity are reflected in the BOLD signal (Goldman et al., 2002; Laufs et al., 2003; Moosmann et al., 2003; Laufs, 2008; Rosa et al., 2010). We hypothesized that frequency content of the resting state BOLD signal extracted from the seed regions would be different in PD off L-DOPA compared to controls and to PD on L-DOPA. Furthermore, we predicted that the L-DOPA associated change in the frequency content would modulate the L-DOPA associated change in cortico-striatal functional connectivity.

MATERIALS AND METHODS

PARTICIPANTS

Twenty-five mild to moderate stage (Hoehn and Yahr stages 1–2.5) (Hoehn and Yahr, 1967) PD patients (64 ± 8 years, 3 females) and 24 age- and gender-matched healthy controls (63 ± 7 years, 5 females) participated in the study. Patients were evaluated using the motor section of the Unified Parkinson's Disease Rating Scale (UPDRS) (Fahn et al., 1987) by a neurologist. The more affected body side was determined by asking each PD patient and was confirmed by the neurologist's rating. All study participants underwent the Mini-Mental State Exam (MMSE) (Folstein et al., 1975), the Montreal Cognitive Assessment (MOCA) (Nasreddine et al., 2005) and the grooved pegboard test (Lafayette Instruments, Lafayette, IN) to measure general cognitive and motor abilities. Performance on the grooved pegboard test has been shown to be associated with individual PD patients' dopaminergic denervation levels, as indicated by [^{11}C]beta-CFT PET scans (Bohnen et al., 2007). These clinical assessments were acquired for patients in both the ON and OFF medication states on separate days in a counterbalanced order. The demographic and clinical characteristics of the patients are listed in **Table S1** in Supplementary Material. All of our participants were diagnosed within 15 years and were in the mild to moderate stage of the disease as shown by the Hoehn and Yahr scale (Hoehn and Yahr, 1967). Participants signed a consent form approved by the Institutional Review Board of the University of Michigan prior to participation, and were compensated for their participation. All experimental procedures were conducted in accordance with the Institutional Review Board of the University of Michigan.

PROCEDURE

Parkinson's disease patients completed two testing days corresponding to the ON and OFF medication states. Thirteen patients were tested ON first and 12 OFF first. We used a single-blind placebo controlled design using a single dose of L-DOPA. PD patients attended both testing days in the OFF state achieved by withdrawal from medication 12–18 h prior to testing. For the ON testing day, patients received a 50 mg dose of carbidopa followed by a single dose of L-DOPA in combination with carbidopa (200 mg of L-DOPA and an additional 50 mg of carbidopa). For the OFF testing day, they received placebo medications following the same time schedule in combination with the 50 mg of carbidopa. All study procedures began 1 h after the patient had taken either L-DOPA or the placebo, by which time L-DOPA reaches its peak plasma dose. Control participants underwent a single testing session without any medication procedure.

fMRI DATA ACQUISITION

fMRI data were collected from a 3 T GE Signa MRI scanner at the University of Michigan. A single-shot gradient-echo (GRE) reverse spiral pulse sequence (Glover and Law, 2001) was used to collect 240 T2* – weighted BOLD images (TR = 2 s, TE = 30 ms, flip angle = 90°, FOV = 220 mm × 220 mm, voxel size = 3.4 mm × 3.4 mm × 3.2 mm, 40 axial slices). For the structural images, a

3D T1 axial overlay (TR = 8.9 ms, TE = 1.8 ms, flip angle = 15°, FOV = 260 mm × 260 mm, slice thickness = 1.4 mm, 124 slices; matrix = 256 × 160) was acquired for anatomical localization. To facilitate normalization, a 110 sliced (sagittal) inversion-prepped T1-weighted anatomical image using spoiled gradient-recalled acquisition in steady state (SPGR) imaging (flip angle = 15°, FOV = FOV = 260 mm × 260 mm, 1.4 mm slice thickness) was acquired. A visual fixation cross was presented to the subject using a rear projection visual display. Participants were instructed to keep their eyes centered on the cross and to not think about anything in particular. The duration of data collection was 8 min. A pressure belt was placed around the abdomen of each subject to monitor the respiratory signal. A pulse oximeter was placed on the subject's finger to monitor the cardiac signal. The respiratory, cardiac, and fMRI data collection were synchronized.

fMRI DATA ANALYSIS

The acquired functional MRI data were preprocessed as part of the standard processing stream at the University of Michigan. First, k-space outliers in the raw data time course greater than two standard deviations from the mean were replaced with the average of their temporal neighbors. Second, images were reconstructed using field map correction to remove distortions from magnetic field inhomogeneity. Third, physiological variations in the data from the cardiac and respiratory rhythms were removed using a regression analysis (Glover et al., 2000). This approach removed the effects of the first and second order harmonics of the externally collected physiological waveforms. Fourth, slice timing differences were then corrected using local sinc interpolation (Oppenheim et al., 1999). Finally, we used MCFLIRT in the fMRIB Software Library (Jenkinson et al., 2002) to perform motion correction (using the 10th image volume as the reference). For all participants, head motion was less than 3 mm in the *x*, *y*, or *z* direction.

The preprocessed data were then normalized to MNI space using SPM5 (Wellcome Department of Cognitive Neurology, London, UK; http://www.fil.ion.ucl.ac.uk). We first registered the 3D T1 axial overlay to the functional images and then registered the high-resolution SPGR image to T1 overlay. The transformation to align the SPGR image to the MNI template was finally applied to the functional data. In order to have all of the PD patients' predominantly disease affected hemisphere aligned, we flipped the *x* direction (i.e., left–right direction) of both the 240 functional images and the anatomical images for the 7 left-side more affected patients before spatial normalization. The results are presented with the left side of the images reflecting patients' more affected brain hemisphere. The same proportion of control subject images was also flipped in the *x* direction.

The following procedures were used to generate functional connectivity images (low frequency time course correlation maps). First, the data were low-pass filtered by convolving the time courses with a rectangular filter with a cutoff frequency of 0.08 Hz, in order to examine the frequency band of interest and to exclude higher frequency sources of noise such as heart rate and respiration (Biswal et al., 1995; Peltier et al., 2003). Second, the time course of activity was extracted from the six striatal seed regions, selected from Di Martino et al. (2008, MNI *x y z* coordinates presented and depicted in **Figure S1** in Supplementary Material: inferior ventral striatum (VSi (±) 9 9 −8), superior ventral striatum (VSs (±) 10 15 0), dorsal caudate (DC (±) 13 15 9), dorsal caudal putamen (DCP (±) 28 1 3), dorsal rostral putamen (DRP (±) 25 8 6), and ventral rostral putamen (VRP (±) 20 12 −3). A four voxel square on the axial plane was placed around these coordinates for the seed. Third, the time course of the seed was unit normalized to remove differences in variance between subjects. Fourth, the seed region time course from the filtered data (averaged across the four voxels) was used in a correlation analysis with all other low-pass filtered voxels in the brain to form functional connectivity maps for each striatal seed region in each participant. *Z* scores from each participant were entered into the group-level random effects analyses, which were carried out using SPM5. We first evaluated the functional connectivity maps associated with each seed region in PD OFF, PD ON, and controls separately, using a threshold of $p < 0.05$ family-wise error (FWE) correction and an extent voxel threshold of 100 (Nichols and Hayasaka, 2003). At FWE <0.05, control group results showed significant clusters across the whole brain for all seed regions; thus, connectivity maps generated from the different seed regions were indistinguishable. Thus we report the control group results with a more stringent threshold of FWE <0.001. An uncorrected threshold of $p < 0.001$ and extent voxel threshold of 10 was used for between group comparisons of connectivity maps. Comparisons of either PD OFF or PD ON to the control group were performed with between subjects *t*-tests, whereas comparison of PD OFF and PD ON was done using a within subjects *t*-test. We also performed an regions of interest (ROI) analysis comparing the connectivity strengths between PD OFF versus PD ON in the brain regions identified from the PD OFF versus control group comparison in order to determine whether L-DOPA corrects for the elevated connectivity in these regions. ROIs were defined as the voxel clusters identified from the PD OFF versus control group comparison of connectivity maps. For example, for the inferior ventral striatum network, the whole cluster in the dorsomedial thalamus (see **Figure 3** and **Table S5** in Supplementary Material.) was used as an ROI and the mean connectivity strength across all voxels within this region was compared between PD OFF and PD ON using a paired *t*-test. In cases in which there were multiple ROIs associated with one seed region (i.e., dorsal caudal putamen and dorsal rostral putamen), repeated measures ANOVA using ROI and medication status as within subject factors was performed.

We also combined the connectivity maps associated with the three caudate seed regions (inferior ventral striatum, superior ventral striatum, and dorsal caudate) and the three putamen seed regions (dorsal caudal putamen, dorsal rostral putamen, and ventral rostral putamen) using the ImCalc applet in SPM5 to perform numerical addition of the three connectivity maps (Di Martino et al. 2008). Direct comparison of the caudate and putamen connectivity maps were performed in controls, PD OFF and PD ON separately using an uncorrected threshold of $p < 0.001$ and extent voxel threshold of 10.

FREQUENCY CONTENT ANALYSIS OF THE fMRI BOLD SIGNAL

The extracted fMRI BOLD timecourses from the six striatal seeds were transformed into the frequency domain using Fast Fourier Transformation in Matlab. We low pass filtered our data

at 0.08 Hz, and thus we were only able to look at the power spectrum between 0.0 and 0.08 Hz. For the normalization of the frequency data we took the following steps. We first divided the 0.08 Hz spectrum into eight frequency bands of approximately 0.01 Hz bandwidth each. We then computed the percentage of the total power contained within each frequency band. Repeated measures ANOVA was used to compare the normalized power content across the eight frequency bands for PD ON and OFF medication, and a mixed model ANOVA was used for the comparison of the PD patients to the controls using frequency bands as a within subject factor and group (PD OFF versus controls) as a between subject factor. The Huynh–Feldt epsilon (Huynh and Feldt, 1970) was used to determine whether the repeated measures data met the assumption of sphericity ($\Sigma > 0.75$). In cases where the sphericity assumption was not met, the *F* statistic was evaluated for significance using the Huynh–Feldt adjusted degrees of freedom.

RESULTS

BEHAVIORAL DATA

We evaluated patients' performance on the UPDRS, MMSE, MOCA, and grooved pegboard tests between the ON and OFF L-DOPA states using paired *t*-tests. Pegboard performance was analyzed separately for the more and less affected sides. Motor symptoms measured by UPDRS were significantly worse in PD OFF than PD ON ($t_{24} = -2.33$, $p < 0.05$), and pegboard performance for the more affected side was significantly worse for PD OFF than PD ON ($t_{24} = -2.88$, $p < 0.01$). These results indicate that L-DOPA significantly improved motor functioning of the patients, and the improvement was most apparent in the more affected side.

STRIATAL FUNCTIONAL CONNECTIVITY IN CONTROLS, PD OFF, AND PD ON

We present our connectivity analyses using the seeds placed in the more affected hemisphere; results were generally similar in the less affected hemisphere. We first identified striatal functional connectivity maps for the control group to evaluate the anatomical plausibility of the networks (FWE correction of <0.001). In general, the results paralleled previous findings (Di Martino et al., 2008; Kelly et al., 2009) (**Figure 1**). Networks for the three caudate seeds followed the ventral–dorsal distinction of cortico-striatal connectivity, such that the inferior ventral striatum showed connectivity with the ventral medial prefrontal areas and anterior cingulate cortex while the superior ventral striatum and dorsal caudate showed connectivity with the more dorsal and lateral areas of the prefrontal cortex including the dorsolateral prefrontal cortex (BA 46) (**Table S2** in Supplementary Material). The three putamen seeds showed connectivity with the primary and secondary motor cortical areas as well as prefrontal and parietal association cortical regions (**Table S2** in Supplementary Material). Our data also showed that there was less specificity of cortico-striatal connectivity across the six striatal seed regions compared to previous studies (Di Martino et al., 2008). For example, we found motor cortical areas associated with the caudate seeds and significant involvement of prefrontal areas associated with the three putamen seeds. This may be due to the effect of age-related decreases in the specificity of functional networks in older adults, since our control group mean age was 63 years (cf. Park and Reuter-Lorenz, 2009; Seidler et al., 2010). This remains to be evaluated in future studies.

We found relatively similar cortico-striatal connectivity patterns in each of our patient groups (**Figure S2** in Supplementary Material, **Tables S3** and **S4** in Supplementary Material). The decreased specificity of the functional connectivity patterns of the six striatal seed regions was also present in the patient groups. In order to determine the distinctiveness of the cognitive and motor networks we directly compared the connectivity maps for caudate and putamen seeds in each group. In the control group, the regions showing greater correlations with the caudate seeds than the putamen seeds included the ventromedial prefrontal cortex, posterior cingulate and the parahippocampal gyrus (**Figure 2**, **Table 1**). The regions showing greater correlation with the putamen seeds than the caudate seeds included the primary and supplementary motor areas (**Figure 2**, **Table 1**). In PD OFF and PD ON however we did not find any regions other than the caudate and putamen themselves to be more correlated with caudate or putamen seed regions, with the exception of the dorsal prefrontal cortex (BA 8) in PD OFF and

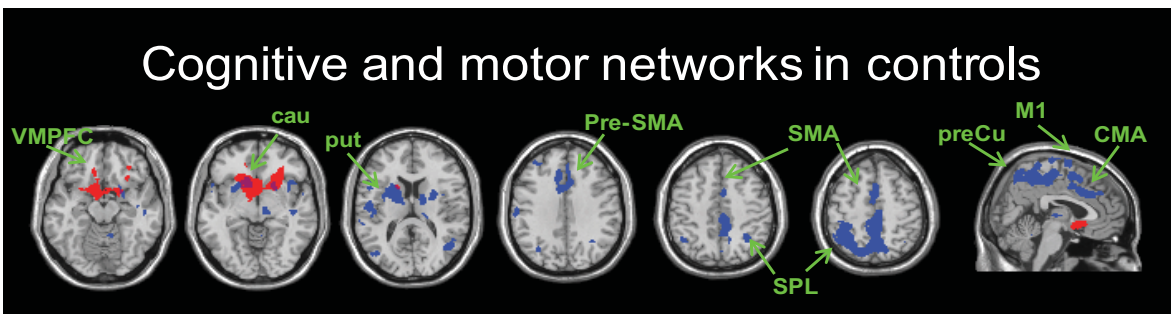


FIGURE 1 | An example of cognitive (seed: inferior ventral striatum, red) and motor (seed: dorsal rostral putamen, blue) networks in controls. $z = -15, -5, 15, 35, 45, 55$ and $x = 5$ from left to right (FWE-corrected $p < 0.001$). VMPFC, ventromedial prefrontal cortex; cau, caudate; put, putamen; Pre-SMA, pre-supplementary motor area; SMA, supplementary motor area; SPL, superior parietal lobule; M1, primary motor area; CMA, cingulate motor area; preCu, precuneus.

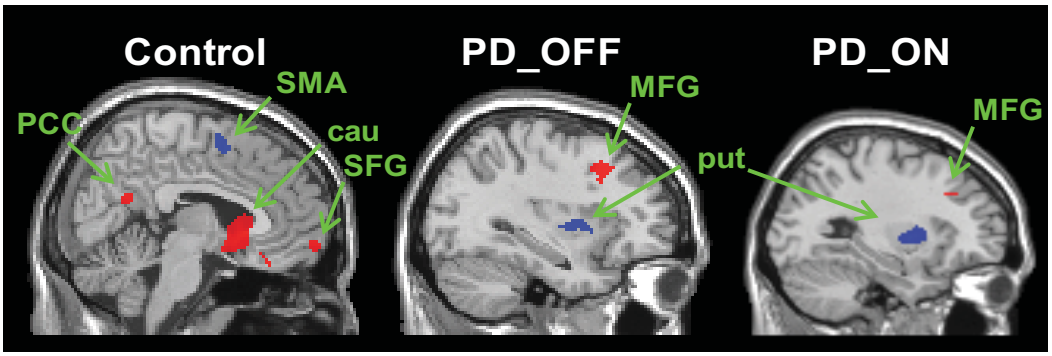


FIGURE 2 | Regions showing greater connectivity with caudate seeds (VSi, VSs, and DC combined) than with putamen seeds (DCP, DRP, and VRP combined) in red and regions showing greater connectivity with putamen seeds than with caudate seeds in blue ($p < 0.001$, uncorrected). PCC, posterior cingulate cortex; SMA, supplementary motor area; SFG, superior frontal gyrus; MFG, middle frontal gyrus; cau, caudate; put, putamen.

Table 1 | Direct comparisons between caudate seeds combined and putamen seeds combined.

Contrast	Region	BA	MNI coordinates			*T*-value
			x	*y*	*z*	
CONTROL						
Caudate > putamen	Caudate		–12	14	8	264.45
	Inferior temporal gyrus	20	–68	–20	–14	6.13
	Parahippocamal gyrus	36	–26	–18	–22	5.75
	Middle frontal gyrus	11	34	38	–14	4.92
	Rectal gyrus	11	8	32	–18	4.14
	Superior frontal gyrus	10	–28	66	14	4.48
	Posterior cingulate gyrus	23	6	–58	20	4.19
	Inferior frontal gyrus	47	–52	32	–12	3.96
Putamen > caudate	Putamen		–28	0	2	276.94
	Precentral gyrus	6	46	12	6	6.02
	Medial frontal gyrus (pre-SMA)	6	6	4	56	4.32
	Superior frontal gyrus	9	32	50	34	5
	Precuneus	7	18	–58	46	4.59
	Postcentral gyrus	7	28	–54	70	3.9
	Superior temporal gyrus	22	66	–8	6	4.64
	Inferior frontal gyrus	47	54	36	–2	4.25
	Inferior parietal lobule	40	–56	–38	46	3.87
	Ventral posterior medial thalamus		18	–22	4	3.75
PD OFF						
Caudate > putamen	Caudate		6	12	12	4.61
	Middle frontal gyrus	8	–30	10	40	4.23
Putamen > caudate	Putamen		–26	–2	–2	4.33
PD ON						
Caudate > putamen	Caudate		–6	20	4	Inf
	Middle frontal gyrus	9	–28	26	34	3.66
Putamen > caudate	Putamen		–22	6	–6	4.33

Inf, infinite T-value.

the dorsolateral prefrontal cortex (BA 9) in PD ON which exhibited greater correlated activity with the caudate than the putamen (**Figure 2**, **Table 1**). These results indicate that in both PD OFF and PD ON there is decreased specificity of the caudate and putamen functional connectivity patterns.

COMPARISON OF CAUDATE VERSUS PUTAMEN FUNCTIONAL CONNECTIVITY IN CONTROLS, PD OFF, AND PD ON

Next, we compared the connectivity maps associated with each seed region between groups. We first compared PD OFF to controls. We found increased functional connectivity in PD OFF compared

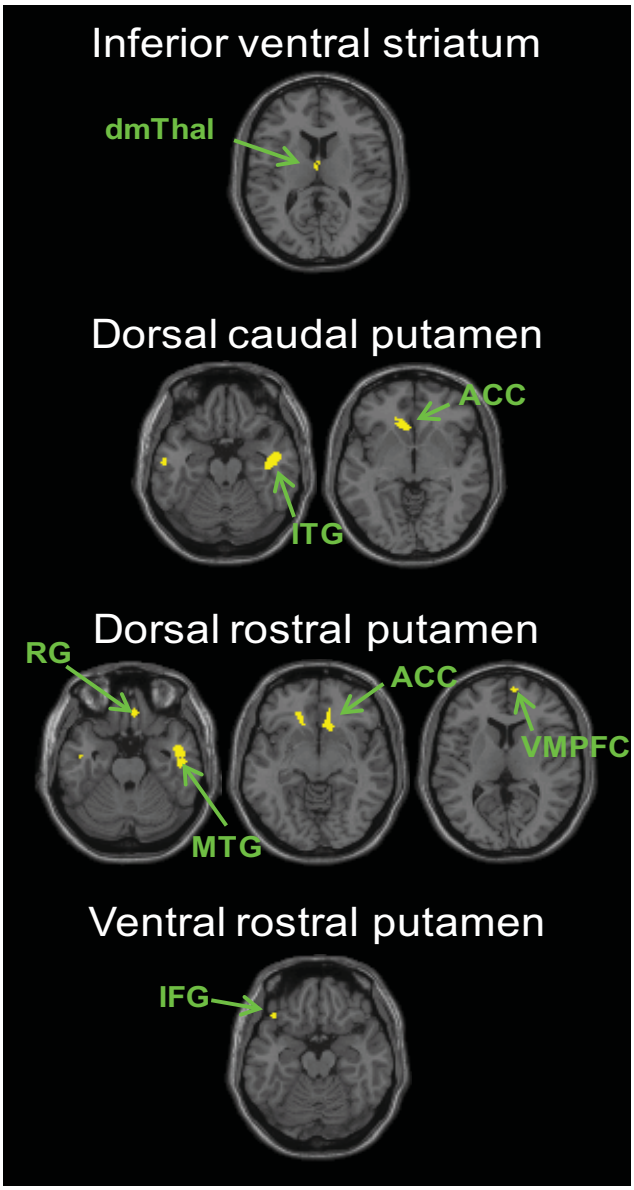


FIGURE 3 | Regions showing greater connectivity with the striatal seeds for PD OFF than controls ($p < 0.001$, uncorrected). No results were found in the other seeds or for the contrast of controls greater than PD OFF. dmThal, dorsomedial thalamus; ACC, anterior cingulate cortex; VMPFC, ventromedial prefrontal cortex; IFG, inferior frontal gyrus; RG, rectal gyrus; MTG, middle temporal gyrus.

to controls with the following seed regions: inferior ventral striatum, ventral rostral putamen, dorsal caudal putamen, and dorsal rostral putamen (**Figure 3**, **Table S5** in Supplementary Material). Regarding the first two seeds, connectivity between the inferior ventral striatum and the dorsomedial thalamus and connectivity between the ventral rostral putamen and the ventromedial prefrontal gyrus was increased in PD OFF compared to controls. For dorsal caudal putamen, the inferior temporal gyrus, anterior cingulate cortex and superior frontal gyrus showed greater connectivity in PD OFF than controls. For dorsal rostral putamen, the ventromedial prefrontal cortex, the anterior cingulate, and the middle and inferior temporal gyrus showed greater connectivity in PD OFF than controls. The increased connectivity in PD OFF was most significantly found in the two dorsal putamen seeds, and we did not find any regions showing greater connectivity for the caudate seeds except for inferior ventral striatum. There were no regions that showed greater connectivity in controls than PD OFF. These results indicate that PD patients show greater cortico-striatal functional connectivity compared to controls specifically in the dorsal putamen seeds. It is of note that the denervation of dopamine in PD is most prominent in the dorsal and posterior striatum, including the dorsal putamen, which is selectively affected in the earlier stages of the disease (Braak et al., 2003, 2006). Considering that the PD patients in the current study were all in the relatively early stages of the disease, our results indicate that increases in functional connectivity are more prominent in the early disease affected striatal subregions.

We also compared PD ON to controls. In general we found decreased cortico-striatal functional connectivity in PD ON compared to controls (**Figure 4**, **Table S6** in Supplementary Material). Decreases in connectivity were found in the primary and supplementary motor areas and the associative prefrontal and parietal regions irrespective of seed location. No regions exhibited greater connectivity for any of the striatal seeds in PD ON than controls.

Lastly, we compared connectivity maps for PD OFF versus PD ON. We found increased connectivity of the striatal seeds in PD OFF compared to PD ON, and the brain regions showing increased connectivity with each seed were part of the functional network associated with that particular seed (**Figure 5**, **Table S7** in Supplementary Material). That is, for the caudate seeds, increased connectivity in PD OFF compared to PD ON was found in the ventromedial prefrontal (BA 11) and orbitofrontal (BA 10) regions for inferior ventral striatum, dorsolateral prefrontal (BA 46) and frontal eye field (BA 8) regions for superior ventral striatum and dorsal caudate. For the putamen seeds, increased connectivity in PD OFF compared to PD on was observed in the primary and secondary motor areas (BA 4, BA 6). There were no regions that showed greater connectivity in PD ON than PD OFF. These results indicate that L-DOPA decreases the abnormally high functional connectivity in PD, with specific effects on the functional networks associated with each cortico-striatal seed. However, our findings indicate that L-DOPA reduces cortico-striatal connectivity in PD to a greater extent than is necessary as evidenced by overall decreased connectivity in PD ON compared to controls.

The brain regions identified in the voxel-wise comparison of connectivity maps between PD OFF and PD ON did not necessarily overlap with the regions identified by the PD OFF versus control group comparison. That is, from the voxel-wise comparison results we could not determine whether L-DOPA corrected the aberrantly elevated functional connectivity in PD. In order to address this, we performed an ROI analysis comparing the connectivity strengths between PD OFF and PD ON in the brain regions identified from the PD OFF versus control group comparison. The mean connectivity strengths across all voxels within the ROIs were compared between PD OFF and PD ON. For the inferior ventral striatum seed region, we found that mean connectivity strength with the dorsomedial thalamus was significantly lower in PD ON than PD OFF ($t_{24} = 2.44$, $p < 0.05$, **Figure S3A** in Supplementary

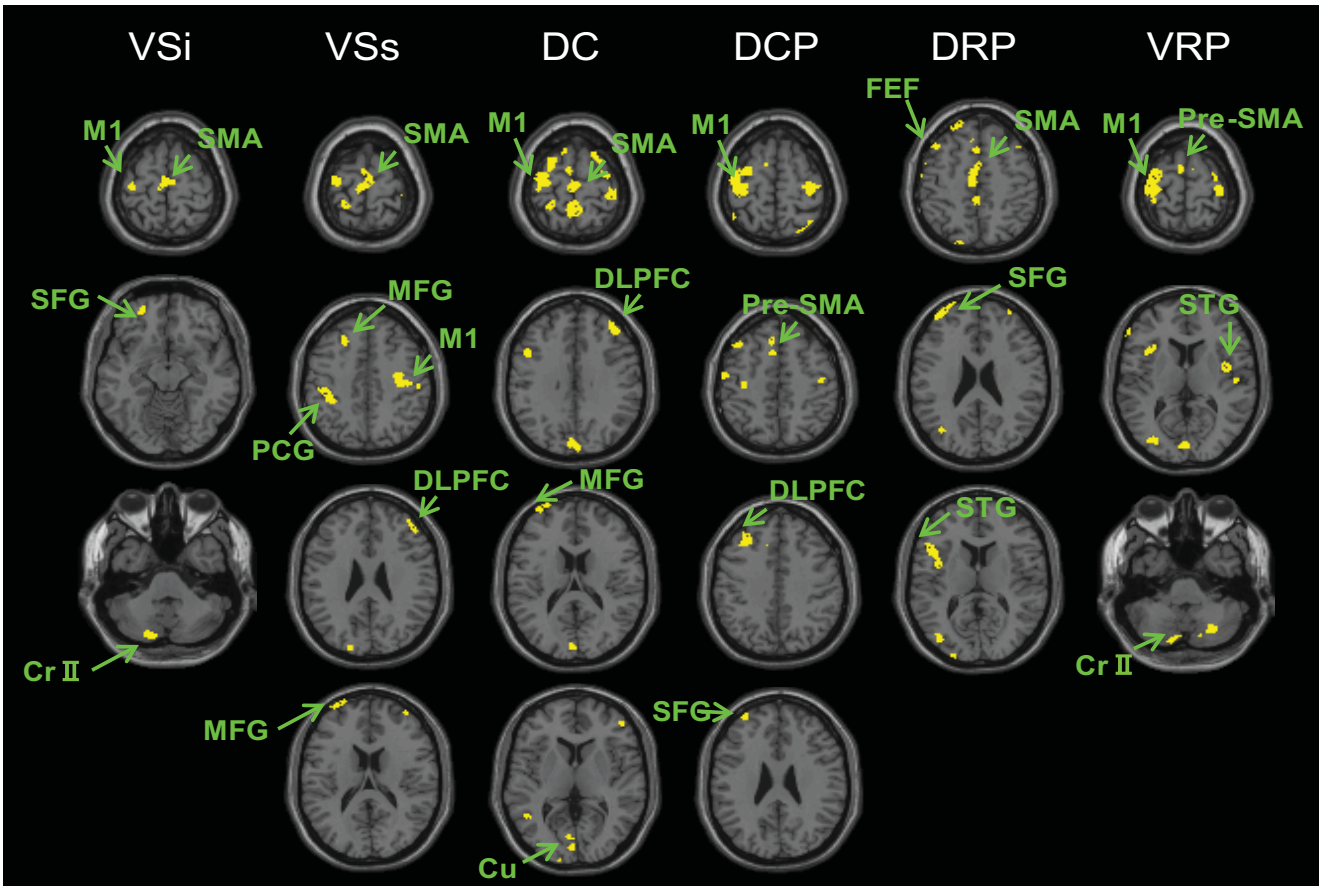


FIGURE 4 | Regions showing greater connectivity with the striatal seeds in controls than PD ON ($p < 0.001$, uncorrected). No results were found for the contrast of PD ON greater than controls. VSi, inferior ventral striatum; VSs, superior ventral striatum; DC, dorsal caudate; DCP, dorsal caudal putamen; DRP, dorsal rostral putamen; VRP, ventral rostral putamen; M1, primary motor cortex; SMA, supplementary motor area; pre-SMA, pre-supplementary motor area; DLPFC, dorsolateral prefrontal cortex; Cr II, cerebellum Crus II, STG, superior temporal gyrus; SFG, superior frontal gyrus; FEF, frontal eye field; cu, cuneus; MFG, middle frontal gyrus; PCG, postcentral gyrus.

Material). For dorsal caudal putamen, which had multiple ROIs associated with it, repeated measures ANOVA showed a significant main effect of medication status ($F_{1,24} = 9.22$, $p < 0.01$, **Figure S3B** in Supplementary Material), reflecting an overall decrease in connectivity strength in PD ON compared to PD OFF. For dorsal rostral putamen we found a marginally significant main effect of medication status ($F_{1,24} = 3.66$, $p = 0.068$, **Figure S3C** in Supplementary Material), reflecting an overall decrease in connectivity strength in PD ON compared to PD OFF. For ventral rostral putamen, connectivity strength with inferior frontal gyrus was lower in PD ON than PD OFF but was only marginally significant ($t_{24} = 1.81$, $p = 0.08$, **Figure S3D** in Supplementary Material). These results demonstrate that L-DOPA indeed corrects for the elevated connectivity in the brain regions that show increased connectivity for PD OFF compared to controls.

FREQUENCY CONTENT ANALYSIS

Comparison of connectivity maps between groups showed that there was an overall elevation of cortico-striatal functional connectivity in PD and that L-DOPA decreased this heightened connectivity. In order to determine whether increased connectivity in PD is associated with a change in oscillatory activity of the striatal BOLD signal in the resting state, we performed a frequency content analysis of the BOLD signal time course extracted from the six striatal seed regions. We first compared PD OFF to controls using a mixed between and within subjects ANOVA with group as a between subjects factor and frequency bands as a within subjects factor in each seed separately. Since we analyzed the normalized power (total power of the eight frequency bands being 100%) there was inherently no main effect of group. We found significant group by frequency band interactions for the inferior ventral striatum ($F_{4.49,\ 210.84} = 2.39$, $p < 0.05$), dorsal caudate ($F_{7,\ 329} = 2.01$, $p = 0.05$) and dorsal caudal putamen ($F_{7,\ 329} = 2.46$, $p < 0.05$). We followed these up with two sample *t*-tests comparing the frequency content of PD OFF and controls in each frequency band for these seed regions. We found significant differences in the frequency content in 0.02–0.03 Hz for inferior ventral striatum ($t_{47} = 2.45$, $p < 0.05$) and dorsal caudate ($t_{47} = 2.11$, $p < 0.05$), and in 0.03–0.04 Hz for dorsal caudal putamen ($t_{47} = 2.27$, $p < 0.05$). Normalized mean signal power was significantly greater in PD OFF than controls in these frequency ranges (**Figure 6**). A concomitant decrease in signal power for PD OFF was seen in the range of 0–0.02 Hz, although it did not reach significance.

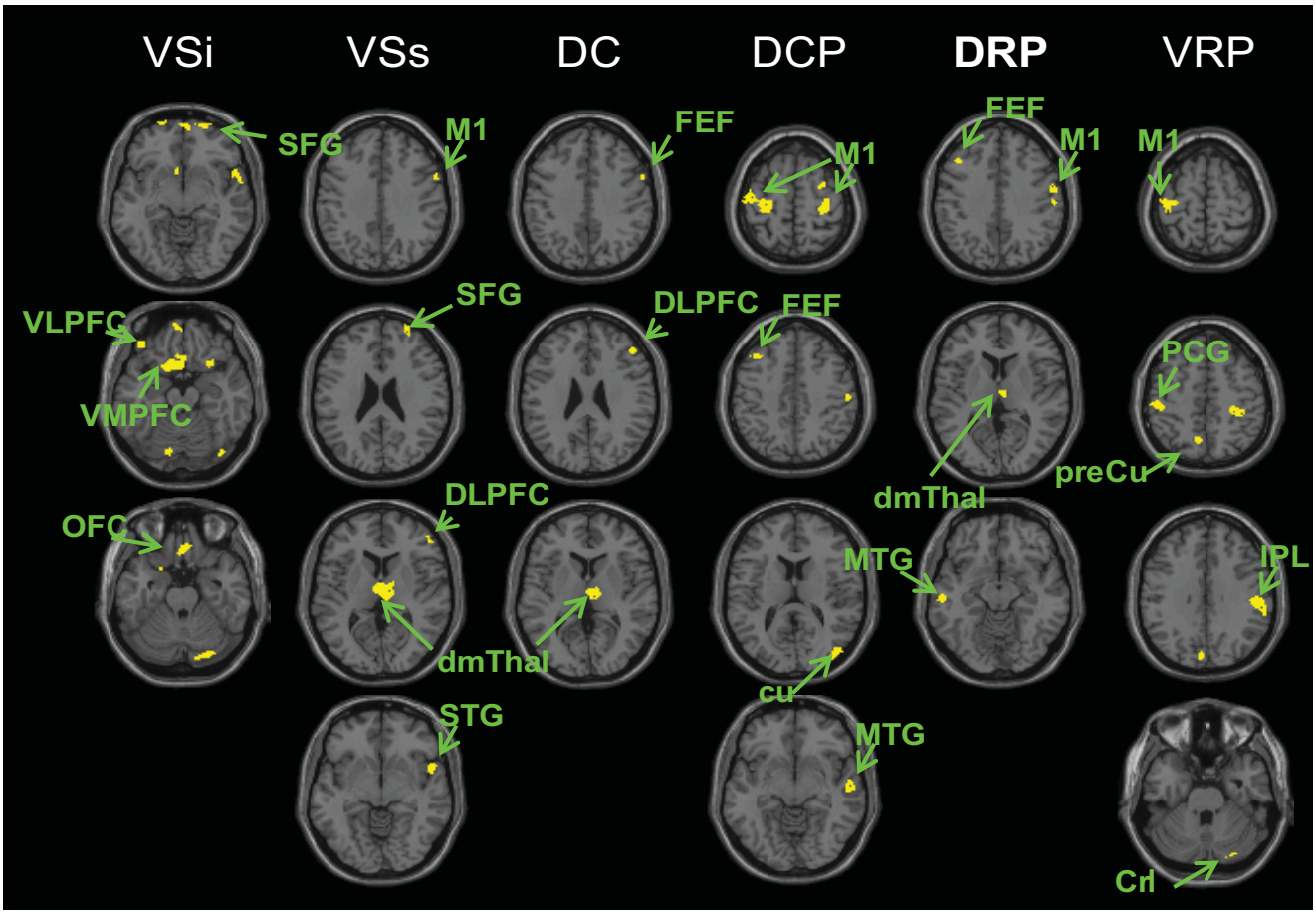


FIGURE 5 | Regions showing greater connectivity with the striatal seeds in PD OFF than PD ON ($p < 0.001$, uncorrected). No results were found for the contrast of PD ON greater than PD OFF. VSi, inferior ventral striatum; VSs, superior ventral striatum; DC, dorsal caudate; DCP, dorsal caudal putamen; DRP, dorsal rostral putamen; VRP, ventral rostral putamen; OFC, orbital frontal cortex; VLPFC, ventrolateral prefrontal cortex; VMPFC, ventromedial prefrontal cortex; DLPFC, dorsolateral prefrontal cortex; FEF, frontal eye field; M1, primary motor cortex; SFG, superior frontal gyrus; STG superior temporal gyrus; dmThal, dorsomedial thalamus; MTG, middle temporal gyrus; cu, cuneus; Cr I, cerebellum crus I; IPL, inferior parietal lobule; PCG, post central gyrus; preCu, precuneus.

We also compared the power content for PD OFF versus PD ON across the eight frequency bands for each striatal seed region using repeated measures ANOVA. We found significant medication by frequency band interactions for superior ventral striatum ($F_{7,168} = 3.53, p < 0.005$), dorsal caudate ($F_{3.97,95.18} = 4.42, p < 0.005$), dorsal caudal putamen ($F_{4.34,104.15} = 2.73, p < 0.05$) and a marginally significant interaction for dorsal rostral putamen ($F_{5.12,122.93} = 2.2$, $p = 0.057$) (**Figure 7**). We followed up with paired *t*-tests comparing the frequency content of the signals for PD OFF versus PD ON in each frequency band for these seed regions. The results showed that across the four seeds, there was a significant difference between PD OFF and PD ON in the frequency range 0–0.02 Hz and 0.03–0.05 Hz. In general, signal power in 0.03–0.05 Hz was greater in PD OFF than PD ON with a concomitant decrease in power in the 0–0.02 Hz range (VSs: 0–0.01 Hz, $t_{24} = -3$, $p < 0.01$; DC: 0–0.01 Hz, $t_{24} = -2.44$, $p < 0.05$, 0.01–0.02 Hz, $t_{24} = -2.75$, $p < 0.05$, 0.04–0.05 Hz, $t_{24} = 2.62$, $p < 0.05$; DCP: 0–0.01 Hz, $t_{24} = -2.03$, $p = 0.053$, 0.03–0.04 Hz, $t_{24} = 2.48$, $p < 0.05$; DRP: 0.03–0.04 Hz, $t_{24} = 2.58$, $p < 0.05$). Taken together with the results arising from the comparison of PD OFF to controls, these data demonstrate that there is relatively greater power for the resting state BOLD signal oscillations in the 0.02–0.05 Hz frequency band for PD OFF, and L-DOPA decreases the elevated oscillations in this frequency range.

In order to determine whether this L-DOPA-associated change in power content within these specific frequency bands modulates L-DOPA-associated connectivity differences in any brain regions, we performed an exploratory voxel-wise correlation analysis. In this analysis, we performed a voxel-wise regression using the OFF and ON difference in the normalized signal content and the OFF and ON connectivity difference. Considering that both the comparisons of PD OFF to controls and PD OFF to PD ON showed significantly increased power in the 0.02–0.05 Hz range, we used the OFF–ON normalized signal content of the frequency bands that showed significantly greater power for PD OFF than PD ON (i.e., 0.04–0.05 Hz for dorsal caudate, 0.03–0.04 Hz for dorsal caudal putamen and dorsal rostral putamen) and the OFF–ON connectivity maps. Analyses were performed within brain regions

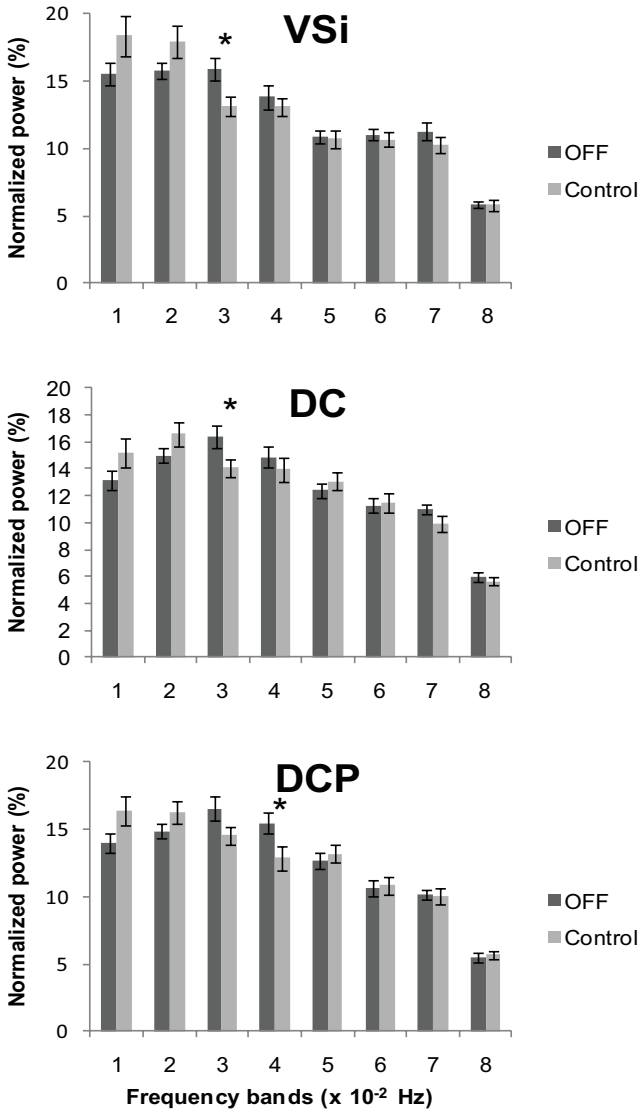


FIGURE 6 | Normalized power across the eight frequency bands in controls and PD OFF. Each band consists of approximately 0.01 Hz bandwidth. A significant group by frequency band interaction was found in inferior ventral striatum (VSi), dorsal caudate (DC), and dorsal caudal putamen (DCP) with PD OFF showing greater signal content in the 0.02–0.04 Hz range of the frequency band than controls. Error bars indicate standard error. *$p < 0.05$.

that showed greater OFF than ON functional connectivity using an explicit mask of the OFF–ON connectivity map thresholded at $p < 0.05$, uncorrected. The correlation analyses within these masks were thresholded at $p < 0.005$ uncorrected with a voxel extent threshold of 10. The results showed that for dorsal caudate, the OFF–ON frequency content difference in 0.04–0.05 Hz was positively correlated with OFF–ON connectivity differences within the dorsomedial thalamus. That is, greater L-DOPA-associated decreases in power in this frequency band were associated with greater decreases in connectivity strength between the dorsal caudate and the dorsomedial thalamus (**Figure 8**). A similar result was found for dorsal caudal putamen, which exhibited a significant positive correlation between the OFF–ON frequency content difference in 0.03–0.04 Hz and OFF–ON connectivity with the dorsomedial thalamus (**Figure 9**).

We also performed a correlation analysis between the OFF and ON difference in frequency content of the 0.03–0.05 Hz and the OFF and ON difference in behavioral measures to determine whether the change in frequency content is correlated with the medication-associated changes in behavior. We used OFF–ON frequency content and OFF–ON behavioral performance measured with MOCA, grooved pegboard, and UPDRS. We only found a significant negative correlation between OFF–ON frequency content of 0.04–0.05 Hz in dorsal caudate with the OFF–ON difference in MOCA score ($r = -0.44$, $p < 0.05$) (**Figure 10**). That is, the greater the L-DOPA-associated decrease in power in this frequency band of dorsal caudate, the greater the improvement in MOCA performance.

Collectively, the results from our frequency content analyses of the resting state BOLD time course in the six striatal seed regions indicate that there is a relative increase in BOLD signal oscillations in the 0.02–0.05 Hz range in PD, and L-DOPA mitigates this effect. The L-DOPA-associated decrease in the frequency content in this range modulated the change in connectivity strength between dorsal caudate and thalamus and dorsal caudal putamen and thalamus. Moreover, for dorsal caudate, the change in frequency content due to medication also modulated the L-DOPA associated change in cognitive performance.

DISCUSSION

We observed hyperconnectivity of the cortico-striatal networks in PD patients, which was mitigated by L-DOPA. Comparisons of connectivity maps between PD OFF and PD ON showed decreased connectivity with L-DOPA in brain regions that are known to be anatomically connected to each of the seed regions. Additional ROI analyses comparing connectivity strength between PD OFF and PD ON within the regions that showed hyperconnectivity in PD OFF compared to controls also revealed a general decrease in connectivity strength with L-DOPA. It is of note however, that down-regulation of connectivity strength in these ROIs was not observed across the board. Therefore, although L-DOPA normalized the PD-associated hyperconnectvity it was more effective in some ROIs than others. Hyperconnectivity in PD patients is explained by the shift in the frequency content of the resting state striatal BOLD signal oscillations in PD patients. More specifically, we found that PD patients OFF L-DOPA had increased functional connectivity between striatal seed regions and cortical areas compared to controls in the two dorsal putamen seeds, which are known to be the most disease-affected subregions of the striatum in the early disease state (Bernheimer et al., 1973; Kish et al., 1988; Frey et al., 1996; Rakshi et al., 1999; Braak et al., 2003, 2006). This hyperconnectivity for PD OFF was also seen in a whole-brain comparison relative to PD ON. Furthermore, the regions showing greater functional connectivity for PD OFF than ON reflected the specificity of the reward, cognitive and motor circuitry of the cortico-striatal pathways. For example, the regions showing greater connectivity with the inferior ventral striatum in PD OFF than PD ON were structures typically involved in reward processing such as the orbital frontal and ventromedial prefrontal cortex (Haber and Knutson, 2010). The regions showing greater connectivity with the dorsal

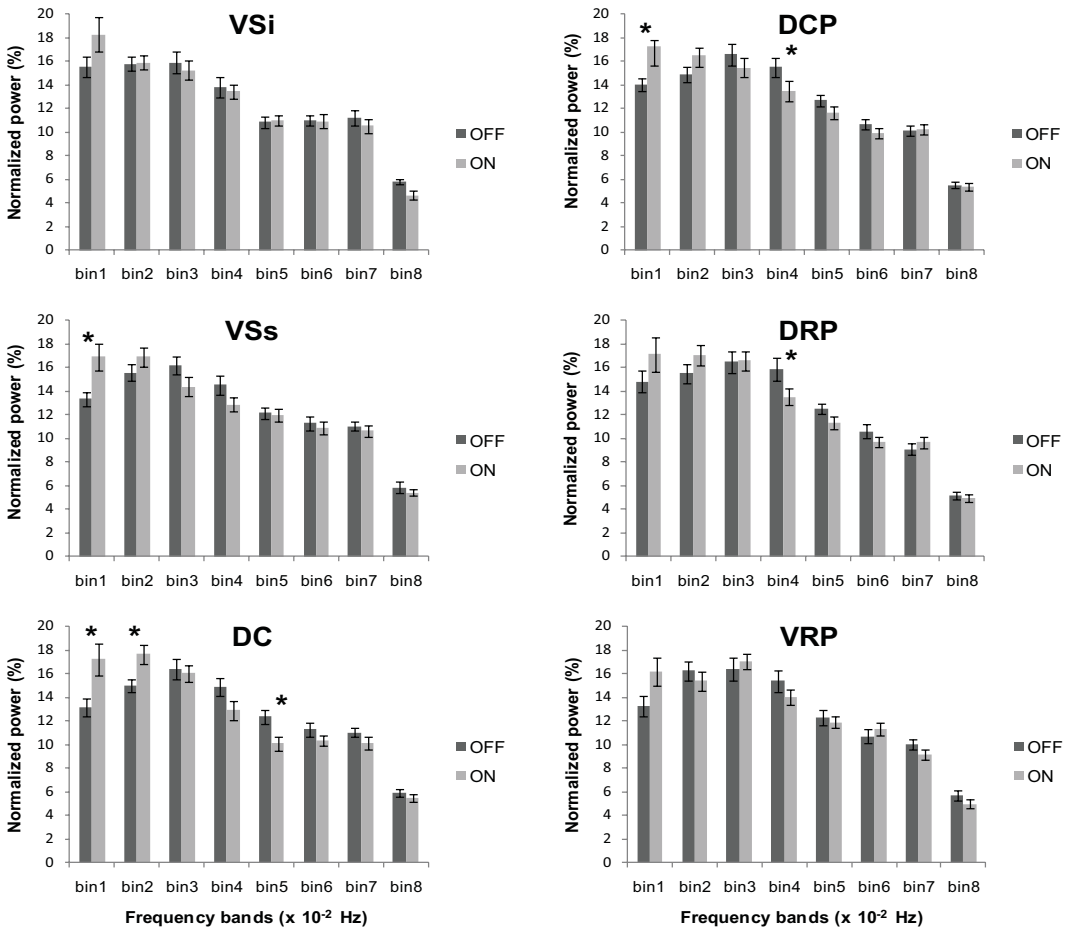


FIGURE 7 | Normalized power across the eight frequency bands in PD ON and PD OFF. Significant group by frequency band interactions were observed for the superior ventral striatum (VSs), dorsal caudate (DC), dorsal caudal putamen (DCP) and dorsal rostral putamen (DRP). Error bars indicate standard error. $*p < 0.05$.

caudate in OFF than ON included the dorsolateral prefrontal cortex which is part of the cognitive cortico-striatal loop (Alexander et al., 1986), whereas for the putamen seeds, differences in connectivity strength were found with the primary and secondary motor cortical areas. These results indicate that there is an increase in the level of connectivity between striatal regions and their selective cortical targets in PD patients.

The increased connectivity we found in PD patients compared to controls is somewhat unique to this clinical group since other studies have widely shown *disrupted* connectivity in patients with autism, depression, schizophrenia, and stroke (Greicius, 2008; Monk et al., 2009; van Meer et al., 2010; Vercammen et al., 2010). However, our observation of hyperconnectivity in PD patients OFF medication and down-regulation of this hyperconnectivity by administration of L-DOPA, is in alignment with previous studies reporting increased oscillatory neural activity of the basal ganglia and heightened synchronous activity across the basal ganglia thalamocortical networks in dopamine depleted states including PD (Costa et al., 2006; Gatev et al., 2006; Hammond et al., 2007; Eusebio et al., 2009). According to these reports, the pathological state of dopamine depletion results in increased synchronous oscillatory activity in the basal ganglia and its associated networks. Therapeutic measures such as dopaminergic medications and deep brain stimulation have been shown to reduce these oscillations and the associated increase in coherent neural activity across networks (Brown et al., 2001; Williams et al., 2002; Priori et al., 2004; Silberstein et al., 2005). The increase in cortico-cortical coupling seen in EEG data from PD patients has been shown to be associated with symptom severity (Silberstein et al., 2005). Additionally, decreases in cortico-cortical coupling due to L-DOPA and deep brain stimulation correlate with clinical improvement (Silberstein et al., 2005). The effect of dopaminergic modulation on coherence of oscillations in the basal ganglia thalamocortical networks has been shown in healthy individuals as well (Honey et al., 2003). Honey et al. (2003) assessed the changes in cortico-striatal network connectivity associated with different states of dopaminergic transmission caused by drug administration in healthy older adults. The authors observed increased functional connectivity between caudate and thalamus/ventral midbrain in decreased dopamine transmission states caused by Sulpiride, a dopamine D2 antagonist (Honey et al., 2003).

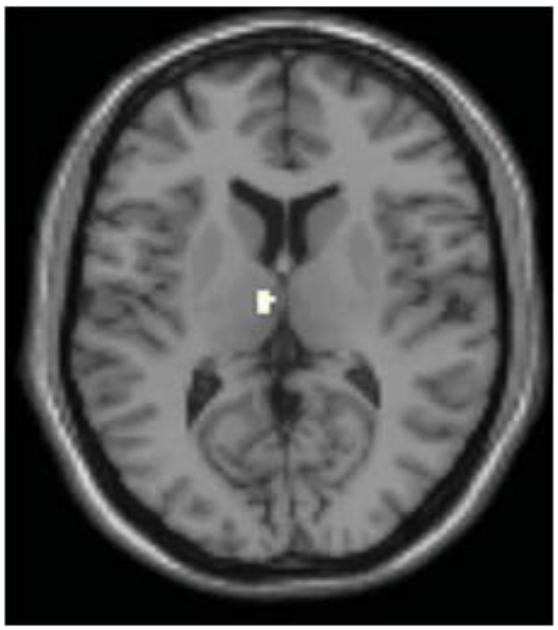


FIGURE 8 | Correlation between the difference in OFF and ON frequency content and OFF and ON connectivity in dorsal caudate. OFF–ON frequency content difference in 0.04–0.05 Hz of dorsal caudate was positively correlated with OFF–ON connectivity within the dorsomedial thalamus ($p < 0.005$ uncorrected using the OFF–ON connectivity map as a mask).

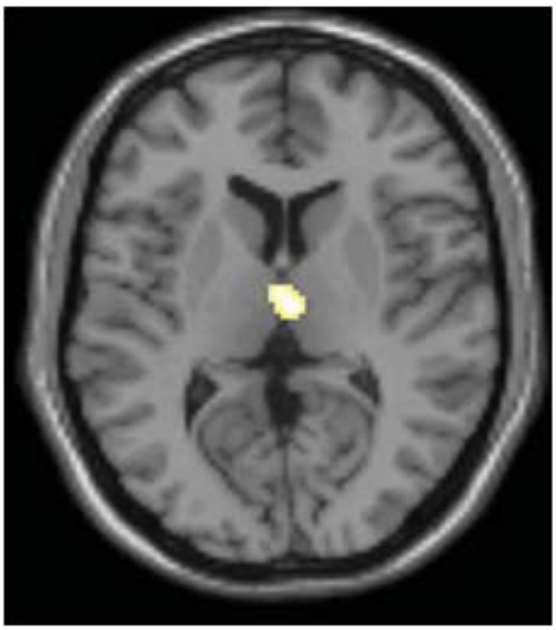


FIGURE 9 | Correlation between the difference in OFF and ON frequency content and OFF and ON connectivity in dorsal caudal putamen. OFF–ON frequency content difference in 0.03–0.04 Hz was positively correlated with OFF–ON connectivity differences within the dorsomedial thalamus ($p < 0.005$, uncorrected using OFF–ON connectivity map as a mask).

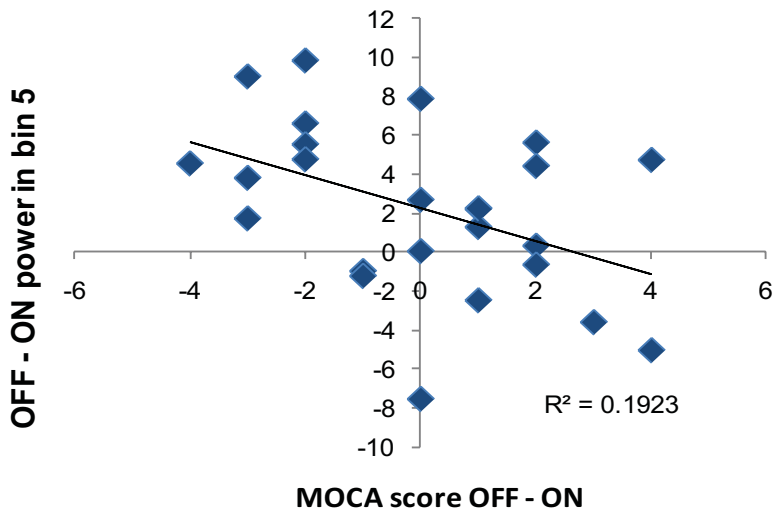


FIGURE 10 | Correlation between the difference in OFF and ON frequency content and OFF and ON MOCA performance difference. OFF–ON frequency power in 0.04–0.05 Hz of dorsal caudate (DC) negatively correlated with OFF–ON performance difference in MOCA ($r = 0.44$, $p < 0.05$).

Oscillatory neural activity in PD and its modulation by drug and deep brain stimulation therapies have been examined by analyzing the frequency content of local field potential recordings or EEG/MEG data (Silberstein et al., 2003, 2005; Kuhn et al., 2004, 2006; Priori et al., 2004; Foffani et al., 2005; Weinberger et al., 2006; Stoffers et al., 2008). Some of these studies report that the PD-related increase in signal frequency content is most prominent in the beta frequency band (10–35 Hz) (Kuhn et al., 2004, 2006; Foffani et al., 2005; Weinberger et al., 2006). Others have found increased power in lower frequency bands including theta, alpha 1 and alpha 2 in PD (Stoffers et al., 2008). Studies evaluating the effect of dopaminergic therapy on modulation of brain signal frequency content have also

shown that with medication, power decreases in the frequency range close to the beta band and concomitantly increases in the lower frequency band (2–7 Hz) (Silberstein et al., 2003; Priori et al., 2004).

In the current study, we compared the frequency content of the BOLD signal time course extracted from the striatal seed regions across medication states and between PD patients and controls. Due to the rate of fMRI data acquisition and BOLD signal preprocessing including low pass filtering, we were only able to look at the frequency range below 0.08 Hz. However, given the sluggish nature of the hemodynamic response function (Haller and Bartsch, 2009), this should be sufficient to capture the frequency range of interest. We found an increase in power content of frequency bands in the range of 0.02–0.05 Hz and a decrease in power in the range of <0.02 Hz for PD OFF compared to PD ON and controls. Furthermore for the comparison of PD OFF and PD ON, there were no significant interactions between medication and frequency bands for the inferior ventral striatum and the ventral rostral putamen. These two regions are the most ventral among the six seed locations, and are thus relatively intact in the early stages of PD (Bernheimer et al., 1973; Kish et al., 1988; Frey et al., 1996; Rakshi et al., 1999; Braak et al., 2003, 2006). Given this, our results suggest that L-DOPA affects a specific frequency range of resting state BOLD signal oscillations, and this effect is present in the more disease affected subregions of the striatum.

An exploratory analysis was performed to determine whether the L-DOPA-associated change in the resting state BOLD frequency content modulated the L-DOPA-associated connectivity differences in any brain regions. We used the frequency bands that showed a significant difference in signal content between PD ON and OFF. Our results showed that differences in signal content of the frequency band modulated the difference in connectivity strength between dorsal caudate and dorsomedial thalamus and also between dorsal caudal putamen and dorsomedial thalamus. That is, the more L-DOPA reduced power in the particular frequency band, the greater the reduction in connectivity between the striatal seed regions (i.e., dorsal caudate and dorsal caudal putamen) and dorsomedial thalamus. It is of note that the dorsomedial thalamus was commonly found in these analyses. Dorsomedial thalamus has traditionally been considered as the relay station for prefrontal and limbic connections and is involved in attention and alertness (Smythies, 1997). However, recent studies report the involvement of the dorsomedial thalamus in cortico-striatal circuitries (Cheatwood et al., 2003; Kunzle, 2006). Considering that our approach was exploratory, future studies are warranted to confirm these particular L-DOPA modulation effects in dorsomedial thalamus.

The L-DOPA-associated change in frequency content of the dorsal caudate signal was correlated with change in MOCA performance between ON and OFF L-DOPA. In other words, the more that L-DOPA reduced signal content in the frequency band the greater MOCA performance improved. To our knowledge, this is the first finding that shows L-DOPA associated shift in neural oscillation affects change in cognitive performance. Previously studies have shown that change in neural oscillation due to medication is correlated with motor improvement (Silberstein et al., 2005), however there has been no reports in terms of the relationship with cognitive improvements. Notably, the seed region we found this relationship with cognitive improvement in is the dorsal caudate, which predominantly has connections with the lateral prefrontal areas including the dorsolateral prefrontal cortex (Di Martino et al., 2008).

Our data showed some parallel findings to previous studies demonstrating changes in oscillatory neural activity in PD patients. Specifically we found changes in the low-frequency spontaneous fluctuations of the BOLD signal in PD patients at rest. A careful interpretation of our data is necessary however since the nature of BOLD signal oscillations could be different from oscillatory activity represented in local field potentials or EEG in previous studies (Silberstein et al., 2003, 2005; Kuhn et al., 2004, 2006; Priori et al., 2004; Foffani et al., 2005; Stoffers et al., 2008). The frequency range in our resting state BOLD signal was limited to below 0.08 Hz due to the nature of the neurovascular coupling (Haller and Bartsch, 2009) whereas the frequency range for local field potentials or EEG recordings is not limited to this low frequency range. Recently efforts have been made to understand the nature of the BOLD signal, in particular its relationship to neural activity. Simultaneous intracortical recordings and fMRI have demonstrated that the BOLD signal correlates with both local field potentials and multi-unit activity, but it is more accurately predicted by local field potentials (Logothetis et al., 2001; Goense and Logothetis, 2008). Simultaneous EEG and fMRI studies have also shown that patterns of fMRI activation can be explained by the frequency content of the EEG signal (Moosmann et al., 2003; Laufs, 2008; de Munck et al., 2009; Britz et al., 2010; Musso et al., 2010; Rosa et al., 2010). Additionally, studies have shown that the frequency content of the fMRI BOLD signal has behavioral relevance (Horovitz et al., 2008; Wu et al., 2008).

One interesting finding associated with the effect of L-DOPA in our patient group was that it seemed to overcorrect the hyperconnectivity of the cortico-striatal pathways as shown by our results comparing PD ON to controls. That is, there was an overall *decrease* in the level of cortico-striatal connectivity in PD ON compared to healthy controls. Irrespective of the striatal seed locations, there was a predominant decrease in connectivity between the striatum and the primary and secondary motor areas in PD ON, which was true even for seed regions that did not exhibit a relative hyperconnectivity for PD OFF relative to controls. Whether this hypoconnectivity for PD ON relative to controls is another side effect of L-DOPA that results in deleterious performance outcomes similar to the "dopamine-overdose effect" (see Cools, 2006 for review; Kwak et al., 2010) needs further investigation. The pattern of results may also be due to L-DOPA's selective effects on the more denervated striatal regions, typically the sensorimotor striatum and its motor cortical targets (Bernheimer et al., 1973; Kish et al., 1988; Rakshi et al., 1999; Braak et al., 2003, 2006).

As mentioned in the Results section, the resting state cortico-striatal functional connectivity patterns in our data are in line with previous findings. That is, separable "cognitive" and "motor" circuitries were identified in healthy older adults and PD patients ON and OFF L-DOPA. However, one thing we did notice was that the cognitive and motor circuitries were less separable in our older adult group compared to what has been reported in previous studies conducted in healthy younger adults (Di Martino et al., 2008; Kelly et al., 2009). The reduced specificity of the cognitive and motor circuitries was even more apparent in our patient

groups. One possible explanation for this discrepancy from previous findings is that the data processing and analysis streams were not identical to these previous studies, although we used the same MNI coordinates for the seed regions. Another possible explanation would be that the reduced specificity of the networks is due to age-related changes in neural recruitment considering that our participants were in their 60 s on average. Given this, the decrease in the exclusiveness of the cortico-striatal circuitries may be due to the age-related dedifferentiation of neural networks (Park and Reuter-Lorenz, 2009; Seidler et al., 2010). This topic awaits further investigation. With regards to PD, a decrease in the relative separation of the cognitive and motor networks was even more apparent. That is, direct comparison of the caudate and putamen connectivity maps in the patient group demonstrated that the relative separation of the striatal networks present in controls was not observed in PD in either the ON or OFF L-DOPA state. This suggests that the cognitive and motor cortico-striatal networks become more diffuse and overlapping in PD in both the ON and OFF medication states.

We found that PD and L-DOPA were associated with shifts in the frequency content of resting state striatal signals, and this was correlated with connectivity strength and cognitive performance change, but not with changes in UPDRS scores. In fact the controlled dose of L-DOPA we used across all patients did not always improve UPDRS score, which suggests that it may have not been clinically efficient for some patients. Additionally, we cannot directly link the frequency range in resting state BOLD signal to the frequency ranges that were reported in EEG or local field potential studies. A further investigation combining EEG and resting state fMRI in PD patients will be required to address this issue.

In conclusion, our results showing a PD-associated increase in cortico-striatal functional connectivity and shifts in the power content of striatal signals parallel previous findings of increased coupled neural oscillatory activity in PD, as measured with local field potentials and EEG. Moreover we found that the L-DOPA associated changes in BOLD signal oscillations modulate changes in connectivity and cognitive performance associated with L-DOPA. It is particularly interesting that our analysis of the low frequency fcMRI signal parallels previous EEG analyses of neural signal content at much higher frequencies. Considering that local field potential recordings can only be done in surgical settings and that EEG only captures cortical activity with low spatial resolution, whereas we found significant changes with fcMRI in mild to moderate stage patients, resting state fcMRI has great potential to be applied to further clinical research investigating the pathophysiology, progression, and treatment of PD.

ACKNOWLEDGMENTS

This study was supported by a grant from the Gustavus and Louise Pfeiffer Foundation (Rachael D. Seidler). We thank Darcy Huismann, Halley Feldman, Melissa Tan, Sarah Shin, Melanie Sottile, Mona Ramlawi, and Keith Newnham for assistance with data collection and analyses. We also thank J. Wayne Aldridge, Joshua Berke, and Bruno Averbeck for their insightful comments on an earlier draft of the manuscript.

REFERENCES

Alexander, G. E., DeLong, M. R., and Strick, P. L. (1986). Parallel organization of functionally segregated circuits linking basal ganglia and cortex. *Annu. Rev. Neurosci.* 9, 357–381.

Bernheimer, H., Birkmayer, W., Hornykiewicz, O., Jellinger, K., and Seitelberger, F. (1973). Brain dopamine and the syndromes of Parkinson and Huntington. Clinical, morphological and neurochemical correlations. *J. Neurol. Sci.* 20, 415–455.

Biswal, B., Yetkin, F. Z., Haughton, V. M., and Hyde, J. S. (1995). Functional connectivity in the motor cortex of resting human brain using echo-planar MRI. *Magn. Reson. Med.* 34, 537–541.

Biswal, B. B., Mennes, M., Zuo, X. N., Gohel, S., Kelly, C., Smith, S. M., Beckmann, C. F., Adelstein, J. S., Buckner, R. L., Colcombe, S., Dogonowski, A. M., Ernst, M., Fair, D., Hampson, M., Hoptman, M. J., Hyde, J. S., Kiviniemi, V. J., Kotter, R., Li, S. J., Lin, C. P., Lowe, M. J., Mackay, C., Madden, D. J., Madsen, K. H., Margulies, D. S., Mayberg, H. S., McMahon, K., Monk, C. S., Mostofsky, S. H., Nagel, B. J., Pekar, J. J., Peltier, S. J., Petersen, S. E., Riedl, V., Rombouts, S. A., Rypma, B., Schlaggar, B. L., Schmidt, S., Seidler, R. D., Siegle, G. J., Sorg, C., Teng, G. J., Veijola, J., Villringer, A., Walter, M., Wang, L., Weng, X. C., Whitfield-Gabrieli, S., Williamson, P., Windischberger, C., Zang, Y. F., Zhang, H. Y., Castellanos, F. X., and Milham, M. P. (2010). Toward discovery science of human brain function. *Proc. Natl. Acad. Sci. U.S.A.* 107, 4734–4739.

Bohnen, N. I., Kuwabara, H., Constantine, G. M., Mathis, C. A., and Moore, R. Y. (2007). Grooved pegboard test as a biomarker of nigrostriatal denervation in Parkinson's disease. *Neurosci. Lett.* 424, 185–189.

Braak, H., Bohl, J. R., Muller, C. M., Rub, U., de Vos, R. A., Del Tredici, K. (2006). Stanley Fahn Lecture 2005: the staging procedure for the inclusion body pathology associated with sporadic Parkinson's disease reconsidered. *Mov. Disord.* 21, 2042–2051.

Braak, H., Del Tredici, K., Rub, U., de Vos, R. A., Jansen Steur, E. N., and Braak, E. (2003). Staging of brain pathology related to sporadic Parkinson's disease. *Neurobiol. Aging* 24, 197–211.

Britz, J., Van De Ville, D., and Michel, C. M. (2010). BOLD correlates of EEG topography reveal rapid resting-state network dynamics. *Neuroimage* 52, 1162–1170.

Brown, P., Oliviero, A., Mazzone, P., Insola, A., Tonali, P., and Di Lazzaro, V. (2001). Dopamine dependency of oscillations between subthalamic nucleus and pallidum in Parkinson's disease. *J. Neurosci.* 21, 1033–1038.

Caballol, N., Marti, M. J., and Tolosa, E. (2007). Cognitive dysfunction and dementia in Parkinson disease. *Mov. Disord.* 22, S358–S366.

Cheatwood, J. L., Reep, R. L., and Corwin, J. V. (2003). The associative striatum: cortical and thalamic projections to the dorsocentral striatum in rats. *Brain Res.* 968, 1–14.

Cools, R. (2006). Dopaminergic modulation of cognitive function-implications for L-DOPA treatment in Parkinson's disease. *Neurosci. Biobehav. Rev.* 30, 1–23.

Costa, R. M., Lin, S. C., Sotnikova, T. D., Cyr, M., Gainetdinov, R. R., Caron, M. G., and Nicolelis, M. A. (2006). Rapid alterations in corticostriatal ensemble coordination during acute dopamine-dependent motor dysfunction. *Neuron* 52, 359–369.

de Munck, J. C., Goncalves, S. I., Mammoliti, R., Heethaar, R. M., and Lopes da Silva, F. H. (2009). Interactions between different EEG frequency bands and their effect on alpha-fMRI correlations. *Neuroimage* 47, 69–76.

Di Martino, A., Scheres, A., Margulies, D. S., Kelly, A. M., Uddin, L. Q., Shehzad, Z., Biswal, B., Walters, J. R., Castellanos, F. X., and Milham, M. P. (2008). Functional connectivity of human striatum: a resting state fMRI study. *Cereb. Cortex* 18, 2735–2747.

Eusebio, A., Pogosyan, A., Wang, S., Averbeck, B., Gaynor, L. D., Cantiniaux, S., Witjas, T., Limousin, P., Azulay, J. P., and Brown, P. (2009). Resonance in subthalamo-cortical circuits in Parkinson's disease. *Brain* 132, 2139–2150.

Fahn, S., Elton, R., and Committee., M.o.t.U.D. (1987). "The Unified Parkinson's Disease Rating Scale," in *Recent Developments in Parkinson's Disease*, Vol. 2, eds S. Fahn, C. D. Marsden, D. B. Calne, M. Goldstein (Florham Park, NJ: Macmillan Healthcare Information), 293–304.

Foffani, G., Bianchi, A. M., Baselli, G., and Priori, A. (2005). Movement-related frequency modulation of beta oscillatory activity in the human subthalamic nucleus. *J. Physiol.* 568, 699–711.

Folstein, M. F., Folstein, S. E., and McHugh, P. R. (1975). "Mini-mental state". A practical method for grading the cognitive state of patients for the clinician. *J. Psychiatr. Res.* 12, 189–198.

Fox, M. D., and Raichle, M. E. (2007). Spontaneous fluctuations in brain activity observed with functional

magnetic resonance imaging. *Nat. Rev. Neurosci.* 8, 700–711.

Frey, K. A., Koeppe, R. A., Kilbourn, M. R., VanderBorght, T. M., Albin, R. L., Gilman, S., and Kuhl, D. E. (1996). Presynaptic monoaminergic vesicles in Parkinson's disease and normal aging. *Ann. Neurol.* 40, 873–884.

Gatev, P., Darbin, O., and Wichmann, T. (2006). Oscillations in the basal ganglia under normal conditions and in movement disorders. *Mov. Disord.* 21, 1566–1577.

Glover, G. H., and Law, C. S. (2001). Spiral-in/out BOLD fMRI for increased SNR and reduced susceptibility artifacts. *Magn. Reson. Med.* 46, 515–522.

Glover, G. H., Li, T. Q., and Ress, D. (2000). Image-based method for retrospective correction of physiological motion effects in fMRI: RETROICOR. *Magn. Reson. Med.* 44, 162–167.

Goense, J. B., and Logothetis, N. K. (2008). Neurophysiology of the BOLD fMRI signal in awake monkeys. *Curr. Biol.* 18, 631–640.

Goldman, R. I., Stern, J. M., Engel, J. Jr., and Cohen, M. S. (2002). Simultaneous EEG and fMRI of the alpha rhythm. *Neuroreport* 13, 2487–2492.

Greicius, M. (2008). Resting-state functional connectivity in neuropsychiatric disorders. *Curr. Opin. Neurol.* 21, 424–430.

Greicius, M. D., Kiviniemi, V., Tervonen, O., Vainionpaa, V., Alahuhta, S., Reiss, A. L., and Menon, V. (2008). Persistent default-mode network connectivity during light sedation. *Hum. Brain Mapp.* 29, 839–847.

Greicius, M. D., Supekar, K., Menon, V., and Dougherty, R. F. (2009). Resting-state functional connectivity reflects structural connectivity in the default mode network. *Cereb. Cortex* 19, 72–78.

Haber, S. N., and Knutson, B. (2010). The reward circuit: linking primate anatomy and human imaging. *Neuropsychopharmacology* 35, 4–26.

Haller, S., and Bartsch, A. J. (2009). Pitfalls in fMRI. *Eur. Radiol.* 19, 2689–2706.

Hammond, C., Bergman, H., and Brown, P. (2007). Pathological synchronization in Parkinson's disease: networks, models and treatments. *Trends Neurosci.* 30, 357–364.

Helmich, R. C., Derikx, L. C., Bakker, M., Scheeringa, R., Bloem, B. R., and Toni, I. (2010). Spatial remapping of cortico-striatal connectivity in Parkinson's disease. *Cereb. Cortex* 20, 1175–1186.

Hoehn, M. M., and Yahr, M. D. (1967). Parkinsonism: onset, progression and mortality. *Neurology* 17, 427–442.

Honey, G. D., Suckling, J., Zelaya, F., Long, C., Routledge, C., Jackson, S., Ng, V., Fletcher, P. C., Williams, S. C., Brown, J., and Bullmore, E. T. (2003). Dopaminergic drug effects on physiological connectivity in a human cortico-striato-thalamic system. *Brain* 126, 1767–1781.

Horovitz, S. G., Fukunaga, M., de Zwart, J. A., van Gelderen, P., Fulton, S. C., Balkin, T. J., and Duyn, J. H. (2008). Low frequency BOLD fluctuations during resting wakefulness and light sleep: a simultaneous EEG-fMRI study. *Hum. Brain Mapp.* 29, 671–682.

Huynh, H., and Feldt, L. S. (1970). Conditions under which the mean square ratios in repeated measures designs have exact F-distributions. *J. Am. Stat. Assoc.* 65, 1582–1589.

Jenkinson, M., Bannister, P., Brady, M., and Smith, S. (2002). Improved optimization for the robust and accurate linear registration and motion correction of brain images. *Neuroimage* 17, 825–841.

Kelly, C., de Zubicaray, G., Di Martino, A., Copland, D. A., Reiss, P. T., Klein, D. F., Castellanos, F. X., Milham, M. P., and McMahon, K. (2009). L-DOPA modulates functional connectivity in striatal cognitive and motor networks: a double-blind placebo-controlled study. *J. Neurosci.* 29, 7364–7378.

Kish, S. J., Shannak, K., and Hornykiewicz, O. (1988). Uneven pattern of dopamine loss in the striatum of patients with idiopathic Parkinsons disease: pathophysiologic and clinical implications. *N. Engl. J. Med.* 318, 876–880.

Kuhn, A. A., Kupsch, A., Schneider, G. H., and Brown, P. (2006). Reduction in subthalamic 8–35 Hz oscillatory activity correlates with clinical improvement in Parkinson's disease. *Eur. J. Neurosci.* 23, 1956–1960.

Kuhn, A. A., Williams, D., Kupsch, A., Limousin, P., Hariz, M., Schneider, G. H., Yarrow, K., and Brown, P. (2004). Event-related beta desynchronization in human subthalamic nucleus correlates with motor performance. *Brain* 127, 735–746.

Kunzle, H. (2006). Thalamo-striatal projections in the hedgehog tenrec. *Brain Res.* 1100, 78–92.

Kwak, Y., Muller, M. L., Bohnen, N. I., Dayalu, P., Seidler, R. D. (2010). Effect of dopaminergic medications on the time course of explicit motor sequence learning in Parkinson's disease. *J. Neurophysiol.* 103, 942–949.

Laufs, H. (2008). Endogenous brain oscillations and related networks detected by surface EEG-combined fMRI. *Hum. Brain Mapp.* 29, 762–769.

Laufs, H., Kleinschmidt, A., Beyerle, A., Eger, E., Salek-Haddadi, A., Preibisch, C., and Krakow, K. (2003). EEG-correlated fMRI of human alpha activity. *Neuroimage* 19, 1463–1476.

Levy, R., Ashby, P., Hutchison, W. D., Lang, A. E., Lozano, A. M., and Dostrovsky, J. O. (2002). Dependence of subthalamic nucleus oscillations on movement and dopamine in Parkinson's disease. *Brain* 125, 1196–1209.

Logothetis, N. K., Pauls, J., Augath, M., Trinath, T., and Oeltermann, A. (2001). Neurophysiological investigation of the basis of the fMRI signal. *Nature* 412, 150–157.

Monk, C. S., Peltier, S. J., Wiggins, J. L., Weng, S. J., Carrasco, M., Risi, S., and Lord, C. (2009). Abnormalities of intrinsic functional connectivity in autism spectrum disorders. *Neuroimage* 47, 764–772.

Moosmann, M., Ritter, P., Krastel, I., Brink, A., Thees, S., Blankenburg, F., Taskin, B., Obrig, H., and Villringer, A. (2003). Correlates of alpha rhythm in functional magnetic resonance imaging and near infrared spectroscopy. *Neuroimage* 20, 145–158.

Musso, F., Brinkmeyer, J., Mobascher, A., Warbrick, T., and Winterer, G. (2010). Spontaneous brain activity and EEG microstates. A novel EEG/fMRI analysis approach to explore resting-state networks. *Neuroimage* 52, 1149–1161.

Nasreddine, Z. S., Phillips, N. A., Bedirian, V., Charbonneau, S., Whitehead, V., Collin, I., Cummings, J. L., and Chertkow, H. (2005). The Montreal Cognitive Assessment, MoCA: a brief screening tool for mild cognitive impairment. *J. Am. Geriatr. Soc.* 53, 695–699.

Nichols, T., and Hayasaka, S. (2003). Controlling the familywise error rate in functional neuroimaging: a comparative review. *Stat. Methods Med. Res.* 12, 419–446.

Oppenheim, A., Schafer, R., and Buck, J. (1999). *Discrete-Time Signal Processing*. Upper Saddle River, NJ: Prentice Hall.

Park, D. C., and Reuter-Lorenz, P. (2009). The adaptive brain: aging and neurocognitive scaffolding. *Annu. Rev. Psychol.* 60, 173–196.

Peltier, S. J., LaConte, S. M., Niyazov, D. M., Liu, J. Z., Sahgal, V., Yue, G. H., and Hu, X. P. (2005). Reductions in interhemispheric motor cortex functional connectivity after muscle fatigue. *Brain Res.* 1057, 10–16.

Peltier, S. J., Polk, T. A., and Noll, D. C. (2003). Detecting low-frequency functional connectivity in fMRI using a self-organizing map (SOM) algorithm. *Hum. Brain Mapp.* 20, 220–226.

Priori, A., Foffani, G., Pesenti, A., Tamma, F., Bianchi, A. M., Pellegrini, M., Locatelli, M., Moxon, K. A., and Villani, R. M. (2004). Rhythm-specific pharmacological modulation of subthalamic activity in Parkinson's disease. *Exp. Neurol.* 189, 369–379.

Rakshi, J. S., Uema, T., Ito, K., Bailey, D. L., Morrish, P. K., Ashburner, J., Dagher, A., Jenkins, I. H., Friston, K. J., and Brooks, D. J. (1999). Frontal, midbrain and striatal dopaminergic function in early and advanced Parkinson's disease – A 3D [F-18]dopa-PET study. *Brain* 122, 1637–1650.

Rogers, B. P., Morgan, V. L., Newton, A. T., and Gore, J. C. (2007). Assessing functional connectivity in the human brain by fMRI. *Magn. Reson. Imaging* 25, 1347–1357.

Rosa, M. J., Kilner, J., Blankenburg, F., Josephs, O., and Penny, W. (2010). Estimating the transfer function from neuronal activity to BOLD using simultaneous EEG-fMRI. *Neuroimage* 49, 1496–1509.

Seidler, R. D., Bernard, J. A., Burutolu, T. B., Fling, B. W., Gordon, M. T., Gwin, J. T., Kwak, Y., and Lipps, D. B. (2010). Motor control and aging: links to age-related brain structural, functional, and biochemical effects. *Neurosci. Biobehav. Rev.* 34, 721–733.

Shohamy, D., Myers, C. E., Geghman, K. D., Sage, J., and Gluck, M. A. (2006). L-DOPA impairs learning, but spares generalization, in Parkinson's disease. *Neuropsychologia* 44, 774–784.

Silberstein, P., Kuhn, A. A., Kupsch, A., Trottenberg, T., Krauss, J. K., Wohrle, J. C., Mazzone, P., Insola, A., Di Lazzaro, V., Oliviero, A., Aziz, T., and Brown, P. (2003). Patterning of globus pallidus local field potentials differs between Parkinson's disease and dystonia. *Brain* 126, 2597–2608.

Silberstein, P., Pogosyan, A., Kuhn, A. A., Hotton, G., Tisch, S., Kupsch, A., Dowsey-Limousin, P., Hariz, M. I., and Brown, P. (2005). Cortico-cortical coupling in Parkinson's disease and its modulation by therapy. *Brain* 128, 1277–1291.

Smythies, J. (1997). The functional neuroanatomy of awareness: with a focus on the role of various anatomical systems in the control of intermodal attention. *Conscious. Cogn.* 6, 455–481.

Stam, C. J. (2010). Use of magnetoencephalography (MEG) to study functional brain networks in neurodegenerative disorders. *J. Neurol. Sci.* 289, 128–134.

Stoffers, D., Bosboom, J. L., Deijen, J. B., Wolters, E., Stam, C. J., and Berendse, H. W. (2008). Increased cortico-cortical functional connectivity in early-stage Parkinson's disease: an MEG study. *Neuroimage* 41, 212–222.

van Meer, M. P., van der Marel, K., Wang, K., Otte, W. M., El Bouazati, S., Roeling,

T. A., Viergever, M. A., Berkelbach van der Sprenkel, J. W., and Dijkhuizen, R. M. (2010). Recovery of sensorimotor function after experimental stroke correlates with restoration of resting-state interhemispheric functional connectivity. *J. Neurosci.* 30, 3964–3972.

Vercammen, A., Knegtering, H., Liemburg, E. J., Boer, J. A., and Aleman, A. (2010). Functional connectivity of the temporo-parietal region in schizophrenia: effects of rTMS treatment of auditory hallucinations. *J. Psychiatr. Res.* 44, 725–731.

Vincent, J. L., Patel, G. H., Fox, M. D., Snyder, A. Z., Baker, J. T., Van Essen, D. C., Zempel, J. M., Snyder, L. H., Corbetta, M., and Raichle, M. E. (2007). Intrinsic functional architecture in the anaesthetized monkey brain. *Nature* 447, 83–86.

Weinberger, M., Mahant, N., Hutchison, W. D., Lozano, A. M., Moro, E., Hodaie, M., Lang, A. E., and Dostrovsky, J. O. (2006). Beta oscillatory activity in the subthalamic nucleus and its relation to dopaminergic response in Parkinson's disease. *J. Neurophysiol.* 96, 3248–3256.

Williams, D., Tijssen, M., Van Bruggen, G., Bosch, A., Insola, A., Di Lazzaro, V., Mazzone, P., Oliviero, A., Quartarone, A., Speelman, H., and Brown, P. (2002). Dopamine-dependent changes in the functional connectivity between basal ganglia and cerebral cortex in humans. *Brain* 125, 1558–1569.

Wu, C. W., Gu, H., Lu, H., Stein, E. A., Chen, J. H., and Yang, Y. (2008). Frequency specificity of functional connectivity in brain networks. *Neuroimage* 42, 1047–1055.

Wu, T., Wang, L., Chen, Y., Zhao, C., Li, K., and Chan, P. (2009). Changes of functional connectivity of the motor network in the resting state in Parkinson's disease. *Neurosci. Lett.* 460, 6–10.

Conflict of Interest Statement: The authors declare that the research was conducted in the absence of any commercial or financial relationships that could be construed as a potential conflict of interest.

Received: 13 May 2010; paper pending published: 04 June 2010; accepted: 23 August 2010; published online: 15 September 2010.

*Citation: Kwak Y, Peltier S, Bohnen NI, Müller MLTM, Dayalu P and Seidler RD (2010) Altered resting state cortico-striatal connectivity in mild to moderate stage Parkinson's disease. Front. Syst. Neurosci. **4**:143 doi:10.3389/fnsys.2010.00143*

Copyright © 2010 Kwak, Peltier, Bohnen, Müller, Dayalu and Seidler. This is an open-access article subject to an exclusive license agreement between the authors and the Frontiers Research Foundation, which permits unrestricted use, distribution, and reproduction in any medium, provided the original authors and source are credited.

SUPPLEMENTARY MATERIAL

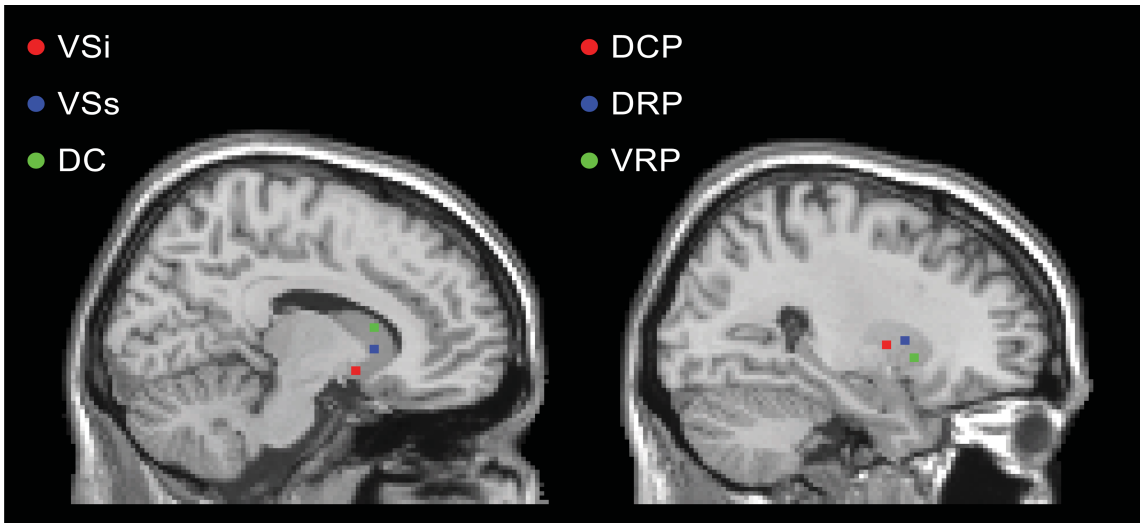


FIGURE S1 | Location of the six striatal seed regions. The left shows ($x = 11$) the location of the three caudate seeds: inferior ventral striatum (VSi), superior ventral striatum (VSs), and dorsal caudate (DC). The right ($x = 28$) shows the locations of the three putamen seeds: dorsal caudal putamen (DCP), dorsal rostral putamen (DRP), and ventral rostral putamen (VRP).

Table S1 | Demographic and clinical variables of PD patients.

	Age	Gender	Disease duration (years)	Affected body side	H and Y	UPDRS_ON	UPDRS_OFF
PD_01	62	M	6	R	2.5	15	16
PD_02	70	M	8	L	2	23	19
PD_03	70	M	7	R	2	14	21
PD_04	52	M	6	R	2.5	16	20
PD_05	71	M	13	R	2.5	18	24
PD_06	69	M	12	R	2	20	24
PD_07	60	M	3	R	1.5	10	9
PD_08	65	M	8	R	2.5	21	27
PD_09	63	M	7	L	2.5	28	28
PD_10	69	M	9	R	2	24	23
PD_11	66	M	1	L	2	9	9
PD_12	67	M	9	R	2.5	14	14
PD_13	73	M	2	R	2.5	18	14
PD_14	51	M	2	R	2	9	8
PD_15	68	M	2	L	2	25	27
PD_16	72	M	4	L	2.5	27	26
PD_17	59	F	2	R	2	5	6
PD_18	64	M	7	R	2	8	6
PD_19	64	M	3	L	2	28	30
PD_20	80	M	6	R	2	11	13
PD_21	50	M	3	R	1.5	13	13
PD_22	62	M	2	R	2	10	17
PD_23	51	M	3	R	2.5	32	37
PD_24	56	F	1	L	2	11	21
PD_25	55	F	3	R	2	15	14
Mean	63.6		5.2		2.1	17.0	18.6
S.D.	7.8		3.4		0.3	7.4	8.1

Table S2 | MNI coordinates of the local maxima of brain regions showing functional connectivity with the six striatal seed regions in controls.

Seed	Region	BA	MNI coordinates			*T*-value
			x	*y*	*z*	
Inferior ventral striatum	Medial frontal gyrus	32	–6	8	–8	34.22
	Superior temporal gyrus	42	56	16	8	10.2
Superior ventral striatum	Lingual gyrus	18	–4	72	–4	13.59
	Superior parietal lobule	7	26	62	54	12.58
	Inferior parietal lobule	40	46	34	54	12.4
	Middle frontal gyrus	6	30	–2	56	11.89
	Paracentral gyrus	6	–6	28	76	10.82
Dorsal caudate	Supramarginal gyrus	40	48	50	30	13.65
	Middle frontal gyrus	46	54	28	22	11.45
	Middle frontal gyrus	10	32	54	18	11.34
	Superior frontal gyrus	8	28	20	48	11.23
	Middle temporal gyrus	21	56	30	–2	10.34
	Postcentral gyrus	2	42	26	40	10.16
	Cerebellum Cr I		22	84	26	10.19
Dorsal caudal putamen	Anterior cingulate gyrus	32	6	14	36	10.54
	Postcentral gyrus	7	14	54	50	10.39
	Precentral gyrus	4	34	18	58	10.21
Dorsal rostral putamen	Insula	13	38	8	6	13.49
	Superior frontal gyrus	9	36	46	30	12.63
	Superior parietal lobule	7	10	68	56	12.52
	Inferior parietal lobule	40	62	30	22	12.25
	Middle temporal gyrus	19	46	74	18	11.05
	Inferior frontal gyrus	44	52	4	22	10.16
	Cerebellum lobule V		12	56	26	12.12
Ventral rostral putamen	Superior temporal gyrus	21	58	24	12	17.79
	Medial frontal gyrus (SMA/pre-SMA)	6	-2	0	56	15.22
	Precentral gyrus	4	44	12	54	12.14
	Superior frontal gyrus	9	40	40	32	11.84
	Middle frontal gyrus	9	32	44	26	11.04
	Parahippocampal gyrus	30	4	48	4	10.81
	Cuneus	19	16	92	28	14.41
	Medulla		4	30	36	10.91

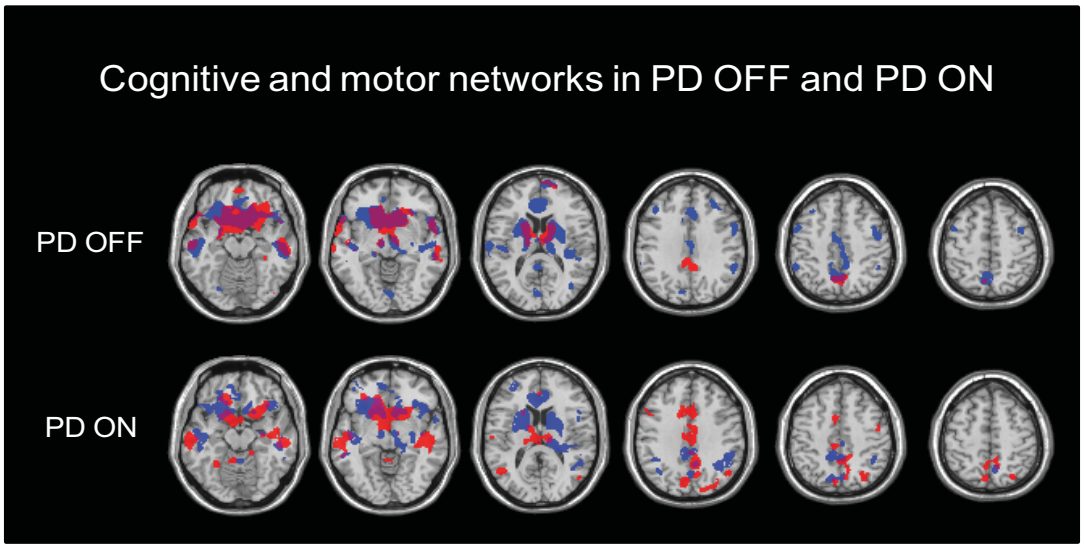


FIGURE S2 | Cognitive (seed: inferior ventral striatum, red) and motor (seed: dorsal rostral putamen, blue) networks in PD OFF (top) and PD ON (bottom). $z = -15, -5, 15, 35, 45, 55$. FWE-corrected $p < 0.05$.

Table S3 | MNI coordinates of the local maxima of brain regions showing functional connectivity with the six striatal seed regions in PD OFF.

Seed	Region	BA	MNI coordiates			*T*-value
			x	*y*	*z*	
Inferior ventral striatum	Superior frontal gyrus	10	4	66	10	6.92
	Superior frontal gyrus	11	–6	60	–20	6.84
	Posterior cingulate gyrus	23	0	–50	22	6.54
	Superior temporal gyrus	41	44	–32	8	6.43
	Cerebellum Cr I		24	–84	–26	8.35
Superior ventral striatum	Medial frontal gyrus	10	4	68	10	10.08
	Superior frontal gyrus	9	–26	48	28	7.3
	Inferior frontal gyrus	9	56	12	24	6.58
	Middle frontal gyrus	6	–44	6	54	6.54
	Paracentral lobule	5	–8	–44	56	5.96
	Precuneus	7	–8	–66	52	6.86
	Cerebellum lobule VI		42	–70	–18	6.66
Dorsal caudate	Inferior temporal gyrus	20	–54	–26	–14	8.39
	Posterior cingulate gyrus	31	–2	–46	26	7.03
	Supramarginal gyrus	40	–50	–54	36	6.76
	Superior frontal gyrus	10	–32	64	–2	6.71
	Superior temporal gyrus	13	52	–40	20	6.69
	Middle frontal gyrus	8	–34	26	46	6.28
	Precuneus	7	–8	–58	44	6.25
Dorsal caudal putamen	Medial frontal gyrus (SMA)	6	–2	–8	76	7.59
	Middle frontal gyrus	6	38	2	56	7.45
	Middle frontal gyrus	9	–42	28	34	6.93
	Intraparietal lobule	40	48	–46	26	6.54
	Medulla		8	–26	–34	7.16
Dorsal rostral putamen	Posterior cingulate gyrus	30	–2	–48	18	7.22
	Middle frontal gyrus	6	32	0	62	7.14
	Precentral gyrus	4	50	–6	44	6.71
	Precuneus	7	–4	–62	54	6.95
	Lingual gyrus	18	2	–82	–6	6.76
	Intraparietal lobule	40	–56	–46	44	6.62
	Superior frontal gyrus	9	26	50	28	6.62
	Middle frontal gyrus	9	–42	30	36	6.55
	Cuneus	19	–14	–76	30	6.35
	Middle temporal gyrus	39	42	–72	10	6.25
	Cerebellum Cr I		–24	–82	–24	7.68
Ventral rostral putamen	Middle frontal gyrus	9	–30	40	36	8.62
	Middle frontal gyrus	10	38	54	0	6.57
	Superior frontal gyrus	10	12	58	22	7.79
	Medial frontal gyrus (SMA)	6	–2	–10	78	7.47
	Lingual gyrus	19	14	–60	2	6.76
	Middle occipital gyrus	19	34	–90	16	6.28
	Pons		6	–18	–24	9.51

Table S4 | MNI coordinates of the local maxima of brain regions showing functional connectivity with the six striatal seed regions in PD ON.

Seed	Region	BA	MNI coordinates			*T*-value
			x	*y*	*z*	
Inferior ventral striatum	Middle temporal gyrus	21	46	–12	–12	10.23
	Postcentral gyrus	7	–4	–60	64	9.89
	Middle frontal gyrus	8	–48	12	42	9.61
	Middle frontal gyrus	6	44	4	40	7.58
	Superior temporal gyrus	39	–46	–60	18	9.32
	Anterior cingulate gyrus	24	6	12	36	8.64
	Inferior frontal gyrus	45	–54	30	4	8.19
	Angular gyrus	39	48	–64	36	7.85
	Inferior parietal lobule	7	30	–72	48	7.7
	Cerebellum lobule III		–12	–40	–22	9.39
	Cerebellum lobule IV		–30	–50	–20	8.86
Superior ventral striatum	Fusiform gyrus	20	–62	–18	–22	14.32
	Superior temporal gyrus	22	–62	12	–2	9.98
	Precentral gyrus	6	44	–2	26	8.98
	Supramarginal gyrus	40	–56	–54	36	7.82
Dorsal caudate	Middle temporal gyrus	21	–50	–16	–12	10.12
	Supramarginal gyrus	40	–40	–56	36	9.13
	Inferior parietal lobule	40	36	–52	38	9
	Medial frontal gyrus (pre-SMA)	6	0	12	44	9.01
	Middle frontal gyrus	9	40	8	42	8.96
	Middle frontal gyrus	10	26	54	2	7.57
	Posterior cingulate gyrus	31	–10	–50	28	8.69
Dorsal caudal putamen	Inferior frontal gyrus	47	58	16	–2	11.06
	Posterior cingulate gyrus	31	10	–40	30	7.91
	Supramarginal gyrus	40	60	–48	22	7.86
Dorsal rostral putamen	Posterior cingulate gyrus	31	–12	–46	28	11.27
	Inferior temporal gyrus	20	–60	–20	–26	10.38
	Inferior parietal lobule	40	38	–52	38	9.65
	Supramarginal gyrus	40	–42	–44	36	7.58
	Red nucleus		–10	–18	–2	10.44
	Cerebellum lobule IV		2	–48	–10	7.44
Ventral rostral putamen	Superior temporal gyrus	22	52	–14	0	11.37
	Supramarginal gyrus	40	60	–52	22	10.33
	Fusiform gyrus	37	52	–66	–16	10.31
	Precuneus	7	10	–60	44	9.37
	Anterior cingulate gyrus	32	0	46	–4	9.14
	Superior frontal gyrus	8	–14	40	38	8.15
	Middle frontal gyrus	9	–40	8	38	6.99
	Pons		–6	–20	–24	8.77

Table S5 | MNI coordinates of the local maxima of brain regions showing greater functional connectivity in PD OFF than controls.

Seed	Region	BA	MNI coordinates			*T*-value
			x	*y*	*z*	
Inferior ventral striatum	Dorsomedial thalamus		0	–8	12	4.35
Dorsal caudal putamen	Inferior temporal gyrus	20	48	–10	–20	4.47
	Inferior temporal gyrus	21	–58	–16	–16	3.73
	Middle temporal gyrus	21	54	–18	–8	3.52
	Anterior cingulate gyrus	24	–12	28	–4	4.02
Dorsal rostral putamen	Rectal gyrus	11	12	30	–18	4.42
	Middle temporal gyrus	21	50	–6	–24	3.93
	Inferior temporal gyrus	20	–46	–8	–32	3.81
	Anterior cingulate gyrus	32	–18	34	–8	3.62
	Orbital frontal gyrus	47	–38	26	–22	3.93
	Medial frontal gyrus	10	10	60	8	3.43
Ventral rostral putamen	Inferior frontal gyrus	11	–40	28	–18	3.54

Table S6 | MNI coordinates of the local maxima of brain regions showing greater functional connectivity in controls than PD ON.

Seed	Region	BA	MNI coordinates			*T*-value
			x	*y*	*z*	
Inferior ventral striatum	Precentral gyrus	4	–34	–20	66	4.13
	Superior frontal gyrus	11	–24	52	–12	3.87
	Superior frontal gyrus	10	–22	66	–8	3.82
	Medial frontal gyrus (SMA)	6	–6	–22	68	3.73
	Lingual gyrus	18	18	–92	–6	3.73
	Cerebellum Cr II		–18	–82	–40	4.63
Superior ventral striatum	Postcentral gyrus	3	38	–30	64	5.25
	Precentral gyrus	4	–30	–16	68	4.93
	Superior frontal gyrus	6	–26	2	64	3.54
	Medial frontal gyrus (SMA)	6	–6	–22	72	4.07
	Middle frontal gyrus	6	–32	10	50	3.7
	Middle frontal gyrus	9	42	40	30	4.53
	Middle frontal gyrus	10	–26	66	18	3.91
	Middle frontal gyrus	8	–22	26	44	3.84
	Inferior frontal gyrus	46	48	48	4	4.23
	Superior parietal lobule	7	18	–74	54	3.88
	Cuneus	18	–18	–90	26	3.68
	Lingual gyrus	17	6	–92	–4	3.85
	Globus pallidus		–18	–8	–6	3.78
Dorsal caudate	Postcentral gyrus	3	38	–30	70	5.99
	Precentral gyrus	4	–30	–16	70	5.68
	Precentral gyrus	6	32	–10	68	3.99
	Middle frontal gyrus	9	42	42	30	5.17
	Middle frontal gyrus	10	–36	62	18	4.11
	Inferior frontal gyrus	46	48	46	4	4.07
	Inferior frontal gyrus	44	–48	14	32	3.97
	Superior parietal lobule	7	18	–74	54	4.89
	Inferior parietal lobule	40	–50	–40	28	3.77
	Middle temporal gyrus	21	–46	–54	6	3.61
	Cuneus	18	–16	–102	–2	3.59
	Caudate		–18	–18	24	3.86
Dorsal caudal putamen	Precentral gyrus	4	–36	–24	64	4.78
	Precentral gyrus	6	22	–16	74	4.23
	Medial frontal gyrus (pre-SMA)	6	–6	14	52	3.97
	Medial frontal gyrus	6	18	–16	50	3.84
	Medial frontal gyrus	32	–10	28	34	4.06
	Middle frontal gyrus	8	–30	34	40	3.96
	Middle frontal gyrus	9	36	12	34	3.46
	Superior frontal gyrus	10	–32	54	26	3.71
	Superior parietal lobule	7	–42	–54	62	4.17
	Lingual gyrus	17	–4	–92	–4	3.67
	Postcentral gyrus	2	–40	–78	–2	3.46
	Putamen		–18	–10	0	3.87
Dorsal rostral putamen	Precentral gyrus	4	–58	–20	40	3.57
	Paracentral lobule	5	16	–36	48	3.47
	Postcentral gyrus	2	–68	–24	34	3.76
	Superior frontal gyrus	6	–36	–8	70	7.28
	Superior frontal gyrus	10	–36	56	26	4.68
	Superior frontal gyrus	8	–20	48	50	4.4
	Middle frontal gyrus	8	46	22	46	4.06
	Medial frontal gyrus	32	–10	24	36	3.7

(Continued)

Table S6 | ***Continued***

Seed	Region	BA	MNI coordinates			*T*-value
			x	*y*	*z*	
	Middle frontal gyrus	9	40	48	28	3.73
	Middle frontal gyrus	10	34	58	22	3.56
	Inferior frontal gyrus	44	–44	16	12	4.23
	Superior parietal lobule	7	–18	–82	52	4.41
	Superior temporal gyrus	22	–56	–32	6	4
	Middle temporal gyrus	39	–36	–70	24	3.7
	Middle occipital gyrus	19	–40	–74	8	4.01
	Lingual gyrus	18	–4	–92	–4	3.91
	Precuneus	7	–4	–62	68	3.67
Ventral rostral putamen	Precentral gyrus	4	–36	–26	70	4.9
	Precentral gyrus	6	–38	16	8	4.39
	Medial frontal gyrus (pre-SMA)	6	–2	4	56	4.32
	Middle frontal gyrus	9	–40	42	36	4.27
	Inferior frontal gyrus	46	–58	36	8	4.08
	Superior parietal lobule	5	16	–36	52	4.66
	Lingual gyrus	18	18	–92	–6	4.45
	Cuneus	17	–32	–78	10	3.89
	Fusiform gyrus	37	–48	–48	–10	4.06
	Transverse temporal gyrus	41	52	–16	12	3.85
	Cerebellum lobule VIIIA		22	–72	–48	4.42
	Cerebellum Cr II		–8	–78	–42	3.87

Table S7 | Brain regions showing greater functional connectivity in PD OFF than PD ON.

Seed	Region	BA	MNI coordinates			*T*-value
			x	*y*	*z*	
Vsi	Orbital gyrus	47	4	32	–24	4.81
	Rectal gyrus	11	–2	16	–18	4.75
	Inferior frontal gyrus	47	–10	18	–18	4.41
	Superior frontal gyrus	10	26	66	–8	4.74
	Superior frontal gyrus	11	–20	68	–10	4.62
	Lingual gyrus	18	6	–80	–4	4.05
	Cerebellum Cr II		26	–84	–26	4.99
	Cerebellar lobe VI		–14	–78	–18	4.01
	Putamen		–30	–8	2	3.96
VSs	Superior temporal gyrus	38	52	8	–6	4.94
	Inferior frontal gyrus	46	52	44	6	4.36
	Superior frontal gyrus	10	28	60	24	4.33
	Precentral gyrus	6	58	8	36	3.88
	Dorsomedial thalamus		4	–12	8	5.54
DC	Middle frontal gyrus	46	48	36	26	4.27
	Middle frontal gyrus	8	58	8	38	4.06
	Dorsomedial thalamus		6	–14	6	4.48
DCP	Precentral gyrus	4	32	–26	62	4.32
	Precentral gyrus	6	–44	–16	64	4.52
	Middle frontal gyrus	6	32	0	60	4.54
	Middle frontal gyrus	8	–36	26	44	3.81
	Middle temporal gyrus	21	58	–14	–8	4.34
	Middle occipital gyrus	19	44	–80	14	4.08
	Cuneus	19	–18	–90	32	3.92
	Postcentral gyrus	2	56	–20	44	3.9
DRP	Middle temporal gyrus	21	–56	–22	–12	4.52
	Middle frontal gyrus	8	–40	30	46	4.11
	Precentral gyrus	4	58	–18	42	4.07
	Precentral gyrus	6	58	–6	38	3.96
	Dorsomedial thalamus		6	–16	8	4
VRP	Inferior parietal lobule	40	56	–26	32	4.43
	Postcentral gyrus	3	–40	–28	60	4.25
	Postcentral gyrus	1	–54	–24	54	4.15
	Precentral gyrus	6	–42	–18	64	3.94
	Cuneus	19	–4	–80	32	3.79
	Precuneus	7	–8	–64	50	3.69
	Cerebellum Cr I		26	–84	–28	4.09

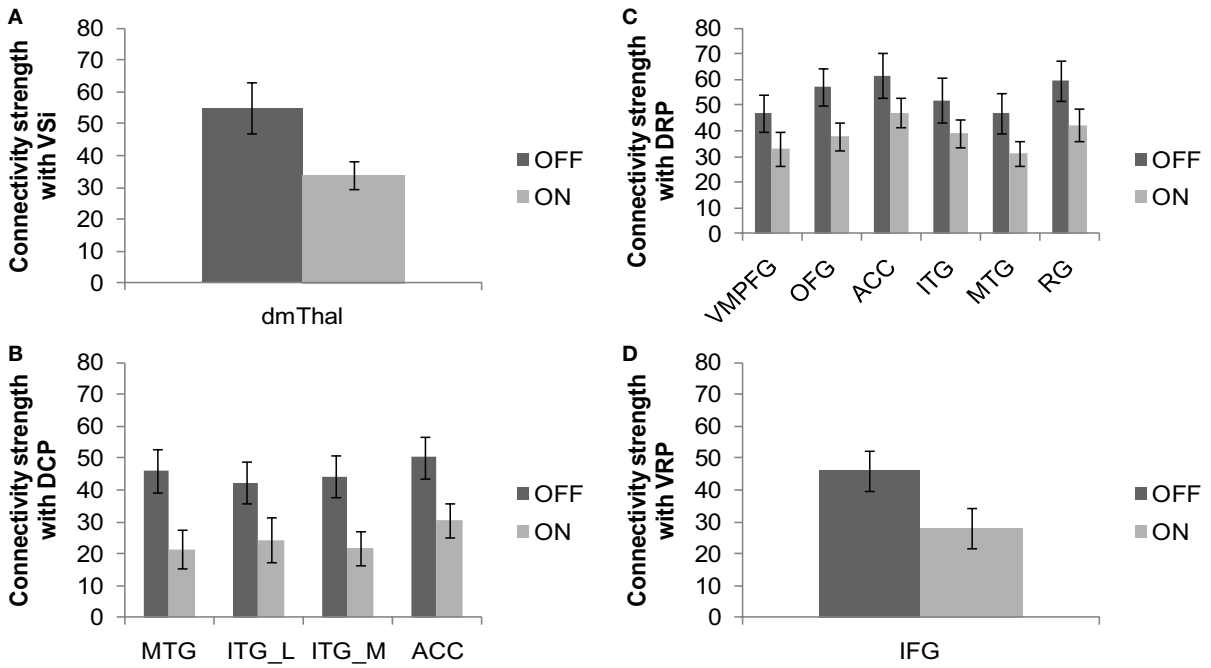


FIGURE S3 | Connectivity strength difference between PD OFF and PD ON in ROIs defined in PD OFF versus controls comparison. Connectivity strength between VSi **(A)**, VSs **(B)**, DRP **(C)**, and VRP **(D)** and each of the ROIs are compared across PD OFF and PD ON. VSi, inferior ventral striatum; dmThal, dorsomedial thalamus; DCP, dorsal caudal putamen; MTG, middle temporal gyrus; ITG_L, inferior temporal gyrus in the less affected side; ITG_R, inferior temporal gyrus in the more affected side; ACC, anterior cingulated cortex; DRP; dorsal rostral putamen; VMPFC, ventromedial prefrontal gyrus; OFG, orbital frontal gyrus; RG, rectal gyrus; VRP, ventral rostral putamen; inferior frontal gyrus. Error bars indicate standard error. For all comparisons we found significant main effect of medication status showing decrease in strength of connectivity in PD ON compared to PD OFF with the exception of DRP and VRP which showed marginally significant medication main effects.

frontiers in
SYSTEMS NEUROSCIENCE

ORIGINAL RESEARCH ARTICLE
published: 20 September 2010
doi: 10.3389/fnsys.2010.00041

Whole brain resting-state analysis reveals decreased functional connectivity in major depression

Ilya M. Veer[1,2,3], Christian F. Beckmann[4,5], Marie-José van Tol[1,6], Luca Ferrarini[7], Julien Milles[7], Dick J. Veltman[8], André Aleman[9], Mark A. van Buchem[1,2], Nic J. van der Wee[1,6] and Serge A.R.B. Rombouts[1,2,3]*

[1] *Leiden Institute for Brain and Cognition, Leiden, Netherlands*
[2] *Department of Radiology, Leiden University Medical Center, Leiden, Netherlands*
[3] *Institute of Psychology, Leiden University, Leiden, Netherlands*
[4] *Oxford Centre for Functional Magnetic Resonance Imaging of the Brain, University of Oxford, Oxford, UK*
[5] *Department of Clinical Neuroscience, Imperial College London, London, UK*
[6] *Department of Psychiatry, Leiden University Medical Center, Leiden, Netherlands*
[7] *Department of Radiology, Division of Image Processing, Leiden University Medical Center, Leiden, Netherlands*
[8] *Department of Psychiatry, VU Medical Center, Amsterdam, Netherlands*
[9] *BCN NeuroImaging Center, University of Groningen, Groningen, Netherlands*

Edited by:
Silvina G. Horovitz, National Institutes of Health, USA

Reviewed by:
Cameron Craddock, Department of Neuroscience, Baylor College of Medicine, USA
Martin Walter, Otto-von-Guericke-Universität Magdeburg, Germany

****Correspondence:***
Ilya M. Veer, Department of Radiology, Leiden University Medical Center, Postzone C2-S, P.O. Box 9600, 2300 RC Leiden, Netherlands.
e-mail: i.m.veer@lumc.nl

Recently, both increases and decreases in resting-state functional connectivity have been found in major depression. However, these studies only assessed functional connectivity within a specific network or between a few regions of interest, while comorbidity and use of medication was not always controlled for. Therefore, the aim of the current study was to investigate whole-brain functional connectivity, unbiased by *a priori* definition of regions or networks of interest, in medication-free depressive patients without comorbidity. We analyzed resting-state fMRI data of 19 medication-free patients with a recent diagnosis of major depression (within 6 months before inclusion) and no comorbidity, and 19 age- and gender-matched controls. Independent component analysis was employed on the concatenated data sets of all participants. Thirteen functionally relevant networks were identified, describing the entire study sample. Next, individual representations of the networks were created using a dual regression method. Statistical inference was subsequently done on these spatial maps using voxel-wise permutation tests. Abnormal functional connectivity was found within three resting-state networks in depression: (1) decreased bilateral amygdala and left anterior insula connectivity in an affective network, (2) reduced connectivity of the left frontal pole in a network associated with attention and working memory, and (3) decreased bilateral lingual gyrus connectivity within ventromedial visual regions. None of these effects were associated with symptom severity or gray matter density. We found abnormal resting-state functional connectivity not previously associated with major depression, which might relate to abnormal affect regulation and mild cognitive deficits, both associated with the symptomatology of the disorder.

Keywords: major depression, resting-state functional magnetic resonance imaging, functional connectivity, independent component analysis, amygdala

INTRODUCTION

Patients suffering from a major depressive episode typically show pervasive depressed mood or anhedonia, accompanied by several cognitive and physical symptoms (American Psychiatric Association, 1994). The apparent heterogeneity in depressive symptom domains (i.e., mood, cognition, motor, and vegetative) is unlikely to be explained by the (functional) breakdown of a single brain area (Davidson et al., 2002). It has thus been proposed that depressive symptoms are associated with dysregulation of a brain network encompassing large parts of the prefrontal cortex (PFC), limbic areas, and subcortical structures (Mayberg, 1997, 2003; Drevets et al., 2008).

Based on data from blood flow and glucose metabolism SPECT and PET studies, and more recently task-related functional MRI (fMRI) studies, current models for depression postulate that ventral and dorsal subsystems of this brain network are differentially affected in this disease (Mayberg, 2003; Drevets et al., 2008). An imbalanced functional integration of these subsystems may lead to a heightened response to negative information in ventral regions (bottom–up) on the one hand and a failure to regulate this response through dorsal regions (top–down) on the other (Phillips et al., 2003). For example, engagement of lateral PFC regions has been linked to efficient top–down regulation of affective responses (Dolcos et al., 2006; Pessoa, 2008), a mechanism that has been shown to fail in patients suffering depression (Johnstone et al., 2007).

Over the last decade, studying such functional interactions between brain regions or systems has become increasingly important for understanding the dynamic interactions between neural systems in both health and disease (Stephan et al., 2008). In depression, several studies have shown abnormal functional connectivity (FC) during both cognitive and emotional task paradigms (Urry et al., 2006; Johnstone et al., 2007; Chen et al., 2008; Matthews et al., 2008),

which have already provided valuable insights on how dysfunctional interactions between brain regions may relate to abnormal behavioral response patterns in depressed patients. However, it might also be beneficial to explore whether these connections are compromised in the absence of goal-directed (i.e., task-induced) behavior. For example, resting-state (RS; i.e., without external task demands) FC may be able to predict how the brain responds to an externally cued task (Mennes et al., 2010). Studies employing RS-FC have shown to be successful in mapping large-scale connectivity patterns in the brain (Biswal et al., 1995; Lowe et al., 1998; Fox and Raichle, 2007). In addition, these so-called resting-state networks (RSNs) are found consistently across participants and over time (Damoiseaux et al., 2006; Shehzad et al., 2009) and show a remarkable overlap with patterns of task-induced activity (Smith et al., 2009).

RS-fMRI studies in major depression have recently reported on altered FC in several areas within the proposed network model of depression (Mayberg, 1997; Drevets et al., 2008). Decreased connectivity of the dorsal anterior cingulate cortex (ACC) with the medial thalamus and left pallidostriatum was found in patients suffering from depression, and a trend for decreased connectivity between the ACC and the amygdala (Anand et al., 2005a,b). In another study, depressive patients were found to show increased connectivity of the subgenual ACC (cg25) and the thalamus within the default mode network (DMN) (Greicius et al., 2007), a canonical RSN (Raichle et al., 2001; Greicius et al., 2003). This finding was partially confirmed by a recent study showing unique cg25, but not thalamic, connectivity within the DMN in the depression group (Zhou et al., 2009). It must be noted, however, that for this effect only qualitative comparisons were carried out between the groups. Additionally, these researchers found increased intra-network connectivity in depression between regions of the DMN, and within the task positive network (TPN), which is associated with attention and working memory (Fox et al., 2005), together with increased anticorrelations between regions of the two networks (Zhou et al., 2009). A last study did not show any FC differences between major depressive disorder (MDD) patients and controls using conventional statistics (Craddock et al., 2009). However, the authors were able to discriminate between patients and controls using support vector classification. In addition to the altered FC found in several task-related fMRI studies, these RS findings further support the idea of dysfunctional interactions as a core feature of depressive symptomatology.

To date, RS-fMRI studies focusing on depression examined connectivity in a limited number of predefined regions or networks of interest, thereby not fully exploring the data as acquired with RS-fMRI. That is, recent studies have identified several other networks of simultaneously oscillating brain regions (Beckmann et al., 2005; Damoiseaux et al., 2006), which may represent multiple functional domains. Furthermore, in some of the studies in MDD, comorbidity and use of medication could not be ruled out as potential confounders.

The aim of the present study was to investigate FC patterns using RS-fMRI in medication-free patients with MDD without comorbidity, and carefully matched healthy controls. Rather than focusing on predefined regions or networks of interest, we adopted an inclusive (exploratory) approach by investigating whole-brain RS-fMRI FC at the network level, ensuring the optimal use of the wealth of information present in the data. Based on the current neurobiological models for depression and the RS studies described above, we expected that altered connectivity would be observed in those RSNs that include areas known to be associated with affective (including ventral prefrontal cortex and limbic areas) and more cognitive (including lateral prefrontal and parietal areas) processing, as well as RSNs that show cortico–striatal connectivity.

MATERIALS AND METHODS

PARTICIPANTS

Participants were selected from the MRI study of the large-scale longitudinal multi-center Netherlands Study on Depression and Anxiety (NESDA)[1] (Penninx et al., 2008), which is designed to examine the long-term course and consequences of depression and anxiety disorders. Participants were recruited through general practitioners, primary care and specialized mental care institutions. For the current study, all participants were required to be fluent in Dutch and right-handed. Patients were included when they met the following criteria: (1) a recent diagnosis (i.e., within 6 months before inclusion) of MDD as indexed by the fourth edition of the diagnostic and statistical manual of mental disorders (DSM-IV) (American Psychiatric Association, 1994) based on the Composite Interview Diagnostic Instrument (CIDI; lifetime version 2.1), administered by a trained clinical interviewer, (2) no current comorbidity with other DSM-IV axis-1 disorders, and (3) no use of psychotropic medication. Exclusion criterion for controls was a history of any DSM-IV axis-1 disorder based on the CIDI. Axis-2 disorders were not assessed in this study. Exclusion criteria for all participants were: (1) daily use of medication or other substances known to affect the central nervous system; (2) the presence or history of major internal or neurological disorders; (3) history of dependency on or recent abuse of alcohol and/or drugs (i.e., in the past year) as diagnosed with the CIDI; (4) hypertension; (5) general MRI-contraindications. None of the included patients underwent treatment for depression.

For the present study, imaging data were available from 23 MDD patients who fulfilled the aforementioned criteria. Two patients were removed from the sample due to excessive head motion during scan acquisition (>3 mm in any of the acquired volumes). Two other patients were removed because no proper age-matched healthy control (HC) was available. For each of the remaining 19 MDD patients, we included in a pair-wise fashion an age- and sex-matched healthy control subject, although education was higher in controls (see **Table 1**). The mean Montgomery–Asberg depression rating scale (MADRS) (Montgomery and Asberg, 1979) symptom severity score for the MDD group was 14.21, SD 9.62, with five participants considered to be in remission (MADRS score <10) at the time of the imaging study. Written informed consent was obtained from all participants and none received compensation except for reimbursement of travel expenses. The study was approved by the Central Ethics Committees of the three participating medical centers (i.e., Leiden University Medical Center [LUMC], Amsterdam Medical Center [AMC], and University Medical Center Groningen [UMCG]).

DATA ACQUISITION

Participants were scanned at one of the three participating centers within 8 weeks after completion of NESDA baseline interview (Penninx et al., 2008). RS-fMRI data were acquired at the end of

[1]www.nesda.nl

Table 1 | Demographic and clinical characteristics for the study sample.

	Healthy controls ($n = 19$)	Major depressive disorder ($n = 19$)
Age	36.11 ± 10.56 (21–53) years	36.21 ± 9.7 (20–57) years
Gender	8 male/11 female	8 male/11 female
Education *	14 ± 2.67 (9–18) years	12.21 ± 2.35 (9–18) years
MADRS **	0.63 ± 1.07 (0–3)	14.21 ± 9.62 (0–33)

*Note: MADRS, Montgomery–Asberg depression rating scale. Except for sex, all values are mean ± SD (range). *p < 0.05, **p < 0.001, using independent sample t-tests.*

the fixed imaging protocol: after completion of three task-related functional MRI runs (to be reported elsewhere) and the acquisition of an anatomical scan (scan sequence: Tower of London, word encoding, T_1-weighted scan, word recognition, perception of facial expression). In the darkened MR room participants were instructed to lie still with their eyes closed and not to fall asleep. Compliance to these instructions was verified as part of the exit interview.

Imaging data were acquired on a Philips 3.0-T Achieva MRI scanner using a six- (Amsterdam) or eight-channel (Groningen and Leiden) SENSE head coil (Philips Medical Systems, Best, The Netherlands). RS-fMRI data were acquired using T_2^*-weighted gradient-echo echo-planar imaging with the following scan parameters in Amsterdam and Leiden: 200 whole-brain volumes; repetition time (TR) = 2300 ms; echo time (TE) = 30 ms; flip angle = 80°; 35 axial slices; no slice gap; FOV = 220 × 220 mm; in plane voxel resolution = 2.3 mm × 2.3 mm; slice thickness = 3 mm; same in Groningen, except: TE = 28 ms; 39 axial slices; in plane voxel resolution = 3.45 mm × 3.45 mm. For registration purposes and analysis of gray matter density, a high resolution T_1-weighted image was acquired with the following scan parameters: repetition time (TR) = 9 ms; echo time (TE) = 3.5 ms; flip angle = 8°; 170 sagittal slices; no slice gap; FOV = 256 × 256 mm; in plane voxel resolution = 1 mm × 1 mm; slice thickness = 1 mm.

DATA PREPROCESSING

The preprocessing of RS-fMRI images was carried out using FEAT (FMRI Expert Analysis Tool) Version 5.90, part of FSL (FMRIB's Software Library[2]) (Smith et al., 2004). The following processing steps were applied: motion correction (Jenkinson et al., 2002), removal of non-brain tissue (Smith, 2002), spatial smoothing using a Gaussian kernel of 4-mm full width at half maximum, grand-mean intensity normalization of the entire 4D dataset by a single multiplicative factor, high-pass temporal filtering (Gaussian-weighted least-squares straight line fitting, with sigma = 50 s; 0.01 Hz cut-off) and registration to the high resolution T_1 and MNI-152 standard space (T_1 standard brain averaged over 152 subjects; Montreal Neurological Institute, Montreal, QC, Canada) images (Jenkinson and Smith, 2001; Jenkinson et al., 2002). Normalized 4D data sets were subsequently resampled to 4-mm isotropic voxels to reduce computational burden in the following analysis steps.

EXTRACTING RESTING-STATE NETWORKS

Standard group independent component analysis (ICA) was carried out using probabilistic ICA (PICA) (Beckmann and Smith, 2004) as implemented in FSL's Multivariate Exploratory Linear Decomposition into Independent Components (MELODIC) Version 3.09. Default group PICA processing steps were applied to the individual preprocessed and normalized data sets: masking out non-brain voxels, voxel-wise de-meaning of the data, and normalization of the voxel-wise variance based on all data sets. Subsequently, data sets from both MDD patients and HCs were concatenated in time to create a single 4D data set, which was then projected into a 20-dimensional subspace using principal component analysis. Next, the data set was decomposed into 20 sets of independent vectors which describe signal variation across the temporal (time-courses) and spatial (maps) domain by optimizing for non-Gaussian spatial source distributions using the FastICA algorithm (Hyvarinen, 1999). At this model order selection, it has been shown that most of the frequently observed large-scale RSNs can be discerned in the data when using this method (Abou-Elseoud et al., 2010). The resulting estimated component maps were divided by the standard deviation of the residual noise and thresholded at a posterior probability threshold of $p > 0.5$ (i.e., an equal loss is placed on false positives and false negatives) by fitting a Gaussian/Gamma mixture model to the histogram of intensity values (Beckmann and Smith, 2004).

STATISTICAL ANALYSES

Subject specific statistical maps were created to test for differences between the MDD and HC groups in the identified components. This was done adopting a dual regression procedure (as previously described in: Filippini et al., 2009). In short, multiple linear regression of the *z*-thresholded Group PICA maps against the preprocessed individual 4D resampled data sets yielded a subject specific time course for each component separately. Next, multiple linear regression of these time courses was carried out against the pre-processed individual 4D data sets in the standard space resolution (i.e., 2 mm), thereby providing better spatial specificity. This resulted in subject specific *z*-maps for each of the 20 components.

Prior to statistical inference 13 out of the 20 components were identified as anatomically and functionally relevant RSNs upon visual inspection, the seven others reflecting distinct artifacts resulting from head motion, fluctuations in cerebrospinal fluid, and physiological or scanner noise. Criteria for inclusion were: signal within the low frequency range of 0.1–0.01 Hz (Lowe et al., 1998; Cordes et al., 2001), connectivity patterns were mainly located in gray matter, and presence of coherent clusters of voxels (De Martino et al., 2007). Inference was carried out only on the subject specific *z*-maps of the 13 relevant RSNs. Statistical difference was assessed non-parametrically using FSL's Randomize tool, Version 2.1, incorporating threshold-free cluster enhancement (TFCE) (Smith and Nichols, 2009). Besides modeling regressors for each of the two groups, additional nuisance regressors describing scanner location and age were

[2]www.fmrib.ox.ac.uk/fsl

added to the model. Separate null distributions of *t*-values were derived for the contrasts reflecting the between and within group effects by performing 5000 random permutations and testing the difference between groups or against zero for each iteration (Nichols and Holmes, 2002). For each RSN, the resulting statistical maps were thresholded at $p \leq 0.05$ (TFCE-corrected for family-wise errors) for the group main effects. Between-group effects were thresholded controlling the local false discovery rate (FDR) (Efron, 2004; Filippini et al., 2009) at $q \leq 0.01$ and subsequently spatially masked with a binary representation of the conjunction of the group main effects images. Note that we applied a more stringent FDR threshold than the more generally accepted $q \leq 0.05$, together with masking for the group main effects, to decrease susceptibility to type 1 errors when testing multiple RSNs.

GRAY MATTER MORPHOLOGY

Major depressive disorder-related gray matter (GM) abnormalities have been found previously in several regions of the brain, although not always consistently (Sheline, 2003; Lorenzetti et al., 2009). To test whether altered FC in the present study might be explained by MRI-detectable loss of gray matter, a VBM style analysis was run on the acquired high resolution T_1-weighted data sets (Ashburner and Friston, 2000; Good et al., 2001). Using FSL's VBM toolbox, all structural images were first brain extracted, then tissue-type segmented, normalized to MNI-152 standard space and non-linearly registered to each other (e.g., Douaud et al., 2007). Next, standard space binary masks were created from the voxels that covered each RSN (conjunction of the FWE-corrected HC > 0 and MDD > 0 contrast maps) as well as from voxels showing differences between the two groups within the separate networks (local FDR controlled HC > MDD and MDD > HC contrast maps). The binary masks were then used to extract mean gray matter intensity scores within these masks for each of the participants. To rule out the influence of any subtle GM density variations, we included the GM values, from both the difference masks and the RSN as a whole, as regressors in the statistical model (see, e.g., Damoiseaux et al., 2008). Additionally, between-group *t*-tests were carried out on the participants' mean intensity scores derived from each mask using SPSS Version 16.0 (SPSS Inc., Chicago, IL, USA) to test whether the two groups differed in GM density on average. Note that whole brain VBM results of a large sample (including MDD) from the NESDA study will be reported elsewhere.

RESULTS

RESTING-STATE FUNCTIONAL CONNECTIVITY

Thirteen functionally relevant RSNs were found using the group PICA analysis (**Figure 1**). Most of these networks have been described in previous studies using similar methodology and were shown to be stable across participants and over time (Beckmann et al., 2005; Damoiseaux et al., 2006). The assemblies of brain areas shown in these networks covered the primary [1], lateral [2] and medial visual cortex [3], sensory-motor cortex [4], ventral stream [8] auditory cortex [12], the hippocampus–amygdala complex [9], precuneus [7] together with the DMN [13], a network associated with salience processing (Seeley et al., 2007) [10], and networks encompassing areas associated with higher order cognition such as attention [11] and working memory [5, 6].

The presence of all 13 networks found with PICA was confirmed in both the HC and MDD group by testing the main effects of group on the subject specific *z*-maps of these networks (all $p \leq 0.05$, TFCE and FWE-corrected). Between-group differences in the voxel-wise spatial distribution of the FC maps were subsequently revealed in three networks (local FDR-corrected at $q \leq 0.01$) (see **Figure 2** and **Tables 2–4**). Within these networks nearly all differences indicated decreased FC in the MDD group. The first network showed an assembly of functionally connected regions in the auditory cortex (Heschl's gyrus) bilaterally, extending into the pre- and postcentral gyri, as well as more ventral areas known to be involved in affective processing, including the insula and temporal poles bilaterally, the medial PFC (BA 10) and bilateral amygdala. Whereas the amygdala and left insula showed connectivity with the rest of the network in HCs, these regions showed decreased FC in the depressed group. In addition, increased FC in the MDD group was found in the right inferior frontal gyrus (IFG) within this RSN (**Figures 2A,B**, RSN 12). The second network mainly showed FC within the lateral parietal cortex, temporal–occipital junction, and precentral gyrus, which are areas involved in attention and working memory. In addition, the frontal poles were found to be negatively associated with the time course of this network. Reduced FC of the left frontal pole was demonstrated in the MDD group (**Figures 2A,B,** RSN 11). The third network showed functionally integrated areas within the medial occipital cortex, mostly covering Brodmann area 19, involved in visual processing. Although both controls and depressed participants demonstrated this connectivity pattern, a consistent decrease in functional integration of the lingual gyrus was found bilaterally in the MDD group in this RSN (**Figures 2A,B,** RSN 3).

The wide range in MADRS scores in the patient group allowed us to examine the relation between current symptom severity and the strength of the functional connections with the areas showing abnormal connectivity in this study. Within the depression group, Pearson product–moment correlation coefficients were calculated between the MADRS scores and the individual *z*-scores obtained from the affected areas within the corresponding individual component maps. However, no association was found between strength of the FC and symptom severity in any of the affected regions.

GRAY MATTER RESULTS

No differences in mean gray matter were observed between controls and depressed participants in either of the three RSNs as a whole, or in the areas showing between-group differences within these RSNs (all $t_{36} < 1$, all $p > 0.3$). In addition, adding GM density values as covariates in the statistical model did not change the functional connectivity results as described in the previous section. This indicates that the altered FC within the three networks is unlikely to be related to macroscopic (i.e., MRI observable) gray matter abnormalities.

DISCUSSION

In the present study we set out to investigate differences in whole brain FC between medication-free MDD patients without comorbidity, and a group of age- and sex-matched healthy controls using RS-fMRI. It was expected that altered connectivity would be observed in those RSNs which contain regions previously described to show altered RS-FC in depres-

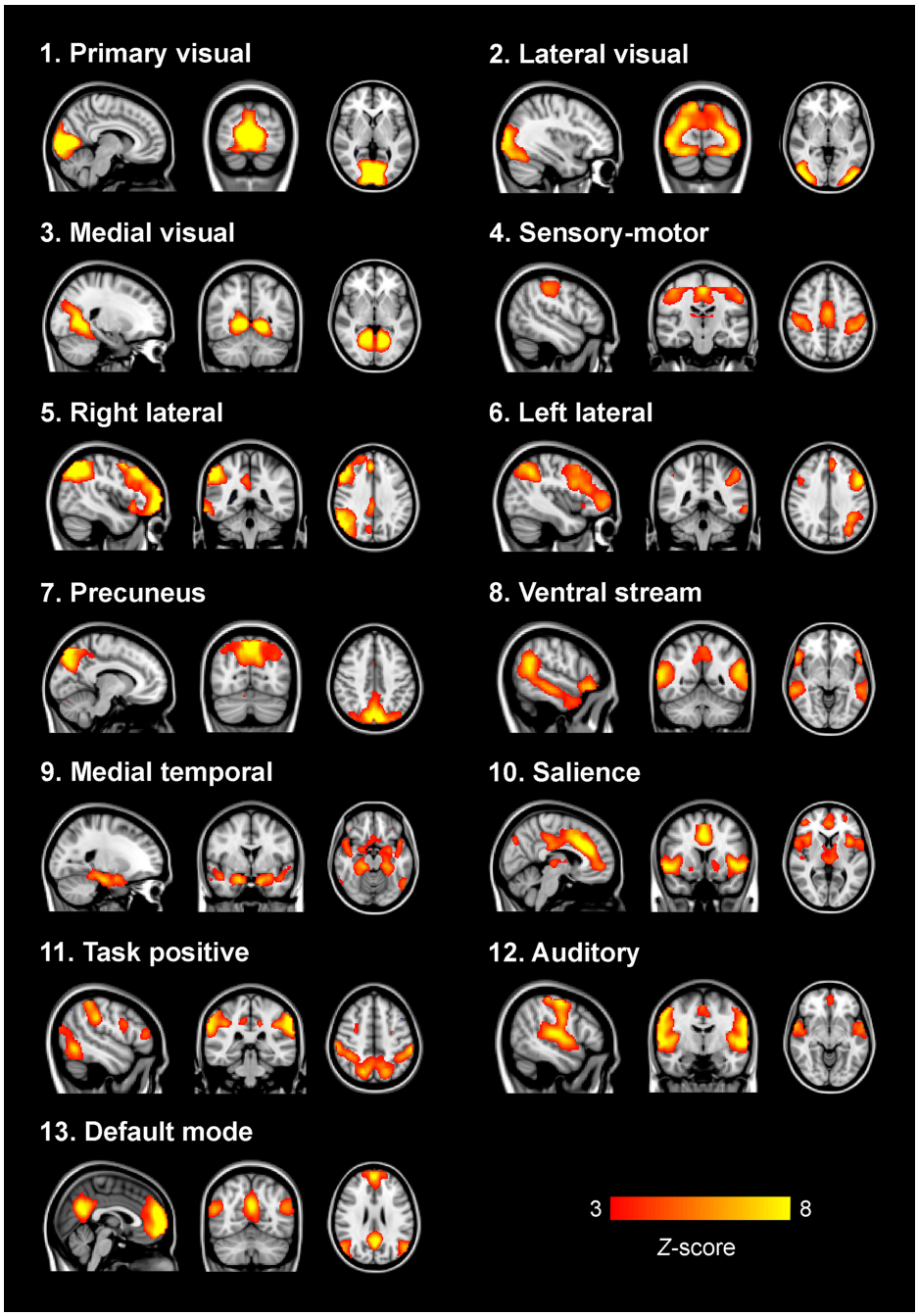


FIGURE 1 | Group ICA functionally relevant resting-state networks. Depicted here are the 13 functionally relevant RSNs resulting from the group PICA step carried out on the concatenated data sets from both patients and controls. Most networks have previously been described (for example in: Beckmann et al., 2005; Damoiseaux et al., 2006) and show assemblies of regions associated with sensory processing, affective processing, and higher order cognitive processes. Images are *z*-statistics, ranging from 3 to 8, overlaid on the MNI-152 standard brain. The left hemisphere of the brain corresponds to the right side in this image.

sion (Anand et al., 2005a,b; Greicius et al., 2007; Zhou et al., 2009), as well as in other regions known to be involved in affective pathology (Phillips et al., 2003; Urry et al., 2006; Johnstone et al., 2007; Chen et al., 2008; Matthews et al., 2008). In this study we mainly found evidence for MDD-related *decreased* FC within three RSNs. These alterations have not been associated with major depression before.

First, altered FC was found in a network with regions known to be involved in emotional processing and affect regulation, such as the anterior insula, dorsal anterior cingulate cortex (dACC), ventromedial prefrontal cortex (vmPFC), temporal poles and amygdala (Pessoa, 2008). MDD patients showed strongly reduced connectivity with the amygdala within this RSN. Coupling between the vmPFC and amygdala has previously been found during downregulation of

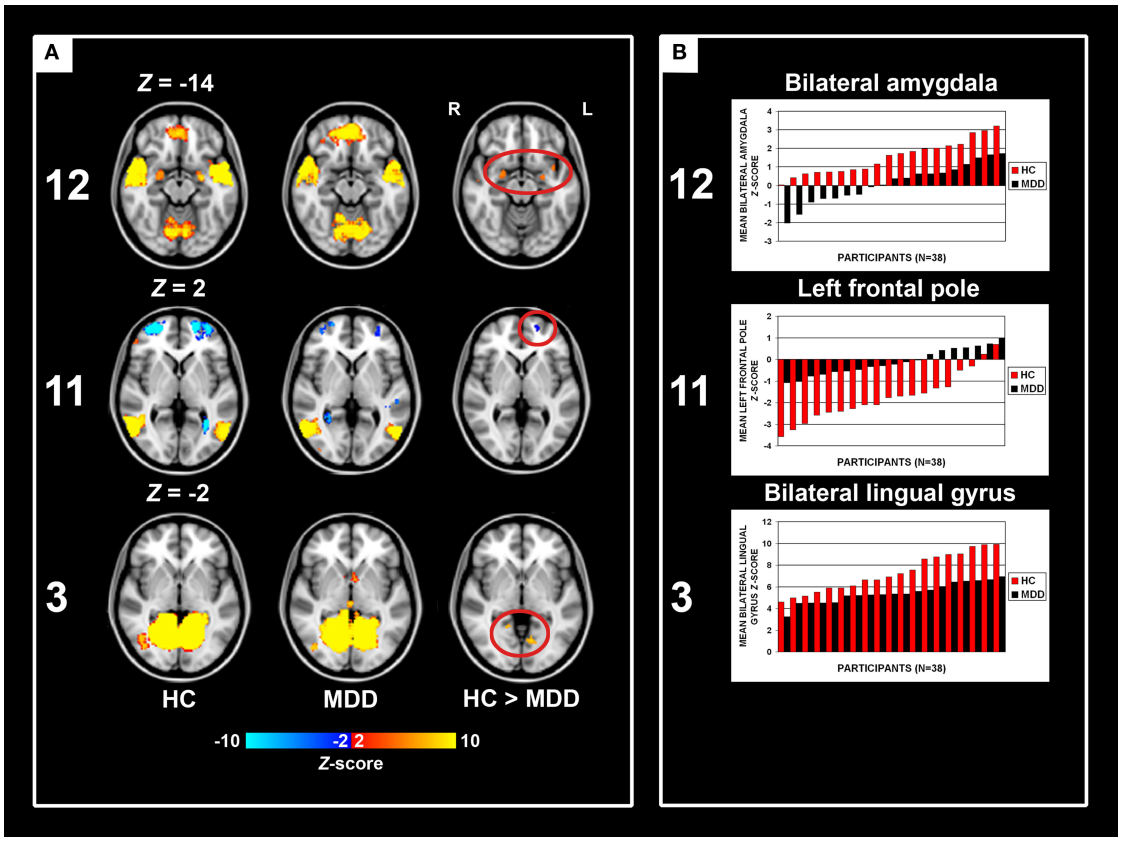


FIGURE 2 | Group main effects and between-group effects. Numbering corresponds to the networks depicted in **Figure 1**. **(A)** Depicted here are the group main and between-group effects for three RSNs. Group main effects are corrected for family-wise errors ($p < 0.05$) and between-group effects are corrected according to a local false discovery rate of 1%. RSN 12 shows an assembly of ventral affective regions, such as temporal poles, insula, medial prefrontal cortex, and amygdala, the latter two regions demonstrating decreased connectivity within the MDD group. RSN 11 shows brain regions linked to attention, of which the left frontal pole shows decreased connectivity in the MDD group. RSN 3 shows MDD-related decreased connectivity of the bilateral lingual gyrus with other medial visual areas. Images are *z*-statistics, ranging from 2 to 10, overlaid on the MNI-152 standard brain. The left hemisphere of the brain corresponds to the right side in this image. HC, healthy controls; MDD, major depressive disorder. **(B)** Distribution of the mean individual *z*-scores within the bilateral amygdala (12), left frontal pole (11), and bilateral lingual gyrus (3). Depicted in red are the controls, in black the MDD group, both sorted from smallest to highest *z*-value.

negative affect in healthy controls (Urry et al., 2006), as was reflected by decreasing amygdala activation with increasing vmPFC activation. In a similar study in depression, MDD patients showed altered coupling between these regions, potentially reflecting impaired top–down control over amygdala responses and inability to down-regulate negative affect (Johnstone et al., 2007). Involvement of the anterior insula along with dACC and somatosensory regions in this network may furthermore underscore its potential role in interoceptive awareness and emotional experience (Critchley et al., 2004). Besides regions showing decreased FC in this RSN, the depression group also demonstrated increased connectivity of the rIFG. This region has been implicated in coping with exertion of both cognitive (Aron et al., 2004) and emotional (Dolcos et al., 2006) control. Recently, IFG function was found compromised in MDD when executive control had to be exerted in minimizing emotional distraction (Wang et al., 2008). Abnormal recruitment of the rIFG within the current RSN may indicate a higher propensity towards inhibition of emotional responses in depression, although the neurocircuitry to successfully do this is compromised. Taken together, the observed decoupling of the amygdala, decreased left insula connectivity and increased rIFG connectivity within this network may be related to the impaired regulation and integration of affective responses observed in MDD patients.

Second, we found reduced involvement of the left lateral frontal pole in a network often referred to as the TPN (Fox et al., 2005), its constituent regions commonly found activated during tasks that require cognitive effort or attention (Corbetta and Shulman, 2002). The lateral frontal poles are thought to play a key role in executive function and stimulus oriented behavior (Burgess et al., 2007a,b), which would complement the proposed function of this RSN. Reduced FC of the left lateral frontal pole, as was found in depression within this network, may thus reflect a suboptimally integrated attention system or reduced externally oriented attention in MDD. This abnormal connectivity pattern may relate to the cognitive deficiencies often observed in depressed patients (Rogers et al., 2004; Ebmeier et al., 2006), yet this relation should be assessed in task-related imaging studies designed to address this question more directly.

Table 2 | RSN 12 characteristics and statistics.

Region	Brodmann area	Center coordinates (MNI space; LPI)			P_{FWE}		$P_{local\ FDR}$ $q < 0.01$	$P_{local\ FDR}$ $q < 0.01$
		x	*y*	*z*	HC	MDD	HC > MDD	MDD > HC
POSITIVE								
Left cerebellum		–16	–68	–22	0.002	<0.001	ns	ns
Right cerebellum		18	–68	–22	<0.001	<0.001	ns	ns
Left superior temporal gyrus	38	–44	0	–14	<0.001	<0.001	ns	ns
	22,41,42	–46	–30	6	<0.001	<0.001	ns	ns
Right superior temporal gyrus	38	56	–10	–8	<0.001	0.002	<0.001	ns
	22,41,42	58	–32	6	<0.001	<0.001	ns	ns
Left amygdala		–24	–6	–14	0.007	ns	<0.001	ns
Right amygdala		24	–4	–16	0.02	ns	<0.001	ns
Left/right medial prefrontal cortex	10	0	48	–14	0.005	<0.001	ns	ns
Left insula		–40	–6	–2	<0.001	<0.001	ns	ns
		–36	4	–18	<0.001	ns	<0.001	ns
Right insula		38	–6	6	<0.001	<0.001	ns	ns
Right thalamus		12	–22	0	ns	0.008	ns	ns
Left/right anterior cingulate gyrus	24	0	2	38	<0.001	<0.001	ns	ns
Left pre- and postcentral gyrus	1,2,3,4	–44	–20	44	<0.001	<0.001	ns	ns
Right pre- and postcentral gyrus	1,2,3,4	48	–16	44	<0.001	<0.001	ns	ns
Left/right postcentral gyrus	5	0	–26	50	0.002	<0.001	ns	ns
Right inferior frontal gyrus	45	56	24	16	ns	<0.001	ns	<0.001
NEGATIVE								
Left thalamus		–12	–6	12	ns	0.039	ns	ns
Left middle frontal gyrus	46	–28	32	36	0.01	ns	ns	ns
Left precentral gyrus	6	–28	6	48	ns	0.026	ns	ns

Note: Group main effects are FWE-corrected for multiple comparisons, between-group contrasts are corrected for multiple comparisons using a local false discovery rate (FDR) of 1%. HC, healthy controls; MDD, major depressive disorder; ns, not significant.

Finally, we demonstrated decreased FC of the bilateral lingual gyrus in MDD in a network including ventromedial occipitotemporal areas. Although both groups showed strong connectivity with the bilateral lingual gyrus within this network, MDD patients revealed a consistent decrease in connectivity strength. Abnormalities in the visual stream are not commonly reported in MDD, and the interpretation of this effect in the depressed patients in the current study must therefore remain speculative.

In the present study we did not find abnormalities in regions previously reported to show altered RS FC in MDD. For example, increased involvement of the subgenual ACC and thalamus in the DMN has been found in MDD (Greicius et al., 2007; Zhou et al., 2009), but was not observed in the current study. Previous work furthermore reported increased connectivity of multiple brain regions within the TPN (Zhou et al., 2009). In the present study, in contrast, we showed MDD-related *reduced* connectivity of the frontal poles, which is at variance with previously found increases in connectivity in this network. In addition, support for reduced coupling between the dorsal ACC and seeds from the pallidostriatum and thalamus in MDD was not found, as has been described in previous studies (Anand et al., 2005a,b).

The discrepancy in results between these studies and ours could be ascribed to differences in patient samples and analysis methods. In contrast to other studies, we report on a sample of medication-free MDD patients without comorbidity and with carefully age- and gender-matched controls. Secondly, for the current study we employed ICA analysis at the group level to obtain whole brain patterns of FC. It is conceivable that this method yields different results compared to approaches using correlations with, or between *a priori* defined regions of interest, or even when using ICA on individual data sets, although little is at present known about cross-validity between the methods.

A limitation of the present study was that our patient sample was mildly depressed on average. In addition, some patients already showed a clinically significant decrease in symptom severity because of the delay between the diagnostic assessment and the time of scanning. While this may have decreased the overall sensitivity of the study, the method applied was still successful in detecting brain functional correlates of depression, even in a mildly affected patient sample. Moreover, the effects found here were shown not to be associated with the current state of symptom severity, indicating that the observed alterations in FC may not be specific to the active state of the disorder and may not cease to exist during the remitted state.

Another limitation of the current study was the possible influence of between-group differences in heart rate variability and breathing on the results. The sampling rate used in this study (2.2 seconds per volume) was too low to avoid aliasing of these physiological signals in the data acquired. Applying a high-pass

Table 3 | RSN 11 characteristics and statistics.

Region	Brodmann area	Center coordinates (MNI space; LPI)			P_{FWE}		$P_{local\ FDR}$ $q < 0.01$	$P_{local\ FDR}$ $q < 0.01$
		x	*y*	*z*	HC	MDD	HC > MDD	MDD > HC
POSITIVE								
Left inferior temporal gyrus	37	–48	–62	–12	<0.001	<0.001	ns	ns
Right inferior temporal gyrus	37	54	–60	–8	<0.001	<0.001	ns	ns
Left lateral occipital cortex	19	–40	–80	18	<0.001	<0.001	ns	ns
Right lateral occipital cortex	19	44	–72	14	<0.001	<0.001	ns	ns
Left supramarginal gyrus	40	–56	–28	24	<0.001	<0.001	ns	ns
	40	–46	–38	40	<0.001	<0.001	ns	ns
Right supramarginal gyrus	40	58	–40	24	<0.001	<0.001	ns	ns
	40	40	–38	40	<0.001	<0.001	ns	ns
Left posterior cingulate cortex	31	–10	–38	40	<0.001	<0.001	ns	ns
Right posterior cingulate cortex	31	12	–38	42	<0.001	<0.001	ns	ns
Left middle frontal gyrus	46	–46	36	12	0.025	ns	ns	ns
Right middle frontal gyrus	46	50	40	8	0.028	ns	ns	ns
Right precentral gyrus	6	48	8	26	0.035	ns	ns	ns
Left/right anterior cingulate gyrus	24	2	2	32	0.037	ns	ns	ns
NEGATIVE								
Left hippocampus		–28	–24	–16	0.002	ns	ns	ns
Left middle temporal gyrus	21	–58	–30	–10	0.002	0.002	ns	ns
Right middle temporal gyrus	21	58	–20	–10	0.003	ns	ns	ns
Left frontal pole	10	–24	56	–4	<0.001	ns	ns	<0.001
Right frontal pole	10	32	56	–2	<0.001	<0.001	ns	ns
Left paracingulate gyrus	32	–8	32	36	0.003	ns	ns	ns
Right paracingulate gyrus	32	4	32	38	0.003	0.003	ns	ns
Left middle frontal gyrus	8	–36	16	38	ns	<0.001	ns	ns
Left/right cuneus	19	2	–78	36	<0.001	<0.001	ns	ns

Note: Group main effects are FWE-corrected for multiple comparisons, between-group contrasts are corrected for multiple comparisons using a local false discovery rate (FDR) of 1%. HC, healthy controls; MDD, major depressive disorder; ns, not significant.

Table 4 | RSN 3 characteristics and statistics.

Region	Brodmann area	Center coordinates (MNI space; LPI)			P_{FWE}		$P_{local\ FDR}$ $q < 0.01$	$P_{local\ FDR}$ $q < 0.01$
		x	*y*	*z*	HC	MDD	HC > MDD	MDD > HC
POSITIVE								
Left lingual gyrus	19	–10	–68	–2	<0.001	<0.001	<0.001	ns
Right lingual gyrus	19	16	–68	–2	<0.001	<0.001	ns	ns
	19	16	–50	–2	<0.001	<0.001	<0.001	ns
Left lateral occipital cortex	19	–38	–76	22	<0.001	<0.001	ns	ns
Right lateral occipital cortex	19	50	–72	16	0.013	<0.001	ns	ns
Left cuneus	19	–14	–76	22	<0.001	<0.001	ns	ns
Right cuneus	19	18	–76	22	<0.001	<0.001	ns	ns
Right precentral gyrus	6	40	8	28	ns	0.03	ns	ns
Left caudate nucleus		–6	8	4	ns	0.011	ns	ns
Right caudate nucleus		8	8	4	ns	0.016	ns	ns

Note: Group main effects are FWE-corrected for multiple comparisons, between-group contrasts are corrected for multiple comparisons using a local false discovery rate (FDR) of 1%. HC, healthy controls; MDD, major depressive disorder; ns, not significant.

temporal filter will therefore not remove all variance caused by these signals. Since physiological activity was not monitored in the current study, it remains unclear if any difference between the two groups has influenced the results. However, it has been shown that ICA is capable of detecting signal sources associated with confounding physiological signals and that it can

successfully split these from the signals of interest (Beckmann et al., 2005). We therefore think that it is unlikely that any of the differences found in this study were introduced by these physiological signals.

Because MDD-related gray matter (GM) abnormalities have been reported elsewhere (Sheline, 2003; Lorenzetti et al., 2009), we investigated whether our MDD sample showed regions of altered GM density, potentially biasing FC within the RSNs. However, no differences were observed in average GM density between controls and patients in either of the affected RSNs as a whole, nor in the regions showing altered FC within these RSNs. In addition, GM density variance did not contribute to the altered FC patterns observed. Therefore, it is unlikely that the differences in FC were related to global or focal changes in GM density within the current study sample.

Our MDD group furthermore consisted of both first episode and recurrent episode MDD patients. Recurrency of depressive episodes can be considered an aggravation of MDD, which might cause – or conversely be caused by – an exacerbation of abnormal FC patterns. However, the small size of both subgroups, as well as the cross-sectional nature of the current study, prevented us to address this question and compare the two groups in a meaningful way. Nevertheless, follow-up data are currently being collected as part of the NESDA study. Analysis of these data should allow us to shed more light on this matter and to test whether the RS-FC at baseline may have a predictive value in determining which patients are more vulnerable to develop recurrent depressive episodes. To this end, support vector classification of individual RS-FC maps could be employed (Craddock et al., 2009).

In conclusion, we showed that (a history of) major depression is associated with altered FC within multiple RSNs, which could reflect less integrated processing of affective information in ventral (limbic) areas and compromised cognitive functional pathways in dorsal (PFC) regions. The current findings thereby complement previous findings on both affective and cognitive abnormalities in depression and will further increase our knowledge about the pathophysiology of the disorder.

ACKNOWLEDGMENTS

The infrastructure for the NESDA study is funded through the Geestkracht programme of the Netherlands Organization for Health Research and Development (ZonMw, grant number 10-000-1002) and is supported by participating universities and mental health care organizations (VU University Medical Center, GGZ inGeest, Arkin, Leiden University Medical Center, GGZ Rivierduinen, University Medical Center Groningen, Lentis, GGZ Friesland, GGZ Drenthe, IQ Healthcare, Netherlands Institute for Health Services Research (NIVEL) and Netherlands Institute of Mental Health and Addiction (Trimbos). The authors gratefully acknowledge Ramona Demenescu and Anita Kuiper for MRI operation, and Evelinda Baerends for useful discussions on the methods.

REFERENCES

Abou-Elseoud, A., Starck, T., Remes, J., Nikkinen, J., Tervonen, O., and Kiviniemi, V. (2010). The effect of model order selection in group PICA. *Hum. Brain Mapp.* 31, 1207–1216.

American Psychiatric Association (1994). *Diagnostic and Statistical Manual of Mental Disorders*, 4th Edn. Washington, D.C.: American Psychiatric Association.

Anand, A., Li, Y., Wang, Y., Wu, J., Gao, S., Bukhari, L., Mathews, V. P., Kalnin, A., and Lowe, M. J. (2005a). Activity and connectivity of brain mood regulating circuit in depression: a functional magnetic resonance study. *Biol. Psychiatry* 57, 1079–1088.

Anand, A., Li, Y., Wang, Y., Wu, J., Gao, S., Bukhari, L., Mathews, V. P., Kalnin, A., and Lowe, M. J. (2005b). Antidepressant effect on connectivity of the mood-regulating circuit: an FMRI study. *Neuropsychopharmacology* 30, 1334–1344.

Aron, A. R., Robbins, T. W., and Poldrack, R. A. (2004). Inhibition and the right inferior frontal cortex. *Trends Cogn. Sci.* 8, 170–177.

Ashburner, J., and Friston, K. J. (2000). Voxel-based morphometry – the methods. *Neuroimage* 11, 805–821.

Beckmann, C. F., DeLuca, M., Devlin, J. T., and Smith, S. M. (2005). Investigations into resting-state connectivity using independent component analysis. *Philos. Trans. R. Soc. Lond. B Biol. Sci.* 360, 1001–1013.

Beckmann, C. F., and Smith, S. M. (2004). Probabilistic independent component analysis for functional magnetic resonance imaging. *IEEE Trans. Med. Imaging* 23, 137–152.

Biswal, B., Yetkin, F. Z., Haughton, V. M., and Hyde, J. S. (1995). Functional connectivity in the motor cortex of resting human brain using echo-planar MRI. *Magn. Reson. Med.* 34, 537–541.

Burgess, P. W., Dumontheil, I., and Gilbert, S. J. (2007a). The gateway hypothesis of rostral prefrontal cortex (area 10) function. *Trends Cogn. Sci.* 11, 290–298.

Burgess, P. W., Gilbert, S. J., and Dumontheil, I. (2007b). Function and localization within rostral prefrontal cortex (area 10). *Philos. Trans. R. Soc. Lond. B Biol. Sci.* 362, 887–899.

Chen, C. H., Suckling, J., Ooi, C., Fu, C. H., Williams, S. C., Walsh, N. D., Mitterschiffthaler, M. T., Pich, E. M., and Bullmore, E. (2008). Functional coupling of the amygdala in depressed patients treated with antidepressant medication. *Neuropsychopharmacology* 33, 1909–1918.

Corbetta, M., and Shulman, G. L. (2002). Control of goal-directed and stimulus-driven attention in the brain. *Nat. Rev. Neurosci.* 3, 201–215.

Cordes, D., Haughton, V. M., Arfanakis, K., Carew, J. D., Turski, P. A., Moritz, C. H., Quigley, M. A., and Meyerand, M. E. (2001). Frequencies contributing to functional connectivity in the cerebral cortex in "resting-state" data. *Am. J. Neuroradiol.* 22, 1326–1333.

Craddock, R. C., Holtzheimer, P. E., III, Hu, X. P., and Mayberg, H. S. (2009). Disease state prediction from resting state functional connectivity. *Magn. Reson. Med.* 62, 1619–1628.

Critchley, H. D., Wiens, S., Rotshtein, P., Ohman, A., and Dolan, R. J. (2004). Neural systems supporting interoceptive awareness. *Nat. Neurosci.* 7, 189–195.

Damoiseaux, J. S., Beckmann, C. F., Arigita, E. J., Barkhof, F., Scheltens, P., Stam, C. J., Smith, S. M., Rombouts, S. A. (2008). Reduced resting-state brain activity in the "default network" in normal aging. *Cereb. Cortex* 18, 1856–1864.

Damoiseaux, J. S., Rombouts, S. A., Barkhof, F., Scheltens, P., Stam, C. J., Smith, S. M., and Beckmann, C. F. (2006). Consistent resting-state networks across healthy subjects. *Proc. Natl. Acad. Sci. U. S. A.* 103, 13848–13853.

Davidson, R. J., Pizzagalli, D., Nitschke, J. B., and Putnam, K. (2002). Depression: perspectives from affective neuroscience. *Annu. Rev. Psychol.* 53, 545–574.

De Martino, F., Gentile, F., Esposito, F., Balsi, M., Di, S. F., Goebel, R., and Formisano, E. (2007). Classification of fMRI independent components using IC-fingerprints and support vector machine classifiers. *Neuroimage* 34, 177–194.

Dolcos, F., Kragel, P., Wang, L., and McCarthy, G. (2006). Role of the inferior frontal cortex in coping with distracting emotions. *Neuroreport* 17, 1591–1594.

Douaud, G., Smith, S., Jenkinson, M., Behrens, T., Johansen-Berg, H., Vickers, J., James, S., Voets, N., Watkins, K., Matthews, P. M., and James, A. (2007). Anatomically related grey and white matter abnormalities in adolescent-onset schizophrenia. *Brain* 130, 2375–2386.

Drevets, W. C., Price, J. L., and Furey, M. L. (2008). Brain structural and functional abnormalities in mood disorders: implications for neurocircuitry models of depression. *Brain Struct. Funct.* 213, 93–118.

Ebmeier, K., Rose, E., and Steele, D. (2006). Cognitive impairment and fMRI in major depression. *Neurotox. Res.* 10, 87–92.

Efron, B. (2004). Large-scale simultaneous hypothesis testing: the choice of a null hypothesis. *J. Amer. Statistical Assoc.* 99, 96–104.

Filippini, N., MacIntosh, B. J., Hough, M. G., Goodwin, G. M., Frisoni, G.

B., Smith, S. M., Matthews, P. M., Beckmann, C. F., and Mackay, C. E. (2009). Distinct patterns of brain activity in young carriers of the APOE-epsilon4 allele. *Proc. Natl. Acad. Sci. U. S. A.* 106, 7209–7214.

Fox, M. D., and Raichle, M. E. (2007). Spontaneous fluctuations in brain activity observed with functional magnetic resonance imaging. *Nat. Rev. Neurosci.* 8, 700–711.

Fox, M. D., Snyder, A. Z., Vincent, J. L., Corbetta, M., Van, E., and Raichle, M. E. (2005). The human brain is intrinsically organized into dynamic, anticorrelated functional networks. *Proc. Natl. Acad. Sci. U. S. A.* 102, 9673–9678.

Good, C. D., Johnsrude, I. S., Ashburner, J., Henson, R. N., Friston, K. J., and Frackowiak, R. S. (2001). A voxel-based morphometric study of ageing in 465 normal adult human brains. *Neuroimage* 14, 21–36.

Greicius, M. D., Flores, B. H., Menon, V., Glover, G. H., Solvason, H. B., Kenna, H., Reiss, A. L., and Schatzberg, A. F. (2007). Resting-state functional connectivity in major depression: abnormally increased contributions from subgenual cingulate cortex and thalamus. *Biol. Psychiatry* 62, 429–437.

Greicius, M. D., Krasnow, B., Reiss, A. L., and Menon, V. (2003). Functional connectivity in the resting brain: a network analysis of the default mode hypothesis. *Proc. Natl. Acad. Sci. U. S. A.* 100, 253–258.

Hyvarinen, A. (1999). Fast and robust fixed-point algorithms for independent component analysis. *IEEE Trans. Neural Netw.* 10, 626–634.

Jenkinson, M., Bannister, P., Brady, M., and Smith, S. (2002). Improved optimization for the robust and accurate linear registration and motion correction of brain images. *Neuroimage* 17, 825–841.

Jenkinson, M., and Smith, S. (2001). A global optimisation method for robust affine registration of brain images. *Med. Image Anal.* 5, 143–156.

Johnstone, T., van Reekum, C. M., Urry, H. L., Kalin, N. H., and Davidson, R. J. (2007). Failure to regulate: counterproductive recruitment of top-down prefrontal-subcortical circuitry in major depression. *J. Neurosci.* 27, 8877–8884.

Lorenzetti, V., Allen, N. B., Fornito, A., and Yucel, M. (2009). Structural brain abnormalities in major depressive disorder: a selective review of recent MRI studies. *J. Affect. Disord.* 117, 1–17.

Lowe, M. J., Mock, B. J., and Sorenson, J. A. (1998). Functional connectivity in single and multislice echoplanar imaging using resting-state fluctuations. *Neuroimage* 7, 119–132.

Matthews, S. C., Strigo, I. A., Simmons, A. N., Yang, T. T., and Paulus, M. P. (2008). Decreased functional coupling of the amygdala and supragenual cingulate is related to increased depression in unmedicated individuals with current major depressive disorder. *J. Affect. Disord.* 111, 13–20.

Mayberg, H. S. (1997). Limbic-cortical dysregulation: a proposed model of depression. *J. Neuropsychiatry Clin. Neurosci.* 9, 471–481.

Mayberg, H. S. (2003). Modulating dysfunctional limbic-cortical circuits in depression: towards development of brain-based algorithms for diagnosis and optimised treatment. *Br. Med. Bull.* 65, 193–207.

Mennes, M., Kelly, C., Zuo, X. N., Di, M. A., Biswal, B. B., Castellanos, F. X., and Milham, M. P. (2010). Inter-individual differences in resting-state functional connectivity predict task-induced BOLD activity. *Neuroimage* 50, 1690–1701.

Montgomery, S. A., and Asberg, M. (1979). A new depression scale designed to be sensitive to change. *Br. J. Psychiatry* 134, 382–389.

Nichols, T. E., and Holmes, A. P. (2002). Nonparametric permutation tests for functional neuroimaging: a primer with examples. *Hum. Brain Mapp.* 15, 1–25.

Penninx, B. W., Beekman, A. T., Smit, J. H., Zitman, F. G., Nolen, W. A., Spinhoven, P., Cuijpers, P., De Jong, P. J., Van Marwijk, H. W., Assendelft, W. J., Van Der Meer, K., Verhaak, P., Wensing, M., De Graaf, R., Hoogendijk, W. J., Ormel, J., and Van Dyck, R. (2008). The Netherlands Study of Depression and Anxiety (NESDA): rationale, objectives and methods. *Int. J. Methods Psychiatr. Res.* 17, 121–140.

Pessoa, L. (2008). On the relationship between emotion and cognition. *Nat. Rev. Neurosci.* 9, 148–158.

Phillips, M. L., Drevets, W. C., Rauch, S. L., and Lane, R. (2003). Neurobiology of emotion perception II: implications for major psychiatric disorders. *Biol. Psychiatry* 54, 515–528.

Raichle, M. E., MacLeod, A. M., Snyder, A. Z., Powers, W. J., Gusnard, D. A., and Shulman, G. L. (2001). A default mode of brain function. *Proc. Natl. Acad. Sci. U. S. A.* 98, 676–682.

Rogers, M. A., Kasai, K., Koji, M., Fukuda, R., Iwanami, A., Nakagome, K., Fukuda, M., and Kato, N. (2004). Executive and prefrontal dysfunction in unipolar depression: a review of neuropsychological and imaging evidence. *Neurosci. Res.* 50, 1–11.

Seeley, W. W., Menon, V., Schatzberg, A. F., Keller, J., Glover, G. H., Kenna, H., Reiss, A. L., and Greicius, M. D. (2007). Dissociable intrinsic connectivity networks for salience processing and executive control. *J. Neurosci.* 27, 2349–2356.

Shehzad, Z., Kelly, A. M., Reiss, P. T., Gee, D. G., Gotimer, K., Uddin, L. Q., Lee, S. H., Margulies, D. S., Roy, A. K., Biswal, B. B., Petkova, E., Castellanos, F. X., and Milham, M. P. (2009). The resting brain: unconstrained yet reliable. *Cereb. Cortex* 19, 2209–2229.

Sheline, Y. I. (2003). Neuroimaging studies of mood disorder effects on the brain. *Biol. Psychiatry* 54, 338–352.

Smith, S. M. (2002). Fast robust automated brain extraction. *Hum. Brain Mapp.* 17, 143–155.

Smith, S. M., Fox, P. T., Miller, K. L., Glahn, D. C., Fox, P. M., Mackay, C. E., Filippini, N., Watkins, K. E., Toro, R., Laird, A. R., and Beckmann, C. F. (2009). Correspondence of the brain's functional architecture during activation and rest. *Proc. Natl. Acad. Sci. U. S. A.* 106, 13040–13045.

Smith, S. M., Jenkinson, M., Woolrich, M. W., Beckmann, C. F., Behrens, T. E., Johansen-Berg, H., Bannister, P. R., De, L. M., Drobnjak, I., Flitney, D. E., Niazy, R. K., Saunders, J., Vickers, J., Zhang, Y., De, S. N., Brady, J. M., and Matthews, P. M. (2004). Advances in functional and structural MR image analysis and implementation as FSL. *Neuroimage* 23 (Suppl. 1), S208–S219.

Smith, S. M., and Nichols, T. E. (2009). Threshold-free cluster enhancement: addressing problems of smoothing, threshold dependence and localisation in cluster inference. *Neuroimage* 44, 83–98.

Stephan, K. E., Riera, J. J., Deco, G., and Horwitz, B. (2008). The brain connectivity workshops: moving the frontiers of computational systems neuroscience. *Neuroimage* 42, 1–9.

Urry, H. L., van Reekum, C. M., Johnstone, T., Kalin, N. H., Thurow, M. E., Schaefer, H. S., Jackson, C. A., Frye, C. J., Greischar, L. L., Alexander, A. L., and Davidson, R. J. (2006). Amygdala and ventromedial prefrontal cortex are inversely coupled during regulation of negative affect and predict the diurnal pattern of cortisol secretion among older adults. *J. Neurosci.* 26, 4415–4425.

Wang, L. H., Labar, K. S., Smoski, M., Rosenthal, M. Z., Dolcos, F., Lynch, T. R., Krishnan, R. R., and McCarthy, G. (2008). Prefrontal mechanisms for executive control over emotional distraction are altered in major depression. *Psychiatry Res.* 163, 143–155.

Zhou, Y., Yu, C., Zheng, H., Liu, Y., Song, M., Qin, W., Li, K., and Jiang, T. (2009). Increased neural resources recruitment in the intrinsic organization in major depression. *J. Affect. Disord.* 121, 220–230.

Conflict of Interest Statement: The authors declare that the research was conducted in the absence of any commercial or financial relationships that could be construed as a potential conflict of interest.

Received: 29 April 2010; paper pending published: 25 June 2010; accepted: 23 July 2010; published online: 20 September 2010.
*Citation: Veer IM, Beckmann CF, van Tol M-J, Ferrarini L, Milles J, Veltman DJ, Aleman A, van Buchem MA, van der Wee NJ and Rombouts SARB (2010) Whole brain resting-state analysis reveals decreased functional connectivity in major depression. Front. Syst. Neurosci. **4**:41. doi: 10.3389/fnsys.2010.00041*
Copyright © 2010 Veer, Beckmann, van Tol, Ferrarini, Milles, Veltman, Aleman, van Buchem, van der Wee and Rombouts. This is an open-access article subject to an exclusive license agreement between the authors and the Frontiers Research Foundation, which permits unrestricted use, distribution, and reproduction in any medium, provided the original authors and source are credited.

frontiers in
SYSTEMS NEUROSCIENCE

ORIGINAL RESEARCH ARTICLE
published: 22 November 2010
doi: 10.3389/fnsys.2010.00152

Is Social Phobia a "mis-communication" disorder? Brain functional connectivity during face perception differs between patients with Social Phobia and healthy control subjects

Sabrina Danti[1,2], Emiliano Ricciardi[1,3], Claudio Gentili[2,3], Maria Ida Gobbini[4], Pietro Pietrini[1]* and Mario Guazzelli[2]

[1] *Laboratory of Clinical Biochemistry and Molecular Biology, Department of Laboratory Medicine and Molecular Diagnostics, University Hospital of Pisa, Pisa, Italy*
[2] *Department of Psychiatry, Neurobiology, Pharmacology and Biotechnologies, University of Pisa, Pisa, Italy*
[3] *MRI Lab, Fondazione Regione Toscana/CNR "G. Monasterio," Pisa, Italy*
[4] *Department of Psychology, University of Bologna, Bologna, Italy*

Edited by:
Barry Horwitz, National Institutes of Health, USA

Reviewed by:
Chris I. Baker, National Institutes of Health, USA
Paolo Frigio Nichelli, Università Degli Studi Di Modena E Reggio Emilia, Italy

****Correspondence:***
Pietro Pietrini, Department of Laboratory Medicine and Molecular Diagnostics, University of Pisa Medical School, Via Roma, 67 I-56126 Pisa, Italy.
e-mail: pietro.pietrini@med.unipi.it

Recently, a differential recruitment of brain areas throughout the distributed neural system for face perception has been found in social phobic patients as compared to healthy control subjects. These functional abnormalities in social phobic patients extend beyond emotion-related brain areas, such as the amygdala, to include cortical networks that modulate attention and process other facial features, and they are also associated with an alteration of the task-related activation/deactivation trade-off. Functional connectivity is becoming a powerful tool to examine how components of large-scale distributed neural systems are coupled together while performing a specific function. This study was designed to determine whether functional connectivity networks among brain regions within the distributed system for face perception also would differ between social phobic patients and healthy controls. Data were obtained from eight social phobic patients and seven healthy controls by using functional magnetic resonance imaging. Our findings indicated that social phobic patients and healthy controls have different patterns of functional connectivity across brain regions within both the *core* and the *extended systems* for face perception and the default mode network. To our knowledge, this is the first study that shows that functional connectivity during brain response to socially relevant stimuli differs between social phobic patients and healthy controls. These results expand our previous findings and indicate that brain functional changes in social phobic patients are not restricted to a single specific brain structure, but rather involve a *mis-communication* among different sensory and emotional processing brain areas.

Keywords: social phobia, functional connectivity, face perception, fMRI

INTRODUCTION

According to the Diagnostic and Statistical Manual of Mental Disorders IV-TR (APA, 2000), Social Phobia is defined as "*the persistent fear of one or more situations in which the person is exposed to possible scrutiny by others*". Among others, human faces may represent "potentially threatening" social stimuli (Stein et al., 2002). Distinctive behavioral and brain functional responses to face perception and recognition have been reported in various anxiety disorders (Rauch et al., 2000; Stein et al., 2002; Straube et al., 2004). In particular, abnormal neural responses to face perception have been described in social phobic patients as compared to healthy controls, mainly in the amygdala (Birbaumer et al., 1998; Stein et al., 2002; Killgore and Yurgelun-Todd, 2005; Phan et al., 2006), in the "extended amygdala" including uncus and parahippocampus (Stein et al., 2002), in the anterior cingulate cortex (Amir et al., 2005), and in the superior temporal sulcus (STS) (Straube et al., 2004).

However, face perception represents a complex cognitive ability that involves multiple operations, including for instance recognition of identity, processing of facial expression and eye gaze, and it is subserved by a distributed network of brain areas within the *core* and the *extended systems* for face recognition (Haxby et al., 2000; Ishai et al., 2005; Benuzzi et al., 2007; Fairhall and Ishai, 2007; Ishai, 2008, 2010). In a recent fMRI investigation of brain response to recognition of angry, fearful, disgusted, happy, and neutral faces, we showed that these integrated and distributed systems for face perception are differentially recruited in social phobic patients as compared to healthy controls (Gentili et al., 2008). Specifically, differences in task-related activations between social phobic patients and healthy controls were not limited merely to brain areas related to the processing of emotional expressions and personality traits (e.g., amygdala), but rather extended also to cortical areas that are involved in attention and processing of other facial features, including the left fusiform, left dorsolateral prefrontal, and bilateral intraparietal cortical areas (Gentili et al., 2008).

Furthermore, brain regions of the so-called default mode network (DMN), that is, those cortical areas that show higher activity while subjects are in a passive resting condition as compared to when they are engaged in an active task (Gusnard et al., 2001; Raichle et al., 2001; Greicius et al., 2003), and specifically the precuneus/posterior cingulate region, showed a differential activity between social phobic patients and healthy controls. This differential recruitment of the distributed system for

face perception in social phobic patients may be coupled to an alteration of the task-related activation/deactivation trade-off (Gentili et al., 2009).

Functional connectivity, as measured by fMRI (fcMRI), reflects the temporal correlation between neurophysiological events that may occur in regions spatially distant and even not anatomically connected (Friston, 1994; Biswal et al., 1995). Thus, functional connectivity represents a powerful tool to understand the functional architecture of the brain and to examine how components of large-scale distributed neural systems are coupled together in performing a specific function (Rogers et al., 2007; Stephan et al., 2008; Esposito et al., 2009). In other words, by using functional connectivity one can measure how distinct brain areas communicate among each other while subjects perform a given cognitive task (Horwitz et al., 2000, 2005; Horwitz, 2003). In patients with a variety of psychiatric disorders, functional correlation analysis has shown a *mis-communication* among brain areas for face perception. For instance, Wang et al. (2009) showed a significantly reduced functional connectivity between the amygdala and perigenual anterior cingulate cortex in patients with Bipolar Disorder as compared to healthy controls during processing of face stimuli. Similarly, a reduced functional connectivity between the left amygdala and right posterior cingulate, precuneus, right fusiform, and parahippocampal cortex has been found in pediatric bipolar disorder patients as compared to healthy children during a face perception task (Rich et al., 2008).

Based on the findings discussed above, which indicate a wider distribution of brain functional abnormalities in patients with Social Phobia, the present study was designed to test the hypothesis that also functional regional correlations within the distributed network for face recognition would be different between healthy controls and patients with Social Phobia. Specifically, we reanalyzed our fMRI data – previously acquired and evaluated with a more conventional general linear model (GLM) analysis in Gentili et al. (2008, 2009) – by using a functional connectivity approach considering as seeds those cortical areas that had shown a differential activity in social phobic patients as compared to healthy controls in response to a face perception task with emotional and neutral stimuli (Gentili et al., 2008).

MATERIALS AND METHODS

SUBJECTS

For this study, we utilized brain functional data originally reported in our previous manuscript (Gentili et al., 2008). In brief, eight right-handed subjects (4 males/4 females) (mean age 39 ± 7 years) with a diagnosis of Social Phobia according to the DSM IV-TR criteria (APA, 2000) and seven right-handed healthy controls (4 males/3 females) (mean age 30 ± 7 years) were recruited. All subjects received a clinical examination to exclude any medical, neurological or psychiatric disorder (other than Social Phobia in the patient group) that could affect brain function or metabolism. They also underwent a brain structural MRI scan exam to rule out any brain morphological abnormality or pathology. No subject in either group had taken any drug for at least 4 weeks prior to the clinical evaluation and the fMRI study. In particular all social phobic patients, as they had never received any pharmacological and/or psychotherapeutic treatment before, were completely drug-naïve. Prior to the enrollment into the study, all subjects signed a written informed consent, under a protocol approved by the Ethics Committee of the University of Pisa, Italy. All subjects retained the right to withdraw from the study at any time.

The psychiatric interview included also the following rating scales: the Liebowitz Scale for Social Phobia (Liebowitz, 1987), the Interaction Anxiousness Scale (Leary and Kowalski, 1993) and the Audience Anxiousness Scale (Leary, 1983) to assess the degree of social anxiety. In addition, before and after the fMRI session each subject completed the State-Trait-Anxiety-Scale (Spielberger et al., 1970) to assess state anxiety during the experiment.

STIMULI AND TASK

Stimuli comprised faces and non-sense pictures. Faces with emotional expressions belonging to ten different subjects were taken from the Ekman and Friesen's (1976) standardized set. We selected faces with angry, fearful, disgusted, and happy expressions as well as faces with neutral expressions. As control stimuli we used non-sense pictures, which were phase-scrambled images of the faces and were matched to the faces in terms of spatial frequencies, luminance, and contrast. Both faces and non-sense scrambled pictures were in gray scale.

A fast event-related design in which each stimulus was presented for 2,000 ms with an inter-stimulus interval (ISI) of 1,500 ms was used. During the fMRI sessions, participants were asked to perform a one-back repetition detection task based on face identity. For the control scrambled pictures a one-back repetition detection task also was performed to control for sensorimotor activations. During the task for faces, the subjects had to indicate whether each presented face image was the same individual as in the immediately preceding image by pressing a hand-held button with their right or left hand for matches and non-matches, respectively. For scrambled pictures the subjects had to indicate whether the successive pictures were identical or not using the same response buttons. In this way the subjects maintained attention to the stimuli, but the emotional task remained implicit. Subjects were instructed to respond during the ISI, when a fixation point appeared on the screen. Faces and scrambled pictures were presented in a pseudo-randomized order: a face with an emotional expression was presented after two to four faces with a neutral one. In each run, two blocks of 38 face stimuli were presented. The two face blocks were separated by an interval of 15 s of rest, a block of eight scrambled pictures and another 15 s interval of rest. Accuracy and reaction times were recorded by computer.

DATA ACQUISITION, PREPROCESSING, AND FUNCTIONAL CONNECTIVITY ANALYSIS

Responses to different faces and scrambled pictures and emotional vs. neutral faces were measured using blood oxygen level dependent (BOLD) contrast fMRI with the acquisition of $T2^*$-weighted gradient echo planar images (EPI) in a 1.5T GE scanner (General Electric, Milwaukee, WI, USA). In each time series, the whole brain volume was acquired 188 times, and each volume consisted of 26 contiguous 5 mm thick axial slices (TR = 2 s, TE = 40 ms, flip angle 90°, FOV = 24 cm, matrix resolution = 64 × 64 pixels). Eight runs were obtained in each fMRI session. Each time series began with 30 s of rest before the presentation of the stimuli. High-resolution T1-weighted spoiled gradient recall images (SPGR) (1.2 mm thick

axial slices, TR = 12.1 ms, TE = 5.22 ms, flip angle = 20°, FOV = 24 matrix resolution = 256 × 256 pixels) were obtained for each subject to provide detailed brain anatomy; the SPGR images were used as an anatomical underlay for the statistical maps derived from the analysis on the EPI sequences.

Data analysis was performed using the AFNI package (http://afni.nimh.nih.gov/afni) (Cox, 1996). Functional connectivity was defined for each subject on the correlation between the mean BOLD signal of the seed region of interest (ROI) and the BOLD time-series of all the other voxels in the brain (Friston et al., 1997; Greicius et al., 2003). Indeed, after spatial realignment and slice time correction, time series for each voxel were normalized to the mean, and then spatially smoothed (Gaussian kernel 6 mm half-width). Linear and quadratic trend of the signal were removed and the images were normalized to the Talairach–Tournoux space (Talairach and Tournoux, 1988). A temporal low-pass filter at 0.1 Hz on the whole signal was applied, to diminish the effect of high-frequency noises and to restrict our analysis to an informative frequency range for functional connectivity analysis (Cordes et al., 2001). Averaged time series extracted from each seed ROI were considered as regressors of interest. Task-related regressors, together with the six regressors for the estimated head movement (6° of motions: left–right, anterior–posterior, superior–inferior, roll, pitch, yaw) and the global signal, were considered as regressors of no interest in the multiple regressions analysis to compute the correlations maps (Deary et al., 2004; Whalley et al., 2005). To remove task-related effects, the task conditions (six regressors, one for each face expression, including the neutral one) were modeled with the canonical gamma-variate hemodynamic response function (Cohen, 1997). We have modeled the task as regressors of no interest exactly as in the GLM analysis of Gentili et al. (2008). The global signal was calculated as the average of BOLD signal across all voxels of the whole brain for each subject. The global signal was considered in the correlation analysis as regressor of no interest to remove artifacts related to physiological noise (e.g., heart or respiratory rate), or variations in scanner sensitivity (Desjardins et al., 2001; Macey et al., 2004).

Definition of seed ROIs for the functional connectivity analysis relied on brain regions that showed a significant recruitment during a face recognition task in social phobic patients and healthy controls, as defined in our previous study (Gentili et al., 2008). Relying on the functional results of group analysis of variance (Gentili et al., 2008), we selected seed ROIs among brain regions involved in the early perception of faces (Haxby et al., 2000), such as the fusiform gyrus, or specifically responding to facial expressions, such as the STS and the amygdala (Winston et al., 2003, 2004; Campbell et al., 2007; Engell and Haxby, 2007). In details, bilateral fusiform gyri (FG) were selected as those clusters that showed a significant ($P < 0.01$) response to faces in both healthy controls and social phobic patients. The right superior temporal sulcus (R-STS) seed ROI was derived from the comparison between emotional and neutral faces ($P < 0.01$) in both social phobic patients and healthy controls. The left amygdala (L-Amy) was selected on the basis of the contrast between faces vs. scrambled pictures as a seed ROI showing a significant ($P < 0.01$) higher response in social phobic patients as compared to healthy controls (**Table 1**).

A multiple regression analysis was performed to examine the whole brain functional connectivity of each seed ROI time series. In order to run group analysis, correlation coefficients were converted to Z scores, using Fisher's Z transformation. For each ROI, individual Z-score correlation coefficient maps were computed by multiplying the cross-run average Z correlation coefficient values by the square root of the number of runs.

In each group, a one-sample t-test was used to define brain regions significantly correlated with the seed ROIs (**Figure 1**). The correction for multiple comparisons was made using Monte-Carlo simulations (AFNI AlphaSim, http://afni.nimh.nih.gov/afni/doc/manual/AlphaSim) with a voxel-wise threshold of 0.05 which resulted in a minimum cluster volume of 5,852 μL and cluster connection radius 1.01 mm for a corrected P value <0.05. Results of the one-sample t-test contrasts were superimposed onto the anatomical regions of Talairach–Tournoux Atlas (Lancaster et al., 1997, 2000) to report brain networks significantly correlated to distinct seed ROIs, as labeled in **Figures 1A–C**.

An unpaired t-test between social phobic patients and healthy controls was performed to identify the regions differentially correlated within the functional networks of the two groups for each seed ROI at an uncorrected $P < 0.05$ and a minimum cluster volume of 1,000 μL for the right FG (R-FG) and R-STS, and of 500 μL for the seed L-Amy (**Figure 2**). Due to the complexity of evaluating the combinations of positive and negative correlations as resulted from the unpaired t-test, we restricted our search volumes to brain regions significantly correlated to a specific seed ROI in the two groups. Search volumes were defined with a binary mask (logical OR) that merged the one-sample t-tests of each seed ROI for each group (uncorrected $P < 0.05$), thus defining overall correlated voxels in either social phobic patients or healthy controls.

Table 1 | Seed ROIs for the functional connectivity analysis, as derived from social phobic patients (SPP) and healthy controls (HC) group contrasts (uncorrected $P < 0.01$).

Seed ROIs	Hemisphere	Brodmann area	Talairach coordinates			Contrasts	Findings
			x	*y*	*z*		
Fusiform gyrus	R	37	35	–58	–11	Faces vs. baseline	SPP and HC
	L	37	–40	–55	–10		SPP and HC
Superior temporal sulcus	R	41	47	–52	16	Emotional vs. neutral faces	SPP and HC
Amygdala	L		–27	–3	–16	Emotional faces vs. scrambled	SPP > HC

See Gentili et al. (2008) for further details.

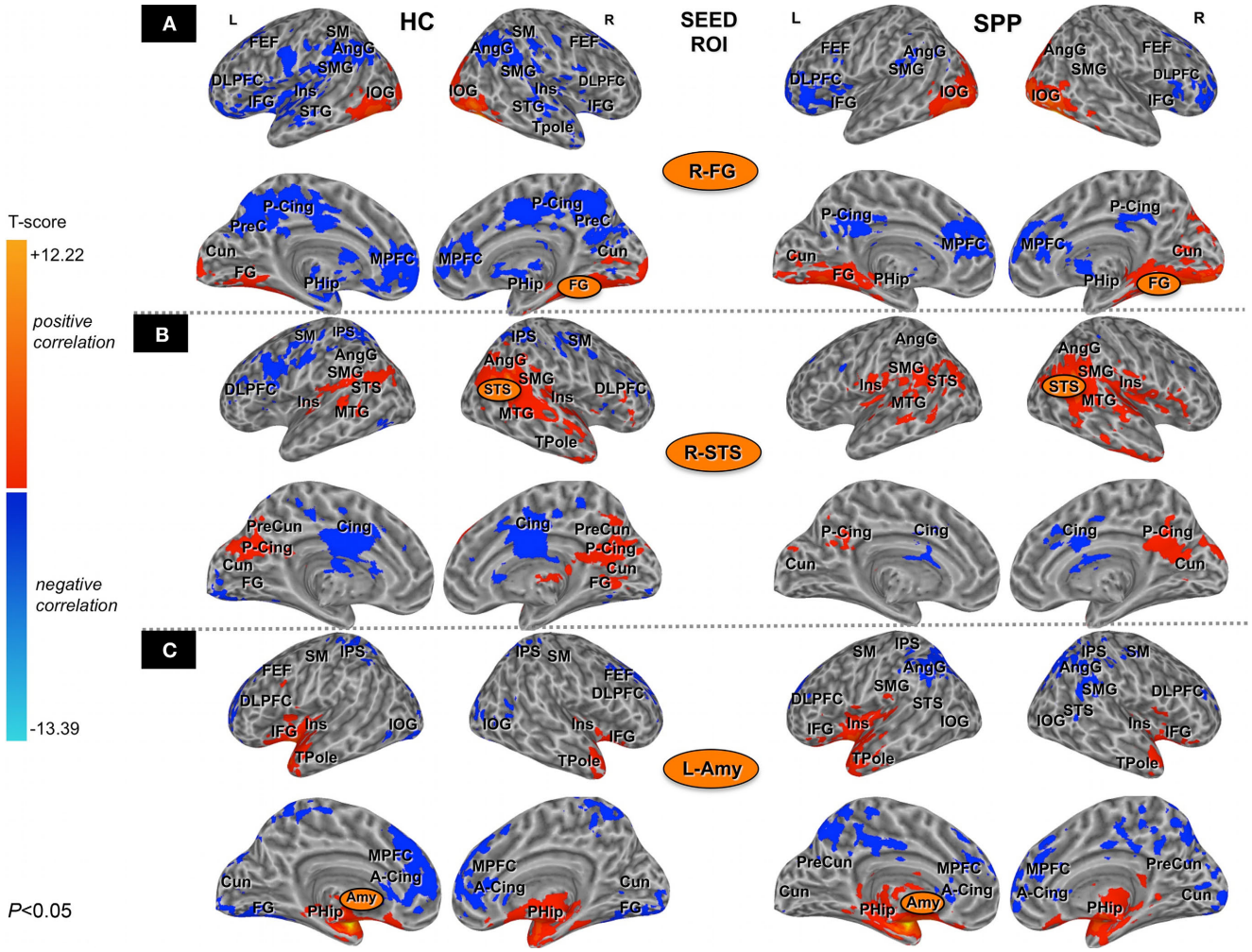


FIGURE 1 | Brain areas positively (red) or negatively (blue) correlated (one-sample *t*-test; corrected $P < 0.05$) with the seed ROIs [right fusiform gyrus/R-FG (A), right superior temporal sulcus/R-STS (B) and left Amygdala/L-Amy (C) in healthy controls (HC) (on the left) and social phobic patients (SPP) (on the right), respectively]. Please note that brain inflated view could distort some clusters of significant correlation. DLPFC, dorsolateral prefrontal cortex; MPFC, medial prefrontal cortex; FEF, frontal eye field; SM, sensorimotor cortex; IFG, inferior frontal gyrus; SMG, supramarginal gyrus; AngG, angular gyrus; IPS, intraparietal sulcus; PreCun, precuneus; MTG, middle temporal gyrus; STG, superior temporal gyrus; STS, superior temporal sulcus; Cing, cingulate cortex; A-Cing, anterior cingulate cortex; P-Cing, posterior cingulate cortex; Amy, amygdala; Ins, insula; PHip, parahippocampus; TPole, temporal pole; Cun, Cuneus; FG, fusiform gyrus; IOG, inferior occipital gyrus.

The schemes depicted in **Figures 3 and 4** aimed to simplify and to better characterize the complexity of both the distributed brain regions differentially correlated with each seed ROI separately in the two groups (**Figure 3**), and all the combinations of differential positive and negative correlations as resulted from the comparison between patients and healthy controls (**Figure 4**). An unbiased approach based on an automatic labeling of anatomically defined regions in the human brain was used as the best to provide a simplified report of results. We selected the 3D database of the Talairach–Tournoux Atlas (Lancaster et al., 1997, 2000), and superimposed onto this common atlas either those voxels correlated with a specific ROI in social phobic patients and healthy controls (**Figure 3**), or those voxels differentially recruited between the two groups (**Figure 4**). The simplified schemes of **Figures 3 and 4** derive from correlation maps of **Figures 1 and 2**, respectively. At last differential clusters in the functional networks of the two groups, as defined by the unpaired *t*-test, are reported in terms of significant group similarities or differences across brain regions in **Table 2**.

RESULTS

PSYCHOMETRIC SCALES AND BEHAVIORAL RESULTS

Patients with Social Phobia had significant higher scores ($P < 0.01$) in all the scales for social anxiety, as compared to the healthy control group. In contrast, no significant differences were found in state anxiety between pre- and post-scan sessions within either group or between the two groups. During the one-back face recognition task used in the fMRI study, accuracy (mean ± standard error: SPP = 92.4±0.5%; HC = 93.5±0.5%, $P = 0.15$) was at ceiling level in both groups with no significant difference between the two groups.

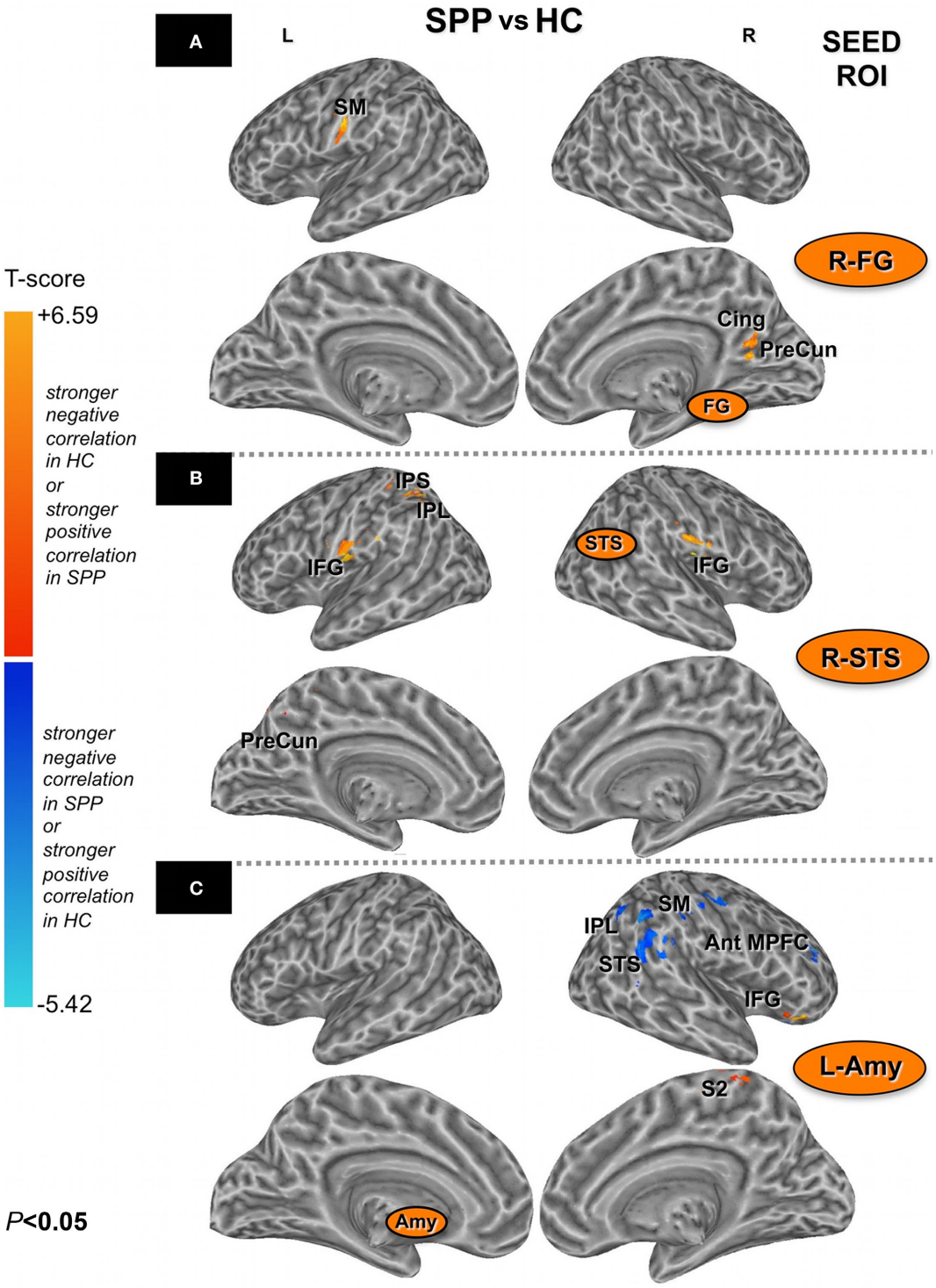


FIGURE 2 | Brain areas with stronger negative correlations in HC or with stronger positive correlation in SPP (red) and brain areas with stronger negative correlations in SPP or with stronger positive correlations in HC (blue) (unpaired *t*-test; uncorrected $P < 0.05$) with the seed ROIs [right fusiform gyrus/R-FG (A), right superior temporal sulcus/R-STS (B) and left Amygdala/L-Amy (C)]. Please note that brain inflated view could distort some clusters of significant correlation. Ant MPFC, anterior middle prefrontal cortex; SM, sensorimotor cortex; S2, secondary somatosensory cortex; IFG, inferior frontal gyrus; IPS, intraparietal sulcus; IPL, inferior parietal lobule; PreCun, precuneus; STS, superior temporal sulcus; Cing, cingulate cortex; Amy, amygdala; FG, fusiform gyrus.

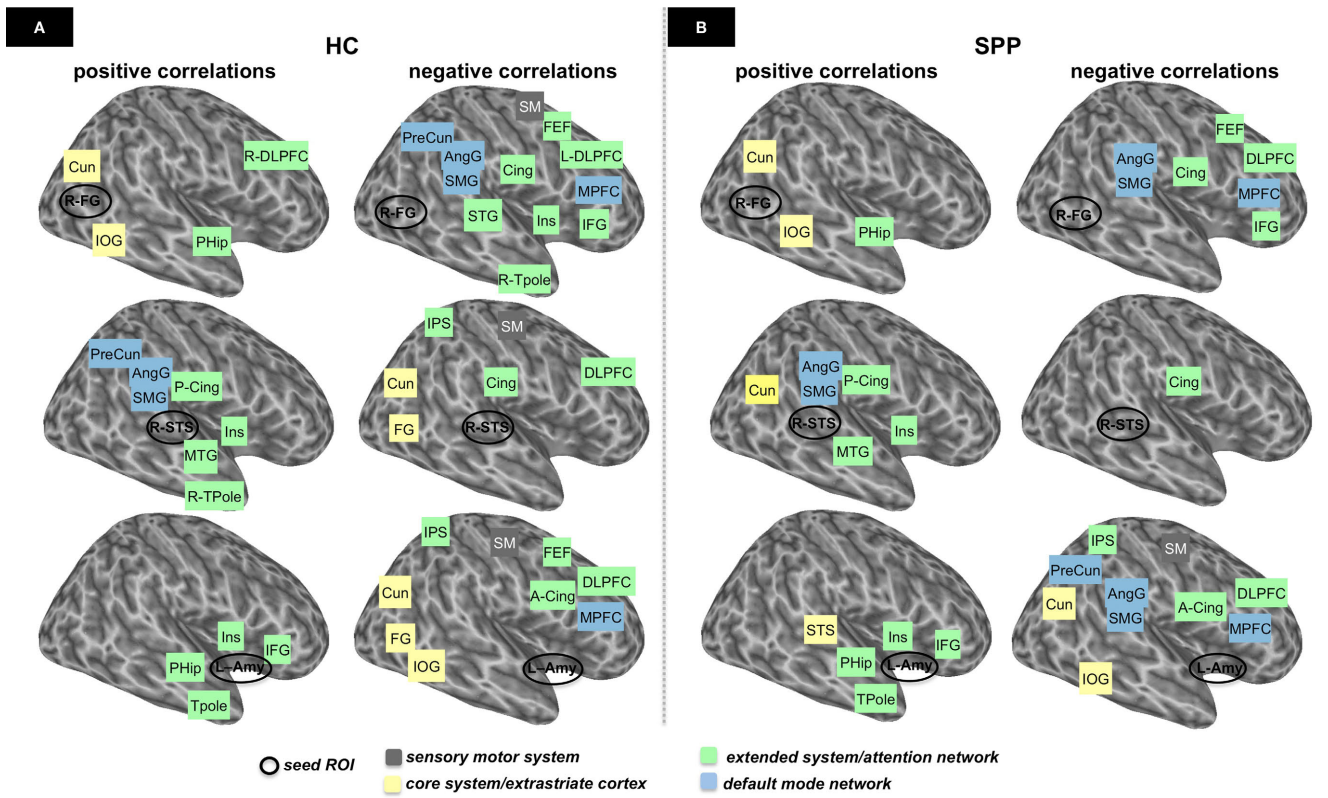


FIGURE 3 | Schematic representation of the functional networks in healthy controls (HC) (A) and social phobic patients (SPP) (B), based on the results reported in **Figure 1**. Positive and negative correlations for these functional networks (one-sample *t*-test; corrected $P < 0.05$) are shown in the first and second columns, respectively. Seed ROIs are indicated with a black circle [top: right fusiform gyrus (R-FG); middle: right superior temporal sulcus (R-STS); bottom: left amygdala (L-Amy), respectively]. Functionally correlated areas of the *core system*/extrastriate cortex (yellow boxes), the *extended*/attention system (green boxes), default mode network (light blue boxes) and sensorimotor areas (gray boxes) are considered bilaterally, unless otherwise indicated. DLPFC, dorsolateral prefrontal cortex; MPFC, medial prefrontal cortex; FEF, frontal eye field; SM, sensorimotor cortex; S2, secondary somatosensory cortex; IFG, inferior frontal gyrus; SMG, supramarginal gyrus; AngG, angular gyrus; IPS, intraparietal sulcus; IPL, inferior parietal lobule; PreCun, precuneus; MTG, middle temporal gyrus; STG, superior temporal gyrus; STS, superior temporal sulcus; Cing, cingulate cortex; A-Cing, anterior cingulate cortex; P-Cing, posterior cingulate cortex; Amy, amygdala; Ins, insula; PHip, parahippocampal regions; TPole, temporal pole; Cun, Cuneus; FG, fusiform gyrus; IOG, inferior occipital gyrus.

Also, no significant difference in reaction time was found between the two groups (SPP = 1120 ± 110 ms; HC = 1031 ± 112 ms, $P = 0.08$) (see Gentili et al., 2008 for further details).

FUNCTIONAL CONNECTIVITY RESULTS

All seed ROIs were strongly connected to their contralateral homologous regions. Furthermore, each ROI showed additional and specific positive and negative correlations with other brain regions.

In **Figures 3A,B,** we depicted a schematic representation of the functional networks previously showed in **Figure 1**. These diagrams represent the functional networks connected with the seed ROIs in the healthy control and the social phobic patient groups, respectively. These networks comprised areas of the *core* and the *extended systems*, as defined in the face recognition model by Haxby et al. (2000). Thus, we grouped brain regions in a *core system*/extrastriate cortex, which includes occipito-temporal extrastriate cortical areas for the visual analysis of faces (yellow boxes), and the *extended*/attention system, which includes fronto-tempo-parietal regions for further processing of the faces (green boxes). Sensorimotor (gray boxes) and DMN regions (light blue boxes) are also included in the functional networks shown in **Figure 3**.

The *core system* regions (bilateral fusiform gyri and R-STS) showed a distinct pattern of positive and negative functional correlations with brain areas of both the *extended system* and the DMN in social phobic patients as compared to healthy controls. Similarly, functional connectivity using the left amygdala as seed ROI showed a differential distributed network of positive and negative correlations with several areas of both the *core* and the *extended systems* in social phobic patients as compared to healthy controls.

Fusiform gyri

Correlation maps for the left and the right fusiform gyrus were consistent across subjects within the two groups, and no differences were identified in paired *t*-test between the left and the right connectivity networks (cluster-level corrected; $P < 0.05$). Thus, only the description of the right fusiform gyrus network was reported. In both healthy controls and social phobic patients, the right fusiform

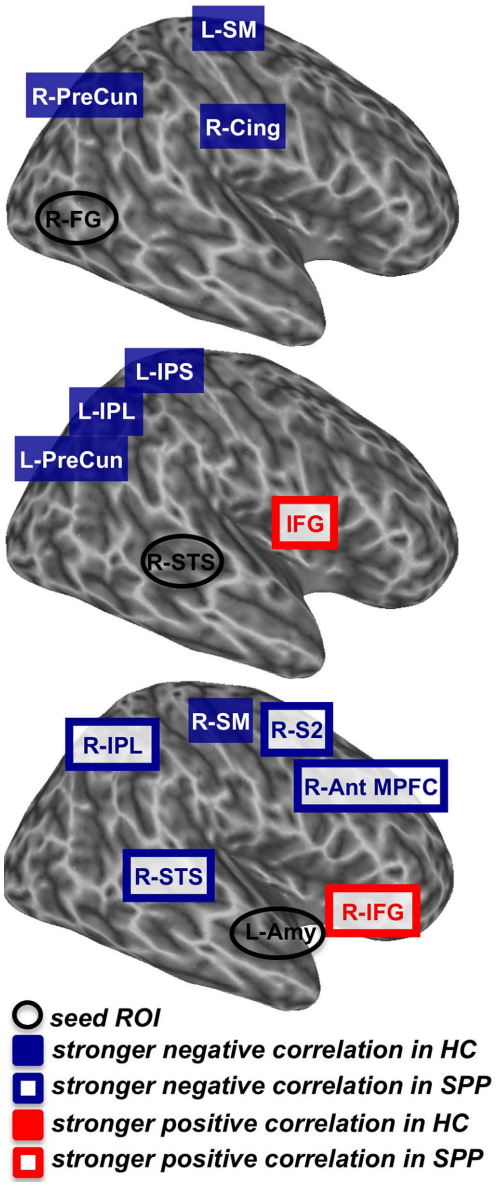


FIGURE 4 | Schematic representation of the differences in functional networks that resulted from the comparison of SPP vs. HC (unpaired *t*-test; uncorrected $P < 0.05$). Seed ROIs are indicated with a black circle [top: right fusiform gyrus (R-FG); middle: right superior temporal sulcus (R-STS); bottom: left amygdala (L-Amy), respectively]. Stronger negative correlations in HC (blue boxes), stronger negative correlations in SPP (white boxes with blue contour), stronger positive correlation in HC (red boxes) and stronger positive correlations in SPP (white boxes with red contour) refer to areas of these functional networks that are considered bilaterally, unless otherwise indicated. Ant MPFC, anterior middle prefrontal cortex; SM, sensorimotor cortex; S2, secondary somatosensory cortex; IFG, inferior frontal gyrus; IPS, intraparietal sulcus; IPL, inferior parietal lobule; PreCun, precuneus; STS, superior temporal sulcus; Cing, cingulate cortex; Amy, amygdala; FG, fusiform gyrus.

gyrus was positively correlated with the areas of the *core system* and of the ventral extrastriate pathway, while it was negatively correlated with large regions of the DMN and of the *extended system*, including the dorsal prefrontal and superior temporal areas. Negative correlations were reported also in the sensorimotor cortical areas in healthy controls (**Figures 3A,B**, top row).

Table 2 | *t*-score (unpaired *t*-test; uncorrected $P < 0.05$) and Talairach–Tournoux Atlas coordinates for the local maxima of brain regions that show significant differences in the functional connectivity during face perception between social phobic patients and healthy controls.

	Brodmann area	Hemisphere	Volume (μL)	Talairach coordinates *x*	*y*	*z*	*t*-score
RIGHT FUSIFORM GYRUS							
Cing	23	R	2,176	7	–60	6	2.3
PreCun	7	R	16,418	14	–58	18	2.6
SM	3	L	2,205	–59	–6	14	2.2
SM	4	L	1,398	–60	–4	16	2.4
RIGHT SUPERIOR TEMPORAL SULCUS							
IPL	40	L	1,448	–34	–51	38	2.4
IPS	7	L	2,360	–26	–49	43	2.9
IFG	44/6	L	1,820	–63	–5	14	2.2
IFG	44/6	R	1,203	55	–8	14	2.2
PreCun	7	L	2,680	–25	–64	39	2.2
LEFT AMYGDALA							
Ant MPFC	10	R	672	41	42	22	–2.2
IFG	47	R	728	35	25	–16	2.3
IPL	40	R	668	46	–40	22	–2.2
SM (paracentral lobule)	5	R	710	5	–42	53	2.2
S2	3	R	607	43	–25	30	–2.3
STS	22	R	1,671	54	–48	10	–2.4

Cing, cingulate cortex; PreCun, precuneus; SM, sensory motor cortex; IPL, inferior parietal lobule; IPS, intraparietal sulcus; IFG, inferior frontal gyrus; Ant MPFC, anterior middle prefrontal cortex; S2, secondary somatosensory cortex; STS, superior temporal sulcus.

When the two groups were compared (uncorrected $P < 0.05$; minimum cluster volume 1,000 μL), differences in the functional connectivity maps were found in the right precuneus (cluster-level corrected $P < 0.05$), the right posterior cingulate and the left sensorimotor (BA3) cortical areas, with a stronger negative correlation in healthy controls as compared to social phobic patients (**Figure 4**, top).

Right superior temporal sulcus

In healthy controls, the R-STS correlated positively with the areas of the *extended system* (including temporal and insular areas, and posterior cingulate) and the DMN (precuneus, angular gyrus and supramarginal cortex), and negatively with the sensorimotor and the dorsal prefrontal regions, the ventral extrastriate areas, the intraparietal sulci and the cingulate cortex. Social phobic patients showed a network of positive connections with the R-STS, whereas a significant negative correlation was found only in the cingulate cortex (**Figures 3A,B,** middle row).

The group comparison (uncorrected $P < 0.05$, minimum cluster volume 1,000 μL) showed a stronger negative correlation in healthy controls as compared to social phobic patients in the left inferior parietal and the anterior intraparietal cortex and the left precuneus. In addition, social phobic patients showed a stronger positive correlation than healthy controls in the bilateral ventral premotor/inferior frontal areas (BA44/6) (**Figure 4**, middle).

Left amygdala

In healthy controls, the left amygdala was positively correlated with areas of the *extended system*, including the parahippocampus, the anterior temporal, the insular and the inferior frontal areas. Conversely, the left amygdala in healthy controls was negatively correlated with a wide network including the anterior cingulate and the posterior parietal areas and the medial frontal cortex (*extended*/attention system and DMN) and the ventral occipito-temporal regions (*core system*/extrastriate cortex). Social phobic patients showed a pattern of functional connectivity similar to healthy controls, though distinct positive and negative correlations were assessed (**Figures 3A,B**, bottom row).

The group comparison (uncorrected $P < 0.05$, minimum cluster volume 500 μL) revealed a differential functional connectivity in several right-sided brain regions related to face recognition. Stronger negative correlations in social phobic patients were found in the superior temporal cortex (BA22), the inferior parietal, the anterior middle prefrontal and the postcentral (BA3) cortex, whereas a stronger positive correlation was found in social phobic patients in the inferior frontal regions (BA47). In contrast, stronger negative correlation in healthy controls was described in the paracentral sensorimotor cortex (BA5) (**Figure 4**, bottom).

DISCUSSION

The present study was designed to examine both positive and negative functional correlations among brain regions within the distributed system for face perception in social phobic patients as compared to healthy controls. Specifically, a whole brain voxel-wise functional connectivity analysis was performed taking as seeds those cortical areas that had shown a differential activity in social phobic patients and in healthy controls in response to a face perception task with emotional and neutral stimuli (Gentili et al., 2008). These areas included the bilateral fusiform gyrus, the R-STS and the left amygdala.

Overall, social phobic patients and healthy controls showed different patterns of functional connectivity across brain regions within both the *core* and the *extended systems* for face perception (Haxby et al., 2000; Ishai et al., 2005; Benuzzi et al., 2007; Fairhall and Ishai, 2007; Ishai, 2008, 2010) as well as within the DMN (Raichle et al., 2001; Gusnard et al., 2001; Greicius et al., 2003). As accuracy and reaction times were similar in the two groups, the differences in brain functional connectivity cannot be due to differences in behavioral performance.

The present results extend our previous findings that regions within the *core* and the *extended systems* for face perception are differentially modulated in patients with Social Phobia as compared to healthy controls (Gentili et al., 2008) by showing that the pattern of functional correlations originated by these brain areas involved in face perception and emotional processing also is altered in patients with Social Phobia.

Functional connectivity of regions of the *core system* for face perception, such as the bilateral fusiform gyri and the R-STS, showed in social phobic patients as compared to the healthy controls a distinct pattern of positive and negative functional correlations with brain areas of both the *extended system* and the DMN. For instance, both the right fusiform gyrus and R-STS showed a stronger negative correlation with the right precuneus in healthy controls as compared to social phobic patients. This is in line with our previous observation of a significantly smaller deactivation in the precuneus during face perception in social phobic patients as compared to healthy controls (Gentili et al., 2009). Consistently, precuneus abnormalities have been shown also in other anxiety disorders (Zhao et al., 2007). As the precuneus is a region of the DMN, this abnormal functional correlation is an additional piece of evidence in support of an impairment of the normal task-related activation/deactivation trade-off in Social Phobia. Since the precuneus plays a role in self-focus perception, its altered connectivity may be related to the attentive bias described in anxiety disorders, which leads anxious subjects to attend to the physiological signs of anxiety and to experience negative self-evaluation, as originally hypothesized by Clark and Wells (1995).

Additionally, the R-STS showed a stronger negative correlation with the left inferior parietal (BA40) and anterior intraparietal (BA7) cortex in healthy controls as compared to social phobic patients. Differences between groups in the patterns of correlations within brain networks associated with attention and other aspects of face processing (e.g., increased visual scanpath length and reduced foveal fixations of the eyes in social phobic patients; Horley et al., 2004) are consistent with our previous findings that in social phobic patients face recognition is associated with decreased activity in parietal areas, independently from the emotional expression of the facial stimuli (Gentili et al., 2008). Functional studies with different social threatening stimuli (e.g., public speech) reported similar results of a reduced recruitment of attentional networks in social phobic patients as compared to healthy controls (Lorberbaum et al., 2004).

Recent studies have shown a stronger amygdala response in social phobic patients during a face recognition task not only with emotional facial expressions, but also with neutral faces (Birbaumer et al., 1998; Stein et al., 2002; Straube et al., 2004; Cooney et al., 2006; Phan et al., 2006; Gentili et al., 2008). Here, functional connectivity using the left amygdala as a seed ROI showed a differential distributed network of positive and negative correlations that involved several areas within both the *core system* (superior temporal cortex) and the *extended system* (frontal and parietal cortical areas) for face recognition. Interestingly, the left amygdala was positively correlated with the inferior frontal/insular cortical regions only in patients with Social Phobia but not in healthy controls, in line with previous findings of a significantly increased response in the amygdala and insula during face recognition in social phobic patients as compared to healthy controls (Straube et al., 2004; Amir et al., 2005; Gentili et al., 2008). In particular, since the insular cortex is involved in the processing of socially threatening stimuli including anger, fear and disgust (Straube et al., 2004; Amir et al., 2005), the abnormal activity found in this brain region in social phobic patients as well as in patients with other anxiety disorders (Stein et al., 2007) may be associated to the dysfunctional monitoring of the bodily

states of arousal associated with and contributing to the emotional experience of anxiety (Damasio et al., 2000; Critchley et al., 2004). Thus, the specific communication between amygdala and inferior frontal cortex/insula found only in patients with Social Phobia may contribute to explain why anxiety patients process differently the emotional-relevant stimuli as compared to healthy controls.

LIMITATIONS OF THE STUDY AND OF THE FUNCTIONAL CORRELATION APPROACH

The present study of brain regional functional correlations has some limitations, both intrinsic to the specific experimental protocol and, more in general, relative to the fcMRI approach itself.

The main specific limitation of the study is the relatively limited number of subjects. All the social phobic patients, however, had a diagnosis of pure Social Phobia without any other concomitant mental disorder. Equally important, all patients were drug-naïve at the time of the fMRI examinations, as they had never been treated before. These uncommon aspects make this sample of patients optimal to investigate brain functional connectivity in the absence of any interference due to previous exposure to drugs, psychotherapy or to the effects of concomitant psychopathology.

Correlations were run using predefined seed ROIs. While this may somewhat limit the ability to uncover potentially abnormal functional connectivity networks that originate from seeds distinct from those used here, the selection derived from a strong a priori hypothesis that was based on solid evidence in the literature (Birbaumer et al., 1998; Stein et al., 2002; Straube et al., 2004; Phan et al., 2006; Gentili et al., 2008) and it was ideal to pursue the main goal of this hypothesis-driven study. Specifically, here we wished to determine whether or not the functional connectivity networks originating from brain regions involved in face perception and in emotional processing, and found to respond abnormally in social phobic patients as compared to healthy control subjects, also would be abnormal in the patient group.

Finally, from a more general perspective, while most of the processing steps of fcMRI data are widely agreed upon (e.g., Fox et al., 2005), some procedures, such as factoring out task-related regressors, or using the global BOLD signal as a regressor of no interest are still debated, and may limit the interpretation of specific findings, including the neural meaning of negative correlations (Deary et al., 2004; Whalley et al., 2005; Fox et al., 2009; Murphy et al., 2009; Weissenbacher et al., 2009).

For instance, the impact of preprocessing on sensitivity and specificity of functional connectivity was recently investigated both in simulated data and in resting state datasets (Fox et al., 2009; Murphy et al., 2009; Weissenbacher et al., 2009). Though this debate is still ongoing, altogether these studies indicated that negative correlations may be in part introduced by global signal regression, and thus should be interpreted with caution. Moreover, while global signal regression may reduce the sensitivity for detecting true correlations, that is, increase the number of false negatives, it maximizes the specificity of positive resting state correlations, as well as the correction for white matter and ventricular time courses (Fox et al., 2009; Weissenbacher et al., 2009).

Another issue to be considered is the effect of modeling the experimental paradigm in our analysis as regressor of no interest in order to remove task-induced changes in BOLD response (Deary et al., 2004; Whalley et al., 2005). As far as the potential residual task effects are concerned, while we cannot rule out completely that some residual effects may still be present, we would like to emphasize that we have modeled the task-related regressors as regressors of no interest exactly in the same manner that was adopted in the GLM analysis for the previous study by Gentili et al. (2008). Among the possible solutions to mitigate task-related effects, this procedure is certainly among the most valid (Deary et al., 2004; Whalley et al., 2005). The question of whether the correlation maps obtained with a functional connectivity approach can be comparable to the task-related patterns has been previously addressed (Biswal et al., 1995; Hampson et al., 2004; Damoiseaux et al., 2006; Mennes et al., 2010). For example, Hampson et al. (2004) directly compared the correlations between the motion sensitive area MT/V5 and other brain regions while subjects where in a resting state (that is, in the absence of any visual stimulation) and in an active stimulation state (that is, visual perception of concentric moving circles). The patterns of correlations obtained in the two different conditions greatly overlapped: while the active state correlations revealed brain regions more specifically related to visual motion processing (middle temporal and occipital cortex), the resting state correlations revealed a broader network including known functional pathways for general visual processing (lingual gyri and cuneus). Thus, while certainly a correlation analysis using resting state data would have been of interest in social phobic patients, based on the findings from the above studies we would expect a substantially similar picture.

In spite of the above discussed limitations and other issues whose discussion would fall far outside the topic of this study, it is undisputable that functional connectivity has made possible to investigate the neural underpinnings of brain function in terms of cerebral networks rather than of a single, isolated brain structure (Horwitz et al., 2005; Kim and Horwitz, 2008; Stephan et al., 2008). Indeed, we would like to emphasize a concept that applies not only to this specific study but also to the investigations of functional connectivity in general. Disruption of functional connectivity, that is, of the way two or more regions are functionally related among themselves, may precede any measurable alteration of activity in any given region. That is, functional connectivity analysis is a powerful tool to identify brain abnormalities in pre-clinical and sub-clinical stages of a disorder. Indeed, this has been shown since the early days of PET studies (see for instance works by Horwitz et al., 1991; Azari et al., 1993; Pietrini et al., 1993, 2009; Grady et al., 2001; Zhang et al., 2010). Thus, individuals with sub-clinical manifestations of Social Phobia may show abnormal functional connectivity patterns in the absence of any absolute group difference in regional activity, similarly to what has been shown in other neuropsychiatric disorders. Furthermore, measures of functional connectivity may then be used to ascertain the effect of psychological or psychopharmacological therapy.

Similarly, by looking at the spatiotemporal synchrony of BOLD signal among brain regions, functional connectivity studies are providing novel evidence that in anxiety disorders, including Social Phobia, a *mis-communication* among multiple brain areas involved in sensory and emotional processing may underlie the main psychopathological manifestations. This possibility is also sustained by the

evidence that DMN areas are abnormally recruited in the rest/task trade-off in social phobic patients, and thus may be associated to a different baseline-rest neural activity (Gentili et al., 2009).

In conclusion, the results of this study indicate that the dynamic cross talking among different areas of the wide network involved in face perception is altered in drug-naïve social phobic patients as compared to healthy individuals. In this interpretative framework, in social phobic patients hyperactivity of regions engaged in emotional expression (amygdala and insula) and facial recognition (superior temporal areas) may be related to the wariness of the others. At the same time, hypoactivation of regions engaged in face perception (fusiform gyrus) and attention (fronto-parietal network) may be related to a weaker cognitive control on the social situation (Lorberbaum et al., 2004).

It has been hypothesized that in anxiety disorders difficulties in defocusing attention from negative stimuli, or from stimuli that have been decoded as negative, may occur along with an increased fear of negative evaluation of contempt (Clark and Wells, 1995). Altered brain networks in response to threatening social stimuli may represent at a neurobiological level the behavioral impairment reported by these patients when exposed to faces (Clark and Wells, 1995; Winton et al., 1995; Lundh and Ost, 1996; Spurr and Stopa, 2002; Horley et al., 2004; Gentili et al., 2009). From a behavioral point of view, social phobic patients show an increase of the fear of negative evaluation and wariness of the others (Schultz and Heimberg, 2008). Therefore, we speculate that the increasing of amygdala–limbic connectivity may represent the neurobiological correlate of this psychopathological aspect.

ACKNOWLEDGMENTS

This research was supported in part by the Fondazione IRIS, Castagneto Carducci (Livorno, Italy). The authors wish to thank Giulio Perugi for help in recruiting social phobic patients, and Massimo Lombardi for running the MRI Laboratory at the Fondazione "G. Monasterio" (Pisa, Italy). We also thank Domenico Montanaro and Franco Lombardo for neuroradiological examinations, Giacomo Handjaras and Lorenzo Sani for their advice on data analysis.

REFERENCES

American Psychiatric Association (APA). (2000). *Diagnostic and Statistical Manual of Mental Disorders*, 4th Edn., Text Revision. Washington, DC: Masson.

Amir, N., Klumpp, H., Elias, J., Bedwell, J. S., Yanasak, N., and Miller, L. S. (2005). Increased activation of the anterior cingulate cortex during processing of disgust faces in individuals with social phobia. *Biol. Psychiatry* 57, 975–981.

Azari, N. P., Pietrini, P., Horwitz, B., Pettigrew, K. D., Leonard, H. L., Rapoport, J. L., Schapiro, M. B., and Swedo, S. E. (1993). Individual differences in cerebral metabolic patterns during pharmacotherapy in obsessive-compulsive disorder: a multiple regression/discriminant analysis of positron emission tomographic data. *Biol. Psychiatry* 34, 798–809.

Benuzzi, F., Pugnaghi, M., Meletti, S., Lui, F., Serafini, M., Baraldi, P., and Nichelli. P. (2007). Processing the socially relevant parts of faces. *Brain Res. Bull.* 74, 344–356.

Birbaumer, N., Grodd, W., Diedrich, O., Klose, U., Erb, M., Lotze, M., Schneider, F., Weiss, U., and Flor, H. (1998). fMRI reveals amygdala activation to human faces in social phobics. *Neuroreport* 9, 1223–1226.

Biswal, B., Yetkin, F. Z., Haughton, V. M., and Hyde, J. S. (1995). Functional connectivity in the motor cortex of resting human brain using echo-planar MRI. *Magn. Reson. Med.* 34, 537–541.

Campbell, D. W., Sareen, J., Paulus, M. P., Goldin, P. R., Stein, M. B., and Reiss, J. P. (2007). Time-varying amygdala response to emotional faces in generalized social phobia. *Biol. Psychiatry* 62, 455–463.

Clark, D. M., and Wells, A. (1995). "A cognitive model of social phobia," in *Social Phobia: Diagnosis, Assessment and Treatment,* eds R. G. Heimberg, M. R. Liebowitz, D. A. Hope, and F. R. Schneier (New York: Guildford Press), 69–93.

Cohen, M. S. (1997). Parametric analysis of fMRI data using linear systems methods. *Neuroimage* 6, 93–103.

Cooney, R. E., Atlas, L. Y., Joormann, J., Eugène, F., and Gotlib, I. H. (2006). Amygdala activation in the processing of neutral faces in social anxiety disorder: is neutral really neutral? *Psychiatry Res.* 148, 55–59.

Cordes, D., Haughton, V. M., Arfanakis, K., Carew, J. D., Turski, P. A., Moritz, C. H., Quigley, M. A., and Meyerand, M. E. (2001). Frequencies contributing to functional connectivity in the cerebral cortex in "resting-state" data. *Am. J. Neuroradiol.* 22, 1326–1333.

Cox, B. (1996). AFNI: software for analysis and visualization of functional magnetic resonance neuroimages. *Comput. Biomed. Res.* 29, 162–173.

Critchley, H. D., Wiens, S., Rotshtein, P., Ohman, A., and Dolan, R. J. (2004). Neural systems supporting interoceptive awareness. *Nat. Neurosci.* 7, 189–195.

Damasio, A. R., Grabowski, T. J., Bechara, A., Damasio, H., Ponto, L. L., Parvizi, J., and Hichwa, R. D. (2000). Subcortical and cortical brain activity during the feeling of selfgenerated emotions. *Nat. Neurosci.* 3, 1049–1056.

Damoiseaux, J. S., Rombouts, S. A., Barkhof, F., Scheltens, P., Stam, C. J., Smith, S. M., and Beckmann, C. F. (2006). Consistent resting-state networks across healthy subjects. *Proc. Natl. Acad. Sci. U.S.A.* 103, 13848–13853.

Deary, I. J., Simonotto, E., Meyer, M., Marshall, A., Marshall. I., Goddard, N. H., and Wardlaw, J. M. (2004). The functional anatomy of inspection time: an event-related fMRI study. *Neuroimage* 22, 1466–1479.

Desjardins, A. E., Kiehl, K. A., and Liddle, P. F. (2001). Removal of confounding effects of global signal in functional MRI analyses. *Neuroimage* 13, 751–758.

Ekman, P., and Friesen, W. V. (1976). Measuring facial movement. *Environ. Psychol. Nonverbal Behav.* 1, 56–75.

Engell, A. D., and Haxby, J. V. (2007). Facial expression and gaze-direction in human superior temporal sulcus. *Neuropsychologia* 45, 3234–3241.

Esposito, F., Aragri, A., Latorre, V., Popolizio, T., Scarabino, T., Cirillo, S., Marciano, E., Tedeschi, G., and Di Salle, F. (2009). Does the default-mode functional connectivity of the brain correlate with working-memory performances? *Arch. Ital. Biol.* 147, 11–20.

Fairhall, S. L., and Ishai, A. (2007). Effective connectivity within the distributed cortical network for face perception. *Cereb. Cortex* 17, 2400–2406.

Fox, M. D., Snyder, A. Z., Vincent, J. L., Corbetta, M., Van Essen, D. C., and Raichle, M. E. (2005). The human brain is intrinsically organized into dynamic, anticorrelated functional networks. *Proc. Natl. Acad. Sci. U.S.A.* 102, 9673–9678.

Fox, M. D., Zhang, D., Snyder, A. Z., and Raichle, M. E. (2009). The global signal and observed anticorrelated resting state brain networks. *J. Neurophysiol.* 101, 3270–3283.

Friston, K. J. (1994). Functional and effective connectivity in neuroimaging: a synthesis. *Hum. Brain Mapp.* 2, 56–78.

Friston, K. J., Buechel, C., Fink, G. R., Morris, J., Rolls, E., and Dolan, R. J. (1997). Psychophysiological and modulatory interactions in neuroimaging. *Neuroimage* 6, 218–229.

Gentili, C., Gobbini, M. I., Ricciardi, E., Vanello, N., Pietrini, P., Haxby, J. V., and Guazzelli, M. (2008). Differential modulation of neural activity throughout the distributed neural system for face perception in patients with Social Phobia and healthy subjects. *Brain Res. Bull.* 77, 286–292.

Gentili, C., Ricciardi, E., Gobbini, M. I., Santarelli, M. F., Haxby, J. V., Pietrini, P., and Guazzelli, M. (2009). Beyond amygdala: default mode network activity differs between patients with social phobia and healthy controls. *Brain Res. Bull.* 79, 409–413.

Grady, C. L., Furey, M. L., Pietrini, P., Horwitz, B., and Rapoport, S. I. (2001). Altered brain functional connectivity and impaired short-term memory in Alzheimer's disease. *Brain* 124, 739–756.

Greicius, M. D., Krasnow, B., Reiss, A. L., and Menon, V. (2003). Functional connectivity in the resting brain: a network analysis of the default mode hypothesis. *Proc. Natl. Acad. Sci. U.S.A.* 100, 253–258.

Gusnard, D. A., Akbudak, E., Shulman, G. L., and Raichle, M. E. (2001). Medial prefrontal cortex and self-referential mental activity: relation to a default mode of brain function. *Proc. Natl. Acad. Sci. U.S.A.* 98, 4259–4264.

Hampson, M., Olson, I. R., Leung, H. C., Skudlarski, P., and Gore, J. C. (2004). Changes in functional connectivity of human MT/V5 with visual motion input. *Neuroreport* 15, 1315–1319.

Haxby, J. V., Hoffman, E. A., and Gobbini, M. I. (2000). The distributed human neural system for face perception. *Trends Cogn. Sci.* 4, 223–233.

Horley, K., Williams, L.M., Gonsalvez, C., and Gordon, E. (2004). Face to face: visual scanpath evidence for abnormal processing of facial expressions in social phobia. *Psychiatry Res.* 127, 43–53.

Horwitz, B. (2003). The elusive concept of brain connectivity. *Neuroimage* 19, 466–470.

Horwitz, B., Friston, K. J., and Taylor, J .G. (2000). Neural modeling and functional brain imaging: an overview. *Neural Netw.* 13, 829–846.

Horwitz, B., Swedo, S. E., Grady, C. L., Pietrini, P., Schapiro, M. B., Rapoport, J. L., and Rapoport, S. I. (1991). Cerebral metabolic pattern in obsessive-compulsive disorder: altered intercorrelations between regional rates of glucose utilization. *Psychiatry Res.* 40, 221–237.

Horwitz, B., Warner, B., Fitzer, J., Tagamets, M. A., Husain, F. T., and Long, T. W. (2005). Investigating the neural basis for functional and effective connectivity. Application to fMRI. *Philos. Trans. R. Soc. Lond., B. Biol. Sci.* 360, 1093–1108.

Ishai, A. (2008). Let's face it: it's a cortical network. *Neuroimage* 40, 415–419.

Ishai, A. (2010). Seeing faces and objects with the "mind's eye". *Arch. Ital. Biol.* 148, 1–9.

Ishai, A., Schmidt, C. F., and Boesiger, P. (2005). Face perception is mediated by a distributed cortical network. *Brain Res. Bull.* 67, 87–93.

Killgore, W. D., and Yurgelun-Todd, D. A. (2005). Social anxiety predicts amygdala activation in adolescents viewing fearful faces. *Neuroreport* 16, 1671–1675.

Kim, J., and Horwitz, B. (2008). Investigating the neural basis for fMRI-based functional connectivity in a blocked design: application to interregional correlations and psycho-physiological interactions. *Magn. Reson. Imaging* 26, 583–593.

Lancaster, J. L., Rainey, L. H., Summerlin, J. L., Freitas, C. S., Fox, P. T., Evans, A. C., Toga, A. W., and Mazziotta, J. C. (1997). Automated labeling of the human brain: a preliminary report on the development and evaluation of a forward-transform method. *Hum. Brain Mapp.* 5, 238–242.

Lancaster, J. L., Woldorff, M. G., Parsons, L. M., Liotti, M., Freitas, C. S., Rainey, L., Kochunov, P. V., Nickerson, D., Mikiten, S. A., and Fox, P. T. (2000). Automated Talairach atlas labels for functional brain mapping. *Hum. Brain Mapp.* 10, 120–131.

Leary, M. R. (1983). Social anxiousness: the construct and its measurement. *J. Personal Assess.* 47, 66–75.

Leary, M. R., and Kowalski, R. M. (1993). The interaction anxiousness scale: construct and criterion-related validity. *J. Personal Assess.* 61, 136–146.

Liebowitz, M. R. (1987). Social phobia. *Mod. Probl. Pharmacopsychiatry* 22, 141–173.

Lorberbaum, J. P., Kose, S., Johnson, M. R., Arana, G. W., Sullivan, L. K., Hamner, M. B., Ballenger, J. C., Lydiard, R. B., Brodrick, P. S., Bohning, D. E., and George, M. S. (2004). Neural correlates of speech anticipatory anxiety in generalized social phobia. *Neuroreport* 15, 2701–2705.

Lundh, L. G., and Ost, L. G. (1996). Recognition bias for critical faces in social phobics. *Behav. Res. Ther.* 34, 787–794.

Macey, P. M., Macey, K. E., Kumar, R., and Harper, R. M. (2004). A method for removal of global effects from fMRI time series. *Neuroimage* 22, 360–366.

Mennes, M., Kelly, C., Zuo, X. N., Di Martino, A., Biswal, B. B., Castellanos, F. X., and Milham, M. P. (2010). Inter-individual differences in resting-state functional connectivity predict task-induced BOLD activity. *Neuroimage* 50, 1690–1701.

Murphy, K., Birn, R. M., Handwerker, D. A., Jones, T. B., and Bandettini, P. A. (2009). The impact of global signal regression on resting state correlations: are anti-correlated networks introduced? *Neuroimage* 44, 893–905.

Phan, K. L., Fitzgerald, D. A., Nathan, P. J., and Tancer, M. E. (2006). Association between amygdala hyperactivity to harsh faces and severity of social anxiety in generalized social phobia. *Biol. Psychiatry* 59, 424–429.

Pietrini, P., Azari, N. P., Grady, C. L., Salerno, J. A., Gonzales-Aviles, A., Heston, L. L., Pettigrew, K. D., Horwitz, B., Haxby, J. V., and Schapiro, M. B. (1993). Pattern of cerebral metabolic interactions in a subject with isolated amnesia at risk for Alzheimer's disease: a longitudinal evaluation. *Dementia* 4, 94–101.

Pietrini, P., Salmon, E., and Nichelli, P. (2009). "Consciousness and dementia: how the brain loses its self," in *The Neurology of Consciousness: Cognitive Neuroscience and Neuropathology*, eds S. Laureys and G. Tononi (Oxford: Academic Press), 204–216.

Raichle, M. E., MacLeod, A. M., Snyder, A. Z., Powers, W. J., Gusnard, D. A., and Shulman, G. L. (2001). A default mode of brain function. *Proc. Natl. Acad. Sci. U.S.A.* 98, 676–682.

Rauch, S. L., Whalen, P. J., Shin, L. M., McInerney, S. C., Macklin, M. L., Lasko, N. B., Orr, S. P., and Pitman, R. K. (2000). Exaggerated amygdala response to masked facial stimuli in posttraumatic stress disorder: a functional MRI study. *Biol. Psychiatry* 47, 769–776.

Rich, B. A., Fromm, S. J., Berghorst, L. H., Dickstein, D. P., Brotman, M. A., Pine, D. S., and Leibenluft, E. (2008). Neural connectivity in children with bipolar disorder: impairment in the face emotion processing circuit. *J. Child Psychol. Psychiatry* 49, 88–96.

Rogers, B. P., Morgan, V. L., Newton, A. T., and Gore, J. C. (2007). Assessing Functional Connectivity in the Human Brain by fMRI. *Magn. Reson. Imaging* 25, 1347–1357.

Schultz, L. T., and Heimberg, R. G. (2008). Attentional focus in social anxiety disorder: potential for interactive processes. *Clin. Psychol. Rev.* 28, 1206–1221.

Spielberger, C. D., Gorsuch, R. L., and Lushene, R. E. (1970). *Manual for the State-Trait Anxiety Inventory*. Palo Alto, CA: Consulting Psychologists Press.

Spurr, J. M., and Stopa, L. (2002). Self-focused attention in social phobia and social anxiety. *Clin. Psychol. Rev.* 22, 947–975.

Stein, M. B., Goldin, P. R., Sareen, J., Zorrilla, L. T., and Brown, G. G. (2002). Increased amygdala activation to angry and contemptuous faces in generalized social phobia. *Arch. Gen. Psychiatry* 59, 1027–1034.

Stein, M. B., Simmons, A. N., Feinstein, J. S., and Paulus, M. P. (2007). Increased amygdala and insula activation during emotion processing in anxiety-prone subjects. *Am. J. Psychiatry* 164, 318–327.

Stephan, K. E., Riera, J. J., Deco, G., and Horwitz, B. (2008). The brain connectivity workshops: moving the frontiers of computational systems neuroscience. *Neuroimage* 42, 1–9.

Straube, T., Kolassa, I. T., Glauer, M., Mentzel, H. J., and Miltner, W. H. (2004). Effect of task conditions on brain responses to threatening faces in social phobics: an event-related functional magnetic resonance imaging study. *Biol. Psychiatry* 56, 921–930.

Talairach, J., and Tournoux, P. (1988). *Coplanar Stereotaxic Atlas of the Human Brain*. New York: Thieme Medical.

Wang, F., Kalmar, J. H., He, Y., Jackowski, M., Chepenik, L. G., Edmiston, E. E., Tie, K., Gong, G., Shah, M. P., Jones, M., Uderman, J., Constable, R. T., and Blumberg, H. P. (2009). Functional and structural connectivity between the perigenual anterior cingulate and amygdala in bipolar disorder. *Biol. Psychiatry* 66, 516–521.

Weissenbacher, A., Kasess, C., Gerstl, F., Lanzenberger, R., Moser, E., and Windischberger, C. (2009). Correlations and anticorrelations in resting-state functional connectivity MRI: a quantitative comparison of preprocessing strategies. *Neuroimage* 47, 1408–1416.

Whalley, H. C., Simonotto, E., Marshall, I., Owens, D. G., Goddard, N. H., Johnstone, E. C., and Lawrie, S. M. (2005). Functional disconnectivity in subjects at high genetic risk of schizophrenia. *Brain* 128, 2097–2108.

Winston, J. S., O'Doherty, J., and Dolan, R. J. (2003). Common and distinct neural responses during direct and incidental processing of multiple facial emotions. *Neuroimage* 20, 84–97.

Winston, J. S., Henson, R. N., Fine-Goulden, M. R., and Dolan, R. J. (2004). fMRI-adaptation reveals dissociable neural representations of identity and expression in face perception. *J. Neurophysiol.* 92, 1830–1839.

Winton, E. C., Clark, D. M., and Edelmann, R. J. (1995). Social anxiety, fear of negative evaluation and the detection of negative emotion in others. *Behav. Res. Ther.* 33, 193–196.

Zhang, H. Y., Wang, S. J., Liu, B., Ma, Z. L., Yang, M., Zhang, Z. J., and Teng, G. J. (2010). Resting brain connectivity: changes during the progress of Alzheimer disease. *Radiology* 256, 598–606.

Zhao, X. H., Wang, P. J., Li, C. B., Hu, Z. H., Xi, Q., Wu, W. Y., and Tang, X. W. (2007). Altered default mode network activity in patient with anxiety disorders: an fMRI study. *Eur. J. Radiol.* 63, 373–378.

Conflict of Interest Statement: The authors declare that the research was conducted in the absence of any commercial or financial relationships that could be construed as a potential conflict of interest.

Received: 12 July 2010; accepted: 19 October 2010; published online: 22 November 2010.

Citation: Danti S, Ricciardi E, Gentili C, Gobbini MI, Pietrini P and Guazzelli M (2010) Is Social Phobia a "miscommunication" disorder? Brain functional connectivity during face perception differs between patients with Social Phobia and healthy control subjects. Front. Syst. Neurosci. ***4****:152. doi: 10.3389/fnsys.2010.00152*

Copyright © 2010 Danti, Ricciardi, Gentili, Gobbini, Pietrini and Guazzelli. This is an open-access article subject to an exclusive license agreement between the authors and the Frontiers Research Foundation, which permits unrestricted use, distribution, and reproduction in any medium, provided the original authors and source are credited.